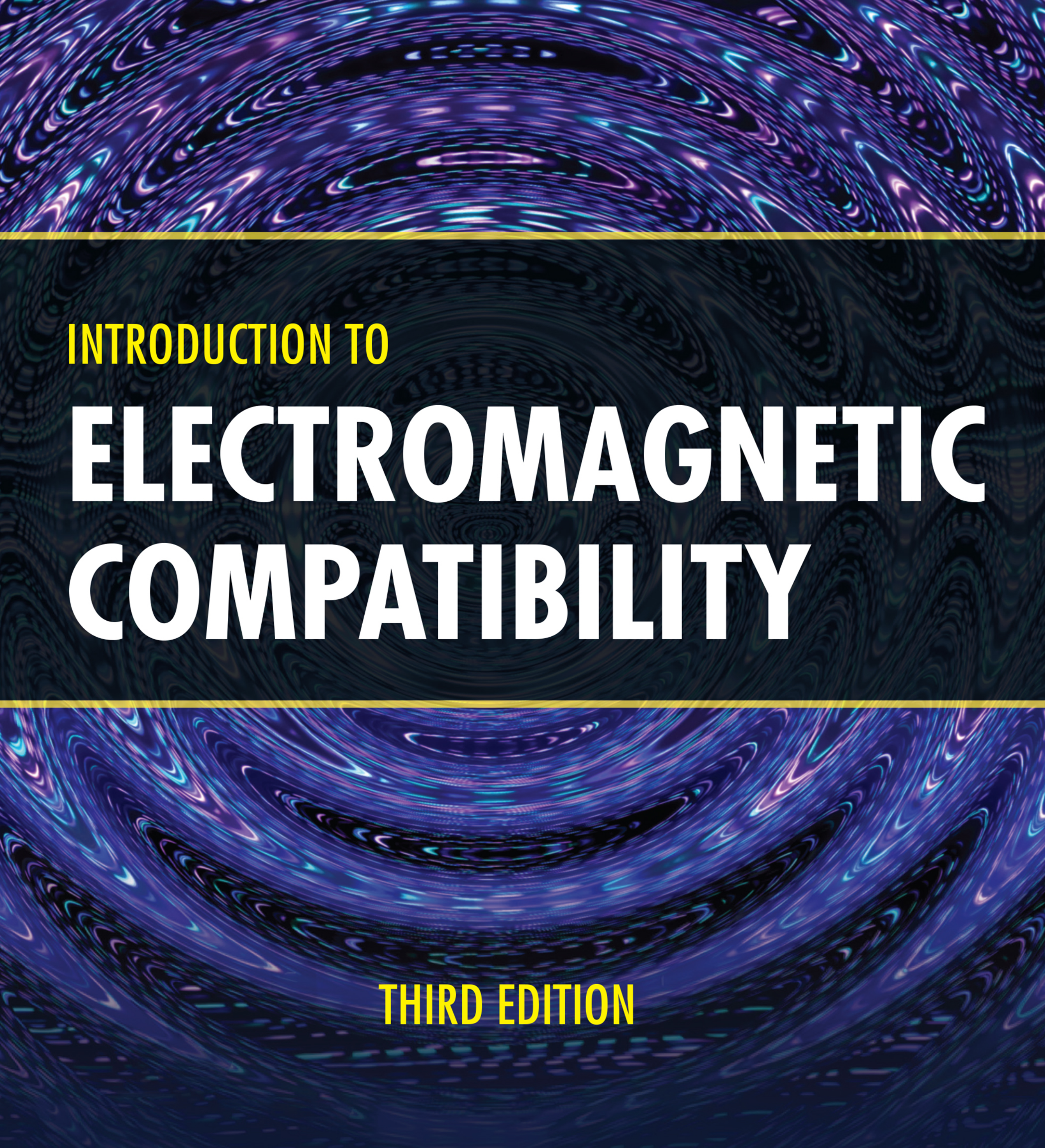

INTRODUCTION TO

ELECTROMAGNETIC COMPATIBILITY

THIRD EDITION

CLAYTON R. PAUL • ROBERT C. SCULLY • MARK A. STEFFKA

WILEY

Introduction to Electromagnetic Compatibility

Introduction to Electromagnetic Compatibility

Third Edition

CLAYTON R. PAUL
ROBERT C. SCULLY
MARK A. STEFFKA

WILEY

This edition first published 2023
© 2023 John Wiley and Sons, Inc.

Edition history:
2e: 2006, Wiley; 1e: 1992, Wiley

All rights reserved. No part of this publication may be reproduced, stored in a retrieval system, or transmitted, in any form or by any means, electronic, mechanical, photocopying, recording or otherwise, except as permitted by law. Advice on how to obtain permission to reuse material from this title is available at http://www.wiley.com/go/permissions.

The right of Clayton R. Paul, Robert C. Scully, and Mark A. Steffka to be identified as the authors of the editorial material in this work has been asserted in accordance with law.

Registered Office
John Wiley & Sons, Inc., 111 River Street, Hoboken, NJ 07030, USA

Editorial Office
111 River Street, Hoboken, NJ 07030, USA

For details of our global editorial offices, customer services, and more information about Wiley products visit us at www.wiley.com.

Wiley also publishes its books in a variety of electronic formats and by print-on-demand. Some content that appears in standard print versions of this book may not be available in other formats.

Limit of Liability/Disclaimer of Warranty
In view of ongoing research, equipment modifications, changes in governmental regulations, and the constant flow of information relating to the use of experimental reagents, equipment, and devices, the reader is urged to review and evaluate the information provided in the package insert or instructions for each chemical, piece of equipment, reagent, or device for, among other things, any changes in the instructions or indication of usage and for added warnings and precautions. While the publisher and authors have used their best efforts in preparing this work, they make no representations or warranties with respect to the accuracy or completeness of the contents of this work and specifically disclaim all warranties, including without limitation any implied warranties of merchantability or fitness for a particular purpose. No warranty may be created or extended by sales representatives, written sales materials or promotional statements for this work. The fact that an organization, website, or product is referred to in this work as a citation and/or potential source of further information does not mean that the publisher and authors endorse the information or services the organization, website, or product may provide or recommendations it may make. This work is sold with the understanding that the publisher is not engaged in rendering professional services. The advice and strategies contained herein may not be suitable for your situation. You should consult with a specialist where appropriate. Further, readers should be aware that websites listed in this work may have changed or disappeared between when this work was written and when it is read. Neither the publisher nor authors shall be liable for any loss of profit or any other commercial damages, including but not limited to special, incidental, consequential, or other damages.

Library of Congress Cataloging-in-Publication Data Applied for:

Hardback ISBN: 9781119404347

Cover Design: Wiley
Cover Image: © optimarc/Shutterstock

Set in 10/12pt TimesLTStd by Straive, Chennai, India

Contents

Preface **xiii**

1 Introduction to Electromagnetic Compatibility (EMC) **1**

1.1 Aspects of EMC 2
1.2 Electrical Dimensions and Waves 9
1.3 Decibels and Common EMC Units 16
  1.3.1 Signal Source Specification 24
1.4 Summary 30
Problems 31
References 34

2 EMC Requirements for Electronic Systems **35**

2.1 Governmental Requirements 36
  2.1.1 Requirements for Commercial Products Marketed in the United States 36
  2.1.2 Requirements for Commercial Products Marketed Outside the United States 40
  2.1.3 Requirements for Military Products Marketed in the United States 44
  2.1.4 Measurement of Emissions for Verification of Compliance 48
    2.1.4.1 Radiated Emissions 49
    2.1.4.2 Conducted Emissions 51
  2.1.5 Typical Product Emissions 54
  2.1.6 A Simple Example to Illustrate the Difficulty in Meeting the Regulatory Limits 60
2.2 Additional Product Requirements 62
  2.2.1 Radiated Susceptibility (Immunity) 62
  2.2.2 Conducted Susceptibility (Immunity) 62
  2.2.3 Electrostatic Discharge (ESD) 62
  2.2.4 Requirements for Commercial Aircraft 63
  2.2.5 Requirements for Commercial Vehicles 63
2.3 Design Constraints for Products 63
2.4 Advantages of EMC Design 64
Problems 66
References 69

3 Signal Spectra—the Relationship between the Time Domain and the Frequency Domain 71

3.1 Periodic Signals 71
    3.1.1 The Fourier Series Representation of Periodic Signals 74
    3.1.2 Response of Linear Systems to Periodic Input Signals 82
    3.1.3 Important Computational Techniques 86
3.2 Spectra of Digital Waveforms 93
    3.2.1 The Spectrum of Trapezoidal (Clock) Waveforms 93
    3.2.2 Spectral Bounds for Trapezoidal Waveforms 96
        3.2.2.1 Effect of Rise/Falltime on Spectral Content 97
        3.2.2.2 Bandwidth of Digital Waveforms 105
        3.2.2.3 Effect of Repetition Rate and Duty Cycle 108
        3.2.2.4 Effect of Ringing (Undershoot/Overshoot) 109
    3.2.3 Use of Spectral Bounds in Computing Bounds on the Output Spectrum of a Linear System 111
3.3 Spectrum Analyzers 113
    3.3.1 Basic Principles 115
    3.3.2 Peak Versus Quasi-Peak Versus Average 117
3.4 Representation of Nonperiodic Waveforms 118
    3.4.1 The Fourier Transform 119
    3.4.2 Response of Linear Systems to Nonperiodic Inputs 121
3.5 Representation of Random (Data) Signals 121
Problems 124
References 132

4 Transmission Lines and Signal Integrity 133

4.1 The Transmission-Line Equations 136
4.2 The Per-Unit-Length Parameters 139
    4.2.1 Wire-Type Structures 141
    4.2.2 Printed Circuit Board (PCB) Structures 151
4.3 The Time-Domain Solution 155
    4.3.1 Graphical Solutions 156
    4.3.2 The Branin Method 167
4.4 High-Speed Digital Interconnects and Signal Integrity 170
    4.4.1 Effect of Terminations on the Line Waveforms 170
        4.4.1.1 Effect of Capacitive Terminations 174
        4.4.1.2 Effect of Inductive Terminations 176
    4.4.2 Matching Schemes for Signal Integrity 177
    4.4.3 When Does the Line Not Matter, i.e., When is Matching Not Required? 179
    4.4.4 Effects of Line Discontinuities 180
4.5 Sinusoidal Excitation of the Line and the Phasor Solution 192
    4.5.1 Voltage and Current as Functions of Position 193
    4.5.2 Power Flow 199
    4.5.3 Inclusion of Losses 200
    4.5.4 Effect of Losses on Signal Integrity 202
4.6 Lumped-Circuit Approximate Models 210
Problems 212
References 219

5 Nonideal Behavior of Components 221

5.1 Wires 222
  5.1.1 Resistance and Internal Inductance of Wires 223
  5.1.2 External Inductance and Capacitance of Parallel Wires 229
  5.1.3 Lumped Equivalent Circuits of Parallel Wires 230
5.2 Printed Circuit Board (PCB) Lands 232
5.3 Effect of Component Leads 235
5.4 Resistors 237
5.5 Capacitors 243
5.6 Inductors 251
5.7 Ferromagnetic Materials—Saturation and Frequency Response 255
5.8 Ferrite Beads 258
5.9 Common-Mode Chokes 261
5.10 Electromechanical Devices 264
  5.10.1 DC Motors 265
  5.10.2 Stepper Motors 267
  5.10.3 AC Motors 267
  5.10.4 Solenoids 268
5.11 Digital Circuit Devices 269
5.12 Effect of Component Variability 270
5.13 Mechanical Switches 270
  5.13.1 Arcing at Switch Contacts 271
  5.13.2 The Showering Arc 274
  5.13.3 Arc Suppression 275
Problems 278
References 284

6 Conducted Emissions and Susceptibility 287

6.1 Measurement of Conducted Emissions 288
  6.1.1 The Line Impedance Stabilization Network (LISN) 288
  6.1.2 Common- and Differential-Mode Currents Again 291
6.2 Power Supply Filters 294
  6.2.1 Basic Properties of Filters 294
  6.2.2 A Generic Power Supply Filter Topology 297
  6.2.3 Effect of Filter Elements on Common- and Differential-Mode Currents 298
  6.2.4 Separation of the Conducted Emissions into Common- and Differential-Mode Currents for Diagnostic Purposes 303
6.3 Power Supplies 310
  6.3.1 Linear Power Supplies 311
  6.3.2 Switched-Mode Power Supplies (SMPS) 312
  6.3.3 Effect of Power Supply Components on Conducted Emissions 315
6.4 Power Supply and Filter Placement 319
6.5 Conducted Susceptibility 321
Problems 321
References 323

7 Antennas 325

7.1 Elemental Dipole Antennas 325
  7.1.1 The Electric (Hertzian) Dipole 325
  7.1.2 The Magnetic Dipole (Loop) 330
7.2 The Half-Wave Dipole and Quarter-Wave Monopole Antennas 332
7.3 Antenna Arrays 342
7.4 Characterization of Antennas 349
  7.4.1 Directivity and Gain 349
  7.4.2 Effective Aperture 354
  7.4.3 Antenna Factor 356
  7.4.4 Effects of Balancing and Baluns 359
  7.4.5 Impedance Matching and the Use of Pads 362
7.5 The FRIIs Transmission Equation 365
7.6 Effects of Reflections 368
  7.6.1 The Method of Images 368
  7.6.2 Normal Incidence of Uniform Plane Waves on Plane, Material Boundaries 368
  7.6.3 Multipath Effects 376
7.7 Broadband Measurement Antennas 381
  7.7.1 The Biconical Antenna 381
  7.7.2 The Log-Periodic Antenna 385
7.8 Antenna Modeling and Simulation 388
  7.8.1 Why Model Antennas? 388
  7.8.2 Modeling Methods 389
  7.8.3 Summary 389
Problems 390
References 395

8 Radiated Emissions and Susceptibility 397

8.1 Simple Emission Models for Wires and PCB Lands 398
  8.1.1 Differential-Mode Versus Common-Mode Currents 398
  8.1.2 Differential-Mode Current Emission Model 402
  8.1.3 Common-Mode Current Emission Model 405
  8.1.4 Current Probes 410
  8.1.5 Experimental Results 414
8.2 Simple Susceptibility Models for Wires and PCB Lands 423
  8.2.1 Experimental Results 433
  8.2.2 Shielded Cables and Surface Transfer Impedance 435
Problems 438
References 443

9 Crosstalk 445

9.1 Three-Conductor Transmission Lines and Crosstalk 446
9.2 The Transmission-Line Equations for Lossless Lines 449
9.3 The Per-Unit-Length Parameters 452
  9.3.1 Homogeneous Versus Inhomogeneous Media 452
  9.3.2 Wide-Separation Approximations for Wires 454
  9.3.3 Numerical Methods for Other Structures 463

9.3.3.1 Wires with Dielectric Insulations (Ribbon Cables) 468
9.3.3.2 Rectangular Cross-Section Conductors (PCB Lands) 472
9.4 The Inductive–Capacitive Coupling Approximate Model 476
9.4.1 Frequency-Domain Inductive–Capacitive Coupling Model 479
9.4.1.1 Inclusion of Losses: Common-Impedance Coupling 481
9.4.1.2 Experimental Results 484
9.4.2 Time-Domain Inductive–Capacitive Coupling Model 490
9.4.2.1 Inclusion of Losses: Common-Impedance Coupling 494
9.4.2.2 Experimental Results 495
9.5 Shielded Wires 500
9.5.1 Per-Unit-Length Parameters 500
9.5.2 Inductive and Capacitive Coupling 503
9.5.3 Effect of Shield Grounding 510
9.5.4 Effect of Pigtails 518
9.5.5 Effects of Multiple Shields 519
9.5.6 MTL Model Predictions 521
9.6 Twisted Wires 529
9.6.1 Per-Unit-Length Parameters 530
9.6.2 Inductive and Capacitive Coupling 533
9.6.3 Effects of Twist 539
9.6.4 Effects of Balancing 546
Problems 549
References 555

10 Shielding 557

10.1 Shielding Effectiveness 561
10.2 Shielding Effectiveness: Far-Field Sources 563
10.2.1 Exact Solution 564
10.2.2 Approximate Solution 567
10.2.2.1 Reflection Loss 568
10.2.2.2 Absorption Loss 570
10.2.2.3 Multiple-Reflection Loss 570
10.2.2.4 Total Loss 573
10.3 Shielding Effectiveness: Near-Field Sources 576
10.3.1 Near Field Versus Far Field 576
10.3.2 Electric Sources 580
10.3.3 Magnetic Sources 580
10.4 Low-Frequency, Magnetic Field Shielding 581
10.5 Effects of Apertures 585
Problems 589
References 590

11 System Design for EMC 593

11.1 Changing the Way we Think About Electrical Phenomena 597
11.1.1 Nonideal Behavior of Components and the Hidden Schematic 597
11.1.2 “Electrons Do Not Read Schematics” 601
11.1.3 What Do We Mean by the Term “Shielding” 603
11.2 What do we Mean by the Term “Ground” 605

11.2.1 Safety Ground 608
11.2.2 Signal Ground 610
11.2.3 Ground Bounce and Partial Inductance 612
11.2.3.1 Partial Inductance of Wires 615
11.2.3.2 Partial Inductance of PCB Lands 620
11.2.4 Currents Return to Their Source on the Paths of Lowest Impedance 621
11.2.5 Utilizing Mutual Inductance and Image Planes to Force Currents to Return on a Desired Path 626
11.2.6 Single-Point Grounding, Multipoint Grounding, and Hybrid Grounding 629
11.2.7 Ground Loops and Subsystem Decoupling 634
11.3 Printed Circuit Board (PCB) Design 636
11.3.1 Component Selection 637
11.3.2 Component Speed and Placement 637
11.3.3 Cable I/O Placement and Filtering 639
11.3.4 The Important Ground Grid 641
11.3.5 Power Distribution and Decoupling Capacitors 641
11.3.6 Reduction of Loop Areas 651
11.3.7 Mixed-Signal PCB Partitioning 652
11.4 System Configuration and Design 655
11.4.1 System Enclosures 655
11.4.2 Power Line Filter Placement 656
11.4.3 Interconnection and Number of Printed Circuit Boards 657
11.4.4 Internal Cable Routing and Connector Placement 658
11.4.5 PCB and Subsystem Placement 659
11.4.6 PCB and Subsystem Decoupling 659
11.4.7 Motor Noise Suppression 660
11.4.8 Electrostatic Discharge (ESD) 661
11.5 Diagnostic Tools 672
11.5.1 The Concept of Dominant Effect in the Diagnosis of EMC Problems 674
Problem 680
References 681

Appendix A The Phasor Solution Method 683

A.1 Solving Differential Equations for their Sinusoidal, Steady-State Solution 683
A.2 Solving Electric Circuits for Their Sinusoidal, Steady-State Response 687
Problems 689
Reference 692

Appendix B The Electromagnetic Field Equations and Waves 693

B.1 Vector Analysis 694
B.2 Maxwell's Equations 701
B.2.1 Faraday's Law 701
B.2.2 Ampere's Law 711
B.2.3 Gauss' Laws 716
B.2.4 Conservation of Charge 719
B.2.5 Constitutive Parameters of the Medium 719
B.3 Boundary Conditions 720
B.4 Sinusoidal Steady State 724
B.5 Power Flow 725
B.6 Uniform Plane Waves 726

B.6.1 Lossless Media 729
B.6.2 Lossy Media 734
B.6.3 Power Flow 737
B.6.4 Conductors versus Dielectrics 738
B.6.5 Skin Depth 740
B.7 Static (DC) Electromagnetic Field Relations—a Special Case 741
B.7.1 Maxwell's Equations for Static (DC) Fields 742
B.7.1.1 Range of Applicability for Low-Frequency Fields 742
B.7.2 Two-Dimensional Fields and Laplace's Equation 743
Problems 744
References 752

Appendix C Computer Codes for Calculating the Per-Unit-Length (PUL) Parameters and Crosstalk of Multiconductor Transmission Lines 753

C.1 WIDESEP.FOR for Computing the PUL Parameter Matrices of Widely Spaced Wires 754
C.2 RIBBON.FOR for Computing the PUL Parameter Matrices of Ribbon Cables 758
C.3 PCB.FOR for Computing The PUL Parameter Matrices of Printed Circuit Boards 760
C.4 MSTRP.FOR for Computing the PUL Parameter Matrices of Coupled Microstrip Lines 761
C.5 STRPLINE.FOR for Computing the PUL Parameter Matrices of Coupled Striplines 762

Appendix D A Spice (PSPICE, LTSPICE, etc.) Tutorial and Applications Guide 765

D.1 Creating a Spice or Pspice Simulation 766
D.1.1 Circuit Description 767
D.1.2 Execution Statements 771
D.1.3 Output Statements 773
D.1.4 Examples 774
D.2 Creating an Ltspice Simulation 777
D.3 Lumped-Circuit Approximate Models 785
D.4 An Exact Spice (Pspice) Model for Lossless, Coupled Lines 788
D.4.1 Computed Versus Experimental Results for Wires 792
D.4.2 Computed Versus Experimental Results for PCBs 798
D.5 Use of Spice (Pspice) in Fourier Analysis 805
D.6 Spicemtl.For for Computing a Spice (Pspice) Subcircuit Model of a Lossless, Multiconductor Transmission Line 815
D.7 Spicelpi.For for Computing a Spice (Pspice) Subcircuit of a Lumped-Pi Model of a Lossless, Multiconductor Transmission Line 817
Problems 818
References 820

Appendix E A Brief History of Electromagnetic Compatibility 823

E.1 History of EMC 823
E.2 Examples 825

Index 827

Preface

Nearly, 30 years have passed since our esteemed colleague, mentor, and friend, Dr. Clayton R. Paul first published his textbook *Introduction to Electromagnetic Compatibility*. One of, if not the, most thorough and highest quality texts of its kind, Dr. Paul's book has become in that nearly 30-year time frame one of the world's most well-known and most widely referenced works on EMC ever written.

Dr. Paul's work has more than survived the "test of time." The foundation he established has enabled two generations (and counting!) of researchers, engineers, and technicians, to not only successfully master the fundamentals of the EMC discipline but to confront the seemingly ever-increasing number of EMC requirements levied against all sorts of systems and products, from the largest power generation and distribution systems to the highly integrated and advanced technologies found in the billions of handheld devices in daily use around the world.

Given the stature and ageless character of Dr. Paul's work, with a strong and abiding sense of humility, it is our great honor and privilege to present this third edition of Dr. Paul's outstanding textbook *Introduction to Electromagnetic Compatibility*.

Our goal in editing this work was to undertake a detailed and critical evaluation of every aspect of the second edition, including the physical and mathematical principles and fundamentals necessary to the practice of the EMC discipline presented in the text, the many and varied analytical tools provided by Dr. Paul to assist in the understanding of the complexities and vagaries of EMC issues, and the plethora of examples used to emphasize and provide insight into the material content.

We are pleased to say we have met our goal and have determined that Dr. Paul's amazing ability to translate and apply his insight and knowledge of the relevant physics, mathematics, and circuit theory, to electrical and electronics systems' EMC remains as essential today as it was at the time of publication of the first edition, and as it will undoubtedly remain into the foreseeable future.

One of the areas that garnered our close attention was how to address the proliferation of computer circuit analysis tools such as SPICE and its many derivatives and iterations, along with the explosion of EMC and antenna modeling simulation tools, having occurred since Dr. Paul's original work. Dr. Paul was an early and staunch advocate of the use of such tools, and it is our opinion that Dr. Paul would be pleased with and highly supportive of their use. The abundance of such tools, however, was something of a two-edged sword for us, as it proved impossible to effectively incorporate the almost certainly countless examples of so many different tools in this text. We ultimately decided not to attempt to do so, electing to maintain the primary thrust of the text as a focused survey of all things EMC as Dr. Paul originally intended it. We did add some brief information regarding the use of antenna modeling tools in Chapter 7. We also elected to retain Appendix D that provides basic information on the use of SPICE, and to expand the Appendix with examples of some of Dr. Paul's excellent tutorials and applications excised from the main body of the text. We took the liberty of adding basic tutorial information for the use of LTSPICE, a freely available, more recent iteration of SPICE. This allowed us to reduce the number of "SPICE" examples in this edition (compared to previous ones) to encourage the reader to use SPICE, LTSPICE, or any other analytical tools with which they are most familiar, to explore and develop their own insight into those methods as applied to EMC analysis.

Many students and practitioners of the EMC discipline have struggled over time with numerical results and how to present them, or interpret them, from the perspective of the "right" number of significant digits to include, and a brief section discussing this important topic has been added to Chapter 1. The section on Power Loss in Cables was deleted in favor of entirely similar information originally included in Sections 4.5.2 through 4.5.4 of Chapter 4. All references in the various chapters were checked and revised as necessary, particularly for EMC standards cited in the text. It is expected those will continue to evolve and be updated many times during the useful lifetime of this edition of the textbook, and the reader is encouraged to keep track of such changes independently. The sections on the History of EMC and some illustrative examples in Chapter 1 have been relocated to Appendix E. Numerous editorial corrections were made to correct spelling, grammatical, and duplicative errors found throughout the text.

We would like to express our heartfelt thanks to our editors, Sarah Keegan and Sarah Lemore, both of whom exhibited seemingly unlimited patience working with us as we navigated this effort though job changes, retirements, relocations, pandemics, and other unexpected challenges. We would also like to thank our spouses for their unstinting support and understanding through long hours of keyboard sessions in the midst of all the foregoing trials and tribulations. We would also like to express our appreciation to Adam Fuchs, one of Mark Steffka's recent students at the *University of Detroit - Mercy*, for his work in revising the content of Chapter 1 and developing the tutorial on the use of LTSPICE. Both of those tasks that he took on will certainly help the reader of this book.

Finally, although Dr. Paul's physical presence with us sadly came to an end a few years ago, it is our fervent wish and desire that his work and legacy live on forever.

ROBERT C. SCULLY
Salida, CO

MARK A. STEFFKA
Canton, MI

December 2021

CHAPTER ONE

Introduction to Electromagnetic Compatibility (EMC)

Since the early days of radio and telegraph communications, it has been known that a spark gap generates electromagnetic waves rich in spectral content (frequency components) and that these waves can cause interference or noise in various electronic and electrical devices such as radio receivers and telephone communications. Numerous other sources of electromagnetic emissions such as lightning, relays, dc electric motors, and fluorescent lights also generate electromagnetic waves that are rich in spectral content and can cause interference in those devices. There are also sources of electromagnetic emissions that contain only a narrow band of frequencies. High-voltage power transmission lines generate electromagnetic emissions at the power frequency [60 Hz; 50 Hz in Europe]. Radio transmitters transmit desired emissions by encoding information (voice, music, etc.) on a carrier frequency. Radio receivers intercept these electromagnetic waves, amplify them, and extract the information that is encoded in the wave. Radar transmitters may transmit pulses of a single-frequency carrier or may transmit a band of frequencies using a chirp modulation scheme. The spectral content of such radar pulse transmissions is distributed over a larger band of frequencies around the carrier than are radio transmissions. Another important and increasingly significant source of electromagnetic emissions is associated particularly with digital computers, and digital electronic devices in general. These digital devices utilize pulses to signify a binary number, 0 (off) or 1 (on). Numbers and other symbols are represented as sequences of these binary digits. The transition time of the pulse from off to on and vice versa is perhaps the most important factor in determining the spectral content of the pulse. Fast (short) transition times generate a wider range of frequencies than do slower (longer) transition times. The spectral content of digital devices generally occupies a wide range of frequencies and can be a major contributor to electromagnetic interference in electrical and electronic devices.

This text is concerned with the ability of these types of electromagnetic emissions to cause *interference* in electrical and electronic devices. The reader has no doubt experienced noise produced in an AM radio by nearby lightning discharges. The lightning discharge is rich in frequency components, some of which pass through the input filter of the radio, causing noise to be superimposed on the desired signal. Also, even though a radio may not be tuned to a particular transmitter frequency, the transmission may be received, causing the reception of an unintended signal. These are

---

Introduction to Electromagnetic Compatibility, Third Edition. Clayton R. Paul, Robert C. Scully, and Mark A. Steffka.
© 2023 John Wiley & Sons, Inc. Published 2023 by John Wiley & Sons, Inc.

examples of interference produced in *intentional receivers*. Of equal importance is the interference produced in *unintentional receivers*. For example, a strong transmission from an FM radio station or TV station may be picked up by a digital computer, causing the computer to interpret it as data or a control signal resulting in incorrect function of the computer. Conversely, a digital computer may create emissions that couple into a TV, causing interference.

This text is also concerned with the design of electronic systems such that interference from or to that system will be minimized. The emphasis will be on *digital* electronic systems. An electronic system able to function compatibly with other electronic systems and not produce or be susceptible to interference is said to be *electromagnetically compatible* with its environment. The objective of this text is to learn how to design electronic systems for *electromagnetic compatibility* (EMC). A system is electromagnetically compatible with its environment if it satisfies three criteria:

1. It does not cause interference with other systems.
2. It is not susceptible to emissions from other systems.
3. It does not cause interference with itself.

Designing for EMC is not only important for the desired functional performance; the device must also meet *legal* requirements in virtually all countries of the world before it can be sold. Designing an electronic product to perform a new and exciting function is a waste of effort if it cannot be placed on the market!

EMC design techniques and methodology have become an integral part of the design of electrical and electronic devices and systems. Consequently, the material in this text has become a fundamental part of an electrical engineer's background. This will no doubt increase in importance as the trend toward increased clock speeds and data rates of digital systems continues.

This text is intended for a university course in electromagnetic compatibility in an undergraduate/graduate curriculum in electrical engineering. There are textbooks available that concern EMC, but these are designed primarily for the industrial professional. Consequently, we will draw on a number of sources for reference material. These will be given at the end of each chapter, and their reference will be denoted in the text by brackets (e.g., [xx]). Numerous trade journals, EMC conference proceedings, and the *Institute of Electrical and Electronics Engineers* (IEEE) *Transactions on Electromagnetic Compatibility* contain useful tutorial articles on various aspects of EMC that we will discuss, and these will similarly be referenced where appropriate. The most important aspect in successfully dealing with EMC design is to have a sound understanding of the basic principles of electrical engineering (circuit analysis, electronics, signals, electromagnetics, linear system theory, digital system design, etc.). We will therefore review these basics so that the fundamentals will be understood and can be used effectively and correctly by the reader in solving the EMC problem. A representative set of such basic texts is [1–3]. A representative but not exhaustive list of texts that cover the general aspects of EMC is represented by [4–13]. The text by Ott [4] will form our primary EMC text reference. Other texts and journal articles that cover aspects of EMC will be referenced in the appropriate chapters. Textbooks on the design of high-speed digital systems are represented by [14–16]. For a discussion of the evolution of this EMC course, see [17, 18].

1.1 ASPECTS OF EMC

As illustrated above, EMC is concerned with the *generation, transmission*, and *reception* of electromagnetic energy. These three aspects of the EMC problem form the basic framework of any EMC design. This is illustrated in Fig. 1.1. A *source* (also referred to as an *emitter*) produces the emission, and a *transfer* or *coupling path* conveys the emission energy to a *receptor (receiver)*, where it is

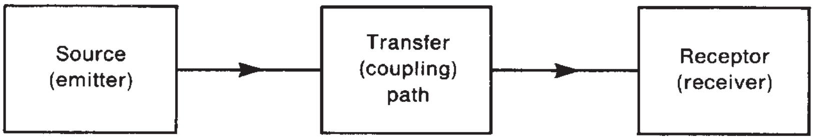

FIGURE 1.1 The basic decomposition of the EMC coupling problem.

processed, resulting in either desired or undesired behavior. Coupling, referred to often in this text, is the desired or undesired transfer of energy from one medium to another. Examples of coupling include capacitive coupling, inductive coupling, or even something as simple as a copper wire connecting two devices. *Interference occurs if the received energy causes the receptor to behave in an undesired manner*. Transfer of electromagnetic energy occurs frequently via unintended coupling modes. However, the unintentional transfer of energy causes interference only if the received energy is of sufficient magnitude and/or spectral content to cause the receptor to behave in an undesired fashion. *Unintentional transmission or reception of electromagnetic energy is not necessarily detrimental; undesired behavior of the receptor constitutes interference*. So the *processing of the received energy* by the receptor is an important part of the question of whether interference will occur. Quite often it is difficult to determine, a priori, whether a signal that is incident on a receptor will cause interference in that receptor. For example, clutter on a radar scope may cause a novice radar operator to incorrectly interpret the desired data, whereas the clutter may not create problems for an operator who has considerable experience. In one case we have interference and in the other we do not, although one could argue that the receptor is the radar operator and not the radar receiver. This points out that it is often difficult to uniquely identify the three aspects of the problem shown in Fig. 1.1!

It is also important to understand that a source or receptor may be classified as intended or unintended. In fact, a source or receptor may behave in both modes. Whether the source or the receptor is intended or unintended *depends on the coupling path, as well as the type of source or receptor*. As an example, a radio station transmitter whose transmission is picked up by a radio receiver that is tuned to that carrier frequency constitutes an intended emitter. On the other hand, if the same radio transmission is processed by another radio receiver that is not tuned to the carrier frequency of the transmitter, then the emission is unintended. (Actually the emission is still intended but the coupling path is not.) There are some emitters whose emissions can serve no useful purpose. An example is the (nonvisible) electromagnetic emission from a fluorescent light.

This suggests that there are three ways to prevent interference:

1. Suppress the emission at its source.
2. Make the coupling path as inefficient as possible.
3. Make the receptor less susceptible to the emission.

As we proceed through the examination of the EMC problem, these three alternative solutions should be kept in mind. The “first line of defense” is to suppress the emission as much as possible at the source. For example, we will find that fast (short) rise/falltimes of digital pulses are the primary contributors to the high-frequency spectral content of these signals. In general, the higher the frequency of the signal to be passed through the coupling path, the more efficient the coupling path. So we should slow (increase) the rise/falltimes of digital signals as much as possible. However, the rise/falltimes of digital signals can be increased only to a point at which the digital circuitry malfunctions. Reducing the high-frequency spectral content of an emission tends to inherently reduce the efficiency of the coupling path and hence reduces the signal level at the receptor. There are “brute force” methods of reducing the efficiency of the coupling path that we will discuss. For example, placing the receptor in a metal enclosure (a shield) will serve to reduce the efficiency of the coupling path. Shielded enclosures are more expensive than reducing the rise/falltime of the emitter, and in practice, their actual performance in an installation may be far less than ideal. Reducing the susceptibility of the receptor is quite often difficult to implement and still preserve the desired function of the product. An example of implementing reduced susceptibility of a receptor to noise would be the use of error-correcting codes in a digital receptor. Although undesired electromagnetic energy is incident on the receptor, the error-correcting codes may allow the receptor to function properly in the presence of a potentially troublesome signal. If the reader will think in terms of reducing the coupling by working from left to right in Fig. 1.1, success will usually be easier to achieve and with less additional cost to the system design. Minimizing the cost added to a system to make it electromagnetically compatible is highly desirable and is an important consideration in EMC design. One can put all electronic products in metallic enclosures and power them with internal batteries, but the product appearance, utility, and cost would very likely be unacceptable to the customer.

We may further break the transfer of electromagnetic energy as it pertains to the prevention of interference, into four subgroups: *radiated emissions, radiated susceptibility, conducted emissions*, and *conducted susceptibility*, as illustrated in Fig. 1.2. A typical electronic system usually consists of one or more subsystems that communicate with each other via cables (bundles of wires). A means for providing power to these subsystems may be a commercial ac (alternating current) power system connected to the installation site. One or more power supplies in a typical electronic system converts the available ac power (may be 120 V, 60 Hz voltage in the US, or 240 V, 50 Hz in Europe) to the various dc (direct current) voltage levels required to power the internal electronic components of the system. For example, 3.3 Vdc to 5 Vdc may be required to power the digital logic, +12 Vdc, and − 12 Vdc voltages may be required to power analog electronics. Other dc voltages may be required to power devices such as motors. Sometimes the input ac power itself may be required to power other components such as small cooling fans. The ac system power is obtained from the commercial power net via a line cord. Other cables are required to interconnect subsystems so that functional signals can be passed between them. All these cables have the potential for emitting and/or picking up electromagnetic energy and are usually quite efficient in doing so. Generally speaking, the longer the cable, the more efficient it is in emitting or picking up electromagnetic energy. Interference signals can also be passed directly between the subsystems via direct conduction on these cables. If the subsystems are enclosed in metallic enclosures, currents may be induced on these enclosures by external signals or internal signals. These induced currents can then radiate to the external environment or to the interior of the enclosure. It is becoming more common, particularly in low-cost systems, to use nonmetallic enclosures, fabricated from non-conductive plastic or composite materials. The electronic circuits contained in these nonmetallic enclosures are, for the most part, completely exposed to electromagnetic emissions, and as such can directly radiate or be susceptible to these emissions. The four aspects of the EMC problem, *radiated emissions, radiated susceptibility, conducted emissions*, and *conducted susceptibility*, illustrated in Fig. 1.2, envelope these considerations.

Electromagnetic emissions can occur from the ac power cord, a metallic enclosure containing a subsystem, a cable connecting subsystems or from an electronic component within a nonmetallic enclosure as Fig. 1.2a illustrates. It is important to understand that "currents radiate." The fundamental process that produces radiated emissions is the acceleration of charge. A time-varying current comprises accelerated charge. Throughout the text we will be trying to replace certain misconceptions that prevent an understanding of this fundamental process. One example is the notion that an ac power cord carries only low-frequency power system signals. Although the primary intent of this cable is to transfer commercial ac power to the system, it is important to realize that *other much higher-frequency signals may and usually do exist on the ac power cord*! These are coupled to the ac power cord from the internal subsystems via a number of coupling paths that we will discuss. Once these higher-frequency currents couple onto this long (typically 1 m or more) cable, they will radiate

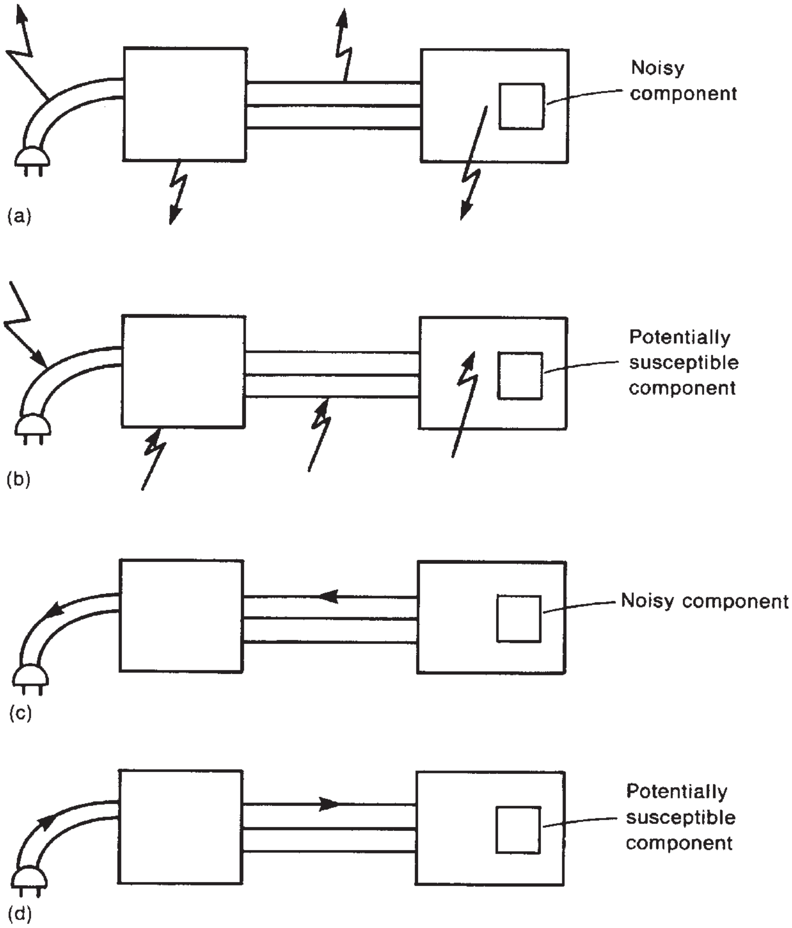
Noisy component
(a)
Potentially susceptible component
(b)
Noisy component
(c)
Potentially susceptible component
(d)

FIGURE 1.2 The four basic EMC subproblems: (a) radiated emissions; (b) radiated susceptibility; (c) conducted emissions; (d) conducted susceptibility.

into the surrounding space quite efficiently. Also, this long cable may function as an efficient "antenna" and pick up radiated emissions from other nearby electronic systems as shown in Fig. 1.2b. Once these external signals are induced onto this cable, as well as any other cables connecting the subsystems, they may be transferred to the internal components of the subsystems, where they may cause interference in those circuits. To summarize, undesired signals may be radiated or picked up by the ac power cord, interconnection cables, metallic cabinets, or internal circuitry of the subsystems, even though these structures or wires are not intended to carry the signals.

Emissions of and susceptibility to electromagnetic energy occur not only by electromagnetic waves propagating through air but also by direct conduction on metallic conductors as illustrated in Fig. 1.2c and d. Usually this coupling path is inherently more efficient than the air coupling path. Electronic system designers realize this, and intentionally place barriers, such as filters, in this path to block the undesired transmission of this energy. It is particularly important to realize that the interference problem often extends beyond the boundaries shown in Fig. 1.2. For example, interference currents conducted out the ac power cord will flow into the power distribution net of the installation. This power distribution net is an extensive array of wires that are directly connected and as such may radiate these signals quite efficiently. In this case, a *conducted emission* produces a *radiated emission*. Consequently, restrictions on the emissions conducted out the product's ac power cord are intended to reduce the radiated emissions from this power distribution system.

Our primary concern will be the design of electronic systems so that they will comply with the *legal* requirements imposed by governmental agencies, or self-imposed limitations by companies in niche markets such as aerospace or automotive manufacturing. Some consumer electronics which traditionally fell into one EMC standard category now might blur the lines between different standards, such as smart appliances. However, there are also a number of other important EMC concerns

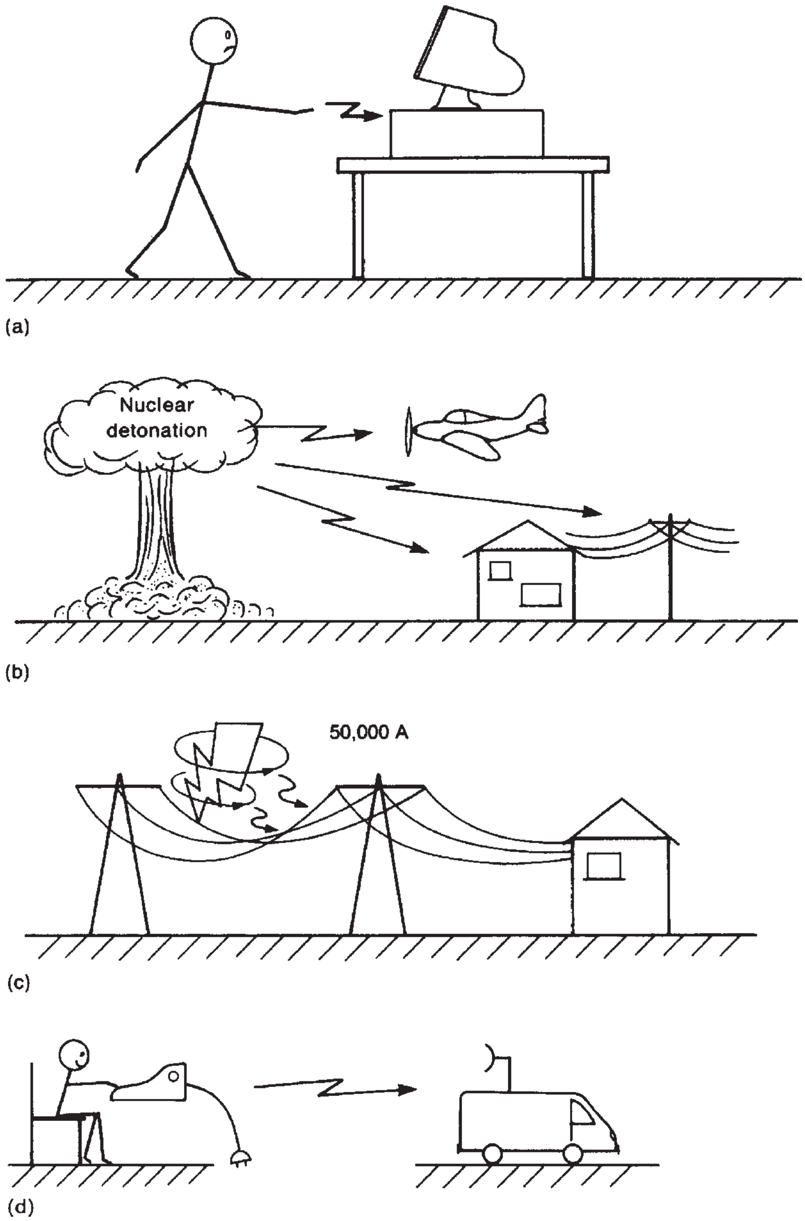

FIGURE 1.3 Other aspects of EMC: (a) electrostatic discharge (ESD); (b) electromagnetic pulse (EMP); (c) lightning; (d) TEMPEST (secure communication and data processing).

that we will discuss. Some of these are depicted in Fig. 1.3. Figure 1.3a illustrates an increasingly common susceptibility problem for today's small-scale integrated circuits, *electrostatic discharge* (ESD). Walking across a nylon carpet with rubber-soled shoes can cause a buildup of static charge on the body. If an electronic device such as a keyboard is touched, this static charge may be transferred to the device, and an arc is created between the fingertips and the device. The direct transfer of charge can cause permanent destruction of electronic components such as integrated circuit chips. The arc also bathes the device in an electromagnetic wave that is picked up by the internal circuitry. This can result in system malfunction. ESD is a very pervasive problem today.

After the first nuclear detonation in the mid-1940s, it was discovered that the semiconductor devices (a new type of amplifying element) in the electronic systems that were used to monitor the effects of the blast were destroyed. This was not due to the direct physical effects of the blast but was caused by an intense electromagnetic wave created by the charge separation and movement within the detonation as illustrated in Fig. 1.3b. Consequently, there is significant interest within the military communities in "hardening" communication and data processing facilities against the effect of this *electromagnetic pulse* (EMP). The concern is not with the physical effects of the blast but with the inability to direct retaliatory action if the communication and data processing facilities are rendered nonfunctional by the EMP. EMP effects can be created by smaller sources that do not require the use of nuclear detonations. Commercial industry, in particular the power industry, is now becoming much more interested in this phenomenon. Nefarious uses have been made of suitcase-sized transmitters that can damage localized targets, and the power industry is concerned about wide-scale effects of outages traced back to EMP events. This represents a radiated susceptibility problem. We will find that the same principles used to reduce the effect of radiated emissions from neighboring electronic systems also apply to this problem, but with larger numbers.

Lightning occurs frequently and direct strikes illustrated in Fig. 1.3c are obviously important. However, the indirect effects on electronic systems can be equally devastating. The "lightning channel" carries upward of 200,000 A of current. The electromagnetic fields from this intense current can couple to electronic systems either by direct radiation or by coupling to the commercial power system and subsequently being conducted into the device via an ac power cord. Consequently, it is important to design and test the product for its immunity to transient voltages on the ac power cord. Most manufacturers inject "surges" onto the ac power cord and design their products to withstand these and other undesired transient voltages that may appear at the entry point of ac power.

It has also become of interest to prevent the interception of electromagnetic emissions by unauthorized persons. It is possible, for example, to determine what is being typed on an electronic typewriter by monitoring its electromagnetic emissions as illustrated in Fig. 1.3d. There are also other instances of direct interception of radiated emissions from which the content of the communications or data can be determined. Obviously, it is imperative for the military to contain this problem, which it refers to as TEMPEST. The commercial community is also interested in this problem from the standpoint of preserving trade secrets, the knowledge of which could affect the competitiveness of the company in the marketplace.

There are several other related problems that fit within the purview of the EMC discipline. It is important to realize that these can all be viewed in terms of the four basic subproblems of radiated emissions, radiated susceptibility, conducted emissions, and conducted susceptibility shown in Fig. 1.2. Only the context of the problem changes.

The primary vehicle used to understand the effects of interference is a *mathematical model*. A mathematical model quantifies our understanding of the phenomenon and also may bring out important properties that are not so readily apparent. An additional, important advantage of a mathematical model is its ability to aid in the design process. *The criterion that determines whether the model adequately represents the phenomenon is whether it can be used to predict experimentally observed results*. If the predictions of the model do not correlate with experimentally observed behavior of the phenomenon, it is useless. However, our ability to solve the equations resulting from the model and extract insight from them quite often dictates the approximations used to construct the model. For example, we often model nonlinear phenomena with linear, approximate models.

Calculations will be performed quite frequently, and correct *unit conversion* is essential. Although the trend in the international scientific community is toward the metric or SI system of units, there is still the need to use other systems. One must be able to convert a unit in one system to the equivalent in another system, as in an equation where certain constants are given in another unit system. A simple and flawless method is to multiply by unit ratios between the two systems *and* cancel the unit names to ensure that the quantity should be multiplied rather than divided and vice versa. This method for converting units is known as dimensional analysis. For example, the units of distance in the English system (used extensively in the USA) are inches, feet, miles, yards, etc. Some representative conversions are 1 in. = 2.54 cm, 1 mil = 0.001 in., 1 ft = 12 in., 1 m = 100 cm, 1 mile = 5280 ft, 1 yard = 3 ft, etc. For example, suppose we wish to convert a distance of 5 miles to kilometers. We would multiply by unity ratios as follows:

$$5\ \text{mi} \times \frac{5280\ \text{ft}}{1\ \text{mi}} \times \frac{12\ \text{in.}}{1\ \text{foot}} \times \frac{2.54\ \text{cm}}{1\ \text{in.}} \times \frac{1\ \text{m}}{100\ \text{cm}} \times \frac{1\ \text{km}}{1000\ \text{m}} = 8.047\ \text{km}$$

Cancelation of the unit names in this conversion avoids the improper multiplication (division) of a unit ratio when division (multiplication) should be used. The inability to properly convert units is a leading reason for numerical errors. Note this text, as do many other technical resources, utilizes rounding to simplify calculations. When working on review exercises and problems, if the reader calculates an answer that does not resemble the book's answer, it is likely a rounding error was made at some point. Many of the problems presented in this text depend on the use of a calculator. It is recommended to use a graphing calculator's features to carry over as many decimal points as possible in calculations.

Review Exercise 1.1 Convert the following dimensions to those indicated: (a) 10 ft. to meters, (b) 50 cm to inches, (c) 30 km to miles.

Answers**:** (a) 3.048 m (meters), (b) 19.685 in. (inches), (c) 18.64 mi (miles).

Note that each of these results may be rounded off, based on the appropriate number of significant digits as (usually) determined by the corresponding standard error. For example, in converting from feet to meters, the number of feet in a meter may be expressed as 3.28, 3.2808, or 3.281. Using these values, the result may be 3.04878, 3.04804, or 3.04785. The number of significant digits used in the calculation for the number of feet in a meter will dictate the number of significant digits in the final result. If 3.28 is used, the result should have 2 digits after the decimal point. If 3.2808 is used, the final result should have 4 digits after the decimal point. If 3.281 is used, the final result should have 3 digits after the decimal point. In all cases, if desired, the final result should be rounded off using standard rules.

Before we set out the standard rules for rounding off, let us agree on what to call the various components of a numeric value.

- The most significant digit is the left most digit (not counting any leading zeros which function only as placeholders and are never significant digits).
- If you are rounding off to n significant digits, then the least significant digit is the nth digit from the most significant digit. The least significant digit can be a zero.
- The first nonsignificant digit is the $n + 1$th digit.

Rounding-off rules

- If the first nonsignificant digit is less than 5, then the least significant digit remains unchanged.
- If the first nonsignificant digit is greater than 5, the least significant digit is incremented by 1.
- If the first nonsignificant digit is 5, the least significant digit can be either incremented or left unchanged (see below!)
- All nonsignificant digits are removed.

Finally, it is important to "sanity-check" any calculations done with a calculator. For example, 10 cm is approximately 4 in. (3.94 in.).

1.2 ELECTRICAL DIMENSIONS AND WAVES

Perhaps the most important concept that the reader should grasp in order to be effective in EMC is that of the *electrical dimensions* of an electric circuit or electromagnetic radiating structure (intentional or unintentional). *Physical dimensions of a radiating structure such as an antenna are not important,* per se*, in determining the ability of that structure to radiate electromagnetic energy. Electrical dimensions of the structure in wavelengths are more significant in determining this.* Electrical dimensions are measured in *wavelengths*. A *wavelength* represents the distance that a single-frequency, sinusoidal electromagnetic wave must travel in order to change phase by 360°. Strictly speaking, this applies to one type of wave: the uniform plane wave. However, other types of waves have similar characteristics, and so this concept has broad application. Appendix B contains a thorough but brief discussion of electromagnetic laws and principles as well as the uniform plane wave and wavelength. All electrical engineering undergraduate curricula require at least one semester of electromagnetic field theory that the material in Appendix B represents. The reader is strongly advised to review this important material in Appendix B or consult [1, 2].

Although Maxwell's equations govern all electrical phenomena, they are quite complicated, mathematically. Hence we use, where possible, simpler approximations to them such as lumped-circuit models and Kirchhoff's laws. The important question here is when we can use the simpler lumped-circuit models and Kirchhoff's laws instead of Maxwell's equations when analyzing a problem. The essence of the answer is when the largest dimension of the circuit is *electrically small*, for example, much smaller than a wavelength at the excitation frequency of the circuit sources. Typically, we might use the criterion that a circuit is electrically small when the largest dimension is smaller than one-tenth of a wavelength.

This notion of electrical dimensions and lumped-circuit models has other significant aspects that we must discuss. Electromagnetic phenomena are truly a *distributed-parameter* process in that the properties of the structure such as capacitance and inductance are, in reality, distributed throughout space rather than being lumped at discrete points. When we construct lumped-parameter electric circuit models, we are ignoring the distributed nature of the electromagnetic fields. For example, consider a lumped-circuit element such as a resistor and its associated *connection leads* as shown in Fig. 1.4. When using lumped-circuit models, we are in effect saying that the connection leads of the elements are of no consequence and their effects may be ignored. When is this valid? In Fig. 1.4, we have shown the element current (assumed cosinusoidal) that enters the left connection lead and exits the right connection lead as a function of time t. This current is actually a wave propagating with velocity v. If the medium surrounding the connection leads (wires) is air, the velocity of propagation

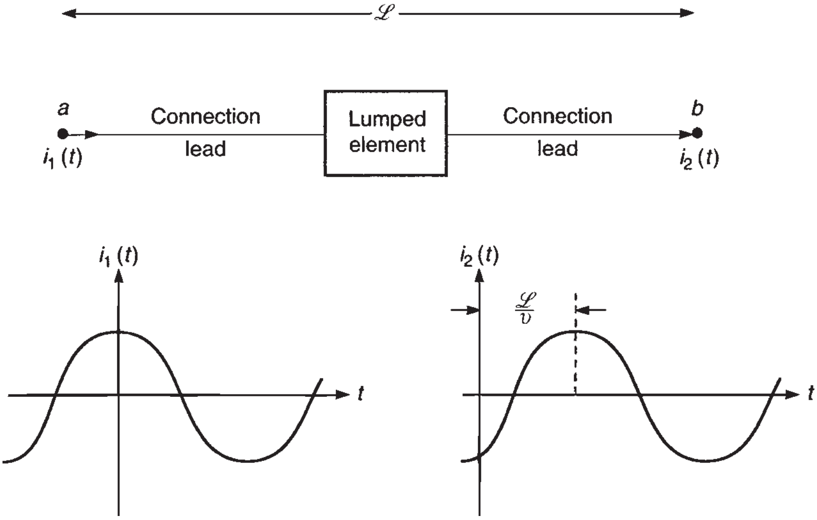

FIGURE 1.4 Illustration of the effect of element interconnection leads.

is the speed of light or $v_0 = 2.99792458 \times 10^8$ m/s or approximately $v_0 \cong 3 \times 10^8$ m/s. Because of this propagation, there is a finite *time delay*

$$T_D = \frac{L}{v} \text{ s} \tag{1.1}$$

required for the current wave to transit element *and* the connection leads and L is the total length of the element and its connection leads. For example, the time delay for a wave propagating in free space (approximately air) over a distance 1 m is approximately 3 ns or about 1 ns per foot. This time delay of propagation is becoming more critical in today's digital electronic circuits because of the ever-increasing speeds (and consequently the higher frequency content) of those digital signals. For example, in the mid-1980s or so the clock speeds of digital devices were on the order of 10 MHz. These digital signals had rise/falltimes in transitioning from a 1 to a 0 and vice versa on the order of 20 ns. Today the clock speeds of personal computers are on the order of 3 GHz or higher and the transition times are on the order of 100–500 ps or less. The velocity of propagation along a printed circuit board (PCB) land that interconnects the components is reduced from that of free space by the presence of the board material that is glass epoxy (FR-4) and is on the order of 1.8×10^8 m/s. Hence, the delay in transiting a 6-in. land on that PCB is on the order of 850 ps. Today this propagation delay can be on the order of the rise/falltimes of the digital signal and can cause timing problems in the digital logic. In the mid-1980s, it was insignificant, and the delay in transiting the digital gates was the only significant delay problem. Today the interconnect connections are drastically impacting *signal integrity*, which we will discuss in Chapter 4. We can look forward to this delay caused by interconnections to become even more critical to the performance of the digital device as clock and data speeds continue to increase seemingly without bound.

Suppose that the current and the associated wave are sinusoidal. Appendix B shows that a sinusoidal propagating wave can be written as a function of time t and position z as (where we have arbitrarily chosen a cosine form)

$$i(z, t) = I \cos(\omega t - \beta z) \tag{1.2}$$

where β is the *phase constant* in radians per meter (rad/m) and $\omega = 2\pi f$, where f is the cyclic frequency in Hz. This is shown in Fig. 1.5 as a function of distance z for fixed times t. As the wave

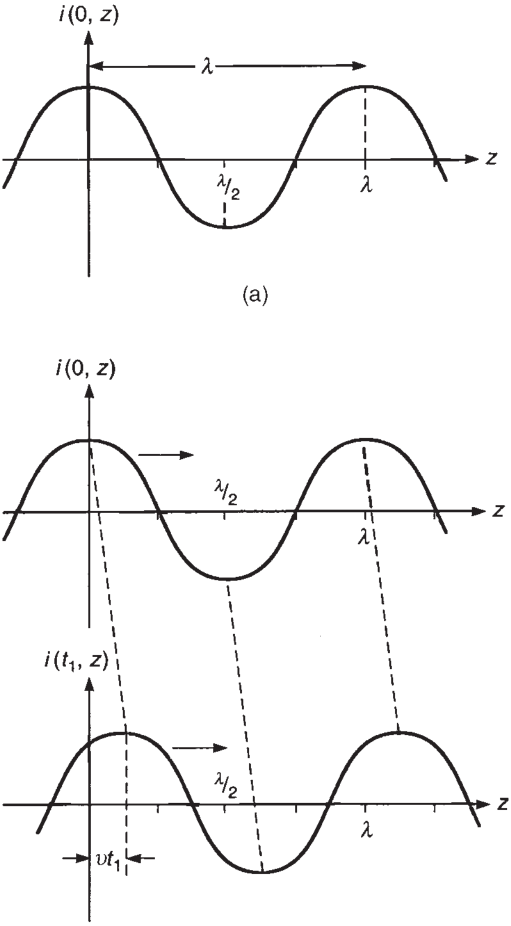

(a)

(b)

FIGURE 1.5 Wave propagation: (a) wave propagation in space and wavelength; (b) wave propagation as time progresses.

propagates from one end of the connection lead, through the element, and exists the other end of the other connection lead it suffers a *phase shift*, which is given in (1.2) by

$$\varphi = \beta L \,\text{rad} \tag{1.3}$$

and L is the total length of the connection leads. The phase shift is alternatively related to wavelength, which is denoted by λ and is *the distance that the wave must travel to change phase by* 2π *radians, which is equivalent to* 360°. Hence, the wavelength and the phase constant are related by

$$\beta\lambda = 2\pi \quad \text{rad} \tag{1.4}$$

Therefore, (1.2) can be written alternatively as

$$i(z, t) = I \cos\left(\omega t - \frac{2\pi}{\lambda} z\right) \tag{1.5}$$

Because distance z appears in this current expression as a ratio with wavelength λ, it becomes clear that physical distance z is not the important parameter; electrical distance in wavelengths z/λ is the critical parameter.

The wavelength of the wave is the distance between successive corresponding points such as the crest of the wave as shown in Fig. 1.5a. For the sinusoidal wave in (1.2), this means that we track points where the argument of the cosine remains constant:

$$(\omega t - \beta z) = \left(\omega t - \frac{2\pi}{\lambda} z\right) = \text{constant} \tag{1.6}$$

It is also clear that the wave in (1.2) is traveling in the $+z$ direction since as time t increases, distance z must also increase to keep the argument of the cosine constant in order to track the movement of a point on the waveform. Differentiating (1.6) gives the velocity of the wave movement as

$$\begin{aligned} v &= \frac{dz}{dt} \\ &= \frac{\omega}{\beta} \\ &= \lambda f \ \frac{\text{m}}{\text{s}} \end{aligned} \tag{1.7}$$

Hence, the wavelength can be written as

$$\lambda = \frac{v}{f} \ \text{m} \tag{1.8}$$

Table 1.1 gives the wavelengths of sinusoidal waves propagating in free space for various frequencies of that wave. Substituting (1.7) into (1.2) yields

$$\begin{aligned} i(z, t) &= I \cos\left(\omega\left(t - \frac{\beta}{\omega} z\right)\right) \\ &= I \cos\left(\omega t - \frac{z}{v}\right) \end{aligned} \tag{1.9}$$

This result illustrates that *the phase shift of a wave is equivalent to time delay*, which is given by z/v seconds.

From (1.3) and (1.4) as the current propagates along the connection leads a distance of one wavelength, $L = \lambda$, it suffers a phase shift of $\varphi = \beta\lambda = 2\pi$ radians or 360°. In other words, if the total length of the connection leads is one wavelength, the current entering the connection leads and the current exiting those leads are in phase but have changed phase 360° in the process of transiting the element. On the other hand, if the total length of the connection leads is one-half wavelength ($L = \lambda/2$), then the current suffers a phase shift of 180° so that the current entering the connection leads and the current exiting those leads are completely *out of phase*. If the length of the connection leads is 0.1 λ, the current suffers a phase shift of 36°. Over a distance of 0.05 λ, it suffers a phase shift of 18°, and over a distance of 0.01 λ it suffers a phase shift of 3.6°. If the effects of the connection leads are to be unimportant as is assumed by the lumped-circuit model, then the total length of the connection leads must be such that this phase shift is negligible. There is no fixed criterion for this, but we will assume that the phase shift is negligible if the lengths are smaller than,

TABLE 1.1 Frequencies of Sinusoidal Waves and Their Corresponding Wavelengths in Free Space (Air)

Frequency (f)	Wavelength (λ)
60 Hz	3107 mi (5000 km)
3 kHz	100 km
30 kHz	10 km
300 kHz	1 km
3 MHz	100 m
30 MHz	10 m
300 MHz	**1 m**
3 GHz	10 cm
30 GHz	1 cm
300 GHz	1 mm

say, 0.1 λ at the excitation frequency of the source. For some situations, the phase shift must be smaller than this to be negligible. Physical dimensions are not as important as *electrical dimensions* in determining the behavior of an electric circuit or device. Electrical dimensions are the physical dimensions in wavelengths. A physical dimension that is smaller than 0.1 λ is said to be *electrically small* in that the phase shift as a wave propagates across that dimension may be ignored. These concepts give rise to the rule of thumb that lumped-circuit models of circuits are an adequate representation of the physical circuit so long as the largest *electrical dimension* of the physical circuit is less than 0.1 λ. Table 1.2 gives the frequencies and corresponding wavelengths for various applications.

TABLE 1.2 Frequencies and Corresponding Wavelengths of Electronic Systems

Frequency Band[a]	Wavelength	Uses
EHF (30–300 GHz)	1 cm–1 mm	Radar, remote sensing, radio astronomy
SHF (3–30 GHz)	10 cm–1 cm	Radar, satellite communication, remote sensing, microwave electronic circuits, aircraft navigation, **digital systems**
UHF (300–3000 MHz)	1 m–10 cm	Radar, TV, microwave ovens, air navigation, cell phones, military air traffic control communication and navigation, **digital systems**
VHF (30–300 MHz)	10 m–1 m	TV, FM broadcasting, police radio, mobile radio, commercial air traffic control (ATC) communication and navigation, **digital systems**
HF (3–30 MHz)	100 m–10 m	Shortwave radio (ham), citizens band
MF (300–3000 kHz)	1 km–100 m	AM broadcasting, maritime radio, ADF direction finding
LF (30–300 kHz)	10 km–1 km	Loran long-range navigation, ADF radio beacons, weather broadcasting
VLF (3–30 kHz)	100 km–10 km	Long-range navigation, sonar
ULF (300–3 kHz)	1 Mm–100 km	Telephone audio range
SLF (30–300 Hz)	6214 mi–621 mi	Communication with submarines, commercial power (60 Hz)
ELF (3–30 Hz)	62 137 mi–6214 mi	Detection of buried metal objects

[a] E = extra, S = super, U = ultra, V = very, H = high, M = medium, L = low, F = frequency.

Broadly speaking, the velocity of propagation of a wave in a nonconductive medium other than free space is determined by the *permittivity* ε and *permeability* μ of the medium. For free space, these are denoted as ε_0 and μ_0 and are given by

$$\begin{aligned}\varepsilon_0 &= \frac{1}{36\pi} \times 10^{-9}\ \frac{\text{F}}{\text{m}} \quad \text{(approximate)}\\ \mu_0 &= 4\pi \times 10^{-7}\ \frac{\text{H}}{\text{m}} \quad \text{(exact)}\end{aligned}$$

The units of ε are farads per meter or a capacitance per distance. The units of μ are henrys per meter or an inductance per distance. We will see these combinations of units several times in later portions of this text and in different contexts. The velocity of propagation in free space (air) is given in terms of these as

$$\begin{aligned}v_0 &= \frac{1}{\sqrt{\varepsilon_0\mu_0}}\ \frac{\text{m}}{\text{s}}\\ &= 3 \times 10^8\ \frac{\text{m}}{\text{s}} \quad \text{(approximate)}\end{aligned} \tag{1.10}$$

Other media through which the wave may propagate are characterized in terms of their permittivity and permeability *relative to that of free space*, ε_r and μ_r, so that $\varepsilon = \varepsilon_r\varepsilon_0$ and $\mu = \mu_r\mu_0$. For example, Teflon has $\varepsilon_r = 2.1$ and $\mu_r = 1.0$. Note that the permeability μ is the same as in free space. This is an important property of *nonferrous or nonmagnetic* materials. On the other hand, the permeability of sheet steel (a ferrous or magnetic material) is 2000 times that of free space, $\mu_r = 2000$, whereas it has a relative permittivity of $\varepsilon_r = 1.0$. Be aware that permeability is affected by the strength of the applied magnetic field and the frequency of that field, and in general decreases rapidly for most materials from the dc value most often quoted in the literature.

For nonconductive media, other than free space, the velocity of wave propagation is

$$\begin{aligned}v &= \frac{1}{\sqrt{\varepsilon\mu}}\\ &= \frac{v_0}{\sqrt{\varepsilon_r\mu_r}}\end{aligned} \tag{1.11}$$

For example, a wave propagating in Teflon ($\varepsilon_r = 2.1$, $\mu_r = 1$) has a velocity of propagation of

$$\begin{aligned}v &= \frac{v_0}{\sqrt{\varepsilon_r\mu_r}}\\ &= \frac{3 \times 10^8\ (\text{m/s})}{\sqrt{2.1 \times 1}}\\ &= 207{,}019{,}667.8\ \frac{\text{m}}{\text{s}}\\ &= 0.69\ v_0\end{aligned}$$

Dielectric materials ($\mu_r = 1$) have relative permittivities (ε_r) typically between 2 and 12, so that velocities of propagation range from 0.7 v_0 to 0.29 v_0 in dielectrics. Table 1.3 gives ε_r for various dielectric materials. Table 1.4 gives the relative permeability and relative conductivity (relative to Copper) for various metals.

TABLE 1.3 Relative Permittivities of Various Dielectrics

Material	ε_r
Styrofoam	1.03
Polyethylene foam	1.6
Cellular polyethylene	1.8
Teflon	2.1
Polyethylene	2.3
Polystyrene	2.5
Nylon	3.5
Silicon rubber	3.1
Polyvinyl chloride (PVC)	3.5
Epoxy resin	3.6
Quartz (fused)	3.8
Epoxy glass (printed circuit substrate)	4.7
Bakelite	4.9
Glass (pyrex)	5.0
Mylar	4.0
Porcelain	6.0
Neoprene	6.7
Polyurethane	7.0
Silicon	12.0

TABLE 1.4 Relative Permeabilities and Conductivities (Relative to Copper) of Various Metals

Conductor	σ_r	μ_r
Silver	1.05	1
Copper-annealed	1.00	1
Gold	0.70	1
Aluminum	0.61	1
Brass	0.26	1
Nickel	0.20	600
Bronze	0.18	1
Tin	0.15	1
Steel (SAE 1045)	0.10	1000
Lead	0.08	1
Monel	0.04	1
Stainless Steel (430)	0.02	500
Zinc	0.32	1
Iron	0.17	1000
Beryllium	0.10	1
Mumetal (at 1 kHz)	0.03	30,000
Permalloy (at 1 kHz)	0.03	80,000

It is very important for the reader to be able to *correctly* calculate the *electrical dimensions* of a structure at a particular frequency. The key to doing this is to realize that *a dimension of 1 m in free space (air) is one wavelength at a frequency of 300 MHz*. Wavelengths in free space can be easily calculated at another frequency by appropriately scaling the dimension, remembering that one wavelength at 300 MHz is 1 m. To do this, it is important to realize that *as frequency increases, a wavelength decreases and* vice versa. For example, a wavelength at 50 MHz is 1 m × 300 MHz/50 MHz = 6 m. A wavelength at 2 GHz (1 GHz = 1000 MHz) in air is 300/2000 = 0.15 m = 15 cm. Table 1.1 gives some representative values.

The electrical dimensions of a circuit or other electromagnetic structure need to be calculated to determine whether it is electrically small ($L < 0.1\ \lambda$). If it is electrically small, we can apply simpler concepts and calculations than would be necessary if it were electrically large ($L > 0.1\ \lambda$). For example, Kirchhoff's voltage and current laws along with the lumped-circuit modeling of elements *are applicable only if the largest dimension of the circuit is electrically small*! If the circuit is electrically large, we have no other recourse but to use Maxwell's equations (or some appropriate simplification of them) in order to describe the problem. Clearly, then, it is important to determine the electrical dimensions of a circuit. One can determine this by first calculating the wavelength at the *highest frequency of interest* and then computing K in relation to $L = K\lambda$ by writing

$$K = \frac{L}{\lambda} \tag{1.12}$$

For example, a circuit or radiating structure whose maximum dimension is 3.6 m and is operated at a frequency of 86 MHz is 3.6/3.49 = 1.03 λ because a wavelength in free space at 86 MHz is 300/86 = 3.49 m. If this structure were immersed in a polyvinyl chloride (PVC) dielectric ($\varepsilon_r = 3.5$, $\mu_r = 1$), its maximum dimension of 3.6 m would be 1.93 wavelength since the wavelength of 86 MHz in PVC is

$$\begin{aligned}\lambda &= \frac{v}{f}\\ &= \frac{v_0}{f\sqrt{\varepsilon_r \mu_r}} = \frac{\lambda_0}{\sqrt{\varepsilon_r \mu_r}}\\ &= \frac{3.49}{\sqrt{3.5 \times 1}} = 1.865\ \text{m}\end{aligned}$$

Review Exercise 1.2 Determine the wavelength at the following frequencies in metric and in English units: (a) 600 MHz in epoxy glass, (b) 3 GHz in air, (c) 5 MHz in polyvinyl chloride.

***Answers*:** (a) 23.1 cm, 9.08 in., (b) 10 cm, 3.94 in., (c) 32.07 m, 105.22 ft.

Review Exercise 1.3 Determine the following physical dimensions in wavelengths: (a) 250 MHz, 5 cm in air, (b) a 1-mile length of 60 Hz power transmission line in air, (c) 10 MHz, 20 ft in PVC.

***Answers*:** (a) 0.042 λ, (b) $3.22 \times 10^{-4}\ \lambda$, (c) 0.38 λ.

1.3 DECIBELS AND COMMON EMC UNITS

The primary quantities of interest in EMC problems are conducted emissions [voltage in volts (V), and current in amperes (A)] and radiated emissions [electric field in volts per meter (V/m) and magnetic field in amperes per meter (A/m)]. Associated with these primary quantities are the quantities of power in watts (W) or power density in watts per square meter (W/m^2). The numerical range of these quantities can be quite large. For example, electric fields can have values ranging from 1 μV/m to 200 V/m. This represents a *dynamic range* of over eight orders of magnitude (10^8). Because these wide ranges in units are common in the EMC community, EMC units are expressed in *decibels* (dB). Decibels have the property of compressing data, e.g., a range of voltages of 10^8 is 160 dB. There are also other reasons for expressing these quantities in dB, as we will see. In order to be effective in EMC, we must be able to express and manipulate units that are expressed in dB. It is also important to conceptualize the values of various EMC units when they are expressed in dB. This is somewhat similar to the conversion from the English system of units (inches, feet, gallons, etc.) to the metric system of units (meters, centimeters, liters, etc.). Those accustomed to the English system have a feel for the length of, for example, 100 yards (the length of a football field in the USA) but may have difficulty visualizing a length of 100 m, although both dimensions are approximately the same. In order to be effective in EMC, it is imperative to be able to convert, understand, and use units expressed in dB. This section is devoted to that objective.

The decibel was originally developed in the telephone industry to describe the effect of noise in telephone circuits [4]. The ear tends to hear logarithmically so describing the effect of noise in dB is natural. To begin the discussion, consider the amplifier circuit shown in Fig. 1.6. A source consisting of an open-circuit voltage V_S and source resistance R_S delivers a signal to an amplifier whose load is represented by R_L. The input resistance to the amplifier is denoted by R_{in} and the power delivered to the amplifier is

$$P_{\text{in}} = \frac{v_{\text{in}}^2}{R_{\text{in}}} \tag{1.13}$$

where the input voltage is expressed as RMS (root-mean-squared) and differs from the peak value of the sinusoidal voltage, v_{peak}, by $v_{\text{RMS}} = v_{\text{peak}}\sqrt{2}$ [3].

There are two common ways of expressing values of voltages and currents: peak and RMS [3]. If we write the equation of a sinusoidal voltage as $V\sin(\omega t)$, the maximum or peak value of the wave form is V. If this voltage is applied across a resistor R, the average power delivered to the resistor is [3] $P_{\text{av}} = V^2/2R$ watts. On the other hand, it is common in industry to express sinusoidal voltages and currents as RMS where $V_{\text{RMS}} = V\sqrt{2}$ and V is the peak value of the waveform. In this case, the average power delivered to a resistor is $P_{\text{av}} = V_{\text{RMS}}^2/R$ watts and no 1/2 factor is required. This is the only consequence of expressing sinusoidal voltages and currents in peak or RMS. For example, household voltages in the United States are 120 V (RMS), which is 170 V (peak). Test and measurement equipment are almost universally calibrated in RMS and not peak.

The power delivered to the load is thus

$$P_{\text{out}} = \frac{v_{\text{out}}^2}{R_L} \tag{1.14}$$

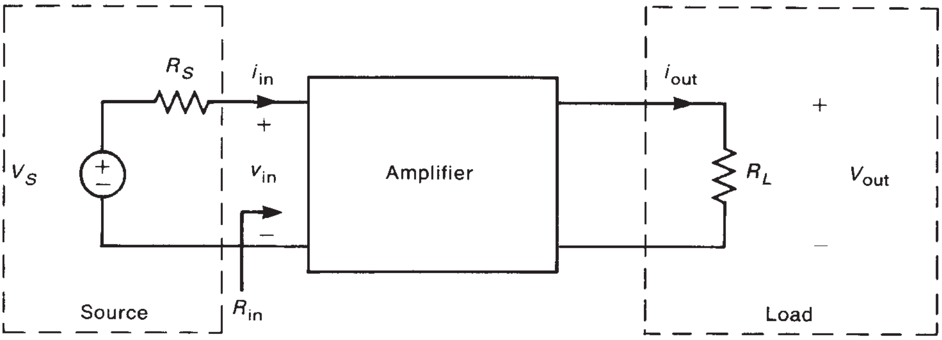

FIGURE 1.6 An illustration of the definition and use of the decibel (dB).

The *power gain* of the amplifier is

$$\begin{aligned} \text{Power gain} &= \frac{P_{\text{out}}}{P_{\text{in}}} \\ &= \frac{v_{\text{out}}^2}{v_{\text{in}}^2} \frac{R_{\text{in}}}{R_L} \end{aligned} \tag{1.15}$$

The power gain expressed in decibels is *defined* as

$$\text{Power gain} \equiv 10\log_{10}\left(\frac{P_{\text{out}}}{P_{\text{in}}}\right) \tag{1.16}$$

where $\log_{10}$ is the logarithm to the base 10.

The related quantities of interest are the *voltage gain* and *current gain* of the amplifier. These are defined by

$$\text{Voltage gain} = \frac{v_{\text{out}}}{v_{\text{in}}} \tag{1.17}$$

$$\text{Current gain} = \frac{i_{\text{out}}}{i_{\text{in}}} \tag{1.18}$$

In dB these are *defined* as

$$\text{Voltage gain} \equiv 20\log_{10}\left(\frac{v_{\text{out}}}{v_{\text{in}}}\right) \tag{1.19}$$

$$\text{Current gain} \equiv 20\log_{10}\left(\frac{i_{\text{out}}}{i_{\text{in}}}\right) \tag{1.20}$$

Note that power gain in dB is defined as 10 $\log_{10}$ of the ratio of the two quantities, whereas voltage gain and current gain in dB are defined as 20 $\log_{10}$ of the ratio of the two quantities! Although this could be taken as simply definition, there is a rationale for it. To see this, observe that *if* the input resistance to the amplifier equals the load resistance, $R_L = R_{\text{in}}$, then (1.15) becomes

$$\text{Power gain} = \left(\frac{v_{\text{out}}}{v_{\text{in}}}\right)^2_{R_L=R_{\text{in}}} \tag{1.21}$$

In dB the power gain becomes, for $R_L = R_{\text{in}}$

$$\text{Power gain}_{\text{dB}} = 20\log_{10}\left(\frac{v_{\text{out}}}{v_{\text{in}}}\right)_{R_L=R_{\text{in}}} \tag{1.22}$$

from which we obtain the defining relation for expressing the voltage gain in dB as in (1.19). In summary, *the ratio of two quantities in dB is given by*

$$\text{dB} \equiv 10\log_{10}\left(\frac{P_2}{P_1}\right) \text{ (power)} \tag{1.23}$$

$$\text{dB} \equiv 20\log_{10}\left(\frac{v_2}{v_1}\right) \text{ (voltage)} \tag{1.24}$$

$$\text{dB} \equiv 20\log_{10}\left(\frac{i_2}{i_1}\right) \text{ (current)} \tag{1.25}$$

Review Exercise 1.4 Determine the ratio of (a) two powers $P_1 = 1\,\text{mW}$ and $P_2 = 20\,\text{W}$, (b) two voltages $v_1 = 10\,\text{mV}$ and $v_2 = 20\,\mu\text{V}$, and (c) two currents $i_1 = 2\,\text{mA}$ and $i_2 = 0.5$ A in dB.

***Answers*:** 43 dB, −54 dB, 48 dB.

Note that *decibels are the ratio of two quantities*. Absolute power, voltage, or current levels are expressed in dB by giving their value *above or referenced to some base quantity*. For example, voltages are commonly expressed relative to 1 μV as dBμV:

$$\text{dB}\mu\text{V} \equiv 20\log_{10}\left(\frac{\text{volts}}{1\,\mu\text{V}}\right) \tag{1.26}$$

For example, a voltage of 1 V is 120 dBμV since

$$\begin{aligned} 20\log_{10}\left(\frac{1\text{ V}}{1\,\mu\text{V} \equiv 10^{-6}\text{ V}}\right) &= 20\log_{10}10^6 \\ &= 120\text{ dB}\mu\text{V} \end{aligned}$$

This is commonly stated as "1 V is 120 dB above a microvolt." As another example, 1 mV is 60 dBμV. Similarly, 350 mV is

$$\begin{aligned} 20\log_{10}\left(\frac{350\times10^{-3}\text{ V}}{10^{-6}\text{ V}}\right) &= 20\log_{10}(350\times10^3) \\ &= 110.88\text{ dB}\mu\text{V} \end{aligned}$$

Conversely, 0.1 μV is −20 dBμV, or 0.1 μV is 20 dB *below* a microvolt.

Some other standard units are dBmV (dB above a millivolt), dBμA (dB above a microamp), and dBmA (dB above a milliamp), where

$$\text{dBmV} \equiv 20\log_{10}\left(\frac{\text{volts}}{1\text{ mV}}\right) \tag{1.27}$$

$$\text{dB}\mu\text{A} \equiv 20\log_{10}\left(\frac{\text{amperes}}{1\,\mu\text{A}}\right) \tag{1.28}$$

$$\text{dBmA} \equiv 20\log_{10}\left(\frac{\text{amperes}}{1\text{ mA}}\right) \tag{1.29}$$

Powers are also expressed relative to a microwatt, dBμW, and dB above a milliwatt, dBmW, or more commonly dBm as

$$\text{dB}\mu\text{W} \equiv 10\log_{10}\left(\frac{\text{watts}}{1\,\mu\text{W}}\right) \tag{1.30}$$

$$\begin{aligned} \text{dBm} &\equiv \text{dBmW} \\ &\equiv 10\log_{10}\left(\frac{\text{watts}}{1\text{ mW}}\right) \end{aligned} \tag{1.31}$$

Note that the pattern for the names follows that for voltage and current except that the very common *dB above a milliwatt is usually denoted as dBm*. Some examples are

$$
\begin{aligned}
15\ \text{mV} &= 15{,}000\ \mu\text{V} \\
&= 83.52\ \text{dB}\mu\text{V} \\
&= 23.52\ \text{dBmV} \\
630\ \text{mA} &= 630{,}000\ \mu\text{A} \\
&= 115.99\ \text{dB}\mu\text{A} \\
&= 55.99\ \text{dBmA} \\
250\ \text{mW} &= 250{,}000\ \mu\text{W} \\
&= 53.98\ \text{dB}\mu\text{W} \\
&= 23.98\ \text{dBm}
\end{aligned}
$$

Note the use of the designation dBm in the last example to designate dBmW.

Review Exercise 1.5 Determine the following quantities in the indicated units: 20 mV (dBμV, 50 μV (dBmV), 100 mA (dBμA), 30 W (dBW), 300 μW (dBm).

***Answers*:** 86 dBμV, −26 dBmV, 100 dBμA, 14.77 dBW, −5.23 dBm.

Radiated electromagnetic fields are given in terms of electric field intensity in units of volts per meter (V/m) or in terms of magnetic field intensity in units of amperes per meter (A/m). The common EMC units reference these to 1 μV/m, 1 mV/m, 1 μA/m, or 1 mA/m as dBμV/m, dBmV/m, dBμA/m, or dBmA/m, respectively. For example, one of the legal limits on radiated electric field is 100 μV/m. This translates to 40 dBμV/m. So these units translate in the same fashion as voltage and current:

$$\frac{\text{dB}\mu\text{V}}{\text{m}} \equiv 20\log_{10}\left(\frac{\text{V/m}}{1\ \mu\text{V/m}}\right) \tag{1.32}$$

$$\frac{\text{dB}\mu\text{A}}{\text{m}} \equiv 20\log_{10}\left(\frac{\text{A/m}}{1\ \mu\text{A/m}}\right) \tag{1.33}$$

It is also important to be able to convert a unit given in dB to its absolute value. To do this, we use the definition of the logarithm of a number to the base m:

$$\log_m A = n \tag{1.34}$$

This denotes the power to which the base m must be raised to give A:

$$m^n = A \tag{1.35}$$

Therefore, we may convert a number given in dB to its absolute value by performing the operation given in (1.35). For example, 108 dBμV is

$$108\ \text{dB}\mu\text{V} = 20\log_{10}\left(\frac{V}{10^{-6}\ \text{V}}\right)$$

Thus, the absolute value of V in this expression is

$$\begin{aligned} V &= 10^{108\ \mathrm{dB\mu V}/20} \times 10^{-6} \\ &= 0.2512\ \mathrm{V} \end{aligned}$$

The common conversions are

$$\mathrm{Volts} = 10^{\mathrm{dB\mu V}/20} \times 10^{-6} \tag{1.36}$$

$$\mathrm{Volts} = 10^{\mathrm{dBmV}/20} \times 10^{-3} \tag{1.37}$$

$$\mathrm{Watts} = 10^{\mathrm{dB\mu W}/10} \times 10^{-6} \tag{1.38}$$

$$\mathrm{Watts} = 10^{\mathrm{dBm}/10} \times 10^{-3} \tag{1.39}$$

The steps are

1. Divide the quantity by 20 (voltage or current) or 10 (power).
2. Raise 10 to that power.
3. Multiply the result by 10^{-6} for dBμV and dBμW or 10^{-3} for dBmV and dBm.

The same rules hold for electric and magnetic field quantities in dBμV/m, dBmV/m, dBμA/m, or dBmA/m, where they are treated like voltage and current, i.e., use $20\log_{10}$. For example, the electric field intensity of 44 dBμV/m translates to

$$\begin{aligned} 10^{(44\ \mathrm{dB\mu V/m})/20} \times 10^{-6} &= 0.00015849\ \frac{\mathrm{V}}{\mathrm{m}} \\ &= 158.49\ \frac{\mu\mathrm{V}}{\mathrm{m}} \end{aligned}$$

Similarly, 56 dBm translates to

$$\begin{aligned} 10^{56\ \mathrm{dBm}/10} \times 10^{-3} &= 398.107\ \mathrm{W} \\ &= 398{,}107.17\ \mathrm{mW} \end{aligned}$$

Review Exercise 1.6 Determine the absolute values of the following quantities: 60 dBμV/m, 120 dBμV/m, 30 dBmV, 66 dBm.

Answers: 1 mV/m, 1 V/m, 31.6 mV, 3981 W.

Referring to the EMC units in dB rather than in absolute quantity has the property of condensing larger numbers into smaller ones. Additional advantages have to do with the properties of the logarithm, so we should review those properties. The primary properties are

$$\log_m(A \times B) = \log_m A + \log_m B \tag{1.40}$$

$$\log_m A^k = k\log_m A \tag{1.41}$$

$$\log_m\left(\frac{A}{B}\right) = \log_m A - \log_m B \tag{1.42}$$

Note that

$$\log_m(A+B) \neq \log_m A + \log_m B$$

These very important properties make the manipulation of EMC units simpler if they are expressed in dB. For example, consider converting a voltage to dBμV:

$$\begin{aligned}20\log_{10}\left(\frac{\text{volts}}{10^{-6}\text{ V}}\right) &= 20\log_{10}(\text{volts}) - 20\log_{10}10^{-6} \\ &= 20\log_{10}(\text{volts}) + 120\end{aligned}$$

We could convert the voltage to dBV (dB relative to 1 V) by taking $20\log_{10}$ of the voltage and then adding 120 to arrive at dBμV.

These properties can also be used to obtain reasonably accurate estimates of a quantity in dB *without the use of a calculator*. In order to show this, let us consider the conversion of some common numbers to dB as given in Table 1.5.

Converting 10 raised to an integer power (positive or negative) is quite easy. Of the numbers 1 through 9, the two most useful are 2 and 3. Note that a ratio of two voltages whose ratio is 2 is *approximately* 6 dB, whereas this same ratio of two powers is *approximately* 3 dB. Similarly, ratios of 3 are *approximately* 10 dB for voltages or currents and 5 dB for power. These can be used to estimate quantities in dB by writing the number as the product of power of 10 and the numbers 2 and 3. For example

$$\begin{aligned}25 &\cong 24 \\ &= 3\times 2\times 2\times 2\end{aligned}$$

TABLE 1.5 Conversion to Decibels

Ratio	V or I in dB	P in dB
10^6	120	60
10^5	100	50
10^4	80	40
10^3	60	30
10^2	40	20
10	20	10
9	19.08	9.54
8	18.06	9.03
7	16.9	8.45
6	15.56	7.78
5	13.98	6.99
4	12.04	6.02
3	9.54	4.77
2	6.02	3.01
1	0	0
10^{-1}	−20	−10
10^{-2}	−40	−20
10^{-3}	−60	−30

Therefore

$$\begin{aligned}
20\log_{10}25 &\cong 20\log_{10}24\\
&= 20\log_{10}(3\times 2\times 2\times 2)\\
&= 20\log_{10}3 + 20\log_{10}2 + 20\log_{10}2 + 20\log_{10}2\\
&\cong 10 + 6 + 6 + 6\\
&= 28\text{ dB }(27.9588)
\end{aligned}$$

The exact value is given in parentheses. Some other examples are

$$\begin{aligned}
20\log_{10}360 &= 20\log_{10}(3\times 2\times 3\times 2\times 10)\\
&= 10 + 6 + 10 + 6 + 20\\
&= 52\text{ dB }(51.126)\\
10\log_{10}\frac{1}{180} &= 10\log_{10}1 - 10\log_{10}180\\
&= 0 - 10\log_{10}(2\times 3\times 3\times 10)\\
&= -3 - 5 - 5 - 10\\
&= -23\text{ dB }(-22.55)
\end{aligned}$$

With these observations, the reader should be able to estimate a number in dB and convert a number expressed in dB to its absolute value. It is common practice for an EMC engineer to be able to quickly make such estimates. For example, an electric field intensity of 86 dBμV/m is $86 = 20+20+20+20+6$. Thus, 86 μV/m represents (approximately) $10\times 10\times 10\times 10\times 2 = 2\times 10^4 = 20,000$ μV/m or 20 mV/m or 0.02 V/m. The exact value is 19 952.62 μV/m.

Review Exercise 1.7 Convert the following voltages to dBμV without a calculator and give the exact result: (a) 120 mV, (b) 0.04 μV, (c) 48 V.

***Answers*:** (a) 102 dBμV (101.58 dBμV), (b) –28 dBμV (−27.96 dBμV), (c) 154 dBμV (153.63 dBμV).

The ability of the dB (and the logarithm) to compress large numbers into smaller ones means that we can make some relatively crude approximations and still arrive at a reasonable estimate of the number in dB. Another example of the utility of expressing EMC units in dB is given in Fig. 1.7. The power gain of the amplifier is the ratio of the output and input power.

$$\text{Gain} = \frac{P_{\text{out}}}{P_{\text{in}}} \tag{1.43}$$

Thus the output power, given the input power, is

$$P_{\text{out}} = \text{Gain}\times P_{\text{in}} \tag{1.44}$$

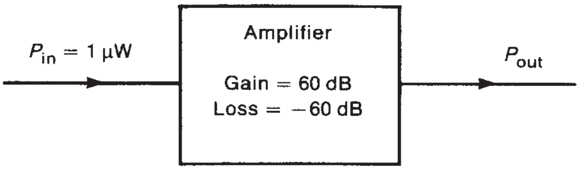

FIGURE 1.7 An illustration of the use of the decibel in computing amplifier performance.

Taking 10 $\log_{10}$ of both sides of (1.44) and using (1.40) gives

$$P_{\text{out dB}} = \text{Gain}_{\text{dB}} + P_{\text{in dB}} \tag{1.45}$$

The reference quantity for P_{out} and P_{in} used to convert them to dB can be any convenient base such as 1 mW. So (1.45) can be written in a number of ways as

$$P_{\text{out dBm}} = \text{Gain}_{\text{dB}} + P_{\text{in dBm}} \tag{1.46a}$$

$$P_{\text{out dB}\mu\text{W}} = \text{Gain}_{\text{dB}} + P_{\text{in dB}\mu\text{W}} \tag{1.46b}$$

Note that Gain in dB is the same in both cases. It is the ratio of two powers and as long as the two powers are expressed in the same units (dBμW, dBm, etc.), gain is unchanged. This makes the computation of powers in a system simple since outputs of signal sources are usually rated in terms of powers (more about this later) and are typically given in dBm. For the example given in Fig. 1.7, $P_{\text{out dBm}} = 60\text{ dB} + -30\text{ dBm}$. Also, $P_{\text{out dB}\mu\text{W}} = 60\text{ dB} + 0\text{ dB}\mu\text{W} = 60\text{ dB}\mu\text{W}$. So *the products of transfer functions become sums when the transfer functions are expressed in dB*. The same holds true when $R_L = R_{\text{in}}$ in Fig. 1.6 and the transfer function is a ratio of two voltages or two currents, or a ratio of a voltage and a current. Because of the way we defined the dB (10 log for power and 20 log for voltage and current), output and input quantities are similarly related with the same Gain in dB that was used for power in (1.45) and (1.46) (assuming $R_L = R_{\text{in}}$):

$$v_{\text{out dB}\mu\text{V}} = \text{Gain}_{\text{dB}} + v_{\text{in dB}\mu\text{V}} \tag{1.47a}$$

$$v_{\text{out dBmV}} = \text{Gain}_{\text{dB}} + v_{\text{in dBmV}} \tag{1.47b}$$

$$i_{\text{out dB}\mu\text{A}} = \text{Gain}_{\text{dB}} + i_{\text{in dB}\mu\text{A}} \tag{1.47c}$$

$$i_{\text{out dBmA}} = \text{Gain}_{\text{dB}} + i_{\text{in dBmA}} \tag{1.47d}$$

1.3.1 Signal Source Specification

Signal sources (pulse and sinusoidal) can be characterized in terms of a Thevenin equivalent as shown in Fig. 1.8. The quantity V_{OC} is the open-circuit voltage and R_S is the source resistance. *Virtually all signal sources today have* $R_S = 50\ \Omega$! Also, *the vast majority of instruments used to measure signals have an input resistance of* 50 Ω *and can be characterized as shown in* Fig. 1.9, *where* $C_{\text{in}} = 0$ and $R_{\text{in}} = 50\ \Omega$. There are exceptions to this latter statement, notably voltmeters and some oscilloscopes. However, it can be said that if the input resistance is not designed to be 50 Ω, it will be designed to

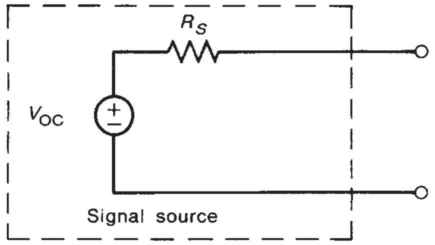

FIGURE 1.8 Specification of a signal source as a Thevenin equivalent circuit.

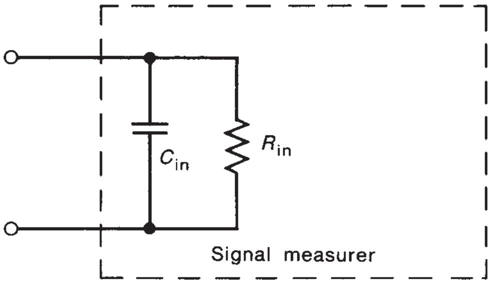

FIGURE 1.9 An equivalent circuit for the input to a signal measurer.

be very large, and its input circuitry can generally be represented as a capacitance in parallel with a large resistance. It is very easy to determine the input representation of a particular signal measurer since the manufacturer will clearly state these parameters near the input connector or in a menu. For example, typical spectrum analyzers used to display the frequency spectrum of a signal have $C_{\text{in}} = 0$ and $R_{\text{in}} = 50\ \Omega$. The high-impedance plug-in for an oscilloscope typically has $C_{\text{in}} = 47$ pF and $R_{\text{in}} = 1\ \text{M}\Omega$. However, there are also other plug-ins available that have $C_{\text{in}} = 0$ and $R_{\text{in}} = 50\ \Omega$.

With these concepts in mind, let us examine the connection of a signal source to a signal measurer with a length of coaxial cable as shown in Fig. 1.10. Suppose the signal measurer has an input impedance that is 50 Ω (purely resistive) and the coaxial connection cable also has a characteristic resistance of $\hat{Z}_c = 50\ \Omega$ (approximately real because of small losses of the cable). Because the load on this cable equals $\hat{Z}_C$, the cable is *matched* and the input impedance, *at any frequency* and *for any length of the cable*, is $\hat{Z}_{in} = 50\ \Omega = \hat{Z}_c$. This shows why signal measurers typically have input resistance of 50 Ω and coaxial cables have $\hat{Z}_c = 50\ \Omega$. Any other choice of characteristic impedance other than 50 Ω would be suitable, but 50 Ω has become the *industry standard. The value* 50 Ω *was determined empirically at Bell Labs through a series of experiments that found* 30 Ω *and* 77 Ω *impedances to be ideal for transmitting maximum power and minimal signal loss, respectively. The arithmetic and geometric means of these two values are* 54.5 Ω *and* 48 Ω*, respectively. A compromise value of* 50 Ω *was established as a result. If the terminal resistance of the cable, which is the input resistance to the signal measurer, had not equaled* $\hat{Z}_C$ *of the cable, the input impedance to the cable as seen by the signal source would not be* 50 Ω *for all frequencies and all lengths L of the cable but would vary with frequency and cable length.* Consequently, it would be very difficult to determine the impedance presented to the source, and furthermore this impedance would vary with frequency and line length so that the source output would vary. (Although the open-circuit voltage of the source in Fig. 1.8 may be stable, the output voltage will depend on the source resistance R_S and the load resistance placed across its terminals.) It is frequently important to be able to perform *swept-frequency measurements*

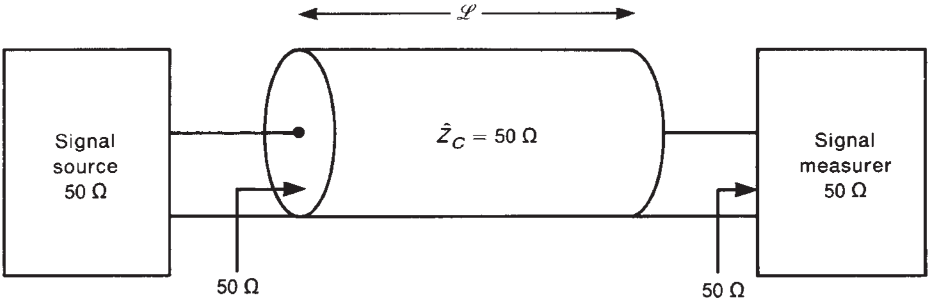

FIGURE 1.10 Use of coaxial cables with matched loads to connect a signal source to a signal measurer.

in which the frequency of the source is swept over a band. If we could not rely on the output being constant with frequency, this swept measurement would be useless since we would not know the output at a particular frequency! This illustrates why *modern EMC test instruments have input and source impedances of pure* 50 Ω *and are connected by* 50 Ω *coaxial cables*!

Another important outcome of this practicality is that it is a simple matter to compute the output of the source and the signal level delivered to the signal measurer. The output of a signal source is usually displayed on a meter of that instrument in terms of output power *to a matched load* in dBm. For example, consider Fig. 1.11, where a signal source is terminated in a load R_L either directly as the input to a device or via the input to a connection cable. If $R_L = R_S$, then the output voltage at the terminals of the source V_{out} is simply one-half of V_{OC}:

$$\begin{aligned} V_{\text{out}|R_L=R_S} &= \frac{R_L}{R_S + R_L} V_{OC} \\ &= \frac{1}{2} V_{OC} \end{aligned} \tag{1.69}$$

Outputs of signal sources typically assume $R_S = R_{\text{L}} = 50\ \Omega$ and are given in terms of the power delivered to the $R_{\text{L}} = 50\ \Omega$ load in dBm:

$$P_{\text{out}} = \frac{V_{\text{out}}^2}{R_L = 50\ \Omega} \tag{1.70}$$

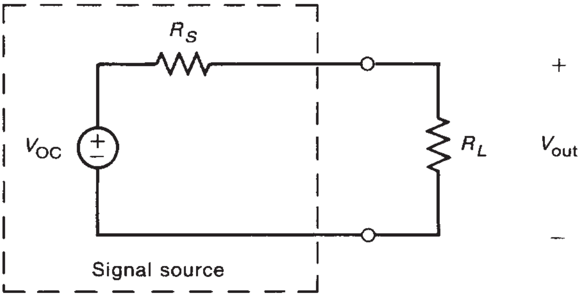

FIGURE 1.11 Calculation of a signal source output for a mismatched load.

Note the absence of the factor of 1/2 in this power expression. This is because the voltage is assumed to be given in its RMS value, $V_{\text{out peak}} = \sqrt{2}V_{\text{out RMS}}$ [3]. This is a typical assumption throughout industry; *voltages and currents of test and measurement equipment are specified in their RMS value and no factor of* 1/2 *is then required in power expressions.* The output power *into an assumed* 50 Ω *load* is given via a meter reading in dBm as

$$P_{\text{out dBm}} = 10\log_{10}\left(\frac{P_{\text{out}}}{1\ \text{mW}}\right) \tag{1.71}$$

For example, if the output voltage across a 50 Ω load is $V_{\text{out}} = 120\ \mu\text{V} = 41.6\ \text{dB}\mu\text{V}$, the power delivered to this 50 Ω load is

$$\begin{aligned} P_{\text{out}} &= \frac{(120 \times 10^{-6}\ \text{V})^2}{50\ \Omega} \times \frac{1000\ \text{mW}}{1\ \text{W}} \\ &= 2.88 \times 10^{-7}\ \text{mW} \\ &= -65.4\ \text{dBm} \end{aligned}$$

Similarly, suppose that the meter reading gives the output power (into an assumed 50 Ω load) of −37 dBm. This can be converted to give V_{out} (in RMS) by the following:

$$\begin{aligned} -37\ \text{dBm} &= 2 \times 10^{-4}\ \text{mW} \\ &= 2 \times 10^{-7}\ \text{W} \end{aligned}$$

Thus,

$$2 \times 10^{-7}\ \text{W} = \frac{V_{\text{out}}^2}{50\ \Omega}$$

Giving $V_{\text{out}} = 3.159\ \text{mV (RMS)} = 70\ \text{dB}\mu\text{V}$.

It is very important to realize that *if the load attached to the source is not* 50 Ω, *then the meter reading does not give the output power across this load.* We can, however, determine the actual output voltage from the meter reading, but this requires some calculation. For example, suppose that a (50 Ω) source is set to put out −26 dBm, *but* is connected across a 150 Ω load. The simplest way to determine the actual output voltage is to (1) determine the V_{OC} of the source and then (2) compute V_{out}. First determine V_{OC} *assuming a load of* 50 Ω (which is what the meter reading is calibrated to assume). The output of −26 dBm *into a* 50 Ω *load* gives a power in that load of 0.002512 mW or 2.512×10^{-6} W. The voltage (in RMS) across a 50 Ω load that would dissipate this power is

$$\begin{aligned} V_{\text{out}|R_L=50\ \Omega} &= \sqrt{50 \times P_{\text{out}}} \\ &= 11.2\ \text{mV} \\ &= 80.99\ \text{dB}\mu\text{V} \end{aligned}$$

So the open-circuit voltage (since all this assumes $R_L = R_S$) is

$$\begin{aligned} V_{OC} &= 2 \times V_{\text{out}|R_L=50\ \Omega} \\ &= 22.3\ \text{mV} \\ &= 87\ \text{dB}\mu\text{V} \end{aligned}$$

Now the actual output voltage can be computed from Fig. 1.11 using $R_S = 50\ \Omega$ and $R_L = 150\ \Omega$ using voltage division as

$$\begin{aligned} V_{\text{out}} &= \frac{150}{50+150} \times 22.4\ \text{mV} \\ &= 16.8\ \text{mV} \\ &= 84.5\ \text{dB}\mu\text{V} \end{aligned}$$

This could be directly obtained in dB. The open-circuit voltage can be immediately obtained as twice the output voltage when the load is 50 Ω:

$$\begin{aligned} V_{OC\ \text{dB}\mu\text{V}} &= 6\ \text{dB} + V_{\text{out dB}\mu\text{V}|R_L=50\ \Omega} \\ &= 6\ \text{dB} + 80.99\ \text{dB}\mu\text{V} \\ &= 87\ \text{dB}\mu\text{V} \end{aligned}$$

Therefore, the output voltage is

$$\begin{aligned} V_{\text{out dB}\mu\text{V}} &= \underbrace{20\log_{10}\left(\frac{150}{50+150}\right)}_{-2.5\ \text{dB}} + V_{OC\ \text{dB}\mu\text{V}} \\ &= -2.5\ \text{dB} + 87\ \text{dB}\mu\text{V} \\ &= 84.5\ \text{dB}\mu\text{V} \end{aligned}$$

Review Exercise 1.8 A 50 Ω signal generator is attached to a signal measurer whose input impedance is 25 Ω. The dial on the signal generator indicates that it is putting out a level of −20 dBm. Determine the voltage at the input to the signal measurer in dBμV.

***Answer*:** 83.5 dBμV.

Most signal measurers such as spectrum analyzers also have their responses specified *assuming a* 50 Ω *input impedance to the instrument*. For example, a level of −25 dBm means that −25 dBm or 0.003162 mW of power is dissipated in the 50 Ω input resistance of the instrument. The voltage (in RMS) across the input terminals can then be computed from the basic power relations above as

$$\begin{aligned} V_{\text{in}} &= \sqrt{50 \times 0.003162\ \text{mW}} \\ &= 12.574\ \text{mV} \\ &= 82\ \text{dB}\mu\text{V} \end{aligned}$$

End-of-chapter Problem 1.8 shows that we can convert power in dBm to a voltage (in RMS) in dBμV *assuming the impedance that it is across is* 50 Ω by

$$\text{dB}\mu\text{V (RMS)} = 107 + \text{dBm} \tag{1.72}$$

Hence, −25 dBm is 107 − 25 = 82 dBμV

For example, a typical calibration signal supplied with a spectrum analyzer is −30 dBm. The level in dBμV can be immediately calculated using (1.72) as 107 − 30 = 77 dBμV.

Finally, we can now use these principles to compute the signal measured by the signal measurer of Fig. 1.10 given the cable loss (at the appropriate frequency) and the output reading of the meter on the signal source. Throughout this we assume a 50 Ω source, cable, and signal measurer. If this is not the case, none of the following makes sense, and, furthermore, the actual level measured by the signal measurer would be extremely difficult to determine *if at all* (without some other measurements being made). Assume that the signal source meter shows the source is putting out a 100 MHz signal with a level of −30 dBm. Suppose the cable (RG58U) is 150 ft. in length. The cable loss at 100 MHz is 4.5 dB/100 ft. The received power is computed from

$$P_{\text{rec}} = \frac{P_{\text{out}} \text{ of cable}}{P_{\text{in}} \text{ to cable}} \times P_{\text{source}} \tag{1.73}$$

Taking 10 log 10 of both sides of this expression gives

$$\begin{aligned} P_{\text{rec dBm}} &= \text{cable gain}_{\text{dB}} + P_{\text{source dBm}} \\ &= \frac{-4.5\ \text{dB}}{100\ \text{ft}} \times 150\ \text{ft} + (-30\ \text{dBm}) \\ &= -36.75\ \text{dBm} \end{aligned} \tag{1.74}$$

This converts to a power of 0.2113 μW or a (RMS) voltage across the 50 Ω load of

$$\begin{aligned} V_{\text{rec}} &= \sqrt{P_{\text{rec}} \times 50} \\ &= 3.25\ \text{mV} \\ &= 70.24\ \text{dB}\mu\text{V} \end{aligned}$$

But this could have been obtained more directly without converting to absolute power by using (1.72):

$$\begin{aligned} V_{\text{rec dB}\mu\text{V}} &= 107 + P_{\text{rec dBm}} \\ &= 107 - 36.75 \\ &= 70.25\ \text{dB}\mu\text{V} \end{aligned}$$

Because of the definition of dB as 10 log 10 for power ratios and 20 log 10 for voltage and current ratios, we can also use the cable loss (a ratio of powers) in dB to convert voltages. However, because this definition for voltages or currents implicitly assumed that $R_L = R_{\text{in}}$ in Fig. 1.5, its use in converting voltages requires a matched load as in Fig. 1.10. For example, the output power of the source in the previous problem of −30 dBm translates to a voltage across its output terminals of 7.07 mV or 77 dBμV. Since the cable is matched, the voltage across the input terminals of the signal measurer can also be computed as

$$V_{\text{rec dB}\mu\text{V}} = \text{cable gain}_{\text{dB}} + V_{\text{source dB}\mu\text{V}} \tag{1.75}$$

For this problem, we compute

$$\begin{aligned} V_{\text{rec dB}\mu\text{V}} &= \frac{-4.5\ \text{dB}}{100\ \text{ft}} \times 150\ \text{ft} + 77\ \text{dB}\mu\text{V} \\ &= -6.75\ \text{dB} + 77\ \text{dB}\mu\text{V} \\ &= 70.25\ \text{dB}\mu\text{V} \end{aligned}$$

as we computed using power.

Review Exercise 1.9 A 50 Ω source is attached to a 50 Ω signal measurer with 300 ft. of RG58U cable. The source is tuned to a frequency of 100 MHz, and the dial indicates an output of −15 dBm. Determine the voltage at the input to the signal measurer in dBμV.

***Answer*:** 78.5 dBμV.

1.4 SUMMARY

EMC is a broad topic with applications in every modern digital electronic device due to the rise in switching speeds and clock rates and the reduction in voltages.

A device's electromagnetic compatibility (EMC) must be considered not only from the perspective of its ability to "stave off" EM issues but also the problems that it introduces into the environment around it. For this reason, we classify EMC in four categories.

Radiated Emissions
Conducted Emissions
Radiated Immunity
Conducted Immunity

Emissions from a device can be further categorized into intentional or unintentional. Both intentional and unintentional emissions must be considered.

Coupling is the desired or undesired transfer of energy from one medium to another.

Unlike the traditional lumped circuit model where physical distances can be ignored, EMC is concerned with the electrical distance, defined by the signal's wavelength. Specifically, we are concerned with the ratio of physical distance to the wavelength of the signal under consideration.

Generally, a path is "electrically small" if it is less than 0.1 λ of a signal traveling it. When greater than 0.1 λ, we can no longer use lumped circuit models, and Maxwell's equations and other EMC methods must be applied to solving these problems.

Propagation of EM waves in nonconductive mediums is determined by the permittivity and permeability of the medium. These can be defined absolutely or relative to the permittivity and permeability of free space.

μ = permeability
μ_r = relative permeability
μ_0 = permeability of free space ($4\pi \times 10^{-7}$ H/m)
$\mu_r = \mu/\mu_0$
ε = permittivity
ε_r = relative permittivity
ε_0 = permittivity of free space $1/(36\pi \times 10^9)$ F/m
$\varepsilon_r = \varepsilon/\varepsilon_0$

A measurement in dB is a measurement of the ratio of two values and is therefore unitless. Analysis of a system in dB allows for gain to be calculated as a sum, rather than a product, further simplifying EMC analysis.

dB measurements can also be relative to a known value, such as 1 μV. As such, a measurement of a signal in dBμV is the ratio of the signal's power to 1 μV.

Most signal measurement devices are designed with a 50 Ω load, and electronic circuits are often designed to meet that load impedance.

We look to match the input impedance, load impedance, and characteristic impedance in a source, load, and conductive path model to allow for the maximum transfer of power, and to avoid other issues such as signal reflection. An unmatched circuit will result in power loss and signal degradation.

PROBLEMS

Section 1.1 Aspects of EMC

1.1.1 Reduce each of the following signal transmission situations to a source, coupling path(s), and receptor:

1. AM radio transmission to the human ear.
2. TV transmission to the human eye.
3. Radar target identification.
4. Transfer of 60 Hz power to an air conditioner.
5. Transfer of digital computer data to a printer.
6. Unintended interference between a radar transmitter and a digital computer.
7. Interference between an automobile ignition system and the car radio.
8. Interference in a radio due to lightning.
9. Several other interference situations of your choosing.

1.1.2 Scan the topic index of the following publications to get an appreciation for the various topics of EMC:

1. *IEEE Transactions on Electromagnetic Compatibility*.
2. *Proceedings of the IEEE International Symposia on Electromagnetic Compatibility*.
3. Various trade magazines such as *RF Design*, *EMC Technology*, *ITEM*, *Compliance Engineering*, *EMC Test and Design*, and *Conformity*.

1.1.3 Convert the following dimensions to those indicated:

1. 30 miles to km [48.28 km]
2. 1 ft. to mils [12 000 mils]
3. 100 yds. (length of a US football field) to meters [91.44 m]
4. 1 mm to mils [39.37 mils]
5. μm (micrometer) to mils [0.03937 mils]
6. 880 yd. (race distance) to m [804.67 m]
7. 35 786 km (height of a satellite in geostationary orbit) in miles [22 236 mi].
8. 238 857 mi (the distance from the earth to the moon) to km [384 403 km].

Section 1.2 Electrical Dimensions and Waves

1.2.1 Determine the wavelength at the following frequencies in metric and English units:

1. 850 MHz, free space [35.3 cm, 13.9 in.]
2. 430 MHz, Teflon [48.1 cm, 18.95 in.]
3. 250 kHz, air [1200 m, 3937 ft]
4. 20 kHz (RS-232 data transmission), air [15 000 m, 9.32 mi]
5. 450 kHz–1.5 MHz AM radio transmission, air [667 m – 200 m, 2187 ft. – 656 ft]
6. 108 MHz FM transmission, air [2.78 m, 9.11 ft]
7. 1 GHz computer clock fundamental frequency, glass epoxy ($\varepsilon_r = 4.7$) [13.84 cm, 5.45 in.]
8. 15 GHz microwave signal, air [2 cm, 0.787 in.]

1.2.2 Determine the following physical dimensions in wavelengths:

1. 120 MHz, 18 cm, air [0.072 λ]
2. 100 MHz, 6 ft., air [0.61 λ]
3. 500 MHz, 10 in., glass epoxy ($\varepsilon_r = 4.7$) [0.918 λ]
4. A 6-ft printer cable at 80 MHz in air [0.49 λ]
5. The 3 m measurement distance of the FCC regulations at the lower frequency (30 MHz) and upper frequency (1 GHz) of the limit in air [0.3 λ, 10 λ]
6. A 10 mi length of 60 Hz power transmission line in air [3.22×10^{-3} λ]
7. An automobile (12 ft) at the lower frequency of the AM band (450 kHz) [5.5×10^{-3} λ]

1.2.3 Determine the wavelength at the following frequencies in metric and in English units:

1. LORAN C long-range navigation 90 Hz [3333.3 km, 2071.2 mi]
2. Submarine communication 1 kHz [300 km, 186.41 mi]
3. Automatic direction finder in aircraft 350 kHz [857.14 m, 0.533 mi]
4. AM radio transmission 1.2 MHz [250 m, 820.2 ft]
5. Amateur radio 35 MHz [8.57 m, 28.12 ft]
6. FM radio transmission 88 MHz [3.41 m, 11.18 ft]
7. Instrument landing system 335 MHz [89.55 cm, 2.94 ft]
8. Satellite 6 GHz [5 cm, 1.97 in.]
9. Remote sensing 45 GHz [6.67 mm, 262.5 mils]

1.2.4 Determine the following physical dimensions in wavelengths, that is, their electrical dimension:

1. A 50 mi length of a 60 Hz power transmission line [(1/62) λ]
2. A 500 ft. AM broadcast antenna broadcasting at 500 kHz [0.254 λ]
3. A 4.5 ft. FM broadcast antenna broadcasting at 110 MHz [0.5 λ]
4. A 2-in. land on a printed circuit board (assume a velocity of propagation of 1.5×10^8 m/s) at 2 GHz [0.677 λ]

1.2.5 A sinusoidal current wave is described below. Determine the velocity of propagation and the wavelength. If the wave travels a distance d determine the time delay and phase shift.

1. $i(z, t) = I_0 \cos(2\pi \times 10^6\, t - 2.2 \times 10^{-2}\, z)$, $d = 3$ km
   $v = 2.856 \times 10^8$ m/s, $\lambda = 285.6$ m, $TD = 10.5$ μs, $\varphi = 3781.5^\circ$
2. $i(z, t) = I_0 \cos(6\pi \times 10^9\, t - 75.4\, z)$, $d = 4$ in.
   $v = 2.5 \times 10^8$ m/s, $\lambda = 83.3$ mm, $TD = 0.41$ ns, $\varphi = 438.9^\circ$
3. $i(z, t) = I_0 \cos(30\pi \times 10^7\, t - 3.15\, z)$, $d = 20$ ft.
   $v = 2.99 \times 10^8$ m/s, $\lambda = 1.995$ m, $TD = 20.4$ ns, $\varphi = 1100.2^\circ$

4. $i(z, t) = I_0 \cos(6\pi \times 10^3\, t - 0.126 \times 10^{-3}\, z)$, $d = 50$ mi
   $v = 1.5 \times 10^8$ m/s, $\lambda = 50$ km, $TD = 0.54$ ms, $\varphi = 580.9^\circ$

Section 1.3 Decibels and Common EMC Units

1.3.1 Determine the following voltages in dBμV and dBm:

1. 23 mV [87.2 dBμV, −19.8 dBm]
2. 670 μV [56.5 dBμV, −50.5 dBm]
3. 3.2 V [130 dBμV, 23.1 dBm]
4. 0.1 μV [−20 dBμV, −127 dBm]
5. 1 mV [60 dBμV, −47 dBm]
6. 300 mV [110 dBμV, 2.55 dBm]
7. 21 mV [86.4 dBμV, −20.6 dBm]
8. 30 V [149.5 dBμV, 42.5 dBm]
9. 48 mV [93.6 dBμV, −13.36 dBm]
10. 0.3 V [109.5 dBμV, 2.55 dBm]
11. 0.5 μV [−6.02 dBμV, −113 dBm]
12. 200 mV [106 dBμV, −0.97 dBm]

1.3.2 Convert the following quantities to V:

1. −26 dBμV [0.05 μV]
2. −35 dBm [4 mV]
3. −16 dBm [35 mV]
4. 36 dBμV [63.1 μV]
5. −28 dBm V [39.8 μV]
6. 20 dBm [2.24 V]

1.3.3 Determine a simple expression to convert (RMS) voltage in dBμV to dBm [dBμV = 107 + dBm]

1.3.4 Determine the following electric field intensity levels in dBμV/m:

1. 100 μV/m [40 dBμV/m]
2. 1 mV/m [60 dBμV/m]
3. 200 V/m [166 dBμV/m]

1.3.5 Estimate the following ratios of currents or voltages in dB. Give exact values.

1. 200 [46.02, 46]
2. 640 [56.12, 56.1]
3. 32×10^{-3} [−29.9, −30]
4. 5.7×10^{-6} [−104.88, −104]

Section 1.3.1 Signal Source Specification

1.3.6 A 50 Ω source is tuned to 100 MHz and attached to a 50 Ω spectrum analyzer with 200 ft. of 50 Ω coaxial cable that has a loss of 4.5 dB/100 ft at 100 MHz. The spectrum analyzer reads a level of signal at 100 MHz of 56.5 dBμV. If the cable is removed and the signal source is attached directly to a 100 Ω load, determine the voltage across this load in dBμV. [67.98 dBμV]. Determine the reading on the meter of the source in dBm. [−41.5 dBm]

1.3.7 A 50 Ω source is attached to a 50 Ω receiver with 200 ft. of RG58U coaxial cable (4.5 dB/100 ft loss at 100 MHz). The source is tuned to 100 MHz and the meter indicates that the output is −30 dBm. Determine the voltage at the receiver input in dBμV. [68 dBμV]. If the voltage at the output terminals of the source is measured and found to be 30 mV, determine the voltage at the input to the receiver in dBm. [−26.45 dBm]. If the received voltage at the terminals of the receiver is measured and found to be −50 dBm, determine the voltage at the output terminals of the source in dBμV. [66 dBμV]

1.3.8 A 50 Ω source is attached to a 300 Ω receiver with a 100 ft. length of twin lead ($Z_C = 300\ \Omega$). The twin lead has a loss of 10 dB/100 ft at the frequency of the source. Determine the voltage at the input to the receiver in dBμV if the source indicates an output of −30 dBm. [71.7 dBμV]

1.3.9 A 50 Ω oscillator is putting out a signal level of −20 dBm according to the meter on the instrument. If a 150 Ω load is placed across its terminals, determine the output voltage in dBμV. [90.5 dBμV]

1.3.10 A 50 Ω oscillator is attached to the high-impedance input of an oscilloscope ($C_{\text{in}} = 47$ pF, $R_{\text{in}} = 1$ MΩ; see Fig. 1.9). The source is tuned to 100 MHz and the level set to −30 dBm. Determine the voltage level (peak) of the sinusoid seen on the oscilloscope face. [11.22 mV]

REFERENCES

1. C. R. Paul and S. A. Nasar, *Introduction to Electromagnetic Fields*, 2, McGraw-Hill, New York, 1987.
2. C. R. Paul, *Electromagnetics for Engineers: with Applications to Digital Systems and Electromagnetic Interference*, Wiley, Hoboken, NJ, 2004.
3. C. R. Paul, *Fundamentals of Electric Circuit Analysis*, Wiley, New York, 2001.
4. H. W. Ott, *Noise Reduction Techniques in Electronic Systems*, 2 Wiley-Interscience, New York, 1986. (See also the Website: http://www.hottconsultants.com).
5. D. D. Gerke and W. D. Kimmel (2002). *EDN's Designer's Guide to EMC*, 2. Elsevier Science and Technology, Cambridge, MA.
6. B. Keiser, *Principles of Electromagnetic Compatibility*, 3, Artech House, Dedham, MA, 1987.
7. N. Violette, D. R. J. White, and M. Violette, *Electromagnetic Compatibility Handbook*, Van Nostrand-Reinhold, New York, 1987.
8. J. R. Barnes, *Electronic System Design: Interference and Noise Control Techniques*, Prentice-Hall, Englewood Cliffs, NJ, 1987.
9. E. R. Freeman and M. Sachs, *Electromagnetic Compatibility Design Guide*, Artech House, Dedham, MA, 1982.
10. T. A. Jerse, *Designing for Electromagnetic Compatibility*, Hewlett-Packard, Palo Alto, CA, 1989.
11. F. M. Tesche, M. V. Ianoz, and T. Karlson, *EMC Analysis Methods and Computational Models*, Wiley-Interscience, New York, 1997.
12. J. J. Goedbloed, *Electromagnetic Compatibility*, Prentice-Hall, Englewood Cliffs, NJ, 1992.
13. R. Perez, ed., *Handbook of Electromagnetic Compatibility*, Academic Press, New York, 1995.
14. H. J. Johnson and M. Graham, *High-Speed Digital Design*, Prentice-Hall PTR, New York, 1993.
15. H. Johnson and M. Graham, *High-Speed Signal Propagation*, Prentice-Hall PTR, New York, 2003.
16. S. H. Hall, G. W. Hall, and J. A. McCall, *High-Speed Digital Design*, Wiley-Interscience, New York, 2000.
17. C. R. Paul (1986). An undergraduate course in electromagnetic compatibility. *1986 IEEE International Symposium Electromagnetic Compatibility*, San Diego, CA.
18. C. R. Paul, Establishment of a university course in electromagnetic compatibility (EMC), *IEEE Trans. Educ.* 33, 111–118 (1990).

CHAPTER TWO

EMC Requirements for Electronic Systems

In this chapter, we will discuss the *motivation* for studying the subject of EMC. This motivation results from the imposition of additional design objectives for electronic systems over and above those required for the functional performance of the system. These additional design objectives stem from the overall requirement that the system be *electromagnetically compatible* with its environment. There are basically two classes of EMC requirements that are imposed on electronic systems:

1. Those mandated by governmental agencies
2. Those imposed by the product manufacturer

The requirements imposed by governmental agencies are *legal* requirements and generally cannot be waived. These requirements are imposed in order to minimize the interference produced by the product. However, compliance with these EMC requirements does not guarantee that the product will not cause interference. It only allows the country imposing the requirement to control the amount of "electromagnetic pollution" that the product generates. In order for the product to be marketed (advertised and sold) in a country, the product must comply with these requirements. If a product cannot be legally sold because of its inability to comply with the governmental EMC requirements, the fact that it may perform a function that gives it significant sales potential is unimportant!

On the other hand, EMC requirements that manufacturers voluntarily impose on their products are intended to result in customer satisfaction. They are imposed for the purpose of ensuring a reliable, quality product. For example, if a new digital computer turns out to be highly susceptible to electrostatic discharge (ESD), the company will obtain a poor reputation from the standpoint of quality control of its product, resulting in loss of future sales on this and other products. Maintaining a good reputation in the marketplace is clearly of critical importance. We will be able to discuss these company-mandated requirements only in general terms since most are proprietary and not available to the public. Nevertheless, most manufacturers impose a set of requirements, often derived in some fashion from existing commercial and/or military standards, which we will discuss.

Compliance with both of these types of EMC requirements is critical to the success of the product in the marketplace. We will begin this discussion with governmental requirements and then discuss those requirements that are imposed by the manufacturing company.

Introduction to Electromagnetic Compatibility, Third Edition. Clayton R. Paul, Robert C. Scully, and Mark A. Steffka.
© 2023 John Wiley & Sons, Inc. Published 2023 by John Wiley & Sons, Inc.

2.1 GOVERNMENTAL REQUIREMENTS

With the availability of rapid, global transportation, and communications, the marketplace today encompasses the entire world. Consequently, the EMC requirements of all countries are of importance to manufacturers of electronic equipment. We will divide these into two sectors: those imposed on products marketed in the United States (USA) and those imposed on products marketed outside its borders. The regulatory requirements of each country are further subdivided into those for commercial use and those for military use.

In this section, we will give a brief overview of the typical regulatory requirements. There are a number of technical nuances in each regulation that will not be discussed so that we can focus on the general requirements without getting involved in minutiae of technical detail. It should be emphasized that the governmental requirements are in a constant state of change. The regulations that we will discuss are those in effect as of this writing. The reader should consult the most current issue of those regulations. Most companies that manufacture electronic products have an “EMC regulation guru” whose job is to keep track of the latest EMC requirements mandated by all governmental agencies worldwide. Hence, we will not describe in this chapter all such regulations. Only the major requirements on conducted and radiated emissions will be described.

2.1.1 Requirements for Commercial Products Marketed in the United States

In the United States, the Federal Communications Commission (FCC) is charged with the regulation of radio and wire communication. A significant part of that responsibility is to control interference from and to wire and radio communication. The FCC Rules and Regulations contained in Title 47 of the Code of Federal Regulations have several parts that apply to nonlicensed electronic equipment. Part 15 applies to radio-frequency devices and will be of primary concern here [1]. The range of frequencies defined by the FCC to be “radio frequencies” extends from 9 kHz to 3000 GHz. A *radio-frequency device* is any device that is capable of emitting radio-frequency energy by radiation, conduction, or other means whether intentionally or not. The purpose of Part 15 is to control the interference from these emitters. Transmitters operating under a radio station license are covered in another part. Some examples of “radio-frequency devices” are dc motors where arcing at the brushes generates a wide spectrum of energy that includes this band of frequencies, digital computers whose “clock” signals generate radiated emissions in this band, electronic typewriters that also employ digital circuitry, etc. Our discussion of the FCC regulations will be brief but will cover the essential points and will concern those parts that affect digital devices.

In 1979, the FCC published, under Part 15 of its Rules and Regulations, a requirement that has had and will continue to have considerable impact on the electrical engineering community and the electronics industry. With the increasing proliferation of computers and other digital devices, the FCC realized that some limits on the electromagnetic emissions from these devices was necessary in order to minimize their potential for interfering with radio and wire communications. Numerous instances of such interference had begun to surface with increasing regularity. This resulted in the publication of the above rule, which has the force of law. It basically sets limits on the radiated and conducted emissions of a *digital device*. The FCC defines a digital device as

> *Any unintentional radiator (device or system) that generates and uses timing pulses at a rate in excess of 9000 pulses (cycles) per second and uses digital techniques …* .

Any electronic device that has digital circuitry and uses a clock signal in excess of 9 kHz is covered under the rule, although there are a limited number of exemptions. This rule includes, for example, electronic typewriters, calculators, point-of-sale terminals, printers, and modems, as well as personal computers.

It is *illegal* to market a “digital device” in the United States unless its radiated and conducted emissions have been measured and do not exceed the limits of the regulation. The FCC considers *marketing* as shipping, selling, offering for sale, etc. Monetary fines and/or jail terms can be imposed for the willful violation of this rule. Companies that manufacture these products are not as much concerned about these consequences as they are the devastating publicity resulting from a “minor infraction.” They are also concerned about the financial impact of a potential recall of a product if some units are randomly tested by the FCC and found to exceed the limits. So it is not sufficient to construct one sample that complies with the regulation.

The FCC further breaks the digital device class of products into Class A and Class B. Class A digital devices are those that are marketed for use in a commercial, industrial, or business environment. Class B digital devices are those that are marketed for use in a residential environment, notwithstanding their use in a commercial, industrial, or business environment. The Class B limits are more stringent than the Class A limits under the reasonable assumption that interference from the device in an industrial environment can be more readily corrected than in a residential environment, where the interference source and the susceptible device are likely to be in proximity. Further, the owner of the interfering device in a residential environment is not as likely to have the expertise or financial resources to correct the problem as would an industrial user. Hence, the potential for interference is more closely controlled for the residential market. Personal computers and their peripherals are a subcategory of Class B digital devices. They must be tested for compliance by the manufacturer and the test data submitted to the FCC for *certification*. For all other “digital devices,” the manufacturer must test the device for compliance, and no test data are required to be submitted to the FCC. The FCC employs random sampling to verify compliance. In this subsection, we will discuss the limits. The measurement procedure to verify compliance will be discussed in Section 2.1.4.

The FCC limits of this rule concern the conducted and radiated emissions of the digital product. Conducted emissions are those currents that are passed out through the unit’s ac power cord and placed on the common power net, where they may radiate more efficiently because of the much larger expanse of this “antenna” and thus cause interference with other devices. The frequency range for conducted emissions extends from 150 kHz to 30 MHz. Compliance is verified by inserting a line impedance stabilization network (LISN) into the unit’s ac power cord. Although the emission to be controlled is current passing out the ac line cord, the limits are given in volts. This is because the test device (LISN) described in Section 2.1.4.2 measures a voltage that is directly related to the interference current. Radiated emissions concern the electric and magnetic fields radiated by the device that may be received by other electronic devices, causing interference in those devices. The FCC, as well as other regulatory agencies, requires measurement of the radiated electric field, and the regulatory limits are given in terms of that field in dBμV/m. The frequency range for radiated emissions begins at 30 MHz and extends to 40 GHz. Compliance is verified by measuring the radiated electric fields of the product either in a semianechoic chamber or at an open-field test site. The radiated emissions must be measured with the measurement antenna in both the vertical and horizontal polarizations with respect to the ground plane of the test site, and the product must comply for both polarizations.

FCC Part 15 requirements include several subparts. Subpart A concerns General Requirements, Subpart B concerns Unintentional Radiators (such as digital devices), and Subpart C concerns Intentional Radiators (such as radio transmitters). Hence, our concern will be with Subpart B. The limits on conducted emissions (out the unit’s power cord) are given for Class B digital devices in Table 2.1, and the limits for Class A digital devices are given in Table 2.2. These emissions are to be measured with a line impedance stabilization network (LISN) inserted into the unit’s power cord. LISNs are discussed in Section 2.1.4.2. There are two levels to be satisfied: QP refers to a quasi-peak detector

TABLE 2.1 FCC and CISPR 32 Conducted Emission Limits for Class B Digital Devices

Frequency (MHz)	μV QP (AV)	dBμV QP (AV)
0.15	1995 (631)	66 (56)
0.5	631 (199.5)	56 (46)
0.5–5	631 (199.5)	56 (46)
5–30	1000 (316)	60 (50)

TABLE 2.2 FCC and CISPR 32 Conducted Emission Limits for Class A Digital Devices

Frequency (MHz)	μV QP (AV)	dBμV QP (AV)
0.15–0.5	8912.5 (1995)	79 (66)
0.5–30	4467 (1000)	73 (60)

in the measurement receiver, whereas AV refers to an average detector in the measurement receiver. See Section 3.3.2 of Chapter 3 for a discussion of these detectors. These limits are plotted in Fig. 2.1.

The upper frequencies of applicability for radiated emissions are given in Table 2.3 and are based on the highest frequency of use in the product. For example, a present-day personal computer having a clock frequency of 3 GHz would be required to have its radiated emissions measured up to 15 GHz. The limits on radiated emissions for Class B digital devices are given in Table 2.4, and the limits on radiated emissions for Class A digital devices are given in Table 2.5. They are plotted in Fig. 2.2. These levels are for a quasi-peak detector in the measurement receiver. For measurements above 1 GHz, the limits are 54 dBμV/m (average detector) and 74 dBμV/m (peak detector) for Class B digital devices and 49.5 dBμV/m (average detector) and 69.5 dBμV/m (peak detector) for Class A digital devices. The measurement distances for radiated emissions are 3 m for Class B measurements and 10 m for Class A measurements. In addition, the measurements must be made with the measurement antenna in horizontal and in vertical polarizations (parallel to and perpendicular to the ground plane of the test site, respectively). The antenna must be elevated above the ground-plane distances of 1–4 m and the maximum emission recorded.

It is informative to compare the radiated emission limits for Class A and Class B products in order to determine how much less stringent the Class A limits are. However, the radiated emissions for Class B devices are to be measured at a distance of 3 m from the product, whereas the radiated emissions for Class A products are to be measured at a distance of 10 m. A common way of scaling these measurement levels for different measurement distances is the *inverse distance method*, in which the emissions are assumed to fall off linearly with increasing distance to the measurement antenna. Thus, the emissions at 3 m are assumed to be reduced by 3/10th if the measurement distance is moved to a further distance of 10 m and vice versa. To translate the Class A limits from a distance of 10 to 3 m, we *add* $20 \log_{10} (10/3) = 10.46 \cong 10$ dB to the Class A limits since moving the measurement point closer to the emitter is expected to increase the electric field levels that are measured. These are compared in Fig. 2.3 and shown, according to this extrapolation, that the Class A limits are some 10 dB less stringent than the Class B limits. It should be pointed out that, as we shall see in Chapter 7, the emissions from antennas fall off inversely with distance only if the measurement points are in the *far field* of the emitter. An approximate criterion for the far-field boundary is three

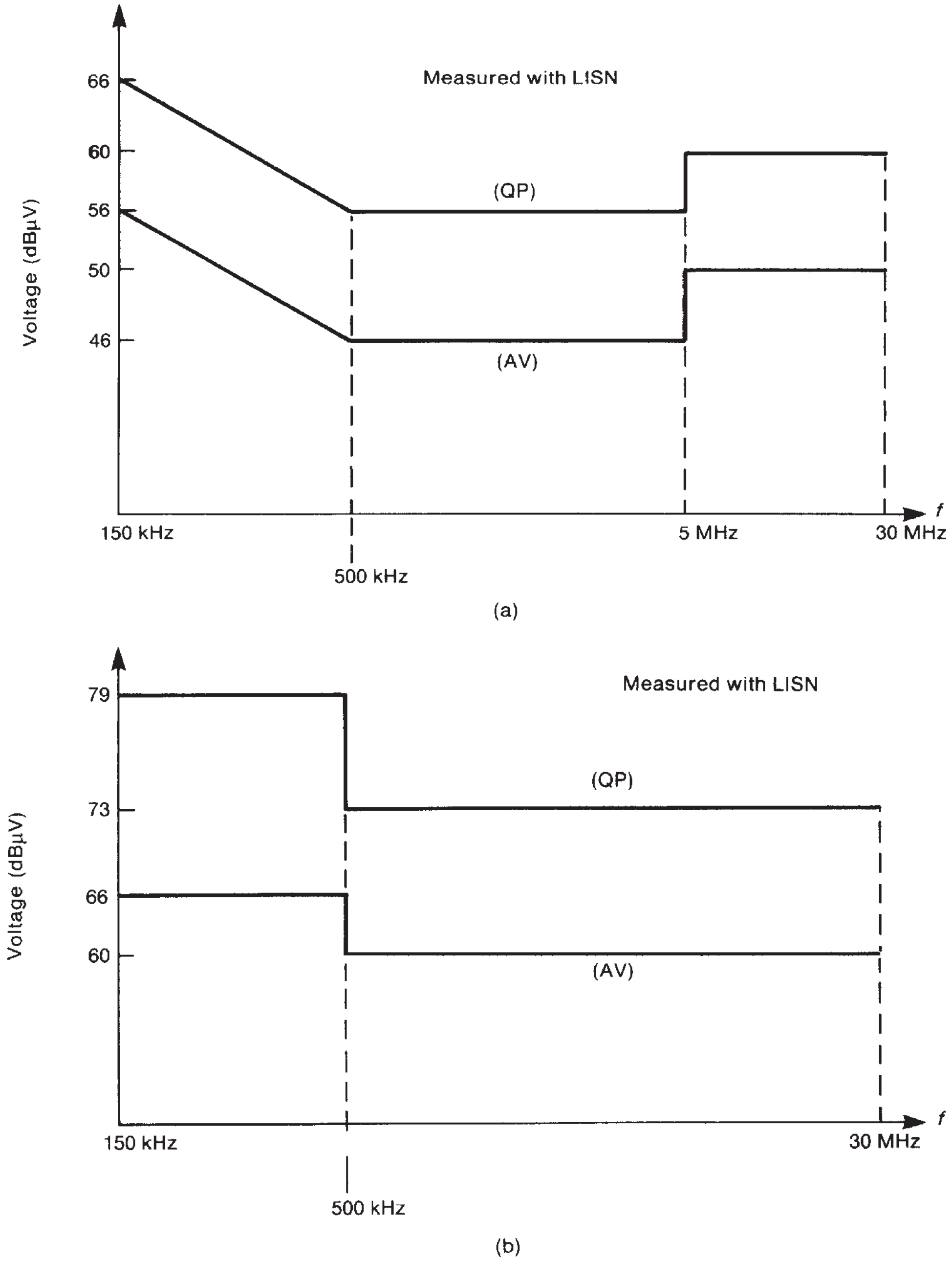

FIGURE 2.1 The FCC and CISPR 32 conducted emission limits: (a) Class B; (b) Class A.

wavelengths (3λ). Based on this criterion the near-field–far-field boundary at the lowest measurement frequency of 30 MHz is 30 m but is 90 cm at 1 GHz. Thus, the measurement distance of 3 m is likely in the near field of the product at 30 MHz, and this extrapolation of the Class A limit at 30 MHz to 3 m (or the extrapolation of the Class B limit out to 10 m) is not technically valid. This comparison, although somewhat approximate, nevertheless illustrates the fact that emissions of Class A devices are controlled to a lesser degree than are those of Class B devices.

TABLE 2.3 Upper Limit of Measurement Frequency

Highest Frequency Generated or Used in the Device or on Which the Device Operates or Tunes (MHz)	Upper Frequency of Measurement Range (MHz)
<1.705	30
1.705–108	1000
108–500	2000
500–1000	5000
>1000	5th harmonic of highest frequency or 40 GHz, whichever is lower

TABLE 2.4 FCC Emission Limits for Class B Digital Devices

	Measured at 3 m	
Frequency (MHz)	μV/m	dBμV/m
30–88	100	40
88–216	150	43.5
216–960	200	46
>960	500	54
>1 GHz	500 (AV)	54 (AV)

TABLE 2.5 FCC Emission Limits for Class A Digital Devices

	Measured at 10 m	
Frequency (MHz)	μV/m	dBμV/m
30–88	90	39
88–216	150	43.5
216–960	210	46.4
>960	300	49.5
>1 GHz	300 (AV)	49.5 (AV)

Review Exercise 2.1 Calculate the levels in Fig. 2.3.

2.1.2 Requirements for Commercial Products Marketed Outside the United States

The majority of the governmental EMC requirements for markets outside the United States are initiated by the International Special Committee on Radio Interference (CISPR), which is a committee of the International Electrotechnical Committee (IEC). Although CISPR writes standards, they are not mandatory. However, most international countries adopt the CISPR recommendations. The most widely used standard is CISPR 32 that sets limits on the radiated and conducted emissions of multimedia equipment (MME), including information technology equipment (ITE), which

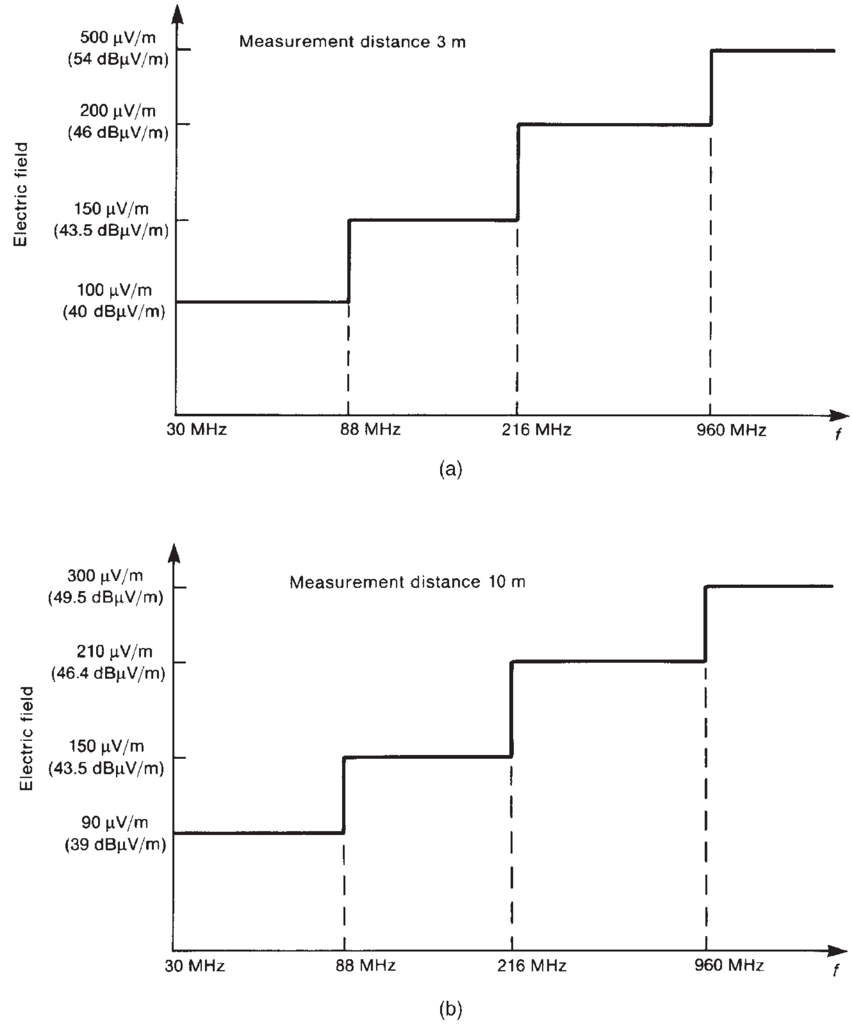

FIGURE 2.2 FCC radiated emission limits: (a) Class B; (b) Class A.

basically includes *digital devices* in the similar meaning as for the FCC. The limits are divided into Class A and Class B equipment, and their meaning is essentially the same as the FCC definitions. The majority of the markets are the European Economic Area (EEA), which includes the 25 members of the European Union (EU), which was formerly known as the European Community (EC) or the European Economic Community (EEC). The EEA also includes three members of the European Free Trade Association. The European EMC Directive 2014/30/EU of the European Parliament and of the Council of February 26, 2014, revised by the Regulation (Eu) 2018/1139 Of The European Parliament and of the Council of July 4, 2018 [2] applies to members of the EEA. If a product satisfies the requirements of the Directive, the manufacturer or importer affixes the "CE" mark to the product, and it is deemed to be legal for sale in states of the EEA with regard to compliance with the EMC directive. The FCC has recently harmonized the conducted emission limits with those of the Directive. Although there are a large number of EMC standards in the Directive, the primary one we will discuss is the CISPR 32 standard published by the IEC [3].

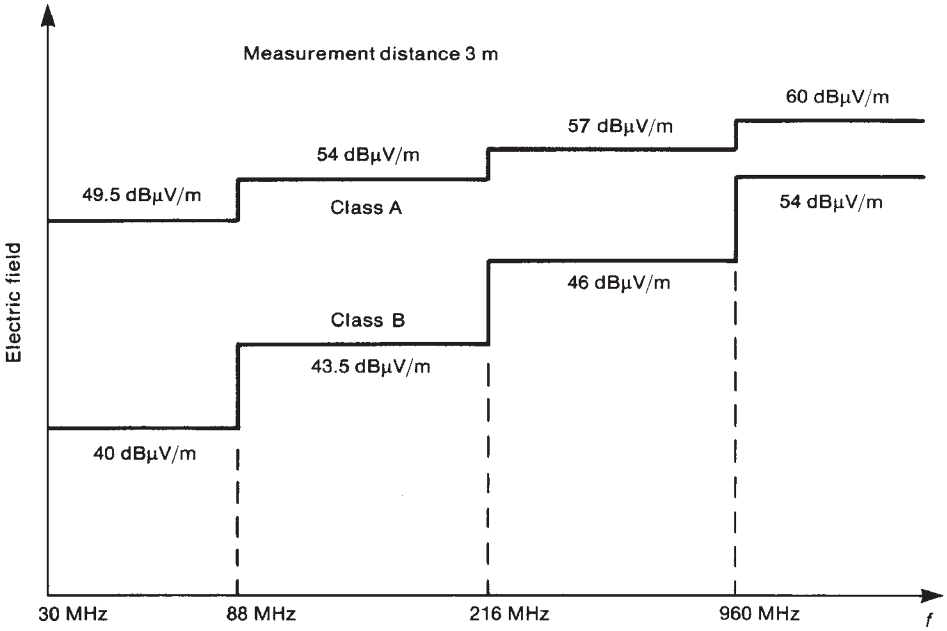

FIGURE 2.3 A comparison of the FCC Class A and FCC Class B radiated emission limits for a measurement distance of 3 m.

The CISPR 32 conducted emission limits are given in Tables 2.1 and 2.2 and shown in Fig. 2.1. They are the same as the FCC conducted emission limits.

The CISPR 32 radiated emission limits are tabulated in Table 2.6 for Class B ITE equipment and in Table 2.7 for Class A ITE equipment. The Class B emissions are to be measured at a distance of 10 m, as are the Class A levels. Like the FCC radiated emission limits, these are to be measured with a CISPR 32 receiver having a quasi-peak detector (QP). The FCC and CISPR 32 radiated emission limits are compared in Fig. 2.4. Note the figure shows the solid line limit as CISPR 22, but this limit

TABLE 2.6 CISPR 32 Radiated Emission Limits for Class B ITE Equipment (10 m) OATS/SAC

Frequency (MHz)	μV/m	DBμV/m
30–230	31.6	30
230–1000	70.8	37

TABLE 2.7 CISPR 32 Radiated Emission Limits for Class A ITE Equipment (10 m) OATS/SAC

Frequency (MHz)	μV/m	dBμV/m
30–230	100	40
230–1000	224	47

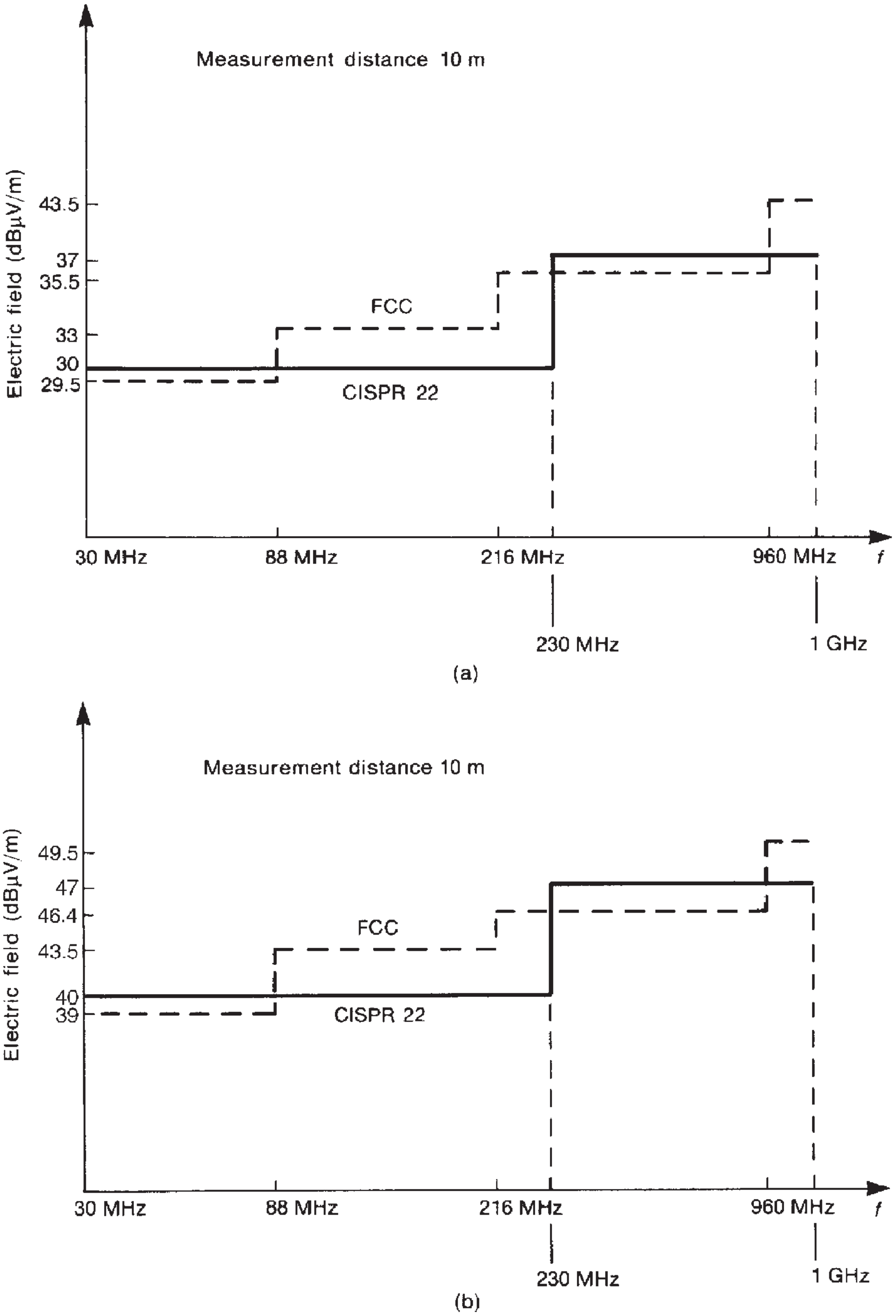

FIGURE 2.4 The CISPR 32 radiated emission limits compared to the FCC radiated emission limits: (a) Class B; (b) Class A.

matches that in CISPR 32. Since the FCC and CISPR 32 limits for Class A equipment are both to be measured at 10 m, no scaling is required. However, the FCC Class B emissions are to be measured at a distance of 3 m. In order to scale these to the CISPR 32 Class B measurement distance of 10 m using the inverse distance rule, we subtract $20 \log_{10}(10/3) = 10.46$ dB from the FCC Class B limits at 3 m. Or we could add 10.46 dB to the CISPR 32 Class B limits at 10 m to scale to the FCC Class B limits at 3 m. We have chosen to scale the FCC Class B limits at 3 m to a distance of 10 m by subtracting 10.46 dB. From this comparison, we see that the CISPR 32 Class B limits are somewhat more restrictive than the FCC Class B limits in the frequency range of 88–230 MHz. From 88 to 216 MHz, the CISPR 32 limits are 3 dB more restrictive, and from 216 to 230 MHz they are 5.5. dB more restrictive. From 230 to 960 MHz, the FCC limits are more restrictive by about 1.5 dB. Again we see that the CISPR 32 limits for Class A digital devices are more restrictive than the FCC limits in the frequency range of 88–216 MHz by some 4 dB and 6 dB in the range of 216–230 MHz. From 230 to 960 MHz, the CISPR 32 limits are less restrictive than the FCC limits by about 1 dB.

Review Exercise 2.2 Compute the levels shown in Fig. 2.4.

One of the most significant aspects of the European EMC Directive was that it mandated, for the first time in commercial products, the requirement that products be tested for their susceptibility (immunity) to conducted and radiated emissions from other sources. The FCC regulations in the United States do not have such a requirement since the FCC is concerned with the viability of wire and radio communications. These require that the product be tested by exposing it to external sources that simulate its intended electromagnetic environment, and the product's operation must not be degraded by these sources. This represents a quality issue, specifically, the product must be able to operate reliably in the surrounding electromagnetic environment. These susceptibility (immunity) standards are generally those prepared by the IEC under the 61000 series and adopted as EN 61000-4-XXX standards. They cover a wide variety of sources/conditions that may cause the product to malfunction. Some of these are electrostatic discharge (ESD); radiated electromagnetic field (radiated by an external source), electrical fast transient/burst, surge immunity tests, immunity to power frequency (50 Hz, 60 Hz) magnetic fields, pulsed magnetic fields immunity test, damped oscillatory magnetic field test, voltage dips, short interruptions in alternating current, harmonics, and interharmonics at ac port, test for immunity to conducted, common-mode disturbances from 0 Hz to 150 kHz, and power quality tests.

2.1.3 Requirements for Military Products Marketed in the United States

A large portion of the products of commercial firms both within and outside the United States are produced for military applications. Specification of limits on emissions for control of interference is obviously more critical for military products than commercial products since interference can affect mission performance of the system containing the product. In addition, it is important to control the susceptibility (immunity) of the electronic devices in the system to other electromagnetic sources, e.g. high-power radars. The typical electromagnetic environment of a military system is considerably more harsh than that for a commercial product.

The EMC requirements for products that are produced for use by the U.S. military (all branches of the Department of Defense or DoD) are contained in the military standard MIL-STD-461G:2015 [5]. The limits and applicability are much more complicated and span much larger frequency ranges than do those of the FCC or CISPR 32. These requirements have been adopted by NASA and are commonly used by all major aerospace companies for both military and commercial hardware. The MIL-STD-461G requirements have also been adopted for use by a large number of military and aerospace organizations outside the United States. One key difference between these military

TABLE 2.8 Emission and Susceptibility Requirements of MIL-STD-461G

Requirement	Description
CE101	Conducted emissions, audio frequency currents, power leads
CE102	Conducted emissions, radio frequency potentials, power leads
CE106	Conducted emissions, antenna port
CS101	Conducted susceptibility, power leads
CS103	Conducted susceptibility, antenna port, intermodulation
CS104	Conducted susceptibility, antenna port, rejection of undesired signals
CS105	Conducted susceptibility, antenna port, cross-modulation
CS109	Conducted susceptibility, structure current
CS114	Conducted susceptibility, bulk cable injection
CS115	Conducted susceptibility, bulk cable injection, impulse excitation
CS116	Conducted susceptibility, damped sinusoidal transients, cables and power leads
CS117	Conducted susceptibility, lightning induced transients, cables and power leads
CS118	Conducted susceptibility, personnel borne electrostatic discharge
RE101	Radiated emissions, magnetic field
RE102	Radiated emissions, electric field
RE103	Radiated emissions, antenna spurious and harmonic outputs
RS101	Radiated susceptibility, magnetic field
RS103	Radiated susceptibility, electric field
RS105	Radiated susceptibility, transient electromagnetic field

Source: MIL-STD-461G [4]/U.S. Department of Defense/Public domain.

requirements and the commercial requirements (FCC and CISPR 32) is that the military requirements can be *waived* and/or *tailored*. The contracting officer for the military project has the authority to waive certain of the MIL-STD-461G requirements and can also accept changes in them for the specific system, which is called “tailoring.” This same approach is commonly used by aerospace organizations, both US and foreign. Table 2.8 gives the individual requirements in MIL-STD-461G [4]. Table 2.9 gives the applicability of the individual standards to specific military systems [4]. We will show the conducted and radiated emission limits that apply to all systems: conducted emissions CE102, *Power Leads from 10 kHz to 10 MHz*, and radiated emissions RE102, *Electric Fields from 10 kHz to 18 GHz*. The conducted susceptibility requirement for all systems are CS101, *Power Leads from 30 Hz to 150 kHz*, and CS114, *Bulk Cable Injection from 10 kHz to 200 MHz*. See [4] for these limits. The primary radiated susceptibility requirement for all systems is RS103, Electric Field from 2 MHz to 40 GHz. Table 2.10 shows the level of incident electric field intensity that the system is to withstand without malfunction. For other limits consult [4].

For all emission requirements, the receiver must use a peak detector. Conducted emissions are measured with a LISN inserted into the power leads. LISNs are discussed in Section 2.1.4.2. Requirement CE102 concerns the conducted emissions out of power leads from 10 kHz to 10 MHz. The limit is shown in Fig. 2.5. Compare this to the FCC/CISPR 32 limits in Fig. 2.1.

Review Exercise 2.3 Compare the FCC/CISPR 32 conducted emission limits in Fig. 2.1 to the limits for MIL-STD-461G CE102 in Fig. 2.5.

Requirement RE102 concerns the radiated electric field from 10 kHz to 18 GHz. The limit for aircraft and space applications is shown in Fig. 2.6a. The limit for ground applications is shown in Fig. 2.6b. These should be compared to the FCC limits in Fig. 2.2 and the CISPR 32 limits in Fig. 2.4. It is important to note that all radiated electric fields are to be measured at a distance of 1 m

TABLE 2.9 Requirement Matrix of MIL-STD-461G[a]

Equipment and ubsystems Installed in, on, or Launched from the Following Platforms or Installations	Requirement Applicability																		
	CE101	CE102	CE106	CS101	CS103	CS104	CS105	CS109	CS114	CS115	CS116	CS117	CS118	RE101	RE102	RE103	RS101	RS103	RS105
Surface ships		A	L	A	S	S	S		A	L	A	L	S	A	A	L	A	A	L
Submarines	A	A	L	A	S	S	S	L	A	L	A	S	S	A	A	L	A	A	L
Aircraft, army, including flight line	A	A	L	A	S	S	S		A	A	A	L	A	A	A	L	A	A	L
Aircraft, navy	L	A	L	A	S	S	S		A	A	A	L	A	L	A	L	L	A	L
Aircraft, air force		A	L	A	S	S	S		A	A	A	L	A		A	L		A	
Space systems, including launch vehicles		A	L	A	S	S	S		A	A	A	L			A	L		A	
Ground, army		A	L	A	S	S	S		A	A	A	S	A		A	L	L	A	
Ground, navy		A	L	A	S	S	S		A	A	A	S	A		A	L	A	A	L
Ground, air force		A	L	A	S	S	S		A	A	A		A		A	L		A	

[a] Legend: A—applicable; L—limited as specified in the individual sections of this standard; S—procuring activity must specify in procurement documentation.

Source: MIL-STD-461G [4]/U.S. Department of Defense/Public domain.

TABLE 2.10 RS103 Limits[a]

		Limit Level (V/m)[a]							
Frequency Range	Platform	Aircraft (External or Safety-Critical)	Aircraft Internal	All Ships (above Decks) and Submarines (External)[b]	Ships (Metallic) (below Decks)	Ships (Nonmetallic) (below Decks)	Submarines (Internal)	Ground	Space
2–30 MHz	A	200	200	200	10	50	5	50	20
	N	200	200	200	10	50	5	10	20
	AF	200	20	—	—	—	—	10	20
30 MHz–1 GHz	A	200	200	200	10	10	10	50	20
	N	200	200	200	10	10	10	10	20
	AF	200	20	—	—	—	—	10	20
1–18 GHz	A	200	200	200	10	10	10	50	20
	N	200	200	200	10	10	10	50	20
	AF	200	60	—	—	—	—	50	20
18–40 GHz	A	200	200	200	10	10	10	50	20
	N	200	60	200	10	10	10	50	20
	AF	200	60	—	—	—	—	50	20

[a] Key: A=Army; N=Navy; AF=Air Force.

[b] For equipment located external to the pressure hull of a submarine but within the superstructure, use “Ships (Metallic) (below Decks).”

Source: MIL-STD-461G [4]/U.S. Department of Defense/Public domain.

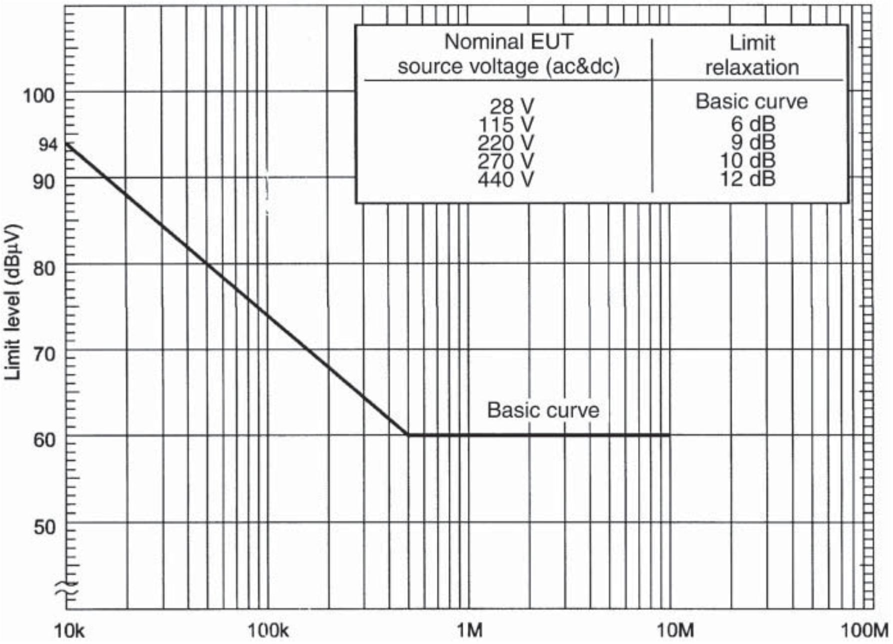

FIGURE 2.5 MIL-STD-461G CE102 limit (EUT power leads, ac and dc) for all applications [4]. Source: MIL-STD-461G [4]/U.S. Department of Defense/Public domain.

when using MIL-STD-461G, whereas the FCC/CISPR 32 radiated electric field emissions are to be measured at distances of 3 and 10 m.

Review Exercise 2.4 Compare the radiated emission limits for FCC shown in Fig. 2.2 and for CISPR 32 shown in Fig. 2.4 to the MIL-STD-461G RE102 emission limits shown in Fig. 2.6. (Remember to scale these by the ratios of the measurement distances in order to compare them.)

2.1.4 Measurement of Emissions for Verification of Compliance

It is as important to clearly specify how one is to measure the product emissions when attempting to verify compliance with the limits as it is to clearly specify the limits. Measurement of radiated and conducted emissions is a complex subject. It is fair to say that if the measurement procedures are not clearly spelled out but are left to the interpretation of the measurement personnel, one can obtain different sets of measured data at different measurement sites *for the same product*! Every standard that sets out limits on radiated and conducted emissions (FCC, CISPR 32, and MIL-STD-461) clearly defines how the data are to be measured. This includes facility characteristics, test procedures, test equipment, measurement bandwidths, and test antennas. Once again, the specification of the method for gathering the data is critically important so that the governing agency can be sure that data gathered on a product at one company's test site can be validly compared to the limits and to data gathered at another test site. Otherwise the governing agency as well as the product manufacturer cannot be assured that the product's emissions comply with the limits. The measurement procedures for FCC measurements is contained in the American National Standards Institute (ANSI) standard ANSI C63.4-2014 [5]. The measurement procedures for CISPR 32 and for MIL-STD-461G are self-contained in the same standard that defines the limits although CISPR 32 references procedures contained in CISPR 16.

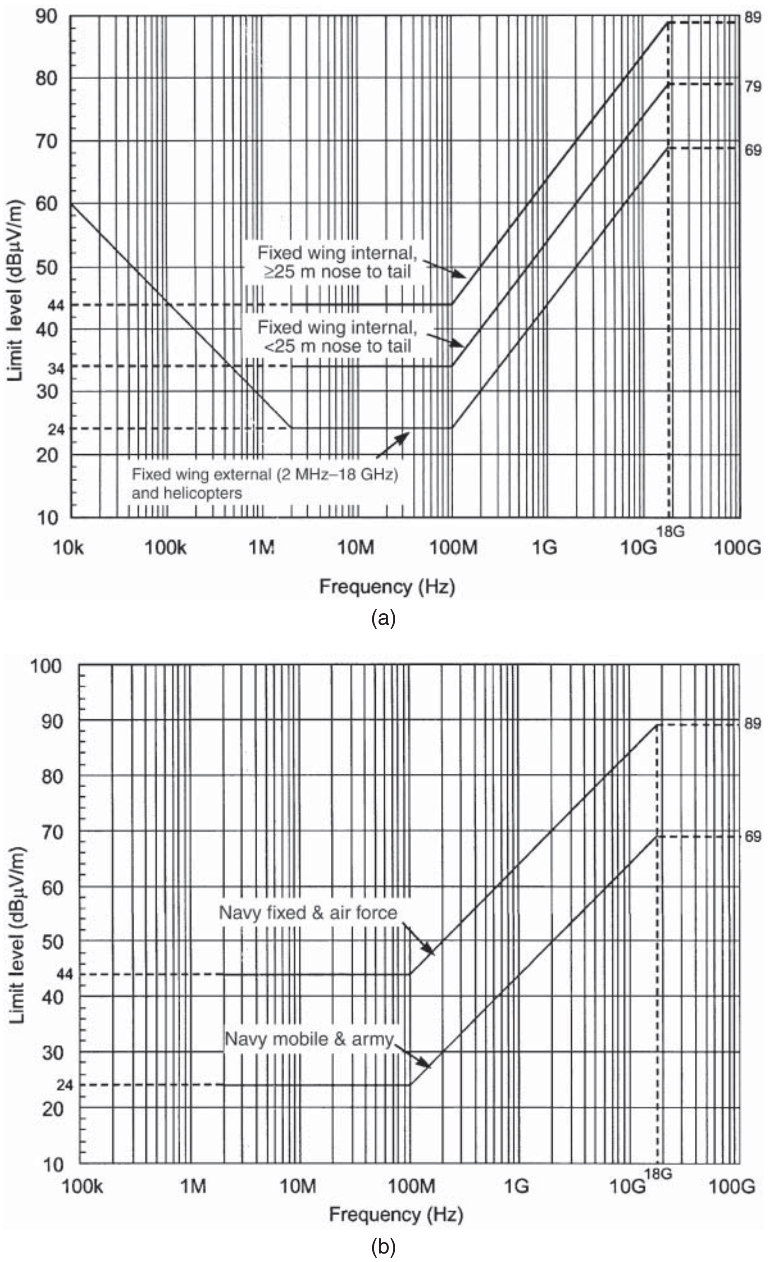

(a)

(b)

FIGURE 2.6 (a) MIL-STD-461G RE102 limit for aircraft and space system applications; (b) MIL-STD-461G RE102 limit for ground applications [4]. Source: MIL-STD-461G [4]/U.S. Department of Defense/Public domain.

2.1.4.1 Radiated Emissions The radiated electric fields for the commercial tests (FCC and CISPR 32) are to be measured either at an open-area test site (OATS) or in a semianechoic chamber (SAC). While the OATS is preferred, the SAC provides all-weather measurement capability, as well as security. A semianechoic chamber is a shielded room having radio-frequency absorber material

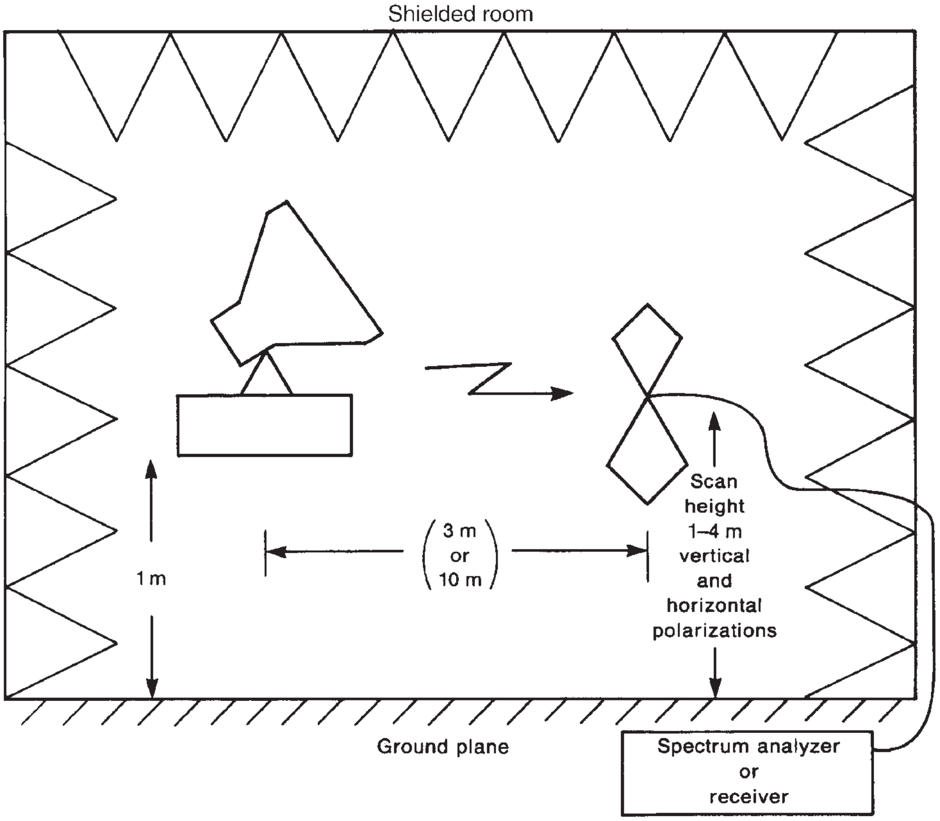
Shielded room
1 m
3 m or 10 m
Scan height 1–4 m vertical and horizontal polarizations
Ground plane
Spectrum analyzer or receiver

FIGURE 2.7 Illustration of the use of a semianechoic chamber for the measurement of radiated emissions.

on the sides and at the top of the room to prevent reflections and simulate free space as illustrated in Fig. 2.7. The product is placed 1 m above the floor of the chamber. A ground plane without absorber constitutes the floor of the room. Hence, there will be reflections (multipath) at the floor. Figure 2.8 shows a typical commercial semianechoic chamber used for compliance testing. There are two purposes for the semianechoic chamber. The first is to prevent electromagnetic emissions from outside the room from contaminating the test. This is provided by the shielded room. The second is to prevent reflections at the walls of the shielded room so as to simulate free space, and this feature is provided by the radio-frequency absorber material that lines the walls. The military standard MIL-STD-461G also provides that the radiated emissions be measured in a shielded room lined with absorber material to prevent reflections. The measurement receiver uses a quasi-peak detector for the FCC and CISPR 32 measurements, whereas the MIL-STD-461G receiver must use a peak detector. The FCC Class B measurement distance is 3 m, and the Class A distance is 10 m. The CISPR 32 measurement distance is 10 m for both Class B and Class A ITE equipment. The MIL-STD-461 measurement distance is 1 m. The preferred measurement antenna for the FCC measurements is a tuned, half-wave dipole. A *half-wave dipole* is a linear antenna whose length is 0.5λ at the measurement frequency. If the frequency is changed, the dipole physical length must also be changed in order to maintain electrical length of 0.5λ. The standards cover a wide frequency range; hence, resizing the dipole for every frequency would be a very time-consuming task. In order to speed the measurement over a wide frequency band, the receiver is swept across the band and the radiated electric field at each frequency is automatically recorded. Because of

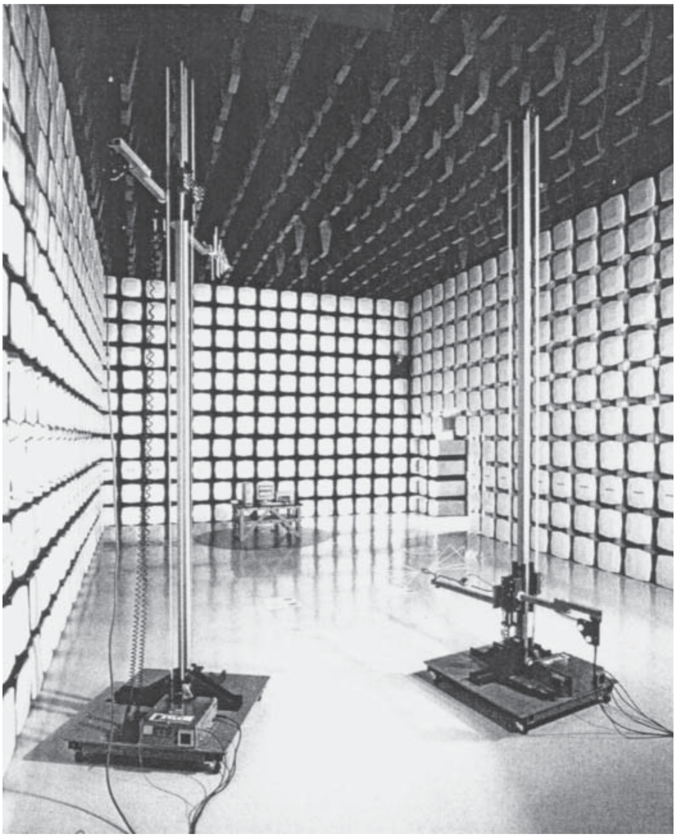

FIGURE 2.8 Illustration of a typical test of a digital device for its radiated emissions as required by various governmental regulations. Source: Courtesy of ETS-Lindgren, Inc.

the inability to use a tuned, half-wave dipole in an automated, swept-frequency measurement, antennas having large bandwidths are used (see Chapter 7). The biconical antenna may be used from 30 to 200 MHz, and the log-periodic antenna is used from 200 MHz to 1 GHz. The biconical and log-periodic antennas are discussed in Section 7.7 of Chapter 7. The CISPR 32 test uses these antennas also. The measurement antennas in the FCC and CISPR 32 tests are to be scanned from a height of 1 m above the floor to 4 m and the maximum level recorded. Also the antennas are to be placed in horizontal polarization (parallel to the floor) and in vertical polarization (perpendicular to the floor) and the maximum recorded emissions in both polarizations must not exceed the standard. The antennas for MIL-STD-461G measurements are specified as a 104-cm rod dipole antenna from 10 kHz to 30 MHz, a biconical antenna from 30 to 200 MHz, and a double-ridge horn antenna above 200 MHz [4]. The antennas used in MIL-STD-461 testing are also used in both horizontal and vertical polarizations above 30 MHz. MIL-STD-461 does not use height scanning for measurements, instead employing a 120 cm height for all antennas [4].

The peak, quasi-peak, and average detectors in the receivers are discussed in the next chapter in Section 3.3.2. The bandwidths of these receivers are also given there.

2.1.4.2 Conducted Emissions The intent of the conducted emission limits is to restrict the noise *current* passing out through the product's ac power cord. The reason for this is that these noise currents will be placed on the common power net of the installation. The common power net of an installation is an array of interconnected wires in the installation walls, and as such represents a large antenna. Noise currents that are placed on this power net will therefore radiate quite efficiently, which can produce interference. An example of this is the lines that appear on a TV set when a blender or other device powered by a universal motor is turned on. The noise generated by the arcing at the brushes of the universal motor pass out through the ac power cord of the blender, are placed on the household ac power system, and are then radiated and picked up by the TV, where they show up as interference.

Therefore the conducted emission that should be measured is the noise current conducted out through the ac power cord of the product. Yet the FCC and CISPR conducted emission limits are given in units of volts. This is because the tests are to be conducted by inserting a line impedance stabilization network (LISN) in series with the ac power cord of the product. In order to understand the performance of this device, we need to discuss the standard ac power distribution system shown in Fig. 2.9. In the United States, ac voltage utilized in residential and business environments has a

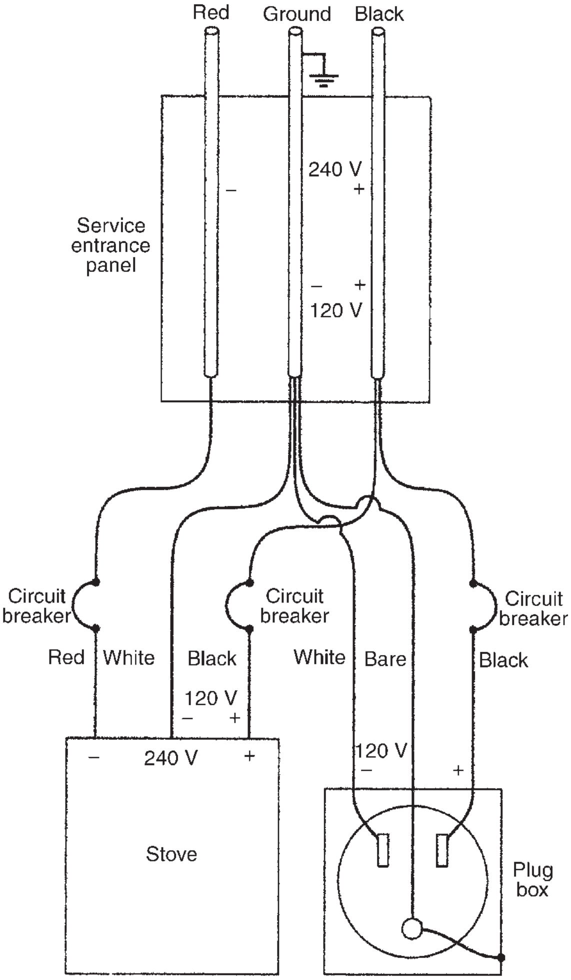

Red
Ground
Black
240 V
–
+
Service entrance panel
– +
120 V
Circuit breaker
Circuit breaker
Circuit breaker
Red
White
Black
White
Bare
Black
120 V
– +
– 240 V +
Stove
120 V
–
+
Plug box

FIGURE 2.9 A typical household power distribution system in the United States.

frequency of 60 Hz and an RMS voltage of 120 V. This power is transmitted to these sites at various other higher voltages. For example, the distribution wiring entering a typical residence is composed of two wires and a ground wire connected to earth. The voltage between the two wires is 240 V. At the service entrance panel in the home, the 120 V is obtained between one wire and the ground and between the other wire and ground. A third or safety wire (referred to as the *green wire*) is carried throughout the residence along with these two wires that carry the desired 60 Hz power. The two wires that carry the desired 60 Hz power are referred to as the *phase* and *neutral* wires. The currents to be measured are those exiting the product via the phase and the neutral wires. Thus, like the radiated emission measurements, two measurements are needed for conducted emissions, phase and neutral.

A typical commercial LISN and its use is illustrated in Fig. 2.10. There are two purposes of the LISN. The first, like the shielded room of the radiated emission measurements, is to *prevent noise external to the test (on the common ac power net) from contaminating the measurement.* The inductor L_1 and capacitor C_2 are for this purpose: L_1 blocks noise, whereas C_2 diverts noise. The value of L_1 is 50 μH, and its impedance ranges from 47 to 9425 Ω over the conducted emission frequency range (150 kHz–30 MHz). The value of C_2 is 1 μF, and its impedance ranges from 1.06 to 0.005 Ω over this frequency range. The second purpose of the LISN is to ensure that measurements made at one test site can be correlated with measurements at another test site. The possibility of this inconsistency between test sites is in the variability of the ac impedance seen looking into the ac power net from site to site. Measurements of the ac impedance seen looking into the ac power net at different locations show variability from site to site in addition to the variability with frequency [6]. (Remember that our interest in this measurement is not the power frequency but noise signals superimposed on the ac power conductors at frequencies from 150 kHz to 30 MHz.) In order to ensure that conducted emissions measured at one site correlate with those measured at another, we must be sure that the impedance seen by the product looking into its power cord is the same from site to site at

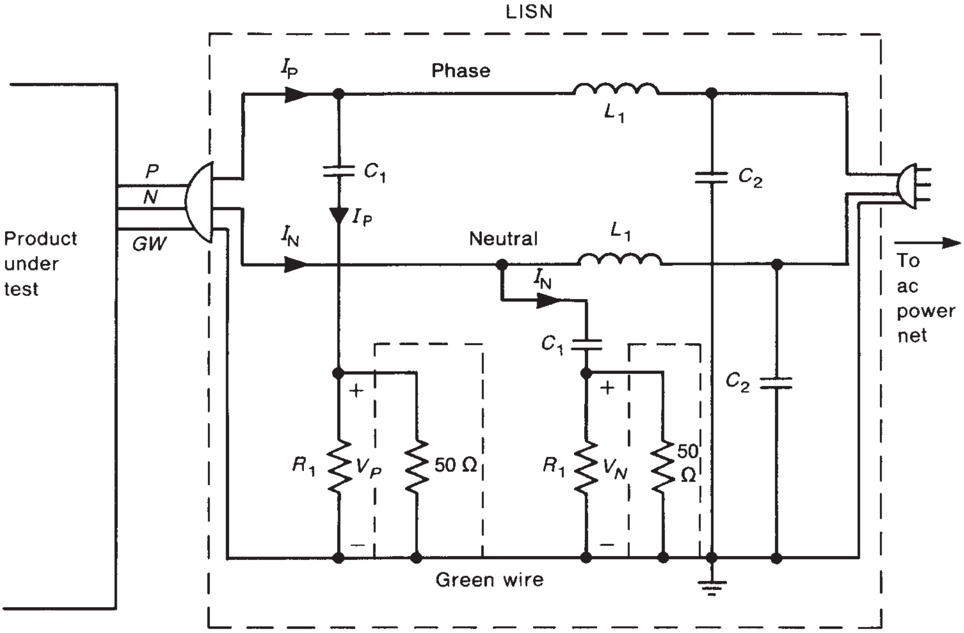

FIGURE 2.10 The line impedance stabilization network (LISN) for the measurement of conducted emissions.

corresponding frequencies. This is the second purpose of the LISN: *to present a constant impedance in frequency and from site to site to the product between phase and ground and between neutral and ground*. The capacitor C_1 and the 50 Ω resistor (which represents the input impedance to the receiver) accomplish this task. The capacitor C_1 is included to prevent any dc from overloading the test receiver, and the $R_1 = 1\ \text{k}\Omega$ resistor is used to provide a discharge path for C_1 in the event that the 50 Ω resistor is disconnected. The value of C_1 is $0.1\ \mu$F, so that the impedance of C_1 over the conducted emission frequency (150 kHz–30 MHz) ranges from 10.6 to 0.05 Ω. The inductor L_1 and capacitor C_2 prevent noise on the commercial power distribution system from being measured, but also pass the required 60 Hz power necessary to operate the product. The impedances of L_1 and C_2 at 60 Hz are 0.019 and 2653 Ω, respectively.

Over the frequency range of the regulatory limit (150 kHz–30 MHz), L_1 and C_2 essentially give an open-circuit looking into the commercial power distribution system. Thus, the impedance seen by the product between phase and green wire (ground) and between neutral and green wire is essentially 50 Ω. Furthermore, this is fairly constant over the frequency range of the conducted emission measurement. The 50 Ω resistors represent the standard 50 Ω input impedance to the spectrum analyzer or receiver that is used to measure the phase V_P and neutral V_N voltages. Now it is clear that these measured voltages are directly related to the noise currents passed out the phase and neutral conductors, I_P and I_N:

$$I_P = \frac{1}{50} V_P$$

$$I_N = \frac{1}{50} V_N$$

Each voltage must be measured over the frequency range of 150 kHz–30 MHz and the emissions must not exceed the limits shown in Fig. 2.1 for either voltage. One of the 50 Ω resistors represents the input impedance of the measurement spectrum analyzer or receiver, and the other 50 Ω termination is a “dummy load.” The FCC Class B conducted emission limit of 46 dBμV (AV) from 500 kHz to 5 MHz therefore represents a current of 12 dBμA or 4 μA.

A typical FCC and CISPR 32 LISN (one-half, phase, or neutral) is shown in Fig. 2.11a, whereas the MIL-STD-461G LISN is shown in Fig. 2.11b. The device being tested is referred to as the *equipment under test* (EUT). An important purpose of the LISN is to present a constant (50 Ω) impedance between phase and ground (green wire) and between neutral and ground (green wire).

2.1.5 Typical Product Emissions

In this section, we will show some examples of radiated and conducted emissions from a typical digital product. These data are included to give the reader an appreciation for the typical range of expected numbers.

The radiated emissions of a typical digital product are shown in Fig. 2.12a for vertical emissions and in Fig. 2.12b for horizontal emissions. Values of quasi-peak measurements at selected frequencies are also shown on the plots. Although we see individual harmonics of the clocks in the system, we do not see them of the same level but instead see certain regions of the spectrum accentuated such as one sees in a resonance situation. Some of this may be due to “tuning” by system cables or other resonance conditions. The FCC Class B and CISPR 32 Class B limits (shown as CISPR 22) are drawn on the plots. The plots include the older German GOP (VDE) limits. These emissions were measured in a semianechoic chamber that is used for product compliance testing.

The conducted emissions of this product are shown in Fig. 2.13, with the phase measurement in (a) and the neutral measurement in (b). This product employs a 45 kHz switching power supply. Note the peaks at the fundamental (45 kHz) and second (90 kHz) and third (135 kHz) harmonics of

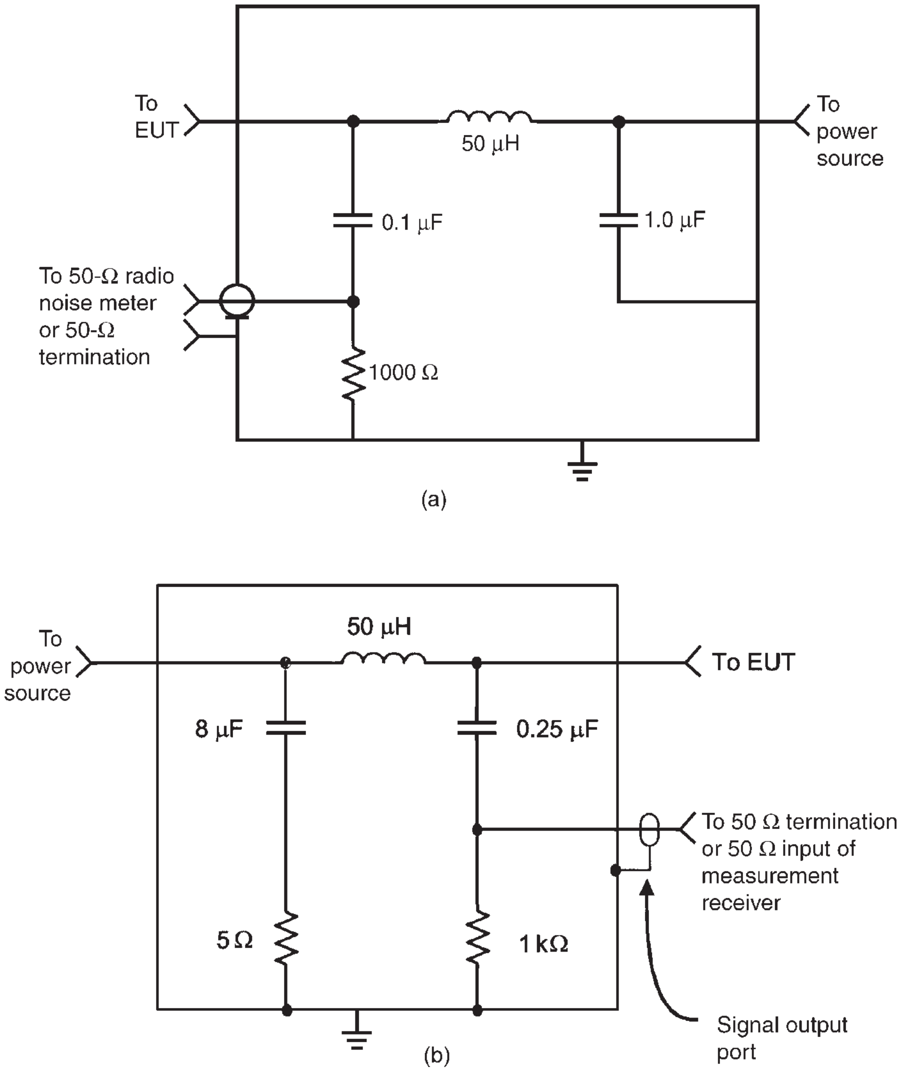
To
EUT
50 μH
To
power
source
0.1 μF
1.0 μF
To 50-Ω radio
noise meter
or 50-Ω
termination
1000 Ω
(a)
To
power
source
50 μH
To EUT
8 μF
0.25 μF
To 50 Ω termination
or 50 Ω input of
measurement
receiver
5 Ω
1 kΩ
Signal output
port
(b)

FIGURE 2.11 LISN element values for (a) FCC and CISPR 32 and (b) MIL-STD-461G conducted emission tests.

the switcher. The switcher frequency was chosen to be 45 kHz rather than a more obvious choice of 50 kHz in order that the third harmonic (135 kHz) occurs prior to the start frequency of the CISPR 32 limit (150 kHz). This moves the third harmonic below the lower frequency limit of CISPR 32 than would a choice of a 50 kHz switch frequency, and only marginally impairs the efficiency of the switcher. Therefore, from the standpoint of satisfying the CISPR 32 (and FCC) requirement, the levels of the first three harmonics of the switcher *are not regulated*! This is a good example of the point that simply being aware of the potential problem can lead to *cost-free* solutions in the early design. Recognizing this later in the design after a 50 kHz switch frequency had been chosen would require changes to be made that may be difficult to implement. Although not apparent on these plots, the harmonics of the system clocks that appear on the ac power cord contribute to the conducted emission levels at the higher frequencies. These may contribute to *radiated emissions* above 30 MHz from this "long antenna."

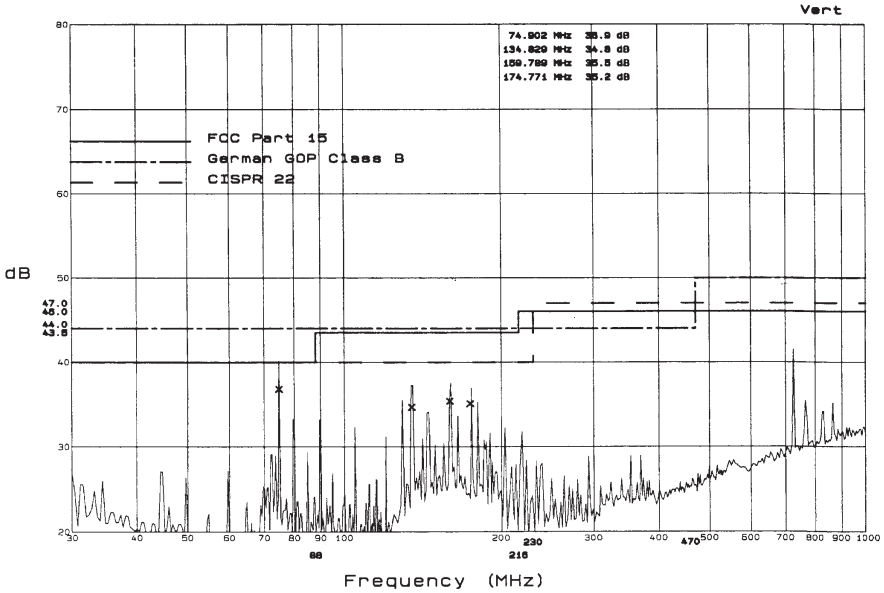

(a)

FIGURE 2.12 Radiated emissions of a typical digital product: (a) vertical emissions; (b) horizontal emissions.

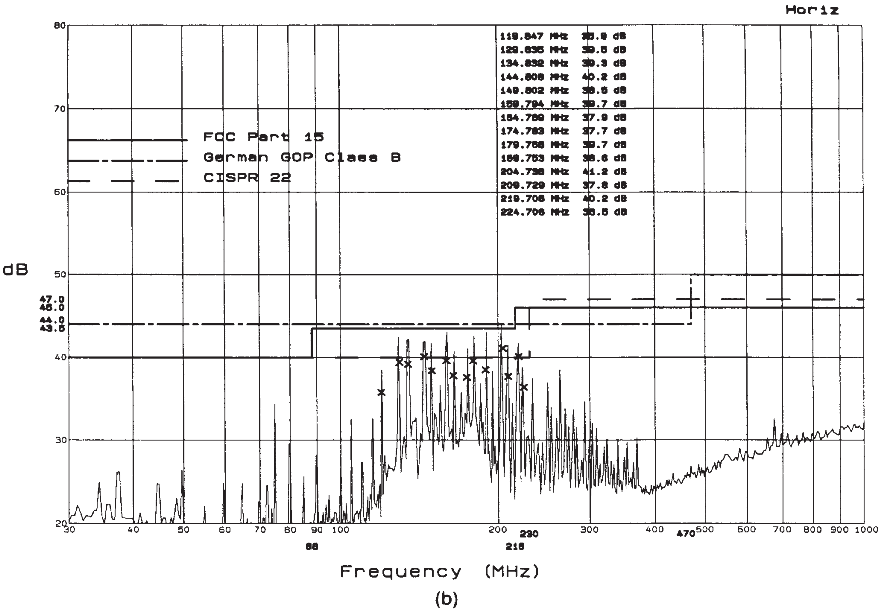

FIGURE 2.12 (*Continued*)

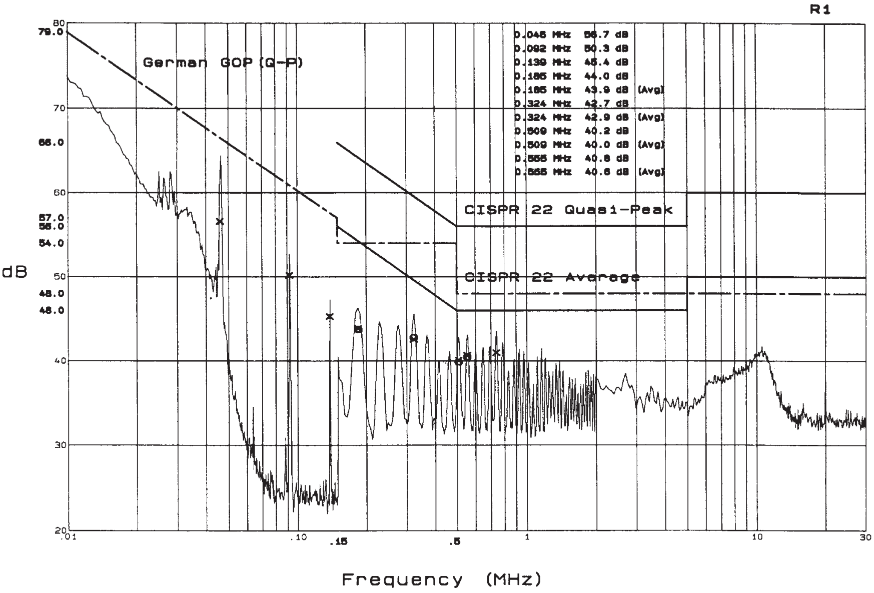

(a)

FIGURE 2.13 Conducted emissions of a typical digital product containing a switching power supply: (a) phase; (b) neutral.

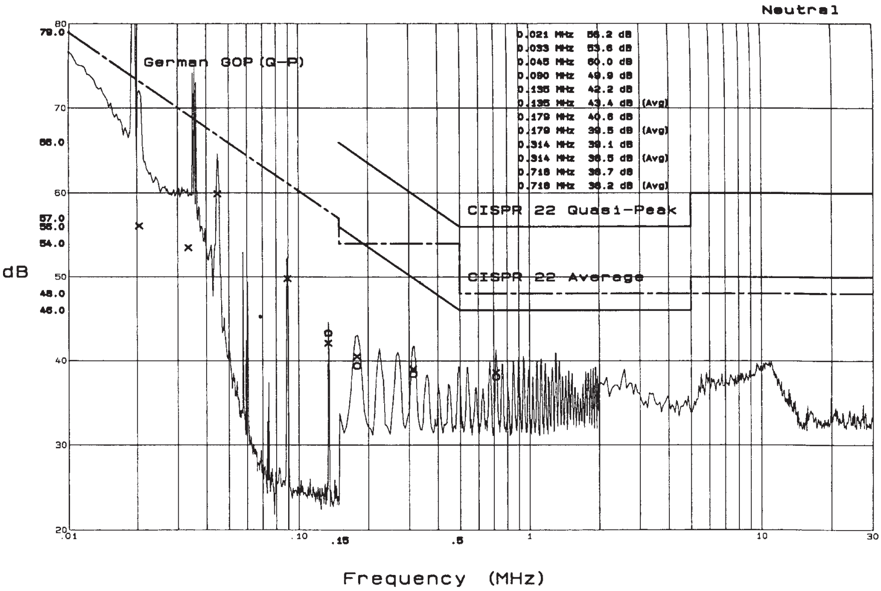

(b)

FIGURE 2.13 (*Continued*)

2.1.6 A Simple Example to Illustrate the Difficulty in Meeting the Regulatory Limits

The measured emissions of a typical product shown in Figs. 2.12 and 2.13 seem to indicate that designing a complex electronic system to satisfy the regulatory requirements is a deceptively simple problem. In this section, we will show data that indicate that this is not true. If one proceeds through a design with no thought given to EMC, it is highly likely, almost a certainty, that the product will not satisfy the regulatory requirements.

In order to illustrate this, a simple experiment was performed. A PCB consisting of two 7 in., parallel, 15 mil lands separated by 180 mils shown in Fig. 2.14 was constructed. A 10 MHz DIP (dual inline package) oscillator drove a 74LS04 inverter that was connected to one end of the pair of lands, and a 74LS04 inverter served as an active load attached to the other end of the pair of lands. Two regulated and compact 5 V power supplies were constructed to power the devices at either end of the line. These consisted of a 9 V battery driving a 7805 regulator chip. Both supplies were very compact (no larger than 2×2 in.) and had no connection to the commercial power system. The horizontal radiated emissions are shown in Fig. 2.15a and the vertical radiated emissions are shown in Fig. 2.15b. Observe that the horizontal emissions exceed the FCC Class B limit by as much as 30 dB! Even though the board is placed parallel to the ground plane of the chamber, the vertical emissions also exceed the FCC Class B limit, but only by some 15 dB.

This very simple experiment is a reasonable approximation to circuitry found on PCBs of products, yet it fails the FCC Class B limit by a large amount. Therefore, even if the device performed some useful function that a consumer would desire, it could not be sold in the United States (or in virtually all other countries in the world, for that matter)! This simple example should serve to illustrate that designing an electronic product to comply with the regulatory limits is a deceptively difficult problem and one that should not be taken lightly.

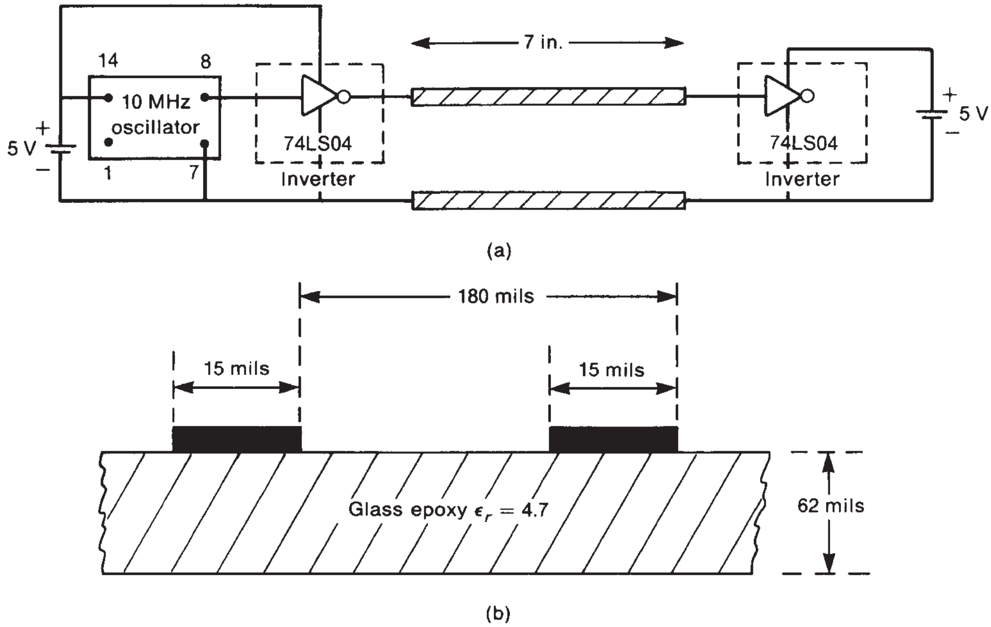

FIGURE 2.14 A simple experiment to demonstrate the difficulty in complying with the radiated emission limits: (a) schematic and dimensions of device tested; (b) cross-sectional dimensions of the printed circuit board (PCB).

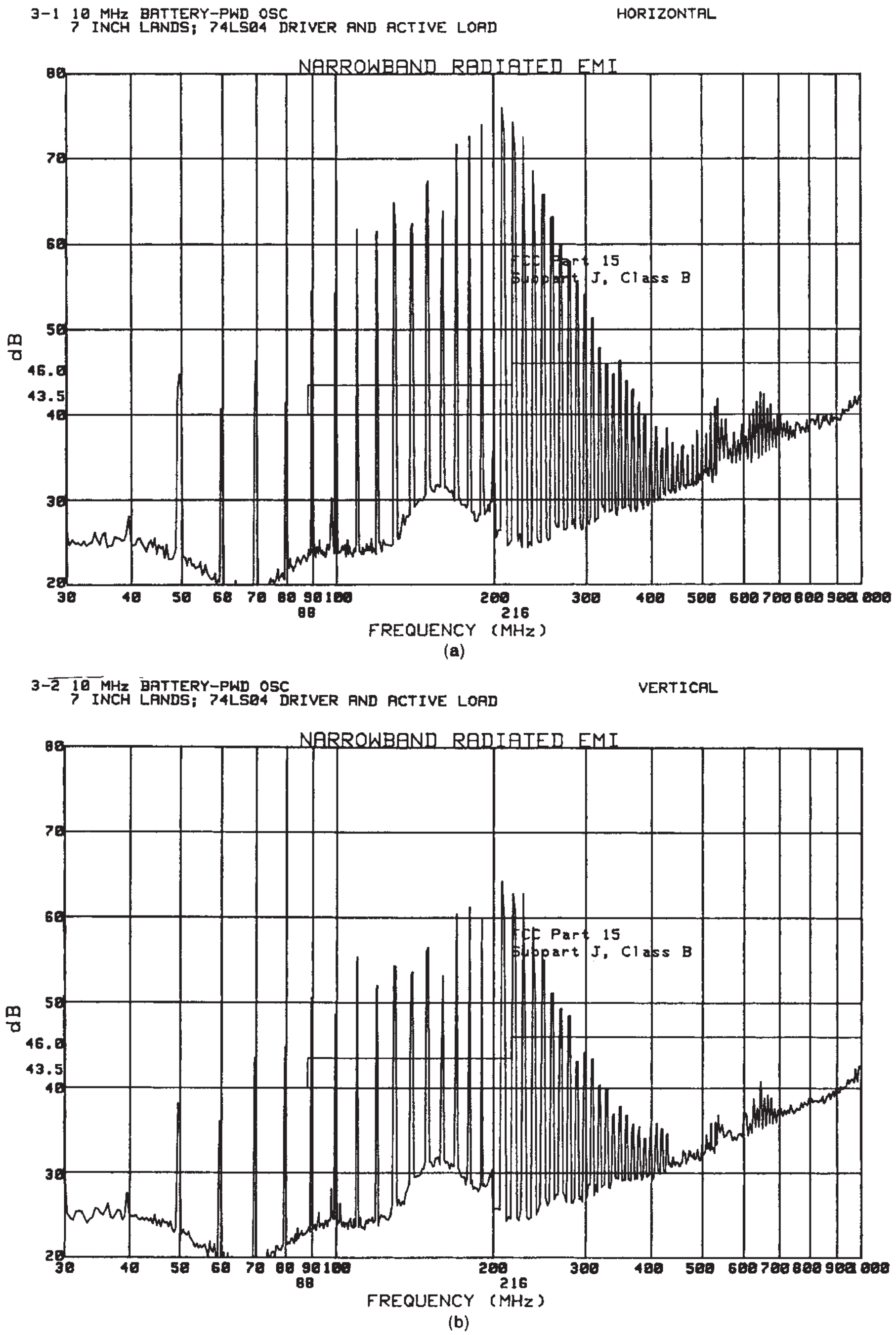

FIGURE 2.15 Radiated emissions at 3 m for the device of Fig. 2.15: (a) horizontal; (b) vertical.

2.2 ADDITIONAL PRODUCT REQUIREMENTS

As pointed out earlier, it is of no benefit to design a product that performs some new and marketable function if it fails to comply with the EMC regulatory requirements. Similarly, it is also of no benefit to design a product that passes the EMC regulatory requirements imposed by governmental agencies but will not operate satisfactorily when placed near an FM radio transmitter or an airport surveillance radar. Consumers do not appreciate the problems these emitters pose on the proper operation of electronic devices. They expect that a product that was purchased in good faith will operate satisfactorily in any residential installation, and the consumer will not appreciate a warning that states "Caution, this computer will not work if your home is within half a mile of an FM transmitting tower." An equally embarrassing event for the product manufacturer is the inability of the product to function properly if the operator walks across a nylon rug in an office situated in a dry climate and touches the product, causing an electrostatic discharge to reset the machine. These examples illustrate the importance of the manufacturer imposing certain tests over and above those required by governmental agencies in order to ensure that the product will perform properly in a wide variety of field installations. We will discuss those requirements in this section. However, these self-imposed requirements are usually proprietary, and the limits and test procedures are not generally made available to the public. Consequently, we will be able to discuss these only in qualitative terms.

2.2.1 Radiated Susceptibility (Immunity)

The purpose of these tests is to ensure that the product will operate properly when it is installed in the vicinity of high-power transmitters. The common types of such transmitters are AM and FM transmitters and airport surveillance radars. Manufacturers test their products to these types of emitters by illuminating the product with a typical waveform and signal level representing the worst-case exposure of the product and determining whether the product will perform satisfactorily. If the product cannot perform satisfactorily in such installations, this deficiency should be determined prior to its marketing so that "fixes" can be applied to prevent a large number of customer complaints and service calls. The EU and MIL-STD-461G standards include a radiated susceptibility test; the FCC requirements do not.

2.2.2 Conducted Susceptibility (Immunity)

Products can be susceptible to a wide variety of interference signals that enter it via the ac power cord. An obvious example is lightning-induced transients. Thunderstorms frequently strike power transmission lines and substations. Circuit breakers are intended to momentarily clear any faults and reclose after a few cycles of the ac waveform. The product must be insensitive to these types of momentary power interruptions, as well as the transient spikes that are generated on the power line. Of course, there is little that the manufacturer can do about a complete power "blackout," but consumers consider it reasonable to expect the product to operate so long as only momentary surges occur. Most manufacturers subject their products to these scenarios by intentionally injecting spikes into the product's ac power cord to simulate lightning-induced transients. The ac voltage is also momentarily reduced and/or interrupted to ensure that the product will operate through any such event. These types of tests represent conducted susceptibility tests. The EU and MIL-STD-461G standards include conducted susceptibility tests; the FCC standards do not.

2.2.3 Electrostatic Discharge (ESD)

This phenomenon has been mentioned previously and is becoming an increasingly important concern with today's integrated circuit technology. The basic phenomenon is the buildup of static charge on a person's body or furniture with the subsequent discharge to the product when the person or the furniture touches the product. The static voltage can approach 25 kV in magnitude. When the discharge occurs, large currents momentarily course through the product. These currents can cause IC memories to clear, machines to reset, etc. Consumers do not view these events as being normal operation of a well-designed product. Consequently, manufacturers test their products for susceptibility to the ESD phenomenon by subjecting their products to a controlled ESD event that represents a typical field scenario and determining whether the product operates successfully. Typical ESD tests used by a manufacturer are described in [7]. The phenomenon of ESD is investigated in more detail in Chapter 11. The EU standards include an ESD test. The FCC and MIL-STD-461G standards do not.

2.2.4 Requirements for Commercial Aircraft

One of the primary voluntary requirements for commercial aircraft is promulgated by the Radio Technical Commission for Aeronautics (RTCA). This is RTCA DO-160G [8]. The RTCA was formed in 1935 and functions as a Federal Aviation Advisory Committee in the United States. Its recommendations are adopted by the Federal Aviation Administration (FAA) and numerous private aircraft manufacturers and airborne electronics manufacturers in the United States. Many non-U.S. government and business interests also belong to RTCA. The RTCA DO-160G standard contains standards and limits for susceptibility, conducted and radiated emissions, ESD, and lightning to which commercial aircraft and airborne electronic equipment are tested to.

2.2.5 Requirements for Commercial Vehicles

Commercial vehicles (automobiles and trucks) are becoming increasingly dependent on onboard electronics (and particularly digital electronics) for their performance. Hence, they are becoming increasingly susceptible to external electromagnetic emissions and also are becoming sources of electromagnetic emissions. In order to ensure that these onboard electronics will not be interfered with or cause interference with themselves or with external receptors, the vehicles are tested to certain standards. The international standards are CISPR 12 and CISPR 25 [9]. The U.S. Society of Automotive Engineers (SAE) also promulgates standards for whole vehicle testing, SAE J551, and for component testing, SAE J1113 [10]. These standards contain limits for emissions, as well as immunity along with standards for testing.

2.3 DESIGN CONSTRAINTS FOR PRODUCTS

Of course, virtually any product can be made to comply with the governmental regulatory limits and the manufacturer's self-imposed susceptibility requirements. For example, a digital device that is susceptible to disturbances on the ac power cord can be made insensitive to this by simply powering the product with internal batteries. The cost to the manufacturer, not only in terms of added cost to the product but also in customer acceptance, is prohibitive. As another example, suppose that the product fails the FCC Class B limits on radiated emissions at a particular frequency. The product can be made to comply with these limits if it is enclosed entirely in a metallic box that has no openings. However, penetrations in the box must be made in order to provide power, as well as data signals from keyboards and other peripheral devices. We will find in later chapters that cables provide efficient antennas for the radiation of high-frequency noise signals. So these penetrations drastically defeat the shielding effect of the enclosure.

A more realistic way of reducing the radiated and conducted emissions of a product is to add suppression components that reduce the levels of emissions. However, these components add extra cost to the product over that required for its functional performance. The manufacturer must add the cost of these components to the manufacturing cost of the product. In today's highly competitive market, any additional cost affects the selling price of the product and the success of the product in the marketplace. Thus, an important consideration is *product cost*. Generally, manufacturers are driven by product cost, with all other considerations being secondary.

Another important design constraint is *product marketability*. For example, market surveys determine what the consumer will be likely to purchase. Product appearance and ease of use are important factors here. It may be possible to enclose a typewriter in a contiguous metal box such that radiated emissions will be reduced. However, the consumer must be able to easily insert paper, type on the keyboard, etc. The acceptability of a product by the consumer is frequently a top priority, otherwise cost savings are inconsequential.

Another design constraint is imposed by the *manufacturability* of the product. Most manufacturers use automated assembly methods to manufacture the final product. Electronic components, as well as other parts of the product, are inserted by robots. Even though today's robots are capable of inserting minute electronic components into printed circuit boards, they are not capable of assembling certain components such as wires that humans can readily place by hand. Thus, any EMC suppression components that are to be added must be such that they can be handled easily in the manufacturing process, or else the cost advantage of automated assembly is not fully realized.

And finally, one of the most important considerations is the *product development schedule*. Manufacturers determine the need for a new product by conducting market surveys. These also serve to indicate the trend in products that will be produced by other manufacturers in the future. In order to take advantage of the interest of the consumer, the product must be placed on the market during a certain timeframe; otherwise competing products will gain an advantage. Product development schedules are developed to not only gauge the progress of the product development but also ensure that the product will be made available to the consumer when his/her interest in that product is at its peak. Delays in this product development schedule obviously affect the marketability of the product, and any delays can be as serious to the manufacturer as cost overruns. EMC problems can and frequently do cause delays in the product's development schedule. The typical scenario is to wait until the end of the development schedule to test the product for its compliance with the governmental EMC requirements, as well as those imposed by the manufacturer. If it is discovered at this late date that the product fails to comply, fixes must be developed. Generally, the difficult part of fixing the problem is the *diagnosis* of the *source of the problem*. For example, even though it is obvious that the product's radiated emissions exceed the FCC Class B limit at a particular frequency, the essential question is "How do we reduce the level of that emission in a cost-effective and manufacturable manner?" Although the original source of the emission is obvious (e.g. one of the system processor clocks), the primary radiation point or mechanism is not known, e.g. which land of a printed circuit board or wire of one of the system's cables is the dominant radiator. Determining the primary or dominant source of the emission is important so that (1) a fix can be efficiently made and (2) unnecessary cost is not added to the product in the way of fixes that do not substantially contribute to the reduction of the emission. We will study this important aspect of *diagnostic tools* in Section 11.5 of Chapter 11. *Diagnosing the problem correctly and quickly is critical to maintaining the product's development schedule,* as well as minimizing the cost of EMC suppression measures.

2.4 ADVANTAGES OF EMC DESIGN

The primary advantages of adequate EMC design are (1) minimizing the additional cost required by suppression elements or redesign in order to satisfy the regulatory requirements (minimizing product cost), (2) maintaining the development and product announcement schedule (minimizing development schedule delays), and (3) ensuring that the product will operate satisfactorily in the presence of the inevitable external noise sources at its installation location (minimizing customer complaints). The reader may not be sensitive to the importance of these issues before entering the workplace. However, the author can assure the reader that these issues are as important as the technical (functional) aspects of the design!

Perhaps the most important factor in ensuring that the product will satisfy the regulatory requirements at the end of the design and will maintain the development schedule is the *early and continuous application of the EMC design principles throughout the entire development cycle of the product.* The longer we proceed into the development of a product, the more aspects are "set in concrete" and cannot be changed without much additional cost and schedule delays. For example, at the early conceptual stages of the design, we can move cables, change locations of cable connectors on PCBs, reorient PCBs in the product, etc., since the design exists only "on paper." Once the design has proceeded to the development of prototypes, it becomes an increasingly difficult and costly matter to make physical changes, since many other aspects of the design must also be changed. For example, suppose someone notices that the clock oscillator on a PCB is located adjacent to a cable connector of that PCB. It should be abundantly clear to the reader, even without reading further in this text, that there exists a strong potential for the oscillator signal to radiate to the cable wires, proceed out the attached cable, and radiate very efficiently from that cable, resulting in serious radiated emission problems. Simply moving the connector away from the oscillator or the oscillator away from the connector may considerably reduce this problem. If this observation is made early in the design, it is *cost-free*! If the change is made later after the PCB has been laid out, it will be extremely costly and will probably result in significant delays in the development of the product, which also represent cost in terms of lost sales. *Early and consistent attention to EMC will minimize cost and schedule delays and will provide the best chance for complying with the regulatory requirements*!

An equally important reason for early and consistent attention to EMC is to make the implementation of any suppression measures that are necessary to comply with the regulatory requirements a much simpler matter. For example, suppose that during the design of a PCB, it is felt that suppression of some of the clock harmonics may be needed when the product is eventually tested for compliance. If the PCB designer will place holes or pads at the output of the clock on the PCB, a capacitor can be easily inserted, if needed, across the clock terminals, thus reducing the emissions of the clock. Also holes may be placed in series with one land of the clock output to provide for later insertion of a series resistor to additionally reduce the clock rise/falltimes and further reduce the high-frequency emissions of the clock signal. In the initial design, the capacitor holes can be left vacant and the series resistor holes can be "wired across" with a 0 Ω resistor. If problems with the clock emissions occur during testing, a capacitor can be inserted and/or a series resistor can be inserted and *only the PCB artwork and the product parts list need to be changed*! If this had not been done, the entire PCB would need to be relaid out, which would be extremely costly and result in significant schedule delays. This represents one of the most effective EMC design principles: *assume that some EMC suppression will be needed for compliance and provide the ability to implement it if it is needed*! It is doubtful that adherence to the EMC design principles of this text will result in a product that exhibits no EMC problems when it is tested. However, adherence to these design principles and maintaining the necessary EMC insight throughout the design will tend to make any necessary suppression easy to apply and at minimal expense. Waiting until that last minute to consider EMC will generally mean that complying with the necessary EMC requirements will be a difficult, time-consuming, and costly experience.

And finally, every electronic design team should include, as an integral partner, an experienced EMC engineer. This person should be consulted on the potential EMC impact of every aspect of the design *early and continuously* in the product design cycle. He/she should be consulted on every detail of the design, no matter how seemingly innocuous it is. For example, the design of the "package," i.e.

the product enclosure(s), is very critical to EMC. Once the product package shape is determined, it cannot usually be changed, yet the shape will determine where PCBs can be placed, where cables can exit the enclosure, where disk drive cables must be routed to the PCB, etc. All these aspects remove some of the EMC designer's "cost-free" fix options. Also, once the first prototype is available, no matter how crude, it should be tested for its EMC problems. Granted, the final product may exhibit less problems than the prototype, but this early test will show where there are significant trouble spots that must be attacked early.

Early and continuous attention to the affect on EMC will give the product the best possible change for minimum cost and schedule delay resulting from EMC. A failure to do this will almost certainly translate to added cost and schedule delay. Managers of products may not be attuned to the fine details of EMC design, but they do understand cost and schedule delay!

PROBLEMS

Section 2.1 Governmental Requirements

Section 2.1.1 Requirements for Commercial Products Marketed in the United States.

2.1.1 Would you consider a network server to be a Class A device or a Class B digital device with regard to the regulatory tests that it must comply with? [Class A; no one would purchase it for use in their home.]

2.1.2 Would you consider a $5000 U.S. high-speed, high-capacity laser printer a Class A or Class B digital device with regard to the regulatory tests it must comply with? [Class B; although this would generally be purchased for use in industry, the FCC might argue (rule) that the price is not high enough to prevent *someone* from purchasing it for use in their home. Hence, to prevent having to retest and recertify this if the FCC should require a recall, we should test it as a Class B product since those limits are more stringent than those for Class A devices.]

2.1.3 The conducted emission limits for Class B digital devices in Table 2.1 are given in voltage that is measured across a 50-Ω resistor, as we will see in Section 2.1.4.2. Determine those levels in μA and in dBμA [0.15 MHz, 39.9 μA (12.6 μA), 32 dBμA (22 dBμA); 0.5 MHz, 12.6 μA (4 μA), 22 dBμA (12 dBμA); 0.5–5 MHz, 12.6 μA (4 μA), 22 dBμA (12 dBμA); 5–30 MHz, 20 μA (6.3 μA), 26 dBμA (16 dBμA)]

2.1.4 The conducted emission limits for Class A digital devices in Table 2.2 are given in voltage measured across a 50-Ω resistor, as we will see in Section 2.1.4.2. Determine those levels in μA and in dBμA. [0.15–0.5 MHz, 178.25 μA (39.9 μA), 45 dBμA (32 dBμA); 0.5–30 MHz, 89 μA (20 μA), 39 dBμA (26 dBμA)]

2.1.5 The FCC radiated emission limits for Class B digital devices in Table 2.4 are to be measured at a distance of 3 m. Some have advocated measuring these at a distance of 5 m. Determine those levels at 5 m in μV/m and in dBμV/m. [30–88 MHz, 60 μV/m, 35.56 dBμV/m; 88–216 MHz, 90 μV/m, 39 dBμV/m; 216–960 MHz, 120 μV/m, 41.56 dBμV/m; >960 MHz, 300 μV/m, 49.56 dBμV/m]

2.1.6 The FCC radiated emission limits for Class A digital devices in Table 2.5 are to be measured at a distance of 10 m. Some have advocated measuring these at a distance of 5 m. Determine those levels at 5 m in μV/m and in dBμV/m. [30–88 MHz, 178 μV/m, 45 dBμV/m; 88–216 MHz, 300 μV/m, 49.5 dBμV/m; 216–960 MHz, 400 μV/m, 52 dBμV/m; >960 MHz, 597 μV/m, 55.5 dBμV/m]

2.1.7 A product is tested for FCC Class B radiated emission compliance as shown in Fig. P2.1.7. The distance between the measurement antenna and the product is 20 ft. The spectrum analyzer is connected to the measurement antenna with 30 ft of RG58U coaxial cable that has a loss of 4.5 dB/100 ft at 100 MHz. The receiving antenna provides an output voltage at 100 MHz of 6.31 V for each V/m of incident electric field. If the spectrum analyzer indicates a level of 53 dBμV at 100 MHz, determine the level of received electric field at the antenna. [38.35 dBμV/m] Determine whether the product will pass or fail the FCC Class B test, and by how much. [No, fails by 1.01 dB]

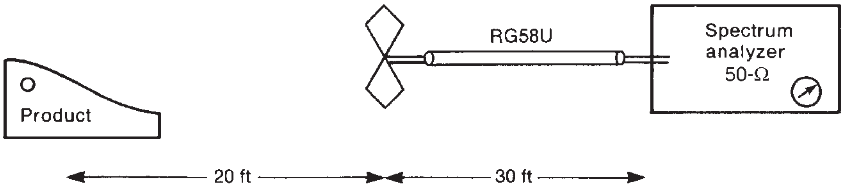

FIGURE P2.1.7

2.1.8 The radiated emissions from a product are measured at 50 MHz at 15 m away and are found to be 21 μV/m. Does the product comply with the FCC Class B limit? [No] By how much does the product pass or fail? [0.424 dB]

2.1.9 The voltage induced at the terminals of an antenna V_{ant} is 5 V for every V/m of incident field E_{ant}. What level in dBμV at the base of the antenna would correspond to the FCC Class B limit at 100 MHz? [57.48 dBμV] Determine the reading of the spectrum analyzer if it is connected to the antenna with 200 ft of RG58U coaxial cable that has 4.5 dB/100 ft of loss at 100 MHz. [48.48 dBμV]

2.1.10 A product emits a radiated electric field level of 36 dBμV/m at 100 MHz when measured at a distance of 30 ft from the product. Determine the emission level when measured at the FCC Class B distance of 3 m. [45.68 dBμV/m]

Section 2.1.2 Requirements for Commercial Products Marketed outside the United States.

2.1.11 An antenna measures the radiated emissions at 220 MHz from a product as shown in Fig. P2.1.11. If the receiver measures a level of −93.5 dBm at 220 MHz, determine the voltage at the base of the antenna in dBμV. The cable loss at 220 MHz is 8 dB/100 ft. [29.5 dBμV] If the product providing these emissions is located at a distance of 20 m and the antenna provides 1.5 V for every V/m of incident electric field at 220 MHz, determine whether the emissions comply with the CISPR 32 Class B and FCC Class B limits and by how much. [Fails CISPR 32 by 2 dB but passes FCC Class B by 3.54 dB]

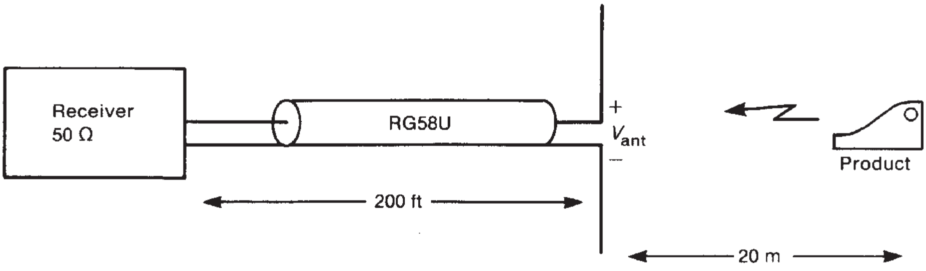

FIGURE P2.1.11

2.1.12 A digital product is being tested for compliance to CISPR 32 Class A requirements. The receiving antenna is placed at a distance of 30 m away and is attached to a 50 Ω receiver with a 100 ft length of 50 Ω cable that has a loss of 10 dB/100 ft at 300 MHz as shown in Fig. P2.1.12. If the receiver indicates a level of −64.5 dBm at 300 MHz, and the antenna provides 4 V at its base for every 1 V/m of electric field incident on it determine whether the product passes or fails and by how much. [Fails by 3 dB]

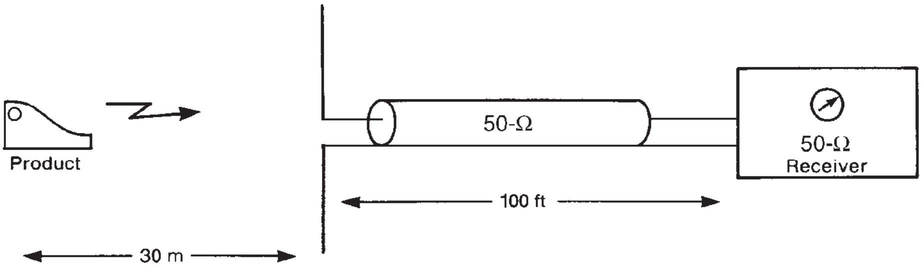

FIGURE P2.1.12

2.1.13 Determine the CISPR 32 Class A conducted emission limit (QP) at 30 MHz when measured with a 50 Ω LISN in dBμA and in μA. [39 dBμA, 89.34 μA]

Section 2.1.3 Requirements for Military Products to Be Marketed in the United States.

2.1.14 The MIL-STD-461G CE102 limits are given in Fig. 2.5. Determine how more stringent these are than the FCC/CISPR 32, Class A QP limits at 150 and 500 kHz for 115-V equipment. [3 dB, 13 dB]

2.1.15 Compare the MIL-STD-461G RE102 radiated emission limits for U.S. Air Force ground applications at 30 MHz and 1 GHz to the FCC Class A radiated emission limits. Is this a valid comparison? [The MIL-STD-461G limits are 15 and 5.5 dB more restrictive. The FCC levels are to be measured with a quasi-peak detector in the receiver, whereas the MIL-STD-461E levels are to be measured with a peak detector in the receiver. Hence, these can't really be compared.]

Section 2.1.4 Measurement of Emissions for Verification of Compliance.

2.1.16 The commercial product radiated emissions are measured in a semianechoic chamber as illustrated in Fig. 2.7. The product is placed 1 m above the floor of the chamber, and the measurement antenna is placed at a distance of 3 or 10 m away. The antenna is to be scanned from 1 to 4 m above the floor and the maximum emission recorded. The ground plane that constitutes the floor of the chamber will give two paths from the product to the measurement antenna. One path is the direct one from the product to the antenna, and the other is reflected at the ground plane. Use the method of images (see Section 7.6.1 of Chapter 7) and compare the two path lengths in wavelengths at 300 MHz for antenna heights of 1 and 4 m and the FCC Class B separation distance [3 λ, $\sqrt{13}\,\lambda$], and [$\sqrt{18}\,\lambda$, $\sqrt{34}\,\lambda$]

2.1.17 Determine the distance farther away that the PCB in Fig. 2.14 must be moved to ensure that its emissions (shown in Fig. 2.15) pass the FCC Class B limits. [126.5 m!]

REFERENCES

1. *Code of Federal Regulations* (2022). Title 47 (47CFR), Part 15, Subpart B: Unintentional Radiators, 2022. These can be accessed from the World Wide Web at the following sites: https://www.ecfr.gov/cgi-bin/ECFR?page=browse, https://www.govinfo.gov/app/collection/cfr.
2. European EMC Directive 2014/30/EU (2014). The European Parliament and of the Council of February 26, 2014, revised by the Regulation (Eu) 2018/1139 Of The European Parliament and of the Council of July 4, 2018. https://eur-lex.europa.eu/legal-content/EN/TXT/?uri=CELEX:32014L0030.
3. International Special Committee on Radio Interference (2019), CISPR 32, Electromagnetic Compatibility of Multimedia Equipment – Emission Requirements, Consolidated Version, edition 2.1, 2019–2010. https://webstore.iec.ch/publication/65836.
4. MIL-STD-461G (2015). Requirements for the Control of Electromagnetic Interference Characteristics of Subsystems and Equipment, December 11, 2015. http://everyspec.com/MIL-STD/MIL-STD-0300-0499/MIL-STD-461G_53571.
5. ANSI C63.4-2014 (2014). Methods of Measurement of Radio-Noise Emissions from Low-Voltage Electrical and Electronic Equipment in the Range of 9 kHz to 40 GHz. www.ansi.org.
6. J. R. Nicholson and J. A. Malack, RF impedance of power lines and line impedance stabilization networks in conducted interference measurements, *IEEE Trans. Electromagn. Compat.* EMC-15, 84–86 (1973).
7. R. J. Calcavecchio and D. J. Pratt (1986). A standard test to determine the susceptibility of a machine to electrostatic discharge. *1986 IEEE International Symposium Electromagnetic Compatibility*, San Diego, CA, September 1986.
8. Radio Technical Commission for Aeronautics, RTCA DO-160G (2010). *Environmental Conditions and Test Procedures for Airborne Equipment*. http://www.rtca.org.
9. CISPR 12 (2021). Vehicles, Boats, and Internal Combustion Engines—Radio Disturbance Characteristics—Limits and Methods of Measurements for the Protection of Off-Board Receivers; CISPR 25, Vehicles, Boats, and Internal Combustion Engines—Radio Disturbance Characteristics—Limits and Methods of Measurement for the Protection of On-Board Receivers. www.iec.ch.
10. Society of Automotive Engineers (2012). *SAE J551, and SAE J1113*. http://www.sae.org.

CHAPTER THREE

Signal Spectra—the Relationship between the Time Domain and the Frequency Domain

The frequency content or *spectrum* of the signals present in an electronic system is perhaps the most important aspect of the ability of that system to not only satisfy any regulatory limits but also perform compatibly with other electronic systems. In this chapter, we will investigate this important aspect of EMC. We will begin the discussion with a general overview of the spectral composition of periodic signals. Once these important concepts are firmly understood, we will specialize these notions to signals that are representative of typical digital products. Bounds will be developed for those spectra that will facilitate the analysis of the effects of the signals. The use of a spectrum analyzer to measure the signal's spectral content will also be discussed, since the ability to use this important instrument correctly is critical to the correct evaluation of the product's compliance (or noncompliance) with governmental regulatory requirements. Finally, we will extend these notions to nonperiodic signals and then to random signals that represent data signals.

3.1 PERIODIC SIGNALS

Time-domain signals or waveforms that occur repetitively in time are referred to as being *periodic*. The more important signals that contribute directly to the radiated and conducted emissions of digital electronic systems are periodic signals. These types of waveforms are representative of clock and data signals that are necessary for the proper function of the system. Data streams in digital products are examples of random signals. The waveform takes on one of two levels during periodic intervals of the clock signal. However, the value in each interval (0 or 1) is a random variable. Signals whose time behavior is precisely known are referred to as *deterministic* signals. Signals whose time behavior is not known but can only be described statistically are referred to as *nondeterministic* or *random* signals. We will examine the frequency-domain description of periodic, deterministic waveforms in this section with the intent of representing clock waveforms of digital products. To some degree, this gives insight into the spectral composition of data signals. However,

---

Introduction to Electromagnetic Compatibility, Third Edition. Clayton R. Paul, Robert C. Scully, and Mark A. Steffka.
© 2023 John Wiley & Sons, Inc. Published 2023 by John Wiley & Sons, Inc.

data signals are nondeterministic; otherwise no information would be conveyed. The spectra of these types of signals will be determined in Section 3.5.

A *periodic* function of time t represented by $x(t)$ is a function (waveform or signal) that has the property [1, 2]

$$x(t \pm kT) = x(t), \quad k = 1, 2, 3, \ldots \tag{3.1}$$

that is, the function repeats itself over intervals of length T, where T is referred to as the *period* of the waveform. An example of a periodic signal is shown in Fig. 3.1. The reciprocal of the period is referred to as the *fundamental frequency* of the waveform, with units of Hertz:

$$f_0 = \frac{1}{T} \tag{3.2a}$$

It can be expressed in radians per second as

$$\omega_0 = 2\pi f_0 = \frac{2\pi}{T} \tag{3.2b}$$

The *average power* in a periodic waveform is defined by

$$P_{av} = \frac{1}{T}\int_{t_1}^{t_1+T} x^2(t)\, dt \tag{3.3}$$

where t_1 is some arbitrary time; that is, we only need to integrate over a time interval of length equal to the period of the signal. The *energy* in a signal is defined by

$$E = \int_{-\infty}^{\infty} x^2(t)\, dt \tag{3.4}$$

Note that a periodic signal has infinite energy, since it must repeat indefinitely, yet the average power is finite. Hence, periodic signals are referred to as *power signals*. Signals that are not periodic are referred to as *nonperiodic*. An example is shown in Fig. 3.2. Nonperiodic signals have zero average power but finite energy. Hence, they are referred to as *energy signals*.

Periodic signals can be represented as *linear combinations* of more basic signals that are referred to as *basis functions* and denoted as $\phi_n(t)$:

$$\begin{aligned} x(t) &= \sum_{n=0}^{\infty} c_n \phi_n(t) \\ &= c_0\phi_0(t) + c_1\phi_1(t) + c_2\phi_2(t) + \cdots \end{aligned} \tag{3.5}$$

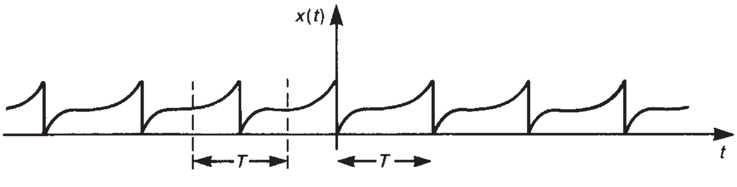

FIGURE 3.1 A periodic signal with period T.

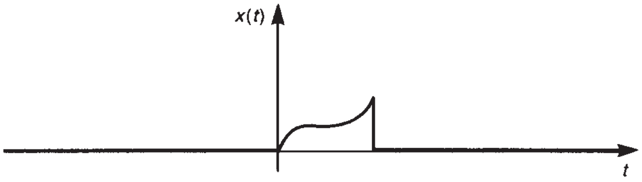

FIGURE 3.2 A nonperiodic signal.

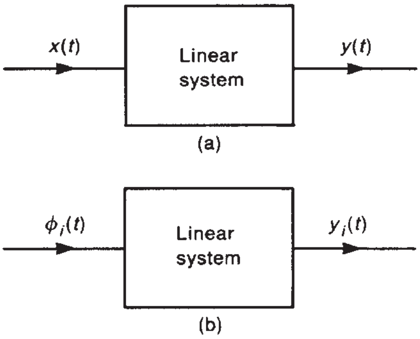

FIGURE 3.3 Processing of a signal by a linear system: (a) input $x(t)$ produces output $y(t)$; (b) a basis function in the expansion of $x(t)$, specifically, $\phi(t)$, produces the corresponding component of the output, $y(t)$.

The basis functions are also periodic, with the same period as $x(t)$. The coefficients c_n are referred to as the *expansion coefficients*. The advantage of such a representation is illustrated in Fig. 3.3. Consider a *linear system* having an input $x(t)$ and an output $y(t)$. This is referred to as a *single-input, single-output system*. The system is *linear* if it possesses the following two properties:

1. If $x_1(t)$ produces $y_1(t)$ and $x_2(t)$ produces $y_2(t)$, then $x_1(t)+x_2(t)$ produces $y_1(t)+y_2(t)$.
2. If $x(t)$ produces $y(t)$, then $kx(t)$ produces $ky(t)$.

These two properties are often collectively referred to as the property of *superposition*. Thus, if we know the response of a linear system to each of the basis functions,

$$\phi_n(t) \to y_n(t) \tag{3.6a}$$

then the response to $x(t)$, which is decomposed into basis functions as in (3.5), is

$$\begin{aligned} y(t) &= \sum_{n=0}^{\infty} c_n y_n(t) \\ &= c_0 y_0(t) + c_1 y_1(t) + c_2 y_2(t) + \cdots \end{aligned} \tag{3.6b}$$

That is, *the response to the original input signal can be found, by superposition, as the sum of the weighted responses to the individual components or basis functions that are used to represent the original input signal.* Quite often it is easier to determine the responses to the simpler basis functions than to the original signal. This then simplifies the determination of the response of the system to the more general input. This not only simplifies the calculation of the response to the original signal, $y(t)$, but also yields considerable insight into how the linear system processes more general inputs. Note that the utility of this result relies on the system being *linear*, since we have used the property of superposition. Although there are a number of choices for the basis set that we could use to expand a general periodic signal, we will concentrate on the sinusoidal basis functions. The sinusoidal basis functions lead to the Fourier series representation that we will discuss next.

3.1.1 The Fourier Series Representation of Periodic Signals

Any periodic function can be represented as in (3.5) as an infinite sum of sinusoidal components. Each sinusoidal component has a frequency that is a multiple of the *fundamental frequency*, $f_0 = 1/T$ and the radian fundamental frequency is $\omega_0 = 2\pi f_0 = 2\pi/T$. There are two versions of the Fourier series. The *trigonometric* form has basis functions $\phi_0 = 1$, and $\phi_n = \cos(n\omega_0 t), \sin(n\omega_0 t)$ for $n = 1, 2, 3, \ldots, \infty$ [1]. The multiples of the fundamental frequency, nf_0, are called *harmonics* of that fundamental frequency.

The *complex-exponential* form is more useful and more easily computed than the trigonometric form and will be what we will use. The complex-exponential form uses as basis functions the complex exponential[1]

$$\begin{aligned}\varphi_n(t) &= e^{j\omega_0 t} \\ &= \cos(n\omega_0 t) + j\sin(n\omega_0 t) \quad \text{for} -\infty, \ldots, -1, 0, 1, \ldots, \infty \end{aligned} \tag{3.7}$$

and we have used Euler's identity

$$e^{j\theta} = \cos(\theta) + j\sin(\theta) \tag{3.8}$$

and $j = \sqrt{-1}$. Hence, the periodic function is decomposed as

$$\begin{aligned} x(t) &= \sum_{-\infty}^{\infty} c_n e^{jn\omega_0 t} \\ &= \cdots + c_{-1}e^{-j\omega_0 t} + c_0 + c_1 e^{j\omega_0 t} + \cdots \end{aligned} \tag{3.9}$$

Note that the summation extends from $-\infty$ to $+\infty$. Each expansion coefficient, c_n, will be, in general, a complex number having a magnitude and an angle. In order to determine the expansion coefficients for a particular $x(t)$, multiply both sides of (3.9) by $\varphi_m^* = e^{-jm\omega_0 t}$ where * denotes the complex conjugate of a complex number (replace j with $-j$ in order to create the conjugate of a complex number) and then integrate over a period:

$$\begin{aligned} \int_{t_1}^{t_1+T} e^{-jm\omega_0 t} x(t)\ dt &= \sum_{-\infty}^{\infty} c_n \int_{t_1}^{t_1+T} e^{-jm\omega_0 t} e^{jn\omega_0 t}\ dt \\ &= c_m T \end{aligned} \tag{3.10}$$

---

[1] Throughout this text, we will denote items that have complex values with a caret $\hat{()}$ over that item. In the complex-exponential form, the expansion coefficients and the basis functions are complex-valued and hence should be denoted as $\hat{c}_n$ and $\hat{\phi}_n$. However, in order to simplify the notation in this chapter, we will omit the carets on these items and denote them simply as c_n and ϕ_n.

This result is due to the fact that, using Euler's identity, the integrand of the right-hand side is

$$\begin{aligned} e^{-jm\omega_0 t} e^{jn\omega_0 t} &= e^{j(n-m)\omega_0 t} \\ &= \cos((n-m)\omega_0 t) + j\sin((n-m)\omega_0 t) \end{aligned} \tag{3.11}$$

which, when integrated over a period T, is zero except for $n = m$, where (3.11) is 1. Hence, the expansion coefficients are given by

$$c_n = \frac{1}{T}\int_{t_1}^{t_1+T} x(t)e^{-jn\omega_0 t}dt \tag{3.12}$$

Note that for $n = 0$,

$$\begin{aligned} c_0 &= \frac{1}{T}\int_{t_1}^{t_1+T} x(t)dt \\ &= \frac{\text{area under curve over one period}}{T} \\ &= \text{average value of } x(t) \end{aligned} \tag{3.13}$$

which is a real number.

Note that the complex-exponential form of the Fourier series contains, in addition to positive-valued harmonic frequencies $\omega_0, 2\omega_0, 3\omega_0, \dots$, negative-valued harmonics $-\omega_0, -2\omega_0, -3\omega_0, \dots$. In addition, the expansion coefficients c_n may be complex-valued, whereas the expansion coefficients in the trigonometric Fourier series are real-valued. At first glance, it may seem that the physical intuition present in the trigonometric Fourier series has been lost in the complex-exponential form. This is not the case. We should realize that for each positive value of n (and harmonic frequency) there is a corresponding negative value of n (and harmonic frequency). The coefficients of these, c_n and c_{-n}, are the conjugates of each other:

$$\begin{aligned} c_{-n} &= \frac{1}{T}\int_{t_1}^{t_1+T} x(t)\, e^{jn\omega_0 t}\, dt \\ &= c_n^* \end{aligned} \tag{3.14}$$

Since c_n may be complex-valued, let us denote it by

$$\begin{aligned} c_n &= |c_n|\underline{/c_n} \\ &= |c_n|e^{j\underline{/c_n}} \end{aligned} \tag{3.15}$$

Thus,

$$c_n^* = |c_n|e^{-j\underline{/c_n}} \tag{3.16}$$

The complex-exponential form in (3.9) may be written as

$$x(t) = c_0 + \sum_{n=1}^{\infty} c_n e^{jn\omega_0 t} + \sum_{n=-1}^{-\infty} c_n e^{jn\omega_0 t} \tag{3.17}$$

Changing the second summation to positive n and using (3.14) gives

$$x(t) = c_0 + \sum_{n=1}^{\infty} c_n e^{jn\omega_0 t} + \sum_{n=1}^{\infty} c_n^* e^{-jn\omega_0 t} \tag{3.18}$$

Substituting (3.15) and (3.16) gives

$$\begin{aligned} x(t) &= c_0 + \sum_{n=1}^{\infty} |c_n| e^{j(n\omega_0 t + \angle c_n)} + \sum_{n=1}^{\infty} |c_n| e^{-j(n\omega_0 t + \angle c_n)} \\ &= c_0 + \sum_{n=1}^{\infty} |c_n| (e^{j(n\omega_0 t + \angle c_n)} + e^{-j(n\omega_0 t + \angle c_n)}) \\ &= c_0 + \sum_{n=1}^{\infty} 2|c_n| \cos(n\omega_0 t + \angle c_n) \end{aligned} \tag{3.19a}$$

In this last relation, we have used Euler's identity in (3.8) to give two important results:

$$\cos(\theta) = \frac{e^{j\theta} + e^{-j\theta}}{2} \tag{3.20a}$$

$$\sin(\theta) = \frac{e^{j\theta} - e^{-j\theta}}{2j} \tag{3.20b}$$

Therefore, *in order to obtain the expansion coefficients for the one-sided spectrum* (*positive frequencies only*), *we double the magnitudes for the double-sided spectrum*, $c_n^+ = 2 \mid c_n \mid$, *and the dc component* c_0 *remains unchanged*. The expansion in (3.19a) is in terms of cosines. Using the identity $\cos(\theta) = \sin(\theta + 90°)$, we can alternatively write it in terms of sines:

$$x(t) = c_0 + \sum_{n=1}^{\infty} 2|c_n| \sin(n\omega_0 t + \angle c_n + 90°) \tag{3.19b}$$

The complex-exponential expansion coefficients are usually more easily computed than are the coefficients in the trigonometric form. For example, consider the square wave of Fig. 3.4. We obtain, using (3.12),

$$\begin{aligned} c_n &= \frac{1}{T} \int_{t_1}^{t_1+T} e^{-jn\omega_0 t} x(t) dt \\ &= \frac{1}{T} \int_{0}^{\tau} e^{-jn\omega_0 t} A dt + \frac{1}{T} \int_{\tau}^{T} e^{-jn\omega_0 t} dt \\ &= \frac{\mathrm{A}}{jn\omega_0 T} (1 - jn\omega_0 \tau) \end{aligned} \tag{3.21}$$

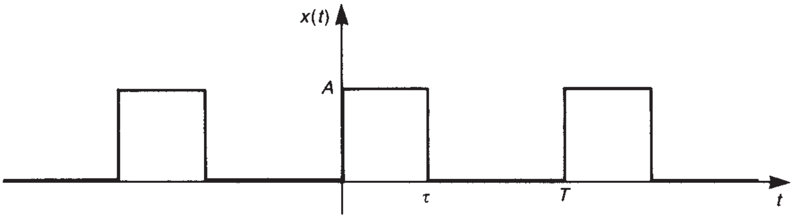

FIGURE 3.4 A periodic "square wave" pulse train.

In calculations of this type, it is often desirable to put the result into a sine or cosine form of function. To do this, we extract $e^{-jn\omega_0\tau}$ from the term in parentheses and use (3.20b) to give

$$\begin{aligned}c_n &= \frac{\mathrm{A}}{jn\omega_0 T} e^{-jn\omega_0\tau/2} \left(e^{jn\omega_0\tau/2} - e^{-jn\omega_0\tau/2}\right)\\ &= \frac{\mathrm{A}}{jn\omega_0 T} e^{-jn\omega_0\tau/2}\, 2j\sin(n\omega_0\tau/2)\\ &= \frac{A\tau}{T} e^{-jn\omega_0\tau/2} \frac{\sin(n\omega_0\tau/2)}{(n\omega_0\tau/2)}\end{aligned}$$

From this result, we see that

$$c_n = \frac{A\tau}{T}\left|\frac{\sin(n\omega_0\tau/2)}{(n\omega_0\tau/2)}\right| \tag{3.23a}$$

$$\angle c_n = \pm\left(\frac{n\omega_0\tau}{2}\right) \tag{3.23b}$$

The ± sign of the angle comes about because the $\sin\left(\frac{1}{2}n\omega_0\tau\right)$ term may be positive or negative (an angle of 180°). This is added to the angle of $e^{-jn\omega_0\tau/2}$. Substituting $\omega_0 = 2\pi/T$ gives

$$|c_n| = \frac{A\tau}{T}\left|\frac{\sin(n\pi\tau/T)}{(n\pi\tau/T)}\right| \tag{3.23a}$$

$$\angle c_n = \pm\left(\frac{n\pi\tau}{T}\right) \tag{3.23b}$$

The amplitude spectrum is given in Fig. 3.5b and the phase spectrum in Fig. 3.5c. The horizontal axes are in terms of cyclic frequency f. The amplitudes of the spectral components lie on an envelope that is

$$\frac{A\tau}{T}\left|\frac{\sin(\pi f\tau)}{(\pi f\tau)}\right|$$

where we have substituted $n/T = f$ to get a continuous envelope. This goes to zero where $\pi f\tau = m\pi$ or at multiples of $1/\tau$. This is a useful and commonly occurring function, usually denoted by

$$\frac{\sin x}{x}$$

At $x = 0$, the function evaluates to unity and is zero when $x = m\pi$ for $m = 1, 2, 3, \ldots$. Although the continuous envelope bounds the spectral amplitudes, the spectral components exist only at

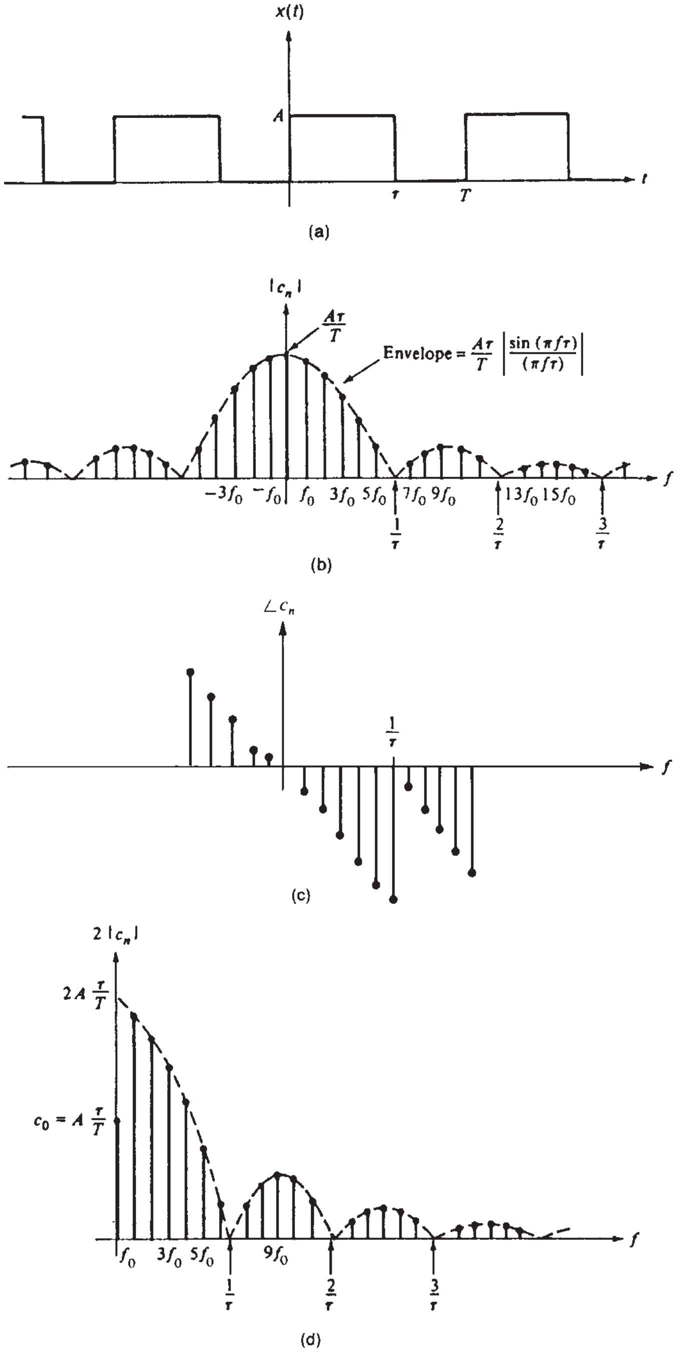

FIGURE 3.5 Frequency-domain representation of a square wave; (a) the signal; (b) the two-sided magnitude spectrum; (c) the phase spectrum; and (d) the one-sided magnitude spectrum.

multiples (harmonics) of the fundamental frequency f = 1/T. The phase is similarly plotted in Fig. 3.5c. The magnitude and phase spectra given in Fig. 3.5b and c are said to be *two-sided spectra*, since both positive and negative frequency components are shown. The *one-sided spectrum* for positive frequencies only is obtained using the result in (3.19) and is shown in Fig. 3.5d. Usually, the one-sided spectra are preferred. Note that all positive frequency components *except the dc component* in the two-sided magnitude spectrum are *doubled* to give the one-sided magnitude spectrum. The one-sided phase spectrum is simply the two-sided phase spectrum for positive frequencies. Suppose that we consider the square wave having a *duty cycle*

$$D = \frac{\tau}{T} \tag{3.25}$$

of 1/2 (or 50%). The expansion coefficients become

$$\begin{aligned}
|c_n| &= \frac{A\tau}{T}\left|\frac{\sin(n\pi\tau/T)}{(n\pi\tau/T)}\right| \quad \frac{\tau}{T} = \frac{1}{2}\\
&= \frac{A}{n\pi} \quad n = 1, 3, 5, \ldots\\
&= 0 \quad 2, 4, 6, \ldots
\end{aligned} \tag{3.26a}$$

$$\begin{aligned}
\angle c_n &= \angle \frac{-n\omega_0\tau}{2} + \sin\left(\frac{n\omega_0\tau}{2}\right)\\
&= \angle \frac{-n\pi}{2} + \sin\left(\frac{n\pi}{2}\right)\\
&= -90^\circ \quad n = 1, 3, 5, \ldots
\end{aligned} \tag{3.26b}$$

And $c_0 = A/2$.

Hence, the complex-exponential Fourier series for a square wave with a 50% duty cycle is

$$\begin{aligned}
x(t) &= \frac{A}{2} + \frac{2A}{\pi}\cos(\omega_0 t - 90^\circ) + \frac{2A}{3\pi}\cos(3\omega_0 t - 90^\circ) + \cdots\\
x(t) &= \frac{A}{2} + \frac{2A}{\pi}\sin(\omega_0 t) + \frac{2A}{3\pi}\sin(3\omega_0 t) + \cdots
\end{aligned} \tag{3.27}$$

Note that (1) we have doubled (3.24a) to give the one-sided spectrum according to (3.19), (2) we have used the trigonometric identity $\cos(\theta) = \sin(\theta + 90^\circ)$, and (3) the even harmonics, n = 2, 4, 6, …, are zero. In order to illustrate how the various components in (3.27) contribute to the overall makeup of the signal, we have shown the summation of the first seven components of a square wave of Fig. 3.4 using (3.27) having $A = 1$, $T = 1$ *s*, and $\tau = 0.5$ *s* in Fig. 3.6. Adding more terms causes a convergence of the total to the time-domain signal.

Example 3.1 Determine the Fourier series (one-sided) for the waveform in Fig. 3.7. Evaluate your result for $A = 2$, $\tau = 2$ *s*, and $T = 4$ *s*.

Solution: The dc (average value) is

$$\begin{aligned}
c_0 &= \frac{1}{T}\left\{\frac{A\tau}{2} + A(T - \tau)\right\}\\
&= A\left[1 - \frac{\tau}{2T}\right]
\end{aligned}$$

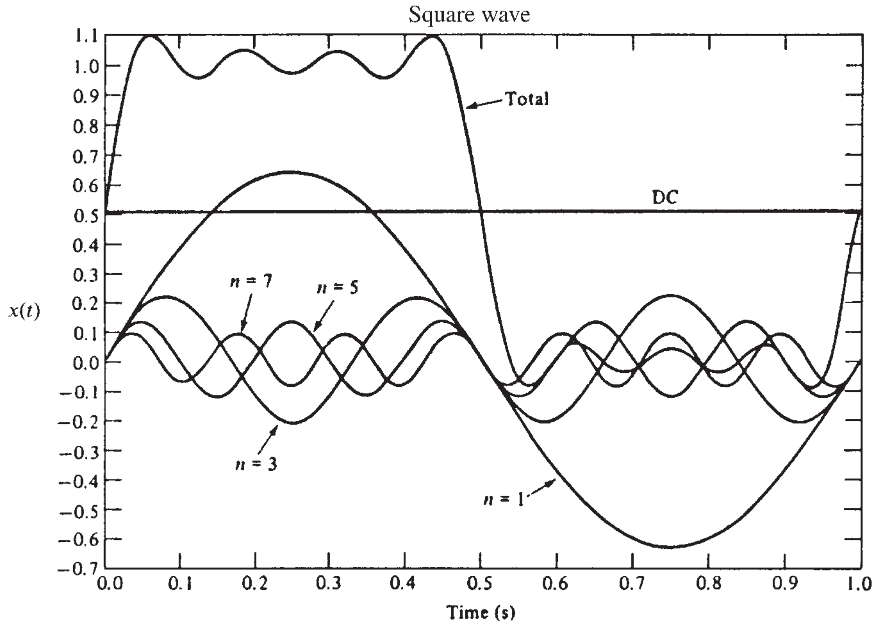

FIGURE 3.6 Illustration of the decomposition of a square wave into its frequency components.

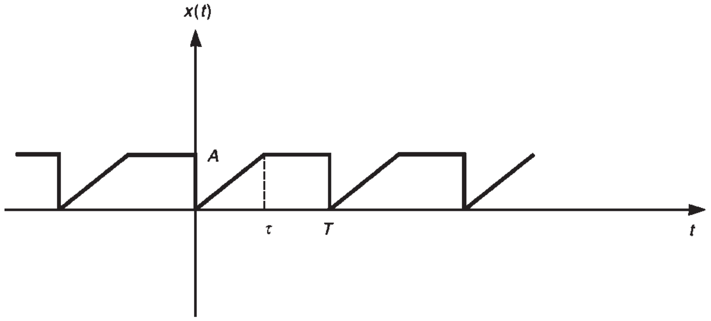

FIGURE 3.7 Example 3.1.

The other coefficients are

$$\begin{aligned} c_n &= \frac{1}{T}\left\{\int_0^{\tau} \frac{At}{\tau} e^{-jn\omega_0 t} dt + \frac{1}{T}\int_{\tau}^{T} Ae^{-jn\omega_0 t} dt\right\} \\ &= \mathrm{j}\frac{\mathrm{A}}{n\omega_0 T}\left[e^{-jn\omega_0 T} - e^{-jn\omega_0 t/2}\left(\frac{\sin(n\omega_0 t/2)}{n\omega_0 t/2}\right)\right] \\ &= \mathrm{j}\frac{\mathrm{A}}{2\pi n}\left[1 - e^{-jn\pi(\tau/T)}\left(\frac{\sin(n\pi\tau/T)}{n\pi\tau/T}\right)\right] \end{aligned}$$

since $e^{-jn\omega_0 T} = e^{-j2\pi n} = 1$.

Evaluating these for $A = 2$, $\tau = 2\ s$, and $T = 4\ s$ gives

$$\begin{aligned} c_0 &= \frac{3}{2} \\ c_n &= -\frac{2}{(n\pi)^2} + j\frac{1}{n\pi} \qquad n = 1, 3, 5, 7, \ldots \\ &= j\frac{1}{n\pi} \qquad n = 2, 4, 6, \ldots \end{aligned}$$

The first seven harmonics become

$$\begin{aligned} c_1 &= 0.3773\underline{/122.48^\circ} \\ c_2 &= 0.1595\underline{/90^\circ} \\ c_3 &= 0.1085\underline{/101.98^\circ} \\ c_4 &= 0.0796\underline{/90^\circ} \\ c_5 &= 0.0642\underline{/97.26^\circ} \\ c_6 &= 0.0532\underline{/90^\circ} \\ c_7 &= 0.0457\underline{/95.2^\circ} \end{aligned}$$

The one-sided spectrum expansion coefficients are obtained by doubling these magnitudes to give

$$\begin{aligned} c_1^+ &= 2c_1 = 0.7547\underline{/122.48^\circ} \\ c_2^+ &= 2c_2 = 0.3183\underline{/90^\circ} \\ c_3^+ &= 2c_3 = 0.2169\underline{/101.98^\circ} \\ c_4^+ &= 2c_4 = 0.1592\underline{/90^\circ} \\ c_5^+ &= 2c_5 = 0.1284\underline{/97.26^\circ} \\ c_6^+ &= 2c_6 = 0.1061\underline{/90^\circ} \\ c_7^+ &= 2c_7 = 0.0913\underline{/95.2^\circ} \end{aligned}$$

Therefore, the one-sided cosine expansion in (3.19a) becomes

$$\begin{aligned} x(t) = 1.5 &+ 0.7547\cos\left(\frac{\pi t}{2} + 122.48^\circ\right) + 0.3183\cos(\pi t + 90^\circ) \\ &+ 0.7547\cos\left(\frac{3\pi t}{2} + 101.98^\circ\right) + 0.7547\cos(2\pi t + 90^\circ) \\ &+ 0.7547\cos\left(\frac{5\pi t}{2} + 97.26^\circ\right) + 0.7547\cos(3\pi t + 90^\circ) \\ &+ 0.7547\cos\left(\frac{7\pi t}{2} + 95.2^\circ\right) + \ldots \end{aligned}$$

The alternative one-sided sine expansion in (3.19b) is obtained by adding 90° to the angles to give

$$\begin{aligned} x(t) = 1.5 &+ 0.7547\sin\left(\frac{\pi t}{2} - 147.52^\circ\right) + 0.3183\sin(\pi t - 180^\circ) \\ &+ 0.7547\sin\left(\frac{3\pi t}{2} - 168.0^\circ\right) + 0.7547\sin(2\pi t - 180^\circ) \\ &+ 0.7547\sin\left(\frac{5\pi t}{2} - 172.74^\circ\right) + 0.7547\sin(3\pi t - 180^\circ) \\ &+ 0.7547\sin\left(\frac{7\pi t}{2} - 174.80^\circ\right) + \ldots \end{aligned}$$

3.1.2 Response of Linear Systems to Periodic Input Signals

Consider the single-input, single-output linear system in Fig. 3.3a. Suppose that the input is a sinusoidal signal:

$$x(t) = X\cos(\omega t + \phi_x) \tag{3.28a}$$

In steady state, the output will also be a sinusoid at the same frequency as the input:

$$y(t) = Y\cos(\omega t + \phi_y) \tag{3.28a}$$

Replacing the time-domain forms with their *phasor* equivalents allows a simple determination of this response [1]. The unit impulse response, denoted by $h(t)$, is the response for the system with a unit impulse function as the input, $x(t) = \delta(t)$, for zero initial conditions [1]. The phasor impulse response is denoted as $|H(j\omega)|\underline{/H(j\omega)}$ and can be easily derived as the *transfer function* of the system [1].[2] In this case, the phasor output becomes

$$Y\underline{/\theta_y} = H(j\omega)X\underline{/\phi_x} \tag{3.29a}$$

Thus, the magnitude of the output becomes

$$Y = |H(j\omega)|X \tag{3.29b}$$

and the phase of the output is

$$\theta_y = \underline{/H(j\omega)} + \phi_x \tag{3.29c}$$

Now, suppose that x(t) is periodic, and its Fourier series has been obtained in the form

$$x(t) = c_0 + \sum_{n=1}^{\infty} 2|c_n|\cos(n\omega_0 t + \underline{/c_n}) \tag{3.30}$$

---

[2] Again, to simplify notation in this chapter, we will omit placing a caret over H(jω) even though it is a complex-valued function.

We may pass each of these components through the system, determine the *sinusoidal steady-state response* to each, $Y(jn\omega_0)$, and add those responses to give the complete sinusoidal steady-state response to $x(t)$.

The magnitude of the response to each component is

$$Y = 2|c_n||H(jn\omega_0)| \tag{3.31a}$$

and the phase of each component response is

$$\underline{/\theta_y} = \underline{/c_n} + \underline{/H(jn\omega_0)} \tag{3.31b}$$

So the time-domain output y(t) becomes

$$y(t) = c_0 H(0) + \sum_{n=1}^{\infty} \left\{ \begin{array}{c} 2|c_n||H(jn\omega_0)| \times \\ \cos[n\omega_0 t + \underline{/c_n} + \underline{/H(jn\omega_0)}] \end{array} \right\} \tag{3.32}$$

as illustrated in Fig. 3.8.

Example 3.2 Consider the application of a 1 V square wave to a lowpass filter as shown in Fig. 3.9a. The output is the voltage across the capacitor $v(t)$. Determine the output waveform by summing the components of the Fourier series.

Solution: The phasor transfer function is computed, using voltage division, as

$$\begin{aligned} H(j\omega) &= \frac{V(j\omega)}{V_s(j\omega)} = \frac{1/j\omega C}{R + (1/j\omega C)} \\ &= \frac{1}{1 + j\omega RC} \end{aligned}$$

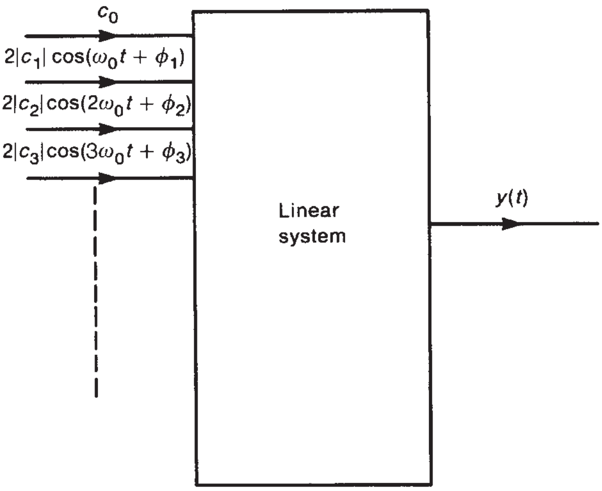
c_0
$2|c_1| \cos(\omega_0 t + \phi_1)$
$2|c_2| \cos(2\omega_0 t + \phi_2)$
$2|c_3| \cos(3\omega_0 t + \phi_3)$
Linear system
$y(t)$

FIGURE 3.8 Illustration of the complete response to a general time-domain signal as the superposition of the responses to the spectral components of the (periodic) input signal.

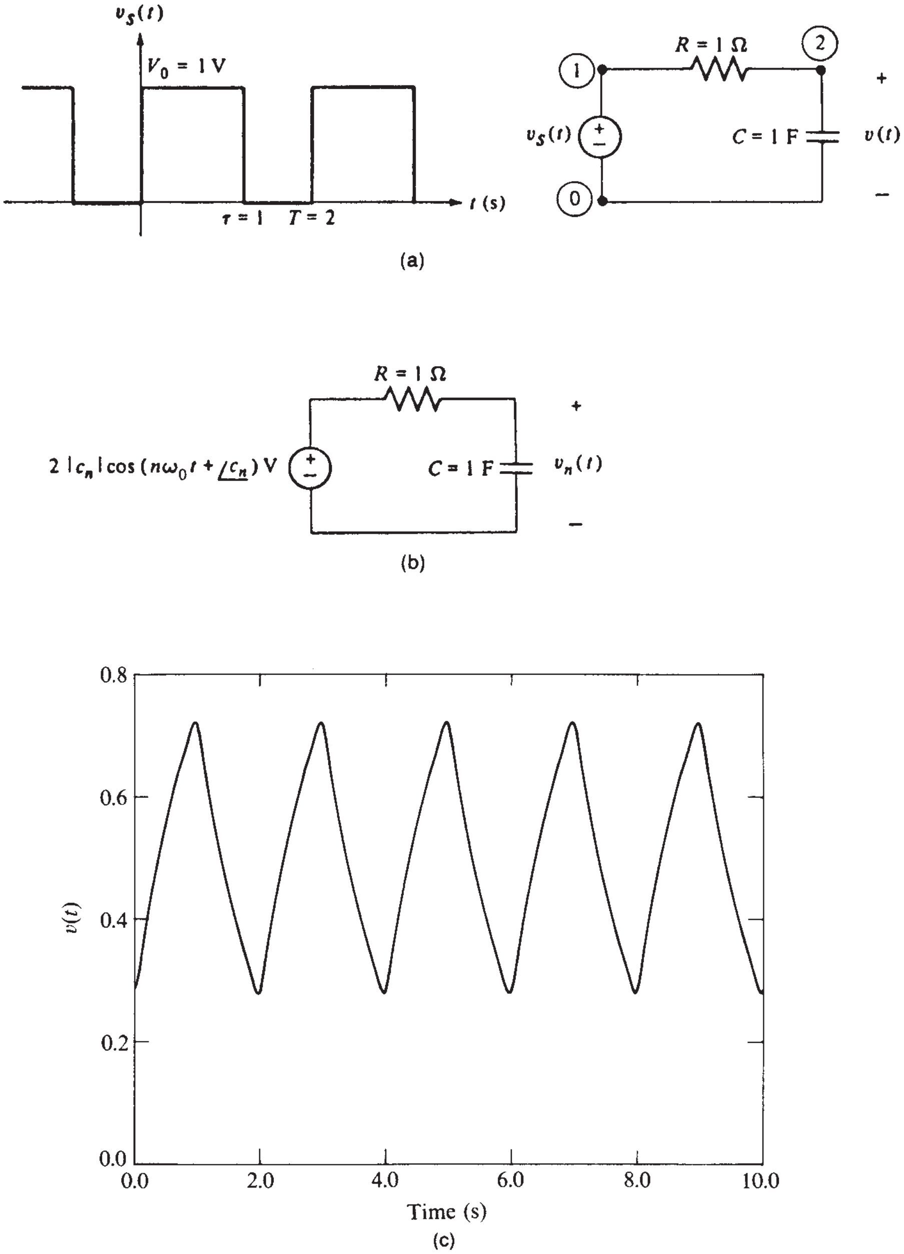

$v_S(t)$
$V_0 = 1$ V
$\tau = 1$
$T = 2$
t (s)
(a)
$R = 1\ \Omega$
①
②
⓪
$v_S(t)$
$C = 1$ F
$v(t)$
+
−
$2\,|c_n|\cos(n\omega_0 t + \angle c_n)$ V
$R = 1\ \Omega$
$C = 1$ F
$v_n(t)$
+
−
(b)
0.8
0.6
0.4
0.2
0.0
$v(t)$
0.0
2.0
4.0
6.0
8.0
10.0
Time (s)
(c)

FIGURE 3.9 Example 3.2 illustrating computation of the steady-state response of a circuit to a periodic signal: (a) the circuit and input signal; (b) computing the response to a spectral component of the input; and (c) computed response.

This transfer function evaluated at the harmonics of $v_S(t)$ is

$$H(jn\omega_0) = \frac{1}{1 + jn\omega_0 RC}$$

Thus,

$$v_n(t) = 2|c_n||H(jn\omega_0)| \cos[n\omega_0 t + \angle c_n + \angle H(jn\omega_0)]$$

and the complete steady-state response is

$$v(t) = c_0 H(0) + \sum_{n=1}^{\infty} v_n(t)$$

As a numerical example, let us choose $R = 1\ \Omega$ and $C = 1\ F$. Thus, the time constant of the circuit is $RC = 1\ s$. It is expected that choosing the pulsewidth of $v_s(t)$ to be less than or greater than this time constant will yield quite different responses. Let us choose $V_0 = 1$ V, $T = 2\ s$, and $\tau = 1\ s$ to give a duty cycle of 50%. The transfer function is

$$H(jn\omega_0) = \frac{1}{1 + jn\pi}$$

The complex-exponential Fourier series coefficients are

$$\begin{aligned} c_n &= \frac{V_0\tau}{T} \frac{\sin(n\pi\tau/T)}{(n\pi\tau/T)} e^{-jn\pi\tau/T} \\ &= \frac{1}{2} \frac{\sin(n\pi/2)}{(n\pi/2)} e^{-jn\pi/2} \end{aligned}$$

Evaluating these for the first seven harmonics gives

$$\begin{aligned}
c_0 &= \tfrac{1}{2} & H(0) &= 1 \\
c_1 &= \tfrac{1}{\pi} e^{-j\pi/2} & H(j\omega_0) &= \tfrac{1}{1+j\pi} \\
&= \tfrac{1}{\pi}\angle -90^\circ & &= 0.3033\angle -72.34^\circ \\
c_2 &= 0 & & \\
c_3 &= -\tfrac{1}{3\pi} e^{-j3\pi/2} & H(j3\omega_0) &= \tfrac{1}{1+j3\pi} \\
&= -\tfrac{1}{3\pi}\angle 90^\circ & &= 0.1055\angle -83.94^\circ \\
&= \tfrac{1}{3\pi}\angle -90^\circ & & \\
c_4 &= 0 & & \\
c_5 &= \tfrac{1}{5\pi} e^{-j\pi/2} & H(j5\omega_0) &= \tfrac{1}{1+j5\pi} \\
&= \tfrac{1}{5\pi}\angle -90^\circ & &= 0.0635\angle -86.36^\circ \\
c_6 &= 0 & & \\
c_7 &= -\tfrac{1}{7\pi} e^{-j7\pi/2} & H(j7\omega_0) &= \tfrac{1}{1+j7\pi} \\
&= -\tfrac{1}{7\pi}\angle 90^\circ & &= 0.04543\angle -87.4^\circ \\
&= \tfrac{1}{7\pi}\angle -90^\circ & &
\end{aligned}$$

Doubling the magnitudes gives the one-sided spectrum of the source voltage as

$$\begin{aligned}
v_s(t) &= \frac{1}{2} + \frac{2}{\pi}\cos(\pi t - 90^\circ) \\
&\quad + \frac{2}{3\pi}\cos(3\pi t - 90^\circ) + \frac{2}{5\pi}\cos(5\pi t - 90^\circ) \\
&\quad + \frac{2}{7\pi}\cos(7\pi t - 90^\circ) + \cdots \\
&= 0.5 + 0.6366\sin(\pi t) \\
&\quad + 0.2122\sin(3\pi t) + 0.1273\sin(5\pi t) \\
&\quad + 0.0909\sin(7\pi t)
\end{aligned}$$

The one-sided spectrum of the output voltage is obtained according to (3.32) as

$$\begin{aligned}
v_s(t) &= 0.5 + 0.1931\cos(\pi t - 162.34^\circ) \\
&\quad + 0.0224\cos(3\pi t - 173.94^\circ) \\
&\quad + 0.0081\cos(5\pi t - 176.36^\circ) \\
&\quad + 0.0041\cos(7\pi t - 177.4^\circ) \\
&\quad + \cdots \\
&= 0.5 + 0.1931\sin(\pi t - 72.34^\circ) \\
&\quad + 0.0224\sin(3\pi t - 83.94^\circ) \\
&\quad + 0.0081\sin(5\pi t - 86.36^\circ) \\
&\quad + 0.0041\sin(7\pi t - 87.4^\circ) \\
&\quad + \cdots
\end{aligned}$$

A plot of this result using the first seven harmonics is shown in Fig. 3.9c. Note that no transient-time interval appears since this result is only the steady-state portion of the solution.

3.1.3 Important Computational Techniques

Although direct computation of the expansion coefficients is straightforward using the previous results, it can become tedious for some waveforms. The purpose of this section is to illustrate four important properties than can be used to make the computation of these coefficients virtually trivial for *piecewise-linear* waveforms. Piecewise-linear waveforms are those that consist of straight-line segments. An example of a periodic, piecewise-linear waveform is shown in Fig. 3.10a.

The first and most important property is that of *linearity*. Any waveform or function can be written as (or decomposed into) a *linear combination* of two or more functions:

$$x(t) = A_1 x_1(t) + A_2 x_2(t) + A_3 x_3(t) + \cdots \tag{3.33}$$

For example, the waveform in Fig. 3.10a can be written as the linear combination of two other waveforms: $x(t) = A_1 x_1(t) + A_2 x_2(t)$, where $x_1(t)$ and $x_2(t)$ are as shown in Fig. 3.10b and $A_1 = A_2 = A$.

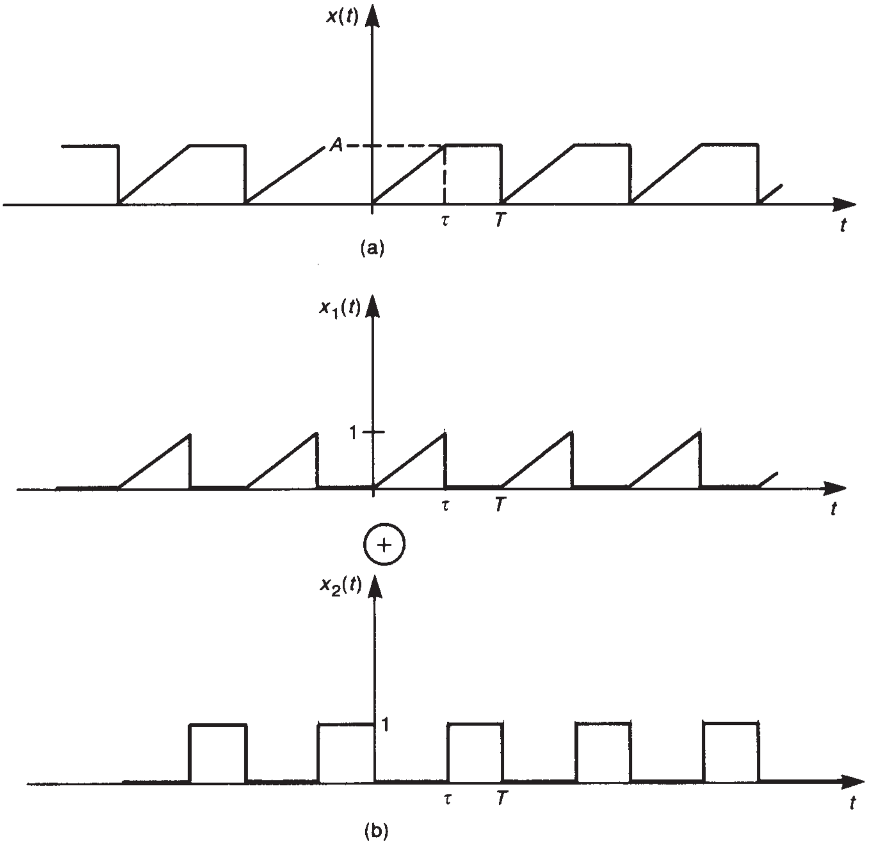

FIGURE 3.10 Illustration of the principle of linear decomposition of a signal: (a) the signal and (b) its decomposition, $x(t) = Ax_1(t) + Ax_2(t)$.

Consequently, the Fourier series of $x_1(t)$ can be written as a linear combination of the Fourier series representations of $x_1(t)$, $x_2(t)$, $x_3(t)$, $\ldots$ according to (3.33). For example, suppose that the complex-exponential forms of $x_1(t)$ and $x_2(t)$ are written as

$$x_1(t) = \sum_{-\infty}^{\infty} c_{1n} e^{jn\omega_0 t} \tag{3.34a}$$

$$x_2(t) = \sum_{-\infty}^{\infty} c_{2n} e^{jn\omega_0 t} \tag{3.34b}$$

If $x(t) = x_1(t) + x_2(t)$, then

$$\begin{aligned} x(t) &= x_1(t) + x_2(t) \\ &= \sum_{-\infty}^{\infty} (c_{1n} + c_{2n}) e^{jn\omega_0 t} \\ &= \sum_{-\infty}^{\infty} c_n e^{jn\omega_0 t} \end{aligned} \tag{3.35}$$

Therefore, the expansion coefficient associated with the nth harmonic of $x(t)$ is the sum of the expansion coefficients of that harmonic associated with $x_1(t)$ and $x_2(t)$. Thus, we can *decompose* a periodic function into a linear combination of perhaps simpler functions. If it is easier to obtain the expansion coefficients of these simpler functions, then the original task of obtaining the expansion coefficients of $x(t)$ will be simplified.

The second important property has to do with *time-shifting a function*. If $x(t)$ is *shifted ahead in t by an amount α* (*delayed in time by α*), it is written as $x(t-\alpha)$. An example is shown in Fig. 3.11c. This is easy to remember if we observe that corresponding points on the waveforms of $x(t)$ and $x(t-\alpha)$ occur where the arguments of $x(t)$ and $x(t-\alpha)$ are identical. For example, the point on $x(t)$ at $t=0$, $x(0)$ corresponds to the point on $x(t-\alpha=0)$ or $t=\alpha$. Thus, $x(t-\alpha)$ is $x(t)$ shifted ahead on the time axis by α (delayed in time). Similarly, $x(t+\alpha)$ is $x(t)$ shifted backward on the time axis by α (advanced in time). An example is shown in Fig. 3.11c. The Fourier series expansion coefficients of $x(t\pm\alpha)$ can be directly found from the expansion coefficients of $x(t)$ as the following shows. First, we recall the complex exponential Fourier series expansion for $x(t)$ given in (3.9), with the expansion coefficients c_n given in (3.12). Suppose that $x(t)$ is *shifted ahead in t* to give $x(t-\alpha)$. Substituting $t-\alpha$ for t in (3.9) gives

$$\begin{aligned} x_1(t-\alpha) &= \sum_{-\infty}^{\infty} c_n e^{jn\omega_0(t-\alpha)} \\ &= \sum_{-\infty}^{\infty} \underbrace{c_n e^{jn\omega_0\alpha}}_{c'_n} e^{jn\omega_0 t} \end{aligned} \tag{3.36}$$

Therefore, *we multiply the expansion coefficients of* $x(t)$ *by* $e^{-jn\omega_0\alpha}$ *to obtain the expansion coefficients of* $x(t-\alpha)$.

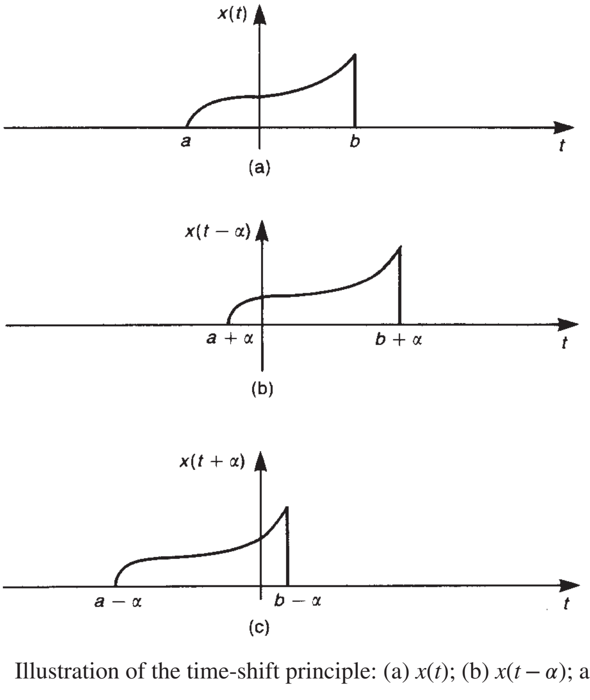

FIGURE 3.11 Illustration of the time-shift principle: (a) $x(t)$; (b) $x(t-\alpha)$; and (c) $x(t+\alpha)$.

The third important property that we will use has to do with the *unit impulse function* $\delta(t)$. This is defined by [1]

$$\delta(t) = \begin{cases} 0 & \text{for } t < 0 \\ 0 & \text{for } t > 0 \\ \int_{0^-}^{0^+} \delta(t)\,dt = 1 \end{cases} \tag{3.37}$$

The notations 0^- and 0^+ denote time immediately prior to and after $t = 0$, respectively; that is, the value of the function is zero except at $t = 0$, where its value is undefined. Intuitively, we say that the unit impulse function has zero width and infinite height such that the *area* under the function is unity [1]. The impulse function is represented by a vertical arrow (whose height is immaterial). The *strength* of the impulse is denoted in parentheses adjacent to this arrow. Figure 3.12 illustrates $A\delta(t-\tau)$. Consider a periodic train of unit impulse functions

$$x(t) = \delta(t \pm kT), k = 0, \pm 1, \pm 2, \pm 3, \ldots \tag{3.38}$$

as shown in Fig. 3.13a. The expansion coefficients are

$$\begin{aligned} c_n &= \frac{1}{T}\int_0^T \delta(t)e^{-jn\omega_0 t}\,dt \\ &= \frac{1}{T}\int_{0^-}^{0^+} \delta(t)e^{-jn\omega_0 t}\,dt = \frac{1}{T}\int_{0^-}^{0^+} \delta(t)\,dt \\ &= \frac{1}{T} \end{aligned}$$

If the pulse train is shifted ahead in t by α as shown in Fig. 3.13b, then, by the time-shift property, the expansion coefficients become

$$c_n = \frac{1}{T}e^{-jn\omega_0\alpha} \tag{3.40}$$

The fourth and final property has to do with the relation between the expansion coefficients for a periodic function $x(t)$ and the expansion coefficients of its various *derivatives*. If $x(t)$ is represented with the complex-exponential Fourier series as

$$x(t) = \sum_{-\infty}^{\infty} c_n e^{jn\omega_0 t} \tag{3.41}$$

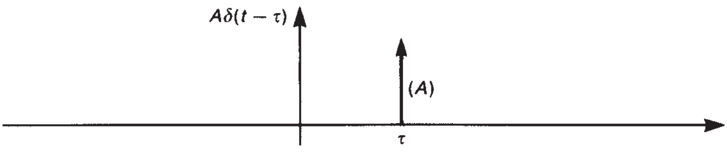

FIGURE 3.12 The impulse function.

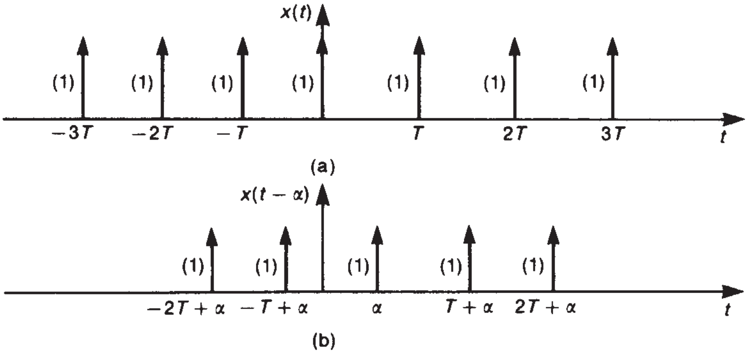

FIGURE 3.13 A periodic train of unit impulses (a) and (b) shifted in time.

and the kth derivative is represented as

$$\frac{d^k x(t)}{dt^k} = \sum_{-\infty}^{\infty} c_n^{(k)} e^{jn\omega_0 t} \tag{3.42}$$

the expansion coefficients are related by

$$c_n = \frac{1}{(jn\omega_0)^k} c_n^{(k)} \quad n \neq 0 \tag{3.43}$$

where $c_n^{(k)}$ is the nth expansion coefficient for the kth derivative of $x(t)$. Note that when we differentiate $x(t)$, the derivative of c_0 is zero. Hence, we may not generally obtain c_0 using this technique. However, c_0 is simple to obtain directly from $x(t)$ as the average value of the waveform. This is simple to show by differentiating (3.41) to yield

$$\frac{d^k x(t)}{dt^k} = \sum_{-\infty}^{\infty} \underbrace{(jn\omega_0)^k\, c_n}_{c_n^{(k)}} e^{jn\omega_0 t} \tag{3.44}$$

We are now ready to utilize these four important properties to simplify the computation of the expansion coefficients in the complex-exponential Fourier series for *piecewise-linear* functions. The technique is to *repeatedly differentiate the function until the first occurrence of an impulse function.* If the differentiated function does not consist solely of impulse functions, write the result as the sum of the part that contains the impulse functions and a part that contains the remainder. Determine the expansion coefficients for the part containing the impulse functions using the results shown above and continue to differentiate the part that did not contain impulses until impulses occur. Repeat the process until the expansion is complete. Divide each part by the required power of $jn\omega_0$ according to (3.43) to return to the expansion coefficient of the original function.

Example 3.3 Determine the Fourier coefficients for the square wave shown in Fig. 3.4.

Solution: The derivative of the waveform is shown in Fig. 3.14 and is a periodic train of impulses of strength A occurring at the rising edge of each pulse and a periodic train of impulses of strength

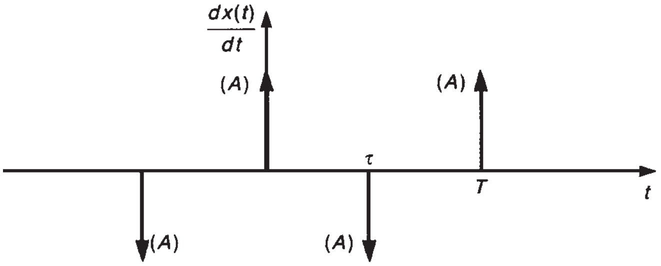

FIGURE 3.14 Example 3.3.

$-A$ occurring at the falling edge of each pulse. The expansion coefficients for the derivative of this function are the sums of the expansion coefficients for each pulse train component:

$$\begin{aligned}c_n^{(1)} &= A\frac{1}{T} - A\frac{1}{T}e^{-jn\omega_0\tau}\\ &= \frac{A}{T}(1-e^{-jn\omega_0\tau})\\ &= \frac{A}{T}(e^{jn\omega_0\tau/2} - e^{-jn\omega_0\tau/2})e^{-jn\omega_0\tau/2}\\ &= jn\omega_0\frac{A\tau}{T}\frac{\sin(n\omega_0\tau/2)}{n\omega_0\tau/2}e^{-jn\omega_0\tau/2}\end{aligned}$$

The expansion coefficients for $x(t)$ are

$$\begin{aligned}c_n &= \frac{1}{jn\omega_0}c_n^{(1)}\\ &= \frac{A\tau}{T}\frac{\sin(n\omega_0\tau/2)}{n\omega_0\tau/2}e^{-jn\omega_0\tau/2}\end{aligned}$$

as before.

Example 3.4 Determine the Fourier series for the waveform of Example 3.1 shown in Fig. 3.7 by differentiation.

Solution: Write the first derivative of the waveform shown in Fig. 3.15b as the sum of two functions shown in Fig. 3.15c:

$$\frac{dx(t)}{dt} = x_1(t) + x_2(t)$$

The expansion coefficients for $x_1(t)$ are easily determined with the preceding properties of the impulse train as

$$c_{1n}^{(1)} = -\frac{A}{T}e^{-jn\omega_0 T} = -\frac{A}{T}$$

The function $x_2(t)$ is differentiated again to yield the result in Fig. 3.15d. The expansion coefficients for this are

$$c_{2n}^{(2)} = \frac{A}{\tau}\frac{1}{T} - \frac{A}{\tau}\frac{1}{T}e^{-jn\omega_0\tau}$$

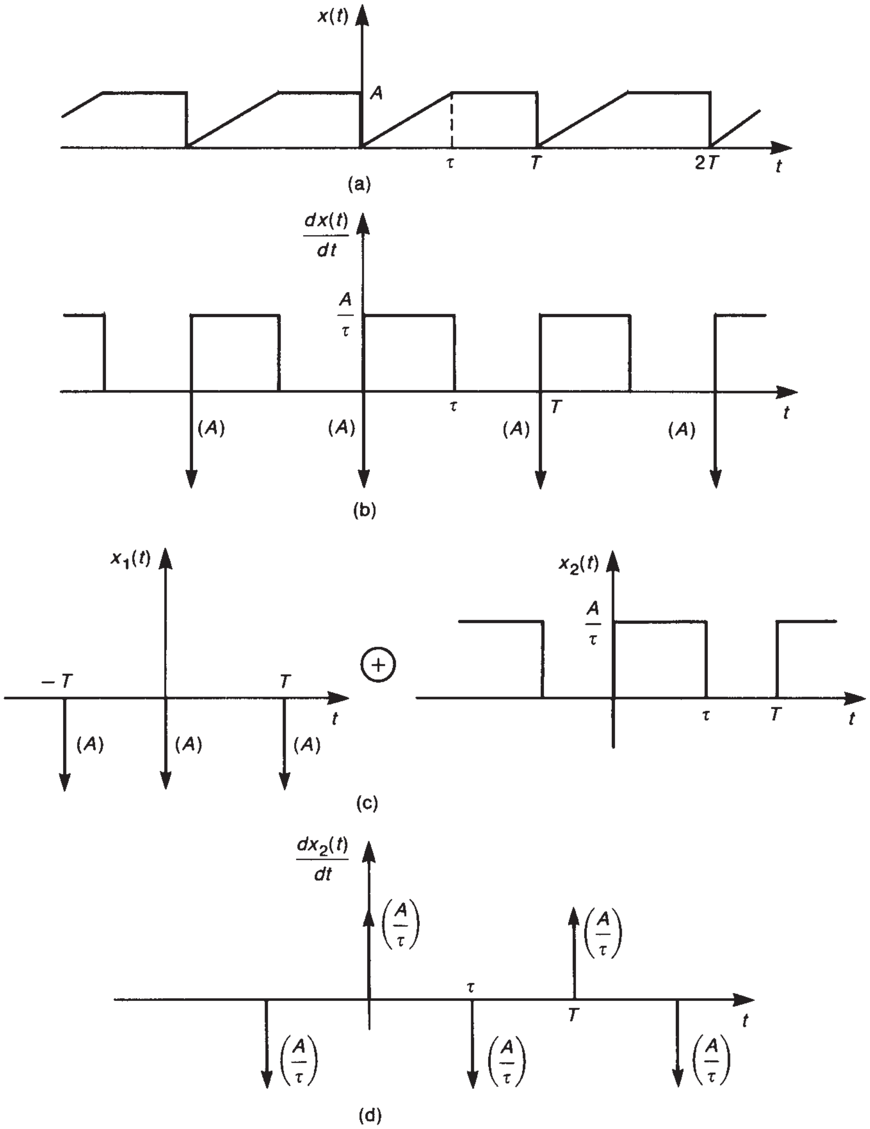
x(t)
A
τ
T
2T
t
(a)
dx(t)/dt
A/τ
τ
T
t
(A)
(A)
(A)
(A)
(b)
x₁(t)
−T
T
t
(A)
(A)
(A)
+
x₂(t)
A/τ
τ
T
t
(c)
dx₂(t)/dt
(A/τ)
(A/τ)
τ
T
t
(A/τ)
(A/τ)
(A/τ)
(d)

FIGURE 3.15 Example 3.4 illustrating the use of differentiation to compute the expansion coefficients for a piecewise-linear, periodic signal: (a) the signal; (b) the first derivative; (c) use of linearity; and (d) repeated differentiation of a component.

Notice in this last result that we have used the properties of linearity and time shift. The expansion coefficients for the original function are then

$$\begin{aligned} c_n &= \frac{1}{jn\omega_0} c_n^{(1)} + \frac{1}{(jn\omega_0)^2} c_n^{(2)} n \neq 0 \\ &= -\frac{1}{jn\omega_0} \frac{A\tau}{T} e^{-jn\omega_0 T} + \frac{1}{(jn\omega_0)^2} \left(\frac{A}{\tau} \frac{1}{T} - \frac{A}{\tau} \frac{1}{T} e^{-jn\omega_0 \tau} \right) \end{aligned}$$

$$
\begin{aligned}
&= j\frac{A}{n\omega_0 T}\left[e^{-jn\omega_0 T} + j\frac{1}{n\omega_0 \tau}(1 - e^{-jn\omega_0 \tau})\right] \\
&= j\frac{A}{n\omega_0 T}e^{-jn\omega_0 T} - j\frac{A}{n\omega_0 T}\frac{\sin(n\omega_0 \tau/2)}{n\omega_0 \tau/2}e^{-jn\omega_0 \tau/2} \\
&= j\frac{A}{2\pi n}\left[1 - e^{-j\frac{n\pi\tau}{T}}\frac{\sin(n\pi\tau/T)}{n\pi\tau/T}\right]
\end{aligned}
$$

since $n\omega_0 T = 2\ \pi n$ and $e^{-jn\omega_0 T} = e^{-j2\pi n} = 1$ as were determined in Example 3.1, but differentiation avoids integration.

3.2 SPECTRA OF DIGITAL WAVEFORMS

As was mentioned earlier, the waveforms of primary importance in digital circuits are those which represent clock and data signals. The clock signals are periodic, deterministic signals and are therefore representable by the methods of the previous sections. Although the clock waveforms resemble square waves as shown in Fig. 3.4, the purpose of this section is to obtain a better representation of them and to simplify that representation to provide insight into the time-domain factors that affect their spectral content. Data waveforms will be considered in Section 3.5.

3.2.1 The Spectrum of Trapezoidal (Clock) Waveforms

Clock waveforms will be represented as periodic trains of trapezoid-shaped pulses shown in Fig. 3.16. Each pulse is described by an amplitude A, a pulse *risetime* τ_r, a pulse *falltime* τ_f, and a *pulsewidth* (between 50% points of the waveform amplitude) τ. For our purposes, we will represent the pulse rise- and falltimes as being the time required for the signal to transition from 0 to A; that is, from the 0% to 100% points. Because actual pulses do not transition as sharply as we have shown, it is common in industry to define the rise- and falltime as being from 0.1 A to 0.9 A; that is, from the 10% to 90% points. The rise/falltime based on the 10–90% points will be 80% of the rise/falltime based on the 0–100% points. The purpose of this section is to investigate the effect of these pulse parameters on the spectrum of the waveform. We will find that *the key parameters that contribute to the high-frequency spectral content of the waveform are the rise- and falltimes of the pulse*. The levels of the emissions in the regulatory frequency range are therefore strongly dependent on the risetimes and falltimes of these pulses.

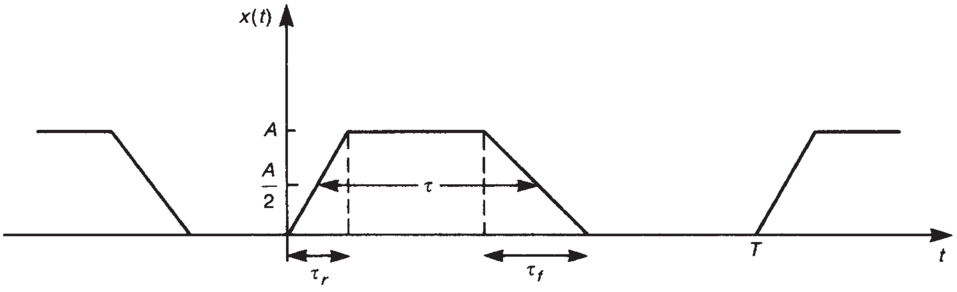

FIGURE 3.16 The periodic, trapezoidal pulse train representing clock and data signals of digital systems.

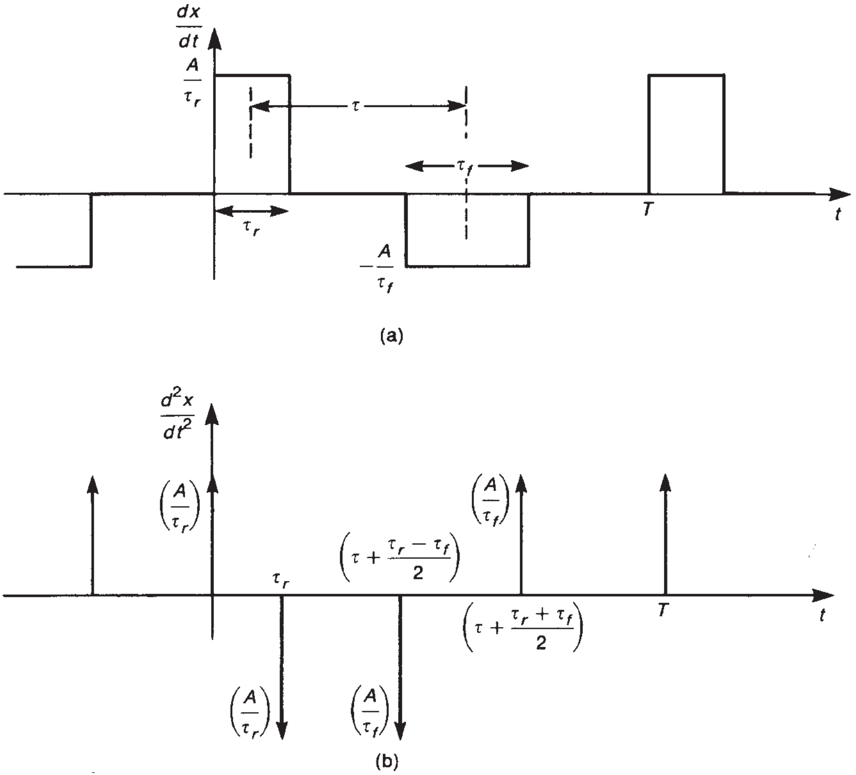

FIGURE 3.17 Various derivatives of the trapezoidal pulse train: (a) first derivative and (b) second derivative.

In order to obtain the complex-exponential Fourier series of this waveform, we will use results of Section 3.1.3. The first derivative of the waveform is shown in Fig. 3.17a. Differentiating this once again to yield impulses gives the waveform in Fig. 3.17b. Since this waveform contains impulses, we expand it to give the expansion coefficients

$$
\begin{aligned}
c_{2n}^{(2)} &= \frac{1}{T}\frac{A}{\tau_r} - \frac{1}{T}\frac{A}{\tau_r}e^{-jn\omega_0\tau_r} - \frac{1}{T}\frac{A}{\tau_r}e^{-jn\omega_0[\tau+(\tau_r-\tau_f)/2]} \\
&\quad + \frac{1}{T}\frac{A}{\tau_r}e^{-jn\omega_0[\tau+(\tau_r+\tau_f)/2]} \\
&= \frac{A}{T}\left[\frac{1}{\tau_r}e^{-jn\omega_0\tau_r/2}(e^{jn\omega_0\tau_r/2} - e^{-jn\omega_0\tau_r/2})\right. \\
&\quad \left. - \frac{1}{\tau_f}e^{-jn\omega_0\tau_r/2}e^{-jn\omega_0\tau}(e^{jn\omega_0\tau_f/2} - e^{-jn\omega_0\tau_f/2})\right] \\
&= j\frac{A}{2\pi n}(n\omega_0)^2 e^{-jn\omega_0(\tau+\tau_r/2)}\left[\frac{\sin(n\omega_0\tau_r/2)}{(n\omega_0\tau_r/2)}e^{jn\omega_0\tau/2} - \frac{\sin(n\omega_0\tau_f/2)}{(n\omega_0\tau_f/2)}e^{-jn\omega_0\tau/2}\right]
\end{aligned}
\tag{3.45}
$$

According to (3.43), the expansion coefficients for the original trapezoidal waveform are

$$\begin{aligned}
c_n &= \frac{1}{(jn\omega_0)^2} c_n^{(2)} n \neq 0 \\
&= -\frac{c_n^{(2)}}{(n\omega_0)^2} \\
&= -j\frac{A}{2\pi n} e^{-jn\omega_0(\tau+\tau_r/2)} \left[\frac{\sin(n\omega_0\tau_r/2)}{(n\omega_0\tau_r/2)} e^{jn\omega_0\tau/2} - \frac{\sin(n\omega_0\tau_f/2)}{(n\omega_0\tau_f/2)} e^{-jn\omega_0\tau/2} \right]
\end{aligned}$$

The result in (3.46) cannot be combined any further to yield useful results. However, *if the pulse risetime equals the falltime*, $\tau_r = \tau_f$, *a very useful result can be obtained*. Substituting $\tau_r = \tau_f$ into (3.46) gives the expansion coefficients as

$$c_n = A\frac{\tau}{T} \frac{\sin(n\omega_0\tau/2)}{(n\omega_0\tau/2)} \frac{\sin(n\omega_0\tau_r/2)}{(n\omega_0\tau_r/2)} e^{-jn\omega_0(\tau+\tau_r/2)} \quad (\tau_r = \tau_f) \tag{3.47}$$

Notice that the result can be placed in the form of the *product* of two (sin *x*)/*x* terms. *If the rise- and falltimes are not equal*, $\tau_r \neq \tau_f$, *the result cannot be placed in the form of the product of two* (sin *x*)/*x* *terms*! There have been attempts to use the above result for $\tau_r \neq \tau_f$ and to replace the risetime in this expression with an average rise/falltime, $1/2(\tau_r + \tau_f)$. Although this would be desirable and reasonably accurate as an approximation if τ_r and τ_f did not greatly differ, the fact is that *this is not correct*! Nevertheless, assuming the rise- and falltimes to be the same will give important insight for the more general case.

Continuing with the assumption that the pulse rise- and falltimes are the same, we may obtain the expansion coefficients for the *one-sided spectrum* (positive frequencies) c_n^+, where

$$x(t) = c_0 + \sum_{n=1}^{\infty} |c_n^+| \cos(n\omega_0 t + \underline{/c_n}) \tag{3.48a}$$

According to (3.19), to obtain this, we *double all the magnitudes of the expansion coefficients for the two-sided spectrum except the* c_0 *term*. From the result in (3.47), we obtain

$$|c_n^+| = 2|c_n| = 2A\frac{\tau}{T} \left| \frac{\sin(n\pi\tau/T)}{(n\pi\tau/T)} \right| \left| \frac{\sin(n\pi\tau_r/2)}{(n\pi\tau_r/2)} \right| \quad \text{for } n \neq 0 \;\; (\tau_r = \tau_f) \tag{3.48b}$$

and

$$c_0 = A\frac{\tau}{T}(\tau_r = \tau_f) \tag{3.48c}$$

where we have substituted $\omega_0 = 2\pi/T$. The angle is

$$\underline{/c_n} = \pm n\pi \frac{\tau + \tau_r}{T} \quad (\tau_r = \tau_f) \tag{3.48d}$$

As a check on this result, substitute $\tau_r = 0$, which gives the result in (3.24) for the square wave.

Several important points can be seen from the result in (3.48). First, suppose that $\tau = (1/2)T$; that is, a 50% duty cycle. In this case, the first sine term becomes $|\sin(n\pi\tau/T)|/|n\pi\tau/T| = |\sin(1/2)n\pi|/|(1/2)n\pi|$, which is zero for even n. Therefore, *there are (theoretically) no even harmonics for a 50% duty cycle*. Digital clock signals tend to approach 50% duty cycle. However, in order for the even harmonics to be absent, the duty cycle must be *exactly 50%*. As a practical matter, the even harmonics can never be completely eliminated, since the duty cycle cannot be set to *exactly 50%*. However, the even harmonics will be increasingly smaller than the odd harmonics the closer we approach a 50% duty cycle. The odd-harmonic levels are quite stable for slight variations in duty cycle. This illustrates that *slight variations in duty cycle from an exact 50% duty cycle can cause the even-harmonic levels to vary widely, and these levels may, in a practical situation, be significant!* This points out a potentially serious difficulty in reproducing measured data on the radiated emissions of a product from one measurement to another *for the same product*. If the offending frequency happens to be an *even harmonic* of a clock in the system, then it is quite likely that a radiated emission at that frequency measured on one day and repeated measurement of the (identical and unchanged) product on a subsequent day will show significant differences in the level! This variation is likely due to the above phenomenon.

Review Exercise 3.1 Determine the magnitudes of the first seven harmonics of a 5 V, 100 MHz, 50%-duty-cycle trapezoidal waveform having rise/falltimes of 1 ns in dBμV. Also, determine the dc component.

***Answers*:** $c_0 = 127.96$ dBμV, $c_1^+ = 129.9$ dBμV, $c_2^+ = 0$, $c_3^+ = 119.19$ dBμV, $c_4^+ = 0$, $c_5^+ = 112.16$ dBμV, $c_6^+ = 0$, $c_7^+ = 104.47$ dBμV.

3.2.2 Spectral Bounds for Trapezoidal Waveforms

Although the result in (3.48) gives the one-sided spectrum expansion coefficients, it is desirable to extract more intuitive information than is apparent in these equations. In order to do this, we will generate *bounds on the magnitude spectrum*. Although these are upper bounds (worst case) on the spectral components and are approximate, their utility will be of considerable benefit in understanding the impact of risetime, falltime, and pulsewidth on the spectrum of the waveform.

To begin this discussion, recall the result for a square wave given in (3.24); this is a trapezoidal pulse train with zero rise/falltime. The magnitudes of the expansion coefficients are in the form of a $(\sin x)/x$ expression. Although the spectral components exist only at frequencies $f = n/T$ for $n = 0, 1, 2, \ldots$, *the envelope* of these spectral components follows a form of $[\sin(\pi f\tau)]/(\pi f\tau)$. This is illustrated in Fig. 3.5b. The envelope has zeros at $f = (m/\tau)$ for $m = 1, 2, 3, \ldots$. This envelope can be bounded as follows [3]. Recall the small-argument expression for $\sin(x)$, which is that $\sin x \cong x$ for small x. Thus, we have

$$\left|\frac{\sin x}{x}\right| \le \begin{cases} 1 & \text{for small } x \\ \frac{1}{|x|} & \text{for large } x \end{cases}$$

This can be drawn as two asymptotes, as shown in Fig. 3.18. The first asymptote is unity and has slope on a logarithmic or *Bode* plot of 0 dB/decade [1]. The second asymptote decreases linearly with x, or − 20 dB/decade [1]. The two asymptotes converge at $x = 1$. In the expansion coefficient for the square wave in (3.24), $x = \pi\tau f$, where $f = n/T$. Thus, for the square wave, the first asymptote has a 0 dB/decade slope out to $f = 1/\pi\tau$ and a − 20 dB/decade slope above that frequency.

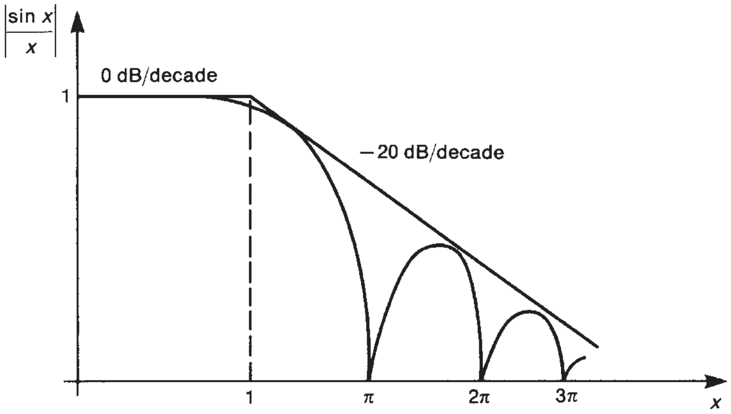

FIGURE 3.18 Bounds on the $(\sin x)/x$ function.

3.2.2.1 *Effect of Rise/Falltime on Spectral Content*

We now are ready to extend these notions to the trapezoidal pulse train. Again, in order to use these results, we must assume that the rise- and falltimes are equal, $\tau_r = \tau_f$, so that the expansion coefficient expression can be put in the form of the product of two $(\sin x)/x$ expressions as given in (3.48). Replacing the discrete spectrum with a continuous envelope by substituting $f = n/T$ gives

$$\text{Envelope} = 2A\frac{\tau}{T}\left|\frac{\sin(\pi\tau f)}{\pi\tau f}\right|\left|\frac{\sin(\pi\tau_r f)}{\pi\tau_r f}\right| \tag{3.49}$$

Recall that the dc term or level is $A\tau/T$. In order to generate bounds for this spectrum, we take the logarithm of (3.49) to give

$$\begin{aligned} 20\log_{10}(\text{envelope}) = 20\log_{10}\left(2A\frac{\tau}{T}\right) + 20\log_{10}\left|\frac{\sin(\pi\tau f)}{\pi\tau f}\right| + \\ 20\log_{10}\left|\frac{\sin(\pi\tau_r f)}{\pi\tau_r f}\right| \end{aligned} \tag{3.50}$$

This shows that the composite plot is the sum of three plots:

$$\text{Plot 1} = 20\log_{10}\left(2A\frac{\tau}{T}\right) \tag{3.51a}$$

$$\text{Plot 2} = 20\log_{10}\left|\frac{\sin(\pi\tau f)}{\pi\tau f}\right| \tag{3.51b}$$

$$\text{Plot 3} = 20\log_{10}\left|\frac{\sin(\pi\tau_r f)}{\pi\tau_r f}\right| \tag{3.51c}$$

Plot 1 has 0 dB/decade slope and a level of $2A\tau/T = 2A\tau f_0$. Plot 2 has two asymptotes. The first asymptote has a 0 dB/decade slope as discussed for the square wave and unit level (0 dB). The second asymptote has −20 dB/decade slope. The two asymptotes join at $f = 1/\pi\tau$. Plot 3 also consists of two asymptotes, one of which has a 0 dB/decade slope and unit level (0 dB) and the other has a −20 dB/decadeslope. The asymptotes of the third plot join at $f = 1/\pi\tau_r$. The composite asymptote

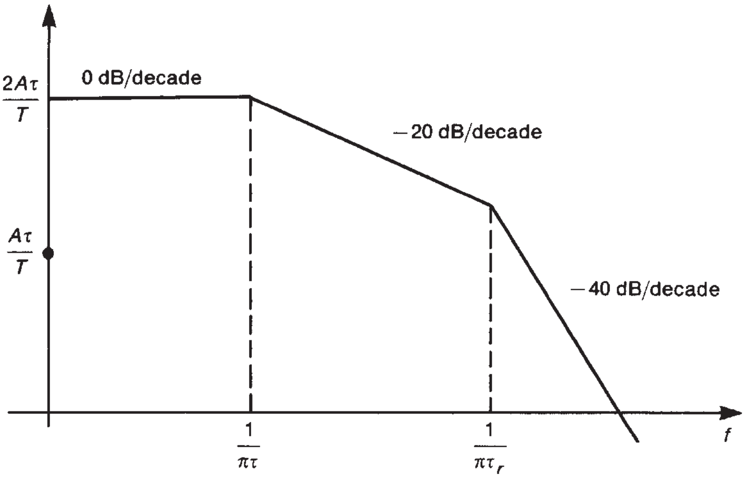

FIGURE 3.19 Bounds on the one-sided magnitude spectrum of a trapezoidal pulse train.

is the sum of these asymptotes, as shown in Fig. 3.19. The composite asymptote thus consists of three straight-line segments. The first is due to plot 1 and has a slope of 0 dB / decade and a starting level of $2A\tau / T$. The second segment has a slope of −20 dB/decade and is due to plot 2. The third segment has a slope of −40 dB / decade and is due to the sum of plots 2 and 3. It is evident that the pulsewidth must be greater than or equal to the pulse rise/falltime: $\tau \geq \tau_r$. Thus, the first breakpoint in the spectral bound will be related to plot 2, whose breakpoint is related to the pulsewidth and is $1/\pi\tau$. The second breakpoint is due to plot 3, whose breakpoint is related to the pulse rise/falltime and is $1/\pi\tau_r$.

From these spectral bounds, it now becomes clear that *the high-frequency content of a trapezoidal pulse train is due primarily to the rise/falltime of the pulse. Pulses having small rise/falltimes will have larger high-frequency spectral content than will pulses having larger rise/falltimes. Thus, in order to reduce the high-frequency spectrum in order to reduce the emissions of a product, increase the rise/falltimes of the clock and/or data pulses.* "Fast" (short) rise/falltimes are the primary contributors to the high-frequency spectral content of the signal and therefore the product's inability to meet the governmental regulatory requirements on radiated and conducted emissions. They are also important in the ability of the product to cause interference. (Recall that the interference potential of a product and whether it complies with the regulatory requirements are not necessarily related; that is, a product that complies with the governmental emission requirements may cause interference.) Figure 3.20 shows the exact spectrum along with the spectral bounds for a 1 V, 1 MHz trapezoidal waveform having a rise/falltime of 20 ns and duty cycles of 50%, 30%, and 10%.

Figure 3.21 shows measured spectra that illustrate these points. Figure 3.21a shows the time-domain waveform and associated spectrum (measured with a spectrum analyzer to be discussed) for a 1 V, 10 MHz trapezoidal pulse train having a 50% duty cycle and rise/falltimes of 20 ns. Figure 3.21b shows the same waveform, but with the rise/falltimes reduced to 5 ns. Note the dramatic increase in the spectral content at the higher frequencies. The span is from essentially dc up to 500 MHz. The center frequency is 250 MHz. The amplitude setting is the same for both spectral plots. The spectrum of the 20 ns rise/falltime pulse train shows very little spectral content above 250 MHz, whereas the spectrum of the 5 ns pulse train shows a significant spectral content up to 500 MHz. Specifically, the 11th harmonic (98 MHz) is increased from 68.0 to 86.1 dBμV, an increase of some 18 dB at 98 MHz! This dramatically illustrates the importance in *using pulses with as large a rise/falltime as possible*!

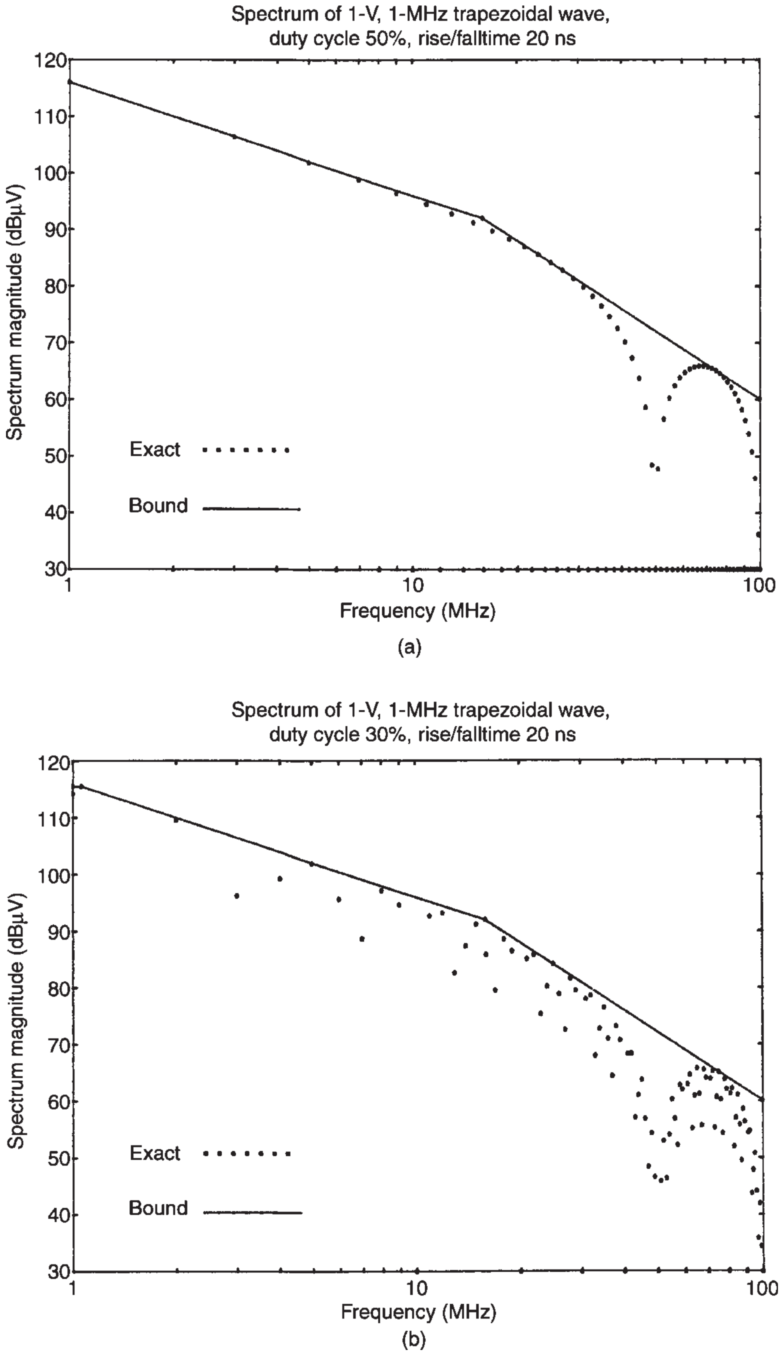

FIGURE 3.20 Examples illustrating the spectral bounds for various duty cycles of a 1 V, 1 MHz, trapezoidal pulse train having rise/falltimes of 20 ns: (a) 50% duty cycle; (b) 30% duty cycle; and (c) 10% duty cycle.

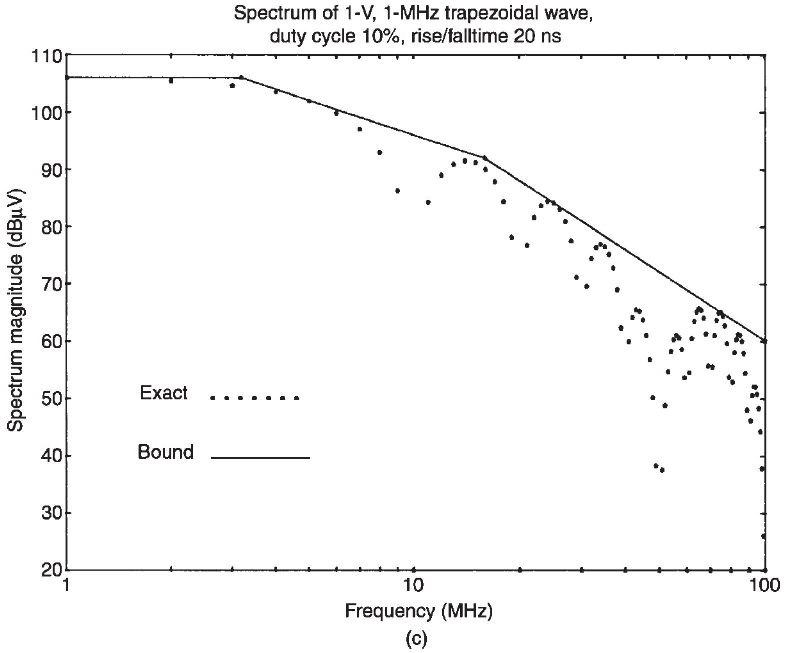

FIGURE 3.20 (*Continued*)

In order to investigate the effect of pulse rise/falltimes as well as other time-domain parameters on spectral content, we must be able to interpolate on log–log or Bode plots. Consider the log–log plot shown in Fig. 3.22a. The slope is given as M dB/decade. The equation for this line is

$$\log_{10}Y_2 - \log_{10}Y_1 = M(\log_{10}f_2 - \log_{10}f_1) \tag{3.52a}$$

or

$$\log_{10}Y_2 = \log_{10}Y_1 + M\log_{10}\left(\frac{f_2}{f_1}\right) \tag{3.52b}$$

This simple but important result allows us to estimate the effect of a higher frequency breakpoint. Consider the trapezoidal spectral bound shown in Fig. 3.22b. The segment breakpoints occur at f and f_3, and it is desired to determine the reduction in dB from the dc level at the frequencies f_2 and f_4. The various reductions are

$$\Delta_1 = -20\log_{10}\left(\frac{f_2}{f_1}\right) \tag{3.53a}$$

$$\Delta_2 = -20\log_{10}\left(\frac{f_3}{f_1}\right) \tag{3.53b}$$

$$\Delta_3 = -20\log_{10}\left(\frac{f_4}{f_3}\right) \tag{3.53c}$$

Therefore, the various levels are

$$\mathrm{K}_2\,\mathrm{dB} = \mathrm{K}\,\mathrm{dB} + \Delta_1 \tag{3.54a}$$

$$\mathrm{K}_4\,\mathrm{dB} = \mathrm{K}\,\mathrm{dB} + \Delta_2 + \Delta_3 \tag{3.54b}$$

Example 3.5 For the 1 V, 10 MHz, 50%-duty-cycle trapezoidal waveform whose measured spectra are shown in Fig. 3.21, determine the level at 98 MHz for the 20 ns rise/falltime and for the 5 ns rise/falltime. In addition, reduce the fundamental frequency to 1 MHz and determine the level at 98 MHz for a 20 ns rise/falltime.

Solution: First, we compute the two break frequencies and draw the spectral bounds. The first break frequency is $1/\pi\tau$. But the pulsewidth τ is related to the duty cycle and fundamental frequency as

$$D = \frac{\tau}{T}$$
$$f_0 = \frac{1}{T}$$

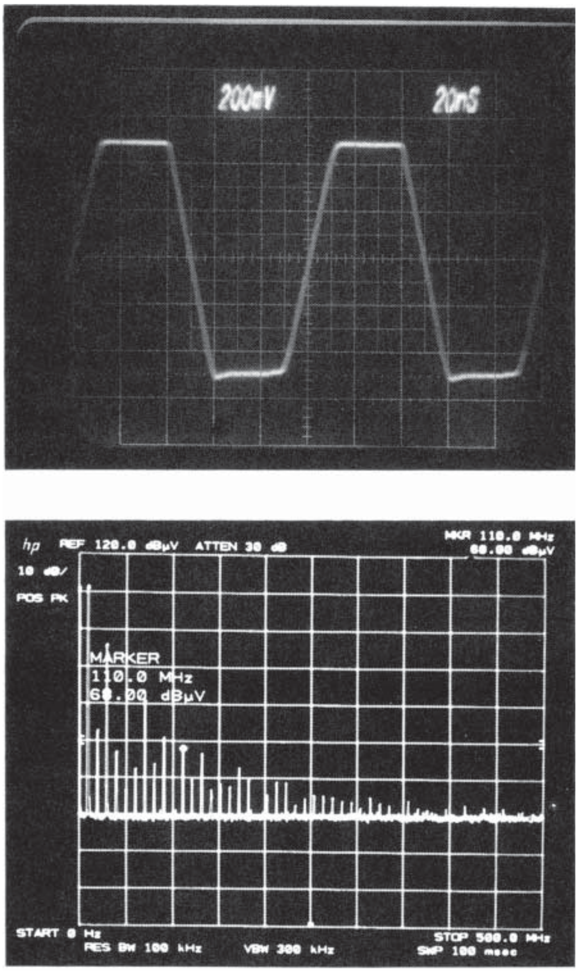

Rise/falltime = 20 ns

(a)

FIGURE 3.21 Experimentally measured spectra of a 1 V, 10 MHz, 50%-duty-cycle trapezoidal pulse train for rise/falltimes of (a) 20 ns and (b) 5 ns.

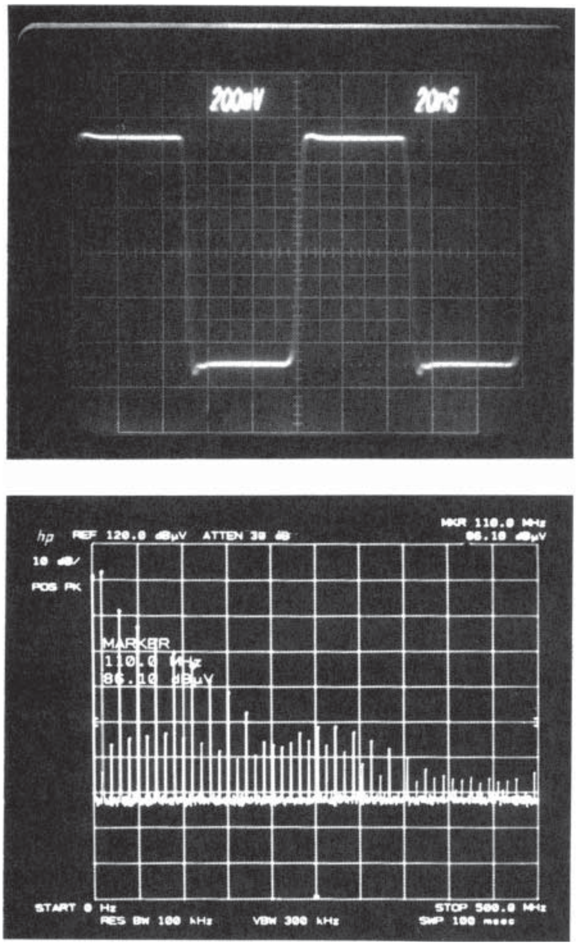

Rise/falltime = 5 ns

(b)

FIGURE 3.21 (*Continued*)

Hence, the first breakpoint is at

$$\frac{1}{\pi\tau} = \frac{f_0}{\pi D}$$

For all three waveforms $D = 1/2$. For the 10 MHz waveform, the first break point occurs at 6.37 MHz. For the 1 MHz waveform, the first break frequency occurs at 637 kHz. The second break frequency occurs at $1/\pi\tau_r$ and depends only on the risetime. For the 20 ns risetime, the second breakpoint occurs at 15.9 MHz, and for the 5 ns risetime, the second breakpoint occurs at 63.66 MHz. These are shown in Fig. 3.23.

Next, we interpolate to find the level at 98 MHz. For the 10 MHz waveform and 20 ns rise/falltimes, the level at 98 MHz is

$$\begin{aligned}
\text{Level}_{110\text{ MHz}} &= 20\log_{10}(10^6\ \mu\text{V}) - 20\log_{10}\left(\frac{15.9\text{ MHz}}{6.37\text{ MHz}}\right) - 40\log_{10}\left(\frac{110\text{ MHz}}{15.9\text{ MHz}}\right) \\
&= 120\text{ dB}\mu\text{V} - 7.95\text{ dB} - 33.6\text{ dB} \\
&= 78.45\text{ dB}\mu\text{V}
\end{aligned}$$

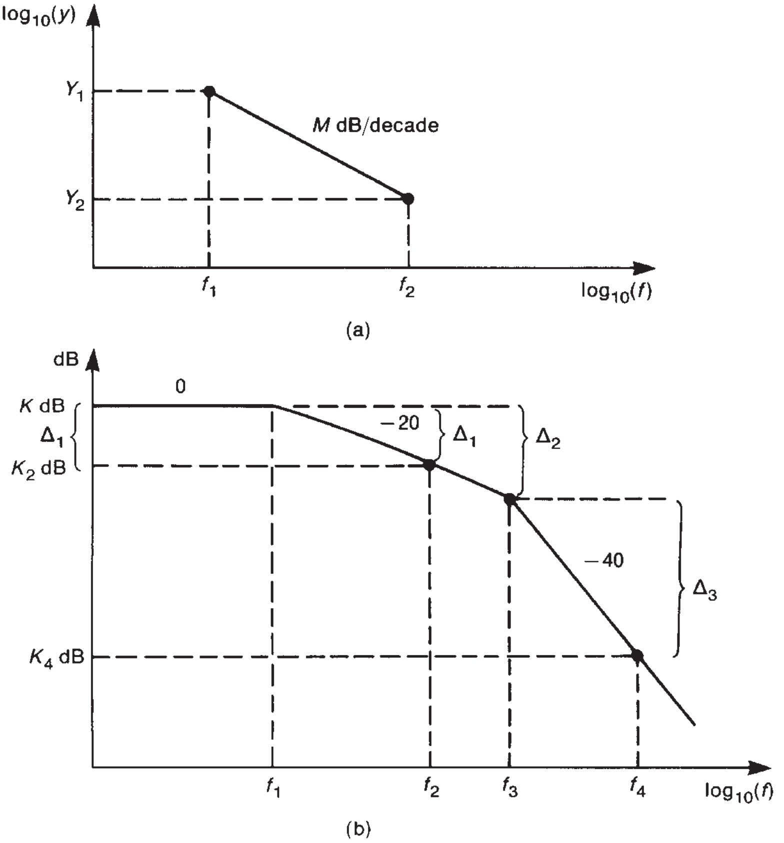

FIGURE 3.22 Illustration of interpolation on log–log (Bode) plots: (a) the general characterization of a linear segment and (b) application to the spectral bounds for a trapezoidal pulse train.

The level at 98 MHz for the 5 ns rise/falltime pulse is

$$
\begin{aligned}
\text{Level}_{110\,\text{MHz}} &= 20\log_{10}(10^6\,\mu\text{V}) - 20\log_{10}\left(\frac{63.7\,\text{MHz}}{6.37\,\text{MHz}}\right) - 40\log_{10}\left(\frac{110\,\text{MHz}}{63.7\,\text{MHz}}\right)\\
&= 120\,\text{dB}\mu\text{V} - 20\,\text{dB} - 9.49\,\text{dB}\\
&= 90.5\,\text{dB}\mu\text{V}
\end{aligned}
$$

which is an increase of 12 dB. The exact values computed using (3.48b) are 73.8 dBμV ($\tau_r = \tau_f = 20$ ns) and 90.4 dBμV ($\tau_r = \tau_f = 5$ ns), which are reasonably close to the bounds. The measured values shown in Fig. 3.21 are reasonably close to these. For example, the measured value for the 11th harmonic (98 MHz) for $\tau_r = \tau_f = 20$ ns is 68.0 dBμV, which is some 6 dB lower than the exact value of 73.8 dBμV. Since the spectrum analyzer measures RMS levels, the computed value of 73.8 dBμV is 70.8 dBμV RMS (subtract 3.01 dB to go from peak to RMS), which is within 2 dB of the measured value! Similarly, the measured value for the 11th harmonic (98 MHz) for $\tau_r = \tau_f = 5$ ns is 86.1 dBμV, which is some 4 dB lower than the exact value of 90.4 dBμV. Again, since the spectrum analyzer measures rms levels, the computed value of 90.4 dBμV is 87.4 dBμV RMS, which is within 1 dB of the measured value!

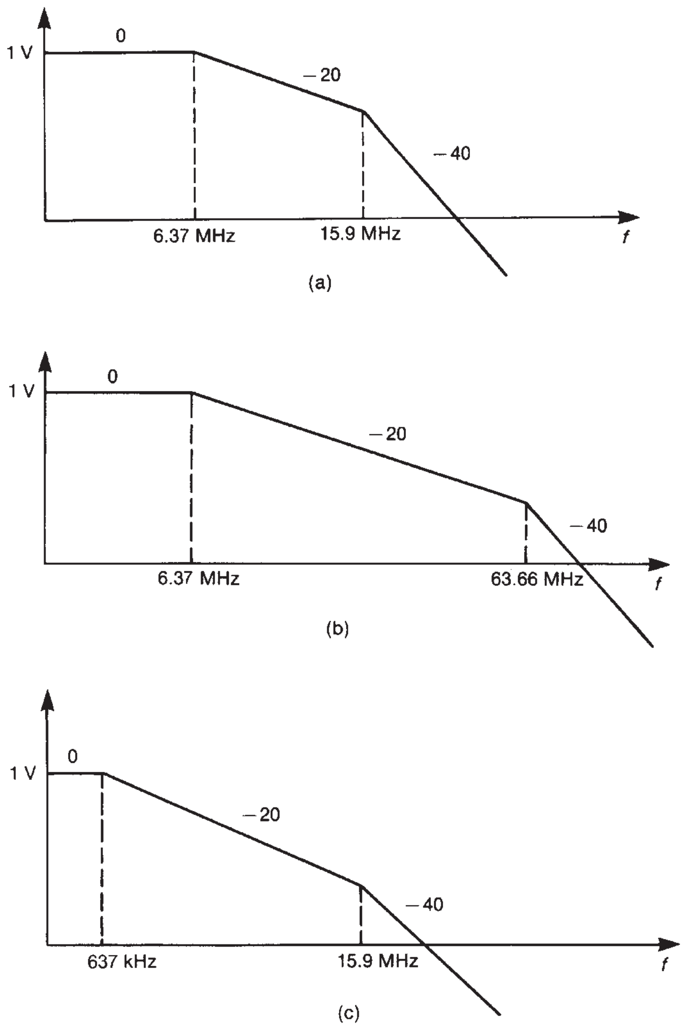

FIGURE 3.23 Example 3.5 illustrating the effect of rise/falltimes and repetition rate on the spectral content of 1 V, 50%-duty-cycle trapezoidal pulse trains; (a) 10 MHz, $\tau_r = \tau_f = 20$ ns; (b) 10 MHz, $\tau_r = \tau_f = 5$ ns; and (c) 1 MHz, $\tau_r = \tau_f = 20$ ns.

Figure 3.23c shows the effect of reducing the repetition rate of the 10 MHz pulse train to 1 MHz (the rise/falltimes remain at 20 ns and the duty cycle remains at 50%). The level at 98 MHz is

$$\begin{aligned}\text{Level}_{110\,\text{MHz}} &= 20\log_{10}(10^6\ \mu\text{V}) - 20\log_{10}\left(\frac{15.9\,\text{MHz}}{637\ \text{kHz}}\right) - 40\log_{10}\left(\frac{110\,\text{MHz}}{15.9\,\text{MHz}}\right)\\ &= 120\,\text{dB}\mu\text{V} - 28\,\text{dB} - 33.6\,\text{dB}\\ &= 58.4\,\text{dB}\mu\text{V}\end{aligned}$$

This is a reduction of 78–58 or 20 dB over the 10 MHz, 20 ns pulse train. So, reducing the fundamental frequency also reduces the high-frequency spectral content. Ordinarily, we do not have the option of changing the fundamental (clock) frequency of the design.

Review Exercise 3.2 Determine the level of the 15th harmonic for a 5 V, 100 MHz, 50%-duty-cycle trapezoidal waveform having rise/falltimes of 1 ns by (a) the exact result in (3.48) and (b) interpolation.

***Answers*:** (a) 93.07 dBμV, (b) 93.07 dBμV.

3.2.2.2 ***Bandwidth of Digital Waveforms*** It is clear from the Fourier series that in order to completely reconstruct a time-domain waveform from its spectral content, we must sum an *infinite* number of harmonics. Clearly, this is not practical. If we continue to add spectral harmonics to the sum, the resulting time-domain waveform gets closer to the actual complete waveform. (There is a phenomenon known as *Gibb's phenomenon*, which occurs at points in a waveform that are discontinuous such as the rising and falling edges of a square wave. The ideal square wave has zero rise/falltimes, and continually adding harmonics will not result in convergence to ideal waveforms at these abrupt discontinuities.) The important question is how many of the harmonics must we add in order to reconstruct a waveform that is in some fashion a reasonable approximation to the actual time-domain waveform? A fundamental property of the Fourier series and the way the coefficients are computed as in (3.12) is that this choice of the coefficients will minimize the integral squared error (ISE) between the actual waveform and the approximate one using the first N coefficients [2]. The ISE is

$$\text{ISE} = \int_{t_1}^{t_1+T} [x(t) - \overline{x}(t)]^2 \, dt$$

where the finite N-term expansion is denoted as

$$\overline{x}(t) = \sum_{n=-N}^{N} c_n \phi_n(t)$$

The expansion coefficients are *orthogonal functions* by choice, and orthogonal basis functions have the important property of minimizing the approximation error when we truncate the expansion; that is, use a finite number of expansion terms or spectral components. The ISE reflects the fact that "positive error" at a particular time t_i [i.e., $x(t_i) > \overline{x}(t_i)$] is as bad as a "negative error" [i.e., $\overline{x}(t_i) > x(t_i)$]. But this does not really give a measure of how close the approximation is to the actual function *at individual points*; that is, we might have very close agreement at almost every time-point but have an extraordinarily large error at a few points and yet the ISE may look "good." Perhaps the best we can do is to include the harmonics up to a point, truncate the sum, and see how well the reconstructed function matches the actual waveform.

If we look at the spectral bound model of a digital (trapezoidal) waveform shown in Fig. 3.19, we see that above the second breakpoint, $1/\pi\tau_r$, the harmonics drop off at a rate of −40 dB/decade. Hence, if we remove spectral components above this, the time-domain waveform would probably not be "sufficiently distorted" from the actual waveform. To be conservative, we might choose a point, say, 3 times this second breakpoint or $3/\pi\tau_r$. But this is approximately $1/\tau_r$. Hence, we might choose as the "bandwidth" of this digital clock signal

$$\text{BW} = \frac{1}{\tau_r} \text{ Hz} \tag{3.55}$$

For example, a signal having a rise/falltime of 1 ns would have, by this criterion, a bandwidth of 1 GHz. Others have chosen a criterion for bandwidth as $0.5/\tau_r$. (See Chapter 1 Ref. 14.) This criterion is not meant to be a hard criterion but is to be used only as a guide to estimate how much of the spectrum is needed to produce an "accurate" reproduction of the time-domain waveform. It is interesting to observe from (3.48) that the first null in the true spectrum occurs at $f = 1/\tau_r$ (substitute $n\pi\tau_r/T \rightarrow \pi f\tau_r$ in the second $\sin x/x$ term).

In order to investigate this behavior, we show, in Fig. 3.24a, a comparison of reconstructing a trapezoidal waveform using only the spectral components up to a frequency of $1/\tau_r$ for a 100-MHz, 50%-duty-cycle, 5 V trapezoidal (clock) waveform having 1 ns rise/falltimes. Typically, the lower frequencies of the spectrum affect the level of the pulse, while the higher frequencies affect the sharp edges. So, eliminating the high-frequency components of the spectrum tends to roll off the sharp edges and hence affect the representation of the pulse transition regions. Eliminating high-frequency components is like passing the waveform through a lowpass filter; the sharp corners at the transitions will be rounded. Using the criterion for bandwidth given in (3.55) gives a bandwidth of $\mathrm{BW} = 1/1\ \mathrm{ns} = 1\ \mathrm{GHz}$. If we discard all harmonics above this and sum the lower 10 harmonics, 100 MHz, 200 MHz, …, 1000 MHz, to reconstruct the waveform, we obtain the result shown in Fig. 3.24a. Observe that the truncated series approximates the actual waveform rather well. The discrepancies occur at the rise/falltimes resulting in slight overshoot or undershoot. Figure 3.24b shows the reconstruction using the alternative bandwidth of $\mathrm{BW} = 0.5/1\ \mathrm{ns} = 500\ \mathrm{MHz}$, that is, summing the first five harmonics. Clearly, this criterion does not reproduce the waveform as well as does the criterion in (3.55).

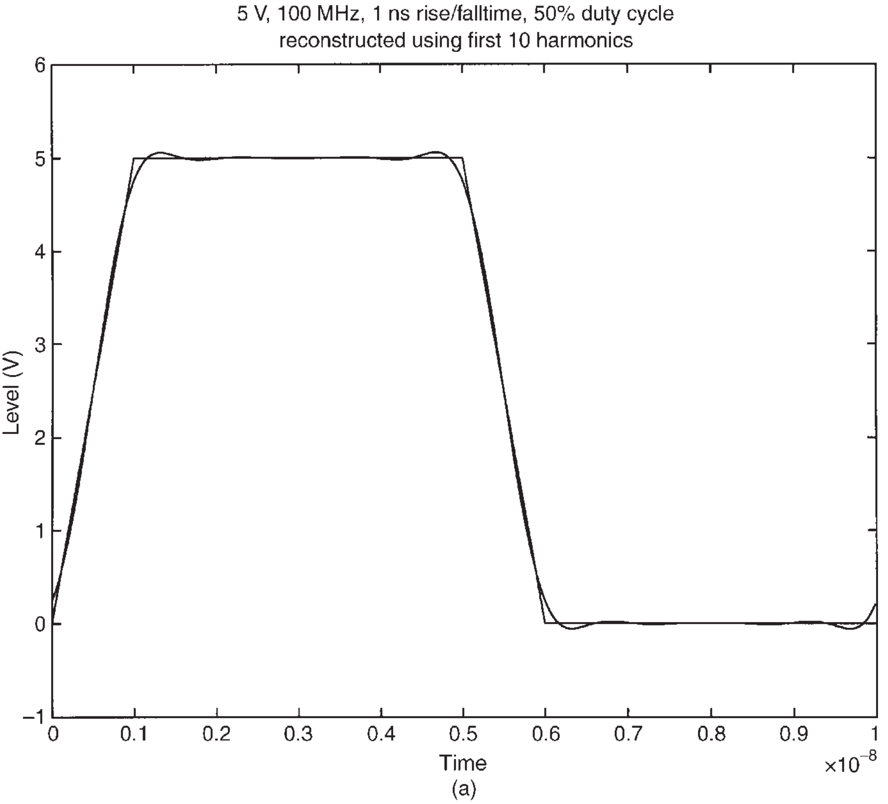

FIGURE 3.24 Reconstruction of a 5 V, 100 MHz, 1 ns rise/falltime, 50%-duty-cycle trapezoidal pulse train: (a) using first 10 harmonics and (b) using first 5 harmonics.

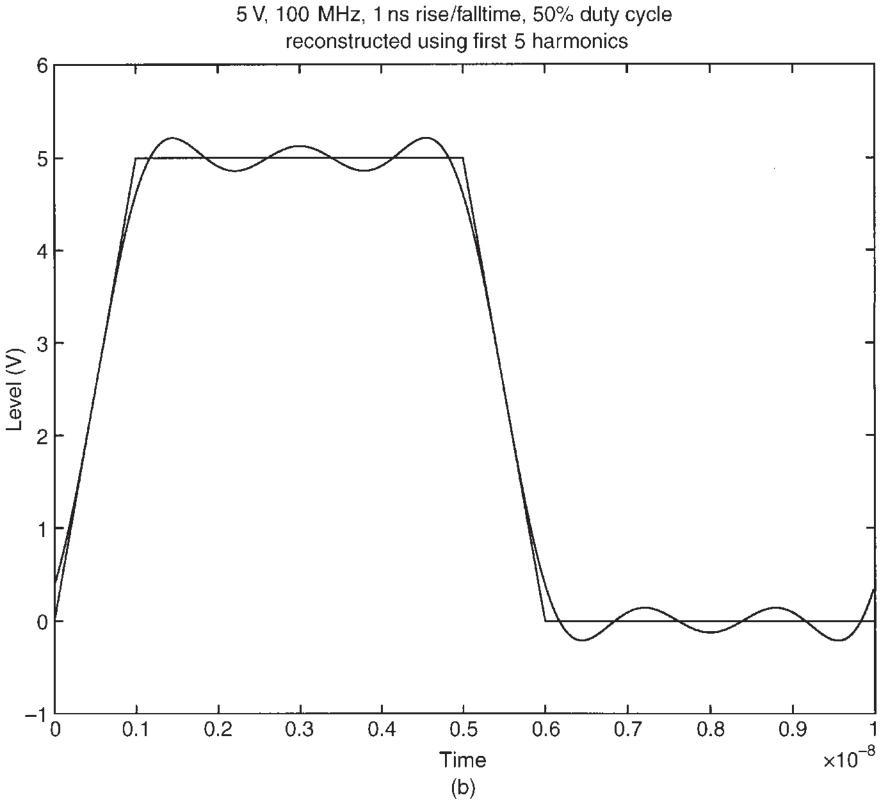

FIGURE 3.24 (*Continued*)

It is interesting to compute the average power in the waveform assuming a 50% duty cycle and $\tau_r = \tau_f$:

$$
\begin{aligned}
P_{av} &= \frac{1}{T}\int_0^T x^2(t)\,dt \\
&= V^2\left[\frac{1}{2} - \frac{1}{3}\frac{\tau_r}{T}\right] \text{ W}
\end{aligned}
\tag{3.56}
$$

Substituting $V = 5$ V, $\tau_r = 1$ ns, $T = 10$ ns gives a total average power in the waveform of 11.667 W. The Fourier coefficients for the first 10 harmonics are, from (3.48b),

$$
\begin{aligned}
c_0 &= 2.5 \\
c_1^+ &= 3.131 \\
c_3^+ &= 0.9108 \\
c_5^+ &= 0.4053 \\
c_7^+ &= 0.1673 \\
c_9^+ &= 0.03865
\end{aligned}
$$

and the even harmonics are zero because of the 50% duty cycle. The average power in the truncated series is the sum of the average powers in the sinusoidal components:

$$\begin{aligned} P_{av} &= c_0^2 + \frac{1}{2}c_1^{+2} + \frac{1}{2}c_3^{+2} + \frac{1}{2}c_5^{+2} + \frac{1}{2}c_7^{+2} + \frac{1}{2}c_9^{+2} \\ &= 11.663\ \mathrm{W} \end{aligned}$$

Hence, the average power in the truncated series is 99.97% of the total average power in the periodic waveform. In the alternative criterion of bandwidth, $\mathrm{BW} = 0.5/\tau_r$, the average power in this truncated sum consisting of 5 harmonics is 11.648 W or 99.84% of the total. In both cases, the truncated series contains virtually all the average power in the complete waveform, so that looking at the average power contained in the truncated series is not a satisfactory criterion for judging its ability to reproduce the waveform and hence the bandwidth. In fact, for this waveform, 96% of the total average power of the waveform is contained in the dc term and the first harmonic.

Review Exercise 3.3 For a trapezoidal waveform having equal rise- and falltimes, determine how much the bound is down at $f = 1/\tau_r$ from the level at the second breakpoint of $1/\pi\tau_r$.

***Answer*:** 19.89 dB.

3.2.2.3 Effect of Repetition Rate and Duty Cycle

One effect of a change in the repetition rate (frequency) of the pulse train is to change the spacing between the discrete harmonics. Also, note that the starting or dc level of the spectral bound is $20\log_{10}(2A\tau/T) = 20\log_{10}(2AD)$, where

$$D = \frac{\tau}{T} \tag{3.57}$$

is the duty cycle. Writing the one-sided spectrum for the trapezoidal waveform given in (3.48b) in terms of the duty cycle D gives

$$\begin{aligned} |c_n^+| &= 2\ AD\left|\frac{\sin(n\pi D)}{n\pi D}\right|\left|\frac{\sin(n\pi\tau_r f_0)}{n\pi\tau_r f_0}\right| \quad \text{for } n \neq 0 \\ c_0 &= AD \end{aligned} \tag{3.58}$$

where $f_0 = 1/T$ is the fundamental frequency of the waveform. Usually, when the frequency of the wave is reduced (the period is increased), the pulsewidth is similarly increased to maintain the same duty cycle, say, 50%. Therefore, reducing the frequency of the pulse train (increasing the period T) does not usually affect the starting level. However, if the frequency of the wave is reduced and the duty cycle remains the same, the pulsewidth will be increased. This has the effect of moving the first breakpoint in the spectral bound, $1/\pi\tau$, down in frequency, so that part of the spectral content in the region of 0 dB/decade now rolls of at a rate of −20 dB/decade.

Figure 3.25 illustrates the effect of the pulse train duty cycle D on the spectral bounds. The first breakpoint in the spectral bound, $1/\pi\tau$, can be written in terms of the duty cycle $D = \tau/T$ and the

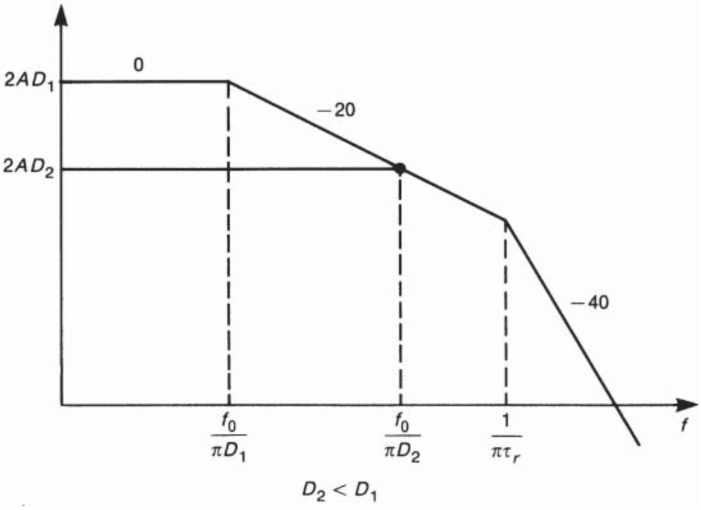

FIGURE 3.25 Illustration of the effect of duty cycle on the spectral bounds of trapezoidal pulse trains.

fundamental frequency of the waveform, $f_0 = 1/T$, as $1/\pi\tau = f_0/\pi D$. Recall that the starting level of the 0 dB/decade segment is $2AD$. Therefore, if we reduce the pulsewidth (reduce the duty cycle), we will lower the starting level and will also move the first breakpoint out in frequency as shown in Fig. 3.25, where $D_1 > D_2$. It is a simple matter to show that the first breakpoint for the smaller duty cycle D_2 will lie on the −20 dB/decade segment for the larger duty cycle D_1, as we have indicated in Fig. 3.25. Therefore, *reducing the duty cycle (the pulsewidth) reduces the low-frequency spectral content of the waveform, but does not affect the high-frequency content*. See the computed results in Fig. 3.20.

3.2.2.4 Effect of Ringing (Undershoot/Overshoot) Inductance and capacitance of PCB lands and wires in a digital system can cause a phenomenon referred to as *ringing*. This is illustrated in Fig. 3.26a for a square wave. As the signal level transitions from one logic level to another, there is a tendency for the signal level to oscillate about the desired level. Losses tend to damp this *ringing*. This type of waveform can be described mathematically as a function of the form $Ke^{-\alpha t}\sin(\omega_r t)$, where α is a damping coefficient and $f_r = \omega_r/2\pi$ is the frequency of the ringing. Quite often a discrete resistor is placed in series with the output land of the driving gate to damp this and provide a smooth transition. An example of the utility of this is given in [1, Example 9.11, p. 550] and in Section 4.4.2 of Chapter 4.

The purpose of this section is to investigate the effect of such ringing on the spectral content of the waveform. We will find that this ringing tends to accentuate or enhance certain regions of the spectrum of the original waveform. This reason combined with the detrimental effect on the functional performance of the system require that we try to prevent this ringing by the use of series resistors or ferrite beads or by matching the transmission line.

Determining the spectrum of the waveform of Fig. 3.26a is made simple by recognizing that it is the sum of three, periodic waveforms: a square wave, a damped sinusoid of the form $Ke^{-\alpha t}\sin(\omega_r t)$, and the same damped sinusoid negated and shifted ahead in t by $(1/2)T$. Using superposition, the

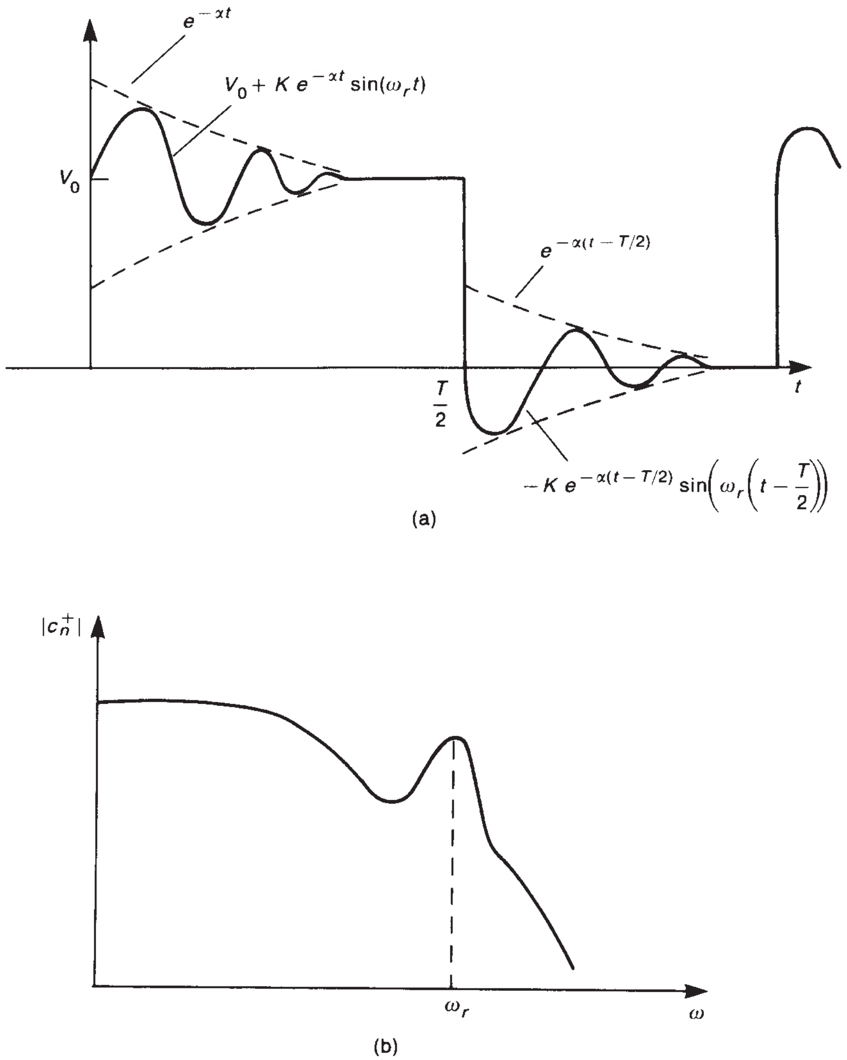

FIGURE 3.26 Illustration of ringing (undershoot/overshoot): (a) time-domain waveform and (b) spectral content.

expansion coefficients of the composite waveform are the sums of the expansion coefficients for the three components:

$$\begin{aligned} c_n &= c_{n\,\text{square wave}} \\ &\quad + \frac{1}{T}\int_0^{T/2} Ke^{-\alpha t}\sin(\omega_r t)e^{-jn\omega_0 t}\,dt \\ &\quad - e^{-jn\omega_0 T/2}\left[\frac{1}{T}\int_0^{T/2} Ke^{-\alpha t}\sin(\omega_r t)e^{-jn\omega_0 t}\,dt\right] \end{aligned}$$

$$
\begin{aligned}
&= c_{n\ \text{square wave}} + (1 - e^{-jn\omega_0 T/2})\frac{1}{T}\int_0^{T/2} K e^{-\alpha t}\sin(\omega_r t) e^{-jn\omega_0 t}\,dt \\
&= \frac{V_0}{2}\frac{\sin(n\omega_0 T/4)}{n\omega_0 T/4}e^{-jn\omega_0 T/4} + \frac{K}{2}\frac{\sin(n\omega_0 T/4)}{n\omega_0 T/4}e^{-jn\omega_0 T/4}\frac{p\omega_r}{p^2 + 2\alpha p + \alpha^2 + \omega_r^2} \\
&= \underbrace{\frac{V_0}{2}\frac{\sin(n\omega_0 T/4)}{n\omega_0 T/4}e^{-jn\omega_0 T/4}}_{c_{n\ \text{square wave}}}\frac{p^2 + [2\alpha + (K/V_0)\omega_r]p + \alpha^2 + \omega_r^2}{p^2 + 2\alpha p + \alpha^2 + \omega_r^2}
\end{aligned}
\tag{3.59}
$$

where $p = jn\omega_0$ in the latter expression and we have assumed, to simplify the result, that $e^{-\alpha T/2} \ll 1$ and a 50% duty cycle. This last result shows that the expansion coefficients are the sum of those for the square wave with no undershoot/overshoot and a similar waveform that is multiplied by a *bandpass* transfer function centered about a radian frequency $\omega = \sqrt{\alpha^2 + \omega_r^2} \cong \omega_r$. Consequently, the spectrum of a square wave with undershoot/overshoot has a part of its spectrum *enhanced* or increased about the *ringing frequency* ω_r, as illustrated in Fig. 3.26b. Consequently, undershoot/overshoot will have the effect of increasing the emissions about the ringing frequency. Quite often we see in the radiated emission profile a seemingly resonant region of enhanced emissions in a narrow frequency band. One possible explanation for this is the undershoot/overshoot present on the digital waveforms. Thus, we should try to eliminate this – if not for functional performance reasons, then certainly for EMC reasons.

Review Exercise 3.4 Determine the increase (in dB) of the spectrum in Fig. 3.26b due to a 1-MHz square wave having $V_0 = 5$ V, a 50% duty cycle, and a ringing waveform having $K = 0.5$ V, $f_r = 30$ MHz, and $\alpha = 10 \times 10^6$.

***Answer*:** 5.76 dB.

3.2.3 Use of Spectral Bounds in Computing Bounds on the Output Spectrum of a Linear System

It is possible to generate spectral bounds for other types of commonly occurring signals. Nevertheless, even though a periodic signal will have frequencies that occur only at multiples of the basic repetition rate, the use of smooth piecewise-linear segments plotted on a log–log format has considerable advantage in estimating the spectral content of the output of a linear system when the signal is the input to the system. This section illustrates this important point and the concepts associated with it.

A linear system having input $x(t)$, output $y(t)$, and impulse response $h(t)$ has an output spectrum

$$Y(jn\omega_0) = H(jn\omega_0)\ X(jn\omega_0) \tag{3.60}$$

Thus, the magnitude and phase spectrum of the output are

$$|Y(jn\omega_0)| = |H(jn\omega_0)| \times |X(jn\omega_0)| \tag{3.61a}$$

$$\underline{/Y(jn\omega_0)} = \underline{/H(jn\omega_0)} + \underline{/X(jn\omega_0)} \tag{3.61b}$$

Eq. (3.61a) shows that the magnitude spectrum of the output is the product of the magnitude spectra of the input and impulse response (transfer function). On a log–log or Bode plot, the output spectrum is the *sum* of the input and transfer function spectra, since

$$20\log_{10}|Y(jn\omega_0)| = 20\log_{10}|H(jn\omega_0)| + 20\log_{10}|X(jn\omega_0)| \tag{3.62}$$

Therefore, we simply add the Bode plots of the input and transfer function magnitude spectra [1].

As an example, consider the circuit shown in Fig. 3.9a. The bound on the magnitude spectrum of the output is the sum of the input and transfer function magnitude bounds, as shown in Fig. 3.27a.

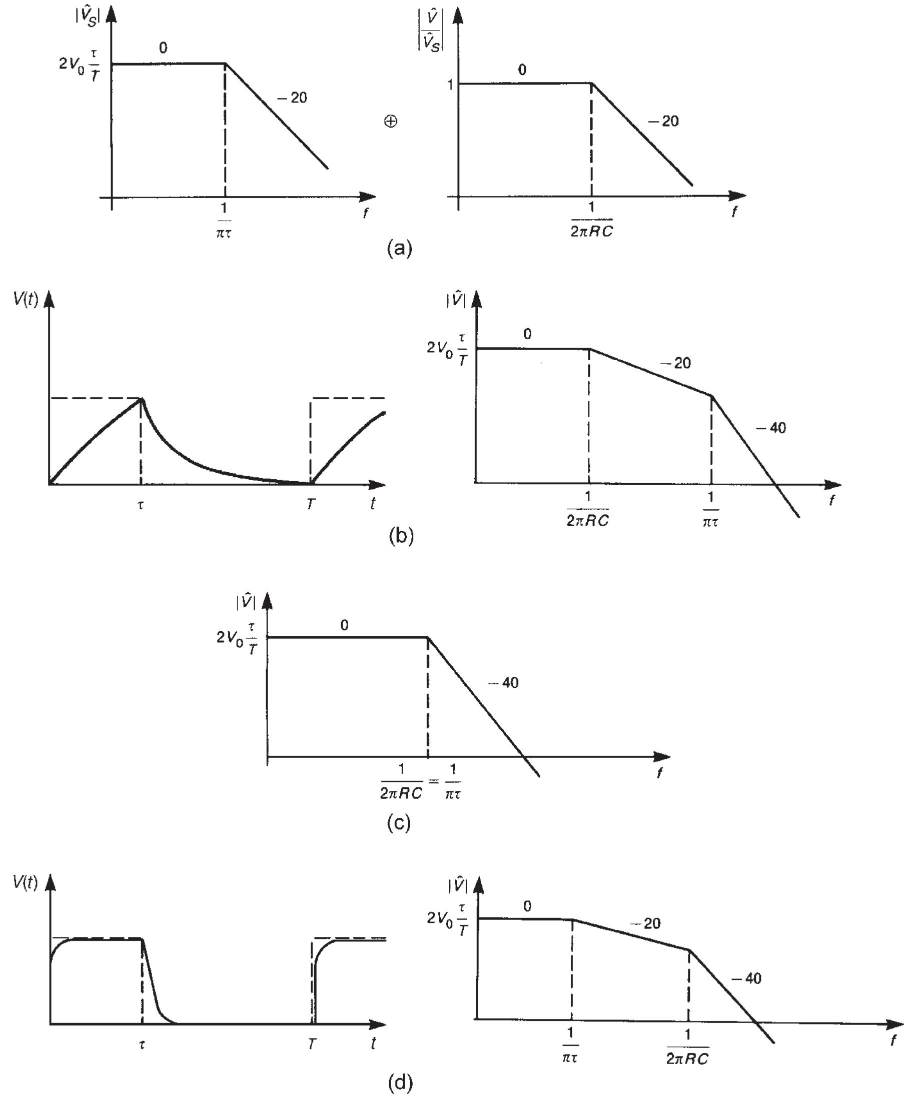

FIGURE 3.27 Illustration of the estimation of processing of a signal by linear systems using spectral bounds and Bode plots for a square-wave input and a lowpass RC circuit: (a) the input and the transfer function; (b) $RC > (1/2)\tau$; (c) $RC = (1/2)\tau$; and (d) $RC < (1/2)\tau$.

Depending on the relative breakpoints, $1/\pi\tau$ and $1/2\pi RC$, we have the three possibilities for the output magnitude spectrum shown in Figs. 3.27b–d. From this result, it is clear that if we want to significantly reduce the high frequency of the output, we would choose the time constant much greater than the pulsewidth: $RC \gg \tau$. This satisfies our intuition, since it will mean that the capacitor has not had sufficient time to charge up to its final value before the pulse switches off. Thus, the output will appear as a "sawtooth" waveform rather than a square wave, and will consequently have less high-frequency spectral content. On the other hand, if we choose the time constant much less than the pulsewidth, $RC \ll \tau$, then only the high-frequency components (above $1/\pi\tau$) will be diminished as shown in Fig. 3.27d. Hence, the output waveform will resemble the input waveform with smoothed transitions.

Review Exercise 3.5 A 10 MHz square wave is passed through a lowpass filter as shown in Fig. E3.5. If the square wave has a duty cycle of 50%, determine the value of R such that output voltage is not significantly distorted.

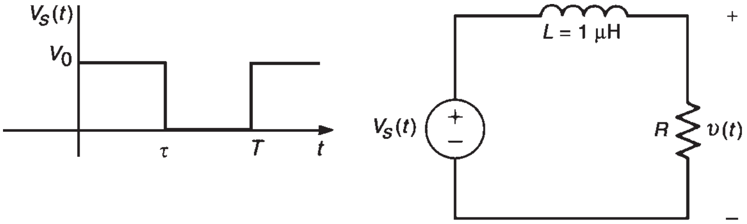

FIGURE E3.5 Review Exercise 3.5.

***Answer*:** $R > 40\ \Omega$.

3.3 SPECTRUM ANALYZERS

Spectrum analyzers are devices that display the *magnitude spectrum for periodic signals*. These devices are basically *radio receivers having a bandpass filter that is swept in time*. (A spectrum analyzer is essentially a superheterodyne receiver wherein the desired signal is mixed with a swept local oscillator and transferred to a lower, fixed intermediate frequency. However, viewing the device as being simply a bandpass filter swept in time gives a simple understanding of the device function.) A photograph of a typical spectrum analyzer is shown in Fig. 3.28a. Figure 3.28b illustrates the point that a bandpass filter whose center frequency is swept in time from the start frequency to the end frequency (chosen by the operator) selects and displays the spectral components of the input signal that are present *within the bandwidth of the instrument at the point in the time of the sweep*. Figure 3.28c shows the measured spectrum of a periodic, trapezoidal 1 MHz, 1 V, 50%-duty-cycle waveform whose rise/falltimes are 12.5 ns (10 ns between the 10% and 90% points). Note the even harmonics of much lower amplitude than the odd harmonics that appear "in the background." Also, observe the typical $(\sin x)/x$ behavior of the envelope. The sweep is from dc to 150 MHz, and a null appears at approximately 80 MHz. This is reasonable to expect, since the magnitude of the one-sided spectrum is given in (3.48). The first $(\sin x)/x$ term is zero where $\pi\tau f = \pi$ or $f = 1/\tau = 2$ MHz. The second $(\sin x)/x$ term is zero where $\pi\tau_r f = \pi$ or $f = 1/\tau_r = 80$ MHz. The deep understanding we now have concerning spectra easily explains seemingly strange results such as these. From the exact result in (3.48), we compute a level at the 15th harmonic (15 MHz) of 92 dBμV, which compares well with the measured value of $87 + 3 = 90$ dBμV (add 3 dB since the spectrum analyzer measures RMS values).

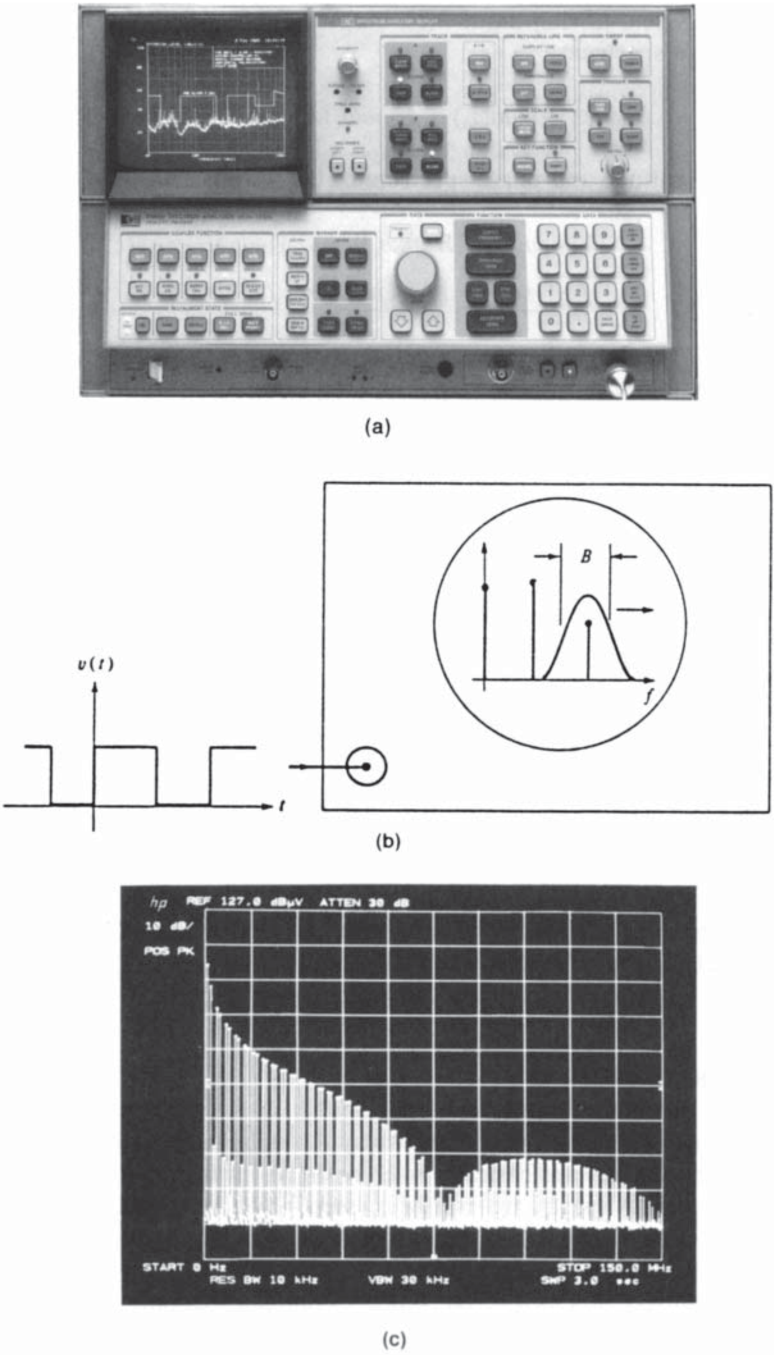
(a)
v(t)
t
B
f
(b)
hp REF 127.0 dBµV ATTEN 30 dB
10 dB/
POS PK
START 0 Hz
RES BW 10 kHz
VBW 30 kHz
STOP 150.0 MHz
SWP 3.0 sec
(c)

FIGURE 3.28 A spectrum analyzer: (a) photograph (courtesy of the Hewlett-Packard Company). Source: Courtesy of the Hewlett-Packard Company; (b) illustration of the function as a swept bandpass filter; and (c) measured spectrum of a 1 V, 1 MHz, 50%-duty-cycle, $\tau_r = \tau_f$ 12.5-ns trapezoidal pulse train.

3.3.1 Basic Principles

Let us now examine more closely the effect of a swept bandpass filter on the “spectrum” that the spectrum analyzer will display. This is critically important in complying with the regulatory limits on conducted and radiated emissions since the ultimate test of success is whether any *measured level* exceeds the regulatory limit at that frequency. We will refer to the term “spectrum analyzer” as SA in this section.

A key ingredient in determining the level that is displayed by the SA at that frequency is the *bandwidth* of the SA (chosen by the operator). This is illustrated in Fig. 3.29. The bandwidth is the 6 dB bandwidth, where the response is reduced by 6 dB from its maximum level at the center frequency. Let us “freeze” the sweep of the SA at some point in its cycle. Suppose at this time that three harmonics are within the bandwidth of the filter at this point in the sweep. The *displayed level at the center frequency of the bandwidth will be the sum of the spectral levels that fall within the bandwidth of the filter at that time*. Thus, even though there are no spectral components at the center

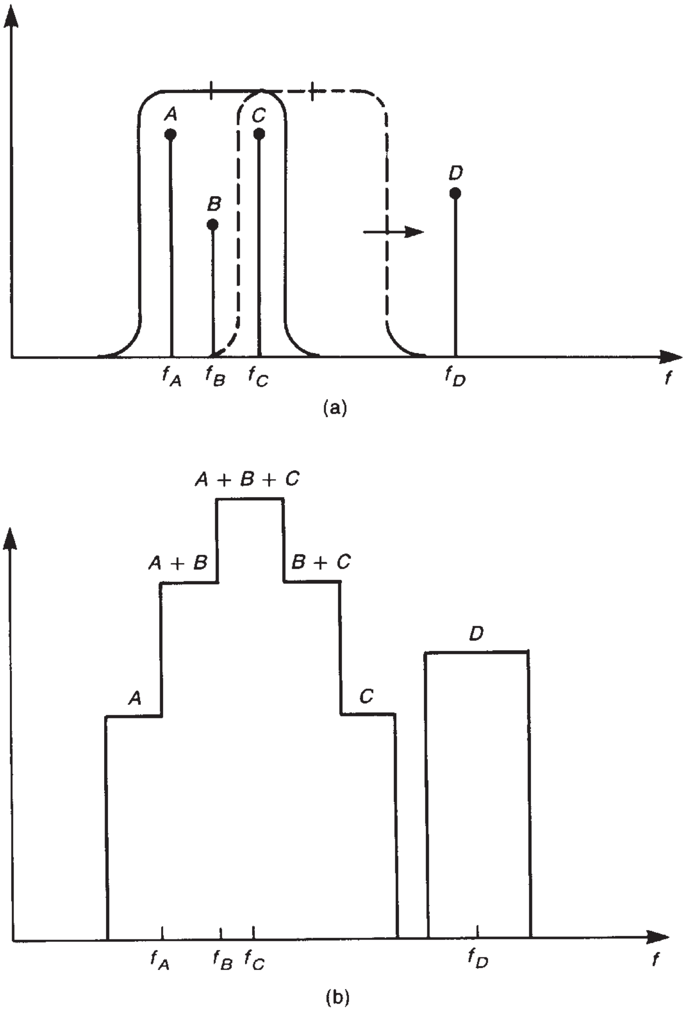

FIGURE 3.29 Illustration of the effect of bandwidth on measured spectrum: (a) a bandwidth that is wide enough to contain several narrowband signals and (b) the resulting display.

TABLE 3.1 FCC Minimum Spectrum Analyzer Bandwidths (6 dB)

Radiated emissions:	30 MHz–1 GHz	120 kHz
Radiated emissions:	> GHz	1 MHz
Conducted emissions:	150 kHz–30 MHz	9 kHz

TABLE 3.2 CISPR 32 Minimum Spectrum Analyzer Bandwidths (6 dB)

Radiated emissions:	30 MHz–1 GHz	120 kHz
Conducted emissions:	150 kHz–30 MHz	9 kHz

frequency of the bandwidth f, the SA will show, *at frequency f*, a level of $A+B+C$. As the filter moves further to the right in its sweep, level A will "drop out" and will show a total of $B+C$. As it moves further to the right, level B will "drop out" and the displayed level will be C. The result is shown in Fig. 3.29b. This shows the important point that *in order to obtain the lowest possible level on the SA display, we should choose as small a bandwidth as possible*! The regulatory agencies realize this so they set a minimum bandwidth to be used for the measurement. (It would not be sensible to use a SA bandwidth larger than this minimum bandwidth, since the measured levels would then be larger.) The minimum bandwidths for the FCC and CISPR 32 regulations are given in Tables 3.1 and 3.2. These are 6 dB bandwidths.

The fact that *the SA adds all spectral levels within the bandwidth of the instrument at that point in its sweep and displays the sum as the level at the center frequency of the filter* illustrates the following important point. *We should attempt to choose clock and data repetition rates such that none of the harmonics of any signal in the system will be closer than the measurement bandwidth of the SA*! As an example, suppose that there are two clock oscillators in the product and we choose both to have a frequency of 10 MHz. Each clock signal may radiate from different parts of the system so that the total received signal at the measurement antenna is the sum of these emissions. Suppose that the received levels at the antenna are due to radiations from two different points in the product and are of equal strength. The displayed signal at 10 MHz, 20 MHz, 30 MHz, … will be 6 dB larger than for one signal. To reduce this, suppose that we have an asynchronous communication channel and do not require clocks of the same frequency. If we choose one clock frequency to be 10 MHz and the other to be 15 MHz, we may still have a problem, although it will not be as severe as for identical clock frequencies. The emissions will now occur at 10 MHz, 15 MHz, 20 MHz, 30 MHz, …. Each one of these comes from a different point in the system, and they are separated by more than the required minimum bandwidth of the SA (103 kHz). On closer examination, we realize that the ninth harmonic of the 10 MHz oscillator, 90 MHz, and the sixth harmonic of the 15 MHz oscillator, also 90 MHz, will add, causing a 6 dB maximum increase in level over that obtained if they did not add within the bandwidth.

Even though the amplitudes of the two harmonics that fall within the bandwidth of the SA are not of the exact same level, a potentially significant increase in measured level will be experienced. Table 3.3 illustrates that even though the two levels are widely different, a significant increase may occur. This occurs because the SA adds the absolute levels and converts the sum to dB. This table is prepared assuming the two signals to be in phase, and thus gives upper bounds on this summation. The results are obtained by first converting the signal amplitudes to absolute levels, adding them, and then converting the result to dB. This represents the way a SA actually adds signals in its bandwidth. Observe that even though two signals differ in level by 10 dB (a ratio of 3.16), they will add to give an increase of 2.39 dB over the level of the large signal! So, it is important to ensure that no two

TABLE 3.3 The Effect of the Addition of Two Unequal Level Signals

Differences in signal levels (dB)	Increase in dB over the larger of the two
0	6.02
1	5.53
2	5.08
3	4.65
4	4.25
5	3.88
6	3.53
7	3.21
8	2.91
9	2.64
10	2.39
18.3	1.0

harmonics are within the bandwidth of the SA of each other. This will make the job of complying with the regulatory limits easier.

A simple method of determining whether two or more signals are adding within the bandwidth of the SA is to narrow the bandwidth of the receiver. (For the purposes of this test, we can lower the bandwidth of the SA below the minimum required by the regulatory agency for this test, since we are only trying to determine whether the viewed signal is due to this addition of two or more harmonics.) If, when the bandwidth is reduced, for example, from 103 to 30 kHz, we see no change in any part of the displayed spectrum, then we are assured that no two signal harmonics are adding within the larger bandwidth.

3.3.2 Peak Versus Quasi-Peak Versus Average

Thus far we have been assuming that the *detector* of the SA is set in the *peak mode*. That is, the maximum (actually RMS) of the sinusoidal harmonic is displayed. A simple peak detector is shown in Fig. 3.30a, where the input sinusoid represents a harmonic whose peak level is V_0. The regulatory requirements, however, dictate that the level that is to be compared with the limit to determine compliance is to be measured with a *quasi-peak detector*. A simple quasi-peak detector is illustrated in Fig. 3.30b. Suppose that the received signal consists of "spikes" that are widely separated in time with regard to the time constant RC of the quasi-peak detector. The capacitor will begin to charge until the first spike turns off. It will then discharge through the R. If the next spike occurs after a length of time that allows the capacitor to completely discharge, we will have the first waveform shown at the output of the SA. However, if the spikes occur more closely than the RC time constant, the capacitor will not have fully discharged before the next spike occurs. Thus, the output signal will continue to increase to some limit. Although this is a simplistic illustration of the function of a quasi-peak detector, it nevertheless illustrates the important point that *infrequently occurring signals will result in a measured quasi-peak level that is considerably smaller than a peak detector would give*. Thus, infrequent events (in relation to the time constant) may be of sufficient magnitude to give distressingly large received levels on a SA that is set to the peak detector function, yet their quasi-peak levels may not exceed the regulatory limit and are therefore of no consequence. However, if the quasi-peak levels exceed the regulatory limit, the peak levels will surely exceed that limit.

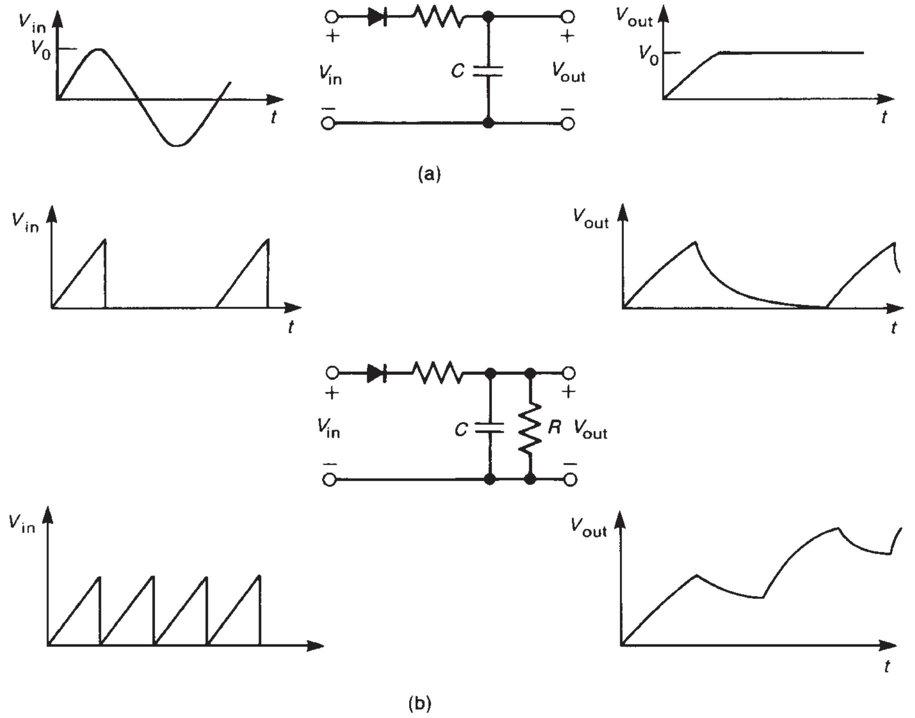

FIGURE 3.30 Two important detectors: (a) the peak detector and (b) the quasi-peak detector.

The reason for the use of a quasi-peak detector function relates to the intent of the regulatory limits, which is to prevent interference in radio and wire communication receivers. Infrequent spikes and other events do not substantially prevent the listener from obtaining the desired information. However, a continuous signal modulation results in a continuous detected signal in the radio and would therefore substantially interfere with the listener's ability to obtain the desired transmitted information.

The FCC and CISPR 22 conducted emission limits are given in quasi-peak (QP) and in average (AV) levels. The average levels are obtained with an average detector. The average detector is basically a 1 Hz lowpass filter, placed after the usual envelope detector, that passes signals whose amplitudes are present for 1 s or more. The problem occurs in digital systems wherein a narrowband emission such as a harmonic of a clock oscillator may be "hiding" under, and at a much lower level than, a broadband emission such as may occur by arcing at the commutator of a dc motor. The average detector will filter out the dc motor noise, revealing the underlying narrowband emission. Of course, we could progressively reduce the SA bandwidth to see the same thing, but that would be a time-consuming process.

3.4 REPRESENTATION OF NONPERIODIC WAVEFORMS

A single pulse occurring only once in time is a nonperiodic signal. Although our major interest will be in periodic signals, which represent the major radiation problems in digital systems, it is of interest to determine the spectral content of nonperiodic signals.

3.4.1 The Fourier Transform

The simplest way to approach this problem of nonperiodic waveforms is to consider a periodic function whose waveshape over one period is the same as the desired nonperiodic signal. Letting the period go to infinity moves the waveforms in adjacent periods further out in time, leaving the desired nonperiodic signal. For example, consider the periodic square-wave pulse train shown in Fig. 3.4, whose spectral components are shown in Fig. 3.5. Suppose that we retain the pulsewidth τ and amplitude A but increase the period T. The complex-exponential Fourier series was obtained earlier. The envelope of spectral components (magnitude) is

$$\text{Envelope} = \frac{A\tau}{T}\frac{\sin(\pi f\tau)}{\pi f\tau} \tag{3.63}$$

Increasing the period lowers the frequency of the fundamental $f_0 = 1/T$ and the harmonics. So, these spectral components move closer together. The basic shape of the envelope remains the same, since it depends on the pulsewidth (which is held constant). As the period is increased indefinitely, individual spectral components merge into a smooth continuous spectrum where the discrete nature of the spectral content disappears. This is the essential result: *The spectrum of a single pulse is a continuum of frequency components.*

This suggests how to handle the case of a single pulse mathematically. First, obtain the complex exponential expansion coefficients, assuming that the pulse repeats itself to give a periodic waveform with period T. Then, let the period go to infinity, $T \to \infty$, in that result, leaving the single pulse. Carrying out this process gives the *Fourier transform* of the signal as [1]

$$\begin{aligned}\mathcal{F}\{x(t)\} &= X(j\omega)\\ &= \int_{-\infty}^{\infty} x(t)e^{-j\omega t}\,dt \end{aligned}\tag{3.64a}$$

where

$$x(t) = \frac{1}{2\pi}\int_{-\infty}^{\infty} X(j\omega)e^{j\omega t}\,d\omega \tag{3.64b}$$

As an application, let us determine the Fourier transform of the single pulse shown in Fig. 3.31a. Directly applying (3.64a) gives

$$\begin{aligned}X(j\omega) &= \int_{0}^{\tau} Ae^{-j\omega t}\,dt\\ &= -\frac{A}{j\omega}(e^{-j\omega t} - 1)\\ &= -\frac{A}{j\omega}e^{-j\omega t/2}(e^{-j\omega t/2} - e^{j\omega t/2})\\ &= A\tau\frac{\sin(\omega\tau/2)}{\omega\tau/2}e^{-j\omega\tau/2}\end{aligned}\tag{3.65}$$

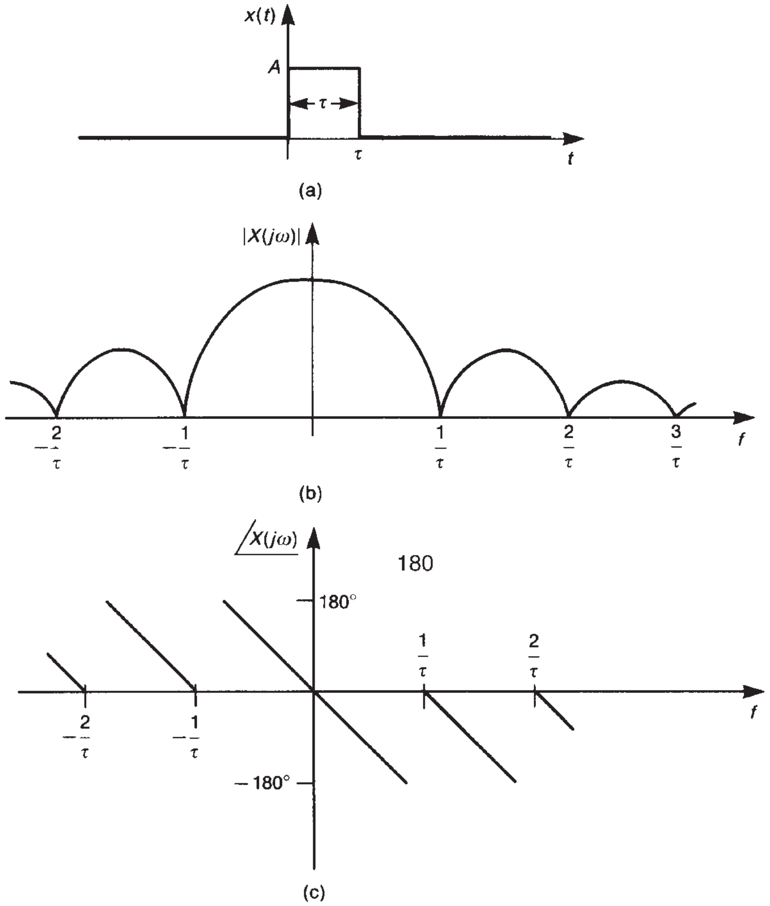

FIGURE 3.31 The Fourier transform of a rectangular pulse: (a) the pulse; (b) the magnitude spectrum; and (c) the phase spectrum.

We have placed the result in the familiar $(\sin x)/x$ form to facilitate plotting. Thus,

$$|X(j\omega)| = A\tau \left| \frac{\sin(\omega\tau/2)}{\omega\tau/2} \right| \tag{3.66a}$$

$$\angle X(j\omega) = \pm\frac{1}{2}\omega\tau \tag{3.66b}$$

These are plotted in Figs. 3.31b, c.

By analogy to the Fourier series, we may view the Fourier transform of a nonperiodic signal as resolving a time function $x(t)$ into a continuum of complex sinusoids. But there is one major difference between the two in this analogy: *The amplitudes of the individual sinusoids are infinitesimally small.* So, it cannot be said that anything is present at a single frequency. But we can visualize individual amplitudes present over some nonzero frequency range $d\omega$ of amplitude $(1/2\pi)\,|X(j\omega)|\,d\omega$ according to Eq. (3.64b).

There are a number of important properties of the Fourier transform that can often be used to simplify its computation. The first of these relates the complex-exponential expansion coefficients and the Fourier transform. *If we know the Fourier transform of a single pulse* $X(j\omega)$*, we can directly obtain the coefficients of the complex-exponential Fourier series of a periodic train of such pulses by replacing* ω *in* $X(j\omega)$*, with* $n\omega_0$ *and dividing the result by the period* T:

$$c_n = \frac{1}{T} X(jn\omega_0) \tag{3.67}$$

There exist a number of tables of Fourier transforms of various pulse shapes. The result in (3.67) allows us to use those tables to obtain the complex-exponential Fourier series expansion coefficients. All of the other properties derived for periodic functions and the Fourier series – linearity, superposition, differentiation, time shifting, impulse functions – apply to the Fourier transform, where we replace the discrete frequency variable $n\omega_0$ with ω and multiply the expansion coefficients c_n by T according to (3.67). Thus, the Fourier transform of piecewise-linear pulses can be easily determined.

Review Exercise 3.6 Determine the Fourier transform of the pulse shown in Fig. E3.6.

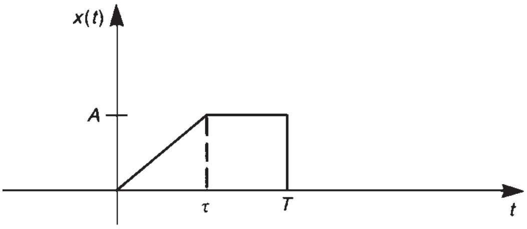

FIGURE E3.6 Review Exercise 3.6.

Answer:

$$X(j\omega) = j\frac{A}{\omega} e^{-j\omega T} - j\frac{A}{\omega} e^{-j\omega\tau/2} \frac{\sin(\omega\tau/2)}{\omega\tau/2}$$

3.4.2 Response of Linear Systems to Nonperiodic Inputs

If we view the Fourier transform of a waveform as resolving that waveform into a continuum of sinusoidal components, it becomes clear that, using superposition, the response of a *linear system* to that waveform is

$$Y(j\omega) = H(j\omega)X(j\omega) \tag{3.68}$$

Therefore, *the Fourier transform of the output of a linear system is the product of the Fourier transforms of the input to that system and the impulse response of that system.* It can be shown that this is the *complete response (transient plus steady state) of the system for zero initial conditions* [1].

3.5 REPRESENTATION OF RANDOM (DATA) SIGNALS

Thus far we have considered only deterministic signals; that is, signals whose time behavior is known a priori. Random signals are those in which the time behavior is described statistically. Digital data waveforms are obviously random signals; otherwise no information would be conveyed. An example of a random signal is the pulse-code modulation–non-return-to-zero (PCM–NRZ) waveform shown in Fig. 3.32a. A PCM–NRZ waveform is one in which two levels are used to represent the two binary

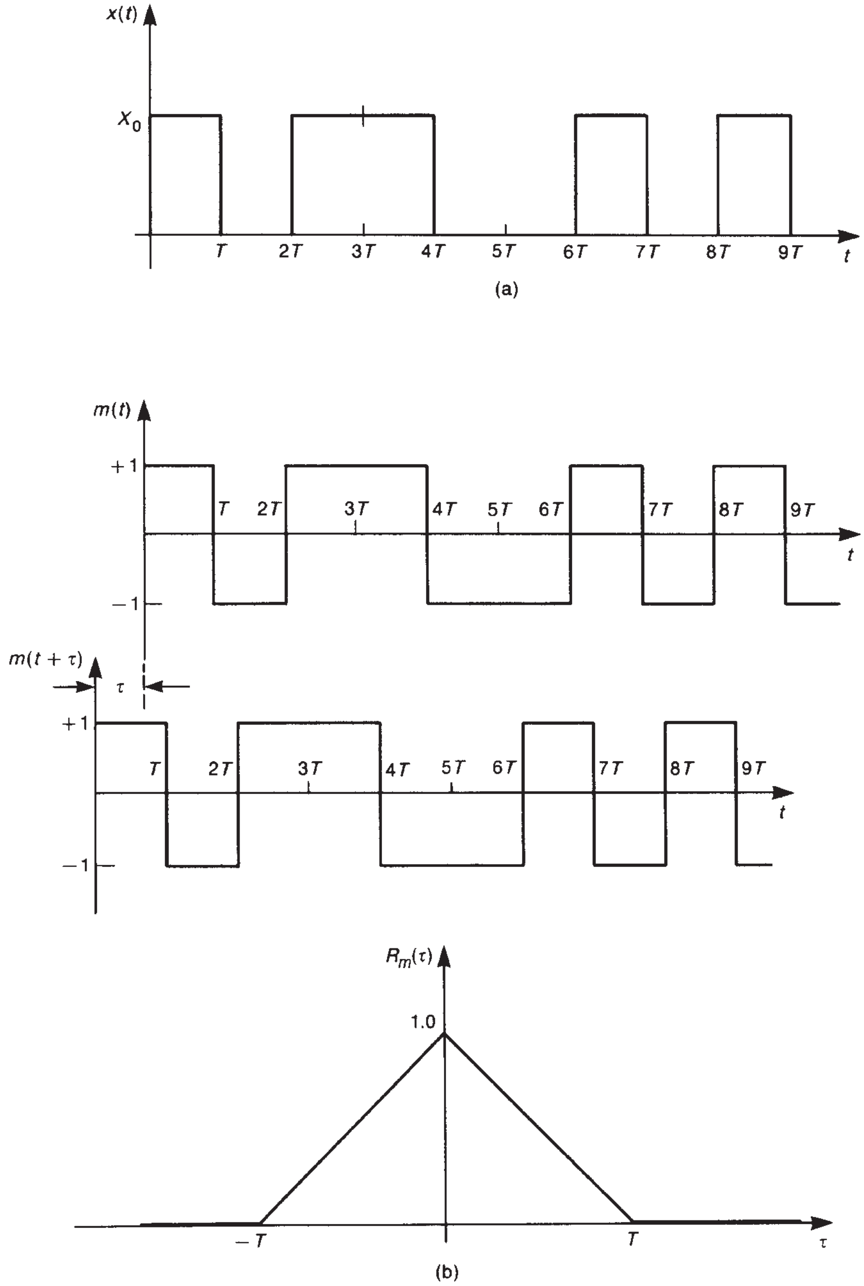
x(t)
X0
T
2T
3T
4T
5T
6T
7T
8T
9T
t
(a)
m(t)
+1
−1
T
2T
3T
4T
5T
6T
7T
8T
9T
t
m(t + τ)
τ
+1
−1
T
2T
3T
4T
5T
6T
7T
8T
9T
t
Rm(τ)
1.0
−T
T
τ
(b)

FIGURE 3.32 Illustration of the computation of the power spectral density of a PCM–NRZ (pulse-code modulation–non-return-to-zero) signal: (a) a typical waveform and (b) the autocorrelation function of $m(t)$.

states of 0 and 1. The NRZ designation means that it is not required that the signal returns to zero between each state transition. A waveform that transitions between 0 and X_0 can be described as

$$x(t) = \frac{1}{2}X_0[1 + m(t)] \tag{3.69}$$

where $m(t)$ is a random variable that assumes values of ±1 with equal probability in the bit interval $nT < t < (n + 1)T$. This signal may give a reasonable approximation to certain digital data signals.

The autocorrelation function $R_x(\tau)$ of a random signal $x(t)$ is defined as the expected value of the product of the signal and that signal shifted in time by τ [4]:

$$R_x(\tau) = \overline{x(t)x(t + \tau)} \tag{3.70}$$

where the overbar indicates the statistical average of all possibilities. Substituting (3.69) into (3.70) gives

$$\begin{aligned} R_x(\tau) &= \frac{1}{4}X_0^2\overline{[1 + m(t)][1 + m(t + \tau)]} \\ &= \frac{1}{4}X_0^2[1 + \overline{m(t)} + \overline{m(t + \tau)} + \overline{m(t)m(t + \tau)}] \\ &= \frac{1}{4}X_0^2[1 + \overline{m(t)m(t + \tau)}] \\ &= \frac{1}{4}X_0^2[1 + R_m(\tau)] \end{aligned} \tag{3.71}$$

where $R_m(\tau)$ is the autocorrelation function of $m(t)$. In the second part of the result, we have assumed that the process is stationary, and in the last part, we have used the fact that the expected (average) value of $m(t)$ is zero [4]. Computation of the autocorrelation function for $m(t)$ illustrated in Fig. 3.32b yields

$$\begin{aligned} R_m(\tau) &= 1 - \frac{|\tau|}{T} \quad \text{for } |\tau| < T \\ &= 0 \quad \text{for } |\tau| > T \end{aligned} \tag{3.72}$$

which is plotted in Fig. 3.32b.

The characterization of a random signal in the frequency domain is accomplished in terms of the *power spectral density* of the signal with the Wiener–Kinchine theorem, which provides that the power spectral density of the signal is the Fourier transform of the autocorrelation function of the signal [4]:

$$G_x(f) = \int_{-\infty}^{\infty} R_x(\tau)e^{-j\omega\tau}d\tau \text{ W/Hz} \tag{3.73}$$

The average power associated with the signal is

$$P_{av} = \int_{-\infty}^{\infty} G_x(f)\, df \text{ W} \tag{3.74}$$

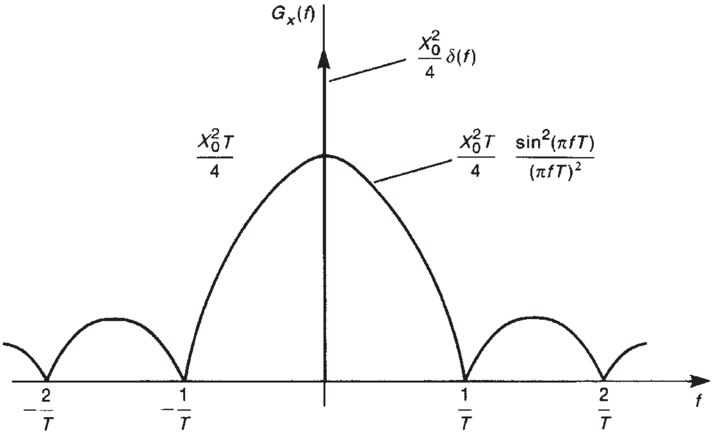

FIGURE 3.33 The power spectral density of the PCM–NRZ signal.

This is the expected or average power dissipated in a 1 Ω resistor by this signal if a statistically large number of samples are taken (signals are applied to the resistor). For the PCM–NRZ waveform, the power spectral density (in W/Hz) becomes

$$G_x(f) = \frac{X_0^2}{4}\delta(f) + \frac{X_0^2 T}{4}\frac{\sin^2(\pi f T)}{(\pi f T)^2} \quad \text{W/Hz} \tag{3.75}$$

which is plotted in Fig. 3.33. Observe that this power spectral density has nulls at the inverse of T (the bit rate). This PCM–NRZ waveform would be a good representation of digital data signals if it were not for the fact that the rise/falltimes are zero in the PCM–NRZ waveform. Digital data signals have nonzero rise/falltimes like those of realistic digital clock waveforms. Observe that the power spectral density in Fig. 3.33 is very similar to the magnitude of the square of the Fourier series coefficients for a square wave shown in Fig. 3.5b, as would be expected. (Replace A, τ in the square wave with X_0, T, respectively, and square the result to give power.) Although we have not derived the power spectral density of a PCM–NRZ waveform having nonzero rise/falltimes (which would represent actual digital data signals), this indicates that concepts about reducing the emissions of digital data signals should carry over from the periodic, clock signal analyses, that is, increase where possible, the rise/falltimes of the bits.

PROBLEMS

Section 3.1 Periodic Signals

3.1.1 Determine the period and fundamental frequency of the waveforms shown in Fig. P3.1.1. In addition, determine the average value and hence c_0.

$$\left[\begin{array}{l} (a)\ T = 4\,\text{ns},\ f_0 = 250\ \text{MHz},\ c_0 = 1;\ (b)\ T = 3\mu s,\ f_0 = 333.3\ \text{kHz},\ c_0 = 2; \\ (c)\ T = 5\mu s,\ f_0 = 200\ \text{kHz},\ c_0 = 2.5;\ (d)\ T = 3\text{ns},\ f_0 = 333.3\ \text{MHz},\ c_0 = 66.7 \end{array}\right]$$

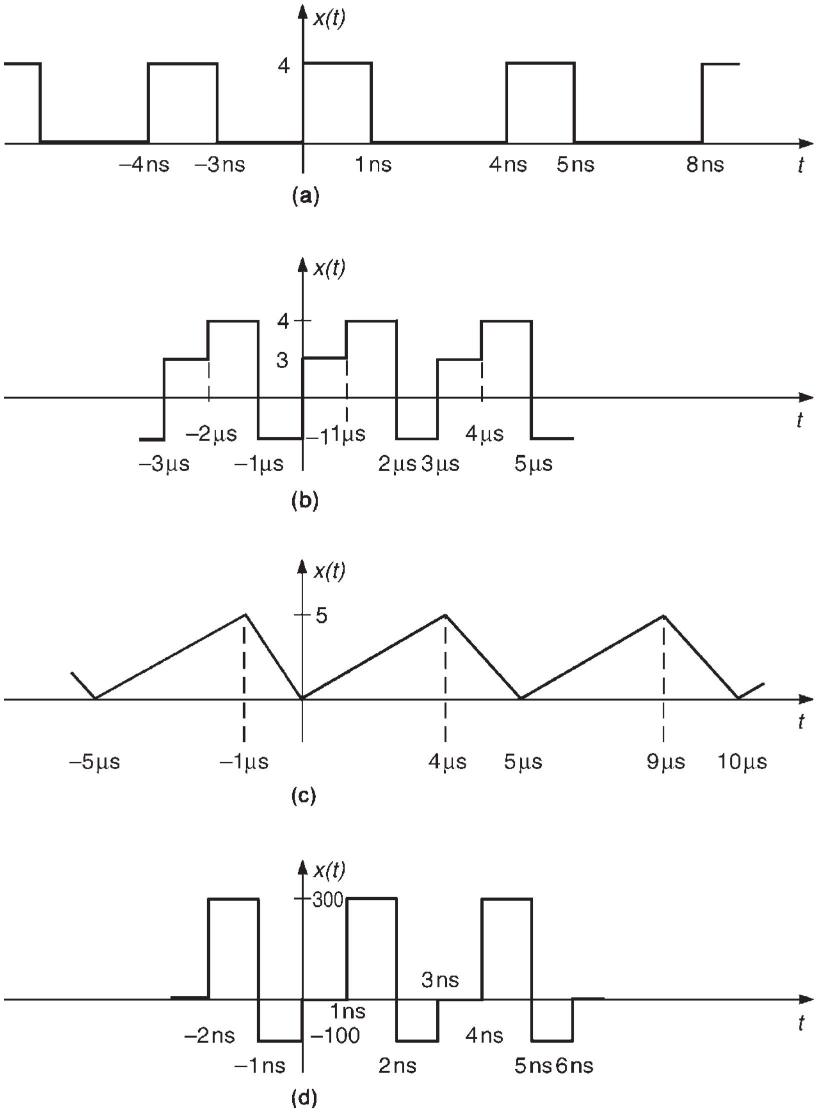

FIGURE P3.1.1

3.1.2 The periodic signal shown in Fig. P3.1.2 is a *full-wave rectified sinusoid* described by

$$x(t) = A \quad \sin\left(\frac{2\pi t}{T}\right) 0 \le t \le \frac{T}{2}$$

It is typical of those obtained from a linear power supply (prior to filtering), as we will see in Section 6.3 of Chapter 6. Determine the Fourier expansion (one-sided) for this waveform.

$$\left[c_n = \frac{2A}{\pi(1-4n^2)} x(t) = \frac{2A}{\pi} - \frac{4A}{3\pi}\cos\left(\frac{4\pi t}{T}\right) - \frac{4A}{15\pi}\cos\left(\frac{8\pi t}{T}\right) - \frac{4A}{35\pi}\cos\left(\frac{12\pi t}{T}\right) - \ldots\right]$$

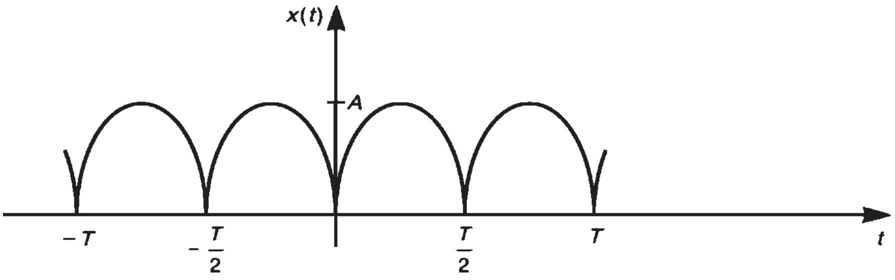

FIGURE P3.1.2

3.1.3 Determine the (one-sided) Fourier series expansion for the waveform in Fig. P3.1.3.

$$\left[c_0 = \frac{A}{2}, c_n = -\frac{2A}{(n\pi)^2} \quad n = \text{odd} \quad x(t) = \frac{A}{2} - \frac{4A}{\pi^2}\cos(\omega_0 t) - \frac{4A}{9\pi^2}\cos(3\omega_0 t) - \ldots\right]$$

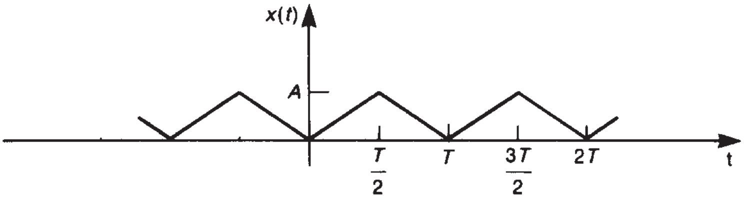

FIGURE P3.1.3

3.1.4 Determine the (one-sided) Fourier series expansion for the waveform in Fig. P3.1.4.

$$\left[c_0 = 0, c_n = \frac{4A}{(n\pi)^2}\angle(-n \times 90^\circ) \quad n = \text{odd},\right.$$

$$\left. x(t) = \frac{8A}{\pi^2}\cos(\omega_0 t - 90^\circ) + \frac{8A}{9\pi^2}\cos(3\omega_0 t + 90^\circ) + \frac{8A}{25\pi^2}\cos(5\omega_0 t - 90^\circ) \ldots\right]$$

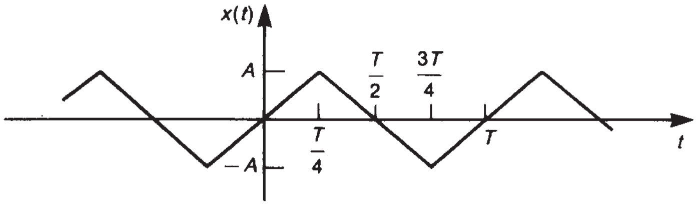

FIGURE P3.1.4

3.1.5 Determine the (one-sided) Fourier series expansion for the waveform in Fig. P3.1.5.

$$\left[c_0 = 0, c_n = 0 n = 4, 8, 12, \ldots, c_n = \frac{3}{n\pi}\angle(-90^\circ) \quad n = 1, 3, 5, \ldots,\right.$$

$$c_n = \frac{2}{n\pi}\angle(90^\circ) \quad n = 2, 6, 10, \ldots, x(t) = \frac{6}{\pi}\cos(\omega_0 t - 90^\circ)$$

$$\left. + \frac{2}{\pi}\cos(2\omega_0 t + 90^\circ) + \frac{2}{\pi}\cos(3\omega_0 t - 90^\circ) + \ldots\right]$$

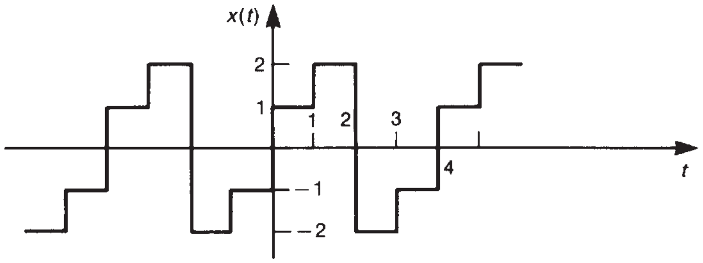

FIGURE P3.1.5

3.1.6 Determine the (one-sided) Fourier series expansion for the waveform in Fig. P3.1.6.

$$\Big[c_0 = \frac{5}{2}, c_n = \frac{5}{2n\pi}\underline{/(90^\circ)}, x(t) = \frac{5}{2} + \frac{5}{\pi}\cos(\omega_0 t + 90^\circ) + \frac{5}{2\pi}\cos(2\omega_0 t + 90^\circ) + \frac{5}{3\pi}\cos\,(3\omega_0 t + 90^\circ) + \ldots\Big]$$

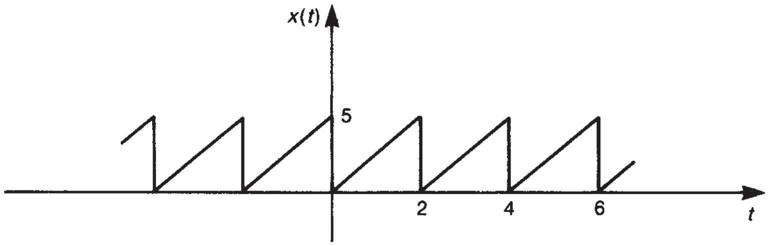

FIGURE P3.1.6

3.1.7 Determine the Fourier series expansion coefficients for the waveform in Fig. P3.1.7.

$$\Big[c_0 = \frac{A}{2}, c_n = \frac{A}{2n\pi}\underline{/(-90^\circ)}, x(t) = \frac{A}{2} + \frac{A}{\pi}\cos(\omega_0 t - 90^\circ) + \frac{A}{2\pi}\cos(2\omega_0 t - 90^\circ) + \frac{A}{3\pi}\cos(3\omega_0 t - 90^\circ) + \ldots\Big]$$

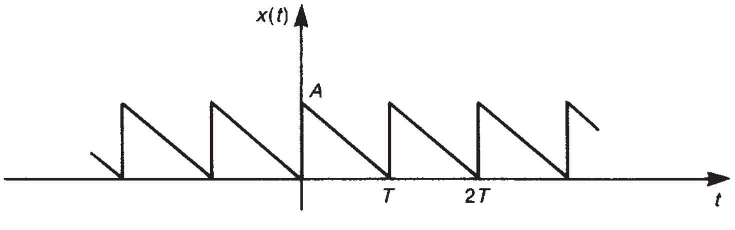

FIGURE P3.1.7

3.1.8 Determine the Fourier series expansion coefficients for the waveform in Fig. P3.1.8.

$$\left[c_0 = \frac{A\tau}{2T}, c_n = -j\frac{A}{2\pi n}\left[1 - e^{-jn\pi\tau/T}\frac{\sin(n\pi\tau/T)}{n\pi\tau/T}\right]\right]$$

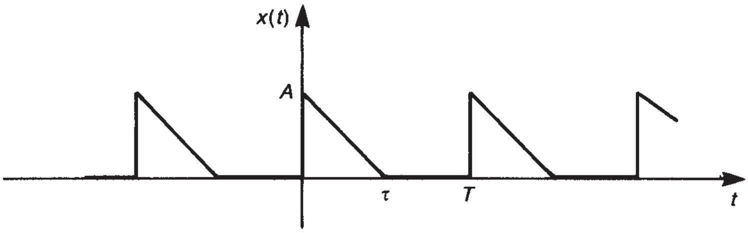

FIGURE P3.1.8

3.1.9 Determine the Fourier series expansion coefficients for the waveform in Fig. P3.1.9.

$$\left[c_0 = \frac{A\tau}{T}\left[1 - \frac{\sigma}{2\tau}\right], c_n = j\frac{A}{2\pi n}\left[e^{-jn2\pi\tau/T} - e^{-jn\pi\sigma/T}\frac{\sin(n\pi\sigma/T)}{n\pi\sigma/T}\right]\right]$$

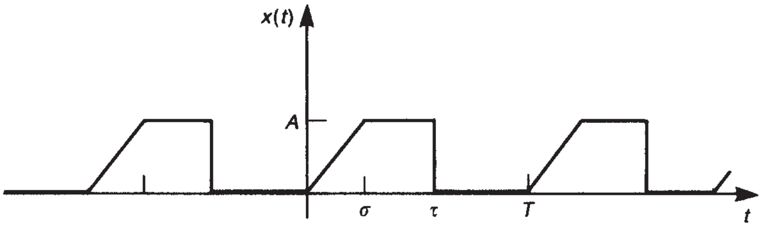

FIGURE P3.1.9

3.1.10 The exponential waveform in Fig. P3.1.10 is often observed in the arcing at the brushes of a dc motor. Determine the Fourier expansion coefficients for this waveform.

$$\left[c_0 = \frac{A}{\alpha T}[1 - e^{-\alpha T}], c_n = \frac{A}{(\sigma T + j2\pi n)}[1 - e^{-\alpha T}]\right]$$

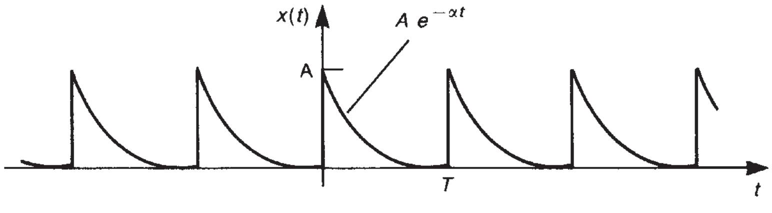

FIGURE P3.1.10

Section 3.2 Spectra of Digital Waveforms

3.2.1 A 10-MHz clock oscillator transitioning from 0 to 5 V with rise/falltimes of 20 ns and a 50% duty cycle is connected to a gate as shown in Fig. P3.2.1. A filter is connected as shown. Determine the level of the 11th harmonic at the gate terminals. Obtain these by using the exact expression and by using the spectral bounds. [73.95 dBμV exact, 78.56 dBμV by interpolation]

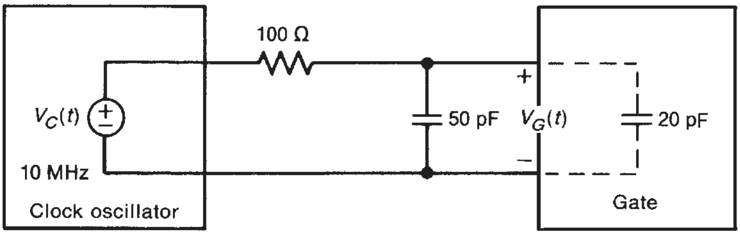
100 Ω
$V_C(t)$
10 MHz
Clock oscillator
50 pF
+
$V_G(t)$
−
20 pF
Gate

FIGURE P3.2.1

3.2.2 Determine the magnitude of the output of the system shown in Fig. P3.2.2 at $\omega = 50 \times 10^6$ rad/s. [102.04 dBμV]

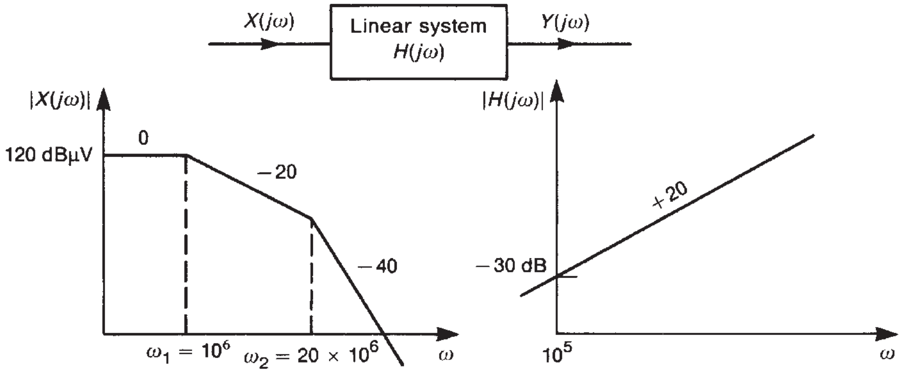
$X(j\omega)$
Linear system
$H(j\omega)$
$Y(j\omega)$
$|X(j\omega)|$
120 dBμV
0
−20
−40
$\omega_1 = 10^6$
$\omega_2 = 20 \times 10^6$
ω
$|H(j\omega)|$
+20
−30 dB
10^5
ω

FIGURE P3.2.2

3.2.3 A periodic waveform with $\omega_0 = 10^5$ rad/s is applied to a circuit as shown in Fig. P3.2.3. Determine the level of the 50th harmonic. [83.01 dBμV]

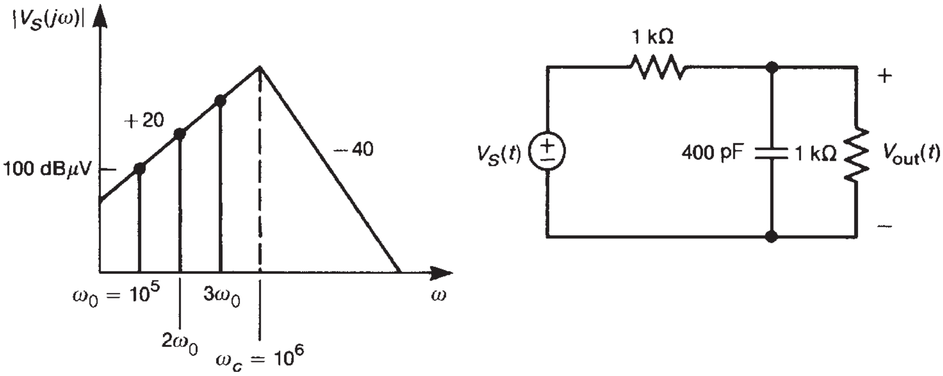
$|V_S(j\omega)|$
+20
100 dBμV
−40
$\omega_0 = 10^5$
$2\omega_0$
$3\omega_0$
$\omega_c = 10^6$
ω
1 kΩ
$V_S(t)$
400 pF
1 kΩ
+
$V_{out}(t)$
−

FIGURE P3.2.3

3.2.4 A 5 V, 10 MHz oscillator having a rise/falltime of 10 ns and a 50% duty cycle is applied to a gate as shown in Fig. P3.2.4. Determine the value of the capacitance such that the fifth harmonic is reduced by 20 dB in the gate voltage $V_G(t)$. [63.34 pF]

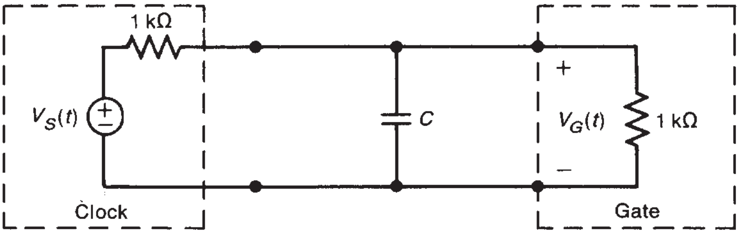

FIGURE P3.2.4

3.2.5 A 10 MHz clock oscillator having a 10 Ω internal resistance has an open-circuit voltage waveform as a trapezoidal pulse train with a 50% duty cycle and rise- and falltimes of 2 ns. Determine the value of a capacitor (an ideal one) that when placed across the oscillator output will reduce the output voltage of the fifth harmonic by 10 dB [955 pF]. Given that the open-circuit voltage transitions from 0 to 5 V, estimate the level of this fifth harmonic [106 dBμV] and give the exact value [105.93 dBμV].

3.2.6 The square-wave current source in Fig. P3.2.6 is applied to the associated circuit. Determine the current $I(t)$ in the form $i(t) = \sum_{n=1}^{7} I_n \sin(n\omega_0 t + \theta_n)$

$$\begin{bmatrix} I_0 = 2.5, I_1 = 0.5, \theta_1 = -80.96^\circ, I_2 = 0, I_3 = 0.0562, \theta_3 = -86.96^\circ, \\ I_4 = 0, I_5 = 0.0203, \theta_5 = -88.17^\circ, I_6 = 0, I_7 = 0.0103, \theta_1 = -88.7^\circ \end{bmatrix}$$

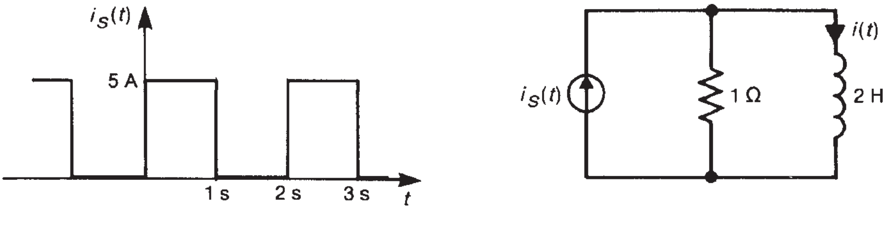

FIGURE P3.2.6

3.2.7 A 5 MHz, 5 V, 30%-duty-cycle trapezoidal waveform having rise/falltimes of 15 ns has the (one-sided) spectral bounds given in Fig. P3.2.7. Determine A, f_1, and f_2. [A = 129.54 dBμV, f_1 = 5.305 MHz, f_2 = 21.221 MHz]. Determine the levels of the first five harmonics. Give exact values and values computed from the spectral bounds both in dBμV. [128.14 (129.54), 105.28 (106.04), 109.58 (103.51), 100.07 (102.02), 101.97 (114.65)]

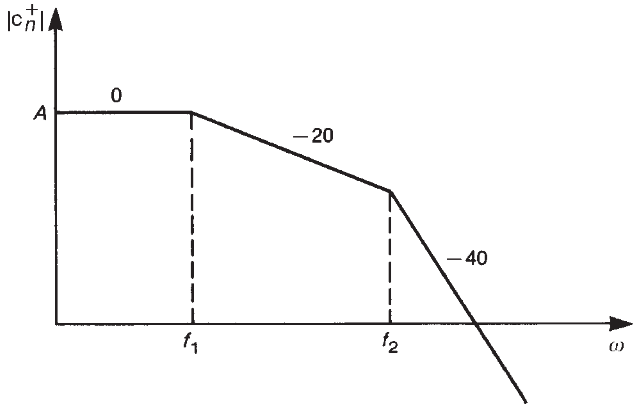

FIGURE P3.2.7

3.2.8 Show that when the duty cycle is varied, the breakpoint of the 0–20 dB/decade segment, $1/\pi\tau$, is always prior to the breakpoint for the −20–40 dB/decade segment, $1/\pi\tau_r$, as shown in Fig. 3.25.

3.2.9 For the ringing waveform shown in Fig. 3.26a, determine the increase in the spectrum (in dB) at the ringing frequency caused by the ringing on the square-wave waveform for $\alpha = 5 \times 10^6$, $f_r = 30$ MHz, $K = 0.5$, $V_0 = 5$. [9.2 dB]

Section 3.3 Spectrum Analyzers

3.3.1 Determine the levels shown in Table 3.3 that give the increase in spectral level shown on the spectrum analyzer when two signals are within the bandwidth and differ in level by those shown.

Section 3.4 Representation of Nonperiodic Waveforms

3.4.1 A frequently used time-domain waveform to represent an electromagnetic pulse (EMP) from a nuclear detonation is the so-called double-exponential pulse given by

$$x(t) = \frac{1}{(\beta - \alpha)}(e^{-\alpha t} - e^{-\beta t})$$

Determine the Fourier transform of this pulse.

$$\left[\frac{1}{\{\alpha\beta + j(\alpha + \beta)\omega - \omega^2\}}\right]$$

3.4.2 Determine the Fourier transform of a pulse given by the waveform over one period of the waveform in Problem 3.9.

$$\left[X(j\omega) = \frac{A}{j\omega} \left[e^{-j\omega\tau} - e^{-j\omega\sigma/2} \frac{\sin\left(\frac{1}{2}\omega\sigma\right)}{\frac{1}{2}\omega\sigma} \right] \right]$$

Section 3.5 Representation of Random (Data) Signals

3.5.1 The "random telegraph" wave is a function that may assume the values of zero or one with equal probability at any instant of time, and it makes random traversals from one value to another. The probability that n traversals occur in a time interval of length T is given by the Poisson distribution $P(n, T) = (aT)^n e^{-(aT/n!)}$, where a is the average number of transversals per unit of time. Determine the autocorrelation function. $\left[R(\tau) = \frac{1}{4}\left(1 + e^{-2a|\tau|}\right)\right]$ Determine the power spectral density of this waveform.

$$\left[G(f) = \frac{1}{4} \left\{ \delta(f) + \frac{a}{(a^2 + \pi^2 f^2)} \right\} \right]$$

REFERENCES

1. C. R. Paul, *Analysis of Linear Circuits*, McGraw-Hill, New York, 1989.
2. C. D. McGillem and G. R. Cooper, *Continuous and Discrete Signal and System Analysis*, Holt, Rinehart and Winston, New York, 1974.
3. S. J. Mason and H. J. Zimmerman, *Electronic Circuits, Signals, and Systems*, Wiley, New York, 1960.
4. A. B. Carlson, *Communication Systems*, McGraw-Hill, New York, 1968.

CHAPTER FOUR

Transmission Lines and Signal Integrity

Transmission of digital and analog signals between two points occurs over a pair of parallel conductors, which is referred to as a *transmission line*. Wires are circular, cylindrical conductors. Some common wire-type transmission lines are shown in Fig. 4.1. Figure 4.1a shows a two-wire line. The signal current travels down one wire and returns to the source on the other. The source (a digital logic gate, a sensor, a transmitter, etc.) is represented as a Thevenin equivalent circuit consisting of an open-circuit voltage $V_s(t)$ and a source resistance R_s. The load, representing the input to, perhaps, a logic gate, is represented as a resistance R_L. We initially investigate sources and loads that are represented as being resistive but will later extend that to dynamic terminations such as inductors, capacitors, and nonlinear terminations. Figure 4.1b illustrates one wire above a "ground plane" where the signal current returns via the ground plane. The third common case is that of a coaxial cable shown in Fig. 4.1c, where an overall, circular–cylindrical shield encloses an interior wire that is located on the axis of the shield. The signal current returns (ideally) on the interior of the shield. In the case of a coaxial cable, the interior is filled with some dielectric such as Teflon. The basic problem here is to determine the currents on the conductors $I(z, t)$ and the voltage between the two conductors $V(z, t)$. The conductors will always be drawn parallel to the z axis of a rectangular coordinate system. The line current and voltage will depend on position along the line z, as well as time t.

Figure 4.2 shows some typical transmission lines composed of conductors of rectangular cross section. Conductors on and within printed circuit boards (PCBs) have a rectangular cross section and are commonly referred to as *lands* with reference to grooves in a rifle barrel that serve to spin the bullet, thereby stabilizing it. Figure 4.2a shows what is commonly referred to as a *stripline*. This represents *innerplanes* that are buried layers within a PCB. The configuration shown in Fig. 4.2b is commonly referred to as a *microstrip* line and is typical of lands on the outer surfaces of a PCB that has innerplanes. Figure 4.2c represents a "one-sided" or "two-sided" PCB not having innerplanes.

In the mid-1980s or so, these connecting conductors were of no consequence; i.e., the voltage and current at the input to the line are almost identical to the voltage and current at the output of the line. Today this is no longer true. As clock and data speeds continue to increase, seemingly without bound, these "interconnect" conductors will have a significant effect on the signal transmission and cannot be ignored. When do the interconnect conductors of the transmission line "not matter"? This

---

Introduction to Electromagnetic Compatibility, Third Edition. Clayton R. Paul, Robert C. Scully, and Mark A. Steffka.
© 2023 John Wiley & Sons, Inc. Published 2023 by John Wiley & Sons, Inc.

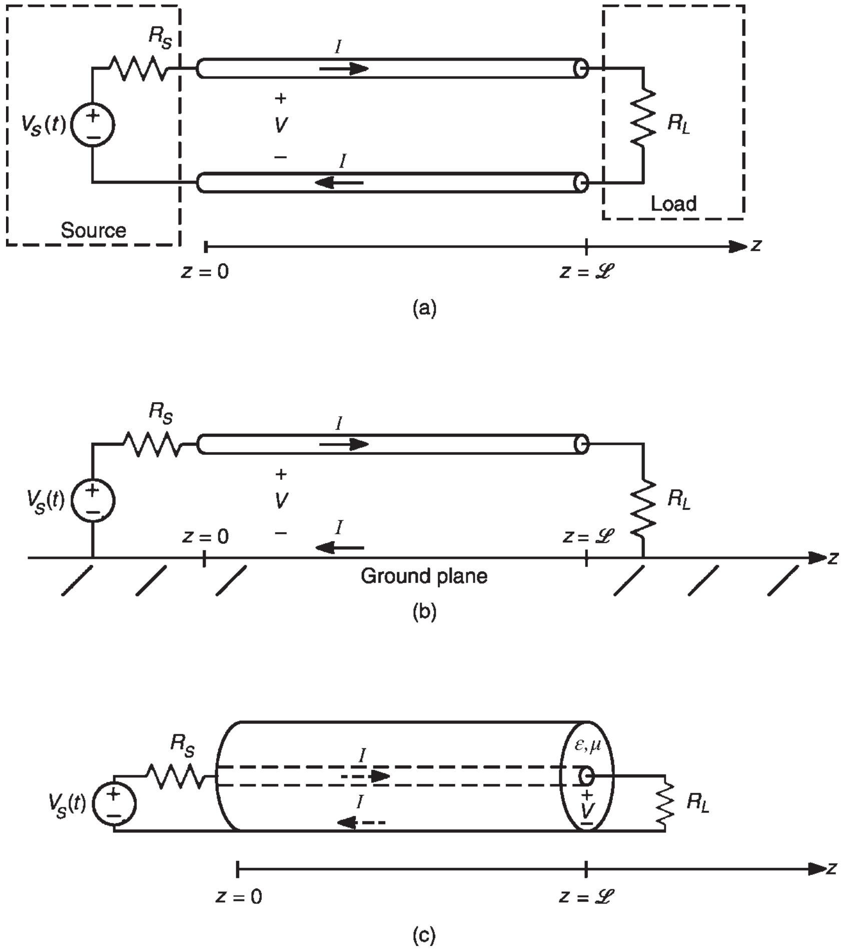

FIGURE 4.1 Illustration of typical wire-type transmission lines: (a) two wires; (b) one wire above an infinite ground plane; (c) a coaxial cable.

chapter will be devoted to understanding the answer to that question. In addition, we will investigate ways of remedying the effect of the conductors on signal transmission quality. All this falls into the category of *signal integrity*. Signal integrity has to do with ensuring that the waveforms at the input and the output of the line are identical or approximately so. These transmission lines carry signals from one point to another. It is critical that these signals not be corrupted by the line. This has to do with the third aspect of a system being electromagnetically compatible and that is with itself.

One rather obvious effect of the line is to impose a *time delay* as the signals propagate from one end to the other. We will find that a transmission line has a *velocity of propagation* v, which dictates the speed of transmission of the signals from one end of the line to the other. The time required for the current and voltage to transit the line, whose total length is denoted by L, is given by the *time delay*:

$$T_D = \frac{L}{v} \text{ s} \tag{4.1}$$

For the parallel wire line of Fig. 4.1a and the wire above ground of Fig. 4.1b, we might assume that free space surrounds the conductors. (Actual wires will have dielectric insulations surrounding the

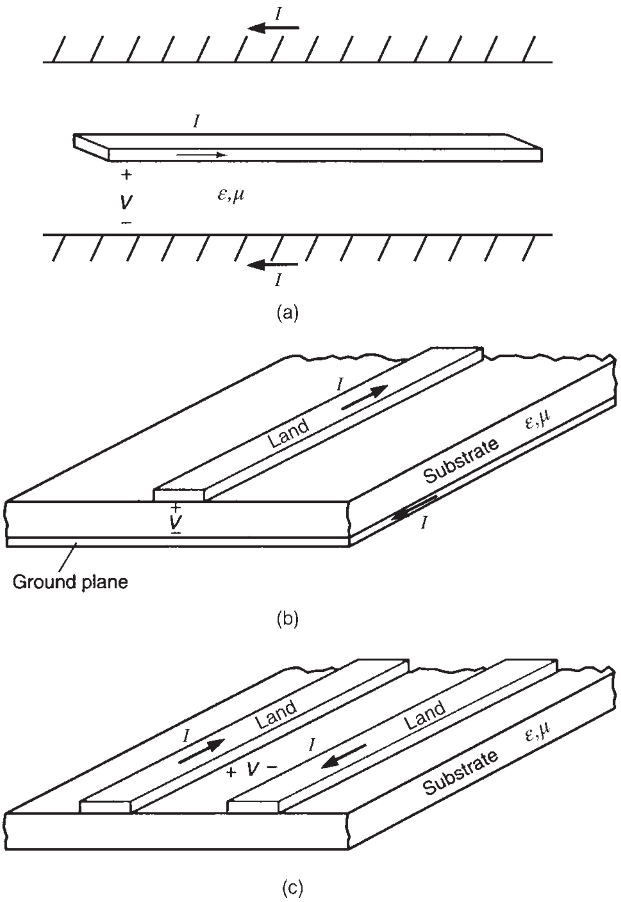

FIGURE 4.2 Illustration of typical printed circuit board (PCB) structures: (a) stripline (innerplane boards); (b) microstrip (outer lands of an innerplane board); (c) PCB (lands on a board without innerplanes).

conductor but we ignore this for the moment.) Hence, the voltage and current waves that propagate along the line will do so at a velocity of $v_0 = (1/\sqrt{\mu_0\varepsilon_0}) \cong 3 \times 10^8$ m/s. Hence the time delay in free space (essentially air) is 3.33 ns/m or 33.3 ps/cm or 85 ps/in. or 1 ns/ft. For the case of a coaxial cable in Fig. 4.1c, the interior is filled with a dielectric, and hence the velocity of propagation is reduced from that of free space $-v = 1/\sqrt{\mu_0\varepsilon_0\varepsilon_r\mu_r} = v_0/\sqrt{\varepsilon_r}$ m/s– and we have recognized that dielectrics are not magnetic and hence $\mu_r = 1$. A coaxial cable filled with Teflon ($\varepsilon_r = 2.1$) has $v = 2.07 \times 10^8$ m/s, and hence time delays of 4.8 ns/m or 48.3 ps/cm or 122.7 ps/in. or 1.47 ns/ft. In the case of the stripline of Fig. 4.2a, the dielectric is that of glass epoxy (FR-4) used to construct PCBs where $\varepsilon_r = 4.7$. Hence, the time delays of a stripline are 7.2 ns/m or 72.3 ps/cm or 183.6 ps/in. or 2.2 ns/ft. In the case of the microstrip in Fig. 4.2b and the PCB in Fig. 4.2c, the computation of the velocity of propagation is complicated by the fact that the electric fields surrounding the lands are partly in air and partly in the dielectric. We can make an estimate of the velocity of propagation by finding an effective relative permittivity as the average of the relative permittivity of air ($\varepsilon_r = 1$) and that of the glass epoxy substrate ($\varepsilon_r = 4.7$) or $\varepsilon_r = [(1 + 4.7)/2] = 2.85$. (This will be discussed in further detail later when we determine an accurate effective permittivity.) Hence, the velocity of propagation on these structures is approximately $v = v_0/\sqrt{\varepsilon_r'} = 1.777 \times 10^8$ m/s. Thus, the time delays on these structures are 5.6 ns/m or 56.3 ps/cm or 143 ps/in. or 1.7 ns/ft. These times may seem to be inconsequential unless one recognizes that clock rise/falltimes today are on the order of picoseconds (1 ns = 1000–500 ps or lower). For example, a 6-in. land on a stripline will incur a total time delay of 1.1 ns! Around the mid-1980s, the only consequential time delay was incurred by the propagation delay through the gates, and the delay of the interconnects was inconsequential. Today and in the future the delay of the interconnects must be considered.

An additional problem these interconnects impose is that of *reflections*. We will find that the second parameter characterizing a transmission line is its *characteristic impedance*, Z_C. For a typical coaxial cable, RG58U, the characteristic impedance is 50 Ω. As was discussed in Chapter 1, if $R_L = Z_C$, there will be no reflections at the load, whereas if the line is mismatched, i.e., $R_L \neq Z_C$, there will be a portion of the signal reflected at the load and traveling back to the source. This phenomenon of reflection on *mismatched* lines will be the major aspect of degrading signal integrity. We will spend considerable time studying how to combat this.

4.1 THE TRANSMISSION-LINE EQUATIONS

Consider a general two-conductor transmission line shown in Fig. 4.3, where the conductors are parallel to the z axis. If we apply a voltage V between the two conductors as in Fig. 4.3a, charge will be deposited on the conductors resulting in an electric field $\boldsymbol{E}_T$, lying in the transverse or xy plane. Since the two conductors separate charge, this suggests that the line has a capacitance per unit of length, c F/m. Now suppose we apply a current I passing to the right in the upper conductor and "returning" on the lower conductor as shown in Fig. 4.3b. This current will cause a magnetic field $\boldsymbol{H}_T$ that also lies in the transverse or xy plane. This magnetic field passes through the loop between the two conductors and suggests that the line has an inductance per unit of length l H/m. This suggests that the line can be modeled as a *distributed parameter* circuit consisting of a sequence of inductors and capacitors as shown in Fig. 4.3c. Note that the total inductance and capacitance in a length Δz of the line is the per-unit-length value multiplied by the length of that section, $l\Delta z$ and $c\ \Delta z$.

Transmission lines have, in addition to inductance and capacitance, losses. The conductors have a finite, nonzero resistance, and the dielectric medium surrounding the conductors has loss. Usually these represent second-order effects and can be neglected. At frequencies in the GHz range, the resistance of the conductors may become significant due to skin effect. We will defer consideration of the effects of losses until Section 4.5.

There is an important point about the line that can be observed from this equivalent circuit. If a pulse is applied to the left end of the line, it will charge the first capacitance and energize the first inductance. As the pulse moves down the line to the right, it will discharge the first capacitor and deenergize the first inductor and then charge and energize the next capacitor and inductor, and so forth. Hence, waves of voltage and current (and their associated transverse electric and magnetic fields) will move down the line with a velocity v. It takes a certain time to energize and deenergize these elements so that it will take a finite, nonzero time for the waves to transit the line. This will result in a *time delay* for a line of total length L of $T_D = L/v$.

Consider a Δz section of the line shown in Fig. 4.4. The line voltage and current are functions of time t and position z. Writing Kirchhoff's voltage law around the outside loop gives

$$V(z + \Delta z, t) - V(z, t) = -l\,\Delta z \frac{\partial I(z, t)}{\partial t}$$

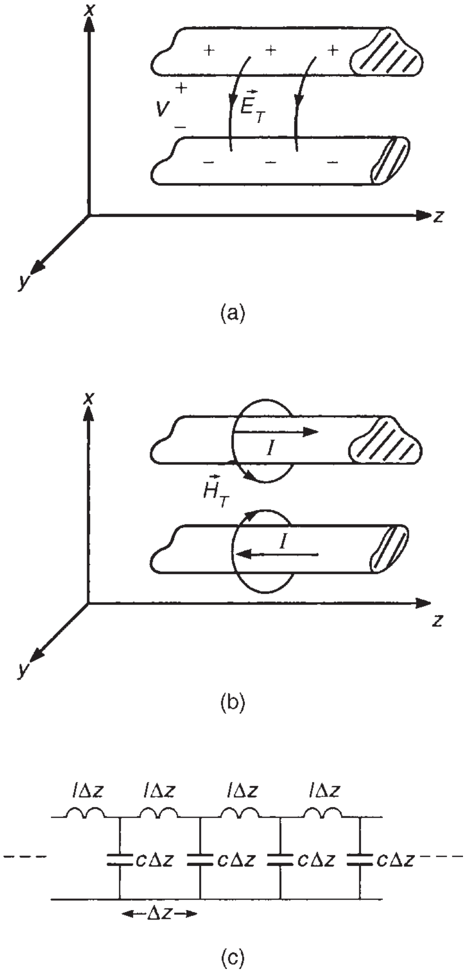
x
+
+
+
+
V
−
$\vec{E}_T$
−
−
−
z
y
(a)
x
I
$\vec{H}_T$
I
z
y
(b)
$l\Delta z$
$l\Delta z$
$l\Delta z$
$l\Delta z$
$c\Delta z$
$c\Delta z$
$c\Delta z$
$c\Delta z$
Δz
(c)

FIGURE 4.3 The two-conductor transmission line: (a) electric field about a transmission line caused by the voltage between the two conductors; (b) magnetic field about a transmission line caused by the current on the conductors; (c) representation of a transmission line as a distributed parameter circuit consisting of cells of per-unit-length inductance l and per-unit-length capacitance c.

Dividing both sides by Δz and taking the limit as $\Delta z \rightarrow 0$ gives

$$\left.\frac{V(z+\Delta z, t) - V(z, t)}{\Delta z}\right|_{\lim_{\Delta z \rightarrow 0}} = \frac{\partial V(z, t)}{\partial t}$$

and we obtain the first transmission-line equation:

$$\frac{\partial V(z, t)}{\partial z} = -l\,\Delta z \frac{\partial I(z, t)}{\partial t} \tag{4.2a}$$

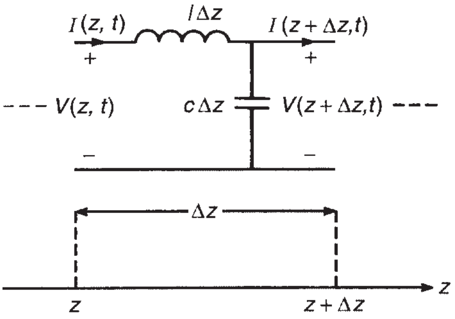

FIGURE 4.4 The per-unit-length equivalent circuit of a transmission line.

Similarly, writing Kirchhoff's current law at the upper node of the capacitor gives

$$I(z+\Delta z,t) - I(z,t) = -c\,\Delta z \frac{\partial V(z+\Delta z,t)}{\partial t}$$

Dividing both sides by Δz and taking the limit as $\Delta z \rightarrow 0$ gives

$$\left.\frac{I(z+\Delta z,t) - I(z,t)}{\Delta z}\right|_{\lim_{\Delta z\rightarrow 0}} = \frac{\partial\, I(z,t)}{\partial t}$$

and we obtain the second transmission-line equation:

$$\frac{\partial\, I(z,t)}{\partial z} = -c\,\Delta z \frac{\partial V(z,t)}{\partial t} \tag{4.2b}$$

Equations (4.2a) and (4.2b) are called the *transmission-line equations*. Observe that they are coupled in that each equation involves both V and I. We can uncouple these equations by, for example, differentiating (4.2a) with respect to z to give

$$\frac{\partial^2\, V(z,t)}{\partial z^2} = -l\,\frac{\partial^2\, I(z,t)}{\partial t\,\partial z}$$

and differentiating (4.2b) with respect to t to give

$$\frac{\partial^2\, I(z,t)}{\partial z\,\partial t} = -c\,\frac{\partial^2\, V(z,t)}{\partial t^2}$$

Substituting the second into the first gives the first uncoupled equation as

$$\frac{\partial^2\, V(z,t)}{\partial z^2} = lc \frac{\partial^2\, V(z,t)}{\partial t^2} \tag{4.3a}$$

Differentiating (4.2b) with respect to z and differentiating (4.2a) with respect to t and substituting gives the second uncoupled equation as

$$\frac{\partial^2 I(z,t)}{\partial z^2} = lc\frac{\partial^2 I(z,t)}{\partial t^2} \tag{4.3b}$$

Once we discuss the important per-unit-length parameters of capacitance and inductance for representative lines in the next section, we will solve these transmission-line equations for various source and load terminations.

4.2 THE PER-UNIT-LENGTH PARAMETERS

The transmission-line equations presented in Section 4.1 contain the per-unit-length parameters of capacitance c (F/m) and inductance l (H/m). All the structural information about the line such as type of conductor, wire radii, and wire separation that distinguish one line from another are contained in these two parameters and nowhere else. Hence, if we wish to solve a particular problem, we must be able to compute c and l for that particular line.

The mode of propagation on a transmission line is the *transverse electromagnetic* (TEM) mode in that the electric and magnetic fields are transverse to the direction of propagation, the z direction. If we write Faraday's law (see Appendix B) in the transverse plane, we have

$$\begin{aligned}\oint_{C_{xy}} \boldsymbol{E}_T \cdot d\boldsymbol{l} &= -\frac{d}{dt}\int_{S_{xy}} \mu \boldsymbol{H}_z \cdot d\boldsymbol{s} \\ &= 0\end{aligned} \tag{4.4}$$

where S_{xy} is a (flat) surface lying in the transverse xy plane and C_{xy} is the closed contour bounding this surface also lying in the transverse xy plane. The right-hand side is zero because the fields are TEM, that is, there are no z or longitudinal components: $E_z = H_z = 0$. But this is identical to the case for static or dc fields (see Section B.7 of Appendix B).

Hence, we can uniquely define a voltage between the two conductors even though the fields are time-varying. This means that *we can compute the per-unit-length capacitance c using dc field computations even though the fields will be varying with time*. There are a number of static field computational packages available that essentially solve Laplace's equation to obtain c for a wide variety of structures such as those shown in Figs. 4.1 and 4.2. Although we can and will obtain exact formulas for c for the wire-type structures in Fig. 4.1, we cannot do so for the rectangular cross-section cases in Fig. 4.2 (although we will show approximate formulas). Hence, these numerical computational packages are particularly valuable in computing c for rectangular cross section conductors. Similarly, writing Ampere's law (see Appendix B) in the transverse plane, we have

$$\begin{aligned}\oint_{C_{xy}} \boldsymbol{H}_T \cdot d\boldsymbol{l} &= I + \frac{d}{dt}\int_{S_{xy}} \varepsilon \boldsymbol{E}_z \cdot d\boldsymbol{s} \\ &= I\end{aligned} \tag{4.5}$$

where, again, S_{xy} is a (flat) surface lying in the transverse xy plane and C_{xy} is the closed contour bounding this surface also lying in the transverse xy plane. The right-hand side is the sum of two currents, a conduction current I and a displacement current due to the z-directed electric field. But the displacement current through the contour and surface is zero because the fields are TEM, that is, there are no z or longitudinal components: $E_z = H_z = 0$. But this is identical to the case for static or dc fields (see Section B.7 of Appendix B). Hence, we can uniquely define a current flowing on each conductor even though the fields are time-varying. This means that *we can compute the per-unit-length inductance l using dc field computations even though the fields will be varying with time*.

This remarkable result simplifies the computation of c and l since only static (dc) field computations are involved. It can also be shown that if the medium surrounding the two conductors is homogeneous, meaning that the permittivity ε and permeability μ are the same everywhere, then c and l are related as

$$lc = \mu\varepsilon \quad \text{homogeneous surrounding medium} \tag{4.6}$$

The wire-type lines in Fig. 4.1, as well as the stripline in Fig. 4.2a, are lines in a homogeneous medium. Logically, the surrounding medium for the case of two wires in Fig. 4.1a and one wire above a ground plane in Fig. 4.1b would be free space (normally wires have dielectric insulations that we neglect for now; otherwise, we would have an inhomogeneous medium). For the case of the coaxial cable in Fig. 4.1c, the fields are confined to the interior of the shield that is some dielectric having $\varepsilon = \varepsilon_r \varepsilon_0$ and $\mu = \mu_0$. (Note that again we use the observation that dielectrics are nonmagnetic so that $\mu_r = 1$.) In the case of the stripline in Fig. 4.2a, the land is immersed in the PCB board material that is glass epoxy (FR-4) having $\varepsilon_r = 4.7$.

For all these cases of a homogeneous medium, the velocity of propagation on the line is

$$\begin{aligned} v &= \frac{1}{\sqrt{\mu\varepsilon}} \\ &= \frac{v_0 = 3 \times 10^8}{\sqrt{\varepsilon_r}} \ \text{m/s} \end{aligned} \tag{4.7}$$

Hence we only need to determine c or l because (4.6) and (4.7) yield

$$l = \frac{1}{cv^2} \tag{4.8a}$$

and

$$c = \frac{1}{lv^2} \tag{4.8b}$$

Most numerical computational packages solve directly for c by solving Laplace's equation and then obtain l from (4.8a). (See Appendix B, Section B7.2.)

For the case of an inhomogeneous medium as is the case for the microstrip in Fig. 4.2b and the PCB in Fig. 4.2c, these relations do not apply. However, for these cases we determine an *effective relative permittivity* ε_r', so that *if the inhomogeneous surrounding medium were replaced by a homogeneous medium having an effective relative permittivity of ε_r', none of the properties of the line would be changed*. In this case, we would obtain

$$lc = \mu_0 \varepsilon_0 \varepsilon_r' \tag{4.9a}$$

$$\begin{aligned} v &= \frac{1}{\sqrt{\mu_0 \varepsilon_0 \varepsilon_r'}} \\ &= \frac{v_0 = 3 \times 10^8}{\sqrt{\varepsilon_r'}} \ \text{m/s} \end{aligned} \tag{4.9b}$$

and (4.8) would hold in terms of this velocity of propagation.

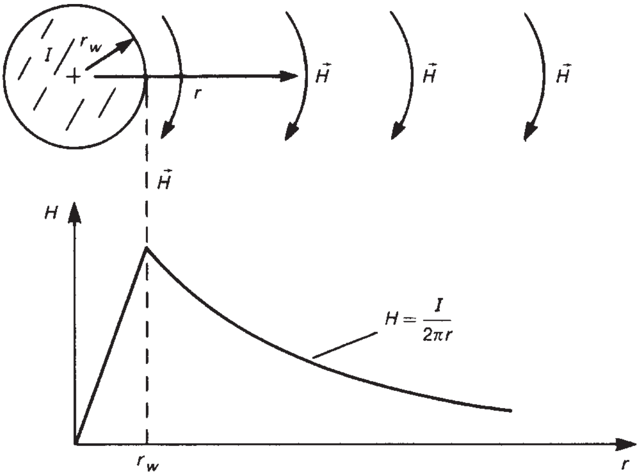

FIGURE 4.5 The magnetic field about a current-carrying wire.

4.2.1 Wire-Type Structures

Consider the two-wire line of Fig. 4.1a. The transverse magnetic field $\boldsymbol{H}_T$ contributes to the per-unit-length inductance of the line. Figure 4.5 shows the magnetic field intensity of a current-carrying wire internal and external to the wire. The portion of the magnetic field internal to the wire contributes to the *internal inductance*, and the portion external to the wire contributes to the *external inductance*. The external inductance is much larger than the internal inductance, and hence the per-unit-length inductance l is approximately the external inductance. The transverse electric field $\boldsymbol{E}_T$ contributes to the per-unit-length capacitance of the line.

The external per-unit-length parameters of inductance and capacitance are derivable in closed form for the three cases of lines in a homogeneous medium shown in Fig. 4.1. Derivations of the inductance and capacitance associated with wires (circular cylindrical conductors) rely on the following two *basic subproblems*. Consider an isolated, current-carrying wire as shown in Fig. 4.5. *An important assumption implicit in the following result is that the current is uniformly distributed across the wire cross section.* If we bring another current-carrying wire in proximity to this wire, the magnetic fields of the two wires will interact, causing the current distributions to be nonuniform; the current density will be greatest on the sides of the wires facing each other. This is referred to as *proximity effect*, and the following result disregards this. Under the assumption of a uniform distribution of current, symmetry shows that the magnetic field intensity vector $\boldsymbol{H}_T$ is transverse to the wire axis, is constant for a fixed radius, and is circumferentially directed according to the right-hand rule. An equation for this magnetic field can be easily derived from Ampere's law that is discussed in Appendix B. Recall that the problem at hand is a static one (dc), so we can omit the displacement current term of Ampere's law. In doing so, we arrive at Ampere's law for the static case given in (4.5):

$$\oint_C \boldsymbol{H}_T \cdot d\boldsymbol{l} = I_{\text{enclosed}} \tag{4.10}$$

Choosing a circular contour C at a radius r from the wire, we observe that, because of symmetry, the magnetic field is tangent to the contour and the dot product can therefore be replaced by the ordinary product and the vector directions removed. Furthermore, it is evident, from symmetry, that the magnetic field will be the same at all points on this constant-radius contour and so can be removed from the integral. Thus, Ampere's law in (4.10) simplifies to

$$\begin{aligned} H_T &= \frac{1}{\oint_C d\boldsymbol{l}} \\ &= \frac{1}{2\pi r} \quad \text{(in A/m)} \end{aligned} \tag{4.11}$$

where the direction of H_T is circumferential about the wire. The transverse magnetic flux density vector is related to this by $\boldsymbol{B}_T = \mu_0 \boldsymbol{H}_T$, where we assume that the surrounding medium is not ferromagnetic. The first basic subproblem is to determine the total magnetic flux ψ_m penetrating a surface S of unit length along the wire direction that lies between a radius R_1 and a radius R_2 from the wire, as shown in Fig. 4.6a. This is obtained by integrating the magnetic flux density vector over the surface, resulting in

$$\begin{aligned} \psi_m &= \int_S \boldsymbol{B}_T \cdot d\boldsymbol{s} \\ &= \int_{S_1} \boldsymbol{B}_T \cdot d\boldsymbol{s} + \underbrace{\int_{S_2} \boldsymbol{B}_T \cdot d\boldsymbol{s}}_{0} + \underbrace{\int_{S_{\text{end}}} \boldsymbol{B}_T \cdot d\boldsymbol{s}}_{0} \\ &= \int_{r=R_1}^{R_2} \frac{\mu_0 I}{2\pi r} dr \\ &= \frac{\mu_0 I}{2\pi} \ln\left(\frac{R_2}{R_1}\right) \quad \text{(in Wb)} \ R_2 > R_1 \end{aligned} \tag{4.12}$$

This simple result is easy to see. Consider the surface S as being, for generality, "tilted" as shown in Fig. 4.6a. Now, consider the *closed* surface consisting of the "wedge-shaped" surface that consists of the original tilted surface S and two other surfaces along with end caps illustrated in Fig. 4.6b. Surface S_1 is the flat surface that is formed by moving radially outward from radius R_1 to R_2. Surface S_2 is formed by moving from the end of this previously constructed surface along a constant radius R_2 down to the edge of the original surface that is at a radius R_2 from the wire. This somewhat wedge-shaped surface along with the end caps forms a closed surface to which we apply Gauss' law, which states that *the total magnetic flux leaving a closed surface is zero; that is, whatever magnetic flux enters a closed surface must leave that closed surface*. The magnetic flux vector is parallel to the end caps, and so no net flux leaves the closed surface through the end caps. Also the magnetic flux vector is tangent to S_2 (the surface at a constant radius R_2 from the wire), so that no flux enters or leaves this surface. This leaves us with the fact that *magnetic flux that penetrates* S_1 *must also penetrate the original surface S*. Therefore, *the total magnetic flux penetrating the original tilted open surface S shown in Fig. 4.6a is the same as the total magnetic flux penetrating the untilted surface S shown in Fig. 4.6c*. This important observation considerably simplifies the determination of the flux penetrating the original (tilted) surface S. Evaluating (4.12) for the untilted surface gives the desired result. It is important to note the direction of the resulting flux through the surface. The direction of the magnetic field is determined by the right-hand rule. For $R_2 > R_1$, the flux is directed through the surface as shown in Fig. 4.6a, so that ψ_m given in (4.12) is a positive quantity. The result in (4.12) should be committed to memory and the resulting direction of the flux through the surface should be firmly understood by the reader, since they will be used on numerous occasions. This is a basic result that will be used to derive the per-unit-length parameters for multiconductor lines.

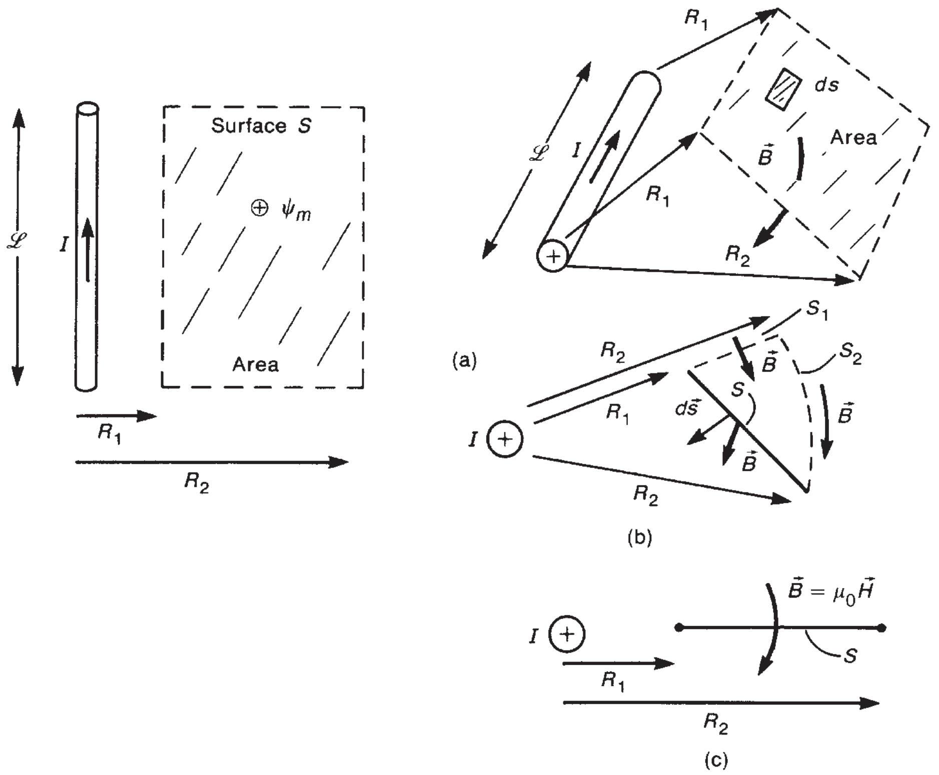

FIGURE 4.6 Illustration of a basic subproblem of determining the magnetic flux of a current through a surface: (a) dimensions of the problem; (b) use of Gauss' law; (c) an equivalent but simpler problem.

The second basic subproblem concerns the voltage between two points due to a wire that is carrying a per-unit-length charge distribution of q C/m that is uniformly distributed around the wire periphery as shown in Fig. 4.7a. As was the case with the previous derivations, an important assumption that is implicit in the following result is that the charge is uniformly distributed around the wire periphery. If we bring another charge-carrying wire in proximity to this wire, the interaction between the fields of the two charge distributions will cause the charge distributions to be largest on the facing sides. This is again referred to as *proximity effect*, and the following result ignores this. We will assume that the medium surrounding the wire is free space with $\varepsilon = \varepsilon_0 \cong 1/36\pi \times 10^{-9}$ F/m. Because of symmetry, the electric field due to this charge distribution $\boldsymbol{E}_T$ is transverse to the wire, is directed away from the wire, and is constant at a constant distance away from the wire. The electric field is obtained by using Gauss' law for the electric field

$$\oint_S \varepsilon_0 \boldsymbol{E}_T \cdot ds = Q_{\text{enclosed}} \tag{4.13}$$

Choosing the closed surface S to be a cylinder of radius r and unit length, with the wire centered on its axis as shown in Fig. 4.7b, we observe that the electric field is parallel to the end caps and so contributes nothing to Gauss' law over the ends. Therefore, we may simply evaluate (4.13) over the sides of the cylinder. But over the sides, the electric field is perpendicular to the sides, and so the dot product can be removed, as can the vector directions. Similarly, because the electric field is, by

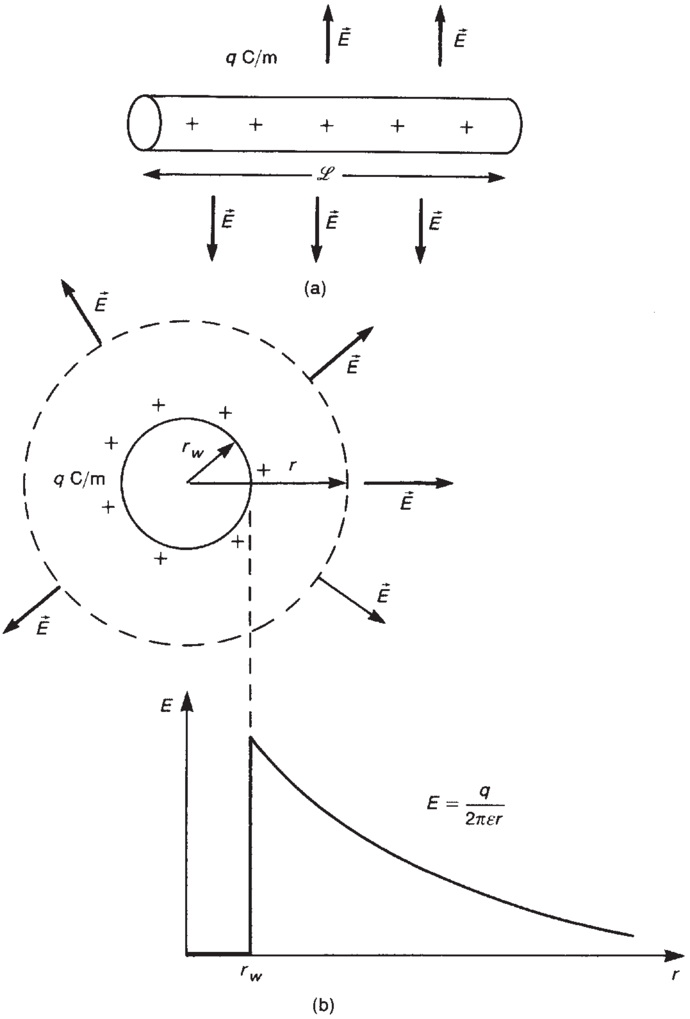

FIGURE 4.7 The electric field about a charge-carrying wire.

symmetry, the same at all points on this surface, the electric field can be removed from the integral, leaving

$$\begin{aligned} \boldsymbol{E}_T &= \frac{q \times 1\ \mathrm{m}}{\varepsilon_0 \int_S ds} \\ &= \frac{q}{2\pi\varepsilon_0 r} \quad (\text{in V/m}) \end{aligned} \tag{4.14}$$

where the field is directed in the radial direction. We now wish to obtain the voltage between two points that are at radial distances R_1 and R_2 from the wire as shown in Fig. 4.8a. The voltage is related to the line integral between point *a*, which is at the larger radius R_2, and point *b*, which is at the smaller radius R_1. The result is

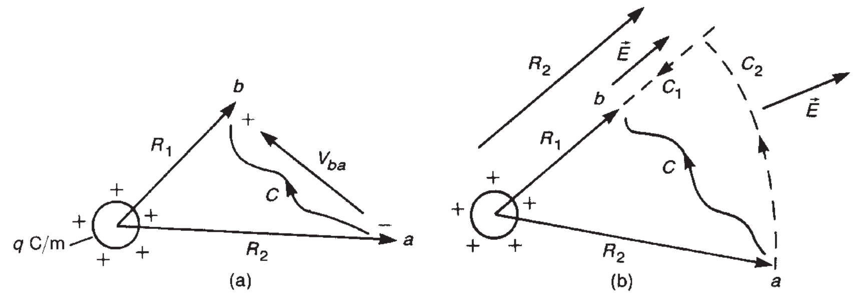

FIGURE 4.8 Illustration of a basic subproblem of determining the voltage between two points: (a) dimensions of the problem; (b) an equivalent but simpler problem.

$$\begin{aligned}
v &= -\int_{C} \mathbf{E}_T \cdot d\mathbf{l} \\
&= -\int_{C_1} \mathbf{E}_T \cdot d\mathbf{l} - \underbrace{\int_{C_2} \mathbf{E}_T \cdot d\mathbf{l}}_{0} \\
&= \int_{r=R_2}^{R_1} \frac{q}{2\pi\varepsilon_0 r}\, dr \\
&= \frac{q}{2\pi\varepsilon_0} \ln\left(\frac{R_2}{R_1}\right) \quad \text{(in V)} \quad R_2 \geq R_1
\end{aligned} \tag{4.15}$$

Again this simple result is due to our choice of the contour over which to perform the integral in (4.15). We choose to integrate along the two contours C_1 and C_2 shown in Fig. 4.8b instead of some general contour between the two points. Because of symmetry, the electric field is perpendicular to the contour C_2, which is at a constant radius R_2 from the wire, and so nothing is contributed to the integral along this *equipotential* contour. Thus the voltage can be obtained by simply integrating from a distance R_2 to a distance R_1 along a radial line between these two points. Observe that the point closer to the positively charged wire is at the higher voltage. This is sensible, since voltage is the work required to move a unit positive charge between the two points. In this case, with the wire positively charged and $R_2 > R_1$, work will be required to move the unit positive charge from R_2 to R_1, so that the closer point will be at the higher potential. Equation (4.15) confirms this observation. It is important for the reader to commit the fundamental result in (4.15) to memory and to be able to perform these types of simple checks on the result, since this result will be used on numerous occasions. Also observe the duality between this result in (4.15) and the result in (4.12).

The two fundamental subproblems and results presented above allow the straightforward derivation of the per-unit-length parameters for the structures of Fig. 4.1. First consider the two-wire line of Fig. 4.1a. Suppose that one wire carries a current I directed into the page and the other wire carries a current of the same magnitude but directed out of the page. Denote the radius of one wire as r_{w1} and the radius of the other as r_{w2}. If the wires are separated by a distance s, the total magnetic flux between the wires is obtained from Fig. 4.9a using (4.12) as

$$\begin{aligned}
\psi_m &= \frac{\mu_0 I}{2\pi} \ln\left(\frac{s - r_{w2}}{r_{w1}}\right) + \frac{\mu_0 I}{2\pi} \ln\left(\frac{s - r_{w1}}{r_{w2}}\right) \\
&= \frac{\mu_0 I}{2\pi} \ln\left[\frac{(s - r_{w2})(s - r_{w1})}{r_{w2} r_{w1}}\right]
\end{aligned} \tag{4.16}$$

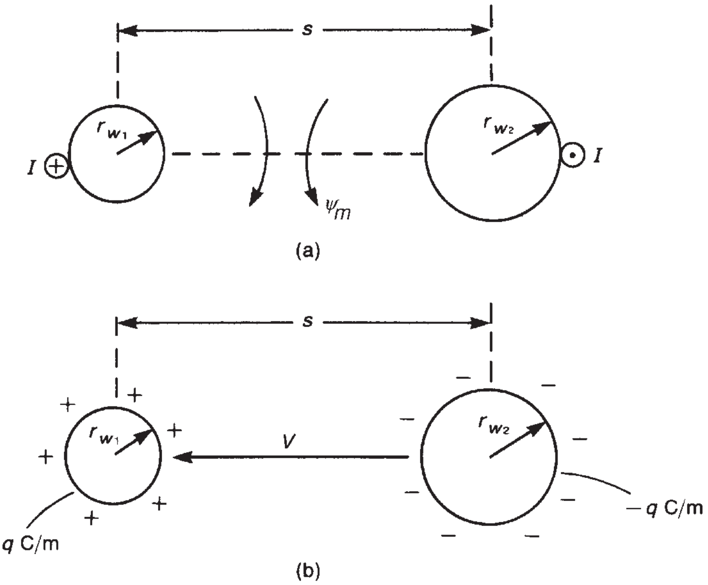

FIGURE 4.9 Determination of the per-unit-length parameters of a two-wire line: (a) inductance; (b) capacitance.

In order to use the basic result in (4.12), the currents must be uniformly distributed around the periphery of each wire, which essentially required that the wires be widely separated [1]. Thus implicit in (4.16) is the requirement that $s \gg r_{w2}, r_{w1}$.

Therefore, the result simplifies to

$$\psi_m = \frac{\mu_0 I}{2\pi} \ln\left(\frac{s^2}{r_{w2} r_{w1}}\right) \quad s \gg r_{w2}, r_{w1} \tag{4.17}$$

Ordinarily, if the ratio of the wire separation to wire radius is greater than approximately 5, i.e., $s/r_{w1} > 5$ and $s/r_{w2} > 5$, Eq. (4.17) gives accuracy within approximately 3% [1]. The per-unit-length external inductance is defined as the ratio of the flux penetrating a unit length surface between the wires. Using (4.17), we obtain

$$\begin{aligned} l &= \frac{\psi_m}{I} \\ &= \frac{\mu_0}{2\pi} \ln\left(\frac{s^2}{r_{w2} r_{w1}}\right) \quad \text{(in H/m)} \quad s \gg r_{w2}, r_{w1} \end{aligned} \tag{4.18}$$

Generally, both wires will have the same radii. For this case, the result in (4.18) becomes

$$\begin{aligned} l &= \frac{\mu_0}{\pi} \ln\left(\frac{s}{r_w}\right), \quad r_{w1} = r_{w2} = r_w \\ &= 0.4 \ln\left(\frac{s}{r_w}\right) \quad \text{(in μH/m)} \\ &= 10.16 \ln\left(\frac{s}{r_w}\right) \quad \text{(in nH/in.)} \end{aligned} \tag{4.19}$$

Although this result gives reasonable approximations for widely separated wires, the exact result is derived in [1] and is

$$
\begin{aligned}
l &= \frac{\mu_0}{\pi}\cosh^{-1}\left(\frac{s}{2r_w}\right) \quad (\text{in H/m}) \\
&= \frac{\mu_0}{\pi}\ln\left[\frac{s}{2r_w} + \sqrt{\left(\frac{s}{2r_w}\right)^2 - 1}\right]
\end{aligned} \tag{4.20}
$$

where $\cosh^{-1}x = \ln\left[x + \sqrt{x^2 - 1}\right]$ and $\cosh^{-1}x \cong \ln(2x)$ for $x \gg 1$. For a separation-to-wire radius of $s/r_w = 4$, the approximate result in (4.19) is higher than the exact result in (4.20) by only 5%.

The next per-unit-length parameter required for the two-wire line is the capacitance. This can be obtained from the per-unit-length inductance using (4.8b) and the exact value of the per-unit-length inductance from (4.20) as

$$
\begin{aligned}
c &= \frac{\mu_0 \varepsilon_0}{l} \\
&= \frac{1}{v_0^2 l} \\
&= \frac{\pi\varepsilon_0}{\cosh^{-1}(s/2r_w)} \quad (\text{in F/m})
\end{aligned} \tag{4.21}
$$

If the ratio of wire separation to wire radius is sufficiently large such that the charge distribution around the peripheries of the wires is essentially constant, then (4.21) simplifies to

$$
c \cong \frac{\pi\varepsilon_0}{\ln(s/2r_w)} \quad (\text{in F/m}) \quad s \geq r_w \tag{4.22}
$$

This approximate result can be derived using the result for the second basic sub problem for the voltage between two points due to a charged wire given in (4.15). In order to use that result, the charge distributions must be uniform around the wire peripheries so that we must implicitly rule out proximity effects and consider widely spaced wires. Consider the two wires of radii r_{w1} and r_{w2} and separated by distance s shown in Fig. 4.9b. The voltage between the wires is given, according to (4.15), by

$$
\begin{aligned}
v &= \frac{q}{2\pi\varepsilon_0}\ln\left(\frac{s - r_{w2}}{r_{w1}}\right) + \frac{q}{2\pi\varepsilon_0}\ln\left(\frac{s - r_{w1}}{r_{w2}}\right) \\
&= \frac{q}{2\pi\varepsilon_0}\ln\left[\frac{(s - r_{w2})(s - r_{w1})}{r_{w2} r_{w1}}\right] \\
&\cong \frac{q}{2\pi\varepsilon_0}\ln\left(\frac{s^2}{r_{w2} r_{w1}}\right)
\end{aligned} \tag{4.23}
$$

For equal radii wires (4.23) reduces to

$$
v = \frac{q}{2\pi\varepsilon_0}\ln\left(\frac{s}{r_w}\right), \quad r_{w1} = r_{w2} = r_w \tag{4.24}
$$

The per-unit-length capacitance is the ratio of the per-unit-length charge to the voltage between the two wires:

$$\begin{aligned} c &= \frac{q}{v} \\ &= \frac{\pi \varepsilon_0}{ln\,(s/r_w)} \\ &= \frac{27.78}{ln\,(s/r_w)} \quad (\text{in pF/m}) \\ &= \frac{0.706}{ln\,(s/r_w)} \quad (\text{in pF/in.}) \end{aligned} \tag{4.25}$$

Review Exercise 4.1 Determine the exact and approximate values for the per-unit-length inductance and capacitance of a two-wire ribbon cable consisting of two 28-gauge 7 × 36 wires ($r_w = 7.5$ mils) separated by 50 mils. Determine the ratio of wire separation to wire radius.

Answers: Exact, 0.75 μH/m = 19.04 nH/in., 14.82 pF/m = 0.3765 pF/in., approximate, 0.759 μH/m = 19.27 nH/in., 14.64 pF/m = 0.372 pF/in. The ratio of wire separation to wire radius is 6.7.

The per-unit-length parameters for the case of one wire above a ground plane shown in Fig. 4.1b can be easily derived from the results for the case of two parallel wires using the method of images [1, 2]. First, consider the per-unit-length capacitance. The wire is at a height h above the ground plane, and the latter can be replaced with the image of the wire, as shown in Fig. 4.10. From this result we can see that the desired capacitance between the wire and the ground plane is twice the capacitance of two wires separated a distance of $2h$, since capacitors in series combine like resistors in parallel. Thus, using the previous results, we obtain

$$c = \frac{2\pi\varepsilon_0}{\cosh^{-1}(h/r_w)} \quad (\text{in F/m}) \tag{4.26}$$

For wires that are sufficiently far from the ground plane, this simplifies to

$$c \cong \frac{2\pi\varepsilon_0}{\ln(2h/r_w)} \quad (\text{in F/m}) \; h \gg r_w \tag{4.27}$$

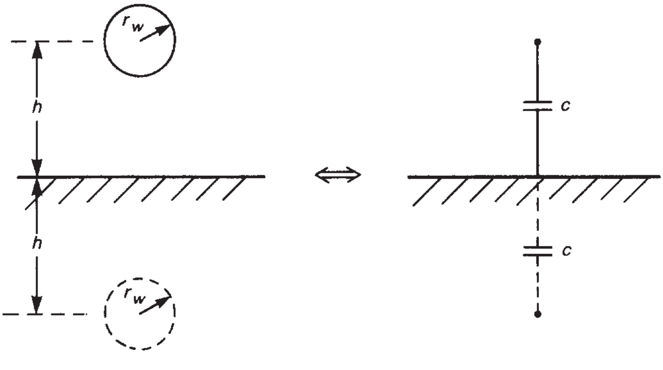

FIGURE 4.10 Determination of the per-unit-length capacitance of a wire above a ground plane with the method of images.

The per-unit-length inductance can be obtained from the per-unit-length capacitance in (4.26) using (4.8b) as

$$\begin{aligned} l &= \frac{\mu_0 \varepsilon_0}{c} \\ &= \frac{\mu_0}{2\pi} \cosh^{-1}\left(\frac{h}{r_w}\right) \quad (\text{in H/m}) \end{aligned} \tag{4.28}$$

If the wires are widely separated, this simplifies to

$$l \cong \frac{\mu_0}{2\pi} \ln\left(\frac{2h}{r_w}\right) \quad (\text{in H/m}) \quad h \gg r_w \tag{4.29}$$

Review Exercise 4.2 Determine the exact and approximate values for the per-unit-length capacitance and inductance of one 20-gauge solid wire of radius 16 mils at a height of 1 cm above an infinite ground plane. Determine the ratio $2h/r_w$.

Answers: Exact, 14.26 pF/m = 0:36 pF/in:, 0:779 μH = m = 19:79 nH/in., approximate, 14:26 pF/m = 0:36 pF/in:, 0:779 μH/m = 19:79 nH/in., The ratio $2h/r_w = 49$. Hence, the exact and approximate results should be the same.

The remaining structure in Fig. 4.1, the coaxial cable shown in part (c), is derived in a similar fashion [1, 2]. Because of symmetry, the electric field is radially directed and magnetic field is circumferentially directed, as shown in Fig. 4.11. Symmetry also shows that if we place a per-unit-length positive charge distribution q C/m on the inner wire and a negative charge distribution $-q$ C/m on the inner surface of the shield, the resulting charge distributions will be uniform around the peripheries of these conductors regardless of the wire radius r_w or the shield interior radius r_s. Similarly, if current I flows along the inner wire surface and returns along the interior surface of the shield, these currents will also be uniformly distributed over the cross section of the conductors. In other words, the proximity effect is not a factor for this structure. Consequently, the *exact* equations for the per-unit-length parameters can be easily derived using the two basic subproblem results in (4.12) and (4.15). For example, the transverse magnetic flux density is circumferentially directed and is obtained from (4.11) as

$$\begin{aligned} B_T &= \mu_0 H_T \\ &= \frac{\mu_0 I}{2\pi r} \end{aligned} \tag{4.30}$$

where the dielectric interior to the shield is assumed to be nonferromagnetic, so that $\mu = \mu_0$. The per-unit-length inductance can be found by determining the total magnetic flux penetrating a unit-length surface between the wire and the shield interior surface shown in Fig. 4.11b as

$$\begin{aligned} \psi_m &= \int_S \boldsymbol{B}_T \cdot d\boldsymbol{s} \\ &= \int_{r=r_w}^{r_s} \frac{\mu_0 I}{2\pi r} \\ &= \frac{\mu_0 I}{2\pi} \ln\left(\frac{r_s}{r_w}\right) \end{aligned} \tag{4.31}$$

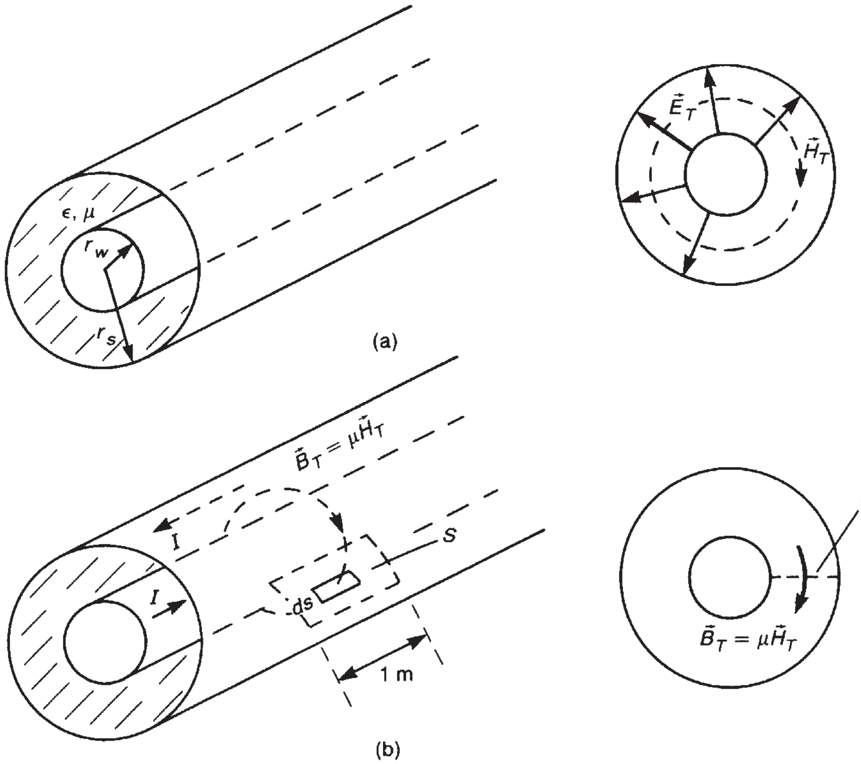

FIGURE 4.11 Determination of the per-unit-length parameters of a coaxial cable: (a) symmetry of the cross-sectional fields; (b) inductance.

Observe that this could have been directly obtained using the fundamental subproblem result given in (4.12). Therefore, the *exact* value of the per-unit-length inductance is

$$\begin{aligned} l &= \frac{\psi_m}{I} \\ &= \frac{\mu_0}{2\pi}\ln\left(\frac{r_s}{r_w}\right) \\ &= 0.2\ln\left(\frac{r_s}{r_w}\right) \quad (\text{in } \mu\text{H/m}) \\ &= 5.08\ln\left(\frac{r_s}{r_w}\right) \quad (\text{in nH/in.}) \end{aligned} \tag{4.32}$$

The per-unit-length capacitance can be obtained using the fundamental result in (4.14) to give

$$E_T = \frac{q}{2\pi\varepsilon} \tag{4.33}$$

where the dielectric interior to the shield has permittivity ε. The voltage between the inner wire and the interior surface of the shield is (assuming the wire is at the higher potential) obtained as

$$\begin{aligned} V &= -\int_{r_s}^{r_w} \boldsymbol{E}_T \cdot d\boldsymbol{l} \\ &= \frac{q}{2\pi\varepsilon} \ln\left(\frac{r_s}{r_w}\right) \end{aligned} \tag{4.34}$$

The per-unit-length capacitance is obtained as

$$\begin{aligned} c &= \frac{q}{v} \\ &= \frac{2\pi\varepsilon}{\ln(r_s/r_w)} \\ &= \frac{55.56\varepsilon_r}{\ln(r_s/r_w)} \quad (\text{in pF/m}) \\ &= \frac{1.4\varepsilon_r}{\ln(r_s/r_w)} \quad (\text{in pF/in}) \end{aligned} \tag{4.35}$$

Observe that

$$\begin{aligned} lc &= \mu\varepsilon \\ &= \frac{\varepsilon_r}{v_0^2} \end{aligned} \tag{4.36}$$

where the medium interior to the shield is homogeneous and characterized by $\mu = \mu_0$, $\varepsilon = \varepsilon_0\varepsilon_r$, and $v_0 = 3 \times 10^8$ m/s.

Review Exercise 4.3 Consider a typical coaxial cable, RG58U, which consists of an inner 20-gauge solid wire ($r_w = 16$ mils) and a shield (braided) having an inner radius of 58 mils. The interior dielectric is polyethylene ($\varepsilon_r = 2.3$). Determine the per-unit-length capacitance and inductance, as well as the velocity of propagation as a percentage of the speed of light.

Answers: 0.2576 μH/m = 6.54 nH/in., 99.2 pF/m = 2.52 pF/in., 66%.

4.2.2 Printed Circuit Board (PCB) Structures

The common printed circuit board (PCB) configurations shown in Fig. 4.2 are shown in cross section in Fig 4.12. Rather than specifying these with a per-unit-length capacitance c and inductance l, it is more common to specify them in terms of an important transmission-line parameter, the characteristic impedance

$$Z_c = \sqrt{\frac{l}{c}} \ \Omega \tag{4.37}$$

The second fundamental transmission-line parameter is the velocity of propagation discussed earlier. The velocity of propagation is given as

$$\begin{aligned} v &= \frac{1}{\sqrt{lc}} \\ &= \frac{1}{\sqrt{\mu_0\varepsilon_0\varepsilon_r'}} \\ &= \frac{v_0}{\sqrt{\varepsilon_r'}} \ \text{m/s} \end{aligned} \tag{4.38}$$

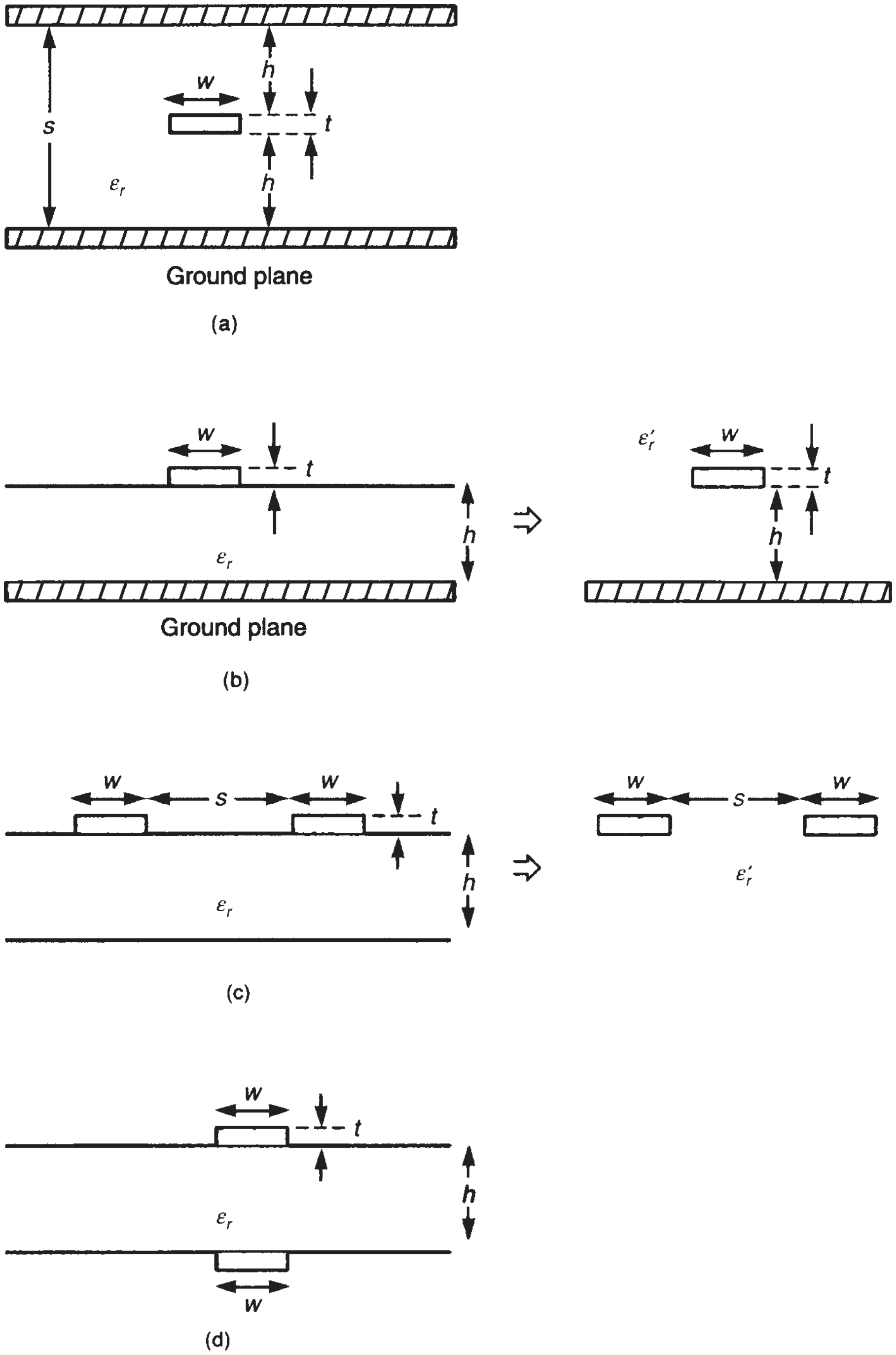
w
h
s
t
h
ε_r
Ground plane
(a)
w
t
h
ε_r
Ground plane
ε′_r
w
t
h
(b)
w
s
w
t
h
ε_r
w
s
w
ε′_r
(c)
w
t
h
ε_r
w
(d)

FIGURE 4.12 Cross-sectional dimensions of lines composed of rectangular cross-section conductors: (a) a stripline; (b) a microstrip line; (c) a printed circuit board (PCB I) consisting of strips on the same side; (d) a printed circuit board (PCB II) consisting of strips on opposite sides.

where ε_r' is an *effective relative permittivity or effective dielectric constant.* The inductance and capacitance per unit length can be determined in terms of the characteristic impedance and velocity of propagation as

$$l = \frac{Z_C}{v} \tag{4.39a}$$

$$c = \frac{1}{vZ_C} \tag{4.39b}$$

Generally, the exact per-unit-length parameters cannot be determined in formula form but can be obtained as approximate relations. Some are obtained by conformal mapping [3], and some are obtained by numerical methods. References [3–9] provide the following results.

The stripline in Fig. 4.12a is in a homogeneous medium, so that the effective relative permittivity is the actual relative permittivity of the dielectric, $\varepsilon_r' = \varepsilon_r$. This configuration represents traces on a PCB that are buried between two innerplanes. The characteristic impedance is as given in [4], where we assume a zero thickness strip, $t = 0$:

$$z_C = \frac{30\pi}{\sqrt{\varepsilon_r}} \frac{1}{\left[\frac{w_e}{s} + 0.441\right]} \tag{4.40a}$$

where the effective width of the center conductor is

$$\frac{w_e}{s} = \begin{cases} \frac{w}{s} & \frac{w}{s} \le 0.35 \\ \frac{w}{s} - \left(0.35 - \frac{w}{s}\right)^2 & \frac{w}{s} \le 0.35 \end{cases} \tag{4.40b}$$

Review Exercise 4.4 Determine the per-unit-length capacitance and inductance of a stripline having dimensions $s = 20$ mils, $w = 5$ mils, and a dielectric having $\varepsilon_r = 4.7$.

***Answers*:** 113.2 pF/m = 2.88 pF/in., 0.461 μH/m = 11.7 nH/in.

The microstrip line shown in Fig. 4.12b has a land of width w placed on a board of thickness h having a relative permittivity of ε_r that has a ground plane on the opposite side. This represents the outer layer and an innerplane of a PCB. The characteristic impedance, assuming the land thickness is zero ($t = 0$) is

$$Z_C = \begin{cases} \frac{60}{\sqrt{\varepsilon_r'}} \ln\left[\frac{8h}{w} + \frac{w}{4h}\right] & \frac{w}{h} \le 1 \\ \frac{120}{\sqrt{\varepsilon_r'}} \left[\frac{w}{h} + 1.393 + 0.667 \ln\left(\frac{w}{h} + 1.444\right)\right]^{-1} & \frac{w}{h} \ge 1 \end{cases} \tag{4.41a}$$

The effective relative permittivity is

$$\varepsilon_r' = \frac{\varepsilon_r + 1}{2} + \frac{\varepsilon_r - 1}{2} \frac{1}{\sqrt{1 + 10h/w}} \tag{4.41b}$$

This effective relative permittivity accounts for the fact that the electric field lines are partly in the substrate dielectric and partly in the air. If this inhomogeneous medium (air and the dielectric) is replaced with a homogeneous one having an effective relative permittivity of ε_r' as shown in Fig. 4.12b, then all properties of the line remain unchanged. But this homogeneous medium case is much easier to analyze and to compute the velocity of propagation as in (4.38). Observe that depending on the strip width relative to the board thickness, we can obtain some extreme approximations:

$$\varepsilon_r' = \begin{cases} \varepsilon_r & h \ll w \\ \frac{\varepsilon_r+1}{2} & h \gg w \end{cases} \tag{4.41c}$$

The first approximation is that the strip width is much larger than the board thickness. Hence, the majority of the electric field is confined to the dielectric. The second approximation is that the strip is very narrow compared to the board thickness so that the electric field lies about equally in the board and the surrounding air. Also a simpler but more approximate relation for the microstrip is obtained in [8] as

$$Z_c = \frac{87}{\sqrt{\varepsilon_r + 1.41}} \ln\left(\frac{5.98h}{0.8w + t}\right) \tag{4.41d}$$

This relation is valid for land thickness-to-width ratios of $0.1 \le t/w \le 0.8$. For 1 ounce copper lands where $t = 1.38$ mils, this restriction is satisfied as long as $1.725 \text{ mils} \le w \le 13.8$ mils. For a microstrip having dimensions of $h = 50$ mils, $w = 5$ mils, and $\varepsilon_r = 4.7$, Eq. (4.41a) yields a characteristic impedance of 151 Ω, whereas (4.41d) (with $t = 0$) yields 151.8 Ω.

Review Exercise 4.5 Determine the per-unit-length capacitance and inductance of a microstrip line having dimensions of $h = 50$ mils, $w = 5$ mils, and $\varepsilon_r = 4.7$.

***Answers*:** 38.46 pF/m = 0.977 pF/m, 0.877 μH/m = 22.3 nH/in. The effective relative permittivity is $\varepsilon_r' = 3.034$.

The PCB I configuration in Fig. 4.12c has two lands of width w placed on one side of a board and separated edge to edge a distance s. This is referred to as the coplanar strips configuration and represents two lands on the outer surfaces of a PCB. The board has thickness h and a relative permittivity of ε_r. Assuming a land thickness of zero ($t = 0$), the characteristic impedance is

$$Z_c = \begin{cases} \dfrac{120}{\sqrt{\varepsilon_r'}} \ln\left(2\dfrac{1+\sqrt{k}}{1-\sqrt{k}}\right) & \dfrac{1}{\sqrt{2}} \le k \le 1 \\ \dfrac{377\pi}{\sqrt{\varepsilon_r'} \ln\left(2\dfrac{1+\sqrt{k'}}{1-\sqrt{k'}}\right)} & 0 \le k \le \dfrac{1}{\sqrt{2}} \end{cases} \tag{4.42a}$$

where k is

$$k = \frac{s}{s + 2w} \tag{4.42b}$$

and $k' = \sqrt{1 - k^2}$. The effective relative permittivity is

$$\varepsilon_r' = \frac{\varepsilon_r + 1}{2} \left\{ \tanh\left[0.775 \ln\left(\frac{h}{w}\right) + 1.75\right] + \frac{kw}{h}[0.04 - 0.7k + 0.01(1 - 0.1\varepsilon_r)(0.25 + k)] \right\} \tag{4.42c}$$

which again accounts for the fact that the electric field lines are partly in air and partly in the substrate dielectric. If this inhomogeneous medium (air and dielectric) is replaced with a homogeneous one having an effective relative permittivity of ε_r' as shown in Fig. 4.12c, all properties of the line remain unchanged.

Review Exercise 4.6 Determine the per-unit-length capacitance and inductance of a PCB I configuration having dimensions $s = 15$ mils, $w = 15$ mils, $h = 62$ mils, and $\varepsilon_r = 4.7$.

Answers: 38.53 pF/m = 0.979 pF/in., 0.804 μH/m = 20.42 nH/in.

The case of two equal-width strips placed on opposite sides of the board shown in Fig. 4.12d is referred to as the *PCB II configuration*. This is not generally found on PCBs because lands on opposite sides of layers are generally routed orthogonal to each other in order to "wire the board." Using vias to jump from one layer to the other, routing blockages can be avoided. The characteristic impedance is given in [9] as (for $t = 0$)

$$\begin{aligned} Z_c &= \frac{377}{\sqrt{\varepsilon_r}\left\{\frac{w}{h} + 0.441 + \frac{\varepsilon_r+1}{2\pi\varepsilon_r}\left[\ln\left(\frac{w}{h} + 0.94\right) + 1.451\right] + 0.082\frac{\varepsilon_r-1}{(\varepsilon_r)^2}\right\}} \\ &= \text{for } \frac{w}{h} > 1 \end{aligned} \tag{4.43a}$$

and

$$\begin{aligned} Z_c &= \frac{377\sqrt{2}}{\pi\sqrt{\varepsilon_r + 1}}\left[\ln\left(\frac{4h}{w}\right) + \frac{1}{8}\left(\frac{w}{h}\right)^2 - \frac{1}{2}\left(\frac{\varepsilon_r - 1}{\varepsilon_r + 1}\right)\left(0.452 + \frac{0.242}{\varepsilon_r}\right)\right] \\ &= \text{for } \frac{w}{h} < 1 \end{aligned} \tag{4.43b}$$

For a glass epoxy board with a wide conductor $w = 200$ mils, and $h = 62$ mils. we obtain from (4.43a) $Z_C = 41.05\ \Omega$. For coplanar strips with $w = 200$ mils, $s = 62$ mils, and $h = 62$ mils we compute from (4.42a) $Z_C = 155.7\ \Omega$. This illustrates the point that *pairs of wide lands placed on opposite sides of the board will give characteristic impedances lower than placing the lands on the same side of the board* (and using a spacing equal to the board width). Low-impedance power distribution circuits can be obtained in this fashion. Power distribution requires lines having low inductance but high capacitance in order to reduce the effect of the $L\ (di\ /\ dt)$ voltage drops caused by sudden changes in the supply current. These voltage drops along the distribution line lower the dc voltages at the modules from, for example, 5 V, possibly causing logic errors. Since the characteristic impedance is $Z_C = 155.7\ \Omega$, a low Z_C indicates low inductance and/or high capacitance. Hence, dc power is often supplied by lands on opposite sides of a substrate (perhaps a substrate different from that of the PCB).

4.3 THE TIME-DOMAIN SOLUTION

The *time-domain solution* of the transmission-line equations refers to the *complete solution of those equations with no assumptions as to the time form of the line excitation*. The other solution of interest is the sinusoidal steady-state or frequency-domain solution considered in a later section, where the time form of the line excitation is restricted to being sinusoidal and furthermore the sinusoidal source is assumed to have been attached a sufficient length of time so that the transients have decayed to zero, leaving the steady-state solution. The time-domain solution is often referred to as being the "transient solution," which is a misnomer since the time-domain solution gives the total solution—transient plus steady state. We will first investigate a graphical method of sketching the terminal voltages of the line versus time. This gives considerable insight into what causes the overall waveform shape.

4.3.1 Graphical Solutions

The transmission-line equations governing lossless lines are given in coupled, first-order form in (4.2) and in uncoupled, second-order form in (4.3).

The solutions of the uncoupled, second-order form are [1, 2]

$$V(z,t) = V^{+}\left(t - \frac{z}{v}\right) + V^{-}\left(t + \frac{z}{v}\right) \tag{4.44a}$$

$$I(z,t) = \frac{1}{Z_C}V^{+}\left(t - \frac{z}{v}\right) + \frac{1}{Z_C}V^{-}\left(t + \frac{z}{v}\right) \tag{4.44b}$$

where Z_c is the characteristic impedance of the line:

$$\begin{aligned} Z_c &= \sqrt{\frac{l}{c}} \\ &= vl \\ &= \frac{1}{vc} \end{aligned} \tag{4.45a}$$

The characteristic impedance Z_c is a real (not complex) number. Hence, it would be more properly called the characteristic *resistance*. The word “impedance” is a frequency-domain (phasor) term, but here the source voltage waveform is not necessarily a single-frequency sinusoid but may have an arbitrary waveform. However, it has become an industry standard to refer to Z_c as the characteristic *impedance*, as we will continue to do here.

The velocity of propagation on the line is

$$\begin{aligned} v &= \frac{1}{\sqrt{lc}} \\ &= \frac{1}{\sqrt{\mu\varepsilon}} \end{aligned} \tag{4.45b}$$

where the medium surrounding the conductors is characterized by μ and ε. These results apply to lines in an inhomogeneous medium, where we would use $\varepsilon = \varepsilon_0\varepsilon_r'$ and ε_r' is the effective dielectric constant. The general forms of the solution given in (4.44) are in terms of the functions $V^{+}(t - z\ /\ v)$ and $V^{-}(t + z\ /\ v)$. The precise forms of these functions will be determined by the functional time-domain form of the excitation source, $V_S(t)$. Nevertheless, they show that time and position must be related as $t - z\ /\ v$ and the $t + z\ /\ v$ in these forms. The function V^{+} represents a *forward-traveling wave* traveling in the $+z$ direction. This is clear, since as time increases, z must also increase to keep the argument of the function constant; that is, in order to track the movement of a point on the wave. Similarly, the function V^{-} represents a *backward-traveling wave* traveling in the $-z$ direction on the line. Thus, the total solution consists of the sum of forward-traveling and backward-traveling waves. The current of each wave is related to the voltage of that wave by the characteristic impedance:

$$I^{+}\left(t - \frac{z}{v}\right) = \frac{1}{Z_C}V^{+}\left(t - \frac{z}{v}\right) \tag{4.46a}$$

$$I^{-}\left(t + \frac{z}{v}\right) = -\frac{1}{Z_C}V^{-}\left(t + \frac{z}{v}\right) \tag{4.46b}$$

We will consider lines of total length L. The forward- and backward-traveling waves are related at the load, $z = L$, by the *load reflection coefficient* as [1, 2]

$$\begin{aligned}\Gamma_L &= \frac{V^-(t + L/v)}{V^+(t - L/v)}\\ &= \frac{R_L - Z_c}{R_L + Z_c}\end{aligned} \tag{4.47}$$

Therefore, the reflected waveform at the load can be found from the incident wave using the reflection coefficient as

$$V^-\left(t + \frac{L}{v}\right) = \Gamma_L V^+\left(t - \frac{L}{v}\right) \tag{4.48}$$

The reflection coefficient given in (4.47) applies to voltages only. A current reflection coefficient can be derived by substituting (4.47) into (4.46), so that

$$I^-\left(t + \frac{L}{v}\right) = -\Gamma_L I^+\left(t - \frac{L}{v}\right) \tag{4.49}$$

Observe that the current reflection coefficient is the negative of the voltage reflection coefficient.

This reflection of waves at the load discontinuity is illustrated in Fig. 4.13. The reflection process can be viewed as a mirror that produces, as a reflected V^-, a replica of V^+ that is "flipped around," and all points on the V^- waveform are the corresponding points on the V^+ waveform multiplied by Γ_L. Note that the total voltage at the load, $V(L, t)$, is the *sum* of the individual waves present at the load at a particular time as shown by (4.44).

Now let us consider the portion of the line at the source, $z = 0$, shown in Fig. 4.14. When we initially connect the source to the line, we reason that a forward-traveling wave will be propagated down the line. We would not expect a backward-traveling wave to appear on the line until this initial forward-traveling wave has reached the load, a time delay of $T_D = L/v$, since the incident wave will not have arrived to produce this reflected wave. The portion of the incident wave that is reflected at the load will require an additional time T_D to move back to the source at $z = 0$. Therefore, for $0 \le t \le 2L/v$, no backward-traveling waves will appear at $z = 0$, and for any time less than $2T_D$ the *total* voltage and current at $z = 0$ will consist only of forward-traveling waves, V^+ and I^+.

Therefore,

$$V(0, t) = V^+\left(t - \frac{0}{v}\right) \tag{4.50a}$$

$$\begin{aligned}I(0, t) &= I^+\left(t - \frac{0}{v}\right)\\ &= \frac{V^+\left(t - \frac{0}{v}\right)}{Z_c} \quad \text{for } 0 \le t \le \frac{2L}{v}\end{aligned} \tag{4.50b}$$

Since the ratio of the *total* voltage and *total* current on the line is Z_c for $0 \le t \le 2L/v$, as shown in (4.50), the line appears to have an input resistance of Z_c over this time interval, as shown in Fig. 4.14b.

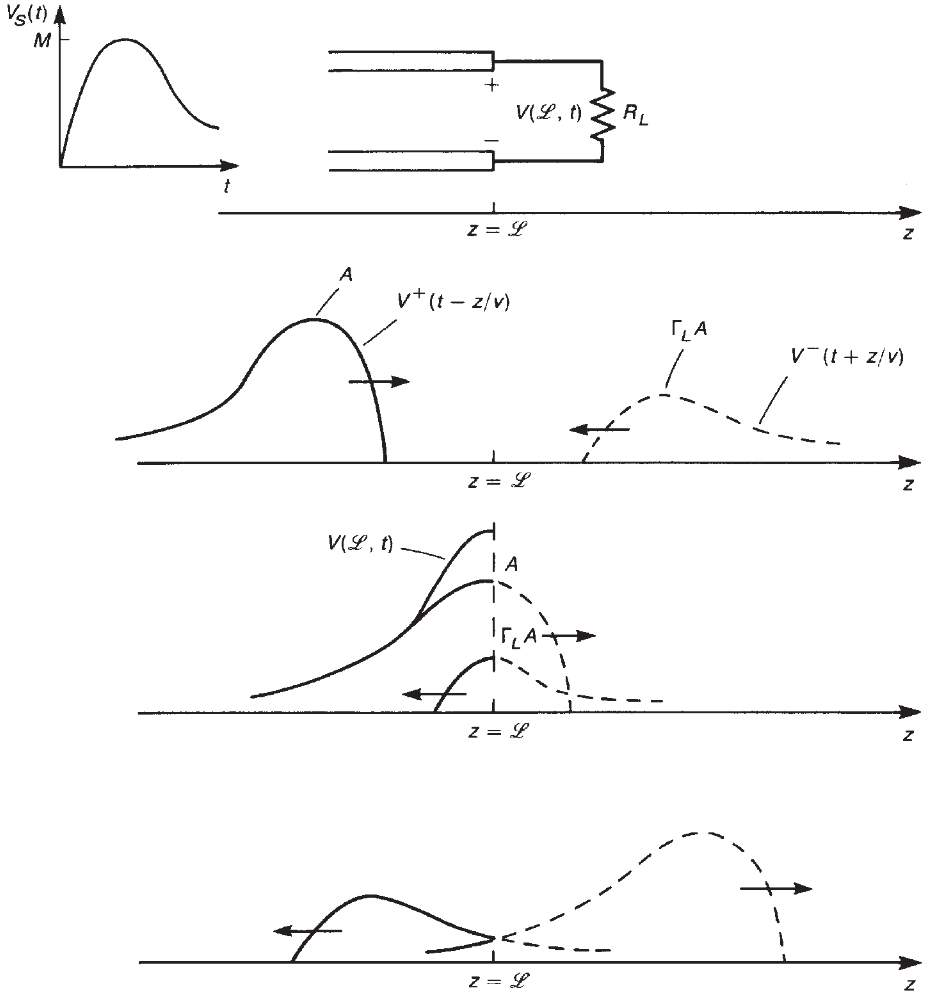
$V_S(t)$
M
t
$+$
$V(\mathscr{L}, t)$
R_L
$-$
$z = \mathscr{L}$
z
A
$V^+(t - z/v)$
$\Gamma_L A$
$V^-(t + z/v)$
$z = \mathscr{L}$
z
$V(\mathscr{L}, t)$
A
$\Gamma_L A$
$z = \mathscr{L}$
z
$z = \mathscr{L}$
z

FIGURE 4.13 Reflection of waves at a termination.

Thus, the forward-traveling voltage and current waves that are initially launched are related to the source voltage by (use voltage division)

$$V(0,t) = \frac{Z_C}{R_S + Z_C} V_S t \tag{4.51a}$$

$$I(0,t) = \frac{V_S(t)}{R_S + Z_C} \tag{4.51b}$$

The initially launched waves have the same shape as the source voltage.

The initially launched wave travels toward the load, requiring a time $T_D = L/v$ for the leading edge of the pulse to reach the load. When the pulse reaches the load, a reflected pulse is initiated, as shown in Fig. 4.13. This reflected pulse requires an additional time $T_D = L/v$ for its leading edge to reach the source. At the source, we can obtain a voltage reflection coefficient

$$\Gamma_S = \frac{R_S - Z_C}{R_S + Z_C} \tag{4.52}$$

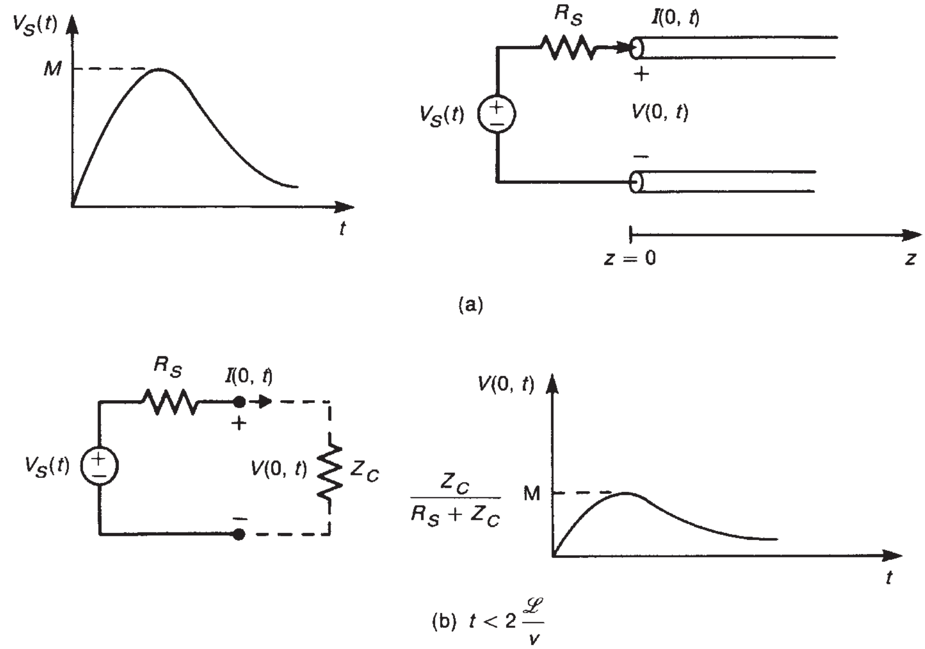

(a)

(b) $t < 2\frac{\mathcal{L}}{v}$

FIGURE 4.14 The equivalent circuit seen at the input to a line before the wave reflected at the load arrives.

as the ratio of the incoming incident wave (which is the reflected wave at the load) and the reflected portion of this incoming wave (which is sent back toward the load). A forward-traveling wave is therefore initiated at the source in the same fashion as at the load. This forward-traveling wave has the same shape as the incoming backward-traveling wave (which is the original pulse sent out by the source and reflected at the load), but corresponding points on the incoming wave are reduced by Γ_S. This process of repeated reflections continue as re-reflections at the source and load. At any time, the total voltage (current) at any point on the line is the sum of all the individual voltage (current) waves existing on the line at that point and time, as is shown by (4.44).

Review Exercise 4.7 Determine the characteristic impedances and velocities of propagation for the wire-type lines in Review Exercises 4.1–4.3

***Answers*:** 225 Ω, 3×10^8 m/s; 234 Ω, 3×10^8 m/s; 51 Ω, 1.98×10^8 m/s.

Review Exercise 4.8 Determine the characteristic impedances and velocities of propagation of the rectangular cross-section lines in Review Exercises 4.4–4.6.

***Answers*:** 63.8 Ω, 1.38×10^8 m/s; 151 Ω, 1.72×10^8 m/s; 144.45 Ω, 1.8×10^8 m/s.

Example 4.1 As an example, consider the transmission line shown in Fig. 4.15a. At $t = 0$ a 30 V battery with zero source resistance is attached to the line, which has a total length of $L = 400$ m, a velocity of propagation of $v = 200$ m/μs, and a characteristic impedance of $Z_C = 50$ Ω. The line is terminated in a 100 Ω resistor, so that the load reflection coefficient is

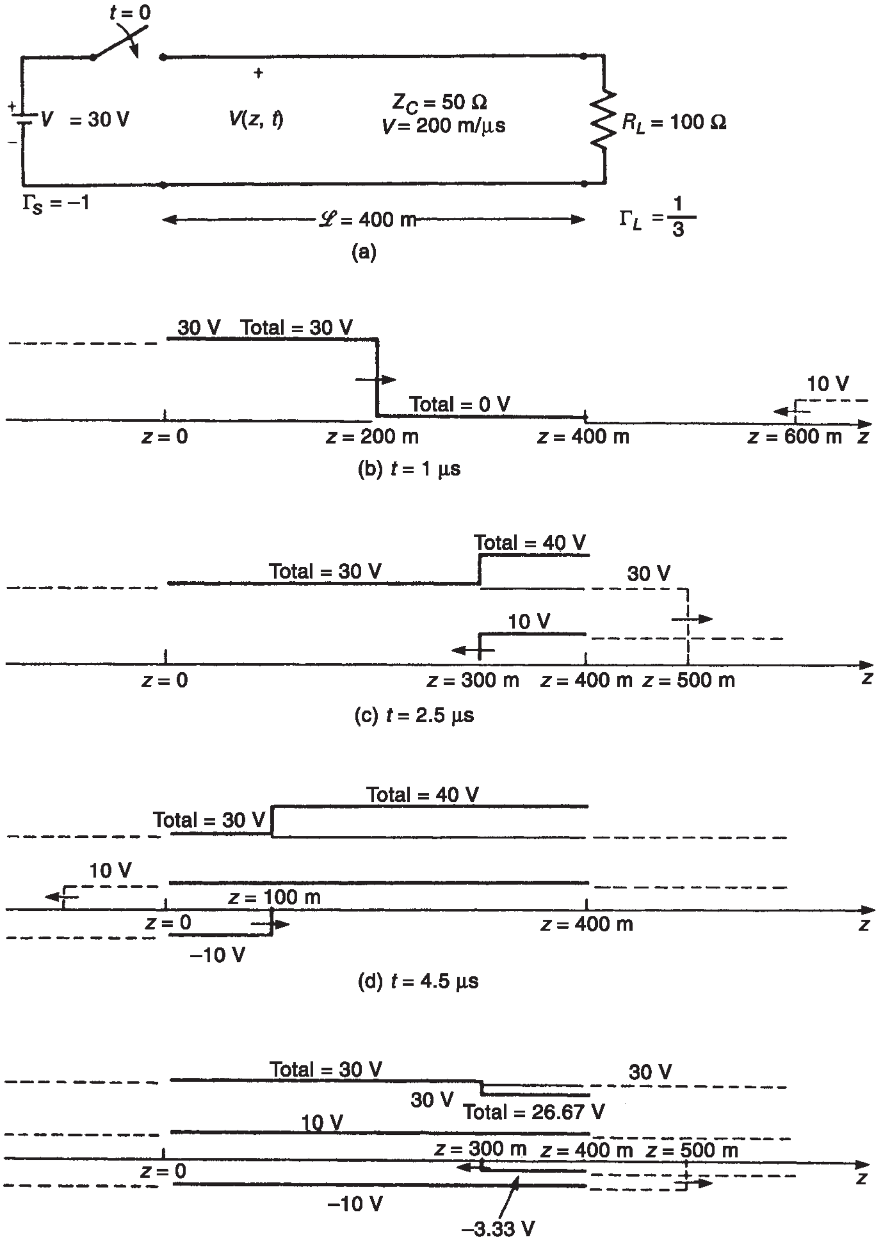
t = 0
+
V = 30 V
V(z, t)
Z_C = 50 Ω
V = 200 m/μs
R_L = 100 Ω
Γ_S = −1
ℒ = 400 m
Γ_L = 1/3
30 V Total = 30 V
Total = 0 V
10 V
z = 0
z = 200 m
z = 400 m
z = 600 m
z
Total = 40 V
Total = 30 V
30 V
10 V
z = 0
z = 300 m
z = 400 m
z = 500 m
z
Total = 40 V
Total = 30 V
10 V
z = 100 m
z = 0
z = 400 m
z
−10 V
Total = 30 V
30 V
30 V
Total = 26.67 V
10 V
z = 300 m
z = 400 m
z = 500 m
z = 0
z
−10 V
−3.33 V

(a)

(b) $t = 1$ μs

(c) $t = 2.5$ μs

(d) $t = 4.5$ μs

(e) $t = 6.5$ μs

FIGURE 4.15 An example to illustrate sketching the voltage on a line as a function of position, Example 4.1; (a) the subject transmission line; (b) voltage on the line at $t = 1$ μs; (c) voltage on the line at $t = 2.5$ μs, following the reflection by the terminating impedance $R_L = 100\ \Omega$; (d) voltage on the line at $t = 4.5$ μs, following the reflection by the source impedance $R_S = 0\ \Omega$; (e) voltage on the line at $t = 6.5$ μs, following the second reflection by the terminating impedance $R_L = 100\ \Omega$.

$$\Gamma_L = \frac{100-50}{100+50}$$
$$= \frac{1}{3}$$

and the source reflection coefficient is

$$\Gamma_S = \frac{0-50}{0+50}$$
$$= -1$$

The one-way transit time is $T_D = (L/v) = 2\ \mu s$. At $t = 0$, a 30 V pulse is sent down the line, and the line voltage is zero prior to the arrival of the pulse and 30 V after the pulse has passed. At $t = 2\ \mu s$, the pulse has arrived at the load, and a backward-traveling pulse of magnitude $30\ \Gamma_L = 10$ V is sent back toward the source. When this reflected pulse arrives at the source, a pulse of magnitude Γ_S of the incoming pulse or $30\ \Gamma_S\Gamma_L = -10$ V is sent back toward the load. This pulse travels to the load, at which time a reflected pulse of Γ_L of this incoming pulse or $30\ \Gamma_L\Gamma_S\Gamma_L = -3.33$ V is sent back toward the source. At each point on the line, the total line voltage is the sum of the waves present on the line at that point.

Example 4.2 The previous example has illustrated the process of sketching the line voltage at various points along the line and at discrete times. Generally, we are interested only in the voltage at the source and load ends of the line, $V(0, t)$ and $V(L, t)$, as continuous functions of time. In order to illustrate this process, let us reconsider the previous example and sketch the voltage at the line output, $z = L$, as a function of time, as is illustrated in Fig. 4.16. At $t = 0$, a 30 V pulse is sent out by the source. The leading edge of this pulse arrives at the load at $t = 2\ \mu s$. At this time, a pulse of $30\ \Gamma_L = 10$ V is sent back toward the source. This 10 V pulse arrives at the source at $t = 4\ \mu s$, and a pulse of $30\ \Gamma_S\Gamma_L = -10$ V is returned to the load. This pulse arrives at the load at $t = 6\ \mu s$, and a pulse of $30\ \Gamma_L\Gamma_S\Gamma_L = -3.33$ V is sent back toward the source. The contributions of these waves at $z = L$ are shown in Fig. 4.16 as dashed lines, and the total voltage is shown as a solid line. Note that the load voltage oscillates during the transient time interval about 30 V, but asymptotically converges to the expected steady-state value of 30 V. If we had attached an oscilloscope across the load to display this voltage as a function of time, and the timescale were set to 1 ms per division, it would appear that the load voltage immediately assumed a value of 30 V. We would see the picture in Fig. 4.16 including the transient time interval only if the time scale of the oscilloscope were sufficiently reduced to, say, 1 μs per division. In order to sketch the load current $I(L, t)$, we could divide the previously sketched load voltage by R_L. We could also sketch this directly by using current reflection coefficients $\Gamma_S = 1$ and $\Gamma_L = -(1/3)$ and an initial current pulse of $30\ \mathrm{V}/Z_C = 0.6$ A. The current at the input to the line is sketched in this fashion in Fig. 4.16c. Observe that this current oscillates about an expected steady-state value of $30\ \mathrm{V}/R_L = 0.3$ A.

Example 4.3 This example shows the effect of pulsewidth on the total voltages. Consider a line of length 0.2 m (7.9 in.) shown in Fig. 4.17a. The source voltage is a pulse of 20 V amplitude and 1 ns duration. The line has a characteristic impedance of 100 Ω and a velocity of propagation of 2×10^8 m/s. The source resistance is 300 Ω ($R_S = 300\ \Omega$) and the load is open-circuited ($R_L = \infty$). Sketch the voltage at the input to the line and at the load.

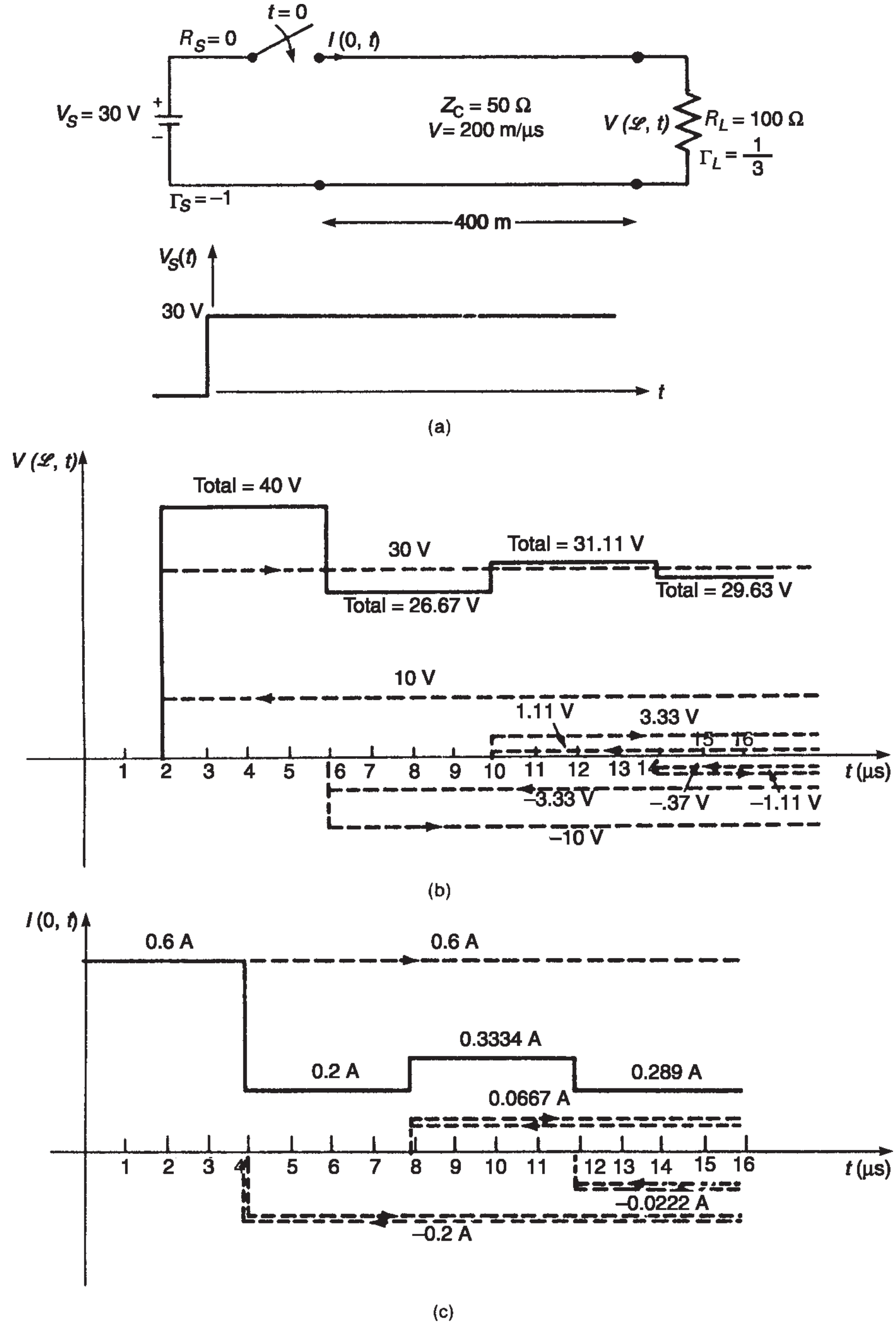
t = 0
$R_S = 0$
$I(0, t)$
$V_S = 30$ V
+
−
$Z_C = 50\ \Omega$
$V = 200$ m/μs
$V(\mathscr{L}, t)$
$R_L = 100\ \Omega$
$\Gamma_L = \frac{1}{3}$
$\Gamma_S = -1$
400 m
$V_S(t)$
30 V
t
(a)
$V(\mathscr{L}, t)$
Total = 40 V
30 V
Total = 31.11 V
Total = 26.67 V
Total = 29.63 V
10 V
1.11 V
3.33 V
1 2 3 4 5 6 7 8 9 10 11 12 13 14 15 16
t (μs)
−3.33 V
−.37 V
−1.11 V
−10 V
(b)
$I(0, t)$
0.6 A
0.6 A
0.3334 A
0.2 A
0.289 A
0.0667 A
1 2 3 4 5 6 7 8 9 10 11 12 13 14 15 16
t (μs)
−0.0222 A
−0.2 A
(c)

FIGURE 4.16 An example to illustrate sketching the voltage and current at the terminations as a function of time, Example 4.2; (a) the subject transmission line and the voltage at the source end $t = 0$ second; (b) voltage at the line termination over time after multiple reflections; (c) current at the line source over time after multiple reflections.

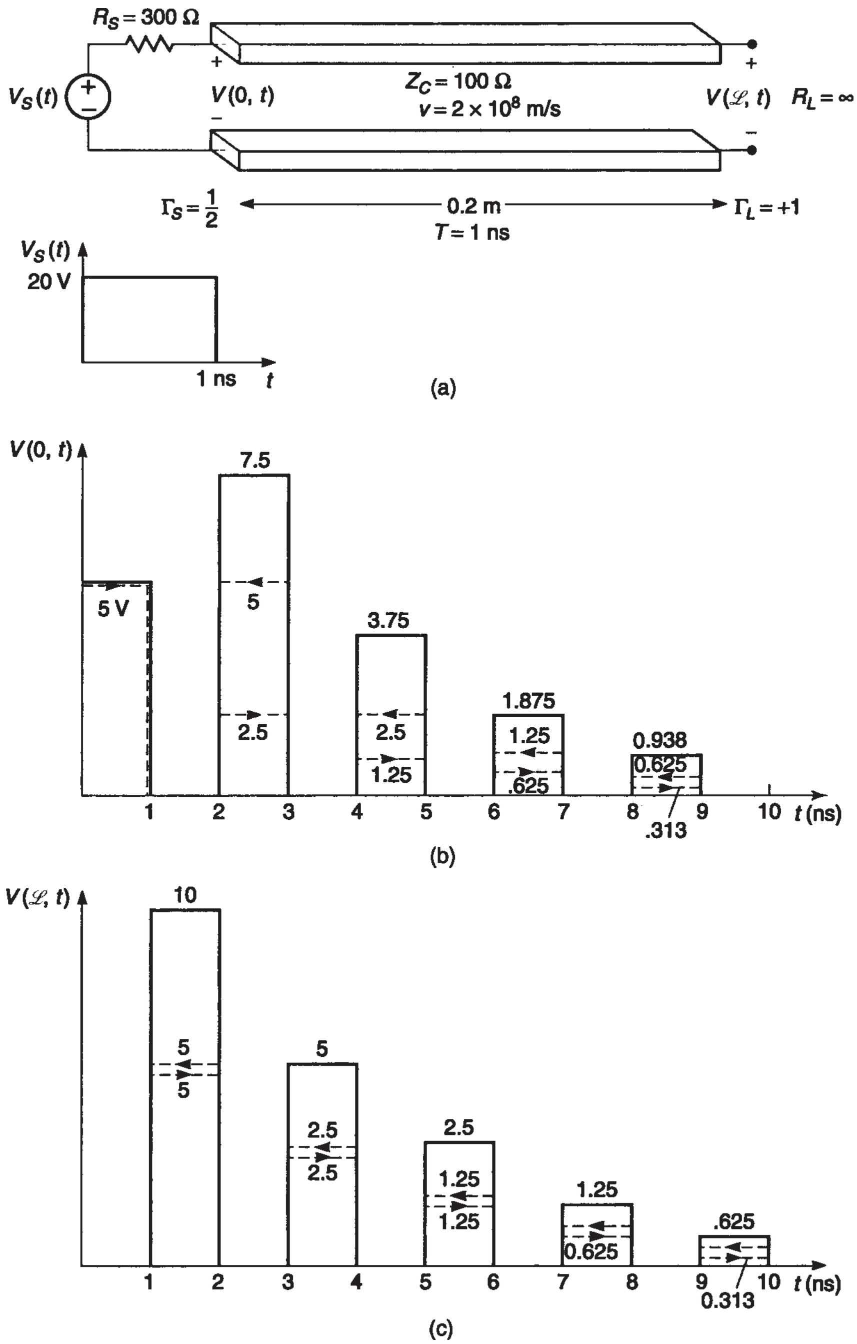
$R_S = 300\ \Omega$
$V_S(t)$
+
$V(0, t)$
−
$Z_C = 100\ \Omega$
$v = 2 \times 10^8$ m/s
+
$V(\mathcal{L}, t)$
−
$R_L = \infty$
$\Gamma_S = \frac{1}{2}$
0.2 m
$T = 1$ ns
$\Gamma_L = +1$
$V_S(t)$
20 V
1 ns
t
(a)
$V(0, t)$
5 V
7.5
5
2.5
3.75
2.5
1.25
1.875
1.25
.625
0.938
0.625
.313
1
2
3
4
5
6
7
8
9
10
t (ns)
(b)
$V(\mathcal{L}, t)$
10
5
5
5
2.5
2.5
2.5
1.25
1.25
1.25
0.625
.625
0.313
1
2
3
4
5
6
7
8
9
10
t (ns)
(c)

FIGURE 4.17 Example 4.3. Illustration of the effect of pulsewidth on the terminal voltages: (a) the problem specification; (b) the voltage at the input to the line; (c) the load voltage.

Solution: The source reflection coefficient is

$$\begin{aligned}\Gamma_S &= \frac{300-100}{300+100}\\ &= \frac{1}{2}\end{aligned}$$

and the load reflection coefficient is

$$\begin{aligned}\Gamma_L &= \frac{\infty-50}{\infty+50}\\ &= 1\end{aligned}$$

The one-way time delay is

$$\begin{aligned}T_D &= \frac{L}{v}\\ &= 1\ \text{ns}\end{aligned}$$

First, we sketch the source voltage, $V(0, t)$. The initially sent out voltage is

$$\frac{100}{300+100}\times 20 = 5\ \text{V}$$

The incident and reflected voltages are again sketched in Fig. 4.17b with dashed lines with an arrow added to indicate whether they are associated with a forward-traveling or a backward-traveling wave. The incident pulse is sent to the load, arriving there after one time delay of 1 ns, where it is reflected as a pulse of 5 V because the load reflection coefficient is $\Gamma_L = 1$. This pulse reflected at the load arrives at the source after an additional 1 ns time delay. This incoming pulse is reflected as $\Gamma_S \times 5\ \text{V} = 2.5\ \text{V}$, which arrives at the load after 1 ns, where it is reflected as 2.5 V, arriving at the source after a 1 ns delay. The process continues as shown. Adding all the incident and reflected pulses at the source, we obtain the total voltage drawn with a solid line. Clearly, this total decays to zero, as it should be in steady state.

Now we sketch the voltage at the load. After a time delay of 1 ns, the initially sent out voltage of 5 V arrives at the load and a reflected voltage of 5 V is sent back toward the source. This reflected voltage arrives at the source after 2 ns, and a reflected voltage of 2.5 V is sent back toward the load and arrives there at 3 ns. When this pulse reflected at the source arrives at the load, a reflected voltage of 2.5 V is sent back toward the source, which is reflected at the source as 1.25 V, arriving at the load at 5 ns. These incident and reflected voltages are sketched in Fig. 4.17c. Adding the voltages present at any one time gives the total as shown by a solid line. Clearly, this load voltage is decaying to zero, as it should in steady state.

Example 4.4 This example illustrates the effect of a pulsewidth that is greater than the round-trip delay. Consider the coaxial cable shown in Fig. 4.18a. The source voltage is a pulse of 100 V amplitude and 6 μs duration. The line is specified by its per-unit-length capacitance and inductance: $c = 100$ pF / m and $l = 0.25$ μH / m. This corresponds to the RG58U coaxial cable whose per-unit-length parameters were computed in Review Exercise Problem 4.3. The line has a characteristic impedance of

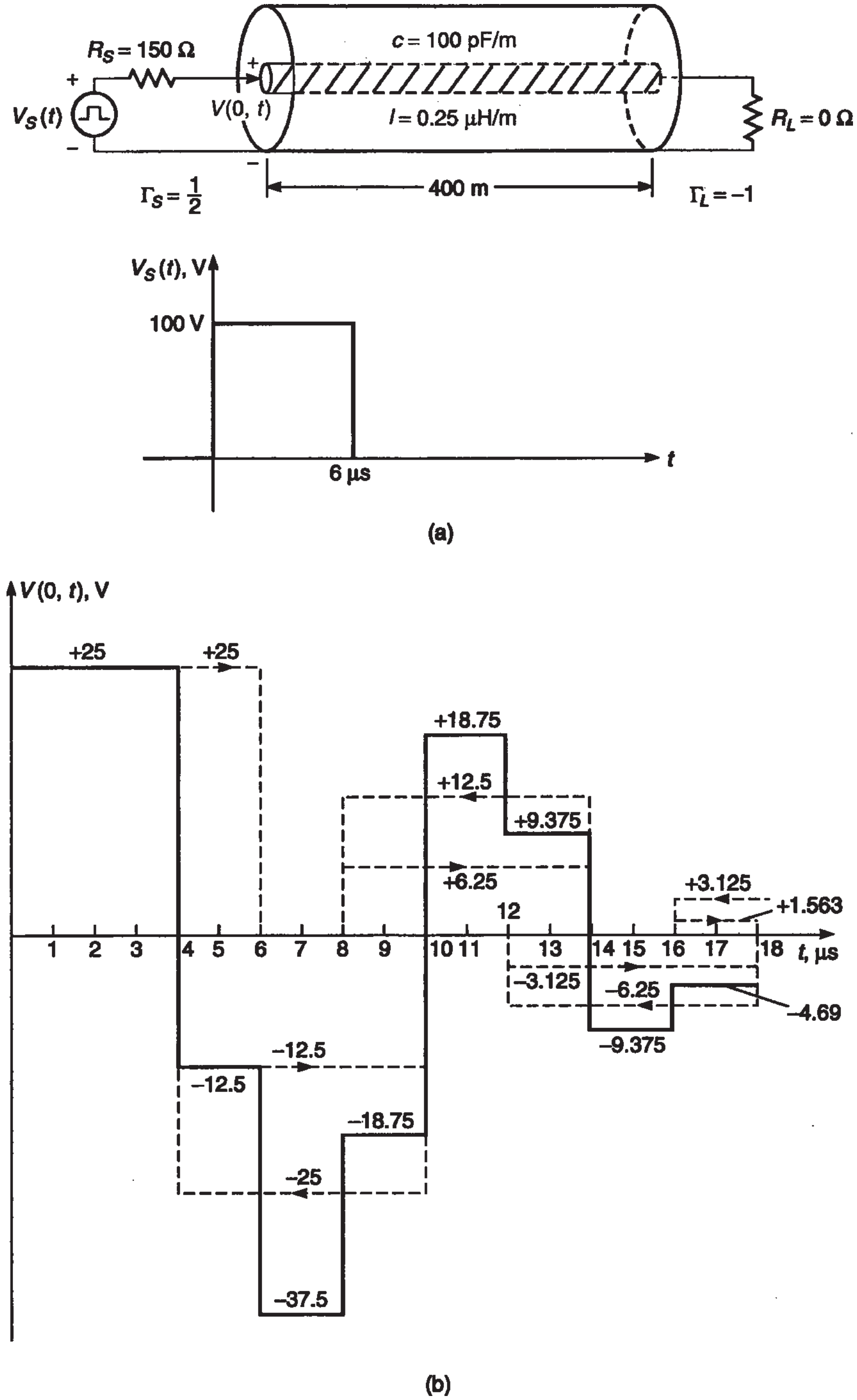
$R_S = 150\ \Omega$
+
$V_S(t)$
−
$V(0, t)$
+
−
$c = 100$ pF/m
$l = 0.25\ \mu$H/m
$R_L = 0\ \Omega$
$\Gamma_S = \frac{1}{2}$
400 m
$\Gamma_L = -1$
$V_S(t)$, V
100 V
6 μs
t
(a)
$V(0, t)$, V
+25
+25
+18.75
+12.5
+9.375
+6.25
+3.125
+1.563
12
1
2
3
4
5
6
7
8
9
10
11
13
14
15
16
17
18
t, μs
−3.125
−6.25
−4.69
−9.375
−12.5
−12.5
−18.75
−25
−37.5
(b)

FIGURE 4.18 Example 4.4. Illustration of the effect of pulsewidth on the terminal voltages: (a) the problem specification; (b) the voltage at the input to the line.

$$\begin{aligned} Z_c &= \sqrt{\frac{l}{c}} \\ &= 50\,\Omega \end{aligned}$$

The velocity of propagation is

$$\begin{aligned} v &= \frac{1}{\sqrt{lc}} \\ &= 200\,\mathrm{m}/\mu\mathrm{s} \end{aligned}$$

The source resistance is 150 Ω ($R_S = 150\ \Omega$), and the load resistance is a short circuit ($R_L = 0\ \Omega$). Sketch the voltage at the input to the line.

Solution: The source reflection coefficient is

$$\begin{aligned} \Gamma_S &= \frac{150-50}{150+50} \\ &= \frac{1}{2} \end{aligned}$$

and the load reflection coefficient is

$$\begin{aligned} \Gamma_L &= \frac{0-50}{0+50} \\ &= -1 \end{aligned}$$

The one-way time delay is

$$\begin{aligned} T_D &= \frac{L}{v} \\ &= 2\ \mu\mathrm{s} \end{aligned}$$

The initially sent out voltage is

$$\frac{50}{150+50} \times 100 = 25\,\mathrm{V}$$

The incident and reflected voltages are again sketched with dashed lines in Fig. 4.18b with an arrow added to indicate whether they are associated with a forward-traveling or a backward-traveling wave. The incident pulse is sent to the load, arriving there after one time delay of 2 μs, where it is reflected as a pulse of –25 V. This pulse reflected at the load arrives at the source after an additional 2 μs time delay. This incoming pulse is reflected as –12.5 V, which arrives at the load after 2 μs, where it is reflected as 12.5 V, arriving at the source after a 2 μs delay. The process continues as shown. Adding all the incident and reflected pulses at the source, we obtain the total voltage drawn with a solid line. Clearly, this total decays to zero, as it should be in steady state.

Observe that in this example, the pulsewidth of 6 μs is three time delays. Hence, the initially sent out pulse and the arriving pulse (which was the sent out pulse reflected at the load) overlap. This overlap creates a rather interesting and complicated waveform.

This graphical process is conveniently shown by the "bounce" or lattice diagram in Fig. 4.19. From this, we can write an expression for the voltage at $z = 0$ and at the load, $z = L$, as

$$\begin{aligned} V(0,t) = \frac{Z_c}{R_S + Z_c} &\left[V_s(t) + (1+\Gamma_S)\Gamma_S V_s(t-2T_D)\right. \\ &+ (1+\Gamma_S)(\Gamma_S\Gamma_L)\Gamma_L V_s(t-4T_D) \\ &\left.+ (1+\Gamma_S)(\Gamma_S\Gamma_L)^2\Gamma_L V_s(t-6T_D) + \cdots\right] \end{aligned} \tag{4.53a}$$

and

$$\begin{aligned} V(L,t) = \frac{Z_c}{R_S + Z_c} &\left[(1+\Gamma_L)V_s(t-T_D) + (1+\Gamma_L)\Gamma_S\Gamma_L V_s(t-3T_D)\right. \\ &+ (1+\Gamma_L)(\Gamma_S\Gamma_L)^2 V_s(t-5T_D) \\ &\left.+ (1+\Gamma_L)(\Gamma_S\Gamma_L)^3 V_s(t-7T_D) + \cdots\right] \end{aligned} \tag{4.53b}$$

So the total voltages are the sum of the source voltage waveforms scaled and delayed by multiples of the one-way time delay, T_D. Although the source and load voltage waveforms could be sketched from (4.53), it is much simpler to "trace the individual incident and reflected waves" and at any time add all those present at that time as was done graphically in the preceding examples. Observe that if the line is matched at the load, $R_L = Z_C$, then the load reflection coefficient is zero, $\Gamma_L = 0$, and (4.53) reduce to

$$V(0,t) = \frac{Z_c}{R_S + Z_c} V_s(t) \qquad R_L = Z_c \tag{4.53c}$$

$$V(L,t) = \frac{Z_c}{R_S + Z_c} V_s(t-2T_D) \quad R_L = Z_c \tag{4.53d}$$

In this case, the only effect of the line is to impose a time delay. The input and output voltages of the line are identical; the line "doesn't matter."

4.3.2 The Branin Method

The previous section has demonstrated a graphical method of sketching the time-domain solution of the transmission-line equations. It is frequently desirable to have a numerical method that is suitable for a digital computer and will handle nonlinear as well as dynamic loads. The following method is attributed to Branin and was originally described in [10]. It is valid only for lossless lines.

In order to obtain the required equations, we simply manipulate the solutions of the lossless transmission-line equations given in (4.44). Rewrite these as

$$V(z,t) = V^+\left(t - \frac{z}{v}\right) + V^-\left(t + \frac{z}{v}\right) \tag{4.54a}$$

$$Z_C I(z,t) = V^+\left(t - \frac{z}{v}\right) - V^-\left(t + \frac{z}{v}\right) \tag{4.54b}$$

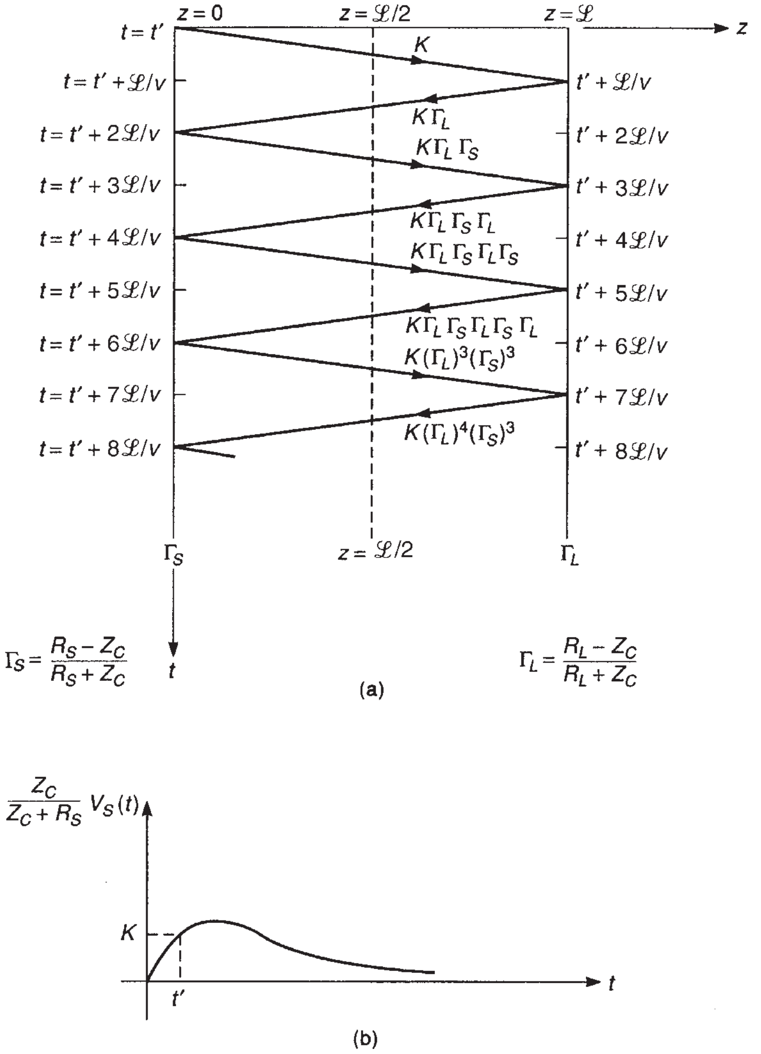
z = 0
z = ℒ/2
z = ℒ
z
t = t′
t = t′ + ℒ/v
t = t′ + 2ℒ/v
t = t′ + 3ℒ/v
t = t′ + 4ℒ/v
t = t′ + 5ℒ/v
t = t′ + 6ℒ/v
t = t′ + 7ℒ/v
t = t′ + 8ℒ/v
K
KΓ_L
KΓ_L Γ_S
KΓ_L Γ_S Γ_L
KΓ_L Γ_S Γ_L Γ_S
KΓ_L Γ_S Γ_L Γ_S Γ_L
K(Γ_L)^3(Γ_S)^3
K(Γ_L)^4(Γ_S)^3
t′ + ℒ/v
t′ + 2ℒ/v
t′ + 3ℒ/v
t′ + 4ℒ/v
t′ + 5ℒ/v
t′ + 6ℒ/v
t′ + 7ℒ/v
t′ + 8ℒ/v
Γ_S
z = ℒ/2
Γ_L
t
Γ_S = (R_S − Z_C)/(R_S + Z_C)
Γ_L = (R_L − Z_C)/(R_L + Z_C)
(a)
Z_C/(Z_C + R_S) V_S(t)
K
t′
t
(b)

FIGURE 4.19 The "bounce diagram" for determining the voltages on the line at different instants of time; (a) diagrammed transits of the signal from end to end of the transmission line showing the individual reflections and capturing the effects of each reflection mathematically one at a time; (b) a composite sketch of the source voltage as a function of time and the line characteristics.

Evaluating these at the source end, $z = 0$, and the load end, $z = L$, gives

$$V(0, t) = V^{+}(t) + V^{-}t \tag{4.55a}$$

$$Z_C I(0, t) = V^{+}(t) + V^{-}t \tag{4.55b}$$

and

$$V(L, t) = V^{+}(t + T_D) + V^{-}(t + T_D) \tag{4.56a}$$

$$Z_C I(L, t) = V^{+}(t - T_D) - V^{-}(t + T_D) \tag{4.56b}$$

where the one-way time delay for the line is

$$T_D = \frac{L}{v} \tag{4.57}$$

Adding and subtracting (4.55) and (4.56) gives

$$V(0,t) + Z_C I(0,t) = 2V^+(t) \tag{4.58a}$$

$$V(0,t) - Z_C I(0,t) = 2V^-(t) \tag{4.58b}$$

$$V(L,t) + Z_C I(L,t) = 2V^+(t - T_D) \tag{4.58c}$$

$$V(L,t) - Z_C I(L,t) = 2V^-(t + T_D) \tag{4.58d}$$

Shifting both (4.58a) and (4.58d) ahead in time by subtracting T_D from t along with a rearrangement of the equations gives

$$V(0,t) = Z_C I(0,t) + 2V^-(t) \tag{4.59a}$$

$$V(L,t) = -Z_C I(L,t) + 2V^+(t - T_D) \tag{4.59b}$$

$$V(0,t - T_D) + Z_C I(0,t - T_D) = 2V^+(t - T_D) \tag{4.59c}$$

$$V(L,t - T_D) - Z_C I(L,t - T_D) = 2V^-(t) \tag{4.59d}$$

Substituting (4.59d) into (4.59a) gives

$$V(0,t) = Z_C I(0,t) + E_0(L,t - T_D) \tag{4.60a}$$

where

$$\begin{aligned} E_0(L,t - T_D) &= V(L,t - T_D) - Z_C(L,t - T_D) \\ &= 2V^-(t) \end{aligned} \tag{4.60b}$$

Similarly, substituting (4.59c) into (4.59b) gives

$$V(L,t) = -Z_C I(L,t) + E_L(0,t - T_D) \tag{4.61a}$$

where

$$\begin{aligned} E_0(0,t - T_D) &= V(0,t - T_D) + Z_C I(0,t - T_D) \\ &= 2V^+(t - T_D) \end{aligned} \tag{4.61b}$$

Equations (4.60) and (4.61) suggest the equivalent circuit of the total line shown in Fig. 4.20. The controlled source $E_L(0, t - T_D)$ is produced by the voltage and current at the input to the line at a time equal to a one-way transit delay earlier than the present time. Similarly, the controlled source $E_0(L, t - T_D)$ is produced by the voltage and current at the line output at a time equal to a one-way transit delay earlier than the present time.

The equivalent circuit shown in Fig. 4.20 is an exact solution of the transmission-line equations for a lossless, two-conductor, uniform transmission line.

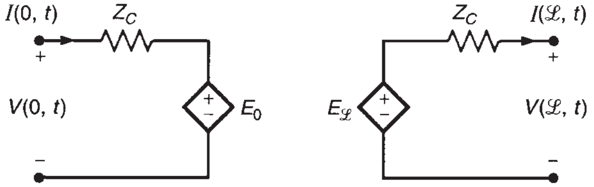

$$E_0 = V(\mathscr{L}, t - T_D) - Z_C I(\mathscr{L}, t - T_D) \qquad E_{\mathscr{L}} = V(0, t - T_D) + Z_C I(0, t - T_D)$$

FIGURE 4.20 The exact model of a transmission line.

4.4 HIGH-SPEED DIGITAL INTERCONNECTS AND SIGNAL INTEGRITY

Clock speeds in digital systems are increasing at a steady rate; PC clocks are on the order of 3 GHz. Digital data transfer rates are similarly increasing. Both of these signals are transferred from one point to another over the PCB lands. Of course, the time delay in traversing the lands is becoming a critical factor in the overall timing budget of the system with the time delays becoming on the order of the pulse rise/falltimes. There are a number of problems associated with time delay, one of which is *clock skew*. Suppose that a clock is fed to two modules as shown in Fig. 4.21. In Fig. 4.21a, the total time delay to module 1 is $TD1 + TD2$. The total time delay to module 2 is $TD1 + TD2 + TD3$, which, because of the longer connection lands, is larger than the delay to module 1. Hence, each module sees the clock shifted in time relative to each other. This is referred to as clock skew. On the other hand, if the land routing is as shown in Fig. 4.21b, the total time delay to each module is the same, $TD1 + TD2 + TD3$.

In addition, there are other perhaps more critical aspects caused by the increasing speeds of digital signal transfer. The clock and data pulses are in the form of trapezoidal pulses transitioning, for example, between 0 and 5 V. The manufacturers of digital gates and other devices provide levels wherein a pulse is guaranteed to be interpreted as a logic 1 or 0. If the pulse level inadvertently lies between the guaranteed levels, the data may be incorrectly interpreted. The term *signal integrity* refers to ensuring that a digital pulse when sent down a pair of lands will arrive at the receiver with the desired level and waveshape. In other words, ideally, we would like to have the line "not matter." We have seen how mismatched lines can cause a distorted signal resulting from reflections at the mismatched load. Also, whenever, the cross-sectional dimensions of the transmission line change, the characteristic impedance of the line will change and hence we will have reflections at that discontinuity. These lands often transition from one layer to another with vias. *Vias* are connections drilled from one layer of a PCB to another and are used to connect two lands on these opposite layers. Clearly, a signal that passes from one layer to another along a via will have encountered a discontinuity and hence a change in characteristic impedance. Around the mid-1980s, these considerations were not of much consequence. Today they are becoming critical to the functionality of the digital device. We will devote this section to learning how to analyze and combat these effects striving for the ultimate goal of having the "line not matter."

4.4.1 Effect of Terminations on the Line Waveforms

Consider a typical clock or data transfer situation shown in Fig. 4.22. A digital gate is represented as a Thevenin equivalent, and the input to the load gate is represented by a load resistor. For typical CMOS gates the gate output resistance (nonlinear) is on the order of $10 - 30\ \Omega$. The input to the

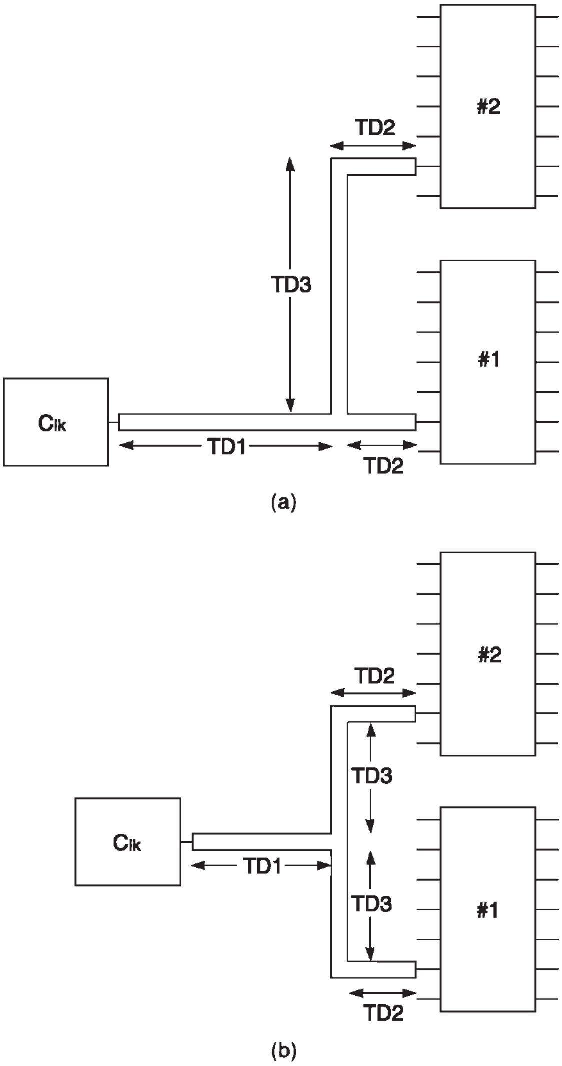

FIGURE 4.21 Illustration of "clock skew" caused by unequal propagation paths: (a) unequal propagation paths; (b) equal propagation paths.

CMOS gate is typically capacitive on the order of 5 – 15 pF. For the moment we will represent the source and load as resistors. One of the detrimental effects of the lands on signal integrity is to produce "ringing" at the termination. This occurs because the line is not matched. In order to demonstrate this, consider modeling the input to a CMOS gate as an open circuit and the driver gate as having a source resistance of 10 Ω as shown in Fig. 4.23. The source voltage transitions from 0 to 5 V. The source reflection coefficient is

$$\begin{aligned}\Gamma_S &= \frac{10-50}{10+50}\\ &= -\frac{2}{3}\end{aligned}$$

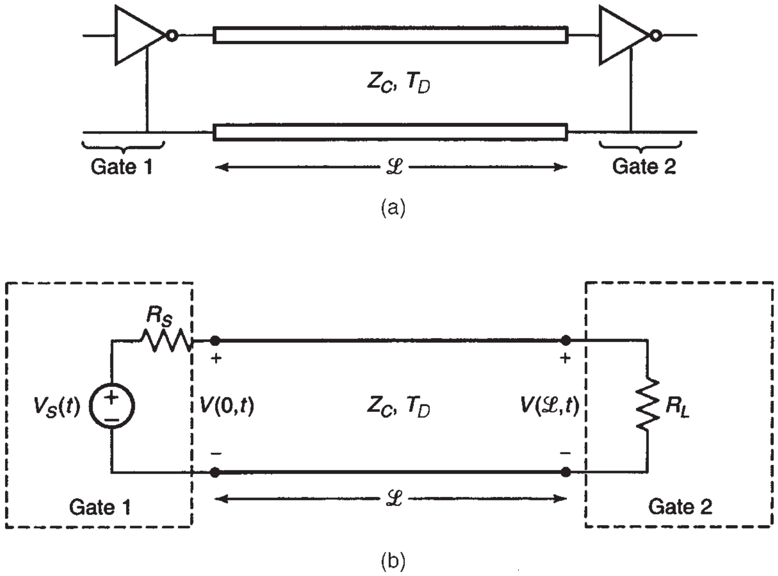

FIGURE 4.22 A typical digital application of transmission lines: (a) the line connects two digital gates; (b) representation of the terminal gates.

The load reflection coefficient at this open circuit is

$$\begin{aligned}\Gamma_L &= \frac{\infty - 50}{\infty + 50}\\ &= +1\end{aligned}$$

The voltage initially sent down the line is

$$V_{\text{init}} = \frac{50}{10+50} \times 5\,\text{V} = 4.17\,\text{V}$$

Wave tracing gives the load voltage as shown in Fig. 4.23b. This shows that the received voltage oscillates about the desired 5 V level between levels of 8.33 and 2.78 V, eventually settling down to 5 V. This constitutes *ringing* and can cause the received voltage to lie outside the levels for a logic 0 and a logic 1 guaranteed by the manufacturer of the gates, thus creating logic errors.

Observe in this last example, the sign of the load and source reflection coefficients are opposite: $\Gamma_S = -$ and $\Gamma_L = +$. Situations such as this represent the majority of source–load terminations in digital logic circuits. When the signs of the source and load reflections coefficients are opposite as in this case, we will always have ringing. On the other hand, when the signs of the source and load reflection coefficients are the same, the load voltage will steadily increase to the steady-state level. This can be readily seen from the exact expression for the load voltage given in (4.53b):

$$\begin{aligned}V(L,t) = {}& \frac{Z_C}{R_S+Z_C}(1+\Gamma_L)[V_S(t-T_D) + \Gamma_S\Gamma_L V_S(t-3T_D)\\ &+ (\Gamma_S\Gamma_L)^2 V_S(t-5T_D) + (\Gamma_S\Gamma_L)^3 V_S(t-7T_D) + \dots]\end{aligned} \tag{4.62}$$

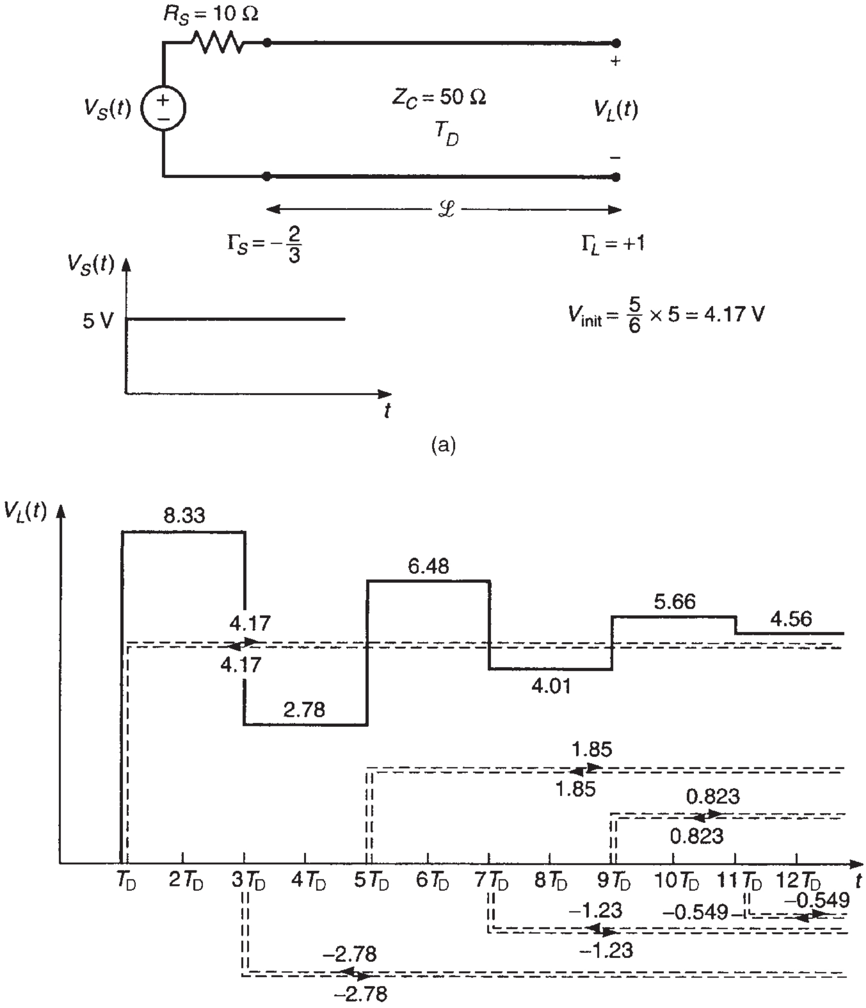
$R_S = 10\ \Omega$
$V_S(t)$
$Z_C = 50\ \Omega$
T_D
$V_L(t)$
+
−
$\mathscr{L}$
$\Gamma_S = -\frac{2}{3}$
$\Gamma_L = +1$
$V_S(t)$
5 V
t
$V_{init} = \frac{5}{6} \times 5 = 4.17$ V
$V_L(t)$
8.33
6.48
5.66
4.56
4.17
4.17
2.78
4.01
1.85
1.85
0.823
0.823
T_D
$2T_D$
$3T_D$
$4T_D$
$5T_D$
$6T_D$
$7T_D$
$8T_D$
$9T_D$
$10T_D$
$11T_D$
$12T_D$
t
−1.23
−0.549
−0.549
−1.23
−2.78
−2.78

(a)

(b)

FIGURE 4.23 Illustration of the phenomenon of "ringing" in transmission lines that interconnect a low-impedance source and a high-impedance load: (a) an example to illustrate the phenonemon; (b) the results of the solution illustrating ringing at the terminals.

Observe that for a source voltage $V_S(t)$ that jumps immediately, say, to 5 V, the load voltage is the sum of this waveform delayed by 1 one-way time delay and successively adding this waveform delayed by 2 one-way time delays *but* multiplied by powers of the products of the source and load reflection coefficients. The source and load reflection coefficients have magnitudes less than one. $|\Gamma_S\Gamma_L| < 1$, and therefore the successive additions are less than $V_S(t - T_D)$. Hence if the source and load reflection coefficients are of the same sign, $\Gamma_S\Gamma_L$ is positive and the load voltage steadily builds up, whereas if the source and load reflection coefficients are of opposite sign, $\Gamma_S\Gamma_L$ is negative with even powers positive and odd powers negative and the load voltage will oscillate about the steady-state value and hence ring. Table 4.1 summarizes these important observations.

TABLE 4.1 Effects of the Signs of the Reflection Coefficients on the Load Voltage

Γ_S	Γ_L	Load Voltage Waveform
$-R_S < Z_C + R_S > Z_C$	$+R_L > Z_C - R_L < Z_C$	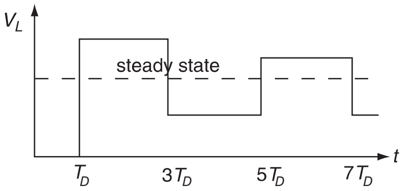
$+R_S > Z_C - R_S < Z_C$	$+R_L > Z_C - R_L < Z_C$	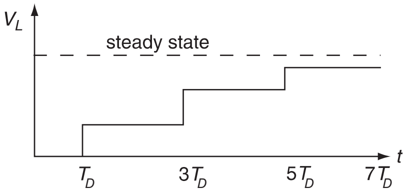

4.4.1.1 *Effect of Capacitive Terminations*

Sketching the source and load voltages on a line that has resistive terminations is quite simple. Sketching these voltages when one or both of the terminations is dynamic (capacitive or inductive) is a bit more complicated. In this section, we will perform an exact analysis of a line having a capacitive termination. Consider the situation shown in Fig. 4.24a, where the source resistance is $R_S = Z_C$ and hence the line is matched at the source. In Section 4.4.2, we will show that this is a common matching scheme. The load, however, is a capacitor representing, perhaps, the input to a CMOS logic gate. The source voltage is a pulse or step function rising to a level of V_0 volts and remaining there, i.e., $V_S(t) = V_0 u(t)$, where $u(t)$ is the unit step function. This represents the transition from a logic 0 to a logic 1. In order to analyze this we transform it with the Laplace transform where s denotes the Laplace transform variable as shown in Fig. 4.24b. The capacitor has an impedance of $Z_L = 1/sC$ [11]. The reflection coefficient at the source is zero since it is matched.

$$\Gamma_S = 0 \tag{4.63a}$$

and the reflection coefficient at the load is

$$\begin{aligned}\Gamma_L &= \frac{Z_L - Z_C}{Z_L + Z_C}\\ &= \frac{\frac{1}{sC} - Z_C}{\frac{1}{sC} + Z_C}\\ &= \frac{1 - sT_c}{1 + sT_c}\end{aligned}$$

and the time constant is denoted as [11]

$$T_C = Z_C C \tag{4.64}$$

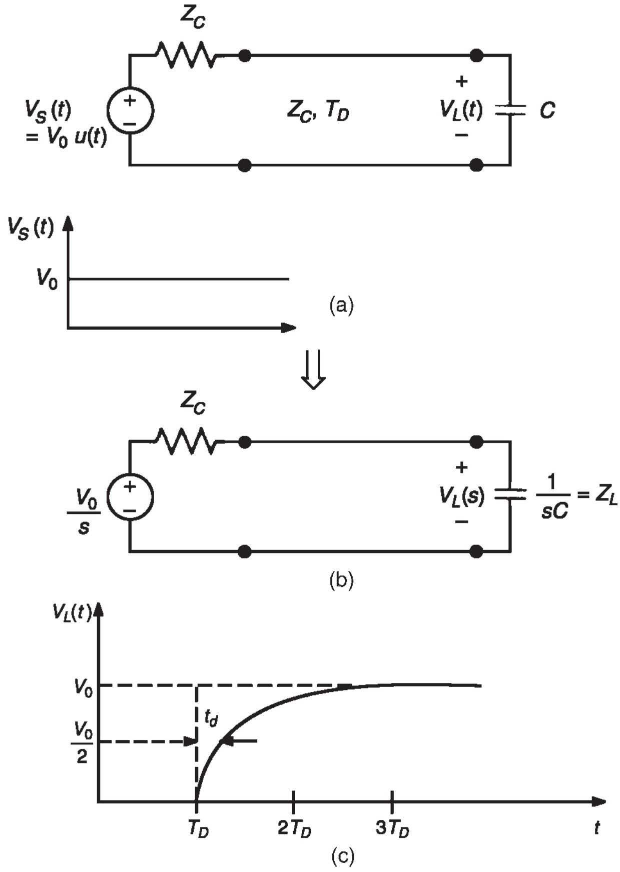
Z_C
$V_S(t) = V_0\,u(t)$
+
−
Z_C, T_D
+
$V_L(t)$
−
C
$V_S(t)$
V_0
(a)
Z_C
$\frac{V_0}{s}$
+
−
+
$V_L(s)$
−
$\frac{1}{sC} = Z_L$
(b)
$V_L(t)$
V_0
$\frac{V_0}{2}$
t_d
T_D
$2T_D$
$3T_D$
t
(c)

FIGURE 4.24 Illustration of the solution for a line terminated in a capacitive load: (a) the problem; (b) the Laplace transform of the problem; (c) the solution for the load voltage.

Since the source is matched, we will only have a forward-traveling wave incident at the load and a reflected wave traveling back to the source. From (4.62) the load voltage is

$$V_L(t) = (1 + \Gamma_L)\frac{Z_C}{(R_S = Z_C) + Z_C}V_0 u(t - T_D) \tag{4.65}$$

Transforming this yields

$$\begin{aligned} V_L(s) &= (1 + \Gamma_L(s))\frac{1}{2}V_S(s)e^{-sT_D} \\ &= \frac{\frac{1}{T_C}}{(s + (1/T_C))s}V_0 e^{-sT_D} \\ &= \left[\frac{1}{s} - \frac{1}{(s + (1/T_C))}\right]V_0 e^{-sT_D} \end{aligned} \tag{4.66}$$

The 1/2 represents the voltage division factor for the initially sent out wave; $Z_C/[(R_S = Z_C) + Z_C] = (1/2)$. The term e^{-sT_D} represents a one-way time delay of T_D. The final result has been expanded in partial fractions. Inverse transforming gives

$$V_L(t) = V_0 u(t - T_D) - e^{-(t-T_D)/T_C} V_0 u(t - T_D) \tag{4.67}$$

This waveform is sketched in Fig. 4.24c. This result makes sense because the incoming traveling wave is a pulse with zero risetime. Initially, the capacitor looks like a short circuit gradually transitioning to an open circuit. Ideally (with an open-circuit load instead of a capacitor) the load voltage should rise abruptly to V_0 at $t = T_D$. The effect of the capacitor is to introduce an additional time delay (measured at the 50% point) t_d, thereby giving the load voltage a risetime when the source had none. Evaluating (4.67) for $V_L(t) = 0.5\ V_0$ gives this time delay as

$$\begin{aligned} t_d &= 0.693T_C \\ &= 0.693CZ_C \end{aligned} \tag{4.68}$$

For example, for a 50 Ω line and a 5 pF load capacitor, we would obtain a time delay of 0.173 ns. Reference [12] gives the result wherein the source voltage has a nonzero risetime. The conclusions are quite similar to the zero-risetime case that we investigated.

4.4.1.2 Effect of Inductive Terminations

Let us replace the capacitive load with an inductive one as shown in Fig. 4.25a. Carrying out the analysis of the previous section but with $ZL = sL$ gives a similar result. The reflection coefficient at the source is again zero since it is matched:

$$\Gamma_S = 0 \tag{4.69a}$$

and the reflection coefficient at the load is

$$\begin{aligned} \Gamma_L &= \frac{Z_L - Z_C}{Z_L + Z_C} \\ &= \frac{sL - Z_C}{sL + Z_C} \\ &= \frac{sT_L - 1}{sT_L + 1} \end{aligned} \tag{4.69b}$$

and the time constant is denoted as [11]

$$\mathrm{T}_L = \frac{L}{Z_C} \tag{4.70}$$

The transformed load voltage is

$$\begin{aligned} V_L(s) &= (1 + \Gamma_L(s))\frac{1}{2}V_S(s)e^{-sT_D} \\ &= \frac{1}{s + (1/T_L)} V_0 e^{-sT_D} \end{aligned} \tag{4.71}$$

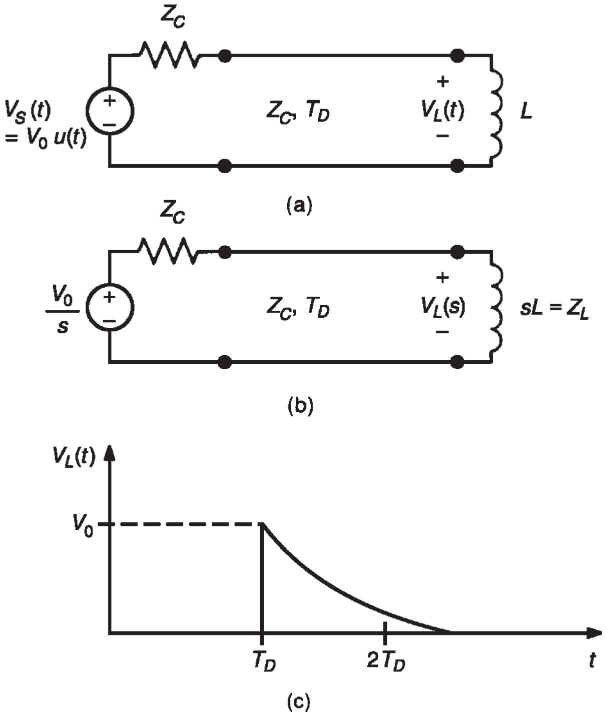

FIGURE 4.25 Illustration of the solution for a line terminated in an inductive load: (a) the problem; (b) the Laplace transform of the problem; (c) the solution for the load voltage.

Inverse transforming this gives

$$V_L(t) = V_0 e^{-(t-T_D)/T_L} u(t - T_D) \tag{4.72}$$

which is plotted in Fig. 4.25c. This makes sense because the incoming traveling wave at the load is a pulse with zero risetime. Initially, the inductor looks like an open circuit gradually becoming a short circuit.

4.4.2 Matching Schemes for Signal Integrity

We have seen how mismatches at the source and/or load of a transmission line can cause the received voltage waveform to differ drastically from what was sent. Hence, mismatches affect signal integrity. How do we remedy this? The most common matching scheme is the *series match* shown in Fig. 4.26a. For typical CMOS gates their source (output) resistances are less than the characteristic impedances of PCB lines. Hence, a resistor R is added to the input of the line (the output of the driving gate) such that

$$R_S + R = Z_C$$

This matches the line at the source. The initially sent out voltage wave will have a level equal to half the source voltage level or $V_0 / 2$. Typically, the load is an open circuit or approximately so, and hence the load reflection coefficient is $\Gamma_L = +1$. In this case, the incident wave is completely

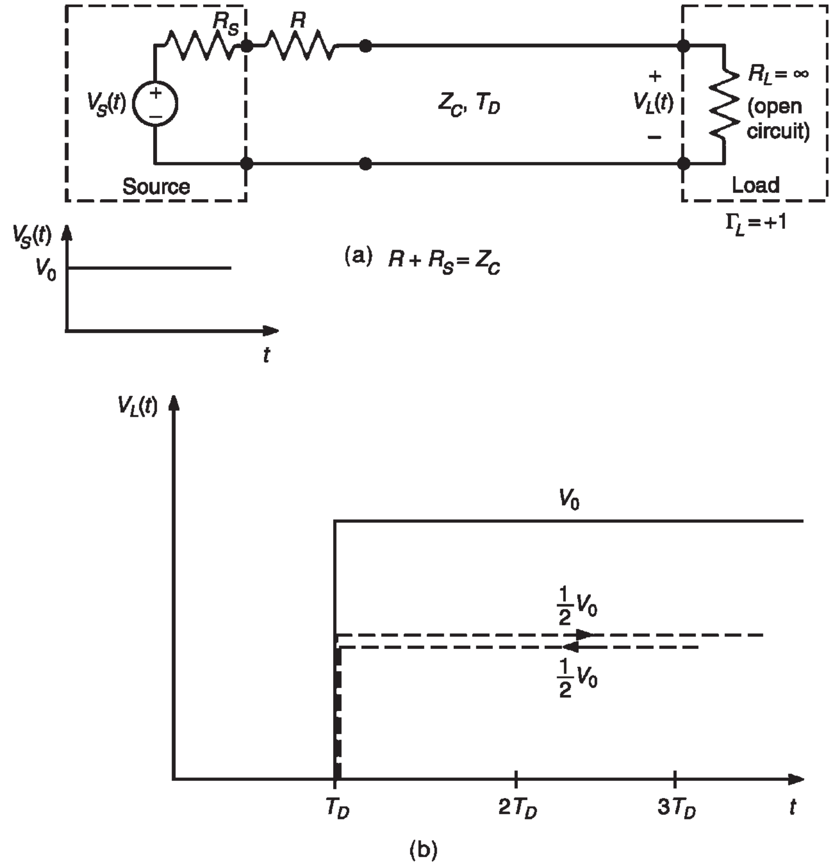

FIGURE 4.26 The series match for matching a transmission line: (a) implementing the series match; (b) explanation of how it works.

reflected at the load, giving a total of $V_0 \;/\; 2 + V_0 \;/\; 2 = V_0$. Hence, the load voltage rises to V_0, immediately giving perfect signal integrity. Another advantage of the series match is that, for an open-circuit load, no current flows in the line and the resistor R and therefore the resistor dissipates no power.

A second scheme for matching is the *parallel match* shown in Fig. 4.27a. Here we place a resistor R in parallel with the load. We choose R such that the line is matched at the load:

$$\begin{aligned} R \parallel R_L &= \frac{RR_L}{R + R_L} \\ &= Z_C \end{aligned}$$

The load voltage is plotted in Fig. 4.27b. Note that the initially sent out voltage has a level of

$$V_{\text{init}} = \frac{Z_C}{R_S + Z_C} V_0$$

This incoming wave at the load is totally absorbed, and there is no reflected wave. There are two disadvantages to the parallel match. First, the load voltage is always less than the source level

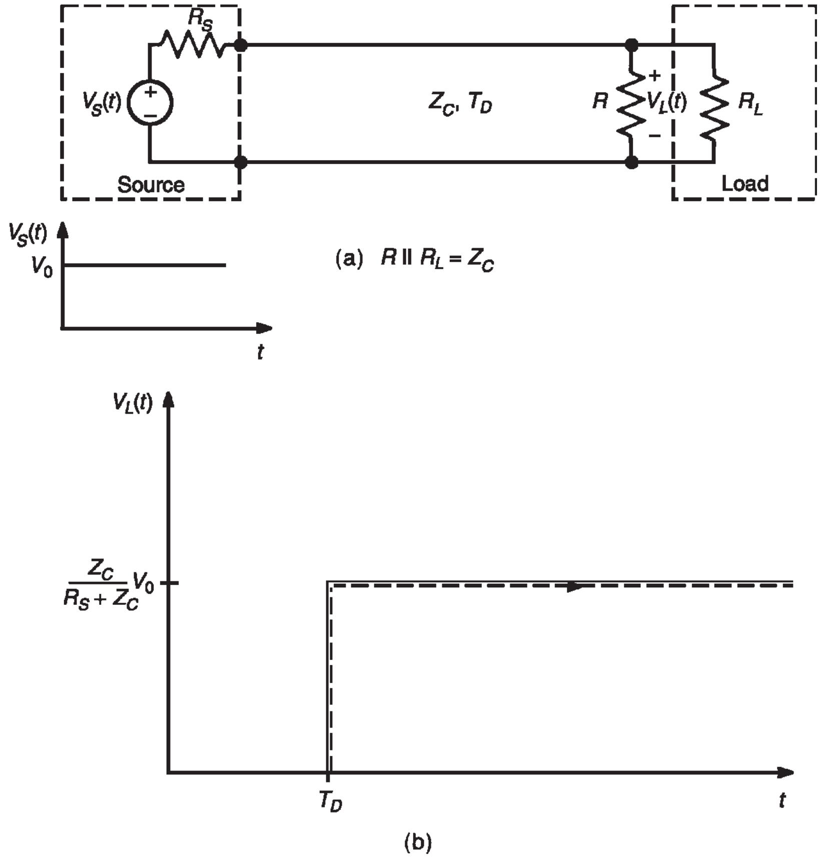

FIGURE 4.27 The parallel match for matching a transmission line: (a) implementing the parallel match; (b) explanation of how it works.

of V_0. For example, suppose that $R_S = 25\ \Omega$, $Z_C = 50\ \Omega$, and $V_0 = 5$ V. The load voltage level will be 3.33 V. In the parallel match case, we have no reflected wave to bring the load voltage up to the source voltage level. The second disadvantage of the parallel match case is that, even for an open-circuited load, the line will draw current when the source is in the high state. Hence, the matching resistor R will consume power.

4.4.3 When Does the Line Not Matter, i.e., When is Matching Not Required?

Matching a line is not always required in order that the voltage at the output of the line be the desired level and waveform. When is it not required to match a line? An obvious case is where the line is very "short." We can obtain a criterion for this by examining the bounds on the spectrum of the trapezoidal pulse given in Fig. 3.19 of Chapter 3. We obtained a criterion on the bandwidth of the pulse, i.e., the significant spectral components of the pulse, as

$$\text{BW} = \frac{1}{\tau_r} \tag{4.73}$$

where τ_r is the pulse risetime. The criterion that the distributed parameter effects of the line be negligible is that it be electrically short at the highest significant frequency:

$$L < \frac{1}{10} \frac{v}{f_{\max}} \tag{4.74}$$

where v is the velocity of propagation on the line. Substituting (4.73), $f_{\max} = 1/\tau_r$ yields

$$T_D = \frac{L}{v} < \frac{1}{10}\tau_r \tag{4.75a}$$

or

$$\tau_r > 10T_D \tag{4.75b}$$

Hence, if the pulse risetime is greater than 10 one-way time delays of the line, the line and any mismatches should not significantly degrade the output waveform.

In order to investigate this criterion, we examine the simple circuit of a line on a circuit board shown in Fig. 4.28a. The source resistance is 20 Ω, and the open-circuit voltage transitions from 0 to 5 V in a risetime τ_r. The load has a 5 pF capacitance. The line has a characteristic impedance of 50 Ω and a one-way time delay of 0.2 ns. Figure 4.28b shows the load voltage when the risetime is equal to the one-way time delay of the line: $\tau_r = 0.2$ ns. The overshoot is 7 V. Figure 4.28c shows the output waveform when the risetime is 5 one-way line delays: $\tau_r = 1$ ns. The overshoot is reduced to around 6 V. Figure 4.28d shows the output waveform when the risetime is 10 one-way line delays: $\tau_r = 2$ ns. The overshoot is reduced to only 5.3 V. Finally, Fig. 4.28e shows the output waveform when the risetime is 20 one-way line delays: $\tau_r = 4$ ns. The overshoot is reduced to 5.2 V and approximates the steady-state voltage of 5 V very well.

If we assume an effective relative permittivity as the average of the board relative permittivity (4.7) and that of air (1.0), this gives an effective relative permittivity of $\varepsilon_r' = 2.85$. The propagation delay is 5.6 ns/m or 0.1429 ns/in. A 7 in. length of PCB land would have a one-way delay of around 1 ns. If we choose as a criterion $\tau_r > 7\ T_D$ instead of (4.75b), then this gives an easily remembered criterion of

$$\tau_r(\text{ns}) > L(\text{in.}) \tag{4.76}$$

A 7-in. land would require the pulse risetime to exceed 7 ns to ensure that the line does “not matter,” and matching would not be required.

Review Exercise 4.9 Derive the criterion given in (4.76).

4.4.4 Effects of Line Discontinuities

Until now there are no discontinuities along the line, that is, there are no changes in cross section along the line and there are no terminations added along the line. In this section, we will investigate the effects of discontinuities along the line. A common discontinuity is where the line cross section changes, for example, if the line width changes at some point as illustrated in Fig. 4.29a. Hence, the first portion has characteristic impedance Z_{C1}, and the second portion has characteristic impedance Z_{C2}. First, consider a wave traveling on line 1 that is incident on the junction. A portion of the incident voltage v_{i1} is reflected back to the left and is given by $v_{r1} = \Gamma_{12} v_{i1}$, where the reflection coefficient is

$$\Gamma_{12} = \frac{Z_{C2} - Z_{C1}}{Z_{C2} + Z_{C1}} \tag{4.77a}$$

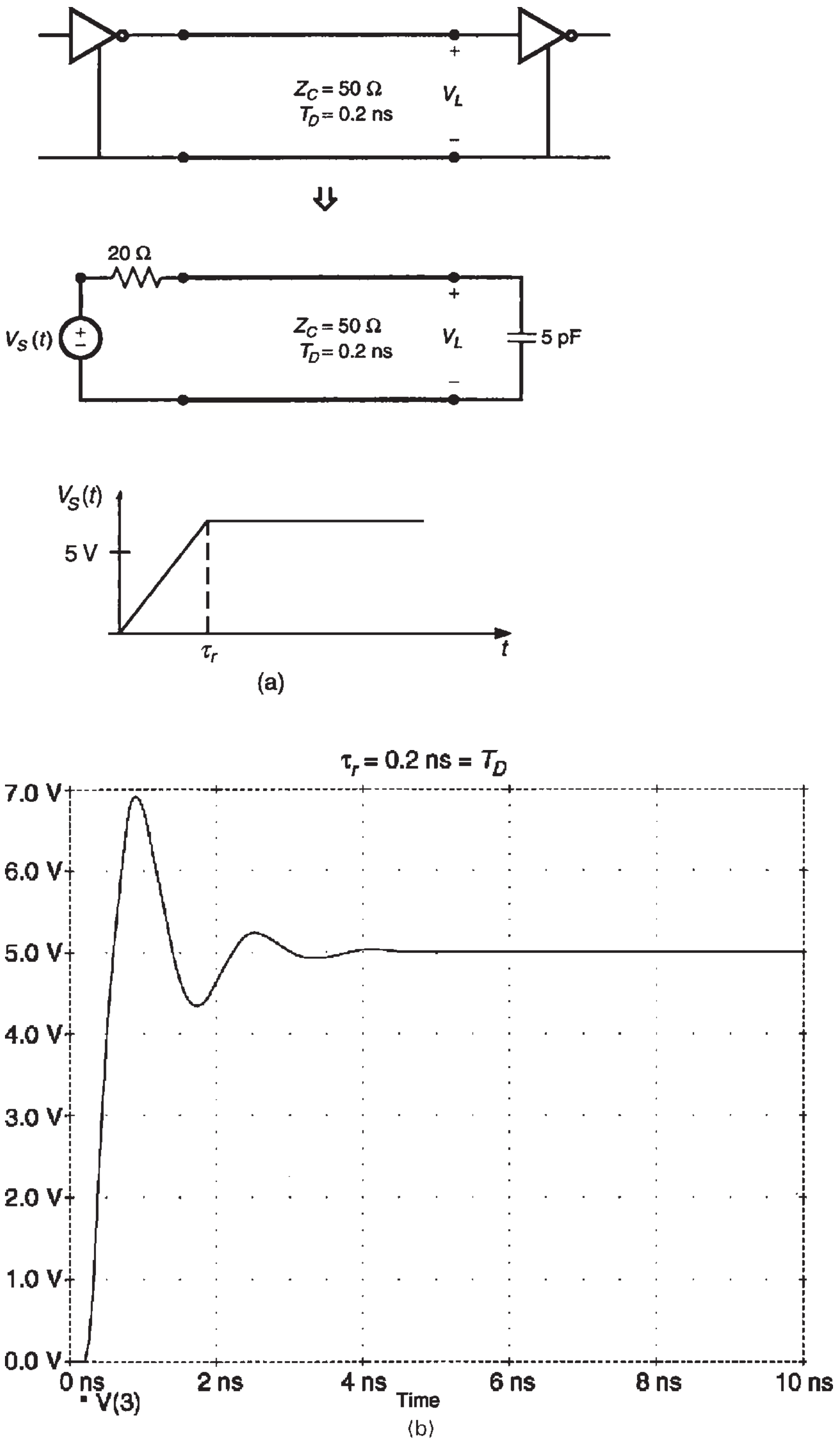

FIGURE 4.28 Determining when "the line doesn't matter": (a) the circuit and the corresponding schematic of the problem; (b) the load voltage for a risetime of $\tau_r = 0.2$ ns $= T_D$; (c) the load voltage for a risetime of $\tau_r = 1$ ns $= 5\ T_d$; (d) the load voltage for a risetime of $\tau_r = 2$ ns $= 10\ T_D$; (e) the load voltage for a risetime of $\tau_r = 4$ ns $= 20\ T_D$.

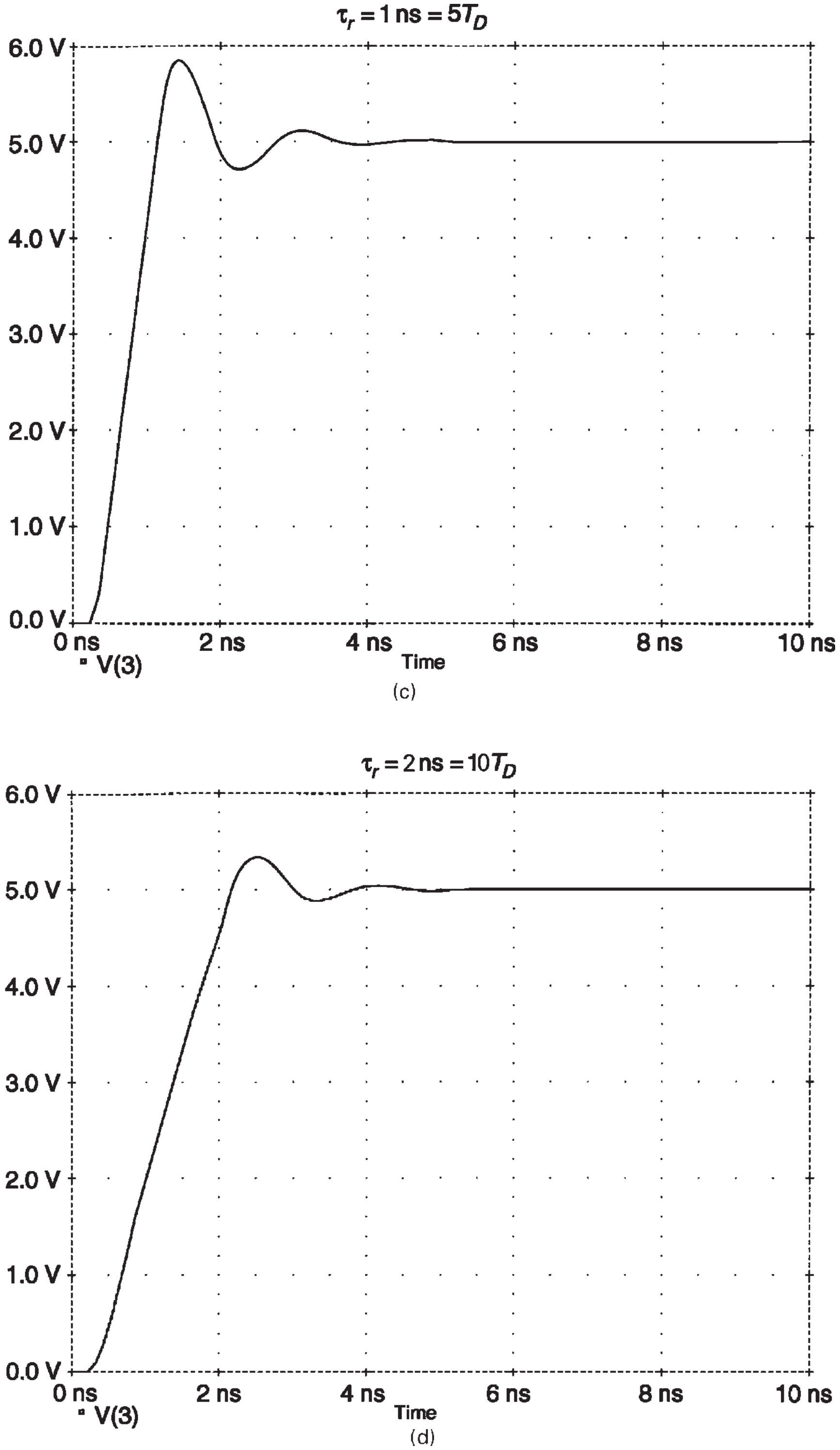

(c)

(d)

FIGURE 4.28 (*Continued*)

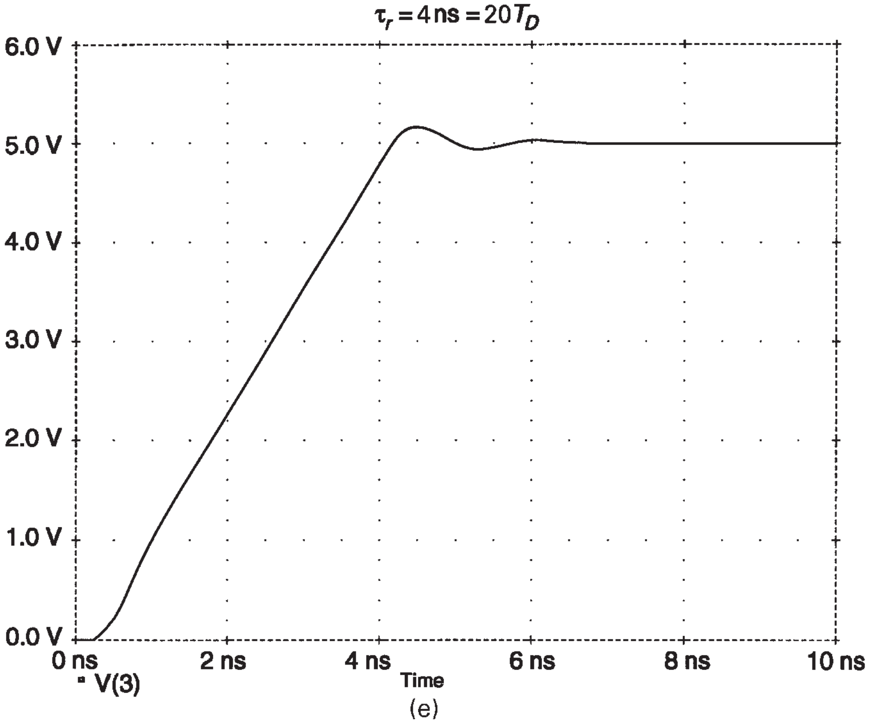

FIGURE 4.28 (*Continued*)

since the incoming wave essentially sees a termination impedance that is the characteristic impedance of the second line. In addition, a portion of the incident voltage v_{t2} is transmitted across the junction onto the second line and is given by $v_{t2} = \mathrm{T}_{12} v_{i1}$. The total voltage on each side of the junction must be equal:

$$v_{i1} + v_{r1} = v_{t2} \tag{4.77b}$$

Hence, the reflection and transmission coefficients are related as

$$1 + \Gamma_{12} = T_{12} \tag{4.77c}$$

and the transmission coefficient is given by

$$T_{12} = \frac{2Z_{c2}}{Z_{c2} + Z_{c1}} \tag{4.77d}$$

This process is illustrated in Fig. 4.29b.

A similar process governs a wave on line 2 that is traveling to the left and strikes the junction as illustrated in Fig. 4.29c. A portion of the incident voltage v_{i2} is reflected back to the right and is given by $v_{r2} = \Gamma_{21} v_{i2}$, where the reflection coefficient is

$$\Gamma_{21} = \frac{Z_{c1} - Z_{c2}}{Z_{c1} + Z_{c2}} \tag{4.78a}$$

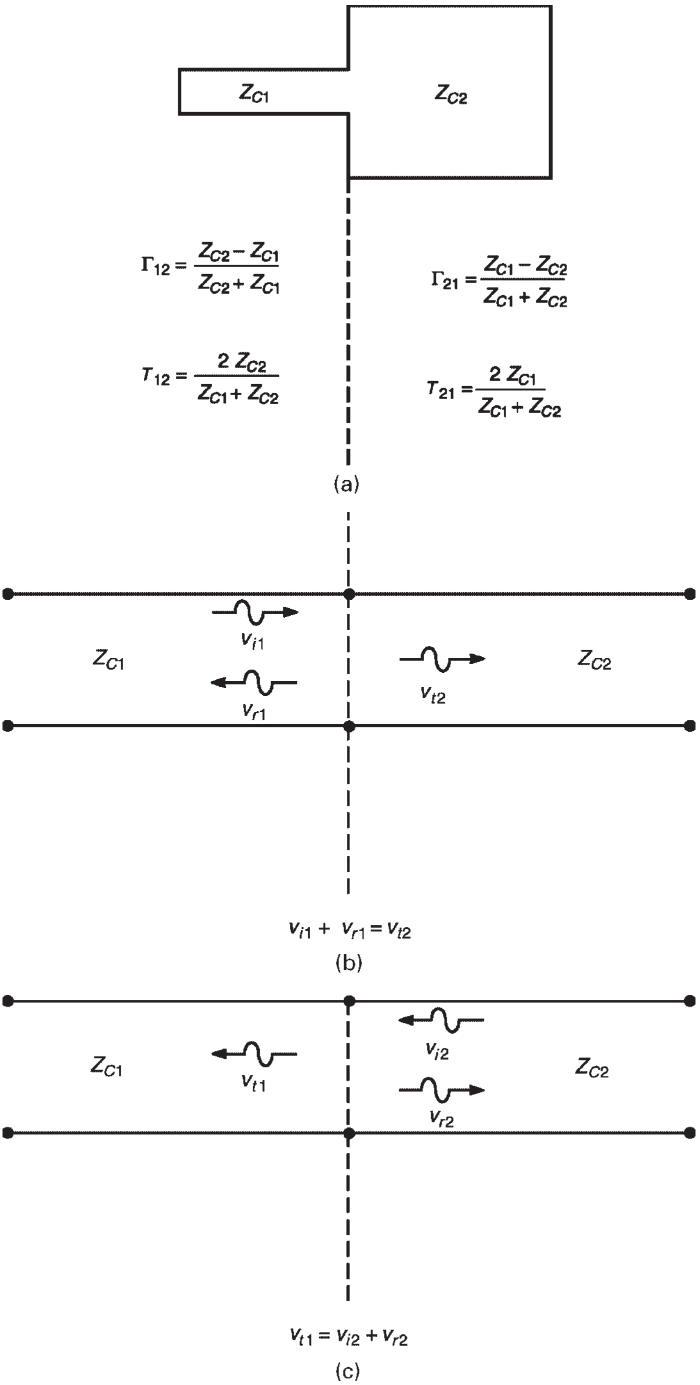
Z_{C1}
Z_{C2}
$\Gamma_{12} = \frac{Z_{C2} - Z_{C1}}{Z_{C2} + Z_{C1}}$
$\Gamma_{21} = \frac{Z_{C1} - Z_{C2}}{Z_{C1} + Z_{C2}}$
$T_{12} = \frac{2Z_{C2}}{Z_{C1} + Z_{C2}}$
$T_{21} = \frac{2Z_{C1}}{Z_{C1} + Z_{C2}}$
(a)
Z_{C1}
V_{i1}
V_{r1}
V_{t2}
Z_{C2}
$V_{i1} + V_{r1} = V_{t2}$
(b)
Z_{C1}
V_{t1}
V_{i2}
V_{r2}
Z_{C2}
$V_{t1} = V_{i2} + V_{r2}$
(c)

FIGURE 4.29 Illustration of line discontinuities caused by different characteristic impedances: (a) problem specification; (b) illustration of computing reflected and transmitted waves for a wave incident from the left; (c) illustration of computing reflected and transmitted waves for a wave incident from the right.

since the incoming wave essentially sees a termination impedance that is the characteristic impedance of the first line. In addition, a portion of the incident voltage v_{t1} is transmitted across the junction onto the first line and is given by $v_{t1} = T_{21} v_{i2}$. The total voltage on each side of the junction again must be equal:

$$v_{i2} + v_{r2} = v_{t1} \tag{4.78b}$$

Hence, the reflection and transmission coefficients are related as

$$1 + \Gamma_{21} = T_{21} \tag{4.78c}$$

and the transmission coefficient is given by

$$T_{21} = \frac{2Z_{C1}}{Z_{C1} + Z_{C2}} \tag{4.78d}$$

This process is again illustrated in Fig. 4.29c.

We can again sketch the voltage waveforms at the load and at the junction by tracing the waves and using the transmission and reflection coefficients given above while noting the direction of travel of the incident wave.

Example 4.5 For the series connection of two different lines illustrated in Fig. 4.30a, sketch the voltage at the load and at the junction. The line is series matched at the source and terminated in an open circuit. Line 1 has a total time delay of 1 ns and a characteristic impedance of 50 Ω, while line 2 has a total time delay of 2 ns and a characteristic impedance of 100 Ω.

Solution: First, we compute the appropriate reflection and transmission coefficients for a wave incident on the junction from line 1 as shown:

$$\begin{aligned}\Gamma_{12} &= \frac{Z_{C2} - Z_{C1}}{Z_{C2} + Z_{C1}}\\ &= \frac{100 - 50}{100 + 50}\\ &= \frac{1}{3}\end{aligned}$$

$$\begin{aligned}T_{12} &= \frac{2Z_{C2}}{Z_{C2} + Z_{C1}}\\ &= \frac{200}{100 + 50}\\ &= \frac{4}{3}\end{aligned}$$

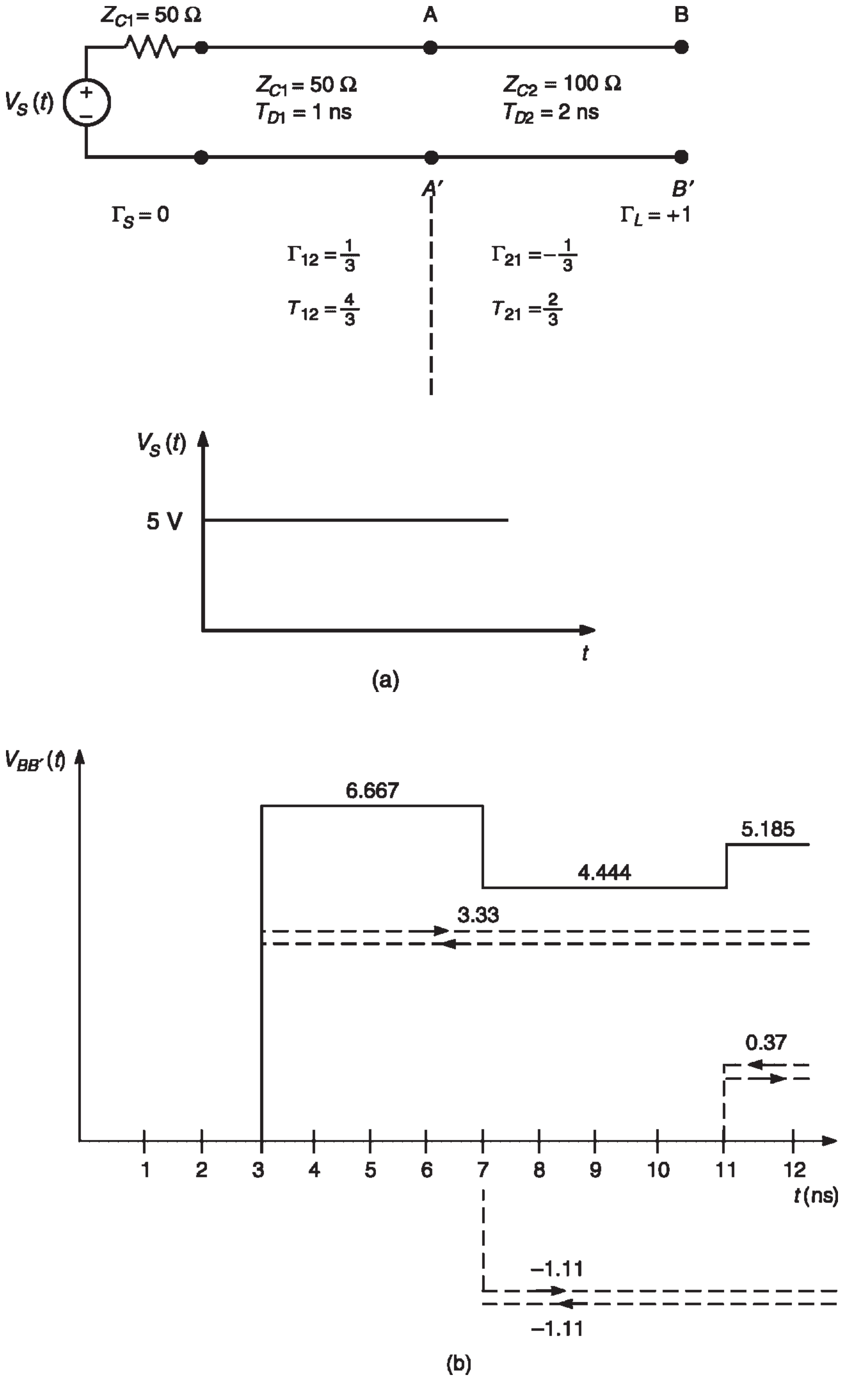
$Z_{C1} = 50\ \Omega$
A
B
$V_S(t)$
+
−
$Z_{C1} = 50\ \Omega$
$T_{D1} = 1$ ns
$Z_{C2} = 100\ \Omega$
$T_{D2} = 2$ ns
A′
B′
$\Gamma_S = 0$
$\Gamma_L = +1$
$\Gamma_{12} = \frac{1}{3}$
$T_{12} = \frac{4}{3}$
$\Gamma_{21} = -\frac{1}{3}$
$T_{21} = \frac{2}{3}$
$V_S(t)$
5 V
t
$V_{BB'}(t)$
6.667
5.185
4.444
3.33
0.37
1
2
3
4
5
6
7
8
9
10
11
12
t (ns)
−1.11
−1.11

(a)

(b)

FIGURE 4.30 Example 4.5: (a) problem specification; (b) the voltage at the end of the line; (c) the voltage at the junction.

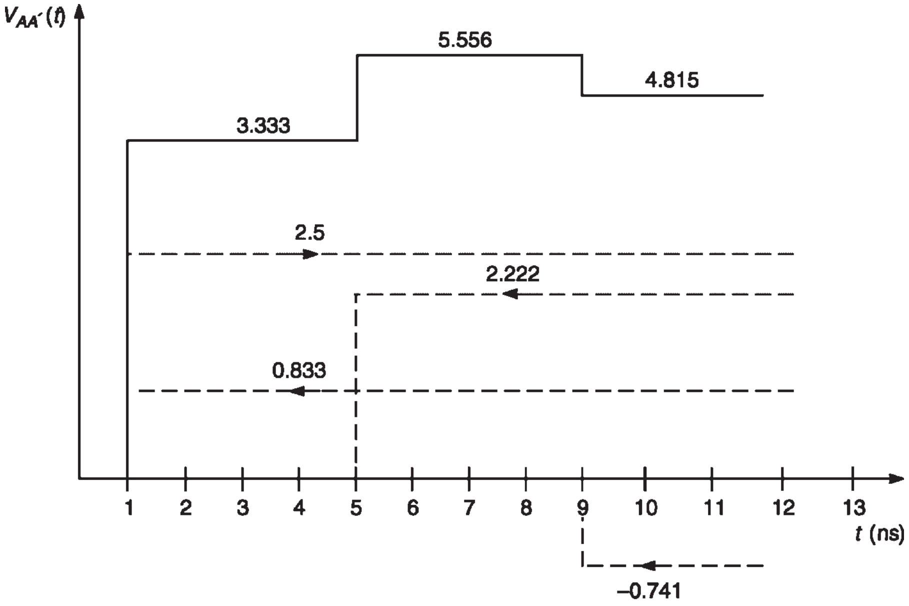

(c)

FIGURE 4.30 (*Continued*)

Observe that $1 + \Gamma_{12} = T_{12}$. Similarly, for a wave incident on the junction from line 2, we obtain

$$\begin{aligned}\Gamma_{21} &= \frac{Z_{C1} - Z_{C2}}{Z_{C1} + Z_{C2}}\\ &= \frac{50 - 100}{50 + 100}\\ &= \frac{1}{3}\end{aligned}$$

Again observe that $1 + \Gamma_{21} = T_{21}$. The initial voltage sent out onto line 1 is

$$V_{\text{init}} = \frac{Z_{C1}}{(R_S = Z_{C1}) + Z_{C1}}(5\,\text{V}) = 2.5\,\text{V}$$

Figure 4.38b shows the load voltage at the end of line 2. The initial voltage of 2.5 V is sent out and at one time delay of line 1, 1 ns, arrives at the junction. A voltage of $\Gamma_{12}2.5$ V = 0.883 V is reflected to the left, arriving at the source after another 1 ns, where it is completely absorbed. A voltage of $T_{12}2.5$ V = 3.333 V is transmitted across the junction onto line 2, arriving at the open-circuit load after an additional 2 ns or 3 ns. The open-circuited load had a reflection coefficient of +1, and hence 3.333 V is reflected. Thus, the total voltage is 6.667 V. This reflected voltage of 3.333 V arrives at the junction incident from the right after another 2 ns, where $T_{21}3.333$ V = 2.222 V is transmitted across the junction and after an additional 1 ns arrives at the source where it is completely absorbed. However, a reflected voltage of $\Gamma_{21}3.333$ V = – 1.111 V is reflected at the junction, sending this back to the right, arriving at the load after a further 2 ns or 7 ns. Since the load reflection coefficient is +1, this is totally reflected, giving a total of 4.444 V. The process continues where the incoming (from the right) wave of 1 (reflected at the load) arrives at the junction after 2 ns more, where $\Gamma_{21}(-1.111)$ V $= +0.37$ V is reflected back to the load, arriving there after an additional 2 ns or 11 ns, where it is completely reflected, giving a total of 5.185 V. This approaches 5 V.

Sketching the voltage at the junction is done in a similar process and is shown in Fig. 4.30c. The initially launched voltage of 2.5 V arrives at the junction at 1 ns, where $\Gamma_{12}2.5$ V $= 0.883$ V is reflected and $T_{12}2.5$ V $= 3.333$ V is transmitted across the junction onto line 2. We can calculate the total voltage at the junction as either $v_{il} + v_{rl} = 2.5 + 0.833 = 3.333$ V or as $v_{t2} = 3.333$ V since the voltages on either side of the junction must be equal. The reflected voltage of 0.833 V is totally absorbed at the matched source, but the transmitted voltage arrives at the load after an additional 2 ns and is totally reflected, giving 3.333 V, arriving at the junction (as an incident wave from the right) after another 2 ns or a total of 1 ns + 2 ns + 2 ns = 5 ns. This is reflected as $\Gamma_{21}3.333$ V $= -1.111$ V and transmitted as $T_{21}3.333$ V $= 2.222$ V. Since the total voltage on either side of the junction must be the same, we obtain either $(1 + \Gamma_{21})$ 3.333 V = 2.222 V or $T_{21}3.333$ V $= 2.222$ V. Adding this to the voltage of 3.333 V already present gives a total voltage of 5.556 V. The 2.222 V is reflected and arrives at the load after another 2 ns, at which time it is completely reflected, arriving at the junction after another 2 ns or a total of 9 ns. This is reflected as $\Gamma_{21}2.222$ V $= -0.741$ V. Adding this to the voltages present from previous reflections gives a total of 4.815 V. This also approaches 5 V in steady state. This is sketched in Fig. 4.30c.

In the previous example, series matching at the source does not eliminate reflections as evidenced in the computed results. This is due to the discontinuity. Reflections at the discontinuity that are sent back to the source are absorbed at the source because of matching, but a portion of the incident wave at the discontinuity is transmitted across the discontinuity and sent to the load. Because the load is not matched to the second part of the line, a reflection is transmitted back to the left that is incident on the discontinuity and hence a portion is transmitted across it toward the source, where it is absorbed. Consider the reverse, specifically suppose that we parallel-match at the load but don't series-match at the source. A wave sent out by the source and incident on the discontinuity will create a reflection that is sent back to the source where it will be reflected. The portion of the incident wave that is transmitted across the discontinuity will be incident on the load but will be completely absorbed because the load is parallel-matched. But the portion of the wave reflected at the source will again be incident on the discontinuity, and a portion will be transmitted across the discontinuity. This will again be incident on the load where it is absorbed. But we will have reflections at the source and at the load. Hence, in order to eliminate reflections on lines having discontinuities, we must series match at the source and parallel-match at the load.

Example 4.6 Sketch the discontinuity and load voltages using symbols rather than numerical values for a line with a discontinuity that is matched at the source and at the load.

Solution: The problem is shown in Fig. 4.31a. The initial voltage sent out is $V_{\text{init}} = V_s / 2$. This arrives at the discontinuity after T_{D1} seconds. A portion of this, $\Gamma_{12}(V_s / 2)$, is reflected back toward the source and a portion of the incident wave, $T_{12}(V_s / 2)$, is transmitted across the discontinuity and is incident on the load after $T_{D1} + T_{D2}$ seconds, where it is absorbed. The waves at the discontinuity and at the load are sketched in Fig. 4.31b. At the discontinuity, the total voltage is

$$\begin{aligned} V_{\text{mid}} &= (1 + \Gamma_{12})\frac{V_s}{2} \\ &= T_{12}\frac{V_S}{2} \\ &= \frac{Z_{C2}}{Z_{C1} + Z_{C2}} V_S \end{aligned}$$

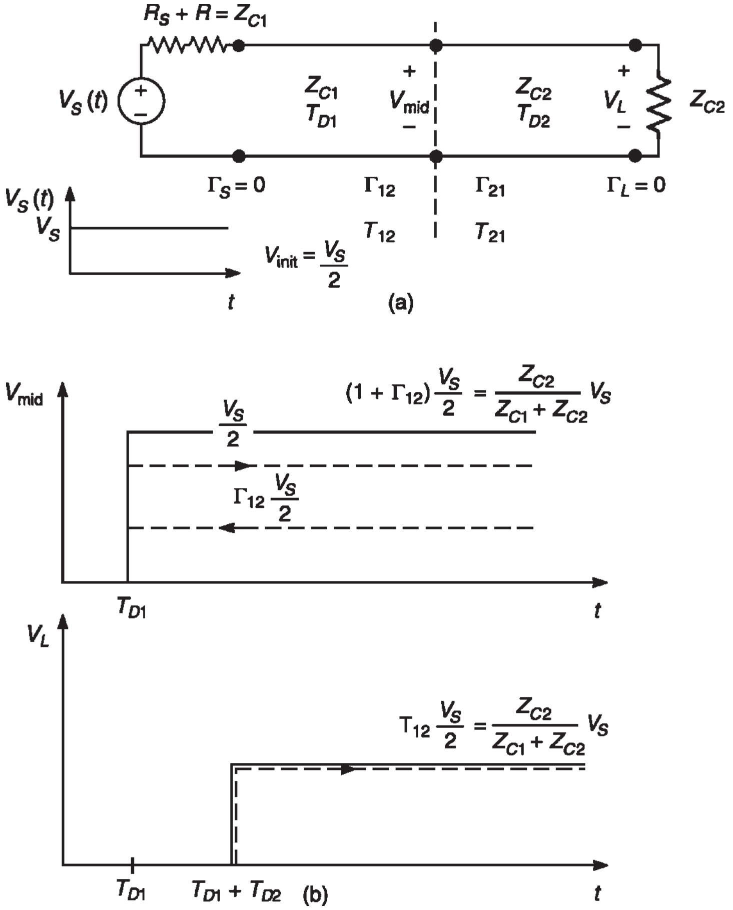

$R_S + R = Z_{C1}$
$V_S(t)$
Z_{C1}
T_{D1}
V_{mid}
Z_{C2}
T_{D2}
V_L
Z_{C2}
$\Gamma_S = 0$
Γ_{12}
Γ_{21}
$\Gamma_L = 0$
T_{12}
T_{21}
$V_S(t)$
V_S
$V_{init} = \frac{V_S}{2}$
t
(a)
V_{mid}
$\frac{V_S}{2}$
$(1+\Gamma_{12})\frac{V_S}{2} = \frac{Z_{C2}}{Z_{C1}+Z_{C2}}V_S$
$\Gamma_{12}\frac{V_S}{2}$
T_{D1}
t
V_L
$T_{12}\frac{V_S}{2} = \frac{Z_{C2}}{Z_{C1}+Z_{C2}}V_S$
T_{D1}
$T_{D1} + T_{D2}$
(b)
t

FIGURE 4.31 Example 4.6. A line with a discontinuity that is matched at the source and at the load: (a) problem specification; (b) symbolic solution.

At the load, the total voltage is

$$\begin{aligned} V_L &= T_{12}\frac{V_S}{2} \\ &= \frac{Z_{C2}}{Z_{C1}+Z_{C2}}V_S \end{aligned}$$

Observe that the voltage at the discontinuity and at the load are identical. This is sensible because these are the steady-state values.

Finally, we consider discontinuities that are introduced by feeding multiple lines either in series or in parallel as shown in Fig. 4.32 [12]. First, consider the series distribution shown in Fig. 4.32a. The analysis of this configuration is essentially the same as the analysis of a line discontinuity considered previously. For simplicity, we have assumed both lines to have the same characteristic impedance Z_C, but the time delays may be different. We show the feeding of two CMOS gates, which we will assume resemble open circuits at their inputs. How shall we match to prevent reflections? Clearly, a series match at the source, $R_S + R = Z_C$, will eliminate all reflections. (This would not be the case if the

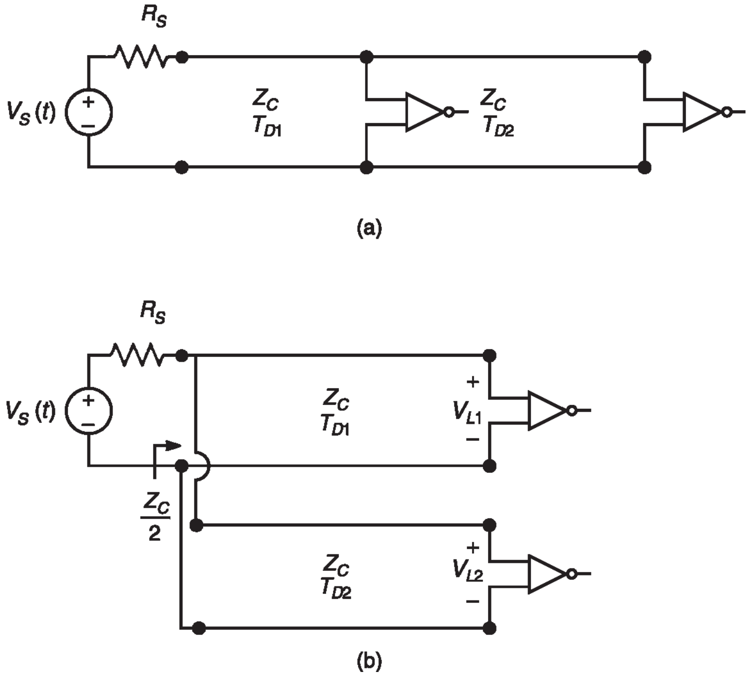

FIGURE 4.32 Effects of feeding multiple lines: (a) series distribution; (b) parallel distribution. Source: Based on Paul [12].

line characteristic impedances were not equal, as we showed earlier.) We could also parallel-match at the load, but this would have consequences as discussed earlier, such as this matching resistor dissipating power in the high state. A frequent mistake made is to parallel-match at the midpoint: at the junction of the two lines. What would be the consequence of placing a resistor $R = Z_C$ at the junction of the two lines as shown in Fig. 4.33? The left line sees the resistor in parallel with the characteristic impedance of the second line for a total of $Z_C / 2$. Hence, at this junction we will have

$$\begin{aligned}\Gamma_{12} &= \frac{(Z_C / 2) - Z_C}{(Z_C / 2) + Z_C} \\ &= \Gamma_{21} \\ &= -\frac{1}{3}\end{aligned}$$

and

$$\begin{aligned}T_{12} &= \frac{2(Z_C / 2)}{(Z_C / 2) + Z_C} \\ &= T_{21} \\ &= \frac{2}{3}\end{aligned}$$

Hence, there will be multiple reflections and transmissions at the junction.

Next, consider the case of parallel distribution shown in Fig. 4.32b, where the source drives two lines that are in parallel. Clearly, the steady-state load voltages are V_S as desired because of the

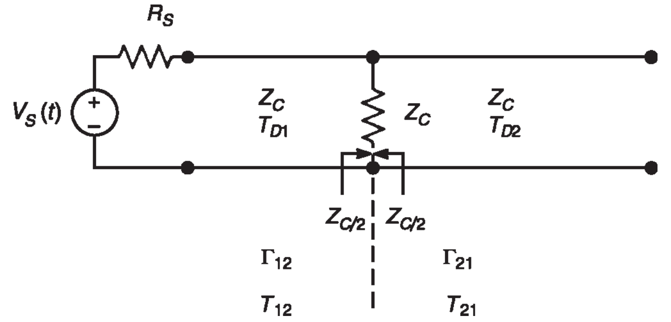
R_S
$V_S(t)$
+
−
Z_C
T_{D1}
Z_C
Z_C
T_{D2}
$Z_{C/2}$
$Z_{C/2}$
Γ_{12}
Γ_{21}
T_{12}
T_{21}

FIGURE 4.33 Matching a series distribution at the line midpoint: a mistake that exacerbates the problem.

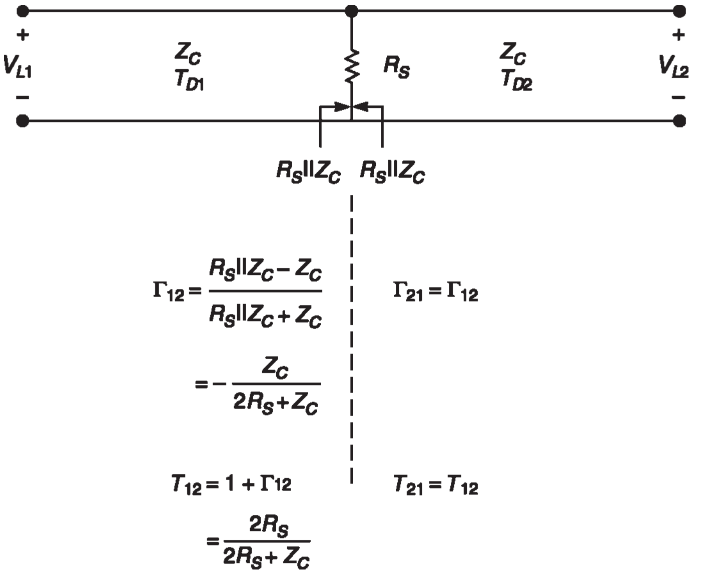
+
V_{L1}
−
Z_C
T_{D1}
R_S
Z_C
T_{D2}
+
V_{L2}
−
$R_S \| Z_C$
$R_S \| Z_C$
$\Gamma_{12} = \dfrac{R_S \| Z_C - Z_C}{R_S \| Z_C + Z_C} = -\dfrac{Z_C}{2R_S + Z_C}$
$\Gamma_{21} = \Gamma_{12}$
$T_{12} = 1 + \Gamma_{12} = \dfrac{2R_S}{2R_S + Z_C}$
$T_{21} = T_{12}$

FIGURE 4.34 Analysis of the parallel distribution of Fig. 4.32b.

open-circuited loads. The source sees two lines in parallel so that the net impedance is $Z_C / 2$. Hence, the initially sent out voltage (for a step voltage of level V_S) is

$$V_{\text{init}} = \frac{Z_C / 2}{R_S + (Z_C / 2)} V_S$$

This is sent out for each line. At the load, it encounters an open circuit (the input to the gate), where it is totally reflected. These arrive at the source after time delays of T_{D1} and T_{D2}. A simple way of seeing what transpires is to redraw the situation as shown in Fig. 4.34. Line 1 on the left sees an impedance at the junction of

$$R_S \parallel Z_C = \frac{R_S Z_C}{R_S + Z_C}$$

Hence, at the junction we have reflection coefficients and transmission coefficients of

$$\begin{aligned}\Gamma_{12} &= \Gamma_{21}\\ &= -\frac{Z_C}{2R_S + Z_C}\end{aligned} \tag{4.80a}$$

and

$$\begin{aligned}T_{12} &= T_{21}\\ &= \frac{2R_S}{2R_S + Z_C}\end{aligned} \tag{4.80b}$$

Review Exercise 4.10 Derive the reflection and transmission coefficients in (4.80).

The initially launched voltage given in (4.79) will be fully reflected at each load and on arriving at the junction will be reflected as $\Gamma_{12} V_{\text{init}} = \Gamma_{21} V_{\text{init}}$ and transmitted across the junction as $\mathrm{T}_{12} V_{\text{init}} = \mathrm{T}_{21} V_{\text{init}}$. This process continues so that we will have continued reflections at the junction and at the loads.

This is undesirable so how can we eliminate these reflections? First suppose that we use a series match at the source, that is, make $R_S = Z_C$. In this case, the reflection coefficients will be –1/3 and the transmission coefficients will be 2/3. Suppose that we series-match at the source but choose $R_S = Z_C / 2$. In this case, the reflection coefficients will be –1/2 and reflections will not be eliminated. However, if the two time delays are equal (an unlikely circumstance), one can show that after two time delays the load voltages reach steady state. An alternative matching scheme would be to parallel match at the loads, placing resistors of value Z_C across the loads. But this would suffer from the undesirable fact that they draw current in the high state as is the case with all parallel matching schemes. Driving many loads in parallel would then begin to draw an exhorbitant current from this one driver. Hence, the parallel distribution is less desirable than the series distribution.

4.5 SINUSOIDAL EXCITATION OF THE LINE AND THE PHASOR SOLUTION

We now consider the case where the source is a single-frequency, sinusoidal waveform

$$V_S(t) = V_S \cos(\omega t) \tag{4.81}$$

and $\omega = 2\pi f$. The solution method (phasor analysis) is the same as for lumped circuits that are driven by a single-frequency sinusoidal source (see Appendix A). Again, we place so much emphasis on single-frequency sinusoidal excitation of lines not because practical sources are single-frequency sinusoids (they are not), but because any periodic (and nonperiodic) waveform can be represented with the Fourier series (Fourier transform) as being composed of a sequence of single-frequency sinusoidal components. Hence, if the system is linear (such as a transmission line having a linear source and load), then we may use superposition to pass each frequency component through it and sum them in time at the output to give the time-domain load voltage. This allows us to obtain great insight into how the line processes the various single-frequency components as is the case with electric filters.

We will also assume that the source has been attached to the line for a length of time so that the transients have decayed sufficiently leaving a steady-state sinusoidal voltage and current along the line. Thus, we replace the source with its phasor equivalent, $\hat{V}_S = V_S\angle 0°$. The resulting line voltages and currents are then given in terms of the phasor line voltages and currents as

$$V(z,t) = \mathscr{R}e\{\hat{V}(z)e^{j\omega t}\} \tag{4.82a}$$

$$I(z,t) = \mathscr{R}e\{\hat{I}(z)e^{j\omega t}\} \tag{4.82b}$$

4.5.1 Voltage and Current as Functions of Position

The phasor transmission-line equations for a *lossless line* are obtained by substituting the phasor forms in (4.82) into the transmission-line equations of (4.2), where we replace time derivatives with $j\omega$ to give

$$\frac{d\hat{V}(z)}{dz} = -j\omega l\hat{I}(z) \tag{4.83a}$$

$$\frac{d\hat{I}(z)}{dz} = -j\omega c\hat{V}(z) \tag{4.83b}$$

Differentiating one with respect to z and substituting the other gives these equations as uncoupled, second-order equations:

$$\frac{d^2\hat{V}(z)}{dz} = -\omega^2 lc\hat{V}(z) = 0 \tag{4.84a}$$

$$\frac{d^2\hat{I}(z)}{dz^2} = -\omega^2 lc\hat{I}(z) = 0 \tag{4.84b}$$

The solutions to these equations are simple to obtain as [1, 2]

$$\hat{V}(z) = \hat{V}^+e^{-j\beta z} + \hat{V}^-e^{j\beta z} \tag{4.85a}$$

$$\hat{I}(z) = \frac{\hat{V}^+}{Z_C}e^{-j\beta z} - \frac{\hat{V}^-}{Z_C}e^{j\beta z} \tag{4.85b}$$

where $\hat{V}^+$ and $\hat{V}^-$ are complex constants that are, as yet, undetermined. The other items are the familiar characteristic impedance and phase constant, given by

$$Z_C = \sqrt{\frac{l}{c}} \tag{4.86}$$

$$\beta = \frac{\omega}{v} \tag{4.87}$$

and v is the velocity of propagation on the line

$$\begin{aligned} v &= \frac{1}{\sqrt{lc}} \\ &= \frac{1}{\sqrt{\mu\varepsilon}} \end{aligned} \tag{4.88}$$

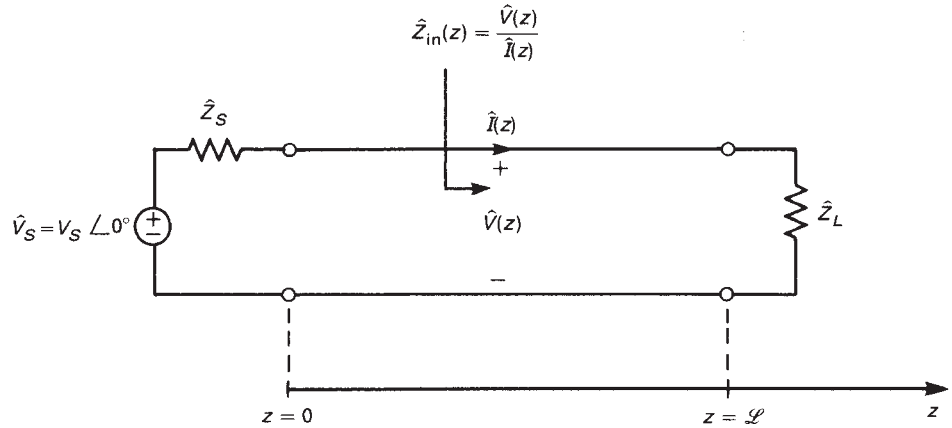
$\hat{Z}_{in}(z) = \frac{\hat{V}(z)}{\hat{I}(z)}$
$\hat{Z}_S$
$\hat{I}(z)$
+
$\hat{V}(z)$
−
$\hat{V}_S = V_S \angle 0°$
$\hat{Z}_L$
$z = 0$
$z = \mathscr{L}$
z

FIGURE 4.35 Definition of terms for the sinusoidal steady-state (phasor) analysis of transmission lines.

and the medium surrounding the line is assumed to be homogeneous and characterized by μ and ε. These results also apply to lines in an inhomogeneous medium such as in Fig. 4.2. These cases are characterized by an effective permittivity $\varepsilon = \varepsilon_0 \varepsilon'_r$.

Consider the transmission line shown in Fig. 4.35. The line is terminated at $z = L$ in a complex impedance $\hat{Z}_L$, and the source is a phasor source with source voltage $\hat{V}s = Vs\angle 0°$ and complex source impedance $\hat{Z}_S$. Let us define a complex voltage reflection coefficient at a particular point z on the line as the ratio of the phasor voltages of the backward- and forward-traveling waves:

$$\begin{aligned}\hat{\Gamma}(z) &= \frac{\hat{V}^- e^{j\beta z}}{\hat{V}^+ e^{-j\beta z}} \\ &= \frac{\hat{V}^-}{\hat{V}^+} e^{j2\beta z}\end{aligned} \tag{4.89}$$

In terms of this reflection coefficient, the voltage and current expressions in (4.85) may be written as

$$\hat{V}(z) = \hat{V}^+ e^{-j\beta z}[1 + \hat{\Gamma}(z)] \tag{4.90a}$$

$$\hat{I}(z) = \frac{\hat{V}^+}{Z_C} e^{-j\beta z}[1 - \hat{\Gamma}(z)] \tag{4.90b}$$

We may also define an *input impedance* to the line at any point on the line as the ratio of the *total* voltage and current at that point on the line, as shown in Fig. 4.35:

$$\begin{aligned}\hat{Z}_{\text{in}}(z) &= \frac{\hat{V}(z)}{\hat{I}(z)} \\ &= Z_C \frac{1 + \hat{\Gamma}(z)}{1 - \hat{\Gamma}(z)}\end{aligned} \tag{4.91}$$

The reflection coefficient at the load is

$$\hat{\Gamma}_L = \frac{\hat{Z}_L - Z_C}{\hat{Z}_L + Z_C} \tag{4.92}$$

The reflection coefficient at some other point on the line is related to the load reflection coefficient as [1, 2]

$$\hat{\Gamma}(z) = \hat{\Gamma}_L e^{j2\beta(z-L)} \tag{4.93}$$

Thus, *the reflection coefficient at any point on the line can be related to the load reflection coefficient, which can be calculated directly from (4.92)*. This gives a general procedure for calculation of the line voltage and current. The procedure is as follows:

1. Compute the load reflection coefficient from (4.92)
2. Compute the reflection coefficient at the line input from (4.93) as

$$\begin{aligned}\hat{\Gamma}(0) &= \hat{\Gamma}_{\text{in}} \\ &= \hat{\Gamma}_L e^{-j2\beta L}\end{aligned} \tag{4.94}$$

3. Compute the input impedance to the line from (4.91) as

$$\hat{Z}_{\text{in}}(0) = Z_C \frac{1 + \hat{\Gamma}(0)}{1 - \hat{\Gamma}(0)} \tag{4.95}$$

4. Compute the phasor input voltage to the line (by voltage division) as

$$\hat{V}(0) = \frac{\hat{Z}_{\text{in}}(0)}{\hat{Z}_{\text{in}}(0) + \hat{Z}_S} \hat{V}_S \tag{4.96}$$

5. Compute the undetermined constant $\hat{V}^+$ from (4.90) as

$$\hat{V}^+ = \frac{\hat{V}(0)}{1 + \hat{\Gamma}(0)} \tag{4.97}$$

6. Finally, compute the line voltage and current at any point on the line from (4.90).

The *time-domain* line voltages and currents can then be found from these phasor voltages and currents using (4.82).

It is also possible to obtain explicit formulas for these results. The preceding results can be combined to obtain equations for the phasor voltage and current at any point on the line in terms of the source voltage:

$$\hat{V}(z) = \frac{1 + \hat{\Gamma}_L e^{-j2\beta L} e^{j2\beta z}}{1 - \hat{\Gamma}_S \hat{\Gamma}_L e^{-j2\beta L}} \frac{Z_C}{Z_C + \hat{Z}_S} \hat{V}_S e^{-j\beta z} \tag{4.98a}$$

$$\hat{I}(z) = \frac{1 - \hat{\Gamma}_L e^{-j2\beta L} e^{j2\beta z}}{1 - \hat{\Gamma}_S \hat{\Gamma}_L e^{-j2\beta L}} \frac{1}{Z_C + \hat{Z}_S} \hat{V}_S e^{-j\beta z} \tag{4.98b}$$

The input impedance can also be written as

$$\begin{aligned} \hat{Z}_{\text{in}}(0) &= Z_C \frac{1 + \hat{\Gamma}_L e^{-j2\beta L}}{1 - \hat{\Gamma}_L e^{-j2\beta L}} \\ &= Z_C \frac{\hat{Z}_L + jZ_C \tan \beta L}{Z_C + j\hat{Z}_L \tan \beta L} \end{aligned} \tag{4.99}$$

Review Exercise 4.11 Derive the relations in (4.98) and (4.99).

A number of interesting properties can be deduced from these results. For example, from (4.92) we see that if the line is matched, $\hat{Z}_L = Z_C$, then the load reflection coefficient is zero, $\hat{\Gamma}_L = 0$. Equations (4.98) then show that for a matched line, the *magnitudes* of the voltage and current are independent of position along the line:

$$\hat{V}(z) = \frac{Z_C}{Z_C + \hat{Z}_S} \hat{V}_S e^{-j\beta z} \quad \hat{Z}_L = Z_C \text{ (matchedline)} \tag{4.100a}$$

$$\hat{I}(z) = \frac{1}{Z_C + \hat{Z}_S} \hat{V}_S e^{-j\beta z} \quad \hat{Z}_L = Z_C \text{ (matchedline)} \tag{4.100b}$$

Where possible, it is desirable to match transmission lines, $\hat{Z}_L = Z_C$, in order to eliminate reflections. This will also cause the magnitudes of the line voltage and current to be constant along the line. Only the phase of these quantities will change between two points along the line as shown by the $e^{-j\beta z}$ factor in (4.100). It is generally not possible to precisely match a line, so a quantitative criterion for the closeness of the match is desired. This is provided by the *voltage standing-wave ratio* (VSWR), which is defined as the ratio of the magnitude of the maximum voltage on the line to the minimum voltage on the line [1, 2]

$$\begin{aligned} \text{VSWR} &= \frac{\left|\hat{V}(z)\right|_{\max}}{\left|\hat{V}(z)\right|_{\min}} \\ &= \frac{1 + \left|\hat{\Gamma}_L\right|}{1 - \left|\hat{\Gamma}_L\right|} \end{aligned} \tag{4.101}$$

[See (4.90)]. The load reflection coefficient for a short-circuit load is $\hat{\Gamma}_L = -1$, whereas that for an open-circuit load is $\hat{\Gamma}_L = 1$. For both cases, the magnitude is unity making the VSWR equal to infinity. For either case, the minimum voltage on the line is zero, which is why the VSWR is infinite. A large VSWR indicates an extreme variation of the voltage and current magnitude along the line, which is undesirable. On the other hand, a matched load gives a reflection coefficient of zero and a VSWR of unity. Therefore, the VSWR of a line will be bounded by unity and infinity:

$$1 \le \text{VSWR} \le \infty$$

The closer the VSWR to unity, the better the match. Equation (4.99) also shows that *the input impedance to a lossless transmission line replicates for line lengths that are multiples of a half-wavelength*; that is, a length of line shows the same input impedance if we add or subtract lengths that are multiples of a half-wavelength. This is seen by observing that $\beta = 2\pi/\lambda$. Equation (4.99) also shows that a *quarter-wavelength line that is terminated in a short circuit (open circuit) appears at its input terminals as an open circuit (short circuit).*

Example 4.7 As a numerical example, consider the parallel-wire line shown in Fig. 4.36a. The per-unit-length parameters of the line are $c = 200$ pF / m and $l = 0.5$ μH / m, from which we compute

$$\begin{aligned} Z_C &= \sqrt{\frac{l}{c}} \\ &= 50\,\Omega \\ v &= \frac{1}{\sqrt{lc}} \\ &= 100 \text{ m}/\mu s \end{aligned}$$

The frequency of the source is 30 MHz, so the line length of 1 m is 0.3 λ in electrical length. The reflection coefficient at the load is

$$\begin{aligned} \hat{\Gamma}_L &= \frac{\hat{Z}_L - Z_C}{\hat{Z}_L + Z_C} \\ &= \frac{100 + j50 - 50}{100 + j50 + 50} \\ &= 0.447\angle 26.6^\circ \end{aligned}$$

and the VSWR is

$$\begin{aligned} \text{VSWR} &= \frac{1 + |\hat{\Gamma}_L|}{1 - |\hat{\Gamma}_L|} \\ &= \frac{1 + 0.447}{1 - 0.447} \\ &= 2.62 \end{aligned}$$

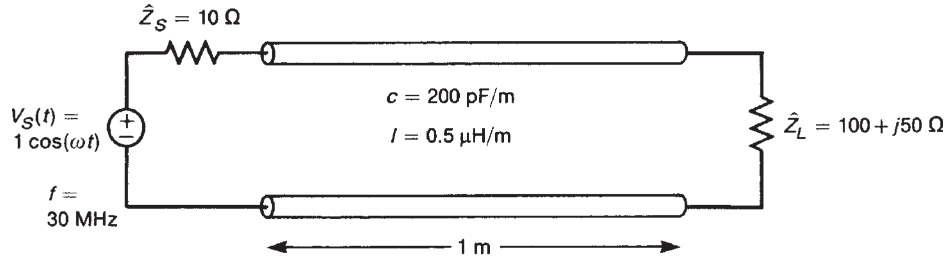

FIGURE 4.36 Example 4.7. An example illustrating the phasor analysis of transmission lines.

The input impedance to the line is computed from the results given above as

$$\begin{aligned}\hat{\Gamma}(0) &= \hat{\Gamma}_L e^{j2\beta(0-L)}\\ &= \hat{\Gamma}_L e^{-j2\beta L}\\ &= 0.447\angle 26.6^\circ\, e^{-j216^\circ}\\ &= 0.447\angle(-189.4^\circ)\end{aligned}$$

Thus,

$$\begin{aligned}\hat{Z}_{\text{in}}(z) &= Z_C\frac{1+\hat{\Gamma}(0)}{1-\hat{\Gamma}(0)}\\ &= 19.54\angle 10.34^\circ\ \Omega\end{aligned}$$

The voltage at the input to the line becomes

$$\begin{aligned}\hat{V}(0) &= \frac{\hat{Z}_{\text{in}}(0)}{\hat{Z}_{\text{in}}(0)+\hat{Z}_S}\hat{V}_S\\ &= 0.664\angle 3.5^\circ\ \text{ V}\end{aligned}$$

and

$$\begin{aligned}\hat{I}(0) &= \frac{\hat{V}(0)}{\hat{Z}_{\text{in}}(0)}\\ &= 34\times 10^{-3}\angle(-6.8^\circ)\ \text{ A}\end{aligned}$$

Thus, the time-domain voltage and current at the input to the line are

$$V(0,t) = 0.664\cos(60\pi\times 10^6 t + 3.5^\circ)\ \text{ V}$$

$$I(0,t) = 0.034\cos(60\pi\times 10^6 t - 6.8^\circ)\ \text{ A}$$

The phasor load voltage and current are obtained by first determining the constant $\hat{V}^+$ as

$$\begin{aligned}\hat{V}^+ &= \frac{\hat{V}(0)}{1+\hat{\Gamma}(0)}\\ &= 1.18\angle(-3.94^\circ)\end{aligned}$$

Thus,

$$\begin{aligned}\hat{V}(L) &= \hat{V}^+ e^{-j\beta z}[1+\hat{\Gamma}_L]\\ &= 1.18\angle(-3.94^\circ)\, e^{-j108^\circ}(1+0.447\angle(26.6^\circ))\\ &= 1.668\angle(-103.8^\circ)\ \text{ V}\end{aligned}$$

Therefore, the time-domain load voltage is

$$V(L,t) = 1.668\cos(60\pi \times 10^6 t - 103.8^\circ)\ \text{V}$$

Review Exercise 4.12 Determine the source and load voltages for a line whose length is 10 m and that has a characteristic impedance of $Z_C = 50\ \Omega$ and a velocity of propagation of $v = 200$ m/ms. The source voltage is $\hat{V}_S = 100\angle 0^\circ$ at 26 MHz and $\hat{Z}_S = 50\ \Omega, \hat{Z}_L = 100 + j50$.

Answers: $\hat{V}(0) = 28.28\angle 7.48^\circ$ V and $\hat{V}(L) = 70.71\angle(-99.84^\circ)$ V

4.5.2 Power Flow

From the transverse nature of the TEM mode of propagation, it is clear that power flow is in the $\pm z$ direction, since the Poynting vector is in this direction. In terms of the line voltage and current, the average power flow in the $+z$ direction is given by

$$P_{\text{av}}(z) = \frac{1}{2}\mathscr{Re}\{\hat{V}(z)\hat{I}^*(z)\} \tag{4.102}$$

where * denotes the complex conjugate. Substituting the forms of the phasor voltages and currents given in (4.90) into (4.102) gives [1, 2]

$$P_{\text{av}}(z) = \frac{1}{2}\frac{|\hat{V}^+|^2}{Z_C}\left(1 - |\hat{\Gamma}_L|^2\right) \tag{4.103}$$

This result could have been derived by adding the average powers of the forward- and backward-traveling waves. If we refer to the forward-traveling wave as the *incident wave* and the backward-traveling wave as the *reflected wave*, the ratio of the powers in these waves is

$$\frac{P_{\text{av,reflected}}}{P_{\text{av,incident}}} = |\hat{\Gamma}_L|^2 \tag{4.104}$$

When the load is either an open circuit or a short circuit, the magnitude of the reflection coefficient is unity, and (4.104) shows that all the incident power is reflected, a sensible result. Similarly, if the line is matched then the reflection coefficient is zero, and (4.104) shows that all the incident power is absorbed in the load.

Example 4.8 For the line shown in Fig. 4.36 and considered in Example 4.7, determine the power delivered to the line input and to the load.

Solution: The average power delivered to the input of the line is

$$\begin{aligned}
P_{\text{av,to line}} &= \frac{1}{2}\mathscr{Re}\{\hat{V}(0)\hat{I}^*(0)\} \\
&= \frac{1}{2}\mathscr{Re}\{(0.664\angle 3.5^\circ)(0.034\angle(-6.8^\circ))\} \\
&= 11.1\,\text{mW} \\
&= \frac{1}{2}\left|\hat{V}(0)\right|\left|\hat{I}(0)\right|\cos(\theta_V - \theta_I) \\
&= \frac{1}{2}(0.664)(0.034)\cos(3.5^\circ + 6.8^\circ)
\end{aligned}$$

Since the line is assumed to be lossless, all of this average power is delivered to the load, which can be checked directly:

$$
\begin{aligned}
P_{\text{av,to load}} &= \frac{1}{2}\mathscr{R}e\{\hat{V}(L)\hat{I}^{*}(L)\} \\
&= \frac{1}{2}\frac{\left|\hat{V}(L)\right|^{2}}{\left|\hat{Z}_{L}\right|}\cos\angle\hat{Z}_{L} \\
&= \frac{1}{2}\frac{(1.668)^{2}}{111.8}\cos 26.57^{\circ} \\
&= 11.1\,\text{mW}
\end{aligned}
$$

4.5.3 Inclusion of Losses

Imperfect line conductors and/or surrounding medium can easily be included in the preceding frequency-domain results in an *exact* manner, as opposed to the time-domain results. Furthermore, skin effect can also be accounted for in an *exact* fashion by simply computing the line resistance at the frequency of interest and including the value as a constant at that frequency. This is not the case for the time-domain results, since inclusion of the line resistance in the transmission-line equations significantly complicates their solution even if we assume that the resistance is independent of frequency (which is not true due to skin effect).

The transmission-line equations were derived for a lossless line from the equivalent circuit in Fig. 4.4 and are given in Eq. (4.2). The per-unit-length equivalent circuit for a lossy line is shown in Fig. 4.37 where we have added the per-unit-length resistance r and conductance g. The per-unit-length resistance r represents losses in the line conductors, whereas the per-unit-length conductance g represents losses in the dielectric surrounding the conductors, From this, we can obtain the transmission-line equations in the limit as $\Delta z \rightarrow 0$ in phasor form as

$$\frac{d\hat{V}(z)}{dz} = -z\hat{I}(z) \tag{4.105a}$$

$$\frac{d\hat{I}(z)}{dz} = -y\hat{V}(z) \tag{4.105b}$$

where the per-unit-length impedance $\hat{z}$ and admittance $\hat{y}$ are given by

$$\hat{z} = r(f) + j\omega l \tag{4.106a}$$

$$\hat{y} = g + j\omega c \tag{4.106b}$$

We have shown the per-unit-length conductor resistance as a function of frequency to emphasize its dependence on skin effect. Equations (4.105) are again a set of coupled differential equations. They may be uncoupled by differentiating one and substituting the other to give

$$\frac{d^{2}\hat{V}(z)}{dz^{2}} - \hat{z}\hat{y}\hat{V}(z) = 0 \tag{4.107a}$$

$$\frac{d^{2}\hat{I}(z)}{dz^{2}} - \hat{y}\hat{z}\hat{I}(z) = 0 \tag{4.107b}$$

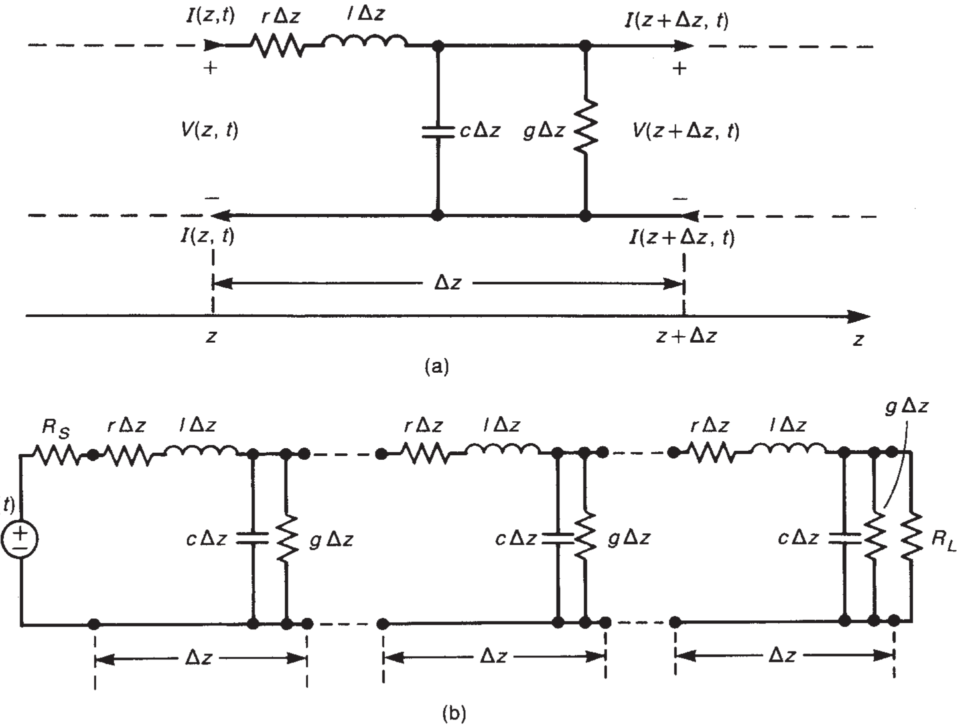

FIGURE 4.37 The per-unit-length equivalent circuit of a two-conductor lossy line: (a) the equivalent circuit for a Δz section; (b) modeling the entire line as a cascade of Δz sections from which the transmission-line equations are derived in the limit as $\Delta z \to 0$.

The general solution of these equations is quite similar in form to that of the lossless case:

$$\hat{V}(z) = \hat{V}^{+} e^{-\alpha z} e^{-j\beta z} + \hat{V}^{-} e^{\alpha z} e^{j\beta z} \tag{4.108a}$$

$$\hat{I}(z) = \frac{\hat{V}^{+}}{\hat{Z}_C} e^{-\alpha z} e^{-j\beta z} - \frac{\hat{V}^{-}}{\hat{Z}_C} e^{\alpha z} e^{j\beta z} \tag{4.108b}$$

where the characteristic impedance is

$$\begin{aligned} \hat{Z}_C &= \sqrt{\frac{\hat{z}}{\hat{y}}} \\ &= \sqrt{\frac{r(f) + j\omega l}{g + j\omega c}} \end{aligned} \tag{4.109}$$

and the propagation constant is

$$\begin{aligned} \hat{\gamma} &= \sqrt{\hat{z}\hat{y}} \\ &= \alpha + j\beta \end{aligned} \tag{4.110}$$

The solution process for lossy lines is virtually unchanged from that for lossless lines. There are, however, some important differences in the behavior of the line voltage and current that are worth pointing out. Observe in (4.108) that the forward- and backward-traveling voltage and current waves are attenuated as they travel alone the line, which is evidenced by the $e^{-\alpha z}$ and $e^{\alpha z}$ amplitude factors. The second important difference between lossy and lossless lines is that average power is dissipated in a lossy line as the waves travel along the line.

4.5.4 Effect of Losses on Signal Integrity

Losses occur in the line conductors and in the surrounding dielectric. Conductor losses are represented by the per-unit-length conductor resistance r in the per-unit-length model shown in Fig. 4.37. Similarly, losses in the surrounding dielectric medium are represented by the per-unit-length conductance, g, in Fig. 4.37. Let us briefly discuss how these two loss mechanisms come about. They will be discussed further in the following chapter. First, consider the wire shown in Fig. 4.38a. At dc, the current will be uniformly distributed over the wire cross section, and the dc resistance per unit length is

$$r_{\mathrm{dc}} = \frac{1}{\sigma \pi r_w^2} \quad \Omega/\mathrm{m} \tag{4.111a}$$

where σ is the metal conductivity and r_w is the wire radius. For copper, the conductivity is $\sigma_{\mathrm{Cu}} = 5.8 \times 10^7$ S/m. As the frequency of the current is increased, the current concentrates near the outer edge of the wire, and the majority of the current is confined to an annulus equal to the *skin depth* [1, 2, 13]:

$$\delta = \frac{1}{\sqrt{\pi f \mu_0 \sigma}} \quad \mathrm{m} \tag{4.112}$$

The permeability of a typical nonmagnetic conductor is that of free space, $\mu_0 = 4\pi \times 10^{-7}$. For $r_w >> \delta$, the per-unit-length resistance is

$$\begin{aligned} r_{\mathrm{hf}} &= \frac{1}{\sigma\left(\pi r_w^2 - \pi (r_w - \delta)^2\right)} \\ &= \frac{1}{\sigma 2\pi r_w \delta} \quad \Omega/\mathrm{m} \end{aligned} \tag{4.111b}$$

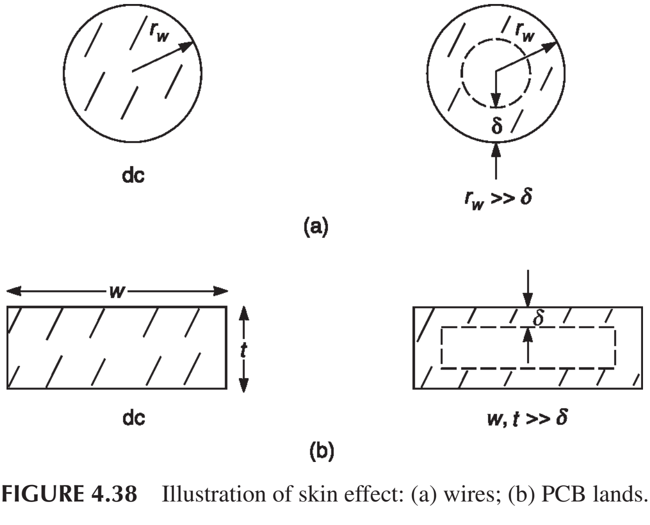

FIGURE 4.38 Illustration of skin effect: (a) wires; (b) PCB lands.

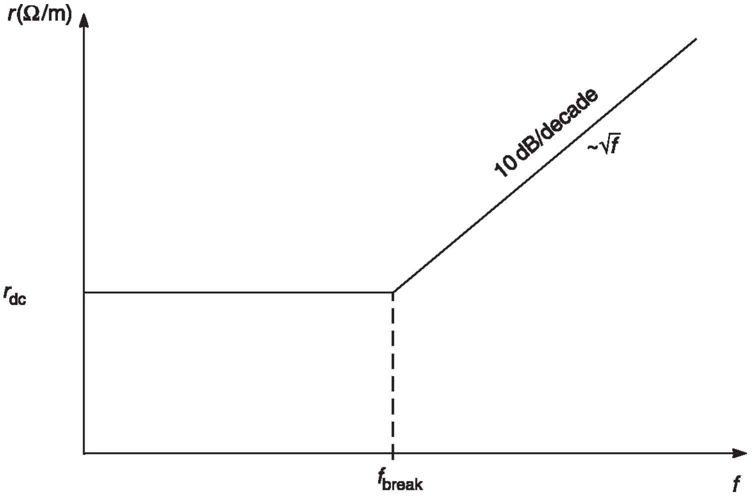

FIGURE 4.39 Frequency response of the per-unit-length resistance of wires.

Observe that the skin depth in (4.112) *decreases* in inverse proportion to the *square root of the frequency*. Observe that the high-frequency per-unit-length resistance has the skin depth in the denominator. Hence, as the frequency increases, the per-unit-length resistance *increases* in direct proportion to the square root of the frequency or 10 dB/decade. This frequency behavior is shown in Fig. 4.39.

Similarly, for the rectangular cross-section PCB land shown in Fig. 4.38b, at dc the current is uniformly distributed over the land cross section and the dc resistance is

$$r_{\mathrm{dc}} = \frac{1}{\sigma w t} \quad \Omega/\mathrm{m} \tag{4.113a}$$

and w and t are the land width and thickness, respectively. For one-ounce copper, the thickness is 1.38 mils. In a fashion similar to that for the wire, as frequency is increased, the current becomes concentrated in a thickness equal to one skin depth at the surface as shown in Fig. 4.38b. Actually, the current also peaks at the corners, but we will ignore this practicality to simplify the computation [13]. Hence

$$\begin{aligned} r_{\mathrm{hf}} &= \frac{1}{\sigma(2\delta t + 2\delta w)} \\ &= \frac{1}{2\sigma\delta(w+t)} \quad \Omega/\mathrm{m} \end{aligned} \tag{4.113b}$$

Again, the high-frequency resistance increases in direct proportion to the square root of the frequency as shown in Fig. 4.39. The dc and high-frequency resistances in (4.113a) and (4.113b) have asymptotes that join at a frequency where [13]

$$\begin{aligned} \delta &= \frac{1}{2}\frac{wt}{(w+t)} \\ &\cong \frac{t}{2} \quad w \gg t \end{aligned} \tag{4.113c}$$

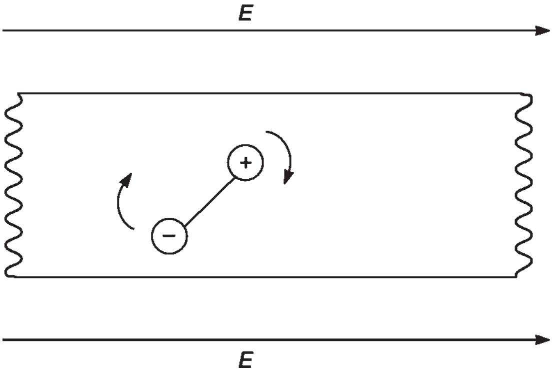

FIGURE 4.40 Illustration of bound charge dipoles in dielectrics and their rotation to align with an applied electric field.

For lands having high aspect ratios, $w \gg t$, the two asymptotes join where the thickness (the smaller dimension) equals two skin depths, which satisfies our intuition.

Now we turn to the loss in the surrounding dielectric medium. Dielectrics are characterized by having *bound charge* in the form of microscopic dipoles and have no appreciable free charge, unlike conductors [1, 2]. When an electric field is applied, these bound charge dipoles tend to rotate so as to align with the applied electric field as illustrated in Fig. 4.40. For high frequencies of the field, the inertia of these dipoles prevents them from being able to completely reverse direction as the (sinusoidal) electric field changes direction. This inability to completely reverse direction provides what is equivalent to a damping loss. If the material also contains a significant number of free charge carriers, the dielectric can contribute an ohmic loss. Dielectric loss that accounts for these damping and ohmic losses is characterized by ascribing a complex relative permittivity to the dielectric as

$$\varepsilon_c = \varepsilon_r' - j\varepsilon_r'' \tag{4.114}$$

The real part, identified as ε_r', refers to the damping loss effect of the permittivity, and is related to power loss in the material related to the fact that work must be done to overcome the damping effect. The imaginary part, identified as ε_r'', refers to ohmic loss in the material related to the fact that work must be done to move free charge carriers from one position to another within the material. In materials that have very low values of ε_r'', ε_r' is often indicated as simply the *relative permittivity* ε_r. Let us consider lines in a *homogeneous* medium such as the coaxial cable in Fig. 4.1c and the stripline shown in Fig. 4.2a. The capacitance of a structure having a surrounding medium that is homogeneous is proportional to the cross-sectional dimensions and the permittivity of the intervening dielectric, giving the per-unit-length capacitive reactance as

$$j\omega c = j\omega\varepsilon K \tag{4.115}$$

Substituting (4.114) gives

$$\begin{aligned} j\omega\,\varepsilon K &= j\omega\,\varepsilon_0\varepsilon_c K \\ &= \underbrace{\omega\,\varepsilon_0\varepsilon_r'' K}_{g} + \underbrace{j\omega\,\varepsilon_0\varepsilon_r' K}_{x_c} \end{aligned} \tag{4.116}$$

The first term of (4.116) is equivalent to a per-unit-length *conductance*, while the second term is equivalent to a per-unit-length capacitive reactance. The ratio of ε_r'' to ε_r' gives the ratio of the ohmic loss term to the damping loss term and is referred to as the *loss tangent* [1]:

$$\tan(\theta) = \frac{\varepsilon_r''}{\varepsilon_r'} \tag{4.117}$$

Numerous handbooks tabulate the loss tangent for different materials and different frequencies. For FR-4, which is used to construct PCBs, the loss tangent is fairly constant at high frequencies and is approximately 0.02. Hence, we may write the per-unit-length conductance as

$$g = \omega c \ \tan(\theta) \tag{4.118}$$

Observe that the per-unit-length conductance *increases directly with frequency* (20 dB/decade), unlike the skin effect resistance. Technically, the result in (4.118) only applies to lines in a *homogeneous* medium and does not apply to, for example, lines in an inhomogeneous medium such as ribbon cables, the microstrip line shown in Fig. 4.2b and the PCB shown in Fig. 4.2c. However, it is possible to include complex permittivities as in (4.114) by including them in a numerical evaluation of the capacitance [13].

Recall that the phasor transmission line equations are given in (4.105) as

$$\frac{d\hat{V}(z)}{dz} = -(r + j\omega l)\hat{I}(z) \tag{4.119a}$$

$$\frac{d\hat{I}(z)}{dz} = -(g + j\omega c)\hat{V}(z) \tag{4.119b}$$

The characteristic impedance is, in general, complex and given by

$$\begin{aligned}\hat{Z}_C &= \sqrt{\frac{r + j\omega l}{g + j\omega c}} \\ &= Z_c \angle \theta_{Z_c} \ \Omega \end{aligned} \tag{4.119c}$$

and the propagation constant is

$$\begin{aligned}\hat{\gamma} &= \alpha + j\beta \\ &= \sqrt{(r + j\omega l)(g + j\omega c)}\end{aligned} \tag{4.119d}$$

from which we compute the exact velocity of propagation as

$$v = \frac{\omega}{\beta} \ \text{m/s} \tag{4.119e}$$

Observe in (4.108) that one of the significant effects of losses is that the amplitude of the sinusoidal wave is attenuated as it travels down the line. This is given by the terms $e^{\pm\alpha z}$. Furthermore, the attenuation constant α as well as the phase constant β are frequency-dependent, as is the characteristic impedance. The characteristic impedance, attenuation constant, and the phase constant as well as the velocity of propagation, $v = \omega / \beta$, will be frequency-dependent even if the per-unit-length resistance r and g were independent of frequency. The velocity of propagation of the sinusoidal waves is $v = \omega / \beta$ and is not constant with frequency in contrast to the lossless case. Digital pulses are composed of a large number of sinusoidal components as we saw in the previous chapter. If each of these sinusoidal components travel down the line at different speeds, they will arrive at the load at different times, resulting in a distortion of the pulse. This is called *dispersion*. In addition, since the attenuation constant is frequency-dependent, each sinusoidal component will be attenuated by a different amount. This also results in dispersion. As we will see, losses attenuate the higher-frequency components more than the lower frequency components. Hence, the bandwidth of the pulse is reduced and the pulse rise/fall-times are increased. If all the sinusoidal components traveled at the same velocity and were attenuated at the same rate, the received pulse would retain its shape and only the amplitude would be lowered.

Typically, losses are small at the significant range of frequencies for typical high-speed digital signals and for typical boards. For example, for a stripline with plate separation of 20 mils and a land of width 5 mils in FR-4 ($\varepsilon_r = 4.7$), we compute $c = 113.2$ pF / m and $l = 0.461$ mH / m (see Review Exercise 4.4). The characteristic impedance for this lossless stripline is $Z_C = \sqrt{l/c} = 63.8\ \Omega$, and the velocity of propagation is $v = 1/\sqrt{lc} = 1.38 \times 10^8$ m / s. Using (4.118), the per-unit-length conductance is $g = (14.2 \times 10^{-12})(f)$ S/m. The high-frequency resistance in (4.113b) dominates the dc resistance in (4.113a) above a frequency given in (4.113c). For this problem, the frequency is 23 MHz. Hence, for frequencies above 23 MHz, the per-unit-length resistance of the land is computed from the high-frequency equation in (4.113b) giving $r = (8.05 \times 10^{-4})\sqrt{f}\ \Omega / \text{m}$.

By “low loss” we mean

$$r \ll \omega l \tag{4.120a}$$

and

$$g \ll \omega c \tag{4.120b}$$

For this stripline problem, r is less than ωl for $f > 1.34$ MHz and g is less than ωc for all frequencies. Observe that since $g = \omega c \tan(\theta)$, g is less than ωc by the loss tangent, which for FR-4 is 0.02. (Actually the loss tangent eventually goes to zero at dc, so it is not correct to assume that the loss tangent is 0.02 for all frequencies.)

Let us consider obtaining a simple formula for the characteristic impedance and the attenuation constant. The propagation constant is given in (4.119d). Rewriting this as

$$\begin{aligned}
\hat{\gamma} &= \alpha + j\beta \\
&= \sqrt{(r + j\omega l)(g + j\omega c)} \\
&= \sqrt{(j\omega l)(j\omega c)\left(1 + \frac{r}{j\omega l}\right)\left(1 + \frac{g}{j\omega c}\right)} \\
&= j\omega\sqrt{lc}\sqrt{\left(1 - \frac{rg}{\omega^2 lc}\right) - j\left(\frac{r}{\omega l} + \frac{g}{\omega c}\right)} \\
&\cong j\omega\sqrt{lc}\sqrt{1 - j\left(\frac{r}{\omega l} + \frac{g}{\omega c}\right)} \qquad \begin{cases} r \ll \omega l \\ g \ll \omega c \end{cases}
\end{aligned} \tag{4.121}$$

We now apply the Taylor's series to expand this

$$(1+x)^n = 1 + \frac{nx}{1!} + \frac{n(n-1)x^2}{2!} + \cdots \quad x\,|< 1$$

to give

$$\hat{\gamma} \cong j\omega\sqrt{lc}\left[1 - j\left(\frac{r}{2\omega l} + \frac{g}{2\omega c}\right)\right] \tag{4.122}$$

from which we identify the attenuation constant as

$$a \cong \frac{1}{2}\left(\frac{r}{Z_c} + gZ_c\right) \tag{4.123a}$$

$$b \cong \omega\sqrt{lc} \tag{4.123b}$$

In a similar fashion, we obtain

$$\begin{aligned} Z_c &= \sqrt{\frac{r+j\omega l}{g+j\omega c}} \\ &\cong \sqrt{\frac{l}{c}} \quad \begin{cases} r \ll \omega l \\ g \ll \omega c \end{cases} \end{aligned} \tag{4.124}$$

Hence for a low-loss line where $r \ll \omega l$ and $g \ll \omega c$, the characteristic impedance and the velocity of propagation are independent of frequency and are essentially the same as for a lossless line. Figure 4.41 shows the magnitude and angle of the characteristic impedance versus frequency from 10 kHz to 1 GHz for the stripline considered previously where the land is of width 5 mils and the plate separation is 20 mils. Observe that above about 5 MHz the characteristic impedance approaches the lossless value of $Z_C = 63.8\ \Omega$. Figure 4.42a shows the attenuation constant, and Fig. 4.42b shows the velocity of propagation, $v = \omega / \beta$. The velocity of propagation approaches the lossless value of $v = 1.38 \times 10^8$ m/s above ~5 MHz. The value of the attenuation constant computed from the approximation in (4.123a) at 100 MHz is $\alpha = 1.085 \times 10^{-1}$, whereas the value computed directly from the exact expression in (4.119d) is the same. Hence for typical board dimensions, the low-loss region where the approximations given above apply is above ~5 MHz. Hence, for today's digital signals, all of their sinusoidal components lie in the low-loss frequency range.

We obtain the power loss in a length of line as $e^{-2\alpha L}$. This assumes the line is matched so that there are only forward-traveling waves on the line. In dB this becomes

$$\text{Loss}_{\text{dB}} = 8.686\,\alpha L \tag{4.125}$$

For the preceding stripline at a frequency of 1 GHz, we obtain

$$\begin{aligned} Z_c &= 63.8\,\Omega \\ \mathrm{r} &= 25.46\ \ \Omega/\mathrm{m} \\ \mathrm{g} &= 1.423 \times 10^{-2}\,\mathrm{S/m} \\ \alpha &= 0.653 \end{aligned}$$

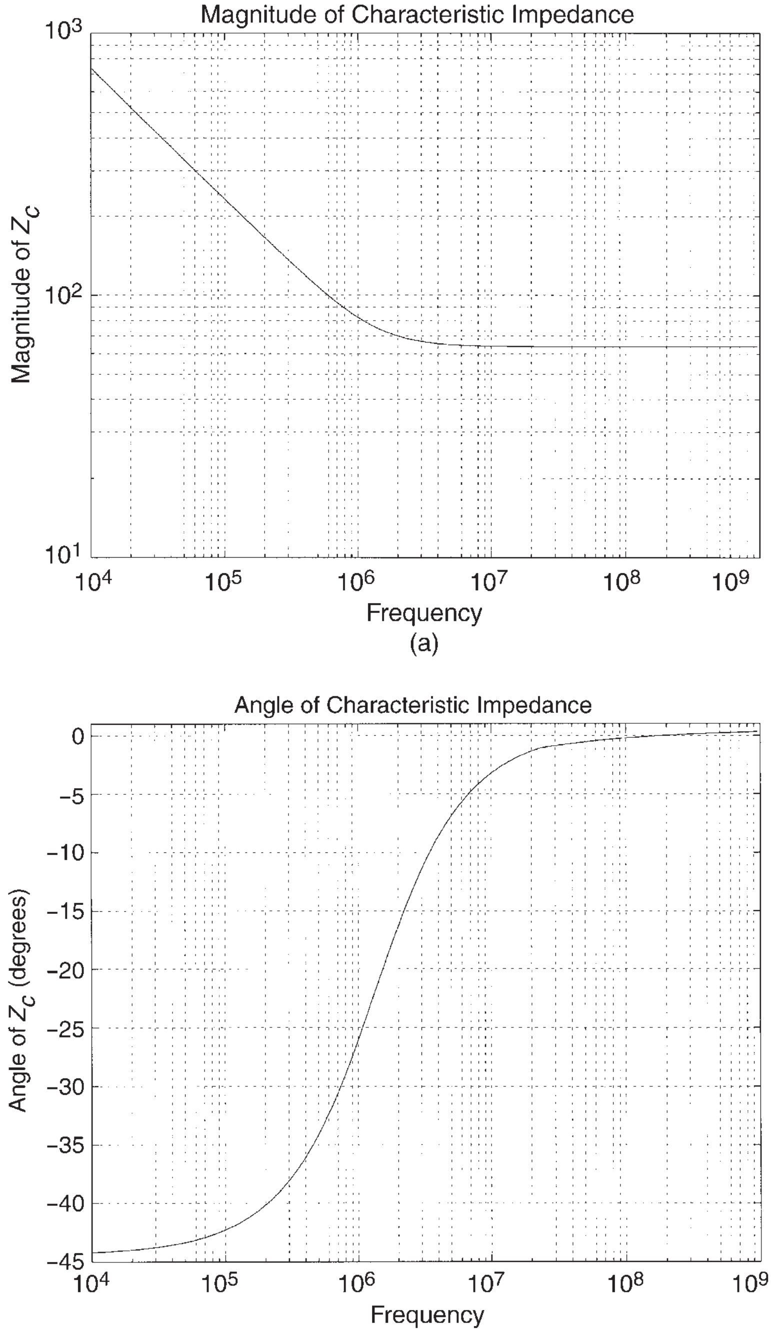

(a)

(b)

FIGURE 4.41 Frequency dependence of the characteristic impedance of a lossy stripline: (a) characteristic impedance magnitude; (b) characteristic impedance angle.

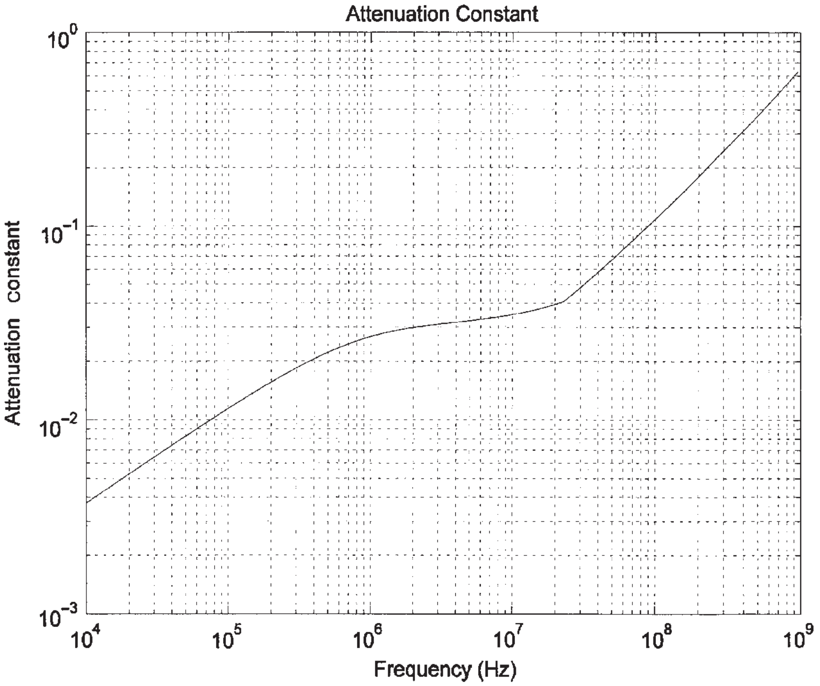

(a)

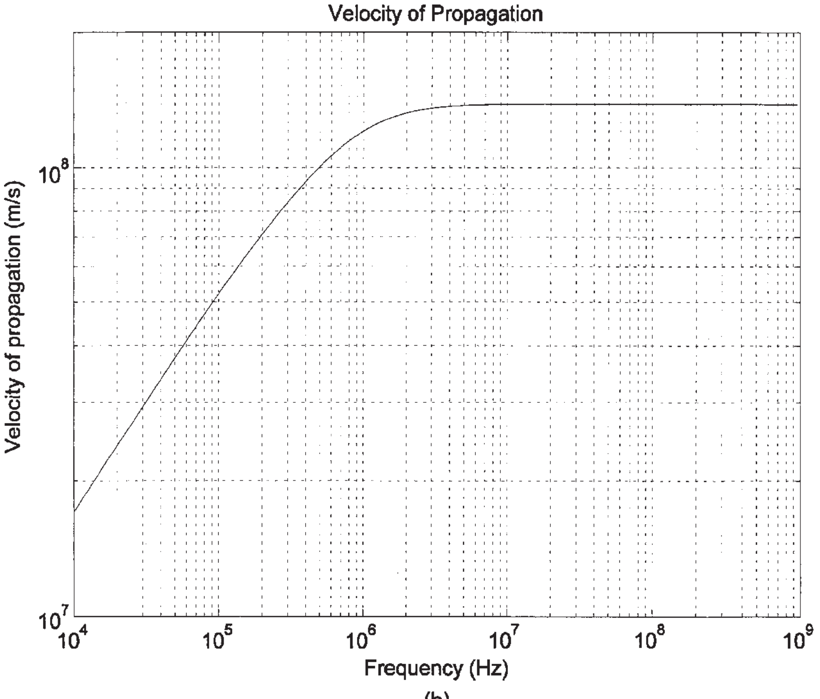

(b)

FIGURE 4.42 Frequency dependence of parameters of a lossy stripline; (a) attenuation constant; (b) velocity of propagation.

The resistive loss is

$$\begin{aligned}\text{Loss}_r &= 4.343\,\frac{r}{Z_c}L \\ &= 1.73\,L \quad \text{dB}\end{aligned} \tag{4.126a}$$

and

$$\begin{aligned}\text{Loss}_g &= 4.343\,gZ_cL \\ &= 3.94\,L \quad \text{dB}\end{aligned} \tag{4.126b}$$

The total attenuation is the sum of these values. For a 6 in. length of this stripline, the total attenuation at 1 GHz is 0.86 dB. This says that the amplitude of a 1-GHz sine wave is reduced by about 1 dB, that is, the input level is reduced to about 90% at the output when traversing a line length of 6 in. Observe that above 1 GHz, the dielectric loss dominates the conductor loss.

Since the velocity of propagation for a low-loss line is approximately frequency-independent, we can obtain a simpler result for the per-unit-length conductance. The characteristic impedance in the low-loss frequency range is essentially the same as for a lossless line: $Z_C = \sqrt{l\,/\,c} = vl = 1\,/\,vc$. Hence, the per-unit-length conductance in (4.118) can be written for a low-loss line as

$$\begin{aligned}g &= \omega c\ \tan(\theta) \\ &= \frac{\omega}{vZ_c}\ \tan(\theta)\end{aligned} \tag{4.127}$$

Once again this simple result holds only for lines in a homogenous medium. The portion of the attenuation due to dielectric loss for a low-loss line becomes

$$\begin{aligned}\text{Loss}_g &= 4.343\,gZ_cL \\ &= 4.343\,\omega\frac{\sqrt{\varepsilon_r}}{v_0}\ \tan(\theta L)\ \ \text{dB}\end{aligned} \tag{4.128}$$

Hence, the attenuation due to dielectric loss is independent of the line cross-section dimensions. On the other hand, the attenuation due to conductor loss depends strongly on the dimensions of the lands such as land width. Once again, the simple result in (4.128) is valid only for lines in a *homogeneous* medium and does not apply to the microstrip or PCB configurations.

4.6 LUMPED-CIRCUIT APPROXIMATE MODELS

Typical circuit analysis computer programs such as SPICE (PSPICE) contain an exact transmission-line model for two-conductor, lossless transmission lines that can be used for either time-domain or frequency-domain analysis of the line as we have observed. Nevertheless, an approximate method of modeling transmission lines that is frequently used is the construction of lumped-circuit models that are intended to be lumped-circuit approximations to the exact per-unit-length distributed-parameter model of Fig. 4.4 The typical such circuits are the lumped-pi or lumped-T circuits shown in Fig. 4.43. These models can be used for either time- or frequency-domain analyses of the line.

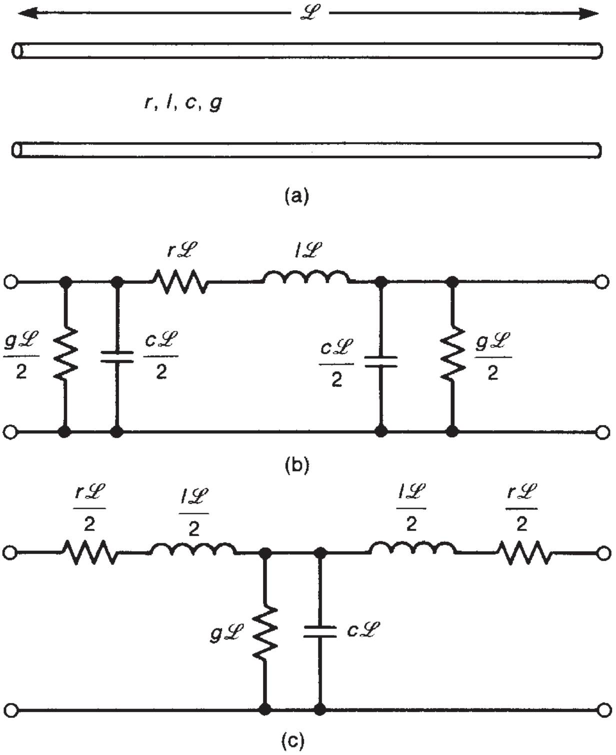

FIGURE 4.43 Modeling the transmission line with lumped circuits: (a) problem definition; (b) the lumped-Pi circuit; (c) the lumped-T circuit.

In order to use the lumped-circuit models in Fig. 4.43 to model the transmission line, the line must be electrically short at the highest frequency of interest of the input source waveform. In other words, *the lumped-circuit model will correctly process only those frequency components of the input source that are below the frequency where the line becomes a significant fraction of a wavelength.* For single-frequency sinusoidal excitations, this presents no problems. However, for time-domain signals such as periodic pulse trains this requires the user to determine whether incorrect processing of those spectral components of the source that are above the frequency where the line becomes electrically long will contribute any significant error. In order to increase the frequency range of validity of the lumped models, one might expect to subdivide the line into several electrically small subsections and model each with a lumped-circuit approximate model such as that in Fig. 4.43. Other work has shown that the gain in the extension of the valid frequency range is not significant, so that modeling a line with a large number of lumped-pi sections, for example, would not give a significant enough extension of the frequency range to make the additional programming required by the large circuit structure worth the trouble [14].

At first glance, it may appear that these lumped-circuit approximate models may be used to simulate losses by simply adding the line resistance r and conductance g to each section. But this will not be able to simulate losses for time-domain inputs because these are frequency-dependent, and it is difficult if not impossible to simulate frequency-dependent r and g in lumped circuits.

PROBLEMS

Section 4.1 The Transmission-Line Equations

4.1.1 For the per-unit-length representations of a lossless transmission line shown in Fig. P4.1.1, derive the transmission-line equations in the limit as $\Delta z \rightarrow 0$. Note that the total per-unit-length inductance and capacitance in each circuit are l and c, respectively. This shows that the *structure* of the per-unit-length equivalent circuit is not important in the limit as $\Delta z \rightarrow 0$.

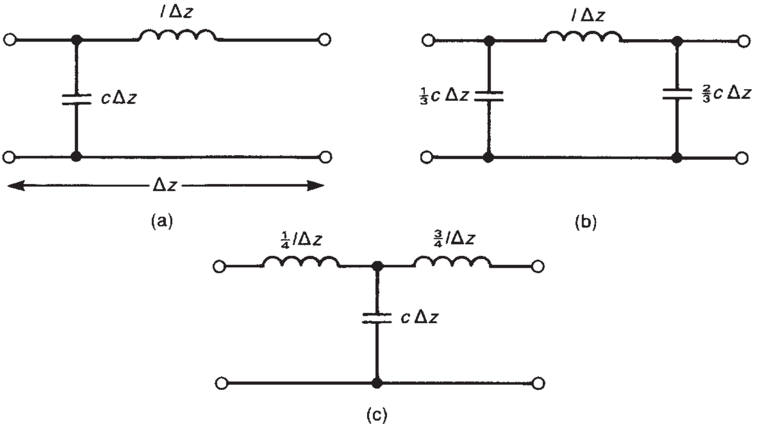

FIGURE P4.1.1

Section 4.2 The Per-Unit-Length Parameters

4.2.1 Two bare 20-guage (radius = 16 mils) wires are separated center-to-center by 50 mils. Determine the exact and approximate values of the per-unit-length capacitance and inductance. [Exact: 27.33 pF / m, 0.4065 μH / m; approximate: 24.38 pF / m, 0.4558 μH / m]

4.2.2 One bare 12-guage (radius = 40 mils) wire is suspended at a height of 80 mils above its return path, which is a large ground plane. Determine the exact and approximate values of the per-unit-length capacitance and inductance. [Exact: 42.18 pF/m, 0.2634 μH/m; approximate: 40.07 pF/m, 0.2773 μH/m]

4.2.3 A typical coaxial cable is RG6U, which has an interior 18-gauge (radius 20.15 mils) solid wire, an interior shield radius of 90 mils, and an inner insulation of foamed polyethylene having a relative permittivity of 1.45. Determine the per-unit-length capacitance, inductance, and the velocity of propagation relative to that of free space. [53.83 pF/m, 0.3 μH/m, 0.83]

4.2.4 Multilayer printed circuit boards (PCBs) consist of layers of board material that is glass epoxy material (FR-4) having a relative permittivity of 4.7 sandwiched between conducting planes. Conductors are buried midway between the conducting planes, which gives a structure resembling a stripline in Fig. 4.2a. Typical dimensions for multiplayer PCBs are a plate separation of 10 mils and a conductor width of 5 mils. Determine the per-unit-length capacitance and inductance for this structure. [156.4 pF/m and 0.334 μH/m]

4.2.5 A microstrip line is constructed on a FR-4 board having a relative permittivity of 4.7. The board thickness is 64 mils and the land width is 10 mils. Determine the per-unit-length capacitance and inductance, as well as the effective relative permittivity [0.7873 μH/m, 43.46 pF/m, $\varepsilon_r = 3.079$]

4.2.6 A PCB shown in Fig. 4.2c has land widths of 5 mils and an edge-to-edge separation of 5 mils. The board is glass epoxy having a relative permittivity of 4.7 and a thickness of 47 mils. Determine the per-unit-length capacitance and inductance, as well as the effective relative permittivity. [0.8038 μH/m, 39.06 pF/m, $\varepsilon_r = 2.825$]

4.2.7 Determine the characteristic impedance and velocity of propagation for the two-wire line in Problem 4.2.1. [122 Ω, 3×10^8 m/s]

4.2.8 Determine the characteristic impedance and velocity of propagation for the one-wire above a ground plane line in Problem 4.2.2. [79 Ω, 3×10^8 m/s]

4.2.9 Determine the characteristic impedance and velocity of propagation for the coaxial line in Problem 4.2.3. [75 Ω, 2.5×10^8 m/s]

4.2.10 Determine the characteristic impedance and velocity of propagation for the stripline in Problem 4.2.4. [46 Ω, 1.38×10^8 m/s]

4.2.11 Determine the characteristic impedance and velocity of propagation for the microstrip line in Problem 4.2.5. [135 Ω, 1.71×10^8 m/s]

4.2.12 Determine the characteristic impedance and velocity of propagation for the PCB line in Problem 4.2.6. [143 Ω, 1.79×10^8 m/s]

4.2.13 Derive the relation between per-unit-length inductance and capacitance and the characteristic impedance and velocity of propagation given in (4.39). [$l = Z_C/v$, $c = 1/vZ_C$]

4.2.14 For the case of two bare wires of radii r_w and separation s, the approximate value of the per-unit-length capacitance, valid for large separations, $s \gg r_w$, is given in (4.22). The exact result is given in (4.21). Plot these two expressions for $2.1 \le s/r_w \le 8$ to show when the approximate relation deviates significantly from the exact result. [At $s/r_w = 5$, the error is 2.7%]

Section 4.3 The Time-Domain Solution

4.3.1 Sketch the load voltage $V(L, t)$ and the input current to the line $I(0, t)$ for the problem depicted in Fig. P4.3.1 for $0 < t < 10$ ns. What should these plots converge to in the steady state [$V(L,t)$, $0 < t < 1$ ns, 0 V, 1 ns $< t <$ 3 ns, 9.375 V, 3 ns $< t <$ 5 ns, 8.203 V, 5 ns $< t <$ 7 ns, 8.35 V, 7 ns $< t <$ 9 ns, 8.331 V, 9 ns $< t <$ 11 ns, 8.334 V, steady state 8.333 V, and $I(0,t)$, $0 < t < 2$ ns, 0.125 A, 2 ns $< t <$ 4 ns, 0.047 A, 4 ns $< t <$ 6 ns, 0.057 A, 6 ns $< t <$ 8 ns, 0.055 A, 8 ns $< t <$ 10 ns, 0.056 A, steady state 0.056 A]

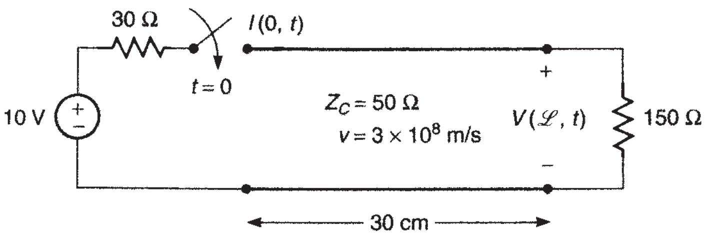

FIGURE P4.3.1

4.3.2 Sketch the load voltage $V(L,t)$ and the input voltage to the line $V(0,t)$ for the problem depicted in Fig. P4.3.2 for $0 < t < 20$ ns. What should these plots converge to in the steady state? [$V(L,t)$, $0 < t < 2$ ns, 0 V, 2 ns $< t <$ 6 ns, 6.667 V, 6 ns $< t <$ 10 ns, 4.444 V, 10 ns $< t <$ 14 ns, 5.185 V, 14 ns $< t <$ 18 ns, 4.938 V, 18 ns $< t <$ 22 ns, 5.021 V, steady state 5 V, and $V(0,t)$, $0 < t < 4$ ns, 3.33 V, 4 ns $< t <$ 8 ns, 5.556 V, 8 ns $< t <$ 12 ns, 4.815 V, 12 ns $< t <$ 16 ns, 5.062 V, 16 ns $< t <$ 20 ns, 4.979 V, steady state 5 V]

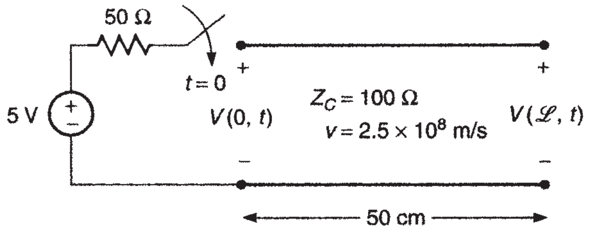

FIGURE P4.3.2

4.3.3 Sketch the input voltage to the line $V(0,t)$, and the load current $I(L,t)$ for the problem depicted in Fig. P4.3.3 for $0 < t < 10$ μs. What should these plots converge to in the steady state? [$V(0,t)$, $0 < t < 2$ μs, 66.67 V, 2 μs $< t <$ 4 μs, 22.22 V, 4 μs $< t <$ 6 μs, 7.407 V, 6 μs $< t <$ 8 μs, 2.469 V, 8 μs $< t <$ 10 μs, 0.823 V, steady state 0 V and $I(L,t)$, $0 < t < 1$ μs, 0 A, 1 μs $< t <$ 3 μs, 1.33 A, 3 μs $< t <$ 5 μs, 1.778 A, 5 μs $< t <$ 7 μs, 1.926 A, 7 μs $< t <$ 9 μs, 1.975 A, 9 μs $< t <$ 11 μs, 1.992 A, steady state 2 A]

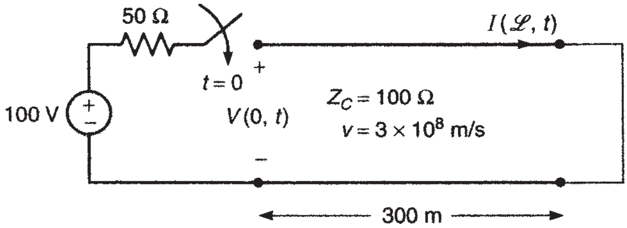

FIGURE P4.3.3

4.3.4 Sketch the input voltage to the line $V(0, t)$ and the load voltage $V(L, t)$ for the problem depicted in Fig. P4.3.4 for $0 < t < 32$ ns. What should these plots converge to in the steady state? [$V(0,t)$, $0 < t < 8$ ns, 10 V, 8 ns $< t <$ 12 ns, 5.556 V, 12 ns $< t <$ 16 ns, −4.444 V, 16 ns $< t <$ 20 ns, −3.951 V, 20 ns $< t <$ 24 ns, 0.494 V, 24 ns $< t <$ 28 ns, 0.439 V, 28 ns $< t <$ 32 ns, −0.055 V, steady state 0 V, and $V(L,t)$, $0 < t < 4$ ns, 0 V, 4 ns $< t <$ 12 ns, 6.667 V, 12 ns $< t <$ 16 ns, 5.926 V, 16 ns $< t <$ 20 ns, −0.741 V, 20 ns $< t <$ 24 ns, −0.658 V, 24 ns $< t <$ 28 ns, 0.082 V, 28 ns $< t <$ 32 ns, 0.073 V, steady state 0 V]

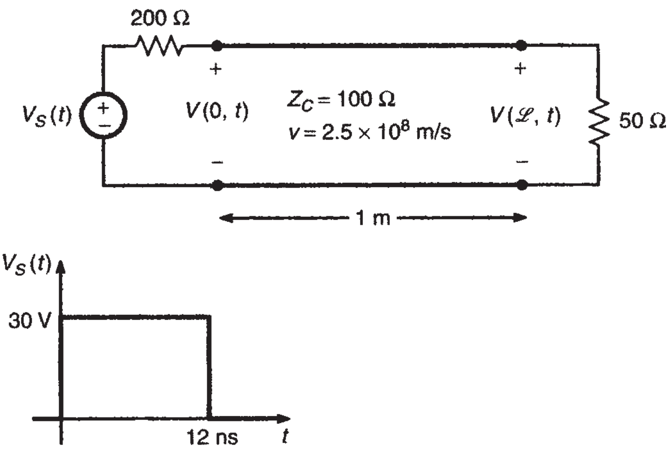

FIGURE P4.3.4

4.3.5 A transmission line having $L = 200$ m, $v = 200$ m/ms, $Z_c = 50\ \Omega$, and $R_L = 20\ \Omega$ is driven by a source that has $R_S = 100\ \Omega$ and an open-circuit source voltage that has a rectangular pulse of 6 V and duration 3 μs. Sketch the input current and output current for the line for a total time of $0 \le t \le 6$ μs. [$I(0, t), 0 \le t \le 2$ μs, 40 mA, 2 μs $\le t \le 3$ μs, 51.43 mA, 3 μs $\le t \le 4$ μs, 11.43 mA, 4 μs $\le t \le 5$ μs, 9.8 mA, 5 μs $\le t \le 6$ μs, -1.63 mA, $I(L, t)$, 1 μs $\le t \le 3$ μs, 57.14 mA, 3 μs $\le t \le 4$ μs, 48.98 mA, 4 μs $\le t \le 5$ μs, -7 mA] What should these converge to? [0 A since the pulse turns off at 3 μs]

4.3.6 A time-domain reflectometer (TDR) is an instrument used to determine properties of transmission lines. In particular, it can be used to detect the locations of imperfections such as breaks in the line. The instrument launches a pulse down the line and records the transit time for that pulse to be reflected at some discontinuity and to return to the line input. Suppose a TDR having a source impedance of 50 Ω is attached to a 50 Ω coaxial cable having some unknown length and load resistance. The dielectric of the cable is Teflon ($\varepsilon_t = 2.1$). The open-circuit voltage of the TDR is a pulse of duration 10 μs. If the recorded voltage at the input to the line is as shown in Fig. P4.3.6, determine (a) the length of the line and (b) the unknown load resistance. [(a) 621.059 m, (b) 75 Ω]

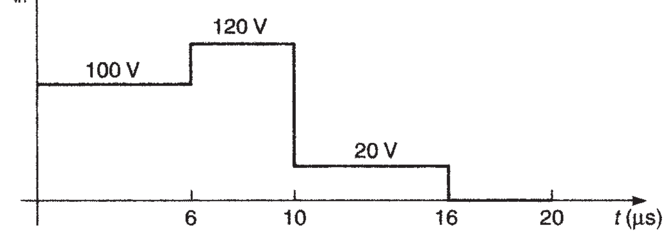

FIGURE P4.3.6

4.3.7 A 12 V battery ($R_S = 0$) is attached to an unknown length of transmission line that is terminated in a resistance. If the input current to the line for 6 μs is as shown in Fig. P4.3.7, determine (a) the line characteristic impedance and (b) the unknown load resistance. [$Z_C = 80\ \Omega$, $R_L = 262.9\ \Omega$]

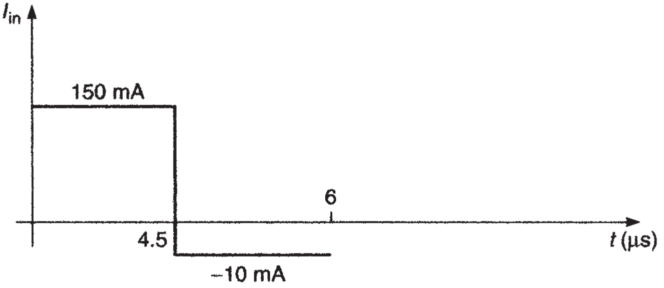

FIGURE P4.3.7

Section 4.4 High-Speed Digital Interconnects and Signal Integrity

4.4.1 Digital clock and data pulses should ideally consist of rectangular pulses. Actual clock and data pulses, however, resemble pulses having a trapezoidal shape with certain rise/falltimes. Depending on the ratio of the rise/falltime to the one-way transit time of the transmission line, the received voltage may oscillate about the desired value, possibly causing a digital gate at that end to switch falsely to an undesired state and cause errors. Matching the line eliminates this problem because there are no reflections, but matching cannot always be accomplished. In order to investigate this problem, consider a line connecting two CMOS gates. The driver gate is assumed to have zero source resistance ($R_S = 0$), and the open-circuit voltage is a ramp waveform (simulating the leading edge of the clock/data pulse) given by $V_S(t) = 0$ for $t < 0$, $V_S(t) = 5(t/\tau_r)$ V for $0 \leq t \leq \tau_r$, and $V_S(t) = 5$ V for $t \geq \tau_r$ where τ_r is the pulse risetime. The input to a CMOS gate (the load on the line here) can be modeled as a capacitance of some 5–15 pF. However, in order to simplify the problem, we will assume that the input to the load CMOS gate is an open circuit, $R_L = \infty$. Sketch the load voltage of the line (the input voltage to the load CMOS gate) for line lengths having one-way transit times T_D such that (a) $\tau_r = T_D/10$, (b) $\tau_r = 2T_D$, (c) $\tau_r = 3T_D$, (d) $\tau_r = 4T_D$. This example shows that in order to avoid problems resulting from mismatch, one should choose line lengths short enough such that $T_D << \tau_r$; that is, the line one-way delay is much less than the risetime of the clock/data pulses being carried by the line.

4.4.2 Highly mismatched lines in digital products can cause what appears to be “ringing” on the signal output from the line. This is often referred to as “overshoot” or “undershoot” and can cause digital logic errors. To simulate this we will investigate the problem shown in Fig. P4.4.2 Two CMOS gates are connected by a transmission line as shown. A 5 V step function voltage of the first gate is applied. Sketch the output voltage of the line (the input voltage to the load CMOS gate) for $0 < t < 9T$. [$0 < t < T, 0\text{ V}, T < t < 3T, 6.944\text{ V}, 3T < t < 5T, 3.858\text{ V}, 5T < t < 7T, 5.23\text{ V}, 7T < t < 9T, 4.62\text{ V};$ steady state 5 V]

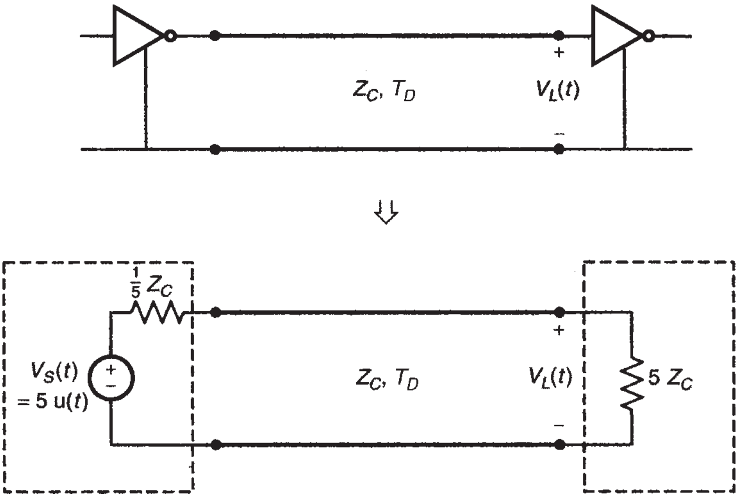

FIGURE P4.4.2

4.4.3 Use series matching and parallel matching in Problem 4.4.2.

Section 4.5 Sinusoidal Excitation of the Line and the Phasor Solution

Note: In the problems of this section, voltages and currents are specified in peak not RMS.

4.5.1 For the transmission line shown in Fig. 4.35, $f = 5$ MHz, $v = 3 \times 10^8$ m/s, $L = 78$ m, $Z_C = 50\ \Omega$, $\hat{V}_S = 50\angle 0°$ V, $\hat{Z}_S = 20 - j30\ \Omega$, $\hat{Z}_L = 200 + j500\ \Omega$. Determine (a) the line length as a fraction of a wavelength, (b) the voltage reflection coefficient at the load and at the input to the line, (c) the input impedance to the line, (d) the time-domain voltages at the input to the line and at the load, (e) the average power delivered to the load, and (f) the VSWR. [(a)1.3, (b)0.9338∠9.866°, 0.9338∠153.9°, (c)11.73∠81.16° Ω (d)20.55 $\cos(10\pi \times 10^6 t + 121.3°)$ V, 89.6 $\cos(10\pi \times 10^6 t - 50.45°)$ V, (e) 2.77 W, (f) 29.21]

4.5.2 For the transmission line shown in Fig. 4.35, $f = 200$ MHz, $v = 3 \times 10^8$ m/s, $L = 2.1$ m, $Z_C = 100\ \Omega$, $\hat{V}_S = 10\angle 60°$ V, $\hat{Z}_S = 50\ \Omega$, $\hat{Z}_L = 10 - j50\ \Omega$. Determine (a) the line length as a fraction of a wavelength, (b) the voltage reflection coefficient at the load and at the input to the line, (c) the input impedance to the line, (d) the time-domain voltages at the input to the line and at the load, (e) the average power delivered to the load, and (f) the VSWR. [(a) 1.4, (b) 0.8251∠(−126.5°), 0.8251∠(−54.5°), (c) 192∠(−78.83°), (d) 9.25 $\cos(4\pi \times 10^8 t + 46.33°)$, (e) 4.738 $\cos(4\pi \times 10^8 t - 127°)$, (f) 43 mW, 12.52

4.5.3 For the transmission line shown in Fig. 4.35, $f = 1$ GHz, $v = 1.7 \times 10^8$ m/s, $L = 11.9$ cm, $Z_C = 100\ \Omega$, $\hat{V}_S = 5\angle 0°$, $\hat{Z}_S = 20\ \Omega$, $\hat{Z}_L = -j160\ \Omega$. Determine (a) the line length as a fraction of a wavelength, (b) the voltage reflection coefficient at the load and at the input to the line, (c) the input impedance to the line, (d) the time-domain voltages at the input to the line and at the load, (e) the average power delivered to the load, and (f) the VSWR. [(a) 0.7, (b) 1∠−64.01°, 1∠152°, (c) 24.94∠90.52°, (d) 3.901 $\cos(2\pi \times 109t + 38.72°)$, 13.67 $\cos(2\pi \times 109t + 38.72°)$, (e) 0 W, (f) ∞]

4.5.4 For the transmission line shown in Fig. 4.35, $f = 600$ MHz, $v = 2 \times 10^8$ m/s, $L =$ 53 cm, $Z_C = 75\ \Omega$, $\hat{V}_S = 20\angle 40^\circ$, $\hat{Z}_S = 30\ \Omega$, $\hat{Z}_L = 100 - j300\ \Omega$. Determine (a) the line length as a fraction of a wavelength, (b) the voltage reflection coefficient at the input to the line and at the load, (c) the input impedance to the line, (d) the time-domain voltages at the input to the line and at the load, (e) the average power delivered to the load, and (f) the VSWR. [(a) 1.59, (b) $0.8668\angle -25.49^\circ$, $0.8668\angle -90.29^\circ$, (c) $74.62\angle -81.84^\circ$, (d) $17.71\cos(12\pi \times 10^8 t + 19.37^\circ)$, (e) $24.43\cos(12\pi \times 10^6 t - 163.8^\circ)$, (f) 0.298 W, 14.02]

4.5.5 For the transmission line shown in Fig. 4.35, $f = 1$ MHz, $v = 3 \times 10^8$ m/s, $L = 108$ m, $Z_C =$ 300 Ω, $\hat{V}_S = 100\angle 0^\circ$, $\hat{Z}_S = 50 + j50\ \Omega$, and $\hat{Z}_L = 100 - j100\ \Omega$. Determine (a) the line length as a fraction of a wavelength, (b) the voltage reflection coefficient at the load and at the input to the line, (c) the input impedance to the line, (d) the time-domain voltages at the input to the line and at the load, (e) the average power delivered to the load, and (f) the VSWR. [(a) 0.36, (b) $0.5423\angle -139.4^\circ$, $0.5423\angle -38.6^\circ$, (c) $657.1\angle -43.79^\circ\ \Omega$, (d) $99.2\cos(2\pi \times 10^6 t - 6.127^\circ)$, $46.5\cos(2\pi \times 10^6 t - 153.3^\circ)$, (e) 5.406 W, (f) 3.37]

4.5.6 A half-wavelength dipole antenna is connected to a 100 MHz source with a 3.6 m length of 300 Ω transmission line (twin lead, $v = 2.6 \times 10^8$ m/s) as shown in Fig. P4.5.6. The source is represented by an open-circuit voltage of 10 V and source impedance of 50 Ω, whereas the input to the dipole antenna is represented by a 73 Ω resistance in series with an inductive reactance of 42.5 Ω. The average power dissipated in the 73 Ω resistance is equal to the power radiated into space by the antenna. Determine the average power radiated by the antenna with and without the transmission line and the VSWR on the line [91.14 mW, 215.53 mW, 4.2]

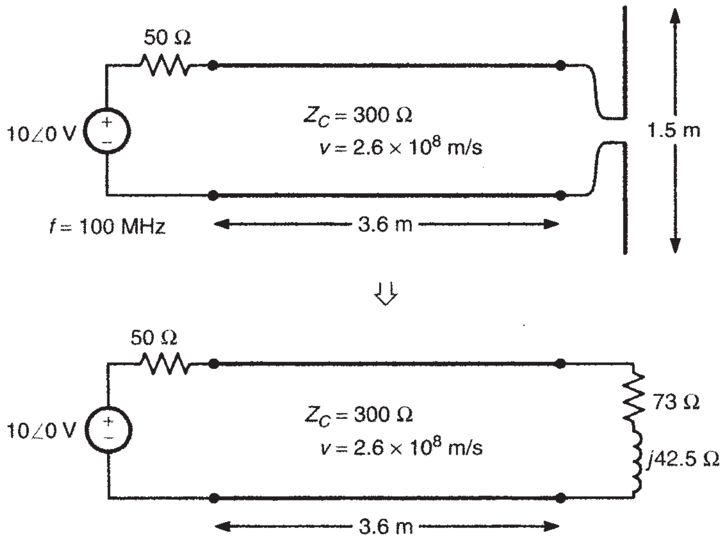

FIGURE P4.5.6

4.5.7 Determine an expression for the input impedance to (a) a transmission line having an open-circuit load and (b) a transmission line having a short-circuit load.

$$\left[-jZ_C \frac{1}{\tan(\beta L)},\ jZ_C \tan(\beta L)\right]$$

4.5.8 Obtain an expression for the input impedance to a quarter-wavelength transmission line. If the line has an open-circuit load, what is its input impedance. If the line has a short-circuit load, what is its input impedance. [$\hat{Z}_{\text{in}} = \hat{Z}_C^2/\hat{Z}_L$, short circuit, open circuit]

4.5.9 A low-loss coaxial case has the following parameters: $Z_C(75 + j0)\ \Omega$, $\alpha = 0.05$, $v = 2 \times 10^8$ m/s. Determine the input impedance to a 11.175 m length of the cable at 400 MHz if the line is terminated in (a) a short circuit, (b) an open circuit, and (c) a 300 Ω resistor. [(a) $90.209\angle(-34.86^\circ)\ \Omega$, (b) $62.355\angle 34.06^\circ\ \Omega$, (c) $66.7\angle 21.2^\circ\ \Omega$]

Section 4.6 Lumped-Circuit Approximate Models

4.6.1 An air-filled line ($v = 3 \times 10^8$ m/s) having a characteristic impedance of 50 Ω is driven at a frequency of 30 MHz and is 1 m in length. The line is terminated in a load of $\hat{Z}_L = (200 - j200)\ \Omega$. Determine the input impedance using (a) the transmission-line model and (b) the approximate, lumped-pi model. [(*a*) $(12.89 - j51.49)\ \Omega$, (*b*) $(13.76 - j52.25)\ \Omega$]

4.6.2 A coaxial cable ($v = 2 \times 10^8$ m/s) having a characteristic impedance of 100 Ω is driven at a frequency of 4 MHz and is 5 m in length. The line is terminated in a load of $\hat{Z}_L = (150 - j50)\ \Omega$ and the source is $\hat{V}_S = 10\angle 0^\circ$ V with $\hat{Z}_S = 25\ \Omega$. Determine the input and output voltages to the line using (a) the transmission-line model and (b) the approximate, lumped-pi model. [Exact: $\hat{V}(0) = 7.954\angle(-6.578^\circ)$ V, $\hat{V}(L) = 10.25\angle(-33.6^\circ)$ V; approximate: $\hat{V}(0) = 7.959\angle(-5.906^\circ)$ V, $\hat{V}(L) = 10.27\angle(-35.02^\circ)$ V]

REFERENCES

1. C. R. Paul and S. A. Nasar, *Introduction to Electromagnetic Fields*, 2nd ed., McGraw-Hill, New York, 1987.
2. C. R. Paul, *Electromagnetics for Engineers with Applications*, Wiley, New York, 2004.
3. R. E. Collin, *Foundations for Microwave Engineering*, 2nd ed., McGraw-Hill, New York, 1992.
4. S. B. Cohn, Problems in strip transmission lines, *IRE Trans. Microwave Theory Tech.* MTT-3, 119–126 (1955).
5. T. C. Edwards, *Foundations for Microstrip Engineering*, Wiley, New York, 1981.
6. K. C. Gupta, R. Garg, and I. J. Bahl, *Microstrip Lines and Slotlines*, Artech House, Dedham, MA, 1979.
7. K. C. Gupta, R. Garg, and R. Chadha, *Computer-Aided Design of Microwave Circuits*, Artech House, Dedham, MA, 1981.
8. H. R. Kaupp, Characteristics of microstrip transmission lines, *IEEE Trans. Electron. Comput.* EC-16, 186–193 (1967).
9. H. A. Wheeler, Transmission line properties of parallel strips separated by a dielectric sheet, *IEEE Trans. Microwave Theory Tech.* MTT-13, 172–185 (1965).
10. F. H. Branin, Jr., Transient analysis of lossless transmission lines, *Proc. IEEE* 55, 2012–2013 (1967).
11. S. Rosenstark, *Transmission Lines in Computer Engineering*, McGraw-Hill, New York, 1994.
12. C. R. Paul, *Analysis of Multiconductor Transmission Lines*, Wiley-Interscience, New York, 1994.
13. C. R. Paul and W. W. Everett, III, *Lumped Model Approximations of Transmission Lines: Effect of Load Impedances on Accuracy*, Technical Report, Rome Air Development Center, Griffiss AFB, NY, RADC-TR-82-286, Vol. IV E, Aug. 1984.

CHAPTER FIVE

Nonideal Behavior of Components

In this chapter we will discuss the typical circuit components used in the design of electronic systems and particularly in digital electronics. Our concentration will be on their role in suppression of radiated and conducted emissions and on their *nonideal* behavior. The latter is critical to their ability to provide adequate suppression. The reader must begin to think in terms not only of the component's *ideal* behavior but also of its *nonideal* behavior. An example is the frequency response of a capacitor's impedance. These components are often used to bypass or divert a high-frequency signal from, for example, a cable where the signal may radiate very efficiently. If the desired frequency of the emission is above the *self-resonant frequency* of the capacitor, the behavior of the capacitor will resemble that of an inductor, and the low impedance desired will not be realized.

Throughout this and later chapters it is critical for the reader to remember: *the primary frequencies of interest are those of the applicable governmental regulations*. For example, if the product is intended to be marketed in the United States, the emissions in the frequency range of the FCC limits (150 kHz–30 MHz for conducted emissions and 30 MHz–40 GHz for radiated emissions) are the *primary* frequencies of interest. A radiated emission occurring at 29 MHz is of no consequence in meeting the FCC regulatory limits! However, we cannot be totally unconcerned about the levels of emissions that are outside the frequency ranges of the regulatory limits, since these emissions may cause interference with other products, which will result in field problems and customer complaints. *Merely satisfying the applicable regulatory requirements does not represent a complete system design from the standpoint of EMC*.

In this chapter we will develop *mathematical models* that yield considerable insight into the *nonideal behavior* of components. Certain approximations will need to be made in developing a relatively simple model. Throughout this text we will frequently show experimentally measured data that serve to illustrate the prediction accuracy of the models that are developed. It is important to keep in mind that *if a postulated model fails to predict experimentally observed phenomena, it is useless*!

Our interest in a component's behavior will focus on the high frequencies of the regulations where it is to be used to reduce conducted and/or radiated emissions. The ultimate test of whether a component will provide the anticipated performance at the desired frequency is to *experimentally measure the desired behavior* (e.g., *impedance*) *of the component at the desired frequency*! There exist a large number of commercially available test instruments that measure the high-frequency

---

Introduction to Electromagnetic Compatibility, Third Edition. Clayton R. Paul, Robert C. Scully, and Mark A. Steffka.

© 2023 John Wiley & Sons, Inc. Published 2023 by John Wiley & Sons, Inc.

behavior of components. Most of these devices are computer-controllable and quite simple to use. One can therefore quickly and accurately determine whether a component will provide the desired EMI suppression through measurement.

5.1 WIRES

The conductors of a system (wires and printed circuit board, PCB, lands) are frequently overlooked as being important *components* of the system. If a pair of conductors is electrically long ($L > \lambda/10$) at the frequency of interest, then the line behaves as a transmission line (see Chapter 4) and cannot be modeled as a lumped circuit with any degree of success. If, on the other hand, the line is electrically short at the frequency of interest, then a lumped-circuit model of it will provide adequate prediction. Their behavior at the regulatory frequencies will be our primary concern here. In the radiated emission range (30 MHz–40 GHz) and to a lesser degree in the conducted emission range (150 kHz–30 MHz), the behavior of these elements is far from the ideal. Perhaps the most important effect, at least in digital circuits, is the conductor *inductance*. The resistance of the conductors is generally more important in the functional design as in determining the required land size and/or wire gauge to ensure minimum voltage drop along them in a power distribution circuit. However, *at the frequencies of the regulatory limits and particularly in the radiated emission range the inductance of the conductors is considerably more important than the resistance*. We examine these topics in this section.

The term *wire* will be used in this text to refer to conductors that consist of one or more *solid, circular, cylindrical conductors*. A single conductor is referred to as a *solid wire*. The wire has radius r_w and conductivity σ. The vast majority of conductor materials are copper (Cu), which has a conductivity $\sigma_{\mathrm{Cu}} = 5.8 \times 10^7$ S/m. Normally the conductor is not ferromagnetic, and as such its permeability μ is that of free space: $\mu = \mu_0 = 4\pi \times 10^{-7}$ H/m. Also, the permittivity of virtually all conductors is that of free space: $\varepsilon = \varepsilon_0 \cong (1/36\pi) \times 10^{-9}$ F/m. Table 5.1 gives the conductivities relative to Cu (σ_r) and permeabilities relative to free space (μ_r) for various conducting materials.

Stranded *wires* are composed of several strands of solid wires of radii r_{ws} that are placed parallel to each other to give flexibility. *As a reasonable approximation, the resistance and internal inductance of a stranded wire consisting of S strands can be computed by dividing the resistance or internal inductance of a single strand of radius r_{ws} by the number of strands S.* Thus we are essentially treating the stranded wire as being *S* identical wires that are connected, electrically, in *parallel. The external parameters of inductance and capacitance can be approximately computed by replacing the stranded wire with a solid wire of equivalent radius.* Consequently, we can obtain the parameters we will need by considering only solid wires.

Numerous handbooks from wire manufacturers list not only the radius and number of strands of stranded wires but also list an equivalent *gauge* that roughly represents the overall radius of the bundle of strands. Wires are referred to by *gauge*, which represents a solid wire of certain radius. Although there are several gauge definitions, the most common is the *American Wire Gauge* (AWG). Manufacturer handbooks also list the wire radius corresponding to the various wire gauges. Wire radii are typically given in the English unit system in terms of *mils*, where 1 mil = $1/1000$ in. = 0.001 in. Table 5.2 gives the wire *diameters* for typical wire gauges.

Stranded wires are typically specified in terms of the number and gauge of the solid wires that make up the stranded wire as (number × gauge). Various tables may include approximate radii and diameters in metric dimensions, and cross-sectional areas in metric dimensions as well as circular mils. It is a simple matter to convert wire radii in mils to wire radii in meters. For example, the

TABLE 5.1 Conductivities (Relative to Copper) and Permeabilities (Relative to Free Space) of Conductors

Conductor	σ_r	μ_r
Silver	1.05	1
Copper—annealed	1.00	1
Gold	0.70	1
Aluminum	0.61	1
Brass	0.26	1
Nickel	0.20	600
Bronze	0.18	1
Tin	0.15	1
Steel (SAE 1045)	0.10	1000
Lead	0.08	1
Monel	0.04	1
Stainless steel (430)	0.02	500
Zinc	0.32	1
Iron	0.17	1000
Beryllium	0.10	1
Mu-metal (at 1 kHz)	0.03	30,000
Permalloy (at 1 kHz)	0.03	80,000

radius of a 20 AWG solid wire is $r_w = 16$ mils. To convert this to meters, we multiply by unit ratios as described in Chapter 1:

$$\begin{aligned} r_{ws} &= 16\,\text{mils} \times \frac{1\,\text{in.}}{1000\,\text{mils}} \times \frac{2.54\,\text{cm}}{1\,\text{in.}} \times \frac{1\,\text{m}}{100\,\text{cm}} \\ &= 16\,\text{mils} \times (2.54 \times 10^{-5}\,\text{m/mil}) \\ &= 0.4064\,\text{mm} \end{aligned}$$

Therefore, *to convert wire radii from mils to meters, multiply by* 2.54×10^{-5}.

Wires are normally covered with a cylindrical dielectric insulation for obvious reasons. The thickness of the dielectric insulation is typically of the order of the wire radius. There are various types of dielectric insulations used by wire manufacturers. Their handbooks list the dc (or low-frequency) values of relative permittivity ε_r for the various insulation materials. Table 5.3 lists ε_r for various insulation materials.

It is important to remember that *the vast majority of dielectric materials are not ferromagnetic and thus have relative permeabilities of free space*, $\mu_r = 1$. Therefore *typical wire insulations do not affect magnetic field properties caused by currents of the wires.*

5.1.1 Resistance and Internal Inductance of Wires

The dc resistance of a round wire of radius r_w, conductivity σ, and total length L is given by

$$R = \frac{L}{\sigma \pi r_w^2} \tag{5.1}$$

TABLE 5.2 Wire Gauges (AWG) and Wire Diameters

	Wire Diameter (mils)	
Wire Gauge	Solid	Stranded
4/0	460.1	522.0 (427 × 23)
		522.0 (259 × 21)
3/0	409.6	464.0 (427 × 24)
		464.0 (259 × 23)
2/0	364.8	414.0 (259 × 23)
		414.0 (133 × 20)
1/0	324.9	368.0 (259 × 24)
		368.0 (133 × 21)
1	289.3	328.0 (2109 × 34)
		328.0 (817 × 30)
2	257.6	292.0 (2646 × 36)
		292.0 (665 × 30)
4	204.3	232.0 (1666 × 36)
6	162.0	184.0 (1050 × 36)
		184.0 (259 × 30)
8	128.5	147.0 (655 × 36)
10	101.9	116.0 (105 × 30)
		115.0 (37 × 26)
12	80.0	95.0 (165 × 34)
		96.0 (7 × 20)
14	64.1	73.0 (105 × 30)
		73.0 (41 × 30)
		73.0 (7 × 22)
16	50.8	59.0 (105 × 36)
		59.0 (26 × 30)
		60.0 (7 × 24)
18	40.3	47.0 (65 × 36)
		49.0 (19 × 30)
		47.0 (16 × 30)
		48.0 (7 × 26)
20	32.0	36.0 (41 × 36)
		36.0 (26 × 34)
		37.0 (19 × 32)
		35.0 (10 × 30)
22	25.3	30.0 (26 × 36)
		31.0 (19 × 34)
		30.0 (7 × 30)
24	20.1	23.0 (41 × 40)
		24.0 (19 × 36)
		23.0 (10 × 34)
		24.0 (7 × 32)
26	15.9	19.0 (7 × 34)
		20.0 (19 × 38)
		21.0 (10 × 36)
28	12.6	16.0 (19 × 40)
		15.0 (7 × 36)
30	10.0	12.0 (7 × 38)
32	8.0	8.0 (7 × 40)
34	6.3	7.5 (7 × 42)
36	5.0	6.0 (7 × 44)
38	4.0	

TABLE 5.3 Relative Permittivities of Insulation Dielectrics

Material	ε_r
Air	1.0005
Styrofoam	1.03
Polyethylene foam	1.6
Cellular Polyethylene	1.8
Teflon	2.1
Polyethylene	2.3
Polystyrene	2.5
Silicone rubber	3.1
Nylon	3.5
Polyvinyl chloride (PVC)	3.5
Epoxy resin	3.6
Quartz (fused)	3.8
Glass (pyrex)	4.0
Epoxy glass (PCB substrate)	4.7
Bakelite	4.9
Mylar	5.0
Porcelain	6.0
Neoprene	6.7
Polyurethane	7.0
Silicon	12.0

As the frequency is increased, the current over the wire cross section tends to crowd closer to the outer periphery because of a phenomenon known as *skin effect*. Essentially, the current can be assumed to be concentrated in an annulus at the wire surface of thickness equal to the skin depth [1]

$$\begin{aligned}\delta &= \frac{1}{\sqrt{\pi f \mu_0 \sigma}}\\ &= \frac{6.6\times 10^{-2}}{\sqrt{f\sigma}}\ \text{m}\\ &= \frac{2.6\times 10^{3}}{\sqrt{f\sigma}}\ \text{mils}\end{aligned} \tag{5.2}$$

when the skin depth is less than the wire radius. Table 5.4 gives the skin depth of copper ($\sigma = 5.8\times 10^7$ S/m, $\varepsilon_r = 1$, $\mu_r = 1$) at various frequencies.

Note that the skin depth becomes extremely small at frequencies in the range of the radiated emission regulatory limits. At 100 MHz, the skin depth is 0.26 mils. Therefore a conductor carrying a high-frequency current utilizes only a very small fraction of the metal of that conductor.

Figure 5.1 illustrates the fact that the current in a round wire is uniformly distributed over the cross section at dc but is increasingly concentrated in a narrow thickness of approximately one skin depth

TABLE 5.4 Skin Depth of Copper

f	δ
60 Hz	8.5 mm
1 kHz	2.09 mm
10 KHz	0.66 mm
100 kHz	0.21 mm
1 MHz	2.6 mils
10 MHz	0.82 mils
100 MHz	0.26 mils
1 GHz	0.0823 mils

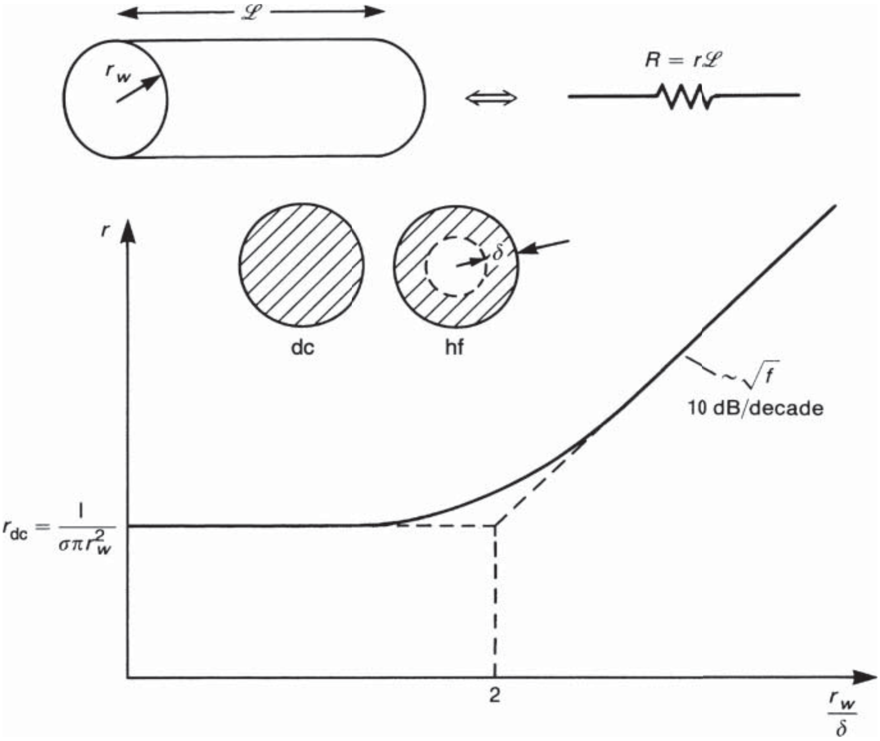

$\mathscr{L}$
r_w
$R = r\mathscr{L}$
r
δ
dc
hf
$\sim\sqrt{f}$
10 dB/decade
$r_{dc} = \frac{1}{\sigma\pi r_w^2}$
2
$\frac{r_w}{\delta}$

FIGURE 5.1 Illustration of the dependence of the per-unit-length resistance of a wire on frequency (skin effect).

near the outer surface for higher frequencies. Since the resistance is proportional to cross-sectional area occupied by the current, the *per-unit-length* resistance becomes

$$\begin{aligned} r_{lf} &= r_{dc} \text{ for } r_w \ll \delta \\ &= \frac{1}{\sigma\pi r_w^2} \text{ (in } \Omega/\text{m)} \\ r_{hf} &= \frac{1}{\sigma[\pi r_w^2 - \pi(r_w - \delta)^2]} \text{ for } r_w \gg \delta \end{aligned} \tag{5.3a}$$

$$
\begin{aligned}
&\cong \frac{1}{\sigma\pi r_w 2\delta} \\
&= r_{\mathrm{dc}}\frac{r_w}{2\delta} \\
&= \frac{1}{2r_w}\sqrt{\frac{\mu_0}{\pi\sigma}}\sqrt{f} \quad (\text{in } \Omega/\mathrm{m}) \qquad (5.3\mathrm{b})
\end{aligned}
$$

This is plotted in Fig. 5.1. Observe from (5.2) that the skin depth decreases with increasing frequency as the inverse square root of the frequency, $\sqrt{f}$. Thus the high-frequency resistance r_{hf} increases at a rate of 10 dB/decade. The resistance remains at the dc value up to the frequency where these two asymptotes meet, or $r_w = 2\delta$. The resistance in (5.3) is a *per-unit-length* resistance, with units of Ω/m. A length L of wire would have a total resistance $R = rL$.

The isolated wire also has an inductance that is frequency-dependent. This is referred to as the *internal inductance* since it is due to magnetic flux internal to the wire. The *dc internal inductance* is derived in [1] as

$$
\begin{aligned}
l_{i,\mathrm{dc}} &= \frac{\mu_0}{8\pi} \quad \text{for } r_w \ll \delta \\
&= 0.5 \times 10^{-7}\ \mathrm{H/m} \\
&= 50\ \mathrm{nH/m} \\
&= 1.27\ \mathrm{nH/in} \qquad (5.4\mathrm{a})
\end{aligned}
$$

This is also a *per-unit-length* parameter. A length L of conductor would have a total internal inductance $L_i = l_i L$. For high-frequency excitation the current again tends to crowd toward the wire surface and tends to be concentrated in a thickness δ. The per-unit-length internal inductance for these higher frequencies is also derived in [1], and becomes

$$
\begin{aligned}
l_{i,hf} &= \frac{2\delta}{r_w} l_{i,\mathrm{dc}} \quad \text{for } r_w \gg \delta \\
&= \frac{1}{4\pi r_w}\sqrt{\frac{\mu_0}{\pi\sigma}}\frac{1}{\sqrt{f}} \qquad (5.4\mathrm{b})
\end{aligned}
$$

Since the skin depth δ decreases with increasing frequency as the inverse square root of the frequency, (5.4b) shows that the high-frequency, per-unit-length internal inductance *decreases* at the rate of -10 dB/decade for $r_w \gg \delta$. This frequency behavior is plotted in Fig. 5.2.

Example 5.1 Determine the resistance and internal inductance of a 2 in. length of 20-gauge solid copper wire at 200 MHz.

Solution: First we determine whether the wire radius is in the dc region on the skin effect region of Fig. 5.1. The skin depth at 200 MHz is

$$
\begin{aligned}
\delta &= \frac{1}{\sqrt{\pi f \mu_0 \sigma}} \\
&= \frac{1}{\sqrt{\pi \times 2 \times 10^8 \times 4\pi \times 10^{-7} \times 5.8 \times 10^7}} \\
&= 4.67 \times 10^{-6}\ \mathrm{m} \\
&= 0.184\ \mathrm{mils}
\end{aligned}
$$

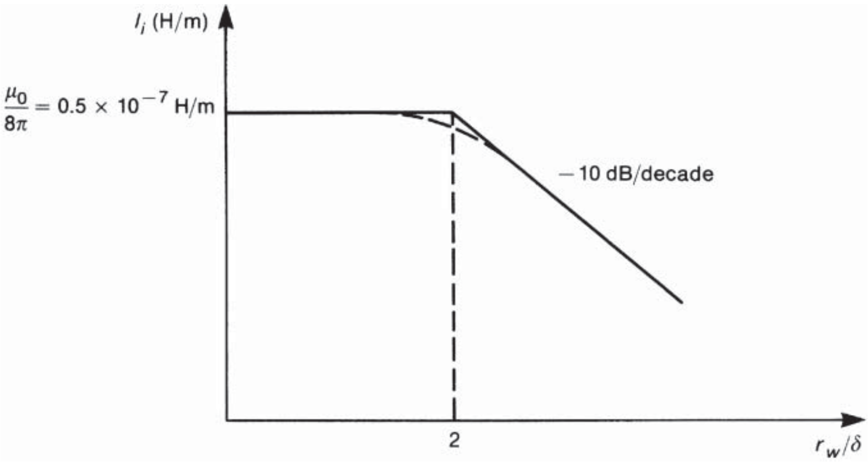

FIGURE 5.2 Illustration of the dependence of the per-unit-length internal inductance of wires on frequency (skin effect).

The radius of a 20-gauge solid wire is, from Table 5.2, 16 mils. Hence we are in the skin effect region since $r_w \gg \delta$. Thus we compute the per-unit-length resistance from (5.3b) as

$$\begin{aligned} r_{hf} &= \frac{1}{2r_w}\sqrt{\frac{\mu_0}{\pi\sigma}}\sqrt{f} \\ &= \frac{1}{2 \times 16 \times 2.54 \times 10^{-5}}\sqrt{\frac{4\pi \times 10^{-7}}{\pi \times 5.8 \times 10^{7}}}\sqrt{2 \times 10^{8}} \\ &= 1.44\ \Omega/\text{m} \\ &= 36.7\ \text{m}\Omega/\text{in.} \end{aligned}$$

Hence the total resistance is

$$\begin{aligned} R &= r_{hf} \times L \\ &= 73.4\ \text{m}\Omega \end{aligned}$$

The internal inductance is computed from (5.4b) as

$$\begin{aligned} l_{i,hf} &= \frac{1}{4\pi r_w}\sqrt{\frac{\mu_0}{\pi\sigma}}\frac{1}{\sqrt{f}} \\ &= \frac{r_{hf}}{2\pi}\frac{1}{\sqrt{f}} \\ &= 1.15\ \text{nH/m} \\ &= 29.2\ \text{pH/in.} \end{aligned}$$

The total internal inductance is

$$\begin{aligned} L_{i,hf} &= l_{i,hf} \times L \\ &= 58.4\ \text{pH} \end{aligned}$$

5.1.2 External Inductance and Capacitance of Parallel Wires

The resistance and internal inductance derived previously are uniquely attributable to or associated with a wire. Currents require a return path. The most common configuration is a pair of parallel wires of equal radii r_w, length L, and separation s, as shown in Fig. 5.3. The magnetic flux external to each wire contributes to the total flux penetrating the area between the two wires. The per-unit-length *external inductance* l_e of a pair of wires is the ratio of the magnetic flux between the two wires ψ_m, per unit of line length to the current producing that flux. This was derived in Chapter 4, and, assuming that the wires are separated sufficiently ($s/r_w > 5$) such that the current is uniformly distributed around the wire peripheries so that *proximity effect* is not a factor, is given as

$$\begin{aligned} l_e &= \frac{(\psi_m/L)}{I} \\ &= \frac{\mu_0}{\pi} \ln\left(\frac{s}{r_w}\right) \quad (\text{in H/m}) \\ &= 0.4 \ln\left(\frac{s}{r_w}\right) \quad (\text{in µH/m}) \\ &= 10.16 \ln\left(\frac{s}{r_w}\right) \quad (\text{in µH/in.}) \end{aligned} \tag{5.5}$$

The total *loop inductance* is the sum of the product of the line length and the internal inductances of the two wires and the product of the per-unit-length external inductance and the line length, i.e., $L_{\text{loop}} = 2l_iL + l_eL$. Note that l_eL is the inductance of the loop bounded by the two wires. Observe that the external inductance is a loop inductance and may be assigned to either wire in the loop.

Charge on the wires contributes to a *per-unit-length capacitance* c between the two wires that depends on the wire separation and radii, as did the external inductance. This *per-unit-length*

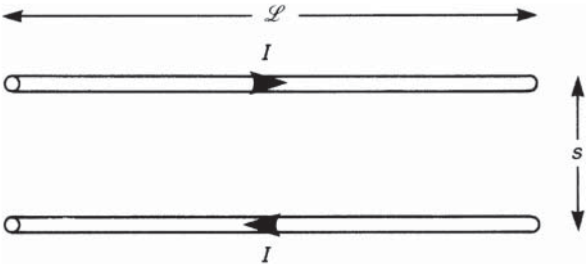

FIGURE 5.3 A pair of parallel wires to be modeled with an equivalent circuit.

capacitance was derived in Chapter 4, and is the ratio of the per-unit-length charge on the wires, Q/L, to the voltage between them:

$$\begin{aligned} c &= \frac{(Q/L)}{V} \\ &= \frac{\pi\varepsilon_0}{\ln(s/r_w)} \text{ (in F/m)} \\ &= \frac{27.78}{\ln(s/r_w)} \text{ (in pF/m)} \\ &= \frac{0.706}{\ln(s/r_w)} \text{ (in pF/in.)} \end{aligned} \tag{5.6}$$

This result assumes that the wires are separated sufficiently ($s/r_w > 5$) such that the charge is uniformly distributed around *the* wire peripheries and *proximity effect* is not a factor. The total capacitance between a pair of parallel wires of total length L is the product of the per-unit-length capacitance and the line length: $C = cL$.

Review Exercise 5.1 Determine the per-unit-length inductance and capacitance of two 20-gauge, solid parallel wires separated by 1/4 in.

Answers: 27.9 nH/in. and 0.257 pF/in.

5.1.3 Lumped Equivalent Circuits of Parallel Wires

Each of these per-unit-length parameters when multiplied by the length gives the total parameter for that length of line. If the total line length L is *electrically short*, i.e., $L \ll \lambda$, at the frequency of excitation, we may lump these distributed parameters and obtain *lumped equivalent circuits* of the pair of wires. On the other hand, if the line is electrically long ($L > \lambda$), then we have no recourse but to model the line as a transmission line (Chapter 4). Combining these elements gives several possible lumped-circuit models of the pair of parallel wires shown in Fig. 5.4. The *lumped-backward gamma* model of Fig. 5.4a is so named because of its resemblance to the Greek letter Γ. The remaining lumped-circuit models, *lumped-Pi*, *lumped-T*, and *lumped-*Γ *models* in the remaining parts of the figure are similarly named. Either of these models would constitute acceptable approximations of the line so long as the line is electrically short. However, depending on the impedance level of the load attached to the endpoint of the wires, one model will extend the prediction accuracy of the model further in frequency than another model. This is discussed and investigated in [2]. For example, if the load impendence Z_L is a "low impedance," i.e., much less than the *characteristic impedance* of the line

$$\begin{aligned} Z_c &= \sqrt{\frac{l_e}{c}} \\ &= 120 \ln\left(\frac{s}{r_w}\right)\ \Omega \end{aligned} \tag{5.7}$$

the lumped-Γ model of Fig. 5.4d and the lumped-T model of Fig. 5.4c would extend the frequency range of adequate prediction slightly higher than the lumped-backward gamma and lumped-Pi models of Fig. 5.4a,b. This is intuitively reasonable because a low impedance load would be in parallel

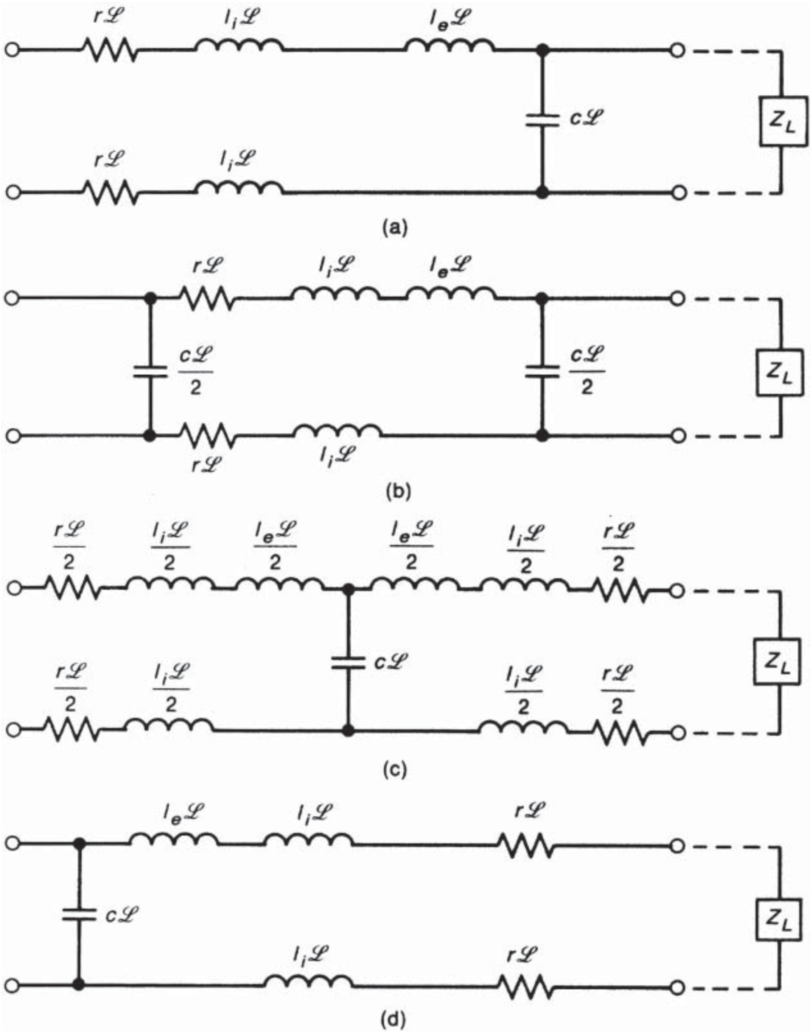
$r\mathscr{L}$
$l_i\mathscr{L}$
$l_e\mathscr{L}$
$c\mathscr{L}$
Z_L
$r\mathscr{L}$
$l_i\mathscr{L}$
(a)
$r\mathscr{L}$
$l_i\mathscr{L}$
$l_e\mathscr{L}$
$\frac{c\mathscr{L}}{2}$
$\frac{c\mathscr{L}}{2}$
Z_L
$r\mathscr{L}$
$l_i\mathscr{L}$
(b)
$\frac{r\mathscr{L}}{2}$
$\frac{l_i\mathscr{L}}{2}$
$\frac{l_e\mathscr{L}}{2}$
$\frac{l_e\mathscr{L}}{2}$
$\frac{l_i\mathscr{L}}{2}$
$\frac{r\mathscr{L}}{2}$
$c\mathscr{L}$
Z_L
$\frac{r\mathscr{L}}{2}$
$\frac{l_i\mathscr{L}}{2}$
$\frac{l_i\mathscr{L}}{2}$
$\frac{r\mathscr{L}}{2}$
(c)
$l_e\mathscr{L}$
$l_i\mathscr{L}$
$r\mathscr{L}$
$c\mathscr{L}$
Z_L
$l_i\mathscr{L}$
$r\mathscr{L}$
(d)

FIGURE 5.4 Lumped equivalent circuits for a pair of parallel wires: (a) lumped-backward Γ; (b) lumped Pi; (c) Lumped T; (d) lumped Γ.

with the rightmost parallel capacitance element of the lumped-backward gamma and lumped-Pi models. Thus these elements will be rendered ineffective by the low impedance load. The converse applies to high-impedance loads; the rightmost resistance and inductance elements of the lumped-Γ and lumped-T models are in series with this high-impedance load and are therefore rendered ineffectual.

Once the per-unit-length parameters of the wires are determined and these lumped circuits are constructed, any lumped-circuit analysis program such as SPICE can be used to analyze the resulting circuit with the loads (gates, etc.) attached. Important time-domain parameters such as risetime, waveshape, and time delay can be easily determined from that simulation.

An important point concerning these models that is frequently misunderstood needs to be discussed. Note that in either of the lumped circuits in Fig. 5.4 the external inductance l_e is in series with the internal inductance l_i. The impedance of the external inductance is $\omega L_e = 2\pi f l_e L$, and therefore increases directly with frequency. (The external inductance is approximately frequency independent.) The impedance of the internal inductance is $\omega L_i = 2\pi f l_i L$ and also appears to increase directly with frequency. However, on closer examination, we recall that the per-unit-length internal inductance decreases with increasing frequency as the inverse square root of the frequency. Thus *the impedance of the internal inductance increases only as the square root of the frequency*. Therefore the impedance of the external inductance increases with frequency at a rate faster than that of the impedance of the internal inductance! Also, the external inductance for typical wire sizes and separations is usually much larger than the internal inductance. For example, consider a pair of 20-gauge solid copper wires that are separated by a distance of 50 mils (typical separation between adjacent conductors in a ribbon cable). The per-unit-length internal inductance is $l_{i,\mathrm{dc}} = 0.05\ \mu\mathrm{H/m} = 1.27\ \mathrm{nH/in.}$, whereas the per-unit-length external inductance is $l_e = 0.456\ \mu\mathrm{H/m} = 11.58\ \mathrm{nH/in.}$, which is larger than the internal inductance by a factor of 10! Consider higher frequencies where $r_w > 2\delta$. The per-unit-length external inductance is larger than the per-unit-length internal inductance by a factor of 10, and above this frequency the difference increases since the external inductance remains constant with increasing frequency but the internal inductance decreases as $1/\sqrt{f}$. Consequently, *the impedance of the internal inductance is usually much smaller than the impedance of the external inductance, and we may therefore neglect the internal inductance in the model*. It is important to make these types of observations where possible based on typical dimensions in order to obtain the simplest model so that qualitative behavior can be more easily extracted from the model.

Several final points need to be discussed. In the above derivations of the per-unit-length external parameters l_e and c we assumed that the medium surrounding the wires was *homogeneous* and was that of free space with permittivity ε_0 and permeability μ_0. Thus we assumed *bare wires in free space*. Wires often have circular dielectric insulation surrounding them to prevent contact with other wires. This type of medium is said to be *inhomogeneous*, since the electric and magnetic fields exist partly in the dielectric insulations (ε_r) and partly in air. Dielectrics are typically not ferromagnetic, and thus have $\mu = \mu_0$. Thus *the presence of inhomogeneous dielectric media typically does not affect the external inductance parameter*. However, since the surrounding medium is inhomogeneous in permittivity ε, Eq. (5.6) for the per-unit-length capacitance of the line *does not apply*. We cannot simply replace ε_0 in that equation with the permittivity of the dielectric insulation since the electric fields are not confined to the dielectric. Derivation of the per-unit-length capacitance for an inhomogeneous medium is a difficult problem and closed-form expressions do not exist for this case—contrary to what some handbooks imply. Numerical methods must be applied in this case [3]. In spite of these technicalities, *we can obtain reasonable approximations for the inhomogeneous medium case ignoring the dielectric insulations* and using the preceding expressions for l_e, (5.5), c, (5.6), for typical wire sizes, dielectric insulation thicknesses, and wire separations.

Review Exercise 5.2 Compute the total internal and external inductances, resistance, and capacitance for a pair of 28-gauge, solid wires that are 5 in. in length and separated by 50 mils at a frequency of 10 MHz.

Answers: 0.209 Ω, 3.32 nH, 105 nH, 1.7 pF.

5.2 PRINTED CIRCUIT BOARD (PCB) LANDS

Wires are generally found in cables that interconnect subsystems and PCBs within systems. The conductors on PCBs have rectangular cross sections, as opposed to wires, whose cross sections are circular. PCBs are composed of a dielectric substrate (typically glass epoxy with $\varepsilon_r \cong 4.7$) on which rectangular cross-section conductors (*lands*) are etched. Typical board thicknesses are of order 47–62 mils. Land thicknesses are specified in terms of the thickness of the board cladding that was

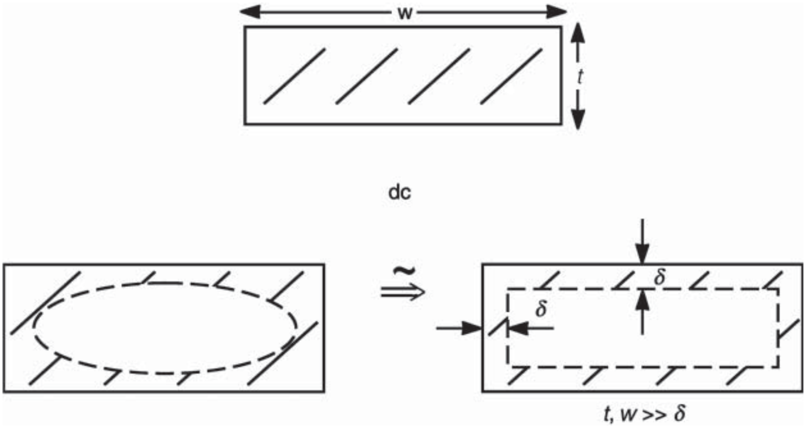

FIGURE 5.5 Illustration of skin effect for PCB lands.

etched away to form the lands. Typical cladding thicknesses are 1 oz Cu and 2 oz Cu. This refers to the weight of that thickness of the copper material that occupies an area of one square foot. For example, the thickness of 1 oz Cu cladding is 1.38 mils, and a 1 ft^2 area would weigh 1 oz. The thickness of 2 oz Cu is double this, or 2.76 mils. Throughout this text we will assume the most common thickness of 1 oz Cu or 1.38 mils.

The current distribution over the land cross section behaves in a manner that is quite similar to that of wires. For dc or low-frequency excitation the current is approximately uniformly distributed over the land cross section as illustrated in Fig. 5.5. Thus the per-unit-length low-frequency resistance of the land is

$$\begin{aligned} r_{lf} &= r_{\mathrm{dc}} \\ &= \frac{1}{\sigma w t} \text{ (in } \Omega/\text{m)} \end{aligned} \tag{5.8a}$$

where w is the land width and t is the thickness (1.38 mils). For high-frequency excitation the current tends to crowd to the outer edges of the land as illustrated in Fig. 5.5. Calculation of the high-frequency resistance is a difficult problem, but can be reasonably approximated by assuming that the current is uniformly distributed over a skin depth δ to give

$$\begin{aligned} r_{hf} &= \frac{1}{\sigma(2\delta w + 2\delta t)} \\ &= \frac{1}{2\sigma\delta[w+t]} \text{ (in } \Omega/\text{m)} \end{aligned} \tag{5.8b}$$

As derived in Section 4.5.4 of Chapter 4, the dc and high-frequency resistances in (5.8a) and (5.8b) have asymptotes that join at a frequency where

$$\begin{aligned} \delta &= \frac{1}{2}\frac{wt}{(w+t)} \\ &\cong \frac{t}{2} \quad w \gg \mathrm{t} \end{aligned} \tag{5.8c}$$

Hence, above this frequency we use (5.8b) to compute the resistance.

The land also possesses an internal inductance due to magnetic flux internal to the land in a fashion similar to that of a wire. However, in the case of a land, computation of this internal inductance is a difficult problem. We will ignore this internal inductance parameter on the assumption that it will be negligible in comparison with the external inductance parameter in any lumped-circuit model.

The computation of the external inductance and capacitance of a pair of parallel lands is much more difficult than for a pair of parallel wires. Generally this can be done using only numerical methods. Approximate formulas for these configurations are developed from these numerical computations and are given in Section 4.2.2 of Chapter 4. The results are given in terms of two parameters: the characteristic impedance of the line

$$Z_c = \sqrt{\frac{l_e}{c}}\ \Omega \tag{5.9a}$$

and effective relative permittivity or dielectric constant ε_r'. The effective relative permittivity accounts for the fact that the electric field lines are partly in air and partly in the PCB board (see Fig. 4.12 of Chapter 4). From this, the velocity of propagation can be computed as

$$\begin{aligned} v &= \sqrt{\frac{1}{l_e c}} \\ &= \sqrt{\frac{1}{\varepsilon_r' \varepsilon_0 \mu_0}} \\ &= \frac{v_0 = 3 \times 10^8}{\sqrt{\varepsilon_r'}}\ \text{m/s} \\ &= \frac{11.8}{\sqrt{\varepsilon_r'}}\ \text{in./ns} \end{aligned} \tag{5.9b}$$

Approximate formulas for typical PCB configurations such as the stripline, the microstrip, and the PCB I and PCB II configurations are given in Section 4.2.2 of Chapter 4. The per-unit-length external inductance and capacitance can be obtained from these as

$$l_e = \frac{Z_c}{v} \tag{5.10a}$$

and

$$c = \frac{1}{v Z_c} \tag{5.10b}$$

Once these parameters are obtained along with the per-unit-length resistance, the lumped equivalent circuits of Fig. 5.4 can be constructed (neglecting the internal inductance of the conductors) for any pair of rectangular cross-section conductors mounted on or in a PCB.

Review Exercise 5.3 Determine the total resistance, external inductance, and capacitance of the PCB I line of Fig. 4.12c (of Chapter 4) whose total length is 5 in. and whose dimensions are $s = 15$ mils, $w = 15$ mils, $h = 62$ mils, $t = 1.38$ mils and $\varepsilon_r = 4.7$. The frequency is 100 MHz.

Answers: 796 mΩ, 102 nH, 4.89 pF.

5.3 EFFECT OF COMPONENT LEADS

We now embark on an examination of the various discrete components, resistors, capacitors, inductors, etc., that are employed in electronic systems. Our emphasis will be on their *nonideal behavior* in the high-frequency range of the regulatory limits. A component must inevitably be connected to the circuit via *leads*. These connection leads usually take the form of bare wires such as the attachment leads of resistors, capacitors, etc. This is referred to as *discrete-lead attachment*. There is an increasing use of other attachment techniques that speed automated assembly of the components on the printed circuit boards (PCBs). Perhaps the most common alternative is the *surface-mount technology* (SMT) method. With this method, flat, rectangular cross-section "tabs" attached to the component package are soldered directly to the PCB. Not only does this reduce the length of the attachment leads (an important factor in achieving the desired behavior of the component), but it also speeds the automated attachment of the component to the PCB. It also allows an increased number of components to be placed on the PCB over the discrete-lead attachment method. Components are normally placed on only one side of a PCB. With the use of SMT components, many of the smaller components such as resistors and capacitors can be placed on the other side of the PCB, thereby increasing the component density. Most PCBs in today's electronic systems could not be "populated" in the allowable board space without the use of SMT components. We will concentrate on the discrete-lead components, although many of our results will also be applicable to SMT components.

One of the most important factors that affect the high-frequency behavior of components is the *length of the component attachment leads*. Unnecessarily long attachment leads cause the component behavior to deviate from the ideal at high frequencies, which often fall in the frequency range of the regulatory limits where we want the component to behave as expected. The *length and separation of the component leads* cause the component to have, in addition to the ideal behavior, an *inductive* element and a *capacitive* element. These elements in combination with the component can give an overall behavior that is far from the desired ideal behavior.

In order to model the inductance of the attachment leads, consider the discrete lead attachment shown in Fig. 5.6a. The inductance of this loop can be obtained using the previous results by multiplying the per-unit-length inductance of the pair of parallel wires given in (5.5) by the lead length. As an example, consider typical component leads that are 20-guage solid wires ($r_w = 16$ mils). Suppose that the leads are 0.5 in. long and are separated by 0.25 in. The expression in (5.5) gives 14 nH. The equivalent circuit becomes as shown in Fig. 5.6b. The inductance we have computed is the inductance of the loop, and as such we may lump it and place it in either lead.

The next effect that we will consider is the capacitance between the leads shown in Fig. 5.7. This may be computed by multiplying the per-unit-length capacitance given in (5.6) by the lead length. As an example, consider two 20-gauge leads of length 0.5 in. separated by 0.25 in. The capacitance is 0.128 pF.

The lumped-circuit model of lead inductance is shown in Fig. 5.6b, and the model of lead capacitance is shown in Fig. 5.7b. How shall we combine these two effects into a single model? There is no unique answer to this question, since these are *distributed parameter elements*. In other words, their effects are distributed along the length of the leads, as illustrated in Fig. 5.8a.

Nevertheless, if the lead length L and separation s are *electrically short* at the frequencies of interest, we may lump L and C (the per-unit-length values multiplied by the lead length L) and produce several *lumped-circuit models* that are identical in structure to those derived for the pair of parallel wires in Section 5.1.3. Figure 5.8b–e again show these four possible equivalent circuits. Again, although either circuit would be an approximate representation of this distributed-parameter phenomenon for electrically short lead lengths, one structure may be a better approximation than the other, depending on the impedance $\hat{Z}$ of the component, as was discussed in Section 5.1.3. In fact, we are interested only in estimates of the effect of the leads, and for this purpose either model would be

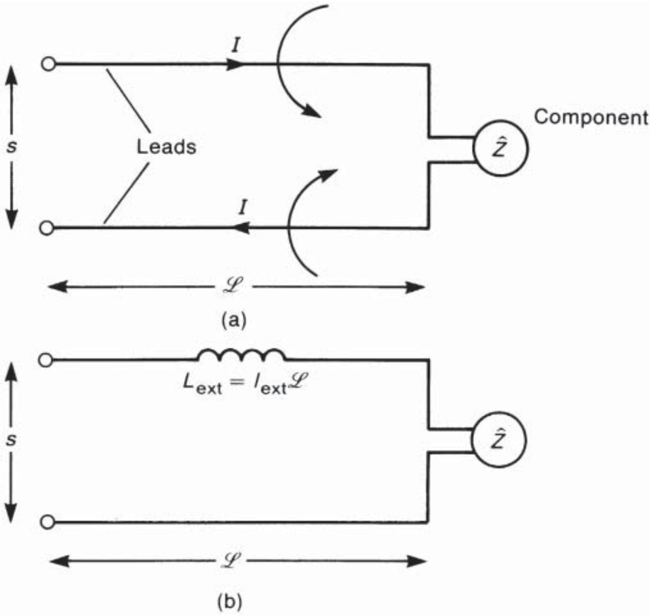
I
Component
s
Leads
$\hat{Z}$
I
$\mathscr{L}$
(a)
$L_{ext} = l_{ext}\mathscr{L}$
s
$\hat{Z}$
$\mathscr{L}$
(b)

FIGURE 5.6 Modeling the effect of magnetic fields of component leads: (a) physical configuration; (b) the equivalent circuit.

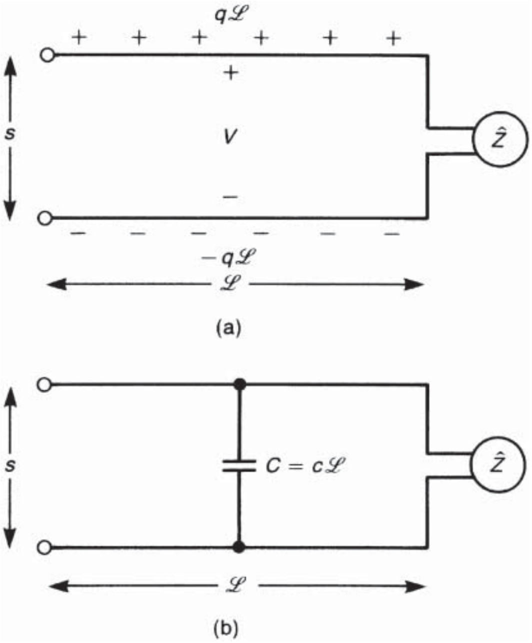
$q\mathscr{L}$
+
s
V
−
$\hat{Z}$
$-q\mathscr{L}$
$\mathscr{L}$
(a)
s
$C = c\mathscr{L}$
$\hat{Z}$
$\mathscr{L}$
(b)

FIGURE 5.7 Modeling the effect of electric fields of component leads: (a) physical configuration; (b) the equivalent circuit.

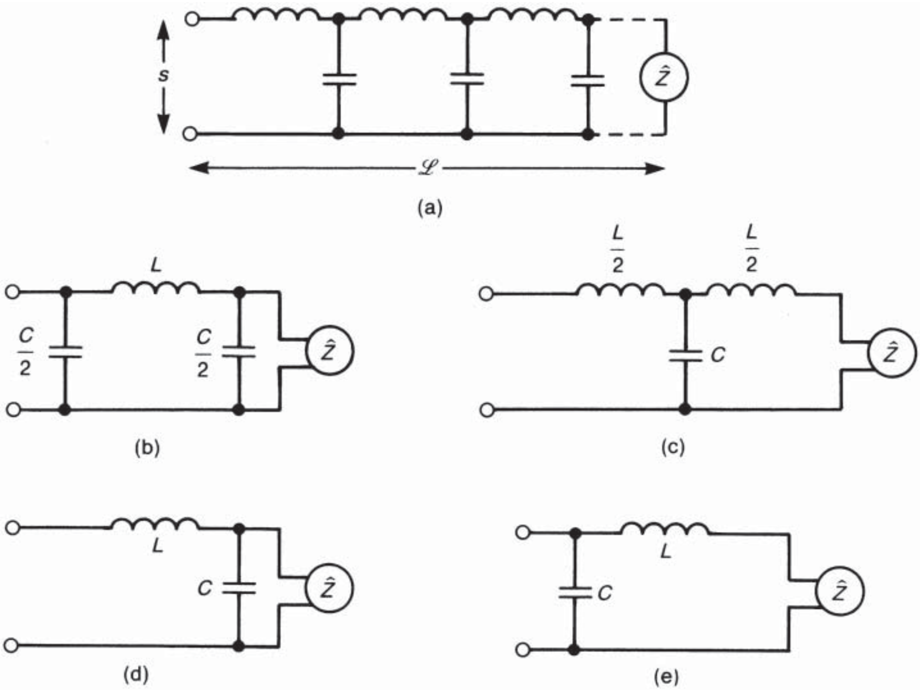

FIGURE 5.8 Equivalent circuits of component leads: (a) distributed parameter; (b) lumped Pi; (c) lumped T; (d) lumped-backward Γ; (e) lumped Γ.

adequate. In these models we have ignored conductor losses on the assumption that these connection leads are short, physically.

5.4 RESISTORS

Resistors are perhaps the most common component in electronic systems. These components are constructed in basically three forms: (1) carbon composition, (2) wire wound, and (3) thin film. Carbon-composition resistors are the most common. They are constructed by forming a cylindrical block of carbon and attaching two wires to the ends. Wire-wound resistors are formed by winding a length of wire that has the desired *dc resistance* on a cylindrical form to conserve space. Wire-wound resistors have a significant amount of inductance due to the construction technique. It is usually difficult to determine whether a resistor is carbon-composition or wire-wound by simply looking at it. The desired length of the wire used to construct a wire-wound resistor can be computed from (5.1). Thin-film resistors are constructed by depositing a thin, metallic film on an insulating substrate. Leads are attached to the ends of the metallic film, and the package resembles an axial-lead resistor. Because of the construction technique, this resistor has more precise values of resistance than does the carbon-composition type but less inductance than does the wire-wound type.

The ideal frequency response of a resistor has a magnitude equal to the value of the resistor and a phase angle of 0° for all frequencies as shown in Fig. 5.9. We denote this as

$$\hat{Z} = R\underline{/0^\circ} \tag{5.11}$$

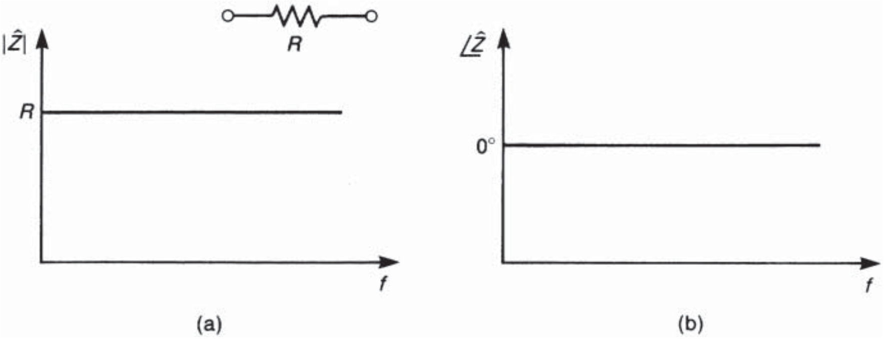

FIGURE 5.9 Frequency behavior of the impedance of an ideal resistor: (a) magnitude; (b) phase.

Actual resistors behave somewhat differently than this ideal at higher frequencies, with the degree to which they differ depending on the construction technique used. For example, since a wire-wound resistor is constructed of turns of wire, we would expect this resistor to have a significant inductive behavior at higher frequencies. Carbon-composition resistors would not be expected to exhibit this behavior to the same degree. Consequently, if the current passing through the resistor has a large *di*/*dt* factor, we would be well advised to use a carbon-composition resistor here instead of a wire-wound resistor. Otherwise, the wire-wound resistor would have a terminal behavior represented by $v(t) = Ri(t) + Ldi(t)/dt$. An example of where this nonideal behavior would be very undesirable would be in the use of this resistor as a "sense resistor" in the source lead of a field-effect transistor that is used as the switch element in a switching power supply. The voltage developed across this resistor is *intended* to be a replica of the current passing out this lead of the transistor and is used as a control to affect the duty cycle of the transistor switch. However, since the current is rapidly changing with time, the inductive nature of a wire-wound resistor may cause the voltage developed across it to resemble the derivative of this current, which would not be desirable.

The advantage of wire-wound resistors over carbon-composition ones is that much tighter tolerances on element value can be obtained. For example, carbon resistors typically have tolerances of 5–10%. This means that the manufacturer guarantees only that, for example, a 1 kΩ resistor would have a value between 1.1 kΩ and 900 Ω for a 10% tolerance. For the *sense* resistor in the abovementioned switching power supply it is important to use a small value of resistance so that the functional performance of the transistor switch will not be impaired. Typical values are of order 1 Ω. The proper operation of the switcher depends on obtaining accurate values of the sampled current, which a 10% tolerance carbon resistor may not give. Consequently a wire-wound resistor might be used in this application. From a functional standpoint, this inductive behavior of the wire-wound resistor can be tolerated. From an EMC standpoint, however, the differentiation of this switch waveform causes pulses of voltage to be developed across the resistor that have a repetition rate of the basic switch frequency *and* very fast rise/falltimes. We saw in Chapter 3 that the spectral content of such signals extends well above the repetition rate of the signal, so that this could cause radiated and/or conducted emission problems.

Both carbon-composition and wire-wound resistors exhibit other nonideal effects. For example, there is a certain "bridging capacitance" from end-to-end due to charge leakage around the resistor body. Usually this is a minor effect. A more significant effect is represented by the *inductance and capacitance of the leads attached to the element*, as was discussed in the previous section. Replacing the leads with a lumped-backward Γ equivalent circuit gives the model shown in Fig. 5.10a. We could have also chosen to use any of the other models of Fig. 5.8 but will choose the lumped-backward Γ model for simplicity. Thus the equivalent circuit of the resistor is as shown in Fig. 5.10b. The lead inductance L_{lead} in this model refers to the inductance of the loop area bounded by the two leads. Values calculated for typical lead lengths of 0.5 in., lead separations of 0.25 in., and lead wires (20-gauge with $r_w = 16$ mils) using (5.5) give L_{lead} of some 14 nH. (The degree of separation is determined largely by the length of the resistor body when the leads are bent at right angles to the body.) The *parasitic* capacitance in this model refers to the parallel combination of the lead and leakage capacitances, $C_{\text{par}} = C_{\text{lead}} + C_{\text{leakage}}$. Typical values are $C_{\text{par}} \cong 1 - 2$ pF. Values of C_{lead} calculated for typical lead lengths of 0.5 in., lead separation of 0.25 in., and lead wires (20-gauge with $r_w = 16$ mils) using (5.6) give C_{lead} of some 0.128 pF. This is probably smaller than the leakage capacitance of the resistor body. It is instructive to calculate the effect of these elements. Consider a 1 kΩ resistor. If we assume a value of the parasitic capacitance of 1 pF, the impedance of C_{par} is 1 kΩ at a frequency of approximately 159 MHz. The inductance and capacitance resonate at a frequency of approximately 1.3 GHz. This illustrates that for high-impedance resistors the parasitic capacitance is the dominant element effect.

In order to examine the frequency response of this model, we first derive the equation for the impedance of the model. A simple way of doing this is described in [4, 5]. (Also see Appendix A.)

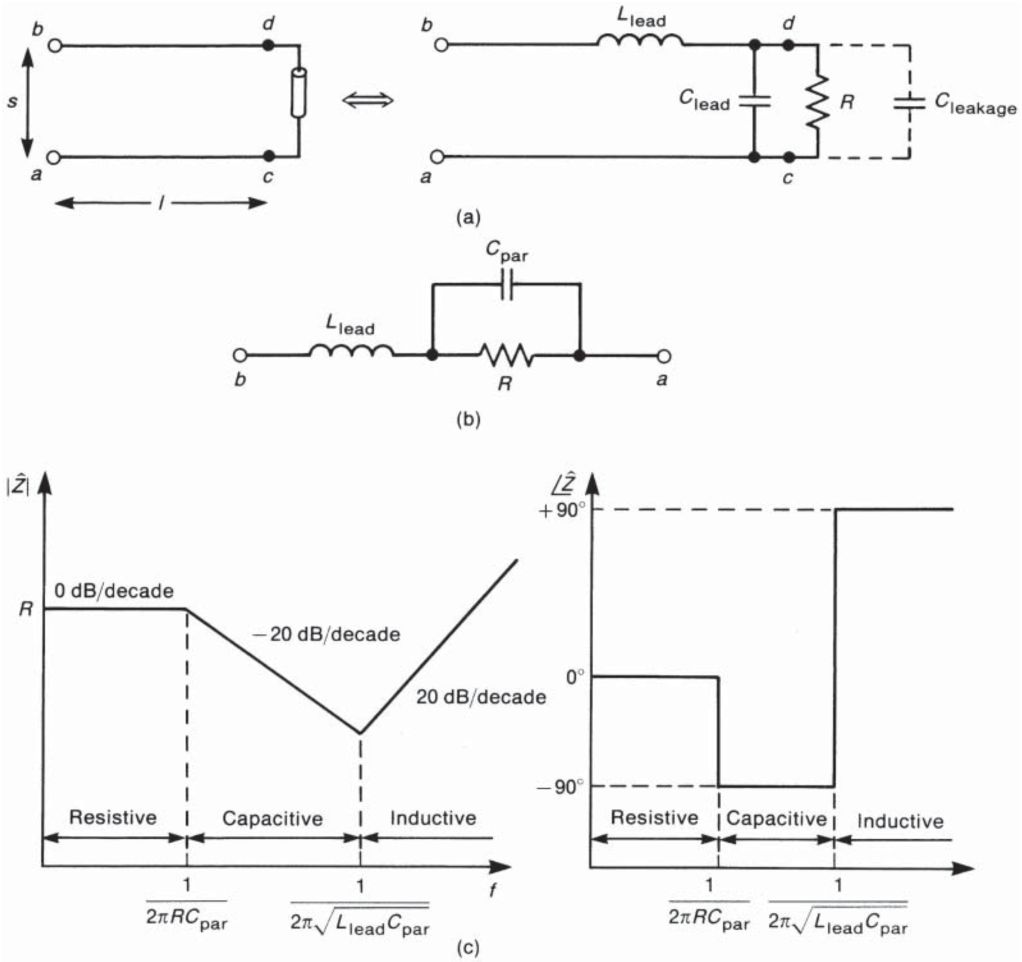
b
d
s
a
c
l
⟺
b
L_{lead}
d
C_{lead}
R
C_{leakage}
a
c
(a)
C_{par}
L_{lead}
b
R
a
(b)
$|\hat{Z}|$
R
0 dB/decade
−20 dB/decade
20 dB/decade
Resistive
Capacitive
Inductive
$\frac{1}{2\pi RC_{\text{par}}}$
$\frac{1}{2\pi\sqrt{L_{\text{lead}}C_{\text{par}}}}$
f
$\angle\hat{Z}$
+90°
0°
−90°
Resistive
Capacitive
Inductive
$\frac{1}{2\pi RC_{\text{par}}}$
$\frac{1}{2\pi\sqrt{L_{\text{lead}}C_{\text{par}}}}$
(c)

FIGURE 5.10 The nonideal resistor including the effects of the leads: (a) equivalent circuit; (b) simplified equivalent circuit; (c) Bode plots of the impedance variation with frequency.

First replace the inductors with their impedances in terms of $p = j\omega$ to give $\hat{Z}_L = pL$, and replace the capacitors with their impedance $\hat{Z}_C = (1/pC)$. Derive the expression for the impedance of the element $\hat{Z}(p)$, and then substitute $p = j\omega$ in that expression. The impedance $\hat{Z}(p)$ here is a general form of a "transfer function" giving the *ratio* of two circuit quantities (current and/or voltage) [4, 5]. The transfer function here is the ratio of the terminal voltage $\hat{V}(p)$ and the terminal current $\hat{I}(p)$ as $\hat{Z}(p) = (\hat{V}(p)/\hat{I}(p))$, where the voltage and current are defined with the passive sign convention. For the resistor model of Fig. 5.10b one can derive

$$\hat{Z}(p) = L_{\text{lead}} \frac{p^2 + (p/RC_{\text{par}}) + (1/L_{\text{lead}}C_{\text{par}})}{p + (1/RC_{\text{par}})} \tag{5.12}$$

Substituting $p = j\omega$ into this expression gives

$$\hat{Z}(j\omega) = L_{\text{lead}} \frac{(1/L_{\text{lead}}C_{\text{par}}) - \omega^2 + (j\omega/RC_{\text{par}})}{j\omega + (1/RC_{\text{par}})} \tag{5.13}$$

The corresponding Bode or asymptotic plot [5] of the magnitude and phase angle of this impedance is given in Fig. 5.10c. We will frequently employ the logarithmic or Bode plot method of displaying the frequency response of elements. The reader should review this method, which is described in any typical circuit analysis text. A complete discussion is given in [5]. The basic method is to plot not the magnitude $|\hat{Z}(j\omega)|$ but the logarithm of the magnitude, $|\hat{Z}(j\omega)|_{\text{dB}} = 20\log_{10}|\hat{Z}(j\omega)|$, in decibels (above or relative to a reference level of 1 Ω). In order that straight lines on the "unlogged" plot translate to straight lines on the log plot, the frequency axis must be plotted as $\log_{10} f$. This is usually more easily accomplished using semilog graph paper where the vertical axis has linear tick mark spacing for plotting $|\hat{Z}(j\omega)|_{\text{dB}} = 20\log_{10}|\hat{Z}(j\omega)|$ and logarithmic spacing of the tick marks on the horizontal axis for plotting the frequency on a logarithmic basis. This is implied when we label the horizontal axes of these plots as simply f. We could also use log–log graph paper with logarithmically spaced tick marks on the vertical axis for plotting the absolute magnitude instead of the magnitude in dB (relative to 1 Ω).

It is important at this point to consider another computational technique. The reader should be able to not only compute the "transfer function" of a circuit but also quickly check the accuracy of the result and determine the gross behavior of the frequency response. In order to do this, we simply check, directly from the circuit, the behavior at two frequencies: dc and infinite frequency. In order to check the behavior at dc, we simply substitute $p = 0$ into any impedance expression. For example, substituting $p = 0$ into $\hat{Z}_L = pL$ and $\hat{Z}_C = (1/pC)$ gives

$$\hat{Z}_L = 0|_{f=0} \tag{5.14a}$$

$$\hat{Z}_C = \infty|_{f=0} \tag{5.14b}$$

In other words, an inductor (an ideal one) is a *short circuit* at dc and a capacitor is an *open circuit* at dc. This can be checked directly from the circuit by replacing the inductor with a short circuit and replacing the capacitor with an open circuit. Once this is done, we see that the behavior of the model at dc is the same as an ideal resistor. As we increase the frequency, the impedance of the capacitor decreases and tends to "short out" the resistor of the model. This begins to occur at a frequency where the impedance of the capacitor equals the resistance, or $\omega_1 = (1/RC_{\text{par}})$. Thus the net impedance decreases at −20 dB/decade and the phase angle approaches −90° above this frequency. At a point where the inductor and capacitor of the model *resonate*, $\omega_0 = (1/\sqrt{L_{\text{lead}}C_{\text{par}}})$, the impedance of the model is at a minimum. (Actually, this minimum occurs at a frequency that is slightly above this resonant frequency, with it approaching this frequency the smaller the value of R).

Above this resonant frequency, the impedance of the inductor becomes dominant and the magnitude of the impedance increases at 20 dB/decade and the phase angle approaches +90°. Finally, as the frequency approaches infinity, the inductor behaves as an open circuit and the capacitor behaves as a short circuit, so that the net impedance of the model approaches that of an open circuit (due primarily to the inductor):

$$\hat{Z}_L = \infty|_{f=0} \tag{5.15a}$$

$$\hat{Z}_C = 0|_{f=0} \tag{5.15b}$$

Since the inductance was dominant for higher frequencies, the phase angle approaches 90°. All of this behavior is borne out by the transfer function that we derived. However, it is always a good idea to perform these simple checks. Also, an understanding of the simple principles described above can be an aid, along with the understanding of the physical construction of the element, in the construction of a suitable model that will represent this nonideal behavior. This examination of the model over distinct frequency ranges is represented in Fig. 5.11. The reader should study this method since it will be used on numerous occasions to examine and construct models of elements and devices.

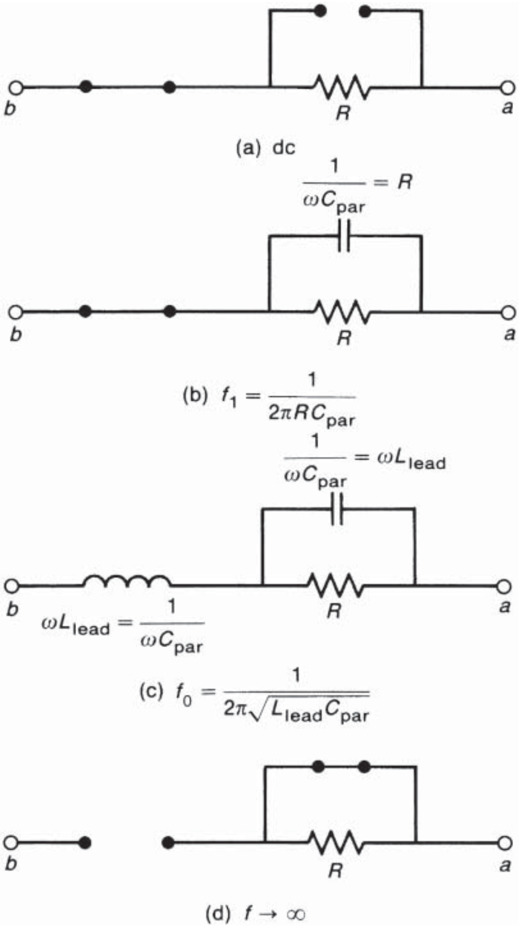
b
R
a
(a) dc
$\frac{1}{\omega C_{\text{par}}} = R$
b
R
a
(b) $f_1 = \frac{1}{2\pi R C_{\text{par}}}$
$\frac{1}{\omega C_{\text{par}}} = \omega L_{\text{lead}}$
b
$\omega L_{\text{lead}} = \frac{1}{\omega C_{\text{par}}}$
R
a
(c) $f_0 = \frac{1}{2\pi\sqrt{L_{\text{lead}} C_{\text{par}}}}$
b
R
a
(d) $f \rightarrow \infty$

FIGURE 5.11 Simplification of the equivalent circuit of a resistor for various frequencies: (a) dc; (b) $f_1 = (1/2\pi R C_{\text{par}})$ (c) $f_0 = (1/2\pi\sqrt{L_{\text{lead}} C_{\text{par}}})$; (d) $f \rightarrow \infty$.

We will frequently present and examine experimentally obtained data. The purpose in doing so is twofold. First, it is not possible to construct one model that will apply to all frequencies, so we will need to accept some approximate behavior in exchange for model simplicity. A model that will predict the behavior of an element for a very wide frequency range can always be constructed. However, that model will of necessity be very complex, and consequently will yield

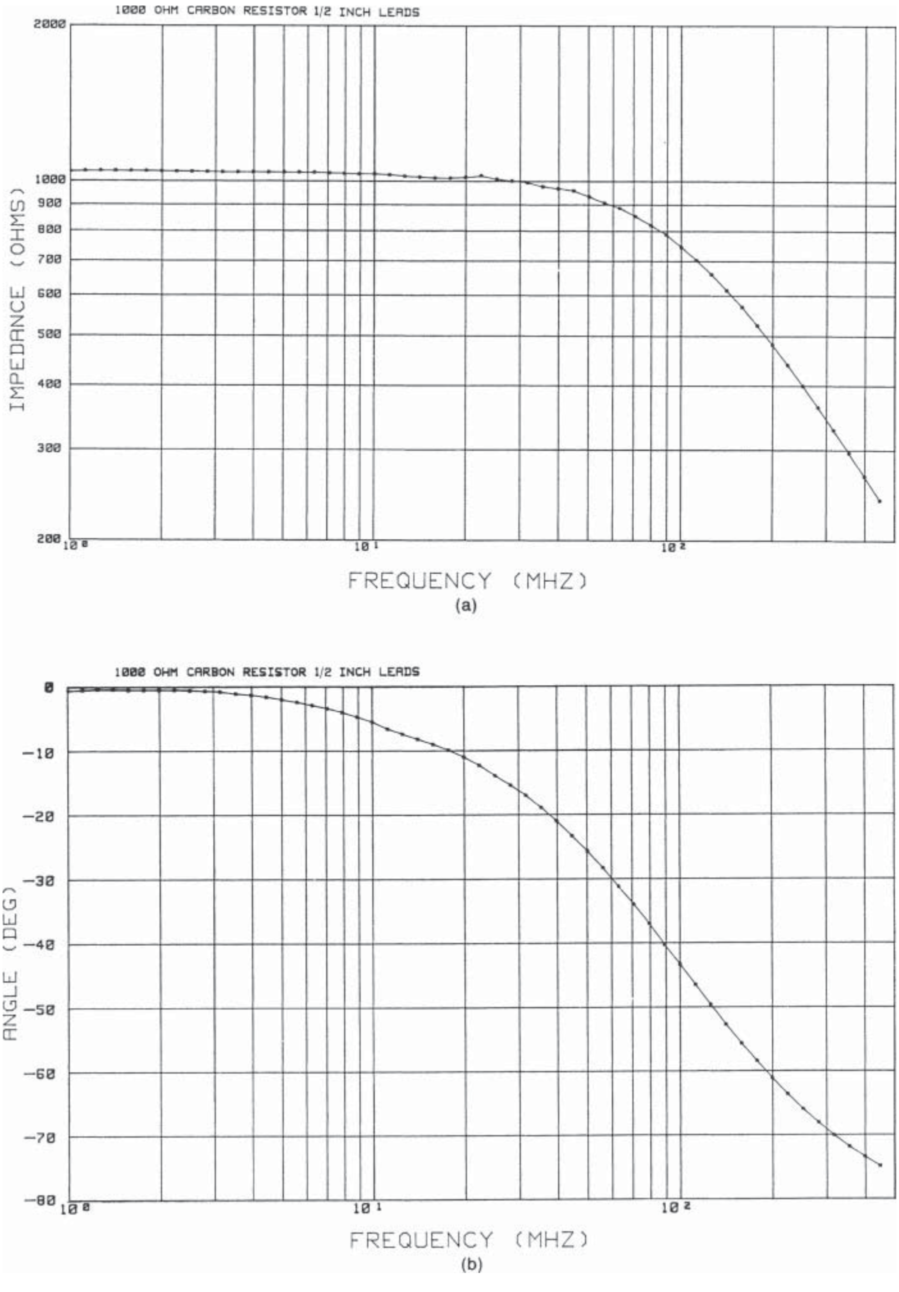

FIGURE 5.12 Measured impedance of a 1000 Ω carbon resistor having 1/2 in. lead lengths: (a) magnitude; (b) phase.

very little insight into the device behavior. Experimental data will reveal the adequacy of the simpler model. Second, it is important for the reader to obtain some appreciation for the typical range of numerical results. Examining experimental data obtained from actual devices will serve this latter purpose. An example of such data is shown in Fig. 5.12, where the measured impedance of a 1 kΩ, 1/8 W carbon resistor having 0.5 in. lead lengths and 0.25 in. lead separation is shown over a frequency range of 1–500 MHz. Comparing Fig. 5.12 with Fig. 5.10c, we see that the first breakpoint f_1 occurs at approximately 120 MHz, but the resonant frequency of the model, f_0, is somewhat above the highest measured frequency of 500 MHz. Nevertheless, the model of Fig. 5.10b gives an adequate description of the resistor if we choose $R = 1.05$ kΩ, $C_{\mathrm{par}} = 1.2$ pF, and $L_{\mathrm{lead}} = 14$ nH.

5.5 CAPACITORS

The ideal behavior of a capacitor is shown in Fig. 5.13. The impedance is $\hat{Z}(p) = (1/pC)$, or, by substituting $p = j\omega$, we obtain

$$\begin{aligned}\hat{Z}(j\omega) &= \frac{1}{j\omega C}\\ &= -j\frac{1}{\omega C}\\ &= \frac{1}{\omega C}\underline{/90^\circ}\end{aligned} \tag{5.16}$$

The magnitude of the impedance decreases linearly with frequency, or −20 dB/decade, and the phase angle is constant at −90°.

There are numerous types of capacitors. For the purposes of EMC suppression, the typical types are ceramic and tantalum electrolytic. Large values of capacitance (1 − 1000 μF) can be obtained in a small package with the tantalum electrolytic capacitor. Ceramic capacitors give smaller values of capacitance (1 μF − 5 pF) than do electrolytic capacitors, yet they tend to maintain their ideal

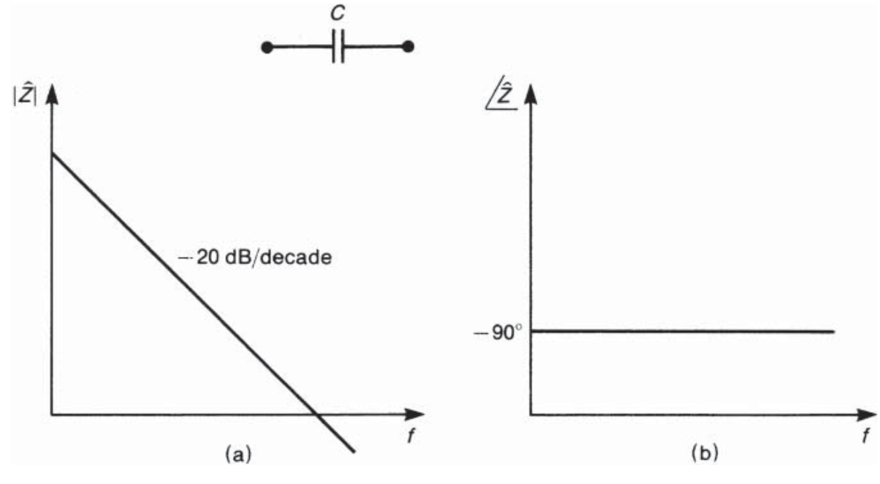

FIGURE 5.13 Frequency response of the impedance of an ideal capacitor: (a) magnitude; (b) phase.

behavior up to a much higher frequency. Thus ceramic capacitors are typically used for suppression in the radiated emission frequency range, whereas electrolytic capacitors, by virtue of their much larger values, are typically used for suppression in the conducted emission band and also for providing bulk charge storage on printed circuit boards as we will see. For a more complete discussion of capacitor types see [6].

Both types of capacitors have similar equivalent circuits, but the model element values differ substantially. This accounts for their different behavior over different frequency bands. Both types of capacitor can be viewed as a pair of parallel plates separated by a dielectric, as illustrated in Fig. 5.14. The loss (polarization and ohmic) in the dielectric is represented as a parallel resistance R_{diel} [1]. Usually this is a large value, as one would expect (hope). The resistance of the plates is represented by R_{plate}. For small ceramic capacitors, this is usually small enough in relation to the other elements to be neglected. Once again, the leads attached to the capacitor have a certain inductance represented by L_{lead} and capacitance C_{lead}. Again, these parasitic element values depend on the configuration of the two leads. If the leads are formed in the shape of a U or bent 90° to the body of the capacitor as is the usual custom then these parasitic lead components are as calculated previously. Usually R_{diel} is so large that it can be neglected. Similarly C_{lead} is usually much less than the ideal capacitance C, and thus may be neglected. Thus the equivalent circuit of the capacitor alone consists of the series combination of C and R_{plate}. The resistance R_{plate} is referred to as the equivalent series resistance or ESR and denoted as R_s. Thus the model consists of the series combination of C, L_{lead}, and R_s, as shown in Fig. 5.15. The ESR is typically several ohms for electrolytic capacitors and varies with frequency. For ceramic capacitors over the regulatory limit frequency range the series resistance is usually negligible. The impedance of this model is

$$\hat{Z}(p) = L_{\mathrm{lead}} \frac{p^2 + (R_s p / L_{\mathrm{lead}}) + (1/L_{\mathrm{lead}} C)}{p} \tag{5.17}$$

Substituting $p = j\omega$ gives

$$\hat{Z}(j\omega) = L_{\mathrm{lead}} \frac{(1/L_{\mathrm{lead}} C) - \omega^2 + (j\omega R_s / L_{\mathrm{lead}})}{j\omega} \tag{5.18}$$

The Bode plots of this impedance are shown in Fig. 5.15. At dc the circuit appears as an open circuit (replace the inductor with a short circuit and the capacitor with an open circuit). As frequency

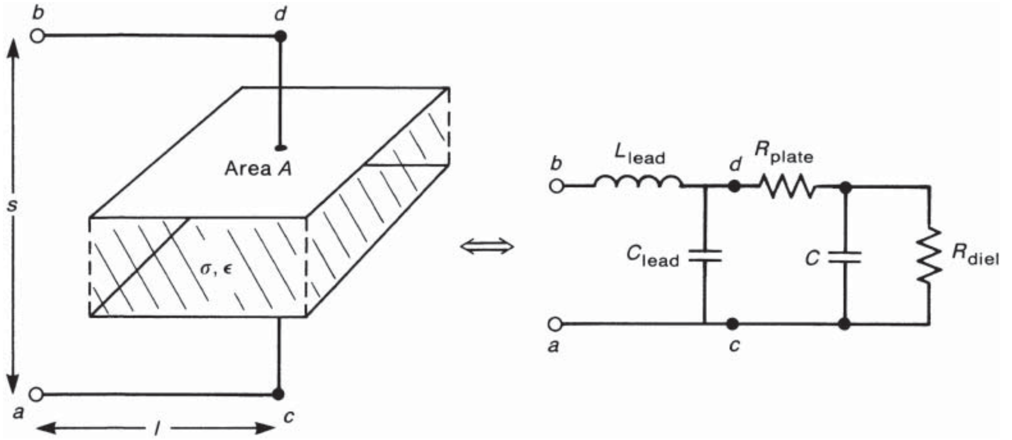

FIGURE 5.14 Modeling of a physical capacitor with an equivalent circuit.

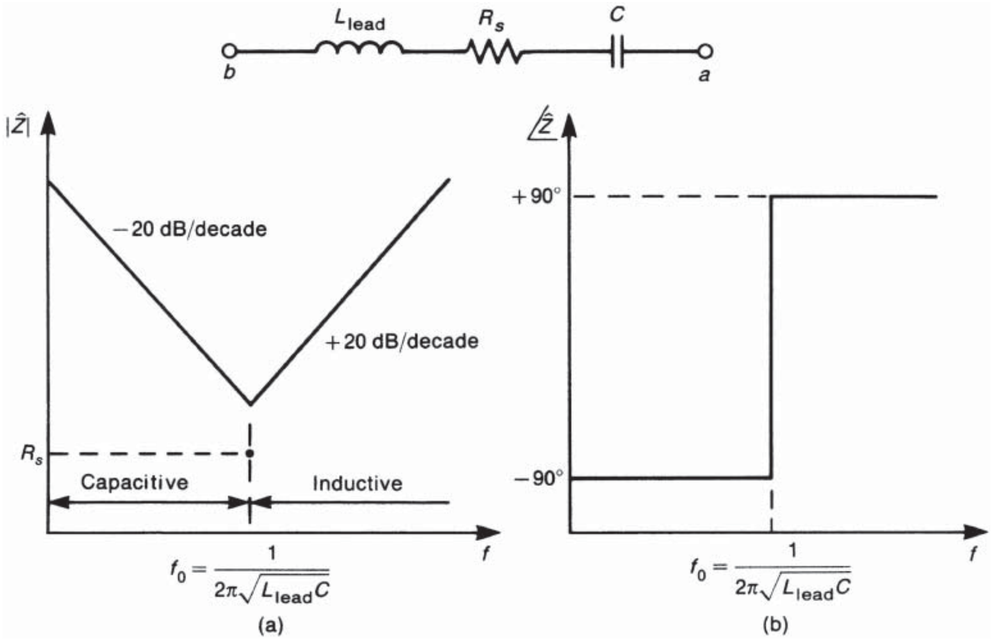

FIGURE 5.15 A simplified equivalent circuit of a capacitor including the effects of lead length showing Bode plots of the impedance: (a) magnitude; (b) phase.

increases, the impedance of the capacitor dominates and decreases linearly with frequency at a rate of −20 dB/decade. The impedance of the inductor increases until it equals that of the capacitor at $f_0 = (1/2\pi\sqrt{L_{\text{lead}}C})$. At this frequency the series combination appears as a short circuit (although the magnitudes of the impedances are equal they are of opposite sign) and the net impedance of the branch is R_s. The frequency f_0 is referred to as the *self-resonant frequency of the capacitor*. For higher frequencies the magnitude of the impedance of the inductor dominates and the impedance increases at a rate of +20 dB/decade, while the phase angle approaches +90°. If one is relying on this element to provide a low impedance such as for shunting noise currents to ground then the frequency of the current to be suppressed must be lower than the *self-resonant frequency* f_0 of the capacitor or else the impedance will be larger than anticipated on the basis of the ideal behavior of the capacitor.

As an example, suppose the leads of a capacitor are formed into a U shape with a separation of 0.25 in. and length 0.5 in. We calculated previously that the inductance of the loop formed by these leads is $L_{\text{lead}} \cong 14$ nH. Therefore a 470 pF capacitor will resonate at a frequency of 62 MHz and 0.1 μF capacitor will resonate at a frequency of 4.25 MHz. This points out the important fact that, *for a fixed lead length and spacing, the larger the capacitance value the lower the self-resonant frequency* (by the square root of the capacitance ratios). Figures 5.16 and 5.17 show measured impedances of a 470 pF ceramic capacitor from 1 to 500 MHz. Two lead lengths are shown: essentially no lead lengths (Fig. 5.16) and 1/2 in. lead lengths (Fig. 5.17). Note that the self-resonant frequency for the 1/2 in. lead length is about 62 MHz, as calculated above. Thus, if one is interested in providing a low impedance to shunt a 200 MHz signal, the 470 pF capacitor with either lead length will give an impedance larger than expected. A 0.15 μF tantalum capacitor was measured, and results are shown from 1 to 500 MHz for essentially no lead lengths and for 1/2 in. lead lengths in Figs. 5.18 and 5.19, respectively. Note that the frequency response of the tantalum capacitor is not as ideal as that of the ceramic capacitor. This is due to the more significant ESR of the tantalum capacitor.

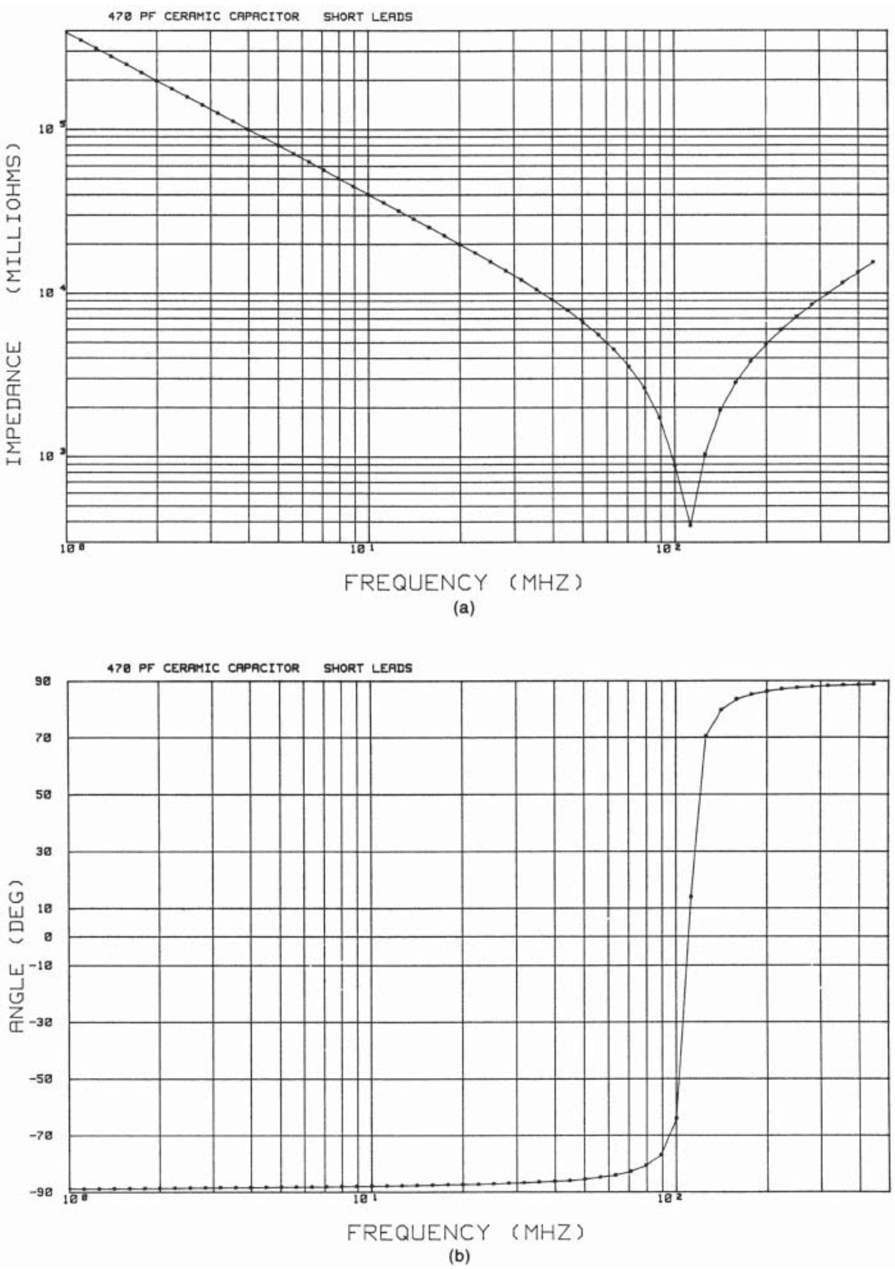

FIGURE 5.16 Measured impedance of a 470 pF ceramic capacitor with short lead lengths: (a) magnitude; (b) phase.

Review Exercise 5.4 Determine the lead inductance for the 0.15 μF tantalum capacitor having 1/2 in. lead lengths directly from the measured impedance magnitude in Fig. 5.19a.

***Answer*:** Impedance at 100 MHz is 10 Ω and inductive, giving 15.9 nH.

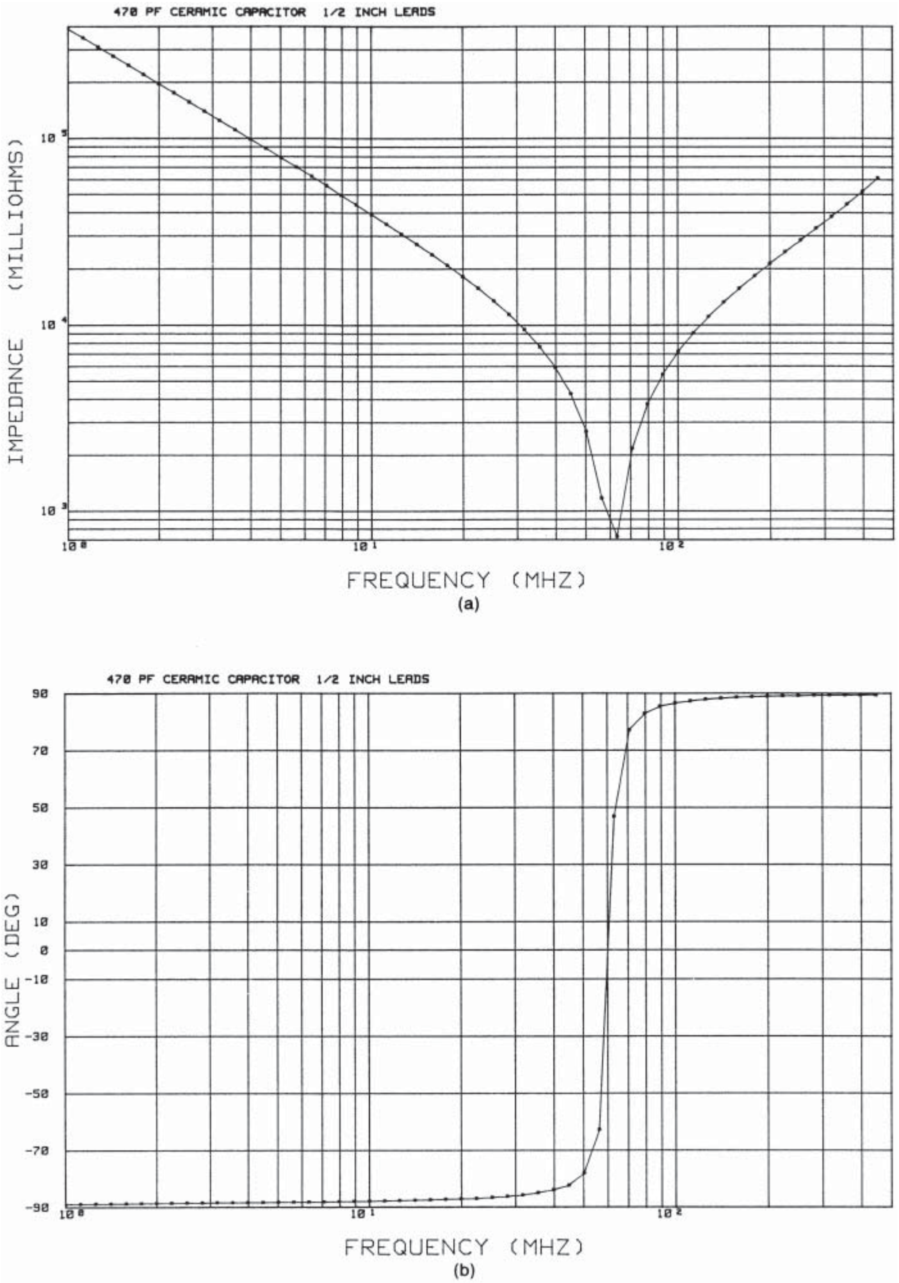

FIGURE 5.17 Measured impedance of a 470 pF ceramic capacitor with 1/2 in. lead lengths: (a) magnitude; (b) phase.

A frequent mistake made in suppression is in the choice and effectiveness of capacitors [7]. Capacitors are generally the common choice for suppression element since they are easily installable after the product is constructed—simply solder them across the two terminals in a connector or on a PCB to provide a low-impedance path to divert the noise current. Suppose that it is desired to reduce the radiated emission at, say, 100 MHz. Also suppose it is found that the noise current present on a

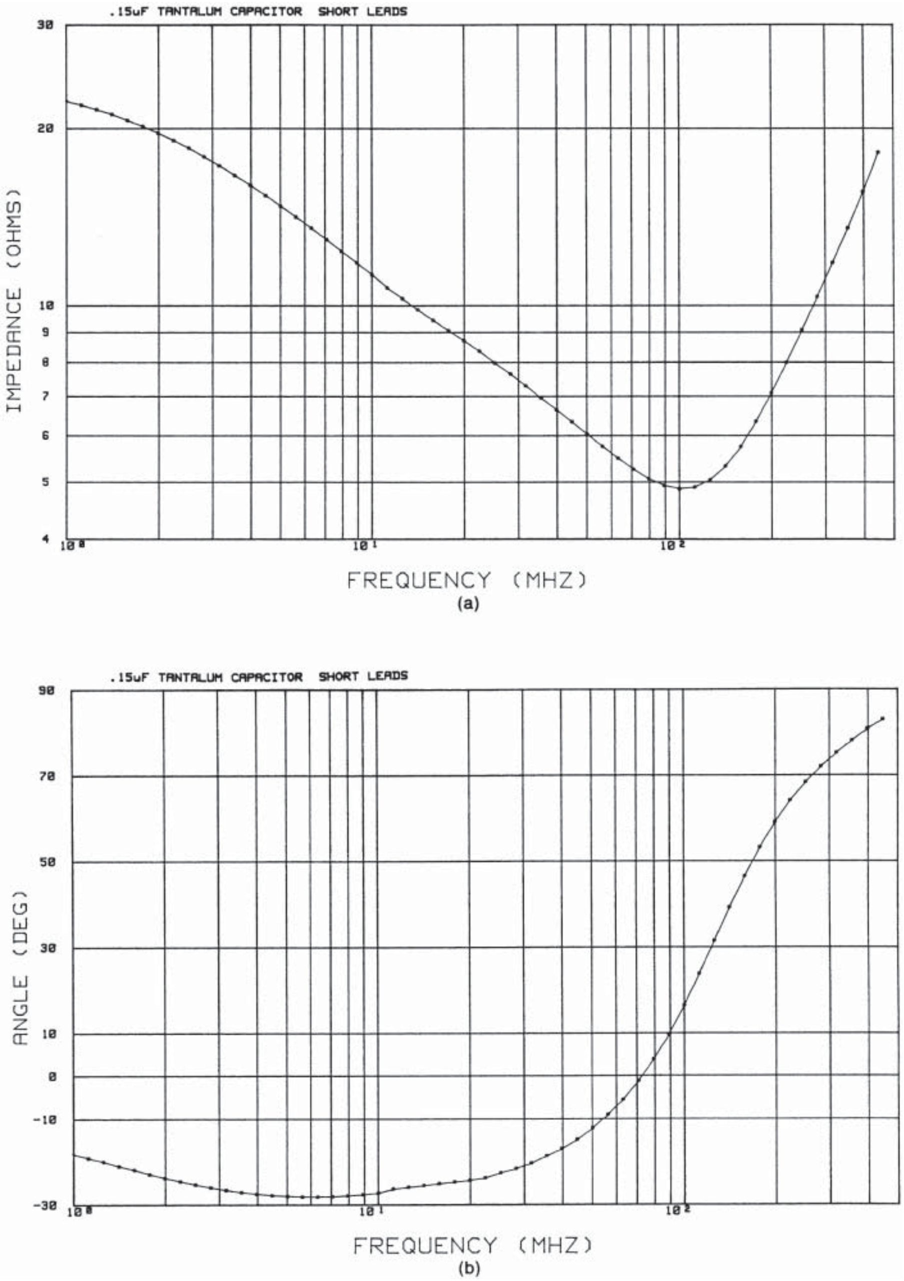

FIGURE 5.18 Measured impedance of a 0.15 μF tantalum capacitor with short lead lengths: (a) magnitude; (b) phase.

particular peripheral cable is the primary radiation source point. One might place a capacitor between the signal and return wires of the cable where it exits the product in order to divert the high-frequency noise current and prevent it from being present on the peripheral cable, where its radiation efficiency will be considerably greater. One might choose a ceramic capacitor of value 100 pF. Suppose that the product's radiated emissions are remeasured and found to be reduced, yet this reduction is still not

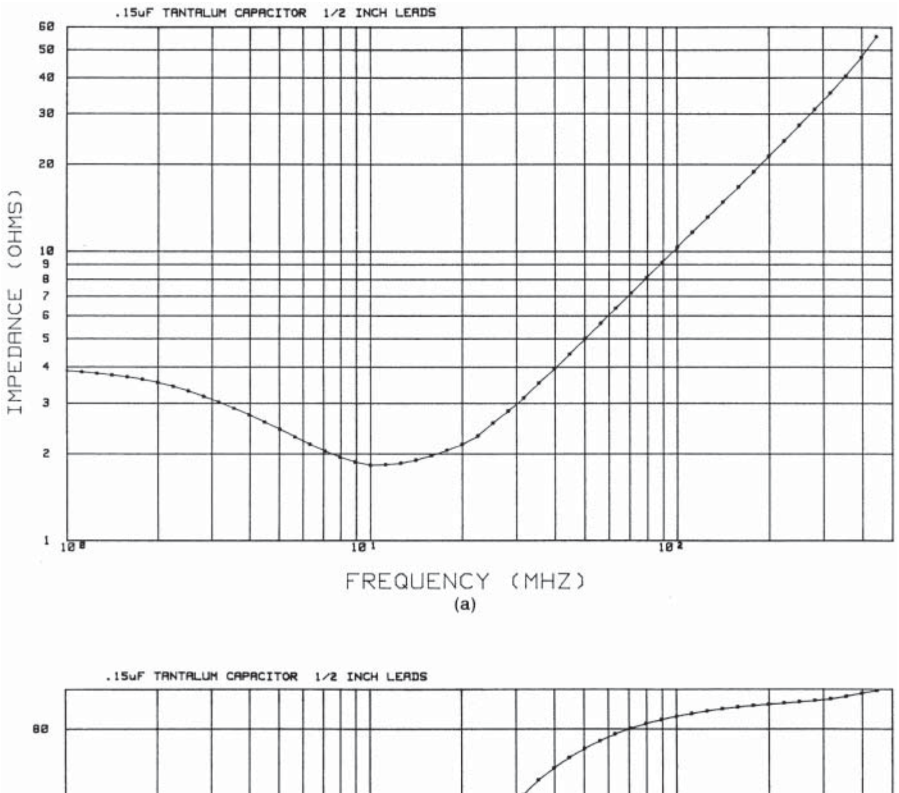

(a)

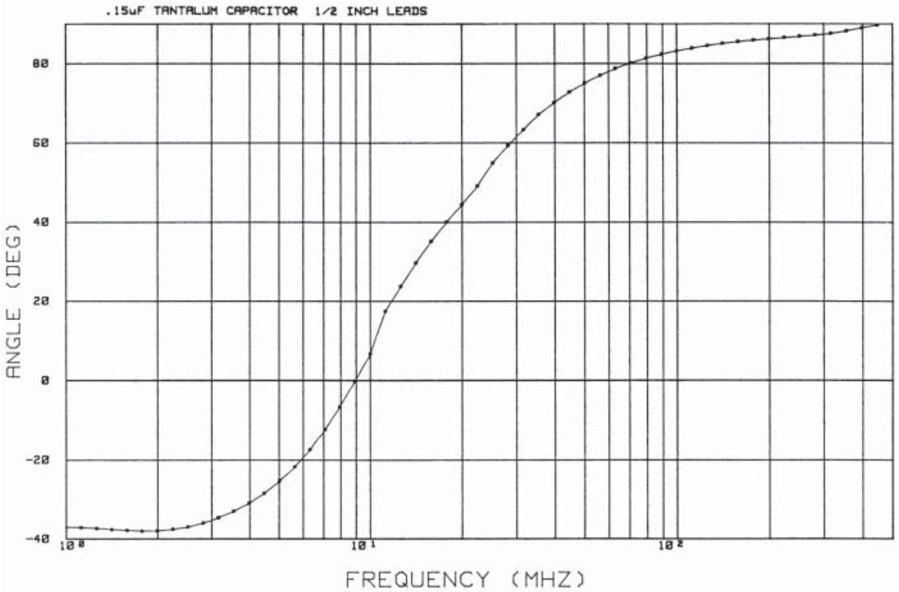

(b)

FIGURE 5.19 Measured impedance of a 0.15 μF tantalum capacitor with 1/2 in. lead lengths: (a) magnitude; (b) phase.

sufficient for the product to comply with the regulatory limit at this frequency. In order to reduce the emission still further, one might be tempted to increase the value of capacitance to, say, 10,000 pF (0.01 μF). When this capacitor is substituted, it will be found that, instead of the radiated emission being reduced (by the expected 40 dB), they are actually increased! What has happened is that the self-resonant frequency of the larger capacitor has been reduced from that of the smaller capacitor not because of any change in L_{lead} but simply because of the larger value of C. Since the self- resonant frequency of the 10,000 pF capacitor is now below the frequency of interest (100 MHz), the capacitor appears inductive, giving an impedance larger than expected. Measured data for 100 and 10,000 pF ceramic capacitors, both having 0.5 in. lead lengths, show that the impedance of the 100 pF capacitor at 100 MHz is 8 Ω, whereas the 10,000 pF capacitor has an impedance of 12 Ω at this frequency!

Review Exercise 5.5 Determine the impedance magnitude and phase of a 10,000 pF ceramic capacitor having attachment leads of 20-gauge wire of length 0.5 in. and separation of 0.25 in. at 50 MHz.

***Answer*:** $4.08\,\underline{/90^\circ}\ \Omega$.

Another caution that should be observed is the effect of the added suppression element on the *functional signals*. Placing a capacitor across the signal and return leads of a cable in order to divert high-frequency signal components from the cable can produce *ringing* by virtue of the resonance created by the capacitor in parallel with the inductance of the cable. Resistors are also frequently inserted in series with the cable in order to block these high-frequency signals. This is frequently implemented by inserting "*RC* packs" in the PCB to provide a low pass filter, where the offboard cable connector exits the PCB. The values of R and C in the implementation described above should be chosen carefully. Suppose that the input to this circuit is a trapezoidal pulse train representing a typical digital signal such as digital data that are being transmitted over the peripheral cable into which the *RC* circuit has been inserted. For the present we will ignore the effect of the peripheral cable. The transfer function of the *RC* circuit so formed is flat out to the break frequency of $1/2\pi RC$ and decreases at a rate of −20 dB/decade above that. Thus we have formed a *lowpass filter*. If the break frequency occurs low enough in the frequency range in comparison with the spectrum of the signal to be passed by the cable due to large values of R or C, the waveform of the signal can be adversely affected, resulting in functional performance problems. On the other hand, if these values are too small, very little filtering of the high-frequency noise on the cable may occur. (See Fig. 3.27 of Chapter 3, which illustrates this.) This indicates two important points: (1) one must be careful to not adversely affect the functional signal with a suppression scheme, or else passing the regulatory limits will be a moot point: and (2) if the added suppression scheme does not produce a sufficient reduction, one should not be confused, since there is a reason why it does not.

It is also important to understand the concept illustrated in Fig. 5.20. Suppose that a capacitor is to be placed in parallel with a cable or a pair of lands on a PCB in order to divert a noise current $\hat{I}_{\text{NOISE}}$. The impedance of the capacitor is represented by $\hat{Z}_{\text{CAP}}$, and the impedance seen looking into the pair of conductors that we wish to divert the noise current from is designated by $\hat{Z}_{\text{LOAD}}$.

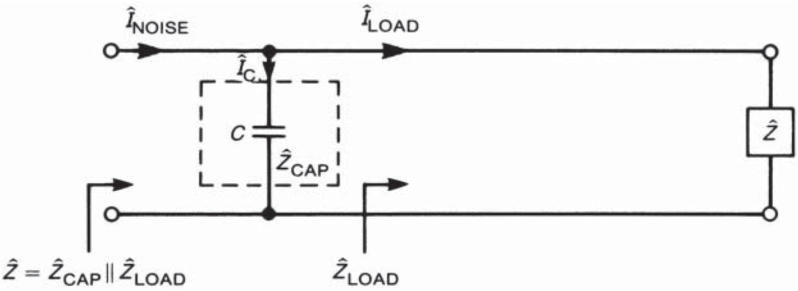

FIGURE 5.20 An important consideration in the diversion of currents with a parallel element: current division and the impedance of the load.

By current division, the portion of the noise current that is diverted through the capacitor is given by [4, 5]

$$\hat{I}_C = \frac{\hat{Z}_{\mathrm{LOAD}}}{\hat{Z}_{\mathrm{CAP}} + \hat{Z}_{\mathrm{LOAD}}} \hat{I}_{\mathrm{NOISE}} \tag{5.19}$$

If $\hat{Z}_{\mathrm{LOAD}}$ is *large* compared with $\hat{Z}_{\mathrm{CAP}}$, then the capacitor will be effective in keeping $\hat{I}_{\mathrm{NOISE}}$ off the cable. On the other hand, if $\hat{Z}_{\mathrm{LOAD}}$ is *small* compared with $\hat{Z}_{\mathrm{CAP}}$, then the capacitor will be ineffective in diverting noise current! This is why the use of parallel capacitors in *low-impedance* circuits is usually *ineffectual*. They are most effective with *high-impedance* loads. *Whenever a parallel suppression component is to be used, the impedance levels of not only the element but also the parallel path should be computed or estimated at the desired frequency. If* $\hat{Z}_{\mathrm{LOAD}} << \hat{Z}_{\mathrm{CAP}}$, *then the suppression component will be ineffectual*. Therefore it is important to remember that *parallel capacitors work best in high-impedance circuits* with regard to diverting noise currents.

Review Exercise 5.6 A capacitor is placed in parallel with a 1000 Ω resistive load as shown in Fig. 5.20. Determine the value of capacitor such that 90% of a 100 MHz current is diverted through it. (Use the current division principle.)

***Answer*:** 3.3 pF.

5.6 INDUCTORS

The impedance of an ideal inductor is plotted against frequency in Fig. 5.21, and is given by

$$\begin{aligned} \hat{Z}_L &= j\omega L \\ &= \omega L \underline{/90^\circ} \end{aligned} \tag{5.20}$$

The magnitude increases linearly with frequency at a rate of +20 dB/decade, and the angle is +90° for all frequencies.

There are numerous variations of the basic construction technique of winding turns of wire on a cylindrical form. The specific construction technique will determine the values of the *parasitic* elements in the model of the nonideal inductor that is shown in Fig. 5.22. The process of winding turns of wire on a cylindrical form introduces resistance of the wire as well as capacitance between neighboring turns. This produces the parasitic elements R_{par} and C_{par} in the nonideal model. Some construction techniques wind the turns of wire in *layers* to shorten the length of the inductor body. But this adds capacitance between layers, which *substantially increases* C_{par}. The nonideal inductor should also include the inductance of the attachment leads L_{lead}, as with all other elements. However since the *intentional element* is an inductance and its value is usually much larger than the lead inductance, we may generally neglect L_{lead} in this nonideal model. Similarly, the lead capacitance C_{lead} is frequently less than the parasitic capacitance C_{par}, so that we may neglect the lead capacitance. Thus the model consists of the series combination of R_{par} and L in parallel with C_{par}. The impedance of this model becomes

$$\hat{Z}_L(p) = R_{\mathrm{par}} \frac{1 + (pL/R_{\mathrm{par}})}{p^2 L C_{\mathrm{par}} + p R_{\mathrm{par}} C_{\mathrm{par}} + 1} \tag{5.21}$$

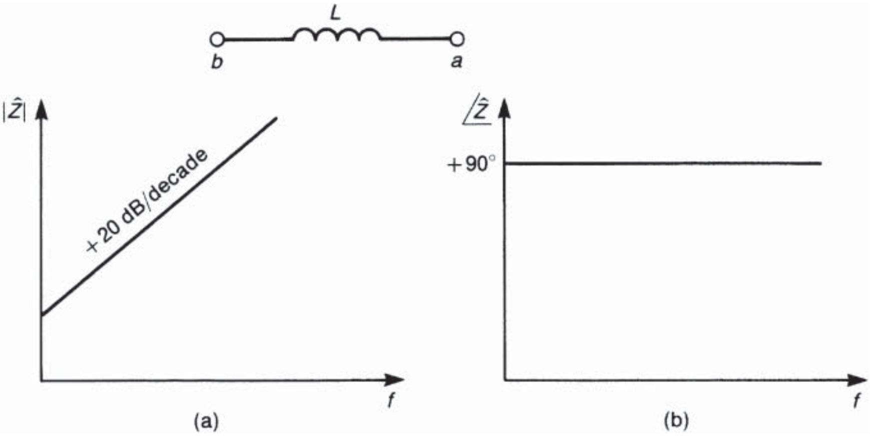

FIGURE 5.21 Frequency response of the impedance of an ideal inductor: (a) magnitude; (b) phase.

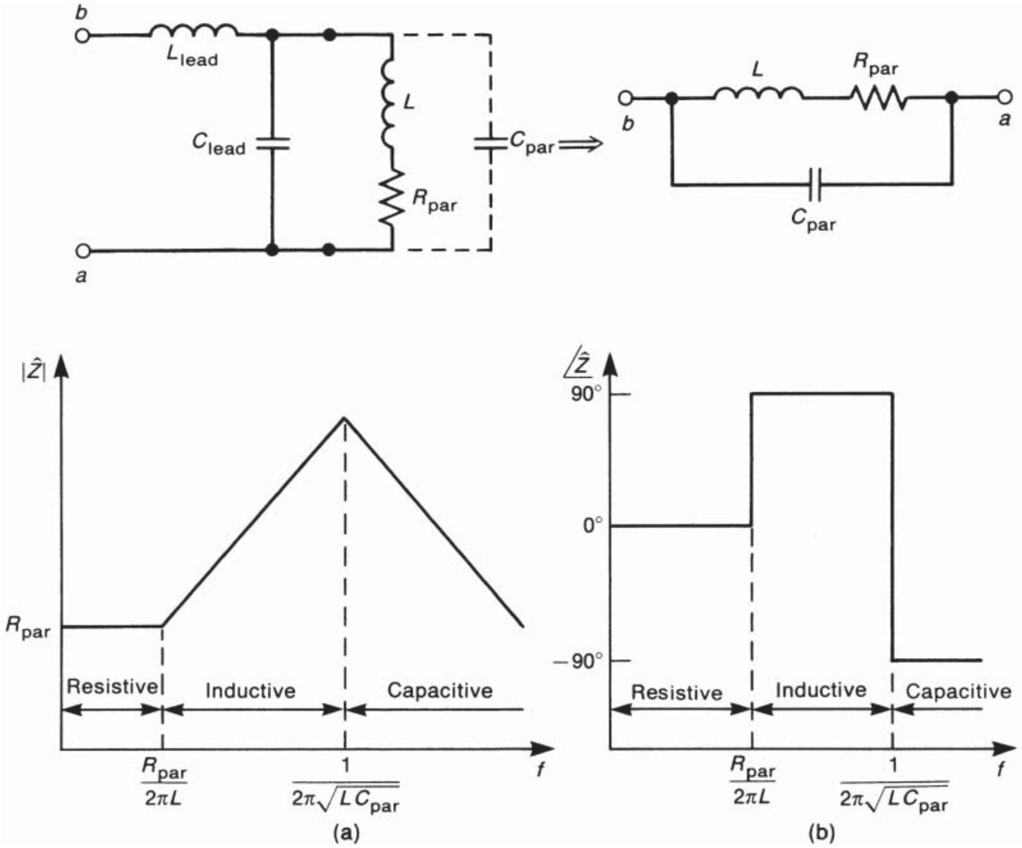
b
L_{lead}
C_{lead}
L
R_{par}
C_{par}
a
L
R_{par}
b
a
C_{par}
$|\hat{Z}|$
R_{par}
Resistive
Inductive
Capacitive
$\frac{R_{\text{par}}}{2\pi L}$
$\frac{1}{2\pi\sqrt{LC_{\text{par}}}}$
f
(a)
$\angle\hat{Z}$
90°
0°
−90°
Resistive
Inductive
Capacitive
$\frac{R_{\text{par}}}{2\pi L}$
$\frac{1}{2\pi\sqrt{LC_{\text{par}}}}$
f
(b)

FIGURE 5.22 A simplified equivalent circuit of an inductor including the effects of lead inductance and capacitance showing Bode plots of the impedance: (a) magnitude; (b) phase.

Substituting $p = j\omega$ gives

$$\hat{Z}_L(j\omega) = R_{\text{par}} \frac{1 + (j\omega L/R_{\text{par}})}{1 - \omega^2 L C_{\text{par}} + j\omega R_{\text{par}} C_{\text{par}}} \tag{5.22}$$

At low frequencies the resistance dominates, and the impedance is R_{par}. As frequency is increased, the inductance of the model begins to dominate at a frequency of $\omega = (R_{\text{par}}/L)$, and the impedance increases at 20 dB/decade while the angle is +90°. As frequency is further increased, the impedance of the parasitic capacitance decreases until its magnitude equals that of the inductor impedance. This occurs at the *self-resonant frequency* of the inductor, $f_0 = (1/2\pi\sqrt{LC_{\text{par}}})$. The Bode plot of the model is also shown in Fig. 5.22.

The measured impedance of a 1.2 μH inductor is shown in Fig. 5.23 from 1 to 500 MHz. The self-resonant frequency of this inductor is of order 110 MHz. This gives a value of C_{par} of 1.7 pF. The measured impedance of a 10 μH inductor gives a value of parasitic capacitance 1.6 pF and a self-resonant frequency of around 40 MHz. This result is reasonable to expect, since the resonant frequency should be reduced by the square root of the ratio of the inductances if the lead lengths and parasitic capacitances are the same. Once again, it is important to remember that *increasing the value of an inductor will not necessarily give a lower impedance at high frequencies, since the larger value of inductance will serve to lower the self-resonant frequency, even though the lead lengths remain identical.*

Review Exercise 5.7 Determine the value of the inductance in the measured data of Fig. 5.23a directly from the data.

***Answer*:** At 4 MHz the impedance is approximately 30 Ω, giving the value of inductance of 1.2 μH.

Capacitors are used to *divert* noise currents, whereas inductors are placed in series with wires or lands to *block* noise currents. This will be effective *if the impedance of the inductor at the frequency of the noise current is larger than the original series impedance seen looking into the wires or lands*, $\hat{Z}_{\text{LOAD}}$, as shown in Fig. 5.24. The choice of whether to use a parallel capacitor to divert noise currents or a series inductor to block noise currents depends strongly on the impedance that it is placed in series or parallel with. *If $\hat{Z}_{\text{LOAD}}$ is large, then a rather large value of inductance will be required in order to increase the net impedance of the circuit and provide any blockage of the noise current*! This is why *series inductors are most effective in low-impedance circuits*. Conversely, parallel capacitors must present a much smaller impedance than $\hat{Z}_{\text{LOAD}}$ in order to divert noise currents, so that *parallel capacitors are most effective in high-impedance circuits*.

As with parallel suppression capacitors, one must be concerned with the effect of the suppression element on the functional signal. Addition of series inductors can cause ringing, which can affect the desired performance of the system. However, they are quite effective in lines that do not carry high-speed signals and operate infrequently, such as reset lines of digital devices and the green wire of power cords.

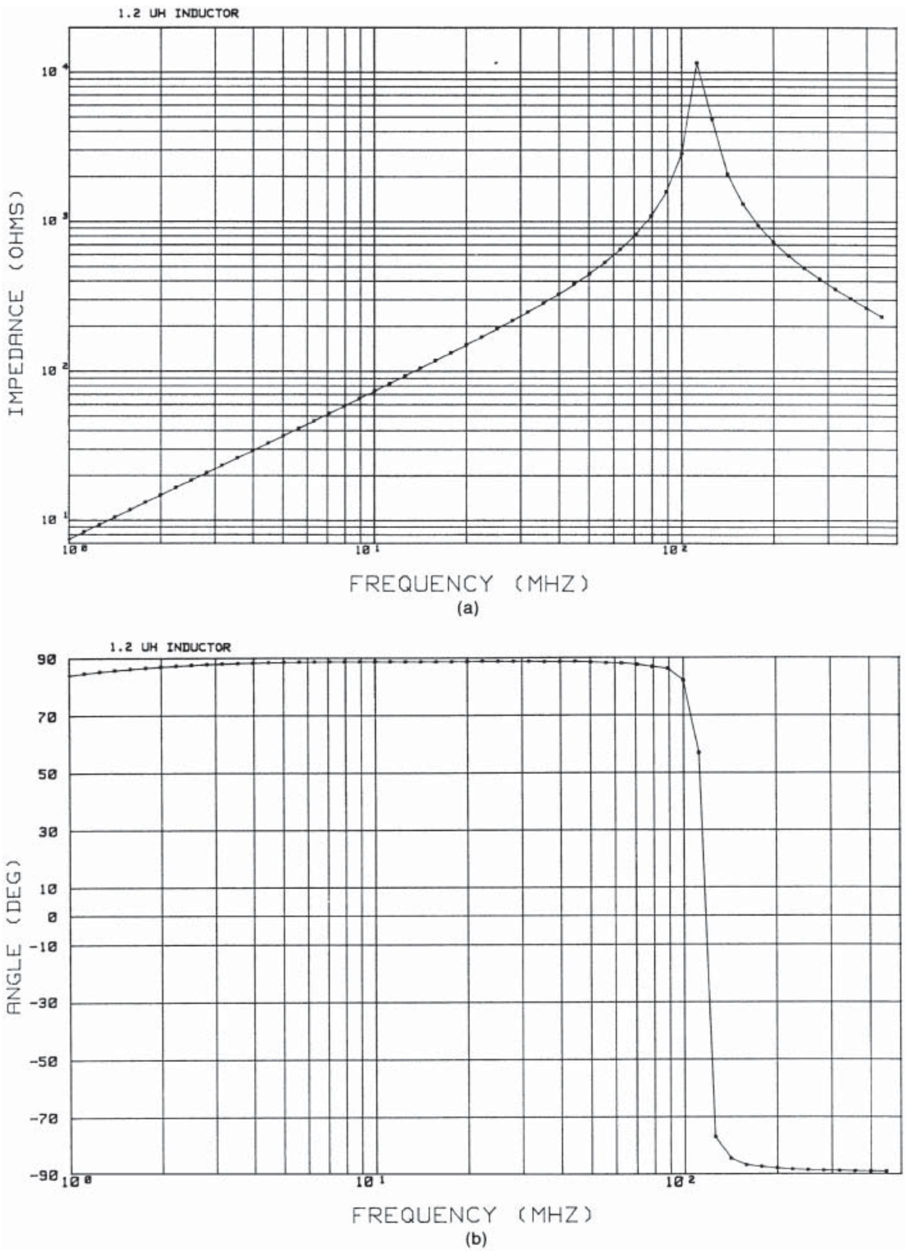

FIGURE 5.23 Measured impedance of a 1.2 μH inductor: (a) magnitude; (b) phase.

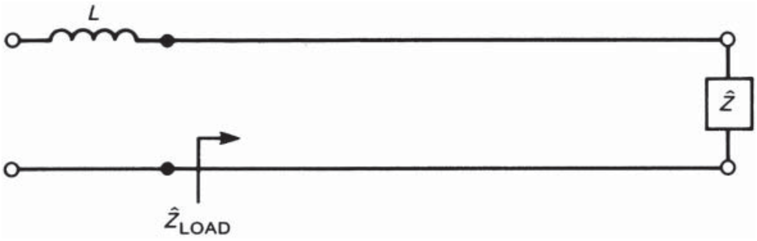

FIGURE 5.24 An important consideration in the blocking of currents with a series element: the impedance of the load.

5.7 FERROMAGNETIC MATERIALS—SATURATION AND FREQUENCY RESPONSE

Ferromagnetic materials are widely used in EMC for noise suppression. All ferromagnetic materials have certain properties that are important to recognize when applying them in EMC applications. The three most important ones are (1) saturation, (2) frequency response, and (3) the ability to concentrate magnetic flux. Consider the toroid inductor shown in Fig. 5.25a. In order to increase the value of inductance of an inductor, inductors are wound on a *ferromagnetic core*. There are numerous types of these ranging from iron to powdered ferrite materials. All types of ferromagnetic materials have large relative permeabilities μ_r, where the permeability is $\mu = \mu_r\mu_0$. For example, steel (SAE 1045) has a relative permeability of $\mu_r = 1000$ and mumetal has $\mu_r = 30,000$. Non-ferromagnetic metals such as copper and aluminum have relative permeabilities of free space, $\mu_r = 1$. The values of relative permeability cited for these materials are values measured at *low currents* and at *low frequencies*, typically 1 kHz or lower. Ferromagnetic materials suffer from the property of *saturation*, illustrated in Fig. 5.25a. Consider a ferro magnetic *toroid* that has N turns of wire wound on it. An approximate value for the inductance of this toroid (assuming that all the magnetic flux is confined to the core) is $L = \mu_r\mu_0 N^2 A/l$, where A is the core cross-sectional area and l is the mean path length of the core [1]. Suppose that a current I is passed through the turns. This current creates a *magnetic field intensity* H that is proportional to the product of the number of turns and the current, NI. A *magnetic flux density* B is produced in the core. The product of B and the cross-sectional area of the core, A, gives the magnetic flux $\psi = BA$, whose units are webers. The relationship between H and B is also shown in Fig. 5.25a. The permeability is the *slope* of this BH curve:

$$\mu = \frac{\Delta B}{\Delta H} \tag{5.23}$$

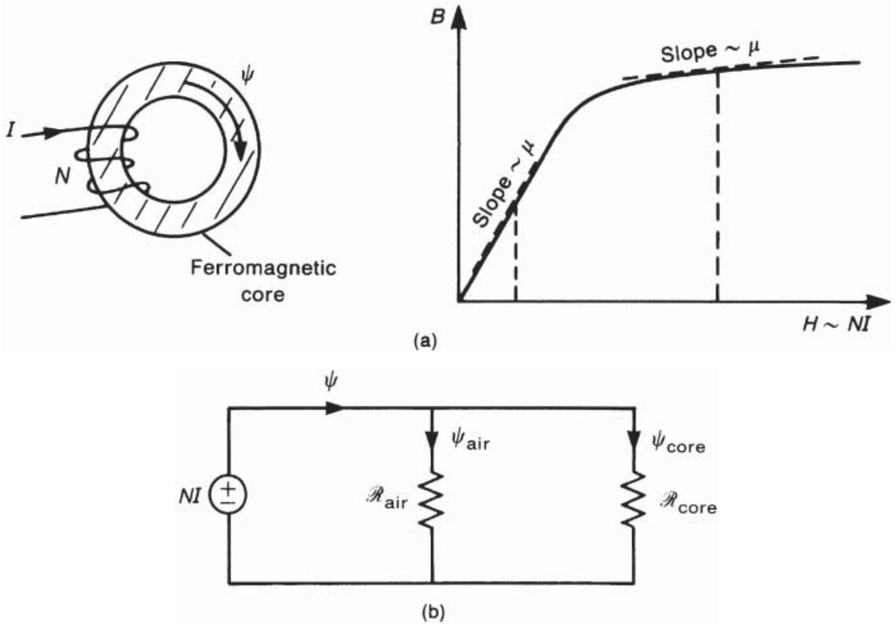

FIGURE 5.25 (a) The nonlinear relationship between magnetic flux density and magnetic field intensity for a ferromagnetic core inductor and (b) an equivalent circuit relating core and air (leakage) fluxes for a ferromagnetic core inductor.

At low values of current I the slope of the BH curve is large, as is the permeability. As current is increased, the *operating point* moves up the curve and the slope decreases. Thus the *permeability decreases with increasing current*. Since the inductance is a direct function of the permeability of the core, the *inductance decreases with increasing current*. We will have numerous occasions to see this phenomenon in the future. This phenomenon of lowering the relative permeability of a ferro magnetic core with increasing current is referred to as *saturation*.

Ferromagnetic materials have a considerable effect on magnetic fields. *Magnetic fields tend to concentrate in high-permeability materials*. For example, in the ferromagnetic-core inductor shown in Fig. 5.25a we indicated that the magnetic flux ψ was confined to the ferromagnetic core. This is correct to a reasonable approximation. Some of the flux *leaks out* and completes the magnetic path through the surrounding air. The division between how much of the total flux remains in the core and how much leaks out depends on the *reluctance* of the core [1, 5]. The quantity of reluctance $\mathcal{R}$ depends on the permeability μ of the magnetic path, its cross-sectional area A, and its length l as [1]

$$\mathcal{R} = \frac{l}{\mu A} \tag{5.24}$$

An important analogy to ordinary lumped circuits can be used to analyze magnetic circuits. It consists of making the analogy of voltage to *magnetomotive force (mmf)*, which is given in ampere turns, NI, and current to magnetic flux ψ as

$$R = \frac{NI}{\psi} \tag{5.25}$$

The equivalent circuit for the toroidal inductor of Fig. 5.25a is given in Fig. 5.25b. By current division, the portion of the total flux ψ that remains in the core is

$$\psi_{\text{core}} = \frac{R_{\text{air}}}{R_{\text{air}} + R_{\text{core}}}\psi \tag{5.26}$$

For high-permeability cores, $R_{\text{core}} \ll R_{\text{air}}$, so that the majority of the flux is confined to the core. The reluctances of the paths are proportional to the permeabilities of the paths, so that the portion of the total flux that remains in the core is proportional to the ratios of the *relative permeabilities* of the

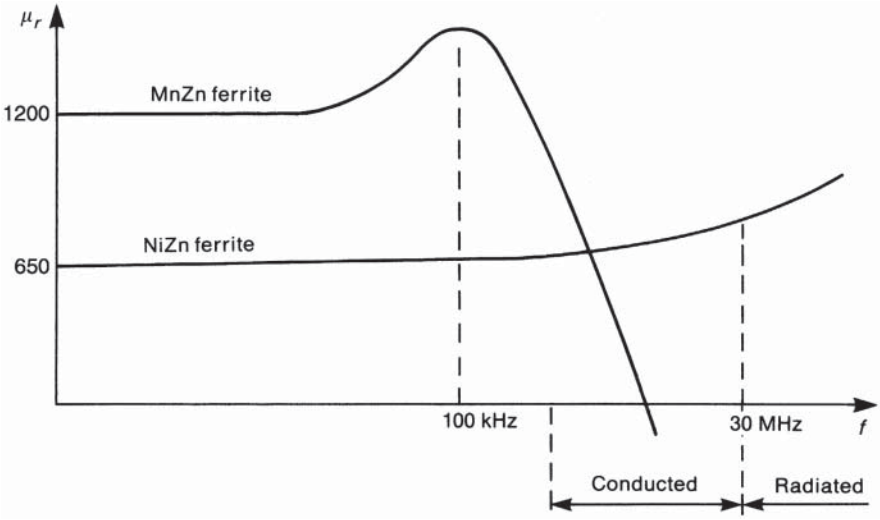

FIGURE 5.26 Frequency response of the relative permeabilities of MnZn and NiZn ferrites.

two paths. Cores constructed from ferromagnetic materials such as steel, which has $\mu_r = 1000$, tend to have small leakage flux. We will use this notion of *lowering the reluctance of a magnetic path in order to concentrate magnetic flux in that path* on numerous occasions in the future.

It seems that we should select a ferrite core material that has the highest *initial permeability* possible in order to concentrate the flux in the core. Ferrite core materials have different frequency responses of their permeability. A core having an initial relative permeability of 2000 at 1 kHz and low current might have that relative permeability reduced to under 100 at frequencies in the frequency range of the regulatory limit *where it is to have an effect*. Figure 5.26 illustrates this

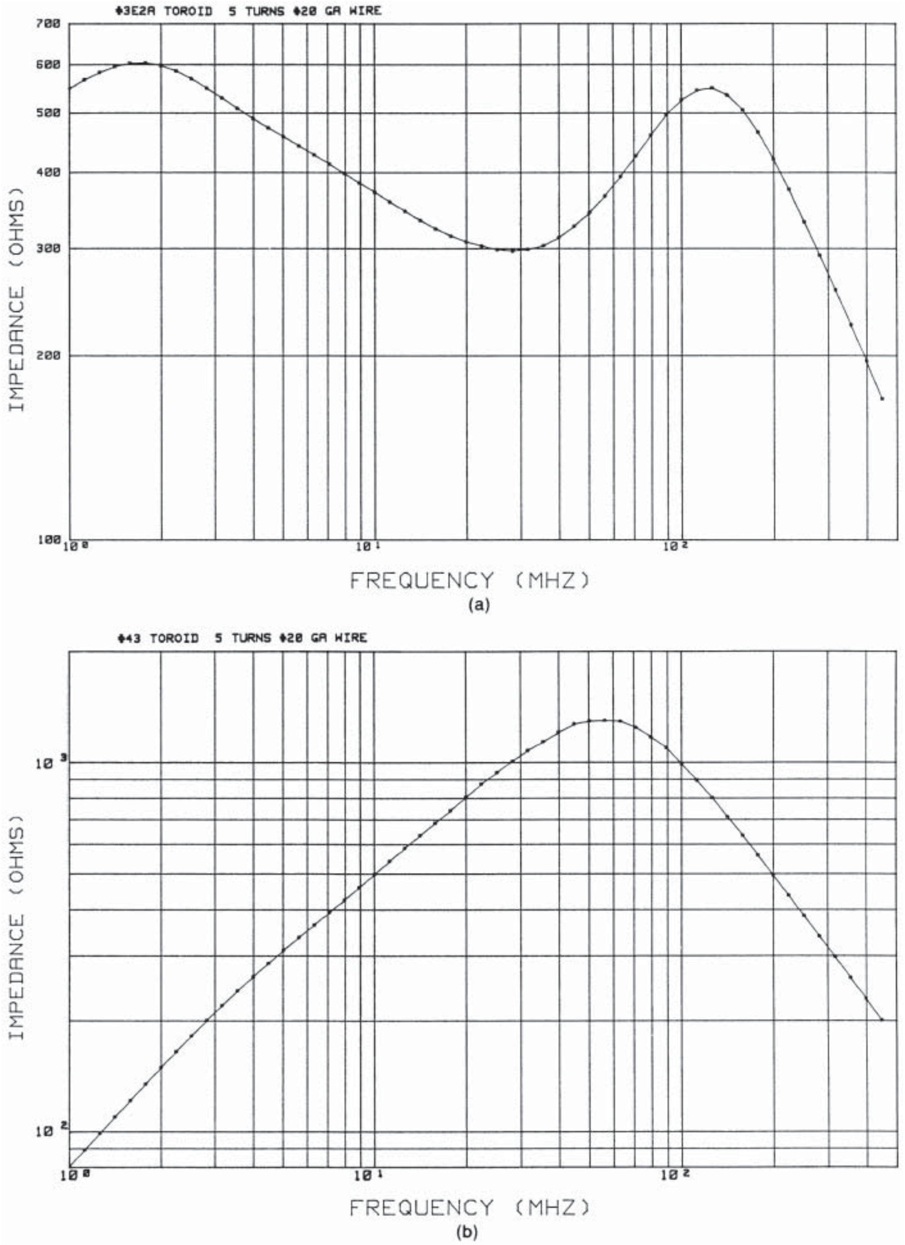

FIGURE 5.27 Measured impedances of inductors formed by winding 5 turns of 28-gauge wire on (a) MnZn and (b) NiZn cores.

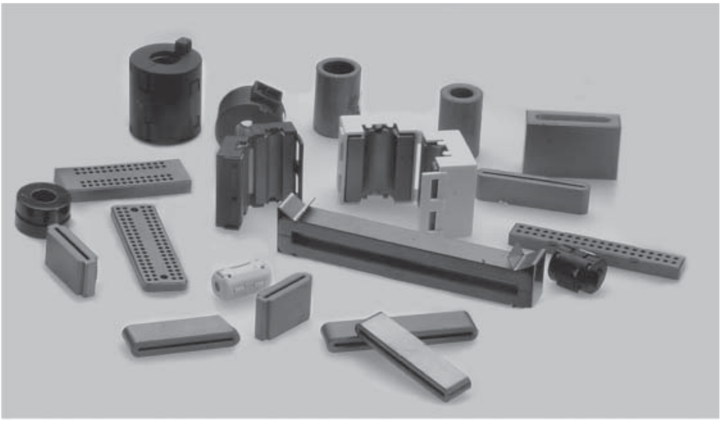

FIGURE 5.28 Photos of various configurations of ferrites for various applications. Source: Courtesy of G-MAG, Inc.

point. Manufacturers of ferrite core materials have their individual mix of materials they use to fabricate the ferrite material. However, ferrites typically are predominantly either of manganese zinc (MnZn) or nickel zinc (NiZn). Manganese zinc ferrites tend to have the high initial permeabilities, *but* their permeabilities deteriorate more rapidly with increasing frequency than do nickel zinc ferrites. Therefore, although a ferrite core having a large initial permeability may seem more attractive than one with a lower value, it should be remembered that in the range of the radiated emission limit (30 MHz–40 GHz) the core having the lower initial permeability may well have the higher permeability of the two and is therefore preferred for use in suppressing the spectral components of currents in this frequency range. Typical EMC laboratories have specific cores to be used for conducted emission suppression and others to be used for radiated emission suppression because of these considerations.

In order to illustrate this frequency dependence, we have shown the frequency response of the impedance of an inductor formed by winding 5 turns of 20-gauge wire on two toroids in Fig. 5.27. Figure 5.27a shows the impedance for a typical MnZn core, while Fig. 5.27b shows the impedance for a typical NiZn core. Note that the MnZn core shows an impedance of some 500 Ω at 1 MHz, whereas the NiZn core shows an impedance of some 80 Ω at 1 MHz. However, at a frequency of 60 MHz, the MnZn core shows an impedance of 380 Ω, whereas the NiZn core shows an impedance of 1200 Ω! This illustrates that the type of core to be used depends on the frequency of application (suppression of conducted emissions or radiated emissions). Unless one is careful to catalog the cores in the inventory such as by painting them with different colors, the proper selection can be difficult.

Figure 5.28 shows photographs of various configurations of ferrite cores. These are available to clamp around round cables such as video cables or ribbon and flat-pack cables.

5.8 FERRITE BEADS

Ferrite materials are basically nonconductive ceramic materials that differ from other ferromagnetic materials such as iron in that they have low eddy-current losses at frequencies up to hundreds of megahertz. Thus they can be used to provide selective attenuation of high-frequency signals that we may wish to suppress from the standpoint of EMC and not effect the more important lower-frequency components of the functional signal. These materials are available in various forms.

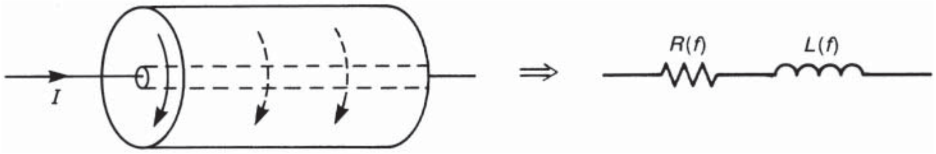

FIGURE 5.29 A ferrite bead.

The most common form is a *bead* as shown in Fig. 5.29. The ferrite material is formed around a wire, so that the device resembles an ordinary resistor (a black one without bands). It can be inserted in series with a wire or land and provide a high-frequency impedance in that conductor.

The current passing along the wire produces magnetic flux in the circumferential direction, as we observed previously. This flux passes through the bead material, producing an internal inductance in much the same way as for a wire considered in Section 5.1.1. Thus the inductance is proportional to the permeability of the bead material: $L_{\text{bead}} = \mu_0 \mu_r K$, where K is some constant depending on the bead dimensions. The bead material is characterized by a complex relative permeability as

$$\mu_r = \mu_r'(f) - j\mu_r''(f) \tag{5.27}$$

The real part μ_r' is related to the stored magnetic energy in the bead material, while the imaginary part μ_r'' is related to the losses in the bead material. Both are shown as being functions of frequency. Substituting this into the general equation for the impedance of the bead inductance gives

$$\begin{aligned} j\omega L_{\text{bead}} &= j\omega\mu_0\mu_r K \\ &= j\omega\mu_0(\mu_r' - j\mu_r'')K \\ &= \underbrace{\omega\mu_r''(f)\mu_0 K}_{R(f)} + \underbrace{j\omega\mu_r'(f)\mu_0 K}_{L(f)} \end{aligned} \tag{5.28}$$

From this result we see that the equivalent circuit consists of a resistance that is dependent on frequency in series with an inductance that is also dependent on frequency. Typical ferrite beads can be expected to give impedances of order 100 Ω above approximately 100 MHz. *Multiple-hole* ferrite beads as illustrated in Fig. 5.30 can be used to increase this high-frequency impedance. The measured impedances of a 1/2-turn (a bead surrounding a wire) ferrite bead and a 2 1/2-turn ferrite bead from 1 to 500 MHz are shown in Fig. 5.31.

Because the impedance of ferrite beads is limited to several hundred ohms over the frequency range of their effectiveness, they are typically used in *low-impedance* circuits such as power supplies. They are also used to construct lossy filters. For example, placing a ferrite bead in series with a wire and placing a capacitor between the two wires will constitute a two-pole, lowpass filter. A series ferrite bead can also act to damp ringing in fast-rise time circuit. Ferrites are available in other forms. A more recent use has been in the placement of ferrite slabs under dual-in-line (DIP) packages. The ferrite slab has holes drilled along its edges that correspond to the pin spacings of the DIP package.

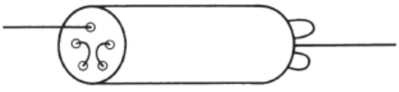

FIGURE 5.30 A multiturn ferrite bead.

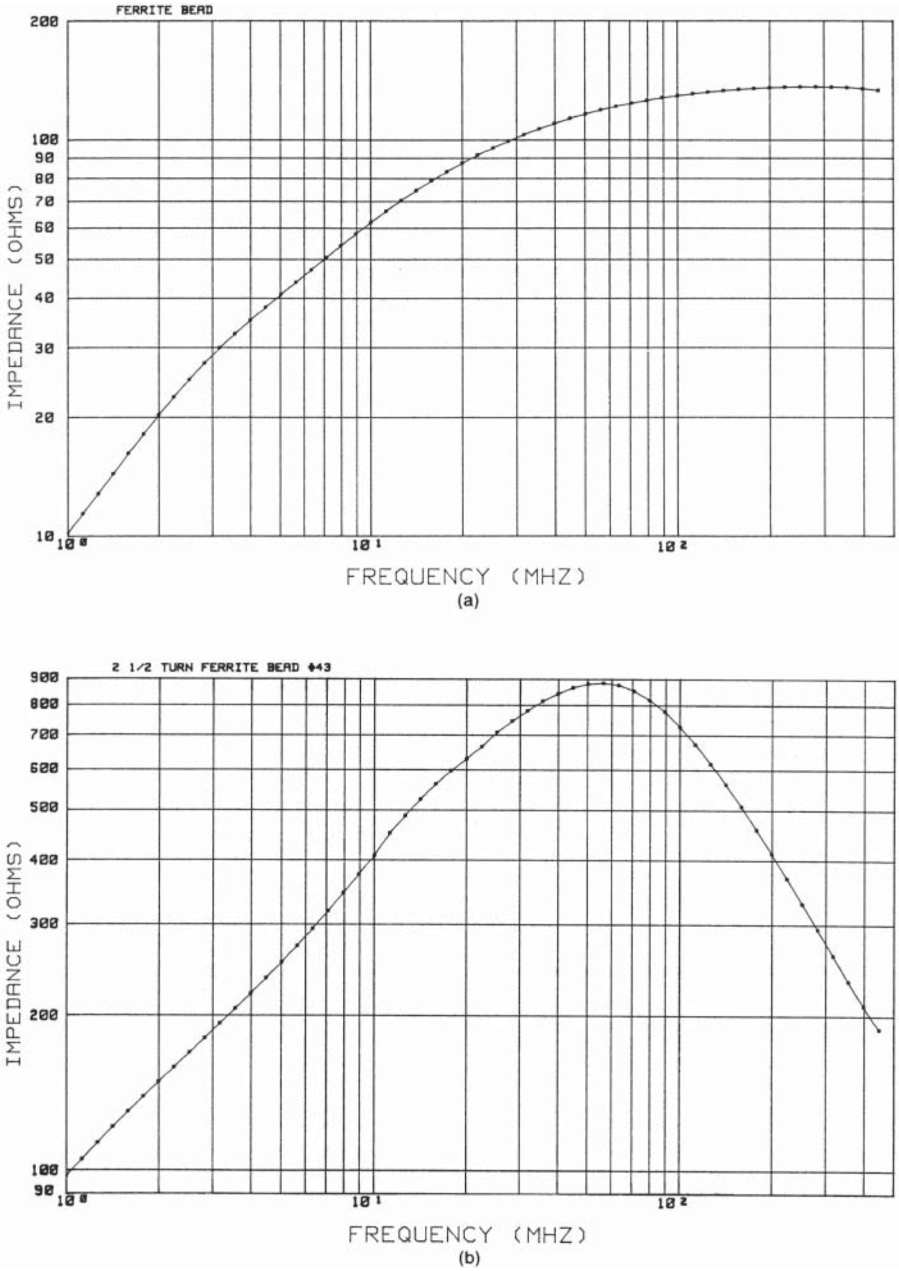

FIGURE 5.31 Measured impedances of (a) a 1/2-turn ferrite bead and (b) a 2 1/2 turn ferrite bead.

The pins of the DIP are placed through these holes and the combination inserted into a carrier or soldered directly to the PCB. An example of this use to damp very high-frequency oscillations is described in [8].

Ferrite beads are no different than other uses of ferrites in that they are susceptible to saturation when used in circuits that pass high-level, low-frequency currents. A ferrite bead placed in series with the 60 Hz power lead would probably be saturated by this high-level (1–10 A) current.

5.9 COMMON-MODE CHOKES

We now embark on a discussion of one of the most important topics affecting the radiated emissions of products, *common-mode* and *differential-mode currents*. Consider the pair of parallel conductors carrying currents $\hat{I}_1$ and $\hat{I}_2$, as shown in Fig. 5.32. We may *decompose* these two currents into two auxiliary currents, which we refer to as *differential-mode* $\hat{I}_D$ and *common-mode* $\hat{I}_C$:

$$\hat{I}_1 = \hat{I}_C + \hat{I}_D \tag{5.29a}$$

$$\hat{I}_2 = \hat{I}_C - \hat{I}_D \tag{5.29b}$$

Solving these two equations gives

$$\hat{I}_D = \frac{1}{2}(\hat{I}_1 - \hat{I}_2) \tag{5.30a}$$

$$\hat{I}_C = \frac{1}{2}(\hat{I}_1 + \hat{I}_2) \tag{5.30b}$$

The differential-mode currents $\hat{I}_D$ are equal in magnitude but oppositely directed in the two wires. These are the desired or functional currents. The common-mode currents $\hat{I}_C$ are equal in magnitude but are directed in the same direction. These are not intended to be present but will be present in practical systems. Standard lumped-circuit theory does not predict these common-mode currents. They are frequently referred to as *antenna-mode currents*.

Let us now investigate the significance of each current on the radiated emissions from this pair of conductors, which may be wires or lands on a PCB. This will be investigated in more detail in Chapter 8. For the present it suffices to give a general discussion. The radiated electric fields $\hat{E}$ due to each current can be superimposed to give the total radiated electric field. First consider the radiated fields due to differential-mode currents, as illustrated in Fig. 5.33a. The differential-mode currents are oppositely directed. Thus the resulting electric field will also be oppositely directed. However, since the two conductors are not collocated, the fields will not exactly cancel, but will subtract to give a small net radiated electric field. On the other hand, since the common-mode currents are directed in the same direction, their radiated field will add, giving a much larger contribution to the total radiated field than will the differential-mode currents, as is illustrated in Fig. 5.33b. Thus *a small common-mode current can produce the same level of radiated electric field as a much larger value of differential-mode current*. In short, *common-mode currents have a much higher potential for producing radiated emissions than do differential-mode currents*! We will find in Chapter 8 that *the predominant mechanisms for producing radiated electric fields in practical products are the common-mode currents on the conductors*! For example, we will find that microamperes of

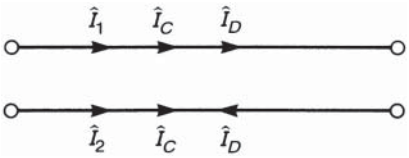

FIGURE 5.32 Decomposition of the currents on a two-wire transmission line into common mode $\hat{I}_C$ and differential-mode $\hat{I}_D$ components.

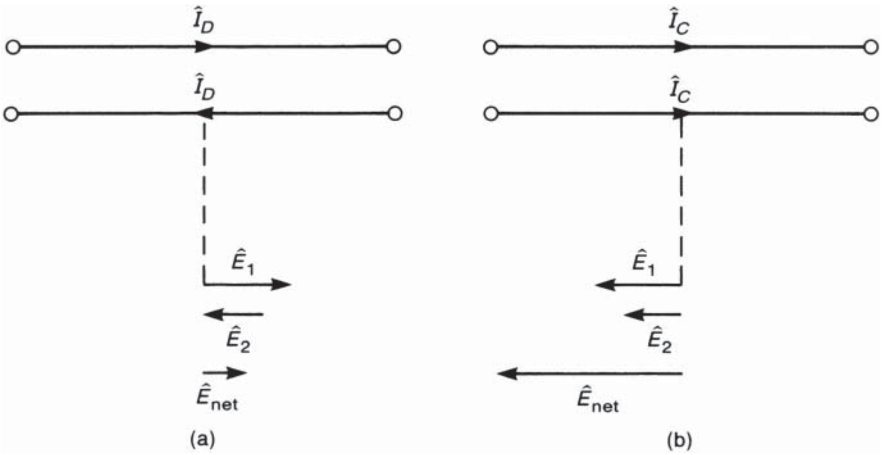

FIGURE 5.33 Illustration of the relative radiated emission potential of (a) differential-mode currents and (b) common-mode currents.

common-mode current will produce the same level of radiated electric field as tens of milliamperes of differential-mode current! Common-mode currents are not intended to be present on the conductors of an electronic system, but nevertheless are present in all practical systems. Because of their considerable potential for producing radiated electric fields, we must determine a method for reducing them.

One of the most effective methods for reducing common-mode currents is with *common-mode chokes*. A pair of wires carrying currents $\hat{I}_1$ and $\hat{I}_2$ are wound around a ferromagnetic core as shown in Fig. 5.36a. Note the directions of the windings. The equivalent circuit is also shown. Here we assume that the windings are identical, such that $L_1 = L_2 = L$. In order to investigate the effect of the core on blocking the common-mode current, we calculate the impedance of one winding:

$$\hat{Z}_1 = \frac{\hat{V}_1}{\hat{I}_1} = \frac{pL\hat{I}_1 + pM\hat{I}_2}{\hat{I}_1} \tag{5.31}$$

Now let us investigate the contribution to the series impedance due to each component of the current. First let us consider common-mode currents in which $\hat{I}_1 = \hat{I}_C$ and $\hat{I}_2 = \hat{I}_C$. Substituting into (5.31) gives

$$\hat{Z}_{CM} = p(L + M) \tag{5.32}$$

The contribution to the series impedance due to differential-mode currents where $\bar{I}_1 = \bar{I}_D$ and $\bar{I}_2 = -\bar{I}_D$ is

$$\bar{Z}_{DM} = p(L - M) \tag{5.33}$$

If the windings are symmetric and all the flux remains in the core, i.e., the flux of one winding completely links the other winding, then $L = M$ and $\hat{Z}_{DM} = 0$! Thus in the ideal case where $L = M$ *a common-mode choke has no effect on differential-mode currents, but selectively places an inductance (impedance)* $2L$ *in series with the two conductors to common-mode currents*. These notions are illustrated in Fig. 5.34.

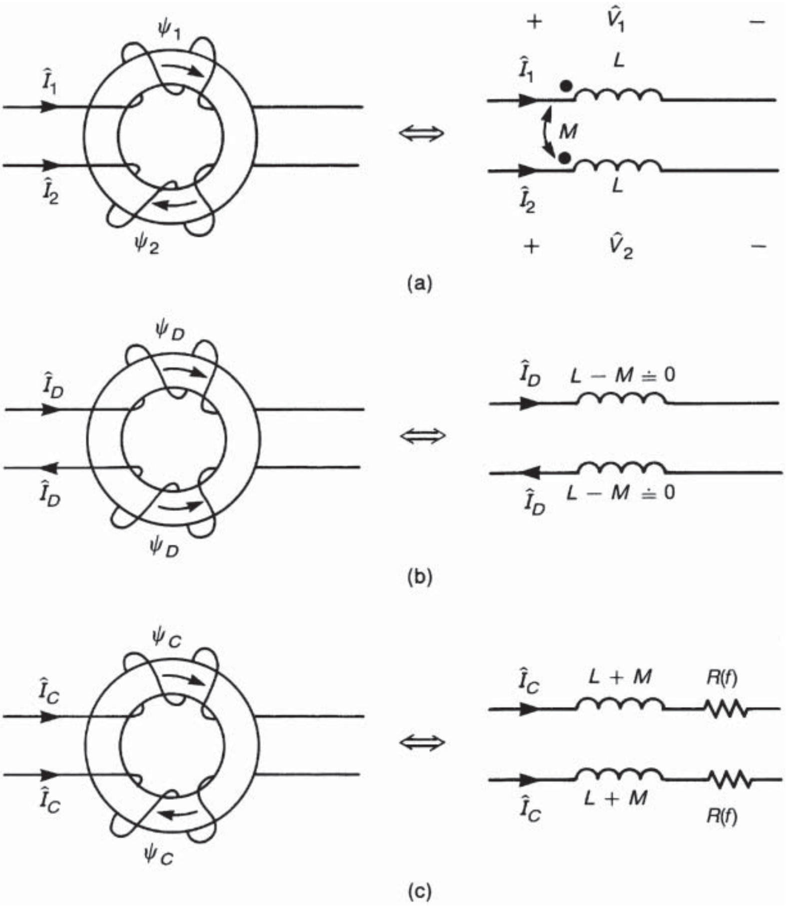

FIGURE 5.34 Modeling the effect of a common-mode choke on (a) the currents of a two-wire line, (b) the differential-mode components, and (c) the common-mode components

In addition to selectively placing inductors $L + M$ in series with the common-mode currents, use of ferrite cores places a frequency-dependent resistance, $R(f)$, in series with the common-mode currents as well. This resistance becomes dominant at the higher frequencies as was the case for a ferrite bead in the previous section. Hence common-mode currents not only are blocked but also have their energy dissipated in the $R(f)$.

Thus common-mode chokes can be effective in blocking and dissipating common-mode currents. In order to provide this impedance to common-mode currents, the wires must be wound around the core such that the fluxes due to the two common-mode currents *add* in the core whereas the fluxes due to the two differential-mode currents *subtract* in the core. Whether the wires have been wound properly can be checked with the *right-hand rule*, where, if one places the thumb of one's right hand in the direction of the current, the fingers will point in the resulting direction of the flux produced by that current. A foolproof way of winding two wires (or any number of wires) on a core to produce this effect is to wind the entire group around the core as illustrated in Fig. 5.35a. In either case one should ensure that the wires entering the winding and those exiting the winding are separated from each other on the core, or else the parasitic capacitance between the input and output will shunt the core and reduce its effectiveness, as illustrated in Fig. 5.35b.

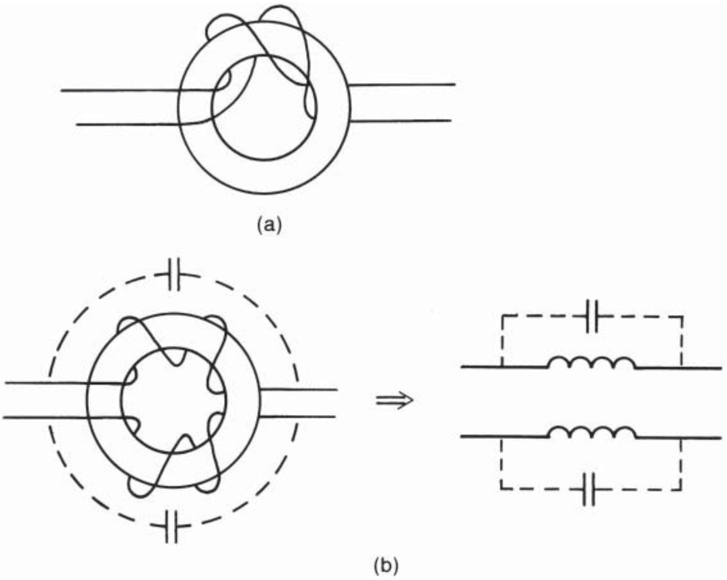

FIGURE 5.35 (a) A simple way of winding a common-mode choke; (b) parasitic capacitance.

The effectiveness of the common-mode choke relied on the assumption that the self and mutual inductances are equal, $L = M$. High-permeability cores tend to concentrate the flux in the core and reduce any leakage flux. Symmetric windings also aid in producing this. Unfortunately, ferromagnetic materials suffer from *saturation* effects at high currents, as discussed earlier, and their permeabilities tend to deteriorate with increasing frequency more than low-permeability cores. One of the most important advantages of the common-mode choke is that *fluxes due to high differential-mode currents cancel in the core and do not saturate it.* The functional or differential-mode currents $\hat{I}_D$ are the desired currents and are usually large in magnitude. If the flux due to these high-level currents did not cancel in the core, the core would tend to saturate, and the high permeability would be lost. Thus more of the flux would leak out into the surrounding air, and the self and mutual inductances would not be approximately equal. Furthermore, since the differential-mode fluxes cancel in the core, the choke does not (ideally) affect the functional signal as do the other suppression components discussed previously. So *the functional signals are not (ideally) affected by the presence of the choke, and also do not affect the performance of the choke*.

5.10 ELECTROMECHANICAL DEVICES

A number of electronic products such as typewriters, printers, and robotic devices use small electromechanical devices such as dc motors, stepper motors, ac motors, and solenoids to translate electrical energy into mechanical motion. These seemingly innocuous (from an EMC standpoint) devices can create significant EMC problems. DC motors create high-frequency spectra due to arcing at the brushes as well as providing paths for common-mode currents through their frames. The purpose of this section is to highlight these problem areas and increase the awareness of the reader for their potential to create EMC problems.

5.10.1 DC Motors

DC motors are used to produce rotational motion, which can be used to produce translational motion using gears or belts. They rely on the property of magnetic north and south poles to attract and like poles to repel. A dc motor consists of stationary windings or coils on the *stator*, along with coils attached to the rotating member or *rotor*, as illustrated in Fig. 5.36a. The coils are wound on metallic protrusions, and a dc current is passed through the windings, creating magnetic poles. A commutator consists of metallic segments that are segmented such that the dc current to the rotor windings can be applied to the appropriate coils to cause the rotor to align with or repel the stator poles as the rotor rotates. Carbon brushes make contact with the rotor segments and provide a means of alternating the current and magnetic fields of the rotor poles using a dc current from a source, as illustrated in Fig. 5.36b. As the current to the rotor coils is connected and disconnected to the dc source through the commutator segments, arcing at the brushes is created as a result of the periodic interruption of the current in the rotor coils (inductors). This arcing has a very high-frequency spectral content, as we saw in Chapter 3. This spectral content tends to create radiated emission problems in the radiated emission regulatory limit frequency range between 200 MHz and 1 GHz, depending on the motor type. In order to suppress this arcing, resistors or capacitors may be placed across the commutator segments as illustrated in Fig. 5.36c. These can be implemented in the form of capacitor or resistor disks that are segmented disks of capacitors or resistors attached directly to the commutator

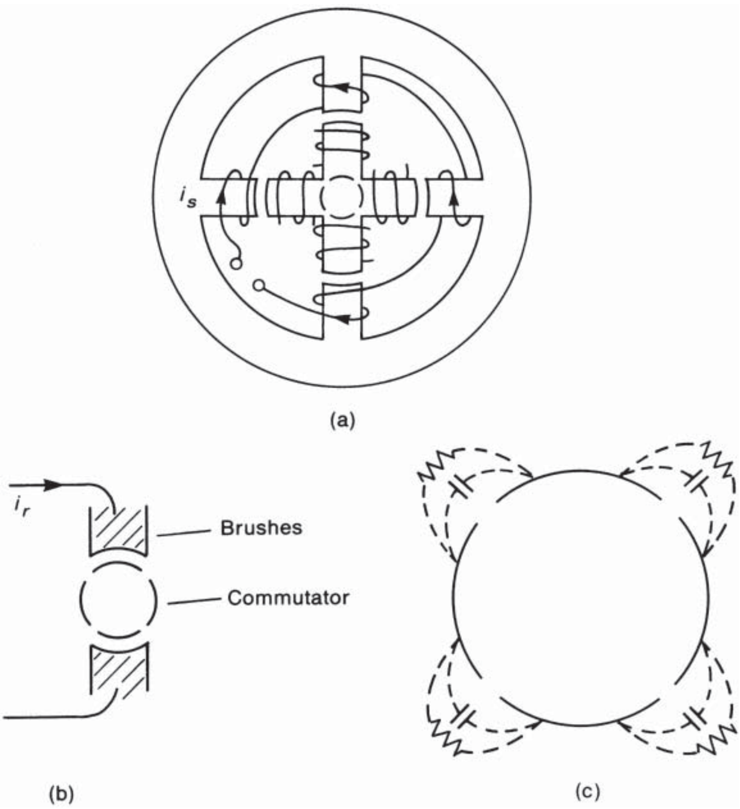

FIGURE 5.36 A dc motor illustrating (a) physical construction, (b) brushes and commutator, and (c) arc suppression elements.

or in resistive ring placed around the commutator. In some cases it may be necessary to insert small inductors in the dc leads to block those noise currents that are not completely suppressed by the capacitor or resistor disks.

An additional source of high-frequency noise and associated radiated and conducted emission comes not from the motors themselves but from the *driver circuits* that are used to change the direction of rotation to provide precise position control of the motor. A typical "H-drive" circuit for a small dc motor is illustrated in Fig. 5.37a. When transistors T_1 and T_1' are turned on, current flows through the commutator and the rotor windings, causing the rotor to turn in one direction. When these are turned off and transistors T_2 and T_2' are turned on, the rotor turns in the opposite direction. This driver circuit is usually connected to the motor via a long pair of wires as shown in Fig. 5.37b. For reasons of thermal cooling of the motor, its housing is usually attached to the metallic frame of the product, which acts as a heat sink. This produces a large capacitance C_{par} between the motor housing and the product frame. This provides a path for *common-mode currents* to pass through the connection wires from the rotor to the stator via capacitance between these windings, and eventually

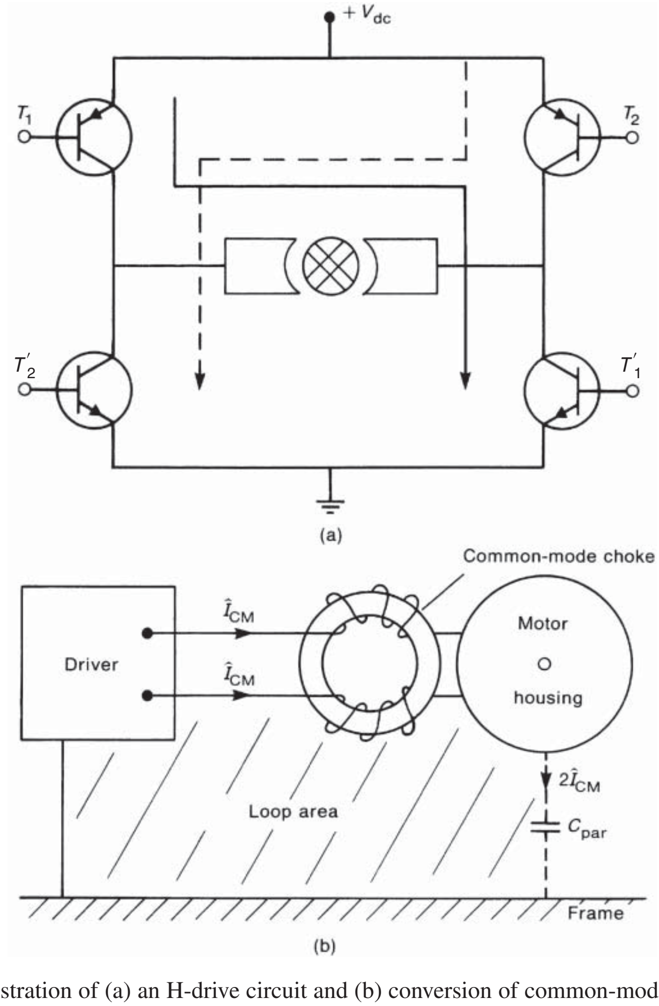

FIGURE 5.37 Illustration of (a) an H-drive circuit and (b) conversion of common-mode driver currents into differential-mode currents with a large loop area because of parasitic capacitance to the motor frame.

to the frame via C_{par}. The current provided to the motor by the driver, although ideally intended to be dc, typically has fast-rise time spikes present on it due to the constant interruption of the current in the driver circuit and in the rotor coils by the commutator. These spikes have very high-frequency spectral content, which is then placed on the product frame and is coupled to other parts of the product radiating in the process. The loop area formed by the leads and their return path (the product frame) also tends to be quite large. We will find in Chapter 8 that the radiation potential tends to be a direct function of the loop area occupied by that current; the larger the loop area, the larger the radiated emission. In order to block this common-mode current, a common-mode choke may be needed to be placed in the driver leads, as is illustrated in Fig. 5.37b. This shows a case where common-mode current (in the driver leads) becomes essentially a differential-mode current flowing around a large loop area. Measured common-mode impedances between the input wires (tied together) and the motor frame for a small dc motor give an impedance null around 100 MHz of about 1 Ω.

5.10.2 Stepper Motors

An alternative to the dc motor for electromechanical positioning is the *stepper motor*. There are basically two types of stepper motors: *permanent magnet* (PM) and *variable reluctance* (VR). Both types have dc current applied to the stationary windings of the stator to produce magnetic poles. The stator and the rotor are segmented into a large number of poles around their peripheries in order to provide fine positioning. The rotor of the PM stepper is permanent magnet made of rare-earth materials. The rotor of the VR stepper consists of shorted turns of wire. Flux from the stator induces currents in these shorted turns, which induces magnetic poles on the rotor. The windings of the stator are arranged in phases to provide various degrees of magnetic pole segmentation. The rotor poles tend to align with those of the stator that are energized in order to reduce the *reluctance* of the magnetic path.

Although there is no arcing to generate high-frequency signals as with the commutator of the dc motor, there remains the problem of common-mode currents between the driver circuit wires and the frame of the motor, which is again attached to the frame of the product for cooling. A typical driver circuit is shown in Fig. 5.38. Turning on transistors T_1 and T_4, for example, causes current to flow through the windings of phase A and phase D in the indicated direction, causing the motor to rotate to one desired position. Constant energization and de-energization of these stator windings again causes high-frequency noise to be passed down the connection wiring. As with other motors, parasitic capacitance exists between the input wires and the motor frame, which is attached to the product frame for thermal reasons. Thus the noise currents on the input wires are placed on the frame of the product and return to the driver via that path. This creates the same problem that was observed for dc motors and may require that a common-mode choke be placed in the driver wires in order to block this path and reduce the radiated emissions of this common-mode current (which becomes a differential-mode current by passing through the large loop created by the driver wires–ground plane circuit). Measurements of the common-mode impedance between the input wires (tied together) and the motor frame for a typical small stepper motor show a null around 70 MHz of some 3 Ω!

5.10.3 AC Motors

AC motors are seldom used to provide positioning of mechanical elements as are dc and stepper motors, but rather are used to provide constant speed and drive small cooling fans. The absence of brushes and the attendant arcing as with dc motors and the noise currents provided by the drivers of both dc and stepper motors tends to diminish the potential of these motors for creating noise problems as opposed to dc or stepper motors. However, because the rotor and stator of these motors

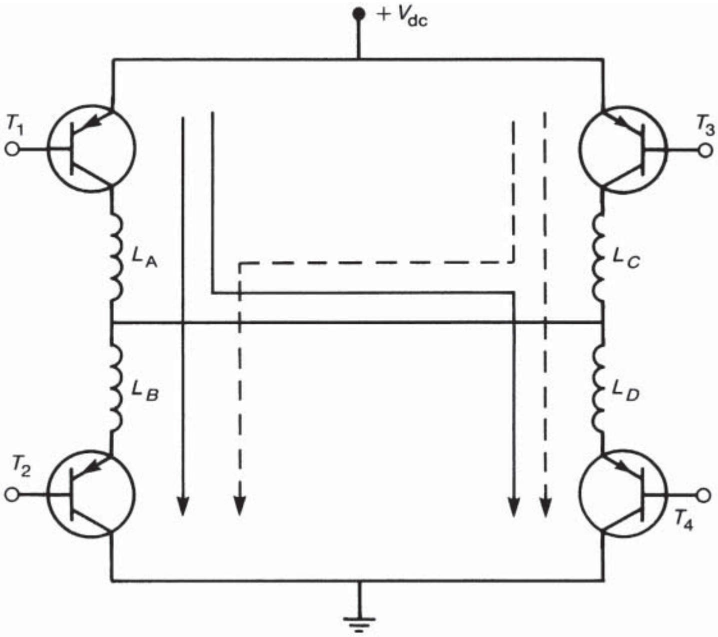

FIGURE 5.38 A typical driver circuit for a stepper motor.

consist of closely spaced inductors, there remains the problem of large parasitic capacitance between the rotor and the stator. If the motor frame is mechanically attached to other mechanical parts of the product, then the potential exists for coupling common-mode currents from the ac power source to the product frame and vice versa. If high-frequency noise is present on the ac waveform feeding these motors or the frame to which the stator is attached, then it is likely that this noise will be coupled to the product frame or to the ac power cord, where its potential for radiated or conducted emissions will usually be enhanced. Chopper drivers are frequently used to control the power to the ac motors. Thus the input current may have a high-frequency spectral content which is transferred via common mode to the product frame. Common-mode chokes in the attachment leads of these types of motors may be needed in order to block this path.

5.10.4 Solenoids

A *solenoid* is essentially a coil of wire with a ferromagnetic slug at its center. Energizing the coil with a dc current causes a magnetic flux to be generated. The ferromagnetic slug tends to move to the center of the coil in a translational fashion in order to minimize the reluctance of the magnetic path. These types of electromechanical devices suffer from many of the problems of the abovementioned motors with the exception of commutation. Sudden energization and de-energization of the winding inductance creates high-frequency noise. Once again, the parasitic capacitance between the windings and the metallic housing of the solenoid creates a potential path for common-mode currents to be placed on the frame of the product, which may require a common-mode choke in the input leads. Measurement of the common-mode impedance between the input wires (tied together) and the solenoid frame for a small solenoid indicate a null at around 150 MHz of 8 Ω!

5.11 DIGITAL CIRCUIT DEVICES

Digital products are very popular today because of their ability to rapidly process data and their inherent noise immunity. However, these attributes pose problems for an EMC standpoint. Data are transmitted and processed in the form of pulses. The transitions between each state (the pulse rise/falltimes) tend to be extraordinarily fast (of order 1 ns). We saw in Chapter 3 that these fast transition times tend to generate high-frequency spectral content in the frequency-domain representation of these signals, which contributes to the high-frequency radiated and conducted emissions of the product. The requirement for increased speeds of data transmission and processing will no doubt cause these EMC concerns to increase in digital products in the future.

Digital products are relatively simple in architecture and typically consist of a central processor in the form of a microprocessor, which performs computation, stores and retrieves data and instructions, and provides sequencing of the entire processes. Various read-only-memory (ROM) modules provide nonvolatile storage of program instructions. Random-access-memory (RAM) modules provide for storage of data, and various drivers or buffers provide the ability to drive peripheral devices or communicate data. One or more *system clocks* provide synchronization of the occurrence of each task within well-defined windows of time. The primary task is to input data and instructions either from external devices such as tape or disk drives or from keyboards and to process this and provide the results as output to displays or signals to drive external processes such as motors or other actuators.

The process seems relatively straightforward from the standpoint of its effect on the EMC profile of the product. However, the subtle aspects of the process have considerable impact. For example, the particular technology and requirements of the product affect the rise/falltime of the clock and data pulses, which affect their high-frequency spectral content. Buffer gates are frequently provided to interface between low-current logic signals and high-current outputs. These have the effect of "squaring up" the signals. Suppose the rise/falltimes of a clock signal have been slowed by the insertion of a lowpass filter such as a shunt capacitor. If a buffer gate has been inserted at some point further down the line, the signal may be "squared up" and have current drive added, thus increasing its high-frequency spectral content.

Conductors that are intended to carry only "rare event" signals that only occur infrequently should not be overlooked since, *although they are not intended to carry high-frequency signals, they may have these present as a result of inadvertent coupling to these lines*. For example, the reset line of a microprocessor may be active only infrequently during machine operation. However, inadvertent coupling of other high-frequency signals to this line can cause very high-frequency signals to be present on this line. If the reset line is routed a long distance around the PCB, it may cause significant radiated emissions, which the EMC engineer may not suspect as being the source of the emissions. It is particularly instructive to probe points on a PCB of a digital product and observe the spectral content of the signals. Virtually all signal lines in a digital product should be suspect with regard to carrying high-frequency signals, although some (such as clock lands) are clearly of more importance. It is this author's experience that the most effective method of reducing radiated and conducted emissions is to affect the source of these emissions. Although this is a seemingly obvious point, it is nevertheless important to keep in mind. Once noise signals are allowed to propagate away from their source, their suppression becomes a problem of suppressing the emanation of the same signal from different points of emission resulting in the need for many more suppression elements.

The active digital components are composed of large number of semiconductor diodes, bipolar junction transistors (BJTs), and field-effect transistors (FETs). These are implemented in integrated circuit form on minute chips. One of the primary parasitic components of these elements that is of concern in EMC is the *parasitic capacitances* formed at the semiconductor junctions [9]. Each of these elements is formed from two types of semiconductor, *n*-type and *p*-type. This junction causes a separation of charge which acts like a capacitance. Once these parasitic capacitances are added to the ideal model of the device, it becomes clear that rise/falltimes of signals will be affected. Of more importance is the effect of these parasitic capacitances in *routing signals around the element*, in effect providing a direct connection at high frequencies from the input of the device to its output.

5.12 EFFECT OF COMPONENT VARIABILITY

It is very important to remember that it will always be required to produce a large number of supposedly identical copies of a product for sale. It is important and relatively simple to produce identical products from a functional standpoint; that is, all products are able to meet the functional performance design goals. This has always been and will continue to be an important criterion in the design process. However, consistency in achieving the EMC design goals among supposedly identical copies of a product is another matter that is not generally assured by achieving consistency in meeting the functional performance design goals. For example, suppose a product prototype is "fine-tuned" to meet the EMC regulatory limits on radiated and conducted emissions. Once the product is placed in production and a large number of copies are made, it is not assured that all of these "copies" will also meet EMC regulatory limits, which require that *all units that are sold must comply*. Changes in parts vendors to reduce product cost can cause a product that previously was in compliance to suddenly be out of compliance, even though it continues to meet the functional performance objectives. One also must realize that the functional performance goals and the EMC performance goals are often in conflict. For example, functional designers are generally concerned about the *maximum rise/falltimes of a digital component*, whereas EMC designers are more concerned about the *minimum rise/falltimes of the digital component* since the shorter the rise/falltime, the larger the high-frequency spectral content of the signal. Manufacturers of components cannot guarantee absolute conformance to specifications of their components, but instead specify bounds. A digital component manufacturer may guarantee maximum rise/falltimes of his/her component for functional performance reasons. A large quantity of these parts used to produce "identical copies" of the product may (and usually do) exhibit variations that, although within the bounds specified by the part manufacturer, may exceed the bounds that are being relied on by the EMC engineer and cause one or more of the "copies" to be out of compliance.

Changing parts vendors to reduce cost at some point in the production cycle of the product can create compliance problems. An example is illustrated in [10]. An RS-232 line driver was tested for this type of variability. Several "equivalent" line drivers from different vendors were tested, and the spectrum present on the −12 Vdc lead to each component was measured over the frequency range of 10–210 MHz. The reader is referred to that publication, which shows extreme variability in the emission present on the −12 V lead from vendor to vendor and within parts of the same vendor. All parts would no doubt meet the functional performance goals. Also observe that the −12 V lead of the line driver "is not supposed to carry these high-frequency signals," but does in fact have these present. This again illustrates that *just because a conductor is not intended to carry high- frequency signals does not rule out the presence of high-frequency signals on that conductor.*

5.13 MECHANICAL SWITCHES

Mechanical switches are often used in electronic products to provide the operator with a quick and easy way of changing the product behavior. On–off switches connect commercial power to the product. Other switches may simply provide a change in the status of the product, for example a reset switch on a personal computer. The EMC problems that may result from the activation of mechanical switches are quite varied and depend strongly on the load that is switched. Arcing at the contacts is the primary interference problem since the arc waveform may contain very high-frequency spectral components of large magnitude, as we will see. Early investigations concerned the interruption of large currents by circuit breakers in power systems [11]. In the early 1940s work concentrated on the behavior of switches in telephone circuits with regard to erosion of the switch contacts as well as the interference produced by these operations [12–16]. In order to subdue this potential interference problem and to ensure longer life for the switch contacts, various protection networks are often used.

In this final section we will discuss the EMC aspects of mechanical switches. The discussion will be brief but will cover the essential points. For a more complete and thorough discussion of the subject the author recommends the text by Ott [6] as well as [11–16]. These references contain virtually all the information one needs to know about mechanical switches from the standpoint of EMC. The following is a condensed summary of that information.

5.13.1 Arcing at Switch Contacts

It has been known from before the days of the Marconi spark-gap transmitter that current in the form of an arc can be conducted between two electrodes that are immersed in air. For example, consider two contacts separated a distance *d* in air shown in Fig. 5.39. The typical voltage–current characteristic is shown. There are three regions shown: the Townsend discharge region named for its discoverer, the glow discharge region, and the arc discharge region. The various voltage levels are denoted as V_B, V_G, and V_A. Typical values for these variables for contacts in air are $V_B \cong 320$ V, $V_G \cong 280$ V, and $V_A \cong 12$ V. The value of V_B depends on contact separation, while that of V_A depends

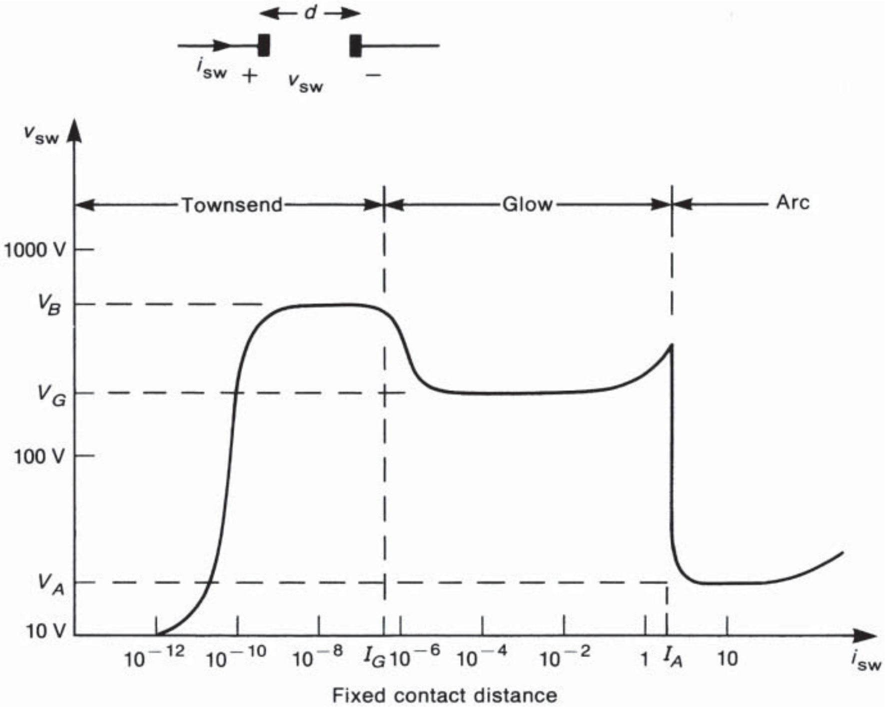

FIGURE 5.39 Illustration of the voltage–current characteristic of arcing at mechanical contacts.

on the contact material. The currents at the transition regions are denoted as I_G and I_A. These are quite variable but are of order $I_G \cong 1 - 100$ mA and $I_A \cong 0.1 - 1$ A.

There are always a few free electrons in the space between the contacts due to cosmic radiation, photon collisions with the gas molecules, etc. As the voltage between the two contacts is increased, the resulting electric field between the contacts accelerates these free electrons, causing them to strike neutral gas molecules. If the free electrons have sufficient kinetic energy imparted by the electric field, they strike the gas molecules, creating additional free electrons as electron–ion pairs. The field accelerates these newly formed electrons, causing them to strike other gas molecules and thereby releasing more free electrons. This produces a multiplicative production of free electrons and positive ions. The positive ions move toward the cathode (the negative terminal of the contact) and the electrons move toward the anode (the positive terminal of the contact). As the positive ions move toward the cathode, they create a space charge around it that increases the local field and the production of free electrons. The positive ions also strike the cathode, liberating more free electrons by secondary emission. This mechanism characterizes the Townsend discharge region of Fig. 5.39. Thermionic heating of the cathode can also liberate electrons, but this mechanism tends to predominate at the higher currents of the arc discharge region. In the early, low-current region all of the electrons emitted at the cathode are collected by the anode. Above a certain voltage level all electrons emitted by the cathode are collected, independently of further increases in voltage, and the curve rises vertically. At still higher voltages the electrons acquire sufficient kinetic energy to create electron–ion pairs in their collisions with the gas molecules, thereby increasing the free electrons and resulting in an avalanche effect. The peak or *breakdown* voltage V_B is dependent on the gas, contact separation and pressure. Paschen found that the breakdown voltage was dependent on the product of the pressure and the contact separation distance as [11]

$$V_B = \frac{K_1 pd}{K_2 + \ln pd} \tag{5.34}$$

where K_1 and K_2 are constants that depend on the gas. For air at standard atmospheric pressure the minimum breakdown voltage is approximately $V_{B,\min} \cong 320$ V and occurs at a contact separation $d_{\min} = 0.3$ mils $= 0.00762$ mm.

At the peak of the Townsend discharge region the production of free electrons and positive ions reaches a self-sustaining, *avalanche* stage wherein the current is sustained by this avalanching process but the voltage across the contacts drops to the lower *glow voltage* designated as V_G. For contacts in air at atmospheric pressure $V_G \cong 280$ V. A region near the cathode develops a faint glow, which is the origin of the term. The voltage drop across the switch remains constant at V_G for a large range of current and is primarily determined by the region between the cathode and the beginning of the glow region: the *cathode fall region*. As the current increases, the dimension of the glow region increases toward the anode, but the voltage drop across the gap remains at V_G.

When the current increases sufficiently such that the cathode fall region encompasses the entire cathode area, further current increases result in higher current density. This leads to heating of the cathode and a slight increase in gap voltage. A point is reached rather quickly where the heating causes vaporization of the contact metal, resulting in a rapid drop in contact voltage, which marks the beginning of the *arc discharge region* where an arc forms between the contacts. The contact voltage drops to a very low voltage of about $V_A \cong 12$ V. The value of V_A is determined by the contact material (since vaporization of the metal is the important process here) but is of about 11–16 V. Once the arc is initiated, a very luminous discharge results where further increases in current do not result in any appreciable change in the contact voltage from V_A. This is the usual visual effect one sees which contacts are opened and an arc forms momentarily.

The formation of an arc as discussed above was initiated by voltages large enough to cause breakdown of the intervening gas. The voltage across the contacts divided by the contact spacing exceeds the breakdown field strength of the gas. This is referred to as a *long arc*. For smaller contact spacings in a vacuum the arc can be initiated by a *field-induced emission* wherein the electric fields at the highest and sharpest points on the cathode liberate electrons. This electron stream fans out as it crosses the gap. Bombardment of the anode by this electron stream causes it to heat to several thousand kelvin, which is sufficient to vaporize the electrode. The cathode may vaporize first, depending on the contact sizes, rate of heating, etc. As the positive ions move toward the cathode, a space charge forms that further promotes the emission, resulting in an avalanche effect. Thus an arc may be formed where the voltage and contact spacing are not sufficient for a gas breakdown. This is referred to as a *short arc* or *metal–vapor arc discharge*. The required field strength is of order $E_B = 10^9$ V/m, although this varies, depending on the cleanliness of the contact surface and surface contaminants.

Figure 5.40 summarizes the breakdown voltage of a switch with air as the intervening medium. The plot is shown as a function of the contact separation distance d. Dividing the separation distance by the velocity of contact closure or opening v gives the axis as a function of time t. For small contact separations less than d_c a short arc may form if the contact voltage divided by the contact separation equals $E_B \cong 10^9$ V/m. The contact voltage drops to $V_A \cong 12$ V. The current through the switch is determined solely by the circuit voltage and impedance. However, a minimum current I_A is required to sustain the arc. This *minimum arc current* is quite variable, and ranges from tens of milliamperes to 1 A. *If the voltage across the contact available from the external circuit drops below V_A and/or the current through the contact available form the external circuit drops below I_A, the arc is extinguished.* For contact separations larger than d_c a glow discharge will form if the contact voltage exceeds the breakdown voltage, which is given by [12]

$$V_{B,\text{glow}} = 320 + 7 \times 10^6\, d \tag{5.35}$$

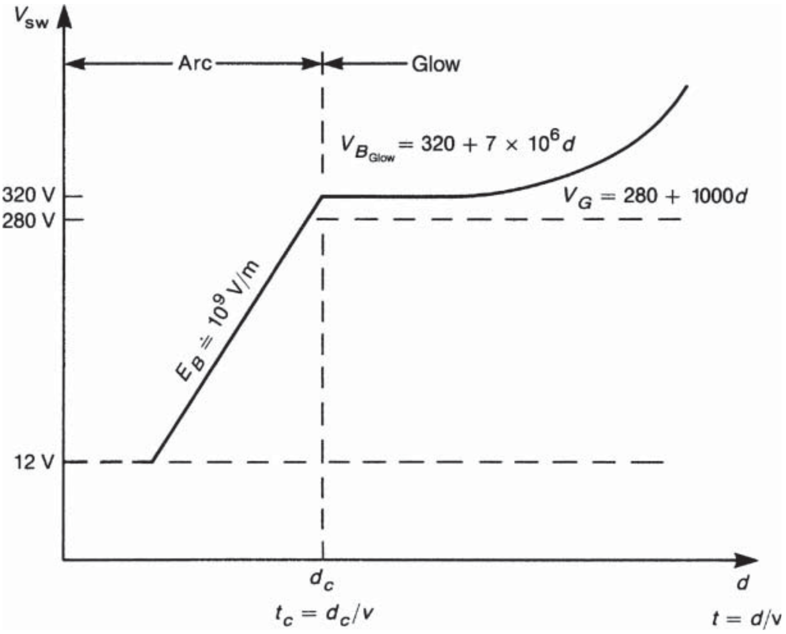

FIGURE 5.40 The breakdown voltage versus contact separation for a mechanical switch.

This is essentially the Paschen voltage curve for $d > d_{\text{min}}$. If the current available from the external circuit exceeds the *minimum glow discharge sustaining current* I_G, a glow discharge will form, and the contact voltage will drop to [12]

$$V_G = 280 + 1000d \tag{5.36}$$

If the current available from the circuit exceeds the minimum arc-sustaining current I_A, the glow discharge will transition to a *long arc*, and the contact voltage will again drop to $V_A \cong 12$ V. It must be reemphasized that, *in order to sustain a glow (arc) discharge, the voltage across and current through the contact that are available from the external circuit must exceed V_G and I_G (V_A and I_A)*. Again, the minimum sustaining voltages are rather predictable as $V_G \cong 280$ V and $V_A \cong 12$ V, whereas the minimum sustaining currents I_G and I_A are quite variable. Some representative ranges are $I_G \cong 1 - 100$ mA and $I_A \cong 100$ mA − A. *The glow discharge is characterized by large voltage and small current, whereas the arc discharge (long or short arc) is characterized by low voltage and large current.*

It is interesting to observe that, although the physics of the two processes are quite different, the arc discharge of a mechanical switch has characteristics very similar to the silicon-controlled rectifier (SCR). Consider the voltage–current characteristic of the switch shown in Fig. 5.39. If we plot this only for large currents above a few milliamperes, the characteristic resembles that of a SCR. In fact, the operation of the two are quite similar. In order to “fire” an SCR, the voltage must be increased to the breakover point. Once the SCR fires, its voltage drops to a low value and the current increases substantially. The SCR can be turned off only by reducing its current below the “hold on current.” The arc discharge of a mechanical switch is similar. In order to create an arc, the voltage across the switch must exceed the breakdown curve shown in Fig. 5.40. Once the arc forms, reducing the switch voltage cannot extinguish the arc (unless it is reduced below the arc voltage V_A). If the current is reduced below the minimum arcing current I_A, the arc will be extinguished!

5.13.2 The Showering Arc

Switches are frequently used to interrupt inductive loads such as solenoids or motors. Interruption of these types of loads leads to an interesting phenomenon known as the “showering arc,” illustrated in Fig. 5.41. The inevitable parasitic capacitance is shown in parallel with the inductive load. When the switch is closed, a steady-state current $I_L = (V_{\text{dc}}/R_L)$ is established in the inductor. When the switch opens, the inductor attempts to maintain this current. It is therefore diverted through the capacitance, charging the latter. The switch voltage $v_{\text{sw}}(t) = v_C(t) + V_{\text{dc}}$, and therefore increases. As this switch voltage increases, it may exceed the switch breakdown voltage, whereby a short arc forms and the switch voltage drops to V_A. The capacitor discharges through the switch, with the current being primarily limited by the local resistance and inductance of the switch wiring. If the switch current exceeds the minimum arc-sustaining current, the arc is sustained. If not, the arc is extinguished, and the capacitor begins to recharge. The switch voltage once again exceeds the switch breakdown voltage, and the switch voltage drops to V_A. If the arc is not sustainable, the capacitor begins to recharge once again. Eventually the energy stored initially is dissipated, and the capacitor voltage decays to zero, leaving $v_{\text{sw}} = V_{\text{dc}}$. This leads to a sequence of rising (as the capacitor charges) and rapidly falling (as the switch breaks down) voltages across the contacts, which has been referred to as the *showering arc* [15, 16]. As the contact separation increases, a glow discharge may develop and may or may not be sustainable, resulting in miniature showering arcs, as illustrated in Fig. 5.41. The number and duration of each showering arc depends on the circuit element values and any delays associated by interconnection transmission lines. A SPICE model useful for predicting the arcing at switches and associated crosstalk is described in [17].

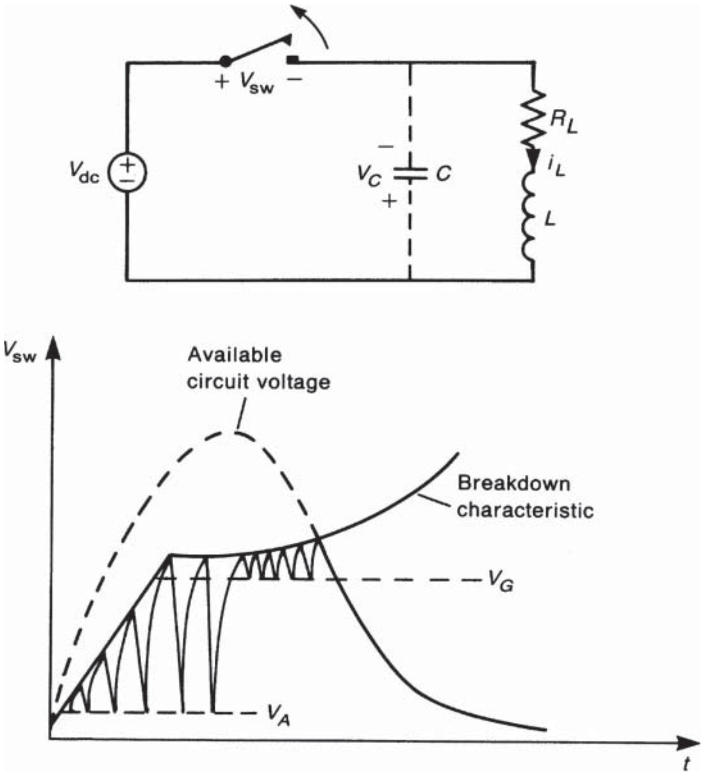

FIGURE 5.41 The showering arc for an inductive load.

5.13.3 Arc Suppression

Showering arcs clearly have significant spectral content and may therefore create EMC problems. The wiring carrying these currents may cause significant radiated emissions, thereby creating interference problems. These signals may also be directly conducted along interconnected wiring paths, creating a potentially more troublesome effect, since the signal levels that are directly conducted to other points will be of the order of the switch voltages, which may be several hundred volts. Since these potential effects are recognized, various suppression measures are usually employed in conjunction with a mechanical switch.

There are so many unknowns involved that it is difficult to make precise calculations. For example, velocity of switch closure or opening has a significant effect on the levels and duration of the showering arc. When the capacitor in Fig. 5.41 discharges through the switch, the discharge current is limited only by the impedance of the local wiring, which is quite small and substantially unknown and variable. Thus contact protection is usually based on simple calculations that reveal starting values to be used and then using an experimental test. In either event, the goal of contact protection is to *prevent the formation of an arc* (*sustained or showering*). Generally, either of two methods may be employed [6]: (1) prevent the switch voltage from exceeding the glow breakdown voltage of the switch (which is approximately 320 V), or (2) ensure that the arc current is below the minimum arc-sustaining current. Technique 1 prevents the arc from forming, while 2 prevents it from being sustained. There are two methods for implementing 1, as illustrated in Fig. 5.42. The contact breakdown voltage profile is plotted against the available circuit voltage (in the absence of breakdown). The slope of the arc breakdown characteristic, $d < d_c$, is obtained as the product of $E_B v$. Choosing

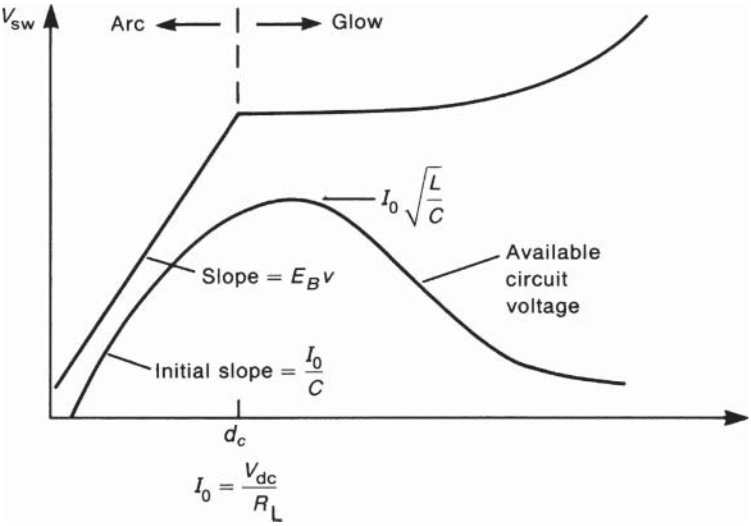

FIGURE 5.42 Contact protection by reducing the circuit available voltage.

$E_B = 10^8$ V/m and a typical switch velocity $v = 0.01$ m/s gives a slope of 1 V/μs. The initial slope of the available circuit voltage for the circuit of Fig. 5.41 can be shown to be I_0/C, where $I_0 = V_{dc}/R_L$ is the initial current through the inductor. Thus the initial rise of contact voltage should be kept below 1 V/μs, although this number is quite variable, depending on the contact surface (which affects E_B) and the contact approach velocity. The peak value of the available circuit voltage can be shown to be $I_0\sqrt{L/C}$ by neglecting the resistance R_L and assuming that all the energy stored in the inductor, $1/2LI_0^2$, is transferred to the capacitor, $1/2\,CV_{\text{peak}}^2$. In addition, the discharge waveform will be non-oscillatory (overdamped) if $\sqrt{L/C} < 1/2\,R_L$ [5]. Even though an arc discharge can be avoided by slowing the initial rise of the available circuit voltage, a glow discharge (which may transition to a long arc discharge) may develop if the peak available circuit voltage exceeds the gas discharge breakdown threshold. Therefore, in order to prevent initiation of an arc, the following two criteria should be satisfied:

$$(a)\quad E_Bv > \frac{V_{dc}}{R_LC}$$

$$(b)\quad \frac{V_{dc}}{R_L}\sqrt{\frac{L}{C}} < V_{B,\text{gas}} \cong 320\text{ V}$$

This can be implemented by placing a sufficiently large capacitor in parallel with the inductor or the switch to increase the net capacitance, thereby reducing the peak available circuit voltage and also reducing the initial rise of the available circuit voltage as shown in Fig. 5.43a. This scheme has a significant drawback in that contact damage during switch closure may be significant because of the large capacitor charging current. When the switch is open, the capacitor charges to the supply voltage V_{dc}. When the switch closes, this initial voltage discharges through the switch, which results in a large current surge through the switch.

Figure 5.43b shows how to remedy this problem caused by a single capacitor across the switch contact—place a resistor in series with the capacitor to limit the discharge current that occurs on contact closure. Limiting this discharge current on switch closure to below I_A gives the minimum value of the resistance. On contact opening, it is desirable to have the resistance as small as possible so as to not limit the arc suppression of the capacitor. The minimum value of R is chosen to limit the discharge current during switch closure to below the minimum arcing current: $V_{dc}/R < I_{A,\text{ min}}$.

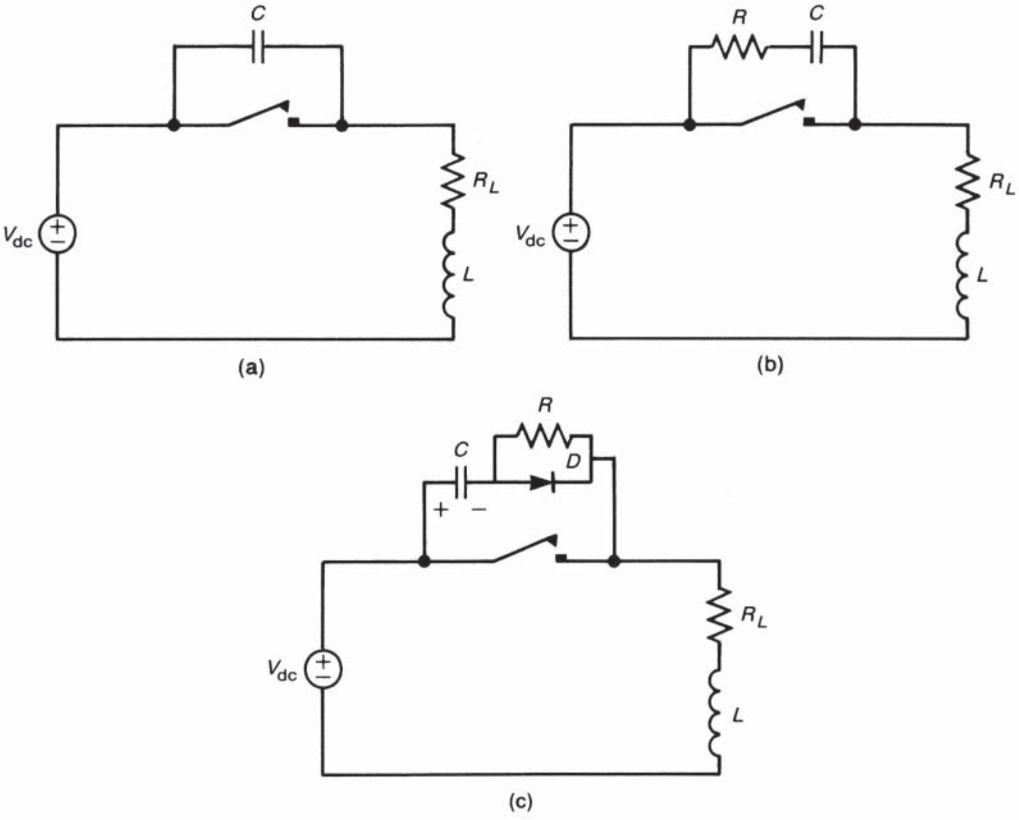

FIGURE 5.43 Various contact protection schemes: (a) capacitor; (b) *RC*, (c) *RC* with a diode. Source: Modified from Ott [6].

The maximum value is determined by the opening of the switch. When the switch opens, the current is diverted through the resistor, and the switch voltage is I_0R, where $I_0 = V_{dc}/R_L$ is the initial current through the inductor. Usually the maximum value of R is chosen to be equal to R_L in order to limit the contact voltage to at most the supply voltage. Therefore the limits on choice of R are [6]

$$\frac{V_{dc}}{I_{A,\min}} < R < R_L \tag{5.37}$$

The capacitor is chosen to satisfy the two criteria mentioned above: (1) the initial rate of voltage rise of the available circuit voltage, I_0/C, is less than 1 V/μs to avoid an arc forming; and (2) the peak available voltage, $I_0\sqrt{L/C}$, is less than 320 V to avoid a gas breakdown, which may transition to an arc. This leads to values C that must satisfy [6]

$$C \geq \left(\frac{1}{320}I_0\right)^2 L \tag{5.38a}$$

$$C \geq I_0 \times 10^{-6} \tag{5.38b}$$

A better but slightly more expensive network is shown in Fig. 5.43c [6]. A diode is placed across the resistor. While the switch is open, the capacitor charges up with polarity shown. When the switch closes, the resistor R limits the discharge current. When the switch opens, the diode shorts out the

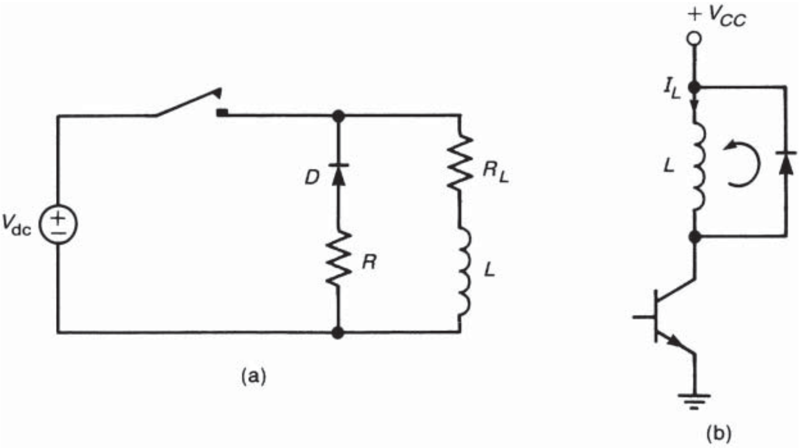

FIGURE 5.44 Diode protection for an inductive load: (a) bypass configuration; (b) free-wheeling diode configuration.

resistor, and the capacitor momentarily diverts the load current as described above. The capacitor value is chosen as above, but the resistor value is chosen to limit the current on closure to be less than the minimum arcing current:

$$R \geq \frac{V_{\text{dc}}}{I_{A,\text{min}}}$$

Contact suppression can be employed across the switch as described previously or across the inductive load, or both: An example of applying a diode across an inductive load is shown in Fig. 5.44a. When the switch opens, the inductor current is diverted through the diode rather than the switch. Contact arcing during switch closure is not affected. A common example of protection of inductive loads with a diode is in switching transistors. A diode ("freewheeling" diode) is placed across the inductive load, which may represent the inductance of a dc motor as shown in Fig. 5.44b. When the transistor switch interrupts the current through the inductance I_L, the inductance kick or Faraday's law voltage across the inductor causes the diode to short out. Thus the diode clamps the collector of the transistor to $+V_{CC}$, preventing large collector–emitter voltages, which may destroy the transistor. Currents of larger magnitude and fast rise times will circulate around the inductor–diode loop. Therefore the diode must be placed very close to the inductor in order to minimize the loop radiation of this current loop.

Contact protection may or may not be required for resistive loads. If the load draws less than the minimum arcing current, no arc can be sustained, and no contact protection is generally required. If the resistive load draws a current greater than the minimum arcing current, a contact protection circuit similar to that of Fig. 5.43 may be required.

PROBLEMS

Section 5.1 Wires

5.1.1 Calculate the per-unit-length dc resistance of the following wires: #6 AWG (solid and 259×30), #20 AWG (solid and 19×32), #28 AWG (solid and 7×36), #30 AWG (solid and 7×38). [1.3 mΩ/m, 1.31 mΩ/m, 33.2 mΩ/m, 28 mΩ/m, 214.3 mΩ/m, 194.4 mΩ/m, 340.3 mΩ/m, 303.8 mΩ/m]

5.1.2 Determine the skin depth of steel (SAE 1045) at 1 MHz, 100 MHz, and 1 GHz. [0.26 mils, 0.026 mils, 0.00823 mils]

5.1.3 Determine the frequency where the resistance of a #20 AWG solid wire begins to increase because of the skin effect. [105.8 kHz] Determine the resistance of this wire at 100 MHz. [1.022 Ω/m]

5.1.4 Determine the frequency where the internal inductance of a #32 AWG solid wire begins to decrease due to skin effect. [1.7 MHz] Determine the internal inductance of this wire at 100 MHz. [6.5 nH/m or 0.165 nH/in.]

5.1.5 Determine the resistance, internal inductance, external inductance and capacitance of a typical ribbon cable consisting of two #28 AWG (7 × 36) wires 2 m in length and separated by 50 mils at 100 MHz. [3.74 Ω, 5.95 nH, 1.518 μH, 29.28 pF] Determine the characteristic impedance of the cable. [227.7 Ω]

5.1.6 Determine the resistance of a 6 in. PCB land of width 5 mils at 1 MHz and at 40 MHz. [0.59 Ω, 0.776 Ω]

Section 5.2 Printed Circuit Board (PCB) Lands

5.2.1 Determine the effective dielectric constant and characteristic impedance of a microstrip line constructed of a glass epoxy board of thickness of 47 mils supporting a 1 oz (ounce) Cu land 100 mils in width. [3.625, 45.3 Ω] Determine the per-unit-length inductance and capacitance. [7.3 nH/in., 3.56 pF/in.]

5.2.2 Determine the effective dielectric constant and characteristic impedance of a coplanar stripline constructed of a glass epoxy board of thickness 47 mils supporting two 1 oz Cu lands 100 mils in width and separated (edge to edge) by 100 mils. [1.96, 172.2 Ω] Determine the per-unit-length inductance and capacitance. [20.4 nH/in., 0.688 pF/in.]

5.2.3 Determine the characteristic impedance of two 1 oz Cu lands 100 mils in width that are located on opposite sides of a 47 mil glass epoxy board. [56.48 Ω]

Section 5.4 Resistors

5.4.1 The magnitude of an impedance is sketched as a Bode plot in Fig. P5.4.1. Determine one possible impedance expression for this. [$\hat{Z}(p) = 0.8(p + 3)/(p^2 + 10p)$]

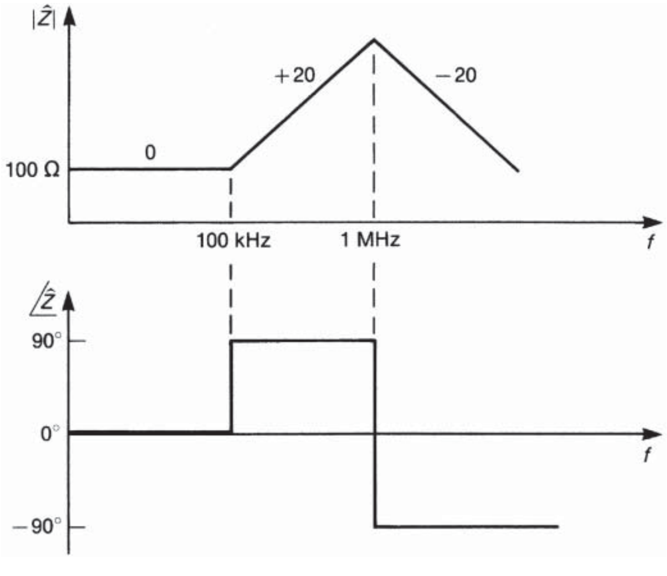

FIGURE P5.4.1

5.4.2 The magnitude of an impedance is sketched as a Bode plot in Fig. P5.4.2. Determine one possible impedance expression for this. [$\hat{Z}(p) = 18p(p+30)/(p+10)^2$]

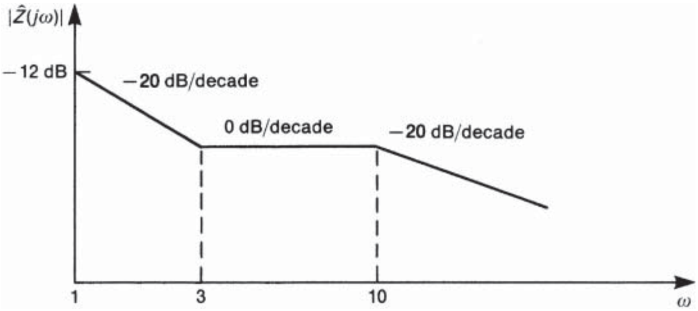

FIGURE P5.4.2

5.4.3 A 1/8 W carbon resistor has the measured Bode plot of the impedance shown in Fig. P5.4.3. Determine the lead inductance and parasitic capacitance. [$L_{\text{lead}} = 12.48$ nH, $C_{\text{par}} = 5.64$ pF]

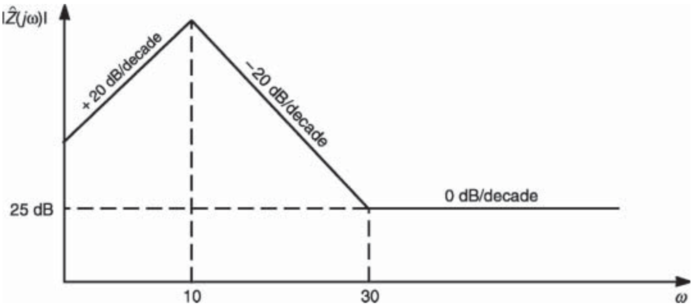

FIGURE P5.4.3

5.4.4 Calculate the parasitic capacitance for the 1000 Ω resistor directly from the measured data in Fig. 5.12a. [$C_{\text{par}} = 1.447$ pF]

5.4.5 A component is measured and found to have the impedance whose magnitude is shown in Fig. P5.4.5. Synthesize an equivalent circuit to represent this impedance. [100 Ω resistor in parallel with 15.92 μH inductor]

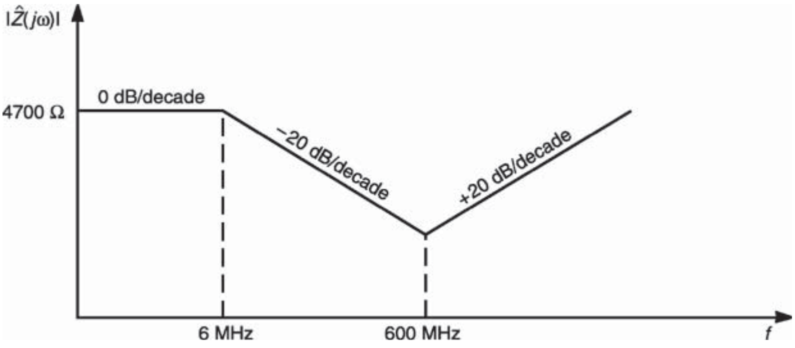

FIGURE P5.4.5

5.4.6 A component is measured and found to have an impedance whose (asymptotic) frequency response is shown in Fig. P5.4.6. Synthesize an equivalent circuit to represent this impedance. [1 nH inductor in series with the parallel combination of a 100 Ω resistor and a 1 μF capacitor]

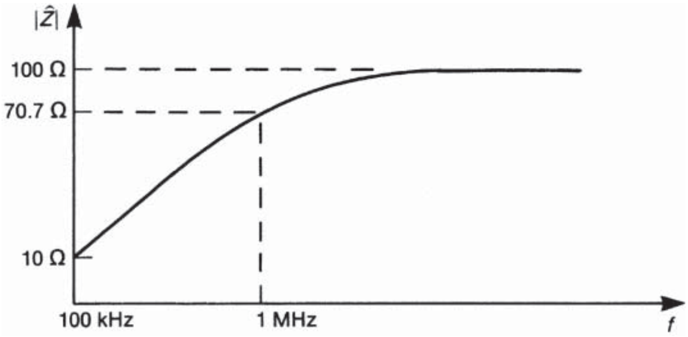

FIGURE P5.4.6

5.4.7 A component has the measured input impedance shown in asymptotic form in Fig. P5.4.7. Synthesize an equivalent circuit to represent this component at its terminals. [A 100 Ω resistor in series with a 0.01 μF capacitor]

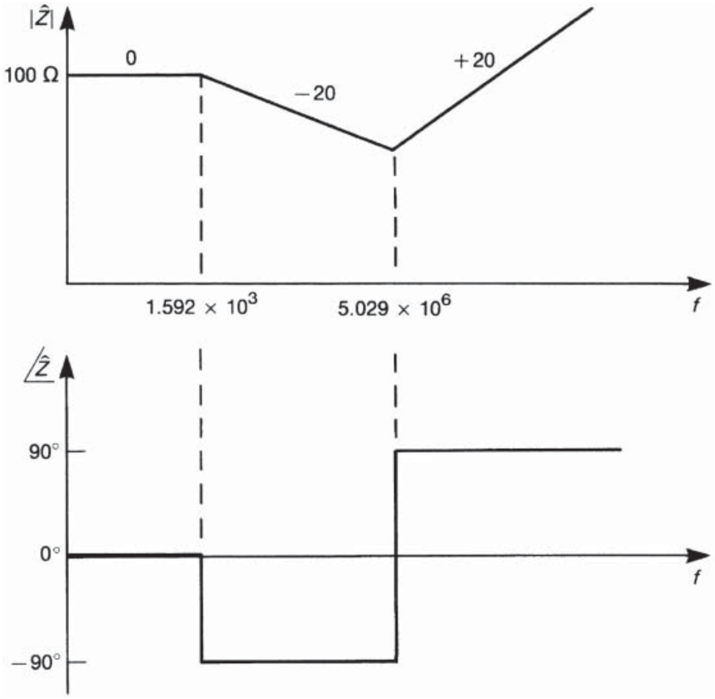

FIGURE P5.4.7

Section 5.5 Capacitors

5.5.1 Determine the lead inductance of the capacitor with very short leads whose measured data are as shown in Fig. 5.16. [4.775 nH]

5.5.2 A 100 MHz noise signal is being applied to the input of a transistor amplifier whose input impedance is $60\underline{/0^\circ}\ \Omega$ at 100 MHz. Determine the value of a capacitor that, when placed across the input, will divert 60% of this current. [20 pF]

5.5.3 A 50 Ω, 100 MHz sinusoidal source is terminated in a 50 Ω load resistor. Determine the value of a capacitor that when placed across the output will reduce the voltage by 20 dB. [633.4 pF]

Section 5.6 Inductors

5.6.1 Determine the parasitic capacitance for the 1.2 μH inductor directly from the measured data in Fig. 5.23. [1.6 pF]

5.6.2 An inductor is to be placed in series with a 50 Ω load to block a 100 MHz noise current. Determine a value for the inductance that will reduce the 100 MHz noise signal across the load by 20 dB. [0.8 μH]

Section 5.7 Ferromagnetic Materials—Saturation and Frequency Response

5.7.1 For the toroid of NiZn whose measured impedance is shown in Fig. 5.25b, model the impedance as an inductor in parallel with a resistance that is in parallel with a parasitic capacitance of the windings. Determine the inductance, resistance, and parasitic capacitance directly from these measured data. [$L = 8\ \mu\text{H}$, $R = 1200\ \Omega$, $C_{\text{par}} = 1.6\ \text{pF}$]

5.7.2 For the NiZn toroid whose measured impedance is shown in Fig. 5.25b, estimate the relative permeability of the material if there are 4 turns of wire, the core cross section is 0.5 × 0.5 cm, and the mean radius of the core is 1 cm. [$\mu_r \cong 1000$]

Section 5.8 Ferrite Beads

5.8.1 For the 1/2-turn ferrite bead whose measured impedance is shown in Fig. 5.31a, determine the equivalent inductance. [$L = 1.6$ mH]

5.8.2 For the 2 1/2-turn ferrite bead whose measured impedance is shown in Fig. 5.31b, determine the stray capacitance. [$C = 1.989$ pF]

Section 5.9 Common-Mode Chokes

5.9.1 An ideal common-mode choke (windings perfectly symmetric and having no losses) is constructed as shown in Fig. P5.9.1. With terminals *AB* connected, the impedance seen looking into terminals *ab* is $300,000\underline{/90^\circ}\ \Omega$ at 50 MHz. With terminals *Ab* connected, the impedance at 50 MHz seen looking into terminals *aB* is $10^6\underline{/90^\circ}\ \Omega$. Determine the self and mutual inductances of the choke. [$L = 1.035$ mH, $M = 0.557$ mH]

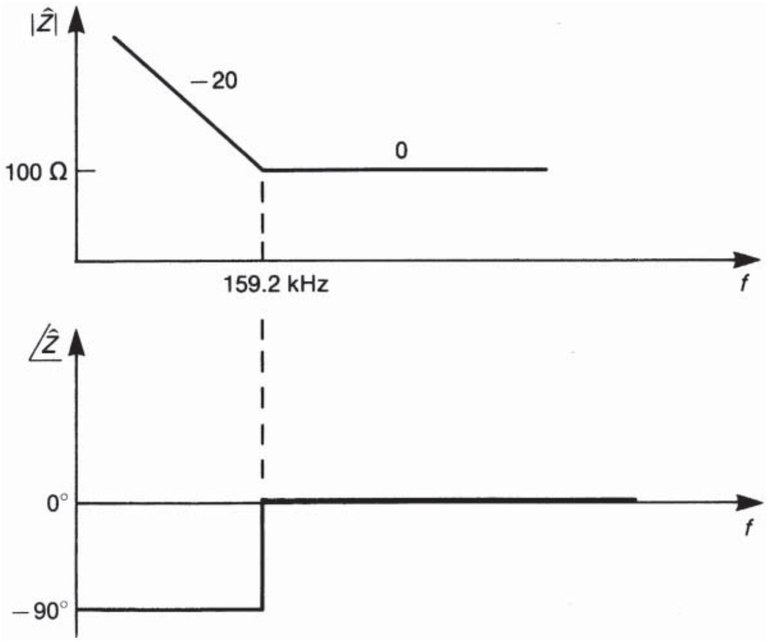

FIGURE P5.9.1

5.9.2 An ideal common-mode choke (windings perfectly symmetric and having no losses) is connected between a source and load as shown in Fig. P5.9.2. Determine the amplitude of the load voltage, assuming that all common-mode currents have been eliminated by the common-mode choke. [2.564 $\underline{/(^{-}75.14\circ)}$ V]

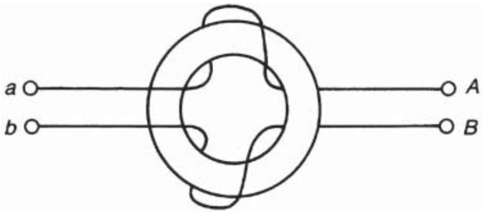

FIGURE P5.9.2

Section 5.10 Electromechanical Devices

5.10.1 A small dc motor has the input impedance frequency response shown in asymptotic form in Fig. P5.10.1. Synthesize an equivalent circuit to represent this motor at its input terminals. [159 pF in parallel with the series combination of 100 Ω and 159 μH]

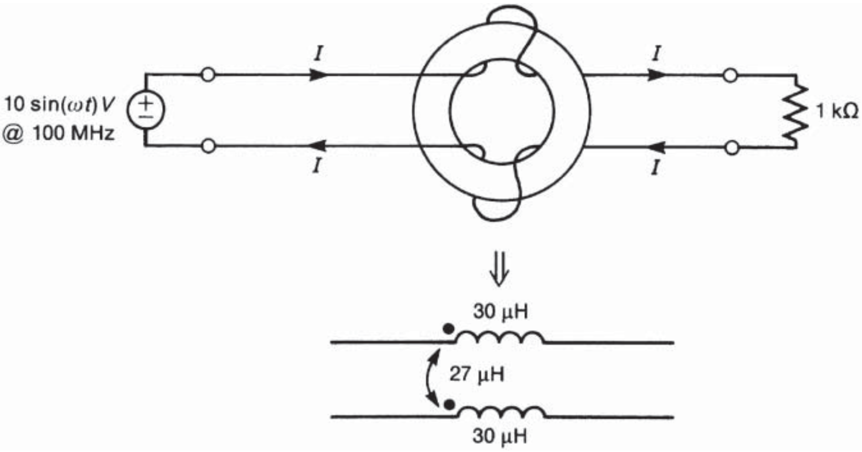

FIGURE P5.10.1

Section 5.13 Mechanical Switches

5.13.1 For the *RC* switch protection network of Fig. 5.43b, suppose that $V_{\mathrm{dc}} = 50$ V, $R_L = 500\ \Omega$, $L = 10$ mH, $I_A = 0.25$ A, and the switch closure/opening velocity is 0.01 m/s. Determine R and C such that the contacts will be protected. [$C > 0.1$ μF, $200\ \mathrm{W} < R < 500\ \mathrm{W}$]

REFERENCES

1. C. R. Paul and S. A. Nasar, *Introduction to Electromangetic Fields*, 2nd ed., McGraw-Hill, New York, 1987.
2. C. R. Paul and W. W. Everett, III, *Lumped Model Approximations of Transmission Lines: Effect of Load Impedances on Accuracy*, Technical Report, Rome Air Development Center, Griffiss AFB, NY, RADC-TR-82-286, Vol. IV. E, Aug. 1984.
3. J. C. Clements, C. R. Paul, and A. T. Adams, Two-dimensional systems of dielectric-coated, cylindrical conductors, *IEEE Trans. Electromagn. Compat.* EMC-17, 238–248 (1975).
4. C. R. Paul, *Fundamentals of Electric Circuit Analysis*, Wiley, New York, 2001.
5. C. R. Paul, *Analysis of Linear Circuits*, McGraw-Hill, New York, 1989.
6. H. W. Ott, *Noise Reduction Techniques in Electronic Systems*, 2nd ed., Wiley-Interscience, New York, 1988.
7. J. C. Englebrecht and K. Hermes, *A Study of Decoupling Capacitors for EMI Reduction*, Technical Report, International Business Machines, TR-51.0152, May 1984.
8. D. M. Hanttula and S. W. Wong, Case study—effect of analog buffer amplifier on radiated emissions, *Proc. 1985 IEEE Int. Symp. Electromagnetic Compatibility*, Wakefield, MA, Aug. 1985.
9. C. R. Paul, S. A. Nasar, and L. E. Unnewehr, *Introduction to Electrical Engineering*, McGraw-Hill, New York, 1986.
10. D. R. Kerns, Integrated circuit construction and its effect on EMC performance, *Proc. 1984 IEEE Symp. Electromagnetic Compatibility*, San Antonio, TX, Apr. 1984.
11. R. Holm, *Electric Contacts, Theory and Application*, 4th ed., Springer-Verlag, Berlin, 1967.
12. H. N. Wagar, Performance principles of switching contacts, *Physical Design of Electronic Systems*, Vol. 3. *Integrated Device and Connection Technology* (Bell Laboratories), Prentice-Hall, Englewood Cliffs, NJ, 1971, Chapter 9.
13. J. D. Cobine, *Gaseous Conductors*, Dover, New York, 1958.

14. A. M. Curtis, Contact phenomena in telephone switching circuits, *Bell Syst. Tech. J.* 19, 40–62 (1940).
15. G. W. Mills, The mechanism of the showering arc, *IEEE Trans. Parts, Mater. Pack.* PMP-5, 47–55 (1969).
16. E. K. Howell, How switches produce electrical noise, *IEEE Trans. Electromagn. Compat.* EMC-21, 162–170 (1979).
17. S. A. Hall, C. R. Paul, K. B. Hardin, and A. E. Nielsen, Prediction of crosstalk due to showering arcs at switch contacts, *Proc. 1991 IEEE Int. Symp. Electromagnetic Compatability*, Cherry Hill, NJ, Aug. 1991.

CHAPTER SIX

Conducted Emissions and Susceptibility

In this chapter, we will investigate the mechanism by which emissions are generated and are conducted out of the product along the product's ac power cord. Regulatory agencies impose limits on these *conducted emissions* because they are placed on the commercial power system net of the installation. The commercial power distribution system in an installation is a large array of wires connecting the various power outlets from which the other electronic systems in the installation receive their ac power. It therefore represents a large "antenna" system from which these conducted emissions can radiate quite efficiently, causing interference in the other electronic systems of the installation. Thus, the conducted emissions may cause radiated emission, which may then cause interference. Ordinarily, the reduction of these conducted emissions is somewhat simpler than the reduction of radiated emissions since there is only one path for these emissions that needs to be controlled: the unit's power cord. However, it is important to realize that *if a product fails to comply with the limits on conducted emissions, it likely will fail to comply with the limits for radiated emissions as well*! Therefore, controlling conducted emissions of a product has equal priority with the control of radiated emissions.

Manufacturers of electronic products realize that simply complying with the regulatory limits on conducted and radiated emissions does not represent a complete design from the standpoint of EMC. A product must be reasonably insensitive to disturbances that are present on the power system net in order to ensure reliable operation of the product. For example, lightning may strike the power transmission lines that feed power to the installation. This may cause disturbances that range from a complete loss of commercial power (which no product is expected to withstand) to momentary power loss due to power system circuit breakers attempting to reclose (which a product is expected to withstand without loss of data or function). The regulatory limits on conducted emissions are intended to control the interference potential of the *radiated emissions* due to the noise currents that are placed on the commercial power wiring by their being conducted out the product along its ac power cord. Normally, these noise currents are too small to cause direct interference by their conduction into a product along its ac power cord. However, disturbances such as those induced by lightning are of sufficient magnitude to cause interference by their direct conduction into a product

---

Introduction to Electromagnetic Compatibility, Third Edition. Clayton R. Paul, Robert C. Scully, and Mark A. Steffka.
© 2023 John Wiley & Sons, Inc. Published 2023 by John Wiley & Sons, Inc.

via its ac power cord. This type of interference represents a *conducted susceptibility* problem and is one that manufacturers realize and try to design a product to withstand.

6.1 MEASUREMENT OF CONDUCTED EMISSIONS

It is important to understand the measurement procedure that is used to verify compliance with the conducted emission regulatory limits. This was discussed in Section 2.1.4. The FCC and CISPR 32, limits on conducted emissions extend from 150 kHz to 30 MHz (see Fig. 2.1). Emissions measured for verification of compliance with the regulatory limits are to be measured with a *line impedance stabilization network* (LISN) inserted between the commercial power outlet and product's ac power cord. A typical test configuration is illustrated in Fig. 6.1. The ac power cord of the product is plugged into the input of the LISN. The output of the LISN is plugged into the commercial power system outlet. AC power passes through the LISN to power the product. A spectrum analyzer is attached to the LISN and measures the "conducted emissions" of the product.

6.1.1 The Line Impedance Stabilization Network (LISN)

The purpose of the conducted emission test is to measure the noise currents that exit the product's ac power cord conductors. These emissions could be simply measured with a current probe. However, the requirement that the measured data be correlatable between measurement sites may render this simple test unrealistic. The impedance seen looking into the ac power system wall outlets varies considerably over the measurement frequency range and from outlet to outlet and building to building [1]. This variability in the loading presented to the product affects the amount of noise that is conducted out the power cord. In order to make this consistent between test sites, the impedance seen by the product looking out the product's ac power cord must be stabilized from measurement site to measurement site. This is the first objective of the LISN—*to present a constant impedance to the product's power cord outlet over the frequency range of the conducted emission test.* Also, the amount of noise that is present on the power system net varies from site to site. This "external" noise

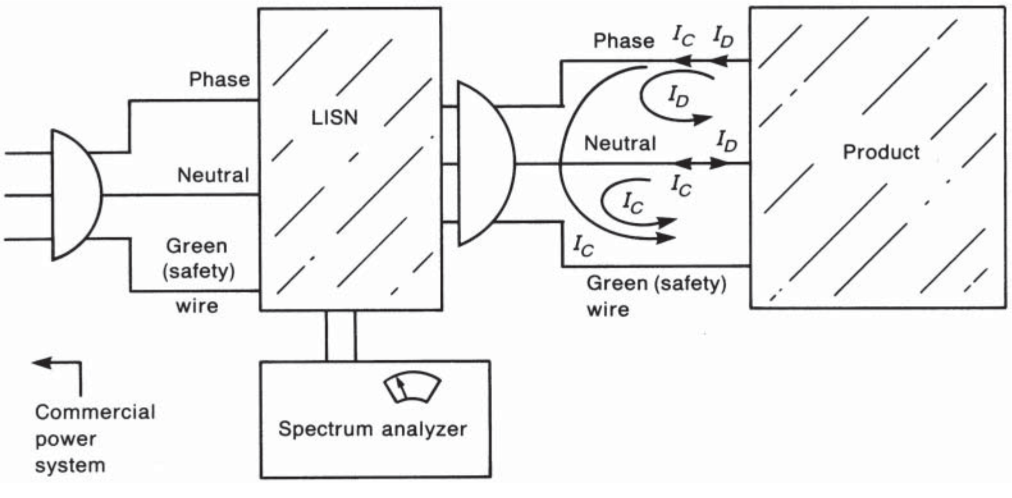

FIGURE 6.1 Illustration of the use of a line impedance stabilization network (LISN) in the measurement of conducted emissions of a product.

enters the product's ac power cord and, unless it is somehow excluded, will add to the measured conducted emissions. It is desired to measure only those conducted emissions that are due to the product, and this gives the second objective of the LISN—*to block conducted emissions that are not due to the product being tested so that only the conducted emissions of the product are measured.* Therefore, the two objectives of the LISN are (1) to present a constant impedance (50 Ω) between the *phase* conductor and the safety wire (the "green wire") and between the *neutral* conductor and the safety wire, and (2) to prevent external conducted noise on the power system net from contaminating the measurement. These two objectives are to be satisfied only over the frequency range of the conducted emission test (150 kHz to 30 MHz). Another subtle but unstated requirement for the LISN is that it will be able to pass the 60 Hz (50 Hz) power required for operation of the product.

The LISN specified for use in the conducted emission measurement is shown in Fig. 6.2. The purpose of the 1 μF capacitors between *phase* and *green wire* and between *neutral* and *green wire* on the commercial power side is to divert "external noise" on the commercial power net and prevent that noise from flowing through the measurement device and contaminating the test data. Similarly, the purpose of the 50 μH inductors is to block that noise. The purpose of the other 0.1 μF capacitors is to prevent any dc from overloading the input of the test receiver. It is instructive to compute the impedances of these elements at the lower frequency limit, 150 kHz, and the upper frequency limit, 30 MHz, of the FCC regulatory limit. These are

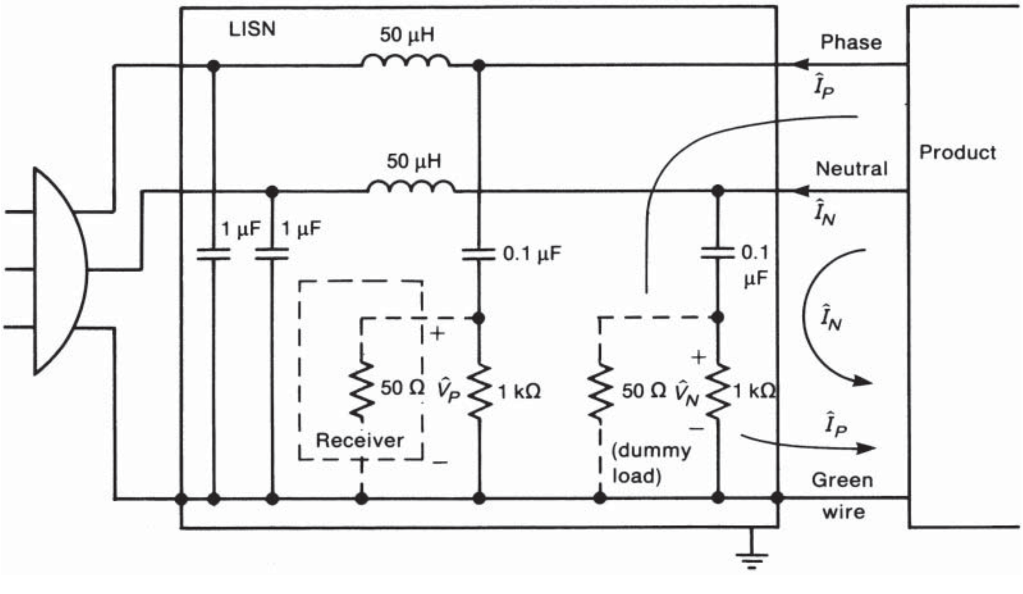

FIGURE 6.2 Illustration of the LISN circuit.

TABLE 6.1 LISN Element Impedances as a Function of Frequency

Element	Z_{150} kHz	Z_{30} MHz
50 μH	47.1 Ω	9424.8 Ω
0.1 μF	10.61 Ω	0.053 Ω
1 μF	1.06 Ω	0.0053 Ω

Thus, the capacitors are low impedances over the measurement frequency range, and the inductor presents a large impedance. The 1-kΩ resistors act as static charge paths to discharge the 0.1 μF capacitors in the event that the 50 Ω resistors are removed. Resistances of 50 Ω are placed in parallel with these 1 kΩ resistors. One 50 Ω resistor is the input impedance of the test receiver (spectrum analyzer), while the other is a 50 Ω dummy load that insures that the impedance between *phase* and the safety wire and between *neutral* and the safety wire is approximately 50 Ω at all times. The measured voltages, denoted by $\hat{V}_P$ and $\hat{V}_n$, are measured between the *phase* wire and the safety wire and between the *neutral* wire and the safety wire. Both the *phase* and the *neutral* voltages must be measured over the frequency range of the conducted emission limit and must be below the specified limit at every frequency in the limit frequency range. Now we see why the conducted emission limits are specified in terms of *voltages* when, in fact, we are interested in conducted emission *currents*. The phase current $\hat{I}_P$ and the neutral current $\hat{I}_N$ are related to the measured voltages by

$$\hat{V}_P = 50\,\hat{I}_P \tag{6.1a}$$

$$\hat{V}_N = 50\,\hat{I}_N \tag{6.1b}$$

where we have assumed that the capacitors of the LISN are short circuits and the inductors are open circuits over the frequency range of the measurement. Therefore, the measured voltages are directly related to the noise currents that exit the product via the phase and neutral wires.

The capacitors (inductors) of the LISN are, as we showed, essentially short (open) circuits throughout the frequency range of the conducted emission test. Therefore, the equivalent circuit of the LISN will be 50 Ω resistors between the *phase* wire and the safety wire and between the *neutral* wire and the safety wire, as shown in Fig. 6.3. At the 60 Hz power frequency, the inductors have impedances of 18.8 mΩ, the 0.1 μF capacitors have impedances of 26.5 kΩ, and the 1 μF capacitors have impedances of 2.7 kΩ. Thus, at the 60 Hz power frequency the LISN has virtually no effect, and ac power for functional operation is provided to the product.

Finally, it is important to point out that *the object of designing for regulatory compliance is to prevent currents in the frequency range of the regulatory limit from flowing through the 50 Ω*

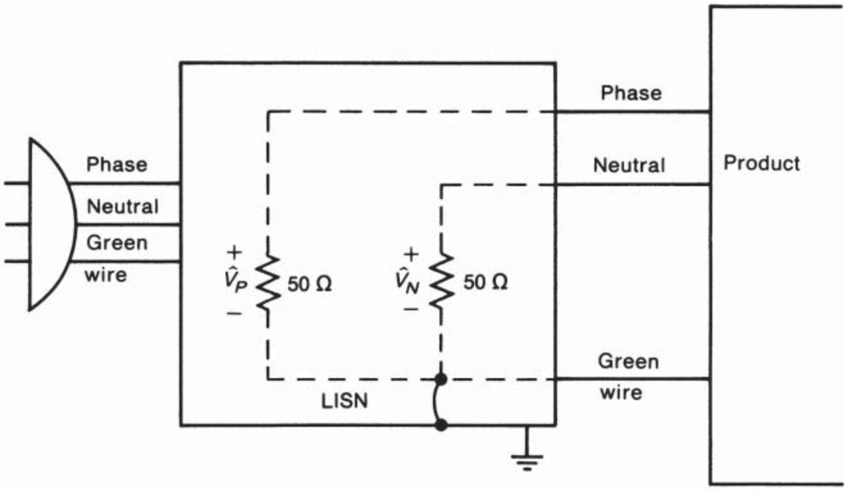

FIGURE 6.3 Equivalent circuit of the LISN as seen by the product over the conducted emission regulatory frequency range.

resistors of the LISN. Emissions outside the frequency range of the regulatory limit are of no concern with regard to meeting the conducted emission limits. They may, however, be important in causing interference with other products and so cannot be completely disregarded in the course of designing a quality product. *Any current in the frequency range of the regulatory limit that exists on the product's power cord will be measured by the LISN and can contribute to the product's failure to comply with that limit*. A common example is the existence of clock harmonics of the system oscillators on the power cord. For example, suppose that a system clock is 10 MHz. If this signal couples to the ac power cord, it will provide signals to the LISN within the regulatory frequency range (10, 20, and 30 MHz). Although the power cord is "not intended" to carry these currents, if they exist on the power cord, they will be measured by the LISN and may contribute to the product's failure to comply with the regulatory limits.

6.1.2 Common- and Differential-Mode Currents Again

Representing the LISN as 50 Ω resistors between phase wire and green wire and between neutral wire and green wire as in Fig. 6.3 (the ideal behavior of the LISN over the frequency change conducted emission regulatory limit) simplifies the analysis of conducted emissions. The voltages that are to be measured for verification of compliance to the regulatory limit are the voltages across these 50 Ω resistors and are denoted as $\hat{V}_P$ and $\hat{V}_N$. These voltages are related to the emission currents via Ohm's law according to (6.1). As was the case for radiated emissions, we may decompose these currents into a differential-mode component that flows out through the *phase* conductor and returns on the *neutral* conductor, and a common-mode component that flows out through the *phase* and *neutral* conductors and returns on the *green wire* as shown in Fig. 6.4:

$$\hat{I}_P = \hat{I}_C + \hat{I}_D \tag{6.2a}$$

$$\hat{I}_N = \hat{I}_C - \hat{I}_D \tag{6.2b}$$

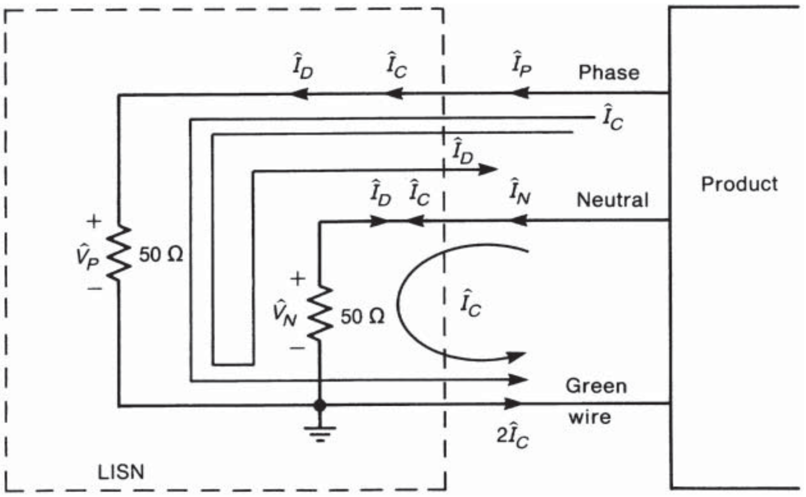

FIGURE 6.4 Illustration of the contributions of differential-mode and common-mode current components on the measured conducted emissions.

Solving these gives

$$\hat{I}_D = \frac{1}{2}(\hat{I}_P - \hat{I}_N) \tag{6.3a}$$

$$\hat{I}_C = \frac{1}{2}(\hat{I}_P + \hat{I}_N) \tag{6.3b}$$

The measured voltages are

$$\hat{V}_P = 50(\hat{I}_C + \hat{I}_D) \tag{6.4a}$$

$$\hat{V}_N = 50(\hat{I}_C - \hat{I}_D) \tag{6.4b}$$

It is important to understand that, as opposed to radiated emissions, *common-mode currents can be of the order of or exceed differential-mode currents in conducted emissions*! We will show experimental results that confirm this important fact. Therefore, *one should not assume that common-mode currents are inconsequential in conducted emissions*. It is also important to remember that differential-mode currents for conducted emission regulatory compliance are not the functional 60 Hz power line currents. Observe that the differential-mode current flows down through one 50 Ω and up through the other, whereas the common-mode currents flow down through both 50 Ω resistors. Therefore, *the contributions due to each current add in* $\hat{V}_P$ *and subtract in* $\hat{V}_N$. Therefore, if the common- and differential-mode currents are of the same magnitude, the phase and neutral voltages will not be the same. Generally, one component dominates the other so that the magnitudes of the phase and neutral voltages are about the same:

$$\hat{V}_P = 50\,\hat{I}_C, \quad \hat{I}_C \gg \hat{I}_D \tag{6.5a}$$

$$\hat{V}_N = 50\,\hat{I}_C, \quad \hat{I}_C \gg \hat{I}_D \tag{6.5b}$$

or

$$\hat{V}_P = 50\,\hat{I}_D, \quad \hat{I}_D \gg \hat{I}_C \tag{6.6a}$$

$$\hat{V}_N = 50\,\hat{I}_D, \quad \hat{I}_D \gg \hat{I}_C \tag{6.6b}$$

Virtually, all products contain a power supply filter as the last circuit that noise currents pass through before they exit the product through the power cord and then pass through the LISN. Power supply filters contain components that are intended to reduce either differential-mode or common-mode currents. The decomposition of the total currents into common-mode and differential-mode components along with this realization that each element of the power supply filter affects one and only one of these components is the key to designing power supply filters that are effective in the reduction of conducted emissions so that the product will comply with the regulatory limits.

Two common methods of blocking the common-mode current path are shown in Fig. 6.5. In many electronic products, an inductor is placed in the green wire, where it enters the product as shown in Fig. 6.5a. This tends to present a high impedance to the common-mode currents that are in the frequency range of the conducted emission regulatory limit, yet a path for fault currents to flow still exists that preserves the shock hazard protection of the green wire. For safety reasons, it is undesirable to physically solder an inductor in the green wire, because the solder joint may become defective, opening the safety wire path and leaving a potential shock hazard. In order to prevent this from happening, the inductor is constructed by winding several turns of the green wire around a

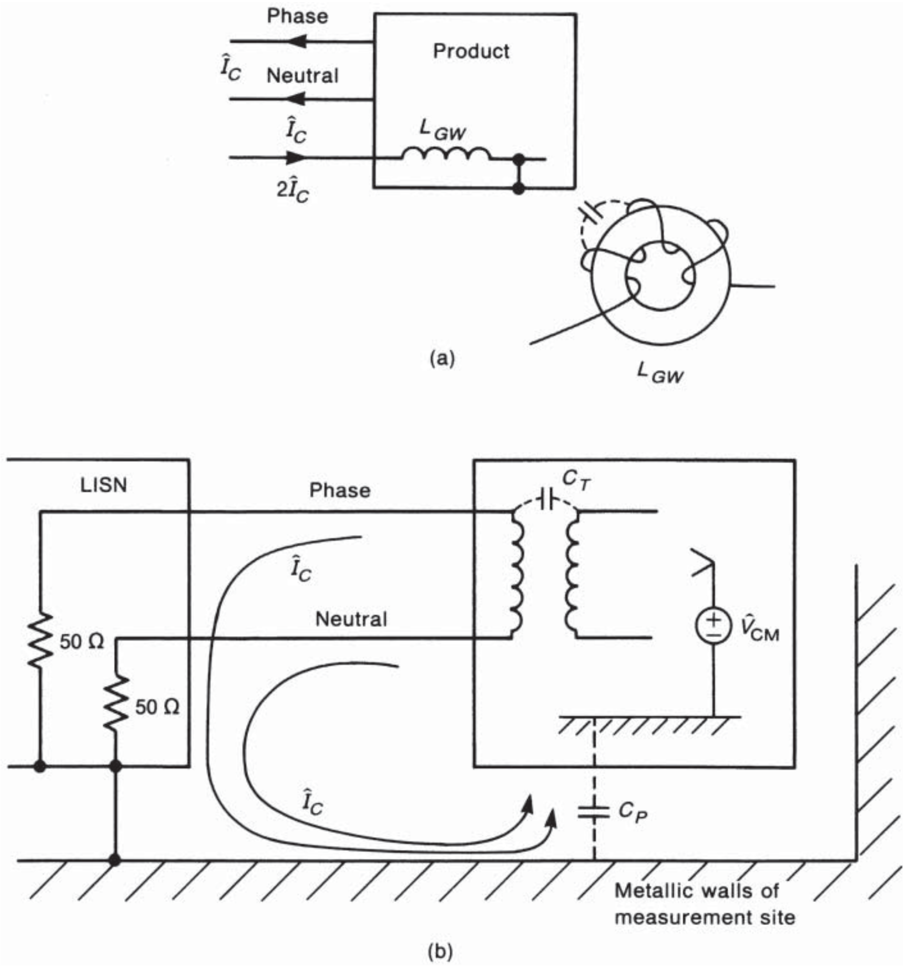

FIGURE 6.5 Methods of reducing the common-mode contribution to conducted emissions: (a) a green-wire inductor; (b) a two-wire product.

ferrite toroid (that has suitable characteristics over the conducted emission limit frequency range). Typical values of this green-wire inductance are of order 0.5 mH, which has an impedance of some 471 Ω at the lower frequency of the regulatory limit (150 kHz). One might expect that this impedance would increase at the upper limit of 30 MHz, but this is not necessarily true. Parasitic capacitances between the windings of the toroid will typically cause its performance to deteriorate at the higher frequencies, as was discussed in Chapter 5.

Another technique for blocking the common-mode path is to construct a so-called "two-wire product." The power cord contains only the phase and the neutral wires, and the safety wire is absent. A two-wire product has an inherent shock hazard because the neutral conductor of the power distribution system is tied directly to earth ground (at the service entrance panel), and the phase conductor is "hot" with respect to the earth ground. It would not be possible to tie the neutral to the product chassis, since we would have no assurance that the consumer would plug the product into the correct holes of the power outlet. If the consumer plugged the product into the wrong holes of the power outlet, the chassis would be "hot" with respect to earth ground, setting up a clear shock hazard. Two-wire products invariably combat this problem by placing a 60 Hz transformer at the power entrance of the product, as shown in Fig. 6.5b. The chassis may be tied to the secondary side of the transformer and would therefore not be directly connected to either the phase or the neutral conductor. The elimination of the green wire in this type of product is frequently thought to eliminate common-mode currents. This is not necessarily true for reasons illustrated in Fig. 6.5b. Stray capacitances between the product chassis and the metallic walls of the test site act to provide the equivalent green-wire path back to the LISN (which must be bonded to the ground plane of the test site). Any common-mode voltage between the electronics of the product and the product frame will tend to drive these common-mode currents through this path. Stray capacitances between primary and secondary of the transformer also exist.

6.2 POWER SUPPLY FILTERS

There are virtually no electronic products today that can comply with the conducted emission regulatory requirements without the use of some form of power supply filter being inserted where the power cord exits the product. Some products may appear not to contain a filter when there is, in fact, one present. An example is the use of a large 60 Hz transformer at the power input of the product in a two-wire product or when using a linear power supply. Properly designed transformers can provide inherent filtering, and so can, in some cases, obviate the need for an "intentional" filter. We will concentrate on the design of intentional power supply filters in this section.

6.2.1 Basic Properties of Filters

We will begin with a discussion of general filter properties. Electric filters occur throughout all branches of electrical engineering such as communications, signal processing, and automatic controls. There is a wealth of design information available for these types of filters. The reader is cautioned that *power supply filters that are intended to reduce conducted emissions are rarely designed using these traditional filter designs*. Nevertheless, a discussion of these basic principles of the traditional filters serves a useful purpose in the illumination of certain basic principles that are common to all filters.

Filters are typically characterized by their *insertion loss* (IL), which is typically stated in dB. Consider the problem of supplying a signal to a load as shown in Fig. 6.6a. A filter is inserted between the source and the load in order to prevent certain frequency components of the source from reaching the load, as shown in Fig. 6.6b. The load voltage without the filter inserted is denoted by $\hat{V}_{L,wo}$ and the load voltage with the filter inserted is denoted as $\hat{V}_{L,w}$. The insertion loss of the filter is defined as

$$\begin{aligned}\mathrm{IL}_{\mathrm{dB}} &= 10\log_{10}\left(\frac{P_{L,wo}}{P_{L,w}}\right)\\ &= 10\log_{10}\left(\frac{V_{L,wo}^2/R_L}{V_{L,w}^2/R_L}\right)\\ &= 20\log_{10}\left(\frac{V_{L,wo}}{V_{L,w}}\right)\end{aligned} \tag{6.7}$$

Note that the voltages in this expression are not denoted with a caret (ˆ) and are therefore the magnitudes of the voltages. The insertion loss gives the reduction in the load voltage *at the frequency of interest* due to the insertion of the filter. Typically, the insertion loss is displayed as a function of frequency.

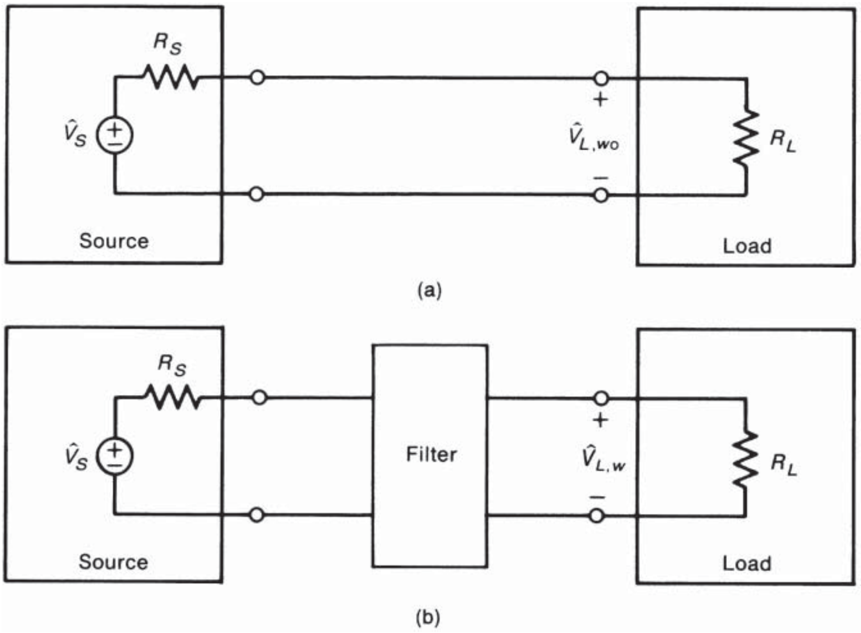

FIGURE 6.6 Definition of the insertion loss of a filter: (a) load voltage without the filter; (b) with the filter inserted.

Some simple filters are shown in Fig. 6.7. These can be analyzed using the techniques discussed in Chapter 5. For example, let us determine the insertion loss of the simple low-pass filter of Fig. 6.7a. The load voltage without the filter can be easily determined from Fig. 6.6a as

$$\hat{V}_{L,wo} = \frac{R_L}{R_S + R_L} \hat{V}_S \tag{6.8}$$

The load voltage with the filter inserted is

$$\begin{aligned} \hat{V}_{L,w} &= \frac{R_L}{R_S + j\omega L + R_L} \hat{V}_S \\ &= \frac{R_L}{R_L + R_S} \frac{1}{1 + j\omega L/(R_S + R_L)} \hat{V}_S \end{aligned} \tag{6.9}$$

The insertion loss is the ratio of (6.8) and (6.9):

$$\begin{aligned} \text{IL} &= 20 \log_{10} \left| 1 + \frac{j\omega L}{R_S + R_L} \right| \\ &= 20 \log_{10}[\sqrt{1 + (\omega\tau)^2}] \\ &= 10 \log_{10}[1 + (\omega\tau)^2] \end{aligned} \tag{6.10}$$

where

$$\tau = \frac{L}{R_S + R_L} \tag{6.11}$$

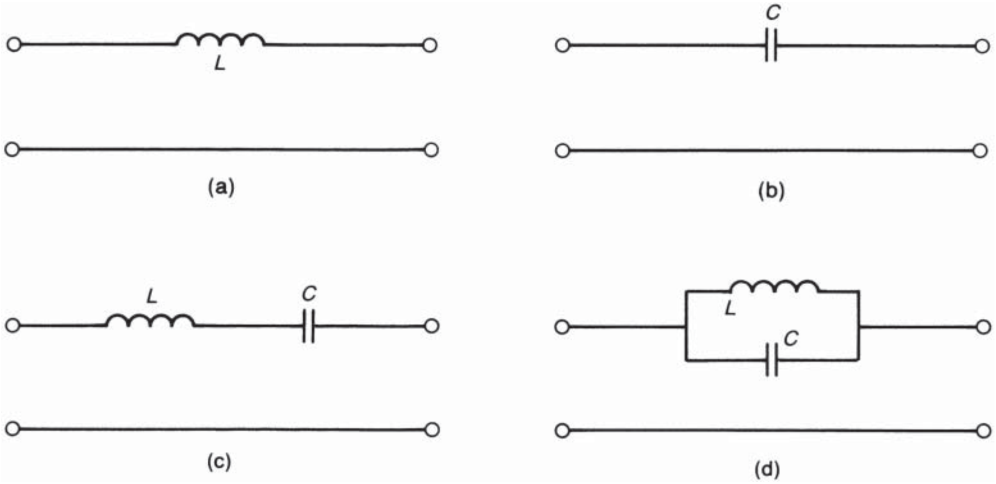

FIGURE 6.7 Four simple filters: (a) low pass; (b) high pass; (c) band pass; (d) band reject.

is the time constant of the circuit. A plot of the insertion loss would show 0 dB from dc to the 3 dB point of $\omega_{3\,\mathrm{dB}} = 1/\tau$ and an increase at a rate of 20 dB/decade above that. Therefore the low-pass filter passes frequency components of the source from dc to $\omega_{3\,\mathrm{dB}}$ and increasingly reduces the frequency components at greater than $\omega_{3\,\mathrm{dB}}$. For frequencies above the 3 dB point, the insertion loss expression simplifies to

$$\begin{aligned} IL &\cong 10\,\log_{10}\left[(\omega\tau)^2\right], \quad \omega \gg \frac{1}{\tau} \\ &= 20\,\log_{10}\omega\tau \\ &= 20\,\log_{10}\left(\frac{\omega L}{R_S + R_L}\right) \end{aligned} \tag{6.12}$$

Other filters are analyzed in a similar fashion.

The example above has illustrated an important point: *The insertion loss of a particular filter depends on the source and load impedances and therefore cannot be stated independently of the termination impedances*. Most filter manufacturers provide frequency response plots of the insertion loss of a particular filter. Since the insertion loss of a filter is dependent on the source and load impedances, what value of source and load impedance is assumed in these specifications? The answer is rather obvious—it is assumed that $R_S = R_L = 50\ \Omega$! This brings up another important point; how does this specification of insertion loss based on $50\,\Omega$ source and load impedances relate to the filter's performance in a conducted emission test? Consider the use of the filter in that test. The "load impedance" corresponds to the $50\,\Omega$ impedances of the LISN between phase and green wire and between neutral and green wire. However, in a typical installation R_L is the impedance seen looking back into the power distribution net. It is highly doubtful that this is $50\,\Omega$! What is the "source impedance R_S" in this usage? The answer is that we do not know, since this is the source impedance seen looking back into the product's power input terminals. It is doubtful that this will be $50\,\Omega$ and furthermore that it will be constant *over the frequency range of the conducted emission test*! So use of the manufacturer's insertion loss data to assess the performance of the filter in a product may not give realistic results in a typical application.

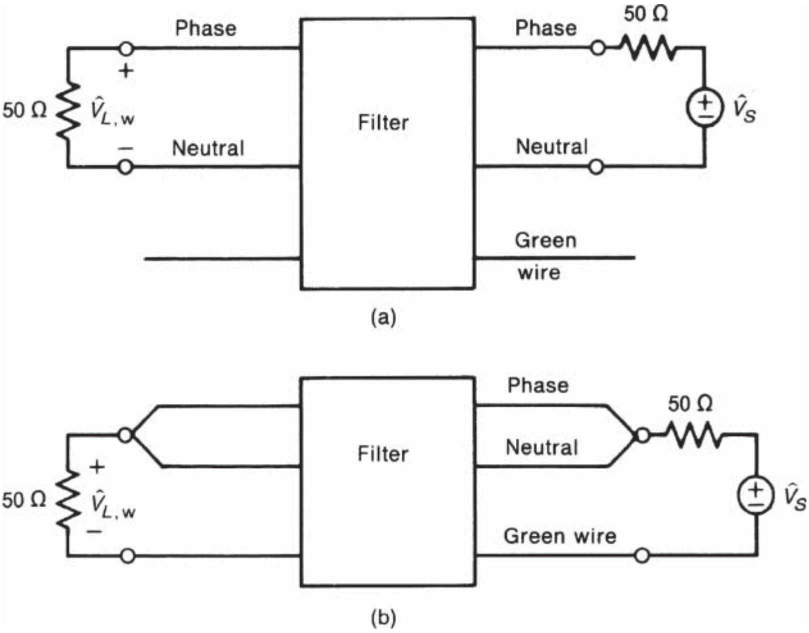

FIGURE 6.8 Insertion loss tests: (a) differential mode; (b) common mode.

Furthermore, there are two currents that must be reduced: common-mode and differential-mode. Filter manufacturers typically give separate insertion loss data for these currents. These data are obtained as shown in Fig. 6.8. For the differential-mode insertion loss measurement, the green-wire terminals are left unconnected and the phase and neutral wires form the circuit to be tested, as shown in Fig. 6.8a, since the differential-mode current, by definition, flows out of the phase wire and returns via the neutral wire, and no differential-mode current returns on the green wire. For the common-mode test, the phase and neutral wires are tied together and form the test circuit with the green wire, as shown in Fig. 6.8b. Once again, *the source and load impedances for each test are assumed to be 50 Ω.*

6.2.2 A Generic Power Supply Filter Topology

The most common power supply filter topology is some version of the generic filter topology shown in Fig. 6.9. The reader should note that this filter topology resembles a Pi structure. The differential- and common-mode currents at the output of the product (usually the input to the product's power supply) are denoted as $\hat{I}_D$ and $\hat{I}_C$, whereas these currents at the input to the LISN (at the output of the filter) are denoted with primes as $\hat{I}'_D$ and $\hat{I}'_C$. The object of the filter is to reduce the unprimed current levels to the primed levels such that the primed currents $\hat{I}'_D$ and $\hat{I}'_C$ give measured voltages

$$\hat{V}_P = 50(\hat{I}'_C + \hat{I}'_D) \tag{6.13a}$$

$$\hat{V}_N = 50(\hat{I}'_C - \hat{I}'_D) \tag{6.13b}$$

which are below the conducted emission limit *at all frequencies in the frequency range of that limit.*

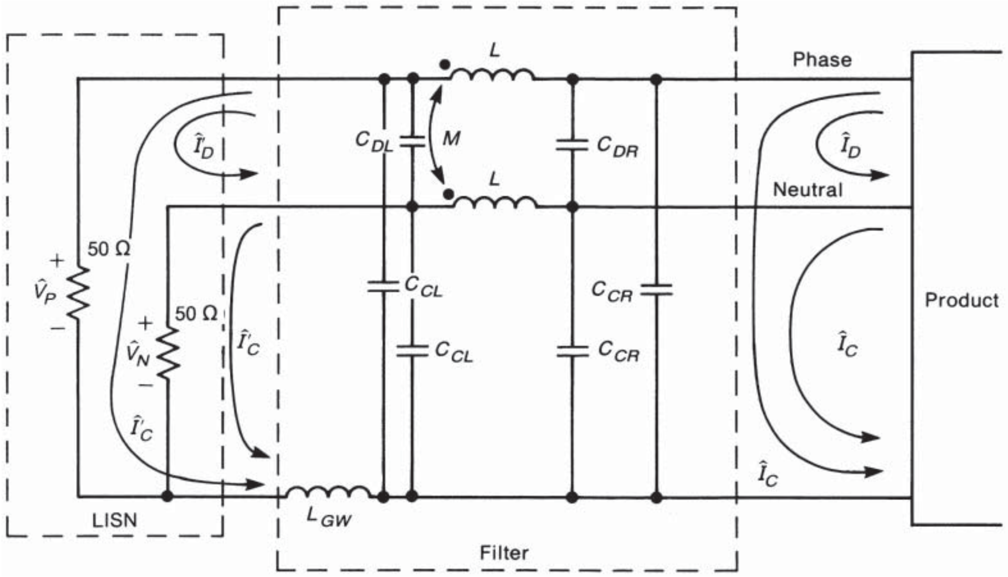

FIGURE 6.9 A typical power supply filter topology.

6.2.3 Effect of Filter Elements on Common- and Differential-Mode Currents

A green-wire inductor L_{GW} is included in the green wire *between the filter output and the LISN input* to block common-mode currents as discussed above. Capacitors between phase and neutral wires, C_{DL} and C_{DR}, are included to *divert differential-mode currents*. These are referred to as *line-to-line capacitors*. Capacitors that have insulation properties approved by safety agencies and are suitable for use as line-to-line capacitors are referred to as "X-caps." The subscripts L and R denote "left" and "right" with regard to the side of the filter on which they are placed. Capacitors C_{CL} and C_{CR} are included between phase and green wire and between neutral and green wire to *divert common-mode currents*. These are referred to as *line-to-ground capacitors*. Capacitors that have insulation properties approved by safety agencies and are suitable for use as line-to-ground capacitors are referred to as "Y-caps." The reason that different capacitors are needed for these tasks is due to safety considerations. For example, suppose that one of the line-to-ground Y-caps shorts out. If this capacitor happens to be connected to the phase wire, 120 V will be tied to the green wire, which is usually tied directly to the product frame, presenting an obvious shock hazard. Also, the safety agencies such as the Underwriters Laboratory (UL) in the United States specify the *maximum leakage current* that may flow through the line-to-ground capacitors at 60 Hz in order to minimize shock hazards due to these leakage currents. This provides an important constraint on the maximum value of the line-to-ground capacitors that may be used in the filter.

Review Exercise 6.1 Determine the maximum line-to-ground capacitance to satisfy a leakage current requirement of 150 μA.

***Answer*:** 3316 pF.

Some filters include only the capacitors on the left or on the right, and some include both sets. Still other filters may, for example, include only C_{DL} and C_{CR} and omit C_{DR} and C_{CL}. Typical values of these capacitorss are $C_D \cong 0.047\ \mu F$ and $C_C \cong 2200\ \mu F$. Observe that the line-to-ground capacitors on the left, C_{CL}, are in parallel with the 50 Ω resistors of the LISN. Therefore, if their impedances at the frequency of interest are not significantly lower than 50 Ω, then these capacitors will be ineffective in diverting the common-mode current. To judge whether the line-to-ground capacitors on the left will be effective, let us compute their impedance for typical values of $C_{CL} = 2200$ pF. The impedances of these capacitors will equal 50 Ω at 1.45 MHz, and so the capacitors C_{CL} will be effective in diverting common-mode currents from the LISN 50 Ω resistors only above this frequency!

One final element is typically included—the *common-mode choke* represented by the coupled inductors. The self-inductances of each winding are represented by L and the mutual inductance is represented by M. Typically, this element consists of two identical windings on a common ferrite core (that has suitable characteristics over the conducted emission frequency range) and so is similar to a transformer, as shown in Fig. 6.10a. Because the windings are identical and are wound tightly on the same core, the mutual inductance is approximately equal to the self-inductance, $L \cong M$, and as such has a coupling coefficient approaching unity:

$$\begin{aligned} k &= \frac{M}{\sqrt{L_1 L_2}} \\ &\cong \frac{M}{L} \\ &\cong 1 \end{aligned} \tag{6.14}$$

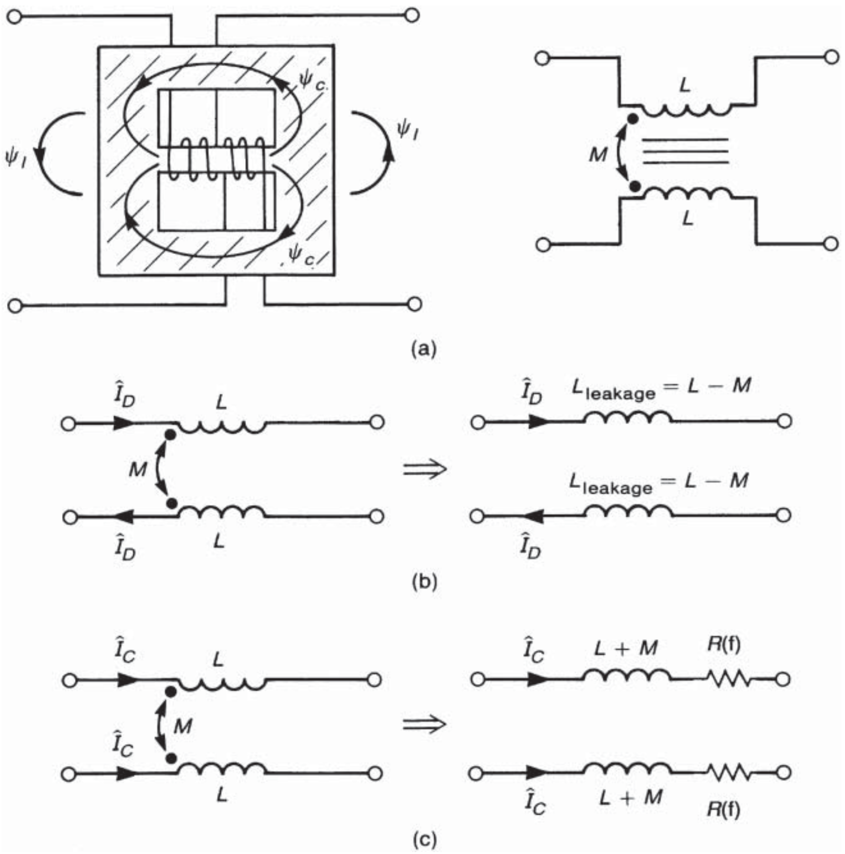

FIGURE 6.10 Use of a common-mode choke to block common-mode conducted emissions: (a) physical construction and equivalent circuit; (b) equivalent circuit for differential-mode currents; (c) equivalent circuit for common-mode currents.

The purpose of the common-mode choke is to block common-mode currents. Ideally, *the common-mode choke does not affect differential-mode currents.* This was shown in Chapter 5, but it is worthwhile to repeat that here. Consider only differential-mode currents through the choke, as shown in Fig. 6.10b. Computing the voltage drop across one side of the choke gives

$$\begin{aligned}\hat{V} &= j\omega L\hat{I}_D - j\omega M\hat{I}_D \\ &= j\omega(L-M)\hat{I}_D \end{aligned} \tag{6.15}$$

Therefore, the element inserts an inductance $L-M$ in each lead with regard to differential-mode currents. This is commonly referred to as the *leakage inductance* and is due to the portion of the magnetic flux that leaks out the core and does not couple between the windings. Ideally this is zero, and the common-mode choke has no effect on differential-mode currents. We will see that this leakage inductance is not zero for actual chokes and has an important role in the blockage of the differential-mode currents. Now consider the effect of the choke on common-mode currents, shown in Fig. 6.10c. Computing the voltage drop across one side of the choke gives

$$\begin{aligned}\hat{V} &= j\omega L\hat{I}_C + j\omega M\hat{I}_C \\ &= j\omega(L+M)\hat{I}_C \end{aligned} \tag{6.16}$$

Therefore, the element inserts an inductance $L+M$ in each lead with regard to common-mode currents. Consequently, the common-mode choke tends to block common-mode currents. Typical values for the inductance are of order 10 mH. Thus, the common-mode current impedance is $j\omega(L+M) = 18,\ 850\ \Omega$ at 150 kHz and 3.77 MΩ at 30 MHz. It is important to emphasize that these are *ideal* values. Parasitic capacitance between the windings as well as the type of core material strongly influence the frequency behavior of the choke. In addition, we have shown the frequency-dependent resistance, $R(f)$, which is also presented to the common-mode currents by a ferrite core.

It is important to reemphasize another important characteristic of the common-mode choke. In addition to the noise signal in the differential-mode current, there is another component—the high-level, 60 Hz power current. Typically, this will be several amps. Currents of this level will easily *saturate* a ferrite core and will therefore reduce its permeability to values approaching that of air. The ability of the choke to block common-mode currents relies on large values of L and M being obtained, which in turn relies on having a large value of the relative permeability of the core. If the core material were saturated by the high-level, 60 Hz current, we would not obtain sufficiently large inductance to provide blocking of the common-mode currents. On the other hand, we do not wish to drop much of the power voltage across the choke. The fact that the differential-mode current flux tends to cancel in the core because of the way the windings are wound on the core means that, ideally, the choke does not provide any impedance to differential-mode currents, and the choke is transparent to these currents (even at 60 Hz). Therefore, *the 60 Hz flux cancels in the core and does not saturate it.* This is an additional benefit of a common-mode choke.

Let us now develop some equivalent circuits to represent the effect of the filter on the common- and differential-mode currents. We will assume a filter that is *symmetric* with regard to phase and neutral. By this it is meant that the phase-green-wire circuit and the neutral-green-wire circuit are identical. This is true for the generic filter shown in Fig. 6.9, in that the line-to-ground capacitors between phase and the green wire are identical to those between neutral and green wire, and the self-inductances of both sides of the common-mode choke are identical. This is normally the case

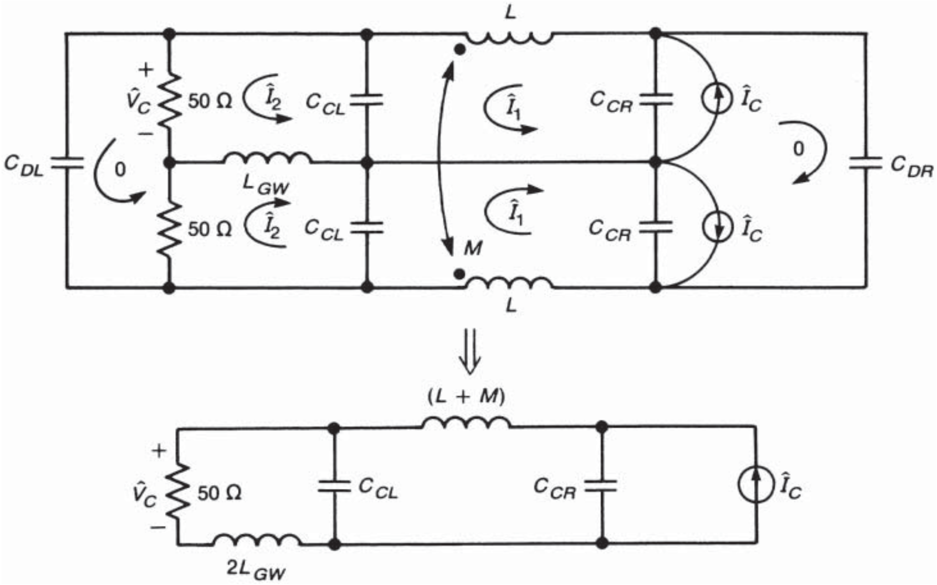

FIGURE 6.11 The equivalent circuit of the filter and LISN for common-mode currents.

since there seems to be no advantage to constructing an unsymmetrical filter. First consider the effect on common-mode currents, shown in Fig. 6.11. We simulate the common-mode currents with current sources. By the symmetry of the structure, we can assume certain currents to be identical as shown. Writing mesh equations, we can demonstrate that the equivalent circuit presented to each common-mode current is as shown. This is intuitively obvious in that the choke appears as an inductance $L+M$ and the line-to-line capacitors have no effect. The green-wire inductor appears twice as large, since $2\hat{I}_C$ flows through it. There is an important observation from this equivalent circuit that illustrates when the green-wire inductor L_{GW} will have an effect in blocking common-mode currents. Suppose the line-to-ground capacitors on the left are absent, $C_{CL}=0$. The equivalent circuit in Fig. 6.11 shows that the equivalent green-wire-inductor $2L_{GW}$ will be in series with the equivalent inductance of the common-mode choke $L+M$ and the 50 Ω of the LISN. Typical value for these are $2L_{GW}=2$ mH and $L+M=55$ mH. This shows that the impedance of the green-wire inductor will be dominated by the impedance of the common-mode choke and hence the green-wire inductor will little or no effect. In order for the green-wire inductor to have any effect, the line-to-ground capacitors on the left must be present, $C_{CL}\neq 0$. To illustrate this we compute, using current division, the ratio of the current through the 50 Ω of the LISN and the current through the choke $L+M$ as

$$\frac{I_{\text{LISN}}}{I_{\text{Choke}}} = \frac{\frac{1}{j\omega C_{CL}}}{50 + j\omega 2L_{GW} + \frac{1}{j\omega C_{CL}}}$$
$$= \frac{1}{1-\omega^2 2L_{GW}C_{CL} + j\omega 50 C_{CL}}$$

If we plot this versus frequency, we see that it consists of a 0 dB/decade ($I_{\text{LISN}}/I_{\text{Choke}}=1$) slope from dc up to a break frequency of

$$f_0 = \frac{1}{2\pi\sqrt{2L_{GW}C_{CL}}}$$

Above this frequency, the plot decreases at −40 dB/decade and the green-wire inductor has a significant effect. For typical values of L_{GW} = 1 mH and C_{CL} = 3300 pF, this break frequency is f_0 = 62 kHz well below the lower limit of the conducted emission regulation of 150 kHz. Suppose the green-wire inductor is absent, $L_{GW} = 0$, but the line-to-ground capacitor on the left is present, $C_{CL} \neq 0$. The ratio of the current through the 50 Ω of the LISN and the current through the equivalent inductance of the choke $L + M$ is

$$\begin{aligned}\frac{I_{\text{LISN}}}{I_{\text{Choke}}} &= \frac{\frac{1}{j\omega C_{CL}}}{50 + \frac{1}{j\omega C_{CL}}}\\ &= \frac{1}{1 + j\omega 50 C_{CL}}\end{aligned}$$

This result plotted versus frequency consists of a 0 dB/decade ($I_{\text{LISN}}/I_{\text{Choke}} = 1$) slope from dc up to a break frequency of

$$f_1 = \frac{1}{2\pi 50 C_{CL}}$$

Above this break frequency, the plot decreases at a rate of only −20 dB/decade. For C_{CL} = 3300 pF, the break frequency is f = 965 kHz or just below 1 MHz. Thus, the line-to-ground capacitor on the left C_{CL} will only have an effect above about 1 MHz when the green-wire inductor is absent. These results show that the green-wire inductor can significantly reduce conducted emissions across the conducted emission regulatory frequency band only if the line-to-ground capacitor on the LISN side of the filter C_{CL} is present. If the line-to-ground capacitor on the LISN side of the filter is absent, the green-wire inductor will have no effect. If the line-to-ground capacitor on the LISN side of the filter is present but the green-wire inductor is absent, $L_{GW} = 0$, then the line-to-ground capacitor will have less effect and only above about 1 MHz. Next, consider the effect on differential-mode currents. We will also simulate these currents as current sources, as shown in Fig. 6.12. Again, the symmetry of the filter dictates

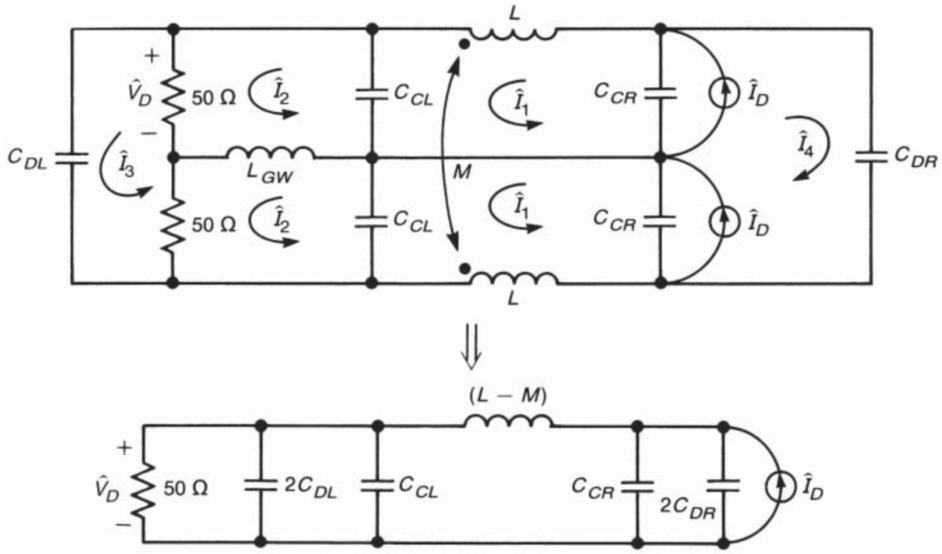

FIGURE 6.12 The equivalent circuit of the filter and LISN for differential-mode currents.

that certain mesh currents will be identical. Writing mesh current equations shows that the equivalent circuit to differential-mode currents appears as shown. Note that the line-to-line capacitors appear twice as large to differential-mode currents. Also note that the line-to-ground capacitors are present, and therefore C_{CL} and C_{CR} also affect differential-mode currents in addition to common-mode currents! This is seldom significant, since the values of the line-to-ground capacitors are typically much smaller than those of the line-to-line capacitors. However, if the line-to-line capacitor with which the line-to-ground capacitor is in parallel is absent, then *the line-to-ground capacitor will affect differential-mode current*. Also note that an ideal common-mode choke, $L = M$, is completely transparent to differential-mode currents as expected. This again illustrates the importance of careful design of the common-mode choke.

6.2.4 Separation of the Conducted Emissions into Common- and Differential-Mode Currents for Diagnostic Purposes

The preceding discussion of the power supply filter concentrated on the *ideal behavior* of the filter. If the line-to-line capacitors behave ideally, then little differential-mode current will reach the LISN. If we can obtain sufficiently large values for the common-mode choke inductance, the line-to-ground capacitors, and the green-wire inductor, then very little common-mode current will reach the LISN. In practice, this almost never occurs, and the product may still fail to comply with the conducted emission regulatory limit even though a careful design of the filter has been completed. When the product is tested for compliance and found to be out of compliance at certain frequencies in the frequency range of the regulatory limit, the next question is how we shall *effectively and efficiently diagnose and correct the problem and bring the conducted emissions into compliance*. In order to illustrate the necessity for this, it is worthwhile to point out that this author has spent many needless hours changing values of the filter components and observing *no change in the levels of the conducted emissions*. Product development schedules cannot tolerate this inefficiency in the correction of the problem. We must be able to quickly and correctly diagnose the root of the problem. Which element of the power supply filter needs to be changed, and what should the element's new value be? There are other ways of reducing the levels of the conducted emissions that will be discussed in Section 6.3 but attacking the power supply filter is a viable first step.

The most important point to realize in the course of changing a power supply element value to effect a reduction in the conducted emissions is illustrated in Fig. 6.13. We have shown a typical plot of the *total* current of the phase or neutral wire. This is decomposed into common- and differential-mode components. Although rather obvious, it is important to point out that the total current is the sum or difference of the common-mode and differential-mode components as shown by (6.2):

$$\hat{I}_{\text{Total}} = \hat{I}_C \pm \hat{I}_D \tag{6.17}$$

If one component is larger than the other component, the total current is the dominant component! This seemingly obvious statement illustrates that one component may dominate over certain frequency ranges. If we change the power supply filter so as to reduce the dominant component, we will reduce the total current. On the other hand, if we change the power supply filter so as to reduce the component that is not dominant, we will cause *no reduction in the total*! Therefore, *if we wish to reduce the total conducted emission at a particular frequency, we must reduce the dominant component at that frequency*. It is also important to observe that one component may be dominant over one frequency range yet not be dominant over another portion of the conducted emission frequency range. (See Section 11.5.1 of Chapter 11 for a further discussion of this important concept of "dominant effect.")

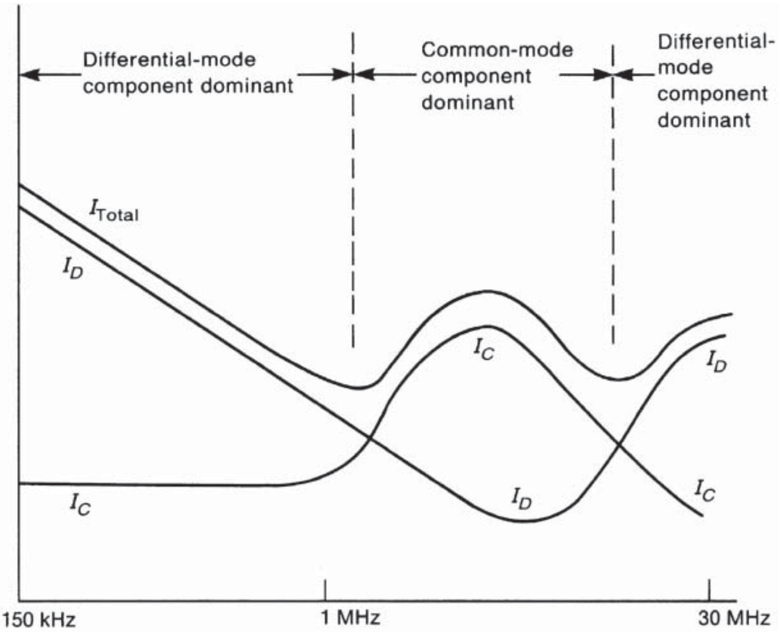

FIGURE 6.13 Illustration of the important observation that one component of current may dominate the other over a particular frequency range of the conducted emission test. In order to reduce the total conducted emission, the dominant component must be reduced.

Now let us consider how we shall reduce a particular component. We saw previously that each element of the power supply filter usually affects only one component: either differential- or common-mode. (The line-to-ground capacitors appear in the differential-mode circuit, yet they are usually much smaller than the line-to-line capacitors that are in parallel with them, and as such do not affect the differential-mode current. However, if the line-to-line capacitor with which they are in parallel is absent, then they will affect the differential-mode current.) So, *if we need to reduce the level of a particular* (*dominant*) *component, we must change the value of a power supply filter element that affects that component*. For example, suppose that the common-mode component dominates the differential-mode component at a frequency where the conducted emission exceeds the regulatory limit. Increasing the value of the line-to-line capacitance will only reduce the differential-mode component and so will not reduce the total conducted emission, since the differential-mode component was not the dominant component at this frequency. Conversely, suppose that the differential-mode component dominates the common-mode component at a particular frequency where the conducted emission exceeds the regulatory limit. Increasing the green-wire inductance by placing more turns on the core may reduce the common-mode component but will not affect a change in the conducted emissions at this frequency, since the differential-mode component was dominant. These observations easily explain the author's experience that *a radical change in the value of an element of the power supply filter may cause absolutely no change in the total conducted emissions; the component that was not dominant was reduced.*

If we are to be able to rapidly and correctly bring about a reduction in the conducted emissions by changing the values of some elements of the power supply filter, we must know which component is the dominant component in the total conducted emission. We need a *diagnostic tool* that can separate the total conducted emission into its common- and differential-mode components at each frequency of the regulatory limit. Such a device was described in [2]. The schematic of the device is shown in

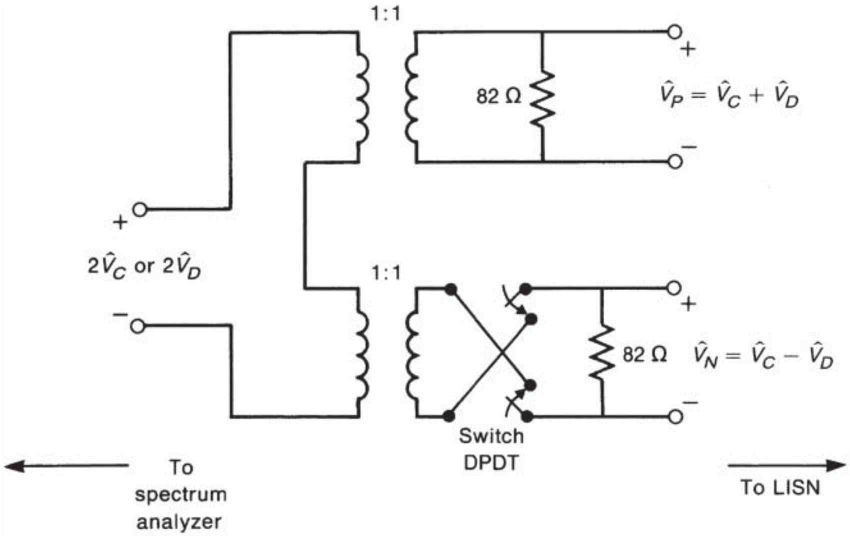
1:1
82 Ω
+
$\hat{V}_P = \hat{V}_C + \hat{V}_D$
−
+
$2\hat{V}_C$ or $2\hat{V}_D$
−
1:1
+
82 Ω
$\hat{V}_N = \hat{V}_C - \hat{V}_D$
−
Switch
DPDT
To
spectrum
analyzer
To LISN

FIGURE 6.14 Schematic of a device to separate the common-mode and differential-mode conducted emission contributions.

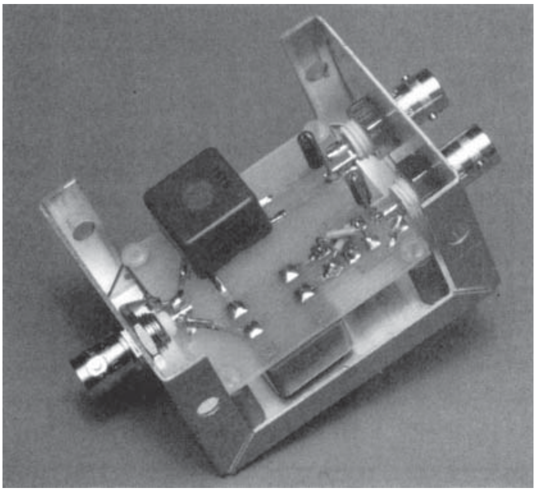

FIGURE 6.15 Photograph of the device of Fig. 6.14.

Fig. 6.14 and a photograph is shown in Fig. 6.15. The device basically adds or subtracts the phase and neutral voltages of the LISN to give only the differential-mode or only the common-mode component of the total conducted emission. It makes use of two wideband transformers (baluns). The phase and neutral output voltages of the LISN are applied to the primaries of the transformers. The secondaries are connected in series, and a switch changes the polarity of the neutral voltage. Since $\hat{V}_P = \hat{V}_C + \hat{V}_N$ and $\hat{V}_N = \hat{V}_C - \hat{V}_N$, the sum gives $\hat{V}_C$ and the difference gives $\hat{V}_D$:

$$\hat{V}_P + \hat{V}_N = 2\hat{V}_C \tag{6.18a}$$

$$\hat{V}_P - \hat{V}_N = 2\hat{V}_D \tag{6.18b}$$

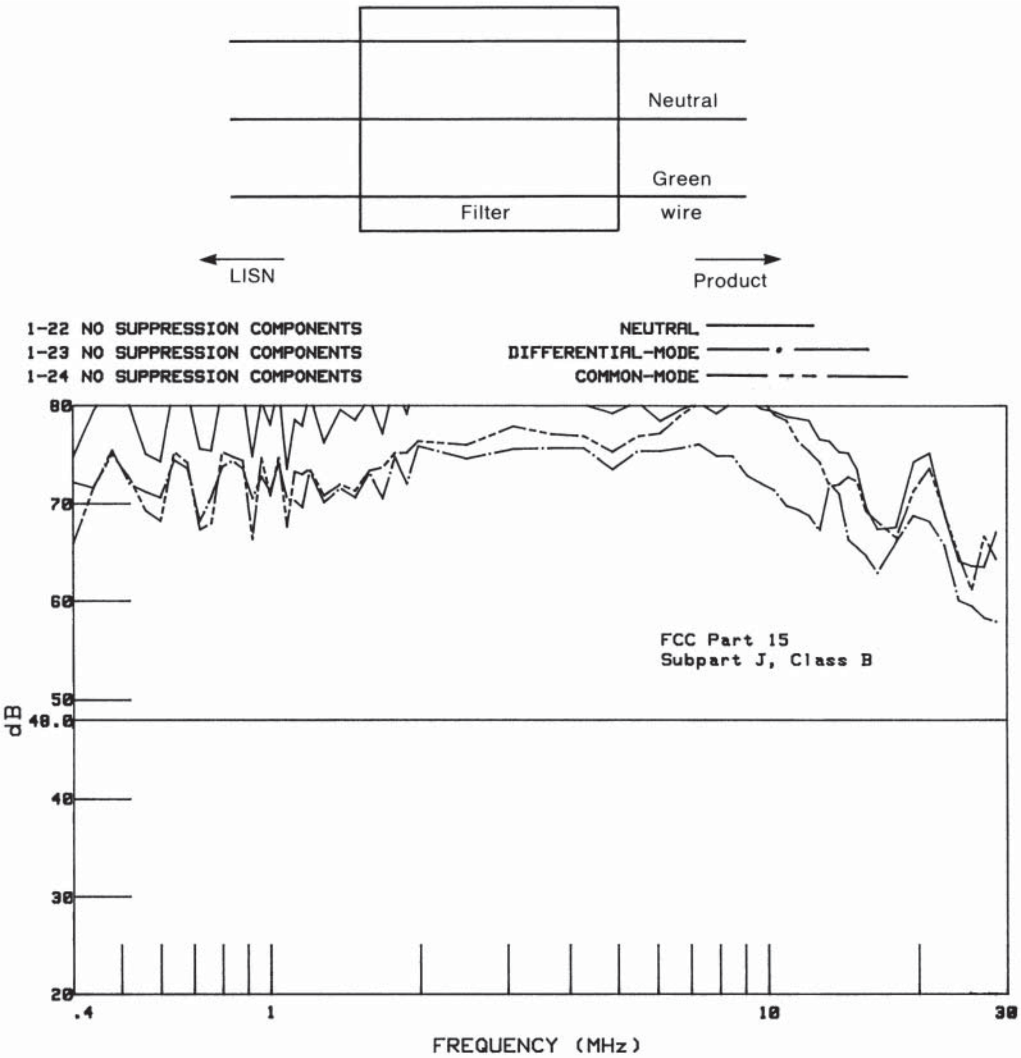

FIGURE 6.16 Measured conducted emissions of a typical digital product separated into differential- and common-mode components with no power supply filter.

In order to demonstrate the effectiveness of the device and to confirm the observations above about the effect of the individual elements of the power supply filter, we will consider an experiment that was described in [2].[1] A typical digital device containing a switching power supply and a power supply filter was tested. The elements of the power supply filter were first removed, and the product's conducted emissions were measured. These data are shown in Fig. 6.16. Observe that the conducted emissions exceed the FCC Class B limit by over 30 dB! The device was inserted at the output of the LISN, and the components are also shown in Fig. 6.16. Observe

---

[1] These measurements were taken before the FCC conducted emission frequency range was reduced from 450 to 150 kHz to harmonize with the CISPR 32 limits.

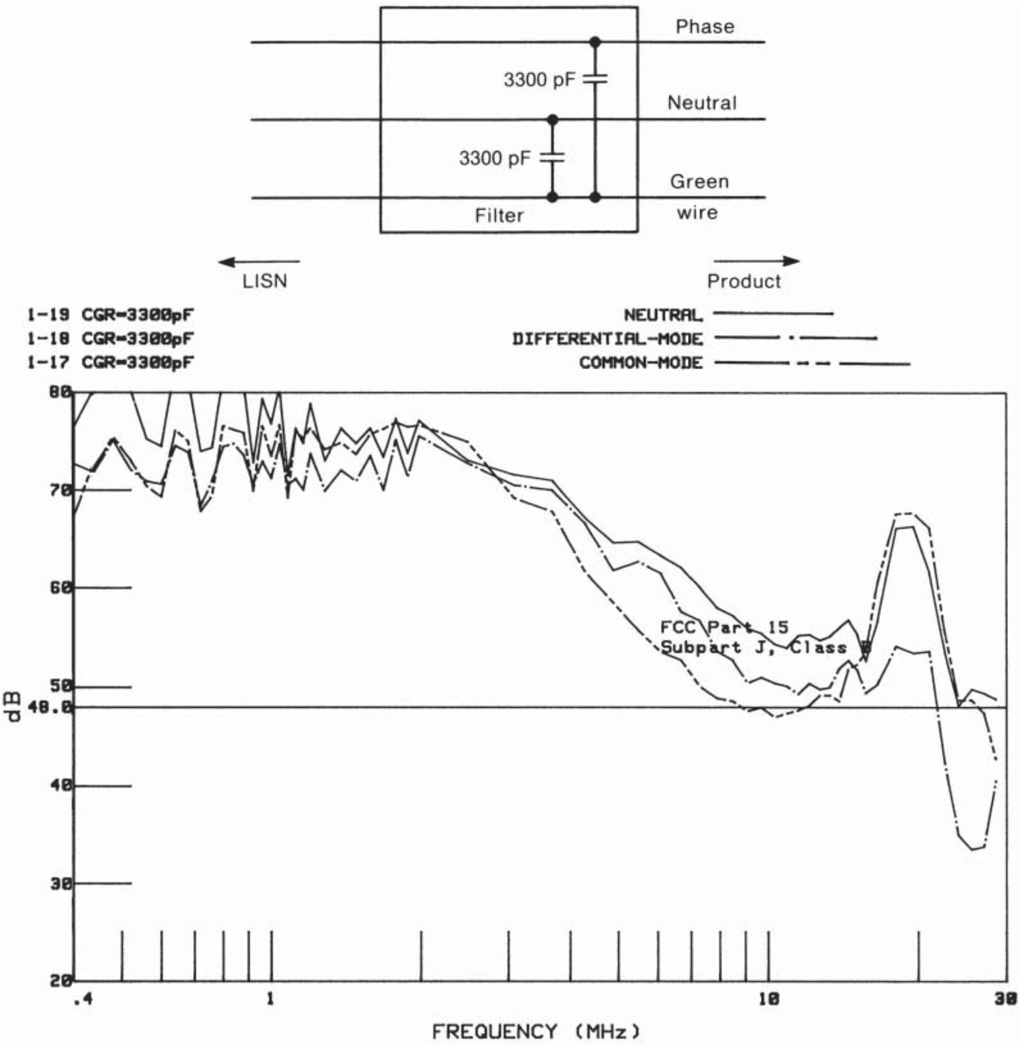

FIGURE 6.17 Measured conducted emissions of a typical digital product separated into differential- and common-mode components with 3300 pF line-to-ground capacitors added.

that the common- and differential-mode components of the total emission as measured with the device are the same order of magnitude. The filter elements were next added one by one and their effect observed. First, 3300 pF line-to-ground capacitors were added. The results are shown in Fig. 6.17. Note that the addition of the line-to-ground capacitors has reduced both the common- and differential-mode components by the same amount, but only above approximately 2 MHz. The 3300 pF line-to-ground capacitors are effectively in parallel with the 50 Ω resistors of the LISN (see Figs. 6.11 and 6.12) and so give a break frequency of order 1 MHz where their impedance equals 50 Ω. Thus, they will begin to shunt both common- and differential-mode currents above this frequency. Next, we add a 0.1 μF line-to-line capacitor. The results are shown in Fig. 6.18. Note that the common-mode component is unchanged, yet the differential-mode component has been reduced considerably. This is sensible to expect since this capacitor should

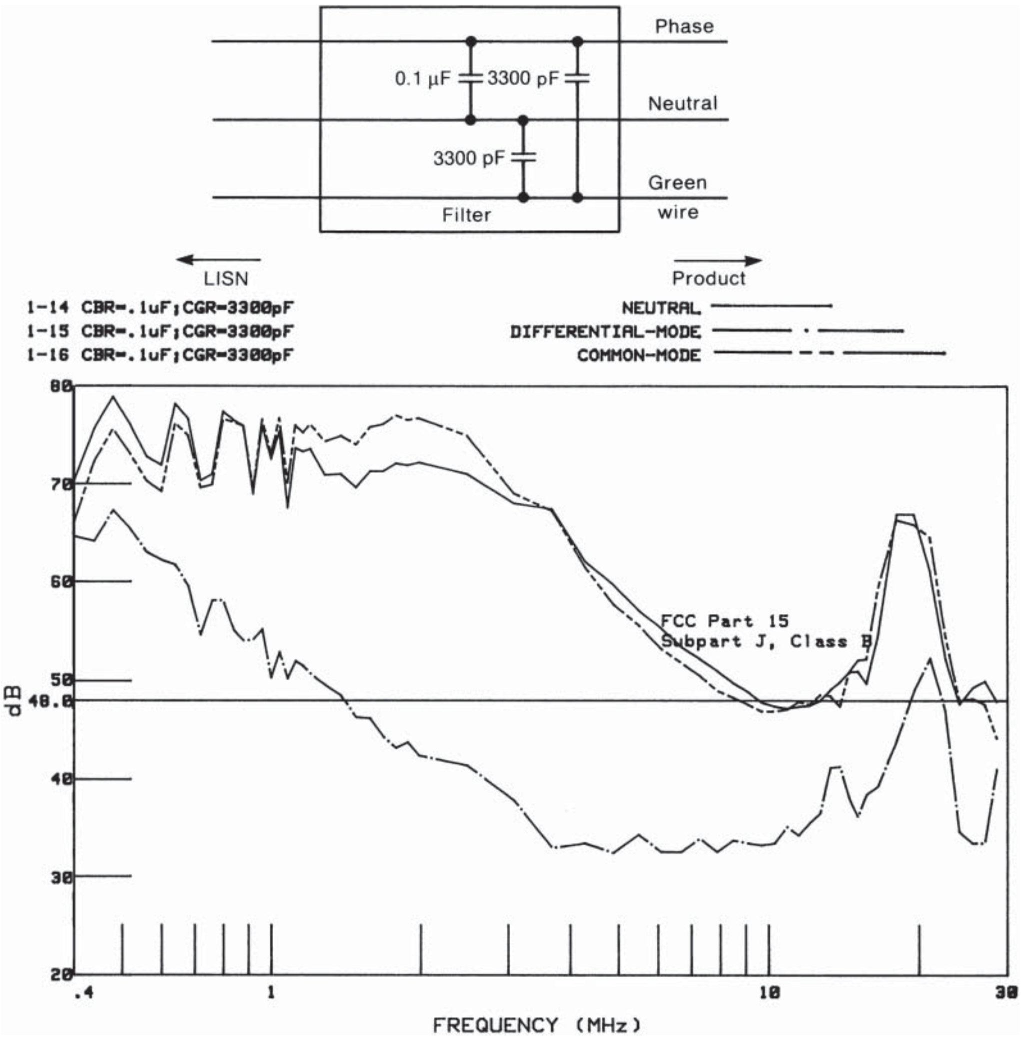

FIGURE 6.18 Measured conducted emissions of a typical digital product separated into differential- and common-mode components with a 0.1 μF line-to-line capacitor added.

affect only the differential-mode component (see Fig. 6.12). According to Fig. 6.12, the break frequency of this effect should be where the impedance of $2C_D + C_C = 0.203$ μF equals 50 Ω. This occurs at 15.7 kHz, which is well below the lower frequency of the plot. Next, we add the 1 mH green-wire inductor. The results are shown in Fig. 6.19. Observe that the differential-mode components are unchanged, but the common-mode components have been substantially reduced. From Fig. 6.11, this should occur where the impedance of $2L_{GW}$ equals 50 Ω, or approximately 4 kHz. And finally, we add the 28 mH common-mode choke. The results are shown in Fig. 6.20. Here, we see that the addition of the common-mode choke does not appear to substantially reduce the common-mode component, yet it drastically reduces the differential-mode component. The reason that it does not seem to reduce the common-mode component, as it was designed to

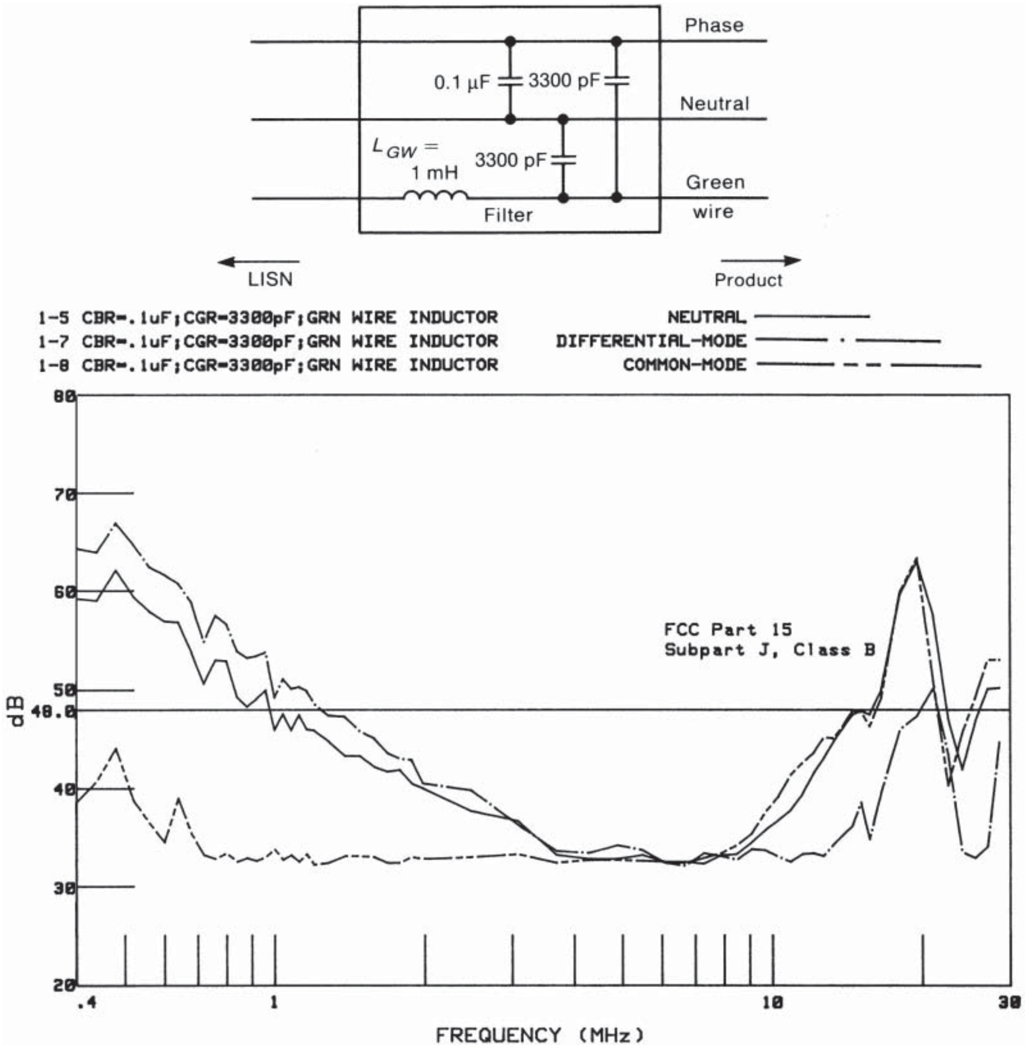

FIGURE 6.19 Measured conducted emissions of a typical digital product separated into differential- and common-mode components with a green-wire inductor added.

do, is that the green-wire inductor has already reduced the common-mode component below the noise floor of the spectrum analyzer, so that no further reduction can be seen. The reason that the differential-mode component has been affected is evidently due to the presence of the nonideal leakage inductance of the choke. Therefore, we have derived an additional benefit from the nonideal behavior of a component that is seldom desired. Some power supplies include small air-core inductors in phase and in neutral to affect the differential-mode current in like fashion. Individual ferrite core inductors should not be used in the phase and neutral lines, since the high-level 60 Hz differential-mode current will saturate the cores, making them no more effective than air-core inductors.

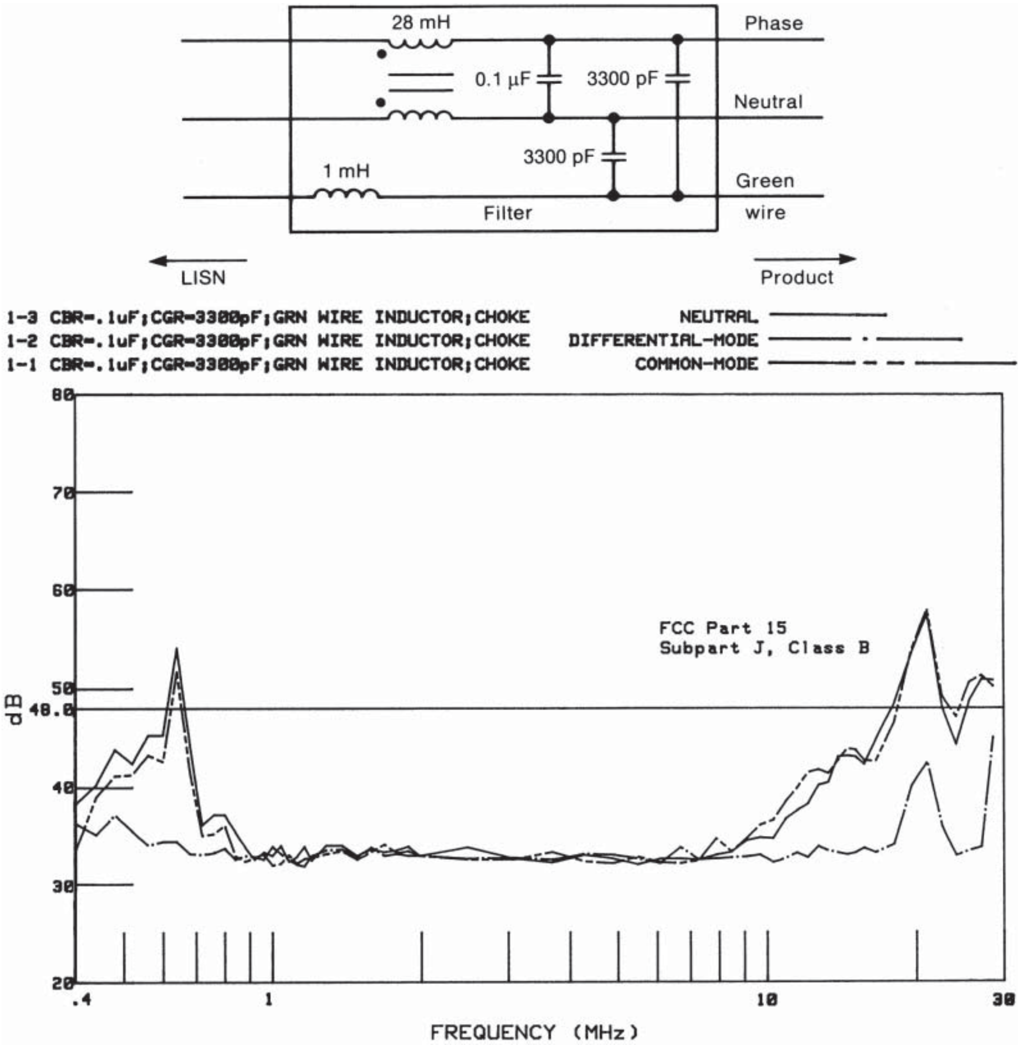

FIGURE 6.20 Measured conducted emissions of a typical digital product separated into differential- and common-mode components with a common-mode choke added.

6.3 POWER SUPPLIES

The primary source of conducted emissions is generally the power supply of the product. There are some important exceptions to this that we will discuss. For example, routing wires carrying digital data or clock signals near the output power wires will cause these digital signals to be coupled to the power cord, where they will be measured by the LISN, possibly causing the product to be out of compliance. For the present, we will address the noise that is generated in the product's power supply. There are numerous points within a power supply that generate noise measured by the LISN. Each particular type of power supply has unique noise-generating properties. In the previous section, we addressed the reduction of conducted emissions by use of a power supply filter. This represents a somewhat "brute force" method of reducing the conducted emissions. However, any power supply filter is capable of reducing the conducted emissions only to a certain degree. The most effective method for reducing conducted emissions is to *suppress them at their source*. This should be attempted where possible. But the noise can be reduced at its source only to a certain degree and still retain the functional performance of the supply. Pulses with sharp rise/falltimes have high-frequency spectral content, as was discussed in Chapter 3. Some power supplies such as switched-mode power supplies (switchers) rely on fast-rise/falltime pulses to operate and to reduce power losses in the supply. These types of noise sources can be reduced only to a certain point, so that compromises must be made between retaining the desired functional performance and reduction of the noise source.

It is worthwhile to consider the purpose of the product's power supply. The electronic components of the product (transistors, gates, microprocessors, memory storage, etc.) require dc voltages for proper operation. For example, the digital electronic components typically require +5 Vdc for proper operation. This voltage must remain within certain tolerances about the nominal value of 5 V, or the logic function will be impaired. Maintaining this output voltage within certain bounds regardless of the changing load on the power supply as the product performs its required function is an important function of a power supply and is referred to as *regulation*. Certain linear electronic components such as operational amplifiers, line drivers and receivers, and comparators require dc voltages of ±12 V. Still other devices within the product, such as dc and stepper motors, require other dc voltages for proper operation. (DC and stepper motors typically require dc voltages on the order of 30 V.) This process of converting 120 V, 60 Hz commercial ac power to the dc voltage levels required by the product's components and maintaining those levels under varying load conditions are the primary functions of the power supply.

6.3.1 Linear Power Supplies

For many years, the *linear power supply* was the predominant method for converting the ac commercial power to the dc voltages needed to power the electronic devices of the product. A typical linear power supply is shown in Fig. 6.21. To begin the discussion, we will disregard the bipolar transistor. A transformer at the input either steps the commercial voltage up or down in magnitude. This is then *rectified* by the two diodes, which form a *full-wave rectifier*. The rectifier converts the sinusoidal commercial voltage to pulsating dc [3]. This pulsating dc resembles the ac waveform of the input, except that the negative half-cycles are made positive [3]. This has an average value or, in

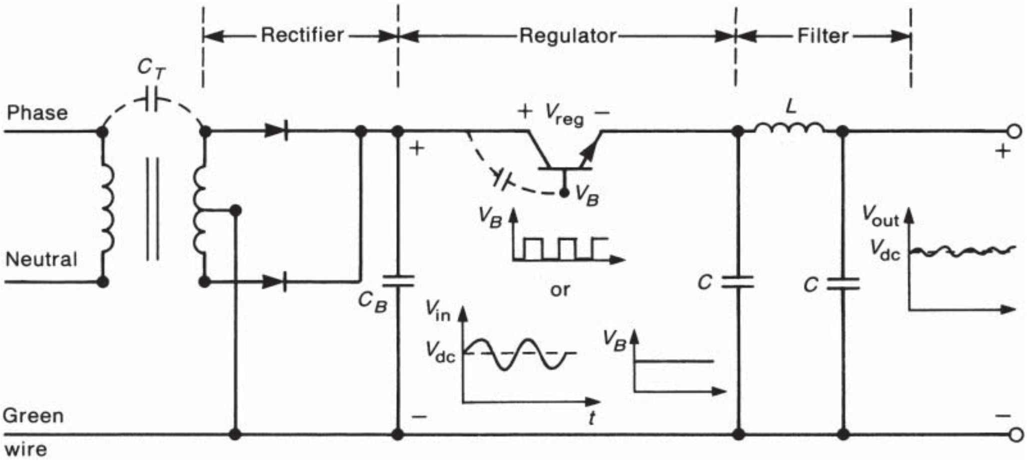

FIGURE 6.21 Illustration of a linear, regulated power supply.

other words, a dc component V_{dc}. A capacitor C_B (denoting the "bulk capacitor") acts to smooth this pulsating dc, giving an essentially constant waveform V_{in} with some variation and a dc level V_{dc}. A low-pass filter shown as a Pi structure consisting of two capacitors C and an inductor L serves to reduce these variations or *ripple* in the output voltage. If we view this waveform in terms of its Fourier components, we see that the filter must be a *low-pass filter* with a cutoff frequency near the fundamental of the pulsating dc waveform (60 Hz) in order to pass the dc level and block the higher harmonics of the waveform. It is not possible to extract only the dc level, so the resulting dc waveform will have a certain amount of *ripple* about the desired dc level. Power supply designs place specifications on the allowed ripple.

If we are satisfied with the level of this dc waveform and if the load on the supply will remain constant, then we do not need the transistor. The transistor acts to maintain the output voltage level in the presence of changes in the load on the supply. The process of maintaining a constant output voltage as the output current of the supply (the load) changes is referred to as *regulation*. In order to maintain the desired output voltage under varying load conditions, the transistor acts as a variable resistor to drop a certain voltage across its collector–emitter terminals. A sample of the dc output voltage is fed back to the base terminal of the transistor. If this dc output voltage becomes lower because of increased loading, the transistor is turned on more strongly, resulting in a lower V_{reg} being dropped across its terminals. The output voltage V_{out} of the supply and the output voltage of the rectifier V_{in} are related by

$$V_{\mathrm{out}} = V_{\mathrm{in}} - V_{\mathrm{reg}} \tag{6.19}$$

Thus, a reduction in the output voltage is compensated for by less voltage being dropped across the regulating transistor. If the output voltage of the supply increases because there is less loading, the transistor drops more voltage across its terminals, reducing the output voltage back to its desired value. Thus, regulation is accomplished under varying load conditions. This represents one of the undesirable features of linear power supplies; power is constantly being dissipated in the regulating transistor in order to maintain a constant dc output voltage of the supply.

Linear power supplies tend to be the quietest of all supply types. The switching power supply discussed in the next section is inherently much noisier but has other advantages over the linear supply from the standpoint of efficiency and lighter weight that make it attractive from a product performance standpoint. From the standpoint of EMC, its performance is less desirable than the linear supply since it is inherently noisier.

6.3.2 Switched-Mode Power Supplies (SMPS)

In this section, we will discuss a popular type of power supply: the *switched-mode power supply* (SMPS). This is frequently referred to as a "switcher." Linear supplies typically have quite low efficiencies of order 20–40%. Switching power supplies discussed in this section have much higher efficiencies of order 60–90%, which explains their popularity. Switching power supplies also tend to be much lighter in weight than linear power supplies. This is because linear supplies require a transformer that will operate efficiently at 60 Hz. Losses due to eddy currents in the transformer are minimized by the use of a large volume of core material. Thus, the 60-Hz transformer tends to be heavy. Switching power supplies require transformers to operate at the switching frequency of the supply, which is of order 20–100 kHz. Consequently, switching power supplies have transformers that are lighter in weight than those of linear supplies. (There are switchers available that operate at frequencies as high as 1 MHz, which further reduces their required weight.) Therefore, switching power supplies are lighter in weight than linear supplies, which is an additional feature that makes them desirable.

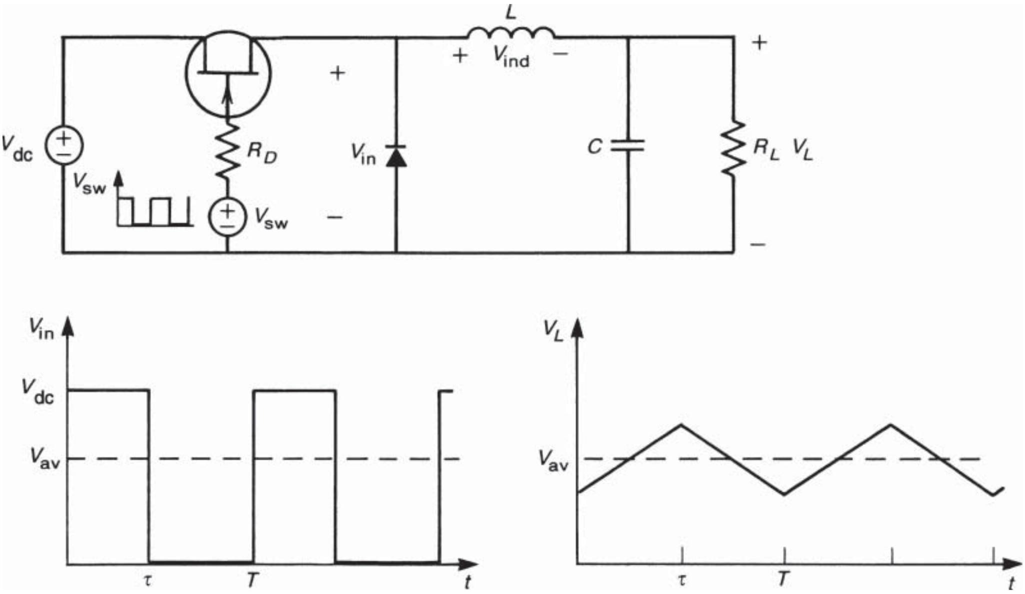

FIGURE 6.22 A simple "buck regulator" switching power supply.

There are numerous versions of switchers. However, in order to illustrate the basic principles, we will begin by discussing the basic *buck regulator* shown in Fig. 6.22. A dc voltage V_{dc} is supplied to a switching element. The switching element shown is a MOSFET. A square-wave pulse train is supplied to the gate of the MOSFET. This waveform has a pulsewidth τ and a period T that is the inverse of the switching frequency, $f_s = 1/T$. This pulse train turns the MOSFET on and off, which supplies a pulsed voltage of the same duty cycle at V_{in}. This waveform has an average (dc) value given by

$$V_{av} = \frac{\tau}{T} V_{dc} \tag{6.20}$$

The duty cycle of the waveform is the ratio of the pulsewidth to the period: $D = \tau/T$. Thus, this pulsed waveform has an average or dc value that can be changed by changing the duty cycle of the switching waveform that is applied to the gate of the switching element. The L and C form a low-pass filter to pass the dc (desired) component of the waveform, and the diode provides a path to discharge the capacitor when the MOSFET turns off. The cycle of operation is described as follows. When the MOSFET is turned on, the diode is open and the dc voltage is applied to the filter. The inductor begins to store energy in its magnetic field, and the capacitor begins to charge up. When the MOSFET is turned off, the voltage across the inductor V_{ind} reverses polarity according to Faraday's law, and the diode closes. The circuit discharges through the diode, giving the waveform across the load resistor shown in Fig. 6.22, which has the desired average or dc value. The advantage of this switcher over a linear regulator is that the switch element, the MOSFET, is either turned full on or full off and as such dissipates very little power as opposed to the linear regulator, where the transistor is always operated in its linear region, dissipating more power. Regulation is accomplished by simply varying the duty cycle of the switching waveform that is applied to the gate of the MOSFET. Typically, a sample of the output voltage V_L is fed to a pulsewidth modulator (PWM). The output of the PWM is a square wave, which is fed to the gate of the MOSFET. The duty cycle of this waveform is varied by the PWM to give the desired dc output voltage in response to changes in load. Other more practical

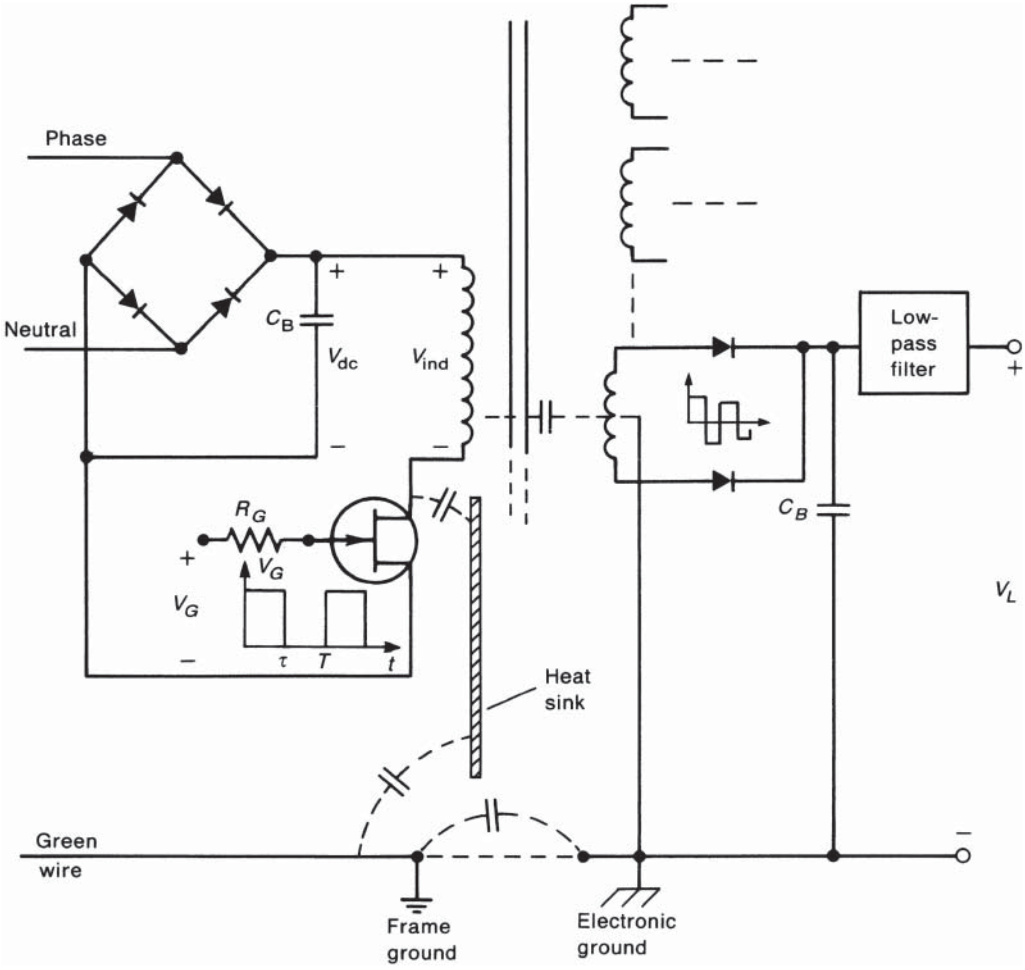

FIGURE 6.23 A typical “flyback” or primary-side switching power supply.

switchers employ this same basic principle of chopping a dc waveform and varying the duty cycle of the waveform to provide regulation.

There are two general types of switchers: the primary-side switcher and the secondary-side switcher. These designations refer to whether the switching occurs on the primary or secondary side of the transformer. Regulation is accomplished by varying the duty cycle of this switching waveform in response to changes in the output voltage of the supply. A primary-side switcher is shown in Fig. 6.23. The version shown is often referred to as a *flyback converter*. A *full-wave bridge rectifier* rectifies the ac commercial power waveform and produces a pulsating dc waveform, which is smoothed by the bulk capacitor C_B to provide an essentially constant waveform that has the value of the peak commercial voltage waveform. This is applied to a transformer that has multiple “taps” or windings on its secondary. A switching element (usually a power MOSFET) opens or closes the connection to the transformer primary. A variable-duty-cycle square-wave waveform is applied to the gate of this switching element. Varying the duty cycle of this waveform provides regulation of the output voltages of the supply. Ordinarily a resistor R_G is placed in series with the gate of the MOSFET switch. The effect of this resistor is to change the rise/falltimes of the pulses that are applied to the gate. Increasing the value of this resistor "rounds the sharp edges" of the waveform. This causes the MOSFET to spend more time in its active region, which increases its power dissipation, an undesirable result from the standpoint of thermal considerations. Increasing the rise/falltimes of the pulsed waveform is desirable from the standpoint of EMC, since the spectral content of the noise that is produced by the switching is directly dependent on these rise/falltimes. So, there is an apparent tradeoff between reduction of the noise spectral content that will contribute to conducted emissions and the thermal heating of the switching element and the related efficiency of the switcher. A heat sink is usually connected to the body of the MOSFET, which acts to dissipate this heat. Ordinarily this heat sink is not directly connected to the MOSFET but is insulated from it by a dielectric washer. This produces a parasitic capacitance between the MOSFET and the heat sink. If the heat sink is attached to the green wire for safety reasons, a path for common-mode currents is provided.

At the secondary side, a pulsating waveform that has alternating polarity pulses is produced. A full-wave rectifier rectifies this waveform, which is smoothed by the bulk capacitor and filtered by the low-pass filter. Because of the ability to have multiple taps on the secondary, numerous dc voltages of different levels can be obtained. For example, we may produce +5 V, +12 V, −12 V, +38 V, etc. Regulation of one of these voltages is accomplished on the primary side of the transformer. Because the transformer is required to carry only the switching frequency (and all its higher harmonics), it can be designed to be smaller and lighter in weight than the 60 Hz transformer. Efficiency is increased over the linear supply due to the switching action (unless the gate resistor is increased to reduce noise emissions). Observe that a major disadvantage of the primary-side switcher is that the switching harmonics are fed directly out the product's ac power cord through the bridge rectifier. There is no 60-Hz transformer present to provide any filtering. Any reduction of this noise that cannot be reduced by changing components in the switcher such as R_G must be eliminated by the power supply filter. This places a larger demand on the necessity for and the careful design of the power supply filter.

6.3.3 Effect of Power Supply Components on Conducted Emissions

As was pointed out earlier, *the most efficient method for the reduction of conducted emissions is to reduce them at their source*. For example, increasing the value of the gate resistor R_G in the primary side switcher shown in Fig. 6.23 will increase the rise/falltimes of the switching waveform and hence reduce their spectral content. However, these rise/falltimes can only be increased to a point because the switching device will spend more time in its active region, which increases its power dissipation.

There are other "noise sources" present in the switcher that should be controlled. One of the major ones comes from the diodes that are used for rectification—particularly the diodes that rectify the switched signal, such as those on the secondary side of the primary-side switcher shown in Fig. 6.23. When a diode is forward-biased, charge is stored at its junction in the junction capacitance. Also, charge carriers in one region are injected into the other region. When the diode is turned off, this charge must be removed. This results in the diode current having the waveform shown in Fig. 6.24a. The diode current passes through zero as the charge is being removed from the junction. Some diodes known as "fast-recovery diodes" snap off sharply. This is referred to as "hard-recovery" and is illustrated in Fig. 6.24a. Other types have soft recoveries where the diode current returns to zero gradually. Obviously, hard-recovery diodes will yield higher-frequency spectra in the current than will soft-recovery diodes, due to the sharp edge of the current waveform when the diode current returns to zero. From the standpoint of efficiency, fast-recovery diodes are more desirable than slow-recovery diodes. In order to reduce this undesirable noise generated in the turnoff of the diode, *snubber circuits* illustrated in Fig. 6.24b are generally placed in parallel with the diodes. The snubber circuit consists of a resistor in series with a capacitor that acts as a path to discharge the charge

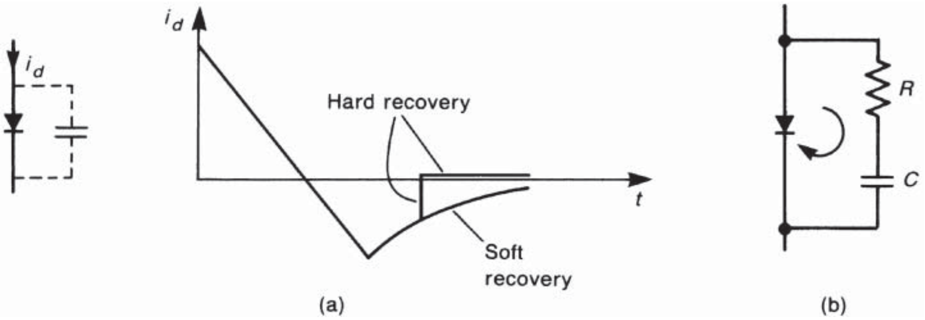

FIGURE 6.24 Illustration of nonideal effects in diodes: (a) various recovery characteristics; (b) an *RC* "snubber" circuit.

stored at the diode junction when the diode turns off. This tends to smooth the diode current waveform, thereby reducing its high-frequency spectral content. Obviously, high-frequency currents will circulate through the snubber circuit, so its leads should be kept short and the elements placed very close to the diode in order to reduce the current loop area and hence the radiated emissions from this loop (see Chapter 8).

Parasitic capacitances provide numerous current paths for noise currents to exit the switcher and contribute to the product's conducted emissions. Capacitance between the switching element and its heat sink will couple switching noise at the element to the heat sink, where it may radiate or be conducted out the line cord. Transformers are used in several places in electronic products. The primary use is in the *power supply* for the product. As discussed above, *linear power supplies* use a transformer to *step down* the 120 V, 60 Hz ac (240 V, 50 Hz ac in Europe) to voltage levels that are *rectified* to produce the dc voltages that power the electronic devices in the product. These types of transformers are of necessity heavy and large in order to reduce the *eddy-current* losses in the core caused by the 60 Hz frequency of the primary ac power. *Switching power supplies* chop this primary power at much higher frequencies (25–100 kHz) to produce the required dc voltages, as discussed earlier. Because of the much higher frequency of the flux in the core, transformers in switching power supplies have much lower eddy-current losses than 60 Hz transformers and can be designed to be much smaller and lighter.

All transformers make use of Faraday's law of induction to change one voltage level to another. Two coils are wound on the same ferromagnetic core as shown in Fig. 6.25a. The voltage v_p across the *primary* generates a current and associated magnetic flux in that winding. Because of the much lower reluctance of the ferromagnetic core compared with that of the surrounding air, the majority of this flux couples to the *secondary*, inducing, by Faraday's law, a voltage v_s across that winding. The ratio of the two voltages is (ideally) proportional to the ratio of the numbers of the turns in each coil:

$$\frac{v_p}{v_s} = \frac{n_p}{n_s} \tag{6.21}$$

There are a number of ways to construct these transformers. The 60-Hz transformers in linear supplies are usually constructed from laminations of steel stacked together. The laminations tend to break up the magnetic flux paths and reduce the eddy-current losses. High-frequency transformers are usually constructed from ferrite cores. There are several transformer core configurations that are different from the simplified version shown in Fig. 6.25a in order to facilitate their assembly. The 60-Hz transformers are constructed from an "I-core" of laminations, with the primary and secondary

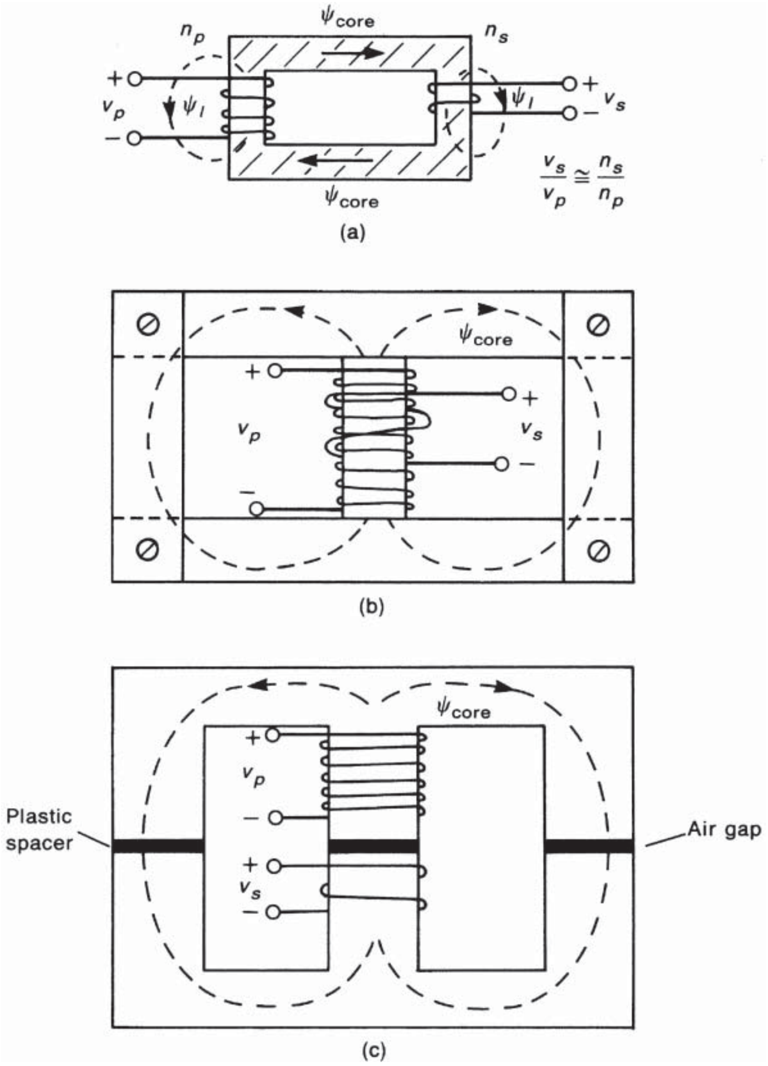

FIGURE 6.25 Construction of transformers: (a) transformer schematic; (b) a 60-Hz transformer; (c) an "E-core" switching power supply transformer.

windings wound on top of each other as shown in Fig. 6.25b. Outer vertical legs of laminations are connected to complete the flux path. Transformers designed to operate at higher frequencies such as in switching power supplies typically use powdered ferrite cores. These are formed into "bobbins" and are available in various configurations. A common one is the "E-core," in which the two halves are shaped like the letter E. The primary and secondary windings are wound on the center legs of each core, and the two halves are placed together to provide a continuous path for the magnetic flux as shown in Fig. 6.25c. Ferrite cores used in these types of transformers are also subject to *saturation* due to high levels of flux caused by high current levels. In order to limit this saturation, thin, plastic spacers are placed in the air gaps when the cores are placed together. This acts to increase the reluctance of the magnetic path, which reduces the flux levels and prevents saturation of the core. Unfortunately, these gaps inadvertently produce large magnetic fields at the switch frequency

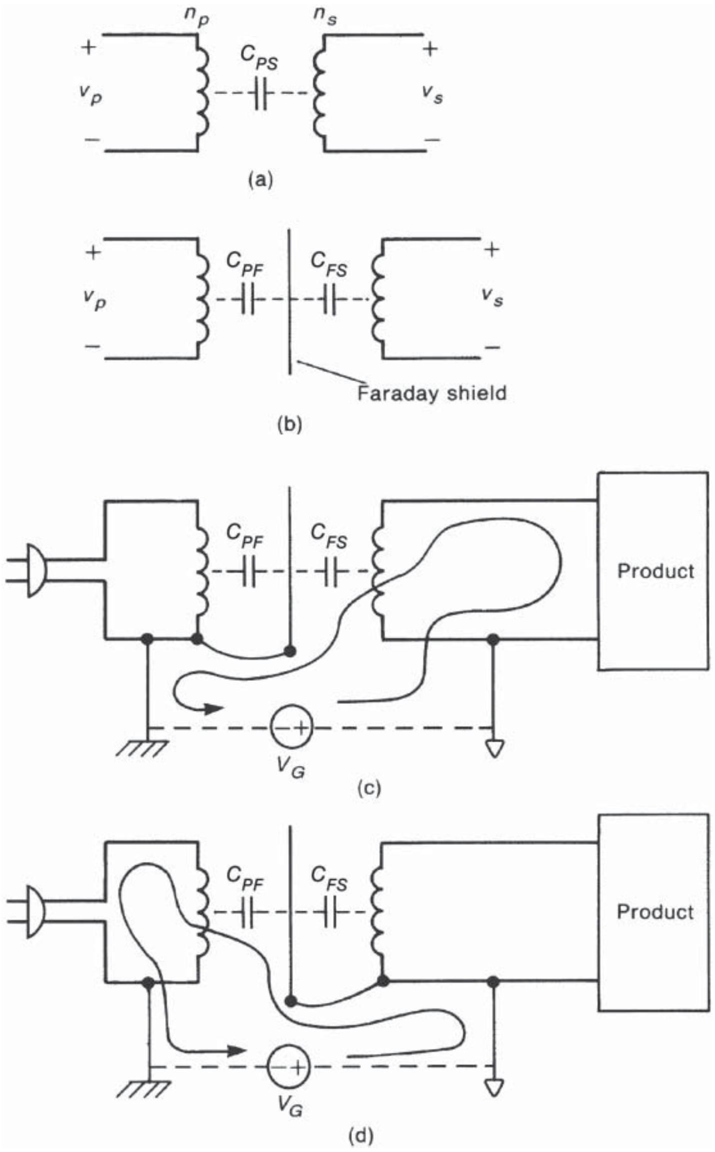

FIGURE 6.26 Illustration of the effect of primary-to-secondary capacitance of a transformer: (a) lumping the parasitic capacitance; (b) use of a Faraday shield; (c) proper connection of the Faraday shield to reduce conducted emissions; (d) improper connection of the Faraday shield.

and its harmonics. This can cause low-frequency-radiated magnetic fields that may cause regulatory compliance problems.

Winding the coils on top of each other (lap winding) as with the I-core of the 60-Hz transformer introduces a *parasitic capacitance* between the primary and secondary as shown in Fig. 6.26a. This primary-to-secondary capacitance can introduce an undesired coupling that allows noise on the secondary side (the electronics side) to be more easily coupled to the primary side (where the system power cord is attached). Once the noise is present on the primary side, it passes out through the power cord and is measured as a conducted emission by the LISN unless a power supply filter is inserted between the power cord and the transformer. Evidently, the efficiency of this coupling due to the parasitic primary-to-secondary capacitance increases at higher noise frequencies. For example, the system processor clock in a digital system (typically greater than 10 MHz) would couple to the primary more easily than would switcher harmonics. In order to reduce this coupling, the primary and secondary coils that are wound on top of each other may have a cylindrical, metallic shield inserted between them. This is referred to as a *Faraday shield*. This effectively breaks up the primary-to-secondary capacitance, as is illustrated in Fig. 6.26b. The question always arises as to which side of the transformer, primary or secondary, should we connect the Faraday shield. The answer depends on where we wish to divert any noise current produced by the difference in potentials of the primary and secondary grounds. The difference between the potentials of the secondary and primary grounds are represented by the voltage source V_G. Figure 6.26c shows connection of the shield to the primary. For this connection, the noise current produced by V_G flows through C_{FS}, the shield, and back through the ground. This is the preferred connection of the shield since the noise current will not flow through the LISN to produce conducted emission problems. Figure 6.26d shows the connection of the shield to the secondary. This connection would cause the noise current to flow through the shield, through C_{PF}, out through the line cord, and back through V_G. Thus, the noise currents would flow through the LISN, possibly resulting in conducted emission problems. The same principle applies to a transformer between an amplifier and a receiver. In order to prevent the noise currents from flowing through the receiver input, the shield should be grounded at the receiver input. Evidently, this desired operation depends also on connecting the Faraday shield to the *grounded side* of the transformer. Proper connection of the Faraday shield is important in reducing the effects of the common-mode voltage between primary and secondary. Ideally, this is what happens, but realistically we observe less than ideal performance due to the resistance and inductance of the shield.

Ferrite beads tend to be effective in blocking noise currents in power supplies. Recall from Chapter 5 that ferrite beads typically have maximum values of impedance of the order of a few hundred ohms. Therefore, in order for them to be effective, they must be in series with impedances that are no larger than the bead impedance, since otherwise the bead impedance would be overshadowed by this larger impedance. The intent is to use the bead to *block noise currents* by adding a significant impedance to the path. Circuit impedances tend to be small in power supplies as opposed to other electronic circuits. Therefore, insertion of a bead tends to provide a significant increase in the circuit impedance in power supply circuits.

6.4 POWER SUPPLY AND FILTER PLACEMENT

Location of components and routing of wires within a product are important considerations in the reduction of conducted and radiated emissions of the product. Being cognizant of some simple notions with regard to the location of components and the routing of wires in a product design (“packaging of the product”) can be an essentially cost-free method of reducing conducted and radiated emissions. A common example is the location of the power supply and its associated power supply filter. *The power supply filter should be placed directly at the exit of the power cord from the product*. The power supply should also be placed as close to the filter as possible. The result of not doing this is illustrated in Fig. 6.27a. There is a wide spectrum of high-frequency noise signals present inside the product. These range from the switching power supply harmonics to harmonics of the clocks used to drive the system’s digital elements and processors. Thus, the spectral content ranges from 20 kHz to well over 500 MHz. These signals tend to be near-field type and die out rapidly with distance from the source. Nevertheless, the higher the frequency of the signals, the

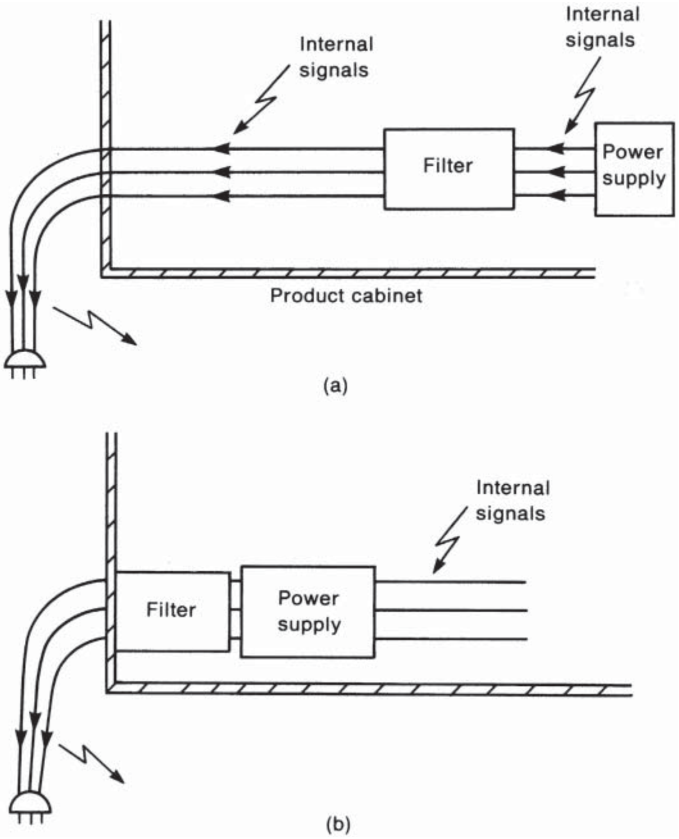

FIGURE 6.27 Illustration of (a) poor filter placement and (b) proper filter placement in the reduction of conducted emissions.

more efficiently are they coupled to the wires inside the product. If the power supply filter is not placed very close to the exit of the power cord, these signals may couple to those wires and exit the product on its power cord. They will therefore be measured as conducted and/or radiated emissions. Note that these signals have bypassed the power supply filter, and as such the filter provides no protection against these signals, causing possible regulatory compliance problems. If the power supply is also placed distant from the power supply filter, these signals may couple to the wires between the filter and the supply. We might expect that the filter would serve to attenuate these. This is not always the case. The power supply filter was designed to attenuate signals in the conducted emission frequency range (150 kHz–30 MHz). Suppose that the system clock has a frequency of 50 MHz. It is doubtful that the power supply filter will provide any filtering to the fundamental frequency of this clock signal, much less to, say, its fifth harmonic of 250 MHz. Once again we must not allow ourselves to overlook these types of undesired performance of the components of the product. Once the clock signal harmonics are present on the product's power cord, they will be measured as conducted emissions (50 MHz) and radiated emissions (100 MHz, 150 MHz, 200 MHz, …). If the power supply filter and the power supply are placed as close to the power cord exit as possible, as shown in Fig. 6.27b, this will minimize the coupling of internal signals to their connection wires and will place a considerable number of possibilities for attenuating these signals in their path.

6.5 CONDUCTED SUSCEPTIBILITY

As we have discussed at several points, the regulatory requirements on conducted emissions are intended to control the radiated emissions from noise currents that are placed on the local power distribution system by conduction out through the product's ac power cord. These signals are generally too small to cause interference by direct conduction from the power net into another product via its ac power cord. However, large transients placed on the power distribution net by such phenomena as lightning strokes can cause EMC problems in a product by direct conduction into that product's ac power cord. Equipment manufacturers realize this and test their products' conducted susceptibility by directly injecting typical such disturbances on the product's ac power cord to ensure that the product will operate satisfactorily through such disturbances.

It goes without saying that a well-designed power supply and its proper placement will tend to provide *some protection* to these types of signals on the ac power cord. However, since the spectral content and signal level of these disturbances tend to be larger than the typical conducted emissions, the power supply filter may not be as effective as desired in this case. Testing will generally reveal when additional protection is required.

PROBLEMS

Section 6.1 Measurement of Conducted Emissions

6.1.1 In order to illustrate that the LISN essentially presents 50 Ω impedances between phase and ground and between neutral and ground, use a circuit analysis software such as LTSPICE to plot the frequency response of the impedance looking into one side of the LISN shown in Fig. P6.1.1 over the conducted emission frequency range of 150 kHz–30 MHz for two cases of impedance seen looking into the power net: (1) short-circuit load and (2) open-circuit load. Determine the values at each end of the frequency band. [Short-circuit: 38.31 and 47.62 Ω; open-circuit: 37.85 and 47.62 Ω]

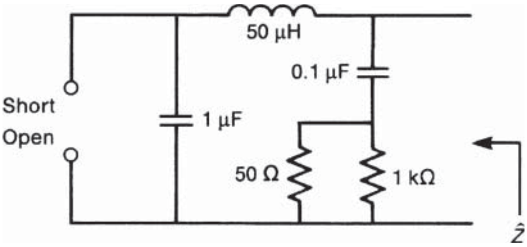

FIGURE P6.1.1

6.1.2 The Class B quasi-peak conducted emission limits at 150 kHz, 500 kHz, and 30 MHz are 66 dBμV, 56 dBμV, and 60 dBμV. Determine these in amperes and dBμA. [32 dBμA, 39.9 μA, 22 dBμA, 12.6 μA, 26 dBμA, 20 μA]

Section 6.2 Power Supply Filters

6.2.1 Use a circuit analysis software such as LTSPICE to plot the frequency response of the differential-mode insertion loss test for a typical power supply filter shown in Fig. P6.2.1a.

Repeat this for the common-mode insertion loss test shown in Fig. P6.2.1b. Determine the insertion loss at 150 kHz and 30 MHz. [Differential mode: 41.7 dB and 179.75 dB; common mode: 49.2 dB and 166.18 dB]

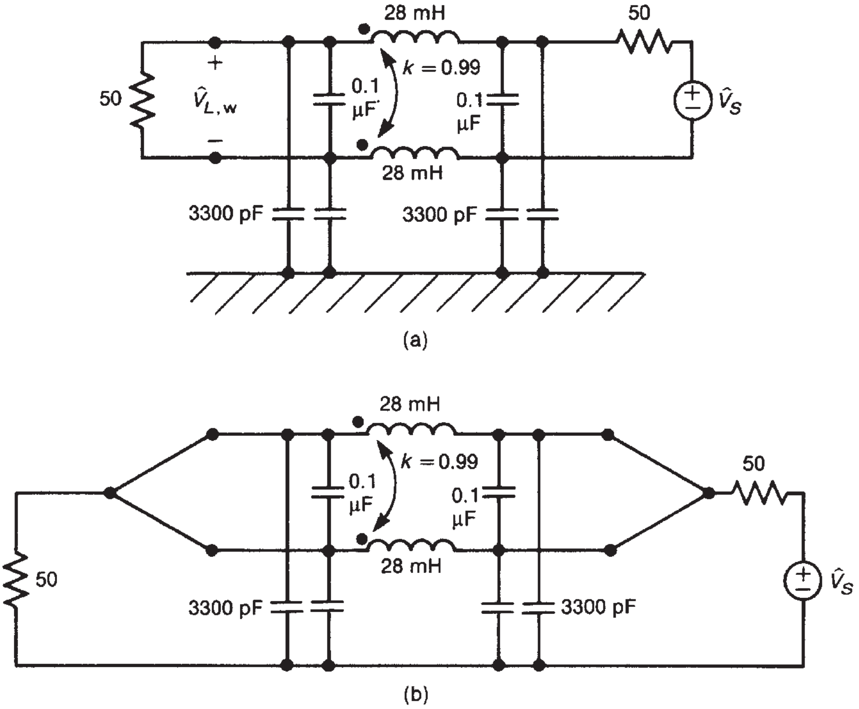

FIGURE P6.1.2

6.2.2 Suppose that a green-wire inductor has an inductance of 1 mH and a parasitic capacitance of 10 pF. Determine the resonant frequency of this inductance and its impedance at 30 MHz. [1.6 MHz, 532 Ω]

6.2.3 Determine an equation for the insertion loss of the high-pass filter shown in Fig. 6.7b. [$\text{IL}_{\text{dB}} = 10 \log 10 \{[1 + (\omega\tau)^2]/(\omega\tau)^2\}$, $\tau = C(R_S + R_L)$]

6.2.4 Determine an equation for the insertion loss of the band-pass filter shown in Fig. 6.7c. [$\text{IL}_{\text{dB}} = 10 \log 10 \{1 + [(\omega/\omega_0)^2 - 1]^2/(\omega\tau)^2\}$, $\tau = C(R_S + R_L)$, $\omega_0 = 1/\sqrt{LC}$]

6.2.5 Determine and equation for the insertion loss of the band-reject filter shown in Fig. 6.7d. [$\text{IL}_{\text{dB}} = 10 \log 10 \{1 + (\omega\tau)^2/[(\omega/\omega_0)^2 - 1]^2\}$, $\tau = L/(R_S + R_L)$, $\omega_0 = 1/\sqrt{LC}$]

6.2.6 Suppose that a common-mode choke has self-inductances of 28 mH and a coupling coefficient of 0.98. Determine the leakage inductance presented to differential-mode currents. [560 μH] Repeat this for a coupling coefficient of 0.95. [1.4 mH]

6.2.7 The effect of a power supply filter on common-mode currents is sometimes characterized by the common-mode impedance as $\hat{Z}_C = \hat{V}_C/\hat{I}_C$ with reference to Fig. 6.11. For $L_{GW} = 1$ mH, $L = 28$ mH, $k = 0.98$, and $C_{CL} = C_{CR} = 3300$ pF, use a circuit analysis software such as LTSPICE to plot this from 150 kHz to 30 MHz. Compute this at 150 kHz and 30 MHz. [−24 dBΩ, −210 dBΩ] Repeat this for the differential-mode impedance with respect to Fig. 6.12 with $C_{DR} = C_{DL} = 0.1$ μF. [−25.6 dBΩ, −164 dBΩ]

6.2.8 For the specifications of Problem 6.2.7 suppose that the common-mode and differential-mode currents at the input to the power supply filter at 150 kHz are equal to 1 mA. Determine the total received voltage across the LISN 50 Ω and which component is dominant. [41.25 dBμV, common-mode]

Section 6.3 Power Supplies

6.3.1 The buck regulator shown in Fig. 6.22 is to be operated at a switching frequency of 50 kHz, an input voltage of 100 V, and an output voltage of 5 V. Determine the required duty cycle. [0.05] Calculate the level of the 25th harmonic (1.25 MHz) of the ideal chopped voltage V_{in}. (Use the asymptotic approximations developed in Chapter 3 and the exact formula.) [Approximate: 128.1 dBμV; exact: 125.1 dBμV]

REFERENCES

1. J. R. Nicholson and J. A. Malack, RF impedance of power lines and line impedance stabilization networks in conducted interference measurements, *IEEE Trans. Electromagn. Compat.* EMC-15, 84–86 (1973).
2. C. R. Paul and K. B. Hardin, Diagnosis and reduction of conducted noise emissions, *IEEE Trans. Electromagn. Compat.* EMC-30, 553–560 (1988).
3. C. R. Paul, S. A. Nasar, and L. E. Unnewehr, *Introduction to Electrical Engineering*, McGraw-Hill, New York, 1986.

CHAPTER SEVEN

Antennas

Antennas are obviously a major ingredient in the discipline of EMC. *Intentional antennas* such as AM, FM, and radar antennas generate electromagnetic fields that couple to electronic devices and result in susceptibility problems. Intentional antennas are also used to measure the radiated emissions of a product for determining compliance to the regulatory limits. *Unintentional antennas* are responsible for producing the radiated emissions that are measured by the measurement antenna and may result in the product being out of compliance. In this chapter, we will review the basics of intentional antennas. This will provide the ability to calculate the electromagnetic field levels *in the vicinity of the product* that will be used to determine its susceptibility to interference. Antennas used to verify regulatory compliance will be discussed. The analysis of intentional antennas also provides understanding of the ability of unintentional antennas to radiate, which is what we are trying to minimize or prevent. A more detailed discussion is found in [1, 2] or other similar texts on elementary electromagnetic field theory.

7.1 ELEMENTAL DIPOLE ANTENNAS

If we know the current distribution over the surface of the antenna, we can obtain the radiated electric and magnetic fields by performing an integral involving this current distribution [1]. Although this result, in principle, allows us to characterize the radiated fields of all antennas, there are two practical complications: the need to obtain the current distribution over the antenna and the need to perform a difficult integration. Typically, we make a reasonable guess as to the current *distribution*. In this section, we will investigate some simple antennas whose radiated fields resemble those of practical antennas so long as the field point is sufficiently distant from the antenna.

7.1.1 The Electric (Hertzian) Dipole

The Hertzian dipole consists of an infinitesimal current element of length dl carrying a phasor current $\hat{I}$ that is assumed to be the same (in magnitude and phase) at all points along the element length, as illustrated in Fig. 7.1. A spherical coordinate system is commonly used to describe antennas. This is because waves radiated from antennas at large distances are spherical waves. The location of a point

---

Introduction to Electromagnetic Compatibility, Third Edition. Clayton R. Paul, Robert C. Scully, and Mark A. Steffka.
© 2023 John Wiley & Sons, Inc. Published 2023 by John Wiley & Sons, Inc.

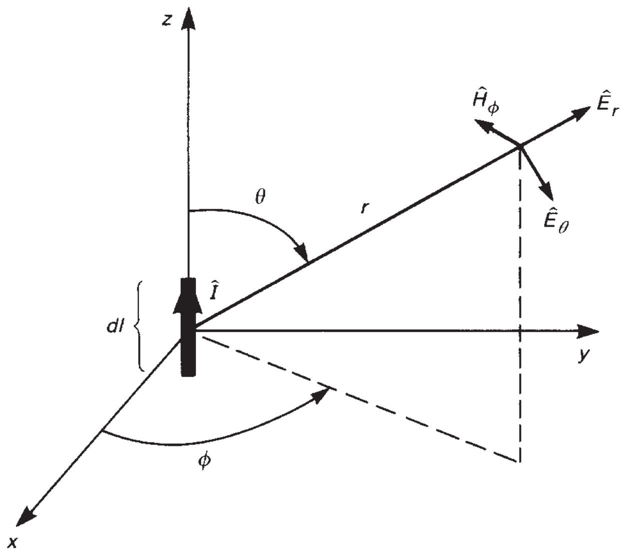

FIGURE 7.1 The electric (Hertzian) dipole.

in this coordinate system is described by the radial distance to the point, r, and the angular positions of a radial line to the point from the z axis, θ, and between its projection on the xy plane and the x axis, ϕ, as shown in Fig. 7.1. Orthogonal unit vectors $\boldsymbol{a}_r$, $\boldsymbol{a}_\theta$, $\boldsymbol{a}_\phi$ point in the directions of increasing values of these coordinates. The components of the magnetic field intensity vector become [1, 2]

$$\hat{H}_r = 0 \tag{7.1a}$$

$$\hat{H}_\theta = 0 \tag{7.1b}$$

$$\hat{H}_\phi = \frac{\hat{I}dl}{4\pi}\,\beta_0^2\,\sin\theta\left(j\frac{1}{\beta_0 r} + \frac{1}{\beta_0^2 r^2}\right)e^{-j\beta_0 r} \tag{7.1c}$$

Similarly, the components of the electric field intensity vector are [1]

$$\hat{E}_r = 2\frac{\hat{I}dl}{4\pi}\eta_0\beta_0^2\cos\theta\left(\frac{1}{\beta_0^2 r^2} - j\frac{1}{\beta_0^3 r^3}\right)e^{-j\beta_0 r} \tag{7.1d}$$

$$\hat{E}_\theta = \frac{\hat{I}dl}{4\pi}\eta_0\beta_0^2\sin\theta\left(j\frac{1}{\beta_0 r} + \frac{1}{\beta_0^2 r^2} - j\frac{1}{\beta_0^3 r^3}\right)e^{-j\beta_0 r} \tag{7.1e}$$

$$\hat{E}_\phi = 0 \tag{7.1f}$$

where $\eta_0 = \sqrt{\mu_0/\varepsilon_0}$ is the intrinsic impedance of free space. Note that the fields in (7.1) can be viewed as functions of *electrical distance from the antenna*, since $\beta_0 r = 2\pi r/\lambda_0$ and $\lambda_0 = v_0/f$ is the wavelength at the frequency of the antenna current. Again, $v_0 = 3 \times 10^8$ m/s is the speed of light.

The complete fields in (7.1) are quite complicated. Our main interest is in the *far fields* where the field point is sufficiently distant from the antenna. How far is "far enough." Note that the $1/r^3$ and

$1/r^2$ terms dominate at very close distances to the antenna. As we move further from the antenna, the $1/r$ terms begin to dominate. The point where the $1/r^3$ and $1/r^3$ terms become insignificant compared with the $1/r$ terms is referred to the boundary between the *near field* and the *far field*. This occurs where $1/(\beta_0 r)^2 = 1/\beta_0 r$ or $r = \lambda_0/2\pi \cong \lambda_0/6$. The reader is cautioned that *the boundary between the near and far fields for other antennas is not simply* $\lambda_0/2\pi$, as is frequently assumed. A more realistic choice for the boundary between the near and far fields will be discussed later but can be summarized as being the larger of $3\lambda_0$ or $2D^2/\lambda_0$, where D is the largest dimension of the antenna. Typically, the first criterion is used for "wire-type" antennas and the second for "surface-type" antennas such as parabolics or horns. This boundary between the near and far fields is not meant to be a precise criterion but is only intended to indicate a general region where the fields transition from complicated to quite simple structure. In the use of antennas for communication, this question of whether the receiving antenna is in the near or far field of the transmitting antenna never arises because these antennas are used for communication over large distances. However, in the area of EMC and interference caused by emissions, the receiver (which may be an intentional antenna used for compliance measurement) is frequently in the near field of the transmitting antenna (which may be the product). This is particularly true for the lower frequencies of the FCC, Class B radiated emission measurement. Nevertheless, for the moment we will assume that the field point is in the far field of the Hertzian dipole. Retaining only the $1/r$ terms in the field expressions in (7.1) gives the *far-field vectors*:

$$\begin{aligned}\hat{\boldsymbol{E}}_{\textbf{far field}} &= j\eta_0\beta_0 \frac{\hat{I}dl}{4\pi}\sin\theta\left(\frac{e^{-j\beta_0 r}}{r}\right)\boldsymbol{a}_\theta \\ &= j\frac{f\mu_0}{2}\hat{I}dl\sin\theta\left(\frac{e^{-j[2\pi(r/\lambda_0)]}}{r}\right)\boldsymbol{a}_\theta\end{aligned} \tag{7.2a}$$

$$\begin{aligned}\hat{\boldsymbol{H}}_{\textbf{far field}} &= j\beta_0 \frac{\hat{I}dl}{4\pi}\sin\theta\left(\frac{e^{-j\beta_0 r}}{r}\right)\boldsymbol{a}_\phi \\ &= j\frac{f\mu_0}{2\eta_0}\hat{I}dl\sin\theta\left(\frac{e^{-j[2\pi(r/\lambda_0)]}}{r}\right)\boldsymbol{a}_\phi\end{aligned} \tag{7.2b}$$

and we have substituted $\beta_0 = 2\pi/\lambda_0 = \omega\sqrt{\mu_0\varepsilon_0}$ and $\eta_0 = \sqrt{\mu_0/\varepsilon_0}$.

The time-domain fields are obtained by multiplying the phasor fields by $e^{j\omega t}$ and taking the real part of the results:

$$\begin{aligned}\boldsymbol{E}_{\textbf{far field}} &= \mathscr{R}e\,\{\hat{\boldsymbol{E}}_{\textbf{far field}}\,e^{j\omega t}\} \\ &= \frac{E_m}{r}\cos\left[\omega\left(t-\frac{r}{v_0}\right)+90^\circ\right]\boldsymbol{a}_\theta \\ &= -\frac{E_m}{r}\sin\left[\omega\left(t-\frac{r}{v_0}\right)\right]\boldsymbol{a}_\theta\end{aligned} \tag{7.3a}$$

$$\begin{aligned}\boldsymbol{H}_{\textbf{far field}} &= \mathscr{R}e\,\{\hat{\boldsymbol{H}}_{\textbf{far field}}\,e^{j\omega t}\} \\ &= \frac{E_m}{\eta_0 r}\cos\left[\omega\left(t-\frac{r}{v_0}\right)+90^\circ\right]\boldsymbol{a}_\phi \\ &= -\frac{E_m}{\eta_0 r}\sin\left[\omega\left(t-\frac{r}{v_0}\right)\right]\boldsymbol{a}_\phi\end{aligned} \tag{7.3b}$$

where

$$\begin{aligned} E_m &= \frac{\eta_0 \beta_0 \hat{I} dl}{4\pi} \sin\,\theta \\ &= \frac{f\mu_0}{2} \hat{I} dl \sin\,\theta \end{aligned} \tag{7.3c}$$

The far fields of the Hertzian dipole satisfy many of the properties of uniform plane waves. (See Appendix B for a discussion of uniform plane waves.) In fact, "locally" the fields resemble uniform plane waves, although they are more correctly classified as spherical waves. These properties are as follows:

1. The fields are proportional to $1/r$, I, dl, and $\sin\theta$.
2. $|\hat{\boldsymbol{E}}_{\text{far field}}| / |\hat{\boldsymbol{H}}_{\text{far field}}| = \eta_0$.
3. $|\hat{\boldsymbol{E}}_{\text{far field}}| / |\hat{\boldsymbol{H}}_{\text{far field}}|$ are *locally orthogonal.*
4. $\hat{\boldsymbol{E}}_{\text{far field}} \times \hat{\boldsymbol{H}}_{\text{far field}} = K\boldsymbol{a}_r$.
5. A phase term $e^{-j\beta_0 r}$ translates to a time delay in the time domain of $\sin[\omega(t - r/v_0)]$.

Property 1 is the origin of the technique of translating fields using the inverse-distance relationship. For example, the electric fields at distances D_1 and D_2 are related by $|\boldsymbol{E}_{D_2}| = (D_1/D_2)|\boldsymbol{E}_{D_1}|$; that is, the fields decay inversely with increasing distance away from the radiator. It is important to remember that *the inverse-distance rule holds only if both D_1 and D_2 are in the far field of the radiating element.* This important restriction is frequently not adhered to. If either of the two distances are in the near field, the inverse-distance rule should not be used.

Example 7.1 A Hertzian dipole has a length of 1 cm and carries a 1 A, 100 MHz current. Determine the magnitude and phase of the electric and magnetic fields at a distance of 1000 m away and broadside to the antenna ($\theta = 90°$).

Solution: A wavelength at 100 MHz is 3 m. The dipole length is $\lambda_0/300$ and satisfies the requirement that it be electrically short. The distance where the fields are to be determined is 333 λ_0 and hence is in the far field of the dipole. Substitution into (7.2) gives

$$\begin{aligned} \hat{E}_\theta &= j\frac{10^8\ \text{Hz} \times 4\pi \times 10^{-7} \times 1\ \text{A} \times 10^{-2}\ \text{m}}{2} \times \frac{e^{-j2\pi[(r=1000\ \text{m}/\lambda_0=3\ \text{m})]}}{r = 1000\ \text{m}} \\ &= 6.28 \times 10^{-4} \angle(-120{,}000°)\ \text{V/m} \end{aligned}$$

and

$$\begin{aligned} \hat{H}_\phi &= \frac{\hat{E}_\theta}{\eta_0 = 120\pi} \\ &= 1.67 \times 10^{-6} \angle(-120{,}000°)\ \text{A/m} \end{aligned}$$

Review Exercise 7.1 The magnitude of the far-field electric field of a Hertzian dipole is measured at a distance of 100 m as 1 mV/m. Determine the magnitude of the electric field at 1000 m.

***Answer*:** 100 μV/m.

We next obtain the total average power radiated by integrating the average power Poynting vector over a suitable closed surface surrounding the antenna. First, we compute the average power density vector using the *total* phasor fields in (7.1) as [1, 2]

$$\begin{aligned} \boldsymbol{S}_{\text{av}} &= \frac{1}{2}\mathscr{Re}\,\{\hat{\boldsymbol{E}} \times \hat{\boldsymbol{H}}^*\} \\ &= \frac{1}{2}\mathscr{Re}\left\{\hat{E}_\theta \hat{H}_\phi^* \boldsymbol{a}_r - \hat{E}_\theta \hat{H}_\phi^* \boldsymbol{a}_\theta\right\} \\ &= 15\pi\left(\frac{dl}{\lambda_0}\right)^2 |\hat{I}|^2 \left[\frac{\sin(\theta)}{r}\right]^2 \boldsymbol{a}_r \quad \text{in W/m}^2 \end{aligned} \tag{7.4}$$

The electric and magnetic fields are assumed here to be in *peak* values and not RMS. Hence, the 1/2 factor is required in the average power expression. This shows that average power is flowing away from the current element: our first hint of “radiation.” It is instructive to note that this average power density vector could have been obtained solely from the far-field expressions given in (7.2). Integrating this result over a sphere of radius r enclosing the current element gives the total average power radiated by the current element [1, 2]:

$$\begin{aligned} P_{\text{rad}} &= \oint_s \boldsymbol{S}_{\text{av}} \boldsymbol{ds} \\ &= 80\pi^2 \left(\frac{dl}{\lambda_0}\right)^2 \frac{|\hat{I}|^2}{2} \quad \text{in W} \end{aligned} \tag{7.5}$$

where $\boldsymbol{ds} = r^2 \sin\,\theta\, d\theta\, d\phi\, \boldsymbol{a}_r$ [1, 2].

Denoting $\hat{I}/\sqrt{2} = \hat{I}_{\text{rms}}$, we can compute a *radiation resistance*:

$$\begin{aligned} R_{\text{rad}} &= \frac{P_{\text{rad}}}{|\hat{I}_{\text{RMS}}|^2} \\ &= 80\pi^2 \left(\frac{dl}{\lambda_0}\right)^2 \quad \text{in } \Omega \end{aligned} \tag{7.6}$$

The radiation resistance represents a fictitious resistance that dissipates the same amount of power as that radiated by the Hertzian dipole when both carry the same value of current.

The Hertzian dipole is a very ineffective radiator. For example, for a length $dl = 1$ cm and a frequency of 300 MHz ($\lambda_0 = 1$ m), the radiation resistance is 79 mΩ. In order to radiate 1 W of power, we require an RMS current of 3.6 A! If the frequency is changed to 3 MHz ($\lambda_0 = 100$ m), the radiation resistance is 7.9 mΩ and the current RMS required to radiate 1 W is 356 A! Nevertheless the Hertzian dipole serves a useful purpose in that the *far fields of a Hertzian dipole are virtually identical to the far fields of most other practical antennas*.

Review Exercise 7.2 A Hertzian dipole is of length 1 cm and carries a peak current of 100 mA at a frequency of 10 MHz. Determine the total radiated power.

***Answer*:** 0.44 μW.

7.1.2 The Magnetic Dipole (Loop)

A dual to the elemental electric dipole is the *elemental magnetic dipole or current loop* shown in Fig. 7.2. A very small loop of radius b lying in the xy plane carries a phasor current $\hat{I}$. It is assumed that the loop circumference is electrically small, i.e., $2\pi b < \lambda_0/10$. This loop constitutes a magnetic dipole moment [1]

$$\hat{m} = \hat{I}\pi b^2 \text{ in A} \cdot \text{m}^2 \tag{7.7}$$

where πb^2 is the area enclosed by the loop. The radiated fields are [1]

$$\hat{E}_r = 0 \tag{7.8a}$$

$$\hat{E}_\theta = 0 \tag{7.8b}$$

$$\hat{E}_\phi = -j\frac{\omega\mu_0\hat{m}\beta_0^2}{4\pi}\sin\theta\left(j\frac{1}{\beta_0 r} + \frac{1}{\beta_0^2 r^2}\right)e^{-j\beta_0 r} \tag{7.8c}$$

and

$$\hat{H}_r = j2\frac{\omega\mu_0\hat{m}\beta_0^2}{4\pi\eta_0}\cos\theta\left(\frac{1}{\beta_0^2 r^2} - j\frac{1}{\beta_0^3 r^3}\right)e^{-j\beta_0 r} \tag{7.8d}$$

$$\hat{H}_\theta = j\frac{\omega\mu_0\hat{m}\beta_0^2}{4\pi\eta_0}\sin\,\theta\left(j\frac{1}{\beta_0 r} + \frac{1}{\beta_0^2 r^2} - j\frac{1}{\beta_0^3 r^3}\right)e^{-j\beta_0 r} \tag{7.8e}$$

$$\hat{H}_\phi = 0 \tag{7.8f}$$

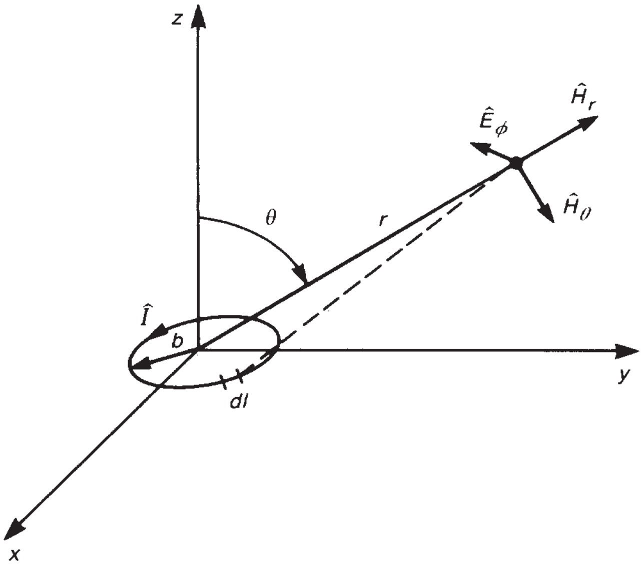

FIGURE 7.2 The magnetic dipole (loop).

Comparing (7.8) with the fields of the Hertzian dipole given in (7.1), we see that duality exists between the fields of these structures. Observations about the electric (magnetic) field of the electric dipole apply to the magnetic (electric) field of the magnetic dipole.

The far field of the magnetic dipole is characterized by the $1/r$-dependent terms:

$$\begin{aligned}\hat{\boldsymbol{E}}_{\text{far field}} &= \frac{\omega\mu_0\hat{m}\beta_0^2}{4\pi}\sin\theta\left(\frac{e^{-j\beta_0 r}}{r}\right)\boldsymbol{a}_\phi \\ &= j\frac{\pi^2 f^2\mu_0\hat{I}b^2}{v_0}\sin\theta\left(\frac{e^{-j[2\pi(r/\lambda_0)]}}{r}\right)\boldsymbol{a}_\phi\end{aligned} \tag{7.9a}$$

$$\begin{aligned}\hat{\boldsymbol{H}}_{\text{far field}} &= -\frac{\omega\mu_0\hat{m}\beta_0^2}{4\pi\eta_0}\sin\theta\left(\frac{e^{-j\beta_0 r}}{r}\right)\boldsymbol{a}_\theta \\ &= -\frac{\pi^2 f^2\mu_0\hat{I}b^2}{\eta_0 v_0}\sin\theta\left(\frac{e^{-j[2\pi(r/\lambda_0)]}}{r}\right)\boldsymbol{a}_\theta\end{aligned} \tag{7.9b}$$

As was the case for the Hertzian (electric) dipole, the far field of the magnetic dipole is such that the fields (1) decay as $1/r$, (2) lie in a (local) plane perpendicular to the radial direction, (3) are orthogonal to each other, and (4) are related by η_0.

As was done for the Hertzian dipole, we may determine a radiation resistance of the magnetic dipole, which becomes [1]

$$\begin{aligned}R_{\text{rad}} &= \frac{P_{\text{rad}}}{|\hat{I}_{\text{RMS}}|^2} \\ &= 31{,}170\left(\frac{A}{\lambda_0^2}\right)^2\end{aligned} \tag{7.10}$$

where $A = \pi b^2$ is the area of the loop. Like the Hertzian dipole, the magnetic dipole is not an efficient radiator. Consider a loop of radius 1 cm. At 300 MHz, the radiation resistance is 3.08 mΩ. In order to radiate 1 W, the loop requires an RMS current of 18 A. At 3 MHz, the radiation resistance is 3.08×10^{-11} mΩ, and the RMS current required to radiate 1 W is 1.8×10^5 A!

Example 7.2 If a loop is electrically small, its shape is not important with respect to the far fields that it generates [1]. In order to illustrate the application of this result to radiated emissions, consider a 1 × 1 cm current loop on a PCB (an equivalent loop radius of 5.64 mm). Suppose that the loop carries a 100 mA current at a frequency of 50 MHz. At a measurement distance of 3 m (FCC Class B), the electric field is a maximum in the plane of the loop and using (7.9) is $|\hat{E}| = 109.6\ \mu V/\text{m} = 40.8$ dBμV/m. Recall that the FCC Class B limit from 30 to 88 MHz is 40 dBμV/m. Therefore, a 1 × 1 cm loop carrying a 50 MHz, 100 mA current will cause a radiated emission that will fail to comply with the FCC Class B regulatory limit! This should serve to illustrate to the reader that passing the regulatory requirements on radiated emissions is not a simple matter, since the dimensions and current levels given above are quite representative of those found on PCBs of electronic products.

7.2 THE HALF-WAVE DIPOLE AND QUARTER-WAVE MONOPOLE ANTENNAS

The Hertzian dipole considered in Section 7.1.1 is an obviously impractical antenna for several reasons. Primarily, the length of the dipole was assumed to be infinitesimal in order to simplify the computation of the fields. Also, the current along the Hertzian dipole was assumed to be constant along the dipole. This latter assumption required the current to be nonzero at the endpoints of the dipole—an unrealistic and, moreover, physically impossible situation since the surrounding medium, free space, is nonconductive. Also, the Hertzian dipole is a very inefficient radiator since the radiation resistance is quite small, requiring large currents in order to radiate significant power. The magnetic dipole suffers from similar problems. In this section, we will consider two practical and more frequently used antennas: the long-dipole and monopole antennas.

The long-dipole antenna (or, simply, the dipole antenna) consists of a thin wire of length l that is fed or excited via a voltage source inserted at the midpoint, as shown in Fig. 7.3a. Each leg is of length $l/2$.

The monopole antenna shown in Fig. 7.3b consists of a single leg perpendicular to a ground plane of height $h = l/2$. The monopole is fed at its base with respect to the ground plane. For purposes of analysis, the ground plane is considered to be infinite and perfectly conducting. In practice, this ideal ground plane is approximated. On aircraft, for example, the metallic fuselage simulates this ground plane. For ground-based stations, the earth simulates, to some degree, this ground plane. Since the earth is much less of an approximation to a perfectly conducting plane than is metal, ground-based stations are usually augmented by a grid of wires lying on the ground to simulate the ground plane. The monopole antenna can be analyzed by replacing the ground plane with the image of the current

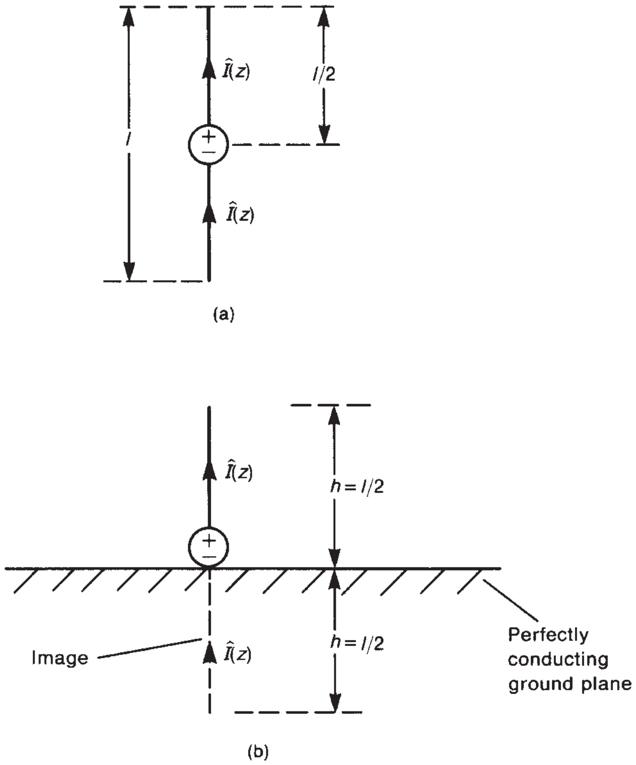

FIGURE 7.3 Illustration of (a) the dipole antenna and (b) the monopole antenna.

element that is above the ground plane, as indicated in Fig. 7.3b. Images are discussed in Section 7.6.1. Once the ground plane is replaced with the image, the problem reduces to the dipole problem so that a separate analysis of the monopole is not needed.

We observed previously that if we know the current distribution over the surface of an antenna, we may compute the resulting radiated fields. In practice, one often makes a reasonable guess as to the *current distribution* over the antenna surface. It can be shown that the current distribution of the long-dipole antenna follows (approximately) the same distribution as on a transmission line; that is, $\hat{I}(z)$ is proportional to sin $(\beta_0 z)$ [1]. Placing the center of the dipole at the origin of a spherical coordinate system as shown in Fig. 7.4a, with the dipole directed along the z axis, we may therefore

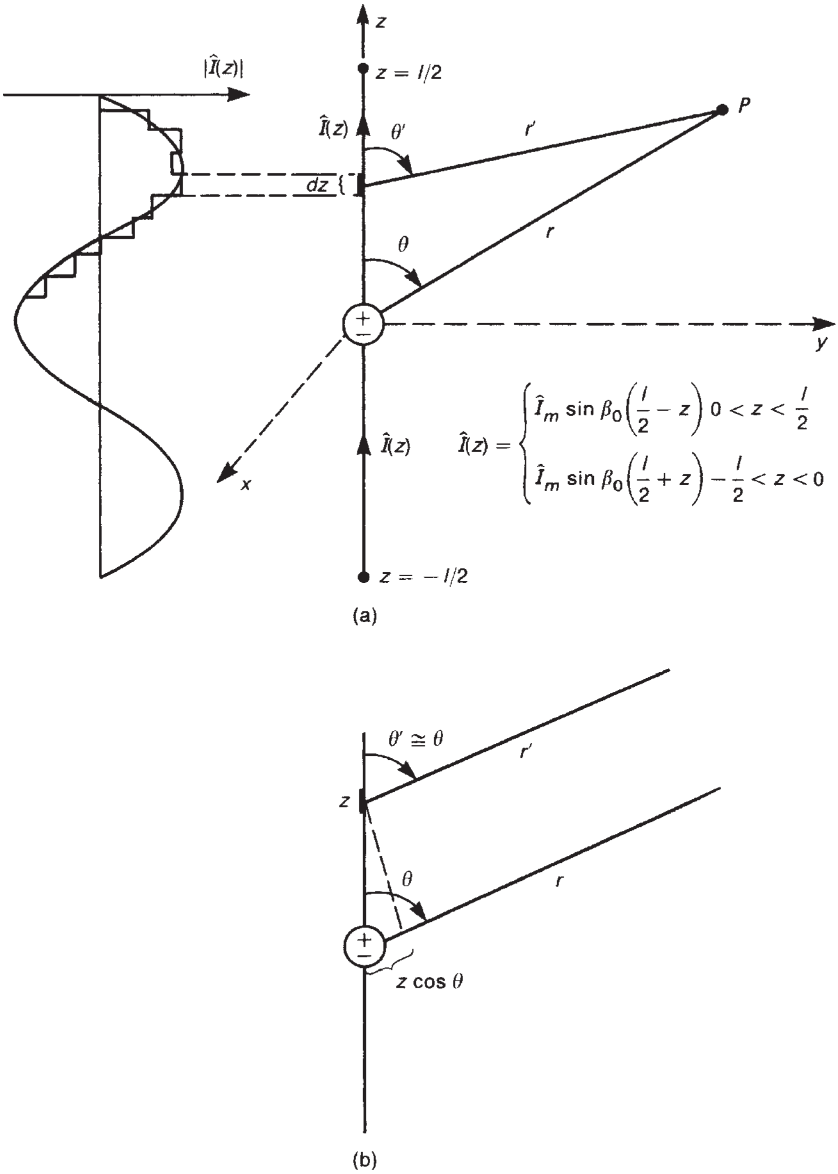

z
$|\hat{I}(z)|$
$z = l/2$
P
$\hat{I}(z)$
θ'
r'
dz
θ
r
y
x
$\hat{I}(z)$
$\hat{I}(z) = \begin{cases} \hat{I}_m \sin \beta_0\left(\frac{l}{2} - z\right) & 0 < z < \frac{l}{2} \\ \hat{I}_m \sin \beta_0\left(\frac{l}{2} + z\right) & -\frac{l}{2} < z < 0 \end{cases}$
$z = -l/2$
(a)
$\theta' \cong \theta$
r'
z
θ
r
$z \cos \theta$
(b)

FIGURE 7.4 Computation of the radiated fields of the dipole antenna: (a) treating the dipole current as a sequence of Hertzian dipoles and superposing the fields; (b) the far-field (parallel-ray) approximation.

write an expression for the current distribution along the wire is

$$\hat{I}(z) = \begin{cases} \hat{I}_m \sin\left[\beta_0\left(\left(\frac{l}{2}\right) - z\right)\right] & \text{for } 0 < z < \left(\frac{l}{2}\right) \\ \hat{I}_m \sin\left[\beta_0\left(\left(\frac{l}{2}\right) + z\right)\right] & \text{for } \left(-\frac{l}{2}\right) < z < 0 \end{cases} \tag{7.11}$$

Note that this current distribution satisfies the necessary criteria: (1) the variation with z is proportional to sin ($\beta_0 z$) and (2) the current goes to zero at the endpoints, $z = -l/2$ and $z = l/2$.

Now that we have assumed the current distribution along the dipole, we may compute the fields of the long dipole as being the superposition of the fields due to many small Hertzian dipoles of length dz having a current that is constant and equal to the value of $\hat{I}(z)$ at that point along the dipole, as shown in Fig. 7.4a. We also assume that the desired field point is in the far field of these current elements, so that we only need the far-field expressions for the Hertzian dipole given in (7.2). For example, the field at point P in Fig. 7.4a due to the segment dz is

$$d\hat{E}_\theta = j\eta_0\beta_0 \frac{\hat{I}(z)\sin\,\theta'}{4\pi r'} e^{-j\beta_0 r'}\,dz \tag{7.12}$$

Our ultimate objective is to obtain the fields at point P in terms of the radial distance r from the midpoint of the dipole and angle θ. Since we are considering only the far field, the radial distance r from the center of the dipole to point P and the distance r from the current element to point P will be approximately equal ($r \cong r'$), and the angles θ and θ' will be approximately equal ($\theta \cong \theta'$), as shown in Fig. 7.4b. This is called the far-field, parallel-ray approximation.

We may substitute $r' = r$ into the denominator of (7.12), but we should not make this substitution into the $e^{-j\beta_0 r'}$ term for the following reason. This term may be written as $e^{-j\beta_0 r'} = 1\angle - 2\pi r'/\lambda_0$, and its value depends not on physical distance r' but on electrical distance r'/λ_0. Therefore, even though r' and r may be approximately equal, the term may depend significantly on the difference in electrical distances. For example, suppose that $r = 1000$ m and $r' = 1000.5$ m and the frequency is $f = 300$ MHz. We have ($\lambda_0 = 1$ m) $\beta_0 r = 2\pi\,(1000) = 360,000°$ and $\beta_0 r' = 2\pi\,(1000.5) = 360,180°$. Note that the fields at 1000 m and those only 0.5 m farther away are 180° out of phase! We will see a more striking example of this in the next section, where the far fields from two antennas that are widely spaced physically but separated on the order of a wavelength may actually be completely out of phase and add destructively to yield a result of zero.

Thus, it is not a reasonable approximation to substitute r for r' in the phase term in (7.12). However, we may still write the result in terms of r. Consider Fig. 7.4b, which shows the two radial distances r and r' as being approximately parallel. Thus, we are assuming that the field point is sufficiently far, physically, from the antenna. From Fig. 7.4b, we may obtain

$$r' \cong r - z\,\cos\,\theta \tag{7.13}$$

Substituting (7.13) into the phase terms in (7.12) and r into the denominator gives

$$d\hat{E}_\theta = j\eta_0\beta_0 \frac{\hat{I}(z)\sin\,\theta}{4\pi r} e^{-j\beta_0(r - z\,\cos\,\theta)}dz \tag{7.14}$$

The total electric field is the sum of these contributions:

$$\hat{E}_\theta = \int_{z=-l/2}^{z=l/2} j\eta\beta_0 \frac{\hat{I}(z)\sin\theta}{4\pi r} e^{-j\beta_0 r} e^{j\beta_0 z\cos\theta}\,dz \tag{7.15}$$

Substituting the expressions for $\hat{I}(z)$ given in (7.11), we obtain [1, 2]

$$\begin{aligned}\hat{E}_\theta &= j\frac{\eta_0 \hat{I}_m e^{-j\beta_0 r}}{2\pi r}F(\theta)\\ &= j\frac{60\hat{I}_m e^{-j\beta_0 r}}{r}F(\theta)\end{aligned} \tag{7.16}$$

where the θ variation term in this result is denoted by

$$F(\theta) = \frac{\cos\left[\beta_0\left(\frac{l}{2}\right)\cos\theta\right] - \cos\beta_0\left(\frac{l}{2}\right)}{\sin\theta} = \frac{\cos\left[\left(\frac{\pi l}{\lambda_0}\right)\cos\theta\right] - \cos\left(\frac{\pi l}{\lambda_0}\right)}{\sin\theta} \tag{7.17}$$

since $\beta_0 = 2\pi/\lambda_0$. The magnetic field in the far-field region of the Hertzian dipole is orthogonal to the electric field and related by η_0. If we carry through the preceding development for the magnetic field, we obtain

$$\hat{H}_\varphi = \frac{\hat{E}_\theta}{\eta_0} \tag{7.18}$$

where $\hat{E}_\theta$ is given by (7.16).

The most frequently encountered case is the half-wave dipole, in which the total dipole length is $l = \lambda_0/2$. Substituting into (7.17), we obtain

$$F(\theta) = \frac{\cos((1/2)\pi\ \cos\ \theta)}{\sin\theta} \quad \text{half-wave dipole, } l = \frac{\lambda_0}{2} \tag{7.19}$$

The electric field will be a maximum for $\theta = 90°$ (broadside to the antenna). For this case, $F(90°) = 1$, and the maximum electric field for the half-wave dipole becomes

$$|\hat{E}|_{\max} = \frac{|\hat{I}_m|}{r} \quad \theta = 90° \tag{7.20}$$

The field is directed in the θ direction and is independent of ϕ, which makes sense from symmetry considerations. For a half-wave dipole, the input current is $\hat{I}_m$ as shown by evaluating (7.11) at $z = 0 : \hat{I}(0) = \hat{I}_m\ \sin[\beta_0 l/2] = \hat{I}_m \sin[\pi/2] = \hat{I}_m$.

The *pattern* of the half-wave dipole antenna is plotted in Fig. 7.5a both in cross section and in three dimensions for a fixed distance r and a function of θ. Observe that the electric field decays inversely with distance. Hence at a fixed distance r, the electric field depends only on angle θ through the pattern factor $F(\theta)$ given in (7.17), which simplifies to (7.19) for the half-wave dipole antenna. The

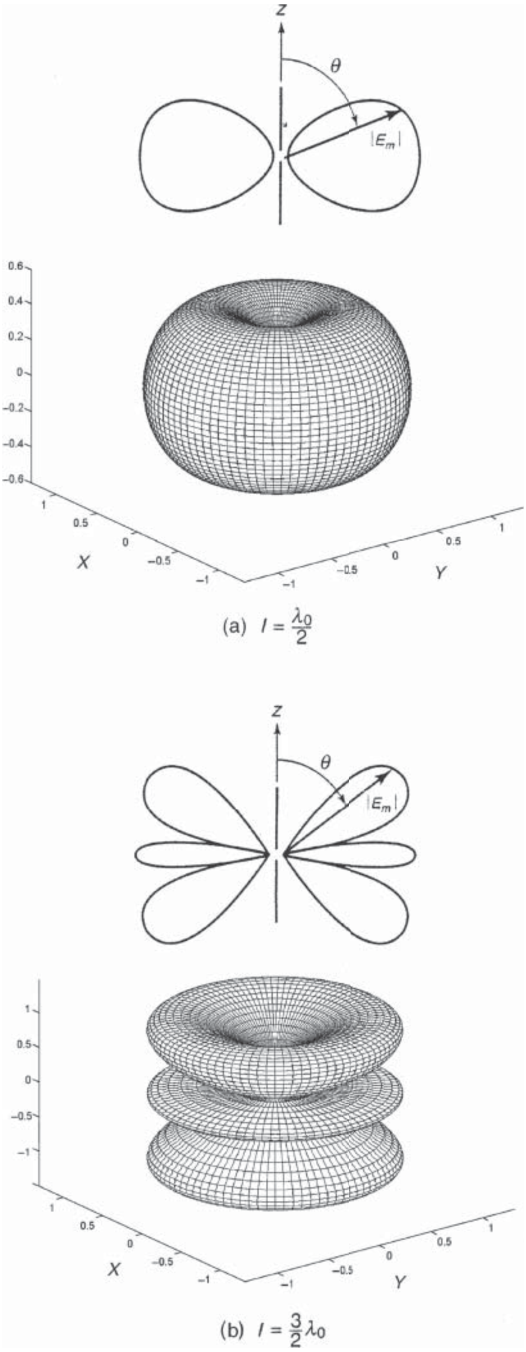

FIGURE 7.5 Radiated electric field patterns of dipoles: (a) a dipole whose length is 1/2 wavelength, $l = \lambda_0/2$; (b) a dipole whose length is 1(1/2) wavelength, $l = 3\lambda_0/2$.

information contained in a plot of the pattern here is as follows. For a fixed value of θ, the distance from the origin to the pattern outline is the *relative magnitude of the electric field for that angle* θ. In other words, a line drawn from the origin to the pattern extremity for that angle θ is proportional to the electric field. This shows that the electric field is zero off the ends of the dipole and is a maximum broadside to it, $\theta = 90°$. For a dipole whose length is one and one-half wavelengths, $l = 3\lambda_0/2$, the pattern factor $F(\theta)$ in (7.17) becomes

$$F(\theta) = \frac{\cos[(3\pi/2)\cos\theta]}{\sin\theta} \quad l = \frac{3\lambda_0}{2}$$

This pattern is plotted in both cross section and three dimensions in Fig. 7.5b. Observe that for this length of the dipole, nulls appear in the pattern off the ends of the dipole and also at other positions. There will be no transmission for these values of θ.

The average power density is

$$\begin{aligned} \boldsymbol{S}_{\text{av}} &= \frac{1}{2}\mathscr{Re}\,\{\hat{\boldsymbol{E}} \times \hat{\boldsymbol{H}}^*\} \\ &= \frac{1}{2}\mathscr{Re}\,\left\{\hat{E}_\theta \hat{H}_\phi^*\right\}\,\boldsymbol{a}_r \\ &= \frac{1}{2}\frac{|\hat{E}_\theta|^2}{\eta_0}\,\boldsymbol{a}_r \\ &= \underbrace{\left(\frac{\eta_0}{8\pi^2}\right)}_{4.77}\frac{|\hat{I}_m|^2}{r^2}F^2(\theta)\,\boldsymbol{a}_r \end{aligned} \tag{7.21}$$

The total radiated power is again obtained by integrating the average power density over a sphere of radius r as [1, 2]

$$\begin{aligned} P_{\text{av}} &= \int_{\phi=0}^{2\pi}\int_{\theta=0}^{\pi} \boldsymbol{S}_{\text{av}} \cdot \underbrace{r^2 \sin\theta\, d\theta\ d\phi\ \boldsymbol{a}_r}_{ds} \\ &= 73\frac{|\hat{I}_m|^2}{2} \end{aligned} \tag{7.22}$$

Now let us compute the average power radiated by the dipole. Once again, integration of the Poynting vector over a sphere of radius r gives the total radiated power [1]:

$$\begin{aligned} P_{\text{rad}} &= 73\frac{|\hat{I}_m|^2}{2} \\ &= 73|\hat{I}_{\text{in,rms}}|^2 \quad \text{in W} \quad \text{(half-wave dipole)} \end{aligned} \tag{7.23}$$

where the RMS current I_{RMS} is related to the peak by $I_{\text{RMS}} = I_m/\sqrt{2}$. Thus, if we know the RMS value of the *input current* at the terminals of a half-wave dipole, we may find the total average power radiated by multiplying the square of the RMS current by 73 Ω. This suggests that we define a radiation resistance of the half-wave dipole as

$$R_{\text{rad}} = 73\ \Omega \quad \text{(half-wave dipole)} \tag{7.24}$$

There is one important difference between the dipole and the monopole. Although the field patterns are the same, the monopole radiates only half the power of the dipole: the power radiated out of the half-sphere above the ground plane. Thus, the radiation resistance for the monopole is half that of the corresponding dipole. In particular, for a quarter-wave monopole of length $h = \lambda_0/4$ (which corresponds to a half-wave dipole), we have

$$R_{\text{rad}} = 36.5\ \Omega \quad \text{(quarter-wave monopole)} \tag{7.25}$$

Up to this point, we have not considered the total input impedance $\hat{Z}_{\text{in}}$ seen at the terminals of the dipole or monopole antenna. The input impedance will, in general, have a real and an imaginary part as

$$\hat{Z}_{\text{in}} = R_{\text{in}} + jX_{\text{in}} \tag{7.26}$$

The input resistance will consist of the sum of the radiation resistance and the resistance of the imperfect wires used to construct the dipole, so that

$$\hat{Z}_{\text{in}} = R_{\text{loss}} + R_{\text{rad}} + jX_{\text{in}} \tag{7.27}$$

Figure 7.6 shows the radiation resistance and reactance referred to the base of a monopole antenna for various lengths of the antenna [3]. Figure 7.6 can be used to give the input impedance for a dipole by doubling the values given in the figure. The input reactance for a half-wave dipole (quarter-wave monopole) is $X_{\text{in}} = 42.5\ \Omega$ ($X_{\text{in}} = 21.25\ \Omega$). The equivalent circuits for the input to a half-wave dipole and a quarter-wave monopole (ignoring losses) are shown in Fig. 7.7. Note that for monopoles that are shorter than one-quarter wavelength (or dipoles shorter than one-half wavelength), the radiation resistance becomes much smaller and the reactive part becomes negative, symbolizing a capacitive reactance. Thus, monopoles that are shorter than one-quarter wavelength appear at their input as a small resistance in series with a capacitance, which is, intuitively, a sensible result. Also observe in Fig. 7.6 that the reactive part of the input impedance is zero for a monopole that is slightly shorter than a quarter-wavelength. Having a zero reactive part is obviously desirable from the standpoint of maximizing the power that is delivered from a source that has a real source resistance (such as 50 Ω) to the antenna and subsequently radiated. This is why monopoles are cut to lengths slightly shorter than a quarter wavelength. If the physical length of a half-wave dipole or a quarter-wave monopole is excessive for the intended installation, it can be shortened, but that introduces a large capacitive reactance to the input impedance, which necessitates a larger value of source excitation voltage to produce the same level of radiated power (dissipated in R_{rad}). In order to overcome this problem, short antennas have "loading coils" or inductors inserted in series with their input to cancel this capacitive reactance and increase the radiated power. This is sometimes referred to as "tuning or loading the antenna."

Review Exercise 7.3 A half-wave dipole carries a 100 MHz current whose magnitude (RMS) at the center of the dipole (the excitation point) is 100 mA. Determine the total power radiated by the dipole and the power density at a distance of 1000 m away broadside to the antenna.

***Answer*:** 0.73 W and 95.4 nW/m^2.

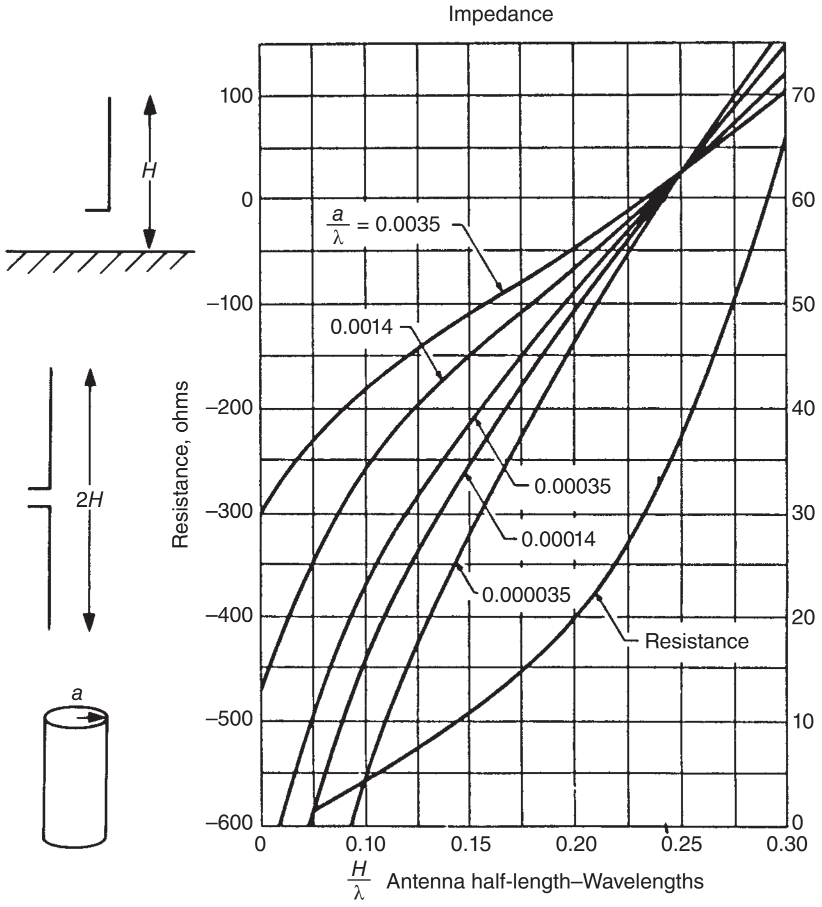

FIGURE 7.6 The radiation resistance and reactance of a dipole antenna as a function of length and wire radius [3]. Source: Jordan and Balmain [3]/Pearson Education.

Example 7.3 The important point to realize here is that, knowing the input impedance of the antenna, we can compute the total average power radiated by the antenna by computing the average power dissipated in R_{rad}. For example, consider the half-wave dipole driven by a 100 V (peak), 150 MHz, 50 Ω source as shown in Fig. 7.8a. Replacing the antenna with its equivalent circuit at its input terminals gives the circuit shown in Fig. 7.8b. The input current to the antenna is

$$\hat{I}_{\text{ant}} = \frac{\hat{V}_S}{R_S + R_{\text{loss}} + R_{\text{rad}} + jX}$$

Assume that the wires are #20 AWG solid copper. The wires have radii much larger than a skin depth at the operating frequency of 150 MHz ($\delta = 5.4 \times 10^{-6}$ m = 0.212 mils), so the high-frequency approximation for wire resistance developed in Chapter 5 can be used to compute R_{loss} as

$$\begin{aligned} r_{\text{wire}} &= \frac{1}{2\pi r_w \sigma \delta} \\ &= 1.25\ \Omega/\text{m} \end{aligned}$$

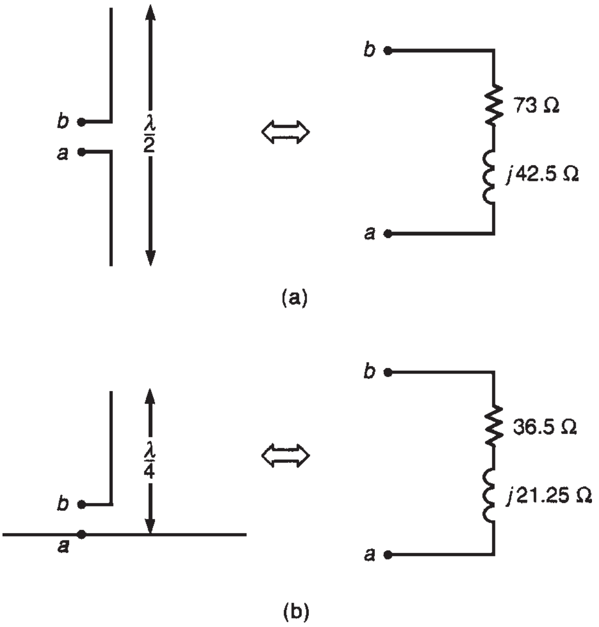

FIGURE 7.7 Representation of the input impedance to an antenna: (a) the input to a half-wave dipole; (b) the input to a quarter-wave monopole.

Using this result, the net ohmic resistance of the wires used to construct the dipole can be obtained as [1]

$$\begin{aligned} R_{\text{loss}} &= r_{\text{wire}}\frac{l}{2} \\ &= 0.63\ \Omega \end{aligned}$$

Since the dipole is a half-wave dipole, its impedance is $(73 + j42.5)\ \Omega$ (see Fig. 7.6), so that

$$\begin{aligned} \hat{Z}_{\text{ant}} &= R_{\text{loss}} + R_{\text{rad}} + jX_{\text{in}} \\ &= (0.63 + 73 + j42.5)\ \Omega \end{aligned}$$

Thus, the current at the antenna input terminals is

$$\begin{aligned} \hat{I}_{\text{ant}} &= \frac{100\angle 0^\circ}{50 + 73.63 + j42.5} \\ &= 0.765\angle(-18.97^\circ)\ \text{A} \end{aligned}$$

The total average power dissipated in antenna losses is

$$\begin{aligned} P_{\text{loss}} &= \frac{|\hat{I}_{\text{ant}}|^2}{2}R_{\text{loss}} \\ &= 184\ \text{mW} \end{aligned}$$

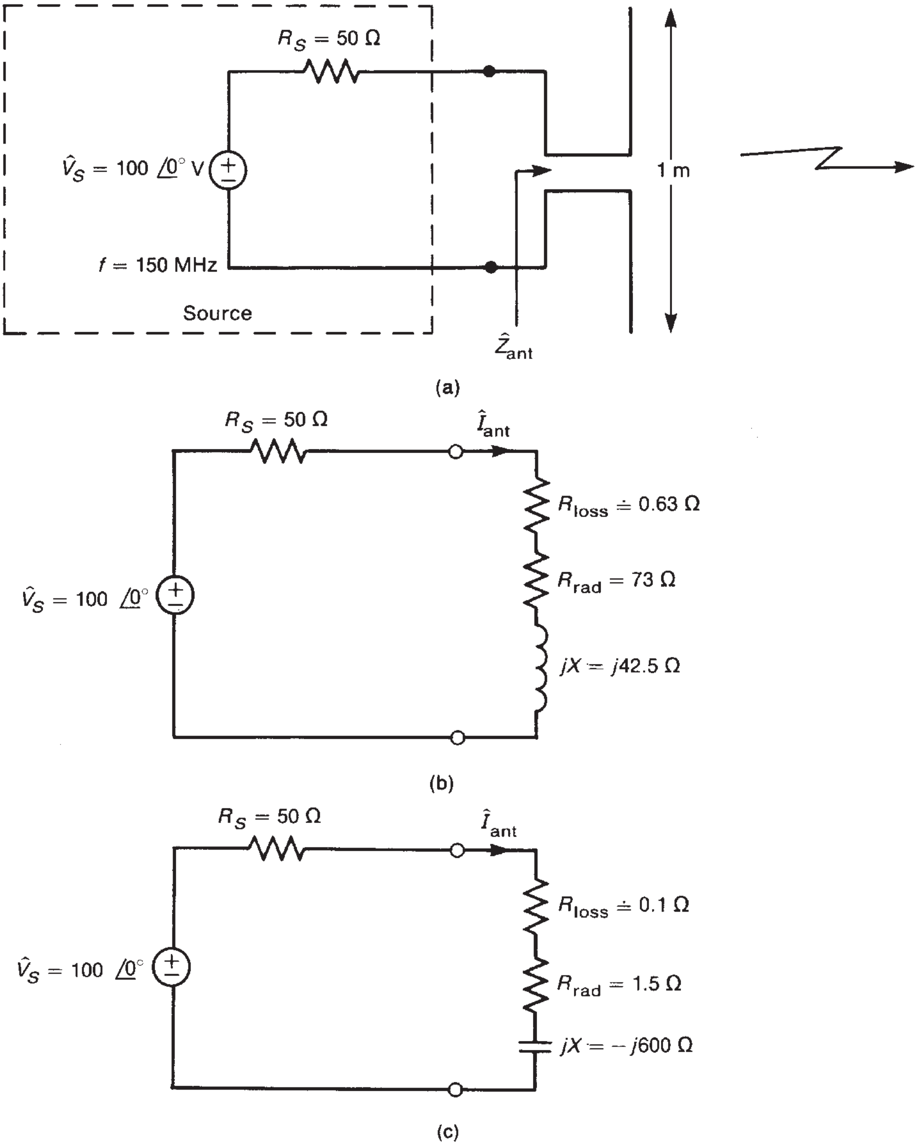
$R_S = 50\ \Omega$
$\hat{V}_S = 100\ \underline{/0^\circ}\ \mathrm{V}$
$f = 150$ MHz
Source
1 m
$\hat{Z}_{\mathrm{ant}}$
(a)
$R_S = 50\ \Omega$
$\hat{I}_{\mathrm{ant}}$
$R_{\mathrm{loss}} \doteq 0.63\ \Omega$
$R_{\mathrm{rad}} = 73\ \Omega$
$jX = j42.5\ \Omega$
$\hat{V}_S = 100\ \underline{/0^\circ}$
(b)
$R_S = 50\ \Omega$
$\hat{I}_{\mathrm{ant}}$
$R_{\mathrm{loss}} \doteq 0.1\ \Omega$
$R_{\mathrm{rad}} = 1.5\ \Omega$
$jX = -j600\ \Omega$
$\hat{V}_S = 100\ \underline{/0^\circ}$
(c)

FIGURE 7.8 An example illustrating the computation of the radiated power of a dipole antenna: (a) the physical configuration with a driving source; (b) equivalent circuit of a half-wave dipole; (c) equivalent circuit of a $\lambda_0/8$ dipole.

The total average power radiated is

$$\begin{aligned} P_{\mathrm{rad}} &= \frac{|\hat{I}_{\mathrm{ant}}|^2}{2} R_{\mathrm{rad}} \\ &= 21.36\ \mathrm{W} \end{aligned}$$

The 1/2 factor in these average power expressions is required because the calculated antenna current is the *peak* value.

In order to illustrate the effect of short antennas on radiated power, consider the problem where the dipole antenna is shortened to $\lambda_0/8$ in total length. From Fig. 7.6, $R_{\mathrm{rad}} \cong 1.5\ \Omega$ and $X_{\mathrm{in}} \cong -600\ \Omega$. The equivalent circuit is shown in Fig. 7.8c. The current at the input to the antenna is

$$\begin{aligned}\hat{I}_{\mathrm{ant}} &= \frac{100\angle 0^\circ}{50 + 0.16 + 1.5 - j600} \\ &= 0.166\angle 85.1^\circ\ \mathrm{A}\end{aligned}$$

Thus, the radiated power is

$$\begin{aligned}P_{\mathrm{av,rad}} &= \frac{|\hat{I}_{\mathrm{ant}}|^2}{2} R_{\mathrm{rad}} \\ &= 20.7\ \mathrm{mW}\end{aligned}$$

Thus, the reduced radiation resistance along with the large increase in reactive part in the input impedance caused by shortening the length of the dipole has significantly reduced the radiated power of the antenna. If an inductor having an inductance of 0.637 μH giving a reactance of $+j600$ is inserted in series with this antenna, the radiated power is increased to 2.81 W! This illustrates the extreme effect of the reactive part of the input impedance.

7.3 ANTENNA ARRAYS

The radiation characteristics of the Hertzian dipole, the magnetic dipole, the long dipole, and the monopole are evidently omnidirectional in any plane perpendicular to the antenna axis, since all fields are independent of ϕ. This characteristic follows from the symmetry of these structures about the z axis. From the standpoint of communication, we may wish to focus the radiated signal since any of the radiated power that is not transmitted in the direction of the receiver is wasted. On the other hand, from the standpoint of EMC, we may be interested in directing the radiated signal away from another receiver in order to prevent interference with that receiver. If the transmitting antenna has an omnidirectional pattern, we do not have these options. In this section, we will investigate how to use two or more omnidirectional antennas to produce maxima and/or nulls in the resulting pattern. This results from phasing the currents to the antennas and separating them sufficiently such that the combined fields will add constructively or destructively to produce these resulting maxima or nulls. This result, although applied to the emission patterns of communications antennas, has direct application in the radiated emissions of products, since it illustrates how multiple emissions may combine. In addition, we will use the simple results obtained here to obtain simple models for predicting the radiated emissions from wires and PCB lands in Chapter 8.

Consider two omnidirectional antennas such as half-wave dipoles in free space or quarter-wave monopoles above ground, as shown in Fig. 7.9a. The current elements lie on the x axis and are directed in the z direction. They are separated by a distance d and are equally spaced about the origin. Assuming the field point P is in the far field of the antennas, the far fields at point P due to each antenna are of the form

$$\hat{E}_{\theta 1} = \frac{\hat{M} I\angle\alpha}{r_1} e^{-j\beta_0 r_1} \tag{7.28a}$$

$$\hat{E}_{\theta 2} = \frac{\hat{M} I\angle 0^\circ}{r_2} e^{-j\beta_0 r_2} \tag{7.28b}$$

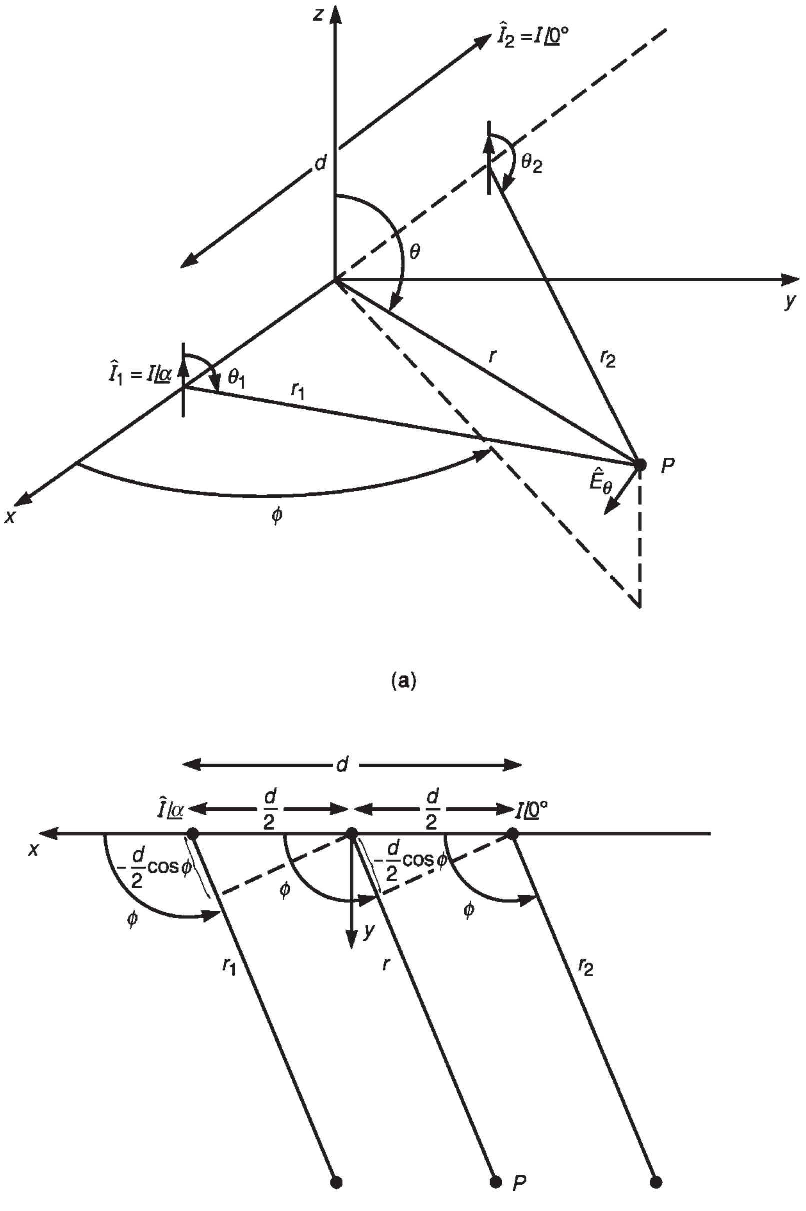
z
$\hat{I}_2 = I\angle 0°$
d
θ_2
θ
y
$\hat{I}_1 = I\angle\alpha$
θ_1
r_1
r
r_2
P
$\hat{E}_\theta$
x
ϕ
(a)
d
$\hat{I}\angle\alpha$
$\frac{d}{2}$
$\frac{d}{2}$
$I\angle 0°$
x
$-\frac{d}{2}\cos\phi$
$-\frac{d}{2}\cos\phi$
ϕ
ϕ
ϕ
y
r_1
r
r_2
P
(b)

FIGURE 7.9 Calculation of the radiated electric field of an array of two antennas: (a) the physical dimensions; (b) the far-field, parallel-ray approximation.

where $\hat{I}_1 = I\angle\alpha$ and $\hat{I}_2 = I\angle 0°$, and we assume that the currents of the two antennas are equal in magnitude but the current in antenna 1 leads that of antenna 2 by α. The factor $\hat{M}$ depends on the type of antennas used. For Hertzian dipoles, $\hat{M} = j\eta_0\beta_0(dl/4\pi)\ \sin\ \theta$ [see (7.2a)]. For long dipoles, $\hat{M} = j60\,F(\theta)$ [see (7.16)].

In this discussion, we will concentrate on determining the fields in the xy plane, $\theta = 90^\circ$, or broadside to the antennas where the fields of the two antennas are a maximum. The total field at point P is the sum of the fields of the two antennas

$$\begin{aligned}\hat{E}_\theta &= \hat{E}_{\theta 1} + \hat{E}_{\theta 2}\\ &= \hat{M}I\left(\frac{e^{-j\beta_0 r_1}}{r_1}e^{j\alpha} + \frac{e^{-j\beta_0 r_2}}{r_2}\right)\\ &= \hat{M}Ie^{j\alpha/2}\left(\frac{e^{-j\beta_0 r_1}e^{j\alpha/2}}{r_1} + \frac{e^{-j\beta_0 r_2}e^{-j\alpha/2}}{r_2}\right) \end{aligned} \tag{7.29}$$

where we have substituted $I\angle\alpha = Ie^{j\alpha}$

In order to simplify this equation, we observe that, since P is sufficiently far from the origin, $r_1 \cong r_2 \cong r$, where r is the distance from the midpoint of the array to point P. This approximation can be used in the denominator terms of (7.29) but cannot be used in the phase terms for reasons discussed in the previous section. If we draw the radius vectors r_1 and r_2 parallel to the radius vector r as shown in Fig. 7.9b, we can obtain a reasonable approximation for the phase terms. To do this, we observe that the path lengths can be written as

$$r_1 \cong r - \frac{d}{2}\cos\,\phi \tag{7.30a}$$

$$r_2 \cong r + \frac{d}{2}\cos\,\phi \tag{7.30b}$$

as illustrated in Fig. 7.9b. Substituting $r_1 \cong r_2 \cong r$ in the denominators of (7.29) and substituting (7.30) into the exponential phase terms yields

$$\begin{aligned}\hat{E}_\theta &= \hat{M}I\frac{e^{-j\beta_0\, r}}{r}\underbrace{\left(e^{j[\beta_0(d/2)\,\cos\,\phi+(\alpha/2)]} + e^{-j[\beta_0(d/2)\,\cos\,\phi+(\alpha/2)]}\right)}_{2\,\cos\,[\beta_0(d/2)\,\cos\,\phi+(\alpha/2)]}e^{j(\alpha/2)}\\ &= 2\hat{M}I\frac{e^{-j\beta_0 r}}{r}e^{j(\alpha/2)}\cos\left(\pi\frac{d}{\lambda_0}\cos\,\phi + \frac{\alpha}{2}\right)\end{aligned} \tag{7.31}$$

where we have substituted the basic relation between the phase constant and wavelength, $\beta_0 = 2\pi/\lambda_0$.

In order to plot the pattern of this "array," we observe that, at a fixed distance r, the electric field depends on angle ϕ as

$$|\,\hat{E}_\theta\,| \propto \cos\left(\frac{\pi d}{\lambda_0}\,\cos\,\phi + \frac{\alpha}{2}\right) \tag{7.32}$$

Hence, the *array factor* for plotting the pattern is

$$F(\phi) = \cos\left(\frac{\pi d}{\lambda_0}\,\cos\,\phi + \frac{\alpha}{2}\right) \tag{7.33}$$

Example 7.4 Suppose that the separation of the two antennas in the array is one-half wavelength, $d = \lambda_0/2$, and the currents are in phase, $\alpha = 0^\circ$. Sketch the pattern of the array.

Solution: The array factor in (7.33) becomes

$$F(\phi) = \cos\left(\frac{\pi}{2}\cos\ \phi\right)$$

which is sketched in Fig. 7.10a. This pattern can be determined with a physical argument with the following observations. The wave propagated from each antenna suffers a phase shift of $\angle(-2\pi r/\lambda_0)$ as it propagates away from the antenna. First examine the direction $\phi = 0^\circ$. A wave propagating to the left from antenna 1 has a relative amplitude of 1 arriving at the point where we desire to determine the field. A wave propagating to the left from antenna 2 suffers a phase shift of $\angle(-2\pi d/\lambda_0) = \angle(-\pi)$ or 180° in propagating from antenna 2 to antenna 1. Hence, it arrives at the field point 180° out of phase with the wave propagating from antenna 1. Thus, the two contributions cancel for the $\phi = 0^\circ$ direction. Similarly, for the $\phi = 180^\circ$, we also have a null in the pattern because the two waves are out of phase when they arrive at the field point. Now consider points broadside to the array, $\phi = 90^\circ$ and $\phi = 270^\circ$. The waves from the two antennas in this case travel the same distances and hence arrive in phase, thus reinforcing each other, giving a maximum in the pattern.

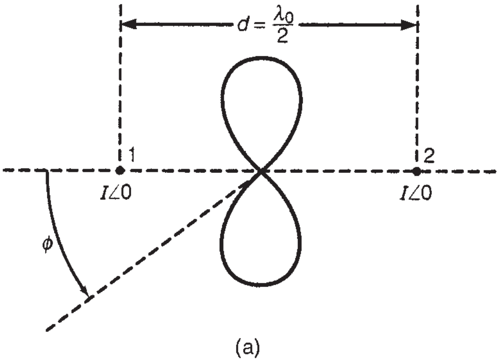

(a)

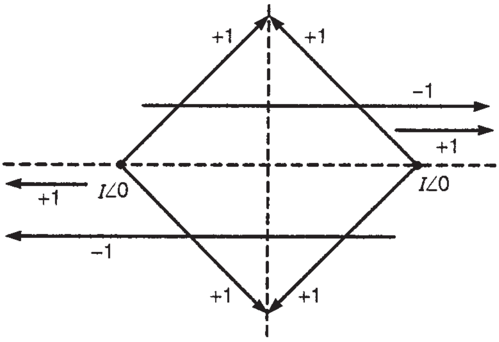

(b)

FIGURE 7.10 Example 7.4. The pattern of an array of two isotropic sources separated by one-half wavelength and having input currents that are in phase: (a) the array factor for this configuration; (b) a diagram depicting the relative phases of each source.

Example 7.5 Suppose that the separation of the two antennas in the array is one-half wavelength, $d = \lambda_0/2$, and the currents are 180° out of phase, $\alpha = \pi$. Sketch the pattern of the array.

Solution: The array factor in (7.33) becomes

$$F(\phi) = \cos\left(\frac{\pi}{2}\cos\,\phi + \frac{\pi}{2}\right)$$

The pattern is sketched in Fig. 7.11a. Again, this pattern is relatively simple to sketch using a physical argument. The wave propagated from each antenna suffers a phase shift of $\angle(-2\pi r/\lambda_0)$ as it propagates away from the antenna. In addition, the current of the antenna may have, as is the case for antenna 1, a phase angle that further shifts the phase of the wave arriving at the field point. First, examine the direction $\phi = 0^\circ$. A wave propagating to the left from antenna 1 has a relative amplitude of -1 arriving at the point where we desire to determine the field. This is due to the fact that the wave starts out with 180° phase angle due to the phase angle of its current. A wave propagating to the left from antenna 2 suffers a phase shift of $\angle(-2\pi d/\lambda_0) = \angle(-\pi)$ or -180° in propagating from antenna 2 to antenna 1. Since the phase angle of the current is zero degrees, there is no additional phase shift incurred. Hence, it arrives at the field point in phase with the wave propagating from antenna 1. Thus, the two contributions add for the $\phi = 0^\circ$ direction. Similarly, for the $\phi = 180^\circ$, we also have a maxima in the pattern because the two waves are in phase when they arrive at the field point.

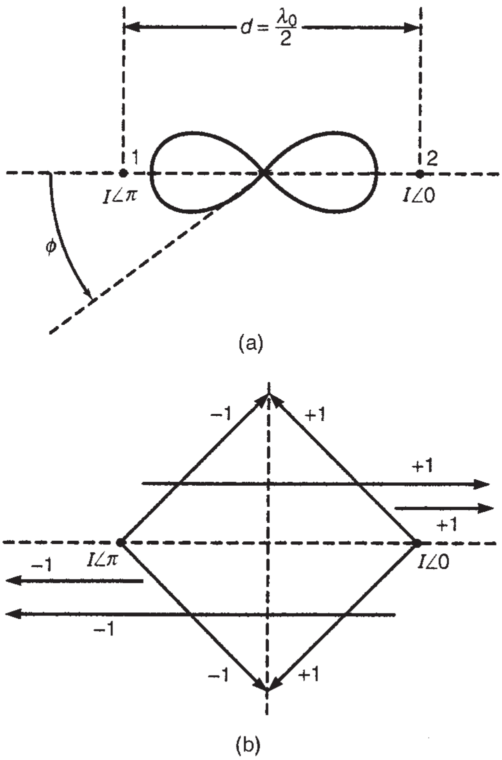

(a)

(b)

FIGURE 7.11 Example 7.5. The pattern of an array of two isotropic sources separated by one-half wavelength and having input currents that are out of phase by 180°: (a) the array factor for this configuration; (b) a diagram depicting the relative phases of each source.

The wave arriving from antenna 1 suffers −180° because it has to propagate a distance $d = \lambda_0/2$ and another 180° because the phase angle of the current is 180°, giving it a net phase shift of 0°. Hence, it arrives in phase with the wave transmitted from antenna 2. Now consider points broadside to the array, $\phi = 90^\circ$ and $\phi = 270^\circ$. The waves from the two antennas in this case travel the same distances but are 180° out of phase because the current of antenna 1 starts out 180° out of phase. Hence, they arrive 180° out of phase, thus giving a null in the pattern.

Example 7.6 Suppose that the separation of the two antennas in the array is one-quarter wavelength, $d = \lambda_0/4$, and the currents are 90° out of phase, $\alpha = \pi/2$. Sketch the pattern of the array.

Solution: The array factor in (7.33) becomes

$$F(\phi) = \cos\left(\frac{\pi}{4}\cos\,\phi + \frac{\pi}{4}\right)$$

The pattern is sketched in Fig. 7.12a. Again, this pattern is relatively simple to sketch using a physical argument. The wave propagated from each antenna suffers a phase shift of $\angle(-2\pi r/\lambda_0)$ as it propagates away from the antenna. In addition, the current of the antenna may have, as is the case

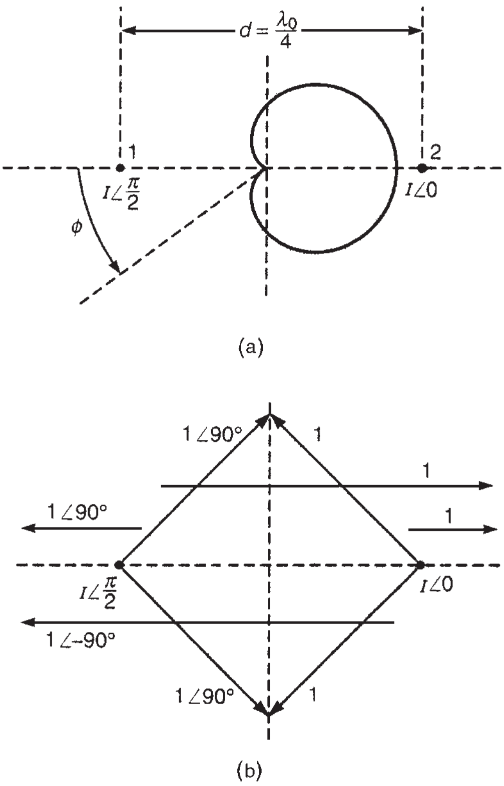

(a)

(b)

FIGURE 7.12 Example 7.6. The pattern of an array of two isotropic sources separated by one-quarter wavelength and having input currents that are out of phase by 90°: (a) the array factor for this configuration; (b) a diagram depicting the relative phases of each source.

for antenna 1, a phase angle that further shifts the phase of the wave arriving at the field point. First examine the direction $\phi = 0^\circ$. A wave propagating to the left from antenna 1 has a phase angle of 90° when it arrives at the point where we desire to determine the field due to the phase angle of the current. A wave propagating to the left from antenna 2 suffers a phase shift of $\angle(-2\pi d/\lambda_0) = \angle(-\pi/2)$ or $-90°$ in propagating from antenna 2 to antenna 1. Since the phase angle of the current is zero degrees, there is no additional phase shift incurred. Hence, it arrives at the field point with a phase angle of $-90°$, which is out of phase with the wave propagating from antenna 1, which arrives with a phase of 90°. Hence, the two waves cancel, giving a null for $\phi = 0^\circ$. Now consider $\phi = 180^\circ$. A wave propagating to the right from antenna 1 starts with a phase angle of 90°. As it propagates from antenna 1 to antenna 2, it suffers a phase shift of $\angle(-2\pi d/\lambda_0) = \angle(-\pi/2)$ or $-90°$. This gives a net phase of $90° - 90° = 0°$ when it arrives at the field point. The wave from antenna 2 arrives at the field point with a relative phase of 0° since it starts out with a phase angle of 0° due to the phase of the current. Hence, the two fields add for $\phi = 180^\circ$. Now consider points broadside to the array, $\phi = 90^\circ$ and $\phi = 270^\circ$. The waves from the two antennas in this case travel the same distances but are 90° out of phase because the currents start out 90° out of phase. Hence, they arrive 90° out of phase, thus giving a total of $1 + j1 = \sqrt{2}\angle 45°$.

The location of nulls in the pattern can be methodically determined by setting the array factor equal to zero:

$$\begin{aligned} F(\phi) &= \cos\left(\frac{\pi d}{\lambda_0}\cos\,\varphi + \frac{\alpha}{2}\right) \\ &= 0 \end{aligned}$$

Thus, the location of nulls in the pattern can be found by solving for

$$\frac{\pi d}{\lambda_0}\cos\,\phi + \frac{\alpha}{2} = \pm\frac{\pi}{2}$$

For example, in Example 7.4, where $d = \lambda_0/2$ and $\alpha = 0^\circ$, we have

$$\frac{\pi}{2}\cos\,\phi = \pm\frac{\pi}{2}$$

giving nulls at $\cos\phi = \pm 1$ or $\phi = 0°, 180°$. For Example 7.5, where $d = \lambda_0/2$ and $\alpha = 180^\circ$, we have

$$\frac{\pi}{2}\cos\,\phi + \frac{\pi}{2} = \pm\frac{\pi}{2}$$

giving nulls at $\cos\phi = 0,\ \cos\ \phi = (-2)$ or $\phi = \pm 90°$, and $\cos\phi = (-2)$ does not represent a physical angle. In Example 7.6, where $d = \lambda_0/4$ and $\alpha = 90^\circ$, we have

$$\frac{\pi}{4}\cos\,\phi + \frac{\pi}{4} = \pm\frac{\pi}{2}$$

giving nulls at $\cos\phi = 1,\ \cos\ \phi = (-3)$ or $\phi = 0°$ and $\cos\phi = (-3)$ does not represent a physical angle.

7.4 CHARACTERIZATION OF ANTENNAS

The antennas we have considered previously are quite simple to analyze. The analysis of other antennas to determine their total radiated power and, more importantly, the shapes of their radiated emission patterns is not so simple. These more complicated antennas are more commonly characterized by measured parameters such as directivity and gain, effective aperture, and/or antenna factor. The purpose of this section is to investigate these criteria.

7.4.1 Directivity and Gain

The *directivity* of an antenna, $D(\theta, \phi)$, is a measure of the concentration of the radiated power in a particular θ, ϕ direction at a fixed distance r away from the antenna. For the elemental dipoles, the half-wave dipole, and the quarter-wave mono pole, we noted that the radiated power is a maximum for $\theta = 90^\circ$ and is zero for $\theta = 0^\circ$ and $\theta = 180^\circ$. To obtain a more quantitative measure of this concentration of radiated power, we will define the radiation intensity $U(\theta, \phi)$.

We found that the far-field, radiated average-power densities for the Hertzian dipole, the magnetic dipole, the long dipole, and the monopole are of the form

$$\begin{aligned} \boldsymbol{S}_{\text{av}} &= \frac{|\hat{\boldsymbol{E}}_{\text{far field}}|^2}{2\eta_0}\boldsymbol{a}_r \quad (\text{in W/m}^2) \\ &= \frac{E_0^2}{2\eta_0 r^2}\boldsymbol{a}_r \end{aligned} \tag{7.34}$$

where E_0 depends on θ, the antenna type and the antenna current. Note that since the far-field electric and magnetic fields depend on the inverse of the distance from them, the power density depends on the square of the inverse distance. To obtain a power pattern relationship that is independent of distance from the antenna, we multiply (7.34) by r^2 and define the resulting quantity to be the *radiation intensity*:

$$U(\theta, \phi) = r^2 S_{\text{av}} \tag{7.35}$$

The radiation intensity will be a function of θ and ϕ but will be independent of distance from the antenna. The total average power radiated will be

$$\begin{aligned} P_{\text{rad}} &= \oint_S \boldsymbol{S}_{\text{av}} \cdot d\boldsymbol{s} \\ &= \int_{\theta=0}^{\pi}\int_{\phi=0}^{2\pi} S_{\text{av}} \underbrace{r^2 \sin\theta\, d\theta\, d\phi}_{ds} \\ &= \int_{\theta=0}^{\pi}\int_{\phi=0}^{2\pi} U(\theta, \phi) \sin\theta\, d\phi\, d\theta \\ &= \oint_S U(\theta, \phi)\, d\Omega \end{aligned} \tag{7.36}$$

where the differential surface in spherical coordinates is [1] $ds = r^2 \sin\theta\, d\phi\, d\theta$.

The quantity $d\Omega = \sin\theta\, d\phi\, d\theta$ is an element of *solid angle* Ω, and the unit of solid angle is the steradian (sr). The units of U are therefore watts per steradian (W/sr). Note that for $U = 1$, (7.36) integrates to 4π. *The total radiated power is therefore the integral of the radiation intensity over a solid angle of* 4π *sr*. Note also that the average radiation intensity is the total radiated power divided by 4π *sr*:

$$U_{\text{av}} = \frac{P_{\text{rad}}}{4\pi} \tag{7.37}$$

The radiation intensity for more complicated antennas is similarly defined. *The directivity of an antenna in a particular direction, $D(\theta, \phi)$, is the ratio of the radiation intensity in that direction to the average radiation intensity*:

$$\begin{aligned} D(\theta,\phi) &= \frac{U(\theta,\phi)}{U_{\text{av}}} \\ &= \frac{4\pi U(\theta,\phi)}{P_{\text{rad}}} \end{aligned} \tag{7.38}$$

The *directivity* of the antenna is often stated for an antenna as a number, which is in the direction of a maximum:

$$D_{\max} = \frac{U_{\max}}{U_{\text{av}}} \tag{7.39}$$

The directivity $D(\theta, \phi)$ of an antenna is simply a function of the shape of the antenna pattern. The *gain* $G(\theta, \phi)$, on the other hand, takes into account the losses of the antenna. For a *lossless* antenna, the directivity and gain are identical. Suppose that a total power P_{app} is applied to the antenna and only P_{rad} is radiated. The difference is consumed in ohmic losses of the antenna, as well as in other inherent losses such as those in an imperfect ground for monopole antennas. If we define an *efficiency factor* e as

$$e = \frac{P_{\text{rad}}}{P_{\text{app}}} \tag{7.40}$$

then the gain is related to the directivity as

$$G(\theta,\phi) = eD(\theta,\phi) \tag{7.41}$$

where we have defined the gain as

$$G(\theta,\phi) = \frac{4\pi U(\theta,\phi)}{P_{\text{app}}} \tag{7.42}$$

For most antennas, the efficiency is nearly 100%, and thus the gain and directivity are nearly equal. Assuming the efficiency is 100%, we will use the term *gain* and *directivity* interchangeably.

We also need to discuss the concept of an isotropic point source. An *isotropic point source* is a fictitious lossless antenna that radiates power equally in all directions. Since this antenna is lossless, its directivity and gain are equal. For an isotropic point source radiating or transmitting a total power P_T, the power density at some distance d away is the total radiated power divided by the area of a sphere of radius d:

$$\boldsymbol{S}_{\text{av}} = \frac{P_T}{4\pi d^2}\boldsymbol{a}_r \tag{7.43}$$

We can also calculate the electric and magnetic fields for the isotropic point source from the realization that the waves resemble (locally) uniform plane waves so that

$$\boldsymbol{S}_{\text{av}} = \frac{|\hat{\boldsymbol{E}}|^2}{2\eta_0} \quad (\text{in W/m}^2) \tag{7.44}$$

Combining (7.43) and (7.44) gives

$$|\hat{\boldsymbol{E}}| = \frac{\sqrt{60P_T}}{d}\,\boldsymbol{a}_\theta \quad (\text{in V/m}) \tag{7.45}$$

where we have substituted $\eta_0 = 120\pi\ \Omega$.

The isotropic point source, although quite idealistic, is useful as a standard or reference antenna to which we refer many of our calculations. For example, since the isotropic point source is lossless, the directivity and gain are equal, and both will be designated by G_0. The gain becomes

$$\begin{aligned} G_0(\theta, \phi) &= \frac{4\pi U(\theta, \phi)}{P_T} \\ &= 1 \end{aligned} \tag{7.46}$$

Figure 7.13 illustrates what *directivity* (gain) of an antenna means. Figure 7.13a shows the pattern of an isotropic point source—the antenna radiates power equally in all directions. Figure 7.13b shows the pattern of an antenna such as a horn or parabolic that strongly focuses its radiated power density in a particular direction, the *main beam*. The directivity is the ratio of the power density of the antenna in the direction of the main beam to the power density of an isotropic point source that is transmitting the same total power P_T in that direction, both measured at the same distance r:

$$D = \frac{S_{\text{av}}(\theta_{\max}, \phi_{\max})}{(P_T/4\pi r^2)} \tag{7.47}$$

which is the same as (7.38):

$$U = r^2 S_{\text{av}}$$

Hence, we can determine the average power density at a distance r from an antenna having gain G or directivity D and having a power P_{app} applied to its input terminals and radiating a total power P_T as

$$\begin{aligned} S_{\text{av}} &= G\frac{P_{\text{app}}}{4\pi r^2} \\ &= D\frac{P_T}{4\pi r^2} \end{aligned} \tag{7.48}$$

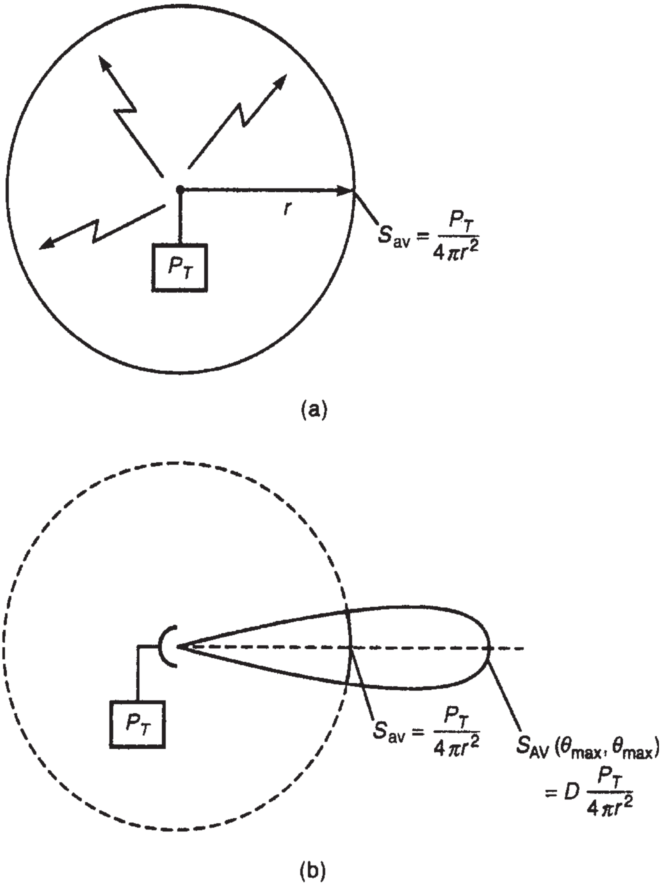
P_T
r
$S_{av} = \frac{P_T}{4\pi r^2}$
(a)
P_T
$S_{av} = \frac{P_T}{4\pi r^2}$
$S_{AV}(\theta_{max}, \theta_{max})$
$= D\frac{P_T}{4\pi r^2}$
(b)

FIGURE 7.13 Illustration of the meaning of antenna directivity: (a) the isotropic point source; (b) directivity of a general antenna.

Example 7.7 Determine the gain of the lossless Hertzian dipole.

Solution: The power density of the Hertzian dipole is given in (7.4) as

$$S_{\text{av}} = 15\pi\left(\frac{dl}{\lambda_0}\right)^2 |\hat{I}|^2 \left[\frac{\sin(\theta)}{r}\right]^2 \text{ W/m}^2$$

which is a maximum in the direction $\theta = 90^\circ$ broadside to the antenna. The total power radiated is given by (7.5) as

$$P_T = 80\pi^2\left(\frac{dl}{\lambda_0}\right)^2 \frac{|\hat{I}|^2}{2} \text{ W}$$

Hence, according to (7.47), since the Hertzian dipole is assumed lossless, the gain is

$$G = 1.5$$

Example 7.8 Determine the gain of a lossless half-wave dipole.

Solution: The power density of a half-wave dipole is given by (7.21) as

$$S_{\text{av}} = 4.77\frac{|\hat{I}_m|^2}{r^2}F^2(\theta)\ \text{W/m}^2$$

which is a maximum in the direction $\theta_{\max} = 90^\circ$, so that $F(\theta_{\max}) = 1$. The total power radiated is given by

$$P_T = 73\frac{|\hat{I}_m|^2}{2}\ \text{W}$$

Hence, the gain is given by (7.47) as

$$G = 1.64$$

According to this, the half-wave dipole is only slightly better than the Hertzian dipole in its ability to focus the radiated power. However, there is a large difference between the two antennas. The radiation resistance of the half-wave dipole is considerably larger than that of the Hertzian dipole, and hence power can be transmitted using a much smaller input current. The quarter-wave monopole radiates half the power of a half-wave dipole (in the space above the location of the ground plane). Hence, the gain of the quarter-wave monopole is twice that of the corresponding half-wave dipole or 3.28.

Gain or directivity of an antenna is often specified in decibels (dB). The gain of an antenna is specified in dB as

$$G_{\text{dB}} = 10\log_{10}(G) \tag{7.49}$$

The gain of the Hertzian dipole is $G = 10\log_{10}(1.5) = 1.76$ dB. The gain of the half-wave dipole is $G = 10\log_{10}(1.64) = 2.15$ dB, and the gain of a quarter-wave monopole is $G = 10\log_{10}(3.28) = 5.17$ dB. Antennas that have considerable focusing ability such as the parabolic or horn antennas have very large gains. A gain of 40 dB is equivalent to a gain of 10,000, that is, the power density in the direction of maximum radiation is 10,000 times the power density if the total transmitted power were radiated equally in all directions, as with an isotropic point source. Satellite antennas such as are used to receive television signals rely on these very large gains (as much as 60 dB) to compensate for the very small power density received on the earth from an orbiting satellite, which can be on the order of 10^{-12} W/m^2.

Gain of an antenna is specified with respect to the gain of some reference antenna. The reference antenna used here is the isotropic point source, which has a gain of unity, $G_0 = 1$. In this case, we say that the gain of the antenna is the gain over an isotropic antenna

$$G_{\text{dB}} = 10\log_{10}\left(\frac{G}{G_0}\right) \tag{7.50}$$

In some instances in industry, the gain of an antenna may be specified with respect to a half-wave dipole. In this case, the gain is over a half-wave dipole:

$$G_{\text{dB}} = 10\log_{10}\left(\frac{G}{1.64}\right) \tag{7.51}$$

We are frequently interested in the coupling between two antennas, one of which is used as a transmitter and the other as a receiver. An important principle in this problem is that of *reciprocity* [1, 3–6]. Reciprocity provides that the source and receiver can be interchanged without affecting the results so long as the impedances of the source and receiver are the same. Several additional properties can be proven. *The impedance seen looking into an antenna terminals when it is used for transmission is the same as the Thevenin source impedance seen looking back into its terminals when it is used for reception. In addition, the transmission pattern of the antenna is the same as its reception pattern.*

7.4.2 Effective Aperture

An additional useful concept is that of an antenna's effective aperture. The *effective aperture* of an antenna is related to the ability of the antenna to extract energy from a passing wave as illustrated in Fig. 7.14a. *The effective aperture of an antenna* A_e *is the ratio of the power received (in its load impedance)* P_R *to the power density of the incident wave* S_{av}

$$A_e = \frac{P_R}{S_{\text{av}}} \qquad (\text{in m}^2) \tag{7.52}$$

The *maximum effective aperture* A_{em} is the ratio in (7.52) when the load impedance is the conjugate of the antenna impedance, $\hat{Z}_L = \hat{Z}_S^*$ in Fig. 7.14b, which means that maximum power transfer to the load takes place and the polarization of the incident wave and the polarization of the antenna are matched. For a linearly polarized incident wave and a receiving antenna such as a dipole or monopole that produces linearly polarized waves when it is used for transmission, the requirement for matched

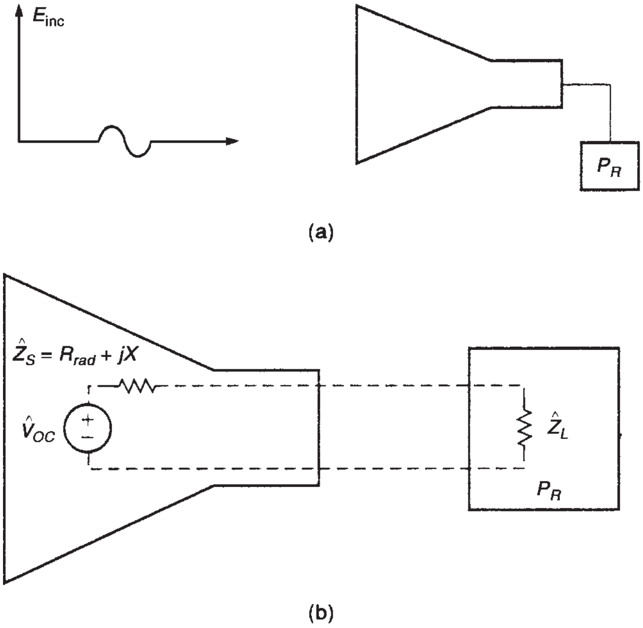

FIGURE 7.14 Receiving properties of antennas: (a) illustration of effective aperture (area); (b) the equivalent circuit of a receiving antenna.

polarization essentially means that the antenna is oriented with respect to the incident wave to produce the maximum response; that is, the electric field vector of the incident wave is parallel to the electric field vector that would be produced by this antenna when it is used for transmission.

Example 7.9 For example, let us compute the maximum effective aperture of a Hertzian dipole antenna. If the dipole is terminated in an impedance $\hat{Z}_L$, we assume that $\hat{Z}_L = R_{\text{rad}} - jX$, where the input impedance to the dipole is $\hat{Z}_{\text{in}} = R_{\text{rad}} + jX$ and the dipole is assumed to be lossless. The maximum induced voltage at the terminals occurs when the electric field vector of the incident wave is aligned with the dipole, $\theta = 90°$, as shown in Fig. 7.15. The open-circuit voltage produced at the terminals of the antenna is

$$|\hat{V}_{OC}| = |\hat{E}_\theta|\, dl \tag{7.53}$$

The power density in the incident wave is

$$S_{\text{av}} = \frac{1}{2}\frac{|\hat{E}_\theta|^2}{\eta_0} \tag{7.54}$$

Since the load is matched for maximum power transfer, the power received is

$$\begin{aligned} P_R &= \frac{|\hat{V}_{OC}|^2}{8R_{\text{rad}}} \\ &= \frac{|\hat{E}_\theta|^2 dl^2}{8R_{\text{rad}}} \end{aligned} \tag{7.55}$$

Substituting the value for R_{rad} given in (7.6) gives

$$P_R = \frac{|\hat{E}_\theta|^2 \lambda_0^2}{640\pi^2} \tag{7.56}$$

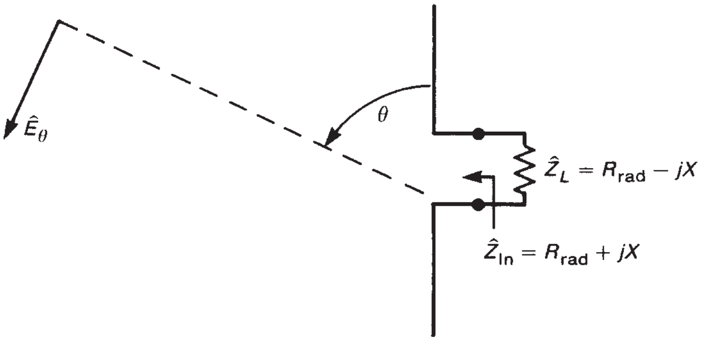
$\hat{E}_\theta$
θ
$\hat{Z}_L = R_{\text{rad}} - jX$
$\hat{Z}_{\text{in}} = R_{\text{rad}} + jX$

FIGURE 7.15 Example 7.9. Illustration of the computation of the maximum effective aperture A_{em} of a linear antenna.

Thus, the maximum effective aperture is

$$\begin{aligned}A_{\mathrm{em}} &= \frac{P_R}{S_{\mathrm{av}}}\\ &= 1.5\frac{\lambda_0^2}{4\pi}\\ &= \frac{\lambda_0^2}{4\pi}G\end{aligned} \tag{7.57}$$

where we have substituted the gain of the Hertzian dipole

$$G = 1.5 \tag{7.58}$$

Observe that the maximum effective aperture of an antenna is not necessarily related to its "physical aperture."

It can be shown that the result in (7.57) is a general result valid for more general antennas; that is, the effective aperture of an antenna used for reception is related to the gain *in the direction of the incoming wave* of that antenna when it is used for transmission as [1, 3–6]:

$$G(\theta, \phi) = \frac{4\pi}{\lambda_0^2}A_e(\theta, \phi) \tag{7.59}$$

The direction for A_e (the direction of the incoming incident wave with respect to the receiving antenna) is the direction of the gain G (the gain of the antenna in this direction when it is used for transmission). We have interchanged directivity D and gain G on the assumption that the antennas are lossless.

Review Exercise 7.4 Determine the maximum effective aperture of a half-wave dipole that is operated at 150 MHz.

***Answer*:** 0.522 m^2.

7.4.3 Antenna Factor

The antenna properties described above are more commonly used in applications of antennas for communication such as signal transmission and radar. In the area of their use in EMC, a more common way of characterizing the reception properties of an antenna is with the notion of its *antenna factor*. Consider a dipole antenna that is used to measure the electric field of an incident, linearly polarized uniform plane wave as shown in Fig. 7.16a. A receiver such as a spectrum analyzer is attached to the terminals of this measurement antenna. The voltage measured by this instrument is denoted as $\hat{V}_{\mathrm{rec}}$. It is desired to relate this received voltage to the incident electric field. This is done with the antenna's *antenna factor*, which is defined as *the ratio of the incident electric field at the surface of the measurement antenna to the received voltage at the antenna terminals*:

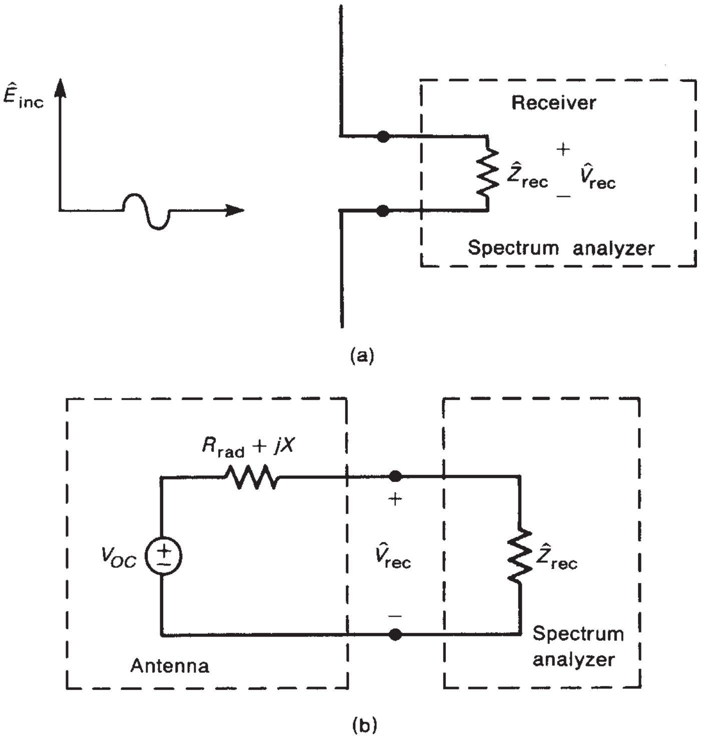
$\hat{E}_{\text{inc}}$
Receiver
+
$\hat{Z}_{\text{rec}}$
$\hat{V}_{\text{rec}}$
−
Spectrum analyzer
(a)
$R_{\text{rad}} + jX$
V_{OC}
+
$\hat{V}_{\text{rec}}$
−
$\hat{Z}_{\text{rec}}$
Antenna
Spectrum analyzer
(b)

FIGURE 7.16 The antenna factor (AF): (a) general circuit; (b) equivalent circuit.

$$\begin{aligned}\text{AF} &= \frac{(\text{V/m}) \text{ in incident wave}}{\text{V received}} \quad (\text{in } 1/\text{m}) \\ &= \frac{|\hat{E}_{\text{inc}}|}{|\hat{V}_{\text{rec}}|}\end{aligned} \tag{7.60}$$

This is frequently expressed in dB as

$$\text{AF}_{\text{dB}} = \text{dB}\mu\text{V/m (incident field)} - \text{dB}\mu\text{V (received voltage)} \tag{7.61a}$$

or

$$\text{dB}\mu\text{V/m (incident field)} = \text{dB}\mu\text{V (received voltage)} + \text{AF}_{\text{dB}} \tag{7.61b}$$

Note that the units of the antenna factor are 1/m (reciprocal meters). The units are frequently ignored, and the antenna factor is stated in dB. The antenna factor is usually furnished by the manufacturer of the antenna as measured data at various frequencies in the range of intended use of the measurement antenna. A typical such plot provided by the manufacturer of a biconical measurement antenna is shown in Fig. 7.17. A known field is provided by some standard antenna at a calibrated test site such as the National Institute of Standards and Technology (NIST) in Boulder, Colorado, in the United States [formerly known as the National Bureau of Standards (NBS)]. The ratio of the known value of the incident field to the measured voltage at the terminals of the antenna in dB according to

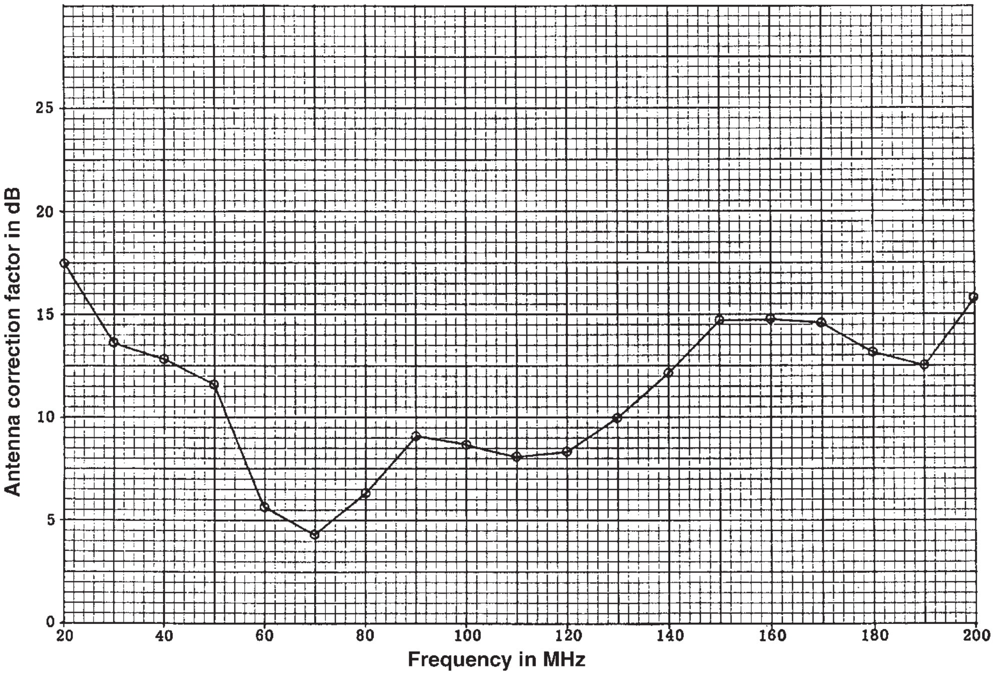

FIGURE 7.17 The antenna factor versus frequency for a typical biconical EMC measurement antenna. Source: Courtesy of the Eaton Corporation.

(7.61) is plotted for the antenna versus frequency. The reciprocal of the antenna factor is referred to as the *antenna effective height* h_e [3–6].

There are several important implicit assumptions in these measured antenna factor data. *If any of these implicit assumptions are not adhered to in the course of using this antenna for measurement, then the measured data are invalid.* The first important assumption is that *the incident field is polarized for maximum response of the antenna.* For a dipole or other wire-type antenna, this means that *the response will be the component of the incident field that is parallel to the antenna axis.* Ordinarily, this is what is desired, since the antenna typically will be used to measure vertical and horizontal fields in testing for compliance with the radiated emission regulatory limits. The second important implicit assumption has to do with *the input impedance of the receiver that is used not only to make the measurement but also to calibrate the antenna.* The most common impedance is the typical input impedance to virtually all spectrum analyzers, and that is 50 Ω. Nevertheless, the antenna manufacturer should explicitly state what termination impedance was used in the calibration. Note that *this does not assume that the receiver is matched to the antenna*, and usually it will not be. However, from the standpoint of using the antenna factor calibration chart for that antenna, it is important only to use a termination impedance that is the same as was used to calibrate the antenna.

On the other hand, suppose that we wish to *calculate* the antenna factor of an ideal antenna such as a dipole from the field equations, maximum effective aperture, etc. for that antenna. Since the spectrum analyzer input impedance is $\hat{Z}_{\text{rec}} = (50 + j0)\ \Omega$ and is therefore not matched, we must use the equivalent circuit of Fig. 7.16b to obtain this. First compute $\hat{V}_{\text{rec, matched}}$ *assuming a matched load*, $\hat{Z}_{\text{rec}} = R_{\text{rad}} - jX$, using the results in the previous sections. Then use this result to obtain the open-circuit voltage $\hat{V}_{OC} = 2\hat{V}_{\text{rec, matched}}$. Then use the equivalent circuit in Fig. 7.16b to compute the actual received voltage $\hat{V}_{\text{rec}}$ and from that the antenna factor.

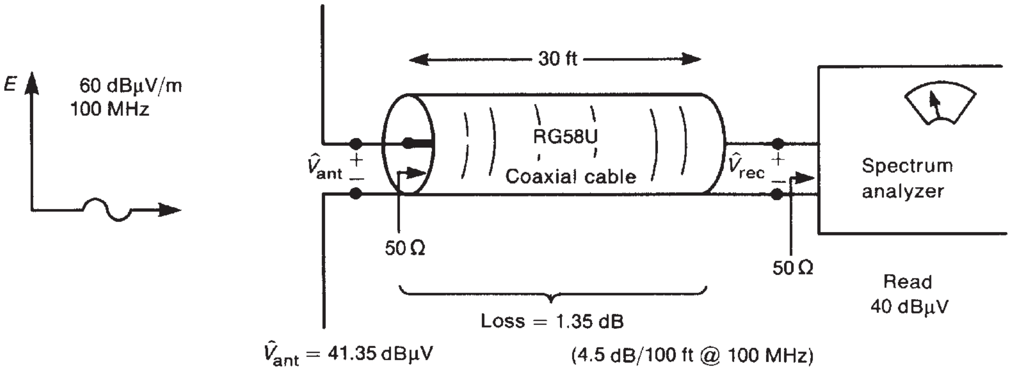

FIGURE 7.18 Example 7.10. An example illustrating the use of the antenna factor to compute the received voltage.

Example 7.10 As an example of the use of measured data to determine the antenna factor, consider the calibration of a measurement antenna shown in Fig. 7.18. A known, incident, linearly polarized, uniform plane wave is incident on the antenna, and the electric field *at the position of the antenna in the absence of the antenna* is 60 dBμV/m. A 30 ft. length of RG58U coaxial cable is used to connect the antenna to a 50 Ω spectrum analyzer. The spectrum analyzer measures 40 dBμV. Since the antenna factor relates the incident electric field to the *voltage at the base of the antenna*, we must relate the spectrum analyzer reading to the voltage at the base of the antenna. The coaxial cable has 4.5 dB/100 ft. loss at the frequency of the incident wave, 100 MHz. Thus, the cable loss of 1.35 dB must be *added* to the spectrum analyzer reading to give the voltage at the antenna terminals of 41.35 dBμV. Therefore, the antenna factor is

$$\begin{aligned}\mathrm{AF_{dB}} &= 60\ \mathrm{dB\mu V/m} - 41.35\ \mathrm{dB\mu V}\\ &= 18.65\ \mathrm{dB}\end{aligned}$$

It is a simple matter to convert the spectrum analyzer readings to the value of incident field; *add the antenna factor in dB to the spectrum analyzer reading in dBμV and add the connection loss in dB to give the incident electric field in dBμV/m*:

$$E(\mathrm{dB\mu V/m}) = \mathrm{AF(dB)} + V_{\mathrm{SA}}(\mathrm{dB\mu V}) + \text{cable loss (dB)} \tag{7.62}$$

Observe that the connection cable loss must be added and not subtracted, since the antenna factor is with respect to the base of the antenna and does not include any connection cable loss (unless explicitly stated by the antenna manufacturer).

7.4.4 Effects of Balancing and Baluns

The ideal antennas that we are considering are inherently *balanced structures*. There are numerous definitions of this concept of *balanced structure*. Generally, but not always, these seemingly different definitions lead to the same result. For example, consider the long dipole antenna shown in Fig. 7.3a. In the analysis of this antenna, we assumed that the current $\hat{I}(z_1)$ at a point z_1 on the upper arm is the same in magnitude as the current at the corresponding position on the lower arm, $-z_1$ (a point that is the same distance from the feedpoint as the point on the upper arm). From this standpoint of *symmetry of the antenna currents*, the antenna is *inherently* a balanced structure. This also inherently assumes that the current entering one terminal of the antenna is equal but opposite to the current entering the other terminal. Nearby metallic obstacles such as ground planes can upset this balance, causing the pattern to deviate substantially from the ideal pattern that was obtained from the assumption of balanced currents on the arms of the antenna [7].

Other factors can upset the balance of the currents on the antenna structure. The most common type of feedline that is used to supply signals to antennas is the coaxial cable (coax). Under ideal conditions, the current returns to its source on the *interior* of the overall shield. If this type of cable is attached to an inherently balanced structure such as a dipole antenna, some of the current may flow *on the outside of the shield*. This current will radiate. The amount of current that flows on the outside of the shield depends on "the impedance to ground" between the shield exterior and the ground, $\hat{Z}_G$, along with the excitation of the shield exterior (unintentional excitation).

The common way of preventing unbalance due to a coaxial feed cable is the use of a *balun*, which is an acronym for *bal*anced to *un*balanced, referring to the transition from an unbalanced coaxial cable to a balanced antenna. The balun is inserted at the input to the antenna, as shown in Fig. 7.19a.

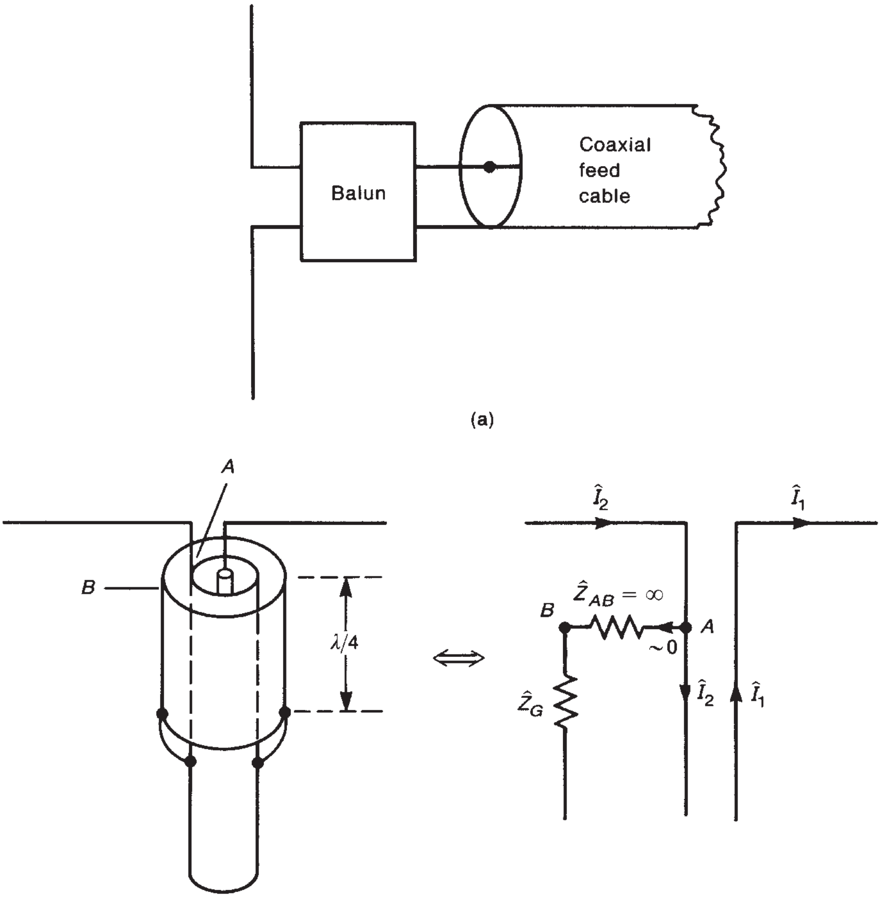

(a)

(b)

FIGURE 7.19 Use of baluns to reduce common-mode currents on antennas: (a) use of a discrete balun to connect an unbalanced coaxial cable to a balanced antenna; (b) the bazooka balun.

In the case of the coaxial feed cable, the intent of the balun is to increase the impedance between the outside of the shield and ground. A common form is the "bazooka balun" shown in Fig. 7.19b. A quarter-wavelength section of shield is inserted over the shield of the original cable, and these are shorted together a quarter-wavelength from the feedpoint. A quarter-wavelength, short-circuited transmission line is formed between the outer coax and the inner coax. We found in Chapter 4 that a short-circuited, quarter-wavelength transmission line appears at its input as an open circuit. Therefore, the impedance between points *A* and *B* is very large (theoretically infinite), so that the impedance between the inner shield and ground is infinite also.

There are other methods of producing balanced feeds. They also seek to block this current on the outside of the shield. One obvious method is to add ferrite sleeves (discussed in Chapter 5) around the feed coax as shown in Fig. 7.20a. The beads act as common-mode chokes [8]. Another way

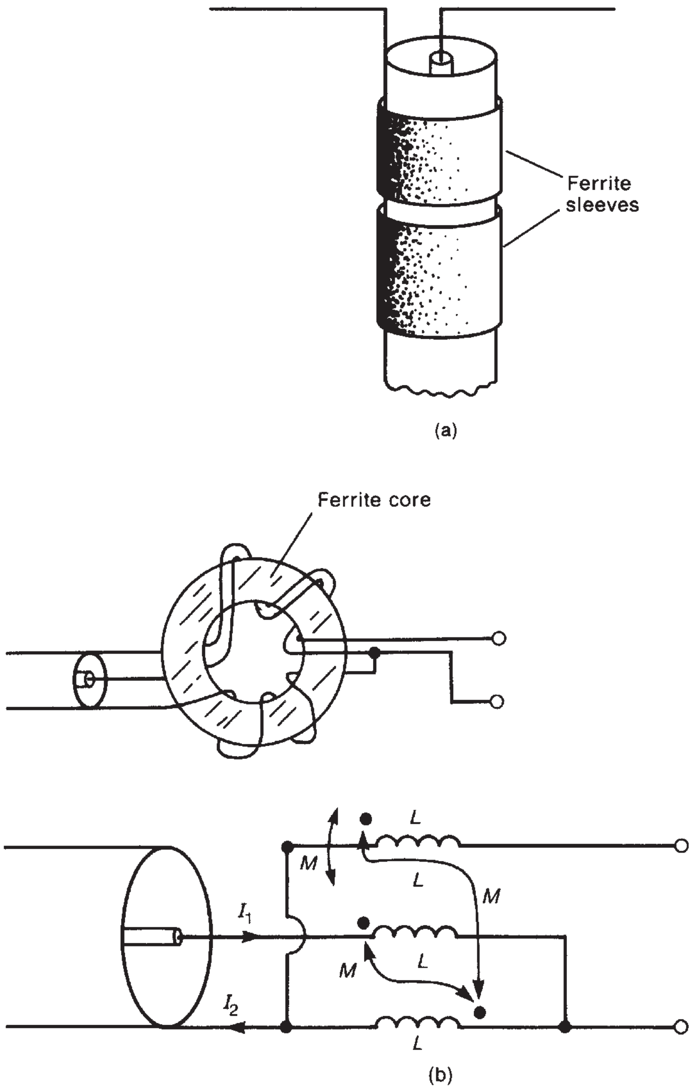

FIGURE 7.20 Other methods of reducing common-mode currents: (a) use of ferrite "sleeves"; (b) use of a ferrite toroid [5]. Source: Balanis [5]/John Wiley & Sons.

of accomplishing this is to custom wind a ferrite toroid as shown in Fig. 7.20b [5]. The equivalent circuit is also shown. Ferrite baluns tend to provide "wideband balancing" over bandwidths of as much as 3 : 1, that is, the ratio of the upper useable frequency to the lowest one is a factor of 3. The bazooka balun works only at the frequency where its length is one-quarter wavelength, so that its bandwidth is limited.

Further discussions of baluns are given in [3–7]. Balancing is a critical factor in the accurate measurement of radiated emissions. If the antenna–feedline combination is not balanced, the measured data may appear to comply with the regulatory limits when in fact they may not because of the pattern distortion caused by the unbalance. Broadband baluns are obviously very desirable in swept frequency measurements for compliance verification, since we do not wish to have to "retune" the balun for each frequency in the test.

7.4.5 Impedance Matching and the Use of Pads

The ability to make *swept-frequency measurements* in the course of measuring the radiated emissions of a product for the verification of compliance with the regulatory limits is obviously important from the standpoint of rapid gathering of the test data. The FCC prefers the use of the half-wave dipole. In order to use this antenna to measure radiated emissions over the frequency range of the limit, 30 MHz to 1 GHz, we must change the length of the dipole at each measurement frequency so that the dipole length is one-half wavelength at that frequency. A more efficient method is to use *broadband measurement antennas* such as the biconical and log-periodic antennas discussed in Section 7.7. These antennas are calibrated as discussed above, and the calibration data usually consist of a plot of the antenna factor for the antenna versus frequency. As pointed out above, the antenna factor data assume that not only is the antenna balanced (measurement antennas are usually provided with built-in baluns) but the *termination impedance seen at the antenna terminals is* 50 Ω. Although the spectrum analyzer or receiver used to measure the antenna terminal voltage usually has an input impedance of 50 Ω, it is almost always necessary to connect it to the antenna with a connection cable such as a coaxial cable, as shown in Fig. 7.18. If the characteristic impedance of the coaxial cable is also 50 Ω (as is usually the case), then the impedance seen looking into the coaxial cable with the receiver attached is also 50 Ω, since this cable is matched at the receiver. Thus, the antenna sees an impedance of 50 Ω for all frequencies, as was assumed in the course of its calibration. If for some reason the termination impedance at the receiver end of the cable is not 50 Ω, then the impedance that the antenna terminals seen looking into the cable is not 50 Ω, because the cable is not matched, and, moreover, the impedance seen looking into the cable will vary with frequency. *The input impedance to a cable will be independent of frequency and equal to its characteristic resistance Z_C (normally* 50 Ω*) only if the cable is terminated in a matched load impedance,* $\hat{Z}_L = Z_C$. A way of providing a matched termination for other values of termination impedances is with the use of a *pad*.

A pad is simply a resistive network whose input impedance remains fairly constant regardless of its termination impedance. A typical topology of a pad is the "Pi" (Π) structure shown in Fig. 7.21a with reference to its resemblance to the symbol π. It is also possible to choose other structures such as the "tee" (T) structure. Being resistive circuits, these pads provide matching over wide frequency ranges (they are said to be broadband devices), but they also give an insertion loss. The resistor values and schematic of a 50 Ω, 6 dB pad are shown in Fig. 7.21b, and a photograph of a commercially available pad is shown in Fig. 7.21c.

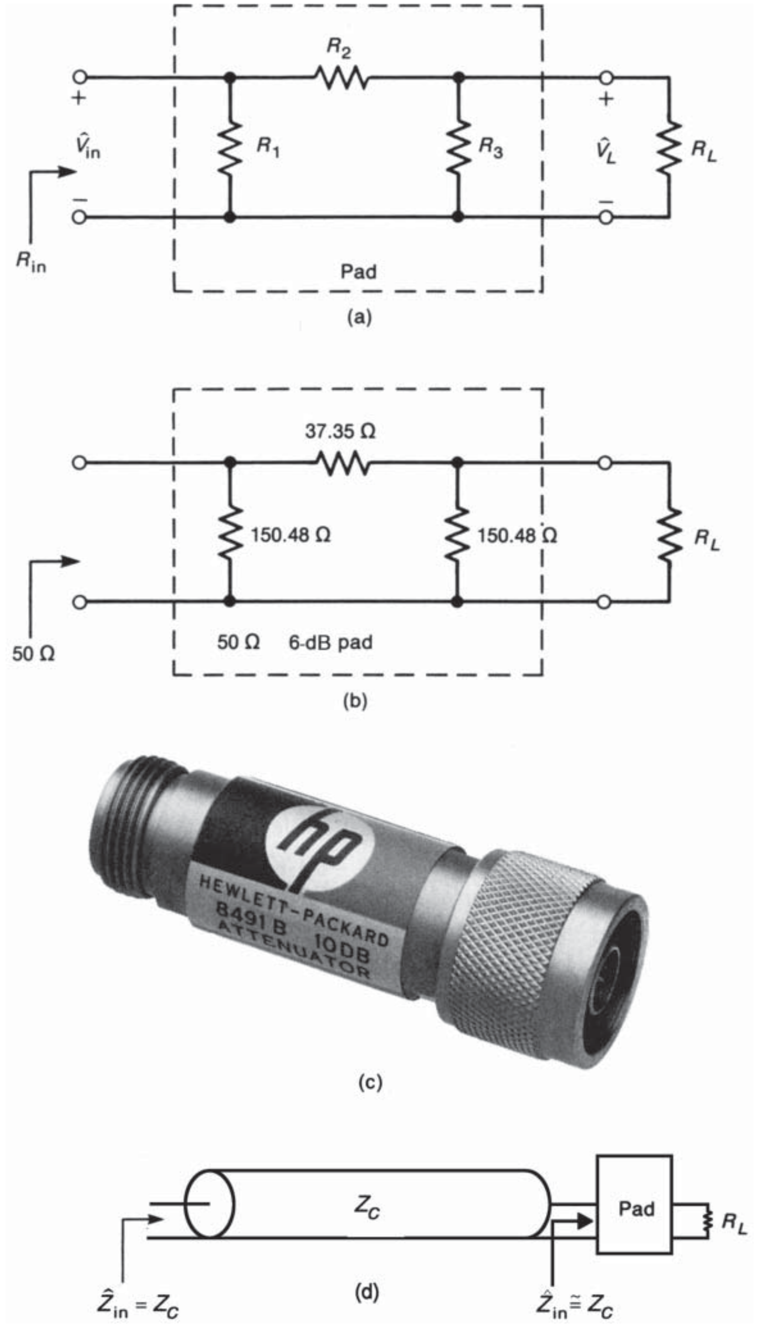
R_2
+
$\hat{V}_{in}$
R_1
R_3
+
$\hat{V}_L$
R_L
−
−
R_{in}
Pad
(a)
37.35 Ω
150.48 Ω
150.48 Ω
R_L
50 Ω
50 Ω 6-dB pad
(b)
HEWLETT-PACKARD
8491 B 10DB
ATTENUATOR
(c)
Z_C
Pad
R_L
$\hat{Z}_{in} = Z_C$
(d)
$\hat{Z}_{in} \cong Z_C$

FIGURE 7.21 Use of pads to match transmission lines: (a) a pi pad structure. Source: Paul and Nasar [1]/McGraw Hill Education; (b) schematic of a 50 Ω, 6 dB pad; (c) a commercially available pad (courtesy of the Hewlett-Packard Corporation). Source: Courtesy of the Hewlett-Packard Corporation; (d) use of a pad to match a coaxial cable.

The insertion loss (IL) is defined as the ratio of the power delivered to the load with and without the pad:

$$\begin{aligned}\mathrm{IL}_{\mathrm{dB}} &= 10\log_{10}\left(\frac{P_{L,\text{without pad}}}{P_{L,\text{with pad}}}\right)\\ &= 20\log_{10}\left(\frac{|\hat{V}_L|_{\text{without pad}}}{|\hat{V}_L|_{\text{with pad}}}\right)\end{aligned} \tag{7.63}$$

Typically, the larger the insertion loss that one can tolerate, the better the matching ability of the pad, i.e., *the wider the range of load impedances such that* $R_{\text{in}} \cong Z_C$. As an illustration of this point, consider the 50 Ω, 6 dB pad shown in Fig. 7.21b. Consider the extreme values of termination impedances: open circuit and short circuit. The open-circuit impedance can be calculated to be

$$\begin{aligned}R_{\text{in,oc}} &= 150.48\|(37.35 + 150.48)\\ &= 83.55\ \Omega\end{aligned}$$

The short-circuit input impedance is

$$\begin{aligned}R_{\text{in,oc}} &= 150.48\|37.35\\ &= 29.92\ \Omega\end{aligned}$$

If this pad is inserted between a 50 Ω coaxial cable and the load as shown in Fig. 7.21d the voltage standing wave ratio (VSWR) on the cable will be less than 1.67 for any load between an open circuit and a short circuit, $|\Gamma_L| = 0.25$ for both cases. Usually, an acceptable VSWR is less than 1.2, which will be more closely achieved for realistic loads. If $R_L = 50\ \Omega$, the insertion loss is 6 dB. A 20 dB, 50 Ω pad will give a smaller range of VSWR at the expense of more loss. For example, the values of resistors for a 20 dB, 50 Ω pad are $R_1 = R_3 = 61.11\ \Omega$ and $R_2 = 247.50\ \Omega$. For the short-circuit load, the input impedance is 49.01 Ω, with a VSWR of 1.02. For the open-circuit load, the input impedance is 51.01 Ω, with a VSWR of 1.02. The insertion loss is obtained for Fig. 7.21a [1]:

$$\mathrm{IL} = 20\log_{10}\left[\left(\frac{R_3\|R_L}{R_2 + R_3\|R_L}\right)^{-1}\right] \tag{7.64}$$

Solving this gives

$$\begin{aligned}R_1 &= R_3\\ &= \frac{R_L(1+X)}{(R_L/Z_C)X - 1}\end{aligned} \tag{7.65a}$$

$$R_2 = (R_3\|R_L)(X-1) \tag{7.65b}$$

where

$$X = 10^{\mathrm{IL}/20} \tag{7.65c}$$

and we are interested in matching to a coaxial cable having a characteristic impedance Z_C as shown in Fig 7.21d for a wide range of loads, R_L.

Review Exercise 7.5 Determine the circuit values for a 10 dB, 75 Ω pad.

Answers: $R_1 = R_3 = 144.37\ \Omega$, $R_2 = 106.73\ \Omega$.

7.5 THE FRIIS TRANSMISSION EQUATION

Exact calculation of the coupling between two antennas is usually a formidable problem. For this reason, many practical calculations of antenna coupling are carried out, approximately, with the Friis transmission equation. Consider two antennas in free space, shown in Fig. 7.22. One antenna is transmitting a total power P_T, and the other is receiving power P_R in its terminal impedance. The transmitting antenna has a gain of $G_T(\theta_T, \phi_T)$ and an effective aperture $A_{eT}(\theta_T, \phi_T)$ in the direction of transmission, (θ_T, ϕ_T). The receiving antenna has a gain and effective aperture of $G_R(\theta_R, \phi_R)$ and $A_{eR}(\theta_R, \phi_R)$ in this direction of transmission, (θ_R, ϕ_R). The power density at the receiving antenna is the power density of an isotropic point source multiplied by the gain of the transmitting antenna *in the direction of transmission*:

$$S_{\text{av}} = \frac{P_T}{4\pi d^2} G_T(\theta_T, \phi_T) \tag{7.66}$$

The received power is the product of this power density and the effective aperture of the receiving antenna *in the direction of transmission*:

$$P_R = S_{\text{av}} A_{eR}(\theta_R, \phi_R) \tag{7.67}$$

Substituting (7.66) into (7.67) gives

$$\frac{P_R}{P_T} = \frac{G_T(\theta_T, \phi_T) A_{eR}(\theta_R, \phi_R)}{4\pi d^2} \tag{7.68}$$

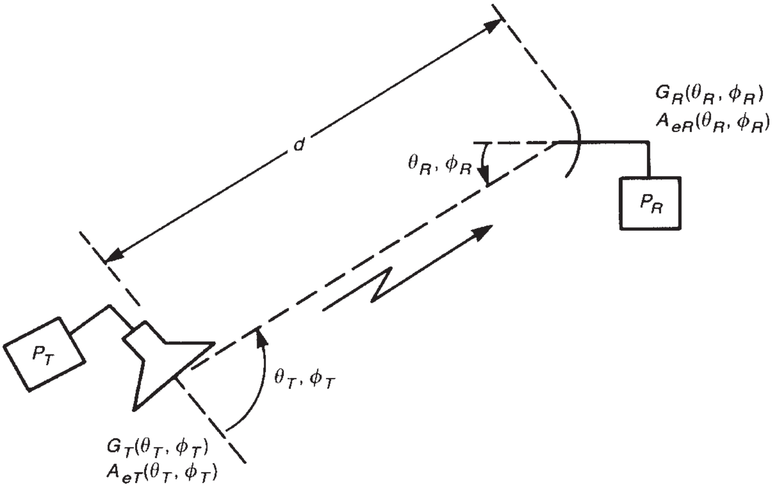

FIGURE 7.22 Illustration of the Friis transmission equation for computing the coupling between two antennas in terms of their gains.

Replacing the effective aperture of the receiving antenna with its gain via (7.59) (assuming a matched load and matched polarization so that the effective apertures are the maximum effective apertures), we obtain the most common version of the *Friis transmission equation*:

$$\frac{P_R}{P_T} = G_T(\theta_T, \phi_T)G_R(\theta_R, \phi_R)\left(\frac{\lambda_0}{4\pi d}\right)^2 \tag{7.69}$$

The electric field intensity of the transmitted field at a distance d from the transmitting antenna can also be computed. The power density in the transmitted wave is that of a uniform plane wave (locally):

$$S_{\text{av}} = \frac{1}{2}\frac{|\hat{E}|^2}{\eta_0} \tag{7.70}$$

Combining this with (7.66) gives

$$|\ \hat{E}\ | = \frac{\sqrt{60P_T G_T(\theta_T, \phi_T)}}{d} \tag{7.71}$$

since $\eta_0 = 120\pi$.

Quite often, in practice, the antenna gains are stated in decibels as is the transmitted power. In decibels, the Friis transmission equation becomes

$$10\log_{10}\left(\frac{P_R}{P_T}\right) = G_{T,\text{dB}} + G_{R,\text{dB}} - 20\log_{10}f - 20\log_{10}d + 147.56 \tag{7.72}$$

There are a number of assumptions inherent in the Friis transmission equation. For the relationship between gain and effective aperture given in (7.59) to be valid, the receiving antenna must be matched to its load impedance and the polarization of the incoming wave; otherwise, the Friis equation will result in an upper limit on the coupling (“worst case”). We also require that the two antennas be in the *far field* of each other. The far-field criterion is usually taken to be the larger of

$$d_{\text{far field}} > \frac{2D^2}{\lambda_0} \quad \text{(surface antennas)}$$

or

$$d_{\text{far field}} > 3\lambda_0 \quad \text{(wire antennas)}$$

where D is the maximum dimension of the antenna [1]. The first criterion is used for “surface-type antennas,” whereas the second criterion is used for “wire-type antennas.” Inherent in the effective-aperture concept is the assumption that the incoming field resembles a uniform plane wave in the vicinity of the receiving antenna. The transmitted wave in the far field of the transmitting antenna resembles a spherical wave from a point source that only locally resembles a uniform plane wave, as is assumed in all of the previous derivations. The criterion that the two antennas be separated by $2D^2/\lambda_0$ ensures that the spherical incoming wave differs in phase from a plane wave at the extremities of the antenna surface by at most $\lambda_0/16$ [1]. The separation criterion of $3\lambda_0$ insures that “wave impedance” of the incoming wave is approximately that of free space.

Example 7.11 As an example, let us calculate the coupling between two half-wave dipole antennas. Assume that the dipoles are separated by a distance of 1000 m, are operated at a frequency of 150 MHz, and are oriented parallel to each other for maximum reception. The transmitting dipole is driven by a 100 V (peak), 50 Ω, source, as shown in Fig. 7.8. The radiated power was calculated in Section 7.2 from the equivalent circuit of Fig. 7.8b to be 21.36 W. The gain of a half-wave dipole in the main beam, broadside to the antenna, is 2.15 dB (1.64 absolute). The electric field at the receiving antenna is calculated from the Friis transmission equation given in (7.71) as

$$\begin{aligned}
|\hat{E}| &= \frac{\sqrt{60 \times 21.36 \times 1.64}}{1000} \\
&= 45.85\ \text{mV/m}
\end{aligned}$$

The value calculated from (7.20) is

$$\begin{aligned}
|\hat{E}|_{\max} &= 60\,\frac{\hat{I}_m}{r} \quad (\theta = 90^\circ) \\
&= 60\,\frac{0.765\ \text{A}}{1000} \\
&= 45.90\ \text{mV/m}
\end{aligned}$$

The average power density at the receiving antenna is

$$\begin{aligned}
S_{\text{av}} &= \frac{1}{2}\frac{|\hat{E}|^2}{\eta_0} \\
&= 2.794\ \mu\text{W/m}^2
\end{aligned}$$

Thus, the average power received in a matched load is

$$\begin{aligned}
P_R &= S_{\text{av}} A_{eR} \\
&= S_{\text{av}} \frac{\lambda_0^2}{4\pi} G_R \\
&= 2.794 \times 10^{-6} \times \frac{2^2}{4\pi} \times 1.64 \\
&= 1.459\ \mu\text{W} \\
&= -28.36\ \text{dBm}
\end{aligned}$$

The radiated power of 21.36 W is 43.3 dBm. Therefore, the ratio of the received and transmitted power is

$$\begin{aligned}
\frac{P_R}{P_T} &= -28.36\ \text{dBm} - 43.3\ \text{dBm} \\
&= -71.66\ \text{dB}
\end{aligned}$$

As an alternative, using the Friis equation in transmission (7.72) gives $\frac{P_R}{P_T} = 2.15 + 2.15 - 20\log_{10}(150 \times 10^6) - 20\log_{10}(1000) + 147.56 = -71.66$ dB

7.6 EFFECTS OF REFLECTIONS

Radiated electromagnetic fields will be reflected at a conducting plane in order to satisfy the boundary conditions. In this section, we will examine this important aspect.

7.6.1 The Method of Images

Consider the point charge Q located at a distance h above a perfectly conducting ground plane shown in Fig. 7.23a. Solving for the fields generated by this charge above the ground plane is a difficult problem unless we replace the ground plane with the *image* of the charge. This image must be such that the electric field distribution in the space above the previous position of the ground plane remains unchanged. Replacing the ground plane with a negative point charge of value Q at a distance h below the ground plane will yield a field distribution above the ground plane that is identical to that before the replacement of the ground plane with the image [1]. This is intuitively clear from the sketch. The boundary condition that the electric field tangent to the ground plane be zero is also satisfied.

Next, consider a current element I parallel to and at a distance h above a perfectly conducting ground plane, as shown in Fig. 7.23b. Since current represents the flow of charge, we can visualize positive charge accumulating at the right end of the current element (in the direction of current flow) and negative charge of equal amount at the left end. This observation allows us to generate the image of the current element by analogy to static charge distributions, as shown in Fig. 7.23b: the current image is located parallel to and at a distance h below the ground plane and is directed opposite to the original current direction. Similarly, a current element vertical to the ground plane, as shown in Fig. 7.23c, is replaced with a vertical current image at the same distance below the ground plane and directed in the same direction as the original current element as the static charge analogy shows. A current that is neither horizontally nor vertically directed can be decomposed into its components as shown in Fig. 7.23d, from which the image components can be constructed as before, resulting in the total image.

7.6.2 Normal Incidence of Uniform Plane Waves on Plane, Material Boundaries

Consider the incidence of a uniform plane wave normal to the plane boundary between two media shown in Fig. 7.24. Intuitively, it is clear that a wave will be reflected at the boundary and a wave will be transmitted across the boundary. We denote the incident wave in phasor form as

$$\hat{\boldsymbol{E}}_i = \hat{E}_i e^{-\hat{\gamma}_1 z}\boldsymbol{a}_y = \hat{E}_i e^{-\alpha_1 z} e^{-j\beta_1 z}\boldsymbol{a}_y \tag{7.73a}$$

$$\hat{\boldsymbol{H}}_r = \frac{\hat{E}_i}{\hat{\eta}_1} e^{-\hat{\gamma}_1 z}\boldsymbol{a}_y = \frac{\hat{E}_i}{\eta_1} e^{-\alpha_1 z} e^{-j\beta_1 z} e^{-j\theta_{\eta 1}}\boldsymbol{a}_y \tag{7.73b}$$

where

$$\hat{\gamma}_1 = \sqrt{j\omega\mu_1(\sigma_1 + j\omega\varepsilon_1)} = \alpha_1 + j\beta_1 \tag{7.73c}$$

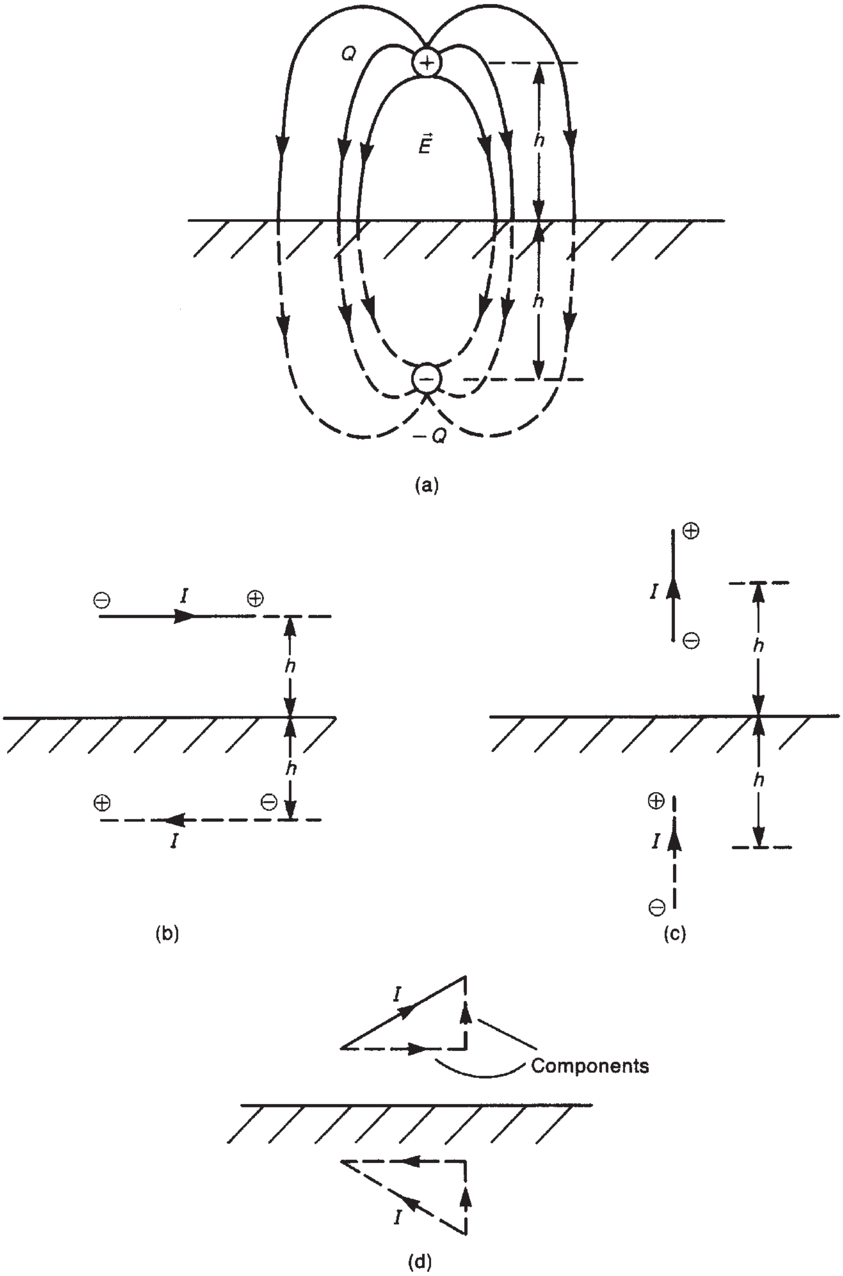

FIGURE 7.23 Illustration of the method of images for charges and currents above infinite, perfectly conducting ground planes: (a) the image of a static charge; (b) the image of a current parallel to the plane; (c) the image of a current perpendicular to the plane; (d) decomposition of a current into its horizontal and vertical components in order to determine its image.

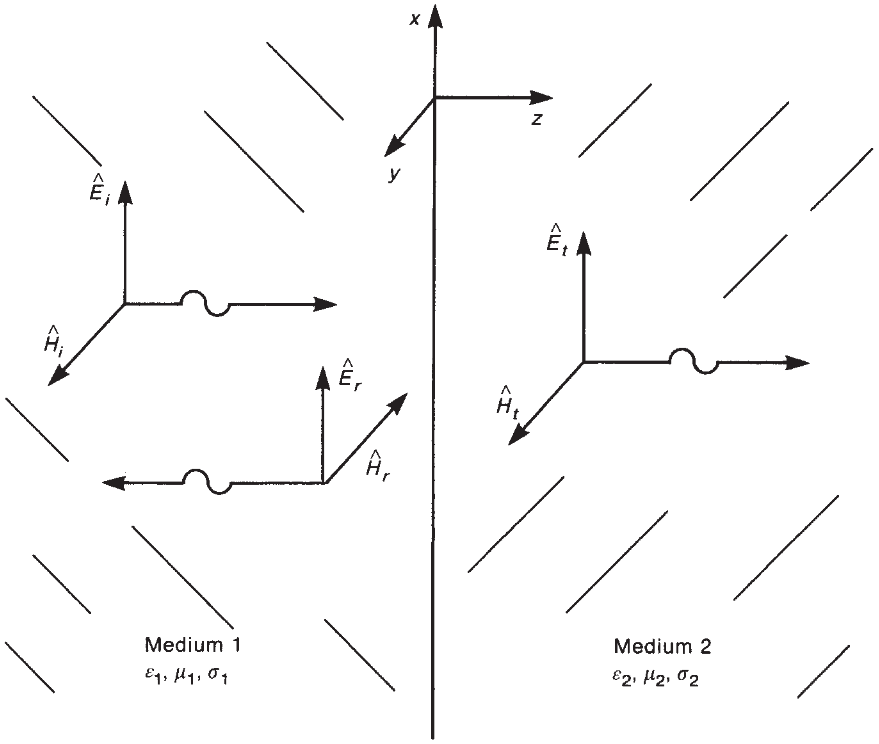

FIGURE 7.24 A uniform plane wave with incidence normal to the interface between two media.

and

$$\hat{\eta}_1 = \sqrt{\frac{j\omega\mu_1}{\sigma_1 + j\omega\varepsilon_1}} = \eta_1 \angle \theta_{\eta 1} \tag{7.73d}$$

(See Appendix B for a discussion of the form of uniform plane waves.)

The reflected wave is represented as

$$\hat{\boldsymbol{E}}_r = \hat{E}_r e^{\hat{\gamma}_1 z} \boldsymbol{a}_x = \hat{E}_r e^{\alpha_1 z} e^{j\beta_1 z} \boldsymbol{a}_x \tag{7.74a}$$

$$\hat{\boldsymbol{H}}_r = -\frac{\hat{E}_r}{\hat{\eta}_1} e^{\hat{\gamma}_1 z} \boldsymbol{a}_y = -\frac{\hat{E}_r}{\eta_1} e^{\alpha_1 z} e^{j\beta_1 z} e^{-j\theta_{\eta 1}} \boldsymbol{a}_y \tag{7.74b}$$

in accordance with the general solution developed in Appendix B. Note that the directions of the electric and magnetic field vectors are such that power flow in the reflected wave is in the negative z direction according to the Poynting vector for that wave, $\hat{\boldsymbol{S}} = \hat{\boldsymbol{E}} \times \hat{\boldsymbol{H}}$, as it must be. The wave transmitted into medium 2 is represented as

$$\hat{\boldsymbol{E}}_t = \hat{E}_t e^{-\hat{\gamma}_2 z} \boldsymbol{a}_x = \hat{E}_t e^{-\alpha_2 z} e^{-j\beta_2 z} \boldsymbol{a}_x \tag{7.75a}$$

$$\hat{\boldsymbol{H}}_t = \frac{\hat{E}_t}{\hat{\eta}_2} e^{-\hat{\gamma}_2 z} \boldsymbol{a}_y = \frac{\hat{E}_t}{\eta_2} e^{-\alpha_2 z} e^{-j\beta_2 z} e^{-j\theta_{\eta 2}} \boldsymbol{a}_y \tag{7.75b}$$

where

$$\hat{\gamma}_2 = \sqrt{j\omega\mu_2(\sigma_2 + j\omega\varepsilon_2)} = \alpha_2 + j\beta_2 \tag{7.75c}$$

and

$$\hat{\eta}_2 = \sqrt{\frac{j\omega\mu_2}{\sigma_2 + j\omega\varepsilon_2}} = \eta_2\theta_{\eta 2} \tag{7.75d}$$

At the boundary, $z = 0$, the boundary conditions require that the total electric field tangent to the boundary be continuous across the boundary. Since the electric fields are defined in the x direction, we obtain

$$\hat{\boldsymbol{E}}_i + \hat{\boldsymbol{E}}_r = \hat{\boldsymbol{E}}_t \quad \text{at} \quad z = 0 \tag{7.76a}$$

Similarly, since neither medium is a perfect conductor, the tangential components of the total magnetic field intensity vector must be continuous across the boundary, resulting in

$$\hat{\boldsymbol{H}}_i + \hat{\boldsymbol{H}}_r = \hat{\boldsymbol{H}}_t \quad \text{at } z = 0 \tag{7.76b}$$

Substituting the forms of the field vectors given above and evaluating them at $z = 0$ gives [1]

$$\hat{\Gamma} = \frac{\hat{E}_r}{\hat{E}_i} = \frac{\hat{\eta}_2 - \hat{\eta}_1}{\hat{\eta}_2 + \hat{\eta}_1} = \Gamma\angle\theta_\Gamma \tag{7.77a}$$

and

$$\hat{T} = \frac{\hat{E}_t}{\hat{E}_i} = \frac{2\hat{\eta}_2}{\hat{\eta}_2 + \hat{\eta}_1} = T\angle\theta_T \tag{7.77b}$$

It is also possible to show that $1 + \hat{\Gamma} = \hat{T}$. The quantities $\hat{\Gamma}$ and $\hat{T}$ are the *reflection* and *transmission coefficients*, respectively, of the boundary. It is a simple matter to also show that $|\hat{\Gamma}| \leq 1$. The magnitude of $\hat{T}$ may exceed unity. Note that $\hat{\Gamma}$ and $\hat{T}$ will be real only if both regions are lossless, i.e., $\sigma_1 = \sigma_2 = 0$; otherwise, $\hat{\Gamma}$ and $\hat{T}$ will in general be complex.

We now assume that the form of the incident wave is $\hat{\boldsymbol{E}} = E_m e^{-\hat{\gamma}_1 z}\boldsymbol{a}_x$, where the magnitude of the incident wave E_m is assumed known. For example, the incident wave may be produced by some distant antenna, and we know how to calculate the value of the electric field at the boundary *in the absence of the boundary* using the Friis transmission equation from the results of Section 7.5. Thus, the phasor forms of the field vectors become, in terms of the incident field magnitude,

$$\hat{\boldsymbol{E}}_i = E_m e^{-\hat{\gamma}_1 z}\boldsymbol{a}_x \tag{7.78a}$$

$$\hat{\boldsymbol{H}}_i = \frac{E_m}{\hat{\eta}_1} e^{-\hat{\gamma}_1 z}\boldsymbol{a}_y \tag{7.78b}$$

$$\hat{\boldsymbol{E}}_r = \hat{\Gamma} E_m e^{-\hat{\gamma}_1 z}\boldsymbol{a}_x \tag{7.78c}$$

$$\hat{\boldsymbol{H}}_r = -\frac{\hat{\Gamma} E_m}{\hat{\eta}_1} e^{-\hat{\gamma}_1 z}\boldsymbol{a}_y \tag{7.78d}$$

$$\hat{\boldsymbol{E}}_t = \hat{T} E_m e^{-\hat{\gamma}_2 z}\boldsymbol{a}_x \tag{7.78e}$$

$$\hat{\boldsymbol{H}}_t = \frac{\hat{T} E_m}{\hat{\eta}_2} e^{-\hat{\gamma}_2 z}\boldsymbol{a}_y \tag{7.78f}$$

Multiplying these phasor forms by $e^{j\omega t}$ and taking the real part of the result gives the time-domain forms of the field vectors:

$$\boldsymbol{E}_i = E_m e^{-\alpha_1 z} \cos(\omega t - \beta_1 z)\boldsymbol{a}_x \tag{7.79a}$$

$$\boldsymbol{H}_i = \frac{E_m}{\eta_1} e^{-\alpha_1 z} \cos(\omega t - \beta_1 z - \theta_{\eta 1})\boldsymbol{a}_y \tag{7.79b}$$

$$\boldsymbol{E}_r = \Gamma E_m e^{\alpha_1 z} \cos(\omega t + \beta_1 z + \theta_\Gamma)\boldsymbol{a}_x \tag{7.79c}$$

$$\boldsymbol{H}_r = -\frac{\Gamma E_m}{\eta_1} e^{\alpha_1 z} \cos(\omega t + \beta_1 z + \theta_\Gamma - \theta_{\eta 1})\boldsymbol{a}_y \tag{7.79d}$$

$$\boldsymbol{E}_t = T E_m e^{-\alpha_2 z} \cos(\omega t - \beta_2 z + \theta_T)\boldsymbol{a}_x \tag{7.79e}$$

$$\boldsymbol{H}_t = \frac{T E_m}{\eta_2} e^{-\alpha_2 z} \cos(\omega t - \beta_2 z + \theta_T - \theta_{\eta 2})\boldsymbol{a}_y \tag{7.79f}$$

The average power density vector of the wave transmitted into the second medium is

$$\begin{aligned}\boldsymbol{S}_{\text{av}} &= \frac{1}{2}\mathscr{R}e\,\{\hat{\boldsymbol{E}} \times \hat{\boldsymbol{H}}^*\} \\ &= \frac{1}{2}\mathscr{R}e\left\{ \hat{T} E_m e^{-\hat{\gamma}_2 z} \frac{\hat{T}^* E_m e^{-\hat{\gamma}_2^* z}}{\hat{\eta}_2^*} \right\} \boldsymbol{a}_z \\ &= \frac{1}{2}\frac{E_m^2 T^2}{\eta_2} e^{-2\alpha_2 z} \cos\,\theta_{\eta 2}\boldsymbol{a}_z \end{aligned} \tag{7.80}$$

where we denote $|\,\hat{T}\,| = T$ and $|\,\hat{\eta}_2\,| = \eta_2$. Note that this is a simple calculation in the second medium because there is only one wave in this medium.

To close this section, we consider incidence on the surface of a perfect conductor, $\sigma_2 = \infty$, from a lossless region, $\sigma_1 = 0$. The intrinsic impedance of the perfect conductor is zero, $\eta_2 = 0$, so that the reflection coefficient is $\hat{\Gamma} = -1$ (and the transmission coefficient is zero, which is a sensible result). Thus, the reflected electric field is equal but opposite to the incident electric field: $\boldsymbol{E}_r = -\boldsymbol{E}_i$. This is a sensible result because the reflected electric field must cancel the incident electric field at the boundary in order to produce zero total tangential electric field at the surface of the perfect conductor, as required by the boundary conditions. Thus, the total fields in region 1 become

$$\begin{aligned}\hat{\boldsymbol{E}}_1 &= \hat{\boldsymbol{E}}_i + \hat{\boldsymbol{E}}_r \\ &= E_m\left(e^{-j\beta_1 z} - e^{j\beta_1 z}\right)\boldsymbol{a}_x \\ &= -2jE_m\,\sin(\beta_1 z)\boldsymbol{a}_x \end{aligned} \tag{7.81a}$$

$$\begin{aligned}\hat{\boldsymbol{H}}_1 &= \hat{\boldsymbol{H}}_i + \hat{\boldsymbol{H}}_r \\ &= \frac{E_m}{\eta_1}\left(e^{-j\beta_1 z} + e^{j\beta_1 z}\right)\boldsymbol{a}_y \\ &= \frac{2E_m}{\eta_1}\cos(\beta_1 z)\boldsymbol{a}_y \end{aligned} \tag{7.81b}$$

The time-domain expressions become

$$\begin{aligned} \boldsymbol{E}_1 &= \mathscr{Re}\{\hat{\boldsymbol{E}}_1 e^{j\omega t}\} \\ &= 2E_m \sin(\beta_1 z)\sin(\omega t)\boldsymbol{a}_x && \text{(7.82a)} \\ \boldsymbol{H}_1 &= \mathscr{Re}\{\hat{\boldsymbol{H}}_1 e^{j\omega t}\} \\ &= \frac{2E_m}{\eta_1}\cos(\beta_1 z)\cos(\omega t)\boldsymbol{a}_y && \text{(7.82b)} \end{aligned}$$

These total fields represent *standing waves*. The magnitudes of the fields are

$$\begin{aligned} |\hat{E}_1| &= 2E_m |\sin(\beta_1 z)| \\ &= 2E_m \left|\sin\left(\frac{2\pi z}{\lambda_1}\right)\right| && \text{(7.83a)} \\ |\hat{H}_1| &= 2\frac{E_m}{\eta_1}|\cos(\beta_1 z)| \\ &= 2\frac{E_m}{\eta_1}\left|\cos\left(\frac{2\pi z}{\lambda_1}\right)\right| && \text{(7.83b)} \end{aligned}$$

These are plotted in Fig. 7.25. Note that the electric field achieves a maximum at distances of $\lambda_1/4, 3\lambda_1/4, \ldots$ and achieves minima (zero) at distances of $\lambda_1/2, \lambda_1, \ldots$ The magnetic field minima

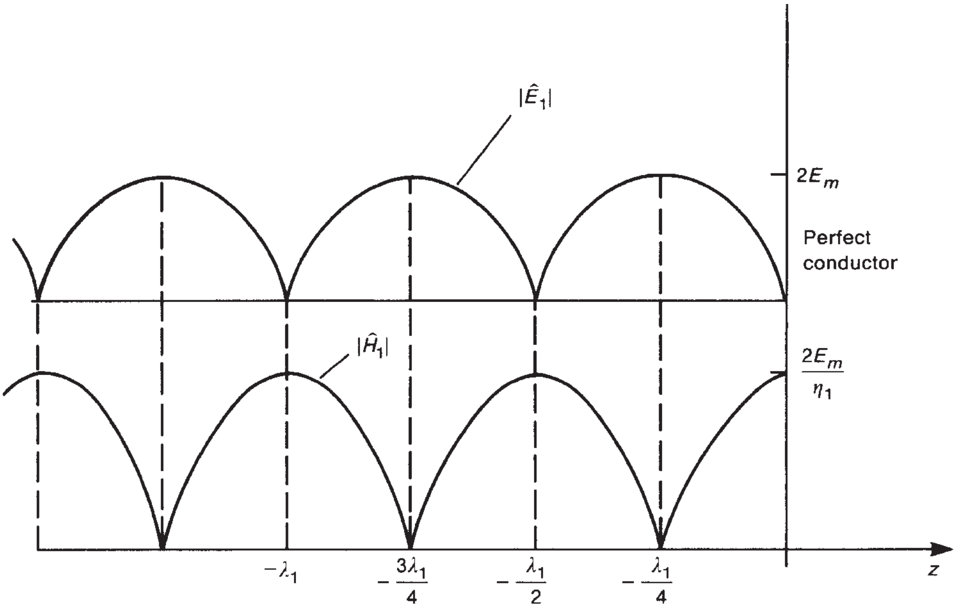

FIGURE 7.25 The total (incident plus reflected) fields for a uniform plane wave of normal incidence on a perfect conductor. The electric field goes to zero at multiples of $\lambda/2$ from the boundary, and the magnetic field goes to zero at odd multiples of $\lambda/4$ from the boundary.

and maxima are separated from the corresponding points of the electric field by $\lambda_1/4$. Also observe that corresponding points on the waveform *replicate for distances that are multiples of* $\lambda_1/2$.

Example 7.12 A 10 V/m, 1 MHz uniform plane wave is traveling in free space and strikes a large block of copper normal to its surface. Determine the power dissipated in a block of the copper having a surface area of 2 m^2 and a depth of one skin depth.

Solution: From (7.73c) and (7.73d), we compute the propagation constant and intrinsic impedance of free space ($\sigma_1 = 0$) as

$$\begin{aligned}\hat{\gamma}_1 &= \sqrt{j\omega\mu_0(j\omega\varepsilon_0)} = j\omega\sqrt{\mu_0\varepsilon_0}\\ &= j\frac{\omega}{v_0}\\ &= j2.09 \times 10^{-2}\end{aligned}$$

and

$$\begin{aligned}\hat{\eta}_1 &= \sqrt{\frac{\mu_0}{\varepsilon_0}}\\ &= 120\pi\\ &= 376.991\ \Omega \cong 377\ \Omega\end{aligned}$$

Thus,

$$\begin{aligned}\alpha_1 &= 0\\ &= 2.09 \times 10^{-2}\\ &\cong 377\ \Omega\\ \theta_{\eta 1} &= 0^\circ\end{aligned}$$

In copper, we compute the following from (7.75c) and (7.75d):

$$\begin{aligned}\hat{\gamma}_2 &= \sqrt{j\omega\mu_0(\sigma + j\omega\varepsilon_0)}\\ &= \sqrt{j2\pi \times 10^6 \times 4\pi \times 10^{-7}\left(5.8 \times 10^7 + j2\pi \times 10^6 \times \frac{1}{36\pi} \times 10^{-9}\right)}\\ &= \sqrt{4.58 \times 10^8 \angle 90^\circ}\\ &= 2.14 \times 10^4 \angle 45^\circ\\ &= 1.51 \times 10^4 + j1.51 \times 10^4\end{aligned}$$

and

$$
\begin{aligned}
\hat{\eta}_2 &= \sqrt{\frac{j\omega\mu_0}{(\sigma + j\omega\varepsilon_0)}} \\
&= \sqrt{\frac{j2\pi \times 10^6 \times 4\pi \times 10^{-7}}{(5.8 \times 10^7 + j2\pi \times 10^6 \times (1/36\pi) \times 10^{-9})}} \\
&= \sqrt{1.36 \times 10^{-7} \angle 90°} \\
&= 3.69 \times 10^{-4} \angle 45°
\end{aligned}
$$

Thus,

$$
\begin{aligned}
\alpha_2 &= 1.51 \times 10^4 \\
\beta_2 &= 1.51 \times 10^4 \\
\eta_2 &= 3.69 \times 10^{-4} \\
\theta_{\eta 2} &= 45°
\end{aligned}
$$

From (7.77b), the transmission coefficient is

$$
\begin{aligned}
\hat{T} &= \frac{2\hat{\eta}_2}{\hat{\eta}_2 + \hat{\eta}_1} \\
&= 1.96 \times 10^{-6} \angle 45°
\end{aligned}
$$

Thus, in copper the average power density is, from (7.80),

$$
S_{\text{av}} = \frac{1}{2} \frac{E_m^2 T^2}{\eta_2} e^{-2\alpha_2 z} \cos\, \theta_{\eta 2} \ \text{W/m}^2
$$

and the average power over the 2-m^2 surface is $P_{\text{av}} = S_{\text{av}} \times 2\ \text{m}^2$ so that

$$
P_{\text{av}} = 7.36 \times 10^{-7} e^{-2\alpha_2 z}
$$

The skin depth is

$$
\begin{aligned}
\delta &= \frac{1}{\sqrt{\pi f \mu_0 \sigma}} \\
&= 66.1\ \mu\text{m}
\end{aligned}
$$

The power dissipated is

$$\begin{aligned} P_{\text{dissipated}} &= P_{\text{in}} - P_{\text{out}} \\ &= 7.36 \times 10^{-7}(1 - e^{-2}) \\ &= 0.637\ \mu\text{W} \end{aligned}$$

Review Exercise 7.6 A 100 V/m, 1 MHz uniform plane wave is traveling in free space and strikes the ocean surface normal to its surface. Determine the power dissipated in a block of that seawater ($\sigma = 4$ s/m, $\varepsilon_r = 1$, $\mu_r = 1$) having a surface area of 10 m^2 and a depth of one skin depth.

***Answer*:** 1.2 W.

7.6.3 Multipath Effects

Radiated fields may travel to the receiving antenna via many different paths. Depending on the electrical length of these paths, the signals may arrive at the receiving antenna in phase, out of phase, or with some gradation in between. The total signal at the receiving antenna will be the phasor/vector sum of all the waves incident on the antenna. Because the electrical lengths of the various paths may be significant, the signals may add constructively or destructively, as with the case of antenna arrays discussed in Section 7.3. Consider the case of a transmitting antenna and a receiving antenna situated above a perfectly conducting ground plane, as illustrated in Fig. 7.26. The received signal at the measurement antenna is a contribution of two signals: a *direct wave* that travels a line-of-sight path between the product emission point and the measurement antenna and a *reflected wave* that is reflected at the ground plane. In the case of measurement of radiated emissions from a product for verification of compliance to the regulatory limits, the test setup is also situated above a ground plane so that the received emission will be the combination of a direct and a reflected wave (see Chapter 2). We will now investigate this phenomenon quantitatively.

Suppose that the electric field intensity *patterns* of the transmitting and receiving antennas are described by $E_T(\theta_T, \phi_T)$ and $E_R(\theta_R, \phi_R)$, respectively. The antennas are at heights h_T and h_R and are separated at a horizontal distance D. The angle of incidence of the reflected wave at the ground plane ψ and the angle of reflection of the reflected wave can be shown to be equal [1]. This is referred to as *Snell's law*. The length of the direct wave path is

$$d = \sqrt{D^2 + (h_R - h_T)^2} \tag{7.84}$$

The reflected wave can be thought of as being due to the image of the transmitting antenna, as shown in Fig. 7.26. Replacing the perfectly conducting ground plane with the image of the transmitting antenna shows that the length of the reflected wave path is

$$d_r = \sqrt{D^2 + (h_R + h_T)^2} \tag{7.85}$$

The received voltage at the base of the receiving antenna and due to the direct wave is proportional to

$$\hat{V}_d = \hat{V}_0 E_T(\theta_{Td}, \phi_{Td}) E_R(\theta_{Rd}, \phi_{Rd}) \frac{e^{-j\beta_0 d}}{d} \tag{7.86}$$

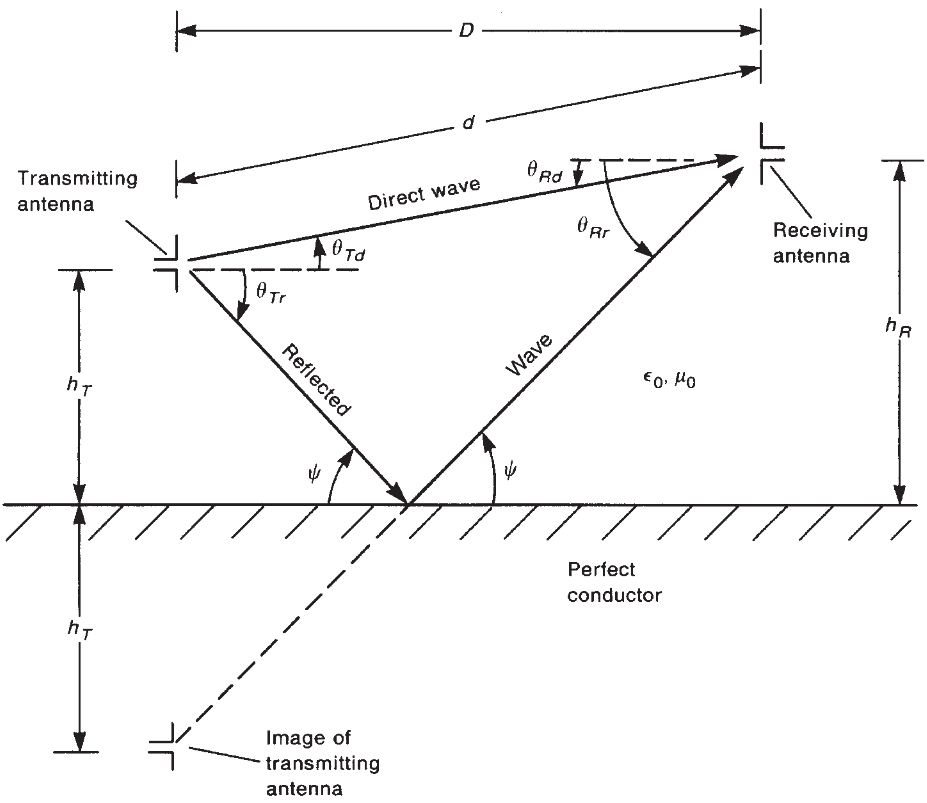
D
d
Transmitting antenna
Direct wave
θ_{Rd}
θ_{Rr}
Receiving antenna
θ_{Td}
θ_{Tr}
h_T
h_R
Reflected
Wave
ϵ_0, μ_0
ψ
ψ
Perfect conductor
h_T
Image of transmitting antenna

FIGURE 7.26 Illustration of the problem of communication between two antennas above a ground plane. The received field is the sum of the contributions due to the direct and the reflected waves.

We have assumed that the antennas are in the far fields of each other so that the electric field at the receiving antenna resembles, locally, a uniform plane wave. This gives the $1/d$ and $e^{-j\beta_0 d}$ dependence. The reflected wave will be the transmitted wave (in the direction θ_{Tr}, ϕ_{Tr}) that is multiplied by the reflection coefficient at the point of reflection, $\hat{\Gamma}$. The form of the received voltage at the base of the receiving antenna is

$$\hat{V}_r = \hat{V}_0 E_T(\theta_{Tr}, \phi_{Tr}) E_R(\theta_{Rr}, \phi_{Rr}) \hat{\Gamma} \frac{e^{-j\beta_0 d_r}}{d_r} \tag{7.87}$$

The total received voltage is the sum of (7.86) and (7.87):

$$\begin{aligned} \hat{V} &= \hat{V}_d + \hat{V}_r \\ &= \hat{V}_0 E_T(\theta_{Td}, \phi_{Td}) E_R(\theta_{Rd}, \phi_{Rd}) \frac{e^{-j\beta_0 d}}{d} \\ &\quad + \hat{V}_0 E_T(\theta_{Tr}, \phi_{Tr}) E_R(\theta_{Rr}, \phi_{Rr}) \hat{\Gamma} \frac{e^{-j\beta_0 d}}{d} \\ &= \hat{V}_0 E_T(\theta_{Td}, \phi_{Td}) E_R(\theta_{Rd}, \phi_{Rd}) \frac{e^{-j\beta_0 d}}{d} \hat{F} \end{aligned} \tag{7.88a}$$

where

$$\hat{F} = 1 + \frac{E_T(\theta_{Tr}, \phi_{Tr})E_R(\theta_{Rr}, \phi_{Rr})}{E_T(\theta_{Td}, \phi_{Td})E_R(\theta_{Rd}, \phi_{Rd})}\hat{\Gamma}\frac{d}{d_r}e^{-j\beta_0(d_r-d)} \tag{7.88b}$$

Thus, the ground reflection modifies the free-space direct wave propagation (the coupling without the ground plane present) by the multiplicative factor $\hat{F}$. Consequently, the Friis transmission equation can be modified to account for the ground reflection by multiplying it by the square of the magnitude of $\hat{F}$ (since the Friis transmission equation involves power).

Let us now consider the reflection coefficient $\hat{\Gamma}$. Two cases arise: *parallel polarization* and *perpendicular polarization*. These cases correspond to the two required measurement antenna polarizations in compliance measurements: *vertical* and *horizontal*. The case of perpendicular (horizontal) polarization is shown in Fig. 7.27a. The term "perpendicular" refers to the fact that the incident electric field is perpendicular to the *plane of incidence*. The plane of incidence contains the propagation vector of the wave and the normal to the surface. The incident and reflected electric field vectors are parallel to the ground plane for this polarization. The reflection coefficient at the ground plane becomes [1]

$$\begin{aligned}\hat{\Gamma}_H &= \frac{\hat{E}_r}{\hat{E}_i} \\ &= -1\end{aligned} \tag{7.89a}$$

where we have used the H subscript to indicate horizontal polarization of the antennas. This result is intuitively obvious if we recall the boundary condition that the total tangential electric field at the surface of a perfect conductor must be zero. The electric fields of the incident and reflected fields are both tangent to the conductor. Thus, the reflected electric field must be opposite to that of the incident wave.

In the case of parallel polarization shown in Fig. 7.27b, the electric field vectors are parallel to the plane of incidence. This corresponds to the case of vertical antenna orientations. The reflection coefficient for this polarization is [1]

$$\begin{aligned}\hat{\Gamma}_V &= \frac{\hat{E}_r}{\hat{E}_i} \\ &= -1\end{aligned} \tag{7.89a}$$

where the V subscript refers to the vertical polarization of the antennas. Again, this result is intuitively obvious if we consider the boundary condition that the total tangential electric field at the surface of a product conductor must be zero. In this case, the tangential components are the z components, which must be equal and opposite at the surface. Therefore, the incident and reflected electric fields must remain unchanged with respect to their propagation vectors, as shown in Fig. 7.27b.

As a practical example, let us compute the ground-plane reflection factor for a current element (a Hertzian dipole) and a linear receiving antenna such as a dipole for a typical FCC Class B measurement. The separation between the current element and the receiving antenna is 3 m. The current element (the product) is placed at a height of 1 m above the ground plane. We will consider the current element and the measurement antenna to be oriented parallel to each other, and the height of the measurement antenna above the ground plane must be scanned from 1 to 4 m. First, consider the case of *horizontal polarization* shown in Fig. 7.28a. The factor in (7.88b) becomes

$$\hat{F}_H = 1 - \frac{d}{d_r}e^{-j(2\pi/\lambda_0)(d_r-d)}$$

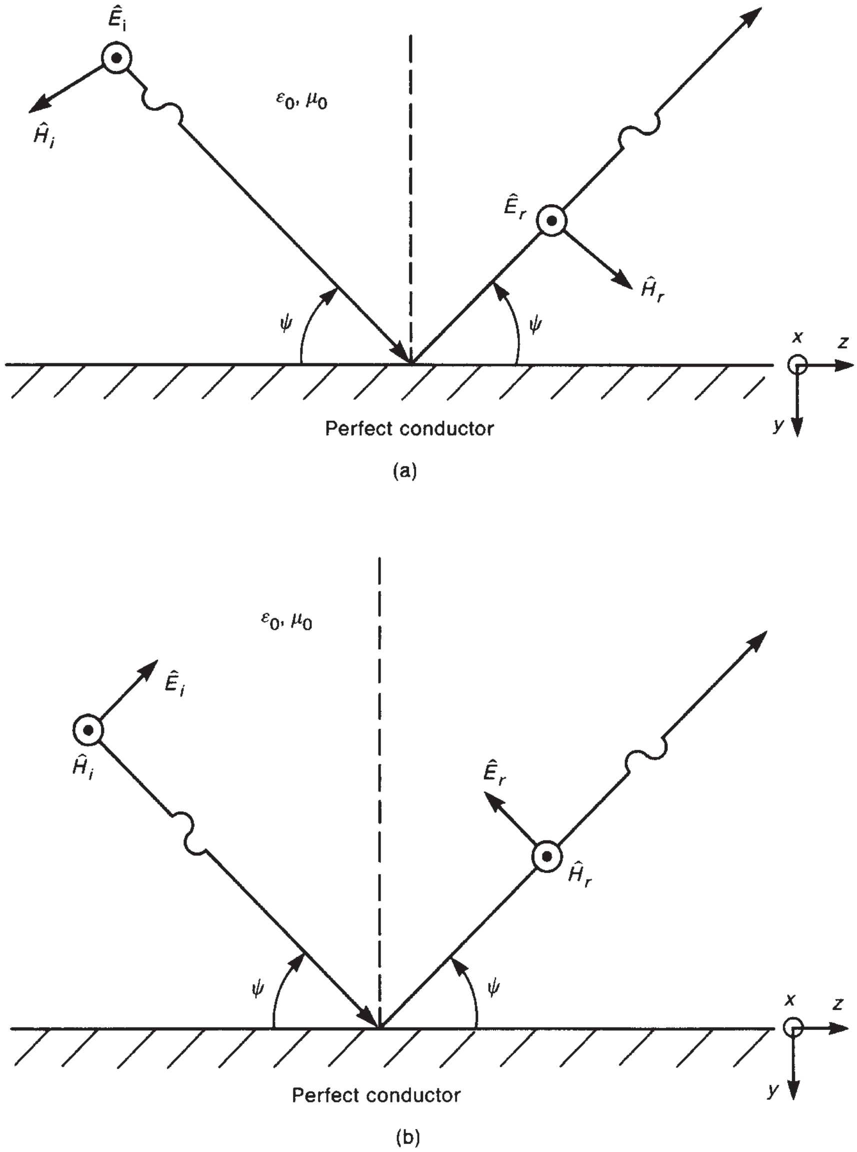
$\hat{E}_i$
$\hat{H}_i$
ε_0, μ_0
$\hat{E}_r$
$\hat{H}_r$
ψ
ψ
x
z
y
Perfect conductor
(a)
ε_0, μ_0
$\hat{E}_i$
$\hat{H}_i$
$\hat{E}_r$
$\hat{H}_r$
ψ
ψ
x
z
y
Perfect conductor
(b)

FIGURE 7.27 Illustration of the determination of the reflection coefficients for a uniform plane wave with oblique incidence on a perfect conductor for (a) perpendicular (horizontal) polarization and (b) parallel (vertical) polarization of the incident wave.

where we have substituted $\beta_0 = 2\pi/\lambda_0$. The reflection coefficient is $\hat{\Gamma}_H = -1$ for this case, and the pattern is omnidirectional in a plane perpendicular to the current element and the horizontally positioned measurement antenna. Thus, the electric field patterns in (7.88b) are unity. The minimum scan height of the measurement antenna of 1 m gives $d = 3$ m ($h_r = 1$ m) and $d_r = \sqrt{13}$ m. The maximum scan height of 4 m gives $d = \sqrt{18}$ m and $d_r = \sqrt{34}$ m. Thus, the factor is

$$\hat{F}_{1\,\mathrm{m}} = 1 - 3\sqrt{\frac{1}{13}}e^{-j(2\pi/\lambda_0)(\sqrt{13}-3)}$$

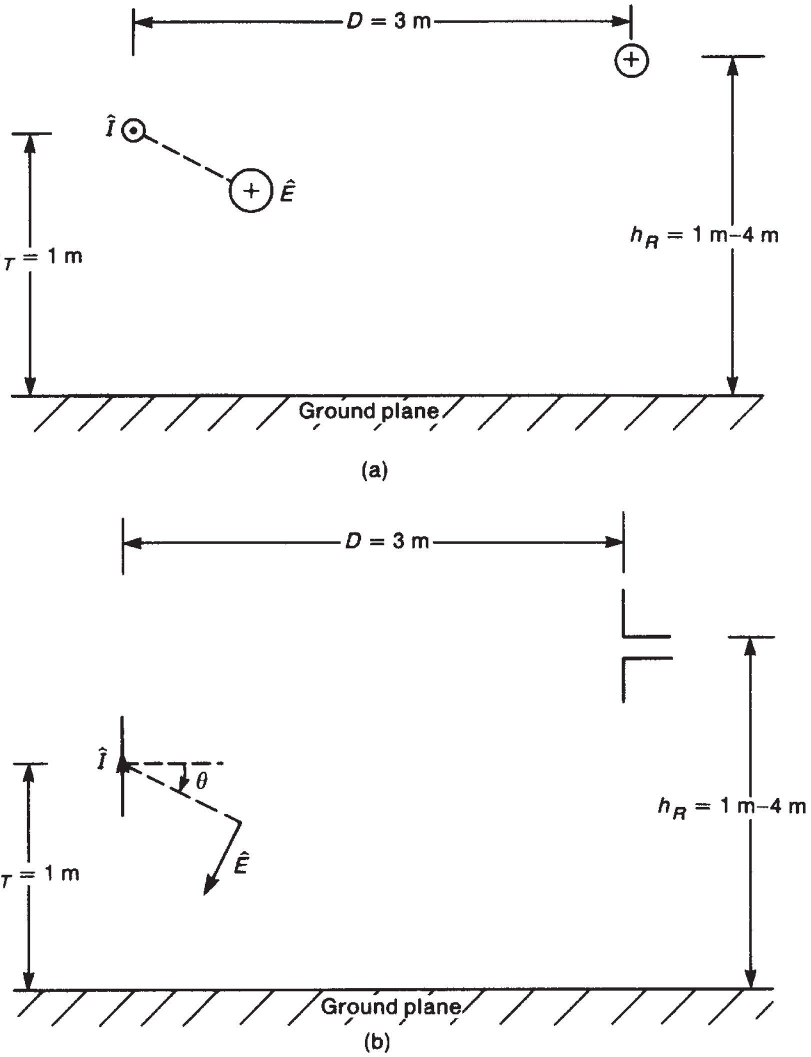

FIGURE 7.28 Determination of the reflected wave correction factor for the FCC Class B radiated emission test: (a) horizontal polarization; (b) vertical polarization.

and

$$\hat{F}_{4\text{ m}} = 1 - \sqrt{\frac{18}{34}} e^{-j(2\pi/\lambda_0)(\sqrt{34}-\sqrt{18})}$$

The factor for *vertical polarization* requires that we consider the pattern for the antenna. Recall that the pattern (for dipole-type antennas) is a maximum broadside to the antenna and is zero off the ends of the antenna. The pattern varies as *cosine* of the various angles in Fig. 7.26: θ_{Tr}, θ_{Td}, θ_{Rr}, and θ_{Rd} as illustrated in Fig. 7.28.

Thus, the factor becomes

$$\hat{F}_V = 1 + \frac{\cos\,\theta_{Tr}\,\cos\,\theta_{Rr}}{\cos\,\theta_{Td}\,\cos\,\theta_{Rd}} \hat{\Gamma}_V \frac{d}{d_r} e^{-j(2\pi/\lambda_0)(d_r-d)}$$

The various cosines are

$$\cos\,\theta_{Tr} = \frac{D}{d_r}$$

$$\cos\,\theta_{Rr} = \frac{D}{d_r}$$

$$\cos\,\theta_{Td} = \frac{D}{d}$$

$$\cos\,\theta_{Rd} = \frac{D}{d}$$

Substituting these along with $\hat{\Gamma}_V = +1$ gives

$$\hat{F}_V = 1 + \left(\frac{d}{d_r}\right)^3 e^{-j(2\pi/\lambda_0)(d_r - d)}$$

7.7 BROADBAND MEASUREMENT ANTENNAS

As has been pointed out, the FCC prefers the use of tuned, half-wave dipoles for measurement of radiated emissions. From the standpoint of rapid and efficient gathering of data over the frequency range of the radiated emission limits of 30 MHz to >1 GHz, the tuned half-wave dipole is not an attractive measurement antenna. Its length must be physically adjusted to provide a total length of $\lambda_0/2$ at each measurement frequency. Also, in the measurement of the vertically polarized emissions at the lowest frequency of the limit, 30 MHz, the dipole length is 5 m or approximately 15 ft. Thus the antenna cannot be scanned from 1 to 4 m at these lower frequencies in the vertical polarization mode.

A more practical measurement technique is the use of *broadband measurement antennas* such as the *biconical* and *log-periodic* antennas. A broadband antenna is an antenna that has the following two characteristics over the band of frequencies of its intended use:

1. The input impedance is fairly constant over the frequency band.
2. The pattern is fairly constant over the frequency band.

In the measurement of radiated emissions for compliance verification, the biconical antenna is typically used in the frequency range of 30–200 MHz, whereas the log-periodic antenna is typically used in the remainder of the band from 200 MHz to 1 GHz. For measurements above 1 GHz, horn antennas are typically used [4–6]. In this section, we will characterize these broadband measurement antennas.

7.7.1 The Biconical Antenna

The *infinite* biconical antenna is constructed of two cones of half angle θ_h with a small gap at the feedpoint, as shown in Fig. 7.29. A voltage source feeds the antenna at this gap. A spherical coordinate system is again appropriate to use for the analysis here. In the space surrounding the cones (assumed free space), $\hat{\boldsymbol{J}} = 0$, and symmetry suggests that the fields are $\hat{\boldsymbol{H}} = \hat{H}_\phi \boldsymbol{a}_\phi$ and $\hat{\boldsymbol{E}} = \hat{E}_\theta \boldsymbol{a}_\theta$. Faraday's and Ampere's laws can be solved to give the forms of the fields as [3–6]

$$\hat{H}_\phi = \frac{H_0}{\sin\,\theta}\frac{e^{-j\beta_0 r}}{r} \tag{7.90}$$

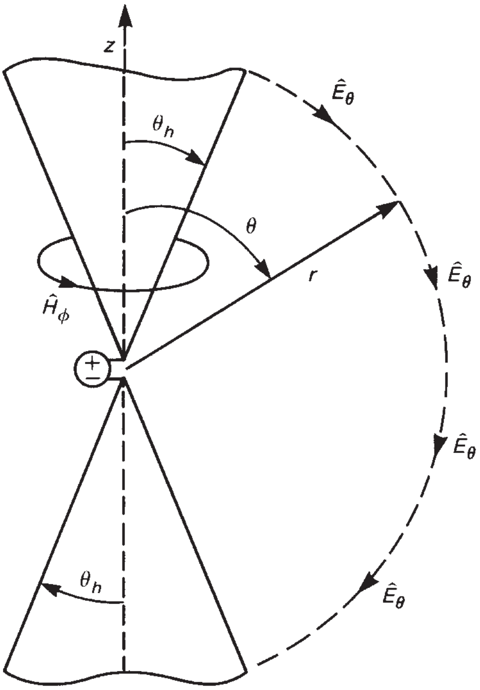

FIGURE 7.29 The infinite biconical antenna.

and

$$\begin{aligned}\hat{E}_\theta &= \frac{\beta_0}{\omega\varepsilon_0}\frac{H_0}{\sin\theta}\frac{e^{-j\beta_0 r}}{r}\\ &= \eta_0\hat{H}_\phi\end{aligned}\tag{7.91}$$

where H_0 is a constant.

Note that the radiated fields are of the *transverse electromagnetic* (TEM) *mode* type in that the electric field and the magnetic field are orthogonal and transverse to the direction of propagation, the r direction, as shown by the presence of the $e^{-j\beta_0 r}$ term. Therefore, we may uniquely define voltage between two points on the cones as was the case for transmission lines. The voltage produced between two points on the two cones that are at a distance r from the feedpoint is

$$\begin{aligned}\hat{V}(r) &= -\int_{\theta=\pi-\theta_h}^{\theta_h} \hat{\boldsymbol{E}}\cdot d\boldsymbol{l}\\ &= 2\eta_0 H_0 e^{-j\beta_0 r}\ln\left(\cot\frac{\theta_h}{2}\right)\end{aligned}\tag{7.92}$$

The current on the surface of the cones is found by using Ampere's law in integral form:

$$\begin{aligned}\hat{I}(r) &= \int_{\phi=0}^{2\pi} \hat{H}_\phi r\sin\theta d\phi\\ &= 2\pi H_0 e^{-j\beta_0 r}\end{aligned}\tag{7.93}$$

The input impedance at the feed terminals can be obtained as the ratio of the voltage and current for $r = 0$

$$\begin{aligned}\hat{Z}_{\text{in}} &= \left.\frac{\hat{V}(r)}{\hat{I}(r)}\right|_{r=0} \\ &= \frac{\eta_0}{\pi} \ln\left(\cot\frac{\theta_h}{2}\right) \\ &= 120 \ln\left(\cot\frac{\theta_h}{2}\right)\end{aligned} \tag{7.94}$$

which is purely resistive. Usually, the cone half angle is chosen to provide a match to the feedline characteristic resistance Z_C. A balun is also normally included at the antenna input. The radiation resistance R_{rad} can be shown to also be equal to $\hat{Z}_{\text{in}}$ given in (7.94), which is a sensible result. To do this, we compute the total radiated average power as

$$\begin{aligned}P_{\text{rad}} &= \oint_S \boldsymbol{S}_{\text{av}} \cdot d\boldsymbol{s} \\ &= \int_{\phi=0}^{2\pi} \int_{\theta=\theta_h}^{\pi-\theta_h} \frac{|\hat{E}_\theta|^2}{2\eta_0} r^2 \sin\theta \, d\theta \, d\phi \\ &= \pi\eta_0 H_0^2 \int_{\theta=0}^{\theta_h} \frac{d\theta}{\sin\theta} \\ &= 2\pi\eta_0 H_0^2 \ln\left(\cot\frac{\theta_h}{2}\right)\end{aligned} \tag{7.95}$$

The radiation resistance is defined by

$$P_{\text{rad}} = \frac{|\hat{I}(0)|^2}{2} R_{\text{rad}} \tag{7.96}$$

Substituting (7.93) evaluated at $r = 0$ into (7.96) shows that

$$R_{\text{rad}} = \hat{Z}_{\text{in}} \tag{7.97}$$

Observe that the radiated fields are spherical waves with $\boldsymbol{E}$ in the θ direction and $\boldsymbol{H}$ in the ϕ direction. For linearly polarized waves incident on the antenna from the broadside direction, $\theta = 90°$, the antenna responds to the component that is parallel to its axis. Thus, this antenna can be used to perform vertical and horizontal field measurements for regulatory compliance verification. Also, observe that the input impedance and pattern are, theoretically, constant over an infinite range of frequencies. Unfortunately, infinite-length cones are obviously not practical, so that practical biconical antennas are constructed of *truncated cones*. Finite-length cones cause discontinuities at the ends, which result in reflections as the waves travel outward along the cones. This produces standing waves on the cones that result in the input impedance having an imaginary part rather than being purely real and independent of frequency. References 3–5 show variations in the input impedance for various cone lengths and half angles. Another practical method of construction for biconicals is

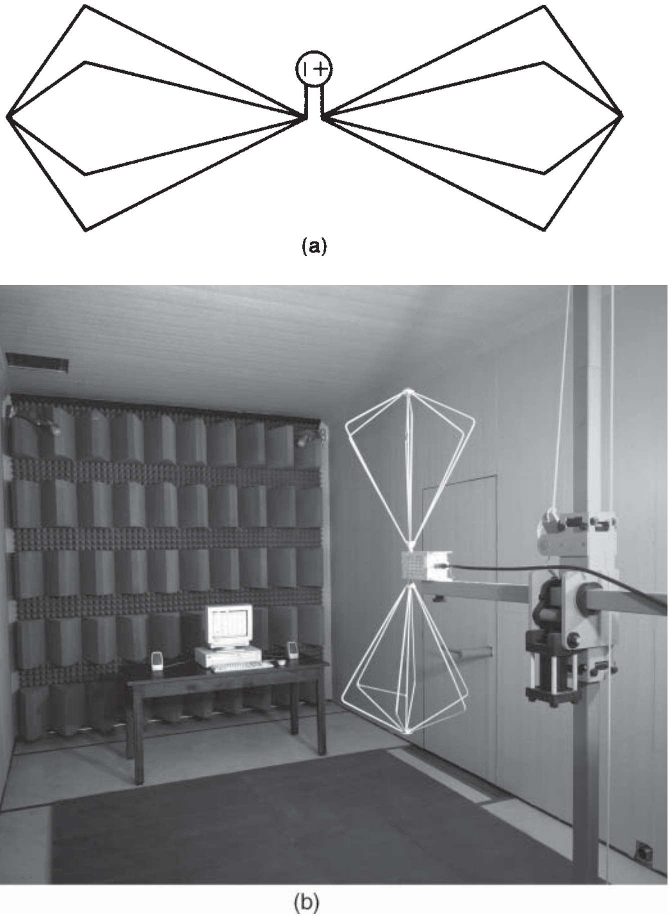

FIGURE 7.30 (a) The truncated biconical antenna composed of wire elements; (b) a photograph of a biconical antenna used in compliance testing. Source: Courtesy of ETS-Lindgren, Inc.

to use wires to approximate the cone surfaces, as illustrated in Fig. 7.30. A photograph of a biconical antenna used in the frequency range of 30–200 MHz is shown in Fig. 7.30b. Other variations are the *discone* antenna shown in Fig. 7.31a consisting of one cone (truncated) above a circular ground plane. This provides a convenient balanced feed with a coaxial cable. The method of images shows that the fields of the discone antenna above the ground plane are the same as those of the biconical antenna. Also, the radiation resistance is one-half that of the biconical, since only one-half of the biconical radiated power is radiated by the discone antenna. Another version is the “bowtie” antenna shown in Fig. 7.31b. This consists of flat, triangular plates, which can be constructed of metal sheets or by using a wire to outline the area of each plate in order to reduce weight and wind loading. The bowtie antenna is frequently used for reception of UHF television signals. Use of wires to outline the triangular sheet reduces the bandwidth over solid metal triangles or cones.

Review Exercise 7.7 Determine the required half-angle of an infinite biconical antenna to give an input impedance of 50 Ω.

***Answer*:** $\theta_h = 66.8^\circ$.

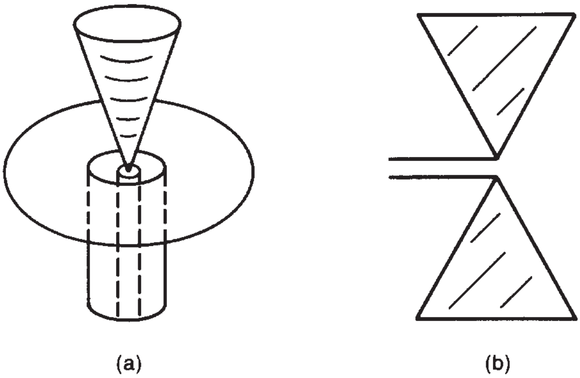

FIGURE 7.31 Other implementations of truncated biconical antennas: (a) the discone antenna; (b) the bow tie antenna.

7.7.2 The Log-Periodic Antenna

The log-periodic antenna is a member of a general class of frequency-independent antennas that rely on repetitive dimensions of their structures. The structural dimensions increase in proportion to the distance from the origin of the structure. This results in the input impedance and radiation properties repeating periodically as the logarithm of frequency. Thus, they are said to be broadband antennas.

The most common form of log-periodic antenna used for the measurement of radiated emissions from 200 MHz to 1 GHz is the *log-periodic dipole array* shown in Fig. 7.32a. This antenna shares the properties of all other log-periodic structures in that the element distances, lengths, and separations are related by a constant such as

$$\tau = \frac{l_n}{l_{n+1}} = \frac{R_n}{R_{n+1}} \tag{7.98}$$

There are two ways of feeding the elements, one of which does not work well. If all the elements are connected in parallel and the antenna fed at the apex as shown in Fig. 7.32b, the currents in the adjacent elements are in the same direction. This can be viewed as dipole array using the techniques of Section 7.3. The elements will be spaced closely in terms of wavelengths so that currents in adjacent elements will interact. Because the current progression is to the right, the pattern will be a beam directed to the right. However, elements to the right will interfere with the radiation from elements to the left, causing interference effects. If the currents to the adjacent elements are reversed in phase by crisscrossing the feed wires as shown inFig. 7.32c, the beam will be directed to the left and negligible interference will be caused by the shorter elements, whose currents have alternate phasing. A practical method of feeding the log-periodic antenna with a coaxial cable and at the same time producing the 180° phase shift between adjacent elements as well as *balanced* operation is illustrated in Fig. 7.33. A coaxial cable is passed through a hollow pipe to which half of the set of elements are attached. The coaxial cable shield is attached to this pipe at point A, whereas its center conductor is connected to the other pipe at the same point, B. This provides the ability to feed the antenna from its rear so that the feedline does not interfere with the pattern and at the same time produces the 180° phase shift between adjacent elements. A photograph of a log-periodic antenna for use in the frequency range of 200 MHz to 1 GHz is shown in Fig. 7.34.

The cutoff frequencies of the log-periodic dipole array (its bandwidth) can be approximately computed by determining the frequency where the shortest elements are one-half wavelength (the highest frequency of operation) and the frequency where the longest elements are one-half wavelength (the

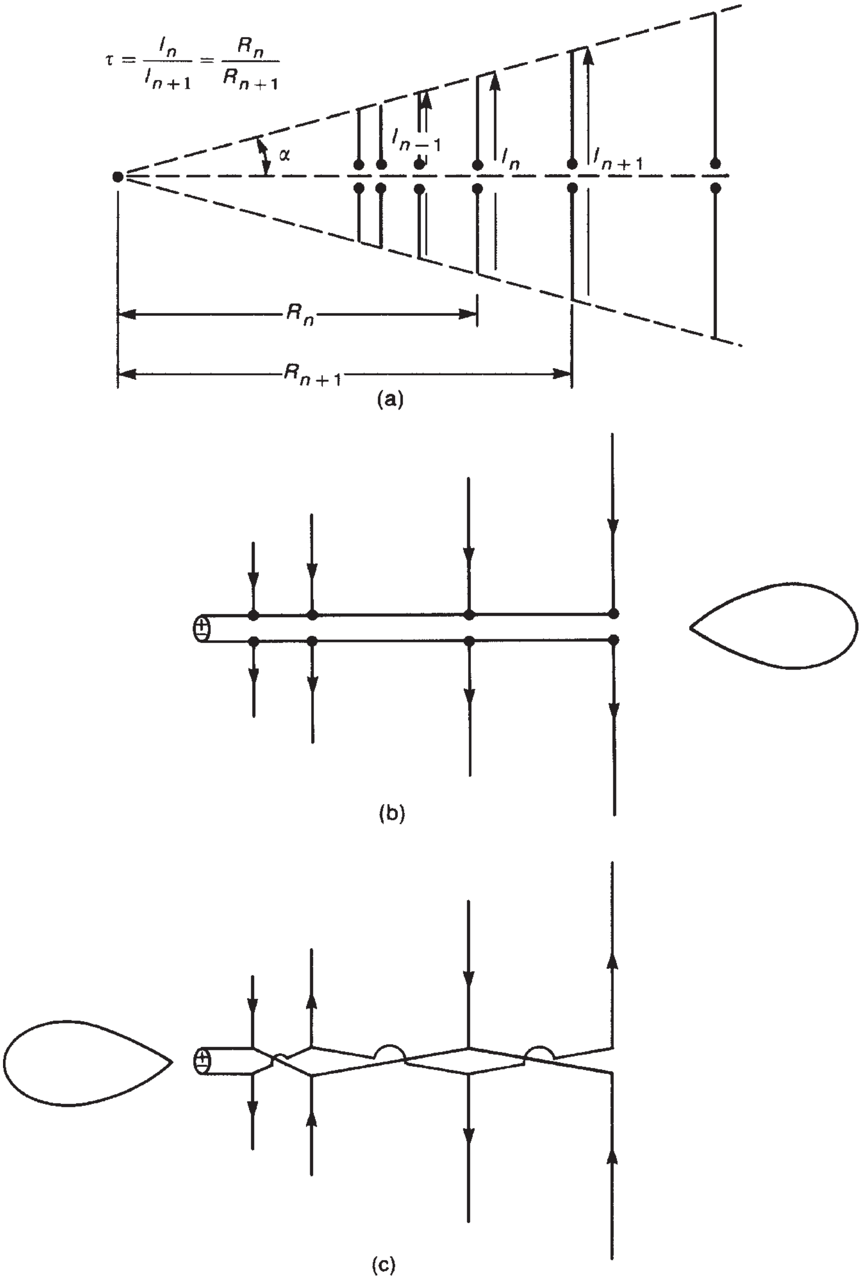

FIGURE 7.32 Log-periodic antennas: (a) periodicity of the structure; (b) nonpreferred excitation method; (c) preferred excitation method.

lowest frequency of operation). For a particular operating frequency, only a few elements will be active, which will be in the vicinity of where the elements are approximately one-half wavelength. So, the active region dynamically adjusts to using the elements that are efficient radiators at the operating frequency. As is somewhat obvious, a linearly polarized uniform plane wave incident along the antenna axis will produce the maximum response when its electric field vector is oriented parallel to

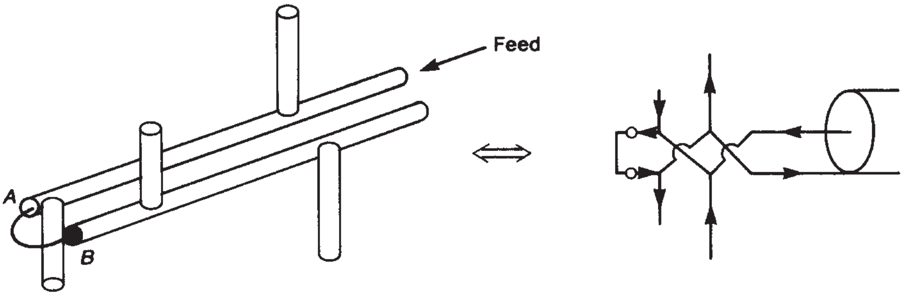

FIGURE 7.33 Practical feed of a log-periodic antenna.

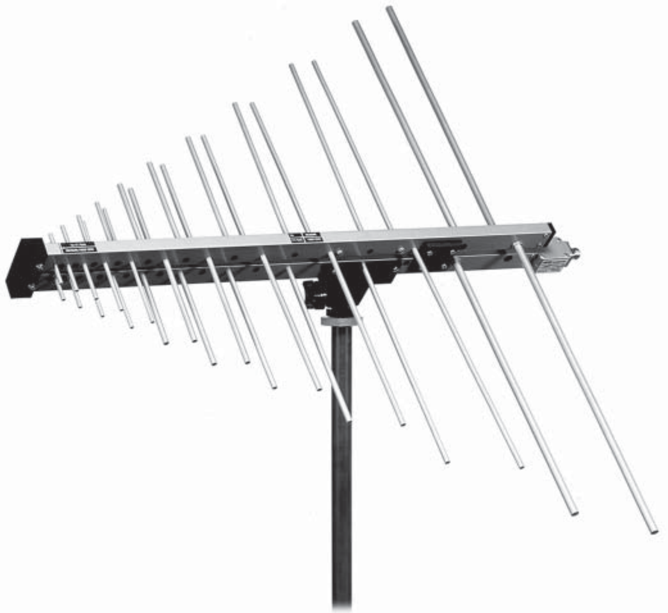

FIGURE 7.34 A photograph of a log-periodic antenna used in compliance testing. Source: Courtesy of ETS-Lindgren, Inc.

the elements of the array. Thus, the antenna can be used to measure vertical and horizontal radiated emissions in the verification of regulatory compliance.

The input impedance to the log-periodic dipole array tends to be resistive, frequency-independent, and between 50 Ω and 100 Ω. A direct analysis is more difficult than for the ideal biconical antenna. Consequently, various design equations are usually employed. For a discussion of these, see [4, 5]. The VSWR can be kept to below 2.0 over the typical frequency range of its use in radiated emission measurements: 200 MHz to 1 GHz.

Review Exercise 7.8 A log-periodic antenna is to be used from 500 MHz to 10 GHz. Determine the lengths of the shortest and longest elements.

***Answers*:** 30 cm and 1.5 cm.

7.8 ANTENNA MODELING AND SIMULATION

After James Clerk Maxwell published his paper “A Dynamical Theory of the Electromagnetic Field” in 1865, the science and discipline associated with the study and application of electromagnetic field theory was fully formed and yet only beginning its infancy. Almost immediately, researchers and experimenters began exploring the science of electromagnetic radiation and its application. In 1887, Heinrich Hertz definitively demonstrated that there could be the transmission and reception of electromagnetic waves, and as a result, “wireless” communication was born. Over the ensuing decades, much work was performed to understand the physical interface between the wireless systems and free space, which is the antenna.

The most perplexing difficulty associated with the analysis and design of antennas was the determination of the current distribution on the structure of the antenna under study. Methods were developed to find the antenna’s impedance without solving for the current distribution, while others were developed to find BOTH the impedance and the current distribution. All these methods encountered similar difficulties, among them the fact not all antennas are made in the same shapes and using the same materials, and the mathematics were challenging.

From the 1880s through approximately 1970, antenna analysis relied on the use of slide rules, nomographs based on empirical data, and laboratory and field experimentation and test. Analytical tools included the use of Pocklington’s and Hallen’s integral equations. Geometries successfully studied and replicated tended to be simple, made of conductors, exhibited similar impedances, and were relatively well understood as to their effects in the far field.

The fundamental physics and relevant mathematics of “intentional” antennas are thus well known and understood, as a brief review of the history discussed previously shows. All the foregoing methods focus ultimately on one key point that is key to an antenna’s performance: the geometry of the conductors that form the structure of the antenna is responsible for the creation of the boundary conditions that either control the electrical current flow responsible for the radiation of energy or the conversion of received energy into electrical current. This is also true of conductors (or even conductive assemblies) that create “unintentional” antennas. While the experienced antenna engineer and the EMC engineer have their background and knowledge in knowing what aspects of antennas create different boundary conditions, those without that background are forced to experience “trial and error” in either the design of intentional antennas or the mitigation of antenna effects in unintentional antennas. Thanks to the efforts of the many researchers who worked tirelessly from Maxwell to the present time, modern computer codes make it possible to analyze antennas and conductive assemblies using the mathematics of electromagnetic fields.

7.8.1 Why Model Antennas?

There are many reasons to model antennas using computational tools. While antennas have deterministic properties, EMC issues are many times nondeterministic. Today’s numerical computational capabilities provide the EMC engineer with insight into antennas and antenna effects responsible for product or system unintentional radiated emissions as compared to EMC requirements or legislated limits, or for unintentional coupling of radiated energy encountered when confronted with susceptibility or immunity considerations. Antenna modeling and simulation computer codes are powerful tools that can be used to address EMC issues. These tools were not widely available only a handful of years ago.

7.8.2 Modeling Methods

To understand how antenna modeling and simulation can be used to solve EMC issues, it is useful to look at the types of modeling that are most common today, along with their advantages and disadvantages.

The common approaches to antenna modeling today are those that are based upon “full wave methods,” which model the exact electromagnetic behavior of the antenna and are based on Maxwell’s equations.

The first of these full-wave methods in use today is known as the “method of moments (MoM),” which utilizes integral equations that describe known incident fields and unknown induced currents. A key aspect is the boundary conditions result from the antenna geometry.

The second of these full-wave methods is the “finite element method” (FEM), which uses the differential form of Maxwell’s equations to determine the solutions. The process consists of utilizing the basic wave equations associated with the electric and magnetic current densities to determine the electric and magnetic fields.

A third method is essentially a combination of the first two and is known as the “hybrid method,” which incorporates aspects of both MoM and FEM. This has the advantage of using each method’s strengths to efficiently determine the solutions.

After about 1960, computer codes based on the MoMs became more widely available, including codes such as AMMP (Antenna Mathematical Modeling Program), TWTD (Thin Wire Time Domain), WAMP (Wire Antenna Modeling Program), and NEC (Numerical Electromagnetic Code).

Many other approaches and codes have been developed since then and those have enabled computational electromagnetics (CEM) to be used for, among other applications, antenna modeling. These methods include the FEM, the finite-difference time-domain (FDTD) method, geometric, physical, and uniform theories of diffraction (GTD, PTD, and UTD) methods, the multiradius bridge-current (MBC) method, and various commercial code packages such as EMA3D, FEKO, WIPL-D, and HOBBIES that combine and/or modify the combination of the various tools that preceded them.

Several versions of an antenna modeling tool known as the “Numerical Electromagnetics Code (NEC)” that was originally written in FORTRAN in the 1970s now exist in the public domain. These public domain packages run on commonly available personal computers, and several are available at no cost.

7.8.3 Summary

No matter which antenna modeling tool is used, the general process is to identify the frequency range of the candidate antenna design, and the necessary design parameters, including gain characteristics, reflection coefficient (or VSWR), and associated antenna factor(s), all as a function of frequency. With this information in hand, computational electromagnetics (CEM) techniques as described previously can be used to provide numerical solutions of Maxwell’s equations and confirmation of the desired antenna design features. Given the high-performance capabilities prevalent today in personal computers and engineering workstations, CEM has become readily available and extremely useful for antenna design and many other electromagnetics applications.

PROBLEMS

Section 7.1 Elemental Dipole Antennas

7.1.1 Consider a Hertzian dipole of length 1 cm carrying a phasor current of $\hat{I} = 10\angle 30°$ A. If the frequency is 100 MHz, determine the electric and magnetic fields at a distance of 10 cm away from the dipole and $\theta = 45°$. [$\hat{E}_r = 2069.67\angle(-60.17°)$, $\hat{E}_\theta = 991.4\angle(-59.64°)$, $\hat{H}_\phi = 0.575\angle(29.83°)$] Compute the ratios $|\hat{E}_\theta| / |\hat{E}_r|$ and $|\hat{E}_\theta| / |\hat{H}_\varphi|$ at this distance. [0.4791724.6] Repeat for distances of 1 m and 10 m, and $\theta = 45°$. [$\hat{E}_r = 4.701\angle(-115.5°)$, $\hat{E}_\theta = 4.033\angle(-31.73°)$, $\hat{H}_\phi = 1.306 \times 10^{-2}\angle(-25.52°)$, 0.8579, 308.8, $\hat{E}_r = 4.247 \times 10^{-2}\angle(-92.73°)$, $\hat{E}_\theta = 0.444\angle(-2.74°)$, $\hat{H}_\phi = 1.18 \times 10^{-3}\angle(-2.7°)$, 10.45, 376.08] Determine these distances in wavelengths. [0.033, 0.33, 3.33]

7.1.2 Determine the far fields of a Hertzian dipole antenna that has a total length of 5 cm, a current of 3 A at a frequency of 1 MHz, at a distance of 2000 m, and an angle of 45°. [$\hat{E}_\theta = 33.3\angle(-150°)$ μV/m, $\hat{H}_\phi = 0.0884\angle(-150°)$ μA/m]

7.1.3 For the Hertzian dipole of Problem 7.1.2, determine the average power density. [1.47 pW/m^2]

7.1.4 For the Hertzian dipole of Problem 7.1.2, determine the radiation resistance and the total average power radiated. [21.9 μΩ, 98.7 μW]

7.1.5 Consider a magnetic dipole (loop) antenna of radius 1 cm carrying a current of $\hat{I} = 10\angle 30°$ A. If the frequency is 100 MHz, compute the electric and magnetic field intensities at $r = 10$ cm, 1 m, 10 m, and $\theta = 45°$.

$$\begin{bmatrix} \hat{E}_\varphi = 14.26\angle(-60.17°),\ 0.324\angle(-115.52°),\ 2.927 \times 10^{-2}\angle(-92.7°) \\ \hat{H}_r = 0.3612\angle 29.83°,\ 8.205 \times 10^{-4}\angle 25.5°,\ 7.412 \times 10^{-6}\angle(-2.73°) \\ \hat{H}_\theta = 0.173\angle 30.36°,\ 7.04 \times 10^{-4}\angle 58.27°,\ 7.746 \times 10^{-5}\angle(-87.26°) \end{bmatrix}$$

Determine the ratios ($|\hat{H}_\theta| / |\hat{H}_r|$) and ($|\hat{E}_\varphi| / |\hat{H}_\theta|$) at these distances. [0.479, 82.43, 0.858, 460.2, 10.45, 377.9]

7.1.6 Determine the far fields of a magnetic dipole (loop) antenna that has a radius of 5 cm, a current of 3 A at a frequency of 1 MHz, at a distance of 2000 m, and an angle of 45°. [0.1096 μV/m $\boldsymbol{a}_\varphi$, 2.908×10^{-10} A/m $\mathbf{a}_\theta$]

7.1.7 For the magnetic loop of Problem 7.1.6, determine the average power density. [1.594×10^{-17} W/m^2]

7.1.8 For the magnetic loop of Problem 7.1.6, determine the radiation resistance and the total average power radiated. [2.374×10^{-10} Ω, 1.068 nW]

Section 7.2 The Half-Wave Dipole and Quarter-Wave Monopole Antennas

7.2.1 Determine the magnitudes of the electric and magnetic fields of a half-wave dipole operated at a frequency of 300 MHz at a distance of 100 m in the broadside plane, that is, $\theta = 90°$. The input current to the terminals is $100\angle 0°$ mA. Determine the total power radiated and the power density in the wave. [60 mV/m, 159.15 μA/m, 365 mW, 4.775 μW/m^2]

7.2.2 A lossless quarter-wave monopole antenna is situated above a perfectly conducting ground plane and is driven by a 100 V 300 MHz source that has a source impedance of 50 Ω. Determine the total average power radiated. Also determine the magnitude of the electric field broadside to the antenna ($\theta = 90°$) and the power density at a distance of 100 m. What is the direction of this electric field vector with respect to the ground plane? [23 W, $E_\theta = 0.674$ V/m, 0.602 mW/m^2, perpendicular]

7.2.3 The quarter-wave monopole antenna of Problem 7.2.2 is replaced by a $\lambda_0/5$ lossless monopole that has an input impedance of $(20 - j50)\ \Omega$. Determine the total average power radiated. [13.51 W]

7.2.4 The quarter-wave monopole antenna of Problem 7.2.2 is replaced by a $\lambda_0/10$ lossless monopole that has an input impedance of $(4 - j180)\ \Omega$. Determine the total average power radiated. [0.566 W]

7.2.5 A lossless dipole antenna is attached to source with a length of lossless 50 Ω coaxial cable. The source has an open-circuit voltage of 100 V (RMS) and a source impedance of 50 Ω. If the frequency of the source is such that the dipole length is one-half wavelength and the transmission-line length is 1.3λ, determine the total average power radiated by the antenna and the VSWR on the cable. [43.1 W, 2.18]

Section 7.3 Antenna Arrays

7.3.1 Two identical monopole antennas are perpendicular to the earth. The antennas are separated by a distance d and fed with currents of equal amplitude as shown in Fig. 7.9. Sketch the pattern of the array in a plane parallel to the earth for the following conditions: (a) $d = \lambda_0/2$, $\alpha = 90°$, (b) $d = 5\lambda_0/8$, $\alpha = 45°$, (c) $d = \lambda_0$, $\alpha = 180°$, (d) $d = \lambda_0/4$, $\alpha = 180°$. [(a) Nulls at 60°, maxima/minima at ±120°, 0°, 180°; (b) nulls at ±53.13°, 180°, maxima/minima at 0°, 180°, ± 101.54°; (c) nulls at 90°, 270°, 180°, 0°, maxima/minima at ±120°, ± 60°; (d) nulls at ±90°, maxima/minima at 0°, 180°]

7.3.2 A standard AM broadcast band transmitting station consists of two vertical monopoles above the earth. The two antennas are separated by 164 ft., and the transmitting frequency is 1500 kHz. The antennas are fed with signals of equal amplitude and a phase difference of 135°. Sketch the electric field pattern at the surface of the earth. Show the location of all maxima and minima and their relative values. [Nulls at $\phi = \pm 60°$ and maxima/minima at $\phi = 0°, 180°$]

7.3.3 Two dipoles are separated by one wavelength. The terminal currents are of equal magnitude but are out of phase by 90°. Sketch the electric field pattern in a plane perpendicular to the dipoles. Show the location of all maxima and minima and their relative values. [Nulls at ±75.52°, ± 138.58°, maxima/minima at 0°, 180°, ± 104.48°, ± 41.41°]

Section 7.4 Characterization of Antennas

7.4.1 A lossless half-wave dipole antenna has an input current to its terminals (peak) of 500 mA. Determine the power density broadside to the antenna at a distance of 3000 m by (a) calculating it directly using the results of Section 7.2 and (b) using the directivity. [0.1326 μW/m^2]

7.4.2 Consider a lossless, half-wave dipole antenna. If the antenna is delivering 1 mW to a matched load, determine the received power if the load is changed to $(10 + j0)\ \Omega$. [0.336 mW]

7.4.3 Determine the maximum effective aperture of a half-wave dipole operated at 300 MHz. [0.1305 m^2]

7.4.4 Determine an expression for the antenna factor of an antenna that is terminated in a matched load. Assume that the antenna input impedance is $\hat{Z}_a = R_a + jX_a$ and its maximum gain is G. [$\mathrm{AF} = (2f/v_0 \mid \hat{Z}_a \mid)\sqrt{\pi\eta_0 R_a/G}$] Write this result in dB. [$\mathrm{AF}_{\mathrm{dB}} = 20 \log f(\mathrm{MHz}) - G(\mathrm{dB}) - 20 \log \mid \hat{Z}_a \mid + 10 \log R_a - 12.79$] Repeat this if the antenna is terminated not in a matched impedance but in a general impedance $\hat{Z}_L$. [$\mathrm{AF} = \left(\frac{|\hat{Z}_a + \hat{Z}_L|}{|\hat{Z}_L|}\right)\left(\frac{f}{v_0}\right)\sqrt{\frac{\pi\eta_0}{GR_a}}$, $\mathrm{AF}_{\mathrm{dB}} = 20 \log f(\mathrm{MHz}) - G\,(\mathrm{dB}) - 20 \log \mid \hat{Z}_L \mid + 20 \log \mid \hat{Z}_a + \hat{Z}_L \mid - 10 \log R_a - 18.81$] [$\log f(\mathrm{MHz}) - G(\mathrm{dB}) - 20 \log \mid \hat{Z}_L \mid + 20 \log \mid \hat{Z}_a + \hat{Z}_L \mid - 10 \log R_a - 18.81$] Compute the antenna factor for a half-wave dipole operated at 300 MHz and terminated in (1) a matched load and (2) 50 Ω. [(1) $\mathrm{AF}_{\mathrm{dB}} = 14.7$, (2) $\mathrm{AF}_{\mathrm{dB}} = 18.26$]. An FM antenna has an impedance of $\hat{Z}_a = 300\,\Omega$ and a gain of 2.15 dB. The matched receiver ($\hat{Z}_L = 300\,\Omega$) requires a minimum signal of 1 μV or 0 dBμV for adequate reception. Determine the minimum electric field intensity at 100 MHz. [$E_{\mathrm{inc,\,min}} = 0.29$ dBμV/m = 1.03 μV/m]

7.4.5 A 1.5-m dipole is connected to a 50 Ω spectrum analyzer with 200 ft. of RG58U coaxial cable. A 100 MHz uniform plane wave is incident on the antenna. Determine the relation between the incident electric field and the voltage received at the input terminals of the spectrum analyzer. [$|\hat{V}_{\mathrm{rec}}|_{\mathrm{dB\mu V}} = -17.72 + |\hat{E}_{\mathrm{inc}}|_{\mathrm{dB\mu V/m}}$] Determine the received voltage level corresponding to the FCC Class B limit. [25.78 dBμV]

7.4.6 Design a 20 dB pad to be used in a 300 Ω system. [$R_1 = R_3 = 366.67\,\Omega$, $R_2 = 1485\,\Omega$]

7.4.7 A quarter-wave transformer illustrated in Fig. P7.4.7 is used to match an antenna to a transmission line. If the input impedance to the terminals of the antenna is purely real and given by R_{in}, show that a $\lambda/4$ length of transmission line with characteristic impedance Z_T will give an input impedance of Z_C if $Z_T = \sqrt{R_{\mathrm{in}} Z_C}$.

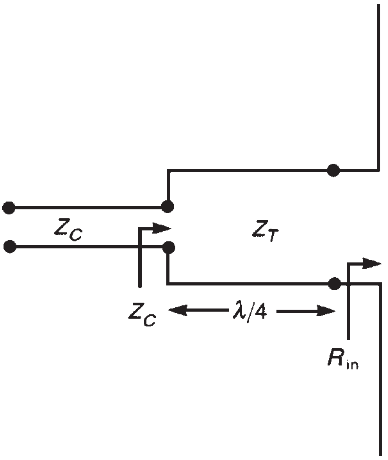

FIGURE P7.4.7

Section 7.5 The Friis Transmission Equation

7.5.1 An aircraft transmitter is designed to communicate with a ground station. The ground receiver must receive at least 1 μW for proper reception. Assume that both antennas are omnidirectional. After takeoff, the airplane flies over the station at an altitude of 5000 ft. When the airplane is directly over the station, a signal of 500 mW is received by the station. Determine the maximum communication range of the airplane. [670 mi]

7.5.2 A telemetry transmitter placed on the moon is to transmit data to the earth. The transmitter power is 100 mW and the gain of the transmitting antenna in the direction of transmission is 12 dB. Determine the minimum gain of the receiving antenna in order to receive 1 nW. The distance from the moon to the earth is 238,857 mi and the transmitter frequency is 100 MHz. [92.14 dB]

7.5.3 A microwave relay link is to be designed. The transmitting and receiving antennas are separated by 30 mi, and the gain in the direction of transmission for both antennas is 45 dB. If both antennas are lossless and matched and the frequency is 3 GHz, determine the minimum transmitter power if the received power is to be 1 mW. [36.81 W]

7.5.4 An antenna on an aircraft is being used as an electronic countermeasure (ECM) to jam an enemy radar. If the antenna has a gain of 12 dB in the direction of transmission and the transmitted power is 5 kW, determine the electric field intensity in the vicinity of the enemy radar, which is 2 mi away. The frequency of transmission is 7 GHz. [0.68 V/m]

7.5.5 A lossless half-wave dipole is being driven by a 10 V (peak), 50 Ω source. Determine the electric field intensity at a distance of 10 km in a plane perpendicular to the antenna. Compute your result by using the Friis transmission equation and check your result by using Eq. (7.20). [0.461 mV/m]

Section 7.6 Effects of Reflections

7.6.1 With reference to Fig. 7.24, medium 1 has $\varepsilon_{r1} = 4$, $\mu_{r1} = 1$ and medium 2 has $\varepsilon_{r2} = 9$, $\mu_{r2} = 4$. Write time-domain expressions for the fields if the incident electric field is $\boldsymbol{E} = 100 \cos(\omega t - 6\pi z)\boldsymbol{a}_x$. Determine the average power transmitted through a 2 m^2 area of the surface.

$$\left[\begin{array}{l}
E_i = 100\cos(9\pi \times 10^8 t - 6\pi z)a_x, \\[6pt]
E_r = \frac{100}{7}\cos(9\pi \times 10^8 t + 6\pi z)a_x, \\[6pt]
E_t = \frac{800}{7}\cos(9\pi \times 100^8 t - 18\pi z)a_x, \\[6pt]
H_i = \frac{100}{188}\cos(9\pi \times 10^8 t - 6\pi z)a_y, \\[6pt]
H_r = -\frac{100}{7\times 188}\cos(9\pi \times 10^8 t + 6\pi z)a_y, \\[6pt]
H_t = \frac{800}{7\times 251}\cos(9\pi \times 10^8 t - 18\pi z)a_y, \\[6pt]
52\ \mathrm{W}
\end{array}\right]$$

7.6.2 With reference to Fig. 7.24, medium 1 has $\varepsilon_{r1} = 4$, $\mu_{r1} = 16$ and medium 2 has $\varepsilon_{r2} = 9$, $\mu_{r2} = 1$. Write time-domain expressions for the fields if the incident electric field is $\boldsymbol{E} = 10 \cos[\omega t - (8\pi/3)z]\boldsymbol{a}_x$. Determine the average power transmitted through a 5 m^2 area of the surface.

$$\left[\begin{array}{l}
E_i = 100\cos(9\pi\times 10^8 t - 6\pi z)a_x,\\
E_r = \frac{100}{7}\cos(9\pi\times 10^8 t + 6\pi z)a_x,\\
E_t = \frac{800}{7}\cos(9\pi\times 100^8 t - 18\pi z)a_x,\\
H_i = \frac{100}{188}\cos(9\pi\times 10^8 t - 6\pi z)a_y,\\
H_r = -\frac{100}{7\times 188}\cos(9\pi\times 10^8 t + 6\pi z)a_y,\\
H_t = \frac{800}{7\times 251}\cos(9\pi\times 10^8 t - 18\pi z)a_y,\\
\text{52 W}
\end{array}\right]$$

7.6.3 With reference to Fig. 7.24, medium 1 has $\varepsilon_{r1} = 9$, $\mu_{r1} = 4$ and medium 2 has $\varepsilon_{r2} = 1$, $\mu_{r2} = 16$. Write time-domain expressions for the fields if the incident magnetic field is $\boldsymbol{H}_i = 0.1 \cos(\omega t - 8\pi z)\boldsymbol{a}_x$. Observe that the incident electric field vector is in the y direction. Determine the average power transmitted through a 3 m^2 area of the surface.

$$\left[\begin{array}{l}
E_i = -25.13\cos(4\pi\times 10^8 t - 8\pi z)a_y,\\
E_r = -17.95\cos(4\pi\times 10^8 t + 8\pi z)a_y,\\
E_t = -43.08\cos\left(4\pi\times 10^8 t - \frac{16\pi}{3}z\right)a_y,\\
H_i = 0.1\cos(4\pi\times 10^8 t - 8\pi z)a_x,\\
H_r = -\frac{5}{7}\times 0.1\cos(4\pi\times 10^8 t + 8\pi z)a_x,\\
H_t = \frac{2}{7}\times 0.1\cos\left(4\pi\times 10^8 t - \frac{16\pi}{3}z\right)a_x,\\
\text{1.85 W}
\end{array}\right]$$

7.6.4 With reference to Fig. 7.24, medium 1 is free space and medium 2 is stainless steel with $\varepsilon_r = 1$, $\mu_r = 500$, and $\sigma = 0.02$ S/m. The incident electric field is given by $\boldsymbol{E}_i = 100 \cos(2\pi\times 10^9 t - 20.94z)\boldsymbol{a}_x$. Write complete time-domain expressions for the fields. Determine the average power dissipated in a volume of material in the stainless steel consisting of a 2 m^2 area of the surface and one skin depth deep.

$$\left[\begin{array}{l}
E_i = 100\cos(2\pi\times 10^9 t - 20.94z)a_x,\\
E_r = 91\cos(2\pi\times 10^9 t + 20.94z + 0.91^\circ)a_x,\\
H_i = 0.265\cos(10\pi\times 10^7 t - 20.94z)a_y,\\
H_r = -0.241\cos(2\pi\times 10^9 t + 20.94z + 0.91^\circ)a_y,\\
E_t = 191e^{-83z}\cos(2\pi\times 10^9 t - 475.62z + 0.43^\circ)a_x,\\
H_t = 2.34\times 10^{-2}e^{-83z}\cos(2\pi\times 10^9 t - 475.62z - 9.47^\circ)a_y,\\
\text{3.8 W}
\end{array}\right]$$

7.6.5 With reference to Fig. 7.24, medium 1 is lossless and has parameters of $\varepsilon_r = 9$, $\mu_r = 1$. Medium 2 is lossy with $\varepsilon_r = 1$, $\mu_r = 1$, and $\sigma = 20$ S/m. The incident electric field is given by $\boldsymbol{E}_i = 5 \cos\,(10\pi \times 10^8 t - 10\pi z)\boldsymbol{a}_x$. Write complete time-domain expression for the fields. Determine the average power dissipated in a volume of material in the second medium consisting of a 1 cm^2 area of the surface and 10 mm deep.

$$\left[\begin{array}{l}
E_i = 5\cos(10\pi \times 10^8 t - 31.4z)a_x,\\
E_r = 4.27\cos(10\pi \times 10^8 t - 31.4z + 170.9^\circ)a_x,\\
H_i = 0.04\cos(10\pi \times 10^8 t - 31.4z)a_y,\\
H_r = -0.034\cos(10\pi \times 10^8 t + 31.4z + 170.9^\circ)a_y,\\
E_t = 10.4e^{-198.69z}\cos(10\pi \times 10^8 t - 198.69z + 40.81^\circ)a_x,\\
H_t = 0.074e^{-198.69z}\cos(10\pi \times 10^8 t - 198.69z - 4.19^\circ)a_y,\\
\\
2.64\ \mu\text{W}
\end{array}\right]$$

7.6.6 Airplanes use radar altimeters to accurately determine their low-level altitude. If an airplane is flying over the ocean ($\varepsilon_r = 81$, $\mu_r = 1$, and $\sigma = 4$ S/m), determine the percent of the transmitted power that is reflected from the ocean surface and the percent of the transmitted power that is lost in the ocean if the radar frequency is 7 GHz. [64.2% and 35.8%]

7.6.7 A radio wave strikes the surface of a copper conductor normal to it. If the total electric field is zero at a distance of 1 m away from the conductor surface, determine the lowest possible frequency of the radio wave. [150 MHz]

7.6.8 Modify the ground reflection factors that were derived for Hertzian dipole antennas for half-wave dipole antennas. [Horizontal—no change; vertical—replace $\cos\,\theta_i$ with $\cos((\pi/2)\sin\,\theta_i)\,\cos\,\theta_i$ in $\hat{F}_V$]

Section 7.7 Broadband Measurement Antennas

7.7.1 A 300 Ω twin-lead transmission line is attached to an infinite biconical antenna. Determine the cone half angle that will match the line to the antenna. [9.38°] Repeat this for a 50 Ω line. [66.79°] Repeat for the discone antenna shown in Fig. 7.31. [0.77°, 47°]

7.7.2 Determine the directivity of the infinite biconical antenna. $\left[D = \left[\sin^2\theta_h \ln\left(\cot\,\frac{\theta_h}{2}\right)\right]^{-1}\right]$ Determine the maximum gain for a cone angle that will match to a 50 Ω line. [2.84]

7.7.3 A log-periodic dipole array is to operate over the frequency band of 200 MHz to 1 GHz. Determine the shortest and longest member lengths. [75 cm, 15 cm]

REFERENCES

1. C. R. Paul and S. A. Nasar, *Introduction to Electromagnetic Fields,* 2nd ed., McGraw-Hill, New York, 1987.
2. C. R. Paul, *Electromagnetics for Engineers*, Wiley, New York, 2004.
3. E. C. Jordan and K. G. Balmain, *Electromagnetic Waves and Radiating Systems,* 2nd ed., Prentice-Hall, Englewood Cliffs, NJ, 1968.

4. W. L. Stutzman and G. A. Thiele, *Antenna Theory and Design*, Wiley, New York, 1981.
5. C. A. Balanis, *Antenna Theory Analysis and Design*, Harper & Row, New York, 1982.
6. J. D. Kraus, *Antennas*, McGraw-Hill, New York, 1950.
7. *ARRL Antenna Book*, 14th ed., American Radio Relay League, Newington, CT, 1984.
8. J. DeMarinis, The antenna cable as a source of error in EMI measurements, *Proc. 1988 IEEE Int. Symp. Electromagnetic Compatibility*, Seattle, WA, Aug. 1988.

CHAPTER EIGHT

Radiated Emissions and Susceptibility

In this chapter, we will discuss the important mechanisms by which electromagnetic fields are generated in an electronic device and are propagated to a measurement antenna that is used to verify compliance to the governmental regulatory limits. Recall that for domestic radiated emissions, the frequency range of measurement is from 30 MHz to over 1 GHz. The FCC measurement distance is 3 m for Class B products and 10 m for Class A products. For CISPR 22 (EN55022), the measurement distance is 10 m for Class B products and 10 m for Class A products. The lower frequency of 30 MHz is one wavelength at 10 m, whereas the frequency of 1 GHz is one wavelength at 30 cm. The product is therefore in the *near field* of the antenna for certain of the lower-frequency ranges of the regulatory limits and in the *far field* for the higher-frequency ranges. We found in the previous chapter that the field structure of the emissions in the near field of an emitter is considerably more complicated that in the far field. Certain simplifications valid for the far field are not valid for the near field, although they are frequently used. An example is the inverse-distance rule that is used to translate an emission measured at one distance to another distance. This assumes that the fields increase (decrease) *linearly* with decreasing (increasing) measurement distances, which is true only in the far field. We will generate some simple models for first-order predictions of the radiated emissions from wires and PCB lands in this chapter. For simplicity, *these models will assume that the measurement antenna is in the far field of the emission* (*the product*), although this is not necessarily the case over the entire frequency range of the regulatory limit.

We will also investigate the ability of the product to be susceptible to radiated emissions from other electronic devices by deriving simple models that give the voltages and currents induced in parallel-conductor lines by an incident uniform plane wave. The incident wave is produced by a distant antenna such as a FM radio station. This aspect of radiated emissions also fits into the company's goal of producing quality products. For example, if a product complies with the relevant regulatory emission requirements but fails to perform properly in dry climates because of susceptibility to electrostatic discharge (ESD) or will not perform properly when installed in a residence near an airport radar, the company's reputation for producing quality products will be significantly degraded.

Introduction to Electromagnetic Compatibility, Third Edition. Clayton R. Paul, Robert C. Scully, and Mark A. Steffka.
© 2023 John Wiley & Sons, Inc. Published 2023 by John Wiley & Sons, Inc.

8.1 SIMPLE EMISSION MODELS FOR WIRES AND PCB LANDS

Our primary interest is to understand the radiation properties of the *unintentional antennas in the system*, which are the wires, PCB lands, and other metallic structures such as cabinets and enclosures. In this section, we will formulate some simple models that allow us to understand the factors that cause the radiated emissions from the currents on wires and PCB lands to exceed the regulatory limits. These will be derived for *ideal situations* such as an isolated pair of wires in free space distant from any other obstacles. The sole purpose of these models is to provide insight into the levels and types of currents with regard to their potential for creating radiated emissions. It is important to keep in mind that time-varying currents are the mechanism that produce radiated electromagnetic fields. Hence currents on wires, PCB lands, or any other conductor in the system *will radiate*. The essential question is how well they radiate. Therefore, our task in reducing radiated emissions is to produce "antennas" having poor emission properties.

8.1.1 Differential-Mode Versus Common-Mode Currents

Differential-mode and common-mode currents were briefly discussed in Chapter 5 in connection with the use of common-mode chokes for suppression purposes. It is important that we review these concepts of differential- and common-mode currents. Consider the pair of parallel wires or PCB lands of length L and separation s shown in Fig. 8.1a. The two conductors are placed in the xz plane and are parallel to the z axis. Suppose that the currents at the same cross section are directed to the right and denoted as $\hat{I}_1$ and $\hat{I}_2$. We will concentrate on frequency-domain emissions, so that the currents will be the phasor currents. These can be decomposed into differential-mode and common-mode components by writing

$$\hat{I}_1 = \hat{I}_C + \hat{I}_D \tag{8.1a}$$

$$\hat{I}_2 = \hat{I}_C - \hat{I}_D \tag{8.1b}$$

Given the currents $\hat{I}_1$ and $\hat{I}_2$, we can decompose them into their differential-mode component $\hat{I}_D$ and their common-mode component $\hat{I}_C$ by solving (8.1) to give

$$\hat{I}_D = \frac{\hat{I}_1 - \hat{I}_2}{2} \tag{8.2a}$$

$$\hat{I}_C = \frac{\hat{I}_1 + \hat{I}_2}{2} \tag{8.2b}$$

At a cross section of the line, the differential-mode currents $\hat{I}_D$ are equal in magnitude but opposite in direction. These are the *functional* or desired currents on the line. Ideal models such as the transmission-line model in Chapter 4 will predict *only* these differential-mode currents. The common-mode currents $\hat{I}_C$ are undesired currents. At cross section of any line, the common-mode currents are equal in magnitude but, unlike the differential-mode currents, the common-mode currents are directed in the same direction. Common-mode currents are sometimes called "antenna-mode currents." They are not necessary for the functional performance of the electronic devices that the line connects. Ideal models such as the transmission line model *will not predict* the common-mode currents [1, 2]. Typically, the common-mode currents will be substantially smaller than the differential-mode currents. However, the reader should not allow this observation to lull him/her into thinking that the radiated emissions of common-mode currents are inconsequential.

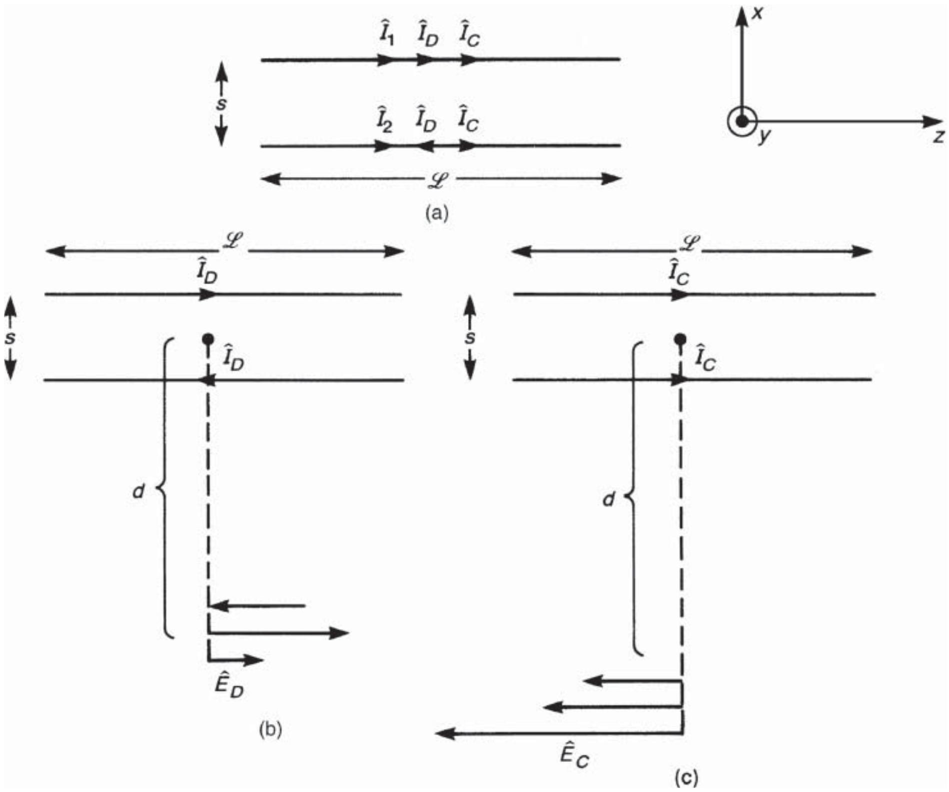

FIGURE 8.1 Illustration of the relative effects of differential-mode currents $\hat{I}_D$ and common-mode currents $\hat{I}_C$ on radiated emissions for parallel conductors: (a) decomposition of the total currents into differential-mode and common-mode components; (b) radiated emissions of differential-mode currents; (c) radiated emissions of common-mode currents.

Common-mode currents are not inconsequential in typical products, and, moreover, they often produce larger radiated emissions than do the differential-mode currents.

In order to see why this occurs, let us consider the radiated electric fields in the plane of the wires and at a point midway along the line and a distance d from the line. The configuration for differential-mode currents is illustrated in Fig. 8.1b. Observe that because the differential-mode currents are equal in magnitude but oppositely directed, the radiated electric fields will also be oppositely directed and will tend to cancel. They will not exactly cancel, since the wires are not collocated, so the net electric field $\hat{E}_D$ will be the difference between these emission components, as indicated in Fig. 8.1b. On the other hand, consider the emissions due to the common-mode currents shown in Fig. 8.1c. Because the common-mode currents are directed in the same direction, their radiated electric field components will add, producing a net radiated electric field $\hat{E}_D$. In the following sections we will show that for a 1 m ribbon cable with wire separation of 50 mils a differential-mode current at 30 MHz of 20 mA will produce a radiated emission just equal to the FCC Class B limit (40 dBμV/m or 100 μV/m from 30 to 88 MHz). On the other hand, a common-mode current of only 8 μA will produce the same emission level! This is a ratio of 2500, or some 68 dB. *Thus seemingly inconsequential common-mode currents are capable of producing significant radiated emission levels*. A number of ideal factors such as proximity to conducting planes and other structural asymmetries can create common-mode currents. The reader is referred to [2] for a more complete discussion of the sources of these common-mode currents.

In this section, we will derive simple emission models for a pair of parallel wires or PCB lands due to the currents on those conductors. Although the case of two parallel wires or PCB lands represents only a subset of the current-carrying conductors of an electronic system, it represents an important and easily analyzed structure. It will therefore provide insight into the radiation mechanism of other structures. Our basic technique to determine the radiated fields of a pair of parallel conductors is to superimpose the radiated fields of each conductor. This technique of treating each conductor as a wire-type, linear antenna (Hertzian dipole, half-wave dipole, etc.), and superimposing the fields of each conductor to determine the net radiated field is virtually identical to the determination of the radiated fields of an array of wire antennas considered in Section 7.3 of the previous chapter. In fact, the two wires of the line shown in Fig. 8.1 can be viewed as an array of linear antennas (see Fig. 7.9), and we will essentially be computing the array factor.

In order to determine this total radiated electric field of the two conductors, consider placing the two currents along the *x* axis and directing them in the *z* direction as shown in Fig. 8.2. Each electric field of these linear antennas will be a maximum broadside to (in a direction perpendicular to) the antenna, that is, in the *xy* plane, $\theta = 90°$. Hence, we will determine the maximum electric field in the *xy* plane. The total radiated electric field will be the sum of each radiated electric field:

$$\hat{E}_\theta = \hat{E}_{\theta,1} + \hat{E}_{\theta,2} \tag{8.3}$$

where the far fields of each antenna are of the form

$$\hat{E}_{\theta,i} = \hat{M}\hat{I}_i \frac{e^{-j\beta_0 r_i}}{r_i} F(\theta) \tag{8.4}$$

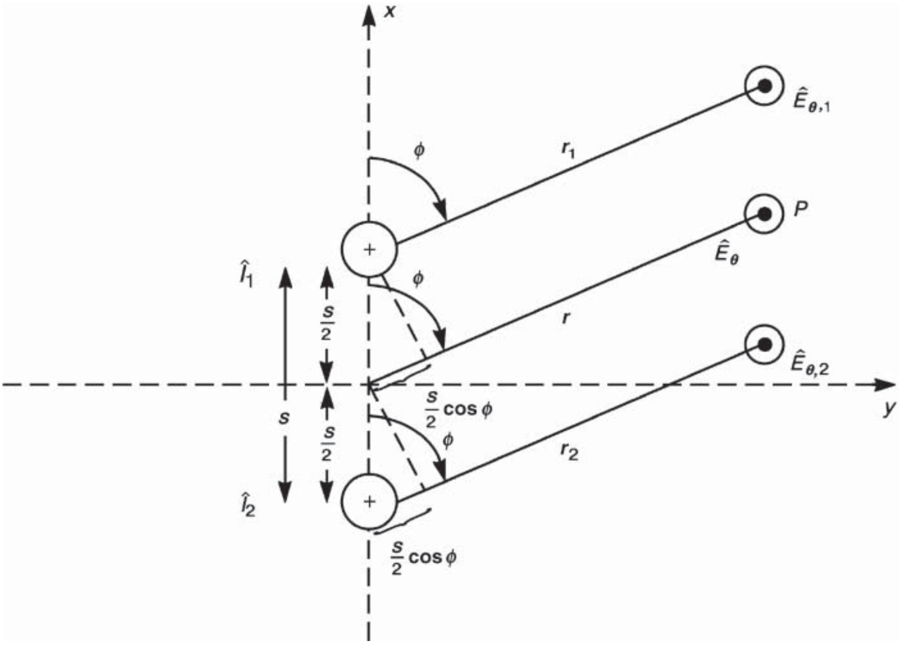

FIGURE 8.2 Calculation of the far fields of the wire currents.

The term $\hat{E}_i$ is the current at the center of the antenna, and the factor $F(\theta)$ has a maximum value of unity and represents the θ variation of the antenna pattern. Observe that, by symmetry, the pattern of each antenna is independent of φ. However, the net pattern of the pair of antennas can be a function of φ, as we will see and as discussed in Section 7.3. The term $\hat{M}$ is a function of the antenna type. For example, for a Hertzian dipole [see Eq. (7.2a)], these are

$$\left.\begin{aligned} \hat{M} &= j\frac{\eta_0\beta_0}{4\pi}L = j2\pi\times 10^{-7}fL \\ F(\theta) &= \sin\,\theta \end{aligned}\right\}\text{(Hertzian dipoles)} \tag{8.5a, b}$$

This result is valid only for current segments that are very short electrically, which allows us to assume that the current at all points along the antenna is the same (magnitude and phase). Similarly, for half-wave dipoles that have a sinusoidal current distribution $\hat{M}$ and $F(\theta)$ are [see Eqs. (7.16) and (7.19)]

$$\left.\begin{aligned} \hat{M} &= j\frac{\eta_0}{2\pi} = j60 \\ F(\theta) &= \frac{\cos\left(\frac{1}{2}\pi\,\cos\,\theta\right)}{\sin\,\theta} \end{aligned}\right\}\left(\text{half-wave dipoles}, L = \frac{1}{2}\lambda_0\right) \tag{8.6a, b}$$

For these linear, wire-type antennas, the radiated electric field is a maximum broadside to the antenna, $\theta = 90°$. Hence, as indicated in Fig. 8.2, each of the radiated electric fields, $\hat{E}_{\theta,i}$, is parallel to the line axis, i.e., out of the page, and hence $F(\theta) = 1$.

In order to determine the total fields, we will again make the “parallel-ray approximation” shown in Fig. 8.2. In terms of the distance r from the midpoint between the lines to point P, the rays are

$$r_1 = r - \frac{s}{2}\cos\,\phi \tag{8.7a}$$

$$r_2 = r + \frac{s}{2}\cos\,\phi \tag{8.7b}$$

Substituting (8.4) into (8.3) gives

$$\hat{E}_\theta = \hat{M}\left(\hat{I}_1\frac{e^{-j\beta_0 r_1}}{r_1} + \hat{I}_2\frac{e^{-j\beta_0 r_2}}{r_2}\right) \tag{8.8}$$

where we assume the two “antennas” are identical (two Hertzian dipoles or two half-wave dipoles, etc.). Substituting (8.7) into the exponential phase terms and letting $r1 = r$ and $r2 = r$ in the denominators for reasons discussed in Section 7.3 gives

$$\hat{E}_\theta = \hat{M}\frac{e^{e^{-j\beta_0 r}}}{r}(\hat{I}_1 e^{+j\beta_0 s/2\,\cos\,\varphi} + \hat{I}_2 e^{-j\beta_0 s/2\,\cos\,\varphi}) \tag{8.9}$$

we will specialize this result for the case of differential-mode currents $\hat{I}_1 = \hat{I}_D$ and $\hat{I}_2 = -\hat{I}_D$ and common-mode currents $\hat{I}_1 = \hat{I}_C$ and $\hat{I}_2 = \hat{I}_C$ in the following two sections. It is important to remind the reader once again that the derivation presented above has the important simplifying *assumption that the measurement point* (*measurement antenna*) *is in the far field of the conductors*. (This is evident in the assumed forms in (8.4), which depend on distance r as $e^{-j\beta_0 r}/r$.) If this assumption is violated, the following simple models are not valid. The radiated fields of a model that applies when the measurement antenna is in the near field of the wires are quite complicated, and the insight we will gain from the simple, far-field models is not as readily obtained [3].

8.1.2 Differential-Mode Current Emission Model

In order to simplify the resulting model, we will model each of the wires as a Hertzian dipole. This model makes three important, simplifying assumptions that were used in Chapter 7 to derive the radiated fields of this antenna: (1) the conductor lengths L are sufficiently short and the measurement point is sufficiently distant that the distance vectors from each point on the antenna to the measurement point are approximately parallel, (2) the current distribution (magnitude and phase) is constant along the line, and (3) the measurement point is in the far field of each antenna. For a measurement distance of 3 m, the first assumption requires that the maximum conductor length be somewhat less than a meter. The assumption of constant distribution of the currents along the conductors is a reasonable approximation so long as the conductors are *electrically short* at the frequency of interest. This simplifies the results considerably and applies to a large number of problems of practical interest. For example, a two-wire cable of length 1 m is one wavelength at 300 MHz. At 100 MHz, the cable is $\lambda_0/3$ in length, and the current distribution is approximately constant. A PCB land 30 cm in length would be $\lambda_0/10$ at 100 MHz, and its current distribution would be reasonably constant below 200 MHz. For shorter wires and PCB lands, the model's applicability should extend to higher frequencies.

We will also determine the radiated fields at a point that is perpendicular to the line conductors and in the plane containing them, as shown in Fig. 8.3. For differential-mode currents, $\hat{I}_2 = -\hat{I}_1$, it is a simple matter to show that a maximum will occur in the plane of the wires and on a line perpendicular to the wires ($\phi = 0°$, $180°$ in Fig. 8.2). In addition, the measurement point is at a distance d from the midpoint of the line. Once again, it is important to emphasize that it is assumed that this measurement point is sufficiently distant from the line that the measurement point is in the *far field* of the line.

The radiated fields can be determined, under the assumption of constant current distributions, by treating each wire as a Hertzian dipole and substituting (8.5) into (8.9). Also we substitute $r = d$ and $\phi = 0°$ (to give the fields in the plane of the wires). And finally, since we are considering differential-mode currents, we substitute

$$\hat{I}_1 = \hat{I}_D \tag{8.10a}$$

$$\hat{I}_2 = \hat{I}_D \tag{8.10b}$$

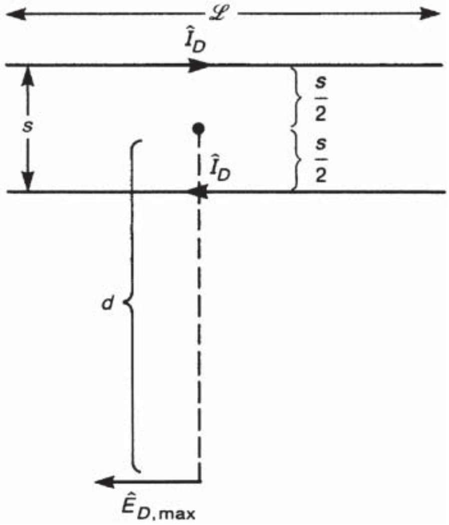

FIGURE 8.3 A simplified estimate of the maximum radiated emissions due to differential-mode currents with constant distribution.

into (8.9). The result becomes

$$\begin{aligned}\hat{E}_{D,\max} &= j2\pi \times 10^{-7} \frac{f\hat{I}_D L}{d} e^{-j\beta_0 d}\{e^{-j\beta_0 s/2} - e^{j\beta_0 s/2}\} \\ &= -4\pi \times 10^{-7} \frac{f\hat{I}_D L}{d} e^{-j\beta_0 d} \sin\left(\frac{1}{2}\beta_0 s\right) \qquad (8.11)\end{aligned}$$

where we replace $e^{jA} - e^{-jA} = 2j \sin A$. Substituting $(1/2)\beta_0 s = (\pi s/\lambda_0) = (\pi sf/c) = 1.05 \times 10^{-8} sf$ and assuming that the wire spacing s is electrically small, so that $\sin((1/2)\beta_0 s) \cong (1/2)\beta_0 s$, the magnitude of (8.11) reduces to

$$|\hat{E}_{D,\max}| = 1.316 \times 10^{-14} \frac{|\hat{I}_D| f^2 L s}{d} \qquad (8.12)$$

and is parallel to the wires.

Example 8.1 As an example, consider the case of a ribbon cable constructed of 28-gauge wires separated a distance of 50 mils. Suppose the length of the wires is 1 m and that they are carrying a 30 MHz differential-mode current. The level of differential-mode current that will give a radiated emission in the plane of the wires and broadside to the cable (worst case) that just equals the FCC Class B limit (40 dBμV/m or 100 μV/m at 30 MHz) can be obtained by solving (8.12) to give

$$100\ \mu\text{V/m} = 1.316 \times 10^{-14} \frac{|\hat{I}_D|(3 \times 10^7)^2(1)(1.27 \times 10^{-3})}{3}$$

or

$$I_D = 19.95\ \text{mA}$$

Generally, the formula for the maximum emission given in (8.12) is sufficient for estimation purposes [4, 5].

Next, we consider the case of a trapezoidal waveform such as a clock or data signal driving a two-wire line as shown in Fig. 8.4. Observe from (8.12) that the *transfer function* relating the maximum received electric field to the current varies with the *loop area* $A = Ls$ and the square of the frequency, so that

$$\left|\frac{\hat{E}_{D,\max}}{\hat{I}_D}\right| = Kf^2 A \qquad (8.13)$$

where the constant is $K = 1.316 \times 10^{-14}/d = 4.39 \times 10^{-15}$ for the FCC Class B measurement distance of $d = 3$ m. Thus, the frequency response of this transfer function increases at a rate of +40 dB/decade. Multiplying this transfer function and the input signal spectrum developed for the trapezoidal waveform in Chapter 3 (adding the Bode plots) gives the resulting spectrum of the received electric field intensity shown in Fig. 8.4. Observe that the resulting electric field spectrum increases at +40 dB/decade up to $1/\pi\tau$, then increases at +20 dB/decade up to $1/\pi\tau_r$, and is flat above that. As an example, consider a 100-MHz pulse train having a 50% duty cycle and rise/falltimes of 1 ns. The various breakpoints are $1/\pi\tau = 63.7$ MHz and $1/\pi\tau_r = 318.3$ MHz. This illustrates that radiated emission problems due to differential-mode currents tend to be confined to the upper frequencies of the radiated emission regulatory limit, typically above 200 MHz.

In summary, the maximum radiation occurs in the plane of the wires broadside to them, as shown in Fig. 8.5a. At a point equidistant from each wire the radiated fields cancel, as shown in Fig. 8.5b.

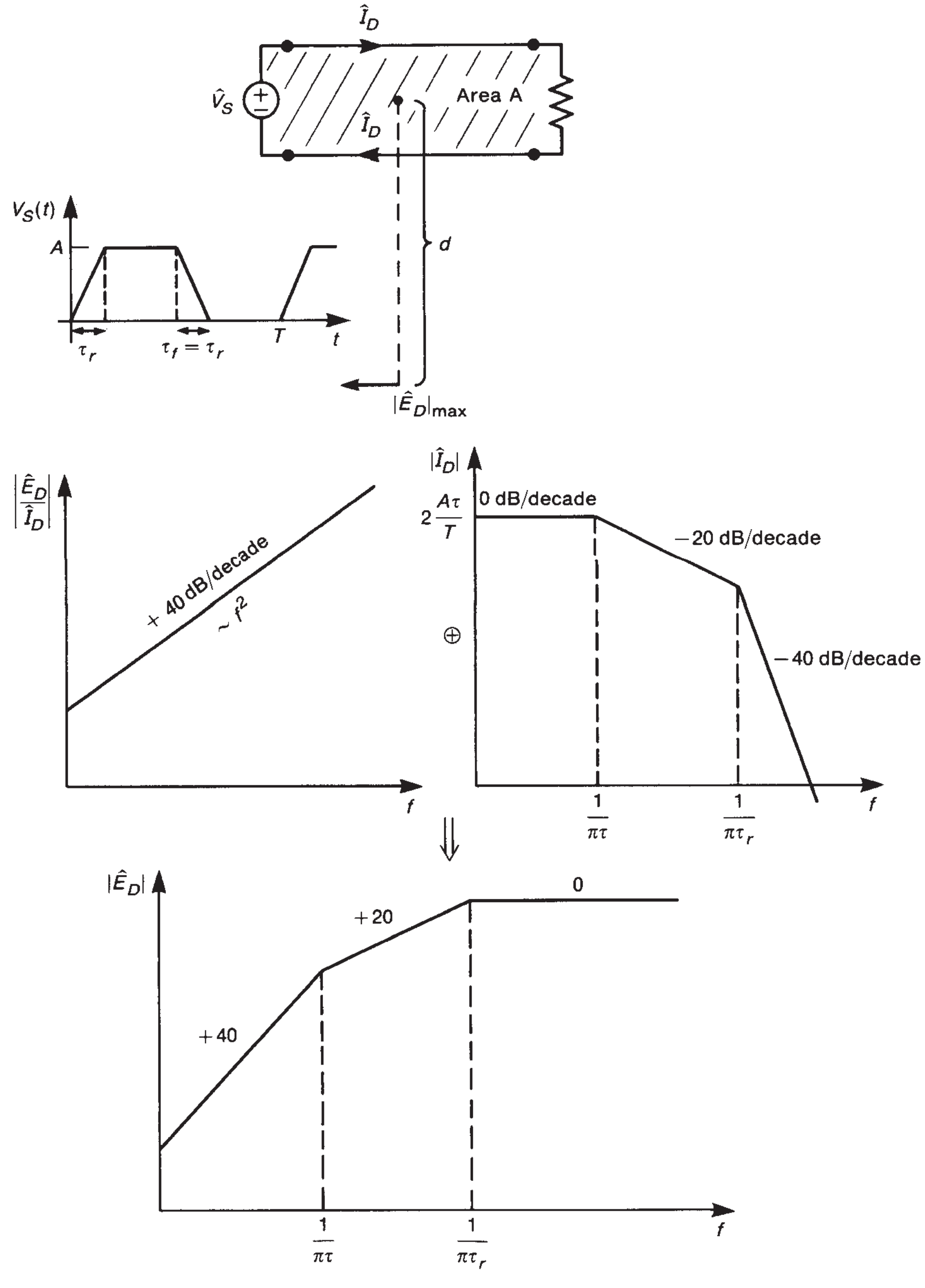
$\hat{I}_D$
$\hat{V}_S$
+
−
Area A
$\hat{I}_D$
d
$|\hat{E}_D|_{max}$
$V_S(t)$
A
τ_r
$\tau_f = \tau_r$
T
t
$\left|\frac{\hat{E}_D}{\hat{I}_D}\right|$
+ 40 dB/decade
~ f^2
f
$|\hat{I}_D|$
$2\frac{A\tau}{T}$
0 dB/decade
−20 dB/decade
−40 dB/decade
⊕
$\frac{1}{\pi\tau}$
$\frac{1}{\pi\tau_r}$
f
⇓
$|\hat{E}_D|$
+40
+20
0
$\frac{1}{\pi\tau}$
$\frac{1}{\pi\tau_r}$
f

FIGURE 8.4 Illustration of the radiated emissions due to the differential-mode currents for a trapezoidal pulse train applied to a two-conductor line: (a) problem definition; (b) spectral content of the radiated emission.

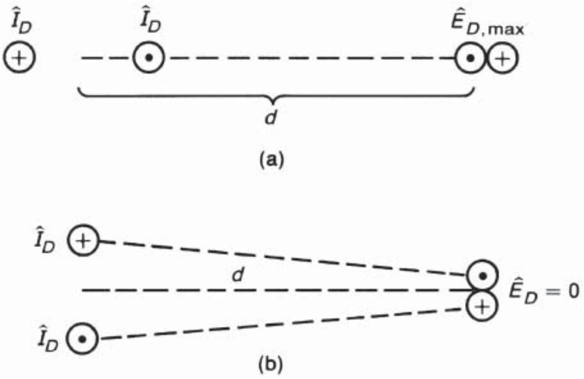

FIGURE 8.5 Illustration of the observation that (a) the fields of differential-mode currents are a maximum in the plane of the wires but (b) cancel broadside to the plane of the wires.

Thus, the radiated emissions of a pair of parallel wires should be quite sensitive to rotation of the cable. The maximum radiated electric fields vary with (1) the square of the frequency, (2) the loop area $A = Ls$, and (3) the current level $\hat{I}_D$. Therefore, in order to reduce the radiated emissions *at a specific frequency* due to differential-mode currents, we have the following options:

1. Reduce the current level.
2. Reduce the loop area.

Option 1 can be achieved by reducing the peak levels of the time-domain currents. Typically, this is not practical since the current levels have been established for functional reasons. Option 1 can also be achieved by slowing (increasing) the pulse rise/falltimes and/or the pulse repetition rate (reducing the pulse train frequency), since these will move the two breakpoints, $1/\pi\tau$ and $1/\pi\tau_r$, of the pulse spectrum shown in Fig. 8.4 lower in frequency, causing the spectrum to "roll off" at a faster rate at this frequency. Option 2, reduction of the loop area, should be addressed early in the design. This tends to be more of a problem on PCBs than in wiring harnesses.

For example, suppose that a clock oscillator is to serve an ASIC or a microprocessor. Routing the clock traces as shown in Fig. 8.6a creates a large loop and enhances the differential-mode radiation. Placing the oscillator close to the ASIC tends to reduce the impact of the tendency of the layout personnel to route lands for wiring purposes rather than EMC considerations, thereby inadvertently creating large loop areas. Judiciously choosing pin assignments in connectors can also reduce the differential-mode current emissions. For example, consider a ribbon cable carrying signals to a stepper motor, as shown in Fig. 8.6b. Perhaps for aesthetic reasons, the pin assignments in the connector at each end of the cable may have been chosen as shown creating a loop for phase A consisting of three wire separations. If the pin assignments had been made as shown in Fig. 8.6c, the radiated emissions due to the differential-mode current of phase A would have been reduced by a factor of 3, or roughly 10 dB! Common-sense considerations such as these provide the EMC designer with "cost-free" methods of reducing radiated emissions.

8.1.3 Common-Mode Current Emission Model

It is quite easy to modify the preceding results to consider the case of common-mode currents shown in Fig. 8.7. Once again, we assume that the conductors can be approximated as Hertzian dipoles and that the measurement point is (for maximum emissions) in the plane of the conductors and a distance

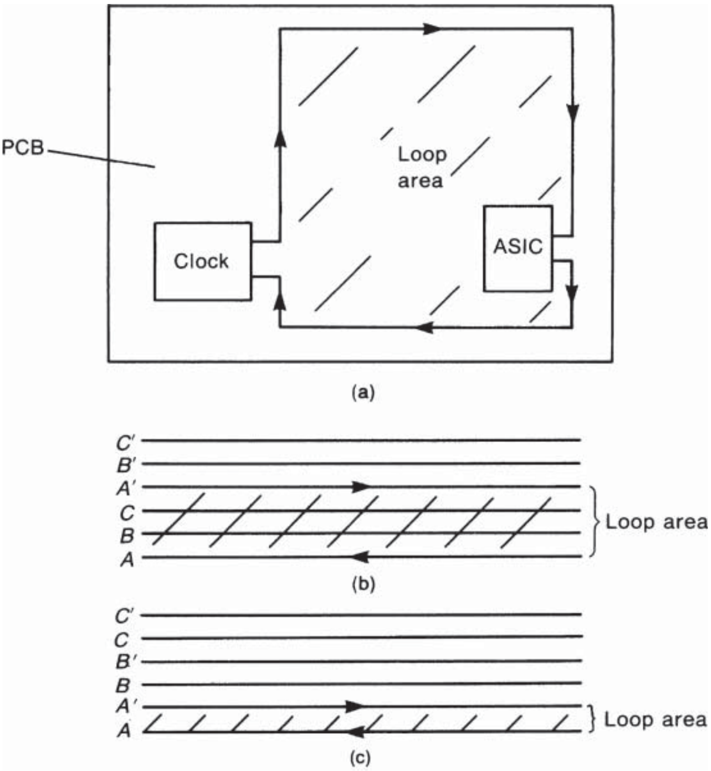
PCB
Loop area
Clock
ASIC
(a)
C′
B′
A′
C
B
A
Loop area
(b)
C′
C
B′
B
A′
A
Loop area
(c)

FIGURE 8.6 Common mistakes that lead to unnecessarily large differential-mode emissions: (a) large clock land areas; (b, c) choices of connector pin assignments in ribbon cables to minimize loop areas.

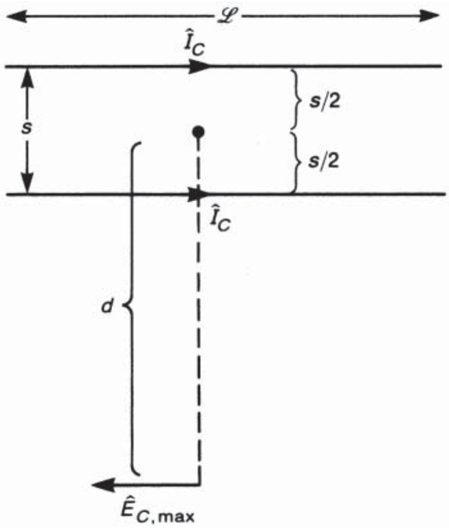
$\mathscr{L}$
$\hat{I}_C$
$s/2$
s
$s/2$
$\hat{I}_C$
d
$\hat{E}_{C,\max}$

FIGURE 8.7 A simplified estimate of the maximum radiated emissions due to common mode currents with constant distribution.

d from a point that is midway between the conductors (and in the far field of the conductors). The common-mode currents at a cross section are equal in magnitude and directed in the same direction:

$$\hat{I}_1 = \hat{I}_C \tag{8.14a}$$

$$\hat{I}_2 = \hat{I}_C \tag{8.14b}$$

Superimposing the fields due to the two Hertzian dipoles as was done above for the differential-mode currents gives (replace the minus sign with a plus sign in (8.11) since the common-mode currents are directed in the same direction)

$$\begin{aligned}\hat{E}_{C,\max} &= j2\pi \times 10^{-7} \frac{f\hat{I}_C L}{d} e^{-j\beta_0 d} \{ e^{-j\beta_0 s/2} + e^{j\beta_0 s/2} \} \\ &= j4\pi \times 10^{-7} \frac{f\hat{I}_C L}{d} e^{-j\beta_0 d} \cos\left(\frac{1}{2}\beta_0 s\right)\end{aligned} \tag{8.15}$$

where we substitute $e^{jA} + e^{-jA} = 2\cos A$. Substituting $(1/2)\beta_0 s = (\pi s/\lambda_0)$ and assuming that the wire spacing s is electrically small, so that $\cos((1/2)\beta_0 s) \cong 1$, the magnitude of (8.15) reduces to

$$|\hat{E}_{C,\max}| = 1.257 \times 10^{-6} \frac{|\hat{I}_C| f L}{d} \tag{8.16a}$$

and is again parallel to the wires.

In the case of common-mode currents, we made the assumption that the maximum radiation occurs in the plane of the wires (Fig. 8.2, $\phi = 0°$, $180°$) as was the case for differential-mode currents. Although this is not the case, since the wire separation is assumed electrically small as it must be in practical cases, $s \ll \lambda_0$, it does not matter. For example, from (8.9) the radiated electric field for common-mode currents is proportional to $\cos(\beta_0 (s/2)\cos\phi) = \cos(\pi(s/\lambda_0)\cos\phi)$. Suppose as is typical in practical situations, $s \leq \lambda_0/100$. In the plane of the wires, $\varphi = 0°, \cos(\pi(s/\lambda_0)\cos\phi) = \cos[(\pi/100) \times 1] = 0.9995$, whereas in a direction that is perpendicular to the plane of the wires, $\varphi = 90°$, $\cos(\pi(s/\lambda_0)\cos\phi) = \cos[(\pi/100) \times 0] = 1.000$. So, for common-mode currents and electrically small wire separations, the "pattern" is virtually omnidirectional around the wires. This makes a great deal of sense because in the case of common-mode currents and closely spaced wires, we may replace the two wires, each carrying current $\hat{I}_C$, with *one wire carrying current* $2\hat{I}_C$ *without substantially changing the radiated fields at any point around it.* In fact, later in this chapter we will measure the common-mode current by placing a current probe around both wires. The current probe will measure a total current of $\hat{I}_{\text{probe}} = 2\hat{I}_C$. Hence, we could modify (8.16a) by replacing $|\hat{I}_C|$ with $|\hat{I}_{\text{probe}}/2|$ and use

$$|\hat{E}_{C,\max}| = 6.283 \times 10^{-7} \frac{|\hat{I}_{\text{probe}}| f L}{d} \tag{8.16b}$$

Note that the coefficient in (8.16a) has been reduced by 1/2.

Example 8.2 As an example, consider the case of a ribbon cable constructed of 28-gauge wires separated a distance of 50 mils that was considered earlier for differential-mode currents. Suppose the length of the wires is 1 m and that they are carrying a 30 MHz common-mode current. The level of common-mode current that will give a radiated emission broadside to the cable (worst case) that just equals the FCC Class **B** limit (40 dBμV/m or 100 μV/m at 30 MHz) can be obtained by solving (8.16a) to give

$$100\ \mu\text{V/m} = 1.257 \times 10^{-6} \frac{|\hat{I}_C|(3 \times 10^7)(1)}{3}$$

or

$$I_C = 7.96\ \mu\text{A}$$

Generally, the formula for the maximum emission given in (8.16a) is sufficient for estimation purposes [4, 5].

Now we reconsider the case of a trapezoidal waveform such as a clock or data signal driving a two-wire line, as shown in Fig. 8.8. Although it is not necessarily the case, we will assume that the waveshape of the common-mode current is the same as that of the differential-mode current. Observe from (8.16a) that the *transfer function* relating the maximum received electric field to the current varies with the line length L and directly with the frequency, so that

$$\left| \frac{\hat{E}_{C,\max}}{I_C} \right| = KfL \tag{8.17}$$

where the constant here is $K = 1.257 \times 10^{-6}/d = 4.19 \times 10^{-7}$ for the FCC Class B measurement distance of $d = 3$ m. Thus, the frequency response of this transfer function increases at a rate of +20 dB/decade. Multiplying this transfer function and the input signal spectrum developed for the trapezoidal waveform in Chapter 3 (adding the Bode plots) gives the resulting spectrum of the received electric field intensity shown in Fig. 8.8. Observe that the resulting electric field spectrum increases at +20 dB/decade up to $1/\pi\tau$, then remains constant up to $1/\pi\tau_r$, and decreases at −20 dB/decade above that. As an example, consider a 100 MHz pulse train having a 50% duty cycle and rise/falltimes of 1 ns. The various breakpoints are $1/\pi\tau = 63.7$ MHz and $1/\pi\tau_r = 318.3$ MHz. This illustrates that radiated emission problems due to common-mode currents tend to be confined to the lower frequencies of the radiated emission regulatory limit, typically below 300 MHz.

In summary, the maximum radiation occurs broadside to the wires and is essentially constant around the cable, i.e., is independent of cable rotation. Thus, the common-mode current radiated emissions of a pair of parallel wires should not be sensitive to rotation of the cable. The maximum radiated electric fields vary with (1) frequency, (2) the line length L, and (3) the current level $\hat{I}_C$. Therefore, in order to reduce the radiated emissions *at a specific frequency* due to common-mode currents, we have the following options:

1. Reduce the current level.
2. Reduce the line length.

Option 1 can again be achieved by reducing the peak levels of the time-domain currents and/or slowing (increasing) the pulse rise/falltimes and/or the pulse repetition rate (reducing the pulse train frequency), since these will move the two breakpoints, $1/\pi\tau$ and $1/\pi\tau_r$, of the pulse spectrum shown in Fig. 8.8 lower in frequency, causing the spectrum to "roll off" at a faster rate at this frequency. Option 2, reduction of the line length, should again be addressed early in the design. This tends to be more of a problem with wiring harnesses, although long lands on PCBs should also be avoided. Thus, to reduce the clock emissions, place the oscillator (or crystal) close to the module it feeds.

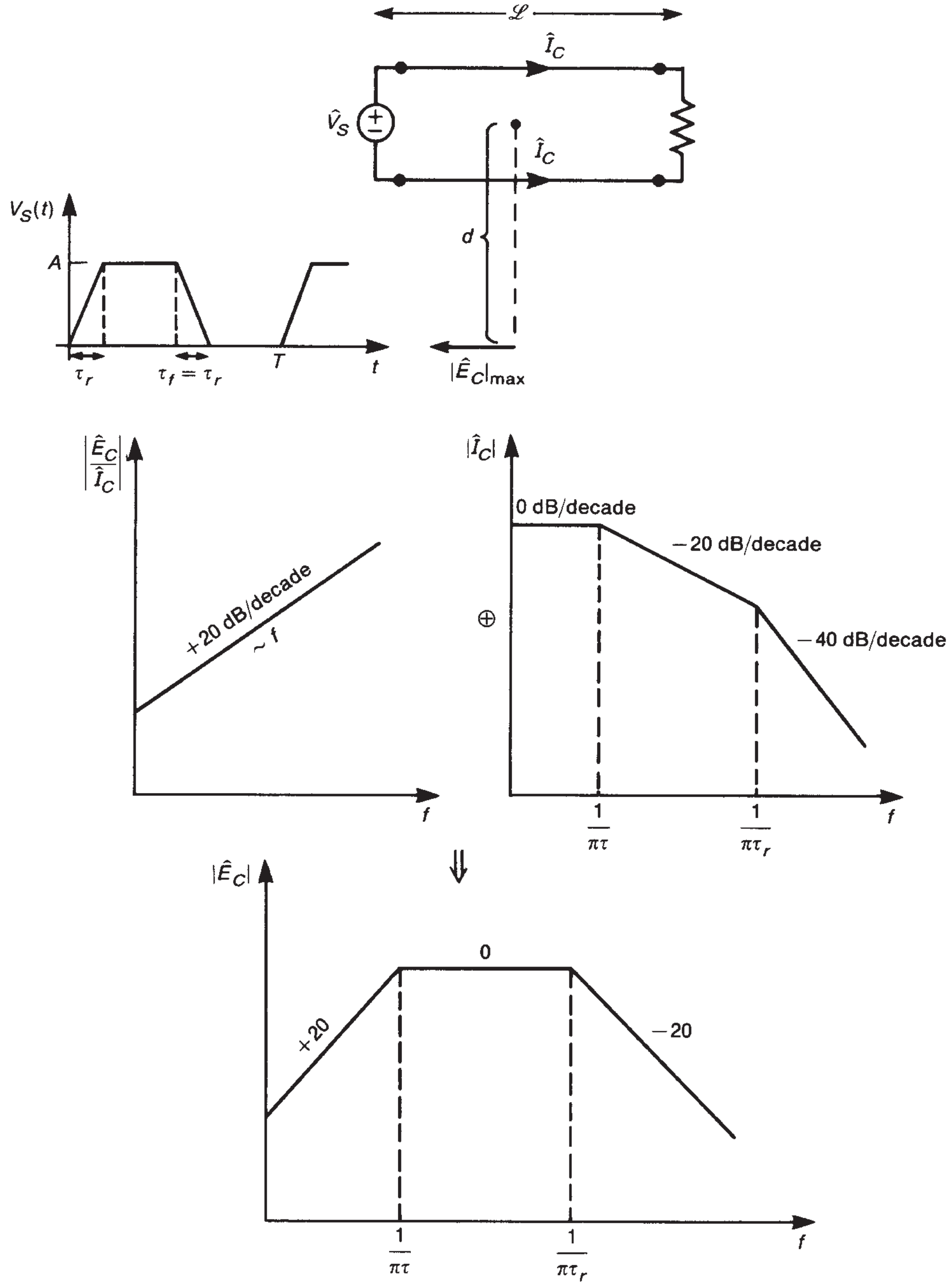
$\mathscr{L}$
$\hat{I}_C$
$\hat{V}_S$
$\hat{I}_C$
d
$|\hat{E}_C|_{max}$
$V_S(t)$
A
τ_r
$\tau_f = \tau_r$
T
t
$\left|\frac{\hat{E}_C}{\hat{I}_C}\right|$
+20 dB/decade
~ f
f
$|\hat{I}_C|$
0 dB/decade
−20 dB/decade
⊕
−40 dB/decade
$\frac{1}{\pi\tau}$
$\frac{1}{\pi\tau_r}$
f
⇓
$|\hat{E}_C|$
+20
0
−20
$\frac{1}{\pi\tau}$
$\frac{1}{\pi\tau_r}$
f

FIGURE 8.8 Illustration of the radiated emissions due to the common-mode currents for a trapezoidal pulse train applied to a two-conductor line: (a) problem definition; (b) spectral content of the radiated emission.

Also route the wires to keep their lengths and loop area small. Cable lengths are usually dictated by system considerations such as the necessary lengths to connect to peripheral devices. In this case, we have the option of blocking the common-mode currents with a toroid, which was discussed in Chapter 5.

8.1.4 Current Probes

Differential-mode currents are the desired or functional currents in the system and as such can be reliably calculated using transmission-line models or, for electrically short lines, lumped-circuit models [1]. Common-mode currents, on the other hand, are undesired currents and are not necessary for functional performance of the system. They are therefore dependent on nonideal factors such as proximity to nearby ground planes and other metallic objects, as well as other asymmetries. Consequently, they are difficult to calculate using ideal models [2]. They can, however, be measured using *current probes*. Current probes make use of Ampere's law (see Appendix B):

$$\oint_C \vec{H} \cdot d\vec{l} = \int_S \vec{J} \cdot d\vec{s} + \frac{d}{dt}\varepsilon \int_S \vec{E} \cdot d\vec{s} \tag{8.18}$$

where C is the contour bounding the open surface S. Ampere's law shows that a magnetic field can be induced around a contour by either conduction current or displacement current that penetrates the open surface S, as illustrated in Fig. 8.9a. A time-changing electric field produces a displacement current. If no time-changing electric field penetrates this surface, the induced magnetic field is directly related to the conduction current passing through the loop. Current probes use this principle in order to measure current. A current probe is constructed from a core of ferrite material that is separated into two halves, which are joined by a hinge and closed with a clip. The ferrite core is used to concentrate the magnetic flux. The clip is opened, the core placed around the wire(s) whose current is to be measured, and the probe closed. The total current that passes through the loop produces a magnetic field that is concentrated in and circulates around the core. Several turns of wire are wound on the core, so that the time-changing magnetic field that circulates around the core induces, by Faraday's law (see Appendix B), an emf that is proportional to this magnetic field. The induced voltage of this loop of wire can therefore be measured and is proportional to the current passing through the probe. A photograph of a typical current probe is shown in Fig. 8.10a.

It is not necessary to carry out precise calculations of the resulting fields and induced emf in order to calibrate the probe. Simply pass a current of known magnitude and frequency through the probe and measure the resulting voltage produced at the terminals. The result is a calibration curve that relates the ratio of the voltage $\hat{V}$ to the current $\hat{I}$ as

$$\hat{Z}_T = \frac{\hat{V}}{\hat{I}} \tag{8.19}$$

The quantity $\hat{Z}_T$ has units of ohms and is referred to as the *transfer impedance* of the current probe. The probe manufacturer provides a calibration chart with the probe that shows the magnitude of the transfer impedance versus frequency. This calibration chart was obtained by passing a current of known amplitude and frequency through the probe and measuring the resulting voltage at the probe terminals. Usually, this is given in dB (relative to 1 Ω) as

$$|\hat{Z}_T|_{\mathrm{dB}\Omega} = |\hat{V}|_{\mathrm{dB}\mu\mathrm{V}} - |\hat{I}|_{\mathrm{dB}\mu\mathrm{A}} \tag{8.20}$$

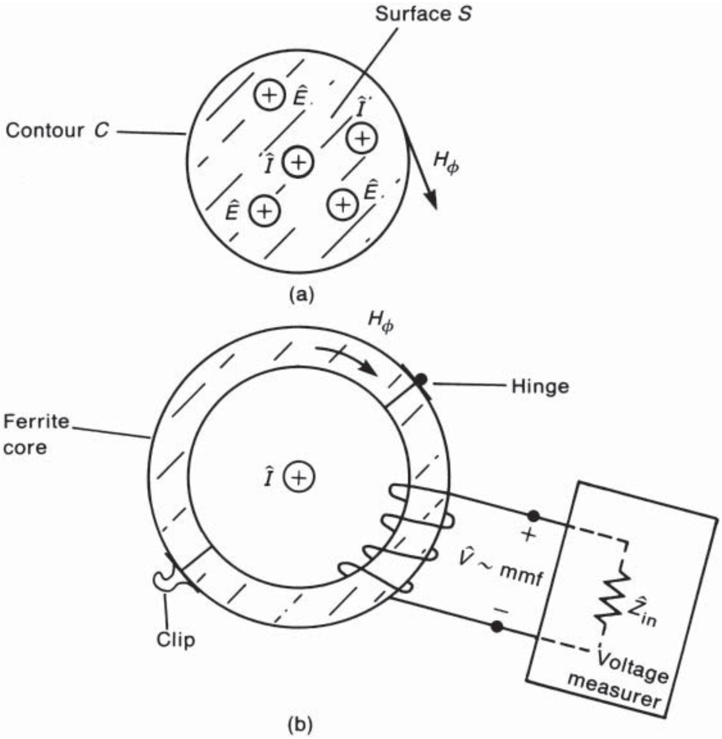

FIGURE 8.9 The current probe: (a) illustration of Ampere's law; (b) use of the current probe to measure currents.

A typical such plot is shown in Fig. 8.10b. For this current probe, the transfer impedance is relatively constant at 12 dBΩ from 10 to 100 MHz. In the following, the probe used to measure common-mode currents had a transfer impedance of 15 dBΩ from 10 to 200 MHz.

There is an important assumption inherent in the transfer impedance calibration curve: the termination impedance of the probe. For example, in the calibration of the probe as illustrated in Fig. 8.9b a voltage measurer such as a spectrum analyzer was used to measure the probe voltage in the course of determining the probe transfer impedance. Therefore the load impedance at the terminals of the probe is the input impedance to the measurement device, which is usually 50 Ω. Thus *the calibration curve of the current probe is valid only when the probe is terminated in the same impedance as was used in the course of its calibration (usually* 50 Ω*).*

For example, consider the problem of determining the level of probe voltage that will correspond to a common-mode current on a cable that will give a radiated emission just meeting a regulatory limit. The probe measures the total or net common-mode current in the cable, and the magnetic fluxes due to the differential-mode currents cancel out in the core. *Thus, the current probe will not measure differential-mode current unless it is placed around each individual wire.* Suppose that the current probe is clamped around a multiwire peripheral cable of a product and the cable length is L. Lumping the net common-mode current into one wire of length L and using the results of the previous section gives the net radiated emission a distance d way as [divide (8.16a) by 2 since this result is for two wires both carrying a current of $\hat{I}_C$]:

$$|\hat{E}_C|_{\max} = 6.28 \times 10^{-7} \frac{|\hat{I}_{C,\text{net}}| f L}{d} \tag{8.21}$$

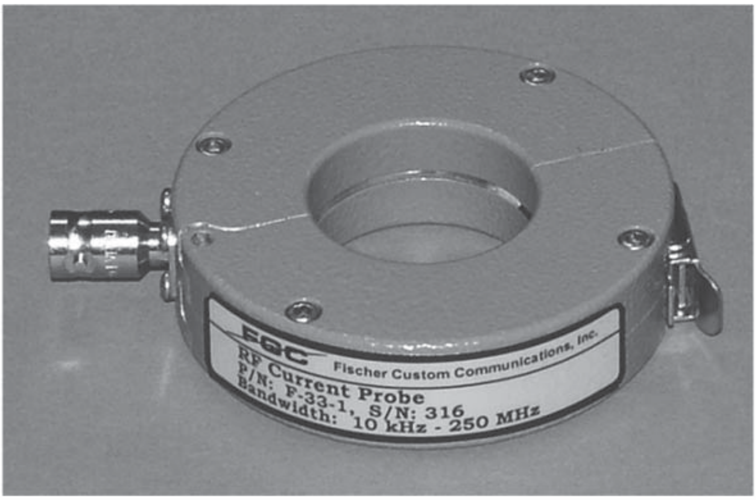
FCC
Fischer Custom Communications, Inc.
RF Current Probe
P/N: F-33-1, S/N: 316
Bandwidth: 10 kHz - 250 MHz

(a) Photograph of current probe.

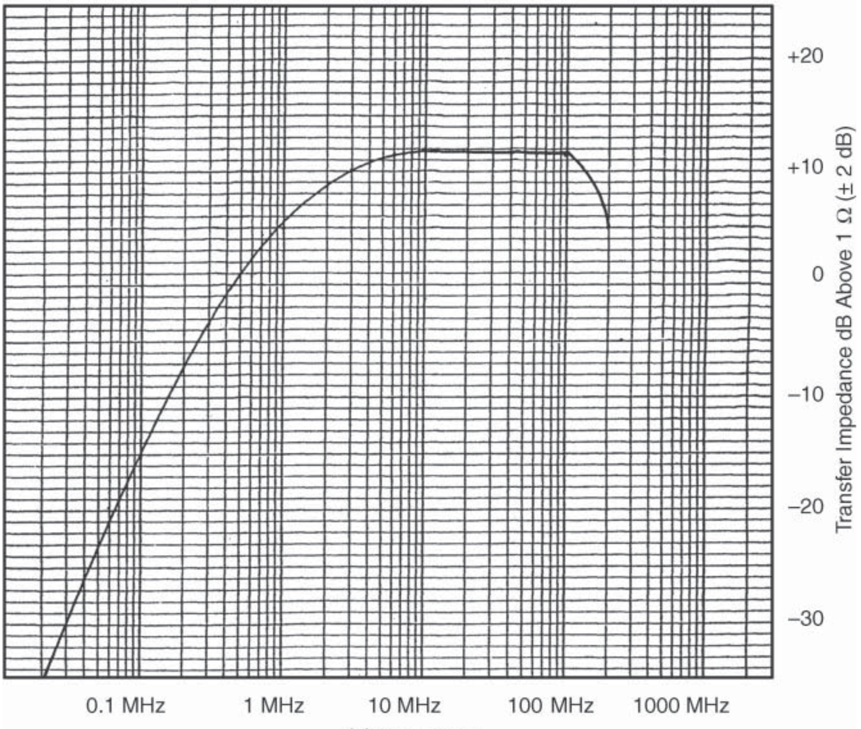

(b) Frequency

FIGURE 8.10 (a) Photograph of a current probe and (b) its measured transfer impedance. Source: Courtesy of Fischer Custom Communications, Inc.

Example 8.3 This result in (8.21) can be solved to give the maximum current to produce a radiated emission that equals the FCC Class B limit (or any other regulatory limit). For example, suppose that the probe is clamped around a 1-m cable and the probe voltage is measured at 30 MHz. Substituting the FCC Class B limit at 30 MHz of 100 μV/m into Eq. (8.21) and solving for the common-mode current gives a net common-mode current of 15.92 μA or 24 dBμA. For a current probe with transfer impedance of 15 Ω, we would measure a voltage of

$$\begin{aligned} |\hat{V}_{SA}|_{\mathrm{dB\mu V}} &= |\hat{I}|_{\mathrm{dB\mu V}} + |\hat{Z}_T|_{\mathrm{dB\Omega}} \\ &= 24\ \mathrm{dB\mu A} + 15\ \mathrm{dB\Omega} \\ &= 39\ \mathrm{dB\mu V} \\ &= 89\ \mathrm{\mu V} \end{aligned} \tag{8.22}$$

where $\hat{V}_{SA}$ denotes the voltage measured by a spectrum analyzer attached to the probe output. Therefore, if we measure a probe voltage greater than 39 dBμV at 30 MHz when the probe is clamped around a 1 m cable, the radiated emissions from the net common-mode current on this cable will (ideally) exceed the FCC Class B regulatory limit. It goes without saying that the radiated emissions from this cable must be reduced! Any other emissions from the product are inconsequential since the emissions from this cable will cause the product to be out of compliance!

In fact, the current probe can be a useful EMC *diagnostic tool* throughout the design of a product. It is a simple matter to measure the net common-mode currents on all peripheral cables of a product or a prototype of the product in the development laboratory using a current probe and an inexpensive spectrum analyzer. This does not require availability of an expensive semi-anechoic chamber in order to determine whether a particular peripheral cable will create serious radiated emission problems. It is also a simple method for determining whether an anticipated “fix” such as adding a toroid on a peripheral cable to reduce the common-mode currents has, in fact, reduced the common-mode current; simply measure the cable’s common-mode current with the probe before and after the installation of the “fix.” This is much more efficient than scheduling the semi-anechoic chamber in the EMC laboratory, taking the product to the lab, setting up the system, and measuring the radiated emissions. It also gives *real-time results* in that one can see rather rapidly if other “fixes” such as attaching grounding straps will affect the cable’s common-mode current (they may increase the common-mode current). This author strongly believes in this type of inexpensive diagnostics. A “calibration chart” for determining the level of probe voltage that will correspond to a current that will equal a regulatory limit can be obtained by substituting (8.19) into (8.21) to give

$$|\hat{E}_C|_{\max} = 6.28 \times 10^{-7} \frac{|\hat{V}_{SA}| f L}{|\hat{Z}_T| d} \tag{8.23}$$

Converting this to dB and solving for the probe voltage gives

$$\begin{aligned} |\hat{V}_{SA}|_{\mathrm{dB\mu V}} = |\hat{E}|_{\mathrm{limit,\ db\mu V/m}} + |\hat{Z}_T|_{\mathrm{db\Omega}} + 20\log_{10} d \\ - 20\log_{10} f_{\mathrm{MHz}} - 20\log_{10} L + 4.041 \end{aligned} \tag{8.24}$$

Example 8.4 For example, consider a 1-m cable, and a current probe with a transfer impedance of 15 dBΩ. In order to comply with the FCC Class B radiated emission limit ($d = 3$ m) at 30 MHz of 40 dBμV/m, Eq. (8.24) gives a probe voltage of

$$\begin{aligned} |\hat{V}_{SA}|_{\mathrm{dB\mu V}} &= 40\ \mathrm{dB\mu V/m} + 15\ \mathrm{dB\Omega} + 20\log_{10}(3) \\ &\quad - 20\log_{10}(30) - 20\log_{10}(1) + 4.041 = 39\ \mathrm{dB\mu V} \end{aligned}$$

as before.

In fact, a calibration chart for the specific probe and regulatory limit to be met can be prepared from (8.24), so that one only needs to compare the spectrum analyzer reading to this level in order to determine if that cable will produce radiated emission problems. For example, considering meeting the FCC Class B limit ($d = 3$ m, 40 dBμV/m from 30 to 88 MHz, 43.5 dBμV/m from 88 to 216 MHz, and 46 dBμV/m from 216 to 960 MHz). If we use the current probe whose transfer impedance is 15 dBΩ, we can determine that the spectrum analyzer reading must be below the limits shown in Fig. 8.11. Note that this current probe is usable up to only approximately 100 MHz. The user must be instructed to scale the values of this chart by the ratio of the actual cable length to a 1 m length by subtracting $20\log_{10}$ (actual length).

8.1.5 Experimental Results

In order to illustrate the relative magnitudes of differential- and common-mode current emissions, as well as to illustrate the prediction accuracy of the above models, we will show experimental results in this section. The reader is again cautioned that the experimental configurations tested are quite

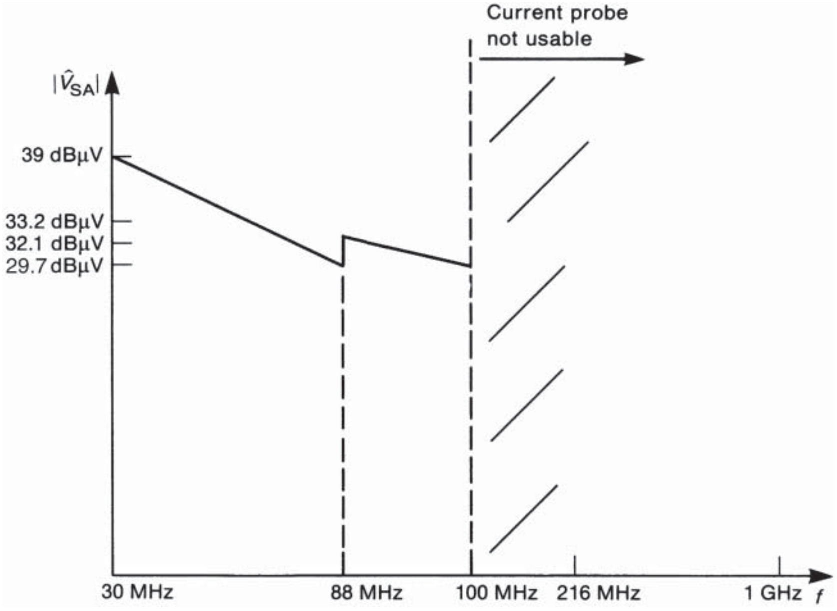

FIGURE 8.11 Illustration of the preparation of a diagram to be used with a current probe and a spectrum analyzer to indicate when a measured cable current would cause emissions exceeding the FCC Class B limits.

simple and may not represent realistic and more complicated electronic products. This is intentional. In order to investigate the accuracy of the prediction models, it is important that the experimental configuration be simple enough so that additional radiation mechanisms will not cloud the interpretation of the data. These data will show that (1) the simple radiated emission prediction models derived in this section are quite accurate *given the currents*, (2) a current probe can be used to provide accurate values of common-mode currents on cables and PCB lands, and (3) a ferrite toroid can be an effective method of reducing the radiated emissions from common-mode currents.

The first experiment is illustrated in Fig. 8.12 and was originally described in [4]. A 10 MHz oscillator packaged in a standard 14-pin dual inline package (DIP) drives a 74LS04 inverter gate. The output of this gate is attached to the input of another 74LS04 inverter gate via a 1 m, three-wire ribbon cable as shown in Fig. 8.12a. The ribbon cable wires are 28-gauge (7 × 32) and have center-to-center separations of 50 mils. The middle wire carried the 10 MHz trapezoidal pulse train output of the driven gate to the gate at the other end, which serves as an active load. An outer wire carries the +5 V power for the inverter active load, and the other outer wire serves as the return for both signals. The +5 V power is derived from a 9 V battery that powers a 7805 regulator as shown in Fig. 8.12b. This provides a compact 5 V source. There is no external connection to the commercial power system. This was intentional, so that radiation from the power cord of a power supply would not contaminate the measurements.

The radiated emissions were measured in a semi-anechoic chamber that is regularly used for developmental and compliance testing. The measured data to be shown were obtained over the

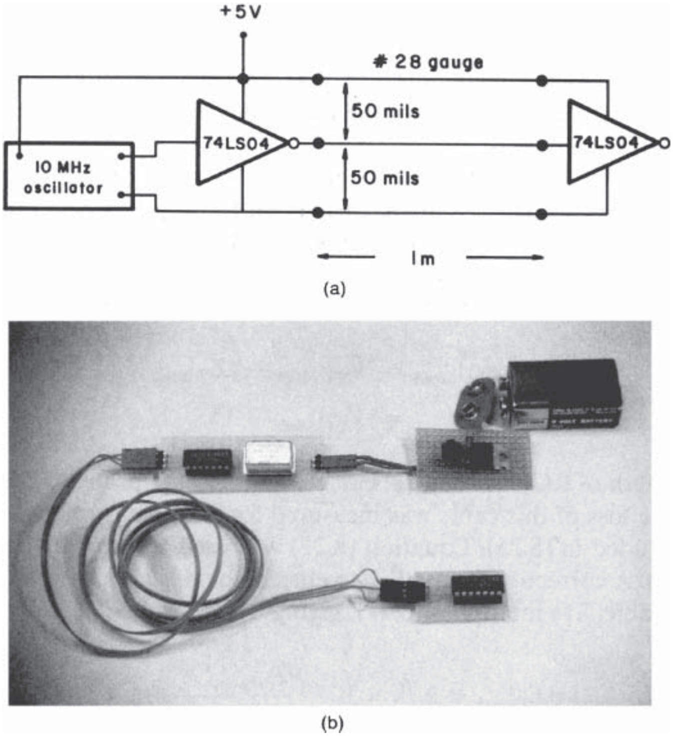

FIGURE 8.12 An experiment to assess the importance of common-mode currents on cables in the total radiated emissions of the cable: (a) schematic of the device tested. Source: Paul and Bush [4]/IEEE; (b) photograph of the device.

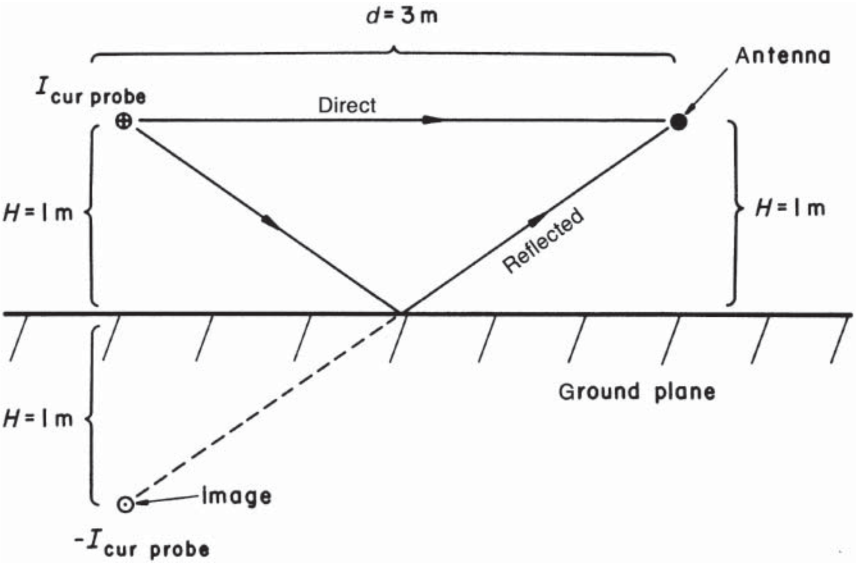

FIGURE 8.13 Physical dimensions of the measurement site, including the effect of the cable image.

frequency range of 30–200 MHz using a biconical antenna. The antenna and the ribbon cable were positioned parallel to the chamber floor, and both were 1 m above the floor, as shown in Fig. 8.13. The separation between them was 3 m. The antenna was oriented parallel to the ribbon cable in order to obtain the maximum radiated emissions from the cable.

A current probe having a probe transfer impedance of 15 dBΩ was used to measure the common-mode current on the cable for the prediction of the common-mode current radiated emissions. The current probe was placed at the midpoint of the cable, and the spectrum of the common-mode current at that point as measured with a spectrum analyzer is shown in Fig. 8.14. Eq. (8.22) was used to relate the spectrum analyzer voltage reading to the common-mode current as

$$\begin{aligned}|\hat{I}_{\text{probe}}|_{\text{dB}\mu\text{A}} &= |\hat{V}_{SA}|_{\text{dB}\mu\text{V}} + \text{cable loss}_{\text{dB}} - |\hat{Z}_T|_{\text{dB}\Omega}\\ &= |\hat{V}_{SA}|_{\text{dB}\mu\text{V}} + \text{cable loss}_{\text{dB}} - 15\ \text{dB}\Omega \end{aligned} \tag{8.25}$$

A 40 ft. length of RG55U coaxial cable connected the probe to the spectrum analyzer. The loss of this cable was measured for each measurement frequency and was included in (8.25). Note that the cable loss must be *added* to the spectrum analyzer, $|\hat{V}_{SA}|_{\text{dB}\mu\text{V}} + \text{cable loss}_{\text{dB}}$, in order to translate the voltage measured at the spectrum analyzer to the base of the current probe. Eq. (8.21) was used to provide the predicted electric fields. A correction factor $\hat{F}_{GP}$ to correct for reflections from the ground plane (see Table 7.1) multiplies (8.21), giving

$$|\hat{E}_C|_{\max} = 6.28 \times 10^{-7} \frac{|\hat{I}_{C,\text{net}}| fL}{d} \hat{F}_{\text{GP}} \tag{8.26}$$

Combining these gives the electric field in dBμV/m as

$$|\hat{E}_C|_{\text{dB}\mu\text{V/m}} = |\hat{V}_{SA}|_{\text{dB}\mu\text{V}} + \text{cable loss}_{\text{dB}} - |\hat{Z}_T|_{\text{dB}\Omega} + 20\log_{10} f_{\text{MHz}} + |\hat{F}_{GP}|_{\text{dB}} - 13.58 \tag{8.27}$$

where $f = f_{\text{MHz}} \times 10^6$, the line length is 1 m, so $20 \log_{10}(L = 1\text{ m}) = 0$, and $d = 3$ m.

The oscillator has a fundamental frequency of 10 MHz, so only harmonics of 10 MHz will appear in the radiated emissions. A plot of the radiated emissions is shown in Fig. 8.15. The predicted

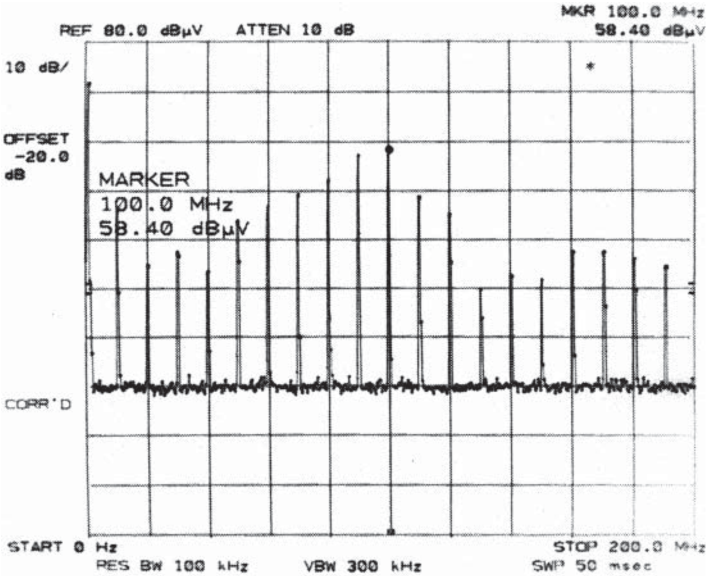

FIGURE 8.14 Measured common-mode current spectral content at the center of the cable.

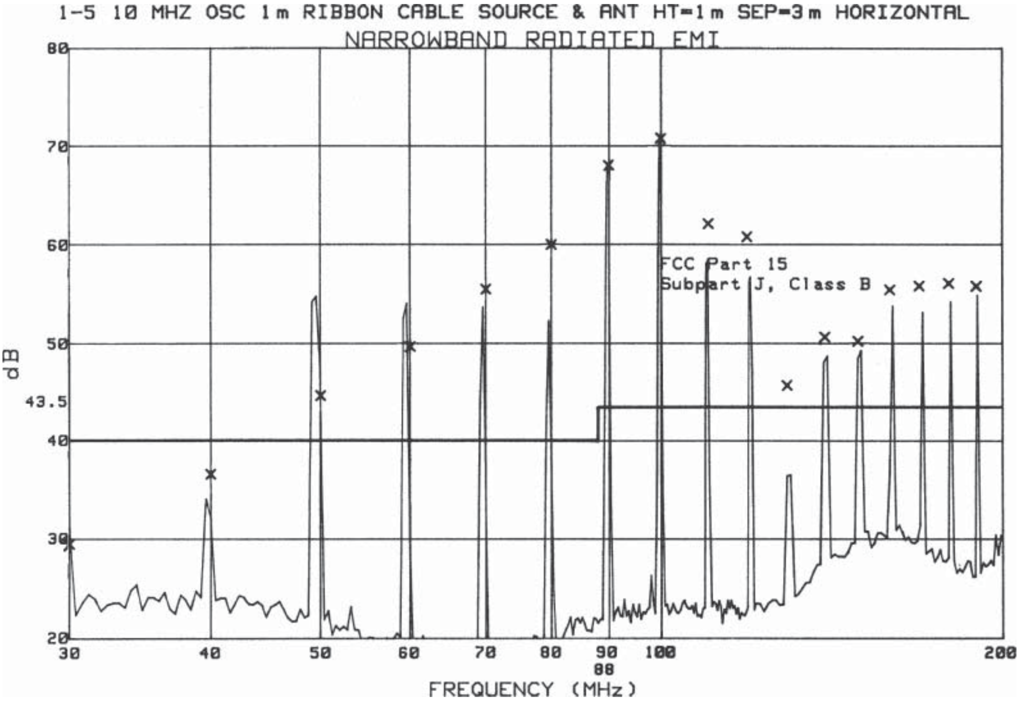

FIGURE 8.15 Measured and predicted emissions of the device of Fig. 8.12.

TABLE 8.1 I_{probe} **versus Position on Cable (*f* = 100 MHz)**

Position of Current Probe from Oscillator End (cm)	$I_{\text{probe, dB}\mu\text{A}}$
5	38.7
10	40.7
15	41.9
20	42.6
25	43.4
30	44.3
35	44.7
40	45.1
45	44.7
50	44.4
55	43.9
60	43.2
65	41.9
70	41.1
75	40.2
80	39.5
85	38.4
90	35.5
95	34.0

values using (8.27) are shown on the plot and are denoted by X. The predictions are within 3 dB of the measured data, except at 50, 80, and 130 MHz.

The common-mode current was then measured at 5 cm intervals along the cable. Table 8.1 shows the levels at these measurement points for the 10th harmonic of 100 MHz. The maximum current of 45.1 dBμA measured at 40 cm corresponds to a current of 180 μA. Note that even though the cable length is $\lambda_0/3$ at 100 MHz, the common-mode current does not display an extreme variation with position, so that the assumption of a constant current along the cable that is inherent in (8.26) seems to be a reasonable assumption. Results obtained in [2] tend to confirm this behavior of common-mode currents.

Example 8.5 Calculate the radiated electric field at 100 MHz as plotted in Fig. 8.15. The current probe is attached to the spectrum analyzer with a 40 ft. length of RG55U coaxial cable. The loss of this length of cable is approximately 1 dB at 100 MHz (2.5 dB/100 ft. at 100 MHz). From Table 7.1 of the preceding chapter, the correction factor for the ground plane (horizontal polarization and 1 m height) at 100 MHz is 0.78 dB. The common-mode current at the midpoint of the cable at 100 MHz is given in Table 8.1 as 44.4 dBμA. From Fig. 8.14, the spectrum analyzer reads 58.4 dBμV at 100 MHz. These are related as

$$|\hat{I}_{\text{probe}}|_{\text{dB}\mu\text{A}} = |\hat{V}_{SA}|_{\text{dB}\mu\text{V}} + \text{cable loss}_{\text{dB}} - |Z_T|_{\text{dB}\Omega}$$

or

$$44.4\ \text{dB}\mu\text{A} = 58.4\ \text{dB}\mu\text{V} + 1\ \text{dB} - 15\ \text{dB}$$

which checks. Hence from (8.27), we have

$$
\begin{aligned}
|\hat{E}_C|_{\text{dB}\mu\text{V/m}} &= \underbrace{|\hat{V}_{SA}|_{\text{dB}\mu\text{V}}}_{58.4} + \underbrace{\text{cable loss}_{\text{dB}}}_{1} - \underbrace{|\hat{Z}_T|_{\text{dB}\Omega}}_{15} \\
&\quad + \underbrace{20\log_{10} f_{\text{MHz}}}_{40} + \underbrace{|\hat{F}_{GP}|_{\text{dB}}}_{0.78} - 13.58 \\
&= 71.6\,\text{dB}\mu\text{V/m}
\end{aligned}
$$

which is the value plotted in Fig. 8.15 at 100 MHz.

Review Exercise 8.1 Compute the radiated electric field for this experiment at 180 MHz and compare to the value plotted in Fig. 8.15.

***Answer*:** **57.9** $\text{dB}\mu\text{V/m}(|\hat{\boldsymbol{V}}_{\boldsymbol{SA}}|_{\text{dB}\mu\text{V}} = \mathbf{36}$, cable loss $= \mathbf{1}$ dB, $|\hat{\boldsymbol{F}}_{\boldsymbol{GP}}|_{\text{dB}} = 4.4$ dB, $|\hat{Z}_T|_{\text{dB}\Omega} = \mathbf{15}$).

In order to confirm that the dominant radiated emission was due to common-mode currents and that the differential-mode current emissions were smaller than these, the 74LS04 load at the far end of the cable was removed and the radiated emissions remeasured. The results are shown in Fig. 8.16. Comparing Figs. 8.15 and 8.16, we see that the levels are essentially the same with or without the load, which tends to further confirm that the *common-mode currents are the dominant radiation mechanism*. As a further confirmation of this, 4 turns of the cable were wound through a toroid of NiZn material. The radiated emissions with the toroid inserted and the load attached along with the common-mode current at the midpoint of the cable was remeasured. The measured data along with the predictions are shown in Fig. 8.17. Comparing Figs. 8.17 and 8.15, we observe that the insertion of the toroid has reduced the radiated emissions by over 20 dB at some frequencies. Also, the emissions can be reliably predicted using (8.27) and the measured common-mode current.

The next set of experimental results concern the emissions from a printed circuit board (PCB) and were described in [5]. The reader may be willing to accept the fact as demonstrated above that common-mode currents tend to be the dominant radiation mechanism for long cables. However, the following set of data show that they may also be the dominant radiation mechanism for much shorter lands on PCBs. A parallel pair of 1 oz. copper lands 25 mils in width and 6 in. in length were etched on a glass epoxy board as shown in Fig. 8.18. The center-to-center spacing was 380 mils, and the board thickness was 62 mils. The characteristic impedance of this configuration was computed to be 342 Ω using a numerical method. A load resistance of 330 Ω was used to provide a matched load. This was confirmed by time-domain measurements of the input and output voltages of the line. The same 10 MHz DIP oscillator and 5 V power supply used in the previous experiment were used to drive this line. This provided a 10 MHz trapezoidal pulse train having a 50% duty cycle, a risetime of approximately 4 ns, and a falltime of approximately 2 ns. It is important to note again that there was no connection to the commercial power system. The entire setup was quite compact and symmetric. One might therefore expect that common-mode currents on the structure would be virtually nonexistent because of this compact size and the symmetry. The measured data will show that is not the case. The radiated emissions and the common-mode current on the lands were measured exactly as for the previous experiment. The measured emissions and

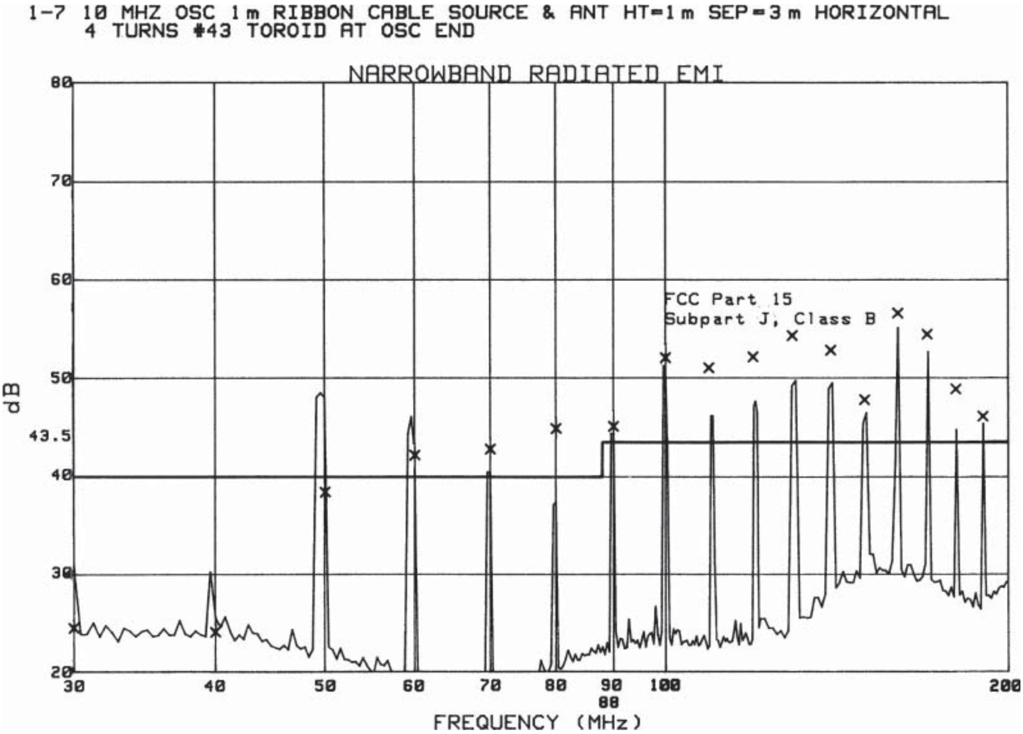

FIGURE 8.16 Measured and predicted emissions of the device of Fig. 8.12, with the load removed. The predicted emissions are virtually unchanged from those with the load attached, illustrating the dominance of common-mode current emissions.

the predictions using (8.27) are shown in Fig. 8.19. Note that using (8.27) and the common-mode currents measured with a current probe at the midpoint of the lands provides reasonable predictions of the radiated emissions. The differential-mode currents were measured with this current probe (the current probe was placed around one of the input wires) and also were predicted with a transmission-line model. The predictions using the differential-mode current prediction model given in (8.12) are also shown on the plot and are some 20 dB below the measured radiated emissions. This further confirms that the radiated emission from the common-mode current is the dominant radiation mechanism.

To further confirm that common-mode currents are the dominant contributor to the radiated emissions, the 330 Ω load was removed and the radiated emissions and common-mode current remeasured. In this case, the differential-mode currents should be considerably less than with the load attached. (The differential-mode currents will not be zero for an open-circuited load due to the displacement current path between the wires.) The radiated emissions with the load removed are shown in Fig. 8.20 and are virtually the same with the load attached! Again, the predictions using measured common-mode currents and (8.27) are reasonably accurate. Finally, the 330 Ω load was reattached, and the board placed on edge with the lands in a vertical plane. The radiated emissions were remeasured and were virtually the same as in Fig. 8.19. If differential-mode current provided any significant contributions to the total radiated emissions, this latter test should show significantly lower emissions, since the differential-mode current emissions from the two lands when the board was placed on edge should cancel at the measurement antenna (see Fig. 8.5b). Such was not the case.

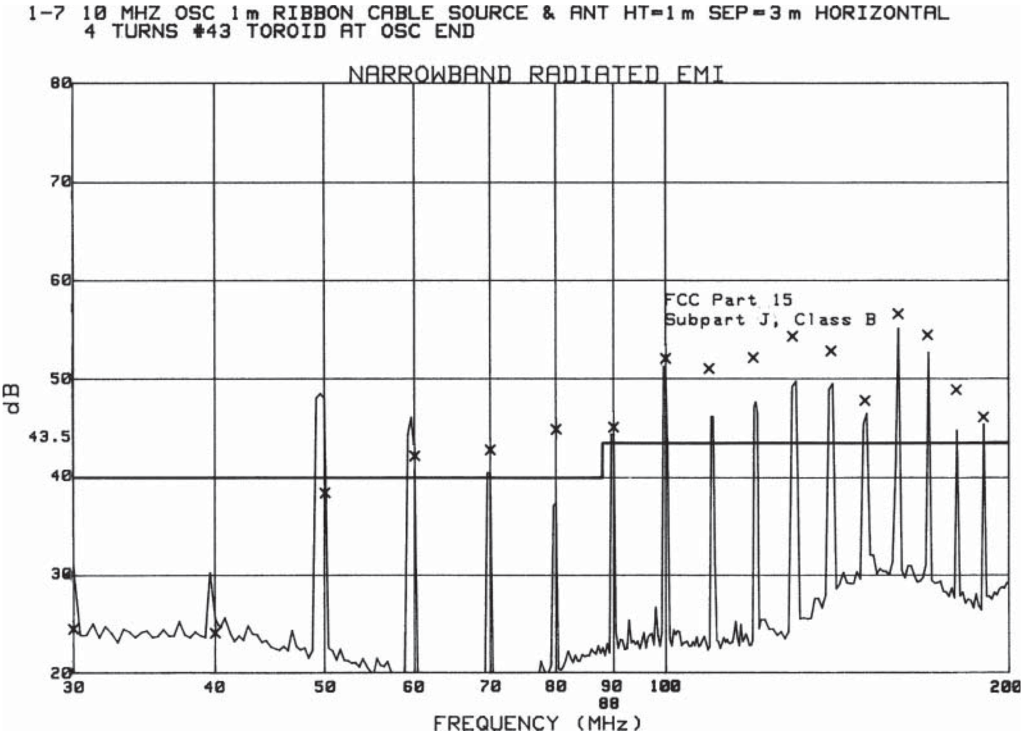

FIGURE 8.17 Measured and predicted emissions of the device of Fig. 8.12 with the cable wrapped 4 turns through a NiZn ferrite toroid, illustrating the effect of a common-mode choke on the reduction of the common-mode current radiated emissions and the dominance of those emissions.

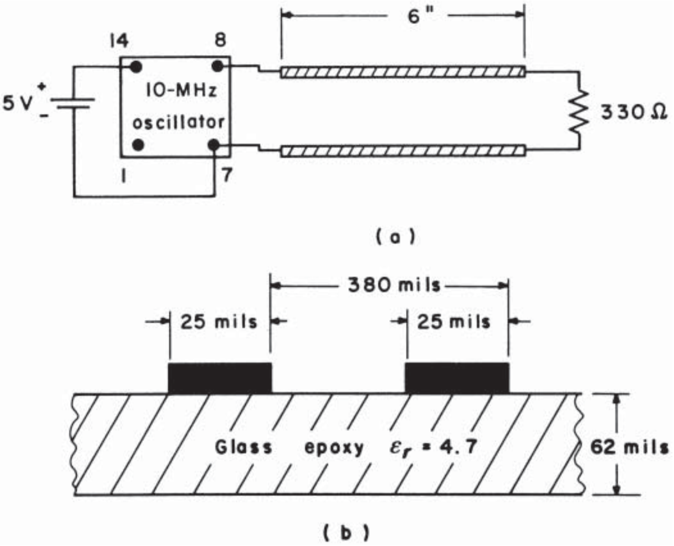
6"
14
8
1
7
10-MHz
oscillator
5 V
+
-
330 Ω
(a)
380 mils
25 mils
25 mils
Glass epoxy $\varepsilon_r = 4.7$
62 mils
(b)

FIGURE 8.18 An experiment illustrating common-mode currents on PCBs: (a) device schematic; (b) the PCB cross-sectional dimensions.

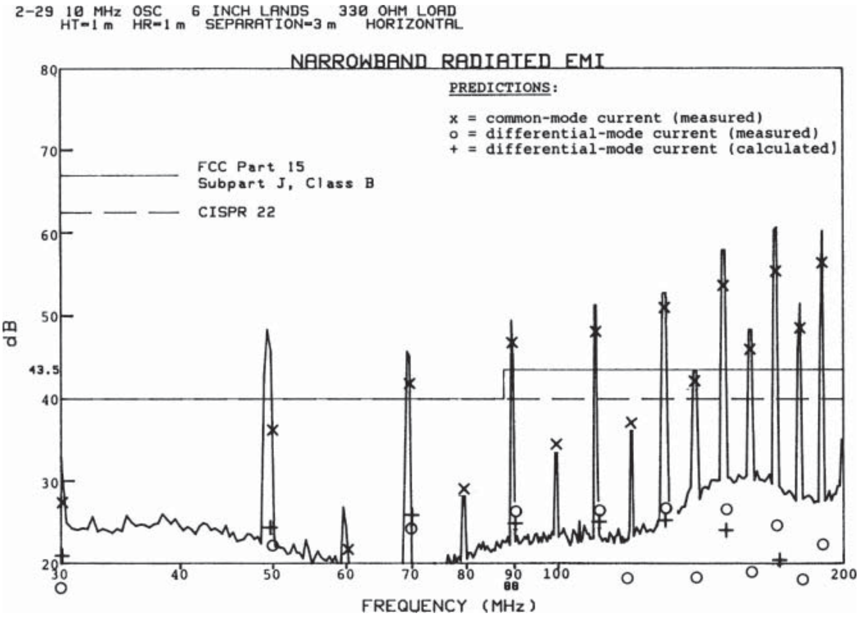

FIGURE 8.19 Measured and predicted emissions of the device of Fig. 8.18.

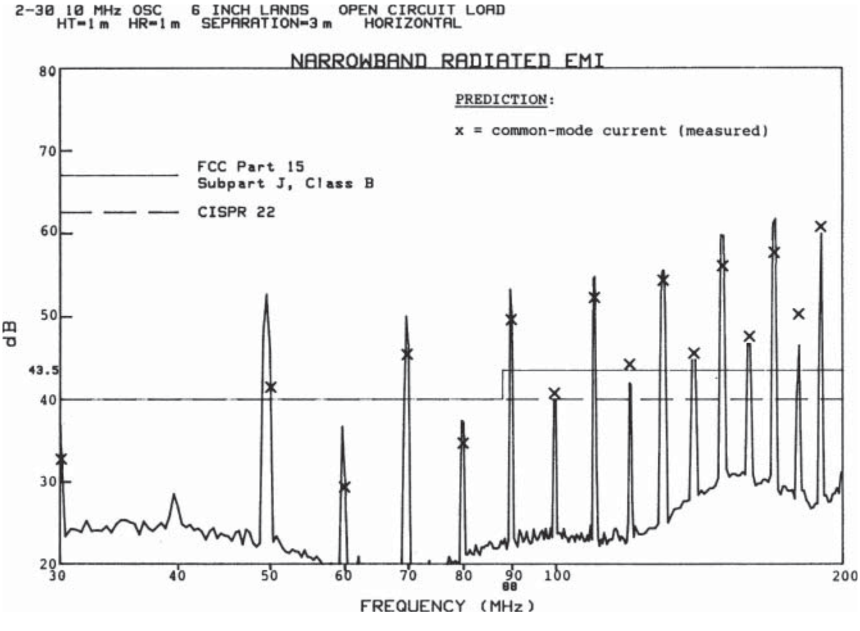

FIGURE 8.20 Measured and predicted emissions of the device of Fig. 8.18, with the load removed. The radiated emissions are virtually unchanged from those with the load attached, illustrating the dominance of common-mode current emissions.

8.2 SIMPLE SUSCEPTIBILITY MODELS FOR WIRES AND PCB LANDS

Complying with the regulatory limits on radiated (and conducted) emissions is an absolute necessity in order to be able to market a digital electronic product. However, as was pointed out previously, *simply being able to comply with regulatory emission limits does not represent a complete product design from the standpoint of EMC*. If a product exhibits susceptibility to external disturbances such as radiated fields from radio transmitters and radars or is susceptible to lightning- or electrostatic-discharge (ESD)-induced transients, then unreliable performance will result and customer satisfaction will be impacted.

The model that we will develop is a simplified version of the more exact transmission line model described in [6–14], but it will be suitable for estimation purposes. A digital computer program for the exact transmission-line model for general multiconductor lines is described in [9,14]. We consider a parallel-wire transmission of length L that has a uniform plane wave incident on it as shown in Fig. 8.21a. (The model also applies to the case of a pair of parallel lands on a PCB, with the

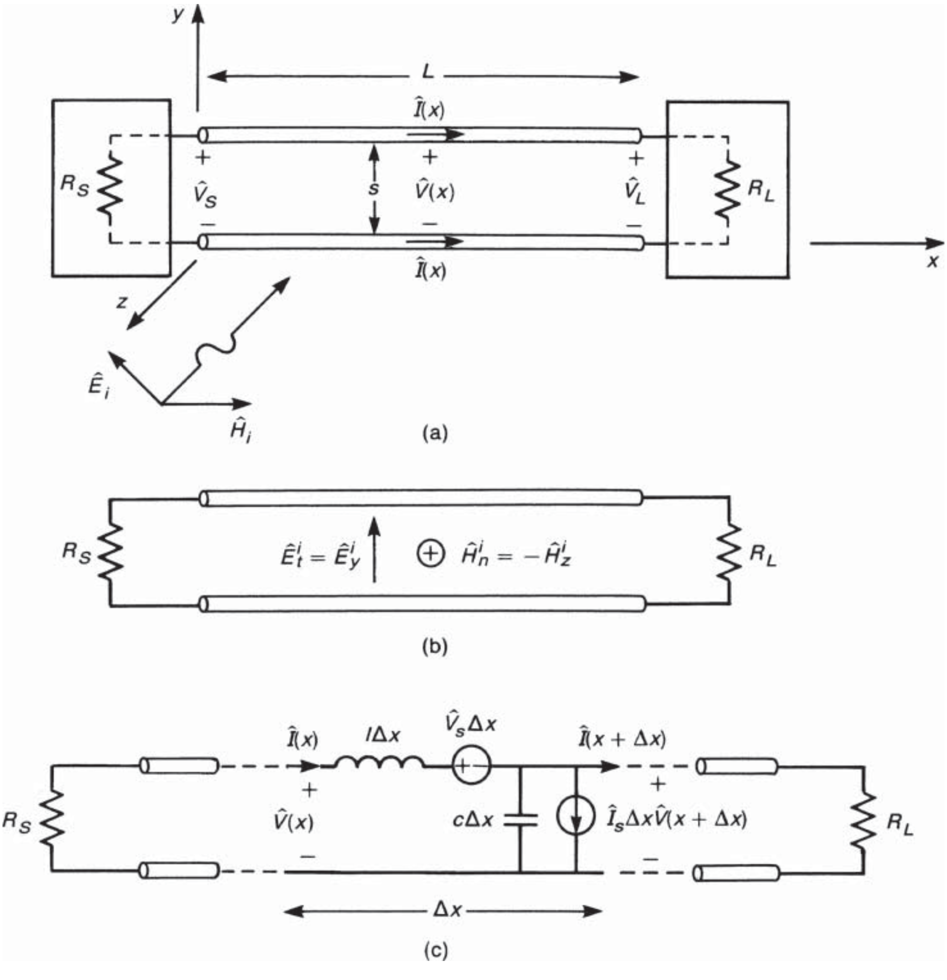
y
L
$\hat{I}(x)$
R_S
+
$\hat{V}_S$
−
s
+
$\hat{V}(x)$
−
+
$\hat{V}_L$
−
R_L
$\hat{I}(x)$
x
z
$\hat{E}_i$
$\hat{H}_i$
(a)
R_S
$\hat{E}_t^i = \hat{E}_y^i$
$\hat{H}_n^i = -\hat{H}_z^i$
R_L
(b)
$\hat{I}(x)$
$l\Delta x$
$\hat{V}_s\Delta x$
$\hat{I}(x+\Delta x)$
R_S
+
$\hat{V}(x)$
−
$c\Delta x$
$\hat{I}_s\Delta x\hat{V}(x+\Delta x)$
+
−
R_L
Δx
(c)

FIGURE 8.21 Modeling a two-conductor line to determine the terminal voltages induced by an incident electromagnetic field: (a) problem definition; (b) effects of the transverse electric field component and the normal magnetic field component; (c) a per-unit-length equivalent circuit.

appropriate change in two parameters.) The wires are separated a distance s and have load resistances R_S and R_L. In order to quantify our results, we will place the two wires in the xy plane, with R_S located at $x = 0$ and R_L at $x = L$. The wires are parallel to the x axis. Our interest is in predicting the terminal voltages $\hat{V}_S$ and $\hat{V}_L$ given the magnitude of a sinusoidal, steady-state incident electric field $\hat{V}_S$ of a uniform plane wave, its polarization, and the direction of propagation of the wave. Two components of the incident wave contribute to the induced voltages. These are the *component of the incident electric field that is transverse to the line axis*, $\hat{E}_t^i = \hat{E}_y^i$ (in the plane of the wires and perpendicular to them and directed upward), and the *component of the incident magnetic field that is normal to the plane of the wires*, $\hat{H}_n^i = -\hat{H}_z^i$ (perpendicular to the plane of the wires and into the page), as shown in Fig. 8.21b. The line will possess per-unit-length parameters of inductance l and capacitance c, as were discussed in Chapter 4. For the parallel-wire line having wires of radius r_w, these per-unit-length parameters were derived in Chapter 4 and are

$$l = \frac{\mu_0}{\pi} \ln\left(\frac{s}{r_w}\right) \quad \text{in H/m} \tag{8.28a}$$

$$c = \frac{\pi \varepsilon_0 \varepsilon_r}{\ln\left(\frac{s}{r_w}\right)} \quad \text{in F/m} \tag{8.28b}$$

where ε_r is the relative permittivity of the surrounding medium (assumed homogeneous and nonferromagnetic). The essential modification required for the following model to apply to two parallel lands on a PCB is the use of the proper per-unit-length parameters of capacitance and inductance. Those elements are also given in Chapter 4. A model of a Δx section of the line is shown in Fig. 8.21(c), where the per-unit-length parameters are multiplied by the length of the section, Δx. The per-unit-length induced sources $\hat{V}_s$ and $\hat{I}_s$ are generated by the incident wave according to the following considerations. First, consider the normal component of the incident magnetic field intensity vector $\hat{H}_n^i$. Faraday's law (see Appendix B) shows that this will induce an emf in the loop bounded by the wires as

$$\begin{aligned} \text{emf} &= j\omega \int_s \hat{B}_n^i ds \\ &= j\omega\, \mu_0 \int_s \hat{H}_n^i ds \\ &= j\omega\mu_0 \Delta x \int_{y=0}^{s} \hat{H}_n^i dy \end{aligned} \tag{8.29}$$

This induced emf can be viewed as an induced voltage source whose polarity, according to Lenz' law, is such that it tends to produce a current and associated magnetic field that opposes any change in the incident magnetic field. Thus, for the incident magnetic field intensity vector, normal to and into the page, the positive terminal of the source will be on the left. For a Δx section, the per-unit-length source will be given by dividing the result in (8.29) by Δx to give

$$\hat{V}_s(x) = j\omega\mu_0 \int_{y=0}^{s} \hat{H}_n^i dy \tag{8.30}$$

The per-unit-length induced current source $\hat{I}_s$ is directed in the $-y$ (downward) direction and is due to the component of the incident electric field intensity vector that is transverse to the line and directed in the $+y$ direction. The result is derived in [6–14] and becomes

$$\hat{I}_s(x) = j\omega c \int_{y=0}^{s} \hat{E}_t^i dy \tag{8.31}$$

This source is the dual of $\hat{V}_s$. The result for the induced current source in (8.31) is reasonable to expect as illustrated in Fig. 8.22. The transverse incident electric field will induce a voltage $\int_{y=0}^{s} \hat{E}_t^i dy$ in the form of a voltage source with its positive voltage terminal at the bottom. This is in series with the per-unit-length capacitance whose impedance is $(1/j\omega c)$ Ω. Converting this to a Norton equivalent, we get a current source (pointing down) of $\hat{I}_s = j\omega c \int_{y=0}^{s} \hat{E}_t^i dy$ in parallel with the per-unit-length capacitance as shown in Fig. 8.22.

The incident fields at the position of the line may be produced by some distant antenna. These incident fields in the vicinity of the line can then be determined using the Friis transmission equation, which was derived in the previous chapter. The antenna producing these incident fields is assumed

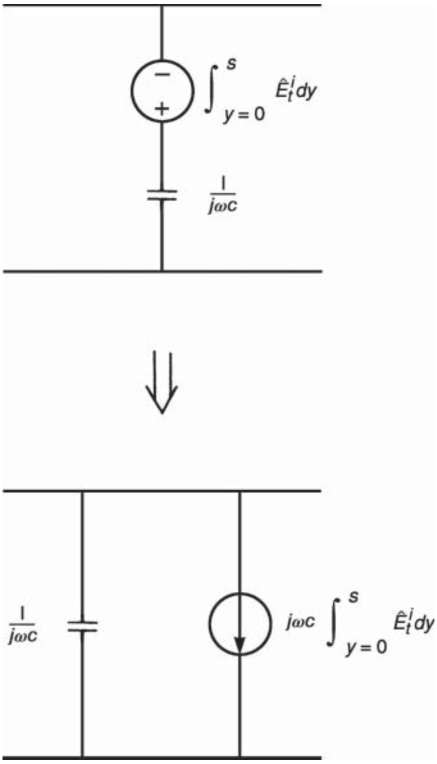
−
+
$\int_{y=0}^{s} \hat{E}_t^i dy$
$\frac{1}{j\omega c}$
$\frac{1}{j\omega c}$
$j\omega c \int_{y=0}^{s} \hat{E}_t^i dy$

FIGURE 8.22 Illustration of the derivation of the parallel current source.

to be transmitting a radiated power P_T, is located a distance d away, and has a gain G in the direction of the line. The incident electric field is [see (7.71) of Chapter 7]

$$|\hat{E}^i| = \frac{\sqrt{60 P_T G}}{d} \tag{8.32a}$$

The incident magnetic field, assuming a uniform plane wave, is obtained by dividing the electric field by the intrinsic impedance of free space, $n_0 = 120\,\pi\ \Omega \cong 377\ \Omega$, to give

$$|\hat{H}^i| = \frac{|\hat{E}^i|}{n_0} \tag{8.32b}$$

Example 8.6 For example, consider a half-wave dipole having a gain in the main beam of 2.15 dB (1.64 absolute), transmitting 1 kW radiated power at 100 MHz. If the line is located a distance of 3000 m from the antenna, the maximum electric and magnetic fields in the vicinity of the line are

$$|\hat{E}^i|_{\max} = \frac{\sqrt{60 \times 1000 \times 1.64}}{3000} = 0.105\ \text{V/m}$$

$$|\hat{H}^i|_{\max} = \frac{|\hat{E}^i|_{\max}}{120\pi} = 0.277\ \text{mA/m}$$

The model in Fig. 8.21 also applies to incident fields that are not uniform plane waves such as magnetic fields from nearby switching transformers, but the incident fields are more difficult to compute in this case [9].

From the per-unit-length model in Fig. 8.21c, we may derive the *transmission-line equations* that relate the voltage $\hat{V}(x)$ and current $\hat{I}(x)$ along the line. To do this, we write, from the per-unit-length equivalent circuit of Fig. 8.21c:

$$\hat{V}(x + \Delta x) + \hat{V}(x) = -j\omega l \Delta x \hat{I}(x) - \hat{V}_s(x)\Delta x \tag{8.33a}$$

$$\hat{I}(x + \Delta x) - \hat{I}(x) = -j\omega c \Delta x \hat{V}(x + \Delta x) - \hat{I}_s(x)\Delta x \tag{8.33b}$$

Dividing both sides by Δx and taking the limit as $\Delta x \to 0$ gives the transmission-line Eqs. [14]:

$$\frac{d\hat{V}(x)}{dx} + j\omega l \hat{I}(x) = -\hat{V}_s(x) = -j\omega\mu_0 \int_{y=0}^{s} \hat{H}_n^i dy \tag{8.34a}$$

$$\frac{d\hat{I}(x)}{dx} + j\omega c \hat{V}(x) = -\hat{I}_s(x) = -j\omega c \int_{y=0}^{s} \hat{E}_t^i dy \tag{8.34b}$$

The solution to these equations is described in [6–14]. This exact solution is not necessary for estimation purposes, and we will obtain an approximate solution.

For many cases of practical interest the line length is *electrically short* at the frequency of interest; this is, $l \ll \lambda_0$. This will be the case of interest here for the purposes of estimating the induced terminal voltages. If the line length is electrically short at the frequency of interest, we may lump the distributed parameters by using one section of the form in Fig. 8.21c to represent the entire line

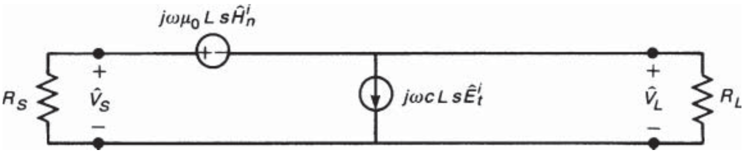

FIGURE 8.23 A simplified, lumped equivalent circuit of the pickup of incident fields for a two-conductor line that is short, electrically.

and replacing Δx with L. Thus, the per-unit-length elements and sources are multiplied by the total line length L. Although the terminal voltages can be calculated from this model for electrically short lines, we will make a final simplification that provides an extremely simple model that is valid for a wide variety of practical situations. In this simple model, we ignore the per-unit-length parameters of inductance and capacitance. Neglecting the line inductance and capacitance is typically valid so long as the termination impedances are not extreme values such as short or open circuits. In addition, since the wire separation is much less than the wire length and is therefore also electrically short, the field vectors do not vary appreciably across the wire cross section, that is, with respect to y. Therefore, the integrals in the sources ((8.30) and (8.31)) with respect to y can be replaced with the wire separation s, giving

$$\hat{V}_s L \cong j\omega\mu_0 \hat{H}_n^i A \tag{8.35a}$$

$$\hat{I}_s L \cong j\omega c \hat{E}_t^i A \tag{8.35b}$$

where A is the area of the loop:

$$A = sL \tag{8.36}$$

The simplified model is shown in Fig. 8.23. From this model, it is a simple matter to compute the induced terminal voltages, using superposition, as

$$\hat{V}_S = \frac{R_S}{R_S + R_L} j\omega\mu_0 Ls\hat{H}_n^i - \frac{R_S R_L}{R_S + R_L} j\omega c Ls\hat{E}_t^i \tag{8.37a}$$

$$\hat{V}_L = -\frac{R_L}{R_S + R_L} j\omega\mu_0 Ls\hat{H}_n^i - \frac{R_S R_L}{R_S + R_L} j\omega c Ls\hat{E}_t^i \tag{8.37b}$$

This is a particularly simple model that will yield useful estimations of the effects of incident fields, as the following examples show.

Example 8.7 Consider, as a first example, the 1 m ribbon cable shown in Fig. 8.24a. The wires are 28 gauge, 7 × 36 ($r_w = 7.5$ mi), and are separated by 50 mils. The termination impedances are $R_S = 50\ \Omega$ and $R_L = 150\ \Omega$. The characteristic impedance of this cable is

$$\begin{aligned} Z_C &= \sqrt{\frac{l}{c}} \\ &= \frac{1}{\pi}\sqrt{\frac{\mu_0}{\varepsilon_0}} \ln\left(\frac{s}{r_w}\right) \\ &= 120 \ln\left(\frac{s}{r_w}\right) \\ &= 228\ \Omega \end{aligned}$$

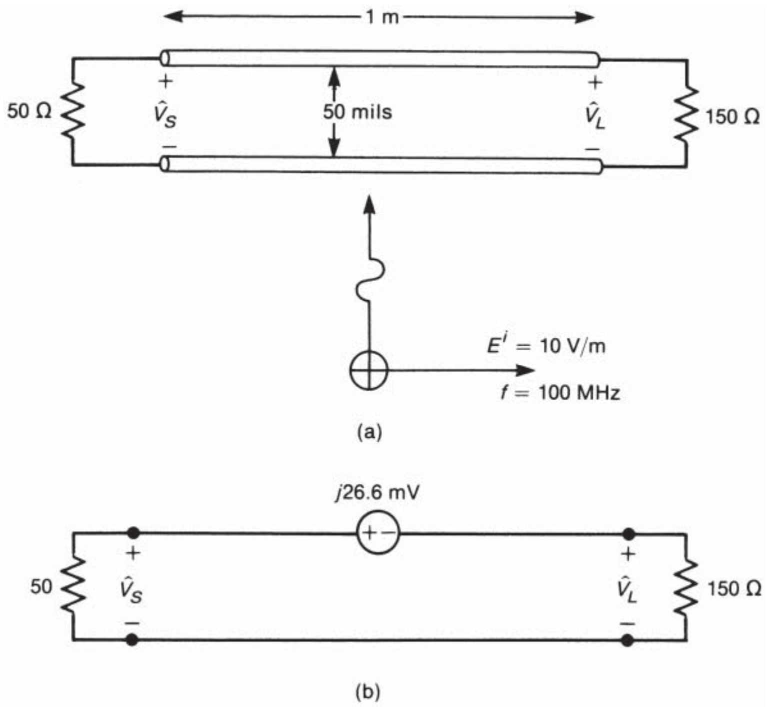

FIGURE 8.24 An example illustrating the computation of induced voltages for a 10 V/m, 100 MHz incident uniform plane wave with broadside incidence: (a) problem definition; (b) the equivalent circuit.

and we have ignored the wire dielectric insulation, $\varepsilon_r = 1$. Thus, the termination impedances are less than the characteristic resistance of the line. They are therefore classified as "low-impedance loads." The line incident uniform plane wave has a frequency of 100 MHz and is traveling in the *xy* plane in the *y* direction and is said to be incident "broadside" to the line. The line is $\lambda_0/3$ at 100 MHz. This is probably marginal for the line to be considered electrically short, and a transmission-line model should perhaps be used. For illustration purposes, we will assume that the line is electrically short and use the simplified model in Fig. 8.23. The electric field intensity vector has a magnitude $E^i = 10$ V/m and is polarized in the *x* direction. The magnetic field intensity vector is therefore directed in the negative *z* direction (into the page) according to the properties of uniform plane waves and is given $H^i = E^i/n_0 = 10/120\pi = 26.5$ mA/m. Thus, the component of the electric field transverse to the line is zero, and the component of the magnetic field that is normal to the plane of the wires is the total magnetic field vector. Therefore, the induced sources are obtained from (8.35) as

$$\begin{aligned}\hat{V}_s L &= j\omega\mu_0 \hat{H}_n^i A \\ &= j \times 2\pi \times 10^8 \times 4\pi \times 10^{-7} \times \frac{E^i}{\eta_0} \times 1 \times 1.27 \times 10^{-3} \\ &= j26.6\,\text{mV}\end{aligned}$$

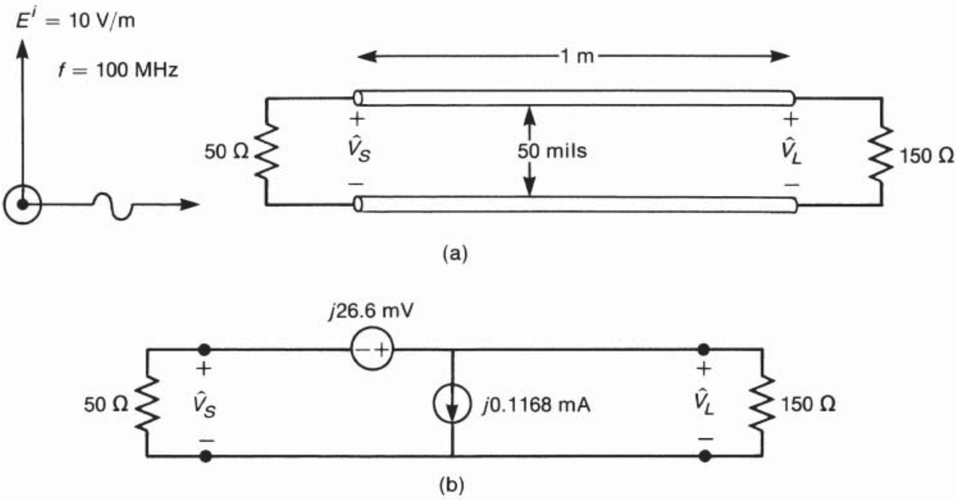

FIGURE 8.25 An example illustrating the computation of induced voltages for a 10 V/m, 100 MHz incident uniform plane wave with endfire incidence: (a) problem definition; (b) the equivalent circuit.

Because there is no component of the electric field that is transverse to the line axis, the current source is absent. The equivalent circuit is shown in Fig. 8.24b, from which we calculate (by voltage division)

$$\begin{aligned}\hat{V}_s &= \frac{50}{50+150}\, j26.6\,\text{mV}\\ &= j6.65\,\text{mV}\\ \hat{V}_L &= -\frac{50}{50+150}\, j26.6\,\text{mV}\\ &= -j19.95\,\text{mV}\end{aligned}$$

Example 8.8 As a second example, consider the same ribbon cable as before but with a different direction of incidence of the wave, as shown in Fig. 8.25a. The wave is propagating in the x direction, along the line axis, and the electric field intensity vector is polarized in the y direction (transverse to the line). The magnetic field intensity vector is therefore directed in the z direction (out of the page) and is normal to the plane of the wires. Therefore, the equivalent sources are given by

$$\begin{aligned}\hat{V}_S L &= j\omega\mu_0 \hat{H}_n^i A\\ &= j\times 2\pi\times 10^8 \times 4\pi\times 10^{-7}\times \frac{E^i}{\eta_0}\times 1\times 1.27\times 10^{-3}\\ &= j26.6\,\text{mV}\end{aligned}$$

$$
\begin{aligned}
\hat{I}_s L &= j\omega c \hat{E}_t^i A \\
&= j\omega \frac{\pi \varepsilon_0 \varepsilon_r}{\ln(s/r_w)} E^i L s \\
&= j2\pi \times 10^8 \times 14.64\ \mathrm{pF/m} \times 10\ \mathrm{V/m} \times 1 \times 1.27 \times 10^{-3} \\
&= j0.1168\ \mathrm{mA}
\end{aligned}
$$

The equivalent circuit is shown in Fig. 8.25b. Note the polarity of the equivalent voltage source. The positive terminal of this source is at the right because the incident magnetic field is directed out of the page. The terminal voltages are given (again by superposition) as

$$
\begin{aligned}
\hat{V}_S &= -\frac{50}{50+150}\, j26.6\ \mathrm{mV} - \frac{50 \times 150}{50+150}\, j0.1168\ \mathrm{mA} \\
&= -j6.65\ \mathrm{mV} - j4.38\ \mathrm{mV} \\
&= -j11.03\ \mathrm{mV} \\
\hat{V}_L &= \frac{150}{50+150}\, j26.6\ \mathrm{mV} - \frac{50 \times 150}{50+150}\, j0.1168\ \mathrm{mA} \\
&= j19.95\ \mathrm{mV} - j4.38\ \mathrm{mV} \\
&= j15.57\ \mathrm{mV}
\end{aligned}
$$

Observe that because of the orientation of the incident magnetic field and the resulting equivalent voltage source, the contributions from the two equivalent sources subtract in $\hat{V}_L$ but add in $\hat{V}_S$. We will find this phenomenon to occur in crosstalk between transmission lines, which will be examined in Chapter 9.

In addition to giving estimates of the induced interference voltages, this simple model gives further insight into the coupling of an electromagnetic wave to a transmission line. Observe that the two induced sources are due to (1) the component of the incident magnetic field that is normal to the loop formed by the transmission line and (2) the component of the incident electric field that is transverse to the transmission line. If either one is zero, then the associated induced source is not present. For example, suppose that the wave is propagating in the plane of the line perpendicular to the conductors with the electric field polarized parallel to the conductors as shown in Fig. 8.26a. In this case, the H field is normal to the loop and induces source V_{ind}, but the electric field is parallel to the conductors and hence the current source is zero, $I_{ind} = 0$. Next, suppose that the wave is propagating perpendicular to the plane of the line as shown in Fig. 8.26b. Here, the H field is parallel to the loop and hence the voltage source is zero, $V_{ind} = 0$. The electric field is completely transverse, so that the current source, I_{ind}, is nonzero. Finally, consider the situation shown in Fig. 8.26c wherein the wave is propagating along the line, but the electric field vector is perpendicular to the loop and the magnetic field vector is transverse to the loop. In this case, both sources are zero, $V_{ind} = 0$ and $I_{ind} = 0$, and no interference voltage is induced across the terminals of the line. This model shows that reorienting the line (where this is feasible) such that no component of the incident magnetic field is perpendicular to the loop and no component of the incident electric field is transverse to the line will (ideally) eliminate any induced interference voltages across the terminations.

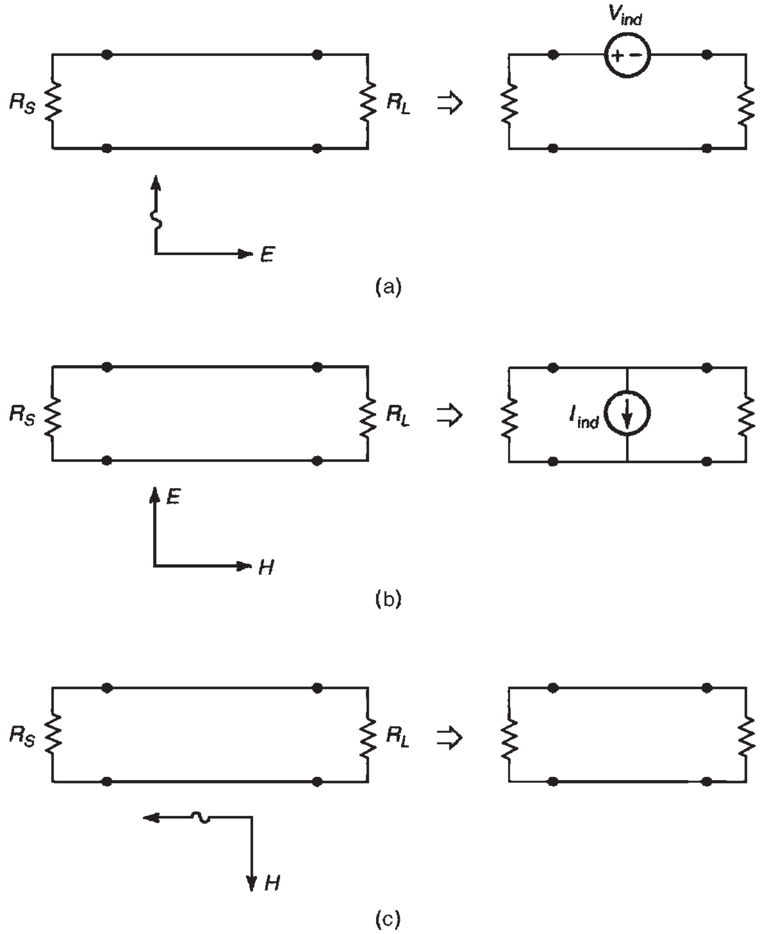

FIGURE 8.26 Illustration of the effect of the direction of incidence of the wave and polarization of its fields with respect to the transmission line: (a) propagation in the plane of the line with the electric field parallel to the line—only the voltage source is induced; (b) propagation perpendicular to the plane of the line with the electric field transverse to the line—only the current source is induced; (c) propagation along the line with the electric field perpendicular to the plane of the line—no sources are induced.

Example 8.9 An example of where this has been useful in the past has to do with susceptibility of electronic typewriters and laser printers to electrostatic discharge (ESD). The industry standard test for susceptibility to ESD consists of placing the product on a metal table and discharging an ESD gun to the table as shown in Fig. 8.27. This creates a wave that propagates across the table and induces noise in the product that may cause improper operation of it. Manufacturers of digital electronic devices such as electronic typewriters, laser printers, and computers routinely test their products for susceptibility to ESD in this fashion before shipment to customers. A particular product was having trouble passing the ESD test. In the presence of the ESD discharge, the product would “lock up” and would only operate when rebooted. That product had one printed circuit board containing the electronics, which was mounted vertically at the rear. Because the ESD table had a metal top, the boundary conditions require that at the table surface, the electric field generated by the spark must be perpendicular to the table and the associated magnetic field must be parallel to it. The pairs

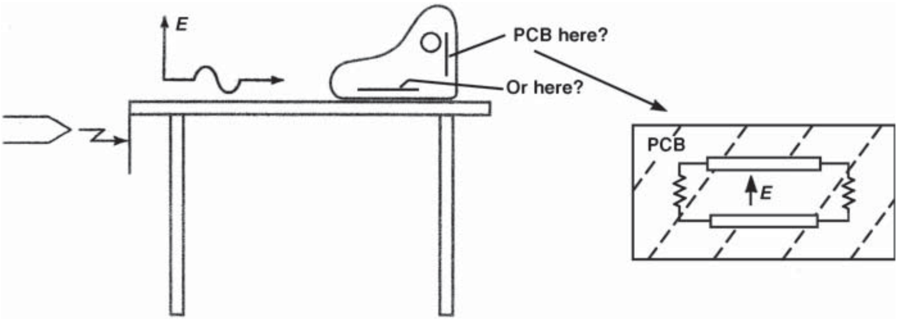

FIGURE 8.27 Illustration of the application of principles described above to design an electronic product to withstand the field of an electrostatic discharge (ESD) pulse.

of lands on the PCB were, because of the placement of the PCB in the vertical plane at the rear of the product such that the electric field was totally transverse to the transmission lines on the PCB formed by the lands. Hence, a current source was induced in those circuits, causing interference. This problem was solved in future designs by placing the PCB flat on the bottom of the product. This had the effect of the incident electric field being perpendicular to the circuits on the PCB and not transverse to them, and the magnetic field, which was parallel to the ESD table, was not normal to the plane of the circuits on the PCB. Hence, both induced sources are zero. Once this design attitude was adopted, most of the ESD problems disappeared.

Example 8.10 As another example of applying these concepts, in the previous example it was too late in the product schedule to move the electronics PCB to the bottom of the product. The electric field from the ESD propagating across the table was transverse to the lands and hence induced a source (current source in this case) in the circuits formed by two parallel lands, thereby creating interference. In order to remedy this, a conductive metal plate was placed behind and very close to the PCB as shown Fig. 8.28. According to the electromagnetic boundary conditions (see Appendix B), electric fields must be normal (perpendicular) to a good conductor since the electric field parallel to the surface of a perfect conductor must be zero. Placing the conducting plate parallel and close to the PCB caused the incident electric field in the vicinity of the PCB to bend to meet the boundary conditions on the conductive plate that is behind and close to the PCB so that now the electric field lines become perpendicular (or approximately so) to the PCB circuit loops instead of transverse to them. Now the induced current source is zero (or approximately so) and the ESD susceptibility is eliminated.

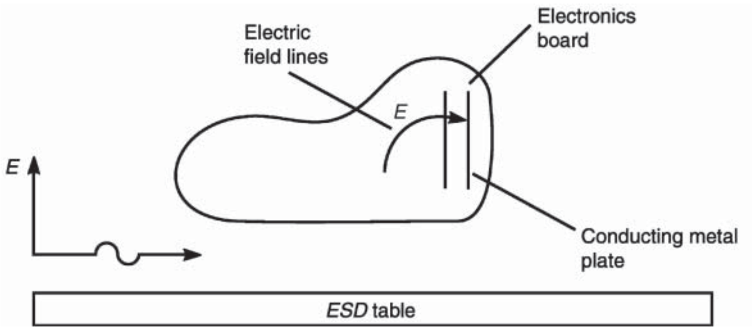

FIGURE 8.28 Use of a conductive plate behind and close to an electronics board to change the orientation of the electric field and minimize ESD pickup.

8.2.1 Experimental Results

In order to illustrate the prediction accuracy of this simple model, an experiment illustrated in Fig. 8.29 was performed and is described in [6]. A parallel-plate, transmission-line antenna was used to generate a known, uniform plane wave traveling along the line axis, with the electric field polarized in the plane of the wires, as shown in Fig. 8.29. The parallel-plate antenna consisted of six pieces of 0.125-in.-thick PC board material held in place by 1 × 4 in. Plexiglas structural members. The top and bottom plates were 29.875 in. wide by 6 ft. long, with the excess copper etched away from the edges, leaving a copper strip 25.625 in. wide. The end pieces were 3 ft. long and tapered from 25.625 in. wide at one end down to 9 in. at the other. However, the copper was etched away, leaving a triangular shape having a 25.625 in. base and a 3 ft. height. All parts of the antenna were held together by large nylon screws (1/4 × 20). Wideband baluns at each end of the antenna provided a balanced structure. The antenna was driven with a wideband power amplifier connected to a frequency synthesizer as a source. A small field-strength meter, optically coupled to the power amplifier, completed a feedback loop and kept the electric field within the line constant at 1 V/m.

The transmission line to be tested consisted of a 1.5 m length of Belden 8285 twin lead, whose characteristic resistance is approximately 300 Ω ($c = 11.8$ pF/m). One end was terminated with

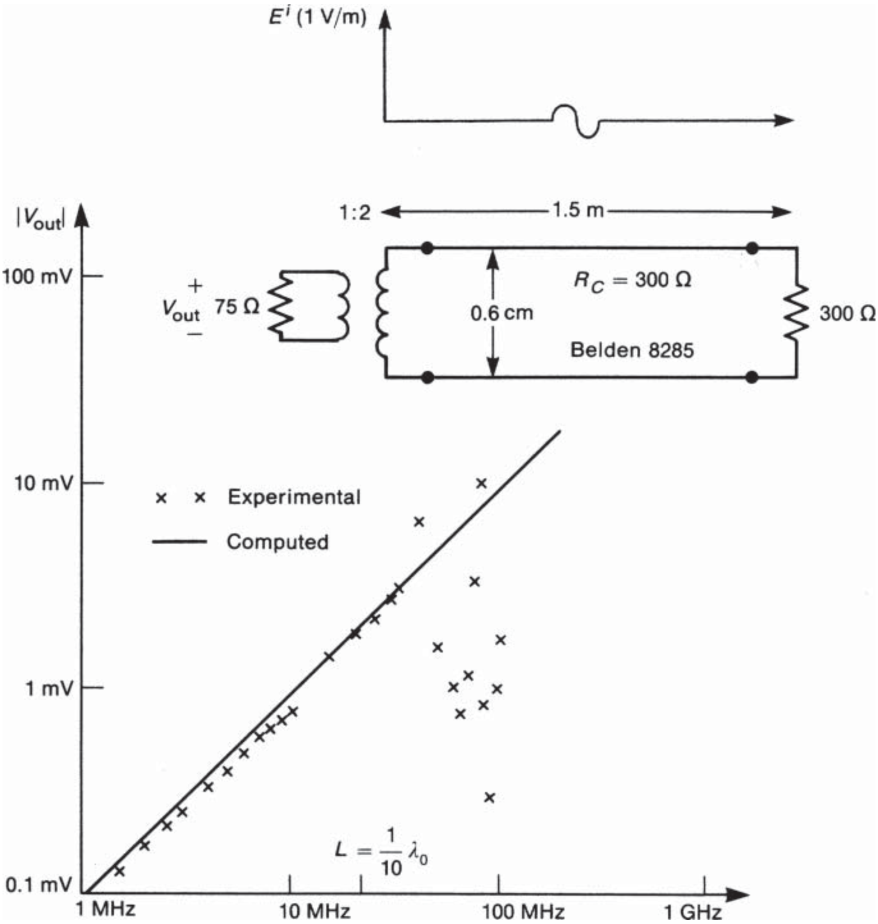

FIGURE 8.29 Measured and predicted results for incident field pickup of a two-conductor line.

a 300 Ω resistor, whereas the other was connected to a 2 : 1 wideband balun. The output of the balun was terminated in 75 Ω. The induced voltage across this side of the balun was measured (see Fig. 8.29).

The transmission line was placed midway between the upper and lower plates of the parallel-plate antenna, with the plane of the two wires perpendicular to the walls of the antenna and on the axis of the direction of propagation. Thus, the incident wave propagated along the line axis, with the electric field intensity vector in the plane of the wires. A Hewlett-Packard 8405 Vector Voltmeter was used to measure the induced voltage across the 75 Ω of the balun. Since this is a relatively high-impedance instrument, the balun at the measured end of the line was terminated with a 75 Ω feedthrough resistor.

These data are shown in Fig. 8.29 along with the predictions of the simple model. The 75 Ω termination reflected through the balun presented a matched 300 Ω load to this end of the transmission line. The received voltage at this end as predicted by the model is reflected through the balun by a factor of 1/2 to give a received voltage of

$$\begin{aligned}
\hat{V}_s &= \frac{1}{2}\left(-\frac{300}{300+300}j\omega\mu_0 Ls\hat{H}_n^i - \frac{300\times 300}{300+300}j\omega cLs\hat{E}_t^i\right)\\
&= \frac{1}{2}\left(-\frac{300}{300+300}j\omega\mu_0 Ls\frac{\hat{E}_t^i}{\eta_0} - \frac{300\times 300}{300+300}j\omega cLs\hat{E}_t^i\right)\\
&= \frac{1}{2}j\omega Ls\hat{E}_t^i\left(-\frac{300}{300+300}\frac{\mu_0}{\eta_0} - \frac{300\times 300}{300+300}c\right)\\
&= \frac{1}{2}j2\pi f\times 1.5\times 0.6\times 10^{-2}\times 1\\
&\quad\times\left(-\frac{300}{300+300}3.33\times 10^{-9} - \frac{300\times 300}{300+300}11.8\times 10^{-12}\right)\\
&= -j9.71\times 10^{-11}f
\end{aligned}$$

Substituting the first frequency of 1 MHz gives $|\hat{V}_S| = 9.71\times 10^{-5}$ V, as opposed to a measured value of 9×10^{-5} V. The predictions of the simple model are within 1 dB up to approximately 40 MHz. Above that, standing waves on the line are predominant, causing a deviation from the 20 dB/decade (linear with frequency) variation of the simple model. It is worth noting that the line is $\lambda_0/10$ at 20 MHz. The measured data clearly follow an increase of 20 dB/decade up to 40 MHz, as predicted by the simple model. This confirms that the simple model is valid for electrically short lines and termination impedances that do not differ substantially from the characteristic impedance of the line.

Additional confirmations of the transmission-line model for predicting the effects of incident fields were carried out in [8, 13]. An experimental verification was conducted in [13] and an analytical investigation in [8]. In [8], a numerical analysis code was used to provide the baseline data. Those data show that the transmission-line model is valid for frequencies so long as the wire separation is small, electrically. In this section, we have concentrated on a simple, approximate version of the basic transmission-line model. This simple model is valid for lines that are electrically short and termination impedances that do not vary significantly from the line characteristic impedance. Including the line inductance and capacitance relaxes the restriction on the termination impedance values but retains the restriction that the line be electrically short. Unless extreme termination impedances are encountered, the simple model that we have concentrated on and that is shown in Fig. 8.23 is usually sufficient for estimation purposes. Other predictions of the exact transmission-line model are given in [14].

8.2.2 Shielded Cables and Surface Transfer Impedance

Coaxial cables consist of a concentric shield enclosing an interior wire that is located on the axis of the shield. The intent of the shield is to completely enclose a circuit in order to prevent coupling to the terminations from incident fields outside the shield, as illustrated in Fig. 8.30. If the shield could be constructed of a solid, perfectly conducting material, this would be the case. Even if this were possible, we would have to ensure that there were no breaks or discontinuities in the shield that would allow the incident field to penetrate to the inner wire and induce signals on that wire. This would require connectors at both ends that *peripherally bond* the shield to the enclosure housing the terminations [15–17]. "Pigtails" are breaks in the shield at the terminations that facilitate termination of the shield at the enclosures. These are common but should be avoided if the full shielding effectiveness of the shield is to be realized. *We will assume that pigtails and other breaks in the shield are not present, so that the only penetration of an external field is through the shield.*

External fields penetrate nonideal shields via *diffusion* of the current that is induced by the external field on the external surface of the shield. A typical way of calculating this interaction is to first calculate the current induced on the shield exterior by the external, incident field, *assuming the shield is a perfect conductor and completely encloses the interior circuitry*. Any interaction between the exterior and the interior of the shield is neglected in this calculation. Once the exterior shield current $\hat{I}_{SH}$ is computed in this fashion, the induced voltages in the terminations $\hat{V}_S$ and $\hat{V}_L$ are computed in the following manner. The shield current *diffuses through the shield wall* to give a voltage drop on the *interior surface of the shield of*

$$d\hat{V} = \hat{Z}_T \hat{I}_{SH} dx \tag{8.38}$$

where the *surface transfer impedance of the shield* is given by [15–18]

$$\hat{Z}_T = \frac{1}{\sigma 2\pi r_{sh} t_{sh}} \frac{\gamma t_{sh}}{\sinh(\gamma t_{sh})} \quad \text{in } \Omega/\text{m} \tag{8.39a}$$

and the propagation constant in the shield material is

$$\gamma = \frac{1 + j1}{\delta} \tag{8.39b}$$

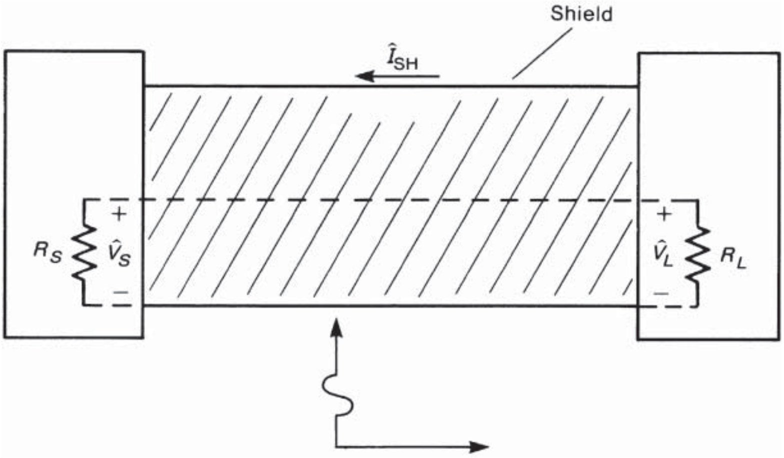

FIGURE 8.30 Illustration of incident field pickup for a shielded cable.

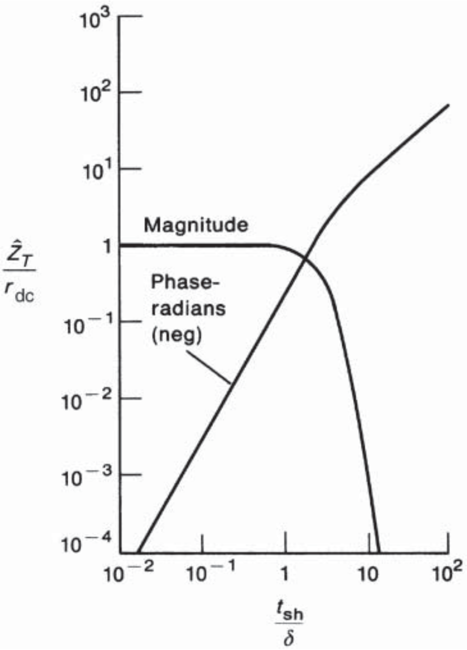

FIGURE 8.31 The surface transfer impedance of a cylinder as a function of the ratio of shield thickness to skin depth [17]. Source: Modified from Hoeft and Hofstra [17].

and $\delta = 1/\sqrt{\pi f \mu_0 \sigma}$ is the skin depth. The shield inner radius is denoted by r_{sh} and the shield thickness is by t_{sh}. A plot of the surface transfer impedance is shown in Fig. 8.31 [17]. This is normalized to the per-unit-length dc resistance of the shield

$$r_{\text{dc}} = \frac{1}{\sigma 2\pi r_{\text{sh}} t_{\text{sh}}} \quad \text{in } \Omega/\text{m} \quad \text{for } t_{\text{sh}} \ll \sigma \tag{8.40}$$

and shows that the shield current on the exterior of the shield completely diffuses through the shield wall for wall thicknesses less than a skin depth, $t_{\text{sh}} \ll \delta$, as we would expect. For wall thicknesses greater than a skin depth, the current on the exterior only partially diffuses through the shield wall, and the transfer impedance decreases with decreasing skin depth (increasing frequencies). Eq. (8.39) gives the per-unit-length surface transfer impedance for solid shields. Shields are frequently constructed of braids of wire woven in a "herringbone" pattern to give flexibility [15, 16, 18]. For braided shields, this becomes [15, 16, 18]

$$\hat{Z}_T = \frac{1}{\sigma \pi r_{bw}^2 BW \cos(\theta_w)} \frac{\gamma 2 r_{bw}}{\sinh(\gamma 2 r_{bw})} \quad \text{in } \Omega/\text{m} \tag{8.41}$$

This is simply the expression in (8.39) with the dc resistance of a solid shield replaced with the dc resistance of the braid and the thickness of the solid shield wall replaced with the diameter of the braid wires. For these *braided shields,* the per-unit-length dc resistance may be approximately

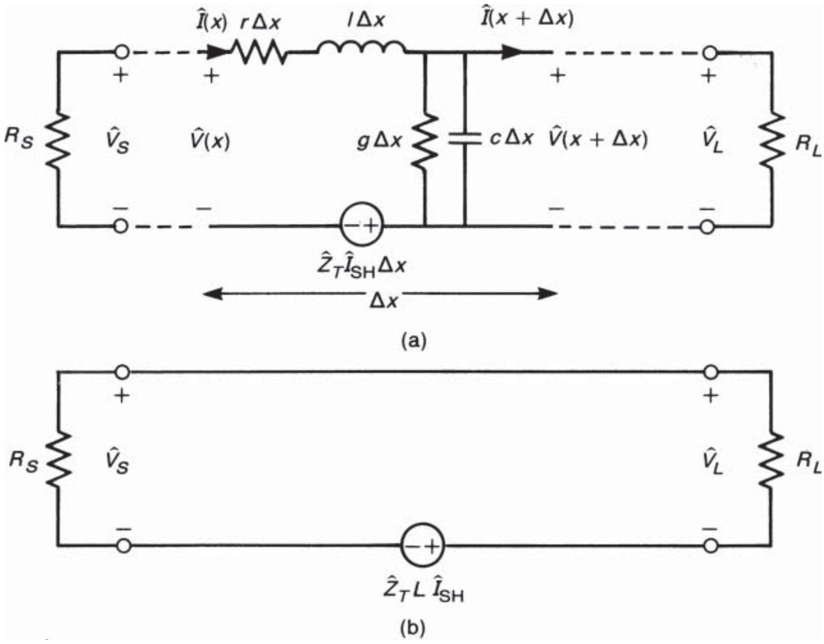
$\hat{I}(x)$ $r\Delta x$
$l\Delta x$
$\hat{I}(x+\Delta x)$
R_S
$\hat{V}_S$
$\hat{V}(x)$
$g\Delta x$
$c\Delta x$
$\hat{V}(x+\Delta x)$
$\hat{V}_L$
R_L
$\hat{Z}_T\hat{I}_{SH}\Delta x$
Δx
(a)
R_S
$\hat{V}_S$
$\hat{V}_L$
R_L
$\hat{Z}_T L \hat{I}_{SH}$
(b)

FIGURE 8.32 The equivalent circuit of the interior of a coaxial cable for computing the pickup of external fields: (a) the per-unit-length equivalent circuit; (b) a simplified equivalent circuit for cables that are short, electrically.

computed by considering the braid wires as being simply connected (electrically) in parallel and becomes [18]

$$r_{\text{dc}} = \frac{r_b}{BW \cos \theta_w} \quad \text{in } \Omega/\text{m} \tag{8.42}$$

where B is the number of *belts* in the shield braid, W is the number of braid wires per belt, θ_w is the weave angle of these belts, and r_b is the per-unit-length dc resistance of the *braid wires*, which have radii r_{bw}:

$$r_b = \frac{1}{\sigma \pi r_{bw}^2} \quad \text{in } \Omega/\text{m} \quad \text{for} \quad r_{bw} \ll \delta \tag{8.43}$$

This voltage drop on the interior surface of the shield acts as a voltage source $\hat{Z}_T\hat{I}_{\text{SH}}\Delta x$ along the longitudinal interior surface of the shield. A per-unit-length equivalent circuit for the circuit enclosed by the shield is shown in Fig. 8.32a, where r, l, g, and c are the per-unit-length resistance, inductance, conductance, and capacitance of the interior wire-shield circuit. The transmission-line equations can again be derived for this per-unit-length equivalent circuit, giving

$$\frac{d\hat{V}(x)}{dx} + (r + j\omega l)\hat{I}(x) = -\hat{Z}_T\hat{I}_{\text{SH}} \tag{8.44a}$$

$$\frac{d\hat{I}(x)}{dx} + (g + j\omega c)\hat{V}(x) = 0 \tag{8.44b}$$

Observe that the driving source is the distributed source $\hat{Z}_T\hat{I}_{\rm SH}$. For an electrically short line, we can approximate the solution by lumping the source and ignoring the per-unit-length parameters of the inner wire–shield circuit, as shown in Fig. 8.32b, to give

$$\hat{V}_S = \frac{R_S}{R_S + R_L}\hat{Z}_T\hat{I}_{\rm SH}L \tag{8.45a}$$

$$\hat{V}_L = -\frac{R_L}{R_S + R_L}\hat{Z}_T\hat{I}_{\rm SH}L \tag{8.45b}$$

In addition to the diffusion source $\hat{Z}_T\hat{I}_{\rm SH}$, two other sources are induced by the external field penetration through the holes in the braided shield [15–18]. The magnetic field of the incident field penetrates, giving a per-unit-length mutual inductance m_{12}, so that the complete surface transfer impedance becomes

$$\hat{Z}_T = \frac{1}{\sigma\pi r_{bw}^2 BW\cos(\theta_w)}\frac{\gamma 2r_{bw}}{\sinh(\gamma 2r_{bw})} + j\omega m_{12} \quad \text{in } \Omega/\text{m} \tag{8.46}$$

In addition, the electric field of the incident field penetrates through these holes in the braided shield to give a per-unit-length mutual capacitance c_{12}, so that a parallel current source must be added to the per-unit-length equivalent circuit of Fig. 8.32a, where [15, 16]

$$\hat{Y}_T = \frac{1}{\hat{V}_{SG}}\frac{d\hat{I}}{dx} \tag{8.47}$$

and $\hat{V}_{SG}$ is the voltage between the shield and the ground plane, and $\hat{I}$ is the current on the interior wire of the shield. The term $\hat{Y}_T$ is referred to as the *surface transfer admittance* of the shield and depends not only on the shield construction but also on the exterior circuit, e.g., the height of the shield above the ground plane. Thus, a source $\hat{Y}_T\hat{V}_{SG}$ must be added to the right-hand side of (8.44b). References [15, 16] give the details of this parameter. Typically, the surface transfer admittance can be neglected except for very large termination impedances.

PROBLEMS

Section 8.1 Simple Emission Models for Wires and PCB Lands

8.1.1 The radiated emissions of a two-wire cable shown in Fig. P8.1.1 are to be predicted at 100 MHz. The currents on the wires at 100 MHz are measured, giving values as shown. Calculate the magnitudes of the maximum radiated emissions due to the differential-mode and the common-mode components of the currents at 10 m. [102.4 dBμV/m, 100 dBμV/m]

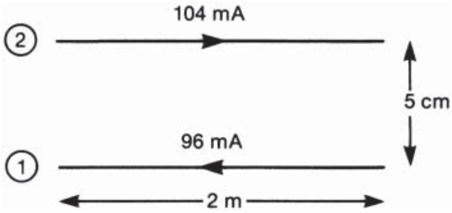

FIGURE P8.1.1

8.1.2 The radiated emissions of a cable are being measured as shown in Fig. P8.1.2 at 100 MHz. Calculate the magnitudes of the radiated electric field due to the differential-mode component and due to the common-mode component measured by the spectrum analyzer at 100 MHz if the antenna factor at 100 MHz is 15 dB and the antenna is oriented parallel to and in the plane of the wires. [90.91 dBμV, 112.3 dBμV]

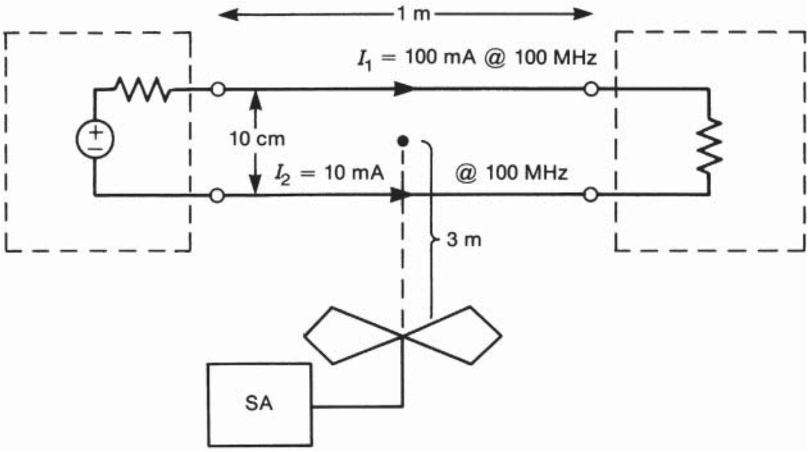

FIGURE P8.1.2

8.1.3 A cable carrying a common-mode current *I* as shown in Fig. P8.1.3 radiates. If a spectrum analyzer reads 32 dBμV at 100 MHz and the antenna has an antenna factor at 100 MHz of 16 dB, determine the current at 100 MHz. [36.6 dBμA]

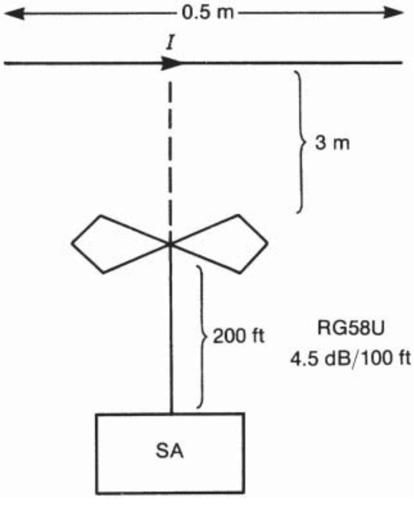

FIGURE P8.1.3

8.1.4 A wire carrying a 1 mA current at 100 MHz is parallel to and 1 cm from an infinite, perfectly conducting ground plane as shown in Fig. P8.1.4. Determine the electric field 3 m above the ground plane. [0.877 mV/m]

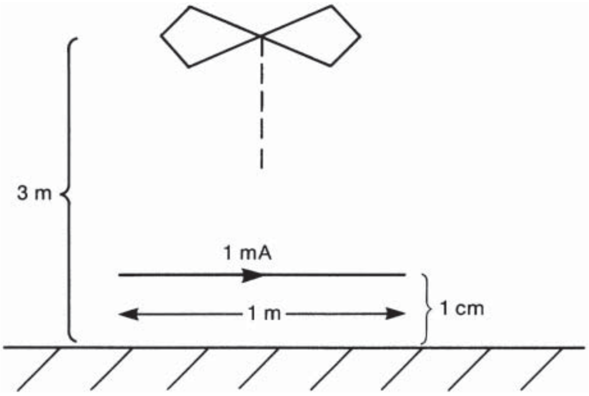

FIGURE P8.1.4

8.1.5 A current probe having $Z_T = 15$ dB Ω at 100 MHz measures a current on a 0.5 m wire as shown in Fig. P8.1.5. The spectrum analyzer is connected to the current probe with a 300 ft. length of RG58U coaxial cable and reads a level of 20 dBμV. Determine the radiated electric field in an FCC Class B radiated emission test. [38.9 dBμV/m]. Will this emission pass Class B? [Yes]

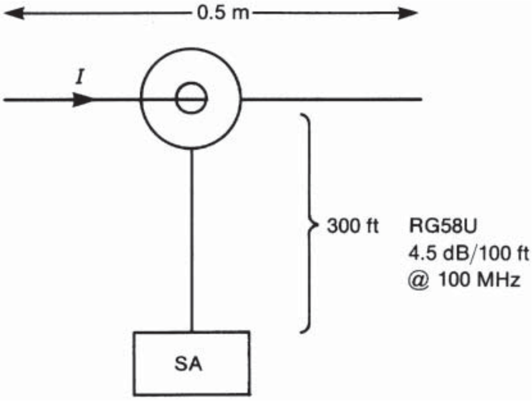

FIGURE P8.1.5

8.1.6 In order to investigate the potential for currents on the ac power cord to impact radiated emissions, consider the typical radiated emission test shown in Fig. P8.1.6. The product has a clock of 10 MHz, and common-mode currents at the harmonics of this clock are inadvertently coupled to the ac power cord. Treat the power cord as a dipole antenna using images and determine the level of current I_C that will barely exceed the FCC Class B limit at the ninth harmonic of the clock. Compare the exact expressions derived assuming sinusoidal current distribution and the approximate expression derived assuming a constant current distribution, which were derived in the previous chapter. To simplify this, compute the fields at the surface of the ground plane. [90 MHz: exact, 5.73 μA; approximate, 3.98 μA]

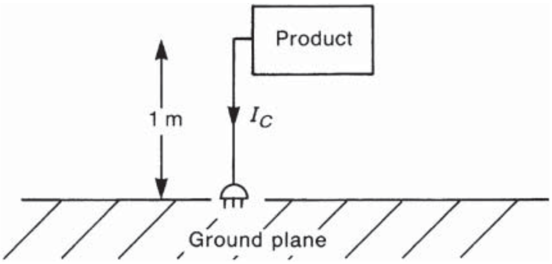
Product
1 m
I_C
Ground plane

FIGURE P8.1.6

8.1.7 Two parallel wires of length 0.5 m and separation of 0.1 mm carry equal and opposite currents (differential mode) of 100 mA at 100 MHz. An antenna with an antenna factor of 20 dB at 100 MHz is used to measure the emissions in an FCC Class B test. If the antenna is parallel to and in the plane of the wires, determine the voltage measured by a spectrum analyzer attached to the antenna. [26.8 dBμV]

8.1.8 The common-mode current in a 1 m cable is measured and consists of a 10 MHz trapezoidal pulse train having a 50% duty cycle and rise/falltimes of 20 ns, as shown in Fig. P8.1.8. The radiated emissions of this cable are measured at a distance of 3 m parallel to the wire using an antenna that has an antenna factor of 8 dB at 30 MHz and 13 dB at 100 MHz. Draw the envelope of the emission as measured on the spectrum analyzer between 30 and 100 MHz. [49 dBμV at 30 MHz and 33.5 dBμV at 100 MHz]

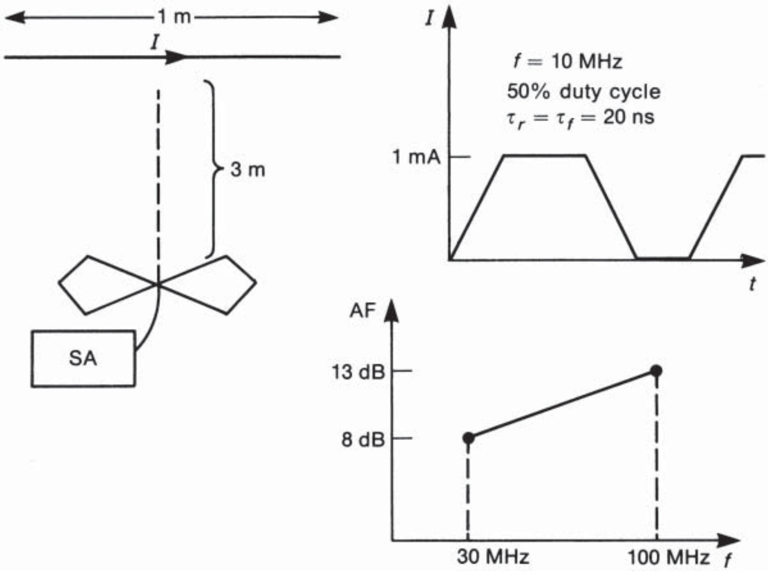
1 m
I
3 m
SA
I
f = 10 MHz
50% duty cycle
$\tau_r = \tau_f$ = 20 ns
1 mA
t
AF
13 dB
8 dB
30 MHz
100 MHz
f

FIGURE P8.1.8

Section 8.2 Simple Susceptibility Models for Wires and PCB Lands

8.2.1 An FM transmitter transmitting at 100 MHz illuminates a two-wire cable in a product at a distance of 300 m away. The transmitter is transmitting an average power of 10 W, and the antenna has a gain in the direction of the product of 20 dB. The cable is 30 cm in length and the wires are separated by 5 cm. The cable per-unit-length capacitance is 20 pF/m. Determine the maximum induced voltage at the cable endpoints if the cable is terminated in 100 Ω resistors at both ends. [21 mV]

8.2.2 An FM antenna that is a half-wave dipole broadcasts 500 W at 108 MHz. Determine the maximum magnetic field intensity 3 mi away. [121.9 μA/m]

8.2.3 A 10 V/m, 100 MHz uniform plane wave is incident on a two-wire line as shown in Fig. P8.2.3. Determine the induced voltage V if the cable has a per-unit-length capacitance of 50 pF/m. [−17.27 mV]

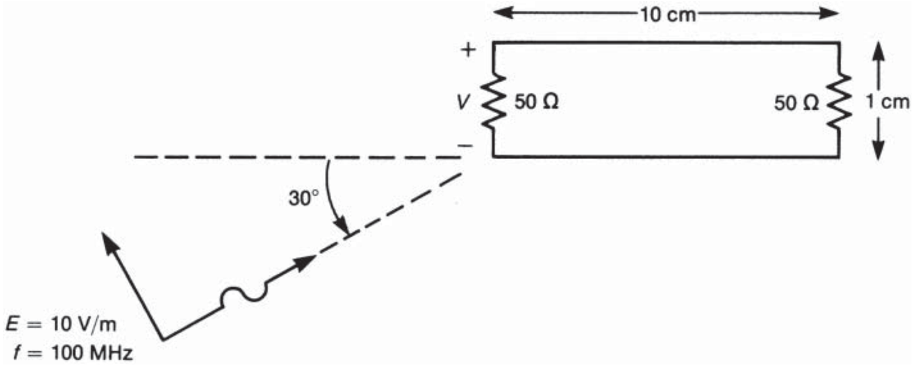

FIGURE P8.2.3

8.2.4 An FM transmitter is transmitting 5 kW at 100 MHz. The gain of the transmitting antenna is 14 dB, and the pattern is omnidirectional in a plane perpendicular to the antenna. Determine the maximum electric field intensity at a distance of 5000 m from the antenna. [114.8 dBμV/m]

8.2.5 A 100-MHz, 10-V/m uniform plane wave is propagating parallel to an air-filled two-wire transmission line as shown in Fig. P8.2.5. The electric field is in the plane of the two wires. Compute the magnitude of the voltage induced across the 50 Ω load. [−9.39 mV]

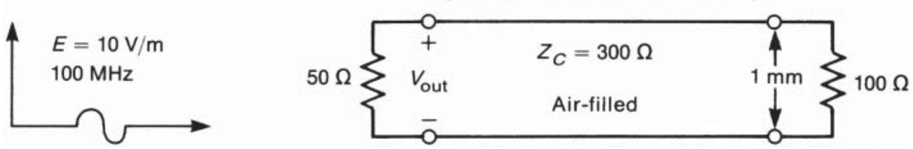

FIGURE P8.2.5

8.2.6 A personal computer is to be installed in an office complex that is one mile from an FM broadcast antenna. The frequency of the transmitter is 100 MHz, and 100 W of power is being transmitted. For maximum coverage, the antenna has an omnidirectional pattern. Determine the electric field in the vicinity of the office complex. [93.6 dBμV/m]

8.2.7 A two-wire ribbon cable is terminated in a 3333 Ω resistor at one end and is open-circuited at the other. The cable is 50 cm in length, and the wires are separated by 1 cm. The per-unit-length capacitance of the cable is 1 pF/m. An airport surveillance radar one mile away illuminates this cable. The radar is transmitting an average power of 1 kW, and the gain in the main beam is 20 dB. Assume the transmission to be a sinusoid at the transmission frequency of 1 GHz and determine the maximum voltage at the line terminations. [0.3187 V]

8.2.8 A 1 m braided shield cable is illuminated by a 1 MHz incident uniform plane wave. The shield is composed of 16 belts with 4 wires per belt of braid wires having radii of 2.5 mils. The weave angle is 30°. The shield interior radius is 35 mils. Determine the net shield resistance (dc). [24.6 mΩ]. Determine the surface transfer impedance of the shield at 1 MHz. [19 mΩ $\angle(-64.3°)$]. The interior circuit is terminated in 300 Ω and 50 Ω resistors. Determine the voltages induced across the loads if the current induced on the exterior of the shield is 31.5 mA. [513 μV, 85.5 μV]

8.2.9 German, Ott, and Paul showed [19] that an image plane placed beneath a PCB can reduce the radiated emissions from both differential-mode and common-mode currents on the PCB lands, as shown in Fig. 8.2. Explain how this is possible. [Use image theory.]

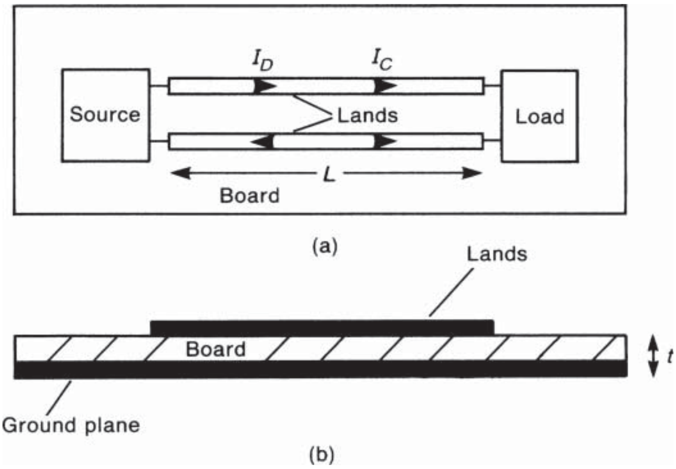

FIGURE P8.2.9 Source: Based on German et al. [19].

REFERENCES

1. C. R. Paul and S. A. Nasar, *Introduction to Electromagnetic Fields*, 2nd ed., McGraw-Hill, New York, 1987.
2. K. B. Hardin, *Decomposition of Radiating Structures to Directly Predict AsymmetricMode Radiation*, Ph.D. Dissertation, University of Kentucky, April 1991.
3. T. J. Dvorak, Fields at a radiation measuring site, *Proc. 1988 IEEE Int. Symp. Electromagnetic Compatibility,* Seattle, WA, Aug. 1988.
4. C. R. Paul and D. R. Bush, Radiated emissions from common-mode currents, *Proc. 1987 IEEE Int. Symp. Electromagnetic Compatibility,* Atlanta, GA, Aug. 1987.
5. C. R. Paul, A comparison of the contributions of common-mode and differential-mode currents in radiated emissions, *IEEE Trans. Electromagn. Compat.* 31, 189–93 (1989).
6. C. R. Paul and D. R. Bush, Bounds on currents induced in transmission lines by incident fields, *Proc. IEEE SouthEasCon,* Louisville, KY, Apr. 1984.

7. C. R. Paul, Frequency response of multiconductor transmission lines illuminated by an electromagnetic field, *IEEE Trans. Electromagn. Compat.* EMC-18, 183–190 (1976).
8. C. R. Paul and R. T. Abraham, Coupling of electromagnetic fields to transmission lines, *Proc. IEEE Int. Symp. Electromagnetic Compatibility,* Boulder, CO, Aug. 1981.
9. C. R. Paul, *Applications of Multiconductor Transmission Line Theory to the Prediction of Cable Coupling*. Vol. VI, *A Digital Computer Program for Determining Terminal Currents Induced in a Multiconductor Transmission Line by an Incident Electromagnetic Field*, Technical Report, Rome Air Development Center, Griffiss AFB, NY, RADC-TR-76-101, Vol. VI, Feb. 1978.
10. C. D. Taylor, R. S. Satterwhite, and C. W. Harrison, The response of a terminated two-wire transmission line excited by a nonuniform electromagnetic field, *IEEE Trans. Anten. Propag.* AP-13, 987–989 (1965).
11. A. A. Smith, A more convenient form of the equations for the response of a transmission line excited by nonuniform fields, *IEEE Trans. Electromagn. Compat.* EMC-15, 151–152 (1973).
12. A. A. Smith, *Coupling of External Electromagnetic Fields to Transmission Lines,* 2nd ed., Interference Control Technologies, Inc., Gainesville, VA, 1987.
13. R. Paul and D. F. Herrick, Coupling of electromagnetic fields to transmission lines, *Proc. 1982 IEEE Int. Symp. Electromagnetic Compatibility,* Santa Clara, CA, Aug. 1982.
14. R. Paul, *Analysis of Multiconductor Transmission Lines*, Wiley-Interscience, New York, 1994.
15. F. Vance, *Coupling to Shielded Cables*, Wiley, New York, 1978.
16. F. Vance, Shielding effectiveness of braided-wire shields, *IEEE Trans. Electromagn. Compat.* EMC-17, 71–77 (1975).
17. L. O. Hoeft and J. S. Hofstra, Measured electromagnetic shielding performance of commonly used cables and connectors, *IEEE Trans. Electromagn. Compat.* EMC-30, 260–275 (1988).
18. C. R. Paul, *Applications of Multiconductor Transmission Line Theory to the Prediction of Cable Coupling*, Vol. VII, *Prediction of Crosstalk Involving Braided-Shield Cables*, Technical Report, Rome Air Development Center, Griffiss AFB, NY, RADC-TR-76-101, Aug. 1980.
19. R. F. German, H. W. Ott, and C. R. Paul, Effect of an image plane on printed circuit board radiation, *Proc. 1990 IEEE Int. Symp. Electromagnetic Compatibility*, Washington, DC, Aug. 1990.

CHAPTER NINE

Crosstalk

In this chapter, we will discuss another important aspect of the design of an electromagnetically compatible product—*crosstalk*. This essentially refers to the *unintended electromagnetic coupling between wires and PCB lands that are in proximity*. Crosstalk is distinguished from antenna coupling in that it is a *near-field coupling problem*. Crosstalk between wires in cables or between lands on PCBs concerns the *intrasystem interference performance* of the product; that is, the *source* of the electromagnetic emission and the *receptor* of this emission are *within the same system*. Thus, this reflects the third concern in EMC: *the design of the product such that it does not interfere with itself*. With clock speeds and data transfer rates in digital computers steadily increasing, crosstalk between lands on PCBs is becoming a significant mechanism for interference in modern digital systems.

There are also cases where crosstalk can affect the radiated and/or conducted emissions of the product. Suppose that a ribbon cable internal to a product is placed in proximity to wires that connect to a peripheral cable that exits the product. Crosstalk between the two cables can induce signals on the peripheral cable that may radiate externally to the product, causing the product to be out of compliance with the radiated emission regulatory limits. If this internal coupling occurs to the power cord of the product, these coupled signals may cause it to fail the conducted emission regulatory requirements. Crosstalk can also affect the susceptibility of a product to emissions from another product. For example, emissions from some other product that are coupled to a peripheral cable of this product may couple, internal to the product, to some other cable internal to it where the susceptibility to this signal may be enhanced.

In order to understand how to model crosstalk, it is important to understand the analysis of two-conductor transmission lines. For a two-conductor transmission line, there is no crosstalk. *In order to have crosstalk, we must have three or more conductors*. However, the notions involved in two-conductor transmission-line theory carry over to a large degree to the case of multiconductor transmission lines and simplify the understanding of the behavior of those lines. It is for this reason that the reader should review conventional two-conductor transmission-line theory given in Chapter 4 and in any undergraduate text on electromagnetic fields, such as [1, 2].

Introduction to Electromagnetic Compatibility, Third Edition. Clayton R. Paul, Robert C. Scully, and Mark A. Steffka.
© 2023 John Wiley & Sons, Inc. Published 2023 by John Wiley & Sons, Inc.

9.1 THREE-CONDUCTOR TRANSMISSION LINES AND CROSSTALK

Virtually all of the techniques developed in Chapter 4 for the analysis of two- conductor transmission lines can be directly extended to the case of coupled transmission lines that consist of any number of parallel conductors. These types of transmission lines are referred to as *multiconductor transmission lines* (MTLs). In this section, we will consider the first logical extension of the two-conductor line results: a three-conductor transmission line. An exhaustive treatment of the solution of the MTL equations for predicting crosstalk is given in the textbook in [3]. Additional short summaries of the solution of the MTL equations for the prediction of crosstalk are given in [4–6].

Adding a third conductor to the two-conductor system provides the possibility of generating interference between the circuits attached to the ends of the line conductors resulting from *crosstalk*. In order to illustrate this important phenomenon, consider the three-conductor line shown in Fig. 9.1. A source consisting of a source resistance R_S and a source voltage $V_S(t)$ is connected to a load R_L via a *generator conductor* and a *reference conductor*. Two other terminations, represented by resistors R_{NE} and R_{FE}, are also connected by a *receptor conductor* and this reference conductor. These terminations represent the input circuitry looking into the terminals of the terminations. Linear, resistive terminations will be shown for illustration, but all results that we will develop will hold for more general terminations, which may include capacitors and/or inductors. The line conductors are assumed to be parallel to the z axis and are of uniform cross section along the line. We will also assume that any surrounding dielectric inhomogeneities also have uniform cross sections along the line axis, so that the lines we will consider will be *uniform lines*. The *generator circuit* consists of the generator conductor and the reference conductor and has current $I_G(z, t)$ along the conductors and voltage $V_G(z, t)$ between them. All the voltages are with respect to the *reference conductor*. The current and voltage associated with the generator circuit will generate electromagnetic fields that interact with the *receptor circuit*, which consists of the receptor conductor and the reference conductor. This interaction will induce current $I_R(z, t)$ and voltage $V_R(z, t)$ along the receptor circuit. This induced current and voltage will produce voltages $V_{NE}(t)$ and $V_{FE}(t)$ at the input terminals of the terminations that are attached to the ends of the receptor circuit. The subscripts *NE* and *FE* refer to "near end" and "far end," respectively, with reference to the end of the line adjacent to the end of the generator circuit that contains the driving source $V_S(t)$. The line is of total length L and extends from $z = 0$ to $z = L$.

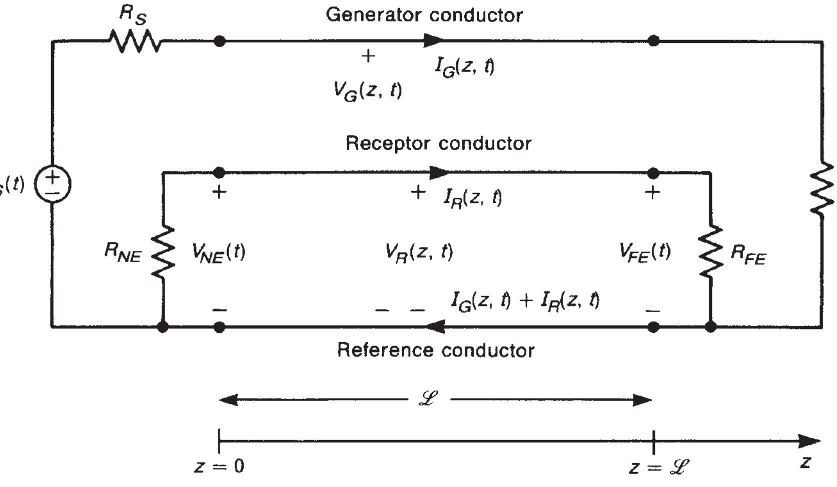

FIGURE 9.1 The general three-conductor transmission line, illustrating crosstalk.

The objective in a crosstalk analysis is to determine (predict) the near-end and far-end voltages $V_{NE}(t)$ *and* $V_{FE}(t)$ *given the line cross-sectional dimensions, and the termination characteristics* $V_S(t)$, R_S, R_L, R_{NE}, *and* R_{FE}. There are two types of analysis that we might be interested in: time-domain analysis and frequency-domain analysis. *Time-domain* crosstalk analysis is the determination of the time form of the receptor terminal voltages $V_{NE}(t)$ and $V_{FE}(t)$ for some general time form of the source voltage $V_S(t)$. *Frequency-domain crosstalk* analysis is the determination of the magnitude and phase of the receptor terminal phasor voltages $\hat{V}_{NE}(j\omega)$ and $\hat{V}_{FE}(j\omega)$ for a sinusoidal source voltage $V_S(t) = V_S \cos(\omega t + \phi)$. Frequency-domain analysis also presumes a steady state, i.e., the sinusoidal source has been attached a sufficient length of time that the transient response has decayed to zero. This is referred to as *phasor* analysis similar to that for electric circuits as described in Appendix A. Of course, these notions are the same as for two-conductor lines, but here we are interested in voltages and currents that are generated in another circuit.

Some typical three-conductor lines representing typical configurations to which this analysis applies are shown in Figs. 9.2 and 9.3. Figure 9.2 shows wire-type lines consisting of conductors of circular cylindrical cross section (wires). Figure 9.2a shows a configuration of three wires where one wire serves as the reference conductor for the line voltages. A ribbon cable is typical of this configuration. Figure 9.2b shows two wires where an infinite, perfectly conducting (ground) plane serves as the reference conductor. The third wire-type configuration shown in Fig. 9.2c consists of two wires within an overall cylindrical shield that serves as the reference conductor. There are many applications where cables are surrounded by an overall shield as in Fig. 9.2c in order to prevent unwanted coupling of external electromagnetic fields to the interior wires. We have shown all these configurations as being *bare wires*, i.e., without dielectric insulations. They are then said to be in a *homogeneous medium* since the surrounding medium has one relative permittivity (that of free space $\varepsilon_r = 1$). Practical wires (with the exception of high-voltage power transmission lines) have cylindrical dielectric insulations surrounding them for obvious reasons. We will need to develop equations for the per-unit-length capacitances and inductances of these configurations. Determining these per-unit-length parameters in simple, closed-form equations is not possible if we include dielectric insulations, and numerical approximation methods must be used [7]. These approximate numerical methods will be discussed for ribbon cables in Section 9.3.3.1. Computer programs for determining the parameters are given in Appendix C. Approximate, simple equations for these parameters for wire-type lines with dielectric insulations ignored will be obtained in Section 9.3.2. For these homogeneous medium cases, all voltage and current waves on the wires will travel down the line with the same velocity:

$$v = \frac{v_0}{\sqrt{\varepsilon_r}} \tag{9.1}$$

where $v_0 \cong 3 \times 10^8$ m/s and ε_r is the relative permittivity of the surrounding (assumed *homogeneous*) medium. If wire insulations are included in the analysis, the surrounding medium will be *inhomogeneous* and the voltage and current waves will travel down the line with different velocities of propagation further complicating the analysis.

Figure 9.3 shows configurations that are typical on printed circuit boards (PCBs). The generator and receptor conductors have rectangular cross section and are referred to as *lands* with reference to grooves in a rifle barrel. Figure 9.3a shows what is referred to as a *coupled stripline*. The reference conductor consists of two infinite planes. The lands are immersed in a *homogeneous medium* between the two planes. This configuration represents PCBs that have *innerplanes*. The lands are buried between these innerplanes. Because the medium surrounding the lands is homogeneous, all voltages and currents on these lands will travel down the line with the same velocity given by (9.1). Typical PCBs are constructed of glass-epoxy, which has a relative permittivity of approximately $\varepsilon_r = 4.7$. Hence, the voltage and current waves on the line travel at velocities of $v = 1.38 \times 10^8$ m/s

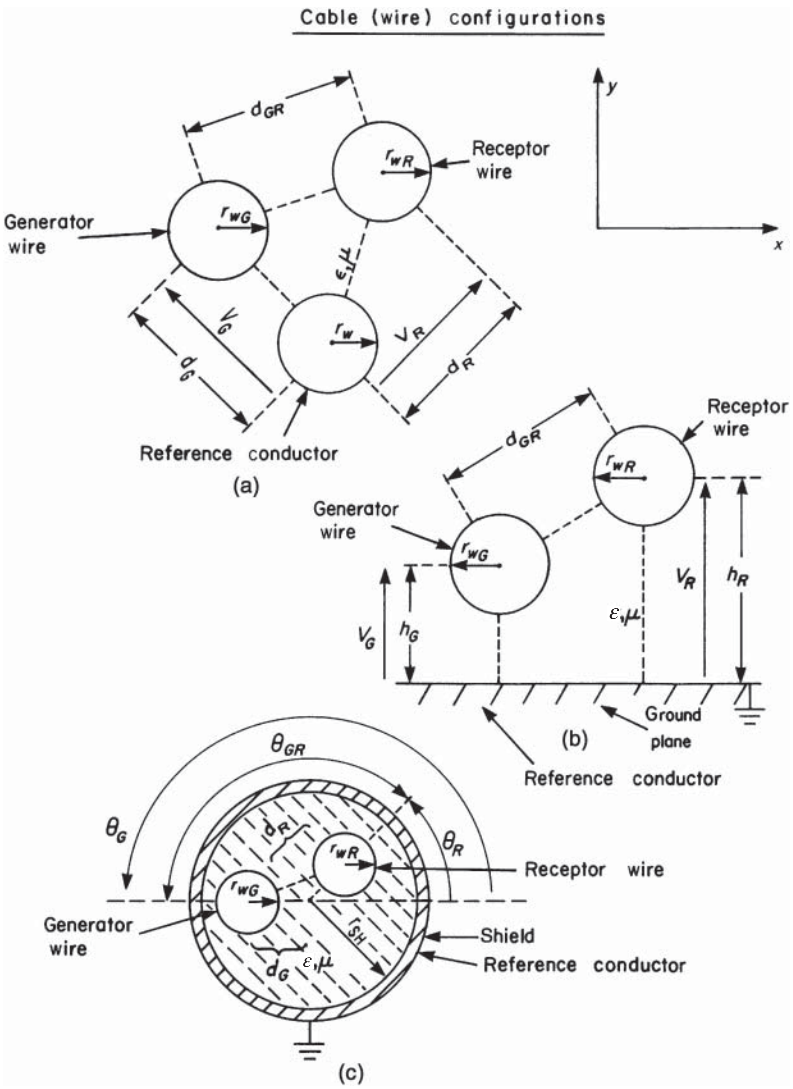
Cable (wire) configurations
d_{GR}
Receptor wire
r_{wR}
Generator wire
r_{wG}
ε,μ
V_G
d_G
r_w
V_R
d_R
Reference conductor
(a)
y
x
d_{GR}
Receptor wire
r_{wR}
Generator wire
r_{wG}
V_G
h_G
V_R
h_R
ε,μ
Ground plane
(b)
Reference conductor
θ_{GR}
θ_G
θ_R
d_R
r_{wR}
Receptor wire
r_{wG}
Generator wire
r_{SH}
Shield
Reference conductor
d_G
ε,μ
(c)

FIGURE 9.2 Wire-type line cross sections whose reference conductors are (a) another wire, (b) an infinite ground plane, or (c) an overall, cylindrical shield.

or $v = 5.45$ in./ns. Figure 9.3b shows what is referred to as a *coupled microstrip*. This is common in microwave circuitry and is represented on PCBs by outer lands of an innerplane board. Because the electric fields lie partly in the board material and partly in the surrounding air, there are two velocities of propagation of the voltage and current waves and both differ from the speed of light. Figure 9.3c represents the lands on the outer surfaces of a PCB where one land serves as the reference conductor. Again, since the electric fields about these lands lie partly in the board material and partly in air, there are two velocities of propagation of the voltage and current waves and neither is the speed of light. The requisite per-unit-length parameters of capacitance and inductance for these three configurations consisting of lands cannot be determined as simple equations. Instead, numerical approximate methods must be used to determine the per-unit-length parameters, and these methods will be discussed in Section 9.3.3.2. Computer programs for determining the parameters are given in Appendix C.

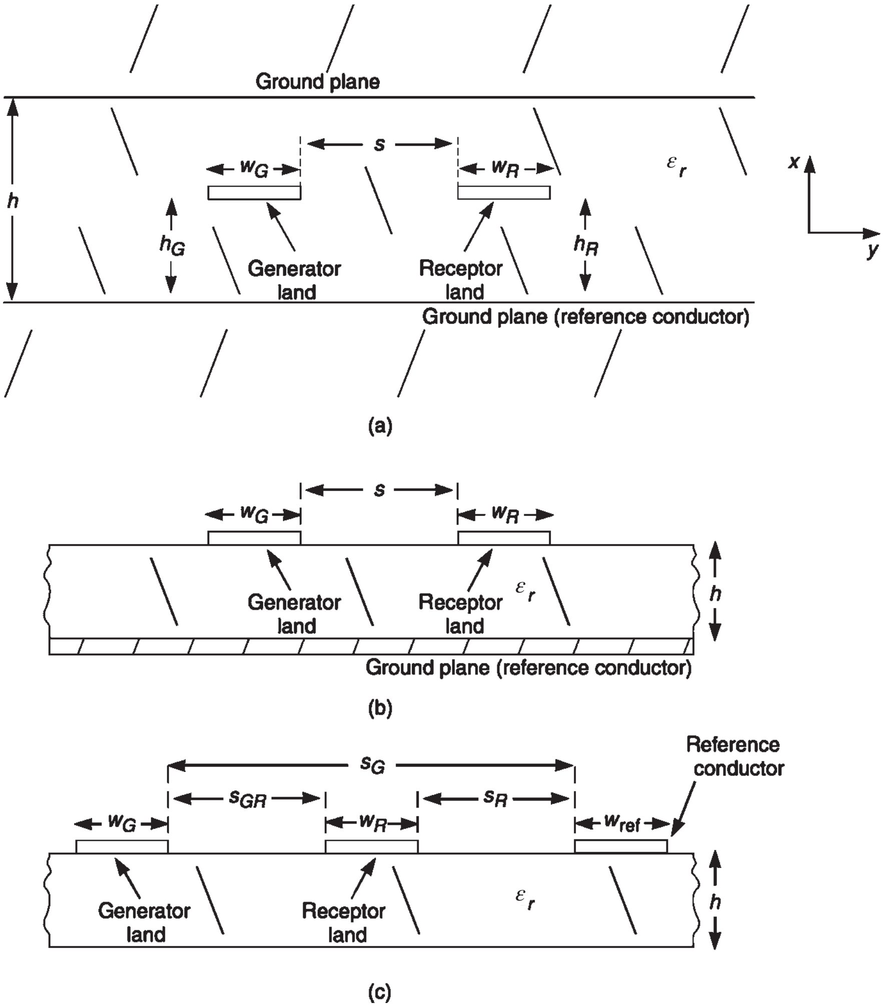
Ground plane
s
w_G
w_R
ε_r
x
y
h
h_G
h_R
Generator land
Receptor land
Ground plane (reference conductor)
(a)
s
w_G
w_R
Generator land
Receptor land
ε_r
h
Ground plane (reference conductor)
(b)
s_G
s_GR
s_R
w_G
w_R
w_ref
Reference conductor
Generator land
Receptor land
ε_r
h
(c)

FIGURE 9.3 Printed circuit board line cross sections: (a) coupled stripline representing innerplane boards; (b) coupled microstrip lines representing innerplane boards and the lands on the outer surface; (c) single-sided PCBs.

9.2 THE TRANSMISSION-LINE EQUATIONS FOR LOSSLESS LINES

The fundamental assumption involved in the analysis of all multiconductor transmission lines is, again, that the *transverse electromagnetic* (TEM) mode of propagation is the only field structure present on the line. The TEM field structure assumes that both the electric and the magnetic field vectors lie in the transverse (xy) plane perpendicular to the line (z) axis, i.e., the electric and magnetic fields do not have a component along the line axis. Under the TEM field structure assumption, line voltages $V_G(z, t)$ and $V_R(z, t)$, as well as line currents $I_G(z, t)$ and $I_R(z, t)$, can be uniquely defined for excitation frequencies other than dc [1, 3, 4]. The total current flowing to the right at any line cross section is zero, so that the currents return through the reference conductor. Furthermore, the TEM field structure is identical to a static (dc) one. This allows the determination of the per-unit-length parameters of inductance and capacitance strictly from dc methods in the cross-section (xy) plane as was the case for two-conductor lines in Chapter 4. The pure TEM field structure cannot exist for (1) imperfect line conductors or (2) an inhomogeneous surrounding medium [3]. Nevertheless, for either case the deviation from a TEM field structure is typically small for "good conductors," typical line cross-sectional dimensions, and frequencies in the lower GHz range. This is referred to as the *quasi-TEM mode assumption,* and we will employ this assumption in our future analyses.

Once again for the TEM field structure, the cross-sectional electric and magnetic field structure is identical to a static (dc) one (see Fig. 4.3 of Chapter 4). Hence, the per-unit-length parameters of inductance and capacitance can be found using static solution methods, which greatly simplifies their determination. This will be considered in the next section. Losses in the line occur via two mechanisms: (1) the losses in the line conductors and (2) losses in the surrounding medium. In order to predict the crosstalk and understand the basic mechanism, as well as the parameters affecting it, we will ignore these losses in formulating the multiconductor transmission-line equations in order to simplify their solution. Ignoring losses gives first-order and reasonably accurate predictions of the crosstalk. To obtain the MTL equations that we must solve in order to predict the crosstalk, we construct the per-unit-length equivalent circuit for a Δz section as shown in Fig. 9.4. The generator and receptor circuits have per-unit-length self-inductances l_G and l_R, respectively, associated with them and a per-unit-length mutual inductance l_m between the two circuits. The line currents produce magnetic fluxes penetrating each loop formed by the conductor and the reference conductor, and these inductances represent the effect of those fluxes via Faraday's law. The line voltages (between each conductor and the reference conductor) produce charges on the conductors that generate electric fields between each pair of conductors. This effect is represented by capacitances. The per-unit-length self-capacitances between the generator conductor and the reference conductor and between the receptor conductor and the reference conductor are represented by c_G and c_R, respectively. The per-unit-length mutual capacitance between the generator and receptor conductors is represented by c_m. In a Δz section of the line, the total inductance or capacitance is the per-unit-length value multiplied by Δz.

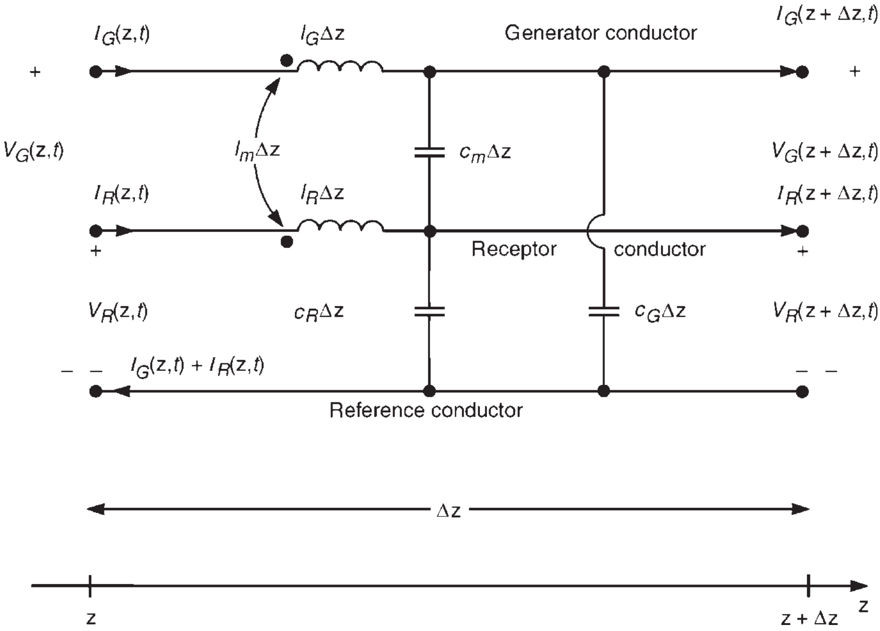

FIGURE 9.4 The per-unit-length equivalent circuit of a three-conductor transmission line.

The MTL equations can again be determined from this per-unit-length equivalent circuit using circuit analysis principles and letting $\Delta \rightarrow 0$, giving [3]

$$\frac{\partial V_G(z,t)}{\partial z} = -l_G \frac{\partial I_G(z,t)}{\partial t} - l_m \frac{\partial I_R(z,t)}{\partial t} \tag{9.2a}$$

$$\frac{\partial V_R(z,t)}{\partial z} = -l_m \frac{\partial I_G(z,t)}{\partial t} - l_R \frac{\partial I_R(z,t)}{\partial t} \tag{9.2b}$$

and

$$\frac{\partial I_G(z,t)}{\partial z} = -(c_G + c_m) \frac{\partial V_G(z,t)}{\partial t} + c_m \frac{\partial V_R(z,t)}{\partial t} \tag{9.2c}$$

$$\frac{\partial I_R(z,t)}{\partial z} = c_m \frac{\partial V_G(z,t)}{\partial t} - (c_R + c_m) \frac{\partial V_R(z,t)}{\partial t} \tag{9.2d}$$

An important observation can be made that aids greatly in the solution of these equations. Writing these equations in matrix form yields [3]

$$\frac{\partial}{\partial z}\mathbf{V}(z,t) = -\mathbf{L}\frac{\partial}{\partial t} I(z,t) \tag{9.3a}$$

$$\frac{\partial}{\partial z}\mathbf{I}(z,t) = -\mathbf{C}\frac{\partial}{\partial t}\mathbf{V}(z,t) \tag{9.3b}$$

where

$$\mathbf{V}(z,t) = \begin{bmatrix} V_G(z,t) \\ V_R(z,t) \end{bmatrix} \tag{9.4a}$$

$$\mathbf{I}(z,t) = \begin{bmatrix} I_G(z,t) \\ I_R(z,t) \end{bmatrix} \tag{9.4b}$$

and the per-unit-length parameter matrices are

$$\mathbf{L} = \begin{bmatrix} I_G \quad I_m \\ I_m I_R \end{bmatrix} \tag{9.5a}$$

$$\mathbf{C} = \begin{bmatrix} (c_G + c_m) - c_m \\ -c_m(c_R + c_m) \end{bmatrix} \tag{9.5b}$$

Observe that *the MTL equations in matrix form in (9.3) have an appearance identical to that of the transmission-line equations for a two-conductor line considered in Chapter* 4. Hence their solution should give similar forms of results but in matrix form. This is a very powerful result that provides great insight into their solution and can be easily extended to lines consisting of more than three conductors [3].

The MTL equations in (9.2) are in the *time domain*. For single-frequency, sinusoidal steady-state excitation (phasor form), we simply replace time derivatives with $j\omega$, where $\omega = 2\pi f$ is the radian frequency of the source and f is its cyclic frequency. This method is identical to the phasor method for solving electric circuits (see Appendix A) and yields

$$\frac{d}{dz}\hat{\mathbf{V}}(z) = -j\omega\mathbf{L}\hat{\mathbf{I}}(z) \tag{9.6a}$$

$$\frac{d}{dz}\hat{\mathbf{I}}(z) = -j\omega\,\mathbf{C}\hat{\mathbf{V}}(z) \tag{9.6b}$$

The phasor voltages and currents are complex numbers that are denoted with a caret (ˆ) over them and now are functions only of position along the line, z. Hence, ordinary derivatives are used. In order to return to the time domain, we multiply the phasor variables by $e^{j\omega t}$ and take the real part of the result as was done in phasor electric circuit analysis (see Appendix A):

$$\mathbf{V}(z,t) = \mathcal{R}e\{\hat{\mathbf{V}}(z)e^{j\omega t}\} \tag{9.7a}$$

$$\mathbf{I}(z,t) = \mathcal{R}e\{\hat{\mathbf{I}}(z)e^{j\omega t}\} \tag{9.7b}$$

In the remainder of this chapter, we will examine an approximate method of solving these equations and predicting the crosstalk. The approximate method is called the *inductive-capacitive coupling model*. An exact solution consisting of a SPICE/PSPICE model is contained in Appendix D. In order to proceed, we must first examine how to obtain the per-unit-length parameters since all the information about the cross-sectional dimensions of a specific line is contained in these and nowhere else.

9.3 THE PER-UNIT-LENGTH PARAMETERS

As was pointed out earlier, it is of no use to solve the MTL equations if the per-unit-length parameters cannot be determined for the particular line cross-sectional configuration. All information about the cross-sectional dimensions of a particular line is contained in these parameters and nowhere else. It remains to determine the entries in **L** and **C.** Approximate equations for the per-unit-length inductances and capacitances for the wire-type lines in a homogeneous medium shown in Fig. 9.2 will be derived for widely separated wires. Corresponding formulas for the PCB-type structures in Fig. 9.3 are difficult to obtain and generally must be found using numerical methods.

9.3.1 Homogeneous Versus Inhomogeneous Media

The configurations in Fig. 9.2 are considered to be lines immersed in a *homogeneous medium*. The surrounding medium for the cases of three wires in Fig. 9.2a or two wires above a ground plane in Fig. 9.2b is logically considered to be free space with parameters ε_0 and μ_0; that is, the wires are considered to be bare. Dielectric insulations severely complicate the determination of the per-unit-length capacitances for wires, but do not affect the per-unit-length inductances since dielectrics have $\mu = \mu_0$. In order to incorporate these types of inhomogeneous media, numerical methods must be used [4, 7]. For the lines in Fig. 9.2 we will ignore the presence of dielectric insulations and consider the wires to be bare, since the dielectric insulations change the capacitances only slightly for widely separated wires, as we will assume. The case of two wires within an overall shield shown in Fig. 9.2c can be analyzed if we assume that the dielectric interior to the shield is homogeneous with ε and μ as we will assume. The inhomogeneity caused by a printed circuit board, as with the structures in Fig. 9.3, is more significant, and closed-form solutions for all the entries in **L** and **C** have not been obtained for these configurations.

If the surrounding medium is *homogeneous*, as for the lines in Fig. 9.2, the per-unit-length parameter matrices given in (9.5) have important, special relationships that parallel those found for two-conductor lines. In particular, these relationships are [3, 4]

$$\mathbf{LC} = \mathbf{CL} = \mu\varepsilon\mathbf{1}_2 \tag{9.8}$$

where the surrounding homogeneous medium is characterized by μ, and ε, and $\mathbf{1}_2$ is the 2×2 identity matrix:

$$\mathbf{1}_2 = \begin{bmatrix} 1 & 0 \\ 0 & 1 \end{bmatrix} \tag{9.9}$$

Therefore we only need to determine one of the parameter matrices, since the other can be found from (9.8) as

$$\begin{aligned} \mathbf{C} &= \mu\varepsilon\mathbf{L}^{-1} \\ &= \frac{1}{v^2}\mathbf{L}^{-1} \end{aligned} \tag{9.10}$$

where $v = 1/\sqrt{\mu\varepsilon}$ is the usual phase velocity for uniform plane waves considered in Appendix B and is also the velocity of waves on the line. For example, for the three-conductor line in a homogeneous medium, we obtain from (9.10)

$$\begin{bmatrix} c_G + c_m & -c_m \\ -c_m & c_R + c_m \end{bmatrix} = \frac{1}{v^2(l_G l_R - l_m^2)} \begin{bmatrix} l_R & -l_m \\ -l_m & l_G \end{bmatrix} \tag{9.11}$$

Comparing the two sides, we obtain the per-unit-length capacitance parameters in terms of the per-unit-length inductance parameters as

$$c_m = \frac{l_m}{v^2(l_G l_R - l_m^2)} \tag{9.12a}$$

$$c_G + c_m = \frac{l_R}{v^2(l_G l_R - l_m^2)} \tag{9.12b}$$

$$c_R + c_m = \frac{l_G}{v^2(l_G l_R - l_m^2)} \tag{9.12c}$$

In the case of lines in an inhomogeneous medium, such as those shown in Fig. 9.3, the per-unit-length inductance matrix $\mathbf{L}$ is not affected by the dielectric inhomogeneity, since $\mu = \mu_0$. Thus, if we designate the per-unit-length capacitance matrix *with the dielectric removed* (*replaced with free space*) by $\mathbf{C}_0$, then the inductance can be found from (9.8) as $\mathbf{L} = \mu_0\varepsilon_0\mathbf{C}_0^{-1}$. Thus for inhomogeneous media, we need to determine the per-unit-length capacitance matrices *with and without the dielectric present*, $\mathbf{C}$ and $\mathbf{C}_0$. Numerical methods are frequently used to obtain these.

Review Exercise 9.1 Show that the inverse of a 2×2 matrix

$$\mathbf{M} = \begin{bmatrix} a & b \\ c & d \end{bmatrix}$$

is

$$\mathbf{M}^{-1} = \frac{1}{(ad - bc)} \begin{bmatrix} d & -b \\ -c & a \end{bmatrix}$$

i.e., $\mathbf{M}\mathbf{M}^{-1} = \mathbf{1}_2$.

That is, the main-diagonal elements are swapped, the off-diagonal elements are negated, and all four entries are divided by the determinant of the matrix, which is the product of the main-diagonal elements minus the product of the off-diagonal elements.

9.3.2 Wide-Separation Approximations for Wires

We will obtain closed-form results for the per-unit-length parameters for three-conductor lines in Fig. 9.2 under *the assumption that the wires are separated sufficiently that the charge and current distributions around the peripheries of the wires are essentially uniform.* This is not a serious restriction for practical configurations, as we will see. In order to derive the per-unit-length parameters for wire-type lines in Fig. 9.2, we will rely on the two basic subproblems discussed for two-conductor lines composed of wires in Chapter 4. It is important that the reader understand these fundamental results, since our deviations will rely on their proper application. The first fundamental subproblem concerns the flux due to a current-carrying wire that penetrates a surface of unit length along the wire and whose edges are at radial distances R_1 and R_2 from the wire where $R_2 \geq R_1$, as shown in Fig. 9.5a. The flux with direction shown is given by Eq. (4.12) and is repeated here:

$$\psi = \frac{\mu_0 I}{2\pi} \ln\left(\frac{R_2}{R_1}\right) \tag{9.13}$$

where the wire carries a current I that is assumed to be uniformly distributed around the wire periphery. *It is very important to determine the correct direction of the resulting flux through*

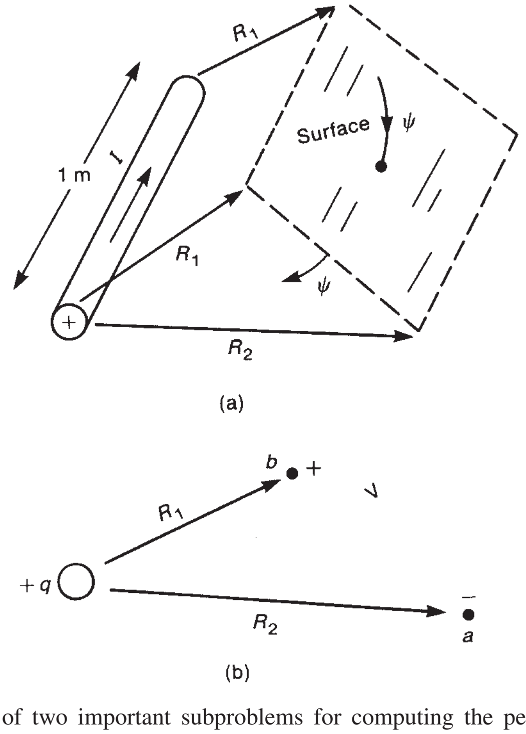

FIGURE 9.5 Illustration of two important subproblems for computing the per-unit-length parameters of wire-type lines: (a) magnetic flux of a current-carrying wire through a surface; (b) voltage between two points for a charge-carrying wire.

the surface. The second fundamental result concerns the voltage between two points that are at radial distances R_1 and R_2 from a charge-carrying wire, where $R_2 \geq R_1$, as shown in Fig. 9.5b. The result is given by Eq. (4.15) and is repeated here:

$$V = \frac{q}{2\pi\varepsilon_0} \ln\left(\frac{R_2}{R_1}\right) \tag{9.14}$$

where the wire carries a per-unit-length charge q that is assumed to be uniformly distributed along the wire and around the wire periphery. Again, as with the determination of the resulting flux, *it is very important to determine the correct direction of the resulting voltage*. The charge distribution on the wire is assumed positive, so that the resulting voltage must be positive at the point closest to the wire.

First, we will consider the case of three wires shown in Fig. 9.2a. The per-unit-length external inductance matrix relates the magnetic fluxes penetrating generator and receptor circuits to the currents of those circuits as

$$\boldsymbol{\psi} = \mathbf{LI} \tag{9.15a}$$

or

$$\begin{bmatrix} \psi_G \\ \psi_R \end{bmatrix} = \begin{bmatrix} l_G & l_m \\ l_m & l_R \end{bmatrix} \begin{bmatrix} I_G \\ I_R \end{bmatrix} \tag{9.15b}$$

The directions of the required fluxes are shown in Fig. 9.6a. Each of the entries in **L** can be obtained in the usual manner for determining two-port parameters by expanding (9.15) to give

$$\psi_G = l_G I_G + l_m I_R \tag{9.16a}$$

$$\psi_R = l_m I_G + l_R I_R \tag{9.16b}$$

First set $I_R = 0$ to give

$$l_G = \left.\frac{\psi_G}{I_G}\right|_{I_R=0} \tag{9.17a}$$

$$l_m = \left.\frac{\psi_R}{I_G}\right|_{I_R=0} \tag{9.17b}$$

Similarly, setting $I_G = 0$ gives

$$l_m = \left.\frac{\psi_G}{I_R}\right|_{I_G=0} \tag{9.17c}$$

$$l_R = \left.\frac{\psi_R}{I_R}\right|_{I_G=0} \tag{9.17d}$$

The results in (9.17) show that the per-unit-length inductances can be found by applying a current on one conductor (and returning on the reference conductor), setting the other current equal to zero, and determining the resulting flux through the appropriate circuit. Fox example, consider finding the self-inductance of the generator circuit. Eq. (9.17a) shows that we place current I_G on the generator

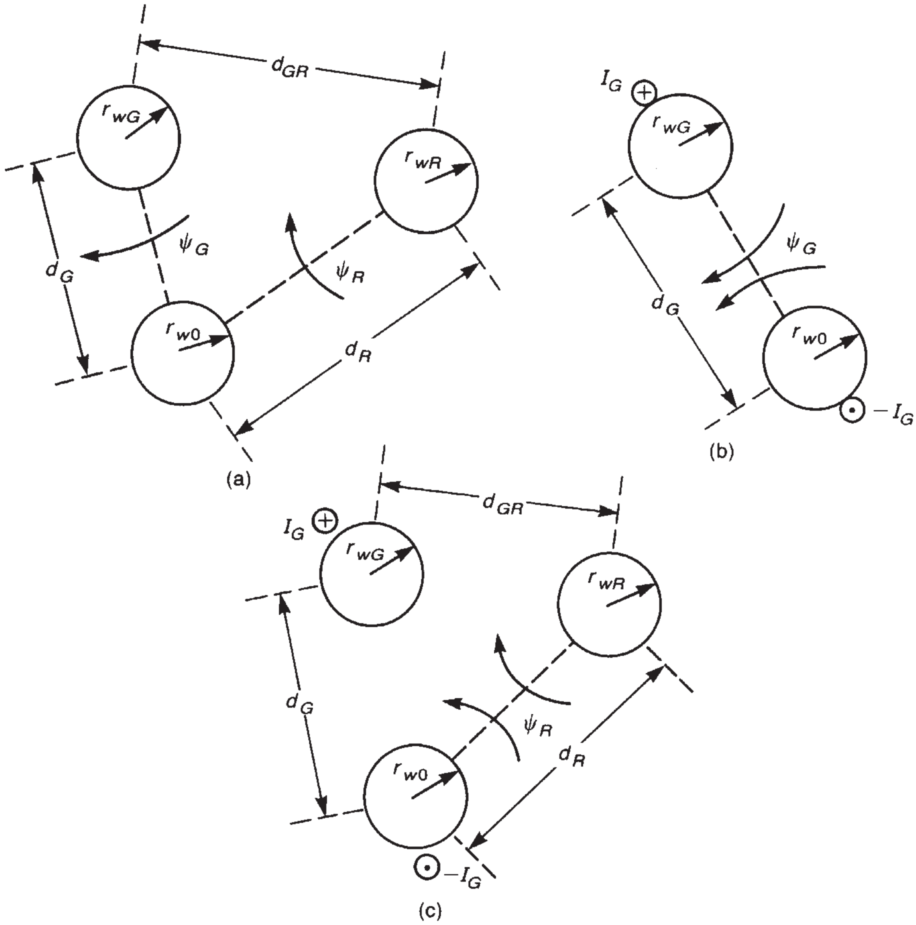

FIGURE 9.6 Computation of the per-unit-length inductances for three-wire lines: (a) definition of circuit magnetic fluxes; (b) computation of the self-inductances; (c) computation of the mutual inductance.

circuit, set $I_R = 0$, and determine the resulting flux through the generator circuit as shown in Fig. 9.6b. Using the fundamental result given in (9.13), we obtain

$$\begin{aligned} l_G &= \frac{\mu_0}{2\pi}\ln\left(\frac{d_G}{r_{wG}}\right) + \frac{\mu_0}{2\pi}\ln\left(\frac{d_G}{r_{w0}}\right) \\ &= \frac{\mu_0}{2\pi}\ln\left(\frac{d_G^2}{r_{wG}r_{w0}}\right) \end{aligned} \tag{9.18}$$

where we have assumed that the intervening medium is not ferromagnetic, $\mu = \mu_0$. Similarly, the self-inductance of the receptor circuit is

$$l_R = \frac{\mu_0}{2\pi}\ln\left(\frac{d_R^2}{r_{wR}r_{w0}}\right) \tag{9.19}$$

The per-unit-length mutual inductance is found from (9.17b) or (9.17c). We apply a current to one circuit and determine the flux penetrating the other circuit as shown in Fig. 9.6c:

$$\begin{aligned} l_m &= \frac{\mu_0}{2\pi}\ln\left(\frac{d_G}{d_{GR}}\right)+\frac{\mu_0}{2\pi}\ln\left(\frac{d_R}{r_{w0}}\right) \\ &= \frac{\mu_0}{2\pi}\ln\left(\frac{d_G d_R}{d_{GR} r_{w0}}\right) \end{aligned} \tag{9.20}$$

The per-unit-length capacitances can be found from the per-unit-length inductances for a homogeneous medium using the result given in (9.8). In order to show the direct derivation, we will use the fundamental result given in (9.14). First we examine the definition of the per-unit-length capacitance matrix **C**. This relates the per-unit-length charges on the generator and receptor conductors to the voltages of these conductors *with respect to the reference conductor* as

$$\begin{bmatrix} q_G \\ q_R \end{bmatrix} = \begin{bmatrix} c_G + c_m & -c_m \\ -c_m & c_R + c_m \end{bmatrix} \begin{bmatrix} V_G \\ V_R \end{bmatrix} \tag{9.21a}$$

or

$$\mathbf{q} = \mathbf{C}\mathbf{V} \tag{9.21b}$$

This form is not convenient for a direct determination, so we invert the expression to give

$$\begin{bmatrix} V_G \\ V_R \end{bmatrix} = \begin{bmatrix} p_G & p_m \\ p_m & p_R \end{bmatrix} \begin{bmatrix} q_G \\ q_R \end{bmatrix} \tag{9.22a}$$

or

$$\mathbf{V} = \mathbf{P}\mathbf{q} = \mathbf{C}^{-1}\mathbf{q} \tag{9.22b}$$

Expanding this gives

$$V_G = p_G q_G + p_m q_R \tag{9.23a}$$

$$V_R = p_m q_G + p_R q_R \tag{9.23b}$$

The entries can be found by setting each of the charges to zero and determining the ratio of voltage to charge producing it. First set $q_R = 0$ to give

$$p_G = \left.\frac{V_G}{q_G}\right|_{q_R=0} \tag{9.24a}$$

$$p_m = \left.\frac{V_R}{q_G}\right|_{q_R=0} \tag{9.24b}$$

Similarly, setting $q_G = 0$ gives

$$p_m = \left.\frac{V_G}{q_R}\right|_{q_G=0} \tag{9.24c}$$

$$p_R = \left.\frac{V_R}{q_R}\right|_{q_G=0} \tag{9.24d}$$

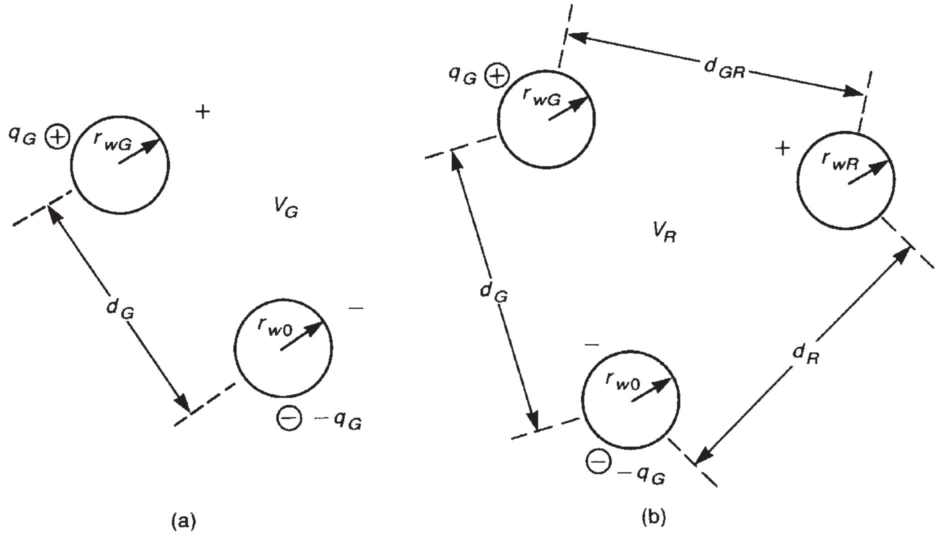

FIGURE 9.7 Computation of the per-unit-length coefficients of potential for a three-wire line: (a) self-term; (b) mutual term.

Inverting (9.22) gives (9.21). In order to obtain the entries in (9.22), we apply the fundamental result given in (9.14) for the voltage produced by a charge-carrying wire. The self-terms can be found for the case of three wires shown in Fig. 9.2a by applying (9.24) as shown in Fig. 9.7. We obtain

$$\begin{aligned} p_G &= \frac{1}{2\pi\varepsilon_0}\ln\left(\frac{d_G}{r_{wG}}\right) + \frac{1}{2\pi\varepsilon_0}\ln\left(\frac{d_G}{r_{w0}}\right) \\ &= \frac{1}{2\pi\varepsilon_0}\ln\left(\frac{d_G^2}{r_{wG}r_{w0}}\right) \end{aligned} \tag{9.25}$$

and

$$\begin{aligned} p_R &= \frac{1}{2\pi\varepsilon_0}\ln\left(\frac{d_R}{r_{wR}}\right) + \frac{1}{2\pi\varepsilon_0}\ln\left(\frac{d_R}{r_{w0}}\right) \\ &= \frac{1}{2\pi\varepsilon_0}\ln\left(\frac{d_R^2}{r_{wR}r_{w0}}\right) \end{aligned} \tag{9.26}$$

Similarly, from (9.24b) and Fig. 9.7(b), we obtain

$$\begin{aligned} p_m &= \frac{1}{2\pi\varepsilon_0}\ln\left(\frac{d_G}{d_{GR}}\right) + \frac{1}{2\pi\varepsilon_0}\ln\left(\frac{d_R}{rw_0}\right) \\ &= \frac{1}{2\pi\varepsilon_0}\ln\left(\frac{d_G d_R}{d_{GR}r_{w0}}\right) \end{aligned} \tag{9.27}$$

Once the entries in (9.22) are obtained as above, the per-unit-length capacitances in (9.21) can be obtained by inverting (9.22). Comparing the entries in **P** in (9.22) obtained in (9.25), (9.26), and (9.27) with the per-unit-length inductances obtained in (9.18), (9.19), and (9.20), we see that $\mathbf{L} = \mu_0\varepsilon_0\mathbf{P}$, which confirms the basic result in (9.8), since $\mathbf{C} = \mathbf{P}^{-1}$.

Example 9.1 A common application of these results is for the case of ribbon cables. Consider the three-wire ribbon cable composed of three 28-gauge (7 × 36) wires whose adjacent separations are 50 mils. It is critical to the correctness of our results that we designate the reference conductor. For our example, we will assume in the following derivation that the center wire is to be the reference wire, as shown in Fig. 9.8a. Determination of the self-inductance l_G is shown in Fig. 9.8b, giving

$$\begin{aligned} l_G &= \frac{\mu_0}{2\pi}\ln\left(\frac{d}{r_w}\right) + \frac{\mu_0}{2\pi}\ln\left(\frac{d}{r_w}\right) \\ &= \frac{\mu_0}{\pi}\ln\left(\frac{d}{r_w}\right) \end{aligned} \tag{9.28}$$

which agrees with (9.18). Similarly, we obtain l_R as

$$l_R = \frac{\mu_0}{\pi}\ln\left(\frac{d}{r_w}\right) \tag{9.29}$$

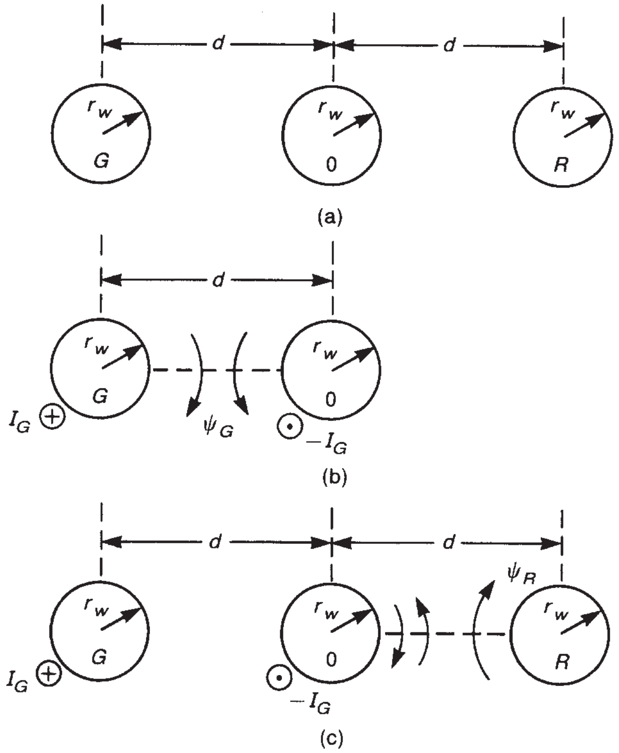

FIGURE 9.8 Computation of the per-unit-length inductances for a ribbon cable where the inner wire is chosen as the reference conductor: (a) problem definition; (b) self-terms; (c) mutual terms.

which agrees with (9.19). The mutual inductance is found from Fig. 9.8c by placing a current I_G on the generator wire (and returning on the reference wire) and finding the total flux through the receptor circuit. Note the defined direction of the receptor circuit flux (upward). Applying the fundamental result to this case gives

$$\begin{aligned} l_m &= -\frac{\mu_0}{2\pi}\ln\left(\frac{2d}{d}\right) + \frac{\mu_0}{2\pi}\ln\left(\frac{d}{r_w}\right) \\ &= \frac{\mu_0}{2\pi}\ln\left(\frac{d}{2r_w}\right) \end{aligned} \tag{9.30}$$

which agrees with (9.20) since $d_G = d_R = d$ and $d_{GR} = 2d$. For the ribbon cable with $r_w = 7.5$ mils and $d = 50$ mils, we obtain $l_G = l_R = 0.759$ μH/m = 19.3 nH/in. and $l_m = 0.24$ μH/m = 6.1 nH/in. We can compute the characteristic impedance of each isolated circuit from $Z_C = v_0 l_G = v_0 l_R = 227.7\,\Omega$. The per-unit-length capacitances can be computed from these results, using (9.12), as $c_G = c_R = 11.1$ pF/m = 0.28 pF/in. and $c_m = 5.17$ pF/m = 0.13 pF/in. We can also compute the characteristic impedance of one circuit *in the presence of the other circuit, using* $Z_C = \sqrt{l_G/(c_G + c_m)} = 216\,\Omega$. Thus, the characteristic impedance of one circuit is affected by the presence of the other circuit.

Next consider the case of two wires above an infinite ground plane, as shown in Fig. 9.9. Replacing the ground plane with the wire images as shown in Fig. 9.9 and applying the fundamental result in (9.13) to (9.17a) gives

$$\begin{aligned} l_G &= \left.\frac{\psi_G}{I_G}\right|_{I_R=0} \\ &= \frac{\mu_0}{2\pi}\ln\left(\frac{h_G}{r_{wG}}\right) + \frac{\mu_0}{2\pi}\ln\left(\frac{2h_G}{h_G}\right) \\ &= \frac{\mu_0}{2\pi}\ln\left(\frac{2h_G}{r_{wG}}\right) \end{aligned} \tag{9.31}$$

Similarly, (9.17d) yields

$$l_R = \frac{\mu_0}{2\pi}\ln\left(\frac{2h_R}{r_{wR}}\right) \tag{9.32}$$

The mutual inductance is found from (9.17b) as

$$\begin{aligned} l_m &= \left.\frac{\psi_R}{I_G}\right|_{I_R=0} \\ &= \frac{\mu_0}{2\pi}\ln\left(\frac{s_1}{s}\right) + \frac{\mu_0}{2\pi}\ln\left(\frac{s_2}{s_3}\right) \\ &= \frac{\mu_0}{2\pi}\ln\left(\frac{s_2}{s}\right) \end{aligned} \tag{9.33}$$

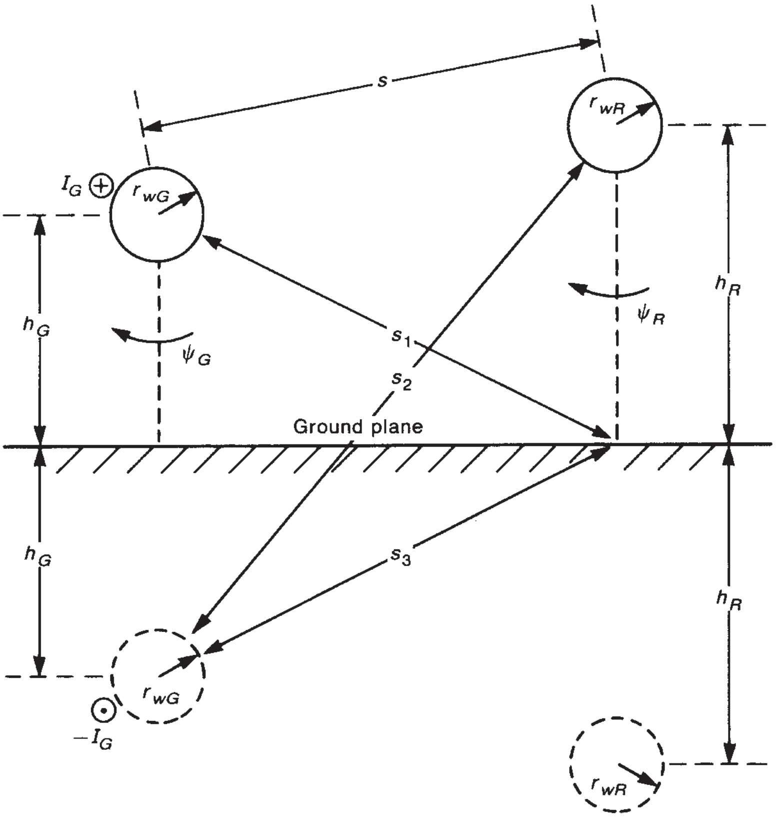

FIGURE 9.9 Computation of the per-unit-length inductances for two wires above a ground plane.

since $s_1 = s_3$. Substituting the dimensions gives

$$s_2 = \sqrt{s^2 + 4h_G h_R} \tag{9.34}$$

so that

$$l_m = \frac{\mu_0}{4\pi} \ln\left(1 + 4\frac{h_G h_R}{s^2}\right) \tag{9.35}$$

Example 9.2 As a numerical example, consider two 20-gauge solid wires (r_w = 16 mils) at a height of 2 cm above a ground plane and separated by 2 cm. The per-unit-length inductances are $l_G = l_R = 0.918$ μH/m = 23.3 nH/in. and $l_m = 0.161$ μH/m = 4.09 nH/in. The characteristic impedance of each isolated circuit is $Z_C = v_0 l_G = v_0 l_R = 275.4\ \Omega$. The per-unit-length capacitances can be obtained from these values, using (9.12), as $c_G = c_R = 10.3$ pF/m and $c_m = 2.19$ pF/m. We can also compute the characteristic impedance of one circuit *in the presence of the other circuit*, using $Z_C = \sqrt{l_G/(c_G + c_m)} = 271\ \ \Omega$. Thus, the characteristic impedance of one circuit is again affected by the presence of the other circuit.

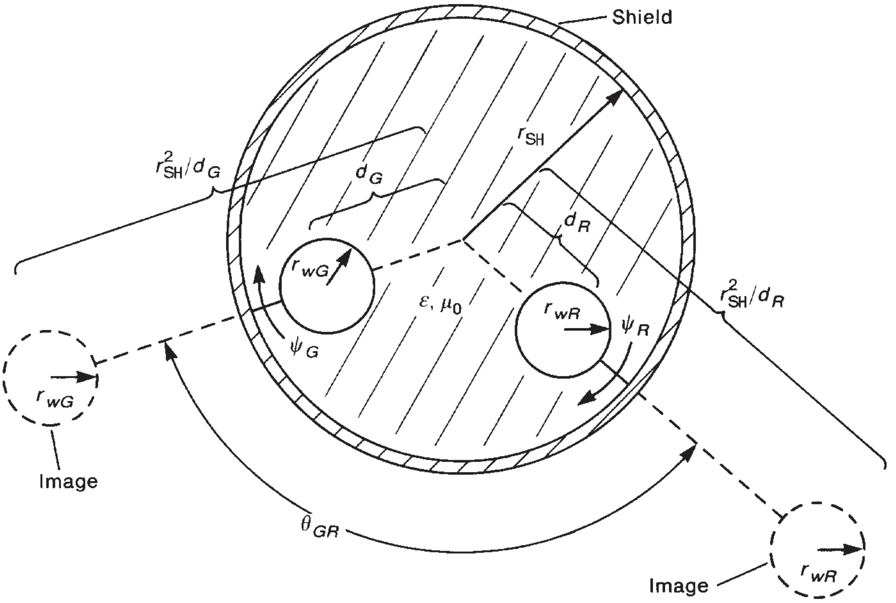

FIGURE 9.10 Computation of the per-unit-length inductances for two wires within an overall cylindrical shield.

The final configuration to be considered is the case of two wires within an overall shield, as shown in Fig. 9.10. The shield has a radius r_{SH} and the wires are located distances d_G and d_R from the shield center and are separated by an angle of θ_{GR}. We may replace the shield with the wire images. Each image lies on a radial line from the shield center and is located a distance r_{SH}^2/d_G and r_{SH}^2/d_R from the shield center [1, 4]. The resulting per-unit-length inductances are derivable in a similar fashion; the derivation is given in [4]. The result is

$$l_G = \frac{\mu_0}{2\pi} \ln\left(\frac{r_{SH}^2 - d_G^2}{r_{SH} r_{wG}}\right) \tag{9.36}$$

$$l_R = \frac{\mu_0}{2\pi} \ln\left(\frac{r_{SH}^2 - d_R^2}{r_{SH} r_{wR}}\right) \tag{9.37}$$

$$l_m = \frac{\mu_0}{2\pi} \ln\left[\frac{d_R}{r_{SH}} \sqrt{\frac{(d_G d_R)^2 + r_{SH}^4 - 2 d_G d_R r_{SH}^2 \cos\theta_{GR}}{(d_G d_R)^2 + d_R^4 - 2 d_G d_R^3 \cos\theta_{GR}}}\right] \tag{9.38}$$

Example 9.3 As an example, consider determining the per-unit-length parameters for a shielded pair of wires consisting of 28-gauge stranded (7 × 36) wires. Also, it is reasonable to assume that $\theta_{GR} = 180°$ in Fig. 9.10. We will also assume that the two wires are separated such that their insulations (not considered here) are touching. Typical insulation thicknesses for wires are on the order of the wire radii. Hence, we will assume $d_G = d_R = 2r_w$ where r_w is the radius of a 28-gauge (7 × 36) stranded wire, which, from Table 5.2, is $r_w = 7.5$ mils. Similarly, we assume that the shield interior radius is four wire radii, $r_{SH} = 4r_w$. Substituting into (9.36)–(9.38) gives

$$
\begin{aligned}
l_G = l_R &= 2 \times 10^{-7} \ln\left(\frac{16r_w^2 - 4r_w^2}{4r_w^2}\right) \\
&= 220\,\text{nH/m} \\
&= 5.58\,\text{nH/in.} \\
l_m &= 2 \times 10^{-7} \ln\left(\frac{2r_w}{4r_w}\sqrt{\frac{((2rw)^2 + (4r_w)^2)^2}{((2r_w)^2 + (2r_w)^2)^2}}\right) \\
&= 44.6\,\text{nH/m} \\
&= 1.13\,\text{nH/in.}
\end{aligned}
$$

The per-unit-length capacitances are computed from (9.12) neglecting dielectric insulations ($\varepsilon_r = 1$) as $c_G = c_R = 42$ pF/m $= 1.07$ pF/in. and $c_m = 10.7$ pF/m $= 0.272$ pF/in. The characteristic impedance of the isolated circuits is $Z_C = v_0 l_G = 65.9\,\Omega$, while the characteristic impedance of one circuit *in the presence of the other* is $Z_C\sqrt{l_G/(c_G + c_m)} = 64.5\,\Omega$. Again, the characteristic impedance of one circuit is affected by the presence of the other circuit.

9.3.3 Numerical Methods for Other Structures

We were able to derive closed-form equations for wire structures in the previous section because we *assumed* that the wires are separated sufficiently so that *the charge distributions around the wire peripheries were constant*. Typically, this is a reasonable approximation if the ratio of wire separation to wire radius is on the order of 5 : 1 or greater. Typical ribbon cables have adjacent wire separations of 50 mils and wire radii of 7.5 mils, giving a ratio of adjacent wire separation to wire radius of 6.67 : 1. Wires that are more closely spaced have charge distributions around the wire peripheries that are not constant but peak on the facing sides of the wires as illustrated in Fig. 9.11a. This is called the *proximity effect*. Figure 9.11b compares the per-unit-length capacitance between two wires using the exact expression [1] and the approximate, wide-separation, expression:

$$c_{\text{exact}} = \frac{\pi\varepsilon_0}{\ln\left[\frac{s}{2r_w} + \sqrt{\left(\frac{s}{2r_w}\right)^2 - 1}\right]} \tag{9.39a}$$

$$c_{\text{approximation}} = \frac{\pi\varepsilon_0}{\ln\left[\frac{s}{r_w}\right]} \qquad s \gg r_w \tag{9.39b}$$

For a separation to wire radius ratio of 5 : 1, the exact value is 17.7 pF/m compared to the approximate value of 17.3 pF/m, a difference of less than 3%. On the other hand, for a separation to wire radius ratio of 2.1 : 1 (the wires are almost touching), the exact value is 88.2 pF/m and the approximate value is 37.4 pF/m, a difference of 236%!

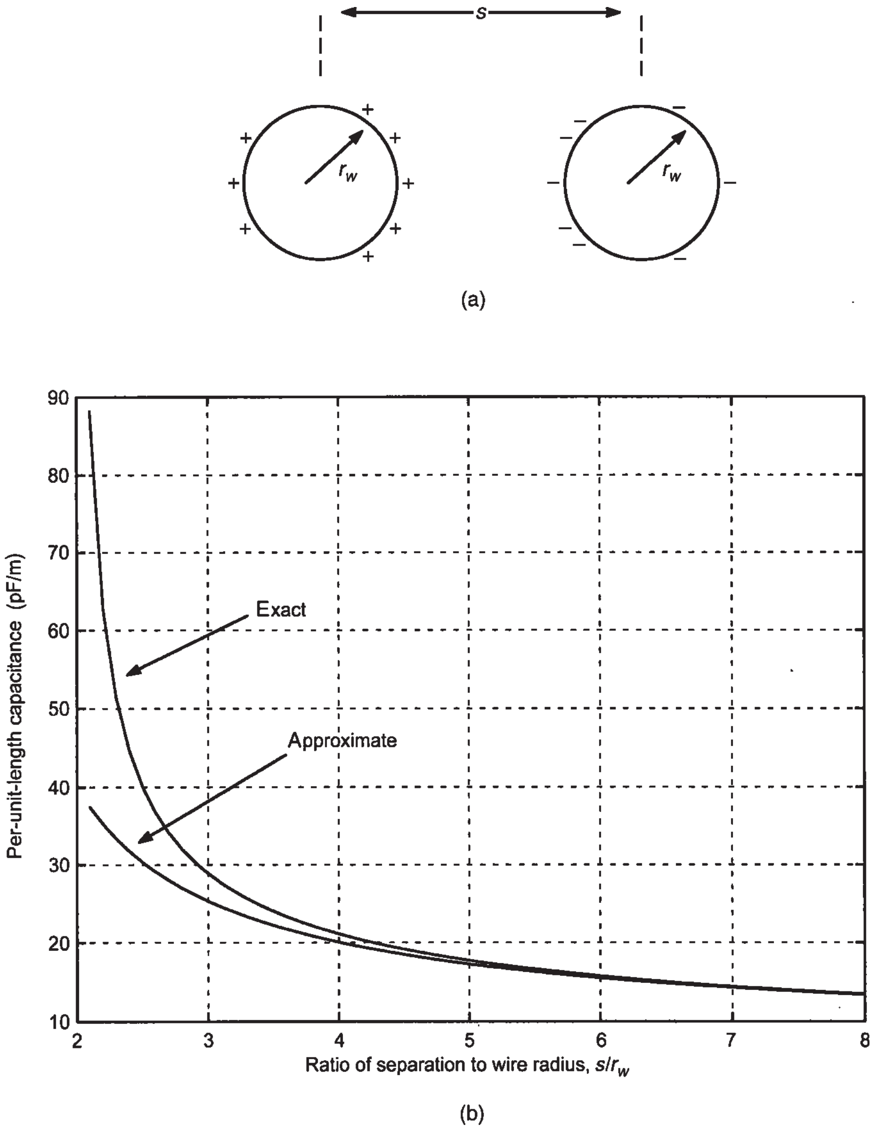

FIGURE 9.11 Illustration of proximity effect for closely spaced wires; (a) representation of charge accumulation on facing sides; (b) plot of the per-unit-length capacitance in terms of the ratio of wire separation to wire radius. Source: Paul and Nasar [1]/McGraw Hill Education.

Although we may derive an exact expression (9.39a) for the per-unit-length capacitance of two bare wires, we cannot derive an exact expression for (1) more than two wires, or (2) wires with dielectric insulations [7]. For these cases, we must use *numerical methods* to obtain the per-unit-length parameters. An important numerical method that we will use to obtain these parameters is generally referred to as the *method of moments* (MoM) [1, 8]. In order to illustrate this powerful method, consider the capacitance of a parallel-plate capacitor shown in Fig. 9.12a. Two square plates of area A and separation d are connected to a battery of voltage V. A total of Q coulombs of charge will be deposited on the plates and the capacitance relates the charge to the voltage as $C = Q/V$. A common *approximate* value for this capacitance is

$$C = \varepsilon \frac{A}{d} \tag{9.40}$$

This is an approximate result and is a reasonable approximation for cases where the plate width is much larger than the separation, i.e., $w \gg d$. The reason that this is an approximation is that its derivation neglects the *fringing* of the electric field at the plate edges illustrated in Fig. 9.12b. For $w \gg d$, the fringing of the electric field has a minor contribution to the capacitance. An exact expression for the capacitance cannot be obtained for this structure. A numerical approximation method, the method of moments, can be used to obtain a very accurate value of the capacitance [1, 8].

In principle, the method of moments is a very simple technique. In order to illustrate this method, let us reconsider the parallel-plate capacitor problem. The approximate relation in (9.40) *assumes* that the charge distribution over each plate is *uniform*, that is, does not vary over the plates. In actuality, the charge distribution will peak at the edges. To model this we break each plate into small rectangular areas Δs_i, and assume the *form of the distribution* of the charge over these subareas but with unknown amplitudes. Two common distributions are shown in Fig. 9.13. In Fig. 9.13a, we approximate the charge over each subarea as being constant with an unknown level, α_i C/m^2. The total charge on each plate having been divided into N subareas is

$$Q \cong \sum_{i=1}^{N} \alpha_i \Delta s_i \quad \text{C (coulombs)} \tag{9.41}$$

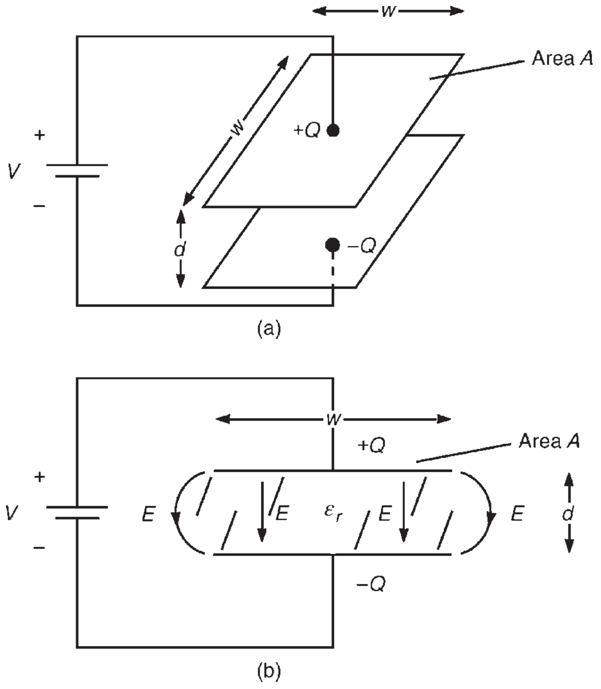

FIGURE 9.12 Calculation of the capacitance of a parallel-plate capacitor: (a) dimensions; (b) illustration of "fringing" of the electric field at the plate edges.

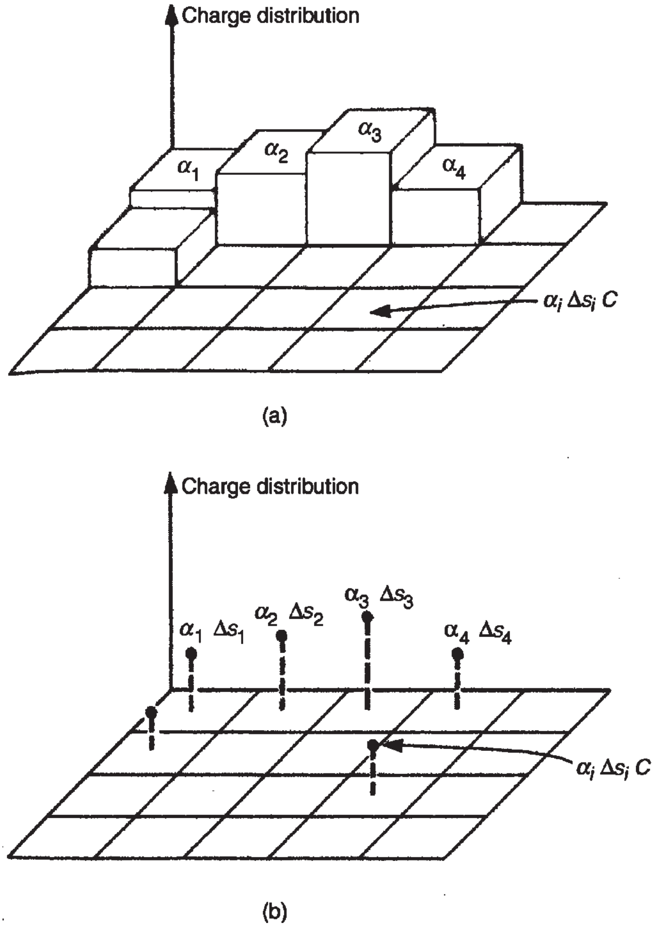
Charge distribution
α_1
α_2
α_3
α_4
$\alpha_i\,\Delta s_i\,C$
(a)
Charge distribution
$\alpha_1\ \Delta s_1$
$\alpha_2\ \Delta s_2$
$\alpha_3\ \Delta s_3$
$\alpha_4\ \Delta s_4$
$\alpha_i\,\Delta s_i\,C$
(b)

FIGURE 9.13 Approximating the charge distribution on the plates of a parallel-plate capacitor: (a) piecewise-constant approximation; (b) pointwise approximation.

Another approximation would be to concentrate all the charge of a subarea at a point at the center of the subarea, $\alpha_i \Delta s_i$ C as illustrated in Fig. 9.13b. The heart of this method is to determine the total voltage of each subarea as the *sum of the contributions from the charges on each subarea* as shown in Fig. 9.14a. Hence, the total voltage of a subarea is the sum of the contributions from all the charges of all the subareas (including the subarea under consideration):

$$V_j = \underbrace{K_{j1}\alpha_1 + \ldots + K_{JN}\alpha_N}_{\text{top-platecontributions}} + \underbrace{K_{JN+1}\alpha_{N+1} + \ldots + K_{j2N}\alpha_{2N}}_{\text{bottom-platecontributions}} \tag{9.42}$$

Each term K_{j1} represents as basic *subproblem* relating the voltage of a subarea V_j to the charge amplitude on another subarea α_i as

$$K_{ji} = \frac{V_j}{\alpha_i} \tag{9.43}$$

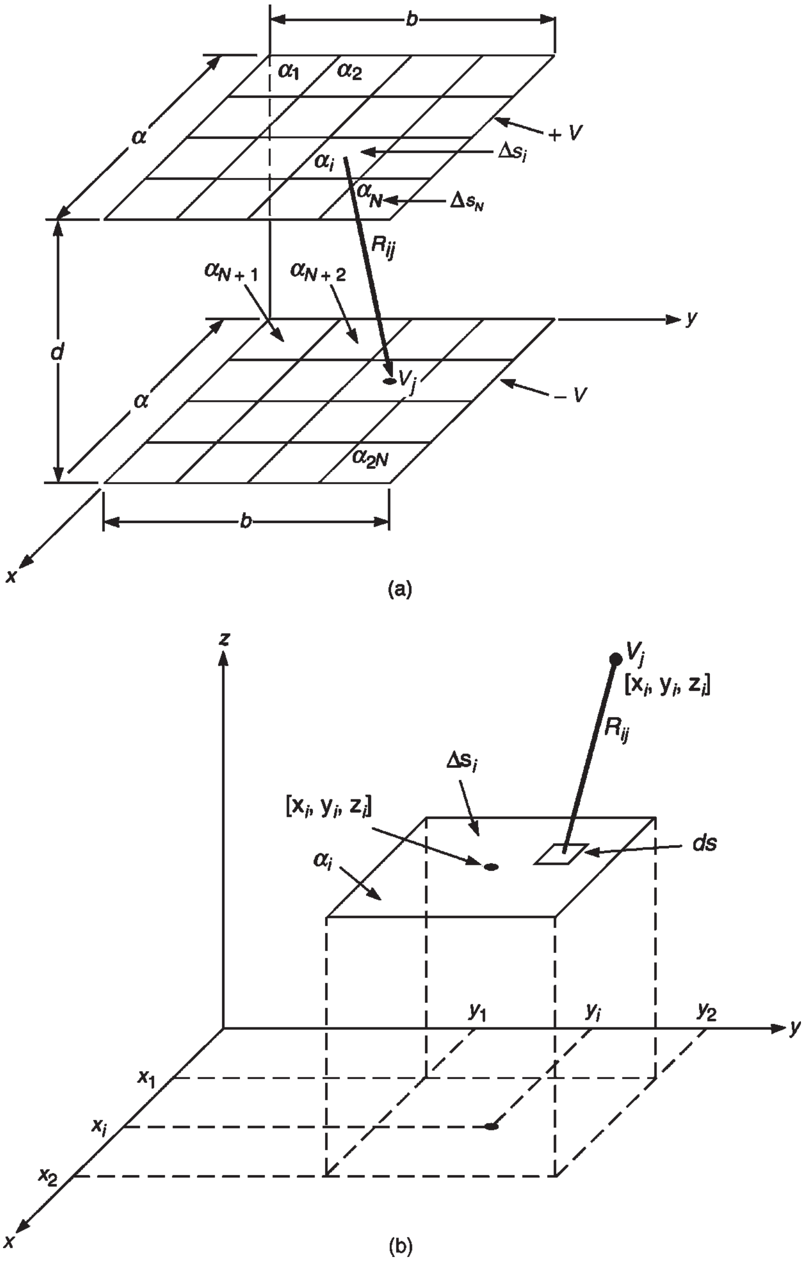
b
α
α_1
α_2
+ V
Δs_i
α_i
α_N
Δs_N
R_{ij}
α_{N+1}
α_{N+2}
d
y
V_j
− V
α
α_{2N}
b
x
(a)
z
V_j
$[x_j, y_j, z_j]$
R_{ij}
Δs_i
$[x_i, y_i, z_i]$
ds
α_i
y_1
y_i
y_2
y
x_1
x_i
x_2
x
(b)

FIGURE 9.14 Illustration of the method of moments (MoM) for numerical solution of the parallel-plate capacitor: (a) enforcing the potential at a subarea due to charge on another subarea; (b) the fundamental canonical problem to be solved.

as illustrated in Fig. 9.14b. Because of symmetry (both plates are identical), we can assign the voltage of the top plate (with respect to infinity) as $+V$ and the voltage of the bottom plate (with respect to infinity) as $-V$. The voltage between the two plates is then $2V$, so that the capacitance is

$$C = \frac{Q}{2V} \tag{9.44}$$

For example, for the pulse approximation of the charge distribution in Fig. 9.13b, it can be shown that [1, 8]

$$K_{ji} = \frac{\Delta s_i}{4\pi\varepsilon R_{ij}} \tag{9.45a}$$

where R_{ij} is the distance between the subarea bearing the unknown charge, $\alpha_i \Delta s_i$, and the subarea where we are evaluating the voltage, V_j. For a self-term, $j = i$, (9.45a) is not usable. Assuming a constant distribution over the subarea, it can also be shown that [1, 8]

$$\begin{aligned} K_{ii} &= \frac{\Delta w}{\pi\varepsilon_0} \ln(1+\sqrt{2}) \\ &= 0.8814 \frac{\Delta w}{\pi\varepsilon_0} \end{aligned} \tag{9.45b}$$

and each subarea is ($\Delta w \times \Delta w$). Grouping (9.42) for all subareas gives a matrix equation to be solved (which is the final result for all such MoM schemes):

$$\begin{bmatrix} K_{11} & K_{12} & \cdots & K_{1(2N)} \\ K_{21} & K_{22} & \cdots & K_{2(2N)} \\ \vdots & \vdots & \cdots & \vdots \\ K_{N1} & K_{N2} & \cdots & K_{N(2N)} \\ \vdots & \vdots & \cdots & \vdots \\ \vdots & \vdots & \cdots & \vdots \\ K_{(2N)1} & K_{(2N)2} & \cdots & K_{(2N)(2N)} \end{bmatrix} \begin{bmatrix} \alpha_1 \\ \alpha_2 \\ \vdots \\ \alpha_N \\ \alpha_{N+1} \\ \vdots \\ \alpha_{2N} \end{bmatrix} = \begin{bmatrix} +V \\ +V \\ \vdots \\ +V \\ -V \\ \vdots \\ -V \end{bmatrix} = \begin{bmatrix} +1 \\ +1 \\ \vdots \\ +1 \\ -1 \\ \vdots \\ -1 \end{bmatrix} \tag{9.46}$$

and we have assigned all subareas on the top plate to have voltages of +1 V and all subareas on the bottom plate have voltages of −1 V. Once (9.46) is solved for all the α_i charge distribution coefficients, the total charge on each plate can be determined from (9.41) and the total capacitance can be determined from (9.44). Figure 9.15 shows the results comparing the MoM result to the approximate capacitance neglecting fringing of the field given in (9.40) for free space between the plates [8]. The result is in terms of the ratio of plate separation d to the width w of the plates. This illustrates that for plates that are closely separated relative to their width, $d/w \ll 1$, the approximate result neglecting fringing given in (9.40) is reasonably accurate. But for larger ratios such as $d = w$, the MoM result gives the more accurate result.

In the following two sections, we will show MoM methods for determining accurate values of the per-unit-length capacitances of common multiconductor transmission lines: (1) ribbon cables including their dielectric insulations, and (2) conductors of rectangular cross section (PCB lands) including the dielectric substrate.

9.3.3.1 Wires with Dielectric Insulations (Ribbon Cables) Ribbon cables consist of dielectric-insulated wires held in a linear array. A five-wire ribbon cable is illustrated in Fig. 9.16 showing typical dimensions. One of the wires (the leftmost wire in this illustration) is chosen as the reference conductor for the line. In order to illustrate the MoM method for determining the per-unit-length parameter matrices for this line, first observe that there will be two charge distributions that we will need to approximate as shown in Fig. 9.17a. At the air–dielectric interface, there is a *bound charge* distribution that exists on the surface of the dielectric. Bound charge is

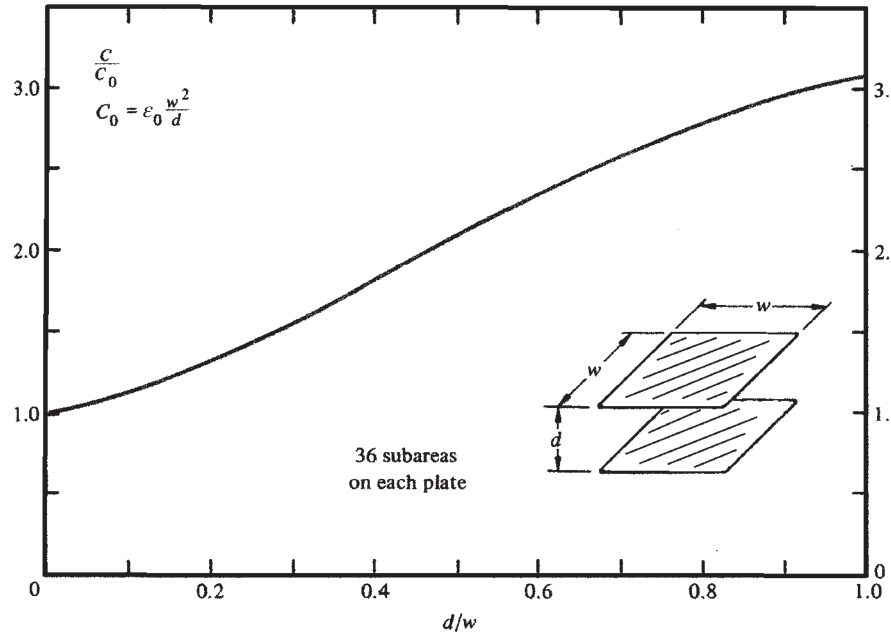

FIGURE 9.15 Plot of the capacitance of a parallel-plate capacitor obtained from the method of moments as a function of the ratio of plate separation to plate width [8]. Source: Harrington [8]/Macmillan.

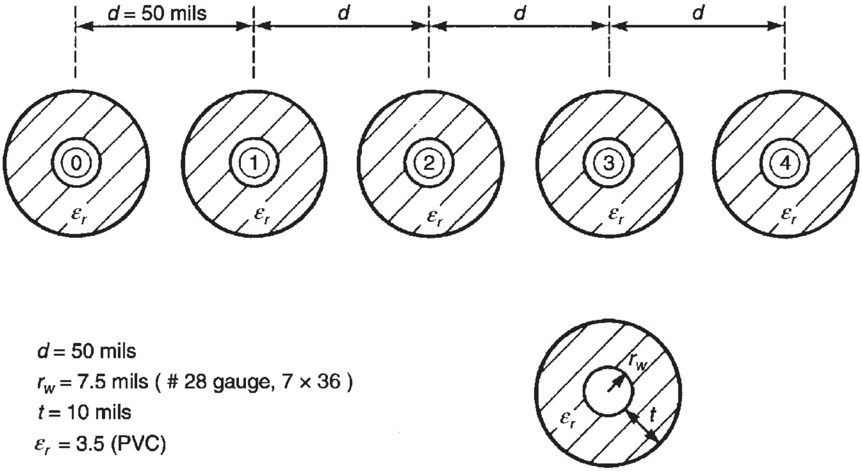

d = 50 mils
d
d
d
0
1
2
3
4
ε_r
d = 50 mils
r_w = 7.5 mils (# 28 gauge, 7 × 36)
t = 10 mils
ε_r = 3.5 (PVC)
r_w
t

FIGURE 9.16 A five-wire ribbon cable illustrating typical dimensions.

caused by rotation of the dipoles of charge in the dielectric to align with any applied electric field as illustrated in Fig. 9.17b [1–3]. To account for proximity effect, we will represent this charge distribution around the dielectric periphery as a Fourier series in the angle θ. For the i^{th} wire, we represent the bound charge distribution as

$$\hat{\rho}_{ib} = \hat{\alpha}_{i0} + \sum_{k=1}^{\hat{N}_i} \hat{\alpha}_{ik} \cos(k\theta_i) \ \ \mathrm{C/m^2} \tag{9.47}$$

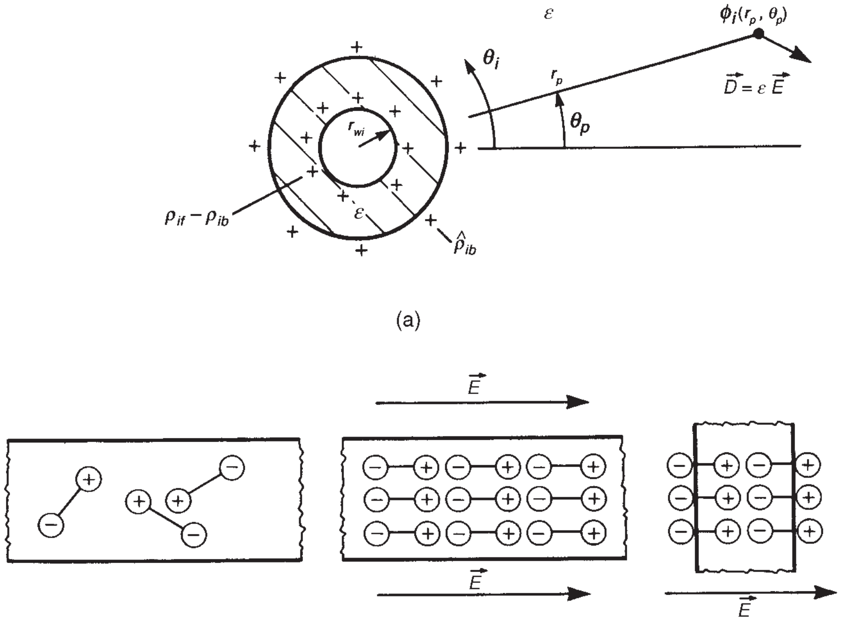

(a)

(b)

FIGURE 9.17 Representation of dielectric with bound charge: (a) illustration of the bound and total charge distributions at the insulation–air interface and the wire–insulation interface; (b) illustration of the alignment of the bound charge dipoles with an applied electric field. Source: Based on Paul and Nasar [1], Paul [2], and Paul [3].

Note that the charge distribution has the units of C/m^2, that is, a distribution around the dielectric periphery *and* along the wire axis. We use $\hat{N}_i + 1$ expansion coefficients (as yet unknown) $\hat{\alpha}_{i0}, \ldots, \hat{\alpha}_{i\hat{N}_i}$. At the interface between the conductor surface and the dielectric insulation, there will be a combination of *free charge* on the conductor surface and *bound charge* on the dielectric surface, which we represent as

$$\rho_{if} - \rho_{ib} = \alpha_{i0} + \sum_{k=1}^{N_i} \alpha_{ik} \cos(k\theta_i) \quad \text{C/m}^2 \tag{9.48}$$

The bound charge around the conductor–dielectric interface is opposite in sign to the bound charge around the dielectric interface. When we determine these expansion coefficients to match the boundary conditions, the total per-unit-length charges can be obtained by integrating the distributions in (9.47) and (9.48) around each periphery. At the air–dielectric periphery, the total per-unit-length charge is

$$\begin{aligned} q_{ib} &= \int_{\theta=0}^{2\pi} \hat{\rho}_{ib}(r_w + t)\, d\theta \\ &= 2\pi\,(r_w + t)\hat{\alpha}_{i0} \quad \text{C/m} \end{aligned} \tag{9.49}$$

and around the conductor–dielectric periphery is

$$\begin{aligned} q_{if} - q_{ib} &= \int_{\theta=0}^{2\pi} (\rho_{if} - \rho_{ib}) r_w d\theta \\ &= 2\pi r_w \alpha_{i0} \quad \text{C/m} \end{aligned} \tag{9.50}$$

Hence, the total per-unit-length charge depends only on the constant term in each charge expansion. The per-unit-length capacitances depend on *free charge* so that

$$q_{if} = 2\pi(r_w + t)\hat{\alpha}_{i0} + 2\pi r_w \alpha_{i0} \text{ C/m} \tag{9.51}$$

Hence, we need to determine the constant terms in the expansions.

Each wire has a total of $N_i + 1 + \hat{N}_i + 1$ unknown expansion coefficients associated with it. In order to determine these, we select $N_i + 1$ *match points* on the conductor–dielectric interface of each wire, where we will impose the requirement that the potential of each point (the voltage with respect to infinity) will be that of the wire ϕ_i and select $\hat{N}_i + 1$ *match points* around the dielectric–free-space interface of each wire where we will impose the boundary condition (see Appendix B) that the components of the electric flux density vector **D** must be continuous across the boundary. Hence, we have two basic subproblems illustrated in Fig. 9.17a: (1) determination of the potential at some point that is a distance r_P and angle θ_P from each charge distribution on the i^{th} wire, $\phi_i(r_P, \theta_P)$; and (2) determination of the electric flux density vector as some point that is a distance r_P and angle θ_P from each charge distribution on the ith wire, $\mathbf{D}(r_P, \theta_P)$. It is a simple matter to determine the solutions for these basic subproblems [1, 3, 7]. Applying these conditions on all the wires in the cable gives a set of simultaneous equations to be solved as

$$\begin{bmatrix} \mathbf{A} & \mathbf{B} \\ \mathbf{C} & \mathbf{D} \end{bmatrix} \begin{bmatrix} \sigma \\ \hat{\sigma} \end{bmatrix} = \begin{bmatrix} \phi \\ 0 \end{bmatrix} \tag{9.52}$$

Expanding these gives

$$\mathbf{A}\sigma + \mathbf{B}\hat{\sigma} = \phi \tag{9.53a}$$

$$\mathbf{C}\sigma + \mathbf{D}\hat{\sigma} = 0 \tag{9.53b}$$

The first set in (9.53a) enforce the potentials on the conductors from all charge distributions, and the second set in (9.53b) enforces continuity of the normal components of the electric flux density vector across the dielectric–free-space boundary due to all charge distributions. Inverting (9.52) gives the charge expansion coefficients in terms of the potentials from which we can obtain the per-unit-length capacitance matrix. See [3] and [9] for the details.

Appendix C describes a FORTRAN computer program, RIBBON.FOR, that implements this method and can be used to compute the per-unit-length capacitance matrix, **C** and the per-unit-length inductance matrix **L**. Tables 9.1 and 9.2 show the results for a three-wire ribbon cable where *the outer wire is chosen as the reference conductor* and 10 expansion coefficients are used around

TABLE 9.1 The Transmission-Line Capacitances for the Three-Wire Ribbon Cable with and without the Insulation Dielectrics. Outer Wire Chosen as the Reference

Entry	With Dielectric (pF/m)	Without Dielectric (pF/m)	Effective Dielectric Constant, ε_r'
$c_G + c_m$	37.432	22.494	1.664
$-c_m$	−18.716	−11.247	1.664
$c_R + c_m$	24.982	16.581	1.507

TABLE 9.2 The Transmission-Line Inductances for the Three-Wire Ribbon Cable Computed Exactly and Using the Wide-Separation Approximations. Outer Wire Chosen as the Reference

Entry	Exact (μH/m)	Wide Separation, Approximation (μH/m)	Percent Error
l_G	0.74850	0.75885	1.38
l_m	0.50770	0.51805	2.04
l_R	1.0154	1.0361	2.04

each dielectric–free-space interface and 10 coefficients are used around each conductor–dielectric interface. Hence for this three-wire cable, the simultaneous equations in (9.52) will be 60×60. The per-unit-length inductances in Table 9.2 can be rather accurately calculated using the wide-separation approximations of the previous section (of course, the dielectric insulations have no effect on inductance), but Table 9.1 shows that the dielectric insulations cannot be ignored in computing the per-unit-length capacitances.

9.3.3.2 Rectangular Cross-Section Conductors (PCB Lands) We next apply the method of moments to the PCB structures shown in Fig. 9.3. We will illustrate the method for the PCB structure of Fig. 9.3c consisting of three conductors of rectangular cross section (lands) on the surface of a PCB substrate shown in Fig. 9.18a. One of the lands will be chosen for the reference conductor. First let us consider computing this with the board removed as illustrated in Fig. 9.18b. Again, because of proximity effect, the charge distribution across each land will not be constant but will tend to concentrate toward the edges of each land as illustrated in Fig. 9.19. The basic idea is to approximate this charge variation across each land by breaking each land into subsections over which we assume the charge distribution is constant with unknown level, α_{ij} C/m^2 (the pulse expansion approximation) as

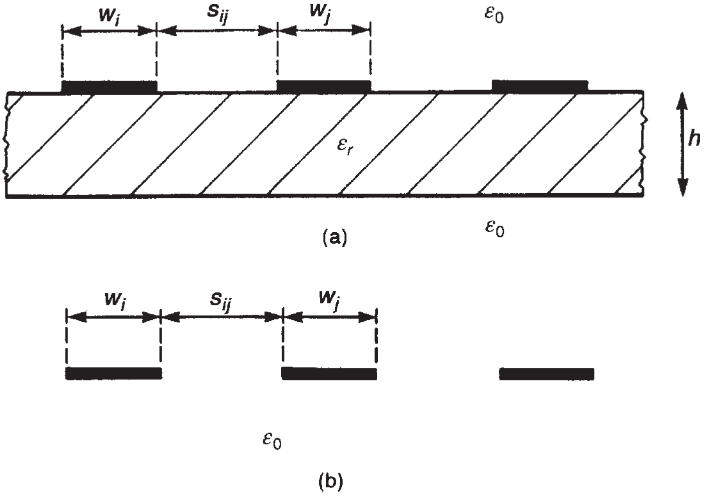

FIGURE 9.18 A printed circuit board (PCB) for illustration of the determination of the per-unit-length capacitances: (a) three conductors of rectangular cross section (lands) on the surface of a PCB substrate; (b) three lands from (a) with board removed.

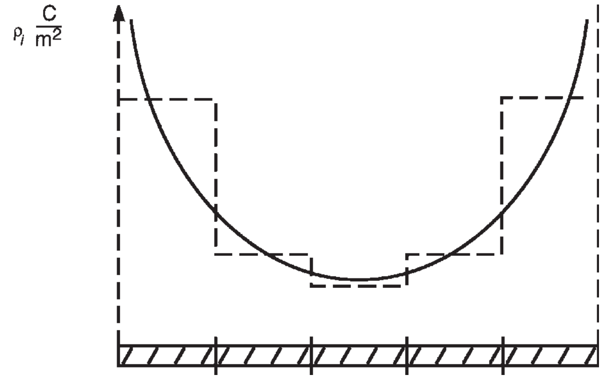
$\rho_i\ \frac{C}{m^2}$

FIGURE 9.19 Illustration of peaking of the charge distribution at the edges of the lands.

illustrated in Figs. 9.19 and 9.20a. If each strip is divided into N_i subsections, the total per-unit-length charge on that strip is determined by summing the products of the expansion coefficient times the width of that subsection, w_{ik}:

$$q_i = \sum_{k=1}^{N_i} \alpha_{ik} w_{ik} \ \text{C/m} \tag{9.54}$$

In order to generate a set of simultaneous equations to be solved for these unknown expansion levels over the land subsections, we must enforce the boundary condition that the potential (voltage with respect to infinity) of each subsection *due to all charge distributions* is that of the land

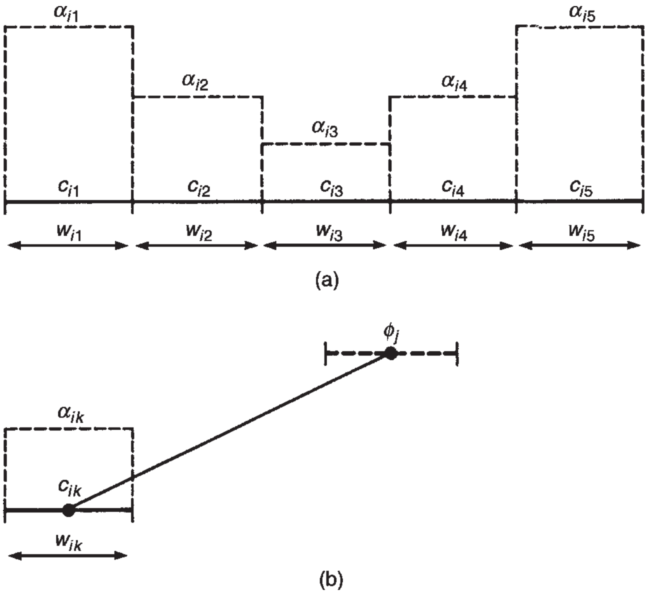
α_{i1}
α_{i2}
α_{i3}
α_{i4}
α_{i5}
c_{i1}
c_{i2}
c_{i3}
c_{i4}
c_{i5}
w_{i1}
w_{i2}
w_{i3}
w_{i4}
w_{i5}
(a)
ϕ_j
α_{ik}
c_{ik}
w_{ik}
(b)

FIGURE 9.20 Illustration of the pulse expansion of a charge distribution on a flat strip: (a) expanded view of land subsections over which the charge variation is constant; (b) potential of each subsection is the integral of the contributions of all charge distributions for the land under consideration.

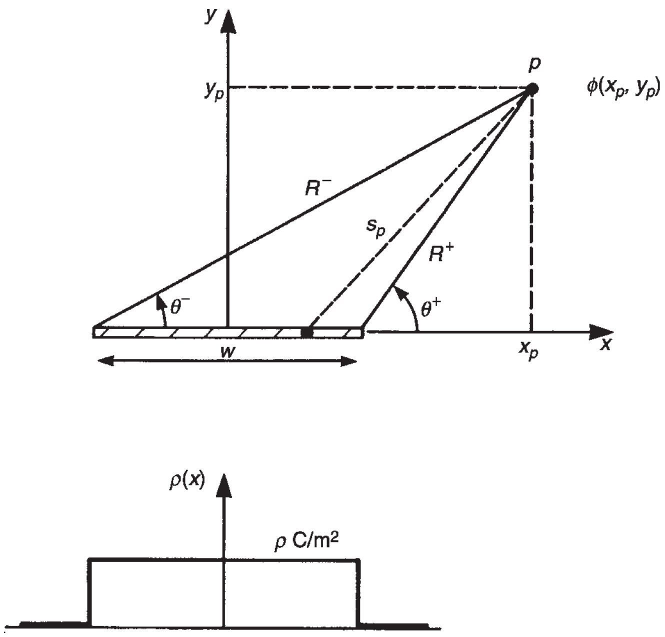

FIGURE 9.21 Calculation of the potential due to a constant charge distribution on a flat strip. Source: Paul [3]/John Wiley & Sons.

being considered. Hence, we need to solve the basic subproblem illustrated in Fig. 9.20b. This basic subproblem has a fairly simple solution illustrated in Fig. 9.21 as [3]

$$\begin{aligned}\phi(w, x_p, y_p) &= -\frac{\rho}{2\pi\varepsilon}\int_{x=-w/2}^{w/2} \ln\left[\sqrt{(x_p - x)^2 + (y_p)^2}\right] dx \\ &= -\frac{\rho}{4\pi\varepsilon}\left\{\left(x_p + \frac{w}{2}\right)\ln\left[\left(x_p + \frac{w}{2}\right)^2 + y_p^2\right]\right. \\ &\quad - \left(x_p - \frac{w}{2}\right)\ln\left[\left(x_p - \frac{w}{2}\right)^2 + y_p^2\right] - 2w \\ &\quad \left. + 2y_p\left[\tan^{-1}\left(\frac{x_p + \frac{w}{2}}{y_p}\right) - \tan^{-1}\left(\frac{x_p - \frac{w}{2}}{y_p}\right)\right]\right\}\end{aligned} \tag{9.55}$$

Again, in order to generate the same number of equations as we have unknown subsection distributions, we match the potential at the center of each subsection strip due to all charge distributions, giving

$$\begin{bmatrix}\mathbf{\Phi}_0 \\ \vdots \\ \mathbf{\Phi}_i \\ \vdots \\ \mathbf{\Phi}_n\end{bmatrix} = \begin{bmatrix}\mathbf{D}_{00} & \dots & \mathbf{D}_{0j} & \dots & \mathbf{D}_{0n} \\ \vdots & \vdots & \vdots & \vdots & \vdots \\ \mathbf{D}_{i0} & \dots & \mathbf{D}_{ij} & \dots & \mathbf{D}_{in} \\ \vdots & \vdots & \vdots & \vdots & \vdots \\ \mathbf{D}_{n0} & \dots & \mathbf{D}_{nj} & \dots & \mathbf{D}_{nn}\end{bmatrix}\begin{bmatrix}\mathbf{A}_0 \\ \vdots \\ \mathbf{A}_j \\ \vdots \\ \mathbf{A}_n\end{bmatrix} \tag{9.56a}$$

and we have shown a general result for a total of n lands. The vector of potentials at the match points on the i^{th} land is denoted as

$$\mathbf{\Phi}_i = \begin{bmatrix} \phi_i \\ \vdots \\ \phi_i \\ \vdots \\ \phi_i \end{bmatrix} \tag{9.56b}$$

and the vector of expansion coefficients is denoted as

$$\mathbf{A}_i = \begin{bmatrix} \alpha_{i1} \\ \vdots \\ \alpha_{ik} \\ \vdots \\ \alpha_{iN_i} \end{bmatrix} \tag{9.56c}$$

and each land is broken into N_i segments. Once (9.56a) is inverted, we can determine the unknown expansion coefficients and hence the total per-unit-length charge on each land as in (9.54).

In order to include the PCB dielectric substrate into these calculations, we could represent, as with ribbon cables, the bound charge at the dielectric surfaces in the same fashion. But this would not be appropriate for this case since each surface extends to infinity. So instead we resolve the basic subproblem *with the dielectric included* by imaging across the dielectric surfaces as illustrated in Fig. 9.22. The details are given in [3], but once this is solved, the procedure described above remains the same. Appendix C describes a FORTRAN program that implements this method for the PCB structure in Fig. 9.3c, PCB.FOR. The coupled stripline of Fig. 9.3a has a similar FORTRAN program, STRPLINE.FOR, described in Appendix C, whereas the FORTRAN program for the coupled microstrip in Fig. 9.3b is implemented in the program MSTRP.FOR that is also described in Appendix C. Hence, accurate, numerical results can be obtained for the per-unit-length capacitance matrix $\mathbf{C}$ with these codes. In addition, the per-unit-length capacitance matrix with the PCB substrate removed and replaced with free space $\mathbf{C}_0$ is also obtained with these codes so that the per-unit-length inductance matrix is obtained as $\mathbf{L} = \mu_0\varepsilon_0\mathbf{C}_0^{-1}$. These programs, like the one for ribbon cables, are designed to handle lines with more than three conductors, although the compiled codes, XXXX.EXE, are dimensioned for three conductors. If one wishes to use these codes for lines consisting of more than three conductors, one must change the dimensions in the XXXX.FOR program (directions for doing this are included in those programs) and recompile them.

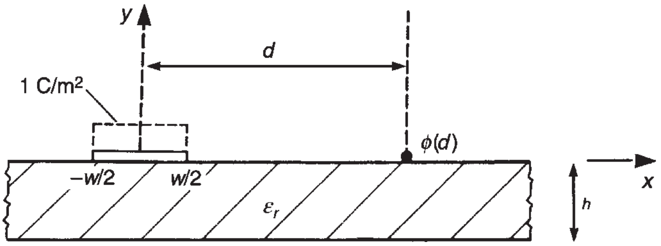

FIGURE 9.22 Calculation of the contribution to the potential at a point due to the charge distribution on a land.

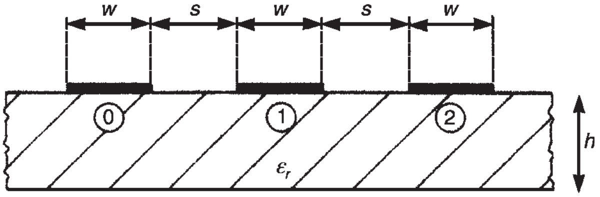

FIGURE 9.23 A PCB consisting of identical conductors with identical separations for computation of numerical results.

Consider the three-conductor PCB structure where the leftmost land is designated as the reference conductor as shown in Fig. 9.23 and having dimensions typical of PCBs of $w = 15$ mils, $s = 15$ mils, $h = 47$ mils, and $\varepsilon_r = 4.7$ (glass epoxy). The per-unit-length inductance and capacitance matrices, computed with each land divided into 30 subsections with the code PCB.FOR, are

$$\mathbf{L} = \begin{bmatrix} 1.105 & 0.691 \\ 0.691 & 1.381 \end{bmatrix} \ \mu\text{H/m}$$

and

$$\mathbf{C} = \begin{bmatrix} 40.6 & -20.3 \\ -20.3 & 29.7 \end{bmatrix} \ \text{pF/m}$$

9.4 THE INDUCTIVE–CAPACITIVE COUPLING APPROXIMATE MODEL

Solution of the coupled MTL equations in (9.3) is, in general, a difficult task. The typical method of solution is to decouple them with a matrix transformation [3, 10]. This is considered in more detail for the generation of a SPICE program in Appendix D. The exact solution in literal form (symbols instead of numbers) can be obtained for three-conductor, lossless lines *in homogeneous media*. That solution is given in [3, 11]. However, this does not apply for the PCB lines in Fig. 9.3, which are in an inhomogeneous medium. Solution of the MTL equations for lines in an inhomogeneous medium for PCB configurations rarely can be obtained in literal form. However, it is possible to obtain a literal solution if we make the assumption that the lines are *weakly coupled* [12]. The condition of weak coupling is described as follows. The current and voltage of the generator circuit will induce voltages and currents in the receptor circuit through the mutual inductance l_m and mutual capacitance c_m. In turn, these induced currents and voltages in the receptor circuit will, as a second-order effect, induce currents and voltages back into the generator circuit. By assuming weak coupling, we mean that these voltages and currents induced in the generator circuit due to the currents and voltages that were induced in the receptor circuit *may be ignored*, that is, the induction of currents and voltages from one circuit to another is a *one-way effect* (from the generator circuit to the receptor circuit). From the standpoint of the MTL equations in (9.2), the condition of *weak coupling* means that the equations for the generator circuit are approximated, by neglecting the mutual terms, as

$$\frac{\partial V_G(z,t)}{\partial z} + l_G \frac{\partial I_G(z,t)}{\partial t} = 0 \tag{9.57a}$$

$$\frac{\partial I_G(z,t)}{\partial z} + (c_G + c_m) \frac{\partial V_G(z,t)}{\partial t} = 0 \tag{9.57b}$$

and the equations for the receptor circuit are unchanged:

$$\frac{\partial V_R(z,t)}{\partial z} + l_R \frac{\partial I_R(z,t)}{\partial t} = -l_m \frac{\partial I_G(z,t)}{\partial t} \tag{9.58a}$$

$$\frac{\partial I_R(z,t)}{\partial z} + (c_R + c_m) \frac{\partial V_R(z,t)}{\partial t} = c_m \frac{\partial V_G(z,t)}{\partial t} \tag{9.58b}$$

The equations have also been rewritten by moving the self-terms to the left-hand side in order to present them in the form of those for isolated two-conductor lines as discussed in Chapter 4. Observe in the equations governing the current and voltage of the generator circuit (the circuit being driven by the source) in (9.57), we have omitted the mutual coupling terms $l_m \partial I_R(z, t)/\partial t$ and $c_m \partial V_R(z, t)/\partial t$, which cause the back interaction of inducing voltages and currents in the generator circuit due to currents and voltages in the receptor circuit. (See Eqs. (9.2a) and (9.2c).) Thus, we can solve for the voltage and current in the generator circuit, $V_G(z, t)$ and $I_G(z, t)$, as though it were an isolated, two-conductor transmission line using the methods of Chapter 4.

Once the voltage and current of this (isolated) generator circuit are obtained, we place induced sources due to these via the mutual inductance and mutual capacitance into the receptor circuit [12]. The sources induced in the receptor circuit are represented by the terms on the right-hand-sides of the equations in (9.58):

$$-l_m \frac{\partial I_G(z,t)}{\partial t} \tag{9.59a}$$

$$c_m \frac{\partial V_G(z,t)}{\partial t} \tag{9.59b}$$

These sources induced in the receptor circuit are visualized as shown in Fig. 9.24. The source in (9.59a) is essentially a Faraday-law-induced source. From (9.15), the per-unit-length magnetic flux penetrating the receptor circuit is given by

$$\psi_R = l_R I_R + l_m I_G \tag{9.60}$$

Faraday's law (see Appendix B) provides that a per-unit-length voltage will be induced in the receptor circuit that is due to the *time rate of change of the magnetic flux penetrating the loop formed by the conductors of the receptor circuit*. Hence, two per-unit-length sources will be induced in the receptor circuit:

$$V_{S1} = l_R \frac{\partial I_R}{\partial t} \tag{9.61a}$$

and

$$V_{S2} = l_m \frac{\partial I_G}{\partial t} \tag{9.61b}$$

Source V_{S1} is produced by the self-inductance of the receptor circuit. Source V_{S2} is produced by the mutual inductance between the two circuits and the current of the generator circuit. As a first-order model, we will ignore the effect of V_{S1}. Hence, we may represent the receptor circuit with one source, V_{S2}, as illustrated in Fig. 9.24a. Because this source is due to magnetic field coupling, it is referred to as *inductive coupling*. The total for a Δz section length will be the per-unit-length source multiplied by Δz.

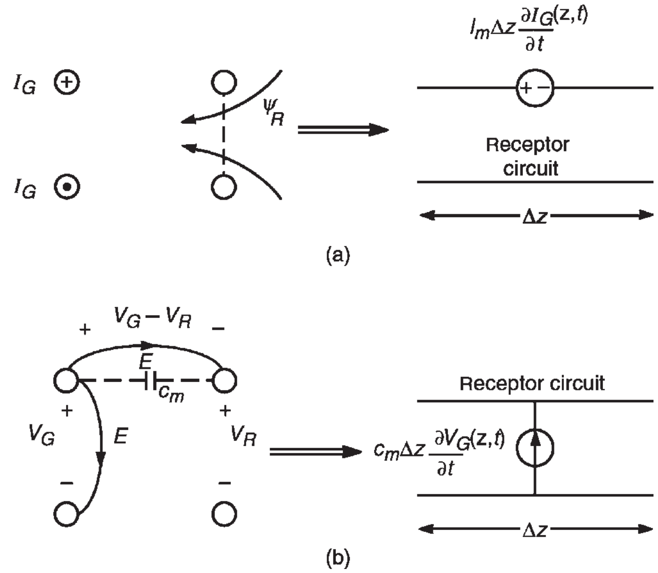

FIGURE 9.24 Explanation of the two components of crosstalk: (a) magnetic field or inductive coupling; (b) electric field or capacitive coupling.

Similarly, the charges on the two circuits are related to the voltages of the two circuits by the per-unit-length capacitance matrix in (9.21). From this, we write the per-unit-length charge induced on the receptor circuit as

$$\begin{aligned} q_R &= (c_R + c_m)V_R - c_m V_G \\ &= c_R V_R - c_m (V_G - V_R) \end{aligned} \tag{9.62}$$

Current is the time rate-of-change of charge and hence per-unit-length current sources will be induced between the two conductors of the receptor circuit of

$$I_{S1} = (c_R + c_m)\frac{\partial V_R}{\partial t} \tag{9.63a}$$

$$I_{S2} = -c_m \frac{\partial V_G}{\partial t} \tag{9.63b}$$

The first current source, I_{S1}, in (9.63a) is simply the current source induced by the receptor circuit self-capacitance. Source I_{S2} is produced by the mutual capacitance between the two circuits. Again, as a first-order model, we will ignore the effect of I_{S1}. Hence we will represent the receptor circuit with one source, I_{S2}, as illustrated in Fig. 9.24b. Because this source is due to electric field coupling, it is referred to as *capacitive coupling*. Hence we will represent the receptor circuit by combining the two sources in (9.61b) and (9.63b) and lumping them together to represent the entire line with total mutual inductance and total mutual capacitance of $L_m = l_m \mathcal{L}$ and $C_m = c_m \mathcal{L}$, respectively, where $\mathcal{L}$ is the total line length as shown in Fig. 9.25a. Although this is a distributed parameter effect, we may

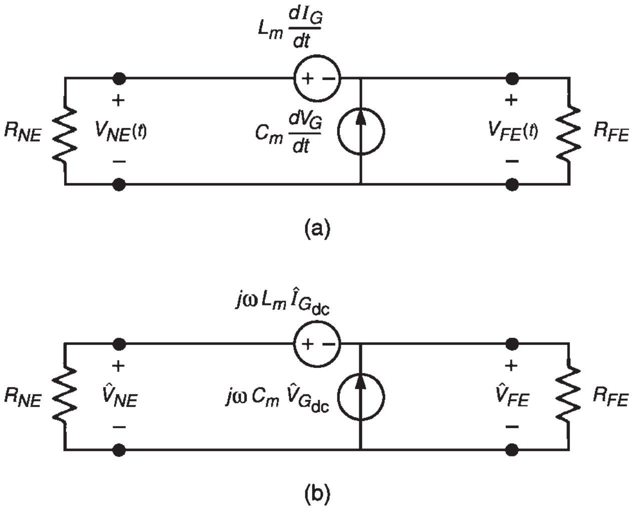

FIGURE 9.25 The simplified inductive–capacitive coupling crosstalk model: (a) time-domain model; (b) frequency-domain model.

lump them as shown on the assumption that the line is *electrically short* at the frequency of the driving source in the generator circuit.

This is referred to as the *inductive–capacitive coupling model*. The crosstalk takes place via two distinct coupling mechanisms: magnetic field coupling due to mutual inductance between the two circuits and electric field coupling due to mutual capacitance between the two circuits. There are two key assumptions in this model: (1) *we assume weak coupling between the generator and receptor circuits, that is, the coupling is a one-way effect from the generator circuit to the receptor circuit; and* (2) *the line is assumed to be electrically short at the frequency of the driving source in the generator circuit,* V_S*, that is,* $L \ll \lambda = (v/f)$.

9.4.1 Frequency-Domain Inductive–Capacitive Coupling Model

Our first main interest is for driving sources in the generator circuit, $V_S(t)$ in Fig. 9.1, that are single-frequency sinusoids; that is, we first determine the *frequency-domain response*. To do this we form the *phasor circuit* by replacing time derivatives with $j\omega$, where $\omega = 2\pi f$ and f is the frequency of the driving source (see Appendix A). The resulting equivalent circuit for the receptor circuit is given in Fig. 9.25b. In that circuit, we show the current and voltage of the generator circuit as being effectively the same as though the driving source was dc:

$$\hat{I}_{G_{\mathrm{dc}}} \cong \frac{1}{R_S + R_L} \hat{V}_S \tag{9.64a}$$

$$\hat{V}_{G_{\mathrm{dc}}} \cong \frac{R_L}{R_S + R_L} \hat{V}_S \tag{9.64b}$$

This is because we assume that *the line is electrically short* at the frequency of the driving source, i.e., $L \ll \lambda$, where $\lambda = (v/f)$ is a wavelength at the frequency f of the driving sinusoidal source, and hence the voltage and current do not vary appreciably in magnitude along the generator line. Hence, they are virtually the same as those produced by a dc source. From this equivalent circuit we may determine the near-end and far-end phasor crosstalk voltages using superposition as

$$\hat{V}_{NE} = \underbrace{\frac{R_{NE}}{R_{NE}+R_{FE}} j\omega L_m \hat{I}_{G_{\mathrm{dc}}}}_{\text{inductive coupling}} + \underbrace{\frac{R_{NE}R_{FE}}{R_{NE}+R_{FE}} j\omega C_m \hat{V}_{G_{\mathrm{dc}}}}_{\text{capacitive coupling}} \tag{9.65a}$$

$$\hat{V}_{FE} = \underbrace{-\frac{R_{FE}}{R_{NE}+R_{FE}} jwL_m \hat{I}_{G_{\mathrm{dc}}}}_{\text{inductive coupling}} + \underbrace{\frac{R_{NE}R_{FE}}{R_{NE}+R_{FE}} jwC_m \hat{V}_{G_{\mathrm{dc}}}}_{\text{capacitive coupling}} \tag{9.65b}$$

and $L_m = l_m L$ and $C_m = c_m L$ are the total mutual inductance and mutual capacitance of the line, respectively. Substituting (9.64) gives the final result

$$\hat{V}_{NE} = \underbrace{\frac{R_{NE}}{R_{NE}+R_{FE}} j\omega L_m \frac{1}{R_S+R_L} \hat{V}_S}_{\text{inductive coupling}} + \underbrace{\frac{R_{NE}R_{FE}}{R_{NE}+R_{FE}} j\omega C_m \frac{R_L}{R_S+R_L} \hat{V}_S}_{\text{capacitive coupling}} \tag{9.66a}$$

$$\hat{V}_{FE} = \underbrace{-\frac{R_{FE}}{R_{NE}+R_{FE}} j\omega L_m \frac{1}{R_S+R_L} \hat{V}_S}_{\text{inductive coupling}} + \underbrace{\frac{R_{NE}R_{FE}}{R_{NE}+R_{FE}} jwC_m \frac{R_L}{R_S+R_L} \hat{V}_S}_{\text{capacitive coupling}} \tag{9.66b}$$

The crosstalk can be viewed as a *transfer function* between the input $\hat{V}_S$ and the outputs $\hat{V}_{NE}$ and $\hat{V}_{FE}$. These transfer functions can be obtained by factoring out $\hat{V}_S$ and $j\omega$ to give

$$\frac{\hat{V}_{NE}}{\hat{V}_S} = j\omega \left(\frac{R_{NE}}{R_{NE}+R_{FE}} \frac{L_m}{R_S+R_L} + \frac{R_{NE}R_{FE}}{R_{NE}+R_{FE}} \frac{R_L C_m}{R_S+R_L} \right) \tag{9.67a}$$

$$\frac{\hat{V}_{FE}}{\hat{V}_S} = j\omega \left(-\frac{R_{FE}}{R_{NE}+R_{FE}} \frac{L_m}{R_S+R_L} + \frac{R_{NE}R_{FE}}{R_{NE}+R_{FE}} \frac{R_L C_m}{R_S+R_L} \right) \tag{9.67b}$$

These can be written as

$$\frac{\hat{V}_{NE}}{\hat{V}_S} = j\omega (M_{NE}^{\mathrm{IND}} + M_{NE}^{\mathrm{CAP}}) \tag{9.68a}$$

$$\frac{\hat{V}_{\mathrm{FE}}}{\hat{V}_S} = j\omega (M_{FE}^{\mathrm{IND}} + M_{FE}^{\mathrm{CAP}}) \tag{9.68b}$$

where

$$M_{NE}^{\mathrm{IND}} = \frac{R_{NE}}{R_{NE}+R_{FE}} \frac{L_m}{R_S+R_L} \tag{9.69a}$$

$$M_{NE}^{\mathrm{CAP}} = \frac{R_{NE}R_{FE}}{R_{NE}+R_{FE}} \frac{R_L C_m}{R_S+R_L} \tag{9.69b}$$

$$M_{FE}^{\text{IND}} = -\frac{R_{FE}}{R_{NE}+R_{FE}}\frac{L_m}{R_S+R_L} \tag{9.69c}$$

$$M_{FE}^{\text{CAP}} = M_{NE}^{\text{CAP}} = \frac{R_{NE}R_{FE}}{R_{NE}+R_{FE}}\frac{R_L C_m}{R_S+R_L} \tag{9.69d}$$

The inductive coupling dominates the capacitive coupling in the near-end crosstalk voltage in (9.68a), i.e., $M_{NE}^{\text{IND}} > M_{NE}^{\text{CAP}}$, if $(L_m/C_m) > R_{FE}R_L$. Similarly, the inductive coupling dominates the capacitive coupling in the far-end crosstalk voltage in (9.68b), i.e., $M_{FE}^{\text{IND}} > M_{FE}^{\text{CAP}}$, if $(L_m/C_m) > R_{NE}R_L$. It can be shown [3, 11] that for a homogeneous medium, these translate to

$$\frac{R_{FE}R_L}{(L_m/C_m)} = \frac{R_{FE}R_L}{Z_{CG}Z_{CR}} < 1 \tag{9.70a}$$

and

$$\frac{R_{NE}R_L}{(L_m/C_m)} = \frac{R_{NE}R_L}{Z_{CG}Z_{CR}} < 1 \tag{9.70b}$$

where the *characteristic impedances of each circuit in the presence of the other circuit* are defined by [3, 11]

$$Z_{CG} = \sqrt{\frac{l_G}{c_G + c_m}} \tag{9.71a}$$

and

$$Z_{CR} = \sqrt{\frac{l_R}{c_R + c_m}} \tag{9.71b}$$

Capacitive coupling dominates if the inequalities in (9.70) are reversed. Hence, we say that inductive coupling dominates capacitive coupling for termination impedances that are *low impedances* (with respect to the circuit characteristic impedance). Similarly, we say that capacitive coupling dominates inductive coupling for termination impedances that are *high impedances* (with respect to the circuit characteristic impedance). This makes sense because in "low-impedance circuits," currents tend to be the larger effect and inductive coupling is due to currents. Similarly, in "high-impedance circuits," voltages tend to be the larger effect and capacitive coupling is due to voltages.

Observe that *the inductive and capacitive coupling contributions are direct functions of the excitation frequency*. Therefore, they increase linearly with an increase in frequency, so that their frequency responses increase at a rate of +20 dB/decade, as shown in Fig. 9.26. Also *the total crosstalk transfer functions increase at 20 dB/decade. Depending on the load impedances, this frequency response may be due totally to one component or the other, as is illustrated in* Fig. 9.27. This observation will explain the effectiveness (or non-effectiveness) of shielded wires or twisted pairs in the reduction of crosstalk, which will be considered in Sections 9.7 and 9.8.

9.4.1.1 *Inclusion of Losses: Common-Impedance Coupling* The foregoing has assumed a lossless line—perfect conductors and a lossless medium. The assumption of a lossless medium is usually a reasonable assumption for frequencies below the low GHz range. However, imperfect conductors can produce significant crosstalk *at the lower frequencies*. This is referred to as *common-impedance coupling* and is easily seen from the following.

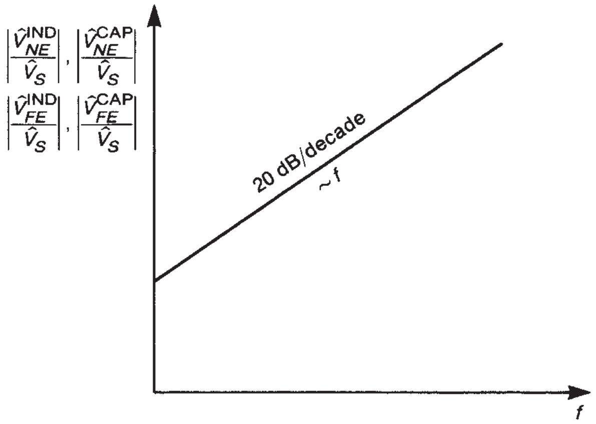

FIGURE 9.26 Frequency response of the crosstalk transfer function.

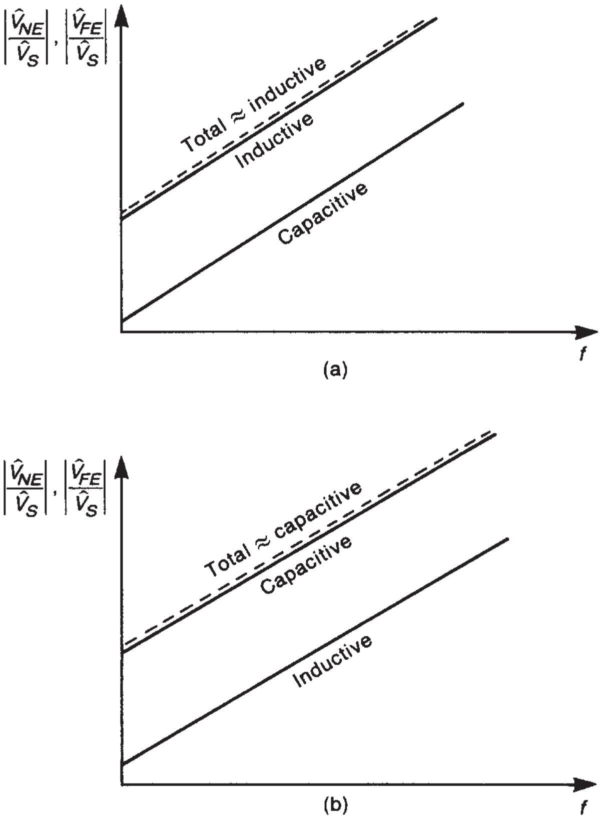

FIGURE 9.27 Effect of load impedance on the dominance of either inductive or capacitive coupling: (a) low-impedance loads; (b) high-impedance loads.

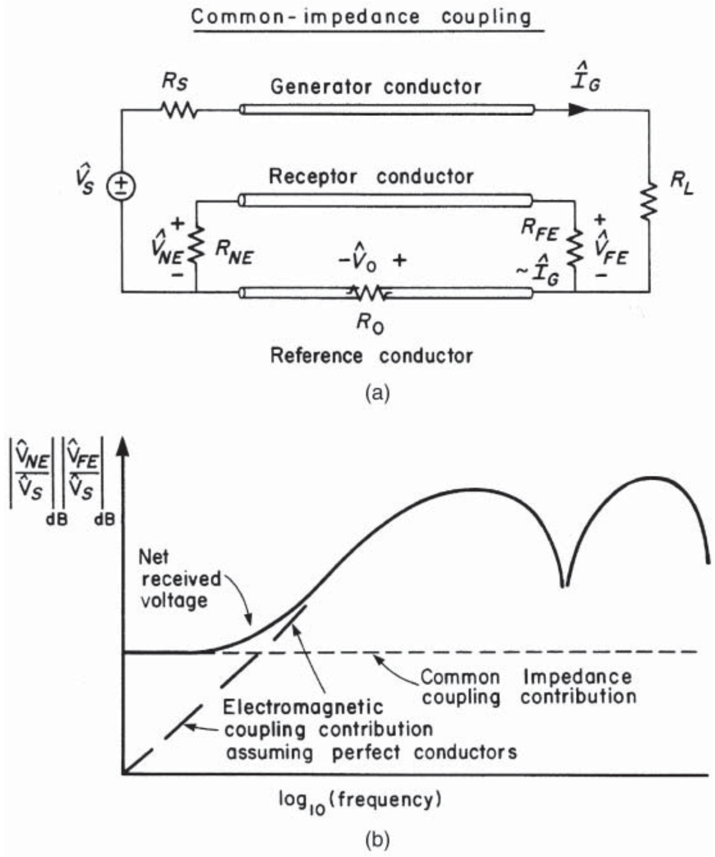
Common-impedance coupling
R_S
Generator conductor
$\hat{I}_G$
$\hat{V}_S$
Receptor conductor
R_L
+
$\hat{V}_{NE}$
−
R_{NE}
$-\hat{V}_0$ +
R_{FE}
$\sim\hat{I}_G$
+
$\hat{V}_{FE}$
−
R_0
Reference conductor
(a)
$\left|\frac{\hat{V}_{NE}}{\hat{V}_S}\right|_{dB}$ $\left|\frac{\hat{V}_{FE}}{\hat{V}_S}\right|_{dB}$
Net received voltage
Common Impedance coupling contribution
Electromagnetic coupling contribution assuming perfect conductors
$\log_{10}$(frequency)
(b)

FIGURE 9.28 Illustration of common-impedance coupling due to nonzero impedance of the reference conductor: (a) model; (b) frequency response of the crosstalk transfer function showing the common-impedance coupling floor at the lower frequencies.

Consider the circuit shown in Fig. 9.28a. For typical loads and low frequencies, the resistance of the reference conductor is usually much smaller than these load resistances, so that the majority of the generator wire current returns through the reference conductor. This produces a voltage drop V_0 across that conductor. For an electrically short line, we may lump the per-unit-length resistance of the reference conductor, r_0, as a single resistance $R_0 = r_0 L$. The voltage drop across the reference conductor is given by

$$\begin{aligned}\hat{V}_0 &= R_0 \hat{I}_G \\ &= \frac{R_0}{R_S + R_L}\hat{V}_S\end{aligned} \tag{9.72}$$

This voltage appears directly in the receptor circuit, producing contributions to the crosstalk transfer functions at low frequencies of

$$\frac{\hat{V}_{NE}^{CI}}{\hat{V}_S} = M_{NE}^{CI} \tag{9.73a}$$

$$\frac{\hat{V}_{FE}^{CI}}{\hat{V}_S} = M_{FE}^{CI} \tag{9.73b}$$

where

$$M_{NE}^{CI} = \frac{R_{NE}}{R_{NE} + R_{FE}} \frac{R_0}{R_S + R_L} \tag{9.74a}$$

$$M_{FE}^{CI} = -\frac{R_{FE}}{R_{NE} + R_{FE}} \frac{R_0}{R_S + R_L} \tag{9.74b}$$

This produces an essentially frequency independent “floor” at the lower frequencies, as shown in Fig. 9.28b.

The total coupling is approximately the sum of the inductive, capacitive, and common-impedance coupling:

$$\frac{\hat{V}_{NE}}{\hat{V}_S} = j\omega(M_{NE}^{\text{IND}} + M_{NE}^{\text{CAP}}) + M_{NE}^{CI} \tag{9.75a}$$

$$\frac{\hat{V}_{FE}}{\hat{V}_S} = j\omega(M_{FE}^{\text{IND}} + M_{FE}^{\text{CAP}}) + M_{FE}^{\text{CI}} \tag{9.75b}$$

9.4.1.2 Experimental Results As an example, consider the three-wire ribbon cable shown in Fig. 9.29. The cable consists of three 28-gauge (7 × 36) wires of total length $L = 4.737$ m (15.54 ft). The center wire is the reference conductor. The radii of the wires is 7.5 mils, the adjacent wire separation is 50 mils, the dielectric thicknesses are 10 mils, and the insulation is polyvinyl chloride (PVC) ($\varepsilon_r = 3.5$). Assuming free-space velocity of propagation, the line is a wavelength at 63.3 MHz. Hence, the line is electrically short for frequencies below approximately 6 MHz. The load resistors are equal, $R_L = R_{NE} = R_{FE} = R$, and $R_S = 0$. We will investigate two values for R: 50 Ω and 1 kΩ. The per-unit-length parameters were computed previously in Example 9.1 using the wide-separation approximation and ignoring the dielectric insulations as $l_G = l_R = 0.76$ μH/m, $l_m = 0.24$ μH/m, $c_G = c_R = 11.1$ pF/m, and $c_m = 5.17$ pF/m. Alternatively, these per-unit-length parameters were computed using the numerical MoM code RIBBON.FOR (described previously and in Appendix C) as $l_G = l_R = 0.749$ μH/m, $l_m = 0.24$ μH/m, $c_G = c_R = 18$ pF/m, and $c_m = 6.27$ pF/m. We will use the more accurate parameters computed with the numerical method. The characteristic impedance of each circuit in the presence of the other is $Z_{CG} = Z_{CR} = 173$ Ω. Therefore, we expect that inductive coupling will dominate for the 50 Ω loads and capacitive coupling will dominate for the 1 kΩ loads. The per-unit-length resistance of the reference wire is computed by determining the per-unit-length resistance of one of the 36-gauge strands and dividing this by 7 (the number of strands that are electrically in parallel). This gives $r_0 = 0.194$ Ω/m, so that the total resistance of the reference wire is $R_0 = 0.921$ Ω.

Note: A large amount of experimental data will be shown in this Chapter in order to confirm the validity of the prediction models that we will obtain. In the case of the frequency response of the crosstalk, the data will be measured at discreet frequencies of 1, 1.5, 2, 2.5, 3, 4, 5, 6, 7, 8, 9 in each decade. Hence, the reader can determine the precise frequency of a data point in these plots.

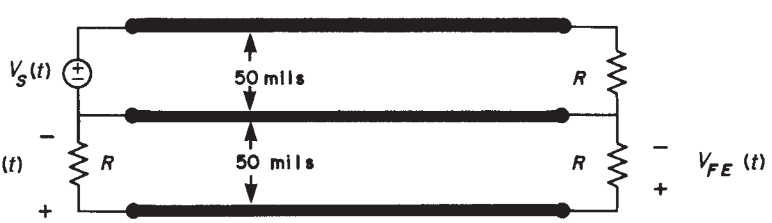

FIGURE 9.29 An experiment illustrating

For $R = 50\,\Omega$, we compute the contributions of the near-end crosstalk transfer function to be

$$\begin{aligned}
M_{NE}^{\mathrm{IND}} &= \frac{R_{NE}}{R_{NE}+R_{FE}}\frac{L_m}{R_S+R_L} \\
&= 1.14\times10^{-8} \\
M_{NE}^{\mathrm{CAP}} &= \frac{R_{NE}R_{FE}}{R_{NE}+R_{FE}}\frac{R_L C_m}{R_S+R_L} \\
&= 7.43\times10^{-10} \\
M_{NE}^{CI} &= \frac{R_{NE}}{R_{NE}+R_{FE}}\frac{R_0}{R_S+R_L} \\
&= 9.21\times10^{-3}
\end{aligned}$$

The inductive coupling component dominates the capacitive coupling component, as expected. The total coupling is

$$\begin{aligned}
\frac{\hat{V}_{NE}}{\hat{V}_S} &= j\omega\,(M_{NE}^{\mathrm{IND}} + M_{NE}^{\mathrm{CAP}}) + M_{NE}^{CI} \\
&= j2\pi f(1.14\times10^{-8} + 7.43\times10^{-10}) + 9.21\times10^{-3} \\
&= j7.61\times10^{-8} f + 9.21\times10^{-3}
\end{aligned}$$

The near-end crosstalk transfer function was measured, and the results are shown in Fig. 9.30a. The exact predictions of the transmission-line model (including losses) are also shown. Those predictions are within 3 dB of the experimental results for frequencies up to 10 MHz, where $L \cong \lambda_0/6$. Observe the common-impedance coupling level of $20\log_{10}(9.21\times10^{-3}) = -40.7$ dB at the lower frequencies. The level of the inductive and capacitive coupling at 1 MHz is computed to be $20\log_{10}(7.61\times10^{-8}\times10^{6}) = -22.4$ dB, which is quite close to the experimental value of approximately −23 dB. Also note the +20 dB/decade region between 100 kHz and 1 MHz, as well as the resonances above 10 MHz, where the line is electrically long.

For $R = 1$ kΩ, we compute the contributions for near-end crosstalk to be

$$\begin{aligned}
M_{NE}^{\mathrm{IND}} &= \frac{R_{NE}}{R_{NE}+R_{FE}}\frac{L_m}{R_S+R_L} \\
&= 5.7\times10^{-10} \\
M_{NE}^{\mathrm{CAP}} &= \frac{R_{NE}R_{FE}}{R_{NE}+R_{FE}}\frac{R_L C_m}{R_S+R_L} \\
&= 1.49\times10^{-8} \\
M_{NE}^{CI} &= \frac{R_{NE}}{R_{NE}+R_{FE}}\frac{R_0}{R_S+R_L} \\
&= 4.61\times10^{-4}
\end{aligned}$$

The capacitive coupling component dominates the inductive coupling component as expected. The total coupling is

$$\begin{aligned}
\frac{\hat{V}_{NE}}{\hat{V}_S} &= j\omega\,(M_{NE}^{\mathrm{IND}} + M_{NE}^{\mathrm{CAP}}) + M_{NE}^{CI} \\
&= j2\pi f(5.7\times10^{-10} + 1.49\times10^{-8}) + 4.61\times10^{-4} \\
&= j9.69\times10^{-8} f + 4.61\times10^{-4}
\end{aligned}$$

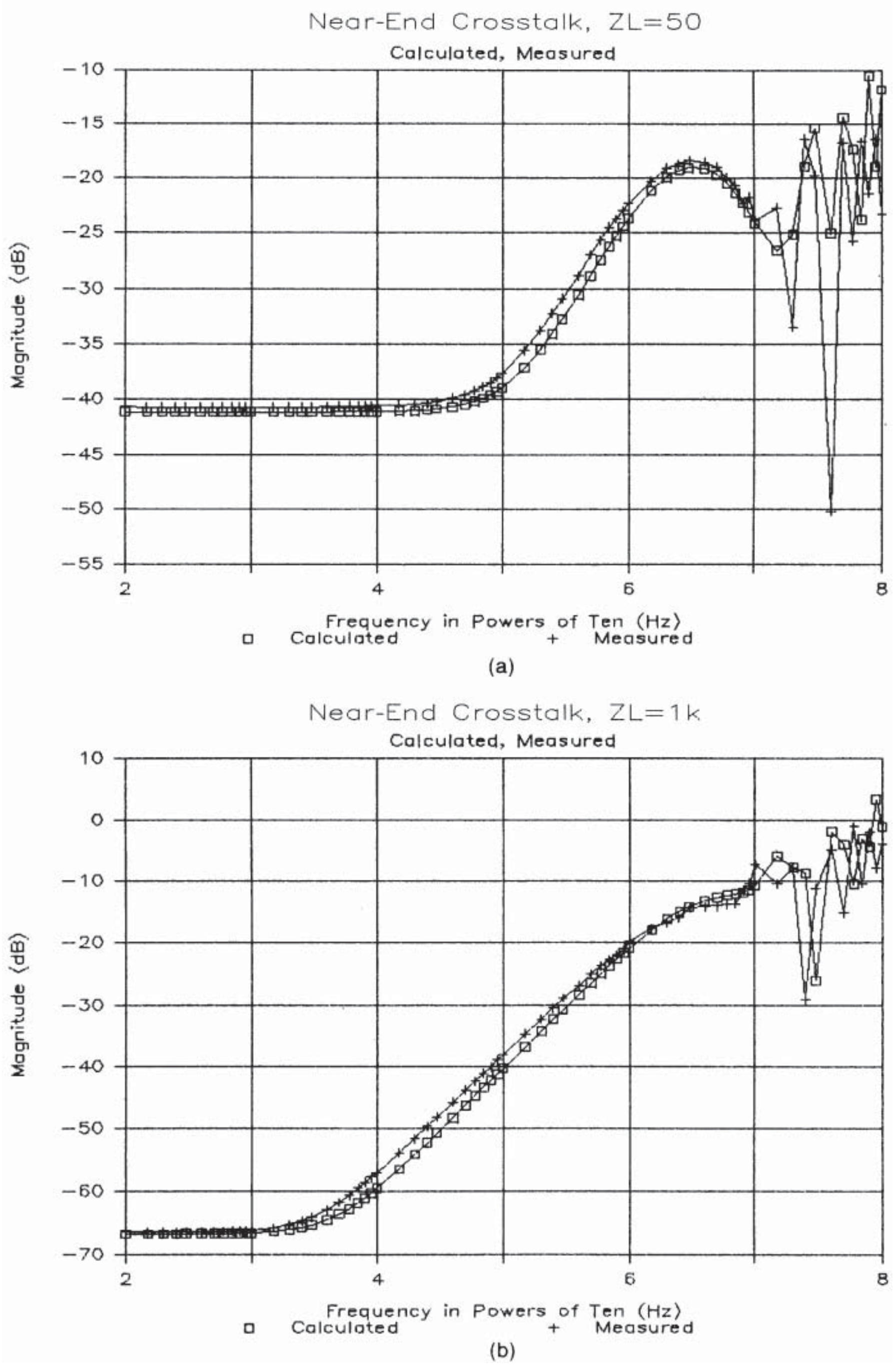

FIGURE 9.30 Frequency response of the near-end crosstalk for the ribbon cable of Fig. 9.29 comparing measured data and the predictions of the transmission-line model for (a) $R = 50\,\Omega$ and (b) $R = 1\,\Omega$.

The near-end crosstalk transfer function was measured, and the results are shown in Fig. 9.30b. The exact predictions of the transmission-line model (including losses) are also shown. Those predictions are also within 3 dB up to 10 MHz. Again observe the common-impedance coupling level of $20\log_{10}(4.61\times10^{-4}) = -66.7$ dB at the lower frequencies. The level of the inductive and capacitive coupling at 1 MHz is computed to be $20\log_{10}(9.69\times10^{-8}\times10^{-6}) = -20.3$ dB, which is quite close to the experimental value of approximately −20 dB. Again note the +20 dB/decade region between 10 kHz and 1 MHz, as well as the resonances above 10 MHz, where the line is electrically long. Transmission-line modeling of ribbon cables that consist of more than three wires is given in [3, 13].

Review Exercise 9.2 For the case of 50 Ω loads in Fig. 9.30a, suppose that instead of choosing the middle wire as the reference conductor, we choose one of the outer wires as the reference conductor. The other outer wire is the receptor wire, and the middle wire is the generator wire. The per-unit-length parameters are given in Tables 9.1 and 9.2. Recompute the near-end crosstalk ratio at 1 MHz.

Answer: −15.65 dB so that this choice of reference wire has increased the crosstalk from −22.4 dB.

Review Exercise 9.3 Repeat Review Exercise 9.1 for 1 kΩ loads.

Answer: −10.87 dB so that this choice of reference wire has increased the crosstalk from −20.3 dB.

As another example of frequency-domain crosstalk prediction, consider the *coupled microstrip* shown in Fig. 9.31. Two 1 oz copper lands of width 100 mils and separated (edge to edge)

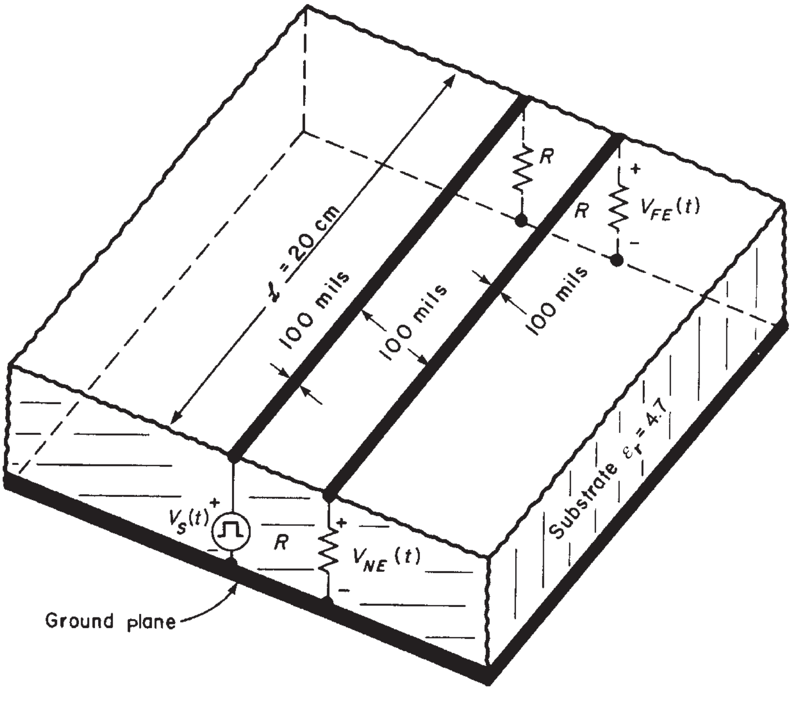

FIGURE 9.31 An experiment illustrating crosstalk using a printed circuit board.

by 100 mils were etched on one side of a glass epoxy PCB ($\varepsilon_r = 4.7$). The board thickness was 62 mils, and a ground plane was placed on the other side. The total length of the lands was 20 cm. The per-unit-length parameters were computed as described in Section 9.3.3.2 using numerical methods. The per-unit-length capacitance matrix with the dielectric substrate present **C** and with the dielectric substrate removed and replaced with air $\mathbf{C}_0$ were computed. The per-unit-length inductance matrix was then obtained as $L = \mu_0\varepsilon_0 C_0^{-1}$. The effective dielectric constant was found to be $\varepsilon_r \cong 3.5$. The lands are $\lambda/10$ at approximately 80 MHz. Once again, the termination impedances will be equal, $R_L = R_{NE} = R_{FE} = R$ and $R_S = 0$, and two values of R will be investigated: 50 Ω and 1 kΩ. The predictions of the multiconductor transmission-line model are shown for $R = 50\,\Omega$ in Fig. 9.32a and for $R = 1$ kΩ in Fig. 9.32b [3]. The prediction accuracies are within 1 dB up to 250 MHz for $R = 50\,\Omega$ and within 3 dB up to 100 MHz for $R = 1$ kΩ. The 1 kΩ loads were constructed by inserting 1 kΩ resistors into BNC cable termination connectors, so that these loads could be easily removed. This places a capacitance of some 10 pF in parallel with the 1 kΩ resistance, which degrades its high-frequency behavior more than for the 50 Ω loads, which were likewise constructed. This explains the seeming deterioration of the predictions for the 1 kΩ loads at a frequency lower than for the 50 Ω loads. Using the measured (or computed) data in the frequency range where the crosstalk varies at 20 dB/decade, we can determine that

$$M_{NE} = 1.06 \times 10^{-10} \quad \text{for} \quad R = 50\,\Omega$$

and

$$M_{NE} = 6.37 \times 10^{-10} \quad \text{for} \quad R = 1\,\text{k}\Omega$$

These crosstalk coefficients are obtained by observing that in the region where the inductive and capacitive coupling dominates (the frequency response increases at 20 dB/decade) the magnitude of the transfer function is, according to (9.67a)

$$\begin{aligned}\left|\frac{\hat{V}_{NE}}{\hat{V}_S}\right| &= \omega\left(\frac{L_m}{2R} + \frac{R}{2}C_m\right) \\ &= \omega(M_{NE}^{\text{IND}} + M_{NE}^{\text{CAP}}) \\ &= 2\pi f\, M_{NE} \end{aligned} \tag{9.76}$$

Thus, we simply determine the value of the transfer function at a frequency f_0 in this range and divide that value by $2\pi f_0$. In fact, using two values of M_{NE} obtained for $R = 50\,\Omega$ and for $R = 1$ kΩ, we can determine the total mutual inductance L_m and capacitance C_m from (9.76) and determine the per-unit-length values as

$$\begin{aligned} l_m &= \frac{L_m}{L} \\ &= 37.2\ \text{nH/m} \\ &= 0.944\ \text{nH/in.} \end{aligned}$$

and

$$\begin{aligned} c_m &= \frac{C_m}{L} \\ &= 6.33\ \text{pF/m} \\ &= 0.161\ \text{pF/in.} \end{aligned}$$

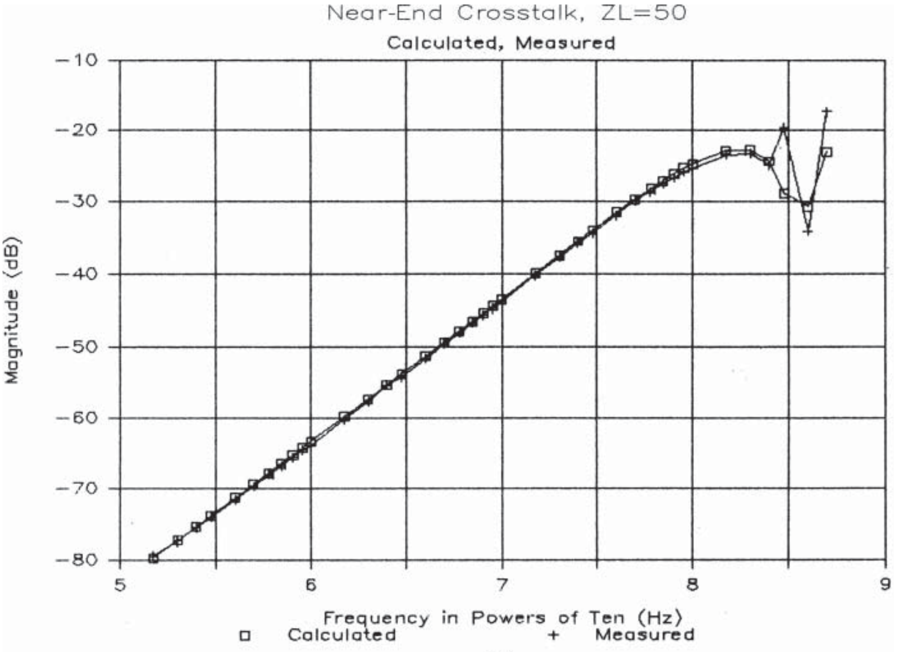

(a)

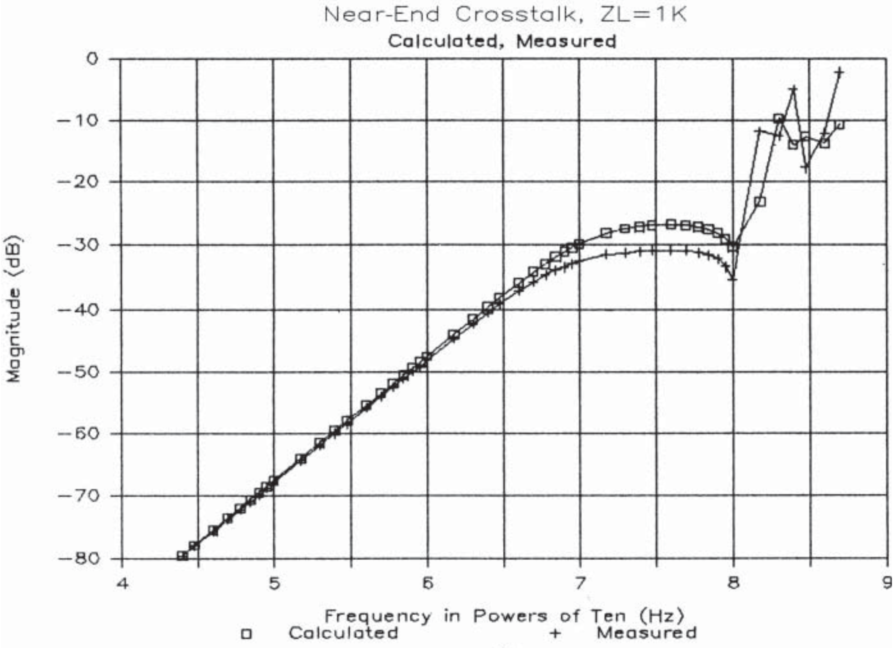

(b)

FIGURE 9.32 Frequency response of the near-end crosstalk for the printed circuit board of Fig. 9.31 comparing measured data and the predictions of the transmission-line model for (a) $R = 50\,\Omega$ and (b) $R = 1\ \text{k}\Omega$. Source: Paul [3]/John Wiley & Sons.

These are very close to the values computed with the numerical MoM code, MSTRP.FOR, described earlier and in Appendix C as

$$l_m = 37.15\,\text{nH/m}$$

and

$$c_m = 4.93\,\text{pF/m}$$

The other parameters computed with the MoM code are

$$l_G = l_R = 0.335\,\mu\text{H/m}$$

and

$$c_G = c_R = 110.6\,\text{pF/m.}$$

Hence, the characteristic impedance of each circuit in the presence of the other is

$$\begin{aligned} Z_C &= \sqrt{\frac{l_G}{(c_G + c_m)}} \\ &= 53.85\,\Omega \end{aligned}$$

Review Exercise 9.4 For a three-conductor PCB shown in Fig. 9.23 where an outside land is chosen as the reference conductor, the middle land is chosen as the generator conductor, and the other outside land is chosen as the receptor conductor. The dimensions are $w = s = 15$ mils, $h = 47$ mils, and $\varepsilon_r = 4.7$. The per-unit-length mutual capacitance and mutual inductance computed with PCB.FOR are $c_m = 20.3$ pF/m and $l_m = 0.691$ μH/m. The line length is 20 cm. Determine the far-end crosstalk transfer ratio for $R_S = 50\,\Omega$, $R_L = 100\,\Omega$, and $R_{NE} = 500\,\Omega$, $R_{FE} = 200\,\Omega$ and 10 MHz. Assume perfectly conducting lands.

***Answer*:** −42.2 dB.

These experimental data have shown that the exact multiconductor transmission-line model gives accurate predictions for frequencies where the line is electrically short. Resonances due to standing waves for frequencies where the line is electrically long accurate predictions are very difficult. The approximate model consisting of the superposition of inductive, capacitive, and common-impedance coupling contributions gives accurate predictions for almost the same frequency range as the transmission-line model, and the calculations are considerably simpler. There are cases in which the termination impedances differ considerably from the line characteristic impedances where the simple model predictions differ from those of the transmission-line model at a frequency where the line is electrically short [14].

9.4.2 Time-Domain Inductive–Capacitive Coupling Model

We can modify the frequency-domain inductive–capacitive approximate model of the previous section to predict time-domain crosstalk where the driving source on the generator line $V_S(t)$ has an arbitrary waveshape. Our major interest will be in periodic pulse trains having a trapezoidal pulse shape in order to represent digital clock and data waveforms.

The phasor crosstalk relations are given previously by

$$\hat{V}_{NE}(j\omega) = j\omega M_{NE}\hat{V}_S(j\omega) \tag{9.77a}$$

$$\hat{V}_{FE}(j\omega) = j\omega M_{FE}\hat{V}_S(j\omega) \tag{9.77b}$$

where the crosstalk transfer coefficients are

$$M_{NE} = \underbrace{\frac{R_{NE}}{R_{NE}+R_{FE}}\frac{L_m}{R_S+R_L}}_{M_{NE}^{\text{IND}}} + \underbrace{\frac{R_{NE}R_{FE}}{R_{NE}+R_{FE}}\frac{R_L C_m}{R_S+R_L}}_{M_{NE}^{\text{CAP}}} \tag{9.78a}$$

$$M_{FE} = \underbrace{-\frac{R_{FE}}{R_{NE}+R_{FE}}\frac{L_m}{R_S+R_L}}_{M_{FE}^{\text{IND}}} + \underbrace{\frac{R_{NE}R_{FE}}{R_{NE}+R_{FE}}\frac{R_L C_m}{R_S+R_L}}_{M_{FE}^{\text{CAP}}} \tag{9.78b}$$

The term $j\omega$ in the frequency domain translates to d/dt in the time domain:

$$j\omega \rightarrow \frac{d}{dt} \tag{9.79}$$

Thus, the frequency-domain results given above translate to the time domain as

$$V_{NE}(t) = M_{NE}\frac{dV_S(t)}{dt} \tag{9.80a}$$

$$V_{FE}(t) = M_{FE}\frac{dV_S(t)}{dt} \tag{9.80b}$$

This important result shows that *the frequency components of the input signal for which the line is electrically short are processed by the line to give an output that is the derivative of the source voltage multiplied by the crosstalk coefficients* M_{NE} and M_{FE}! The time-domain crosstalk is the sum of inductive- and capacitive-coupling contributions due to the mutual inductance and capacitance between the generator and receptor circuits. A simple time-domain equivalent circuit for the receptor circuit is shown in Fig. 9.33. Figure 9.34 shows the crosstalk voltage for a periodic, trapezoidal

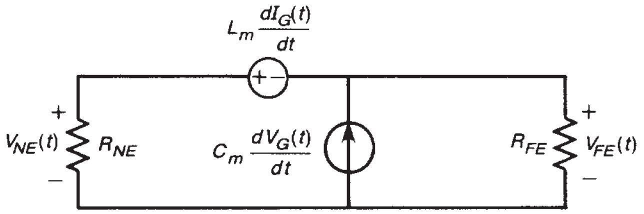

FIGURE 9.33 The simple inductive–capacitive coupling model of the receptor circuit for a general, time-domain excitation.

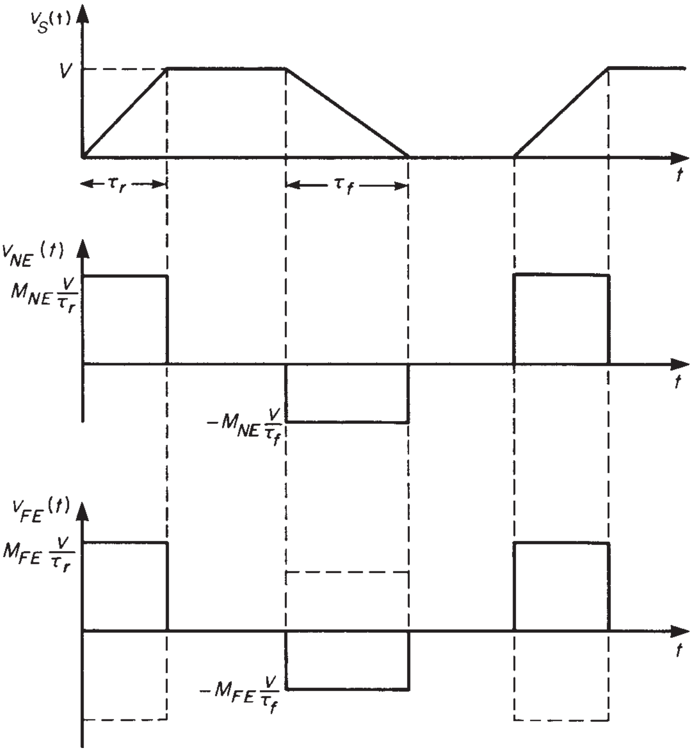

FIGURE 9.34 Time-domain crosstalk prediction of the inductive–capacitive coupling model for a trapezoidal pulse train excitation.

pulse train source voltage that may represent a clock or data signal. Observe that the crosstalk signal appears as pulses occurring during the transitions of the source voltage. During the risetime of the pulse, the crosstalk voltage is a positive pulse if the crosstalk coefficient is positive. During the falltime, where the slope of the source is negative, the crosstalk voltage is a negative pulse if the crosstalk coefficient is positive. The crosstalk coefficient for near-end crosstalk M_{NE} is always positive, as shown by (9.78a). The far-end crosstalk coefficient M_{FE}, given in (9.78b), is positive if capacitive coupling dominates inductive coupling. If inductive coupling dominates capacitive coupling, the far-end crosstalk coefficient is negative.

The *primary restrictions on the use of this simple result are that the line* be *electrically short and weakly coupled.* For a time-domain signal that contains frequency components from dc to (theoretically) infinite frequency only those components of this signal that are below the frequency where the line is electrically short will be correctly processed by this simple model. The higher-frequency components will not be correctly processed. For a given line length and velocity of propagation, this places restrictions on the spectral content of the signal. In order to obtain some relation between the frequency-domain and corresponding time-domain restriction, consider the spectrum of a periodic, trapezoidal pulse train shown in Fig. 9.35 that was obtained in Chapter 3. The actual spectrum consists of discrete frequency components at the fundamental frequency $f_0 = 1/T$ and the higher harmonics that follow an envelope that is the product of two $(\sin x)/x$ variations. We developed bounds on that exact spectrum, as shown in Fig. 9.35b. In order to do that, we assumed that the rise- and falltimes of the pulse are equal, $\tau_r = \tau_f$. The frequency response of the line is shown in Fig. 9.36. Let us assume that the line is "electrically short" for frequencies below f_u. The spectrum of the crosstalk

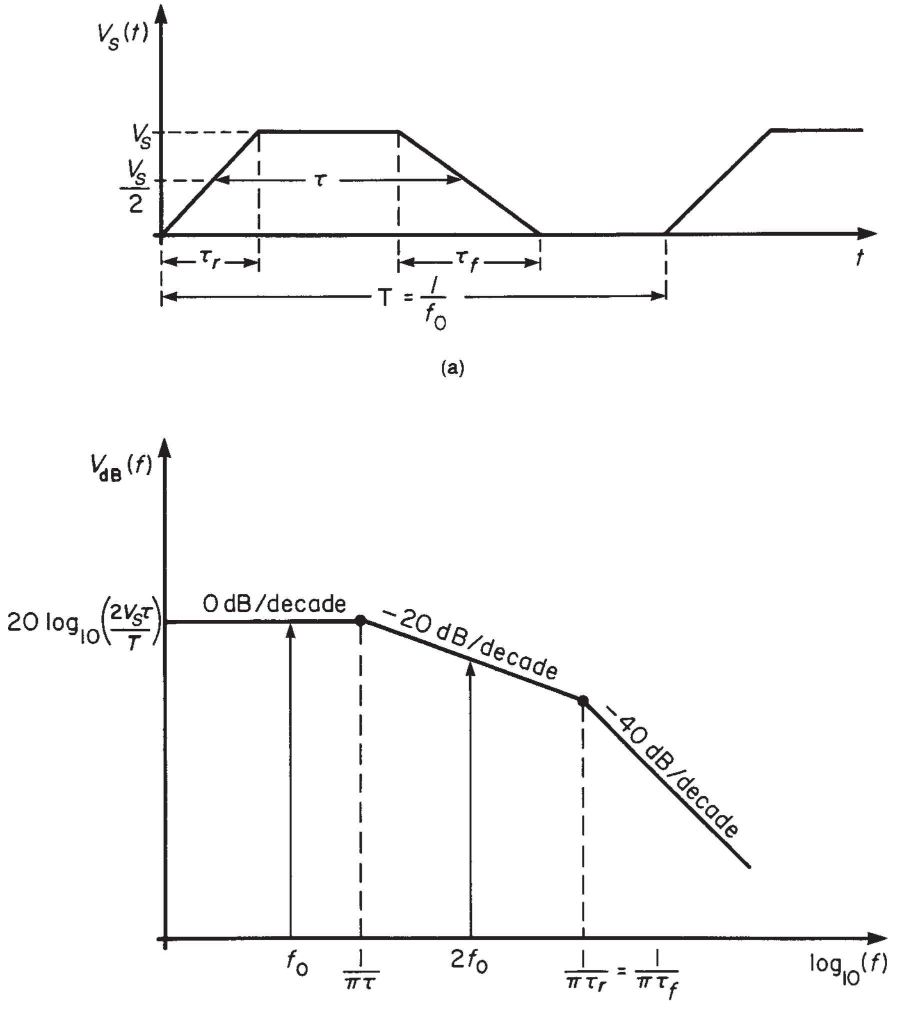
$V_S(t)$
V_S
$\frac{V_S}{2}$
τ
τ_r
τ_f
$T = \frac{1}{f_0}$
t
$V_{dB}(f)$
$20\log_{10}\left(\frac{2V_S\tau}{T}\right)$
0 dB/decade
−20 dB/decade
−40 dB/decade
f_0
$\frac{1}{\pi\tau}$
$2f_0$
$\frac{1}{\pi\tau_r} = \frac{1}{\pi\tau_f}$
$\log_{10}(f)$

(a)

(b)

FIGURE 9.35 Bounds on the spectrum of a periodic, trapezoidal pulse train. (a) Definition of trapezoidal pulse. (b) Spectral content of trapezoidal pulse.

pulse is given by the sum (Bode plots) of the spectrum of the input signal and the spectrum of the transfer function, as shown in Fig. 9.37. It is reasonable to assume that those components of the input spectrum at some point past the second breakpoint in the −40 dB/decade region do not contribute significantly to the overall pulse amplitude. Therefore, incorrect processing of these components will not significantly affect the resulting crosstalk prediction.

In Chapter 3, we showed that a reasonable criterion for the bandwidth of this signal is the reciprocal of the rise/falltime:

$$f_u = \frac{1}{\tau_r} \tag{9.81}$$

In order for our approximate model to be valid, the line length must be electrically short at this frequency:

$$L < k\lambda|_{f=f_u} \tag{9.82}$$

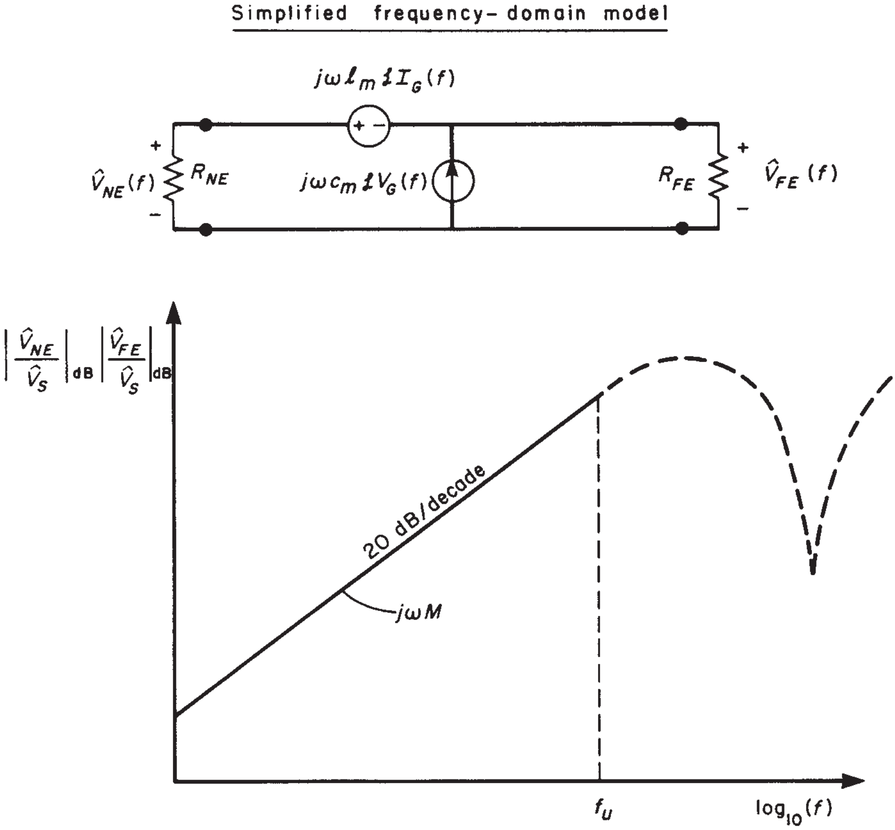
Simplified frequency- domain model
jωl_m l I_G(f)
+ −
jωc_m l V_G(f)
+
V̂_NE(f)
−
R_NE
R_FE
+
V̂_FE(f)
−
|V̂_NE / V̂_S|dB |V̂_FE / V̂_S|dB
20 dB/decade
jωM
f_u
log10(f)

FIGURE 9.36 Frequency response of the simple inductive–capacitive coupling model.

Substituting (9.81) into (9.82) along with the fundamental relation $\lambda = (v/f)$ gives

$$\tau_r > \frac{1}{k} T_D \tag{9.83}$$

where $T_D = (L/v)$ is the one-way transit time (time delay) of the line. A reasonable choice for this constant would be $k = (1/10)$. This gives the restriction on the pulse rise/falltime as

$$\tau_r, \tau_f > 10 T_D \tag{9.84}$$

This criterion is not meant to be precise but is only intended to give a notion about those pulse trains that will or will not be processed correctly by the simple model.

9.4.2.1 Inclusion of Losses: Common-Impedance Coupling Once again, we may include the resistance of the line conductors in an approximate manner by adding the common-impedance coupling coefficients to the inductive and capacitive coupling contributions presented above:

$$V_{NE}(t) = (M_{NE}^{\mathrm{IND}} + M_{NE}^{\mathrm{CAP}}) \frac{dV_S(t)}{dt} + M_{NE}^{CI} V_S(t) \tag{9.85a}$$

$$V_{FE}(t) = (M_{FE}^{\mathrm{IND}} + M_{FE}^{\mathrm{CAP}}) \frac{dV_S(t)}{dt} + M_{FE}^{CI} V_S(t) \tag{9.85b}$$

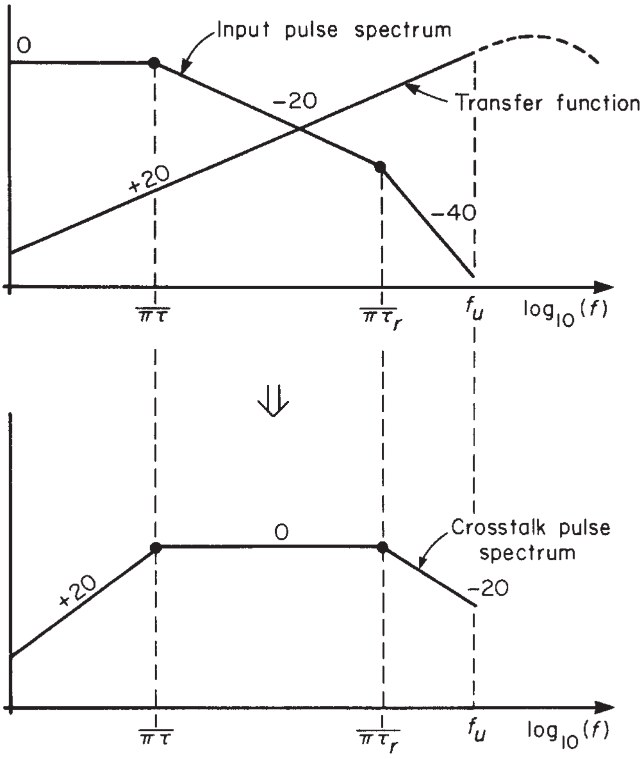

FIGURE 9.37 Output crosstalk spectrum as the sum of the trapezoidal pulse train spectral bounds of Fig. 9.35 and the transfer function of Fig. 9.36.

where the common-impedance coupling M_{NE}^{CI} and M_{FE}^{CI} are given by (9.74):

$$M_{NE}^{CI} = \frac{R_{NE}}{R_{NE} + R_{FE}} \frac{R_0}{R_S + R_L} \tag{9.86a}$$

$$M_{FE}^{CI} = -\frac{R_{FE}}{R_{NE} + R_{FE}} \frac{R_0}{R_S + R_L} \tag{9.86b}$$

The effect is to add a reduced replica of $V_S(t)$, $M_{NE}^{CI} V_S(t)$, and $M_{FE}^{CI} V_S(t)$, to the weighted derivative of that waveform, $(M_{NE}^{\mathrm{IND}} + M_{NE}^{\mathrm{CAP}})\, dV_S(t)/dt$ and $(M_{FE}^{\mathrm{IND}} + M_{FE}^{\mathrm{CAP}}) dV_S(t)/dt$.

9.4.2.2 Experimental Results We will now show some experimental results that illustrate the prediction accuracy of the model. These are the configurations that were considered for the frequency-domain results in Section 9.4.1.2. First, consider the ribbon cable shown in Fig. 9.29. The source voltage $V_S(t)$ will be a 2.5 V, 20 kHz trapezoidal pulse train having a 50% duty cycle and rise/falltimes of 400 ns. This is typical of a RS-232 serial data stream. The one-way time delay is

$$T_D = \frac{L}{v_0} = \frac{4.737}{3 \times 10^8} = 15.8\ \mathrm{ns}$$

where we have ignored the wire insulations in computing this. The maximum rise/falltimes that may be considered are

$$\tau_r, \tau_f > 150\ \mathrm{ns}$$

which this waveform satisfies. The near-end crosstalk coefficients were computed for this case previously for $R_S = 0$ and $R_L = R_{NE} = R_{FE} = 50\,\Omega$ as

$$M_{NE}^{\text{IND}} = 1.14 \times 10^{-8}$$

$$M_{NE}^{\text{CAP}} = 7.43 \times 10^{-10}$$

$$M_{NE}^{CI} = 9.21 \times 10^{-3}$$

Therefore, the near-end crosstalk waveform is given by

$$V_{NE}(t) = 1.21 \times 10^{-8} \frac{dV_S(t)}{dt} + 9.21 \times 10^{-3} V_S(t)$$

The "slew rate" of the pulse train is

$$\left| \frac{dV_S(t)}{dt} \right| = \frac{2.5\text{ V}}{400\text{ ns}} = 6.25 \times 10^6 \text{ V/s}$$

which gives peak pulse amplitudes (ignoring losses) of 75 mV. The total coupling is sketched in Fig. 9.38a, and the measured values are shown circled. The experimentally observed waveform is shown in Fig. 9.38b. Comparing the two shows good prediction, which is a direct result of the choice of rise/falltimes. Observe the crosstalk pulses occurring during the transition of the source waveform. Also observe the 23 mV "offset" created by the common-impedance coupling during the time where the input pulse is at its maximum level of 2.5 V.

We next consider the ribbon cable with 1 kΩ loads: $R_S = 0$ and $R_L = R_{NE} = R_{FE} = 1\text{ k}\Omega$. The coupling coefficients were computed previously as

$$M_{NE}^{\text{IND}} = 5.7 \times 10^{-10}$$

$$M_{NE}^{\text{CAP}} = 1.49 \times 10^{-8}$$

$$M_{NE}^{CI} = 4.61 \times 10^{-4}$$

Therefore, the near-end crosstalk waveform is given by

$$V_{NE}(t) = 1.54 \times 10^{-8} \frac{dV_S(t)}{dt} + 4.61 \times 10^{-4} V_S(t)$$

The "slew rate" of the pulse train remains

$$\left| \frac{dV_S(t)}{dt} \right| = \frac{2.5\text{ V}}{400\text{ ns}} = 6.25 \times 10^6 \text{ V/s}$$

which gives peak pulse amplitudes (ignoring losses) of 96.4 mV. The total coupling is sketched in Fig. 9.39a, and the measured values are shown circled. The experimentally observed waveform is shown in Fig. 9.39b. Comparing the two shows good prediction, which again is a direct result of the

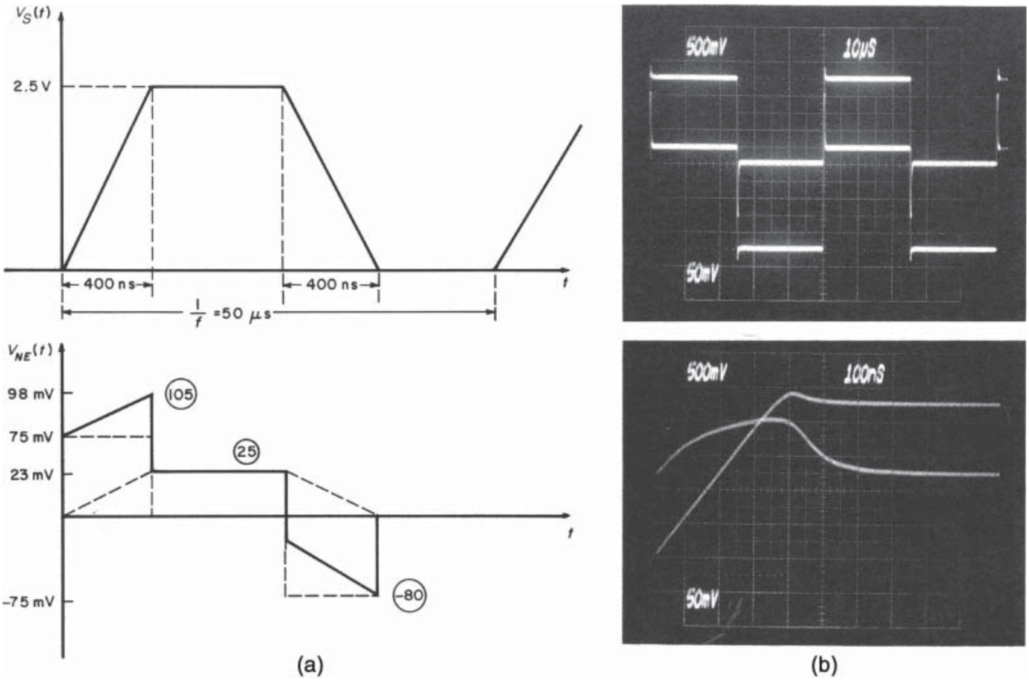

(a) (b)

FIGURE 9.38 The time-domain, near-end crosstalk for the ribbon cable of Fig. 9.29 for a trapezoidal pulse train input for $R = 50\,\Omega$: (a) predicted waveform; (b) measured waveform.

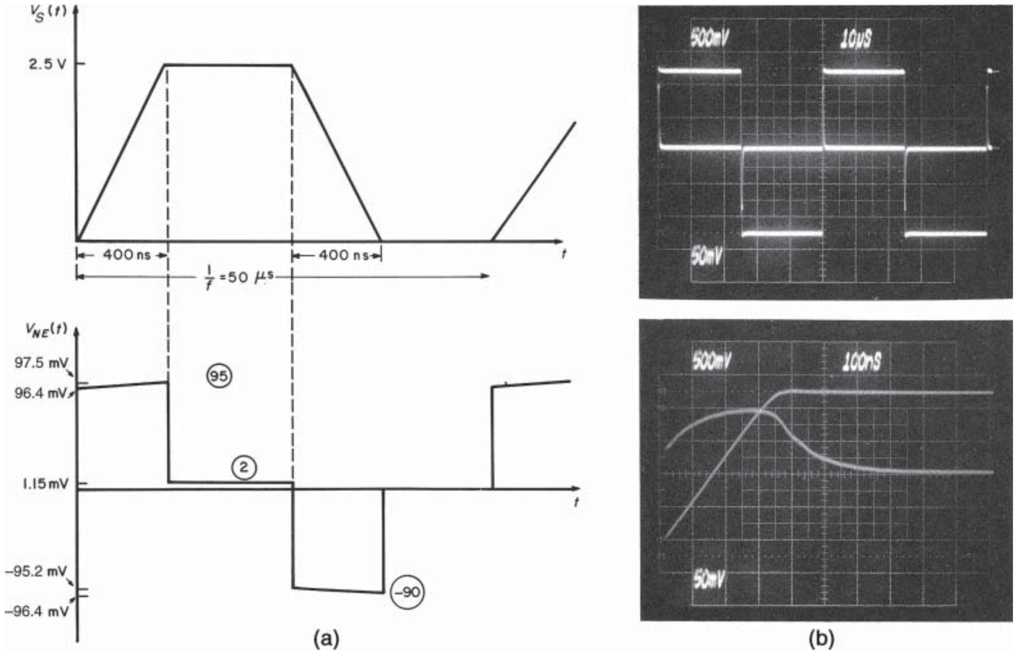

(a) (b)

FIGURE 9.39 The time-domain, near-end crosstalk for the ribbon cable of Fig. 9.29 for a trapezoidal pulse train input for $R = 1\ \text{k}\Omega$: (a) predicted waveform; (b) measured waveform.

choice of rise/falltimes. Observe the crosstalk pulses occurring during the transition of the source waveform. Also observe that the small 1.15 mV "offset" created by the common-impedance coupling during the time where the input pulse is at its maximum level of 2.5 V is too small to be observed.

Review Exercise 9.5 For the ribbon cable in Fig. 9.29 and the same source waveform as in the experiment, determine the peak far-end crosstalk voltage ignoring losses for 50 Ω and 1 kΩ loads.

Answers**:** −66 mV, −89 mV.

Next, we will consider the printed circuit board shown in Fig. 9.31 that was considered previously. The source voltage $V_S(t)$ will be a 2.5 V, 1 MHz trapezoidal pulse train having a 50% duty cycle and rise/falltimes of 50 ns. The one-way delay is

$$T_D = \frac{L}{v} = \frac{20\text{ cm}}{3 \times 10^8} \sqrt{2.85} = 1.125\text{ ns}$$

where we have assumed an effective relative permittivity as the average of free space and the board, $\varepsilon_r' = (1 + 4.7)/2 = 2.85$.

The maximum rise/falltimes that may be considered are

$$\tau_r, \tau_f \mathrel{\tilde{>}} 12\text{ ns}$$

which this waveform satisfies. The near-end crosstalk coefficient was obtained from the frequency-domain experimental results for this case previously for $R_S = 0$ and $R_L = R_{NE} = R_{FE} = 50\,\Omega$ as

$$M_{NE} = 1.06 \times 10^{-10}$$

The common-impedance coupling was too small to observe, so it will be assumed to be zero. Therefore, the near-end crosstalk waveform is given by

$$V_{NE}(t) = 1.06 \times 10^{-10} \frac{dV_S(t)}{dt}$$

The "slew rate" of the pulse train is

$$\left| \frac{dV_S(t)}{dt} \right| = \frac{2.5\text{ V}}{50\text{ ns}} = 5.0 \times 10^7 \text{ V/s}$$

which gives peak pulse amplitudes (ignoring losses) of 5.3 mV. The experimentally observed waveform is shown in Fig. 9.40. Observe the crosstalk pulses occurring during the transition of the source waveform. The peak measured voltage is 5.5 mV.

We next consider the PCB with 1 kΩ loads: $R_S = 0$ and $R_L = R_{NE} = R_{FE} = 1\text{ k}\Omega$. The coupling coefficient was obtained previously from the measured frequency-domain data as

$$M_{NE} = 6.37 \times 10^{-10}$$

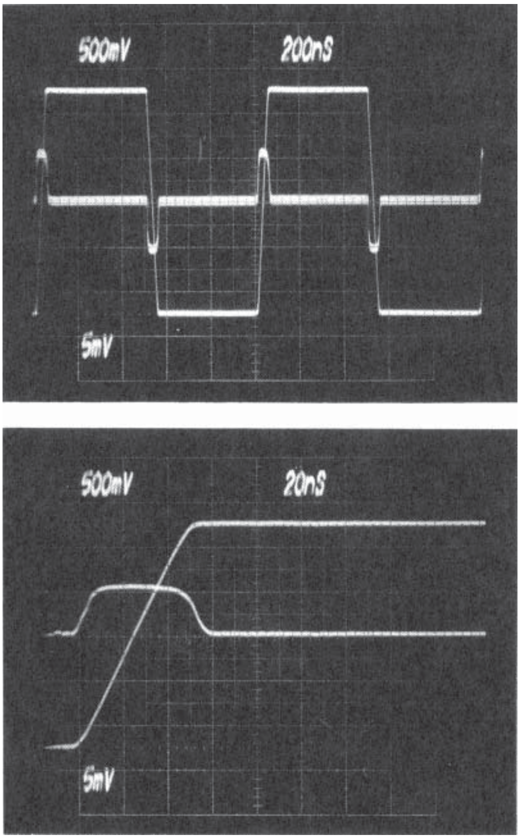

FIGURE 9.40 Measured near-end crosstalk waveforms for the printed circuit board of Fig. 9.31 for $R = 50\ \Omega$.

Therefore, the near-end crosstalk waveform is given by

$$V_{NE}(t) = 6.37 \times 10^{-10} \frac{dV_S(t)}{dt}$$

The "slew rate" of the pulse train remains

$$\left| \frac{dV_S(t)}{dt} \right| = \frac{2.5\ \text{V}}{50\ \text{ns}} = 5.0 \times 10^7\ \ \text{V/s}$$

which gives peak pulse amplitudes (ignoring losses) of 31.9 mV. The experimentally observed waveform is shown in Fig. 9.41. Observe the crosstalk pulses occurring during the transition of the source waveform. The measured peak voltage is 24 mV, which is somewhat lower than the predicted value of 31.9 mV. It appears that the crosstalk pulse has not reached steady state when the source reaches its maximum value of 2.5 V.

Review Exercise 9.6 For the coupled microstrip board in Fig. 9.31 and the same source waveform, as in the experiment, determine the peak far-end crosstalk voltage ignoring losses for 50-Ω and 1-k Ω loads.

***Answers*:** −2.14 mV, 31.5 mV.

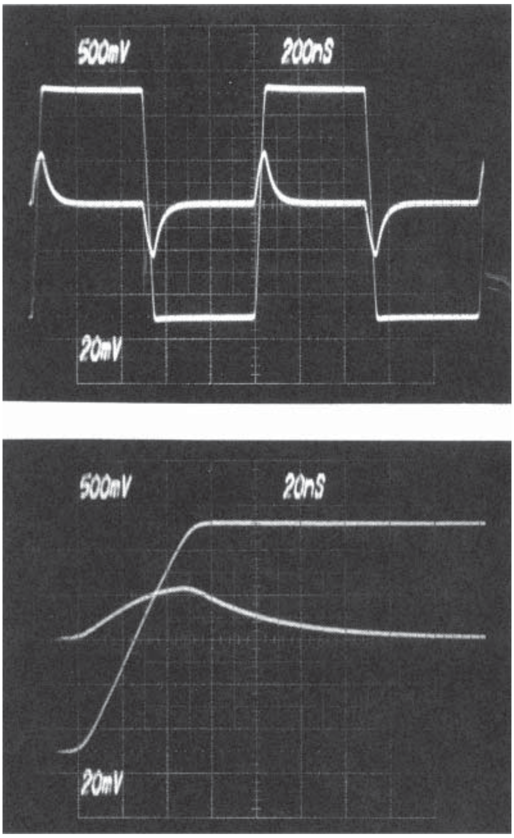

FIGURE 9.41 Measured near-end crosstalk waveforms for the printed circuit board of Fig. 9.31 for $R = 1\ \text{k}\Omega$.

9.5 SHIELDED WIRES

We now consider methods for reducing the crosstalk in a three-conductor line. Suppose the near- or far-end crosstalk in the previous three-conductor line exceeds desired levels, causing interference with the terminations at the ends of the receptor circuit. For wire-type lines, there are two common methods for reducing the crosstalk; replace the generator and/or receptor wire with a shielded wire or a twisted pair. Consider replacing the receptor wire with a shielded wire, as shown in Fig. 9.42. In order to illustrate the effect of a shielded wire on crosstalk, we will use an infinite ground plane as the reference conductor. Other choices of reference conductors such as another wire will give the same conclusions.

9.5.1 Per-Unit-Length Parameters

The per-unit-length resistances of the generator and receptor wires, r_G and r_R, can be computed in the usual manner. The per-unit-length resistance of the shield, r_S, depends on the construction technique. For braided-wire shields, we can compute the resistance by computing the resistance of one of the braid wires and placing all braid wires in parallel. The result is [15, 16]

$$r_S = \frac{r_b}{BW \cos \theta_w} \tag{9.87}$$

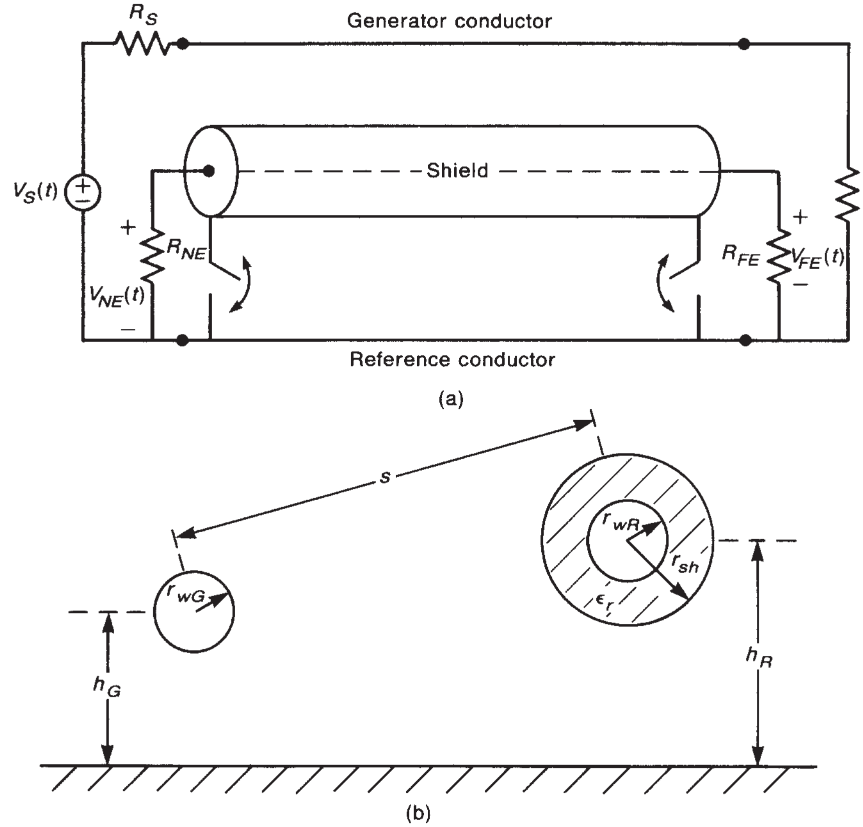

FIGURE 9.42 Adding a shield around the receptor circuit wire to reduce crosstalk: (a) the configuration; (b) cross-sectional dimensions where the reference conductor is a ground plane.

where r_b is the per-unit-length resistance of a braid wire, θ_w is the weave angle, B is the number of belts, and W is the number of braid wires per belt. The per-unit-length resistance of a solid shield such as are used in flatpack, coaxial cables is computed as a solid wire with well-developed skin effect [17, 18]. In other words, we assume the shield current to be uniformly distributed over the shield cross section, so that the shield resistance is its dc value:

$$r_S = \frac{1}{\sigma 2\pi r_{\text{sh}} t_{\text{sh}}} \tag{9.88}$$

where r_{sh} is the shield interior radius and t_{sh} the shield thickness.

The per-unit-length inductance parameters are simply computed from the flux–current methods used earlier. We will compute these parameters for the ground plane reference conductor shown in Fig. 9.42b. The self-inductances are computed by placing a current on that wire (or shield) and returning through its image and computing the magnetic flux passing through the circuit (between that wire and the ground plane). The self-inductance of the generator circuit is simply that of a wire above a ground plane computed earlier [see (9.31)]:

$$l_G = \frac{\mu_0}{2\pi} \ln\left(\frac{2h_G}{r_{wG}}\right) \tag{9.89}$$

Similarly, the self-inductance of the shield ground plane circuit is computed as that of a “fat wire” above ground:

$$l_S = \frac{\mu_0}{2\pi} \ln\left(\frac{2h_R}{r_{\text{sh}} + t_{\text{sh}}}\right) \tag{9.90}$$

where r_{sh} is the shield interior radius and t_{sh} the shield thickness. The self-inductance of the receptor circuit is computed as the self-inductance of a wire above ground (the receptor voltage is defined between the receptor wire and the ground plane and the receptor current returns through the ground plane):

$$l_R = \frac{\mu_0}{2\pi} \ln\left(\frac{2h_R}{r_{wR}}\right) \tag{9.91}$$

The mutual inductance between the generator wire and the shield l_{GS} and that between the generator wire and the receptor wire l_{GR} are computed in the previous fashion as being between two wires above ground [see (9.35)]:

$$\begin{aligned} l_{GS} &= \frac{\mu_0}{4\pi} \ln\left(1 + 4\frac{h_G h_R}{s^2}\right) \\ &= l_{GR} \end{aligned} \tag{9.92}$$

In order for these to be equal, we assume that the shield and generator wire are widely separated, which is implicit in all these results. The mutual inductance between the shield and receptor wire circuit is

$$\begin{aligned} l_{RS} &= \frac{\mu_0}{2\pi} \ln\left(\frac{2h_R}{r_{\text{sh}} + t_{\text{sh}}}\right) \\ &= l_S \end{aligned} \tag{9.93}$$

Hence, the mutual inductance between the receptor wire–ground plane circuit and the shield–ground plane circuit l_{RS} *is identical to the self-inductance of the shield–ground plane circuit* l_S.

This result is very important and deserves further explanation. Consider the shield-receptor wire above ground shown in Fig. 9.43. The shield circuit is between the shield and the ground plane. The mutual inductance between the shield and receptor circuits can be obtained by placing a current on the shield and determining the magnetic flux through the receptor circuit or by placing a current on the receptor wire and determining the magnetic flux through the shield circuit:

$$\begin{aligned} l_{RS} &= \left.\frac{\psi_S}{I_R}\right|_{I_S=0} \\ &= \left.\frac{\psi_R}{I_S}\right|_{I_R=0} \end{aligned} \tag{9.94}$$

Consider placing a current on the receptor wire and computing the magnetic flux through the shield–ground plane circuit. This can be obtained by placing all of the receptor wire current on the shield, and thus $l_{RS} = l_S$. This important observation allows a shield to eliminate inductive coupling, as we will see.

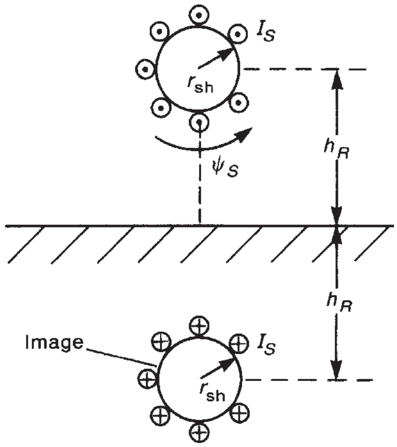

FIGURE 9.43 Calculation of the per-unit-length self-inductances of the shield–ground plane circuit for a shielded wire above a ground plane.

The capacitances are obtainable through the use of the important reciprocal relationship between the inductance and capacitance matrices given in (9.8). The medium interior to the shield can have $\varepsilon_r \neq 1$, whereas the medium outside is logically assumed to be free space, where we neglect any dielectric insulation around the generator wire and the shield. Thus, the capacitance between the shield and receptor wire is the same as for a coaxial cable given in Chapter 4:

$$c_{RS} = \frac{2\pi\varepsilon_0\varepsilon_r}{\ln(r_{\text{sh}}/r_{wR})} \tag{9.95}$$

The other capacitances can be found using the reciprocal relationship for conductors in a homogeneous medium by considering only the generator wire and the shield as

$$\begin{bmatrix} c_G + c_{GS} & -c_{GS} \\ -c_{GS} & c_S + c_{GS} \end{bmatrix} = \mu_0\varepsilon_0 \begin{bmatrix} l_G & l_{GS} \\ l_{GS} & l_S \end{bmatrix}^{-1} \tag{9.96}$$

Observe from Fig. 9.44 that certain of the self and mutual capacitances are eliminated by the presence of the shield. The shield acts as a Faraday cage in that electric field lines external to the shield terminate on the shield and cannot terminate on conductors interior to the shield. Hence, the mutual capacitance between the generator and receptor wire circuits is zero, $c_{GR} = 0$. Similarly, the self-capacitance of the receptor circuit is zero, $c_R = 0$.

9.5.2 Inductive and Capacitive Coupling

The multiconductor transmission-line (MTL) equations for the shielded receptor wire configuration in Fig. 9.42 (a four-conductor line) can be solved numerically via computer modeling [15–20]. We will show those predictions in this section. This yields an exact solution for the problem. In addition, these MTL equations have been solved in literal form (symbols instead of number) in [21, 22]. This shows, once again, that for weakly coupled lines that are electrically short, we may compute the crosstalk as the sum of an inductive-coupling contribution due to mutual inductances and a capacitive coupling contribution due to mutual capacitances.

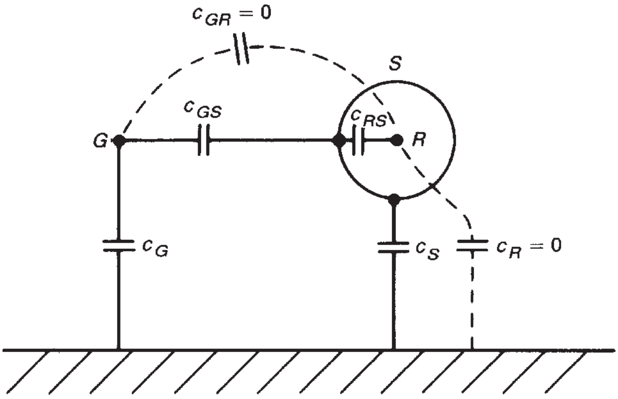
$c_{GR} = 0$
S
c_{GS}
c_{RS}
G
R
c_G
c_S
$c_R = 0$

FIGURE 9.44 The cross-sectional capacitance equivalent circuit for the shielded receptor wire above a ground plane.

First consider the capacitive coupling with the circuit shown in Fig. 9.45. We have retained only the mutual capacitances between the generator, shield, and receptor circuits and ignored the self-capacitances c_G and c_S. The element values are the per-unit-length values multiplied by the line length: $C_{RS} = c_{RS}L$ and $C_{GS} = c_{GS}L$. The capacitive coupling is (by voltage division)

$$\begin{aligned}\hat{V}_{NE}^{\text{CAP}} &= \hat{V}_{FE}^{\text{CAP}} \\ &= \frac{j\omega R C_{RS} \parallel C_{GS}}{1 + j\omega R C_{RS} \parallel C_{GS}} \hat{V}_G \end{aligned} \tag{9.97}$$

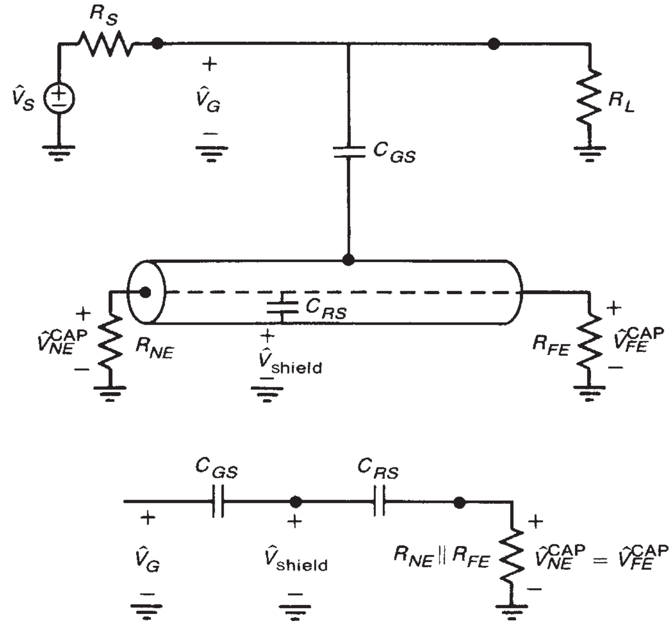
R_S
$\hat{V}_S$
+
$\hat{V}_G$
−
R_L
C_{GS}
+
$\hat{V}_{NE}^{CAP}$
−
R_{NE}
C_{RS}
+
$\hat{V}_{\text{shield}}$
−
R_{FE}
+
$\hat{V}_{FE}^{CAP}$
−
C_{GS}
C_{RS}
+
$\hat{V}_G$
−
+
$\hat{V}_{\text{shield}}$
−
$R_{NE} \parallel R_{FE}$
+
$\hat{V}_{NE}^{CAP} = \hat{V}_{FE}^{CAP}$
−

FIGURE 9.45 A lumped equivalent circuit for capacitive coupling for the shielded receptor wire of Fig. 9.42.

where

$$R = \frac{R_{NE}R_{FE}}{R_{NE} + R_{FE}} \tag{9.98a}$$

$$C_{RS} \parallel C_{GS} = \frac{C_{RS}C_{GS}}{C_{RS} + C_{GS}} \tag{9.98b}$$

This result could be easily seen by reducing the two capacitors to an equivalent, and capacitors in series add like resistors in parallel. For a sufficiently small frequency, this reduces to

$$\begin{aligned}\hat{V}_{NE}^{\text{CAP}} &= \overline{V}_{FE}^{\text{CAP}} \\ &= j\omega\frac{R_{NE}R_{FE}}{R_{NE} + R_{FE}}\frac{C_{RS}C_{GS}}{C_{RS} + C_{GS}}\overline{V}_{G_{\text{dc}}}\end{aligned} \tag{9.99a}$$

and

$$\hat{V}_{G_{\text{dc}}} = \frac{R_L}{R_S + R_L}\hat{V}_S \tag{9.99b}$$

is the dc or “low-frequency” value of the generator line voltage. In effect, this is the same as the capacitive coupling between two wires where the mutual capacitance between them is $C_{RS} \parallel C_{GS}$ since capacitors in series add like resistors in parallel. Observe that the capacitive coupling contribution in (9.116a) increases at 20 dB/decade as for unshielded wires. Also, for typical shielded wires $C_{RS} \gg C_{GS}$, so that $C_{RS} \parallel C_{GS} \cong C_{GS} \cong C_{GR}$. Thus, the capacitive coupling is basically unchanged from the unshielded case.

Typically, the shield is connected to the reference conductor (“grounded”) at one end or at both ends. Observe that *if the shield is connected to the reference conductor at either end, the shield voltage is reduced to zero and the capacitive coupling contribution is removed:*

$$\begin{aligned}\hat{V}_{NE}^{\text{CAP}} &= \hat{V}_{FE}^{\text{CAP}} \\ &= 0 \quad \left(\begin{array}{c}\text{shield connected to the} \\ \text{reference conductor at either end}\end{array}\right)\end{aligned} \tag{9.100}$$

This is the origin of the notion that a shielded wire eliminates electric field or capacitive coupling wherein the electric field lines from the generator circuit terminate on the shield and not on the receptor wire. In order for the shield to eliminate capacitive coupling, the shield voltage $\hat{V}_{\text{shield}}$ must be zero. For an electrically short line, grounding the shield at either end will cause the voltage all along the shield to be approximately zero. As the line length increases, electrically, the shield must be grounded at multiple points spaced some $\lambda/10$ along it in order to approximate this.

Next, we consider inductive coupling. We have seen that the shield inherently eliminates capacitive coupling so long as it is “grounded” at either end. *A shield must be grounded at both ends in order to eliminate inductive coupling*. To show this, consider the magnetic fields generated by the generator wire current as shown in Fig. 9.46. The generator wire current $\hat{I}_G$ produces a magnetic flux ψ_G in the shield–ground plane circuit. This induces, by Faraday’s law, an emf in the shield circuit that produces a secondary current $\hat{I}_S$ flowing back along the shield. The flux of this induced shield current tends to cancel that of the generator wire current. It is this process that allows a shielded

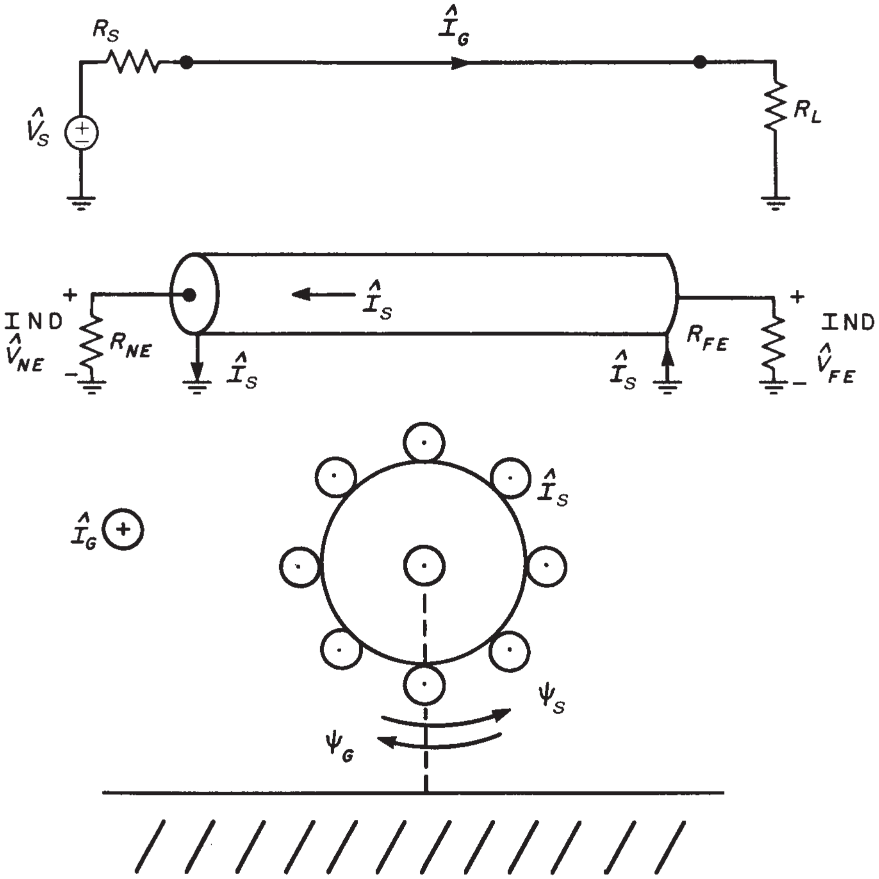

FIGURE 9.46 Illustration of the effect of placing a shield around a receptor wire on inductive coupling.

wire to eliminate inductive or magnetic field coupling. Observe that if the shield is not grounded at *both ends*, then there is no path for allowing a current, $\hat{I}_S$, to flow back along the shield, thereby generating a magnetic flux through the shield–ground plane loop that counter-acts the flux due to the generator wire loop. Hence, if the shield is not grounded at *both ends*, inductive coupling will not be eliminated.

In order to quantify this effect, consider the inductive equivalent circuit shown in Fig. 9.47. *The values of the elements in this circuit are the per-unit-length values multiplied by the total line length* L, e.g., $L_{GR} = l_{GR}L$, *and are denoted with capital letters*. The current in the generator circuit induces two sources via Faraday's law. A source $j\omega L_{GR}\hat{I}_G$ is induced in the receptor wire–ground plane loop, and a source $j\omega L_{GS}\hat{I}_G$ is induced in the shield–ground plane loop.

This latter induced source produces the current flowing back along the shield:

$$\hat{I}_S = \frac{j\omega L_{GS}}{R_{\text{SH}} + j\omega L_{\text{SH}}}\hat{I}_G \tag{9.101}$$

where R_{SH} is the total resistance of the shield, $R_{\text{SH}} = r_S L$, and L_{SH} is the total self-inductance of the shield–ground plane loop, $L_{\text{SH}} = l_S L$. This induced current in the shield induces, as a secondary

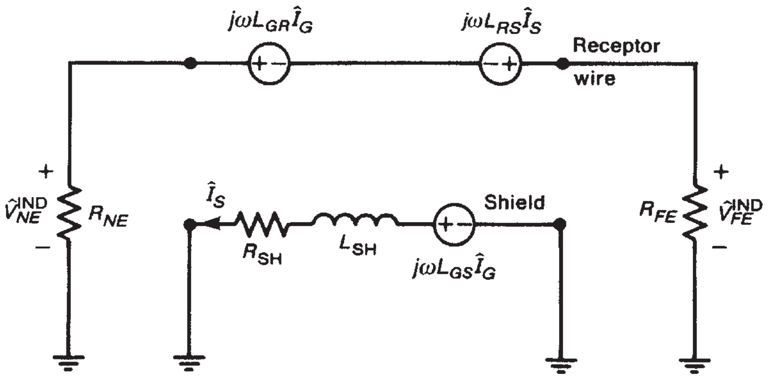

FIGURE 9.47 A lumped equivalent circuit for inductive coupling for the shielded receptor wire of Fig. 9.42.

effect, the induced source $j\omega L_{RS}\hat{I}_S$ in the receptor wire–ground plane loop. The near-end-induced crosstalk voltage is

$$\hat{V}_{NE}^{\mathrm{IND}} = \frac{R_{NE}}{R_{FE}+R_{NE}} j\omega\ (L_{GR}\hat{I}_G - L_{RS}\hat{I}_S) \tag{9.102}$$

Substituting (9.101) into (9.102) gives

$$\hat{V}_{NE}^{\mathrm{IND}} = \frac{R_{NE}}{R_{FE}+R_{NE}} \frac{j\omega R_{\mathrm{SH}} L_{GR} + \omega^2 (L_{GS}L_{RS} - L_{GR}L_{\mathrm{SH}})}{R_{\mathrm{SH}} + j\omega L_{\mathrm{SH}}} \hat{I}_G \tag{9.103}$$

Substituting the important relationships previously determined:

$$L_{GR} = L_{GS} \tag{9.104a}$$

$$L_{RS} = L_{\mathrm{SH}} \tag{9.104b}$$

gives

$$\hat{V}_{NE}^{\mathrm{IND}} = \underbrace{\frac{R_{NE}}{R_{FE}+R_{NE}} j\omega L_{GR}\hat{I}_G}_{\substack{\text{crosstalk}\\ \text{with shield}\\ \text{removed}}} \underbrace{\frac{R_{\mathrm{SH}}}{R_{\mathrm{SH}}+j\omega L_{\mathrm{SH}}}}_{\substack{\text{effect of}\\ \text{shield}}} \tag{9.105a}$$

$$\hat{V}_{FE}^{\mathrm{IND}} = \underbrace{-\frac{R_{FE}}{R_{FE}+R_{NE}} j\omega L_{GR}\hat{I}_G}_{\substack{\text{crosstalk}\\ \text{with shield}\\ \text{removed}}} \underbrace{\frac{R_{\mathrm{SH}}}{R_{\mathrm{SH}}+j\omega L_{\mathrm{SH}}}}_{\substack{\text{effect of}\\ \text{shield}}} \tag{9.105b}$$

where

$$\hat{I}_G = \frac{1}{R_S + R_L} \hat{V}_S \tag{9.105c}$$

is the dc or low-frequency current of the generator circuit, which is approximately constant along the generator circuit since the line is presumed to be electrically short. But (9.105) is *the result for the same case with the shield removed but multiplied by the shielding factor*

$$\mathrm{SF} = \frac{R_{\mathrm{SH}}}{R_{\mathrm{SH}} + j\omega L_{\mathrm{SH}}} \tag{9.106}$$

This factor can be written as

$$\mathrm{SF} = \frac{1}{1 + j(f/f_{\mathrm{SH}})} \tag{9.107a}$$

where the *shield break frequency* is

$$f_{\mathrm{SH}} = \frac{R_{\mathrm{SH}}}{2\pi L_{\mathrm{SH}}} \tag{9.107b}$$

This shielding factor is approximated by

$$\mathrm{SF} \cong \begin{cases} 1 & \text{for} \quad f < f_{\mathrm{SH}} \\ \dfrac{R_{\mathrm{SH}}}{j\omega L_{\mathrm{SH}}} & \text{for} \quad f > f_{\mathrm{SH}} \end{cases} \tag{9.107c}$$

Hence, the inductive coupling contribution in (9.105) can be summarized as three cases.

Case I: The shield is not grounded at both ends:

$$\hat{V}_{NE}^{\mathrm{IND}} = j\omega \left\{ \frac{R_{NE}}{R_{NE} + R_{FE}} \frac{L_{GR}}{R_S + R_L} \right\} \hat{V}_S \tag{9.108a}$$

$$\hat{V}_{FE}^{\mathrm{IND}} = j\omega \left\{ -\frac{R_{FE}}{R_{NE} + R_{FE}} \frac{L_{GR}}{R_S + R_L} \right\} \hat{V}_S \tag{9.108b}$$

A shield that is not grounded at both ends does not allow a shield current to flow back along the shield to produce a counteracting magnetic flux.

Case II: The shield is grounded at both ends and $f < f_{\mathrm{SH}}$:

$$\hat{V}_{NE}^{\mathrm{IND}} = j\omega \left\{ \frac{R_{NE}}{R_{NE} + R_{FE}} \frac{L_{GR}}{R_S + R_L} \right\} \hat{V}_S \tag{9.109a}$$

$$\hat{V}_{FE}^{\mathrm{IND}} = j\omega \left\{ -\frac{R_{FE}}{R_{NE} + R_{FE}} \frac{L_{GR}}{R_S + R_L} \right\} \hat{V}_S \tag{9.109b}$$

Case III: The shield is grounded at both ends and $f > f_{\mathrm{SH}}$:

$$\hat{V}_{NE}^{\mathrm{IND}} = \frac{R_{NE}}{R_{NE} + R_{FE}} \frac{L_{GR}}{R_S + R_L} \frac{R_{\mathrm{SH}}}{L_{\mathrm{SH}}} \hat{V}_S \tag{9.110a}$$

$$\hat{V}_{FE}^{\mathrm{IND}} = -\frac{R_{FE}}{R_{NE} + R_{FE}} \frac{L_{GR}}{R_S + R_L} \frac{R_{\mathrm{SH}}}{L_{\mathrm{SH}}} \hat{V}_S \tag{9.110b}$$

Observe for case III where the shield is grounded at both ends and the frequency is above the shield break frequency, $f > f_{SH}$, the shielding factor in (9.124c) has a $j\omega$ in the denominator that cancels with the $j\omega$ in the expression for the coupling with the shield removed. Hence, the crosstalk is *independent of frequency* and is flat above this frequency.

A qualitative description of this effect is as follows. For $f < f_{SH}$, the generator current finds the lowest-impedance return path through the ground plane, and so the flux from this current threads the entire receptor circuit. For $f > f_{SH}$, the generator current finds the lowest-impedance return path to be back along the shield instead of through the ground plane, $\hat{I}_S = \hat{I}_G$ [15–20]. Eq. (9.101) confirms this. For $f > f_{SH}$, Eq. (9.101) shows that $\hat{I}_S = (L_{GS}/L_{SH})\hat{I}_G$.

Later, we will show that $L_{GR} = L_{GS} \cong L_{SH}$, and hence the majority of the generator current returns along the shield instead of through the ground plane, resulting in no additional magnetic flux threading the receptor circuit for increasing frequencies, which is illustrated in Fig. 9.48.

The total crosstalk transfer function is the sum of the inductive and capacitive coupling contributions:

$$\frac{\hat{V}_{NE}}{\hat{V}_S} = \frac{\hat{V}_{NE}^{\text{IND}}}{\hat{V}_S} + \frac{\hat{V}_{NE}^{\text{CAP}}}{\hat{V}_S} \tag{9.111a}$$

$$\frac{\hat{V}_{FE}}{\hat{V}_S} = \frac{\hat{V}_{FE}^{\text{IND}}}{\hat{V}_S} + \frac{\hat{V}_{FE}^{\text{CAP}}}{\hat{V}_S} \tag{9.111b}$$

In summary, *if the shield is grounded at least one end, the capacitive coupling contribution is zero, and the inductive coupling is affected by the shield only if the shield is grounded at both ends and the frequency is greater than the break frequency, shield* $f > f_{SH} = (R_{SH}/2\pi L_{SH})$.

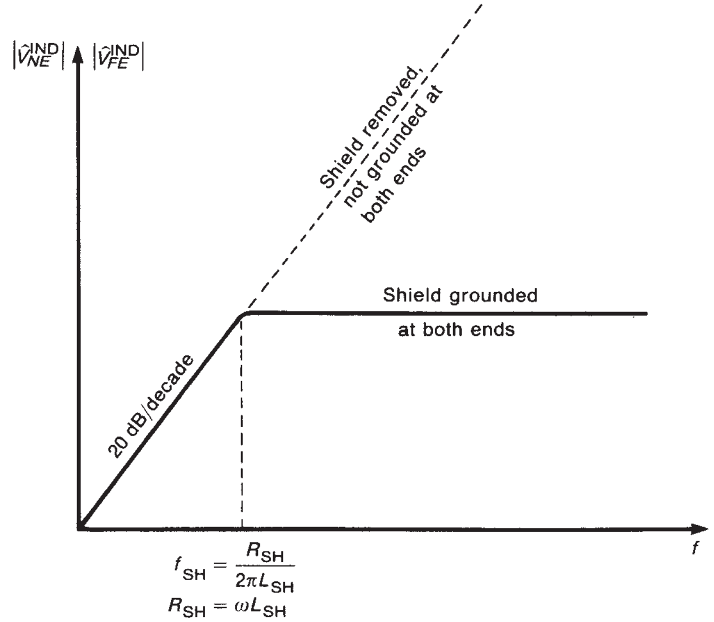

FIGURE 9.48 Illustration of the effect of shield grounding on the inductive coupling to a shielded wire.

9.5.3 Effect of Shield Grounding

In order to illustrate these results, we will consider experimental results. Consider the shielded receptor circuit shown in Fig. 9.49. The line length is 3.6576 m (12 ft) and the conductors are suspended a height of 1.5 cm above a ground plane. Two values of termination resistance will be used to accentuate the inductive and capacitive coupling: $R = 50\,\Omega$ and $R = 1\,\mathrm{k}\Omega$. The generator wire and shield insulations are in contact, giving a separation of approximately 0.2 cm. This will be referred to on the plots as SEPARATION: TOUCHING. The generator wire is a 20-gauge solid wire ($r_{wG} = 15$ mils). The characteristics of the shielded wire are $r_{wR} = 15$ mils (22 gauge stranded, 7×30), $\varepsilon_r = 2.1$ (Teflon), $r_{\mathrm{sh}} = 35$ mils, $r_{\mathrm{braid}} = 2.5$ mils (36-gauge wires), $\theta_w = 30°$, $B = 16$, $W = 4$, and $t_{\mathrm{sh}} \cong 5$ mils $= 2\, r_{\mathrm{braid}}$. The resistance of the shield is

$$R_{\mathrm{SH}} = \frac{L}{\sigma \pi r_{\mathrm{braid}}^2 B W \cos \theta_w}$$
$$= 89.8\,\mathrm{m}\Omega$$

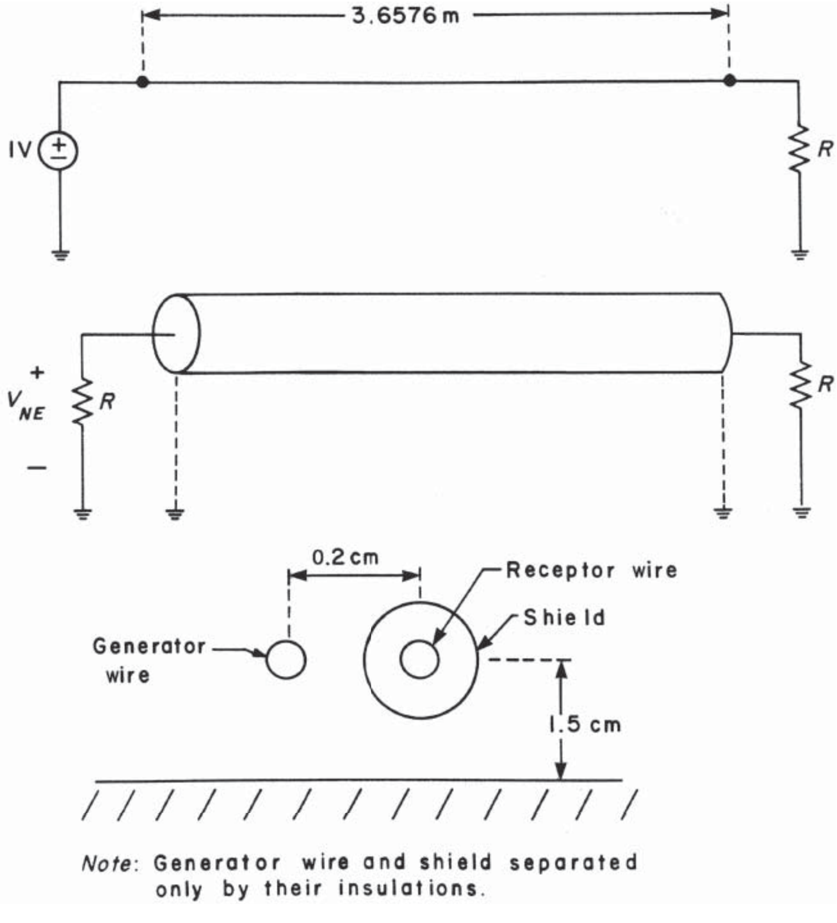
3.6576 m
IV
R
+
V_{NE}
R
−
R
0.2 cm
Receptor wire
Shield
Generator wire
1.5 cm
Note: Generator wire and shield separated only by their insulations.

FIGURE 9.49 An experiment to illustrate the effect of shield grounding on crosstalk to a shielded wire.

The total inductances are obtained by multiplying the per-unit-length inductances given by (9.89)–(9.93) by the line length L to give

$$\begin{aligned}L_G &= 3.15\ \mu\text{H}\\ L_R &= 3.19\ \mu\text{H}\\ L_{\text{SH}} &= 2.48\ \mu\text{H}\\ L_{\text{GR}} &= 1.98\ \mu\text{H}\\ &= L_{\text{GS}}\end{aligned}$$

The capacitance C_{RS} is obtained by multiplying (9.112) by the line length to yield

$$C_{RS} = 503.6\ \text{pF}$$

The mutual capacitance C_{GS} is found from (9.113) as

$$\begin{aligned}C_{GS} &= \frac{l_{GS}L}{v_0^2(l_G l_S - l_{GS}^2)}\\ &= 76.3\ \text{pF}\end{aligned}$$

The shield time constant gives a break frequency of

$$\begin{aligned}f_{\text{SH}} &= \frac{R_{\text{SH}}}{2\pi L_{\text{SH}}}\\ &= 5.8\ \text{kHz}\end{aligned}$$

With the shield removed, the mutual inductance between the generator and receptor wires is unchanged, $L_{GR} = 1.98$ mH, but the mutual capacitance must be recomputed as

$$\begin{aligned}C_{GR} &= \frac{l_{GR}L}{v_0^2(l_G l_R - l_{GR}^2)}\\ &= 48.2\ \text{pF}\end{aligned}$$

The experimental results are shown for $R_S = 0$ and $R_L = R_{NE} = R_{FE} = R$ in Fig. 9.50a for $R = 50\ \Omega$ and in Fig. 9.50b for $R = 1\ \text{k}\Omega$. The results show the magnitude of the measured near-end crosstalk transfer ratio, $|\ \hat{V}_{NE}/\hat{V}_S\ |$, for four grounding configurations of the shield. The shield terminations are represented as “O,” meaning “open,” or “S,” meaning “shorted (short-circuited) to ground.” The result for the shield present but ungrounded at either end is denoted as “OO.” The result for the shield grounded at the left (source) end but ungrounded at the right (load) end are designated as “SO,” whereas the result for the shield grounded at the right (load) end but ungrounded at the left (source) end are designated as “OS.” The result for the shield grounded at both ends is denoted as “SS.”

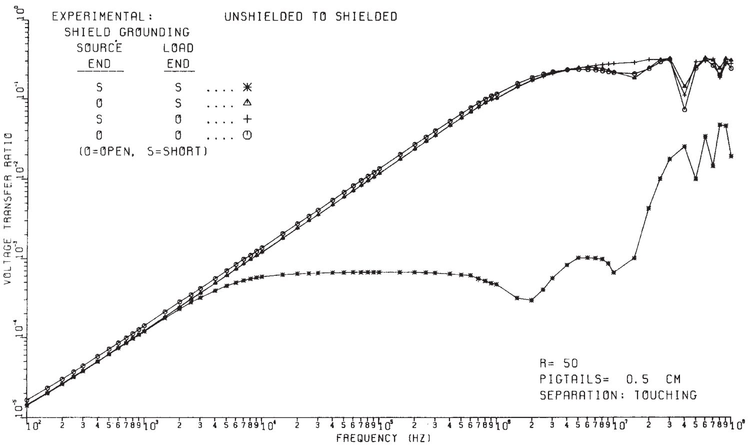

(a)

FIGURE 9.50 Measured near-end crosstalk for the configuration of Fig. 9.49 for the shield ungrounded, grounded at the left end, grounded at the right end, and grounded at both ends for (a) $R = 50\,\Omega$ and (b) $R = 1\,\mathrm{k}\Omega$.

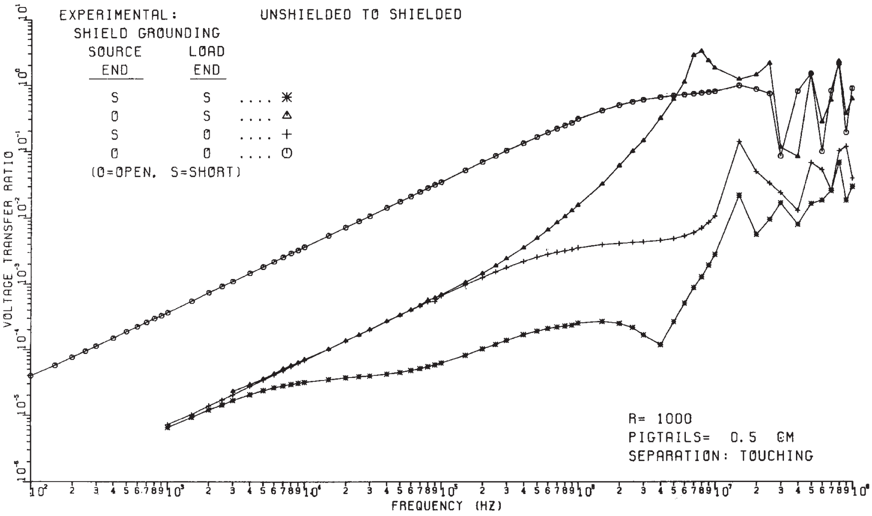

(b)

FIGURE 9.50 (*Continued*)

The results in Fig. 9.50 can be explained with reference to Fig. 9.51. The crosstalk transfer ratio is

$$\frac{\hat{V}_{NE}}{\hat{V}_S} = j2\pi f\left[M_{NE}^{\text{IND}} + M_{NE}^{\text{CAP}}\right]$$
$$\frac{\hat{V}_{FE}}{\hat{V}_S} = j2\pi f\left[M_{FE}^{\text{IND}} + M_{FE}^{\text{CAP}}\right]$$

If the shield is not grounded at either end, the capacitive coupling is essentially the same as with the shield removed since $C_{RS} \| C_{GS} \cong C_{GS \cong} C_{GR}$:

$$\begin{aligned} M_{NE}^{\text{CAP}} &= M_{FE}^{\text{CAP}} \\ &= \frac{R_{NE}R_{FE}}{R_{NE}+R_{FE}} \frac{C_{RS}C_{GS}}{C_{RS}+C_{GS}} \frac{R_L}{(R_S=0)+R_L} \\ &= \frac{R}{2}\frac{C_{RS}C_{GS}}{C_{RS}+C_{GS}} \\ &\cong \frac{R}{2}C_{GR} \quad \text{OO} \end{aligned}$$

If the shield is grounded at least at one end, the capacitive coupling is eliminated.

$$\begin{aligned} M_{NE}^{\text{CAP}} &= M_{FE}^{\text{CAP}} \\ &= 0 \quad \text{OS, SO, SS} \end{aligned}$$

Next consider the inductive coupling. If the shield is not grounded at both ends, the inductive coupling is essentially the same as with the shield removed since there is no path for the shield current to traverse:

$$\begin{aligned} M_{NE}^{\text{IND}} &= \frac{R_{NE}}{R_{NE}+R_{FE}} \frac{L_{GR}}{(R_S=0)+R_L} \\ &= \frac{L_{GR}}{2R} \quad \text{OO, OS, SO} \\ &= -\frac{R_{FE}}{R_{NE}+R_{FE}} \frac{L_{GR}}{(R_S=0)+R_L} \\ &= -\frac{L_{GR}}{2R} \quad \text{OO, OS, SO} \end{aligned}$$

If the shield is grounded at both ends, then a shielding factor

$$\text{SF} = \frac{1}{1+j(f/f_{\text{SH}})}$$

where the break frequency of the shielding factor

$$\begin{aligned} f_{\text{SH}} &= \frac{R_{\text{SH}}}{2\pi L_{\text{SH}}} \\ &= 5.8\,\text{kHz} \end{aligned}$$

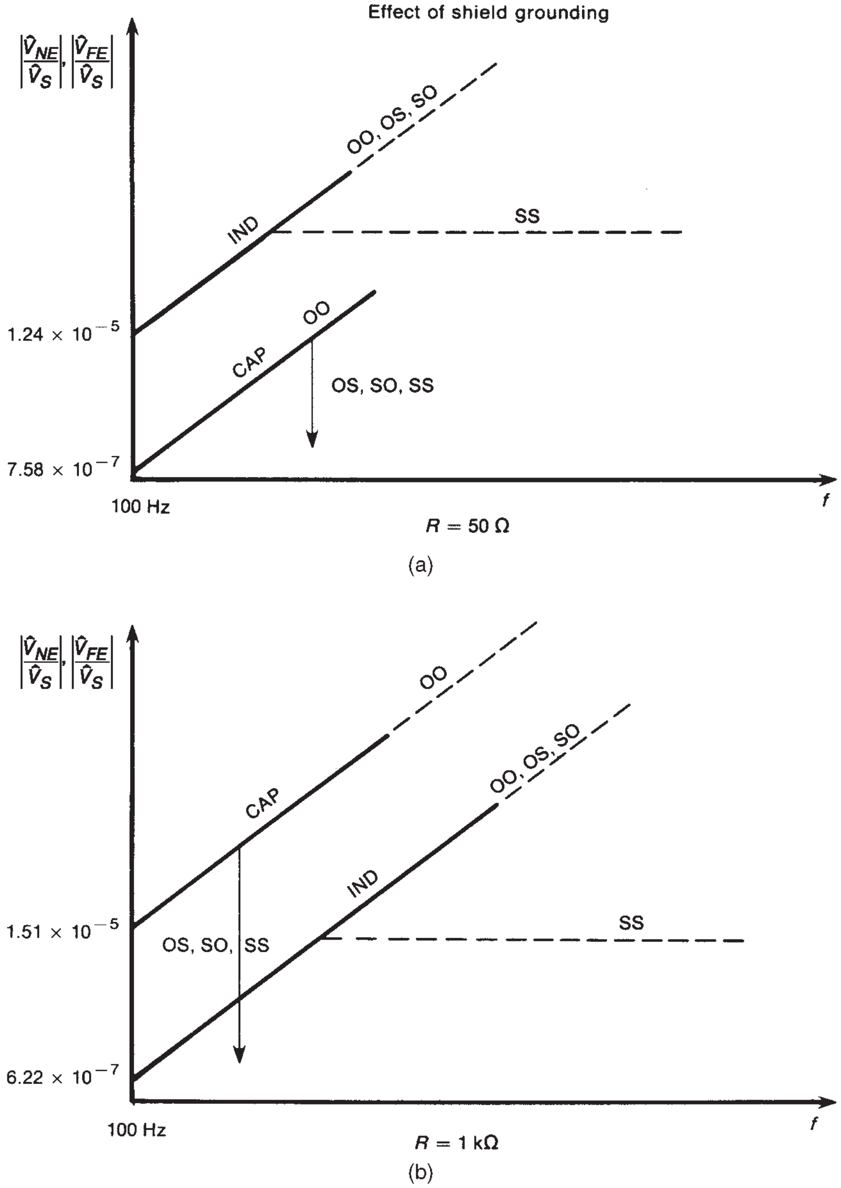

FIGURE 9.51 Explanation of the effect of shield grounding in the experimental results of Fig. 9.50 in terms of inductive and capacitive coupling for (a) $R = 50\,\Omega$ and (b) $R = 1\,\text{k}\Omega$.

is multiplied by the inductive coupling:

$$\begin{aligned} M_{NE}^{\text{IND}} &= \frac{R_{NE}}{R_{NE}+R_{FE}}\frac{L_{GR}}{(R_S=0)+R_L}\text{SF} \\ &= \frac{L_{\text{GR}}}{2R}\text{SFSS} \\ &= -\frac{R_{\text{FE}}}{R_{\text{NE}}+R_{\text{FE}}}\frac{L_{\text{GR}}}{(R_S=0)+R_L}\text{SF} \\ &= -\frac{L_{\text{GR}}}{2R}\text{SFSS} \end{aligned}$$

The characteristic impedance for the isolated wires above ground can be calculated as $Z_{CG} = v_0 l_G = 258\,\Omega$ and $Z_{CR} = v_0 l_R = 262\,\Omega$. Hence, we expect that *with the shield removed*, inductive coupling will dominate capacitive coupling for $R = 50\,\Omega$ loads, but capacitive coupling will dominate inductive coupling for $R = 1\ \text{k}\Omega$ loads. First, consider the case for $R = 50\,\Omega$ shown in Fig. 9.50a and analyzed in Fig. 9.51a. If a shield is placed around the receptor wire *but is not grounded at either end* (OO), the crosstalk is virtually the same as with the shield removed. Placing a shield around the receptor wire and grounding it at least at one end will remove the capacitive coupling:

$$M_{NE}^{\text{CAP}} = 0 \quad \text{OS, SO, SS}$$

Since inductive coupling dominates capacitive coupling *with the shield removed for* $R = 50\,\Omega$, we see *no reduction in the crosstalk:*

$$\begin{aligned}\frac{\hat{V}_{NE}}{\hat{V}_S} &= j2\pi f M_{NE}^{\text{IND}} \\ &= j2\pi f \frac{L_{GR}}{2R} \quad \text{OO, OS, SO}\end{aligned}$$

If the shield is grounded at both ends, then the shielding factor multiplies this:

$$M_{NE}^{\text{IND}} = \frac{L_{GR}}{2R} \frac{1}{1 + j(f/f_{\text{SH}})} \qquad \text{SS}$$

For frequencies below f_{SH}, the shielding factor is unity and the inductive coupling is unaffected by the shield even though the shield is grounded at both ends:

$$\begin{aligned}\frac{\hat{V}_{NE}}{\hat{V}_S} &= j2\pi f M_{NE}^{\text{IND}} \\ &= j2\pi f \frac{L_{GR}}{2R} \quad \text{SS} \quad f < f_{\text{SH}} = 5.8\,\text{kHz}\end{aligned}$$

For frequencies above the shield break frequency, the shielding factor becomes

$$\text{SF} \cong \frac{R_{\text{SH}}}{j\omega L_{\text{SH}}} \qquad f > f_{\text{SH}} = 5.8\,\text{kHz}$$

and the inductive coupling becomes constant:

$$\begin{aligned}\frac{\hat{V}_{NE}}{\hat{V}_S} &= j2\pi f M_{NE}^{\text{IND}} SF \\ &= j2\pi f \frac{L_{GR}}{2R} \frac{R_{\text{SH}}}{j2\pi f L_{\text{SH}}} \\ &= \frac{L_{GR}}{2R} \frac{R_{\text{SH}}}{L_{\text{SH}}} \quad \text{SS} \quad f > f_{\text{SH}} = 5.8\,\text{kHz}\end{aligned}$$

Hence for the shield grounded at both ends and frequencies above the shield break frequency, the crosstalk is independent of frequency and hence levels off at a level of 7.17×10^{-4} above $f_{\text{SH}} = 5.8$ kHz. The results in Fig. 9.502a verify this exactly.

Review Exercise 9.7 Compute the crosstalk transfer ratio at 100 kHz for $R = 50\,\Omega$ and compare to the experimental result.

***Answer*:** OO 1.348×10^{-2} (1.3×10^{-2}), OS, SO 1.24×10^{-2} (1×10^{-2}), SS 7.17×10^{-4} (7×10^{-4}).

Next consider the case of $R = 1\,\text{k}\Omega$ shown in Fig. 9.50b and analyzed in Fig. 9.51b. For this case, *capacitive coupling will dominate inductive coupling with the shield removed*. Placing a shield around the receptor wire and grounding it at least at one end will remove the capacitive coupling:

$$M_{NE}^{\text{CAP}} = 0 \quad \text{OS, SO, SS}$$

Because the capacitive coupling dominated the inductive coupling with the shield removed, the total crosstalk drops to the underlying inductive coupling:

$$\begin{aligned}\frac{\hat{V}_{NE}}{\hat{V}_S} &= j2\pi f M_{NE}^{\text{IND}} \\ &= j2\pi f \frac{L_{GR}}{2R} \quad \text{OO, OS, SO}\end{aligned}$$

If the shield is grounded at both ends, then the shielding factor multiplies this as follows:

$$M_{NE}^{\text{IND}} = \frac{L_{GR}}{2R} \frac{1}{1 + j\frac{f}{f_{\text{SH}}}} \text{SS}$$

For frequencies below f_{SH}, the shielding factor is unity and the inductive coupling is unaffected by the shield even though the shield is grounded at both ends:

$$\begin{aligned}\frac{\hat{V}_{NE}}{\hat{V}_S} &= j2\pi f M_{NE}^{\text{IND}} \\ &= j2\pi f \frac{L_{GR}}{2R} \quad \text{SS} \quad f < f_{\text{SH}} = 5.8\,\text{kHz}\end{aligned}$$

For frequencies above the shield break frequency, the shielding factor again becomes

$$\text{SF} \cong \frac{R_{\text{SH}}}{j\omega L_{\text{SH}}} \quad f > f_{\text{SH}} = 5.8\,\text{kHz}$$

and the inductive coupling again becomes constant:

$$\begin{aligned}\frac{\hat{V}_{NE}}{\hat{V}_S} &= j2\pi f M_{NE}^{\text{IND}} SF \\ &= j2\pi f \frac{L_{GR}}{2R} \frac{R_{\text{SH}}}{j2\pi f L_{\text{SH}}} \\ &= \frac{L_{GR}}{2R} \frac{R_{\text{SH}}}{L_{\text{SH}}} \quad \text{SS} \quad f > f_{\text{SH}} = 5.8\,\text{kHz}\end{aligned}$$

Hence for the shield grounded at both ends and frequencies above the shield break frequency, the crosstalk is independent of frequency and hence levels off at a level of 3.59×10^{-5} above $f_{SH} = 5.8$ kHz. The results in Fig. 9.50b verify this exactly. Above approximately 100 kHz, this begins to increase. We will see in the next section that this is due to the "pigtails" (exposed sections) at the end. Also observe that the crosstalk for $R = 1$ kΩ in Fig. 9.50b for the shield grounded only at the right end (OS) begins to differ from, and becomes greater than, the crosstalk for the shield grounded only at the left end (SO) above approximately 200 kHz. This is because the line is becoming electrically long (the line is $L \cong \lambda_0/400$ at 200 kHz). Hence, grounding the shield at the left end where the measurement of the crosstalk voltage is being made only makes the shield voltage zero *at that end*. Grounding the shield only at the right end makes the voltage of the shield zero only at that end and not necessarily at the left end.

Review Exercise 9.8 Compute the crosstalk transfer ratio at 100 kHz for $R = 1$ kΩ and compare to the experimental result.

***Answer*:** OO 2.144×10^{-2} (3×10^{-2}), OS, SO 6.22×10^{-4} (6×10^{-4}), SS 3.59×10^{-5} (5×10^{-5})

The results above can be shown to remain true whether the shield is placed around the receptor wire or around the generator wire [19–22]. If a shield is placed around the generator wire and around the receptor wire, the results are essentially unchanged in that capacitive coupling can be eliminated by grounding *either shield at either end*. The inductive coupling is the product of the inductive coupling with both shields removed multiplied by two *shield factors* of the form of (9.123) [19, 20]. In summary, *connecting either end of a shield to the reference conductor eliminates capacitive coupling. In order to affect inductive coupling, the shield must be connected to the reference conductor at both ends. The inductive coupling will become constant with frequency above the shield break frequency given by* $f_{SH} = (R_{SH}/2\pi L_{SH})$.

9.5.4 Effect of Pigtails

The term "pigtail" is commonly used to refer to the break in a shield required to terminate it to a "grounding point." Shield connections are commonly passed through a connector by connecting the shield to a connector pin with another wire (the pigtail wire), as shown in Fig. 9.52. This exposes the interior, shielded wire over the length of the pigtail wire. Pigtail lengths of over 5 in. are not uncommon.

The effect of the exposed, pigtail section is to allow the direct coupling to the interior shielded wire over the length of the pigtail section. For electrically short lines, we can superimpose the coupling over the two pigtail sections at the ends of the cable and the coupling over the shielded section (which we considered in the previous section), as illustrated in Fig. 9.53. If the line is electrically short, we can reflect the termination impedances to the ends of each section and treat the individual couplings as separate problems, for example [15, 23],

$$\hat{V}_{NE} = \hat{V}_{NE}^{\text{left pigtail}} + \hat{V}_{NE}^{\text{shielded section}} + \hat{V}_{NE}^{\text{right pigtail}} \tag{9.112}$$

We can compute each of these contributions using the previous methods. Each contribution is the sum of a capacitive and an inductive coupling component. If the shield is grounded at either end, the capacitive coupling is eliminated from $\hat{V}_{NE}^{\text{shielded section}}$.

As an experimental example, consider the experiment considered previously for the illustration of shielding. We will investigate the near-end crosstalk transfer function for the shield grounded at both ends and for two values of terminations impedances, $R = 50\,\Omega$ and $R = 1$ kΩ. Three lengths of

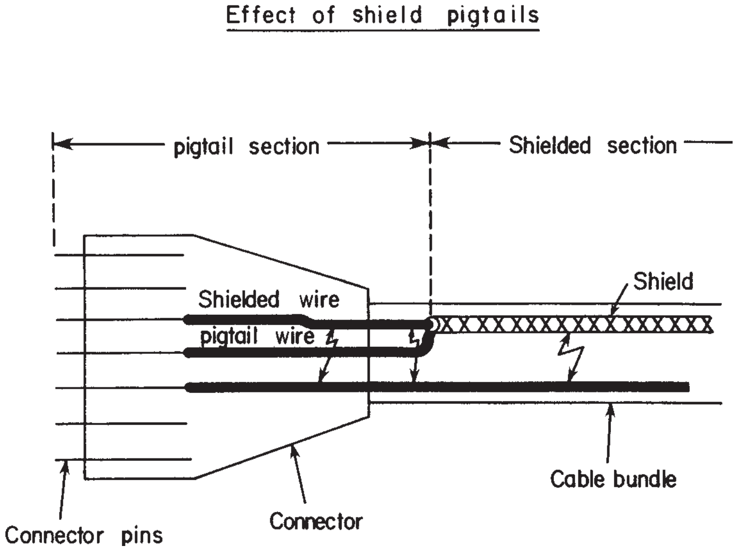

FIGURE 9.52 Illustration of “pigtails” used to terminate shields in a cable connector.

pigtail sections on both ends will be used, as illustrated in Fig. 9.54. The first length is 0.5 cm and is as small as reasonably possible without using a peripheral bonding of the shield. The second length is 3 cm, which is only 1.6% of the total line length. The third length is 8 cm, which is only 4.4% of the total line length. The experimental data are shown in Fig. 9.55. Observe that for $R = 50\,\Omega$ shown in Fig. 9.55a and frequencies above 1 MHz, the longest length of pigtail causes the crosstalk to be as much as some 30 dB larger than for the shortest pigtail length. The reason for this is illustrated in Fig. 9.56, where we have shown the components given in (9.112). Observe that the contributions over the pigtail sections are inductive and much smaller than the contribution over the shielded section below 100 kHz. Above the shield break frequency (6 kHz), the generator wire current flows back along the shield, and the coupling over the shielded section flattens out. The pigtail coupling continues to increase at 20 dB/decade and becomes greater than the coupling over the shielded section above 100 kHz. For the case of $R = 1\ \mathrm{k}\Omega$ shown in Fig. 9.55b, we see a similar effect, but it extends to a frequency much lower than that for $R = 50\,\Omega$. This is because the inductive coupling over the shielded section is reduced to a much lower level for $R = 1\ \mathrm{k}\Omega$, and the pigtail section contributions begin to dominate at a much lower frequency.

The result is that *pigtails reduce the shielding effectiveness of a shielded wire over that which could be obtained if the shield were peripherally bonded at each end, thereby causing no exposure of the interior wire*. Pigtails do not eliminate the effect of a shield; they just reduce it from its ideal effect.

9.5.5 Effects of Multiple Shields

We observed that the effect of placing a shield around a wire is to eliminate capacitive coupling if the shield is terminated to the reference conductor at one or both ends. The shield acts to reduce inductive coupling above the break frequency, $f_{SH} = (R_{SH}/2\pi L_{SH})$ only if the shield is terminated to the reference conductor at *both ends*.

Suppose that we place shields around *both* the generator *and* receptor wires. Also let us terminate both ends of each shield to the reference conductor. The capacitive coupling will be eliminated, and we are left with the inductive coupling to consider. The inductive coupling *with the shields removed*

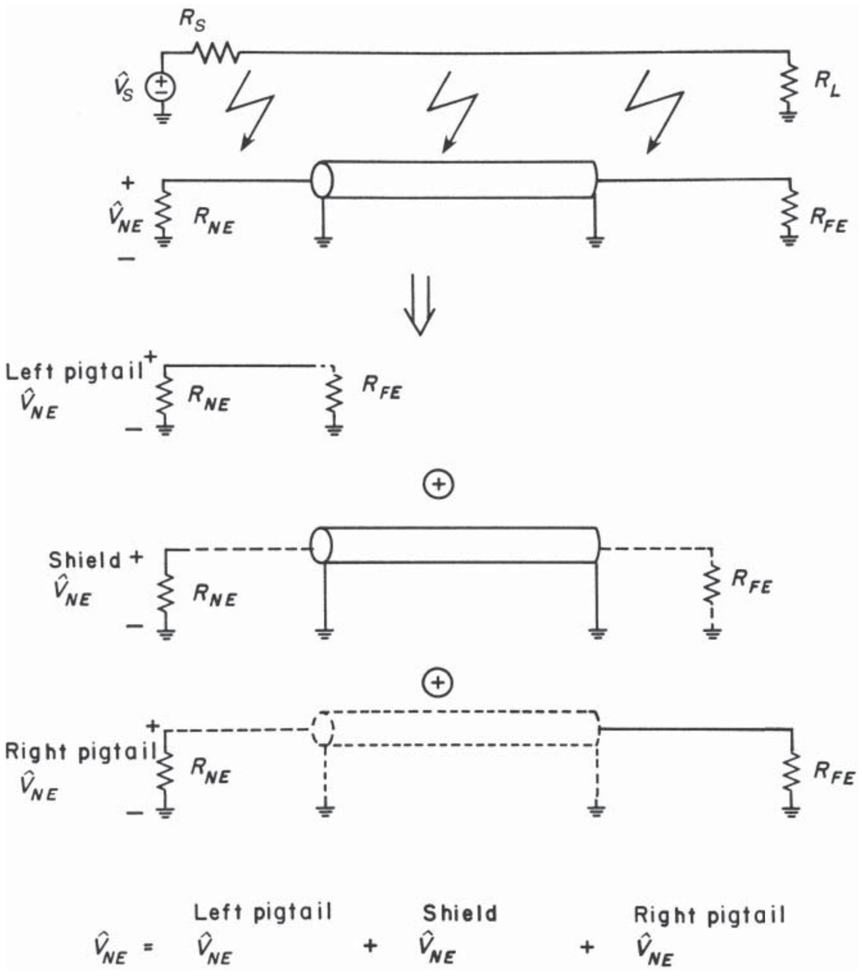
R_S
$\hat{V}_S$
R_L
+
$\hat{V}_{NE}$
R_{NE}
−
R_{FE}
Left pigtail
+
$\hat{V}_{NE}$
R_{NE}
−
R_{FE}
Shield +
$\hat{V}_{NE}$
R_{NE}
−
R_{FE}
+
Right pigtail
$\hat{V}_{NE}$
R_{NE}
−
R_{FE}
Left pigtail
Shield
Right pigtail
$\hat{V}_{NE} = \hat{V}_{NE} + \hat{V}_{NE} + \hat{V}_{NE}$

FIGURE 9.53 An approximate method of computing the effect of pigtails on crosstalk by superimposing the inductive and capacitive coupling over each section.

will be multiplied by two shielding factor terms, each of the form of (9.106). Thus, the total coupling is inductive and is given by [15, 19, 20, 23].

$$\frac{\hat{V}_{NE,FE}}{\hat{V}_S} = \underbrace{\frac{\hat{V}^{\text{IND}}_{NE,FE}}{\hat{V}_S}}_{\substack{\text{with both}\\ \text{shields}\\ \text{removed}}} \frac{R_{\text{SH}G}}{R_{\text{SH}G} + j\omega L_{\text{SH}G}} \frac{R_{\text{SH}R}}{R_{\text{SH}R} + j\omega L_{\text{SH}R}} \tag{9.113}$$

where $R_{\text{SH}G}$ and $L_{\text{SH}G}$ ($R_{\text{SH}R}$ and $L_{\text{SH}R}$) are the shield total resistance and self-inductance of the generator circuit (receptor circuit) shield. Thus, the crosstalk transfer ratio will be as shown in Fig. 9.57, where the break frequencies are given by

$$f_{\text{SH}G} = \frac{R_{\text{SH}G}}{2\pi L_{\text{SH}G}} \tag{9.114a}$$

$$f_{\text{SH}R} = \frac{R_{\text{SH}R}}{2\pi L_{\text{SH}R}} \tag{9.114b}$$

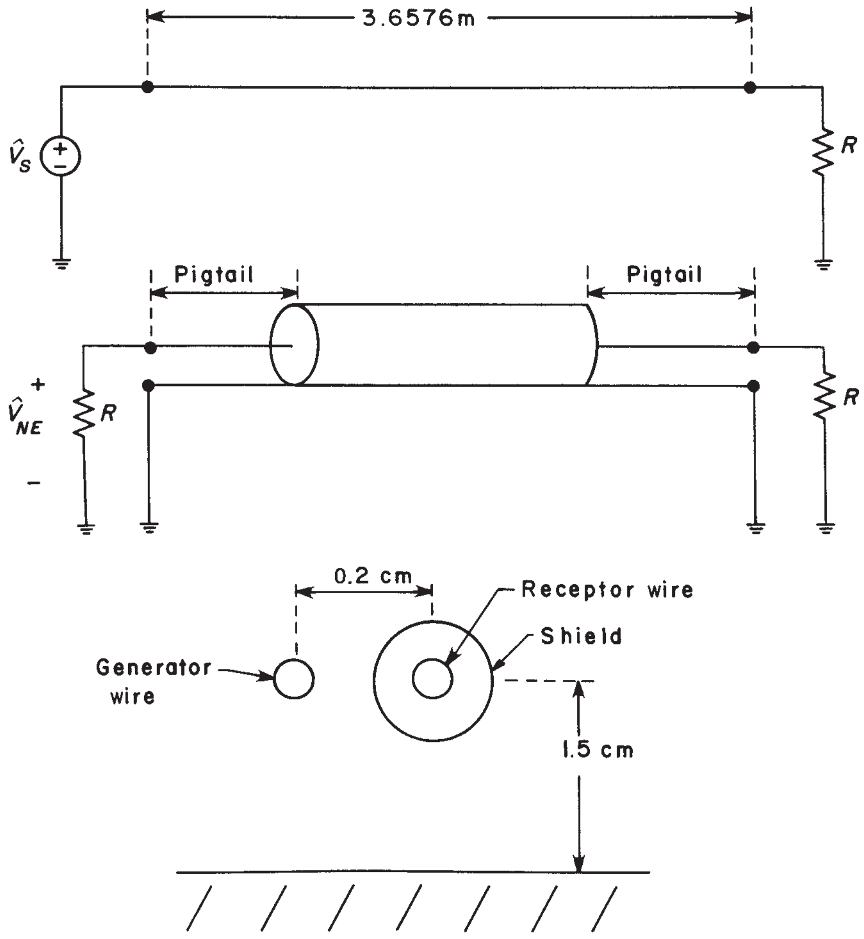

FIGURE 9.54 An experiment to illustrate the effect of pigtail lengths on crosstalk.

Therefore, the presence of shields on both wires (and grounded at both ends) causes the crosstalk to roll off at −20 dB/decade above the second break frequency.

In order to illustrate this effect, we will show the experimentally observed results for (a) no shields, (b) one shield around the receptor wire, and (c) shields on both the generator and the receptor wires. The experimental cross-sectional configurations are shown in Fig. 9.48. The separation between generator and receptor wires is $s = 1.5$ cm, which is denoted on the graphs as SEPARATION: WIDE. The pigtail lengths for both shields are 8 cm. Data for other separations and pigtail lengths are given in [19, 20]. The experimental data are shown in Fig. 9.59 for $R = 50\ \Omega$. Since both shields are identical and are at the same height above the ground plane (h = 1.5 cm), $R_{\mathrm{SH}G} = R_{\mathrm{SH}R}$ and $L_{\mathrm{SH}G} = L_{\mathrm{SH}R}$, so that the break frequencies are the same, $f_{\mathrm{SH}G} = f_{\mathrm{SH}R} \cong 6$ kHz. The behavior of the inductive coupling illustrated in Fig. 9.48 for one shield and in Fig. 9.57 for shields on both wires is evident in the experimental data. Observe that for shields on both wires, the −20 dB/decade behavior extends to 100 kHz. Above this, the response increases at +20 dB/decade. This is clearly due to the coupling over the 8 cm pigtail sections becoming dominant.

9.5.6 MTL Model Predictions

The exact solution of the multiconductor transmission-line (MTL) equations is described in [15, 19, 20, 23]. The solution technique is to treat the two pigtail

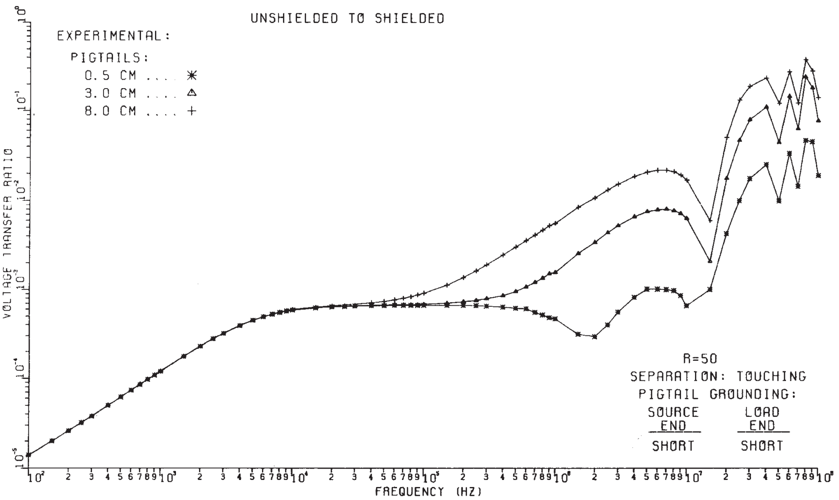

(a)

FIGURE 9.55 Experimental results for the configuration of Fig. 9.54 for pigtail lengths of 0.5, 3, and 8 cm for (a) $R = 50\,\Omega$ and (b) $R = 1\ \text{k}\Omega$.

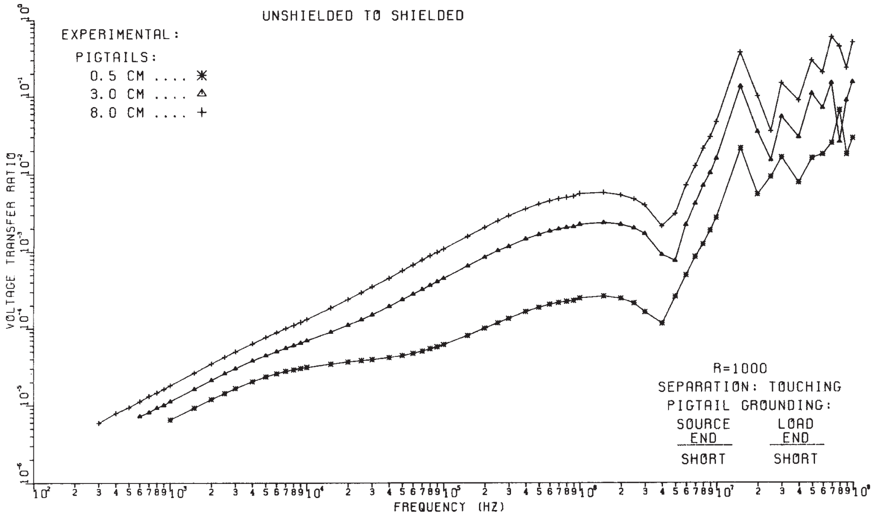

(b)

FIGURE 9.55 (*Continued*)

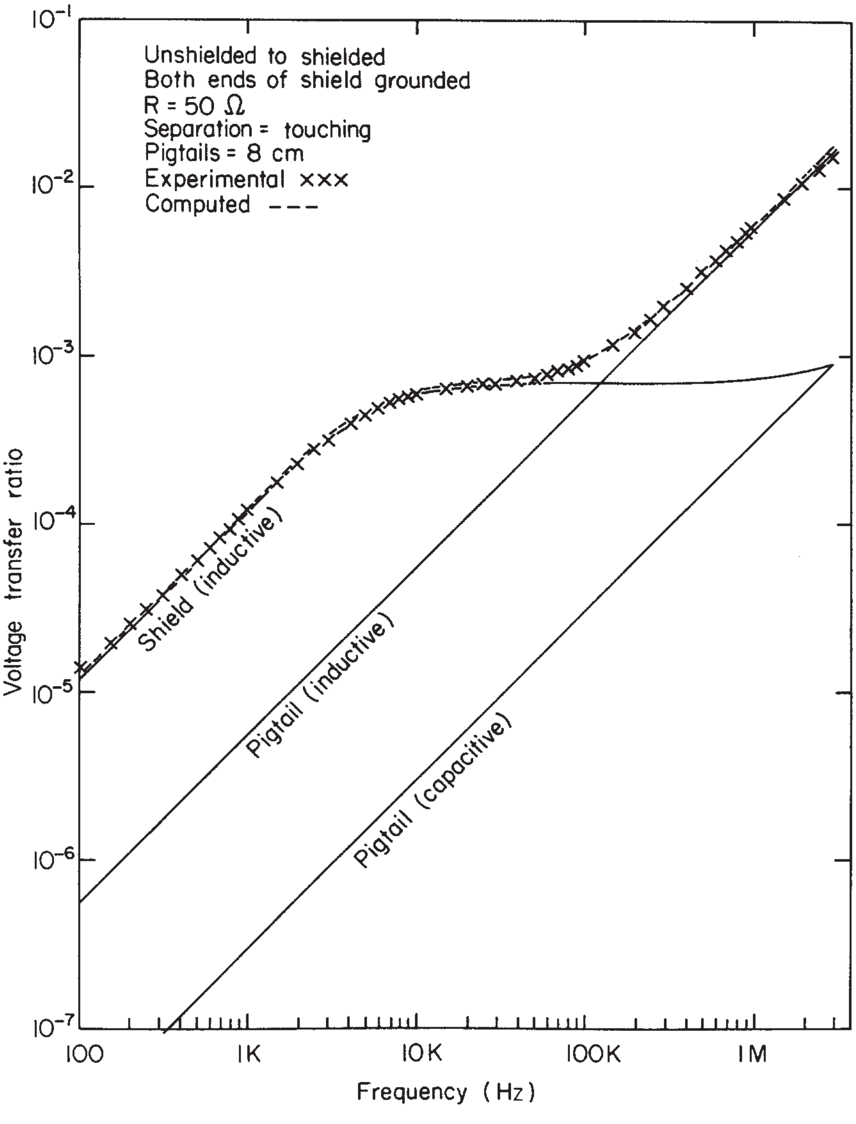

FIGURE 9.56 The near-end crosstalk for the configuration of Fig. 9.54 for 8 cm pigtail lengths and $R = 50\,\Omega$ in terms of contributions according to Fig. 9.53.

transmission lines and determine the exact chain parameter matrix (CPM) of each section. Multiplying these chain parameter matrices together (in the proper order) gives the CPM of the overall line. The terminal conditions are incorporated [3, 4, 20, 23] in order to solve for the terminal voltages. This has been implemented in a FORTRAN computer program described in [20] that considers a number of nonideal effects such as coupling through holes in the shield. In order to illustrate the prediction accuracy of this exact solution method, we will show the predictions for the data that were given in Fig. 9.59. These results are given for $R = 50\,\Omega$ in Fig. 9.60a for one shield around the receptor wire and in Fig. 9.60b for shields around both the generator and receptor wires. Both shields are grounded at both ends, the pigtail lengths at each end are 8 cm, and the generator and receptor circuits are separated by 1.5 cm (SEPARATION: WIDE). The MTL model shows excellent predictions of the experimental results.

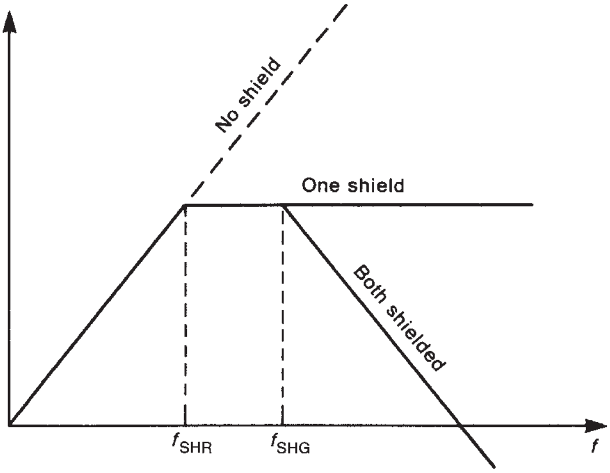

FIGURE 9.57 Frequency response of crosstalk for no shields, one shield (on the generator wire or on the receptor wire), and shields on both wires.

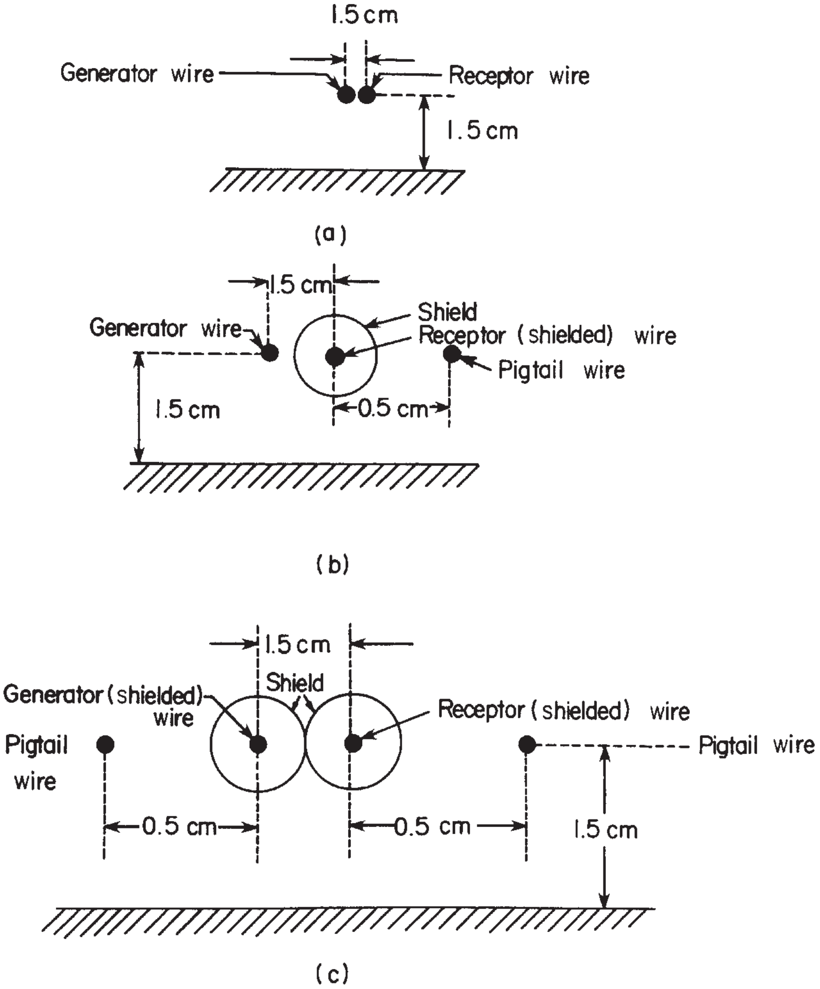
1.5 cm
Generator wire
Receptor wire
1.5 cm
(a)
1.5 cm
Generator wire
Shield
Receptor (shielded) wire
Pigtail wire
1.5 cm
0.5 cm
(b)
1.5 cm
Shield
Generator (shielded) wire
Receptor (shielded) wire
Pigtail wire
Pigtail wire
0.5 cm
0.5 cm
1.5 cm
(c)

FIGURE 9.58 Cross section of an experiment to illustrate the effect of placing shields on neither wire [(a) unshielded to unshielded], one wire [(b) unshielded to shielded],

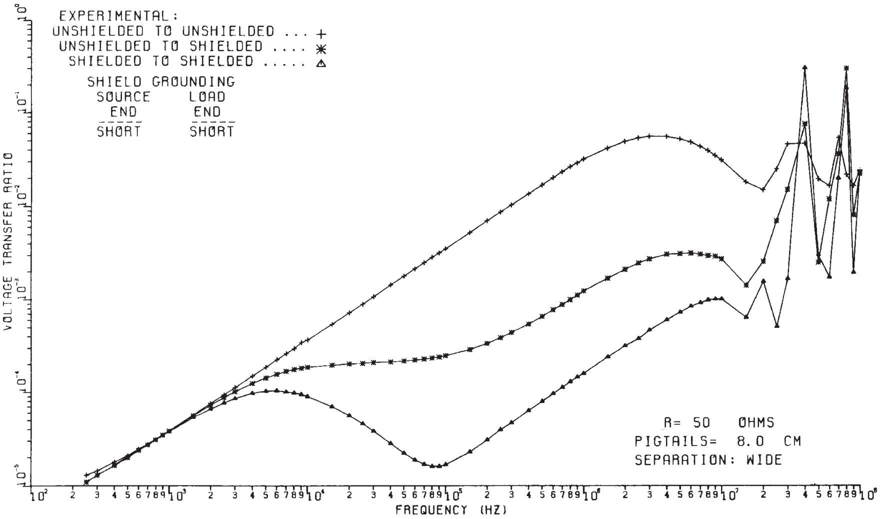

FIGURE 9.59 Experimental results for $R = 50\,\Omega$ and 8-cm pigtails for the configurations of Fig. 9.46.

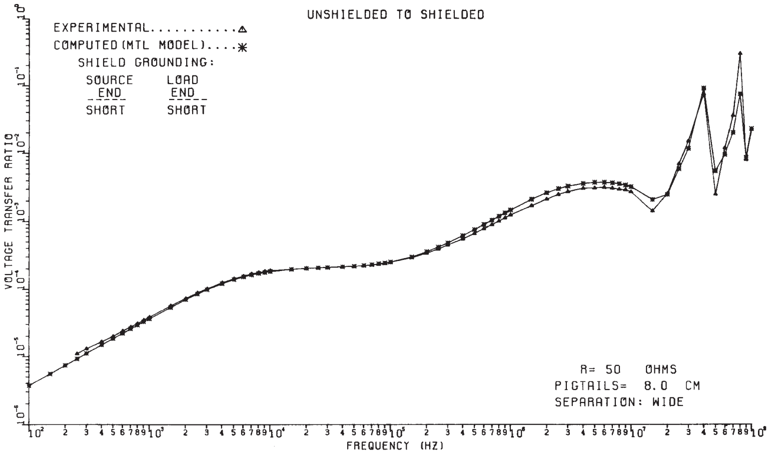

(a)

FIGURE 9.60 Predictions of the transmission-line model versus experimental results for the configuration of Fig. 9.46 for (a) a shield on the receptor wire and (b) shields on both the generator and the receptor wires.

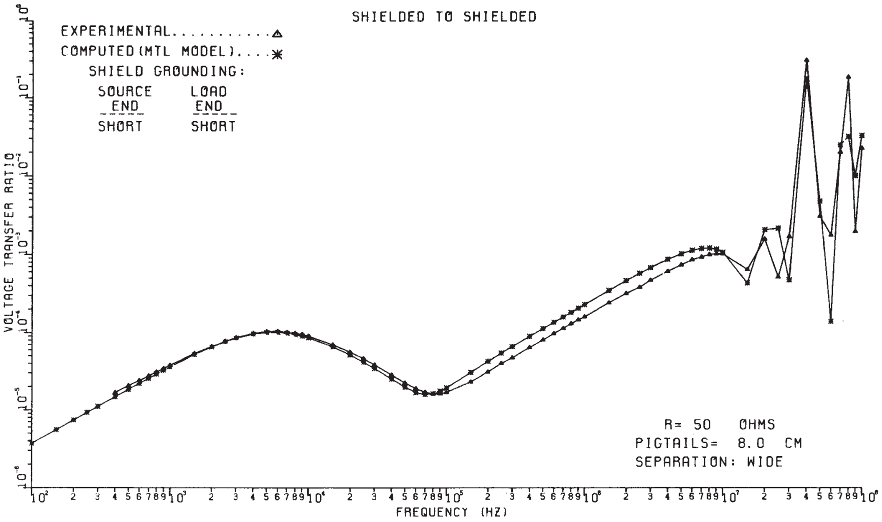

(b)

FIGURE 9.60 (*Continued*)

9.6 TWISTED WIRES

We now turn our attention to the use of a *twisted pair of wires* to reduce crosstalk. A twisted pair is the *dual* to a shielded wire in the following sense. We observed that placing a shield around a receptor wire inherently tends to reduce *capacitive or electric field coupling* so long as either end of the shield is attached to the reference conductor. In order to reduce inductive coupling, the shield must be attached to the reference conductor at *both ends* in order to allow a current to flow back along the shield to produce a counteracting magnetic flux to cancel the flux from the generator current. Replacing a receptor wire with a twisted pair and using one wire of the pair as the return for the receptor circuit inherently reduces *inductive or magnetic field coupling* because of the twist. The twisted pair reduces capacitive coupling only if the terminations at both ends are *balanced with respect to the reference conductor*.

In reality, a twisted pair of wires is a *bifilar helix*. In order to model the twisted pair, we will approximate it as a cascade of alternating loops as shown in Fig. 9.61. The essential way in which the twisted pair reduces *inductive or magnetic field coupling* is as follows. Consider the magnetic flux from the generator wire current. This flux threads the loops of the twisted pair, inducing emfs in each loop. But because the loops alternate in polarity, the induced emfs tend to cancel in the adjacent loops. Thus, the net induced emf induced in the receptor circuit (the twisted pair) is that of one half-twist. (A loop is referred to here as a *half-twist*.) The twist does not, inherently, affect capacitive coupling.

A simple *topological model* for the twisted pair is shown in Fig. 9.62. We will again illustrate this for the case where a ground plane is the reference conductor for both circuits. This model assumes that the twisted pair can be approximated as a cascade of alternating rectangular loops in the vertical plane (or in the horizontal plane). The *exact transmission-line model for this approximation of the bifilar helix* is solved in [24–26] by modeling each half-twist whose length is denoted by L_{HT} along with the adjacent generator wire with a chain parameter matrix (CPM) for this section. The overall chain parameter matrix of the cascade is the product of all these chain parameter matrices of the half-twist sections with an appropriate reversal of the twisted wires at the junctions between the half-twists. This is similar to the process used in the previous section to incorporate pigtail sections of a shielded wire line. The reader is referred to the implementation of this transmission-line model to [24, 26]. Predictions of this exact MTL model will be shown in the following sections.

The following approximate model makes use of the notions of inductive and capacitive coupling described previously and was originally described in [25, 26]. We assume once again that the line

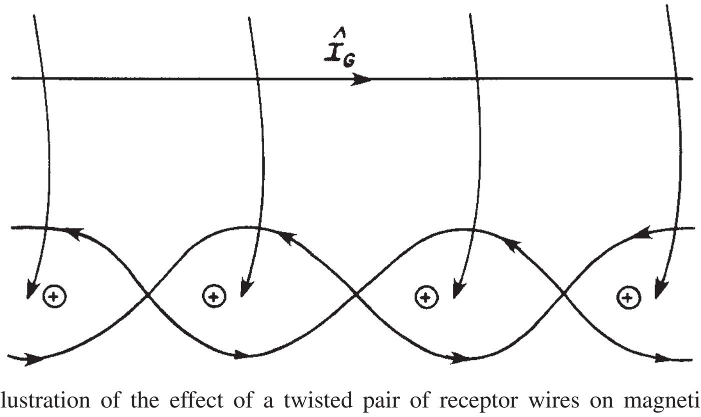

FIGURE 9.61 Illustration of the effect of a twisted pair of receptor wires on magnetic field (inductive) coupling.

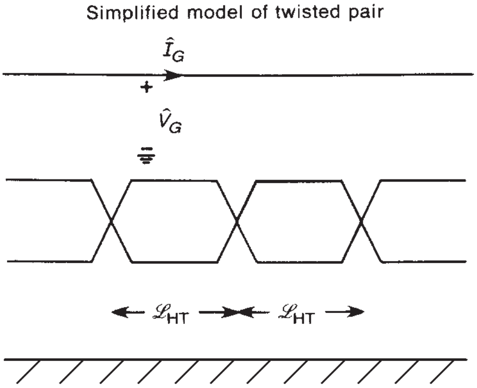
Simplified model of twisted pair
$\hat{I}_G$
+
$\hat{V}_G$
$\mathscr{L}_{HT}$
$\mathscr{L}_{HT}$

FIGURE 9.62 A simple "abrupt loop" model of a twisted pair of receptor circuit wires.

is *electrically short* in using the following lumped model. Also, we assume that the generator and receptor circuits are weakly coupled. Now consider each loop (half-twist) as a parallel-wire line and compute the mutual inductances from the generator circuit to *each circuit formed between each wire of the twisted pair and the reference conductor*. This gives per-unit-length mutual inductances l_{m1} and l_{m2} and per-unit-length mutual capacitances c_{m1} and c_{m2}. The effects of these mutual elements are represented in the usual fashion as voltage and current sources whose values depend on the mutual element *for that length of the half-twist* and the generator circuit voltage or current, as shown in Fig. 9.63. The total inductance or capacitance parameter is the per-unit-length value multiplied by the length of the half-twist (the loop), denoted by L_{HT}.

9.6.1 Per-Unit-Length Parameters

These mutual inductances are computed as shown in Fig. 9.64. For example, consider a generator wire and a twisted pair above a ground plane (the reference conductor), as shown in Fig. 9.65. The generator wire and the twisted pair are at a height h above the ground plane, and the horizontal

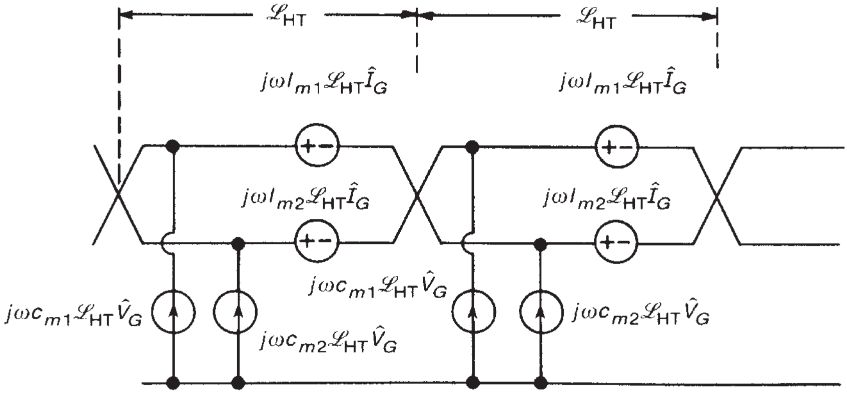
$\mathscr{L}_{HT}$
$\mathscr{L}_{HT}$
$j\omega l_{m1}\mathscr{L}_{HT}\hat{I}_G$
$j\omega l_{m1}\mathscr{L}_{HT}\hat{I}_G$
$j\omega l_{m2}\mathscr{L}_{HT}\hat{I}_G$
$j\omega l_{m2}\mathscr{L}_{HT}\hat{I}_G$
+−
+−
+−
+−
$j\omega c_{m1}\mathscr{L}_{HT}\hat{V}_G$
$j\omega c_{m1}\mathscr{L}_{HT}\hat{V}_G$
$j\omega c_{m2}\mathscr{L}_{HT}\hat{V}_G$
$j\omega c_{m2}\mathscr{L}_{HT}\hat{V}_G$

FIGURE 9.63 The simple inductive–capacitive coupling model for the twisted pair of receptor circuit wires of Fig. 9.62.

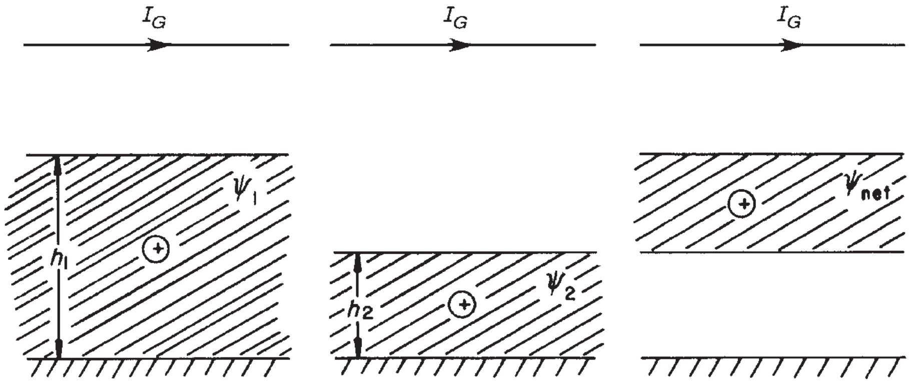

I_G
I_G
I_G
h_1
ψ_1
h_2
ψ_2
ψ_{net}

FIGURE 9.64 Illustration of the per-unit-length mutual inductance to a twisted pair of receptor wires.

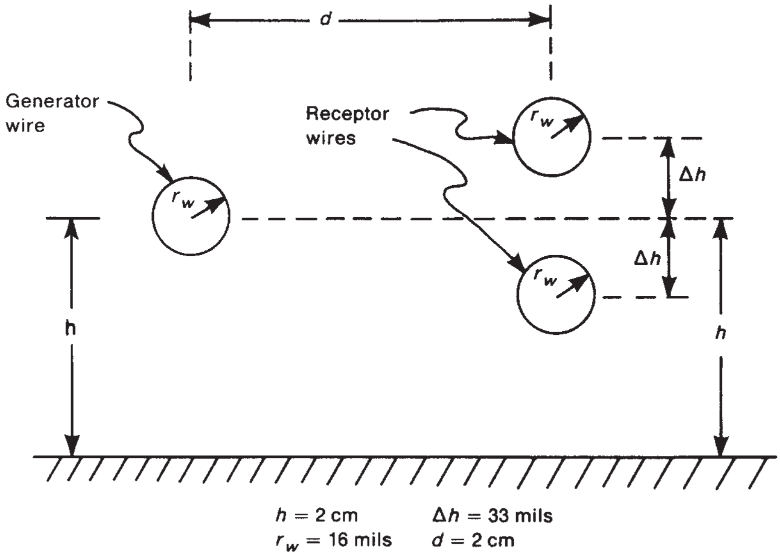

d
Generator wire
Receptor wires
r_w
r_w
r_w
Δh
Δh
h
h
h = 2 cm
r_w = 16 mils
Δh = 33 mils
d = 2 cm

FIGURE 9.65 Cross-sectional dimensions of a twisted receptor wire pair for computing the per-unit-length inductances.

separation between the generator wire and the twisted pair is d. The separation between the two wires of the twisted pair is $2\Delta h$. Assume for illustration that the wires are identical, with radii r_w. The mutual inductances are obtained by treating each wire of the twisted pair with the ground plane as a circuit and using our previously derived results [see (9.35)] to obtain

$$l_{m1} = \frac{\mu_0}{4\pi} \ln \left[1 + \frac{4h(h + \Delta h)}{d^2 + \Delta h^2} \right] \tag{9.115a}$$

$$l_{m2} = \frac{\mu_0}{4\pi} \ln \left[1 + \frac{4h(h + \Delta h)}{d^2 + \Delta h^2} \right] \tag{9.115b}$$

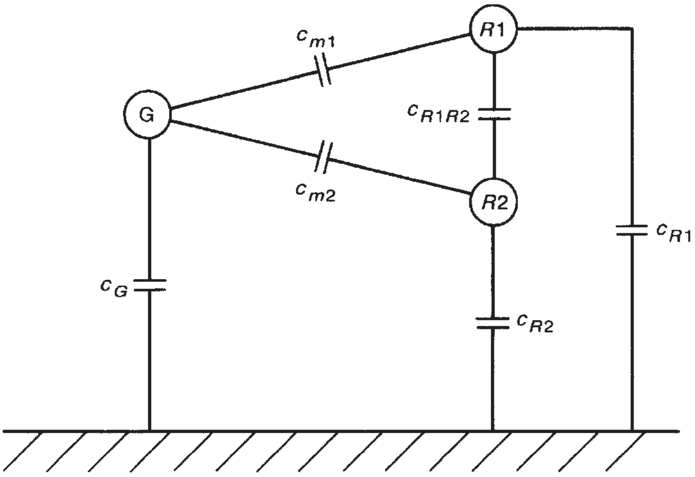

FIGURE 9.66 The per-unit-length capacitances for a twisted receptor pair.

In order to determine the mutual capacitances, we invert the per-unit-length inductance of the line. The self-inductances are [see (9.31) and (9.32)]

$$l_G = \frac{\mu_0}{2\pi} \ln\left(\frac{2h}{r_w}\right) \tag{9.115c}$$

$$l_{R1} = \frac{\mu_0}{2\pi} \ln\left[\frac{2(h+\Delta h)}{r_w}\right] \tag{9.115d}$$

$$l_{R2} = \frac{\mu_0}{2\pi} \ln\left[\frac{2(h-\Delta h)}{r_w}\right] \tag{9.115e}$$

The remaining mutual inductance is computed by placing a current on one wire of the twisted pair (and returning in the image) and computing the flux through the circuit formed by the other wire and the ground plane using the fundamental result in (9.13):

$$\begin{aligned} l_{R1R2} &= \frac{\mu_0}{2\pi} \ln\left(\frac{h+\Delta h}{2\Delta h}\right) + \frac{\mu_0}{2\pi} \ln\left[\frac{(h+\Delta h)+(h-\Delta h)}{h+\Delta h}\right] \\ &= \frac{\mu_0}{2\pi} \ln\left(\frac{h}{\Delta h}\right) \end{aligned} \tag{9.115f}$$

which is equivalent to using (9.35). For the dimensions of $d = 2$ cm, $h = 2$ cm, $r_w = 16$ mils (20 gauge, solid), and $\Delta h = 33$ mils, we compute

$$\begin{aligned} l_{m1} &= 1.641 \times 10^{-7}\ \text{H/m} \\ l_{m2} &= 1.574 \times 10^{-7}\ \text{H/m} \\ l_g &= 9.179 \times 10^{-7}\ \text{H/m} \\ l_{R1} &= 9.261 \times 10^{-7}\ \text{H/m} \\ l_{R2} &= 9.093 \times 10^{-7}\ \text{H/m} \\ l_{R1R2} &= 6.344 \times 10^{-7}\ \text{H/m} \end{aligned}$$

The difference between l_{m1} and l_{m2} will be needed:

$$l_{m1} - l_{m2} = 6.706 \times 10^{-9}$$

The mutual capacitances are computed by ignoring the dielectric insulations as (see Fig. 9.66)

$$\begin{bmatrix} c_G + c_{m1} + c_{m2} & -c_{m1} & -c_{m2} \\ -c_{m1} & c_{R1R2} + c_{m1} + c_{R1} & -c_{R1R2} \\ -c_{m2} & -c_{R1R2} & c_{R1R2} + c_{m2} + c_{R2} \end{bmatrix} = \mu_0 \varepsilon_0 \begin{bmatrix} l_G & l_{m1} & l_{m2} \\ l_{m1} & l_{R1} & l_{R1R2} \\ l_{m2} & l_{R1R2} & l_{R2} \end{bmatrix}^{-1} \tag{9.116}$$

This gives

$$c_{m1} = 1.411 \text{ pF/m}$$
$$c_{m2} = 1.190 \text{ pF/m}$$

We will also need the sum and difference of c_{m1} and c_{m2}:

$$c_{m1} + c_{m2} = 2.601 \text{ pF/m}$$
$$c_{m1} - c_{m2} = 0.220 \text{ pF/m}$$

9.6.2 Inductive and Capacitive Coupling

The resulting model thus consists of a sequence of sources shown in Fig. 9.67 [24–31]. The induced voltage sources $\overline{E}_1$ and $\overline{E}_2$ are due to the mutual inductance between the generator and the twisted pair receptor and are essentially induced emfs resulting from Faraday's law. The contributions of these sources to the crosstalk voltages at the ends of the twisted pair are referred to as *inductive coupling*. The induced current sources $\overline{I}_1$ and $\overline{I}_2$ are due to mutual capacitance between the generator and twisted-pair receptor, and their contributions to the crosstalk voltages are referred to as *capacitive coupling*. From Fig. 9.63, these sources are given by

$$\hat{E}_1 = j\omega l_{m1} L_{HT} \hat{I}_G \tag{9.117a}$$

$$\hat{E}_2 = j\omega l_{m2} L_{HT} \hat{I}_G \tag{9.117b}$$

$$\hat{I}_1 = j\omega c_{m1} L_{HT} \hat{V}_G \tag{9.117c}$$

$$\hat{I}_2 = j\omega c_{m2} L_{HT} \hat{V}_G \tag{9.117d}$$

where $\hat{V}_G$ and $\hat{I}_G$ are the *low-frequency* values of the generator circuit voltage and current. These may be computed as dc values. Now let us "untwist" the wires, giving the circuit for two adjacent half-twists (one full twist) shown in Fig. 9.68.

We next must consider the termination configurations. There are generally two methods for terminating twisted pairs, as shown in Fig. 9.69. The circuit in Fig. 9.69a is said to be *unbalanced* in the sense that the impedances seen between each wire and ground are not the same. One wire of the

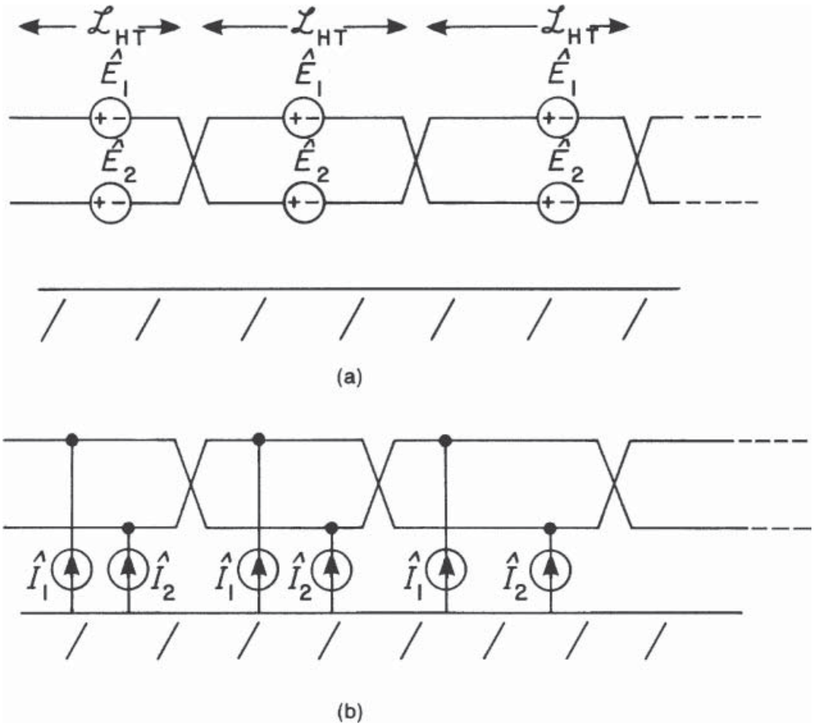

FIGURE 9.67 The simple inductive–capacitive coupling model of a twisted receptor pair: (a) inductive coupling; (b) capacitive coupling. Source: Based on Paul and McKnight [24], Paul and McKnight [25], Paul and McKnight [26], Paul and Jolly [27], Paul and Jolly [28], Paul and Jolly [29], Paul and Koopman [30], and Paul and Koopman [31].

twisted pair is connected to the reference conductor at the near end, while the other end is not connected to the reference conductor in order to avoid *ground loops* between that wire and the reference conductor, which will allow circulating currents to flow in that loop. The circuit shown in Fig. 9.69b is said to be *balanced* in the sense that the impedances seen between each wire and the reference conductor are equal, which is due to the use of a center-tapped transformer. Balanced line drivers and receivers will also produce this effect.

We will consider the unbalanced case shown in Fig. 9.69a in this section, while the balanced case will be considered in Section 9.6.4. The equivalent circuit for the entire line, substituting the simple model for the twisted pair, is given in Fig. 9.70 and shows that the near-end crosstalk is the superposition of the inductive and capacitive coupling contributions. The values of the sources are given in (9.117). Untwisting the twisted pair gives the circuit in Fig. 9.71. This equivalent circuit shows that *the net induced emf in the twisted-pair loop is that of one half-twist for an odd number of half-twists and is zero for an even number of half-twists*. Observe that the current sources that are attached to the wire of the twisted pair that is grounded at the near end are “shorted out,” and thus do not contribute to the solution. The net current source attached to the wire that is not grounded over one complete twist is $\hat{I}_1 + \hat{I}_2 = j\omega c_{m1} L_{HT} \hat{V}_G + j\omega c_{m2} L_{HT} \hat{V}_G$, according to Fig. 9.63. Since the two twisted wires are very close together, $c_{m1} c_{m2}$. Also, $L = NL_{HT}$, where N is the total number of half-twists. Thus, the net current source attached to the ungrounded wire is approximately $j\omega c_m L$, where we may use c_{m1} or c_{m2} for c_m. Essentially, this gives the same capacitive coupling as that of the *untwisted pair*, which we will refer to as the *straight-wire pair* (SWP). The *twisted-wire pair*

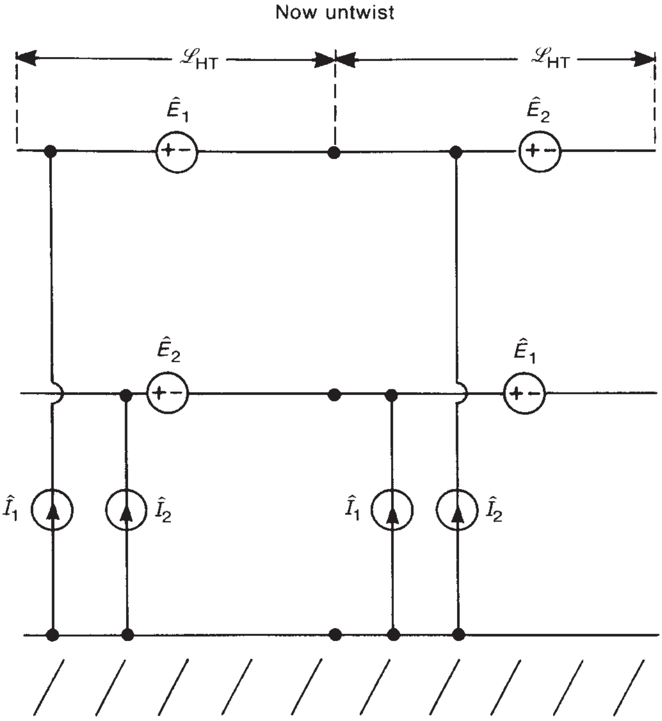
Now untwist
$\mathscr{L}_{HT}$
$\mathscr{L}_{HT}$
$\hat{E}_1$
$\hat{E}_2$
$\hat{E}_2$
$\hat{E}_1$
$\hat{I}_1$
$\hat{I}_2$
$\hat{I}_1$
$\hat{I}_2$

FIGURE 9.68 "Untwisting" the model of Fig. 9.67.

will be referred to as TWP. From this circuit, we can determine the near-end and far-end crosstalk voltage transfer ratios in the usual fashion as

$$\frac{\hat{V}_{NE}}{\hat{V}_S} = \frac{R_{NE}}{R_{NE}+R_{FE}} j\omega(l_{m1}-l_{m2})L_{HT}\frac{1}{R_S+R_L} + \frac{R_{NE}R_{FE}}{R_{NE}+R_{FE}} j\omega(c_m)L\frac{R_L}{R_S+R_L} \tag{9.118a}$$

$$\frac{\hat{V}_{FE}}{\hat{V}_S} = -\frac{R_{FE}}{R_{NE}+R_{FE}} j\omega(l_{m1}-l_{m2})L_{HT}\frac{1}{R_S+R_L} + \frac{R_{NE}R_{FE}}{R_{NE}+R_{FE}} j\omega(c_m)L\frac{R_L}{R_S+R_L} \tag{9.118b}$$

where we have substituted

$$\hat{I}_G = \frac{1}{R_S+R_L}\hat{V}_S \tag{9.119a}$$

$$\hat{V}_G = \frac{R_L}{R_S+R_L}\hat{V}_S \tag{9.119b}$$

Observe in (9.118) that the net mutual inductance is the *difference* of the per-unit-length mutual inductances between the generator circuit and the circuits formed from each wire of the twisted pair

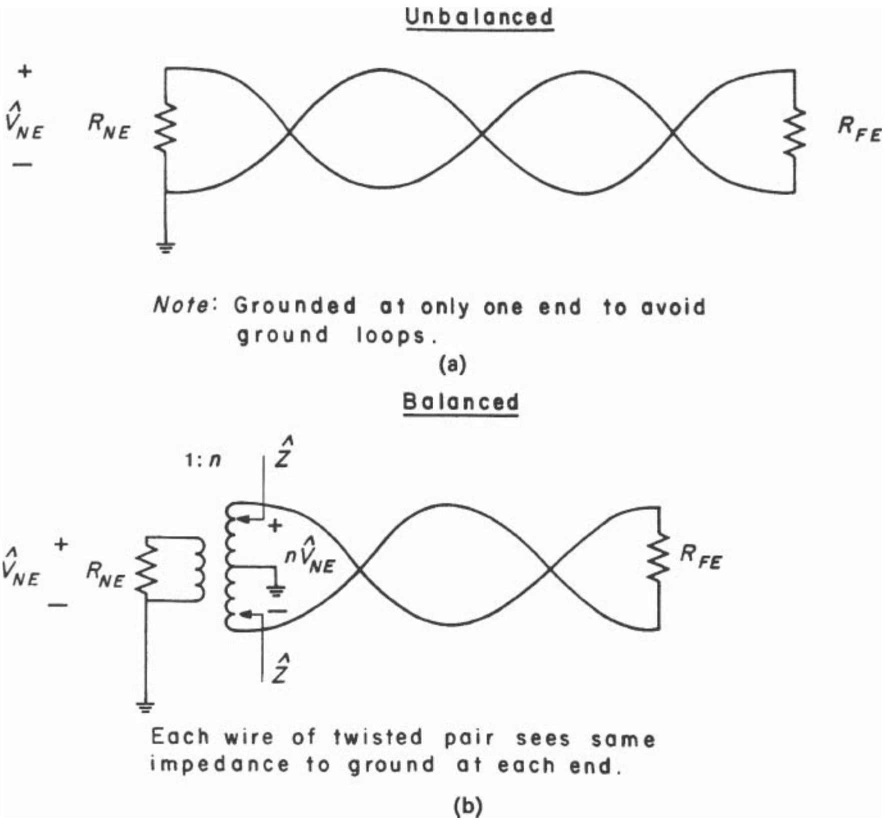
Unbalanced
+
$\hat{V}_{NE}$
R_{NE}
−
R_{FE}
Note: Grounded at only one end to avoid ground loops.
(a)
Balanced
1: n
$\hat{Z}$
+
$n\hat{V}_{NE}$
$\hat{V}_{NE}$
+
R_{NE}
−
−
$\hat{Z}$
R_{FE}
Each wire of twisted pair sees same impedance to ground at each end.
(b)

FIGURE 9.69 Terminating a twisted pair: (a) unbalanced terminations; (b) balanced terminations.

with the ground plane *multiplied by the length of a half-twist*. Thus, the *inductive coupling is the same as to an SWP of total length equal to one half-twist* (a "short line"). However, the net mutual capacitance is the per-unit-length mutual capacitance to the ungrounded wire of an SWP *multiplied by the total line length L*. Therefore, the near-end or far-end crosstalk becomes

$$\frac{\hat{V}_{NE,FE}}{\hat{V}_S} = \underbrace{\left.\frac{\hat{V}^{\text{IND}}_{NE,FE}}{\hat{V}_S}\right|^{SWP}_{L_{SWP}=L_{HT}}}_{\substack{\text{inductive coupling}\\ \text{for SWP whose}\\ \text{length is one}\\ \text{half}-\text{twist}}} + \underbrace{\left.\frac{\hat{V}^{\text{CAP}}_{NE,FE}}{\hat{V}_S}\right|^{SWP}_{L_{SWP}=L}}_{\substack{\text{capacitive coupling}\\ \text{for SWP whose length}\\ \text{is the total line length}}} \tag{9.120}$$

This assumes that there is an *odd number of half-twists*. If the number of half-twists is even, all adjacent induced voltages will cancel, and the total inductive coupling is reduced to zero. In either event, *for this unbalanced termination the capacitive coupling is unaffected by the twist,* i.e., *it is the same as to an* SWP *whose length is the total length of the twisted pair*.

With this understanding, let us consider the significance of the twist illustrated in Fig. 9.72. Consider an untwisted receptor pair (SWP). Suppose that inductive coupling dominates capacitive

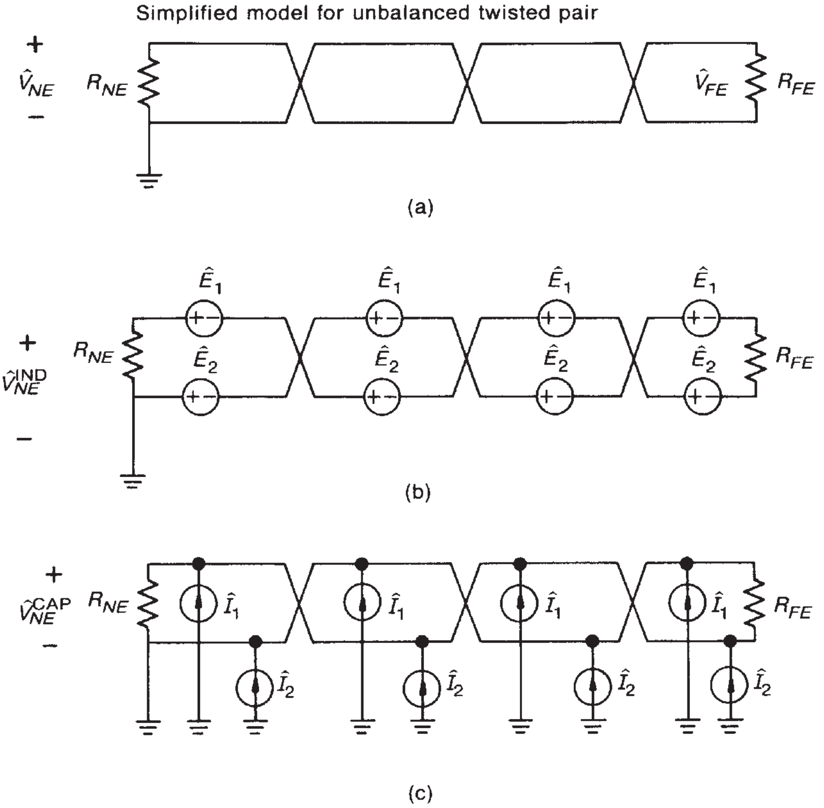
Simplified model for unbalanced twisted pair
+
$\hat{V}_{NE}$
−
R_{NE}
$\hat{V}_{FE}$
R_{FE}
(a)
$\hat{E}_1$
$\hat{E}_2$
+
$\hat{V}_{NE}^{IND}$
−
R_{NE}
R_{FE}
(b)
+
$\hat{V}_{NE}^{CAP}$
−
R_{NE}
$\hat{I}_1$
$\hat{I}_2$
R_{FE}
(c)

FIGURE 9.70 A simplified model for the unbalanced receptor wire pair: (a) physical configuration; (b) inductive coupling model; (c) capacitive coupling model.

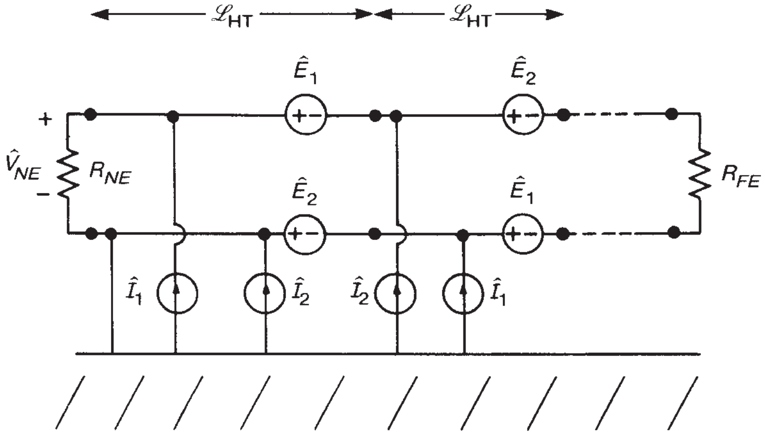
$\mathscr{L}_{HT}$
$\mathscr{L}_{HT}$
$\hat{E}_1$
$\hat{E}_2$
+
$\hat{V}_{NE}$
−
R_{NE}
$\hat{E}_2$
$\hat{E}_1$
R_{FE}
$\hat{I}_1$
$\hat{I}_2$
$\hat{I}_2$
$\hat{I}_1$

FIGURE 9.71 The inductive–capacitive coupling model for the unbalanced twisted receptor wire pair of Fig. 9.70 obtained by "untwisting" the wires.

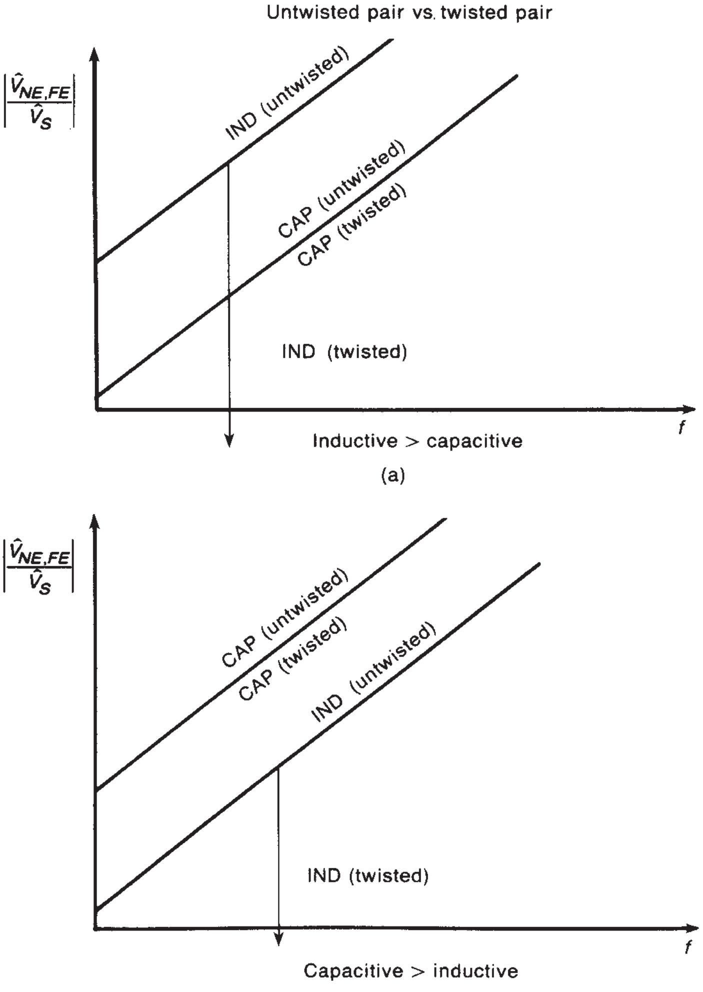

FIGURE 9.72 Explanation of the effect of twist on crosstalk to an unbalanced twisted pair for (a) inductive coupling dominant before twisting and (b) capacitive coupling dominant before twisting.

coupling, as shown in Fig. 9.72a. If we replace the SWP with a twisted pair, the inductive coupling is reduced to that of one half-twist (if there are an odd number of half-twists), but the capacitive coupling is essentially unaffected. Since inductive coupling dominated capacitive coupling prior to the twisting of the wires, the total crosstalk will drop to the level of the capacitive coupling of the untwisted pair. On the other hand, consider the case for high-impedance loads in Fig. 9.72b where capacitive coupling dominates inductive coupling for the untwisted pair. In this case, twisting the wires will drop the inductive coupling contribution, and the capacitive coupling is again unaffected. But since capacitive coupling dominated inductive coupling prior to twisting the wires, *no reduction in the total coupling will be observed.* This illustrates that *for the unbalanced termination twisting the pair of receptor wires will reduce the total coupling for low-impedance terminations but will not change it for high-impedance terminations*! This shows that twisted wires may or may not be effective in reducing crosstalk. They will usually be effective only in *low-impedance circuits*. This is why twisted pairs are typically effective in power distribution circuits, which typically have low-impedance terminations.

9.6.3 Effects of Twist

In order to illustrate the effectiveness or ineffectiveness of a twisted pair in the reduction of crosstalk, we will show some experimental results. We will compare the near-end crosstalk voltage transfer ratio for three configurations shown in Fig. 9.73. The *single-receptor-wire* configuration shown in Fig. 9.73a was considered earlier and should give the largest crosstalk. The SWP shown in Fig. 9.73b should reduce inductive coupling, since the receptor circuit loop area is reduced. The capacitive coupling should not be reduced, since it results from the current source attached to the ungrounded wire of the pair, which is essentially that of the single receptor wire (see Fig. 9.71). The *twisted-wire pair* (TWP) shown in Fig. 9.73c should only reduce inductive coupling.

The experimental configuration is shown in Fig. 9.74 and consists of a line of total length 4.705 m above a ground plane. The wires are 20 gauge and are separated by 2 cm and suspended above the ground plane at a height of 2 cm. The cross-sectional configurations are shown in Fig. 9.75, and the

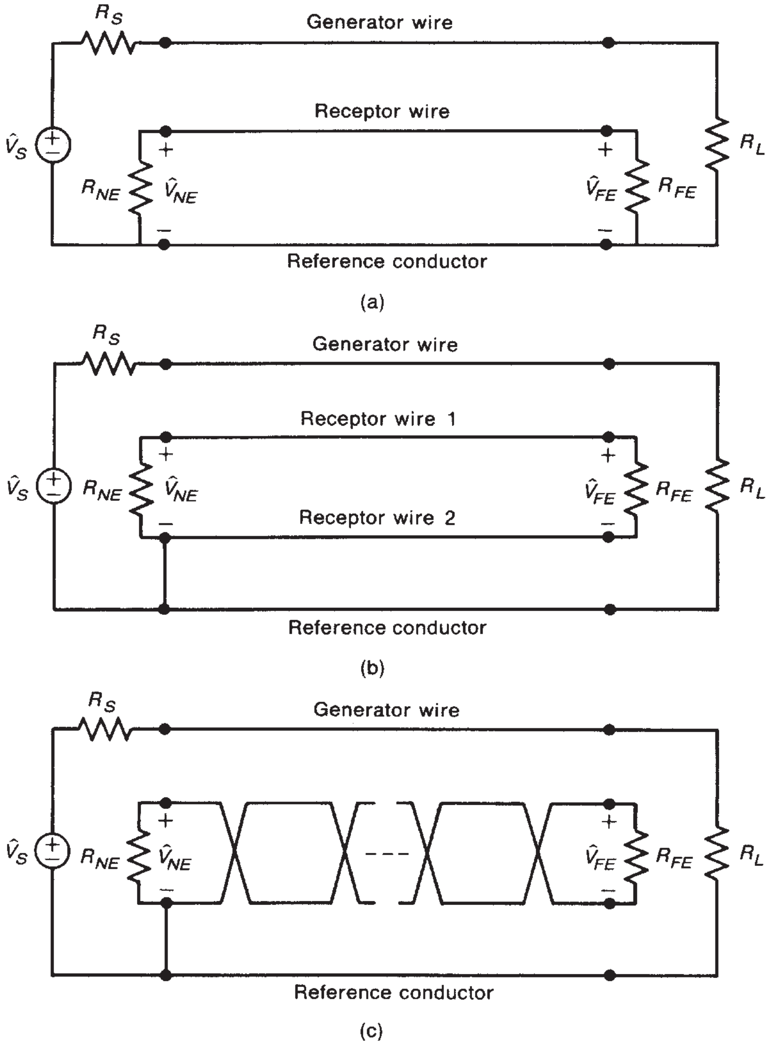

FIGURE 9.73 The three levels of reducing inductive crosstalk: (a) single-receptor wire; (b) straight-wire receptor pair (SWP); (c) twisted-wire receptor pair (TWP).

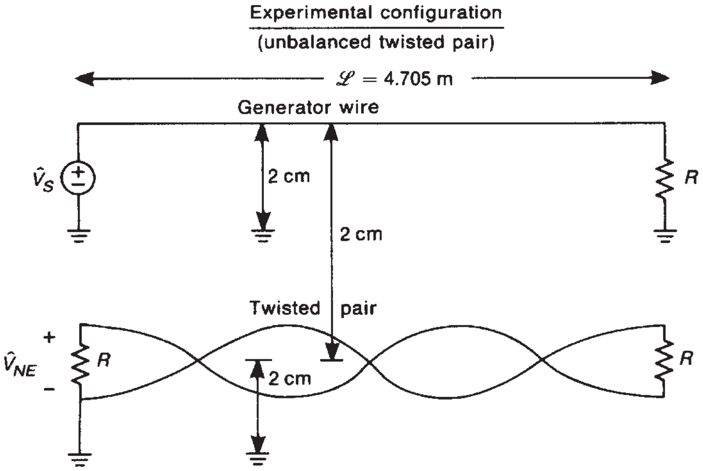
Experimental configuration
(unbalanced twisted pair)
$\mathscr{L} = 4.705$ m
Generator wire
$\hat{V}_S$
+
−
2 cm
2 cm
R
Twisted pair
+
$\hat{V}_{NE}$
−
R
2 cm
R

FIGURE 9.74 An experiment to illustrate the effect of a twisted pair on crosstalk for unbalanced terminations.

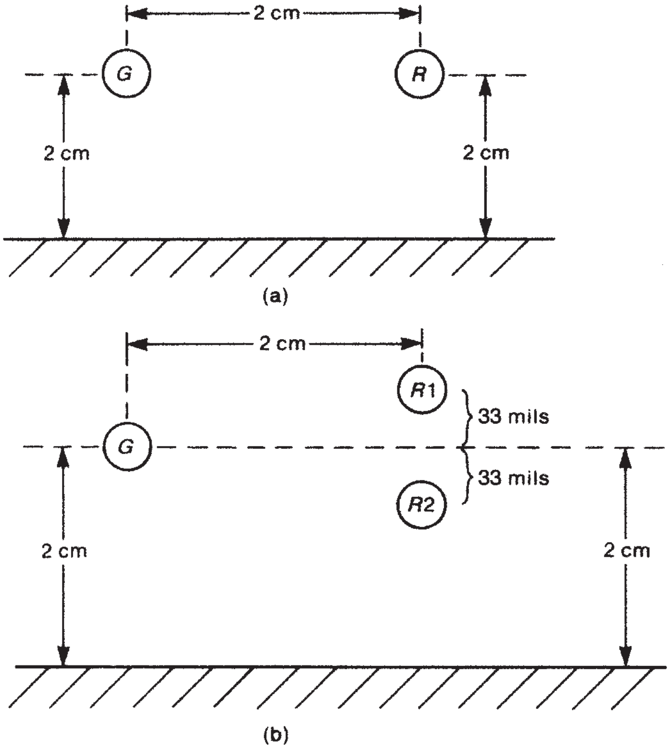
2 cm
G
R
2 cm
2 cm
(a)
2 cm
R1
33 mils
G
33 mils
R2
2 cm
2 cm
(b)

FIGURE 9.75 Cross-sectional dimensions for the experiment of Fig. 9.74: (a) Single-receptor wire; (b) SWP and TWP.

per-unit-length parameters for the SWP and TWP configurations were computed in Section 9.6.1. The number of half-twists was $N = 225$, so that the length of a half-twist was $L_{HT} = 2.09$ cm. This gives a twist rate of slightly over 7 twists per foot, which is typical. We will measure the near-end crosstalk voltage transfer ratio for $R_S = 0$ and $R_L = R_{NE} = R_{FE} = R$, where three values of R will be used: $R = 1$ kΩ, $R = 50\,\Omega$, and $R = 1\,\Omega$. The experimental results will also be compared with the predictions of the multiconductor transmission-line model, which forms the overall chain parameter matrix of the line from the products of the chain parameter matrices of the half-twists with an appropriate interchange of the wires of the twisted pair at the junctions [24]. The inductive–capacitive coupling model in (9.118) gives ($R_S = 0$)

$$\left|\frac{\hat{V}_{NE}}{\hat{V}_S}\right| = 2\pi f\left[\frac{1}{2R}(l_{m1} - l_{m2})L_{HT} + \frac{R}{2}(c_m)L\right] \tag{9.121}$$

where $L_{HT} = 2.09$ cm and $L = 4.705$ m. The data for $R = 1$ kΩ are shown in Fig. 9.76a. Observe that there is little difference in the crosstalk for all three configurations. This confirms our notion that capacitive coupling is dominant for the single-receptor-wire configuration and is unchanged for the SWP and TWP configurations. Eq. (9.121) gives

$$\begin{aligned}\left|\frac{\hat{V}_{NE}}{\hat{V}_S}\right|_{R=1\ k\Omega} &= 2\pi f\left[\frac{1}{2R}(l_{m1} - l_{m2})L_{HT} + \frac{R}{2}c_m L\right]\\ &= f(4.403 \times 10^{-13} + 1.922 \times 10^{-8})\end{aligned}$$

where we have used $c_m = (c_{m1} + c_{m2})/2$. At the lowest measured frequency of 1 kHz, this gives a prediction of 1.9×10^{-5}, which compares well with the measured valued of 2×10^{-5}. The data for $R = 50\,\Omega$ are shown in Fig. 9.76b. Here, we see that the SWP configuration reduces the crosstalk by some 20 dB, and the TWP configuration further reduces that by some 10 dB. Eq. (9.121) gives

$$\begin{aligned}\left|\frac{\hat{V}_{NE}}{\hat{V}_S}\right|_{R=50\ \Omega} &= 2\pi f\left[\frac{1}{2R}(l_{m1} - l_{m2})L_{HT} + \frac{R}{2}c_m L\right]\\ &= f(8.81 \times 10^{-12} + 0.96 \times 10^{-9})\end{aligned}$$

This gives a prediction of 0.97×10^{-6} at 1 kHz, which matches the measured value of 1.8×10^{-6} rather well. Figure 9.76c shows the results for $R = 1\,\Omega$. Observe that the SWP configuration reduces the crosstalk by some 26 dB, whereas the TWP configuration further reduces the crosstalk by some 80 dB. The crosstalk levels for the TWP configuration and $R = 1\,\Omega$ shown in Fig. 9.76c were too small to be measured below 1.5 MHz. The trend of the data at this lowest measurement frequency indicates that the predictions of the MTL model that are shown are reasonable and that there is a large reduction for $R = 1\,\Omega$. Measurements for $R = 3\,\Omega$ and given in [26] confirm this behavior for very low-impedance loads. Eq. (9.138) gives

$$\begin{aligned}\left|\frac{\hat{V}_{NE}}{\hat{V}_S}\right|_{R=1\ \Omega} &= 2\pi f\left[\frac{1}{2R}(l_{m1} - l_{m2})L_{HT} + \frac{R}{2}c_m L\right]\\ &= f(4.40 \times 10^{-10} + 1.92 \times 10^{-11})\end{aligned}$$

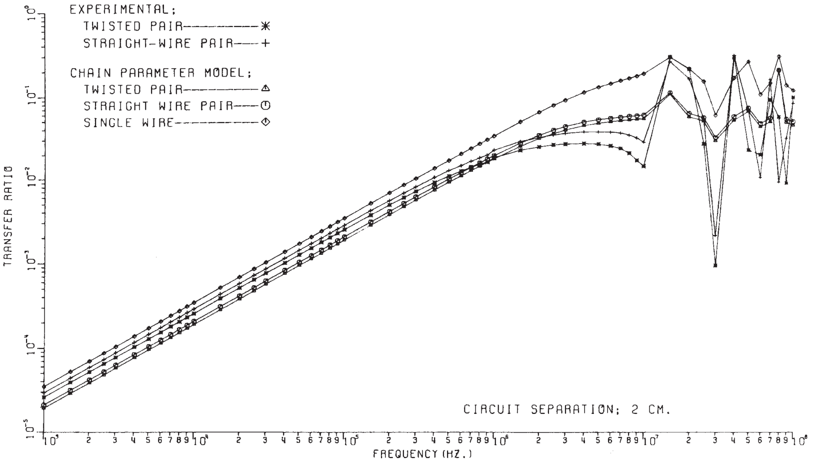

(a)

FIGURE 9.76 Experimental results for the experiment of Fig. 9.74, comparing the predictions of the transmission-line model (chain parameter model) to measured data for a single-receptor wire, a straight-wire pair, and a twisted-wire receptor pair, for (a) $R = 1\ \text{k}\Omega$, (b) $R = 50\ \Omega$, and (c) $R = 1\ \Omega$. (Figure continues on the next two pages)

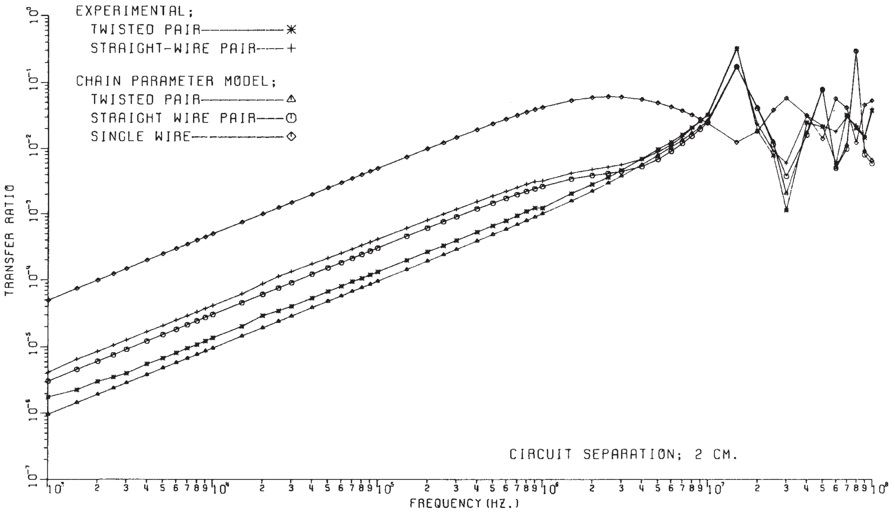

(b)

FIGURE 9.76 (*Continued*)

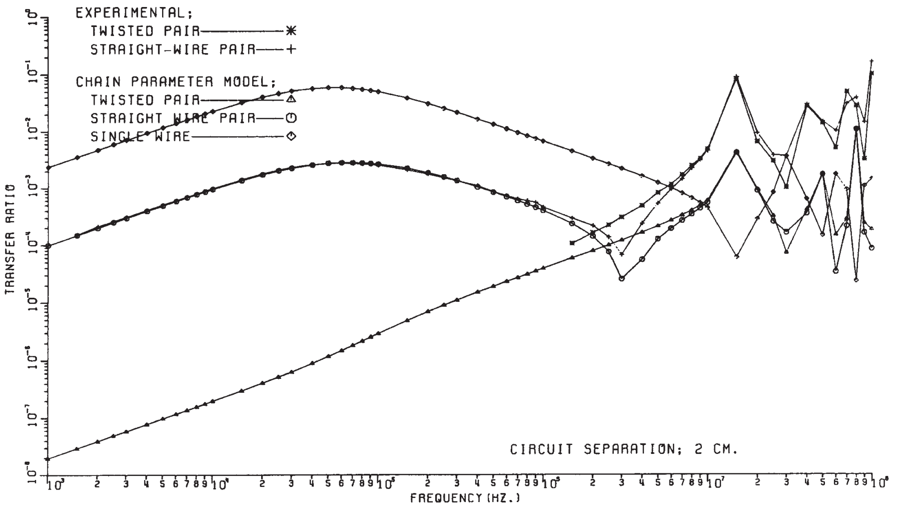

(c)

FIGURE 9.76 (*Continued*)

This gives a predicted value of 4.6×10^{-7} at 1 kHz. The calculated value from the MTL model of 2×10^{-8} is for an even number of half-twists, so that the inductive coupling is not included. Thus, the above capacitive coupling of 1.92×10^{-8} at 1 kHz matches the prediction rather well.

Review Exercise 9.9 Recompute the crosstalk for $R = 1\ \text{k}\Omega$, $R = \mathbf{50}\ \Omega$, and $R = \mathbf{1}\ \Omega$ for the untwisted pair and compare to the experimental results at 1 kHz.

***Answers*:** $R = 1\ \text{k}\Omega$, 1.93×10^{-5} (3×10^{-5}); $R = 50\,\Omega$, 2.9×10^{-6} (4×10^{-6}); $R = 1\,\Omega$, $9.9 \times 10^{-5}(1 \times 10^{-4})$.

The explanation for this effectiveness or ineffectiveness of the TWP in the reduction of crosstalk is illustrated in Fig. 9.77 and results from our notion that the capacitive coupling is the same for all three configurations. The inductive coupling for the SWP configuration is smaller than for the single-receptor wire and is still smaller for the TWP configuration (equivalent to that of one half-twist at most). For $R = 1\ \text{k}\Omega$, capacitive coupling dominates inductive coupling for the single-receptor-wire configuration. So, replacing the receptor wire with a straight-wire pair or a twisted-wire pair should

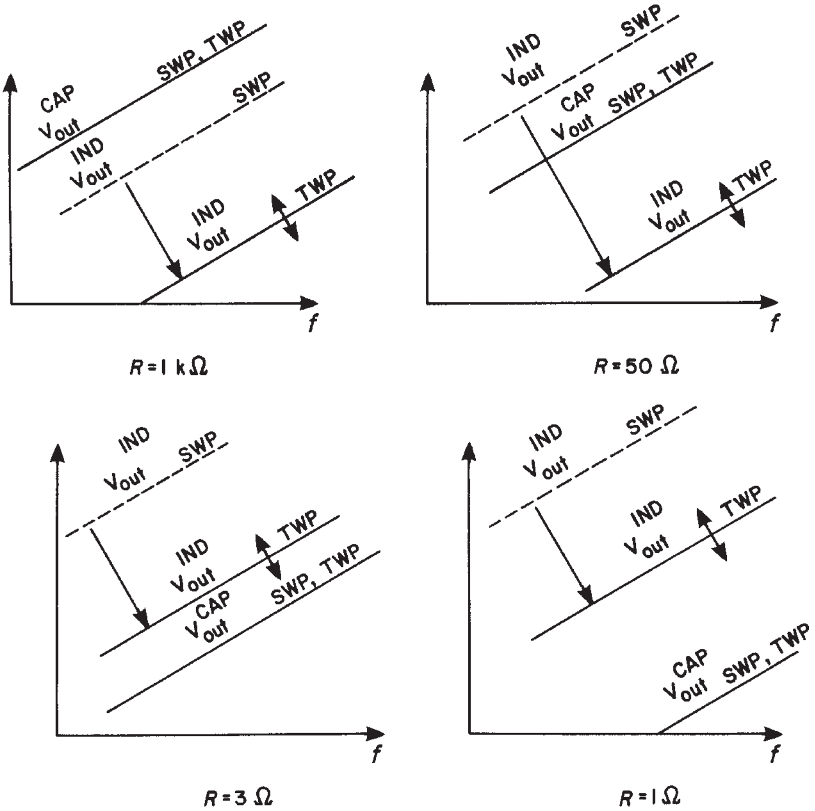
CAP V_{out}
SWP, TWP
IND V_{out}
SWP
IND V_{out}
TWP
f
$R = 1\ \text{k}\Omega$
IND V_{out}
SWP
CAP V_{out}
SWP, TWP
IND V_{out}
TWP
f
$R = 50\ \Omega$
IND V_{out}
SWP
IND V_{out}
TWP
CAP V_{out}
SWP, TWP
f
$R = 3\ \Omega$
IND V_{out}
SWP
IND V_{out}
TWP
CAP V_{out}
SWP, TWP
f
$R = 1\ \Omega$

FIGURE 9.77 Explanation of the results of Fig. 9.76 in terms of inductive and capacitive coupling.

not significantly reduce the *total crosstalk*, as is evident from the experimental data. For $R = 50\,\Omega$, inductive coupling dominates capacitive coupling for the single-receptor-wire case. Replacing the single receptor wire with a straight-wire pair reduces the inductive coupling, so the total crosstalk reduces to the capacitive coupling level. For $R = 3\,\Omega$, the same result is observed, except that the capacitive coupling "floor" is much smaller than for $R = 50\,\Omega$, so that the total crosstalk drops more but is still restricted to being no less than the capacitive coupling. For $R = 1\,\Omega$, the capacitive coupling floor is reduced considerably, so that the inductive coupling reduction caused by the twist can be fully realized. These observations are confirmed with experimental results in [26].

This brings up an important notion: *sensitivity of crosstalk in twisted-pairs to line twist* [27–29]. Consider the previous experiment. For the extremely low impedance of $R = 1\,\Omega$, we pointed out that the capacitive coupling "floor" is reduced substantially, and the inductive coupling of one half-twist, although small, is larger than this floor. We also pointed out that, according to our model of a twisted pair as being a sequence of alternating loops, if the twisted pair consists of an *even number of half-twists,* then the inductive coupling should completely cancel out, leaving *an inductive coupling of zero*! This suggests that for the case of $R = 1\,\Omega$, where the inductive coupling of one half-twist dominates the capacitive coupling floor, we should see an extreme sensitivity of the crosstalk to whether the line consists of an *odd or even number of half-twists*. In order to assess this, we rotated the far end of the twisted pair to give the minimum and maximum crosstalk at each frequency. The data for $R = 3\,\Omega$ are plotted in Fig. 9.78a and those for $R = 1\,\Omega$ in Fig. 9.78b. These data show this extreme sensitivity to line twist (as much as 40 dB)! This suggests that *precise prediction of crosstalk is not feasible for very small values of termination impedances*. The low-frequency predictions for the SWP configuration are shown on these data and indicate that the minimum coupling is not zero but is restricted to the capacitive coupling floor, which is quite small. No such sensitivity to twist was observed for the high-impedance terminations of $R = 1$ kΩ or the case of $R = 50\,\Omega$. This is sensible to expect based on Fig. 9.77, since the capacitive coupling floor is dominant for the twisted pair configuration for $R = 1$ kΩ and $R = 50\,\Omega$.

9.6.4 Effects of Balancing

We will now consider the effect of *balanced loads* on the twisted pair as illustrated in Fig. 9.69b. The model for the twisted-pair of receptor wires is unchanged, but the terminations affect the resulting crosstalk. The inductive and capacitive coupling models are shown in Fig. 9.79. The inductive coupling is unchanged from the unbalanced case, since the total induced emf around the receptor wire loop is the same. However, *because of the balanced loads, the capacitive coupling contributions cancel out*. Thus, *the effect of balancing is to eliminate the capacitive coupling contribution*! The resulting crosstalk voltage transfer ratio is given by the unbalanced case with the capacitive coupling contribution removed:

$$\frac{\hat{V}_{NE,FE}}{\hat{V}_S} = \underbrace{\left.\frac{\hat{V}^{\text{IND}}_{NE,FE}}{\hat{V}_S}\right|^{SWP}_{L_{SWP}=L_{HT}}}_{\substack{\text{inductive coupling}\\ \text{for SWP whose}\\ \text{length is one}\\ \text{half-twist}}} \tag{9.122}$$

where the inductive coupling contribution is given by the inductive coupling portion of (9.118).

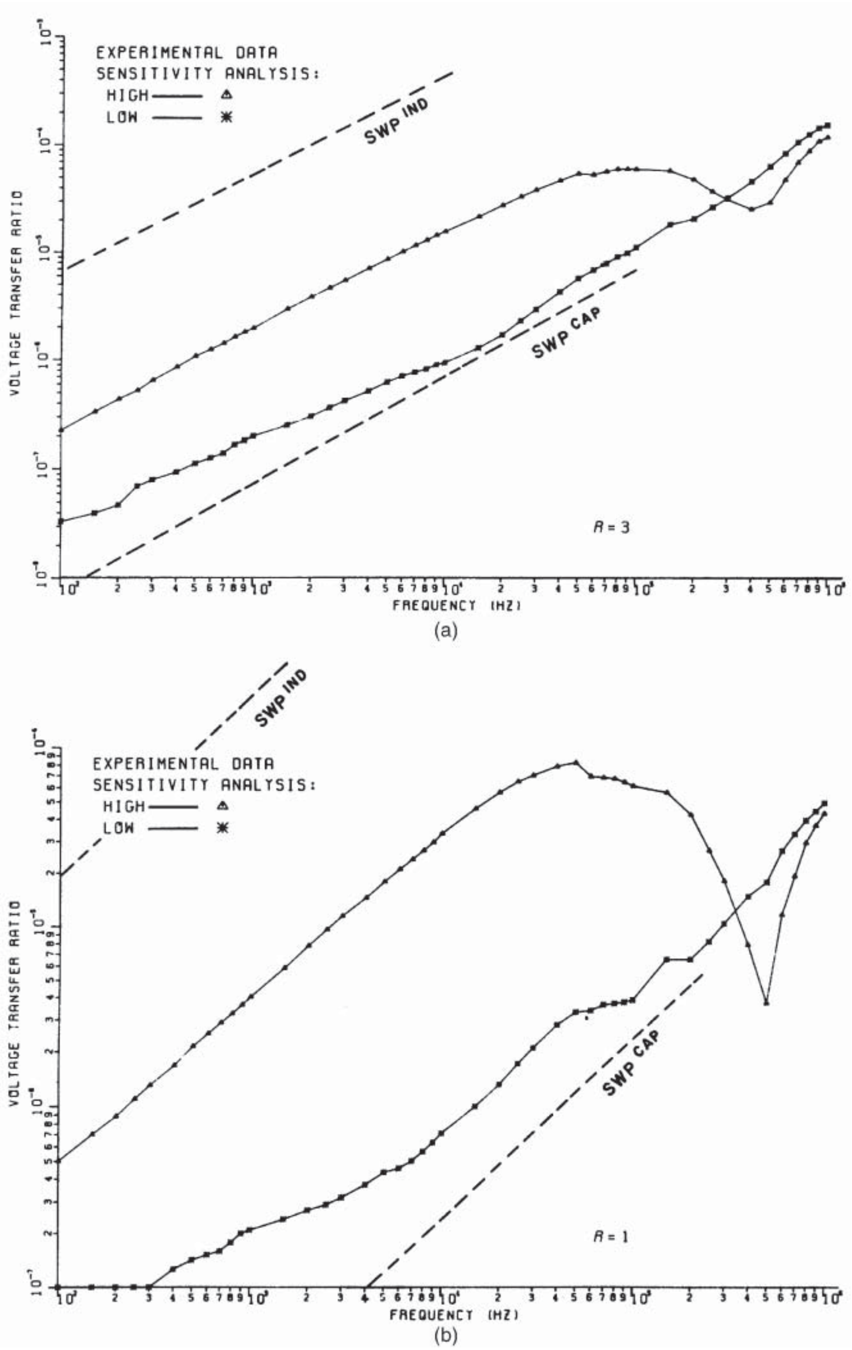

(a)

(b)

FIGURE 9.78 Experimental results for the experiment of Fig. 9.74 obtained by varying the number of twists, showing that for low-impedance loads the inductive coupling can be dominant for an odd number of half-twists and eliminated for an even number: (a) $R = 3\ \Omega$; (b) $R = 1\ \Omega$.

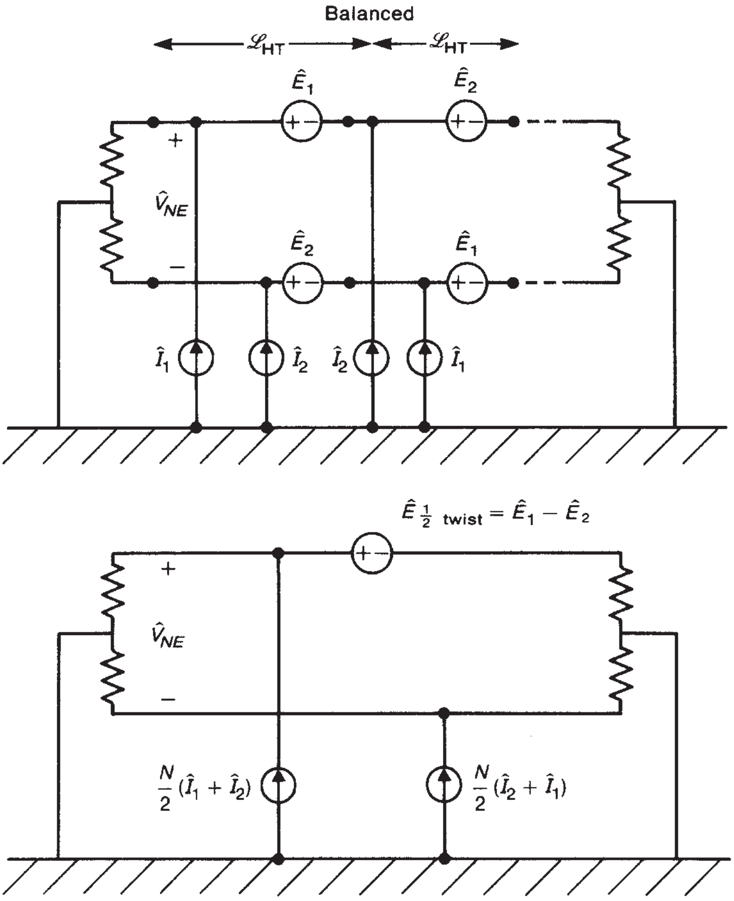
Balanced
$\mathscr{L}_{HT}$
$\mathscr{L}_{HT}$
$\hat{E}_1$
$\hat{E}_2$
+
$\hat{V}_{NE}$
−
$\hat{E}_2$
$\hat{E}_1$
$\hat{I}_1$
$\hat{I}_2$
$\hat{I}_2$
$\hat{I}_1$
$\hat{E}_{\frac{1}{2}\ \text{twist}} = \hat{E}_1 - \hat{E}_2$
+
$\hat{V}_{NE}$
−
$\frac{N}{2}(\hat{I}_1 + \hat{I}_2)$
$\frac{N}{2}(\hat{I}_2 + \hat{I}_1)$

Inductive coupling: → that of one half twist
Capacitive coupling: → cancelled out

FIGURE 9.79 The inductive–capacitive coupling model for a twisted receptor wire pair and balanced terminations.

The previous experiment was repeated for a balanced termination at the near end of the twisted pair. A center-tapped 1 : 2 transformer was used to provide the balance, as shown in Fig. 9.69b. Figure 9.80 illustrates the effect of balance. For $R = 1\,\Omega$ and $R = 3\,\Omega$, where inductive coupling dominated capacitive coupling for unbalanced terminations, eliminating the capacitive coupling contribution by balancing the loads should have no effect on either the crosstalk levels or the sensitivity to line twist. For $R = 1\ \text{k}\Omega$ and $R = 50\,\Omega$, where capacitive coupling dominated inductive coupling for the unbalanced case, balancing the twisted pair terminations and thus eliminating capacitive coupling should affect the crosstalk level and the sensitivity to line twist. Experimental data shown in [30, 31] confirm these observations. This suggests that *sensitivity to line twist should be a significant problem for balanced, twisted pairs for a wide range of termination impedance levels*.

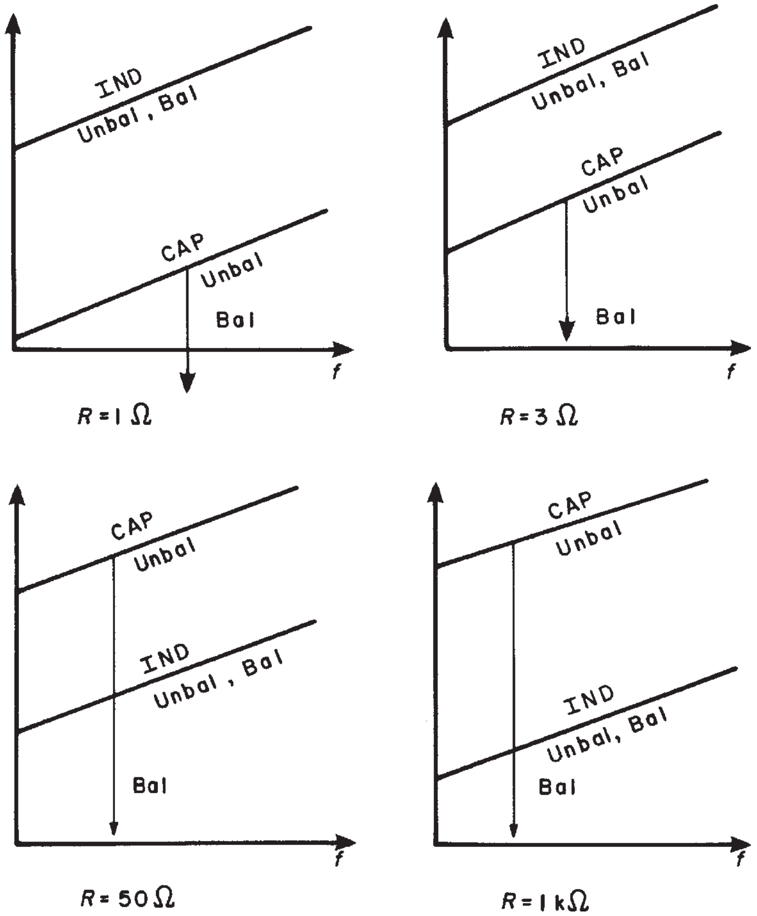

FIGURE 9.80 Explanation of the effect of balanced versus unbalanced terminations on the crosstalk to a twisted receptor wire pair for $R = 1\ \Omega$, $R = 3\ \Omega$, $R = 50\ \Omega$, and $R = 1\ \mathrm{k}\Omega$.

PROBLEMS

Section 9.1 Three-Conductor Transmission Lines and Crosstalk

9.1.1 A high-voltage power transmission line extends 30 m from the generating station to a residence. Determine the time delay of propagation of voltage and current waves on the line. [160.9 μs]

9.1.2 A printed circuit board (PCB) has innerplanes surrounding the embedded lands. This resembles a coupled stripline illustrated in Fig. 9.3a. If the board length is 9 in., determine the propagation delay of voltage and current waves from one end to the other. [1.65 ns]

9.1.3 A PCB has an innerplane as a ground plane. Several of the lands on the PCB surface along with this ground plane constitute a coupled microstrip line illustrated in Fig. 9.3b. Estimate the time delay if the lands have a total length of 5 in. [0.715 ns]

Section 9.2 the Transmission-Line Equations for Lossless Lines

9.2.1 Derive the multiconductor transmission-line equations given in (9.2).

Section 9.3 the per-Unit-Length Parameters

9.3.1 In preparation for determining the per-unit-length capacitance matrix from the inverse of the per-unit-length inductance matrix, determine the inverse of the following 2×2 matrix:

$$M = \begin{bmatrix} 50 & 20 \\ 10 & 30 \end{bmatrix}$$

$$M^{-1} = \begin{bmatrix} 2.31 \times 10^{-2} & -1.54 \times 10^{-2} \\ -7.69 \times 10^{-3} & 3.85 \times 10^{-2} \end{bmatrix}$$

9.3.2 Three bare, 20-gauge solid wires have equal adjacent spacings, so that their cross-sectional locations are at the vertices of a triangle having equal-length sides. Determine the per-unit-length inductances and capacitances if the separation is 50 mils. [$l_G = l_R = 0.456$ μH/m, $l_m = 0.228$ μmH/m, $c_G = c_R = c_m = 16.25$ pF/m]

9.3.3 A 20-gauge, bare generator wire is suspended 1/4 in. above a ground plane. Another identical wire is suspended 1/2 in. above the ground plane and separated horizontally by 3/8 in. from the generator wire. Determine the per-unit-length inductances and capacitances. [$l_G = 0.688$ μH/m, $l_R = 0.827$ μH/m, $l_m = 0.124$ μH/m, $c_m = 2.49$ pF/m, $c_G = 14.1$ pF/m, $c_R = 11.32$ pF/m]

9.3.4 Figure 9.3.4 shows a ribbon cable transmission line where an outside wire is used as the reference wire. Assume that all wires are 28-gauge stranded (7×36) and the adjacent wire spacings are 50 mils. Compute the per-unit-length inductances and capacitances, neglecting the wire insulations. [$l_G = 1.036$ μH/m, $l_R = 0.76$ μH/m, $l_m = 0.518$ μH/m, $c_m = 11.12$ pF/m, $c_G = 5.17$ pF/m, $c_R = 11.12$ pF/m]

9.3.5 Two 20-gauge solid wires are placed inside a shield that is filled with polyvinyl chloride (PVC) insulation ($\varepsilon_r = 4$). The shield interior radius is 250 mils, and each wire is placed at a distance of 100 mils from the shield center and on a line through the shield center ($\theta_{GR} = 180°$). Determine the per-unit-length inductances and capacitances. [$l_G = 0.515$ μH/m, $l_R = 0.515$ μH/m, $l_m = 74.3$ nH/m, $c_m = 12.72$ pF/m, $c_G = 75.4$ pF/m, $c_R = 75.4$ pF/m]

9.3.6 Use the computer program (see Appendix C) STRPLINE.FOR (the executable program is STRPLINE.EXE) to compute the per-unit-length inductance and capacitance of a one-land stripline consisting of one land of width 5 mils situated midway between two ground planes that are separated by 20 mils. The dielectric has a relative permittivity of 4.7. Compare these values to those computed with formulae in Chapter 4, Review Exercise 4.4. [0.4666 μH/m (0.461 μH/m), 112.07 pF/m (113.2 pF/m)]

9.3.7 Use the computer program (see Appendix C) MSTRP.FOR (the executable program is MSTRP.EXE) to compute the per-unit-length inductance and capacitance of a one-land microstrip line consisting of one land of width 5 mils on a board of thickness 50 mils. The dielectric has a relative permittivity of 4.7. Compare these values to those computed with formulas in Chapter 4, Review Exercise 4.5. [0.878799 μH/m (0.877 μH/m), 39.0297 pF/m (38.46 pF/m)]

9.3.8 Use the computer program (see Appendix C) PCB.FOR (the executable program is PCB.EXE) to compute the per-unit-length inductance and capacitance of a two-land printed circuit board consisting of two lands of width 15 mils and edge-to-edge separation of 15 mils lying on top of a substrate whose thickness is 62 mils. The dielectric has a relative permittivity of 4.7. Compare these values to those computed with formulas in Chapter 4, Review Exercise 4.6. [0.809196 μH/m (0.804 μH/m), 38.6188 pF/m (38.53 pF/m)]

9.3.9 Verify the data in Tables 9.1 and 9.2 for a three-wire ribbon cable where an outer wire was chosen as reference and the middle wire is chosen as the generator wire using RIBBON.FOR. The wires are 28 gauge (7 × 36) and are separated by 50 mils. The dielectric insulations have thicknesses of 10 mils and relative permittivities of 3.5.

9.3.10 The per-unit-length parameters for the coupled microstrip line in Fig. 9.31 were obtained from the measured frequency-domain data in Fig. 9.32 as $l_m = 37.2$ nH/m and $c_m = 6.33$ pF/m. Verify these and compute the remaining parameters using MSTRP.FOR. [$l_G = l_R = 0.335327\ \mu\text{H/m}$, $l_m = 37.1527\ \text{nH/m}$, $c_G + c_m = c_R + c_m = 115.511\ \text{pF/m}$, $c_m = 4.92724\ \text{pF/m}$]

9.3.11 Compute the per-unit-length parameters for the PCB in Fig. 9.51 using PCB.FOR. [$l_G = 1.38315\ \mu\text{H/m}$, $l_R = 1.10707\ \mu\text{H/m}$, $l_m = 0.691573\ \mu\text{H/m}$, $c_G + c_m = 29.6949\ \text{pF/m}$, $c_R + c_m = 40.5238\ \text{pF/m}$, $c_m = 20.2619\ \text{pF/m}$]

Section 9.4 the Inductive–Capacitive Coupling Approximate Model

9.4.1 For the ribbon cable shown in Fig. P9.3.4, assume the total mutual inductance and total mutual capacitance to be $L_m = 1$ μH and $C_m = 250$ pF. If $V_S(t)$ is a 1 MHz sinusoid of magnitude 1 V, calculate the magnitude of the far-end crosstalk if the termination impedances are $R_S = 50\,\Omega$, $R_L = 50\,\Omega$, $R_{NE} = 100\,\Omega$, and $R_{FE} = 100\,\Omega$. [7.854 mV] Determine the near-end and far-end inductive and capacitive coupling coefficients. [$M_{NE}^{\text{IND}} = 5 \times 10^{-9}$, $M_{FE}^{\text{IND}} = -5 \times 10^{-9}$, $M_{NE}^{\text{CAP}} = 6.25 \times 10^{-9} = M_{FE}^{\text{CAP}}$].

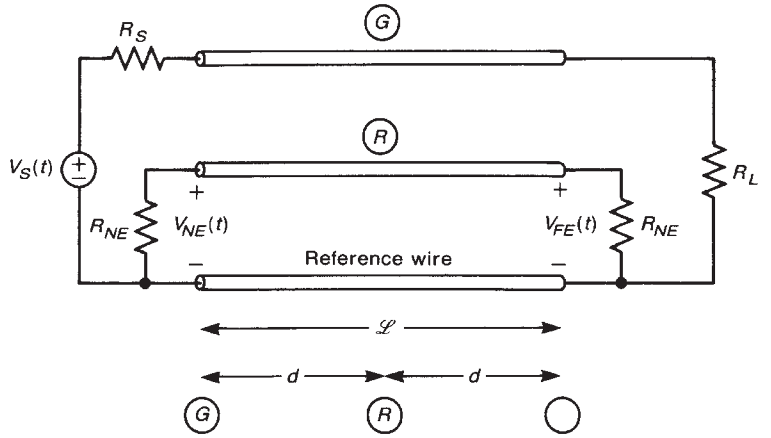

FIGURE P9.3.4

9.4.2 For the ribbon cable shown in Fig. P9.3.4, assume the total mutual inductance and total mutual capacitance to be $L_m = 0.4$ μH and $C_m = 400$ pF. If $V_S(t)$ is a 1 MHz sinusoid of magnitude 1 V, calculate the magnitude of the near-end crosstalk if the termination impedances are $R_S = 50\,\Omega$, $R_L = 50\,\Omega$, $R_{NE} = 50\,\Omega$, and $R_{FE} = 50\,\Omega$. [44 mV] Determine the near-end and far-end inductive and capacitive coupling coefficients. [$M_{NE}^{\mathrm{IND}} = 2 \times 10^{-9}$, $M_{FE}^{\mathrm{IND}} = -2 \times 10^{-9}$, $M_{NE}^{\mathrm{CAP}} = 5 \times 10^{-9} = M_{FE}^{\mathrm{CAP}}$]

9.4.3 For the ribbon cable shown in Fig. P9.3.4, assume the total mutual inductance and total mutual capacitance to be $L_m = 1$ μH and $C_m = 250$ pF. Suppose that the termination impedances are equal: $R_S = R_L = R_{NE} = R$. Determine the value of R for which the inductive and capacitive coupling contributions are exactly equal. [$R = \sqrt{L_m/C_m} = 63.25\,\Omega$]

9.4.4 Consider the case of two wires above a ground plane shown in Fig. P9.4.4. Suppose $l_m = 2$ nH/m, $c_m = 0.6$ pF/m, $L = 2$ m, $R_S = 0$, $R_L = 50\,\Omega$, $R_{NE} = 100\,\Omega$, $R_{NE} = 200\,\Omega$, and $V_S(t) = 1\ \cos\ \omega t\ V$, where $f = 1$ MHz. Determine the time-domain far-end and near-end crosstalk voltages. [$V_{FE}(t) = 0.167\cos(\omega t + 90°)$ mV, $V_{NE}(t) = 0.67\cos(\omega t + 90°)$ mV]. Determine the near-end and far-end inductive and capacitive coupling coefficients. [$M_{NE}^{\mathrm{IND}} = 2.67 \times 10^{-11}$, $M_{FE}^{\mathrm{IND}} = -5.33 \times 10^{-11}$, $M_{NE}^{\mathrm{CAP}} = 8 \times 10^{-11} = M_{FE}^{\mathrm{CAP}}$]

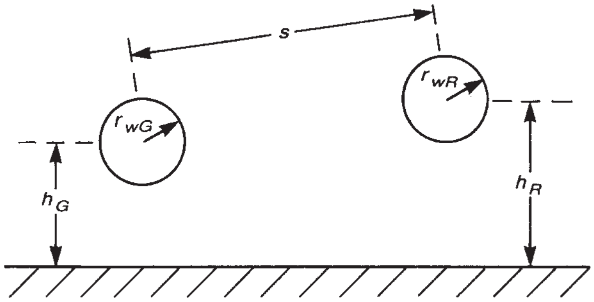

FIGURE P9.4.4

9.4.5 For the ribbon cable of Problem 9.4.1, suppose that the wires are 28-gauge (7 × 36) stranded. Determine the common-impedance coupling level for the near-end crosstalk voltage if the total line length is 3 m and the frequency where this level equals the inductive–capacitive coupling level [$M_{NE}^{CI} = 2.92 \times 10^{-3}$, $M_{FE}^{CI} = -2.92 \times 10^{-3}$, $f_{NE} = 41.26$ kHz, $f_{\mathrm{FE}} = 371.3$ kHz]

9.4.6 -or the ribbon cable of Problem 9.4.2, suppose that the wires are 24-gauge (7 × 32) stranded. Determine the common-impedance coupling level for the near-end crosstalk voltage if the total line length is 2 m and the frequency where this level equals the inductive–capacitive coupling level. [$M_{NE}^{CI} = 7.6 \times 10^{-4}$, $M_{FE}^{CI} = -7.6 \times 10^{-4}$, $f_{NE} = 17.27$ kHz, $f_{\mathrm{FE}} = 40.3$ kHz]

9.4.7 For the case of two wires above a ground plane in Problem 9.4.4, suppose the per-unit-length resistance of the ground plane is 0.001 Ω/m. Determine the near-end and far-end common impedance coupling coefficients and the frequency where this level equals the inductive–capacitive coupling level. [$M_{NE}^{CI} = 1.33 \times 10^{-5}$, $M_{FE}^{CI} = -2.67 \times 10^{-5}$, $f_{NE} = 19.89$ kHz, $f_{FE} = 159.15$ kHz]

9.4.8 For the ribbon cable of Problem 9.4.1, suppose $V_S(t)$ is replaced with a 1 MHz, 5 V, 50% duty cycle trapezoidal pulse train having rise/falltimes of 50 ns. Compute the maximum near- and far-end crosstalk voltages. [$V_{NE,\max} = 1.13$ V, $V_{FE,\max} = 125$ mV]

9.4.9 Repeat Problem 9.4.8 for the ribbon cable of Problem 9.4.2. [$V_{NE,\max} = 0.7$ V, $V_{FE,\max} = 0.3$ V]

9.4.10 Repeat Problem 9.4.8 for the ribbon cable of Problem 9.4.3 where $R_S = R_L = R_{NE} = R_{FE} = 63.25\,\Omega$. [$V_{NE,\max} = 0.791$ V, $V_{FE,\max} = 0.0$ V]

9.4.11 Repeat Problem 9.4.8 for the problem of two wires over a ground plane of problem 9.4.4. [$V_{NE,\max} = 10.7$ mV, $V_{FE,\max} = 2.67$ mV]

9.4.12 Consider the ribbon cable shown in Fig. P9.3.4. The total mutual inductance is $L_m = 1$ μH, and the total mutual capacitance is $C_m = 25$ pF. If $R_S = 0$, $R_L = R_{NE} = R_{FE} = 100\,\Omega$, and the pulse waveform shown in Fig. P9.4.12 is applied, sketch the time-domain near-end crosstalk and determine the maximum crosstalk voltage level. [62.5 mV]

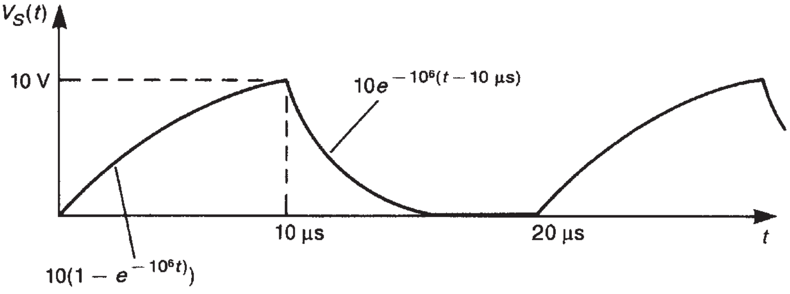

FIGURE P9.4.12

Section 9.5 Shielded Wires

9.5.1 Consider the case of two wires above a ground plane, with the receptor wire shielded, as shown in Fig. 9.54b. Assume that the generator wire is a 22-gauge (7 × 30) stranded wire. The receptor conductor is an RG58U coaxial cable having an inner, solid 20-gauge wire, a shield interior radius of 64 mils, an interior dielectric of polyethylene giving the cable a nominal velocity of propagation of 66% of free space, and a shielded thickness of approximately 15 mils (assume solid copper). The generator wire is suspended a height of 1 in. and the coaxial cable is suspended a height of 1.5 in. The separation between the generator wire and the cable is 1/4 in. Determine the per-unit-length parameters of the line. [$r_S = 4.43$ mΩ/m, $l_G = 0.979$ μH/m, $l_S = 0.727$ μH/m, $l_R = 1.05$ μH/m, $l_{GS} = 0.4575$ μH/m, $c_{RS} = 92.17$ pF/m, $c_{GS} = 10.12$ pF/m, $c_G = 5.97$ pF/m, $c_S = 11.52$ pF/m].

9.5.2 For the line in Problem 9.5.1, determine the frequency where the shield will affect the inductive coupling when it is grounded at both ends. [970 Hz]

9.5.3 If the shield in Problem 9.5.1 is grounded at both ends, the line length is 2 m and $R_S = 0$, $R_L = 1$ kΩ, $R_{NE} = 100\,\Omega$, and $R_{\text{FE}} = 50\,\Omega$, determine the near-end crosstalk transfer ratio at 100 Hz, 1 kHz, 100 kHz, and 10 MHz. [0.38×10^{-6}, 2.67×10^{-6}, 3.72×10^{-6}, 3.72×10^{-6}]

9.5.4 For the ribbon cable shown in Fig. P9.3.4, assume the total mutual inductance and mutual capacitance to be $L_m = 0.4$ μH and $C_m = 400$ pF. If $V_S(t)$ is a 1 MHz sinusoid of magnitude 1 V, and the termination impedances are $R_S = R_L = R_{NE} = R_{FE} = 50\,\Omega$, determine the near-end crosstalk if a shield is placed around the receptor wire and the shield is only connected to the near end of the reference wire. [12.57 mV] How much does the shield reduce the crosstalk. [10.88 dB]

9.5.5 Consider the case of two wires above a ground plane shown in Fig. P9.4.4. The line has parameters of $l_m = 2$ nH/m, $c_m = 0.6$ pF/m, $V_S(t) = 1\cos(\omega t)$ V, $f = 1$ MHz, $L = 2$ m, $R_S = 0$, $R_L = 50\,\Omega$, $R_{NE} = 100\,\Omega$, and $R_{FE} = 200\,\Omega$. A shield is placed around the receptor wire and is connected to the ground plane only at the near end. Determine the near-end crosstalk voltage. [$0.1676\cos(\omega t + 90°)$ mV] By how much does the shield reduce the crosstalk? [12 dB]

9.5.6 The shield of Problem 9.5.5 is connected to the ground plane at both ends and has a per-unit-length resistance of 1 Ω/m and per-unit-length self-inductance of 16 μH/m. Determine the near-end crosstalk voltage. [1.667 cos($\omega t + 0°$) μV]

Section 9.6 Twisted Wires

9.6.1 Consider the case of an unbalanced twisted generator pair shown in Fig. P9.6.1. Assume that the generator wires are 28-gauge stranded (7 × 36), as is the receptor wire, and the heights above the ground plane are 1 in. The separation between the generator and receptor circuits is $s = 1/4$ in. and the generator wires are separated only by their insulations, giving $d = 35$ mils. Ignore the effect of the wire insulations and compute the per-unit-length parameters. [$l_{G1R} = (\mu_0/4\pi)\ \ln[1 + 4h_G h_R/(s + \Delta d)^2] = 0.404\ \mu\text{H/m}, l_{G2R} = (\mu_0/4\pi) \ln[1 + 4h_G h_R/ (s - \Delta d)^2] = 0.432\ \mu\text{H/m}, l_{G1G2} = (\mu_0/4\pi) \ln(1 + 4h_G^2/d^2) = 0.809\ \mu\text{H/m}, l_{G1} = (\mu_0/2\pi) \ln(2h_{G1}/r_{wG1}) = 1.12\ \mu\text{H/m}, l_{G2} = (\mu_0/2\pi) \ln(2h_{G2}/r_{wG2}) = 1.12\ \mu\text{H/m}, l_R = (\mu_0/2\pi) \ln(2h_R/r_{wr}) = 1.12\ \mu\text{H/m}, c_{G1R} = 2.047\ \text{pF}/m, c_{G2R} = 3.112\ \text{pF/m}, c_{G1G2} = 14.61\ \text{pF/m}, c_{G1} = 4.61\ \text{pF/m}, c_{G2} = 4.012\ \text{pF/m}, c_R = 6.73\ \text{pF/m}$] $l_{G2} = (\mu_0/2\pi) \ln$

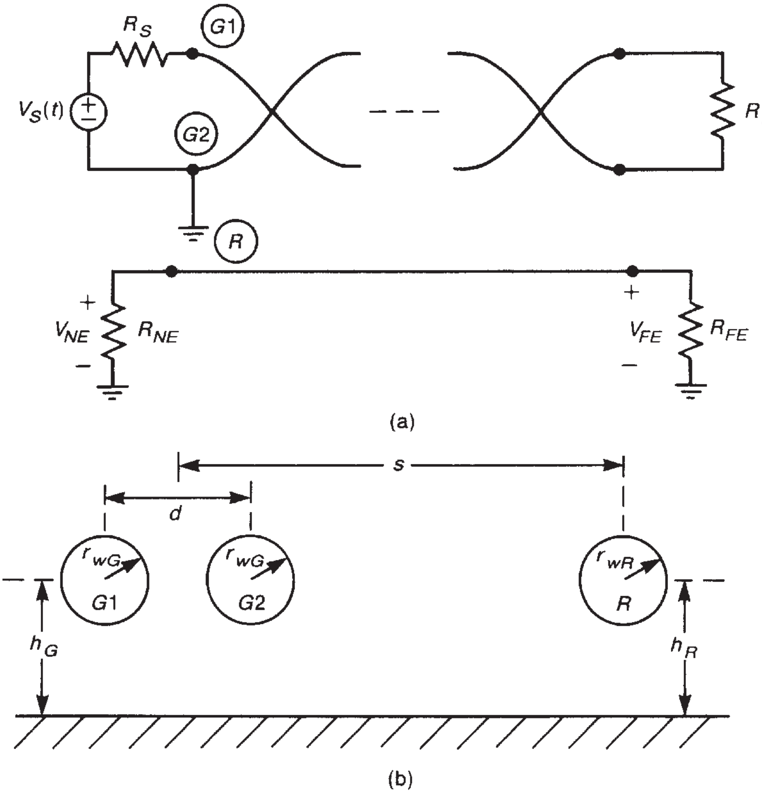

FIGURE P9.6.1

9.6.2 For the unbalanced twisted pair of Problem 9.6.1, determine the near-end and far-end crosstalk transfer ratios if $R_S = R_L = R_{NE} = R_{FE} = 10\,\Omega$ and the line length is 10 m and the twist rate 10 twists/m [$M_{NE}^{\text{IND}} = 3.45 \times 10^{-11}$, $M_{FE}^{\text{IND}} = -3.45 \times 10^{-11}$, $M_{NE}^{\text{CAP}} = M_{FE}^{\text{CAP}} = 6.449 \times 10^{-11}$]] If $V_S(t)$ is a 5 V, 1 MHz sinusoid, determine the near-end and far-end crosstalk voltages. [$V_{NE} = 3.11$ mV, $V_{FE} = 0.941$ mV]

9.6.3 Suppose the generator twisted pair in Problem 9.6.1 is balanced. Determine the crosstalk transfer ratios. [$M_{FE}^{\mathrm{IND}} = 3.45 \times 10^{-11}$, $M_{FE}^{\mathrm{IND}} = -3.45 \times 10^{-11}$, $M_{NE}^{\mathrm{CAP}} = M_{FE}^{\mathrm{CAP}} = 0$] If $V_S(t)$ is a 5 V, 1 MHz sinusoid, determine the near-end and far-end crosstalk voltages. [$V_{NE} = 1.085\ \mathrm{mV} = V_{FE}$]

REFERENCES

1. C. R. Paul and S. A. Nasar, *Introduction to Electromagnetic Fields*, 2nd ed., McGraw-Hill, New York, 1987.
2. C. R. Paul, *Electromagnetics for Engineers: With Applications to Digital Systems and Electromagnetic Interference*, Wiley, New York, 2004.
3. C. R. Paul, *Analysis of Multiconductor Transmission Lines*, Wiley-Interscience, New York, 1994.
4. C. R. Paul, *Applications of multiconductor Transmission Line Theory to the prediction of cable coupling. Vol. I, Multiconductor Transmission Line Theory*, Technical Report, Rome Air Development Center, Griffiss AFB, NY, RADC-TR-76-101, Apr. 1976, (A025028).
5. C. R. Paul, *Crosstalk, Handbook of Electromagnetic Compatibility*, Academic Press, San Diego, CA, 1995, Chapter 2, Part II.
6. C. R. Paul, *Coupled transmission lines, Encyclopedia of RF and Microwave Engineering*, Wiley-Interscience, Hoboken, NJ, 2005, pp. 863–882.
7. J. C. Clements, C. R. Paul, and A. T. Adams, Two-dimensional systems of dielectric-coated, cylindrical conductors, *IEEE Trans. Electromagn. Compat.* **EMC-17**, 238–248 (1975).
8. R. F. Harrington, *Field Computation by Moment Methods*, Macmillan, New York, 1968.
9. C. R. Paul and A. E. Feather, Computation of the transmission-line inductance and capacitance matrices from the generalized capacitance matrix, *IEEE Trans. Electromagn. Compat.* **EMC–18**(4), 175–183 (1976).
10. C. R. Paul, Decoupling the multiconductor transmission-line equations, *IEEE Trans. Microwave Theory Tech.* **MTT-44**(8), 1429–1440 (1996).
11. C. R. Paul, Solution of the transmission line equations for three-conductor lines in homogeneous media, *IEEE Trans. Electromagn. Compat.* **EMC-20**, 216–222 (1978).
12. C. R. Paul, Solution of the transmission-line equations under the weak-coupling assumption, *IEEE Trans. Electromagn. Compat.* **EMC-44**(3) 413–424 (2002).
13. C. R. Paul, Prediction of crosstalk in ribbon cables: comparison of model predictions and experimental results, *IEEE Trans. Electromagn. Compat.* **EMC-20**, 394–406 (1978).
14. C. R. Paul, On the superposition of inductive and capacitive coupling in crosstalk prediction models, *IEEE Trans. Electromag. Compat.*, **EMC-24**, 335–343 (1982).
15. C. R. Paul, Transmission-line modeling of shielded wires for crosstalk prediction, *IEEE Trans. Electromagn. Compat.* **EMC-23**, 345–351 (1981).
16. C. R. Paul, SHIELD – a digital computer for the prediction of crosstalk to shielded cables, *1983 It. Symp. Technical Exhibition on Electromagnetic Compatibility*, Zurich, Switzerland, (March 1983).
17. C. R. Paul and W. E. Beech, Prediction of crosstalk in flatpack, coaxial cables, *1984 IEEE Int. Symp. Electromagnetic Compatibility*, San Antonio, TX, (April 1984).
18. C. R. Paul and W.E. Beech, *Prediction of Crosstalk in Flatpack Coaxial Cables*, Technical Report, Rome Air Development Center, Griffiss AFB, NY, RADC-TR-82-286, Vol. IV F, Dec. 1984.
19. C. R. Paul, *Applications of Multiconductor Transmission Line Theory to the Prediction of Cable Coupling, Vol. VIII, Prediction of Crosstalk Involving Braided, Shield Cables*. Technical Report, Rome Air Development Center, Griffiss AFB, NY, RADC-TR-76-101, Aug. 1980.
20. C. R. Paul, SHIELD, *A Digital Computer Program for Computing Crosstalk between Shielded Cables*, Technical Report, Rome Air Development Center, Griffiss AFB, NY, RADC-TR-82-286, Vol. IV B, Nov. 1982.

21. C. R. Paul and B. A. Bowles, Symbolic solution of the multiconductor transmission-line equations for lines containing shielded wires, *IEEE Trans. Electromagn. Compat.* **EMC-33**, 149–162 (1991); see also B. A. Bowles, *Literal Solution to the Transmission Line Equations for Shielded Wires*. MSEE thesis, University of Kentucky, Dec 1990.
22. C. R. Paul and B. A. Bowles, Literal solution of the transmission-line equations for shielded wires, *IEEE Int. Sym. Electromagnetic Compatibility*, Washington, DC, 21–23 Aug. 1990, pp. 591–599, doi: 10.1109/ISEMC.1990.252838.
23. C. R. Paul, Effect of pigtails on crosstalk to braided-shield cables, *IEEE Trans. Electromagn. Compat.* **EMC-22**, 161–172 (1980).
24. C. R. Paul and J. A. McKnight, Prediction of crosstalk involving twisted pairs of wires, Part I : a transmission line model for twisted wire pairs, *IEEE Trans. Electromagn. Compat.* **EMC-21**, 92–105 (1979).
25. C. R. Paul and J. A. McKnight, Prediction of crosstalk involving twisted pairs of wires, Part II: a simplified, low-frequency prediction model, *IEEE Trans. Electromagn. Compat.* **EMC-21**, 105–114 (1979)
26. C. R. Paul and J. A. McKnight, *Applications of Multiconductor Transmission Line Theory to the Predictions of Cable Coupling. Vol. V, Prediction of Crosstalk Involving Twisted Wire Pairs*, Technical Report, Rome Air Development Center, Griffiss AFB, NY, RADC-TR-76-101, Feb. 1978, (A053559).
27. C. R. Paul and M. B. Jolly, Sensitivity of crosstalk in twisted-pair circuits to line twist, *IEEE Trans. Electromagn. Compat.* **EMC-24**, 359–364 (1982).
28. C. R. Paul and M. B. Jolly, Crosstalk in balanced, twisted-pair circuits, *1981 IEEE Int. Symp. Electromagnetic Compatibility*, Boulder, CO, Aug. 1981.
29. C. R. Paul and M. B. Jolly, *Crosstalk in Twisted-Wire Circuits*, Technical Report, Rome Air Development Center, Griffiss AFB, NY, RADC-TR-82-286, Vol. IV C, Nov. 1982.
30. C. R. Paul and D. Koopman, Sensitivity of coupling to balanced, twisted pair lines to line twist, *1983 Int. Symp. and Technical Exhibition on Electromagnetic Compatibility*, Zurich, Switzerland, Mar. 1983.
31. C. R. Paul and D. Koopman, *Prediction of Crosstalk in Balanced, Twisted Pair Circuits*, Technical Report, Rome Air Development Center, Griffiss AFB, NY, RADC-TR-82-286, Vol. IV D, Aug. 1984.

CHAPTER TEN

Shielding

This chapter addresses the concept of *shielding* of electronic circuits. The term *shield* usually refers to a metallic enclosure that *completely encloses* an electronic product or a portion of that product. There are two purposes of a shield, as illustrated in Fig. 10.1. The first, as shown in Fig. 10.1a, is to prevent the emissions of the electronics of the product or a portion of those electronics from radiating outside the boundaries of the product. The motivation here is to either prevent those emissions from causing the product to fail to comply with the radiated emissions limits or prevent the product from causing interference with other electronic products. The second purpose of a shield, as shown in Fig. 10.1b, is to prevent radiated emissions external to the product from coupling to the product's electronics, which may cause interference in the product. As an example, shielding may be used to reduce the *susceptibility* to external signals such as high-power radars or radio and TV transmitters. A photograph of a shielded room that is used for EMC testing is shown in Fig. 10.1c.

Therefore a shield is, conceptually, a barrier to the transmission of electromagnetic fields. We may view the *effectiveness of a shield* as being the ratio of the magnitude of the electric (magnetic) field that is incident on the barrier to the magnitude of the electric (magnetic) field that is transmitted through the barrier. Alternatively, we may view this as the ratio of the electric (magnetic) field incident on the product's electronics with the shield removed to that with the shield in place. In this latter sense, we may view the quantification of *shielding effectiveness* as being equivalent to an *insertion loss*, as was discussed for filters in Chapter 6. These notions give a qualitative idea about the meaning of the term *shield* and will be made more precise, quantitatively, in the following sections.

We will compute *ideal values of shielding effectiveness* in the following sections and will obtain some rather large values of shielding effectiveness of the order of hundreds of dB. A shielding effectiveness of 100 dB means that the incident field has been reduced by a factor of 100,000 as it exits the shield! In order to realize these ideal and extremely large values of shielding effectiveness, *the shield must completely enclose the electronics and must have no penetrations such as holes, seams, slots, or cables. Any penetrations in a shield unless properly treated may drastically reduce the effectiveness of the shield*. For example, consider a closed metallic box (shield) that has a wire penetrating it as shown in Fig. 10.2a. Suppose a nearby radiating source such as an antenna radiates an electromagnetic field. This field will be coupled to the wire, generating a current in it. This current will flow unimpeded into the enclosure and couple to the internal electronics. The converse is also true; noise internal to the shield will couple to the wire, flow out the enclosure on the wire, and radiate. This type

---

Introduction to Electromagnetic Compatibility, Third Edition. Clayton R. Paul, Robert C. Scully, and Mark A. Steffka.
© 2023 John Wiley & Sons, Inc. Published 2023 by John Wiley & Sons, Inc.

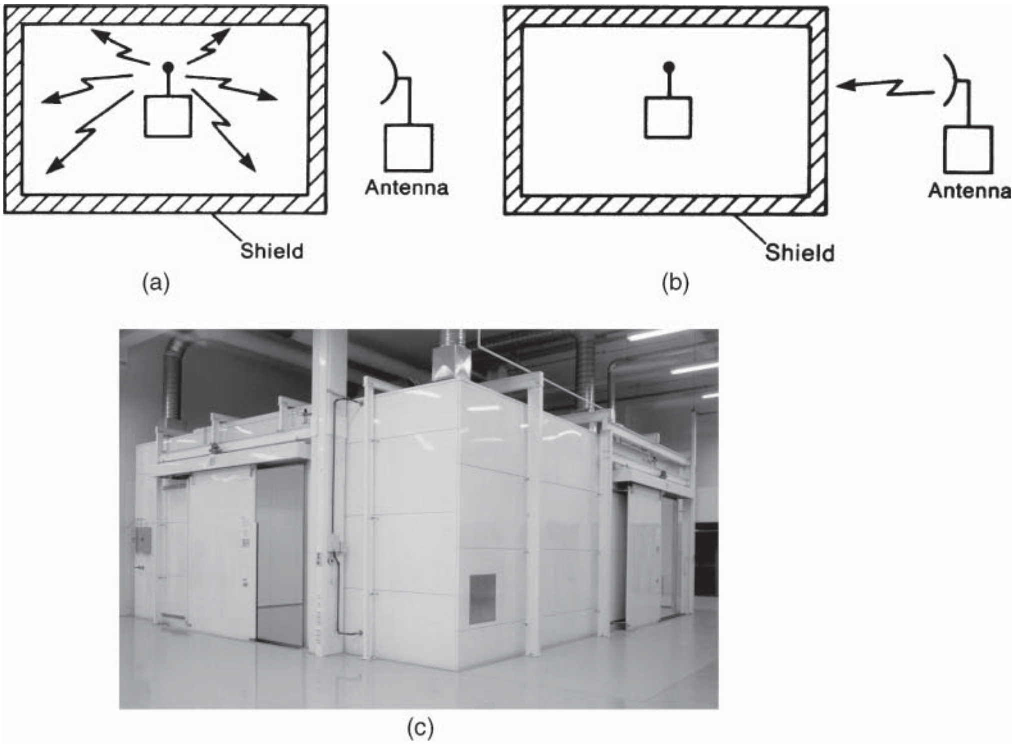

FIGURE 10.1 Illustration of the use of a shielded enclosure: (a) to contain radiated emissions and (b) to exclude radiated emissions; (c) a shielded room. Source: Courtesy of ETSLindgren, Inc.

of penetration of a shield will virtually eliminate any effectiveness of the shield. Cable penetrations such as these must be properly treated in order to preserve the effectiveness of the shield. Some common methods are to provide filtering of the cable at its entry/exit point or to use shielded cables whose shields are peripherally bonded to the product shield as shown in Fig. 10.2b [1]. Observe that the cable will have currents induced on it by the external field. Simply connecting the cable shield to the product shield with another wire as shown in Fig. 10.2b may cause the currents on the cable shield to be conducted into the interior of the product's shield surface, where they may, once again, radiate to the internal electronics of the product, thus reducing the effectiveness of the product shield.

Again, the converse is also true; unless the cable shield is peripherally bonded to the enclosure, the noise currents internal to the enclosure may flow out the enclosure along the exterior of the shield, where they may radiate. *Removing an overall shield from a peripheral cable may actually decrease the radiated emissions of a cable*! The author has seen this happen, for example, with the Centronics printer cable that attaches a personal computer to its printer. As a general rule, *a shield placed around cable wires will not necessarily reduce the radiated emissions of the cable*. The explanation of this phenomenon is illustrated in Fig. 10.2c. *In order to realize the shielding effectiveness of a cable shield in reducing the radiated emissions of the cable, the cable shield must be attached to a zero-potential point* (*an ideal ground*). If the voltage of the point at which the shield "pigtail" is attached, say, the logic ground of an electronics PCB, is varying, as illustrated in Fig. 10.2c, then we will have produced a monopole antenna (the cable shield). If the length of the cable shield is on the order of $\lambda_0/4$, the shield becomes an effective radiator. Peripheral cables such as printer cables for personal computers tend to have lengths of order 1.5 m, which is a quarter-wavelength at 50 MHz. Resonances in the radiated emissions of a product due to common-mode currents on these types of peripheral cables are frequently observed in the frequency range of 50–100 MHz. Disconnecting the

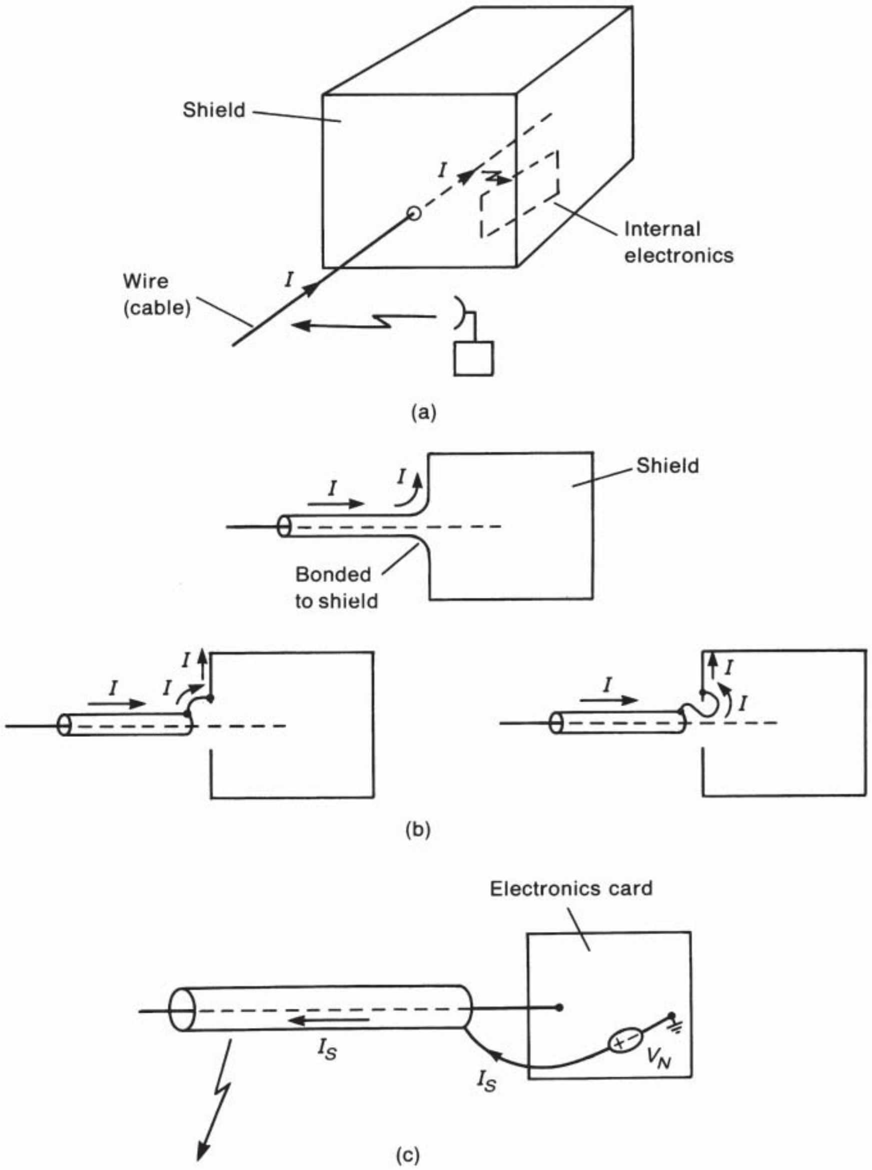

FIGURE 10.2 Important practical considerations that seriously degrade shielding effectiveness: (a) penetration of an enclosure by a cable allowing direct entry (or exit) of external (internal) fields; (b) pigtail termination of a cable shield at the entry point to a shielded enclosure. Source: Based on Vance [1]; (c) termination of a cable shield to a noisy point, causing the shield to radiate.

peripheral cable from the product usually removes these resonances and their accentuated radiated emissions.

Another common penetration is that of a hole or *aperture* in the shield wall. Fields interior to the shield or exterior to it will radiate through this aperture, thus reducing the effectiveness of the shield. This is illustrated by an important theorem known as *Babinet's principle* [2]. In order to illustrate this principle, consider a slot that is cut in a perfectly conducting screen as shown in Fig. 10.3a. A transmission line is connected across two points of the slot and excites it. The far fields that are radiated by this "slot antenna" are denoted by $E_{\theta s}$, $E_{\varphi s}$, $H_{\theta s}$, and $H_{\varphi s}$. Now consider the *complementary*

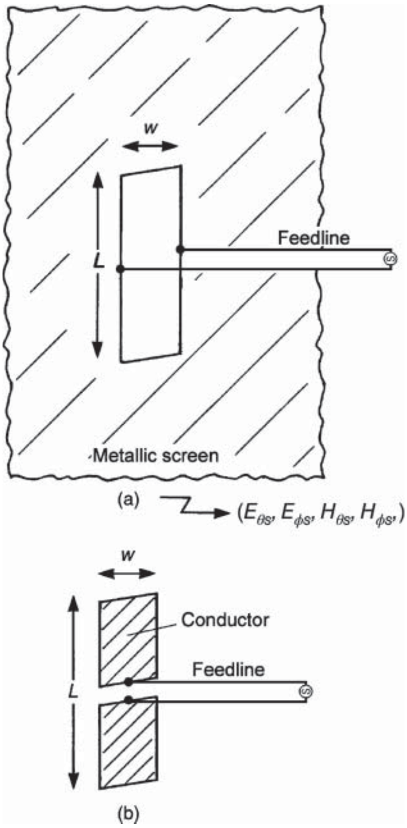

FIGURE 10.3 Illustration of the effect of apertures in a shield (illustration of Babinet's principle): (a) aperture in a metal screen; (b) corresponding physical antenna elements having the same shape and size as the aperture.

structure shown in Fig. 10.3b, which consists of the replacement of the screen with free space and the replacement of the slot with a perfect conductor of the same shape as the slot. The antenna is fed, again, with the transmission line attached to the two halves. The far fields radiated by this complementary structure are denoted by $E_{\theta c}$, $E_{\varphi c}$, $H_{\theta c}$, and $H_{\varphi c}$. *Babinet's principle as modified by Booker provides that the far fields radiated by the original screen with the slot and those radiated by the complementary structure are related by* [2]

$$E_{\theta s} = H_{\theta c} \tag{10.1a}$$

$$E_{\varphi s} = H_{\varphi c} \tag{10.1b}$$

$$H_{\theta s} = -\frac{E_{\theta c}}{\eta_0^2} \tag{10.1c}$$

This illustrates that *apertures can be as effective radiators as antennas whose conductor dimensions are those of the aperture*. This provides considerable insight into the effects of apertures in shields on their reduction of the effectiveness of the shield. For example, suppose that the slot in Fig. 10.3a has linear dimensions that are one-half wavelength, $L = \lambda_0/2$. Babinet's principle provides that the radiation properties of this slot will be the same as (with E and H interchanged) a dipole antenna of the same length as the slot as illustrated in Fig. 10.3b. We are aware that a half-wavelength-long dipole antenna such as in Fig. 10.3b with $L = \lambda_0/2$ is a very efficient radiating structure. Hence, a slot of the same linear dimensions is also a very efficient radiator. Observe also that as the slot width w becomes smaller, the slot and complementary dipole remain efficient radiators. Hence, we should not be caught in the trap of thinking that "If we cannot see much light through a slot, it will not radiate well." This is, of course, not true. Slots such as these occur numerous places in shielded enclosures. Lids that provide access to the interior of the shielded enclosure have these slots around them, as do doors that provide access to anechoic chambers. Hence, these gaps are treated by placing conductive gasketing material in the gap or beryllium finger stock around doors in order to "short out" the slot antennas there.

All these considerations should alert the reader to the fact that shielding should not be relied on to completely eliminate radiated emissions of the product. There are numerous examples of electronic products that do not employ shielded enclosures, yet they are able to comply with the regulatory limits on radiated and conducted emissions. Electronic typewriters and printers are contained in plastic enclosures. The expense and impracticality of a contiguous metallic enclosure rule out their use for these types of products. On the other hand, personal computers and large mainframe computers employ metallic enclosures. Effectively treating all penetrations provides effective use of shields for these types of products. As a cardinal rule, *the EMC designer should incorporate the same EMC design principles into a product whether that product is to be shielded or not.* The following discussion of the principles of shielding will nevertheless serve to illustrate the quantitative aspects of shielding.

10.1 SHIELDING EFFECTIVENESS

In this section, we will begin the quantitative discussion of the shielding effectiveness of a metallic shield. The general notion of shielding effectiveness was discussed above. In order to quantify these notions, we consider the general problem of a metallic barrier of thickness t, conductivity σ, relative permittivity $\varepsilon_r = 1$, and relative permeability μ_r, shown in Fig. 10.4. An electromagnetic wave is incident on this barrier. A reflected wave is produced, and a portion of this incident wave is transmitted through the barrier. The *shielding effectiveness* of the barrier is defined for the electric field, in decibels, as

$$\mathrm{SE} = 20\log_{10}\left|\frac{\hat{E}_i}{\hat{E}_t}\right| \tag{10.2}$$

Note that this will be a positive result, since the incident field is expected to be greater than the field that exits the barrier. For example, a shielding effectiveness of 120 dB means that the magnitude of the transmitted field is reduced from the magnitude of the incident field by a factor of 10^6. Some definitions of shielding effectiveness are in terms of the ratio of the transmitted field to the incident field. This definition would give a negative result in dB, which is the negative of (10.2). In terms of the magnetic field, the shielding effectiveness could be defined as

$$\mathrm{SE} = 20\log_{10}\left|\frac{\hat{H}_i}{\hat{H}_t}\right| \tag{10.3}$$

If the incident field is a uniform plane wave and the media on each side of the barrier are identical, then the two definitions are identical, since the electric and magnetic fields are related by the intrinsic impedance of the medium for a uniform plane wave. For near fields and/or different media

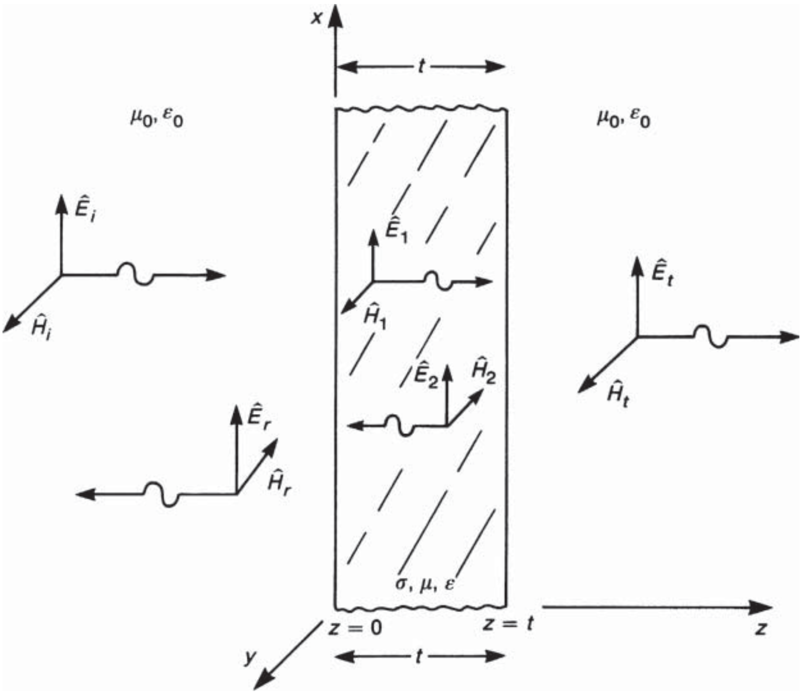

FIGURE 10.4 Illustration of the shielding effectiveness of a conducting barrier to a uniform plane wave that is incident normal to the surface.

on the two sides of the boundary, the two are not equivalent. However, the definition of the shielding effectiveness in terms of the electric field in (10.2) is often taken to be the standard for either situation.

There are several phenomena that contribute to the reduction of the incident field as it passes through the barrier. Consider the diagram shown in Fig. 10.5, which shows these effects. The first effect is *reflection* at the left surface of the barrier. The portion of the incident electric field that is reflected is given by the reflection coefficient for that surface. (See Section 7.6 of Chapter 7.) The portion of the wave that crosses this surface proceeds through the shield wall. As it passes through this conductive medium, its amplitude is attenuated according to the factor $e^{-\alpha z}$, where α is the attenuation constant of the material discussed in Appendix B. This is referred to as *absorption loss*. For barrier materials that constitute good conductors (as is usually the case) the attenuation constant α is related to the skin depth of the material, δ, as $\alpha = 1/\delta$ and $\delta = 1/\sqrt{\pi f \mu \sigma}$, where μ is the permeability of the barrier and σ is its conductivity. Therefore, the amplitudes of the fields are attenuated according to the factor $e^{-z/\delta}$. If the barrier thickness t is much greater than the skin depth of the barrier material at the frequency of the incident wave, then this wave that is transmitted through the first interface is greatly attenuated when it strikes the right interface. This becomes the incident wave for the right interface and is incident on this interface from the metal. A portion of this incident wave is reflected, and a portion is transmitted across the barrier into the medium on the right of the barrier. The reflected portion of this wave is transmitted back through the barrier and strikes the first interface, being incident from the metal. Once again, a portion of this wave is transmitted through the left interface and adds to the total reflected field in the left medium, and a portion is reflected and proceeds to the right. This portion is again attenuated as it passes through the barrier. Once it has passed through the barrier and strikes the right interface, a portion is reflected and a

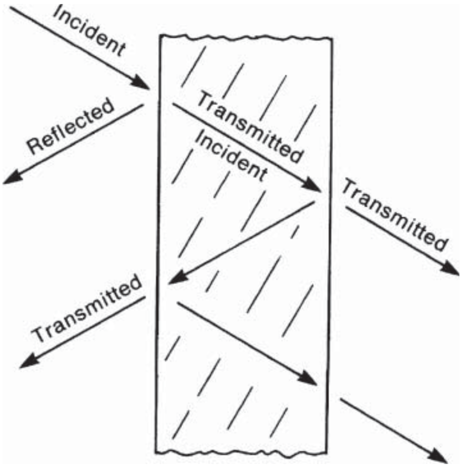

FIGURE 10.5 Illustration of multiple reflections within a shield.

portion is transmitted through the right interface. The portion transmitted through the right interface adds to the total field that is transmitted through the shield. The process continues in like fashion, but the additional reflected and transmitted fields are progressively attenuated by their travel through the conductive barrier. If a shield is designed to have a thickness that is much greater than the skin depth of the material at the frequency of the anticipated incident field, there is little consequence to the continued re-reflection at the interior surfaces of the barrier. These *multiple reflections and transmissions* can therefore generally be disregarded for shield thicknesses that are much greater than a skin depth, and only the initial reflection and transmission at the left and right interfaces need to be considered. Nevertheless, the shielding effectiveness given in (10.2) can be broken into the product of three terms each representing one of the phenomena of *reflection loss, absorption loss, and multiple reflections*. In decibels, these factors add to give

$$\mathrm{SE}_{\mathrm{dB}} = R_{\mathrm{dB}} + A_{\mathrm{dB}} + M_{\mathrm{dB}} \tag{10.4}$$

where R represents the reflection loss caused by reflection at the left and right interfaces, A represents the absorption loss of the wave as it proceeds through the barrier, and M represents the additional effects of multiple re-reflections and transmissions. Observe that the re-reflections will create fields that will add to the initial field transmitted across the right interface. Thus, the multiple-reflection factor M will be a negative number and will, in general, reduce the shielding effectiveness (since R and A will be positive). We now embark on a quantitative determination of these factors that contribute to the shielding effectiveness of a barrier. In addition to the following derivations, the reader is referred to [3–6] for similar developments.

10.2 SHIELDING EFFECTIVENESS: FAR-FIELD SOURCES

In this section, we will assume that the source for the field that is incident on the barrier is sufficiently distant from the barrier that the incident field resembles a uniform plane wave, whose properties are discussed in Appendix B. We first determine the exact solution for the shielding effectiveness and will then determine this in an approximate fashion to show that the two methods yield the same

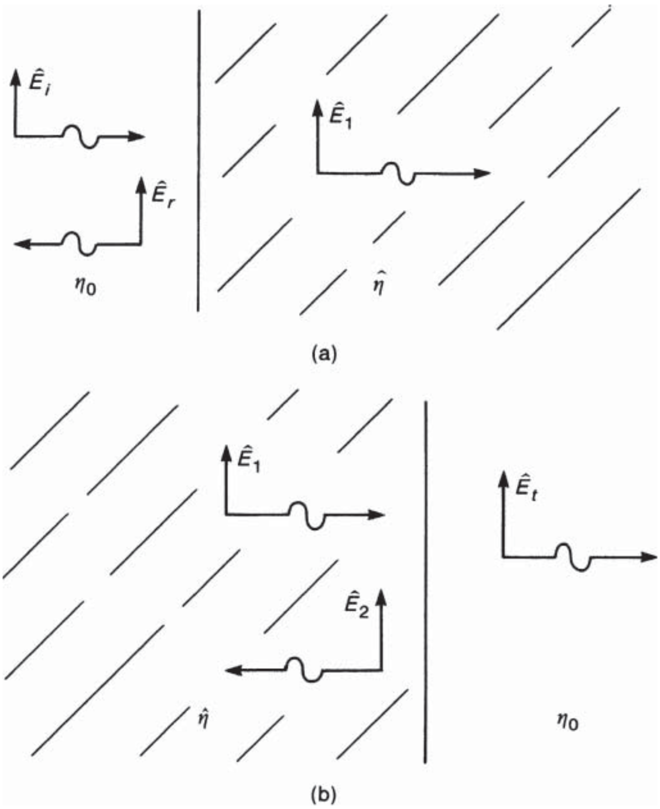

FIGURE 10.6 Approximate calculation of shielding effectiveness for uniform plane waves: (a) incident wavefront entering the shield from the left; (b) wavefront exiting the shield from the left.

results for shields that are constructed from "good conductors" whose thickness t is much greater than a skin depth at the frequency of the incident wave.

10.2.1 Exact Solution

In order to obtain the exact solution for the shielding effectiveness of a metallic barrier, we solve the problem illustrated in Fig. 10.4. A conducting shield of thickness t, conductivity σ, permittivity $\varepsilon = \varepsilon_0$, and permeability μ has an incident uniform plane wave incident on its leftmost surface. The medium on either side of the shield is assumed, for practical reasons, to be free space. A rectangular coordinate system is used to define the problem, with the left surface lying in the xy plane at $z = 0$ and the right surface located at $z = t$. Forward- and backward-traveling waves are present in the left medium and in the shield according to the general properties of the solution of Maxwell's equations. Only a forward-traveling wave is postulated in the medium to the right of the shield, since we reason that there is no additional barrier to create a reflected field. The general forms of these fields are (see Section B6.2 and [6, 7]):

$$\hat{\boldsymbol{E}}_i = \hat{E}_i e^{-j\beta_0 z} \alpha_x \tag{10.5a}$$

$$\hat{\boldsymbol{H}}_i = \frac{\hat{E}_i}{\eta_0} e^{-j\beta_0 z} \alpha_y \tag{10.5b}$$

$$\hat{\boldsymbol{E}}_r = \hat{E}_r e^{-j\beta_0 z}\alpha_x \tag{10.5c}$$

$$\hat{\boldsymbol{H}}_r = -\frac{\hat{E}_r}{\eta_0} e^{j\beta_0 z}\alpha_y \tag{10.5d}$$

$$\hat{\boldsymbol{E}}_1 = \hat{E}_1 e^{-\hat{\gamma} z}\alpha_x \tag{10.5e}$$

$$\hat{\boldsymbol{H}}_1 = -\frac{\hat{E}_1}{\hat{\eta}} e^{-\hat{\gamma} z}\alpha_y \tag{10.5f}$$

$$\hat{\boldsymbol{E}}_2 = \hat{E}_2 e^{-\hat{\gamma} z}\alpha_x \tag{10.5g}$$

$$\hat{\boldsymbol{H}}_2 = -\frac{\hat{E}_2}{\hat{\eta}} e^{\hat{\gamma} z}\alpha_y \tag{10.5h}$$

$$\hat{\boldsymbol{E}}_t = \hat{E}_t e^{-j\beta_0 z}\alpha_x \tag{10.5i}$$

$$\hat{\boldsymbol{H}}_t = -\frac{\hat{E}_t}{\eta_0} e^{-j\beta_0 z}\alpha_y \tag{10.5j}$$

where the phase constant and intrinsic impedance in the free-space regions are

$$\beta_0 = \omega\sqrt{\mu_0\varepsilon_0} \tag{10.6a}$$

$$\eta_0 = \sqrt{\frac{\mu_0}{\varepsilon_0}} \tag{10.6b}$$

and the propagation constant and intrinsic impedance of the shield are

$$\begin{aligned}\hat{\gamma} &= \sqrt{j\omega\mu(\sigma + j\omega\varepsilon)}\\ &= \alpha + j\beta\end{aligned} \tag{10.7a}$$

$$\begin{aligned}\hat{\eta} &= \sqrt{\frac{j\omega\mu}{\sigma + j\omega\varepsilon}}\\ &= \frac{\eta}{\theta_\eta}\end{aligned} \tag{10.7b}$$

The magnitude of the incident field $\hat{E}_i$ is assumed known. In order to determine the remaining amplitudes $\hat{E}_r$, $\hat{E}_1$, $\hat{E}_2$, and $\hat{E}_t$, we need four equations. These are generated by enforcing the boundary conditions on the field vectors at the two boundaries, $z = 0$ and $z = t$. Continuity of the tangential components of the electric field at the two interfaces gives

$$\hat{\boldsymbol{E}}_i|_{z=0} + \hat{\boldsymbol{E}}_r|_{z=0} = \hat{\boldsymbol{E}}_1|_{z=0} + \hat{\boldsymbol{E}}_2|_{z=0} \tag{10.8a}$$

$$\hat{\boldsymbol{E}}_1\Big|_{z=t} + \hat{\boldsymbol{E}}_2|_{z=t} = \hat{\boldsymbol{E}}_t|_{z=t} \tag{10.8b}$$

Continuity of the tangential components of the magnetic field at the two interfaces gives

$$\hat{\boldsymbol{H}}_i|_{z=0} + \hat{\boldsymbol{H}}_r|_{z=0} = \hat{\boldsymbol{H}}_1|_{z=0} + \hat{\boldsymbol{H}}_2|_{z=0} \tag{10.9a}$$

$$\hat{\boldsymbol{H}}_1\Big|_{z=t} + \hat{\boldsymbol{H}}_2|_{z=t} = \hat{\boldsymbol{H}}_t|_{z=t} \tag{10.9b}$$

Substituting the forms given in (10.5) gives the required four equations as

$$\hat{E}_i + \hat{E}_r = \hat{E}_1 + \hat{E}_2 \tag{10.10a}$$

$$\hat{E}_1 e^{-\hat{\gamma}t} + \hat{E}_2 e^{\hat{\gamma}t} = \hat{E}_t e^{-j\beta_0 t} \tag{10.10b}$$

$$\frac{\hat{E}_i}{\eta_0} - \frac{\hat{E}_r}{\eta_0} = \frac{\hat{E}_1}{\hat{\eta}} - \frac{\hat{E}_2}{\hat{\eta}} \tag{10.10c}$$

$$\frac{\hat{E}_1}{\hat{\eta}} e^{-\hat{\gamma}t} - \frac{\hat{E}_2}{\hat{\eta}} e^{\hat{\gamma}t} = \frac{\hat{E}_t}{\eta_0} e^{-j\beta_0 t} \tag{10.10d}$$

Solving these equations gives the ratio of the incident and transmitted waves as [6]

$$\frac{\hat{E}_i}{\hat{E}_t} = \frac{(\eta_0 + \hat{\eta})^2}{4\eta_0\hat{\eta}} \left[1 - \left(\frac{\eta_0 - \hat{\eta}}{\eta_0 - \hat{\eta}}\right)^2 e^{-2t/\delta} e^{-j2\beta t}\right] e^{t/\delta} e^{j\beta t} e^{-j\beta_0 t} \tag{10.11}$$

Equation (10.11) is the *exact expression* for the ratio of the electric field that is incident on the boundary and the electric field that is transmitted through the boundary. We have substituted the relation $\hat{\gamma} = \alpha + j\beta$ from (10.7a) and also $\alpha = 1/\delta$ (assuming that the barrier material is a good conductor), where δ is the skin depth for the barrier material at the frequency of the incident wave:

$$\delta = \frac{1}{\sqrt{\pi f \mu \sigma}} \tag{10.12}$$

We can, however, make some reasonable approximations to reduce this to a result derived by approximate means in the following sections. This will not only simplify the result but also demonstrate that the same result can be derived by approximate methods without any significant loss in accuracy, as we will do in the next section.

In order to simplify (10.11), we will assume that the barrier is constructed from a "good conductor," so that the intrinsic impedance of the conductor is much less than that of free space: $\hat{\eta} \ll \eta_0$ Therefore, we may approximate

$$\frac{\eta_0 - \hat{\eta}}{\eta_0 + \hat{\eta}} \cong 1 \tag{10.13}$$

Also we assume that the skin depth δ is much less than the barrier thickness t. Thus

$$\begin{aligned} e^{-\hat{\gamma}t} &= e^{-\alpha t} e^{-\beta t} \\ &= e^{-t/\delta} e^{-\beta t} \\ &\ll 1 \;\; \text{for} \;\; t \gg \delta \end{aligned} \tag{10.14}$$

Substituting these into the exact result given in (10.11) and taking the absolute value of the result give

$$\begin{aligned}\left|\frac{\hat{E}_i}{\hat{E}_t}\right| &= \left|\frac{(\eta_0+\hat{\eta})^2}{4\eta_0\hat{\eta}}\right| e^{t/\delta}\\ &\cong \left|\frac{\eta_0}{4\hat{\eta}}\right| e^{t/\delta}\end{aligned} \tag{10.15}$$

Taking the logarithm of this result in order to express the shielding effectiveness in dB in accordance with (10.2) gives

$$\mathrm{SE}_{\mathrm{dB}} \cong \underbrace{20\log_{10}\left|\frac{\eta_0}{4\hat{\eta}}\right|}_{R_{\mathrm{dB}}} + \underbrace{20\log_{10} e^{t/\delta}}_{A_{\mathrm{dB}}} + M_{\mathrm{dB}} \tag{10.16a}$$

The multiple-reflection loss in (10.4) is evidently the middle term of (10.11):

$$\begin{aligned}M_{\mathrm{dB}} &= 20\log_{10}\left|1-\left(\frac{\eta_0-\hat{\eta}}{\eta_0+\hat{\eta}}\right)^2 e^{-2t/\delta} e^{j2-\beta t}\right|\\ &\cong 20\log_{10}\left|1-e^{-2t/\delta}e^{j2-\beta t}\right|\end{aligned} \tag{10.16b}$$

which can be neglected for shields that are constructed of good conductors, $\hat{\eta} \ll \eta_0$, and whose thicknesses are much greater than a skin depth, $t \gg \delta$. We have also substituted $\beta = \alpha = 1/\delta$, assuming the barrier is constructed from a good conductor. (See Appendix B, Section B.6.4.) Observe that this term is of the form $1-\hat{\Gamma}_{\mathrm{in}}^2$ where $\hat{\Gamma}_{\mathrm{in}} = [(\eta_0-\hat{\eta})/(\eta_0+\hat{\eta})]e^{-2\hat{\gamma}t}$ is the reflection coefficient at the right boundary referred to the left boundary. The multiple-reflection term is approximately unity ($M_{\mathrm{dB}} \simeq 0$) for barrier thicknesses that are thick compared with a skin depth, $t \gg \delta$, and is of no consequence. However, for barrier thicknesses that are thin compared with a skin depth, $t \ll \delta$, the multiple-reflection factor is negative (in dB). In this case, multiple reflections reduce the shielding effectiveness of the barrier. For example, for $t/\delta = 0.1$, Eq. (10.16b) gives $M_{\mathrm{dB}} = -11.8$ dB.

The separation of the exact result into a component due to reflection, a component due to absorption, and a component due to multiple reflections as in equation (10.4) is evident in (10.16a). This result will be derived by approximate methods in the following section.

10.2.2 Approximate Solution

We now consider deriving the previous result *under the assumption that the barrier is constructed of a good conductor, $\hat{\eta} \ll \eta_0$, and the barrier thickness is much greater than a skin depth at the frequency of the incident wave, i.e., $t \gg \delta$*. These assumptions are usually inherent in a well-designed shield and thus are not restrictive from a practical standpoint. The basic idea is illustrated in Fig. 10.6. First, it is worth noting that this approximate solution is analogous to the problem of analyzing the overall gain of cascaded amplifiers. In that problem, we compute the input impedance of the first stage, using the input impedance of the second stage as the load for the first. Then we can compute the ratio of the output voltage of the first stage to its input voltage. Next, we compute the ratio of the output voltage of the second stage to its input voltage, using the input impedance of the third stage as the load for the second stage. This process continues until we finally compute the gain of the last stage. The overall gain of the cascade is then the product of the gains of the individual stages. This technique takes into account the loading of each stage on the preceding stage, and this loading generally cannot be neglected. However, if the input impedances of the individual stages are quite large, as is generally the case for FET and vacuum-tube amplifiers, then this loading can be ignored and the overall gain of the cascade can be computed as the gains of the individual, *isolated* stages.

10.2.2.1 Reflection Loss The approximate analysis technique we will use is the direct analogy of the method for analyzing cascaded amplifiers described above. Assuming that the barrier thickness is much greater than a skin depth at the frequency of the incident wave, the portion of the incident wave that is transmitted across the left interface in Fig. 10.4, $\hat{E}_1$, is greatly attenuated by the time it reaches the right interface. Thus, the reflected wave $\hat{E}_2$, when it arrives at the left interface, is not of much consequence and so contributes little to the total reflected wave $\hat{E}_r$ ($\hat{E}_2$ is also greatly attenuated as it travels from the second interface back to the left interface). Therefore, we can approximately compute the portion of the incident wave that is transmitted across the left interface, $\hat{E}_1$, by assuming that the barrier is infinitely thick and therefore assuming that $\hat{E}_2 = 0$. This then becomes the basic problem considered in Section 7.6.2 of Chapter 7 and is illustrated in Fig. 10.6a. The transmission coefficient becomes

$$\frac{\hat{E}_1}{\hat{E}_i} \cong \frac{2\hat{\eta}}{\eta_0 + \hat{\eta}} \tag{10.17}$$

The next basic problem occurs at the right interface, as illustrated in Fig. 10.6b, and is again related to the basic problem considered in Section 7.6.2 of Chapter 7. The transmission coefficient for this case gives

$$\frac{\hat{E}_t}{\hat{E}_i} \cong \frac{2\hat{\eta}_0}{\eta_0 + \hat{\eta}} \tag{10.18}$$

Note that for this case, the intrinsic impedance of the medium for the transmitted wave is η_0 and the intrinsic impedance for the incident wave is $\hat{\eta}$. For the first half of this problem, the intrinsic impedance of the medium for the transmitted wave is $\hat{\eta}$ and the intrinsic impedance for the incident wave is η_0. Taking the product of (10.17) and (10.18) gives the ratio of the transmitted field and the incident field *in the absence of attenuation* as

$$\begin{aligned}\frac{\hat{E}_t}{\hat{E}_i} &= \frac{\hat{E}_t}{\hat{E}_1}\frac{\hat{E}_1}{\hat{E}_i} \\ &= \frac{2\hat{\eta}_0}{\eta_0 + \hat{\eta}}\,\frac{2\hat{\eta}}{\eta_0 + \hat{\eta}} \\ &= \frac{4\hat{\eta}_0\hat{\eta}}{(\eta_0 + \hat{\eta})^2} \end{aligned} \tag{10.19}$$

Note that because $\hat{\eta} \ll \eta_0$, (10.17) is much smaller than (10.18). Thus, *the transmission coefficient is very small at the first boundary and is approximately two at the second boundary*. Thus, *very little of the electric field is transmitted through the first* (*left*) *boundary*. The reflection coefficient at the first (left) interface is $\Gamma_1 = (\hat{\eta} - \eta_0)/(\hat{\eta} + \eta_0) \cong -1$, and the electric field is effectively "shorted out" by the good conductor. The reflection coefficient at the second (right) boundary is $\Gamma_2 = (\eta_0 - \hat{\eta})/(\eta_0 + \hat{\eta}) \cong +1$. These are analogous to the voltage reflections at the end of a short-circuited (left boundary) or open-circuited (right boundary) transmission line. Thus, the majority of the electric field that is incident on each interface is reflected. However, because very little of the electric field is transmitted through the first boundary, it is of little consequence that the reflection coefficient at the second boundary is approximately unity! The reflection loss term in (10.4) is therefore

$$\begin{aligned} R_{\mathrm{dB}} &= 20\log_{10}\left|\frac{\hat{E}_i}{\hat{E}_t}\right| \\ &= 20\log_{10}\left|\frac{(\eta_0+\hat{\eta})^2}{4\hat{\eta}_0\hat{\eta}}\right| \\ &= 20\log_{10}\left|\frac{\eta_0}{4\hat{\eta}}\right| \end{aligned} \tag{10.20}$$

where we have substituted the approximation $\hat{\eta} \ll \eta_0$.

It is instructive to consider the magnetic field transmissions. Recall from Chapter 7 that the reflection and transmission coefficients were derived for the electric field only and could not be used for the magnetic field. If we wish to determine the reflected and transmitted magnetic fields, we need to divide the electric fields by the appropriate intrinsic impedances to give

$$\begin{aligned} \frac{\hat{H}_1}{\hat{H}_i} &= \frac{\hat{E}_1/\hat{\eta}}{\hat{E}_i/\eta_0} \\ &= \frac{\hat{E}_1\eta_0}{\hat{E}_i\hat{\eta}} \\ &= \frac{2\eta_0}{\eta_0+\hat{\eta}} \end{aligned} \tag{10.21}$$

Similarly, we obtain

$$\begin{aligned} \frac{\hat{H}_t}{\hat{H}_1} &= \frac{\hat{E}_t/\eta_0}{\hat{E}_1/\hat{\eta}} \\ &= \frac{\hat{E}_t\eta_0}{\hat{E}_1\hat{\eta}} \\ &= \frac{2\hat{\eta}}{\eta_0+\hat{\eta}} \end{aligned} \tag{10.22}$$

Taking the product of (10.21) and (10.22) gives the ratio of the transmitted and incident magnetic field intensities:

$$\begin{aligned} \frac{\hat{H}_t}{\hat{H}_i} &= \frac{\hat{H}_t}{\hat{H}_1}\frac{\hat{H}_1}{\hat{H}_i} \\ &= \frac{2\hat{\eta}}{\eta_0+\hat{\eta}}\frac{2\eta_0}{\eta_0+\hat{\eta}} \\ &= \frac{4\eta_0\hat{\eta}}{(\eta_0+\hat{\eta})^2} \end{aligned} \tag{10.23}$$

Comparing (10.23) and (10.19) shows that *the ratio of the transmitted and incident electric fields is identical to the ratio of the transmitted and incident magnetic fields*. However, there is one important difference: *the primary transmission of the magnetic field occurs at the left interface, whereas the primary transmission of the electric field occurs at the right interface*. [See (10.17), (10.18), (10.21), and (10.22).] Therefore, the attenuation of the magnetic field as it passes through the boundary is more important than is the attenuation of the electric field. This points out that "thick" boundaries have more effect on shielding against magnetic fields than electric fields (because of this attenuation of the magnetic field as it travels through the boundary).

Since the primary transmission of the electric field occurs at the second boundary, shield thickness is not of as much importance as it is for magnetic field shielding, in which the primary transmission occurs at the first boundary. Attenuation of the barrier is of more consequence in magnetic field shielding, since there is considerable transmission of the magnetic field at the first boundary. Therefore, effective shields for electric fields can be constructed from thin shields, which effectively "short out" the electric field at the first boundary.

10.2.2.2 Absorption Loss

The previous result assumed that the barrier thickness was much greater than a skin depth, so that we could "uncouple" the calculation of the reflections and transmissions at the two interfaces. However, in taking the product of the two transmission coefficients as in (10.19), we are assuming that $\hat{E}_1$ is the same amplitude at the left and right interfaces. But the magnitude of $\hat{E}_1$ at the right interface will be reduced substantially from its value at the left interface by the factor $e^{-t/\delta}$. This attenuation can be easily accounted for – simply multiply (10.19) by $e^{-t/\delta}$. Thus, the *absorption factor* accounting for attenuation becomes

$$A = e^{t/\delta} \tag{10.24}$$

In decibels, this becomes

$$A_{\text{dB}} = 20\log_{10} e^{t/\delta} \tag{10.25}$$

10.2.2.3 Multiple-Reflection Loss

In the previous approximate calculations, we have assumed that any "secondary reflections" are of no consequence, since they will have suffered substantial attenuation as they travel back and forth through the barrier. If the barrier thickness is not much greater than a skin depth, as was assumed, then the re-reflections and transmissions may be important. This is particularly true for magnetic fields, since the primary transmission occurs at the first boundary, and thus these multiple reflections can be more significant for magnetic field shielding. In the case of multiple reflections that are significant, they are accounted for with a *multiple-reflection factor* given in (10.16b) and illustrated in Fig. 10.7a. The total transmitted electric field is the sum of the primary and secondary transmitted waves at the right interface as

$$\begin{aligned} \hat{E}_t &= \hat{E}_{t1} + \hat{E}_{t2} + \hat{E}_{t3} + \cdots \\ &= \hat{E}_{t1}(1 + \Delta_2 + \Delta_3 + \ldots) \end{aligned} \tag{10.26}$$

where $\hat{E}_{t1}$ is the first electric field transmitted across the right interface, which was considered to be the total transmitted field in the previous approximate solution that neglected these re-reflections.

Consider the electric field transmitted across the left interface and incident on the right interface, $\hat{E}_{\text{in}}$, in Fig. 10.7. A portion of this is transmitted across the right interface,

$$\hat{E}_{t1} = \frac{2\eta_0}{\eta_0 + \hat{\eta}} \hat{E}_{\text{in}} \tag{10.27}$$

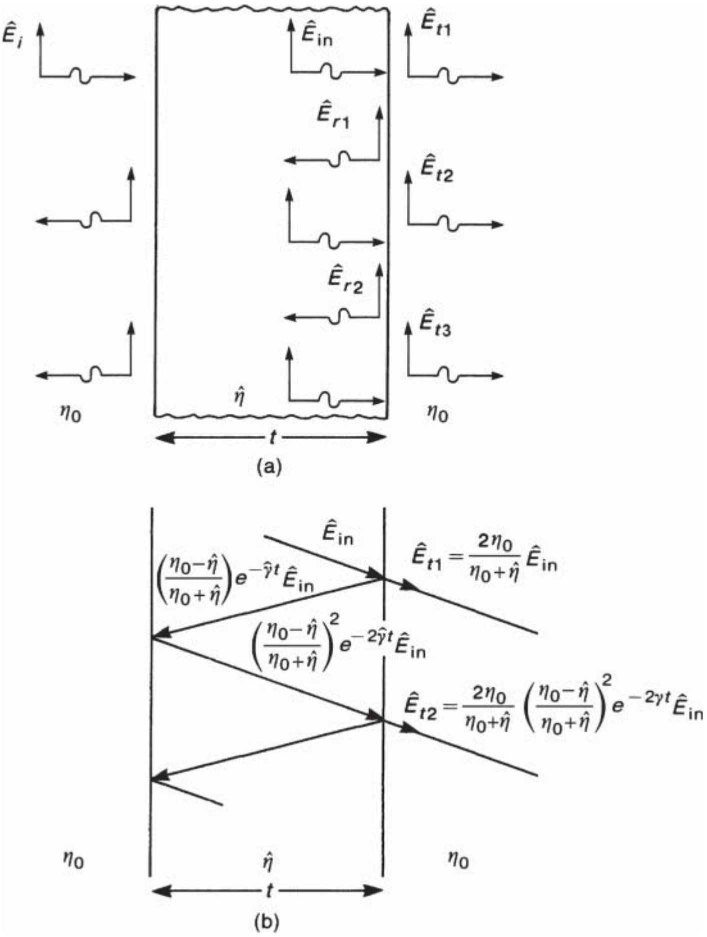
$\hat{E}_i$
$\hat{E}_{in}$
$\hat{E}_{t1}$
$\hat{E}_{r1}$
$\hat{E}_{t2}$
$\hat{E}_{r2}$
$\hat{E}_{t3}$
η_0
$\hat{\eta}$
η_0
t
(a)
$\hat{E}_{in}$
$\left(\frac{\eta_0-\hat{\eta}}{\eta_0+\hat{\eta}}\right)e^{-\hat{\gamma}t}\hat{E}_{in}$
$\hat{E}_{t1}=\frac{2\eta_0}{\eta_0+\hat{\eta}}\hat{E}_{in}$
$\left(\frac{\eta_0-\hat{\eta}}{\eta_0+\hat{\eta}}\right)^2 e^{-2\hat{\gamma}t}\hat{E}_{in}$
$\hat{E}_{t2}=\frac{2\eta_0}{\eta_0+\hat{\eta}}\left(\frac{\eta_0-\hat{\eta}}{\eta_0+\hat{\eta}}\right)^2 e^{-2\gamma t}\hat{E}_{in}$
η_0
$\hat{\eta}$
η_0
t
(b)

FIGURE 10.7 Illustration of the effect of multiple reflections within the barrier: (a) combining multiple transmissions; (b) calculation in terms of reflection and transmission coefficients.

and a portion is reflected and sent back to the left interface,

$$\hat{E}_{r1} = \frac{\eta_0 - \hat{\eta}}{\eta_0 + \hat{\eta}}\hat{E}_{\text{in}} \tag{10.28}$$

These are obtained by multiplying by the transmission coefficient $\hat{T} = 2\eta_0/(\eta_0 + \hat{\eta})$ and the reflection coefficient $\hat{\Gamma} = (\eta_0 - \hat{\eta})(\eta_0 + \hat{\eta})$ at the right interface. (See Section 7.6.2.) The reflected wave $\hat{E}_{r1}$ propagates back to the left interface and in so doing suffers attention and phase shift, $e^{-\hat{\gamma}t}$. At this left interface, the incoming wave

$$\hat{E}_{r1}e^{-\hat{\gamma}t}$$

is reflected as

$$\left(\frac{\eta_0 - \hat{\eta}}{\eta_0 - \hat{\eta}}\right)e^{-\hat{\gamma}t}E_{r1}$$

and propagated back to the second interface. When it arrives there, it has been again multiplied by $e^{-\hat{\gamma}t}$ by virtue of propagating through the barrier again. Hence, this second wave that is incident on the right interface is

$$\left(\frac{\eta_0 - \hat{\eta}}{\eta_0 - \hat{\eta}}\right) e^{-2\hat{\gamma}t} E_{r1}$$

A portion of this is transmitted across the right interface as

$$\hat{E}_{t2} = \frac{2\eta_0}{\eta_0 + \hat{\eta}} \left(\frac{\eta_0 - \hat{\eta}}{\eta_0 + \hat{\eta}}\right) e^{-2\hat{\gamma}t} E_{r1}$$

Substituting (10.27) and (10.28) gives $\hat{E}_{t2}$ in terms of $\hat{E}_{t1}$ as

$$\begin{aligned} \hat{E}_{t2} &= \left(\frac{\eta_0 - \hat{\eta}}{\eta_0 + \hat{\eta}}\right) e^{-2\hat{\gamma}t} \hat{E}_{t1} \\ &= \Delta^2 \hat{E}_{t1} \end{aligned} \tag{10.29a}$$

where

$$\Delta = \left(\frac{\eta_0 - \hat{\eta}}{\eta_0 + \hat{\eta}}\right) e^{-\hat{\gamma}t} \tag{10.29b}$$

This continues giving the total transmitted electric field as

$$\begin{aligned} \hat{E}_t &= \hat{E}_{t1}(1 + \Delta^2 + \Delta^4 + \cdots) \\ &= \frac{\hat{E}_{t1}}{(1 - \Delta^2)} \end{aligned} \tag{10.30}$$

a summation that is valid for $|\Delta| < 1$ as is the case here.

The shielding effectiveness is

$$\begin{aligned} \mathrm{SE}_{\mathrm{dB}} &= 20 \log_{10} \left| \frac{\hat{E}_i}{\hat{E}_t} \right| \\ &= 20 \log_{10} \left| \frac{\hat{E}_i}{\hat{E}_{t1}} \right| + 20 \log_{10} \left| 1 - \Delta^2 \right| \\ &= \underbrace{20 \log_{10} \left| \frac{\hat{E}i}{\hat{E}_{t1}} \right|}_{R_{\mathrm{dB}}+A_{\mathrm{dB}}} + \underbrace{20 \log_{10} \left| 1 - \left(\frac{\eta_0 - \hat{\eta}}{\eta_0 + \hat{\eta}}\right)^2 e^{-2\hat{\gamma}t} \right|}_{M_{\mathrm{dB}}} \end{aligned} \tag{10.31}$$

10.2.2.4 Total Loss Combining the results given above gives the three components of the shielding effectiveness given in (10.4). The reflection loss is given in (10.20). Substituting the approximation for the intrinsic impedance of a good conductor as

$$\begin{aligned}\hat{\eta} &= \sqrt{\frac{j\omega\mu}{\sigma + \omega\varepsilon}} \\ &= \sqrt{\frac{j\omega\mu}{\sigma}\sqrt{\frac{1}{1 + (j\omega\varepsilon/\sigma)}}} \quad \left(\begin{array}{c}\text{barrier is a} \\ \text{good conductor,} \\ (\sigma/\omega\varepsilon) \gg 1\end{array}\right) \\ &\cong \sqrt{\frac{j\omega\mu}{\sigma}} \\ &= \sqrt{\left(\frac{\omega\mu}{\sigma}\right)} \,/45° \end{aligned} \tag{10.32}$$

and

$$\eta_0 = \sqrt{\frac{\mu_0}{\varepsilon_0}} \tag{10.33}$$

into (10.20) gives

$$R_{\text{dB}} = 20 \log_{10} \left(\frac{1}{4}\sqrt{\frac{\sigma}{\omega\mu_r\varepsilon_0}}\right) \tag{10.34}$$

where we have assumed $\mu = \mu_0\mu_r$ and $\varepsilon = \varepsilon_0$. For the conductivity of metals, it is customary to refer to that of copper, which has a conductivity $\sigma_{Cu} = 5.8 \times 10^7$ S/m. Thus, the conductivity of other metals is written as $\sigma = \sigma_{Cu}\sigma_r$, where σ_r is the *conductivity relative to copper*. Substituting this into (10.34) gives

$$R_{\text{dB}} = 168 + 10\log_{10}\left(\frac{\sigma_r}{\mu_r, f}\right) \tag{10.35}$$

Observe that *the reflection loss is greatest at low frequencies and for high-conductivity metals*. Similarly, *magnetic materials*, $\mu_r > 1$, *degrade the reflection loss*. The reflection loss decreases at a rate of −10 dB/decade with frequency. As an example, consider a shield constructed of copper ($\mu_r = 1$). The reflection loss at 1 kHz is 138 dB. At 10 MHz, the reflection loss is 98 dB. On the other hand, sheet steel has $\mu_r = 1000$ and $\sigma_r = 0.1$. At 1 kHz, the reflection loss is 98 dB, and at 10 MHz it is reduced to 58 dB.

The absorption loss is given by (10.25). This can also be simplified. The skin depth is

$$\begin{aligned}\delta &= \frac{1}{\sqrt{\pi f \mu\sigma}} \\ &= \frac{0.06609}{\sqrt{f\mu_r\sigma_r}} \text{ m} \\ &= \frac{2.6}{\sqrt{f\mu_r\sigma_r}} \text{ in.} \\ &= \frac{2602}{\sqrt{f\mu_r\sigma_r}} \text{ mils}\end{aligned} \tag{10.36}$$

where we have written the result in various units. Substituting (10.36) into (10.25) gives

$$\begin{aligned} A_{\mathrm{dB}} &= 20\log_{10} e^{t/\delta} \\ &= \frac{20t}{\delta}\log_{10} e \\ &= \frac{8.686t}{\delta} \\ &= 131.4t\sqrt{f\mu_r\sigma_r} \quad (t \text{ in m}) \\ &= 3.338t\sqrt{f\mu_r\sigma_r} \quad (t \text{ in in.}) \end{aligned} \tag{10.37}$$

Equation (10.37) shows that the absorption loss increases with increasing frequency as $\sqrt{f}$ *on a decibel scale*. This is quite different from the absorption loss being proportional to the square root of frequency so that it increases at a rate of 10 dB/decade on a decibel scale. Therefore, the absorption loss increases quite rapidly with increasing frequency. Ferromagnetic materials where $\mu_r \gg 1$ increase this loss over copper (assuming that $\mu_r\sigma_r \gg 1$). The absorption loss can also be understood in terms of the thickness of the shield relative to a skin depth, as is evident in (10.37):

$$\begin{aligned} A_{\mathrm{dB}} &= \frac{8.686t}{\delta} \\ &= 8.7 \text{ dB for } \frac{t}{\delta} = 1 \\ &= 17.4 \text{ dB for } \frac{t}{\delta} = 2 \end{aligned} \tag{10.38}$$

This illustrates the importance of skin depth in absorption loss.

Observe that the reflection loss is a function of the ratio σ_r/μ_r, whereas the absorption loss is a function of the product $\sigma_r\mu_r$. Table 10.1 shows these factors for various materials.

TABLE 10.1 Relative Conductivity and Permeability, and Approximate Absorption and Reflection Losses, for Various Materials

Material	σ_r	μ_r	$A \sim \mu_r\sigma_r$	$R \sim \sigma_r/\mu_r$
Silver	1.05	1	1.05	1.05
Copper	1	1	1	1
Gold	0.7	1	0.7	0.7
Aluminum	0.61	1	0.61	0.61
Brass	0.26	1	0.26	0.26
Bronze	0.18	1	0.18	0.18
Tin	0.15	1	0.15	0.15
Lead	0.08	1	0.08	0.08
Nickel	0.2	600	120	$3{:}3 \times 10^{-4}$
Stainless steel (430)	0.02	500	10	4×10^{-5}
Steel (SAE 1045)	0.1	1000	100	1×10^{-4}
Mumetal (at 1 kHz)	0.03	30,000	900	1×10^{-6}
Superpermalloy (at 1 kHz)	0.03	100,000	3000	3×10^{-7}

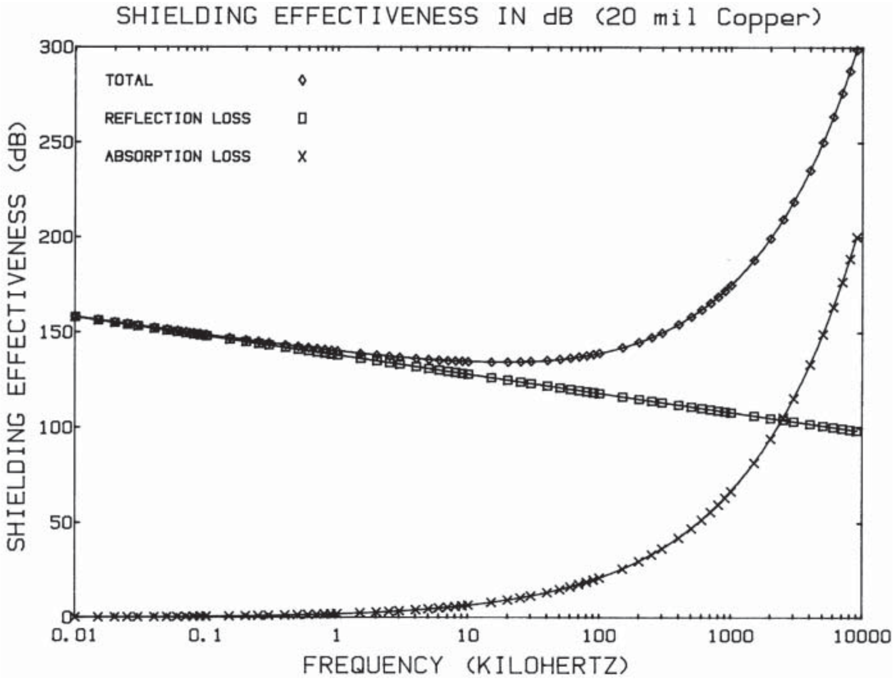

FIGURE 10.8 Shielding effectiveness of a 20-mil thickness of copper.

Figure 10.8 shows the components of the shielding effectiveness for a 20-mil thickness of copper as a function of frequency from 10 Hz to 10 MHz. Observe that the absorption loss is dominant above 2 MHz. Figure 10.9 shows the same data for steel (SAE 1045) for a 20-mil thickness. These data are plotted from 10 Hz to only 1 MHz. Note that for this material reflection loss dominates only below 20 kHz. These data indicate that reflection loss is the primary contributor to the shielding effectiveness at low frequencies for either ferrous or nonferrous shielding materials. At the higher frequencies ferrous materials increase the absorption loss and the total shielding effectiveness. It is worthwhile reiterating that for electric fields the primary transmission occurs at the second boundary, whereas for magnetic fields it occurs at the first boundary, so that absorption is more important for the reduction of magnetic fields.

Review Exercise 10.1 Determine the reflection loss for aluminum, brass, and stainless steel at 1 MHz.

***Answers*:** 106 dB, 102 dB, and 64 dB.

Review Exercise 10.2 Determine the skin depth in mils for aluminum, brass, and stainless steel at 1 MHz.

***Answers*:** 3.33 mils, 5.1 mils, and 0.82 mils.

Review Exercise 10.3 Determine the absorption loss for 1/8 in (125-mil)-thick aluminum, brass, and stainless-steel shields at 1 MHz.

***Answers*:** 326 dB, 213 dB, and 1320 dB.

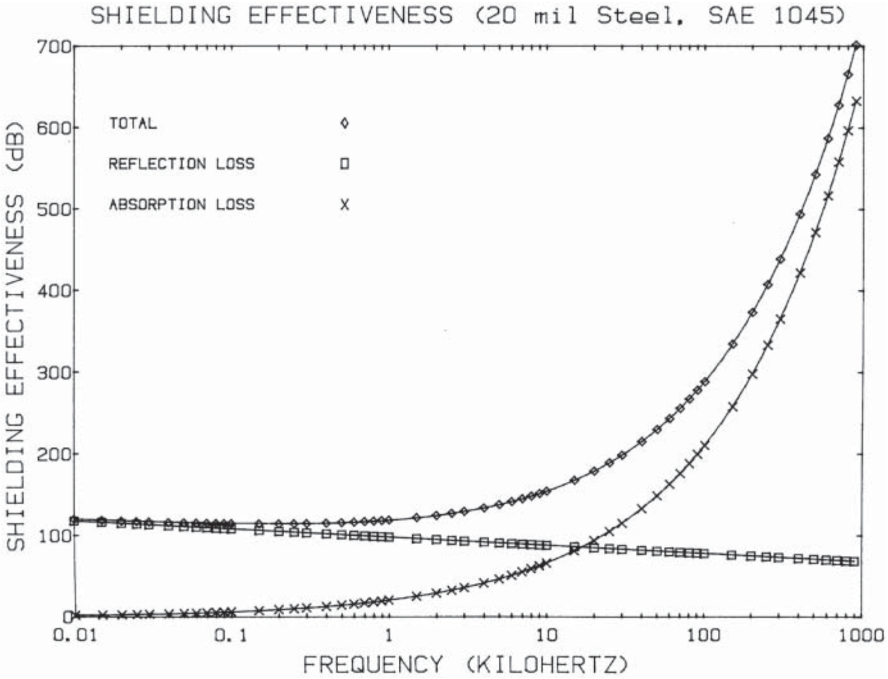

FIGURE 10.9 Shielding effectiveness of a 20-mil thickness of steel (SAE 1045).

10.3 SHIELDING EFFECTIVENESS: NEAR-FIELD SOURCES

The previous analysis of shielding effectiveness assumed a uniform plane wave incident normal to the surface of the shield. This therefore assumes that the shield is in the far field of the source of the incident field. In this section, we will consider *near-field sources*. We will find that the techniques for shielding depend on the *type of source*; whether the source is a *magnetic field source* or an *electric field source*. It must be pointed out that near fields are much more complicated in structure than are far fields (which are simple and resemble uniform plane waves). Hence, analysis of the effects of plane, conducting barriers on near fields is a very complicated process. The reader is referred to the ongoing analysis published in the literature. The near-field shielding for current loops is analyzed in [8, 9], whereas the near-field shielding for line current sources is analyzed in [10].

It is unreasonable to expect that simple and highly accurate formulas can be obtained for near-field shielding as were obtained (exactly) for far-field shielding in the preceding sections. The following results are approximations to the exact results (which are very complicated). The heart of this approximate method is to replace the intrinsic impedance of free space, $\eta_0 = \sqrt{\mu_0/\varepsilon_0}$, with the *wave impedance*, $\hat{Z}_w$, for the Hertzian (electric) dipole and the small magnetic loop (dipole) considered in Chapter 7. Although this is a somewhat crude approximation, it has been investigated in [10] and shown to give reasonably accurate results if we make some simple modifications.

10.3.1 Near Field Versus Far Field

In order to demonstrate why it is important to differentiate between types of sources when they are close to the shield, consider the elemental electric (Hertzian) dipole considered in Section 7.1. We found that at sufficiently distant points from this source, the fields resembled plane waves in that (1) the far-field components E_θ and H_ϕ are orthogonal and (2) the ratio of these two field vectors is the intrinsic impedance of the medium $E_\theta H_\phi = \eta_0$. In the "near field" of this source, these conditions are not satisfied. In particular, one must be of order $3\lambda_0$ from this source in order for these two characteristics to hold, i.e., the far field. In general, the near fields have more field components than these. Furthermore, the field components do not vary simply as inverse distance $1/r$, but also depend on $1/r^2$ and $1/r^3$. The $1/r$ terms equal the $1/r^2$ and $1/r^3$ terms at $r = \lambda_0/2\pi$ or about $\lambda_0/6$. A reasonable criterion for the near-field/far-field boundary would be where the ratio of E_θ to H_ϕ is approximately η_0. This ratio is referred to as the *wave impedance*:

$$\hat{Z}_w = \frac{\hat{E}_\theta}{\hat{H}_\phi} \tag{10.39}$$

It is only in the far field where it is appropriate to use the term "intrinsic impedance" to characterize the wave impedance. The wave impedance is obtained from Eq. (7.1) as the ratio of the total fields:

$$\hat{Z}_w = \eta_0 \frac{j/\beta_0 r + 1/(\beta_0 r)^2 - j/(\beta_0 r)^3}{j/\beta_0 r + 1/(\beta_0 r)^2} \tag{10.40}$$

The magnitude of the wave impedance is plotted against distance from the source in Fig. 10.10a. In the far field, the $1/r$ terms dominate, giving $\hat{Z}_w \cong \eta_0$. Equation (10.40) reduces in the very near field to

$$\begin{aligned} \hat{Z}_w &\cong \eta_0 \left(-j\frac{1}{\beta_0 r} \right) \quad \text{(near field } \beta_0 r \ll 1\text{)} \\ &= \frac{\eta_0}{\beta_0 r} \angle -90^\circ \end{aligned} \tag{10.41}$$

In the near field, the electric field is proportional to $1/r^3$, while the magnetic field is proportional to $1/r^2$:

$$\left. \begin{aligned} \hat{E}_\theta &\sim \tfrac{1}{r^3} \\ \hat{H}_\phi &\sim \tfrac{1}{r^2} \end{aligned} \right\} \quad \text{(electric source, near field)} \tag{10.42a, b}$$

Also, in the near field of the electric dipole, the wave impedance is greater than the intrinsic impedance of the medium. Therefore, the electric dipole is referred to as a *high-impedance source*. The magnitude of the wave impedance for an *electric field source* is therefore

$$\begin{aligned} |\hat{Z}_w|_e &= \frac{1}{2\pi f \varepsilon_0 r} \\ &= 60\frac{\lambda_0}{r} \end{aligned} \tag{10.43}$$

where the subscript e denotes an electric field source (the Hertzian dipole). We have written (10.41) in terms of the free-space wavelength $\lambda_0 = v_0/f$ using $\eta_0 = 120\pi$ and $\beta_0 = 2\pi/\lambda_0$.

The elemental magnetic dipole (loop) is the dual of the elemental electric dipole in that we can interchange the electric and magnetic field quantities and obtain corresponding results. The fields

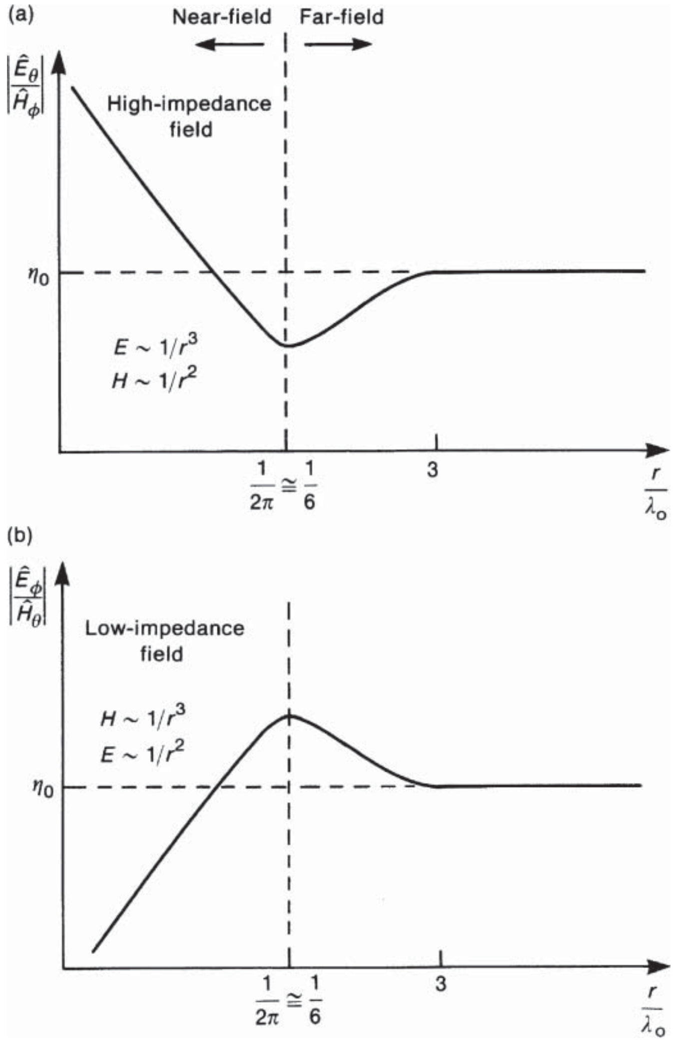

FIGURE 10.10 Wave impedance of (a) the electric (Hertzian) dipole and (b) the magnetic (loop) dipole.

of the elemental magnetic dipole (loop) are given in Eq. (7.8). The far-field components for the elemental magnetic dipole (loop) are E_ϕ and H_θ. The wave impedance for this source is therefore defined as

$$\hat{Z}_w = \frac{\hat{E}_\phi}{\hat{H}_\theta} \tag{10.44}$$

$$\hat{Z}_w = \eta_0 \frac{j/\beta_0 r + 1/(\beta_0 r)^2}{j/\beta_0 r + 1/(\beta_0 r)^2 - j/(\beta_0 r)^3} \tag{10.45}$$

The magnitude of the wave impedance is plotted against distance from the source in Fig. 10.10b. In the far field, the $1/r$ terms dominate, giving $|\hat{Z}_w| \cong \eta_0$.

Equation (10.45) reduces in the very near field to

$$\begin{aligned} \hat{Z}_w &\cong -j\eta_0\beta_0 r \;\; (\text{near field}, \;\; \beta_0 r \ll 1) \\ &\cong \eta_0\beta_0 r\angle -90^\circ \end{aligned} \tag{10.46}$$

In the near field, the magnetic field is proportional to $1/r^3$, while the electric field is proportional to $1/r^2$:

$$\left.\begin{aligned} \hat{H}_\theta &\sim \tfrac{1}{r^3} \\ \hat{E}_\phi &\sim \tfrac{1}{r^2} \end{aligned}\right\} \quad (\text{magnetic source, near field}) \tag{10.47a, b}$$

Also, in the near field of the magnetic dipole, the wave impedance is less than the intrinsic impedance of the medium. Therefore, the magnetic dipole is referred to as a *low-impedance source*. The magnitude of the wave impedance for a *magnetic field source* is therefore

$$\begin{aligned} |\hat{Z}_w|_m &= 2\pi f \mu_0 r \\ &= 2369\frac{r}{\lambda_0} \end{aligned} \tag{10.48}$$

where the subscript m denotes a magnetic field source (the magnetic loop) and we have again substituted $\eta_0 = \sqrt{\mu_0/\varepsilon_0}$, $\beta_0 = \omega\sqrt{\mu_0\varepsilon_0}$, and $\beta_0 = 2\pi/\lambda_0$ into (10.46).

Review Exercise 10.4 A very short wire in a switching power supply is modeled as an electric dipole. Determine the magnitude of the wave impedance of its radiated field at a distance of 15 cm if it carries the fundamental frequency of the switcher of 100 kHz. Evaluate this using the exact expression in (10.40) and the very-near-field approximation in (10.41).

***Answers*:** 1.2×10^6 Ω, 1.2×10^6 Ω.

Review Exercise 10.5 A transformer in a 100 kHz switching power supply is modeled as a small magnetic loop (dipole). Determine the magnitude of the wave impedance of its radiated field at a distance of 15 cm. Evaluate this using the exact expression in (10.45) and the approximate expression in (10.46).

***Answers*:** 0.118 Ω, 0.118 Ω.

The distinction between electric and magnetic sources will allow us to translate much of our results obtained for far-field sources to the case of near-field sources. There are numerous examples of such sources. For example, a transformer is constructed of turns of wire wound on a magnetic core. The electromagnetic field in the vicinity of this source tends to be predominantly magnetic. In fact, the transformer resembles the magnetic loop. For this source, the near fields have the properties that the wave impedance is much less than η_0, and the electric field varies with distance as $1/r^2$, while the magnetic field varies as $1/r^3$. Examples of electric field sources are spark gaps and other points where arcing takes place, such as at the brushes of a dc motor. For this source the near fields have the properties that the wave impedance is much greater than η_0, and the magnetic field varies with distance as $1/r^2$, while the electric field varies as $1/r^3$.

10.3.2 Electric Sources

The basic mechanisms of shielding observed for far-field sources are prevalent for near-field sources, but the type of source is critical to determining effective shielding methodologies. An exact solution for this problem is considerably more difficult than for the uniform plane-wave source case [8–10]. As an approximation, we write the shielding effectiveness as the product of a reflection term, an absorption term, and a multiple-reflection term, and obtain each factor using the previous results but substituting the wave impedance $\hat{Z}_w$ for η_0 in those equations. The absorption loss term is unaffected by the type of source.

The reflection loss is obtained by substituting the wave impedance for intrinsic impedance of the free space in (10.20):

$$\begin{aligned} R_{\text{dB}} &= 20\log_{10}\left|\frac{(\hat{Z}_w+\hat{\eta})^2}{4\hat{Z}_w\hat{\eta}}\right|_{\text{dB}} \\ &\cong 20\log_{10}\left|\frac{\hat{Z}_w}{4\hat{\eta}}\right| \end{aligned} \tag{10.49}$$

Substituting the wave impedance for electric field sources from (10.43) and the approximation for a good conductor from (10.32) gives

$$R_{e,\text{dB}} = 322 + 10\log_{10}\left(\frac{\sigma_r}{\mu_r f^3 r^2}\right) \tag{10.50}$$

The reflection loss for an electric field source is plotted in Fig. 10.11 for a copper shield and various distances from the source to the shield [3]. The reflection loss for a uniform plane-wave source is shown to illustrate the asymptotic convergence as the source-to-shield distance is increased. Observe in this figure that the reflection loss for near-field electric sources is considerably higher than for a uniform plane-wave source. It also increases with decreasing distance between the source and the shield.

10.3.3 Magnetic Sources

Again, the absorption loss is the same as for uniform plane-wave sources. The reflection loss for near-field magnetic sources is obtained by substituting the wave impedance from (10.48) into (10.49) to give

$$R_{m,\text{dB}} = 14.57 + 10\log_{10}\left(\frac{fr^2\sigma_r}{\mu_r}\right) \tag{10.51}$$

Figure 10.11 also shows the reflection loss for near-field, magnetic sources for various source-shield distances and frequency for a copper shield [3]. Observe that the reflection loss decreases for decreasing frequencies and is less than for the plane-wave reflection loss. Consequently, reflection loss is usually negligible for lower frequencies. Also, the absorption loss is small for low frequencies, so that other techniques must be used for shielding against low-frequency, near-field magnetic sources.

Olson et al. [10] have shown that the expression for the near-field reflection loss for magnetic sources in (10.51) provides reasonably accurate predictions if we replace the distance r with $r/2$.

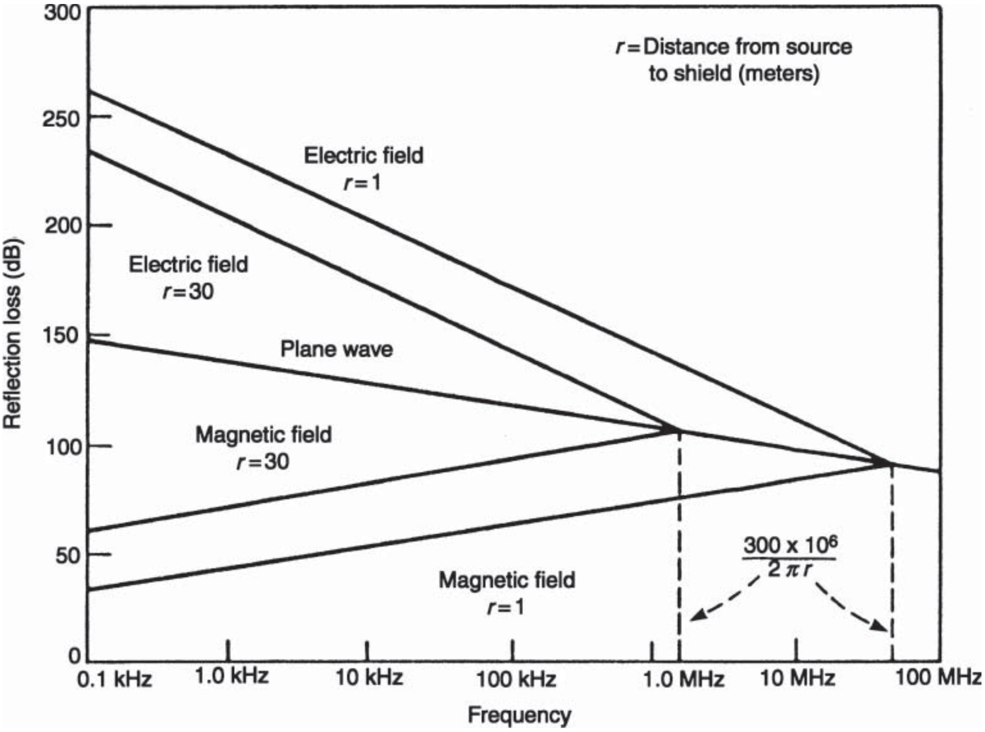

FIGURE 10.11 Reflection loss of near-field electric and magnetic sources [3]. Source: Ott [3]/John Wiley & Sons.

Review Exercise 10.6 Determine the reflection loss for the problem in Review Exercise 10.4 if the shield is aluminum.

***Answer*:** 186 dB.

Review Exercise 10.7 Determine the reflection loss for the problem in Review Exercise 10.5 if the shield is stainless steel.

***Answer*:** 4 dB.

10.4 LOW-FREQUENCY, MAGNETIC FIELD SHIELDING

In the previous sections, we have seen that *for far-field* (*uniform plane-wave*) *sources reflection loss is the predominant shielding mechanism at the lower frequencies, while absorption loss is the predominant shielding mechanism at the higher frequencies. For near-field electric sources*, the situation is to a large degree unchanged from the uniform plane-wave case: *Reflection loss is predominant at the lower frequencies, while absorption loss is predominant at the higher frequencies*. For near-field magnetic sources, the situation is quite different at low frequencies. *Absorption loss tends to be the dominant shielding mechanism for near-field, magnetic sources at all frequencies*. However, both reflection and absorption loss are quite small for near-field magnetic sources at low frequencies,

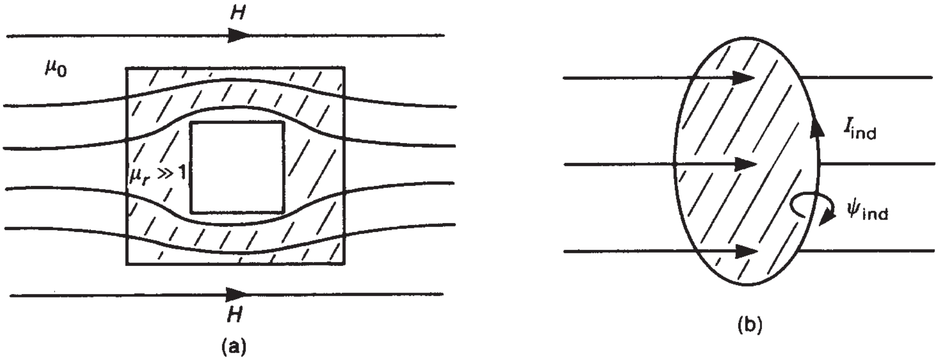

FIGURE 10.12 Two important methods of shielding against low-frequency magnetic fields: (a) using a highly permeable ferromagnetic material to divert the magnetic field; (b) using a "shorted turn" of conductor to generate an opposing magnetic field.

so that other, more effective, methods of shielding against low-frequency magnetic sources must be used.

There are two basic methods for shielding against low-frequency magnetic sources: diversion of the magnetic flux with high-permeability materials and the generation of opposing flux via Faraday's law, commonly known as the "shorted-turn method." The diversion of magnetic flux with a low-reluctance (high-permeability) path is illustrated in Fig. 10.12a. Assuming the external medium is free space with $\mu = \mu_0$ and the shield is constructed of a ferromagnetic material having $\mu = \mu_r \mu_0$ with $\mu_r \gg 1$, the magnetic field will tend to concentrate in the low-reluctance ferromagnetic path and as such will be diverted from affecting the region interior to the shield. In the "shorted-turn" method illustrated in Fig. 10.12b, a conductor loop such as a wire is placed such that the incident magnetic field penetrates the surface bounded by the loop, thereby inducing, according to Faraday's law, a current I_{ind} in the loop, and associated magnetic flux ψ_{ind}. This induced magnetic flux is of a polarity or direction as to counteract the original incident magnetic field, and so the net magnetic field in the vicinity of the loop is reduced. There are numerous applications of these two notions. These represent the majority of situations where shielding can be effective in the reduction of the effect of low-frequency magnetic fields.

There are two factors, however, that may degrade the effectiveness of the flux diversion technique and must be kept in mind:

1. The permeability of ferromagnetic materials decreases with increasing frequency.
2. The permeability of ferromagnetic materials decreases with increasing magnetic field strength.

Manufacturers of ferromagnetic materials tend to specify the relative permeability of the material at a low frequency such as 1 kHz so that the stated value of μ_r may be the largest that will be obtained. For example, Mumetal has a relative permeability of over 10,000 from dc up to around 1 kHz, as shown in Fig. 10.13 [3]. Above 1 kHz, the relative permeability of Mumetal decreases dramatically, and above around 20 kHz, it is no greater than that of cold-rolled steel. Therefore, high-permeability materials such as Mumetal are more effective for magnetic fields than less costly materials such as steel below a few tens of kilohertz. In order to shield against magnetic fields above 20 kHz, steel is as effective as these high-permeability materials. This is why *shielding enclosures for switching power supplies are constructed from steel rather than Mumetal.* Steel is less expensive than Mumetal and is as effective at the switcher fundamental frequency (20–100 kHz) and the harmonics of the switcher.

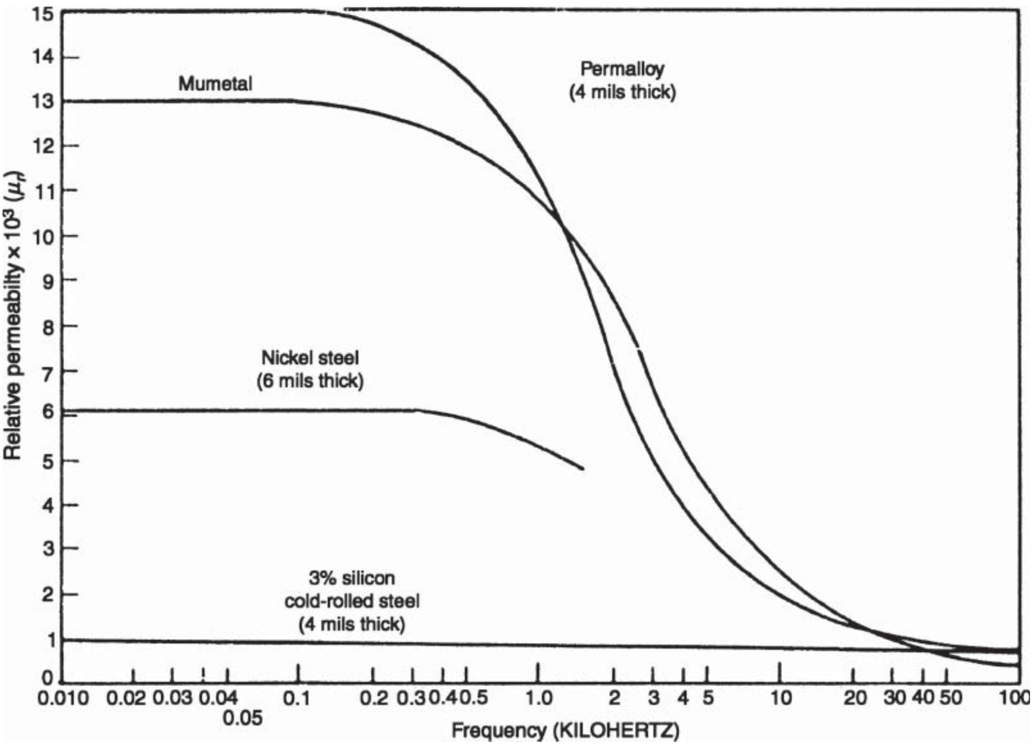

FIGURE 10.13 Illustration of the frequency dependence of various ferromagnetic materials [3]. Source: Ott [3]/John Wiley & Sons.

Shielding the power supply prevents the low-frequency, high-level magnetic fields of the switching transformer from radiating to other PCBs or wires in the product, where they may cause functional problems or be conducted out the power cord, causing conducted emission problems.

On the other hand, shielding against 60 Hz interference is more effective with Mumetal if the field strengths are not too large that they *saturate* the material. This phenomenon of saturation of ferromagnetic materials by high-level magnetic fields was discussed in Chapter 5 and is illustrated in Fig. 10.14a. The slope of the $B-H$ curve is proportional to the relative permeability of the material. The magnetic field intensity is proportional to the ampere turns if a series of turns of wire carrying current I is wound around the material. Thus high currents tend to give high levels of H where the slope of the curve is flatter, resulting in a lowering of μ_r for high levels of magnetic fields. Thus, even though Mumetal may appear to be an effective shielding material for 60-Hz magnetic fields due to its high relative permeability at this low frequency, this may not be realized, since high currents are usually associated with the 60 Hz power frequencies. Manufacturers of ferromagnetic materials typically state the *initial* relative permeability of their materials at (1) a low frequency, typically 1 kHz; and (2) low field levels. A typical way of minimizing the saturation effect is to use two shields, as shown in Fig. 10.14b. The first shield has a low μ_r and low susceptibility to saturation. The purpose of this shield is to reduce the incident magnetic field so that it does not saturate the second shield, which has a high μ_r and a high potential for saturation. Typically, the first layer provides some reflection loss for the electric field.

Although not discussed in Chapter 2, there are some regulatory agencies that impose limits on the low-frequency magnetic field emissions of a product. The radiated magnetic fields are to be

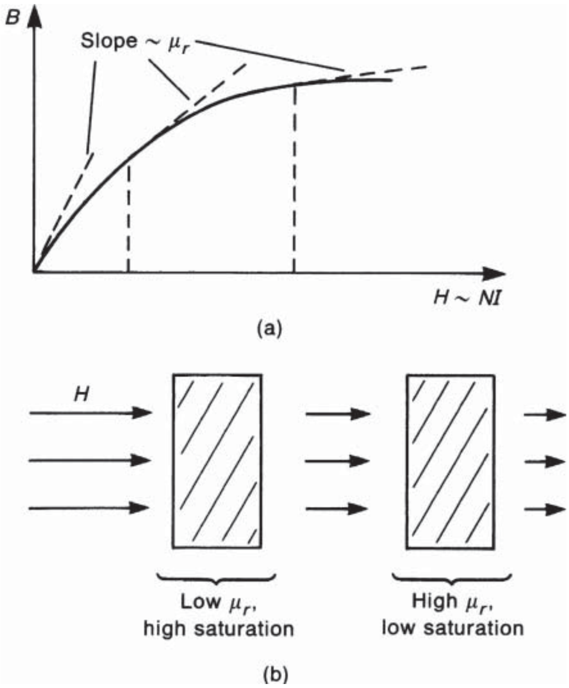

FIGURE 10.14 Illustration of the important phenomenon of saturation of ferromagnetic materials: (a) the *B–H* curve; (b) use of a multilayer magnetic shield to reduce the effects of saturation.

measured with a loop antenna at frequencies below 30 MHz. Low-frequency radiated magnetic fields from transformers of switching power supplies tend to be among the major problems in complying with these legal requirements.

A common application of the “shorted-turn” effect in the reduction of magnetic fields is with transformers of switching power supplies. A conductive “turn” consisting of a contiguous strip of copper tape is wrapped around the transformer as shown in Fig. 10.15a,b. The objective of this “shorted turn” or “band” is to reduce the radiated magnetic field of the leakage flux of the transformer. It is important to place the loop such that the surface bounded by the loop is as perpendicular as possible to the flux that it is intended to cancel, so that the maximum emf will be induced in the band. There are cases where two orthogonal bands must be used. The transformer core is frequently “gapped” in order to reduce the magnetic flux levels and prevent saturation of the core, as discussed in Section 6.3.3. The leakage flux at this gap (which can be quite intense) may lie orthogonal to that from the windings, depending on the location of the gap. If this leakage flux does not penetrate the area bounded by the first band orthogonal to that area, a second band may be needed orthogonal to the first band. This use of bands on transformers, in particular switching transformers of switching power supplies, is quite effective in allowing the product to meet the regulatory limits on low-frequency magnetic fields. It is also effective in preventing interference from the transformer, such as with a video monitor that may be placed on top of the product and close to the transformer. Photographs of switching transformers having these “bands” placed around them are shown in Fig. 10.15c.

Shielding can be an effective suppression method if it is used properly and fits the problem at hand, such as in low-frequency magnetic shielding for power supply enclosures and bands on transformers. Shielding should not be relied on in all instances since it is all too often misapplied and too much is expected of it.

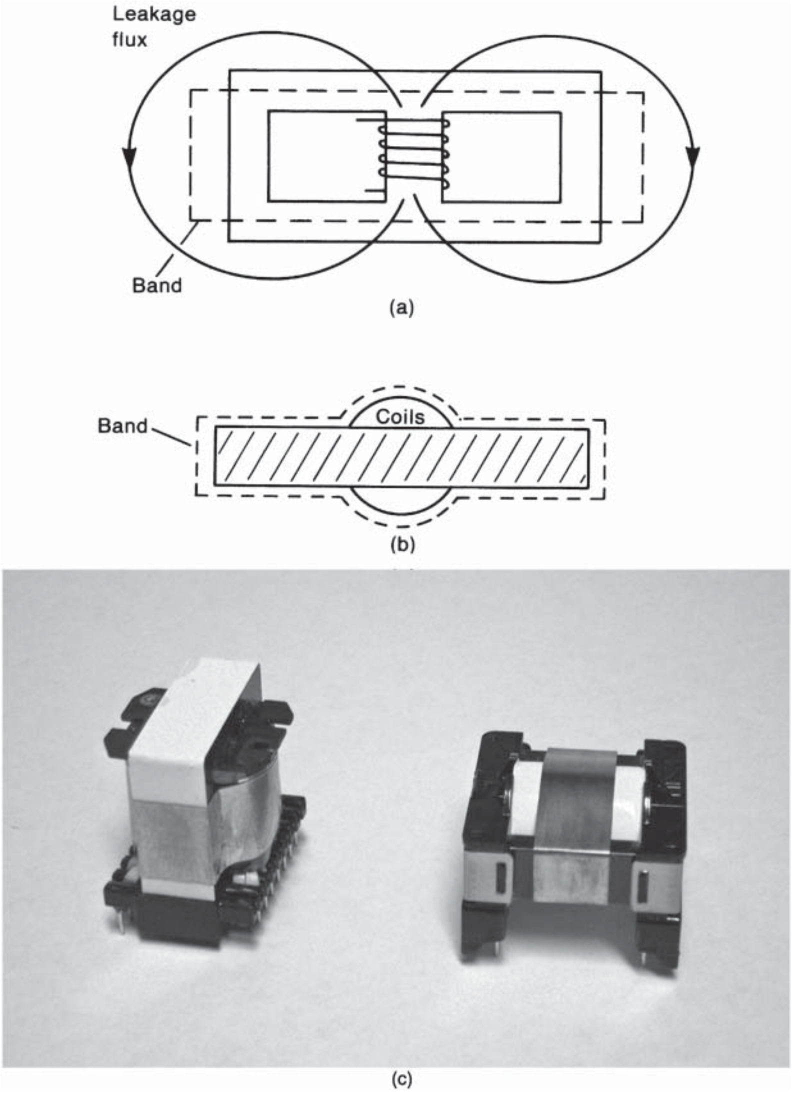

FIGURE 10.15 Use of the shorted-turn effect (bands) to reduce the radiated magnetic fields of transformer leakage flux: (a) side view; (b) top view; (c) photograph of bands on a switching transformer used to reduce the radiated magnetic field due to gaps in the “E-cores”. Source: Courtesy of G-MAG, Inc.

10.5 EFFECTS OF APERTURES

As was pointed out earlier, there are numerous cases where openings in an otherwise contiguous shield cannot be avoided for practical reasons. One of the more common ones is the need to ventilate the internal electronics for thermal reasons. Fans are frequently employed to move hot air inside the shield to the outside. The reader will observe that these types of openings are frequently in the form of a large number of small holes rather than one large hole. There is an important reason for this, which is illustrated in Fig. 10.16. Consider the solid shield shown in Fig. 10.16a. Currents are induced to flow in this shield, and it is these currents and their associated fields that generate “scattered” fields,

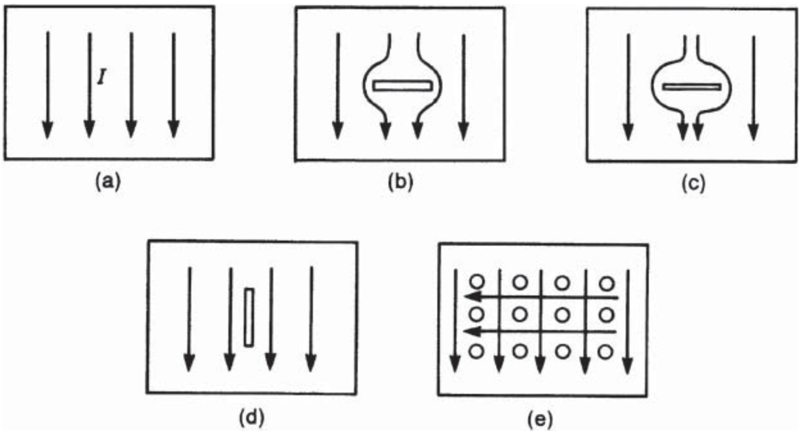

FIGURE 10.16 Illustration of the effects of slots on induced currents on shields. Many small holes provide as much ventilation as does one long slot, but perturb the induced currents much less, thereby reducing the degradation caused by the aperture: (a) no apertures; (b) long, wide slot perpendicular to the direction of induced currents; (c) long, narrow slot perpendicular to the direction of induced currents; (d) long, wide slot parallel to the direction of induced currents; (e) large number of small holes.

which counteract or reduce the effects of incident fields. This was illustrated in Section 7.6.2, where we considered a uniform plane wave incident normally to the surface of a perfect conductor. The incident field induces a surface current, which may be thought of as producing the reflected field. The reflected field is of a polarity such that it tends to cancel the incident field in order to satisfy the boundary condition that the *total electric field* tangent to a perfect conductor must be zero. In order for the shield to perform this cancellation, the induced currents must be allowed to flow unimpeded. Suppose that we place a slot in the shield perpendicular to the direction of these induced currents. The slot will interrupt the current flow and will tend to reduce the shielding effectiveness. The width of the slot does not significantly affect this, as illustrated in Figs. 10.16b,c. On the other hand, if we orient the slot parallel to the direction of the induced current, the slot will have much less effect on the shielding, as illustrated in Fig. 10.16d. Since it is not feasible to determine the direction of the induced current and place the slot direction appropriately, a large number of small holes are used instead, as illustrated in Fig. 10.16e.

It is also necessary to have access doors to allow entry into the shielded enclosure. Where these doors are closed, a gap is produced around the door that can act as a slot antenna, as discussed previously. Even though the gap opening may be quite small, the radiation potential of the gap can be quite large, as is illustrated by Babinet's principle, discussed earlier. For example, suppose that a lid is required on top of a shielded enclosure as illustrated in Fig. 10.17a. Babinet's principle shows that replacement of the gap with a solid conductor whose dimensions are those of the gap will produce the same radiated fields as those from the gap. This illustrates rather dramatically that the *length of the gap is more important than its thickness in determining the radiated emissions of the gap*. If the gap length happens to be of the order of a half-wavelength, it is clear from Babinet's principle that the gap has radiation potential similar to that of a half-wave dipole antenna. This is why it is necessary to place many screws at frequent intervals around a lid in order to break up these potential slot antennas, as illustrated in Fig. 10.17b, since shorter linear antennas tend to radiate less efficiently than do long ones. Metallic *gaskets* are frequently used to close gaps as illustrated in Fig. 10.17c. These are of the form of wire knit mesh or beryllium copper "finger stock." Gaskets should be placed on the inside of any securing screws,

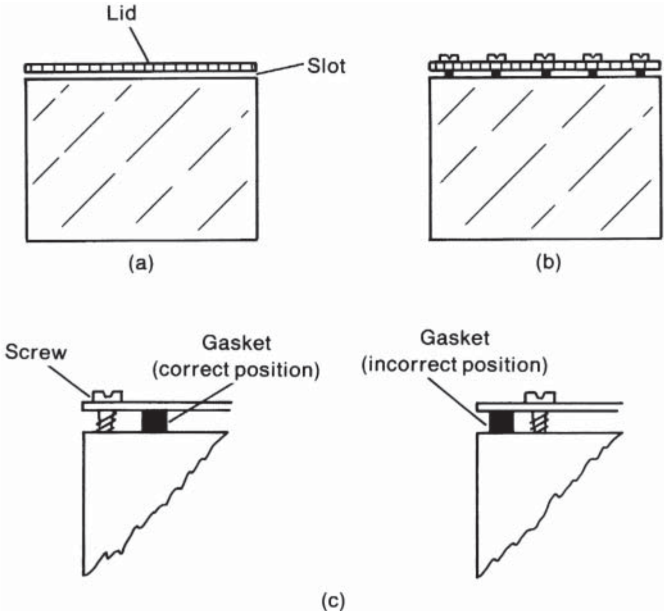

FIGURE 10.17 Illustration of the effects of slots at doors and covers: (a) the slot radiates, according to Babinet's principle, as efficiently as does a conductor of the same dimensions as the slot; (b) many closely spaced screws break up the slot length; (c) illustration of proper and improper gasket placement to reduce the radiated emissions from screws.

since if they are placed outside these screws, radiation from the screw holes will not be protected against.

Openings in shielded enclosures can also be protected by using the "waveguide above cutoff" principle [7]. A square waveguide with side dimensions d has a cutoff frequency for the propagation of higher-order modes TE_{mn} and TM_{mn} given by [7]

$$f_{c,mn} = \frac{v_0}{2d}\sqrt{m^2 + n^2} \tag{10.52}$$

The lowest-order propagating mode is the TE_{10} mode, with cutoff frequency

$$\begin{aligned} f_{c,10} &= \frac{v_0}{2d} \\ &= \frac{1.5 \times 10^8}{d} \quad (d \text{ in m}) \\ &= \frac{5.9 \times 10^9}{d} (d \text{ in in.}) \end{aligned} \tag{10.53}$$

The attenuation of a rectangular waveguide to these higher-order modes can be computed by determining the effective attenuation constant for this guide from [7, 11]

$$\alpha_{mn} = \omega\sqrt{\mu_0\varepsilon_0}\sqrt{\left(\frac{f_{c,mn}}{f}\right)^2 - 1} \tag{10.54}$$

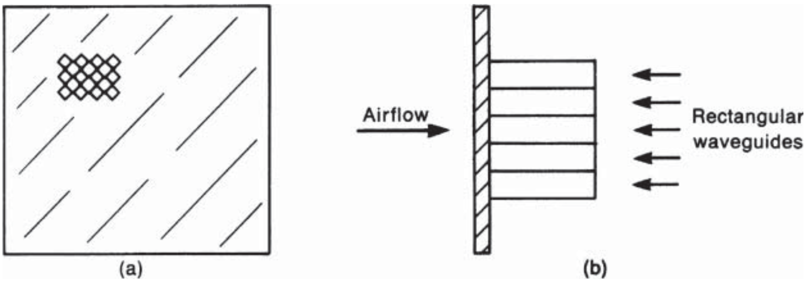

FIGURE 10.18 Use of the waveguide-below-cutoff principle to provide ventilation of an enclosure and to minimize the electromagnetic field penetrations: (a) front view; (b) side view.

where $f_{c,\,mn}$ is the cutoff frequency of the particular mode. Assuming that the frequency of the incident wave is much less than the cutoff frequency for the mode, (10.54) simplifies to

$$\begin{aligned}\alpha_{mn} &\cong \frac{2\pi f}{v_0}\frac{f_{c,mn}}{f} f \ll f_{c,mn} \\ &= \frac{2\pi f_{c,mn}}{v_0} \end{aligned} \tag{10.55}$$

Substituting the relation for the cutoff frequency for the lowest-order TE_{10} mode given in (10.53) gives

$$\alpha_{10} = \frac{\pi}{d} \tag{10.56}$$

The attenuation of a guide of length l is proportional to $e^{-\alpha l}$. Thus, the attenuation or shielding effectiveness afforded by one guide is

$$\begin{aligned}\mathrm{SE}_{\mathrm{dB}} &= 20\log_{10} e^{\alpha_{10} l} \\ &= \alpha_{10}\, l\, 20\log_{10} e \\ &= 27.3\frac{l}{d} \end{aligned} \tag{10.57}$$

This rather simple result shows that TE and TM modes are strongly attenuated in direct proportion to the guide length as they travel along the guide. This is the basis for the use of *waveguides below cutoff* to allow airflow into a shielded enclosure and at the same time prevent the propagation of frequencies lower than the cutoff frequency into the enclosure. Many small waveguides are welded together in a “honeycomb” fashion as illustrated in Fig. 10.18 in order to provide sufficient volume of airflow and to give the appropriate waveguide dimensions. These are placed in the walls of shielded rooms to provide ventilation and also to prevent entry of low-frequency fields.

PROBLEMS

10.1.1 Examine a typical personal computer having a metallic enclosure and list the "penetrations" that allow signals from the inside to pass to the outside, avoiding the shielding of the metallic enclosure.

10.1.2 Model the shield on a 2-m personal computer printer cable as a monopole antenna (with the metallic structure of the computer as the ground plane) and estimate the maximum radiated emissions at a measurement distance of 3 m if the voltage of the shield attachment point with respect to the metallic structure is a 1-mV, 37.5-MHz signal. [53.5 dBμV/m broadside and parallel to the cable]

10.1.3 Consult [11] to show that for the complementary slot problem shown in Fig. P10.3 that the impedance of the complementary dipole, $\hat{Z}_d$, and that of the slot, $\hat{Z}_s$, are related by $\hat{Z}_s\hat{Z}_d = 1/4\eta^2$ where the surrounding medium has intrinsic impedance η. Use this result to determine the impedance of the slot if $L = \lambda/2$ and the slot width is infinitesimally small. [$\hat{Z}_s = [(363 - j211)\ \Omega]$]

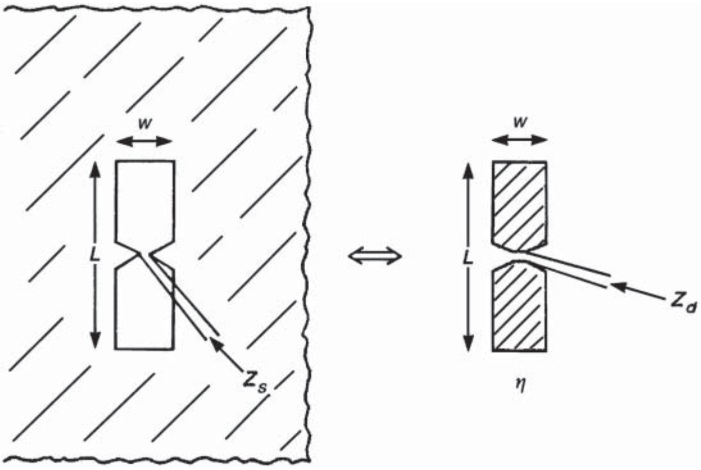

FIGURE P10.3 Source: Jordan and Balmain [11]/Pearson Education.

Section 10.2 Shielding Effectiveness: Far-Field Sources

10.2.1 Determine the skin depth at 30 MHz, 100 MHz, and 1 GHz for steel (SAE 1045). [0.048 mils, 0.026 mils, 0.0082 mils] Repeat for nickel and brass. [0.0434 mils, 0.0238 mils, 0.0075 mils, 0.93 mils, 0.51 mils, 0.16 mils]

10.2.2 Compute the intrinsic impedance of steel (SAE 1045) at 30 MHz, 100 MHz, and 1 GHz. [$0.202\angle 45^\circ\ \Omega$, $0.369\angle 45^\circ\ \Omega$, $1.17\angle 45^\circ\ \Omega$] Repeat for brass. [$3.96\times 10^{-3}\angle 45^\circ\ \Omega$, $7.24\times 10^{-3}\angle 45^\circ\ \Omega$, $2.29\times 10^{-2}\angle 45^\circ\ \Omega$]

10.2.3 Compute the electric field reflection coefficient for an air-steel interface at 30 MHz, 100 MHz, and 1 GHz. [$0.999\angle 180^\circ = -0.999$, $0.999\angle 180^\circ = -0.999$, $0.996\angle 180^\circ$] Compute the electric field transmission co-efficient for an air–steel interface at 30 MHz, 100 MHz, and 1 GHz. [$1.07\times 10^{-3}\angle 45^\circ$, $1.96\times 10^{-3}\angle 45^\circ$, $6.2\times 10^{-3}\angle 44.9^\circ$]

10.2.4 Compute the reflection loss and absorption loss for a 20 mil steel (SAE 1045) barrier at 30 MHz, 100 MHz, and 1 GHz, assuming a far-field source. [53.23 dB, 3656.6 dB, 48 dB, 6676.0 dB, 38 dB, 21,111 dB]

Section 10.3 Shielding Effectiveness: Near-Field Sources

10.3.1 Compute the reflection loss and absorption loss for a 20-mil steel (SAE 1045) barrier at 10 kHz, 100 kHz, and 1 MHz for a near-field electric source that is a distance of 5 cm from the shield. [188.02 dB, 66.76 dB, 158.02 dB, 211.11 dB, 128.02 dB, 667.6 dB]

10.3.2 Compute the reflection loss and absorption loss for a 20-mil steel (SAE 1045) barrier at 10 kHz, 100 kHz, and 1 MHz for a near-field magnetic source that is a distance of 5 cm from the shield. [−11.45 dB use $R = 0$, 66.76 dB, −1.45 dB use $R = 0$, 211.11 dB, 8.55 dB, 667.6 dB]

10.3.3 A transformer consists of 2000 turns of wire with a radius of 5 cm and carries a 50 kHz current at a level of 1 A. Model this as a small loop and compute the magnetic flux density at a distance of 3 m from the loop center in the plane of the loop. [5.8×10^{-8} Wb/m^2]

Section 10.4 Low-Frequency, Magnetic Field Shielding

10.4.1 Discuss the advantageous shielding aspects of a typical paint can that has a press-on lid, a zinc coating, and a tin metal can.

Section 10.5 Effect of Apertures

10.5.1 Determine the length of a waveguide to provide 100 dB attenuation if the guide dimensions are 100 × 100 mils. [9.3 mm] What range of frequencies are attenuated by this guide (at least in the waveguide propagation mode) [dc to 59 GHz]

REFERENCES

1. E. F. Vance, Electromagnetic-interference control, *IEEE Trans. Electromagn. Compat.* EMC-22, 319–328 (1980).
2. C. A. Balanis, *Antenna Theory Analysis and Design*, Harper & Row, New York, 1982.
3. H. W. Ott, *Noise Reduction Techniques in Electronic Systems*, 2nd ed., Wiley-Interscience, New York, 1988.
4. S. A. Schelkunoff, *Electromagnetic Waves*, Van Nostrand, NJ, 1943.
5. R. B. Schulz, V. C. Plantz, and D. R. Brush, Shielding theory and practice, *IEEE Trans. Electromagn. Compat.* EMC-30, 187–201 (1988).
6. C. R. Paul, *Electromagnetics for Engineers*, Wiley, Hoboken, NJ, 2004.
7. C. R. Paul and S. A. Nasar, *Introduction to Electromagnetic Fields*, 2nd ed., McGraw-Hill, New York, 1987.
8. P. R. Bannister, New theoretical expressions for predicting shielding effectiveness for the plane shield case, *IEEE Trans. Electromagn. Compat.* EMC-10, 1–7 (1968).

9. P. R. Bannister, Further notes for predicting shielding effectiveness for the plane shield case, *IEEE Trans. Electromagn. Compat.* EMC-11, 50–53 (1969).
10. R. G. Olsen, M. Istenic, and P. Zunko, On simple methods for calculating ELF shielding of infinite planar shields, *IEEE Trans. Electromagn. Compat.* EMC-45, 538–547 (2003).
11. E. C. Jordan and K. G. Balmain, *Electromagnetic Waves and Radiating Systems*, 2nd ed., Prentice-Hall, Englewood Cliffs, NJ, 1968.

CHAPTER ELEVEN

System Design for EMC

The purpose of this final chapter is to provide an application of the previously discussed principles in the design of an electronic system to achieve electromagnetic compatibility with its environment, specifically, to minimize (1) its potential for interfering with other electronic systems, (2) its susceptibility (maximize its immunity) to electromagnetic emissions from other sources, and (3) its potential for interfering with itself. The word “minimize” is used here rather than “eliminate” since it is virtually impossible to guarantee that these EMC problems will be eliminated from the initial design. There also tends to be a *reciprocity* between interference due to the system’s emissions and its susceptibility to emissions from other systems. If we design a system to minimize its electromagnetic emissions, its susceptibility to electromagnetic emissions from other sources also tends to be reduced, and vice versa.

In the course of the development of an electronic product, we tend to become sensitized to the need to pass the governmental regulations on, for example, the product’s radiated and conducted emissions. This is natural since if we do not comply with the governmental regulations, any other considerations are a moot point—the product cannot be brought to market. However, it is important to keep in mind that a successful EMC design encompasses not only complying with the governmental legal requirements but also making the product a quality one. If, for example, we neglect to ensure that the product will not be immune to electrostatic discharge (ESD) events when this is not a governmental requirement (as in the USA), then the company will acquire a poor reputation and future sales will be affected. Therefore, all three basic EMC design objectives must be kept in mind in order to enable the EMC engineer to identify any aspect of the design that would impact these goals. Producing reliable, quality products is a crucial part of a company’s reputation.

There is a wide spectrum of electronic products that must be designed for EMC. There are a very large number of *low-cost products* such as inkjet printers, laserjet printers, electronic typewriters, and CD, DVD, and VHS players, as well as portable music devices in the market today. The market price for these is typically under $200–$500 U.S. Cost is a paramount issue for these systems. Hence, they do not enjoy the luxury of printed circuit boards (PCBs) having many levels of innerplanes. Typically, these low-cost electronic products contain PCBs that are double-sided, i.e., without innerplanes, or at most Two Sided Two Planes (2S2P) PCBs that have the two outer layers (two sides) for component placement and routing of traces, as well as two innerplanes (two planes): one for power and one for ground. Innerplane boards with more layers become very expensive to design and produce and hence

Introduction to Electromagnetic Compatibility, Third Edition. Clayton R. Paul, Robert C. Scully, and Mark A. Steffka.
© 2023 John Wiley & Sons, Inc. Published 2023 by John Wiley & Sons, Inc.

dramatically affect the selling price of the product. Since selling price is so low, manufacturing cost is a severe constraint in order that the company's offerings remain competitive in today's markets. At the other end of the spectrum are the high-end servers costing thousands of dollars for which innerplane PCBs are required and can be afforded. The emphasis in this chapter will be on low-cost products that typically have PCBs without innerplanes or at most 2S2P boards. For these products, successful EMC design practice is rather simple and can be easily described. This will constitute our major emphasis.

Successful EMC design of a product depends on the *early and continuous* application of the principles outlined in the text. In order to minimize unnecessary costs and schedule delays, it is imperative that an experienced EMC engineer be involved at the very early stages of product development. This involvement should begin as early as the product conceptual development. Decisions about the product enclosure and its packaging are usually the first to be made, but these can dramatically impact a successful EMC design. These and other early decisions that are made remove many of the EMC engineer's options. It is important to realize that virtually all other engineers involved in the product development do not understand or appreciate the EMC engineer's perspective. For example, cable routing can be a serious EMC concern. Figure 11.1 illustrates such a case. A new digital product was being designed, and in order to minimize cost, it was decided to use a system PCB from a previous product. However, when the product enclosure was redesigned, this necessitated that the PCB system board from the previous product be rotated 90° from its use in the previous product. The connector on the PCB for the flat cable from the disk drive in the previous product was designed to be directly beneath the disk drive, and hence the length of flat cable required was minimized. Now, however, because of the board rotation, the disk drive connector is far away from the disk drive so that the flat cable must be lengthened. The EMC engineer would have seen that this could cause radiated emission problems because longer cables tend to radiate better than do short ones. However, the real problem in this new orientation is that the flat cable now lies directly on top of the system clock module. The non-EMC engineers do not see this as a problem since "there is no hard electrical connection between the wires in the cable and the clock module." The EMC engineer would have immediately seen the "hidden schematic"; there is considerable parasitic capacitance between the case of the clock module and the cable allowing coupling between the two that could be as significant as if they were "hard-wired." It turns out that this was not detected early in the design because no EMC engineer was assigned to the project. Toward the end of the design, preliminary EMC testing showed a significant coupling that produced radiated emissions exceeding the regulatory specifications. In order

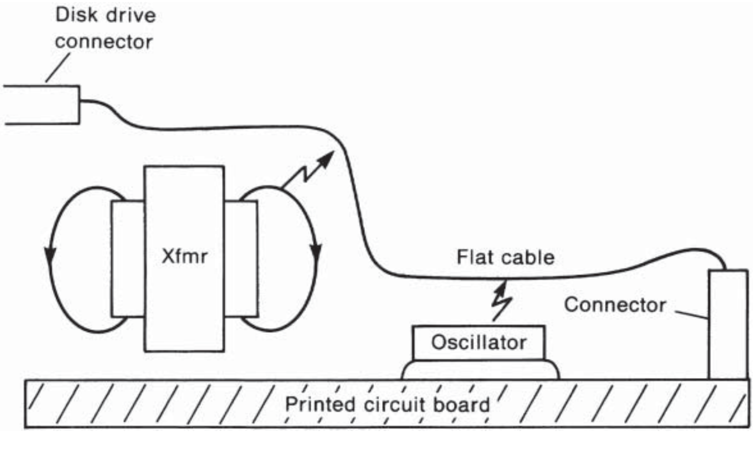

FIGURE 11.1 Packaging considerations that affect radiated and conducted emissions of a product.

to fix this, a thickness of insulation was placed between the clock module and the cable, thereby raising the cable some distance above the module. This, of course, drastically reduced the parasitic capacitance and hence the radiated emissions. Why was this not an acceptable “fix”? The company had a state-of-the-art automated assembly line; the entire product was to be assembled completely by robots. The automated assembly line was a key feature in keeping the manufacturing cost low so that the market price was competitive. Unfortunately, placing the separator beneath the cable was an operation that the automated manufacturing line could not implement and workers were needed to take each unit off the line, remove the product covers, insert the spacer, replace the product covers, and put the product back on the line for further processing. This added cost and production delay that virtually negated the significant cost savings of the automated manufacturing line. If an experienced EMC engineer had been involved early, this would have been an obvious problem and a cost-effective solution could have been identified before the design had proceeded to this point.

Another example of the consequences of early design decisions and the lack of an experienced EMC engineer on the design team at the early stages is illustrated in Fig. 11.2. An electronic typewriter was being developed. The product contained two PCBs: one contained the system electronics and one contained the switching power supply for the product. After the product packaging was designed, the only place where these PCBs could be located was vertically at the rear of the machine and *in proximity*. The switching power supply PCB contained the usual switching transformer, which switched at 50 kHz. The stray magnetic fields around this transformer were intense and extended some distance from that PCB. Because of the proximity of the two PCBs, these magnetic fields coupled strongly to the electronics PCB and created significant interference with the machine function. By the time the prototypes were tested and the problem uncovered, it was too late to change the PCB locations. To fix the problem a shielded cage was constructed around the power supply PCB. It was constructed of steel so that the magnetic fields of the switching transformer were diverted (see Section 10.4 of Chapter 10). But this added cost (for EMC reasons and not for added functional performance) dramatically increased the product cost, thereby impacting the product market price and company profit. The EMC engineer would view the switching transformer as a small current loop (see Section 7.1.2 of Chapter 7). The very near magnetic fields of the small current loop decrease with distance away from the loop as $1/r^3$. Hence, the electronics PCB would not have to be moved very far away from the power supply PCB in order to dramatically reduce this magnetic field coupling and the resulting interference. It is important to point out that the non-EMC engineers on the project did not understand how the signals from one PCB could interact with those of other PCB since they were not “connected”; they did not see the “hidden schematic.”

When the product is tested to determine its compliance to the regulatory limits (usually toward the end of the design cycle), EMC problems will usually surface. Electronic products today are

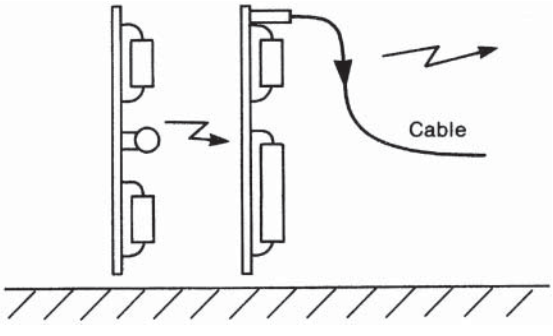

FIGURE 11.2 Illustration of the inadvertent coupling between PCBs due to their proximity.

so complex that it is virtually impossible to consider all EMC issues in the design. However, if attention is paid to EMC throughout the design, the major problems will have been averted, and it will be easier to remedy those problems that do surface without the necessity of adding expensive and difficult-to-implement "fixes." If, for example, the system clock oscillator were placed on the PCB where an input/output (I/O) cable exits the board, parasitic coupling from the oscillator or its lands to the I/O cable lands could result in significant radiated emissions from that cable. During the final testing, there is little that can be done other than to perform a repeated PCB layout, which is expensive and more importantly requires significant delays in the product development schedule. Vigilance to EMC throughout the product design cycle is an important aspect of preventing costly and inconvenient EMC problems.

It is important to keep in mind that the primary objective in applying the EMC design principles and concepts of this text to product design is not to remove all EMC problems from the design. There are always going to be EMC problems that will surface during testing that occurs later into the design cycle. The primary objective is to take care of the major and obvious problems and to leave options for fixing the remaining problems with minimal impact on product cost and schedule delay. For example, we now realize that the rise/falltimes of a clock signal determine the high-frequency spectral content of the signal, and higher frequencies tend to radiate more efficiently than do lower frequencies. Hence, we need a "plan B" for dealing with this potential problem later in the design. In the early layout of the PCB, the layout personnel are instructed to manually place the clock module very close to the ASIC or microprocessor it serves as shown in Fig. 11.3. However, anticipating that the rise/falltimes of this clock may need to be increased to reduce its high-frequency content, pads should be placed so that (a) a series resistor can be inserted in the lands and (b) a capacitor can be inserted across the lands forming a low-pass filter. In the beginning, the capacitor pads would not be populated, and a 0 Ω surface-mount resistor could be placed in series with the clock lands. Later in the design, if problems are uncovered necessitating increasing the clock rise/falltimes, then the capacitor can be added and the value of the series resistor can be changed. Why is this significant? The answer is that no time-consuming repeated PCB layout would be required; only the bill of materials (parts list) need to be changed. This is a virtually cost-free solution. Another similar problem has to do with the proper "grounding" point for the Faraday shield of a switching transformer. (See Section 6.3 of Chapter 6.) Some advocate attaching the shield to the ac power input side of the power supply, while others advocate connecting the shield to the electronics side of the power supply. While there are good arguments for both solutions, it often happens that the best solution does not conform to the best argument. Hence, the "plan B" for this problem would be to place pads in both places and determine the best connection point during preliminary EMC testing. Therefore, *assume that the design will have EMC problems and have a plan B for dealing with them.*

A considerable amount of effective EMC design can be achieved by simply changing the way one thinks about or visualizes electrical and electromagnetic phenomena. This is perhaps the major

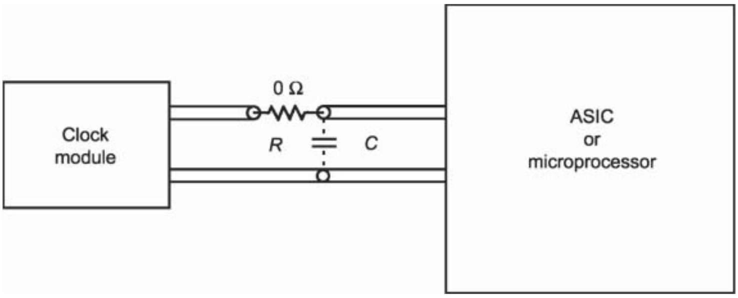

FIGURE 11.3 Having a "plan B" to reduce the spectral content of a clock if needed.

objective that the author has tried to achieve with this text. Now that the reader has studied the previous chapters, he/she can entertain a vast array of new ways to think about or visualize electrical and electromagnetic phenomena. The difference between an EMC engineer and other engineers is that other engineers do not “see this enlarged picture of possibilities” and hence do not suspect that EMC problems can be caused by such a large number of processes and possibilities. Hence, other engineers do not “anticipate these.” The major portion of effective EMC design can be dramatically achieved if we simply “change the way we think about electrical phenomena.”

11.1 CHANGING THE WAY WE THINK ABOUT ELECTRICAL PHENOMENA

Perhaps the most important aspect of becoming effective at EMC design is to begin routinely thinking of the nonideal behavior of electrical components in addition to the ideal behavior that we have been taught to. It is very important to keep in mind the range of frequencies we will be concerned with

Conducted emissions: 150 kHz–30 MHz
Radiated emissions: 30 MHz– > 1 GHz

We are seldom concerned with low frequencies (other members of the design team are concerned with low frequencies). The importance of this is that the electrical and electronic components in the system (wires, PCB lands, resistors, capacitors, inductors, ferrites, and IC modules) typically behave far from the ideal at these frequencies. If we think only in terms of ideal behavior of electrical and electronic components, we will not be able to see or anticipate the nonideal electrical paths and hence will not be able to consider other possible causes for radiated or conducted emissions. Therefore, we will have inadvertently reduced our possibilities for correcting EMC problems; we will not have the ability to see “the hidden schematic.”

11.1.1 Nonideal Behavior of Components and the Hidden Schematic

We discussed in Chapter 5 how a capacitor can act like and become equivalent to an inductor above the self-resonant frequency caused by the lead inductance. Hence, if a capacitor is added for noise suppression purposes to divert noise currents from cables, exactly the opposite may happen if the frequency of the noise current is above the self-resonant frequency of the capacitor. In addition, stray or parasitic capacitance that may be inconsequential at relatively low frequencies will become significant at higher frequencies since a capacitor’s impedance is $\hat{Z} = -j(1/\omega C)$ and $\omega = 2\pi f$. Consequently, the impedance of a capacitor decreases with increasing frequency. Mutual capacitance between sections of a circuit may be inconsequential at low frequencies, but at higher frequencies, these may provide very low impedance connections that are as effective as “hard-wired” connections. An example of this is the parasitic capacitance of a motor (dc, stepper, or ac) between the input leads and the frame of the motor. Because the rotor and the stator of the motor consist of coils of wire that are in proximity (to reduce the reluctance of the magnetic path between them), there is a very large capacitance between the input (rotor) and the frame of the motor (attached to the stator). The frame of the motor is frequently bonded to the structure of the product in order to provide thermal heat sinking of the motor. The consequence here is that high-frequency noise currents from the motor driver electronics can be inadvertently placed on the frame of the product as common-mode currents where they contaminate the machine electronics and radiate efficiently. (See Section 5.10 of Chapter 5.)

The strong *duality* existing in electromagnetics has been pointed out numerous times throughout this text. Hence, if we recognize the effects of parasitic capacitance as pointed out in the previous paragraph, we should also immediately expect to see the dual effects of parasitic inductance. An example of this is the inductance of connection leads of components. There is a tendency to concentrate on parasitic capacitance and neglect inductance, and this should be avoided.

Perhaps the most important "components" of an electronic device from the standpoint of EMC are the wires and PCB lands in it. A very serious mistake is to view them as "perfect conductors," which they are not. As we will see, typical wires and PCB lands have an inductance of some 15–30 nH/in. This parameter is referred to as *partial inductance* and will be discussed in Section 11.2.3. The wire or PCB land will also have a resistance giving the equivalent circuit shown in Fig. 11.4. We examined some of these issues in Chapter 5. A wire of radius r_w will have a per-unit-length resistance and internal inductance (due to magnetic flux internal to the wire) of [1]

$$r_i = \begin{cases} \dfrac{1}{\sigma \pi r_w^2} & r_w < 2\delta \ \Omega/\text{m} \\ \dfrac{1}{\sigma 2\pi r_w \delta} & r_w > 2\delta \ \Omega/\text{m} \end{cases} \tag{11.1a,b}$$

$$l_i = \begin{cases} \dfrac{\mu_0}{8\pi} = 50\ \text{nH/m} = 1.27\ \text{nH/in.} & r_w < 2\delta \\ \dfrac{1}{4\pi r_w}\sqrt{\dfrac{\mu_0}{\pi\sigma}}\dfrac{1}{\sqrt{f}}\ \text{H/m} & r_w > 2\delta \end{cases} \tag{11.1c,d}$$

where δ is the skin depth

$$\begin{aligned} \delta &= \frac{1}{\sqrt{\pi f \mu_0 \sigma}} \\ &= \frac{6.6 \times 10^{-2}}{\sqrt{f}}\ \text{m} \\ &= \frac{2.6}{\sqrt{f}}\ \text{in.} \end{aligned} \tag{11.1e}$$

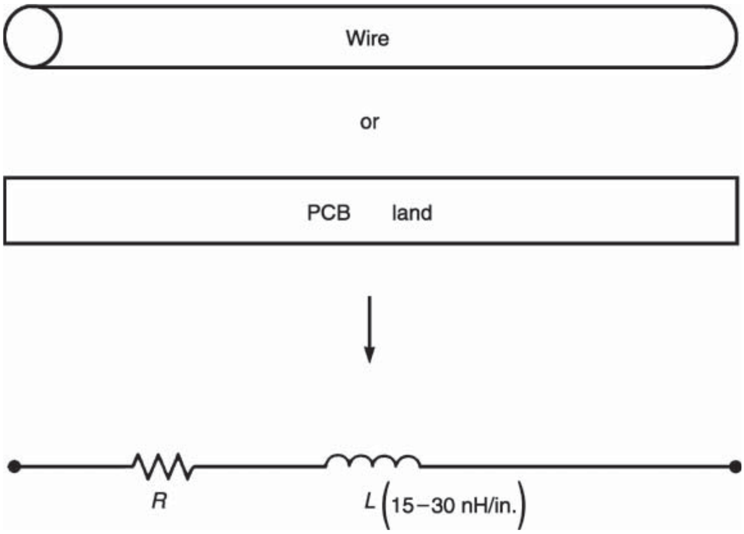

FIGURE 11.4 Illustration of the impedance of a wire or PCB land.

and σ is the conductivity (assuming copper, $\sigma = 5.8 \times 10^7$ S/m), and $\mu_0 = 4\pi \times 10^{-7}$ H/m is the permeability of free space (assuming that the conductor is not ferromagnetic, which copper is not). Observe that the wire resistance starts out at its dc level, but at high frequencies increases rapidly as $\sqrt{f}$. (See Fig. 5.1 of Chapter 5.) For example, a 20-gauge, solid copper wire has a radius of 16 mils, which is equal to two skin depths at a frequency of 106 kHz. Hence, below 106 kHz, the wire has, according to (11.1a), a per-unit-length resistance of 33 mΩ/m = 0.84 mΩ/in. At a frequency of 100 MHz, the wire radius is much larger than a skin depth and (11.1b) applies, giving the per-unit-length resistance as 1.02 Ω/m = 26 mΩ/in. It is very important to observe that the internal inductance of a wire (due to the magnetic flux internal to the wire) starts out at 1.27 nH/in. but decreases after that at a rate of the square root of the frequency. This is because the current crowds to the surface of the wire as frequency increases due to skin effect and hence the magnetic flux internal to the wire decreases to zero. The external inductance (partial inductance) that is due to the magnetic flux external to the wire is on the order of 15–30 nH/in. Hence, the internal inductance of the wire is usually negligible.

We will frequently refer to the *inductance of a conductor*. This is not the internal inductance since the internal inductance is in series with and negligible compared to the external or partial inductance. Inductance is a property of a closed loop. All currents must form closed loops, although the extent of the complete loop may not be obvious. The concept of partial inductance allows one to uniquely ascribe portions of that loop inductance to segments of the loop. There is a large body of work that demonstrates the validity of this concept of partial inductance [2–7]. This is the basis for the highly successful partial element equivalent circuit (PEEC) method for analyzing physical structures by breaking them into small partial elements of resistance, inductance, and capacitance [8]. A wire and a PCB land have the equivalent circuit shown in Fig. 11.4, and the per-unit-length impedance is

$$\begin{aligned} z &= r + j\omega\left(l_i + L\right) \\ &= r + j2\pi f\,(15 - 30\ \text{nH/in.}) \end{aligned}$$

For a 20-gauge, solid copper wire, the impedance at 100 MHz is

$$z = 26 \times 10^{-3} + j\,(9.42 - 18.8)\ \Omega/\text{in.} \qquad \text{(20-gauge, solid, copper wire)}$$

Observe that the inductive reactance *increases with frequency* and far exceeds the resistance! Suppose that we use a 1 ft (30.5 cm) length of 20-gauge, solid, copper wire to "connect" two parts together. In fact this "connection" will have an impedance of 113–226 Ω at 100 MHz that is due almost completely to the wire inductance! The parts are therefore not "connected together"! PCB lands have the same behavior. A PCB land having width w and thickness t will have a per-unit-length resistance of [9]

$$r = \begin{cases} \dfrac{1}{\sigma w t} & t < 2\delta \\ \dfrac{1}{2\sigma\delta\,(w + t)} & t > 2\delta \end{cases} \quad \Omega/\text{m} \tag{11.2}$$

A typical PCB land having a thickness of 1.38 mils (1 oz copper) and width 5 mils will have a per-unit-length resistance of 3.9 Ω/m = 98.4 mΩ/in. below some 14.2 MHz and increasing at a rate of $\sqrt{f}$ above that. Computation of the internal inductance of conductors of rectangular cross section (PCB lands) is very difficult, but the behavior is very similar to that of a wire; above a frequency where the cross-sectional dimensions become on the order of a skin depth, the internal inductance begins to fall off at a rate of $\sqrt{f}$ [9]. Again, the partial inductance dominates the internal inductance and is, as we will see in Section 11.2.3, on the order of 15–30 nH/in.

Review Exercise 11.1 Determine the total impedance of a PCB land of width 10 mils, thickness 1.38 mils, length 3 in. at a frequency of 100 MHz. Assume a partial inductance of 15 nH/in.

Answer**:** $0.344 + j28.27\ \Omega$.

It is very important for the reader to remember that digital signals such as clocks have a spectral content consisting of a dc level and single-frequency sinusoidal components at the clock harmonic and harmonics above that, i.e., f_0, $2f_0$, $3f_0 \cdots$. Hence, a 600 MHz clock will be composed of high-frequency sinusoidal signals, 600 MHz, 1.2 GHz, 1.8 GHz, and so on, so that, with the exception of the dc component, at those frequencies skin effect is pronounced for the conductors in the system. Hence, the currents carried by these conductors will be effectively on or very near to the surfaces of these conductors and will not be carried in the interior of the conductors.

Another important consequence of the frequency range of interest here is that of *electrical dimensions*. Electrical dimensions are physical dimensions in wavelengths discussed in Section 1.4 of Chapter 1. We know that linear antennas such as dipoles or monopoles radiate very well when their lengths are on the order of one-quarter wavelength to one-half wavelength [$(\lambda/4)$ to $(\lambda/2)$]. The consequence of high frequencies here is that physical dimensions that radiate well are becoming shorter as the frequency increases. An example is the parallel-port, Centronics printer cable commonly used to attach a personal computer to a printer. This cable is on the order of 1.5 m. It is between one-quarter and one-half wavelength at frequencies between 50 and 100 MHz. Around the mid-1980s, one of the major radiated emission problems of these systems occurred around 75 MHz. This was caused by common-mode currents on the printer cable radiating very efficiently. This necessitated placing a ferrite toroid around the cable or installing it in the equipment at the cable output to block those currents from getting on the cable. In order to become effective at EMC, the reader must become adept at viewing physical dimensions in terms of wavelengths.

PCB layout is a crucial part of an effective EMC design. We must always be aware of parasitic paths caused by parasitic capacitance and inductance, as well as by near-field radiation. Figure 11.5a shows an example where these parasitic paths can nullify an otherwise well-formulated design. As discussed in Chapter 6, it is always necessary to place a filter at the entrance of the power cord to the product in order to block or divert noise currents inside the product from exiting this power cord, thereby allowing the product to comply with the conducted emission regulatory limits. In laying out the PCB containing the power supply, a power supply filter was placed on the PCB at the immediate entrance of the power cord, as is good practice. However, in order to conserve space, the phase and neutral lands exiting the filter were looped backward as shown in Fig. 11.5a. This caused significant coupling from the phase and neutral lands on one side of the filter to the phase and neutral lands on the other side of the filter. (One can view this coupling path as parasitic mutual capacitances effectively connected between the lands.) This effectively bypassed the filter over certain frequencies of the conducted emission limit, thereby rendering an otherwise effective filter ineffective.

Figure 11.5b shows another example of this inadvertent coupling. In order to make the on/off switch of an electronic typewriter more accessible to the user, it was placed in a “tower” at the rear of the product. The phase wire was routed up to the top of the tower, through the switch, and back down the tower to join with the neutral wire. This essentially made the extended length of the phase wire into an antenna, which picked up the noise emissions inside the typewriter and routed them out the product again, essentially bypassing the product’s power supply filter. Fixing this necessitated wrapping the phase wire several times around a toroid placed inside the tower.

These examples have shown how the EMC engineer can be very effective in essentially a cost-free manner by visualizing and anticipating coupling paths caused by the “hidden schematic.”

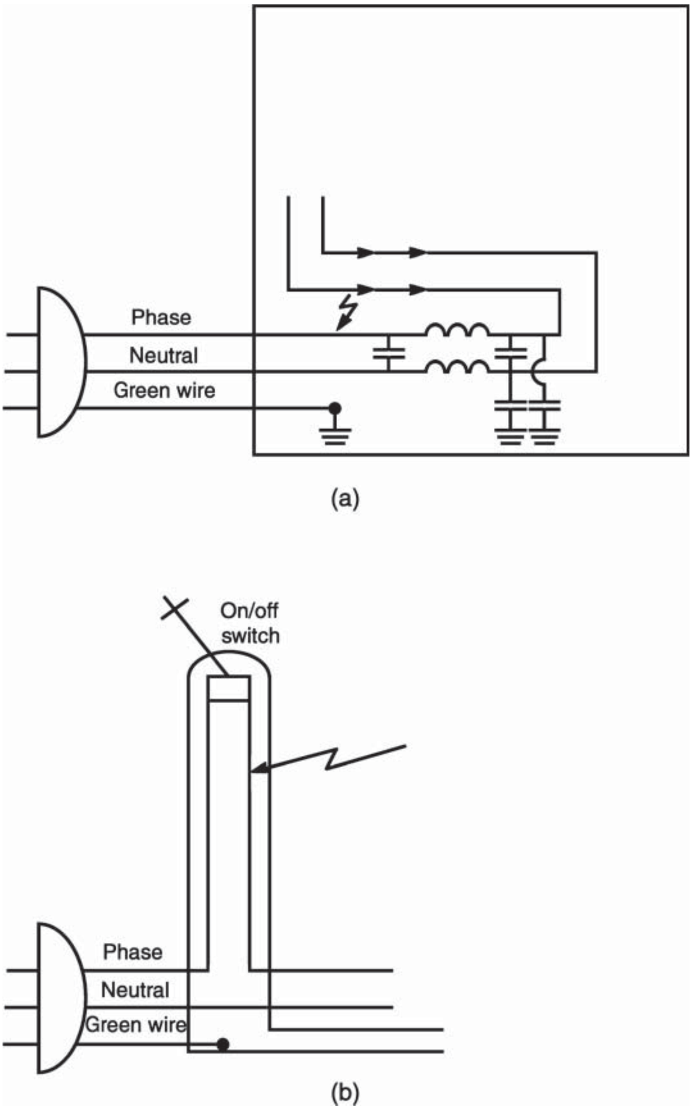

FIGURE 11.5 Configuration considerations: (a) proximity of input and output lands of a conducted emissions filter causes bypassing of it; (b) lengthy wires may act as efficient antennas by picking up internal noise and routing it out through the power cord unimpeded.

11.1.2 "Electrons Do Not Read Schematics"

Currents must always return to their source. But they don't have to return along the path dictated by the schematic. This mindset that currents flow along paths dictated in the schematic is an extremely important mental aspect to remove from one's mind. Perhaps the major aspect of the problem that prevents us from thinking the proper way is the frequency range we are considering. Once again, we are not focused on low frequencies but are interested in frequencies from the low MHz range to the GHz range. At low frequencies, in the low kHz range and at the power frequency, the return paths can be rather easily predicted since the resistance of the conductors is the dominant portion of the conductor impedance, and their inductive reactance is negligible. However, a very important aspect in the diagnosis of an EMC problem is to determine the current return paths [10]. Figure 11.6a illustrates that, although *currents will return to their source along the path of least impedance*, this lowest-impedance path is frequently difficult to determine at the high frequencies of interest here. This is because (1) digital signals have a wide range of frequency components and (2) the path impedance at these high frequencies is dominated by the inductance of the path whose impedance is dependent on frequency, $\hat{Z} = j2\pi f L$. Hence, *some frequency components will return to their source along one path and other frequency components will return along other paths*. This is because the impedances of the paths are frequency dependent. This represents an example of the mental block we may have caused by our mind making ideal assumptions. We have a tendency to assume that all the frequency components of a pulse must "stay together" as they return to their source. An example of this is shown in Fig. 11.6b for a coaxial cable above a ground plane that was discussed in Section 9.7 of Chapter 9. At low frequencies (below the break frequency caused by the shield resistance and the shield to ground plane self-inductance, which was around 6 kHz for the example in Section 9.7), the currents find the lowest-impedance return path to be through the massive, low-resistance ground plane. As frequency is increased, the strong mutual inductance between the shield and its inner wire (caused by their concentric alignment) causes the lowest impedance return path for the current to

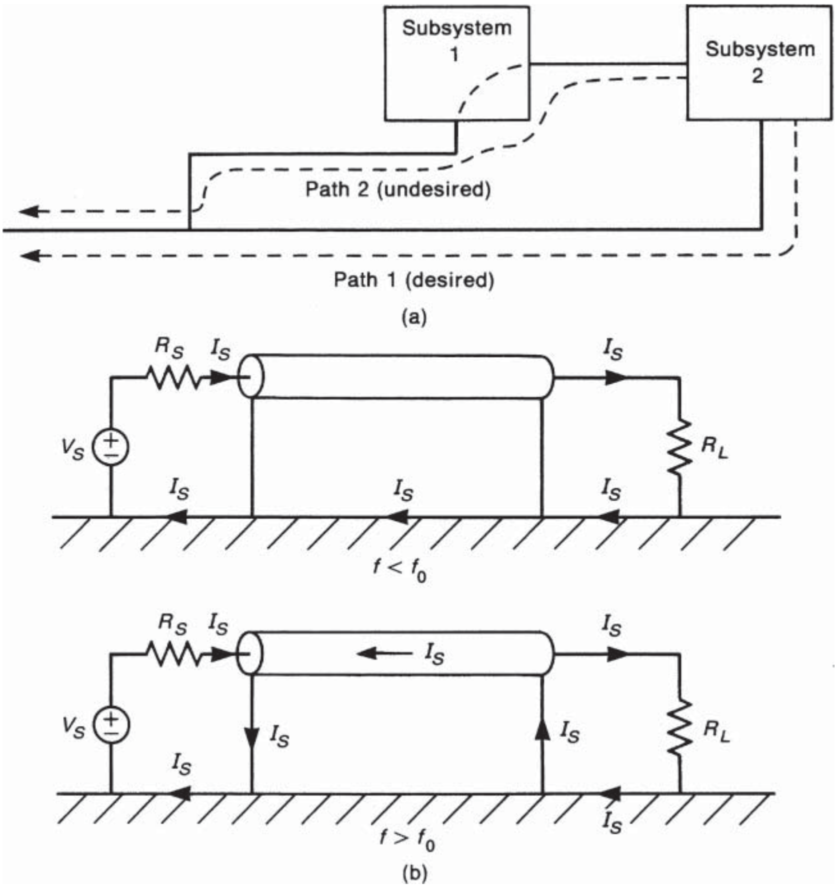

FIGURE 11.6 Illustration of the principle that signals may not return through their desired paths: (a) illustration of the principle; (b) a practical example—a shielded wire above a ground plane. Source: Based on Ott [10].

be back along the shield and not through the ground plane. Hence, some frequency components of the pulse return through the ground plane, and some return back along the shield. This happens in numerous other places.

Also, we frequently assume that the return path is that designated as "ground." In fact, currents can return along conductors designated to carry the dc voltage to the modules, for example, the +5 V power plane. This is another example of making assumptions that "sound right" but, in fact, are not accurate. In order to become effective at EMC, we must be willing to critically examine, using scientifically grounded principles and not intuition, all our assumptions.

Another example of the principle that "electrons don't read schematics" is the following. During the course of testing for radiated emissions, the product was failing the radiated emission test at a frequency around 132 MHz. It was clear that this was the 11th harmonic of the 12 MHz system clock. But the important question was "Where is it radiating from"? In the course of trying to determine this, all cables in the product were disconnected, yet the emission remained. Of course, the remaining cable, the power cord, could not be disconnected. But the product engineer did not suspect this cable because "the power cord is supposed to carry only the 60-Hz power signal." Current probes are handy diagnostic tools for EMC. A current probe (having a frequency response in the desired range) was placed around the power cord, revealing that, in fact, the 132 MHz current was on that cable. Once this current was on the power cord of the product, it radiated very well, causing the product to fail the radiated emission test. While this example may seem contrived and not realistic, it in fact happened and reveals the major problem many non-EMC engineers have that prevent them from anticipating and/or diagnosing EMC problems. We tend to assume certain things because they "sound right." In order to become effective at EMC, we must not get caught in these types of assumptions.

As a final example, it is informative to examine all the pins of ASICs and microprocessors for their spectral content. A high-frequency FET probe attached to a spectrum analyzer works quite well for this purpose. We are not interested in determining the exact levels of the signals but only in their relative levels and presence on the pins. The author encountered an important example of this. A particular microprocessor had the RESET pin very close to the CLOCK pins of that device. In the course of laying out the PCB, the layout personnel assumed that the RESET pin was "quiet" and did not require care in its routing. Hence, its routing was very low in priority, and the land length was allowed to be quite long. During testing it was determined that, due to inadvertent coupling between the internal bonding wires between CLOCK and RESET, the clock signal was placed on the RESET pin and hence routed considerable distances around the PCB on the lengthy RESET land. The incorrect assumption that the RESET pin was "quiet" led to this problem.

11.1.3 What Do We Mean by the Term "Shielding"

Perhaps the two most widely misunderstood and misused terms in electrical engineering are "grounding" and "shielding." A significant reason is that, in a practical situation, these cannot be implemented in the ideal sense that we are usually thinking of. It was pointed out in Chapter 10 that extraordinarily large values of shielding effectiveness can be computed. However, these assume that the shield is a contiguous, conducting enclosure having *no penetrations*. Any penetrations of a shield such as wires and apertures can drastically reduce and sometimes completely negate any such effectiveness of the shield as illustrated in Fig. 11.7. Any such penetrations must be *treated* before exiting the shield with, for example, filters to prevent any bypassing of the shield barrier. All it takes to virtually destroy a shield's effectiveness is to allow one penetration that is not treated. Openings to allow airflow or viewing of a visual display unit (VDU) must be treated with many small holes or honeycomb vents as discussed in Section 10.5. Furthermore, a wide variety of electronic products cannot use metallic enclosures. Plastic enclosures are required in order to give the product an aesthetically pleasing appearance. Sometimes these are made quasi-conducting by the addition of

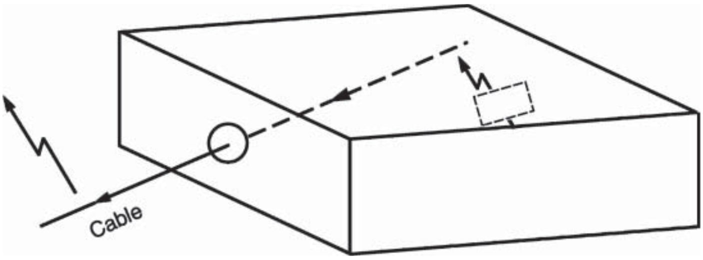

FIGURE 11.7 Reduction of the effectiveness of a shielded enclosure by a cable penetration.

carbon fibers to the plastic or by plating the interior surface with conducting materials. However, these remedies do not necessarily act as effectively as does the desired contiguous, metallic enclosure [11]. Furthermore, most electronic products such as electronic typewriters and printers require large openings to allow access to the interior for purposes of, for example, inserting and retrieving paper. It goes without saying that for these cases, the shielding effectiveness of the enclosure is far from the ideal. Hence, a guiding principle is to *not rely on a shield to cure a bad EMC design caused by not implementing the other concepts of this text such as proper PCB layout.*

Again, we frequently get caught up in the use of words and terms without thinking critically of their meaning. Another example of this regards shielding. The author was involved in the EMC qualification of a combination electronic typewriter/printer. This was connected to a personal computer via the usual parallel-port, Centronics printer cable. In the course of testing, the product failed the radiated emission limits. Using a current probe, it was determined that the cause was common-mode currents on this printer cable. This Centronics printer cable is universally available and contains a braided shield around all the interior wires. The shield is peripherally bonded to the connector at the PC side but often has a “pigtail” at the end to be attached to the typewriter/printer as shown in Fig. 11.8. The concentric shield was added to the cable in the early days of its development for purposes of removing ESD charge and remains to this day an essential and nonremovable part of the cable. The author, out of curiosity, cut and removed the shield from the printer cable and retested the device. The removal of the cable shield did not affect the functional performance of the product but did drop the radiated emissions over 10 dB across the frequency band! At first, this was incomprehensible since the author was trapped in the assumption that “shields are always a good thing and reduce, not increase, radiated emissions.” The answer to why the cable shield increased and not

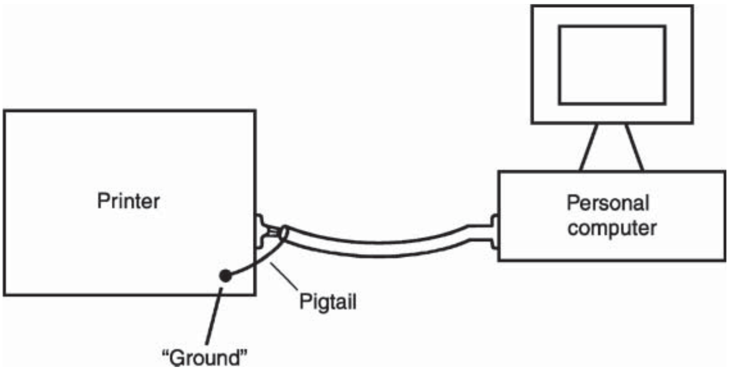

FIGURE 11.8 Illustration of the effect of the Centronics parallel-port printer cable shield. Source: Based on Ruehli [3].

decreased the radiated emissions is that, in order for a cable shield to have any effectiveness, it must be connected to "ground." Here we encounter the next assumption. It is tacitly assumed that the "ground" is "quiet," i.e., is at 0 V potential. In fact, at these frequencies of interest, no conductor in the system is at 0 V potential; even millivolts potentials can drive the cable shield as though it is an antenna. This is what was happening. The answer was not to remove all shields from all Centronic printer cables; this was not possible since the cable part is already in use. The "fix" was to route all of the cable wires and the shield pigtail through a ferrite toroid placed on (and adding unnecessary cost to) the printer. This example provides another important example of being caught up in the use of words without careful examination of their meaning.

Review Exercise 11.2 In the course of testing a personal computer for compliance, it is found that it exceeds the radiated emission limits. It is also found that if the $3\frac{1}{2}$-in. floppy disk drive is disconnected from the cable that connects it to the motherboard and removed from the PC, *the radiated emissions are substantially reduced and the unit passes*! The product engineer (PE) expects that the disk drive is radiating so that "shielding" the disk drive will therefore eliminate the radiated emissions and then applies "sticky copper tape" around the disk drive (even a disk cannot be inserted) and reconnects it to the cable. The PE remeasures the radiated emissions and finds, with much consternation, that the radiated emissions have not been reduced by even a tenth of a dB! Explain why this happened. (This is a true story.)

11.2 WHAT DO WE MEAN BY THE TERM "GROUND"

The conventional notion of "ground" is a zero impedance, equipotential surface, and often it is considered only from the standpoint of its dc performance. Neither of these aspects are applicable to "ground" with regard to its application in EMC. *All conductors have a certain amount of impedance*; consequently, *any currents that pass through that "ground" will cause points on its surface to be at different potentials because of the voltage drop across this impedance*! For example, consider Fig. 11.9, which shows two subsystems such as PCBs that are connected to ground (a metallic plane, wire, or PCB land). These subsystems may be either digital or analog or a combination. In digital subsystems, the +5 V current returns to its source (the dc power supply) through this ground, and this current is constantly changing state when the logic devices switch. In analog subsystems, this current may consist of low-frequency or high-frequency narrowband signals, as well as broadband signals such as are produced by arcing at dc motor brushes. The analog signals also return to their source through a return. The analog signals often have dedicated returns or "grounds" that are different from the digital returns, although this is not always the case. Nevertheless, for the purposes of illustration,

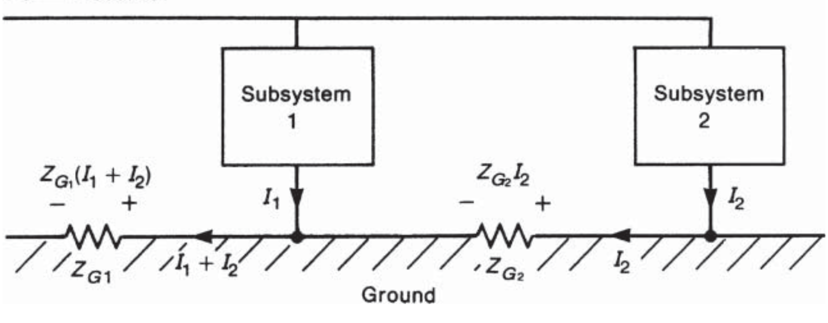

FIGURE 11.9 Illustration of common-impedance coupling.

let us assume that the ground or return of subsystem 2 is attached to the ground of subsystem 1 as shown, and both subsystems subsequently share the same return thereafter. The return current I_2 for subsystem 2 combines with that of subsystem 1, and both pass through the common ground impedance Z_{G1}, developing a voltage drop across that part of the return of $Z_{G1}(I_1 + I_2)$. Observe that the signal fluctuations that are unique to subsystem 2 are contained in I_2 and are therefore included in the voltage drop $Z_{G1}I_2$. Thus, the ground point of subsystem 1 is varying at a rate that is proportional to the signals in subsystem 2. Therefore, the signals in subsystem 2 will couple to subsystem 1 by virtue of this nonzero impedance of the ground and the sharing of the ground return by both signals. Similarly, the voltage of the ground point for subsystem 2 is $Z_{G1}I_1 + (Z_{G1}I_1 + Z_{G1} + Z_{G2})I_2$. Thus, the ground point for subsystem 2 has the signals of subsystem 1 imposed on it through Z_{G1}. This is often referred to as *common impedance coupling* and was discussed in Chapter 9 with regard to crosstalk. This illustrates the importance of the nonideal effect of ground impedance.

Another important misconception is that the ground impedance is its dc or low-frequency resistance. Again, at the frequencies of the radiated emission limit, 30 MHz >1 GHz, the resistance of conductors, even including skin effect, is negligible compared with the inductance of the conductor! For example, consider a 28-gauge solid wire (radius of 6.3 mils), whose dc resistance is 5.4×10^{-3} Ω/in. and whose resistance at 100 MHz is 65.9×10^{-3} Ω/in. Increasing the diameter of the wire to 20 gauge (radius of 16 mils) decreases these only slightly (to 8.44×10^{-4} Ω/in. at dc and to 25.9×10^{-3} Ω/in. at 100 MHz). Therefore, the wire size does not significantly decrease the high-frequency resistance. However, the inductance is on the order of some 15 nH/in. This gives an impedance at 100 MHz of 9.43 Ω/in., which is significantly larger than the portion due to resistance. Now consider the effect of this return inductance on digital signals. Consider a typical "totem-pole" output of a TTL gate shown in Fig. 11.10. The fanout of this gate, including any interconnection wiring capacitance, is represented by the lumped capacitance C_{LOAD}. With the output in the high state, transistor Q_1 is ON and Q_2 is OFF. With the output in the low state, the reverse is true. During the transition from low to high, C_{LOAD} charges up as shown in the figure. When the gate switches off, Q_1 switches OFF and Q_2 switches ON, so that C_{LOAD} discharges through Q_2. This illustrates why the risetime of TTL totem-pole outputs is typically slower than the falltime; the time constant of the charge path is RC_{LOAD} and R is on the order of 100 Ω, whereas the time constant of the discharge path is $R_{\mathrm{SAT}}C_{\mathrm{LOAD}}$, where R_{SAT} represents the saturation resistance of the transistor Q_2. During the low-to-high transition, current is drawn from the dc supply through the inductance of the +5 V supply line and returns through the inductance of the return line to the dc supply. During the transition from high to low, the discharge current of the capacitor passes through the inductance of the "ground connection" between the gate and the load. These sudden changes in the current through those inductances create voltage drops across them. There is also another particularly troublesome current involved in this process. During the transition from OFF to ON and vice versa, there is a brief time during which both Q_1 and Q_2 are ON, resulting in the so-called crossover current that flows from the supply through both transistors and back to the supply through the ground conductor. This crossover current is limited only by the impedance through the Q_1 to Q_2 path and can be quite large (of order 50 mA) with very fast rise/falltimes. Let us consider the voltage developed across the inductance of the return or ground conductor, L_{GND}, between the gate and its load. The current provided is essentially $I_{\mathrm{GND}} = C_{\mathrm{LOAD}}\, dV_{\mathrm{LOAD}}/dt$, with the waveform shown. Current spikes related to the slope of the load voltage occur during the state transitions as shown in the figure. The voltage developed across the ground conductor is essentially $V_{\mathrm{GND}} = L_{\mathrm{GND}}\, dI_{\mathrm{GND}}/dt = C_{\mathrm{LOAD}}\, L_{GND}\, d^2V_{\mathrm{LOAD}}/dt^2$. This results in the voltage waveform developed across the ground conductor as shown in the figure, which is related to the slope of the current. For illustration, let us assume a load capacitance of 10 pF and a voltage transition of 3 V in 5 ns. This produces a current through the ground of 6 mA, which will have a rise/falltime less than that of the original voltage, e.g., 1 ns. Assume that the total length of

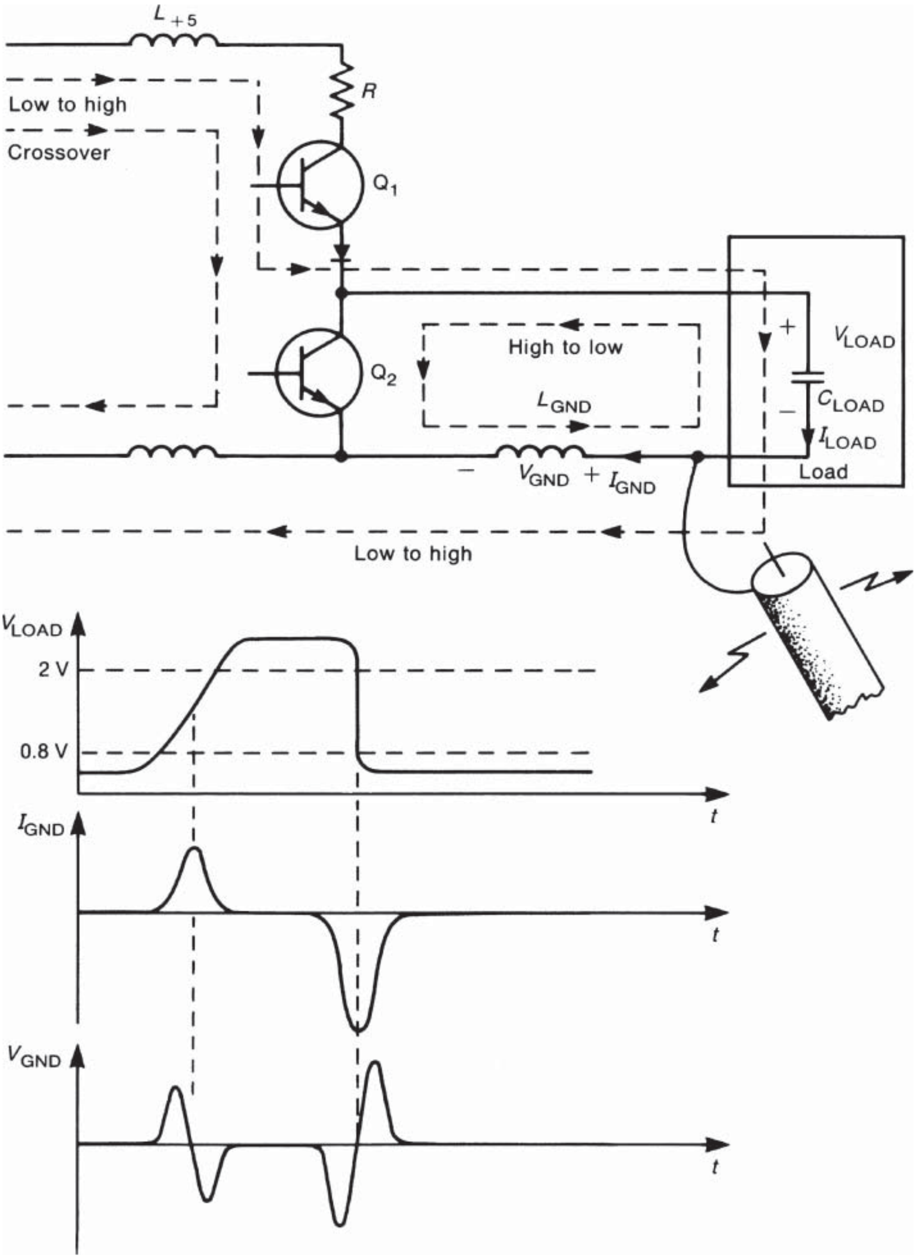
L_{+5}
R
Low to high
Crossover
Q_1
Q_2
High to low
L_{GND}
V_{LOAD}
C_{LOAD}
I_{LOAD}
Load
+
−
−
V_{GND}
+
I_{GND}
Low to high
V_{LOAD}
2 V
0.8 V
t
I_{GND}
t
V_{GND}
t

FIGURE 11.10 Illustration of the effect of conductor inductance on ground voltage ("ground bounce").

the ground or return conductor is 5 in., with a typical value of 15 nH/in., giving a net inductance of the return land of some 75 nH. This will give a voltage drop across the ground conductor of 0.45 V. Doubling the length of the return conductor gives a voltage drop across it approaching the noise margin of TTL. When several gates are switching in this manner, it becomes clear that the inductance of the return conductors may create false logic switching because the reference voltages of two gates may differ by the noise margin. The similar effect occurs along the +5 V supply conductor.

If the shield of a shielded conductor is attached to this assumed "quiet ground" point, it is quite obvious that it will most likely radiate as a very efficient antenna. Clearly, something must be done to mitigate this effect of conductor inductance if digital logic circuits are to operate reliably and systems containing them are to comply with the governmental requirements on radiated emissions. We will find in Section 11.3.4 that a *ground grid* (or a ground plane as with an innerplane (multilayer) PCB) will tend to reduce the inductance of the return path, whereas *decoupling capacitors* will reduce the *effect* of the conductor inductance. Observe that if the switch rate is at the system clock frequency, e.g., 10 MHz, then the currents through the return conductor will consist of pulses at twice this frequency (20 MHz), having rise/falltimes less than 5 ns. Is there any doubt as to the radiated emission potential of even small loops of these currents?

11.2.1 Safety Ground

It is important to realize that *there are several purposes of a ground system*. The concept of a ground as being a zero potential surface may be appropriate at dc or low frequencies, but is never true at higher frequencies, since conductors have significant impedance (inductance) and high-frequency currents flow through these impedances, resulting in points on the ground having different high-frequency potentials. This highlights the distinction between the two types of ground: safety ground and signal ground. As discussed in Chapter 6, commercial power is utilized as 120 V, 60 Hz voltage in the United States (240 V, 50 Hz in Europe). *A safety ground is normally required in order to provide protection against shock hazard*. This safety ground is generally called "chassis ground." In addition to shock protection, it also serves an important role in draining electrostatic discharge (ESD) charge and diverting ESD currents away from vulnerable electronics. A typical commercial power distribution for residences and commercial buildings in the United States is illustrated in Fig. 11.11. The commercial power is provided to the residence as 240 V, 60 Hz between one wire (the "red" wire) and another wire (the "black" wire) from the external power distribution system. This enters the residence through the *service entrance panel* and is distributed on three buses in the service entrance panel. The center bus is referred to as *ground* and is connected to physical earth ground at the service entrance panel via a ground rod inserted into the earth. This is to provide shock and fire hazard protection in the event of a fault. The voltage between the two outer buses (red and black) is 240 V, and the voltage between each of the outer buses and the center ground bus is 120 V. A 240 V service required by ovens and clothes dryers is obtained by connecting to the outer red and black buses. A fuse or circuit breaker is inserted in each of the leads that are connected to that load. Conventional 120 V service is obtained by connecting to either of the outer buses and the center or ground bus. The lead connected to the red (or black) bus is referred to as the *black* or *phase wire* in reference to the conventional color of that wire's insulation in typical cables. It is also at a voltage of 120 V *with respect to earth*. The lead connected to the center ground bus is referred to as the *white* or *neutral wire* in reference to its insulation color and is at earth potential. In addition to these two wires, there is another wire supplied in typical residential wiring cables: the *green* or *ground wire* in reference to its insulation color within an electronic device. The green wire is often referred to as the *safety wire* for the following reason. At an outlet, the black and white wires are connected to the two outlet terminals. Commercial 120 V power is obtained by plugging the power cord of the device into these two holes in the outlet socket. In addition, the green wire that is carried through the residence along with the black and white wires is connected to a third hole in the outlet as well as to the metallic case of the outlet. This is to provide a path for fault currents to flow back to the service entrance panel in order to blow the fuse or open the circuit breaker for that circuit. Suppose that the black wire becomes disconnected inside the outlet and accidentally comes in contact with the metallic enclosure. A path will be provided back to the service entrance panel via the green wire for current to flow, thereby opening the circuit breaker for this circuit.

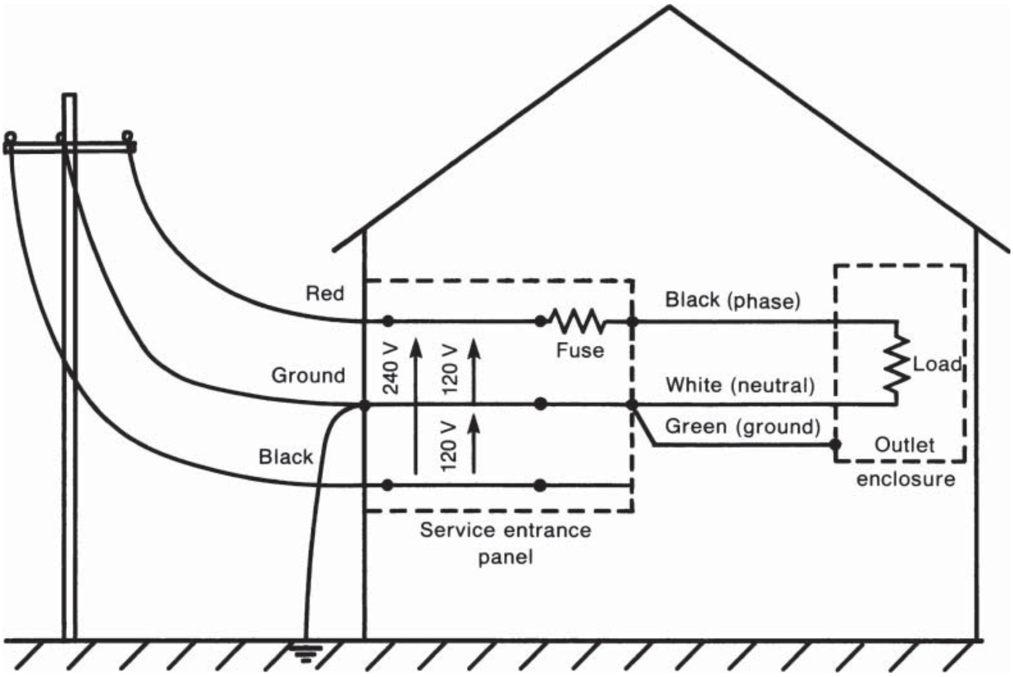

FIGURE 11.11 Residential power distribution in the United States.

If the green wire were not present or were not connected to the outlet enclosure, the outlet enclosure would be placed at 120 V with respect to earth ground, which would pose a potential shock hazard to anyone who might touch the outlet enclosure. The only time the green wire carries current is during such a fault. The current normally returns via the white wire. Because of the rather high voltages, a small voltage drop of several hundred millivolts across any of these conductors due to several amperes of current flowing through the wires is inconsequential. Thus these conductors are essentially equipotential surfaces with regard to the commercial 120 V, 60 Hz power. The concept of ground in this application is that of a *safety ground*.

It is also worth noting the method by which products that receive power from this outlet utilize this ground. The two common methods, referred to as *three wire products* and *two wire products*, are illustrated in Fig. 11.12. The power cord of a three-wire product contains three wires: black, white and green. The green wire is connected directly to the metallic frame of the product in order to provide shock hazard protection in the same manner as within the power outlet enclosure. The black and white wires go to the power supply of the product, where this 120 V, 60 Hz ac voltage is converted to the dc voltages (+5 V, +12 V, −12 V, +38 V, etc.) required to power the product's electronics as well as drive motors and other components. A two wire product illustrated in Fig. 11.12b uses only the black and white wires. Remember that the black wire is at 120 V with respect to earth ground and the white wire is at earth potential. It would not be feasible to connect the white wire to the product frame for shock hazard protection, because the user could insert the plug improperly in the outlet. Most two wire plugs are polarized (one blade is larger than the other), so only one insertion configuration is possible in the outlet holes. However, in order to safeguard against shock, the black and white wires are first passed through a transformer in the product, and one of the output wires of the transformer may be connected to the frame of the product. The transformer essentially removes the distinction between which of the two wires is "hot" with respect to earth on the secondary side.

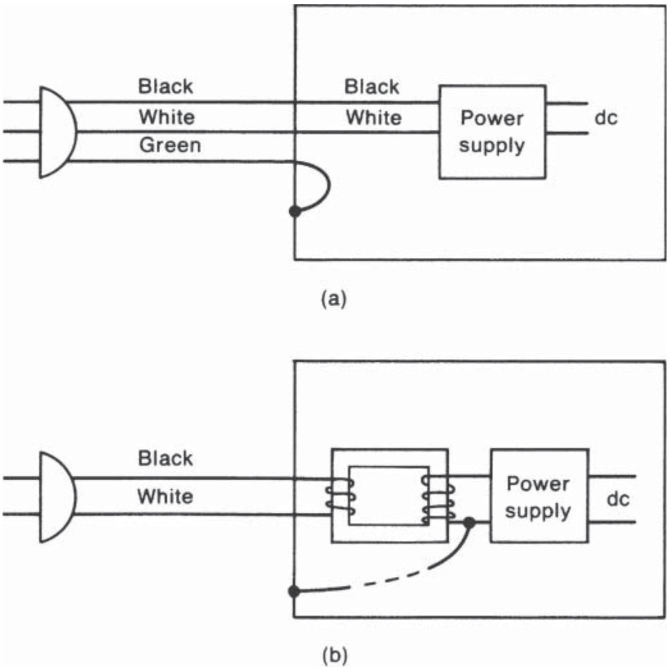

FIGURE 11.12 Illustration of power cord connections for (a) a three-wire product and (b) a two-wire product.

Any fault that occurs to the product frame (the overall metallic enclosure or metallic substructure of a plastic enclosure) will draw a large current, which will trip the circuit breaker for that circuit. As discussed in Chapter 6, the elimination of the green wire in two wire products is thought to remove conducted emission problems due to common-mode currents because there is no *physical circuit* for these components of the noise currents through the 50 Ω impedances of the LISN. This assumption is false, since there remains a path via displacement current between the product and the frame of the LISN (which is connected to the green wire). There may also be an alternate path through the ground wire in a peripheral cable and through the green wire of that peripheral device to the LISN, as illustrated in Fig. 11.6a. Two wire products may lessen conducted emission problems, but they typically do not eliminate them.

11.2.2 Signal Ground

The other type of ground is the *signal ground along which the signal currents return to their source*. So we should think of *signal ground* as the *return path for signal currents* and not as an equipotential conductor surface (which it is not). It is important to emphasize that *although it may be the designer's intent for the signals to return to their source through these designated paths, there is no guarantee that this will occur*! In fact, *some frequency components of that same signal may return through one path, while other frequency components of that same signal may return through another path*. A shielded cable above a ground plane is a good example. The frequency components that are below the cutoff frequency of the shield–ground plane circuit will return along the ground plane, but those above this cutoff frequency will return along the shield and not the ground plane (see Fig. 11.6b). Hence we must remember that *electrons do not read schematics*, that is, currents may return to their source along paths not designated on the schematic and usually do so. So in the case of signal grounds, it is critically important to think of them *as paths for current to flow in order for them to return to their source* as pointed out by Ott [10]. In other words, it is crucially important that we think of signal grounds as *the return path for signal currents*. We often concentrate on the "going down" path that a signal traverses from its source to its "load." However we often give little or no thought to the path(s) these currents return to the source on. In order to be effective at EMC design *we must determine and intentionally design these signal return paths*!

There are two consequences of this way of thinking about *signal ground* [10]: (1) the *total path* has a *loop area*; and (2) the signal return conductors, like the "going down" conductors, have nonzero impedance and hence differences in voltage along their surfaces. Recall that one of, if not the, most important factors that determine how well differential-mode currents radiate, and hence may cause the product to fail the radiated emission test or cause interference with other electronic devices, is the *current loop area. Large loop areas increase the radiated emissions of the signal currents flowing around that loop and hence must be avoided*. Also, *the total loop area consists of the "going down" path and the return path that closes the loop*. Hence we should focus on both the "going down" path *and* the return path. We should, of course, also *minimize the lengths of each path in order to control the radiated emissions of the common-mode currents on these conductors*. In many cases, large loop areas result if the designer has not provided a signal return path (signal "ground") close to the "going down" path, thereby giving the signal current no choice but to flow around a loop that has a large area. This is illustrated in Fig. 11.13. The designer has provided only a long land on a PCB for the signal to return on. This has produced a large loop area, which promotes radiated emissions of this signal. If the alternative path close to the "going down" land had been provided, the loop area would be dramatically reduced as would be the radiated emissions.

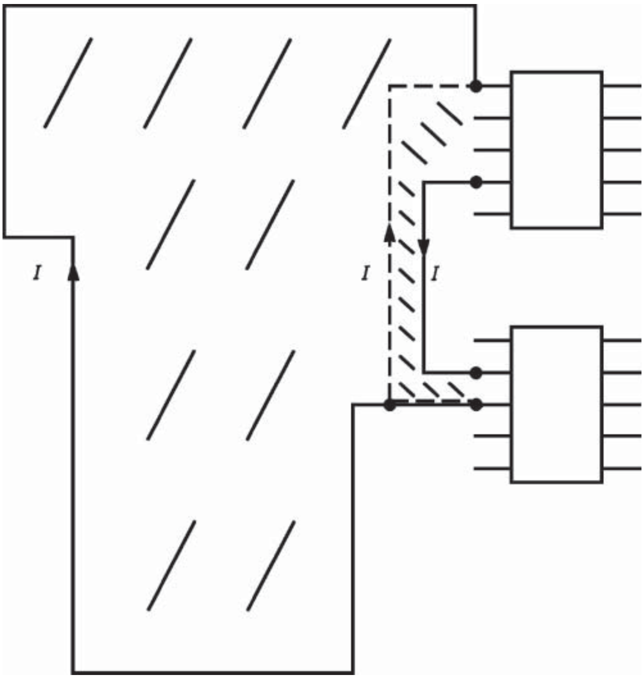

FIGURE 11.13 Illustration of the effect on radiated emissions of providing a return path close to the "going down path."

The second consequence of thinking of signal grounds as paths for the currents to return to their source is that these conductive paths have impedances and high-frequency currents flowing through them. Hence the conductors will not be equipotential surfaces. This promotes coupling of interference between subsystems via *common-impedance coupling* as discussed earlier. We will find that these impedances of the return and "going down" paths are related to the loop impedance, which is primarily inductive at these high frequencies, and the loop inductance can be related to the inductances (partial) of the individual conductors of the path. Hence reducing the loop inductance by either bringing the conductors closer together and/or shortening the lengths of the "going down" and return paths will reduce the inductances and impedances of these individual paths.

11.2.3 Ground Bounce and Partial Inductance

A very significant problem in today's digital electronics is "ground bounce." We often make the mistake of thinking of "ground" as being a conductor where the voltages are the same at all points on its surface and at all frequencies, i.e., an equipotential surface. Nothing could be farther from the truth. Once again, the most important way of thinking of ground (signal grounds) was given by Ott in his important paper "Ground—a path for current to flow" [10]. This paper is so significant because it points out that (1) signal grounds have high-frequency signals flowing through them (returning to their sources) and (2) the signal ground path has significant impedance. These two observations combine to show that any two points on this signal ground will not be at the same voltage; a voltage difference will exist between them. Hence this paper encourages us to change the way we think about "ground." This voltage difference may range from microvolts to millivolts and thereby seem to be inconsequential. With regard to the radiated emission test, these "small voltages" are sufficient to create radiated emissions that cause a product to fail the regulatory limits. Offboard cables attached to these "ground" points act like antennas producing radiated emissions. A common example is the Centronics printer cable that connects printers to a personal computer. The cable has an overall braided shield that is to be "grounded" at both ends. The problem here is to find a "quiet ground point" to attach the shield to. No such point exists in practical digital systems. Figure 11.10 illustrates this important point. As the signals being carried by the conductors switch state, the current also changes with time producing a voltage drop across the inductance of the conductors which drives any cable shield attached to this "ground" and hence making the cable shield a radiating antenna. We previously described the author's personal experience where a printer cable was carrying a common-mode noise current (measured with a current probe) that was causing radiated emission problems. The author cut the overall braided cable shield and removed it. The consequence was that the radiated emissions were reduced some 10 dB with the "shield" removed.

We also discussed the concept that the impedance of wires and PCB lands is, at the high frequencies of interest here, predominantly inductive reactance caused by the *partial inductance* of the conductors. The resistance of wires and PCB lands, even including skin effect, is dominated at these frequencies by the partial inductance that is on the order of 15–30 nH/in. (We will quantify this soon and give important formulas for computing this partial inductance.) The term "ground bounce" stems from this observation. As the logic signal currents flowing through these conductors are changing state, this causes a voltage drop between any two points on the conductor of $L\,(di/dt)$ volts. Hence the voltage of points on the conductor are "bouncing up and down." This can cause not only radiated emission problems, as outlined before, but also functional problems. For the logic to be interpreted correctly, the voltages of the ground pins of two communicating logic modules are required to be approximately the same. Ground bounce causes these to differ, thereby possibly causing logic errors. As speeds of logic signals increases, so does the magnitude of the ground bounce. For example, a 2 in. land would have 30–60 nH of inductance. Suppose that the logic currents transition from 0 to 10 mA with a risetime of 10 ns. This would cause a difference in voltage between the two ends of the conductor of some 30–60 mV. The increasing speeds of logic today make "ground bounce" an ever-increasing problem. For example, suppose that the risetime decreases to 1 ns. This voltage drop increases to 300–600 mV, rapidly increasing to on the order of the noise margin of the digital devices. Today's logic has risetimes approaching 500 ps for which the abovementioned ground drop increases to 600 mV to 1.2 V; an obviously serious problem. As was pointed out earlier, all conductors in the system possess this inductance. Hence other consequences in addition to ground bounce occur. The land carrying the +5 V power signal has this inductance also. Hence the voltage at the power pins of the modules can differ from the desired +5 V at the power supply by this voltage drop, thereby producing other functional problems. This is sometimes referred to as "power rail collapse."

Of course, the rise/falltimes of the digital pulses can be reduced just so much and retain the functionality of the machine. So how can we reduce this inductive voltage drop There are two ways to do this: (1) we can, by design, reduce the inductance, for example, by placing multiple conductors in parallel to reduce the net inductance; or (2) we can reduce the *effect* of the inductance with decouping capacitors placed at the power and ground pins of the modules. This will be discussed in Section 11.3.5.

We now discuss the concept *of partial inductance*. Numerous experimental tests have confirmed that *a voltage exists between two ends of a conductor that is proportional to the time derivative of the current through it* [5]. If we considered the impedance of the conductor as being due only to resistance, then the voltage would be proportional to the current and not its time derivative. Hence, there must be an inductance associated with the conductor. The internal inductance due to magnetic flux internal to the conductor is too small to cause this, and furthermore it reduces to zero as frequency is increased. Inductance is with respect to a closed current loop. *All currents must return to their source and hence must form closed loops*. However, the closed path for their return may be quite extensive and/or may not be obvious. *The concept of partial inductance allows us to break that loop inductance into portions that are uniquely attributable to segments of that loop*. For example, consider the rectangular loop in Fig. 11.14a. The loop inductance is defined as the ratio of the total magnetic flux penetrating the surface s of this loop:

$$\psi = \int_s \boldsymbol{B} \cdot d\boldsymbol{s} \tag{11.3a}$$

to the current that produced that magnetic flux [1, 12]:

$$L = \frac{\psi}{I} \ \mathrm{H} \tag{11.3b}$$

For later purposes, we will identify the currents associated with the individual sides of the loop as I_1, I_2, I_3, I_4, but all are equal to I; $I = I_1 = I_2 = I_3 = I_4$. We now wish to construct the equivalent circuit of the loop shown in Fig. 11.14b. Inductances L_{pii} are referred to as the *self-partial inductances* and L_{pij} with $i \neq j$ are referred to as the *mutual partial inductances* [2, 3]. These may defined in a unique and meaningful way by using an alternative form of (11.3). By Gauss' law, $\nabla \cdot \boldsymbol{B} = 0$, i.e., the magnetic field lines must form closed loops. For this reason, we may write the magnetic flux density $\boldsymbol{B}$ in terms of the magnetic vector potential $\boldsymbol{A}$ as [1]

$$\boldsymbol{B} = \nabla \times \boldsymbol{A} \tag{11.4}$$

because a vector identity provides that $\nabla \cdot \nabla \times \boldsymbol{A} = 0$ for any vector $\boldsymbol{A}$. Substituting this into (11.3) and using Stokes' theorem gives [1]

$$L = \frac{\oint_c \boldsymbol{A} \cdot d\boldsymbol{l}}{I} \tag{11.5}$$

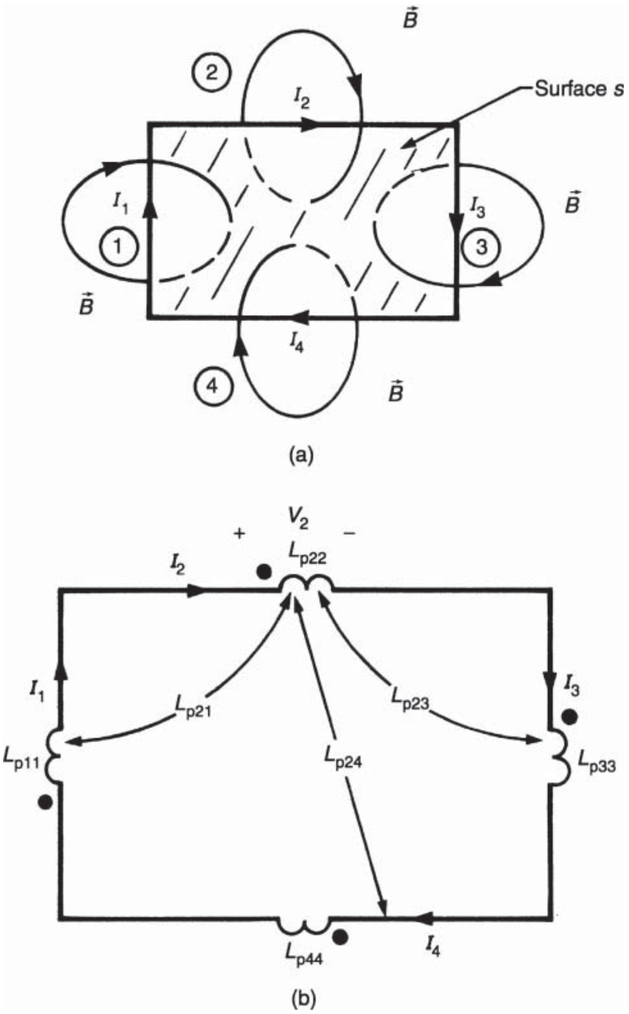

FIGURE 11.14 Illustration of the decomposition of loop inductance into partial inductances: (a) the physical circuit; (b) the equivalent circuit in terms of partial inductances.

where c is the contour of the closed loop. Hence, *the magnetic flux through a closed loop can be found as the line integral of the magnetic vector potential* (*also produced by the current*) *around the loop*. In other words, we sum the products of the differential contour segments and the components of $\boldsymbol{A}$ that are tangent to the loop contour. But this integral can be uniquely broken into the sum of the integrations along each segment of the contour as

$$\begin{aligned} L &= \frac{\int_{c_1} \boldsymbol{A} \cdot d\boldsymbol{l}}{I} + \frac{\int_{c_2} \boldsymbol{A} \cdot d\boldsymbol{l}}{I} + \frac{\int_{c_3} \boldsymbol{A} \cdot d\boldsymbol{l}}{I} + \frac{\int_{c_4} \boldsymbol{A} \cdot d\boldsymbol{l}}{I} \\ &= L_1 + L_2 + L_3 + L_4 \end{aligned} \tag{11.6a}$$

where the subcontours c_i are identified with the four individual segments of the loop and

$$L_i = \frac{\int_{c_i} \boldsymbol{A} \cdot d\boldsymbol{l}}{I} \tag{11.6b}$$

This observation suggests that we may uniquely attribute portions of the loop inductance to segments of the loop.

The alternative result in (11.6) suggests that the *partial inductances* of the equivalent circuit in Fig. 11.14b can be defined as

$$L_{pij} = \frac{\int_{c_i} \boldsymbol{A}_{ij} \cdot d\boldsymbol{l}_i}{I_j} \tag{11.7}$$

where $\boldsymbol{A}_{ij}$ is the magnetic vector potential along segment $\boldsymbol{l}_i$ due to current I_j along segment $\boldsymbol{l}_j$. If $i=j$, these are referred to as the *self-partial inductances*, and if $i \neq j$, these are referred to as the *mutual partial inductances*. It is important to point out that *the magnetic vector potentials are parallel to the currents producing them*. Hence, *the mutual partial inductances between segments that are orthogonal are zero*! With these definitions, the voltage developed across a segment of a conductor can be uniquely and meaningfully obtained. For example, the voltage across segment 2 is

$$V_2 = L_{p22}\frac{dI_2}{dt} + \underbrace{L_{p21}}_{0}\frac{dI_1}{dt} + \underbrace{L_{p23}}_{0}\frac{dI_3}{dt} + L_{24}\frac{dI_4}{dt} \tag{11.8}$$

and mutual partial inductances L_{p21} and L_{p23} are zero because segments 1 and 3 are orthogonal to segment 2 for which this voltage is being written.

We now turn to the important interpretation of the meaning of these partial inductances. Ruehli [3] has shown that an alternative to (11.7) is

$$L_{pij} = \frac{\int_{s_i} \boldsymbol{B}_{ij} \cdot d\boldsymbol{s}_i}{I_j} \tag{11.9}$$

where s_i is the area bounded by the conductor i and infinity and by straight lines that are located at the ends of segment j and are perpendicular to segment j. This is illustrated in Fig. 11.15 for parallel segments. The extension to nonparallel segments is straightforward and is given in [3]. Hence, *the magnetic fluxes involved extend from the conductor to infinity*. This observation provides considerable insight into the meaning and calculation of these partial inductances. It is a simple matter to prove this equivalence. Utilizing the relation between magnetic flux density and the magnetic vector potential, $\boldsymbol{B} = \nabla \times \boldsymbol{A}$, and Stokes' theorem [1], the numerator of (11.9) can be written as

$$\int_{s_i} \boldsymbol{B}_{ij} \cdot d\boldsymbol{s}_i = \oint_{c_i} \boldsymbol{A}_{ij} \cdot d\boldsymbol{l}_i \tag{11.10}$$

Recalling that the magnetic vector potential $\boldsymbol{A}$ is parallel to the current producing it, we see in Fig. 11.15 that along the sides the magnetic vector potential is perpendicular to the path and as such the line integral of $\boldsymbol{A}$ along these paths is zero. It can also be shown that the magnetic vector potential goes to zero at infinity Hence, the line integral of $\boldsymbol{A}$ along this part of the contour is zero, and thus the line integral around the closed paths shown in Fig. 11.15 reduces to only the integral along the conductor segment that was to be proven. We now turn to the calculation of the partial inductances for practical geometries.

11.2.3.1 Partial Inductance of Wires

The self-partial inductance of a wire of radius r_w is the ratio of the external flux passing through the surface between the wire and infinity and the current I in the wire as shown in Fig. 11.16a. Grover [2] states that as

$$L_p = \frac{\mu_0}{2\pi} l \left[\ln\left(\frac{2l}{r_w}\right) - \frac{3}{4} \right] \text{ H} \tag{11.11a}$$

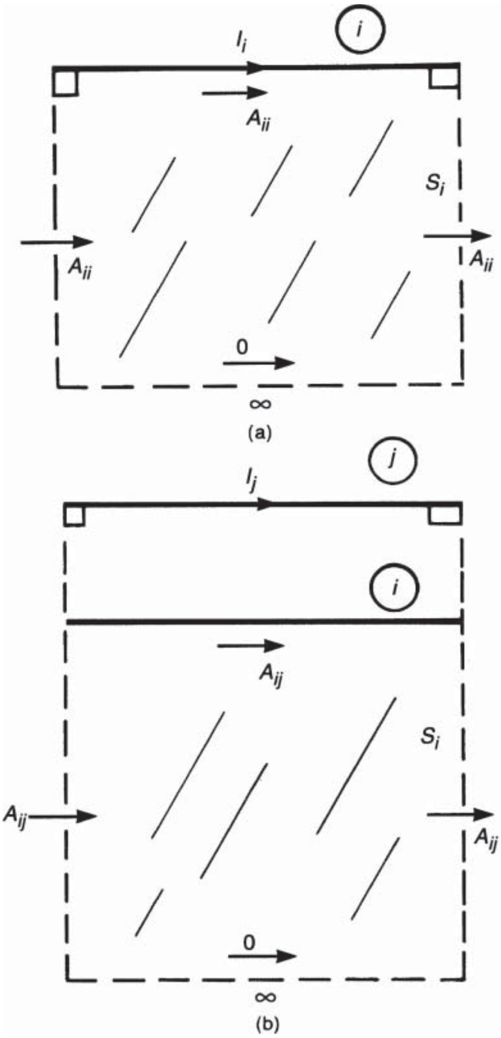

FIGURE 11.15 Illustration of the definition of partial inductances: (a) self-partial inductance; (b) mutual partial inductance.

where l is the wire length. This is the dc inductance. As the frequency of the current goes to infinity, the current crowds to the surface and the self-partial inductance becomes

$$L_p = \frac{\mu_0}{2\pi} l \left[\ln\left(\frac{2l}{r_w}\right) - 1 \right] \text{ H} \quad (f \rightarrow \infty) \tag{11.11b}$$

The mutual partial inductance between two *filaments* shown in Fig. 11.16b can be obtained exactly with the Neumann formula [1] and becomes [2]

$$M_p = \frac{\mu_0}{2\pi} l \left[\ln\left(\frac{l}{d} + \sqrt{1 + \frac{l^2}{d^2}} \right) - \sqrt{1 + \frac{d^2}{l^2}} + \frac{d}{l} \right] \text{ H} \tag{11.12a}$$

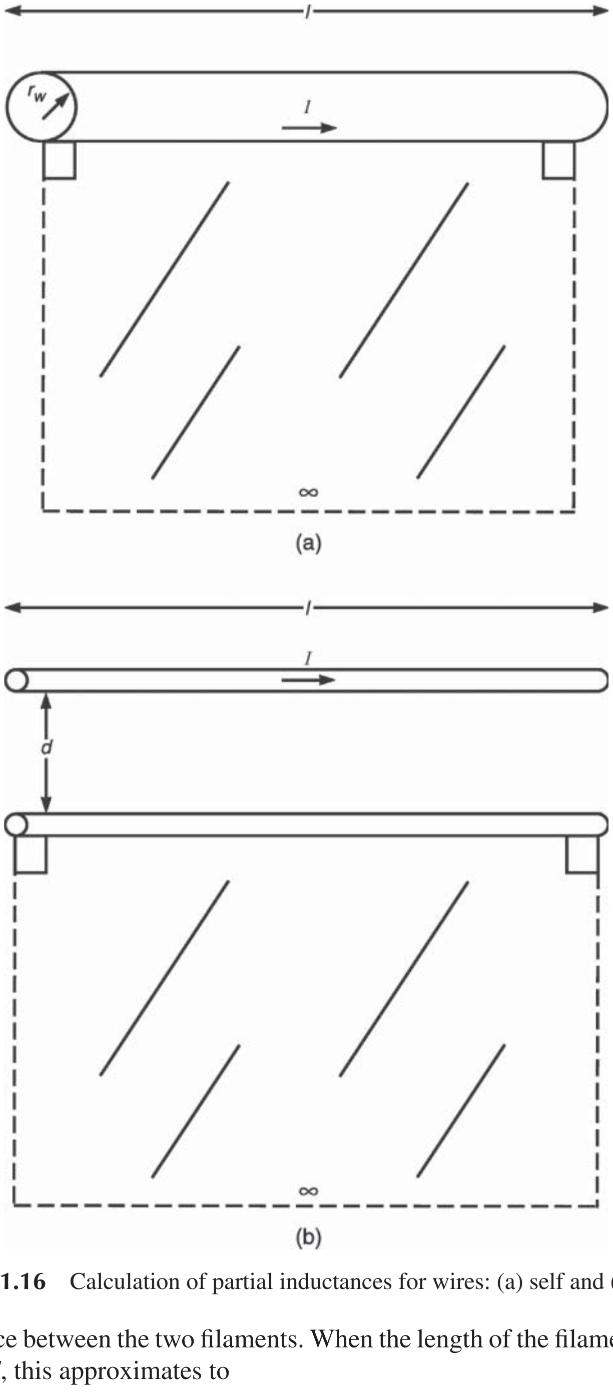

FIGURE 11.16 Calculation of partial inductances for wires: (a) self and (b) mutual.

where d is the distance between the two filaments. When the length of the filaments, l, is much larger than the separation d, this approximates to

$$M_p \cong \frac{\mu_0}{2\pi} l \left[\ln\left(\frac{2l}{d}\right) - 1 \right] \ \text{H} \quad d \ll l \tag{11.12b}$$

Review Exercise 11.3 Determine the self and mutual partial inductances for 20-gauge wires having lengths of 3 in. and separation of 1/4 in.

***Answers*:** 78.9 nH or 26.3 nH/in., 34.44 nH or 11.48 nH/in. (approximate: 33.19 nH or 11.06 nH/in.).

Now we will combine these results to determine the "ground bounce" of a circuit. Consider two parallel, identical wires of length l, separation d, and radius r_w shown in Fig. 11.17a. The equivalent circuit is shown in terms of the self-partial inductances L_p and mutual partial inductance M_p. The voltage drop across each self-partial inductance is

$$\begin{aligned} V_p &= L_p \frac{dI}{dt} - M_p \frac{dI}{dt} \\ &= \left(L_p - M_p\right) \frac{dI}{dt} \end{aligned} \tag{11.13}$$

If we ignore the voltage drop and partial self and mutual inductances of the ends with the assumption that the wire lengths are much greater than the wire separations $d \ll l$, then the total voltage drop around the loop is twice (11.13). Hence, the loop inductance is

$$L_{\text{loop}} = 2\left(L_p - M_p\right) \tag{11.14}$$

Substituting (11.11a) and (11.12b) yields

$$\begin{aligned} L_{\text{loop}} &= 2\left(L_p - M_p\right) \\ &= \frac{\mu_0}{\pi} l \left[\ln\left(\frac{d}{r_w}\right) + \frac{1}{4}\right] \\ &= l\left[\frac{\mu_0}{\pi} \ln\left(\frac{d}{r_w}\right) + \frac{\mu_0}{4\pi}\right] \end{aligned} \tag{11.15}$$

The first term is the transmission-line per-unit-length *loop* inductance given in (4.19), and the second term is the per-unit-length internal inductance of the two wires ($\mu_0/8\pi = 50$ nH/m for each wire) given in (5.4a). If we had substituted the high-frequency self-partial inductance given in (11.11b) instead of the dc result, the internal inductance term in (11.15) would vanish. This is a logical expectation since as frequency increases, the current in the wire crowds to the surface, leaving no flux internal to the wire to produce an internal inductance. Figure 11.17b shows how to interpret the term $(L_p - M_p)$. The self-partial inductance L_p gives the magnetic flux penetrating the area between the wire and infinity per unit of current producing it, while the mutual partial inductance M_p gives the magnetic flux from the first wire current penetrating the area between the second wire and infinity per unit of current producing it. The difference between the two, $(L_p - M_p)$, is the magnetic flux penetrating the area between the first and second wires per unit of current producing it. Thus, the difference between the self and mutual partial inductances is related to the flux penetrating the loop. Hence, it is logical to expect the result in (11.15), which is the usual loop inductance. This supports the idea that we can combine partial inductances to produce a loop inductance.

Review Exercise 11.4 Consider the case of two identical, parallel 20-gauge solid wires of length 3 in. and separation 1/4 in. The two wires connect a source voltage and a load resistance. Suppose that the current is a 100 mA trapezoidal wave of frequency 10 MHz with a 50% duty cycle and a rise/falltime of 10 ns. Determine the "ground bounce" V_{GND} between the two ends of the return wire. Note that the net inductance of the return wire is $(L_p - M_p)$, which from Review Exercise 11.3 is on the order of 14.82 nH/in.

***Answer*:** 445 mV.

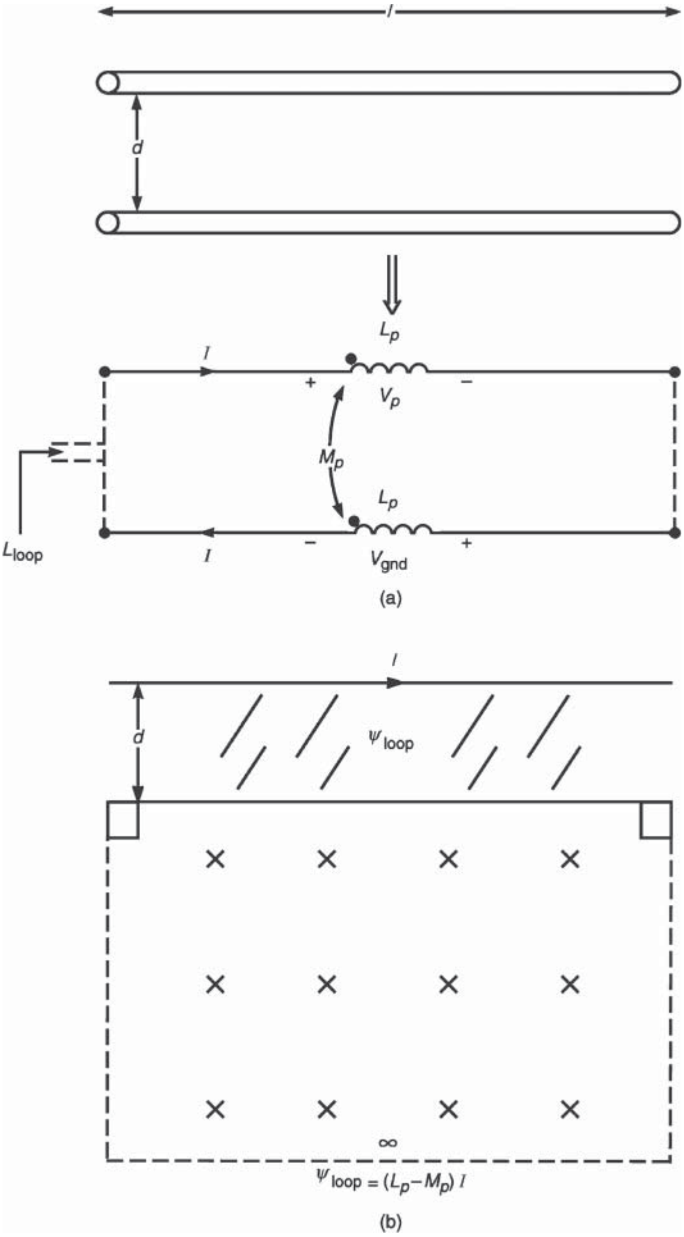
l
d
L_p
I
+
−
V_p
M_p
L_p
L_{loop}
I
−
V_{gnd}
+
(a)
l
d
ψ_{loop}
∞
$\psi_{loop} = (L_p - M_p)\, I$
(b)

FIGURE 11.17 Relating the transmission-line loop inductance of a pair of parallel wires to partial inductances: (a) the equivalent circuit in terms of partial inductances; (b) the loop inductance in terms of partial inductances.

Review Exercise 11.5 What is the consequence of increasing the separation of the wires in Review Exercise 11.4

***Answer*:** The ground bounce voltage increases because the mutual partial inductance decreases. This shows a very important result, which we will use throughout the rest of this chapter. In order to force current to return to its source along an intended path, we take advantage of mutual inductance and place the desired return path very close to the signal line. This also tends to reduce the voltage drop across the return conductor and hence the "ground bounce."

11.2.3.2 Partial Inductance of PCB Lands

The meaning and interpretation of the partial inductances for conductors of rectangular cross section, i.e., PCB lands, is the same as for wires. However, the calculation of them is considerably more complicated. Perhaps the best sources of exact formulae are the papers by Hoer and Love [4] and by Ruehli [3]. The exact formula for the self-partial inductance of a land of width w, thickness t, and length l is very complicated. However, if we examine the case of a land of zero thickness, $t = 0$, the formula for self-partial inductance is fairly simple [3, Eq. (16); 4, Eq. (18)].

$$L_p = \frac{\mu_0}{6\pi} l \left[3 \ln \left(u + \sqrt{(u^2+1)} \right) + u^2 + \frac{1}{u} \right.$$
$$\left. + 3u \ln \left(\frac{1}{u} + \sqrt{\frac{1}{u^2} + 1} \right) - \frac{(u^2+1)^{3/2}}{u} \right] \text{ H } (t = 0) \qquad (11.16)$$

where the parameter u is the ratio of land length to land width, $u = l/w$. For typical cases of interest in PCBs, the land widths vary from 5 to 15 mils and the land lengths, from 1 to 5 in. Hence, the parameter u ranges within $67 < u < 1000$. Ruehli has plotted the exact relation versus the preceding relation for zero-thickness lands (Fig. 5 in Ref. [3]) and shows that the approximation in (11.16) is sufficiently accurate for $u > 10$.

Review Exercise 11.6 Determine the total and per-unit-length self-partial inductance for land length to width ratios of $u = 10$ and $u = 1000$.

***Answers*:** 705.7 nH/m = 17.93 nH/in. and 1.62 μH/m = 41.15 nH/in. Observe that these calculated values correspond to the previously stated rules of thumb of 15–30 nH/in.

For the mutual partial inductance, the exact value for parallel, rectangular cross-section conductors (bars) is given by Hoer and Love [4, Eq. (14)]. But this is very complex and computationally intensive. If the bars are not too close, then a reasonable approximation is to treat them as filaments and use (11.12). A more accurate expression is to divide the cross section of each bar into sub-bars and treat each as a filament and then use the filament approximation of (11.12) to characterize each sub-bar and sum the results

$$M_p = \frac{1}{B_1 B_2} \sum_{i=1}^{B_1} \sum_{i=2}^{B_2} M_{pij} \qquad (11.17)$$

where bar 1 is divided into B_1 sub-bars or filaments and bar 2 is divided into B_2 sub-bars or filaments. The distance d in (11.12) and M_{pij} is the distance between the centers of the respective sub-bars treating them as filaments. Ruehli [3, Fig. 8] has shown that for parallel and aligned bars, the filament expression in (11.12) works as well as the expression in (11.17) for most cases of interest except for extremely close spacings where the bar separation is on the order of the bar thickness. This is, of course, sensible since for separations large compared to the bar width and thickness, the distances between the filaments in (11.17) are approximately the same.

11.2.4 Currents Return to Their Source on the Paths of Lowest Impedance

Perhaps the most important principle in the design of "ground" systems and PCBs is the principle that *currents will return to their source along the paths of lowest impedance*. This is a very simple but incredibly powerful concept. For example, consider the case of a source driving a load as shown in Fig. 11.18. We have shown the impedances of the paths between the source and the load as being resistive to simplify our initial discussion, but we now know that these impedances are predominantly inductive. The current leaving the source and proceeding to the load is [13]

$$I = \frac{V_S}{R_L + 2\ \Omega + 1\ \Omega \parallel 5\ \Omega} \tag{11.18}$$

where $R_1 \parallel R_2 = ((R_1 R_2)/(R_1 + R_2))$ is the resistance of the parallel connection of two resistors R_1 and R_2. For example, $1\ \Omega \parallel 5\ \Omega = 5/6\ \Omega$. Using *current division* [13], we can determine the portion of the current I that flows through each return path:

$$I_1 = \frac{5\ \Omega}{1\ \Omega + 5\ \Omega} I = \frac{5}{6} I \tag{11.19a}$$

$$I_2 = \frac{1\ \Omega}{1\ \Omega + 5\ \Omega} I = \frac{1}{6} I \tag{11.19b}$$

Note that the majority of the current, 5/6 ths of it, returns through the path having the lowest resistance, 1 Ω. This also applies to the case where the paths have reactive (resistive plus inductive) impedances. Hence, we have established the important principle that *currents will return to their source along the path of lowest impedance*. To be strictly correct, we should say that the *majority* of the current will return along the path of lowest impedance.

We now consider the second important principle in the choice of return paths for the currents: *loop area*. Currents will choose the path of lowest impedance to return to the source, but *the path impedance is that of the complete loop—going down and returning*. We established in the previous section that the impedance of a complete path is related to the inductance of that path, which is a complete loop. But the inductance of the loop is directly related to the *area of the loop*. Hence, *the smaller the area of the loop, the lower is the impedance of that complete path*. Currents will *choose* to return to their source along the path of lowest total *loop* impedance, which is the path of *smallest loop area*. Figure 11.19 dramatically illustrates this point. Suppose that a multitude of return paths is provided by "stitching together" conductors into a grid pattern. (This technique is used to create an important *gridded ground* system discussed in Section 11.3.4.) The current I flows from the source to the load, where it has a number of choices for return path back to the source. The *lowest*

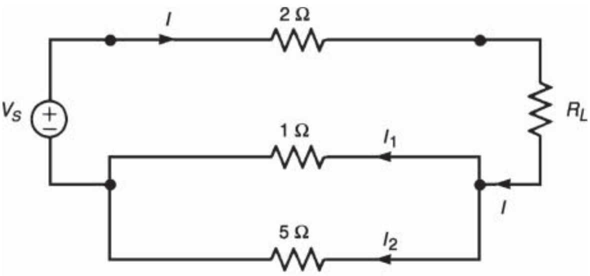

FIGURE 11.18 Illustration of the important principle that currents return to their source along the path of lowest impedance.

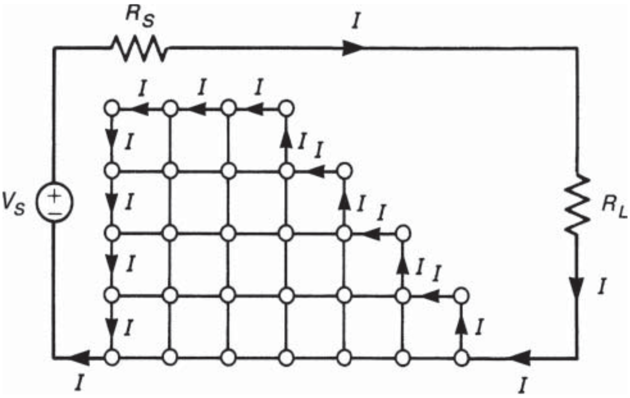

FIGURE 11.19 Effect of a ground grid on the return path of a signal.

impedance path is the one closest to the going-down conductor since this gives the smallest loop area encompassed by the current. Note also that this automatically minimizes the radiated emissions of this current since the radiated emissions of these "differential-mode currents" is related to the loop area they enclose. The problem with PCB designs is when the designer does not "give the current several choices for return path." Hence, the current has few choices. Providing a dedicated "ground" or return for each current that is close to the "going down" current would solve this problem but cannot be feasibly done on today's large and complex PCBs. Hence, a stitched-together ground grid discussed in Section 11.3.4 accomplishes this and dynamically provides choices for the current to make. The "ground" grid in Fig. 11.19 is a simple illustration of this concept.

Consider the case where a "ground plane" is provided for a current return path as shown in Fig. 11.20. This is the case where a signal land is routed along the outer surface of a PCB and a ground plane is buried as an innerplane beneath it. It turns out that, as we will show, the return current will flow predominantly along a path directly below the going-down current, which *minimizes the total loop area of the "going down" – return path.* The closer the going-down land is to the innerplane, the more the return current will concentrate under it. This can be shown as follows. According to the method of images (see Section 7.6.1 of Chapter 7), an infinite, perfectly conducting ground plane can be replaced by its *image*—a current that is oppositely directed and at the same distance below the position of the ground plane as shown in Fig. 11.21. This is a much simpler problem to solve, and the fields above the position of the ground plane are unchanged. However, this shows that the current distribution on the ground plane *will be concentrated directly below the current I.* The magnetic field intensity vector ***H***, which has units of A/ m due to the current above and parallel to the ground plane, can be determined for static currents as (see Section 4.2 of Chapter 4)

$$H = \frac{1}{2\pi r} \tag{11.20}$$

where $r = \sqrt{x^2 + h^2}$ is the distance from the current to a point on the ground plane at a distance x from a point directly beneath the current. Although this is derived for dc currents, it reasonably applies for high-frequency currents that are close to the plane for distances that are electrically small. The direction of this ***H*** field is determined by the right-hand rule (in a circumferential direction around the current). The magnetic field intensity at this position on the ground plane due to the image current has the same value but different direction. The boundary conditions (see Section B.3 of Appendix B) are that the *component of* the magnetic field intensity *tangent to* the surface of a perfect conductor

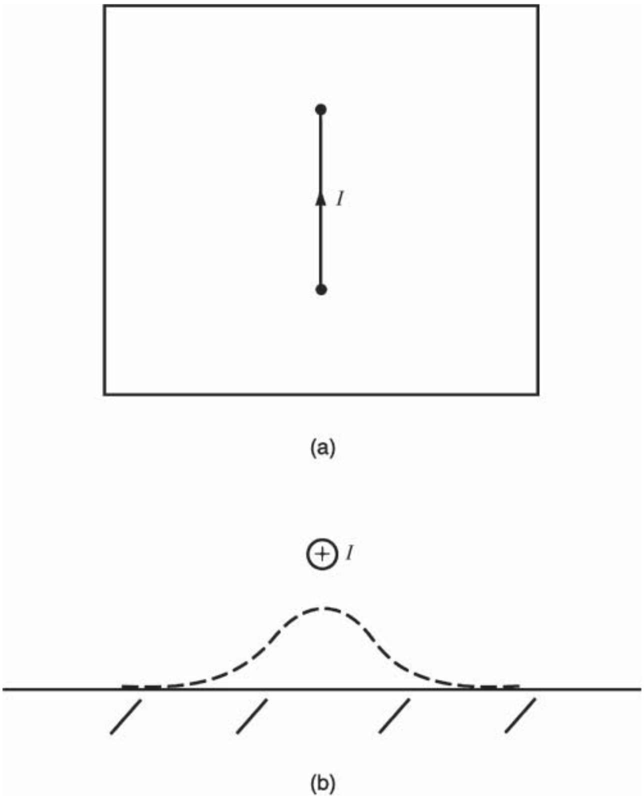

FIGURE 11.20 Illustration of the fact that return currents will concentrate on a ground plane beneath the wire: (a) a wire parallel and referenced to a ground plane; (b) a cross-sectional view of the "going down" and return paths showing the concentration of the majority of the return current beneath the wire.

produces a surface current density on that conductor having units of A/m that is equal to the tangential component of ***H***. This surface current is distributed along the surface of the conductor and is directed out of the page. Its value is

$$\begin{aligned} J_s(x) &= 2H\cos\theta \\ &= \frac{Ih}{\pi\left(h^2+x^2\right)} \quad \text{A/m} \end{aligned} \tag{11.21}$$

Multiplying the magnetic field intensity vector by $\cos\theta = h/r$ gives the tangential component, and the original current and the image current combine to produce double the field of (11.20). The current density is a maximum directly below the current and is

$$J_S(0) = \frac{I}{\pi h} \quad \text{A/m} \tag{11.22}$$

The current density rapidly decays in value as we go away from this point that is directly beneath the current. Figure 11.21b shows this by plotting the ratio of (11.21) and (11.22). In order to show

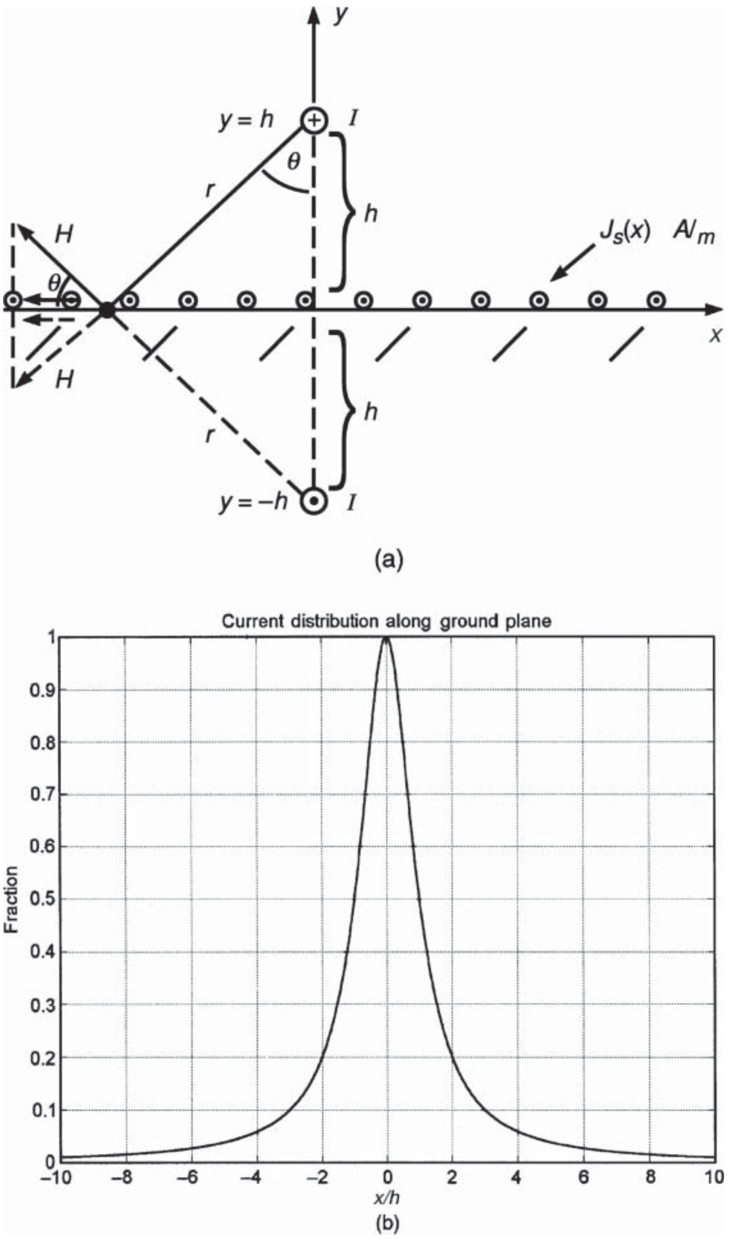

FIGURE 11.21 Determination of the return current distribution on the ground plane: (a) the cross-sectional dimensions; (b) plot of the return current distribution on the ground plane versus the ratio of the distance from beneath the wire and the height of the wire above the ground plane.

how this current distribution is concentrated along the ground below the current I, we integrate (11.21) along the ground plane (with respect to x) as

$$\begin{aligned} I(d) &= \int_{-d}^{d} \frac{Ih}{\pi\left(h^2+x^2\right)}dx \\ &= 2\int_{0}^{d} \frac{Ih}{\pi\left(h^2+x^2\right)}dx \\ &= \frac{2Ih}{\pi}\left[\frac{1}{h}\tan^{-1}\left(\frac{x}{h}\right)\right]_0^d \\ &= \frac{2I}{\pi}\tan^{-1}\left(\frac{d}{h}\right) \end{aligned} \tag{11.23}$$

Observe that as we let $d \to \infty$, this evaluates to I, as it should. Table 11.1 shows this result in terms of the portion of the ground plane current contained beneath the original current over a length $2d$ in the area between $-d < x < d$.

This shows that the current returning on the ground plane is concentrated in a region directly below the going-down current. The reason for this is now rather obvious. *This minimizes the loop area formed by the going down and return paths.* Therefore, we can use an *image* plane to force currents to return on desired paths [14].

An innerplane PCB with a ground plane buried in it serves this purpose and accomplishes a result resembling the ground grid of Fig. 11.19; *it gives the return current a multitude of possible return paths rather than restricting it to only one path.* Furthermore, the return current, when given a choice, will dynamically select a return path that minimizes the total loop area, i.e., one directly beneath the going-down current. Innerplane PCBs having a buried "ground plane" and/or a gridded ground system are crucial in reducing radiated emissions, reducing ground bounce, and forcing currents to return on desired paths.

Figure 11.22 shows a case where the philosophy of this image plane method has been circumvented. A slot is cut in the ground plane and a current passes above the slot. The current has no choice; it will attempt to complete the return path as close to directly beneath the going-down current as possible. But the slot forces the return current around it, creating a large loop area beneath the going-down current and the return current and hence increasing the radiated emissions. Therefore, slots should, in general, not be cut in ground planes. Of course, there may be instances where this is unavoidable for other reasons. But the designer now understands the pros and cons of doing this and can make an informed decision.

It is also a good idea to route cables very close to large conducting planes. Even though there may be no "hard-wired" return path to the plane, displacement current through the inevitable parasitic capacitances can in fact provide such a return path. The closer the cable is to the conducting plane, the lower is the loop area of this return path and hence the lower the radiated emissions.

TABLE 11.1 Results of (11.23) as $d \to \infty$

D/h	$I(d)/I$	%
1	0.5	50
2	0.705	71
5	0.874	88
10	0.9	94

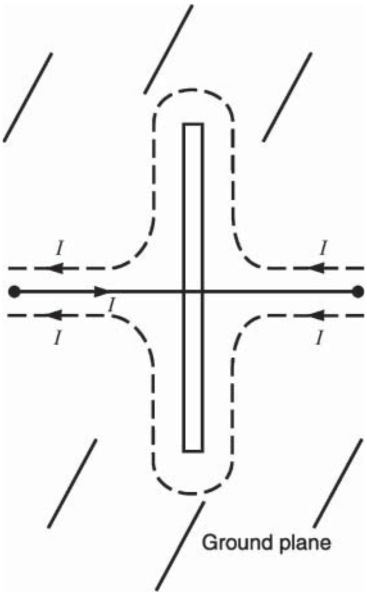

FIGURE 11.22 Effect of a slot in a ground plane showing that the return current creates a large loop caused by flowing around the slot. Source: Based on Smith and Nakauchi [15].

11.2.5 Utilizing Mutual Inductance and Image Planes to Force Currents to Return on a Desired Path

Placing two conductors closer together *increases the mutual inductance between them*. This is a direct consequence of the *reduction of the loop area between them*. We have seen numerous instances where this increased mutual inductance created by placing two conductors close together will reduce the impedance of this return path and hence cause the majority of the current to return to its source along this lowest-impedance path. For example, the case of a coaxial cable surrounding an interior wire is shown in Fig. 11.6b. Above a certain frequency (6 kHz for the experimental results shown), the current will find a lower impedance path back along the shield instead of through the massive ground plane. This is caused by the strong mutual inductance between the shield and its concentrically located inner wire. Another example is shown in Fig. 11.23. If only one return for all three currents is provided, the currents will have only one choice for their return, which will create a large loop area. However, if we provide each current with a dedicated return that is very close to the going-down current, then the impedance of that path will be the lowest because of the small loop area, and the major portion of each current will return through each dedicated return. This is not a case of "electrons reading schematics"; rather, it is "tricking the electrons" into returning along the desired path by taking advantage of their natural inclination to return to their source along the path of lowest impedance and judiciously providing that path.

Figure 11.24 illustrates another application of this important principle using mutual inductance to force currents to return along desired paths. It frequently happens that pin assignments in connectors of ribbon or flat cables or on edge connectors have the returns, "grounds," assigned without any thought given to this principle. Figure 11.24a shows this. All the "grounds" are placed together and far away from their signal conductors. Figure 11.24b shows that simple assignment of the pin assignments such that returns are directly adjacent to the going-down lines will take advantage of the mutual inductance principle. This is frequently referred to as the GSG (ground–signal–ground) or the GSSG (ground–signal–signal–ground) assignment. Again, this is not a case of relying on the

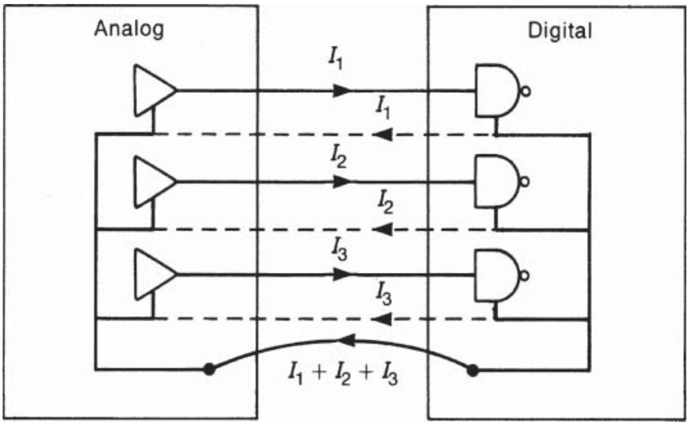
Analog
Digital
I_1
I_1
I_2
I_2
I_3
I_3
$I_1 + I_2 + I_3$

FIGURE 11.23 Effect of providing dedicated returns close to the "going-down" currents on reducing loop areas.

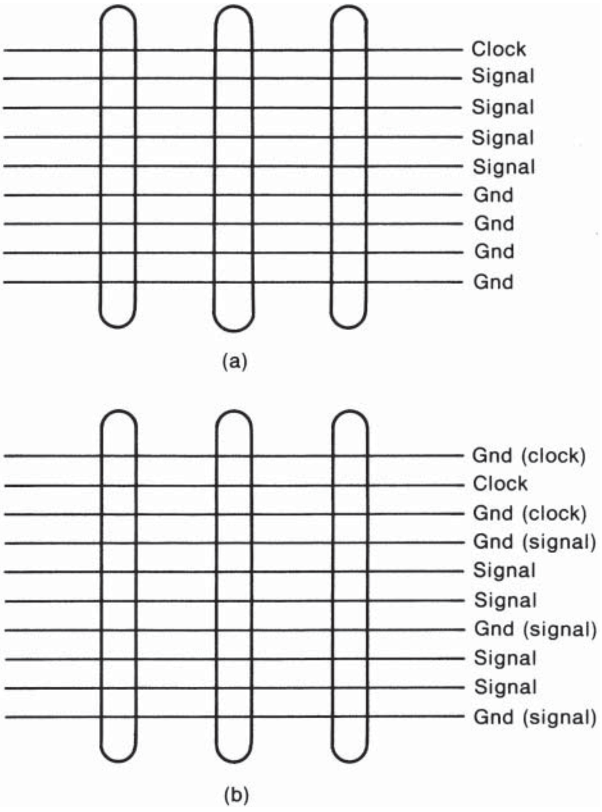
Clock
Signal
Signal
Signal
Signal
Gnd
Gnd
Gnd
Gnd
(a)
Gnd (clock)
Clock
Gnd (clock)
Gnd (signal)
Signal
Signal
Gnd (signal)
Signal
Signal
Gnd (signal)
(b)

FIGURE 11.24 Use of interspersed grounds (returns) on backplanes and in ribbon cables to reduce loop areas: (a) large loop areas; (b) reduced loop areas.

electrons to "read the schematic." However, placing a return close to a signal line will guarantee that the going-down current will find a lowest-impedance path very close to that and hence minimize the signal's loop area. Although we have given names to the various grounds, the electrons do not care what the name of a return path is; they only care about its impedance. Do not allow non-EMC personnel to determine pin assignments in connectors, or the result in Fig. 11.24a will be virtually guaranteed.

Creating an image plane can have the same effect. For example, if we place a metal foil strip beneath a ribbon or flat cable and terminate it to the "ground" connections on the PCB, the currents will have a lowest-impedance path directly beneath each signal line that they will dynamically select to return on. This effect was demonstrated in [14]. Once again, routing wires and cables near large conducting planes will have a similar effect in controlling large loop areas and hence radiated emissions.

Figure 11.25 shows the advantage of the GSG configuration, i.e., placing returns on *both sides* of the going-down conductor. If the return conductors are placed very close to and symmetrically about the going down land, this will virtually guarantee that the return currents will divide equally and return along these two paths. There is another advantage of this; *the radiated fields will tend to be canceled*. Figure 11.25b shows the magnetic fields at a distance d above and perpendicular to the plane containing the conductors and in the plane containing them. Observe that according to the right-hand rule, the magnetic fields from the going-down current are virtually canceled by the magnetic fields of the two return currents. It is important to understand that an important assumption implicit in this is that *the two ground conductors must be connected together at both ends* or else the going-down current will not have the choice to return on both these conductors. Although this visualization of the magnetic fields implicitly assumes dc currents, it can be shown to similarly hold for high-frequency currents since this configuration is essentially an antenna array (see Section 7.3 of Chapter 7).

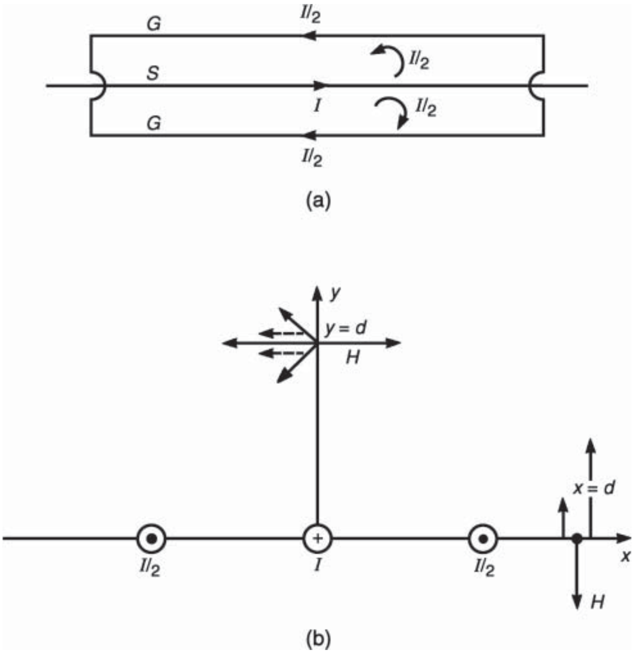

FIGURE 11.25 Effect of providing returns symmetrically about the "going-down" current in reducing radiated emissions: (a) symmetric configuration; (b) magnetic fields in the cross section.

11.2.6 Single-Point Grounding, Multipoint Grounding, and Hybrid Grounding

There are basically two philosophies regarding signal ground schemes: single-point ground systems and multipoint ground systems. A *single-point ground system* is one in which subsystem ground returns are tied to a single point within that subsystem. The intent in using a single-point ground system is to *prevent currents of two different subsystems from sharing the same return path and producing common-impedance coupling*. Figure 11.26 shows typical implementations of a single-point ground philosophy. Three subsystems have the same source. The method shown in Fig. 11.26a is referred to as the "daisy chain" or *series connection method*. This technique has the obvious problem of permitting common-impedance coupling between the grounds of the two subsystems. The connection in Fig. 11.26a will have the signals of SS 2 and SS 3 impressed on SS 1 as discussed previously. This underscores the need to be cognizant of the return paths for the currents where they are possible to determine. The *parallel connection* shown in Fig. 11.26b is the ideal single-point ground connection. However, it, too, suffers from the disadvantage that the individual ground conductors will have a certain impedance dependent on the length of these connections. In a distributed system, these connection wires may need to be long if we strictly adhere to the single-point ground system philosophy. The ground wires will then possess a possibly large impedance that may negate their positive effect. Also, the return currents flowing through these wires may radiate efficiently to other ground wires and produce coupling between the subsystems in a fashion similar to crosstalk, thereby creating radiated emissions compliance problems. The degree to which this occurs depends on the spectral content of these return signals—higher-frequency components will radiate and couple more efficiently than will lower-frequency components. Therefore, a single-point ground philosophy is not a universally ideal ground system philosophy, since it works best for low-frequency subsystems.

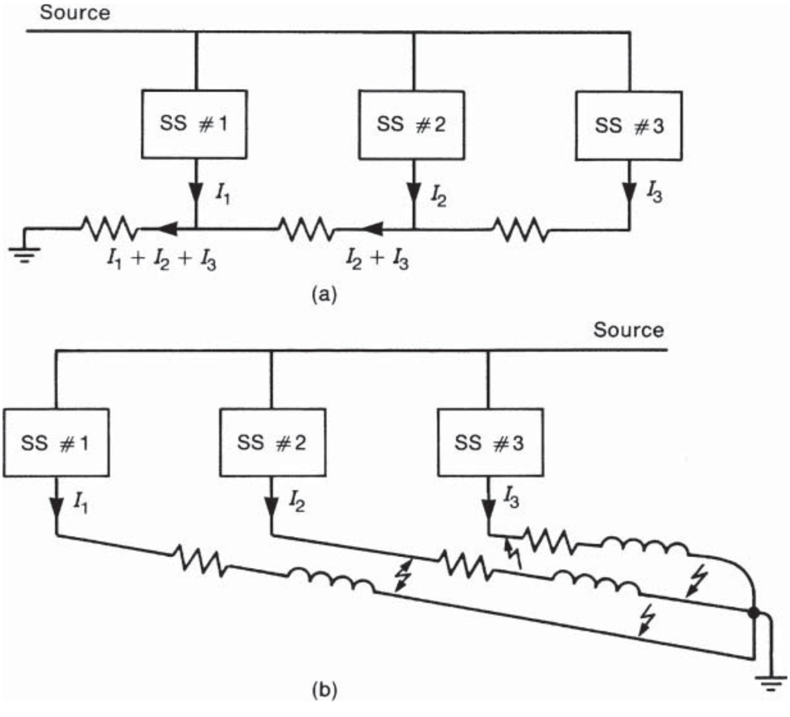

FIGURE 11.26 Illustration of the problems in single-point grounds: (a) common impedance coupling in a "daisy-chain connection"; (b) unintentional coupling between ground wires in a single-point ground system.

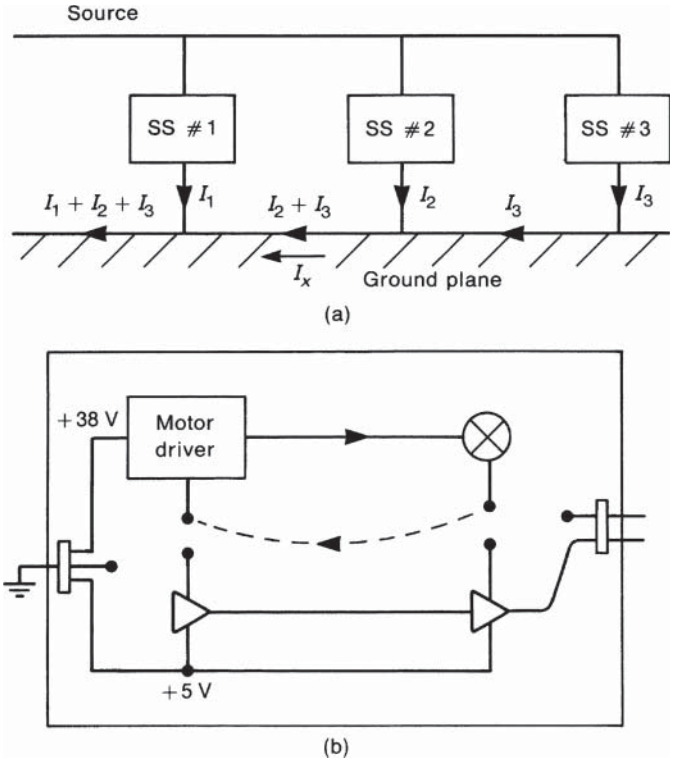

FIGURE 11.27 Illustration of multipoint grounding: (a) the ideal case; (b) illustration of problems that may occur in multipoint ground schemes.

The other type of ground system philosophy is the *multipoint ground system* illustrated in Fig. 11.27a. Typically, a large conductor (often a ground plane) serves as the return in a multipoint ground system. In a multipoint ground system, the individual grounds of the subsystems are connected at different points to the ground conductor. In using a multipoint ground system, *it is assumed that the ground return to which the individual grounds are terminated has a very low impedance between any two points at the frequency of interest.* Otherwise, there would be no technical distinction between this and the series connection, single-point ground system in Fig. 11.26a. The advantage that a multipoint ground system is thought to have over a single-point ground system is that the connection lead lengths can be shorter, since there is a closer available ground point. But this again *presumes* that the ground has zero, or at least very low, impedance *between the ground connection points at the frequency of interest*, which is not necessarily true. If the ground plane in Fig. 11.27a were replaced by a long, narrow land on a PCB, we might believe that we were implementing a multipoint ground system if we attached the subsystem grounds at points along this land, when, in fact, this would more closely resemble the series connection, single-point system of Fig. 11.26a. Quite often, these "semantics" create confusion and misunderstanding. *Simply connecting subsystems to different points on a conductor does not constitute a multipoint ground system unless the spirit of such a system is preserved; that is, the impedance between these connection points along the ground conductor is small at the particular frequency of interest.*

Another problem with a multipoint ground system may be that too little attention is paid to other currents that flow through the ground conductor. For example, suppose that the "ground plane" (to which the subsystems are multipoint-grounded) has other currents intentionally or otherwise routed through it. An example is illustrated in Fig. 11.27b, where a dc motor drive circuit is contained on the same PCB as other digital electronic circuits. The +38 Vdc required to drive the dc motor and the +5 Vdc required to power the digital electronics are provided to the PCB via a connector. Suppose that these circuits are grounded to a common ground net on the PCB. The high-current levels of the motor circuit may pass through this ground, developing potentially large, high-frequency voltages between two points on that ground net as the motor driver switches. If the digital logic circuitry is also terminated to that ground net in a multipoint fashion, these voltages developed across the ground net by the motor return currents may couple into the digital logic circuit via common-impedance coupling, creating problems in its desired performance. In addition, suppose that a signal is routed off the PCB via a connector at the opposite side of the PCB from the power connector. The ground wire in that signal cable will be driven at the varying potential of the noisy ground system and may radiate creating radiated (or conducted) emission problems.

Typically, single-point ground systems are used at frequencies in the kHz range and below and in analog subsystems, where low-level signals are involved. In these cases, millivolt and even microvolt ground drops can create significant common-impedance coupling interference problems for those circuits. Single-point ground systems are also typically employed in high-level subsystems such as motor drivers, where the intent is to prevent these high-level return currents from developing large voltage drops across a common ground net. Digital subsystems, on the other hand, are inherently "immune" to noise from external sources; however, they are quite susceptible to internal noise. They are said to "shoot themselves in the foot" by internal interference via common impedance coupling, as illustrated in Fig. 11.10. *In order to minimize this common impedance coupling, the ground system in digital sub systems tends to be multipoint*, using a large ground plane such as in innerplane board or placing numerous alternate ground paths in parallel such as with a ground grid, thus reducing the impedance of the return path. It is also important to route the signal conductors in proximity to the ground returns, since this will also reduce the impedance of the return as we saw in Section 11.2.4.

Other types of ground systems are used less frequently than the previous ones in special circumstances. These are referred to as *hybrid ground systems* and are a combination of the previous two systems over different frequency ranges. As an example, consider a shielded wire above a ground plane, as shown in Fig. 11.28. In Chapter 9, we discussed the concept that a shielded cable will eliminate inductive coupling to the interior, shielded wire *only if the shield is connected to the ground plane or reference conductor at both ends*. We also pointed out that this permits the possibility of common impedance coupling due to noise currents flowing through the reference conductor generating a voltage across the shield that is coupled to the interior wire. This commonly occurs when low-frequency power currents flow through the reference conductor. A way of selectively implementing the shield grounding and avoiding this low-frequency coupling is illustrated in Fig. 11.28.

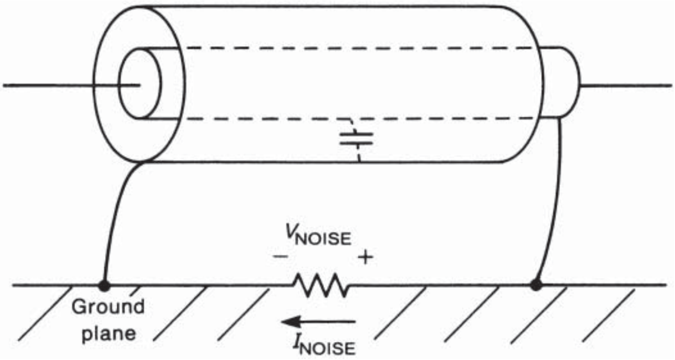

FIGURE 11.28 A way of creating a single-end grounded shield at low frequencies and a shield grounded at both ends at high frequencies to avoid "ground loops."

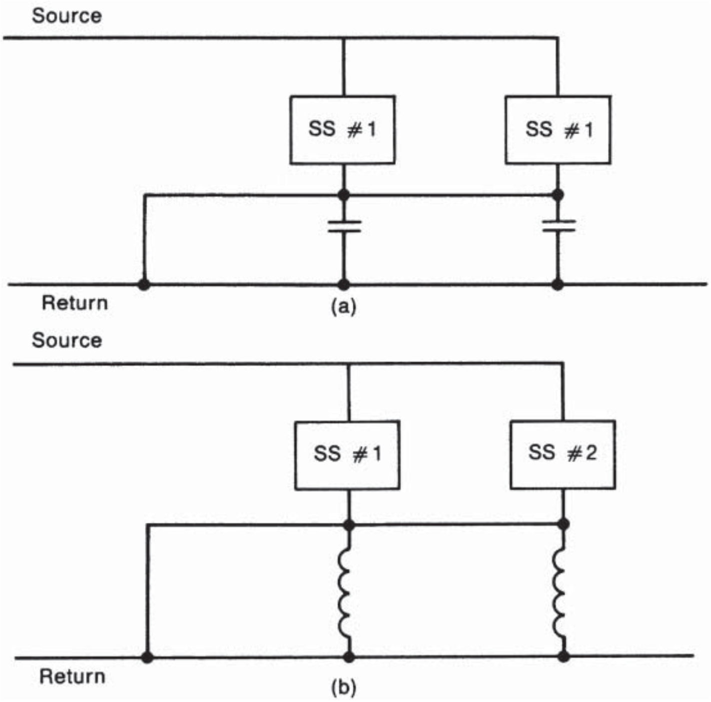

FIGURE 11.29 Hybrid ground schemes: (a) single-point at low frequencies and multipoint at high frequencies; (b) single-point at high frequencies and multipoint at low frequencies [16]. Source: Ott [16]/John Wiley & Sons.

If the cable has two shields with the inner shield attached to the reference conductor at one end and the outer shield connected to the reference conductor at the other end, no low-frequency connection exists between the two shields, thus avoiding the common-impedance coupling problem due to I_{NOISE} flowing through the reference conductor. However, the parasitic capacitance between the two shields (which is quite large because of the concentric nature of the two shields) provides a high-frequency connection between the two shields, so that the shield is effectively connected to the reference conductor at both ends. This represents the *frequency-selective grounding of a hybrid ground scheme*. A single shield can implement this if we attach one end of the shield to the return conductor *via a capacitor*. At low frequencies, the shield will be single-end grounded; whereas at high frequencies the capacitor will present a low impedance, and the shield will be double-end grounded. Typically, this requires a fairly large capacitance. Figure 11.29 depicts two other implementations of a hybrid ground system. The capacitors shown in Fig. 11.29a provide a single-point ground system at low frequencies and a multipoint ground system at high frequencies. The inductors in Fig. 11.29b provide just the opposite. The grounding schemes in Fig. 11.29b is useful when it is necessary to connect the subsystems to green-wire ground for safety purposes and to have a single-point ground system at higher frequencies.

Review Exercise 11.7 A shielded wire with a single overall shield is connected to ground with a wire at one end. In order to avoid low-frequency ground loops, it is connected with a capacitor to ground at the other end. Determine the value of capacitance that will give an impedance of less than 1 Ω above 100 MHz.

***Answer*:** 1.6 nF.

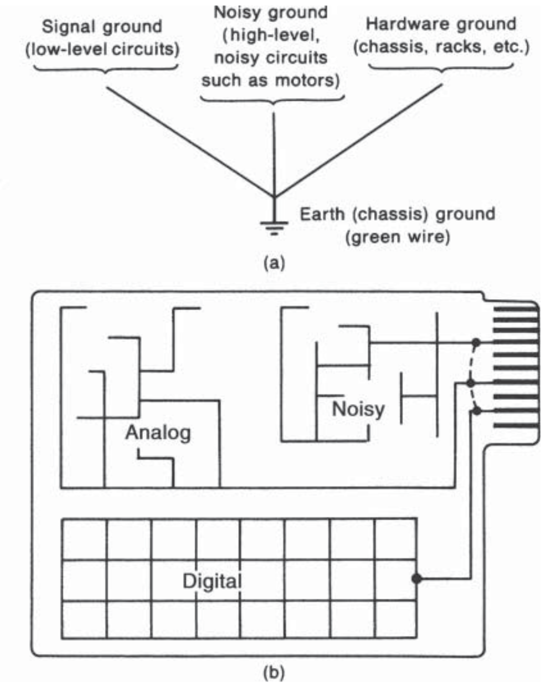

FIGURE 11.30 Segregation of grounds: (a) the ideal arrangement; (b) PCB layout of the ground system [16]. Source: Ott [16]/John Wiley & Sons.

Typical systems require three separate ground systems, as shown in Fig. 11.30a. Low-signal-level (voltage, current, power) subsystems should be tied to a single dedicated ground point. This is referred to as *signal ground*. Within this signal-ground subsystem, the circuits may utilize single-point ground systems, multipoint ground systems, or a combination. The second type of ground system is referred to as the *noisy ground system*. The noisy ground system represents circuits that operate at high-levels and/or generate noise-type signals. A signal may be considered noisy in one instance and not in another. For example, the high-frequency spectral content of digital clock signals may be considered noise in complying with the regulatory limits or interfering with other subsystems, yet this spectral content contains the necessary spectral components of the functional signal. On the other hand, arcing at brushes of dc motors is random noise and is not necessary for the functional performance of the motor. (Arcing can be suppressed as discussed in Chapter 5 and not impede the motor's performance.) For example, Fig. 11.30b shows a PCB that contains digital circuitry, analog circuitry, and noisy, motor driver circuitry. The noisy circuitry ground has a dedicated connection to the board connector that prevents these high-level return currents from passing through the analog or digital ground systems. Similarly, the digital and analog circuitries have dedicated ground returns back to the connector. Note that the ground system within the analog ground system (a signal ground) is essentially a single-point ground system, whereas the ground system within the digital ground system (another signal ground) is essentially a multipoint ground system.

The third type of ground is the *hardware ground* that is connected to chassis, frame, cabinets, equipment racks, etc. This hardware ground is not *intended* to carry current except in the case of a fault or for diversion of ESD signals.

The key to understanding why these different and distinct ground systems are required lies in the fact that *they are intended to prevent common impedance coupling*. If we allow high-level noise from a motor driver circuit to pass through a conductor that also serves as the return for a digital circuit, these high-level currents will generate voltage drops across this common return that will be fed into the digital circuit, creating possible functional problems in the digital circuit as is illustrated in Fig. 11.27b. It is important to separate low-level and high-level returns, since the larger the magnitude of the return current, the larger the common-impedance voltage drop. Several different low-level circuits may share the same return and not cause interference with each other, since the common impedance coupling voltage drops generated across the common ground net may not be large enough to cause interference. Not only are the signal levels important in separating ground systems, but their spectral content is also important. Some subcircuits contain inherent filtering at their inputs. Thus, high-level noise signals that are presented to their inputs will not create interference problems if the spectral content of that noise is outside the passband of the circuit's input filtering. Digital circuits tend to have very wide bandwidth inputs, so the frequency selective protection is not present. On the other hand, analog circuits such as comparators tend to have a degree of high-frequency filtering due to the response time of the operational amplifier (opamp). Parasitics can, however, negate this. The hardware ground is usually separate from the other grounds in order to also avoid the common impedance coupling problem. It is important to not provide a connection between hardware ground and the other grounds, in particular the signal ground, so that voltage drops created by, for example, ESD signal diversion will not cause points within the signal ground system to vary at the noise rate. See section 11.3.7 for a further discussion of this.

11.2.7 Ground Loops and Subsystem Decoupling

The difference in voltage between two ground systems can result in a potentially serious interference problem, which is referred to as a *ground loop*. This is illustrated in Fig. 11.31, where the two subsystems are connected to different ground nets that are at different voltages or are connected to the same ground system where the two connection points are at different voltages, due to the impedance of the ground system. The voltage difference between the two connection points V_G acts like a voltage source and will drive *common-mode currents* I_{C1} and I_{C2} through the signal and return wires between the two systems and between the two connection points. Even if one of the subsystems is not physically connected to a ground point, parasitic capacitance between the subsystem and the ground system can effectively complete the circuit. This is common in small motors, in which the large parasitic capacitance between the motor wiring and the motor frame (which is usually connected to large metallic portions of the frame for thermal considerations) provides a path from the motor input wires through the motor case to the product frame. (See Fig. 5.39b.) These two common-mode currents flow around potentially large loops: the signal wire ground return loop and the return wire

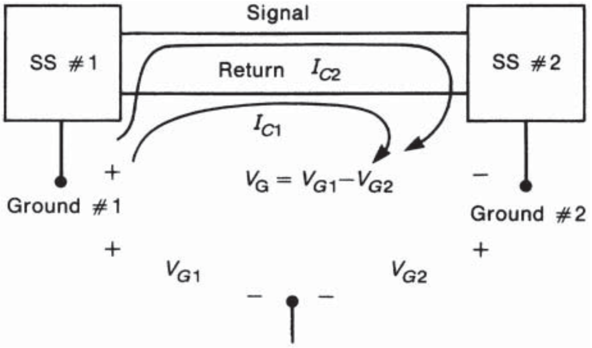

FIGURE 11.31 Illustration of the generation of common-mode currents on interconnect cables due to differences in ground voltages.

ground return loop. These common-mode currents then act like two differential-mode currents from the standpoint of generating radiated emissions. The levels of radiated emissions are proportional to the loop areas, as discussed in Chapter 8.

There are several methods for blocking this path. One of the more common and easily implemented methods is to insert a common-mode choke in the signal return wires as shown in Fig. 11.32. The common-mode choke was discussed in Chapter 5 and can be represented as a pair of coupled inductors as shown in Fig. 11.32. The magnetic fluxes due to the differential-mode (functional) current tend to subtract in the core, so that the common-mode choke *ideally* presents no impedance to these functional signals (if the wires are wound properly on the core). Leakage inductance and parasitic capacitance between the input and output wires tend to degrade the choke's differential-mode performance. The magnetic fluxes due to the common-mode component of the currents (which returns through the connection between the two ground systems) tend to add in the core, and so an inductive impedance is presented in series with the common-mode currents.

Another method of blocking this common-mode current is with the use of an *optical coupler*, as illustrated in Fig. 11.33a, which breaks the direct, metallic path. The ground voltage is between the input and the output of the coupler rather than between the two input terminals, and therefore does not create a common-mode current. This method is particularly suitable where rather large differences of voltage occur between ground systems such as the input to a pulsewidth modulator in a switching power supply. A balanced system, as shown in Fig. 11.33b, also tends to provide immunity to ground drops. The output of subsystem 1 is driven in a balanced mode *with respect to the ground of that subsystem*, so that the voltage of the signal wire and the voltage of its return *with respect to the common ground point* are 180° out of phase. The input to subsystem 2 is also balanced in that the impedance between the signal wire and the common ground for that subsystem equals the impedance between the signal return and this common point. A simple analysis of this circuit shows that the output voltage of subsystem 2, which is the *difference* of the two voltages across the impedances

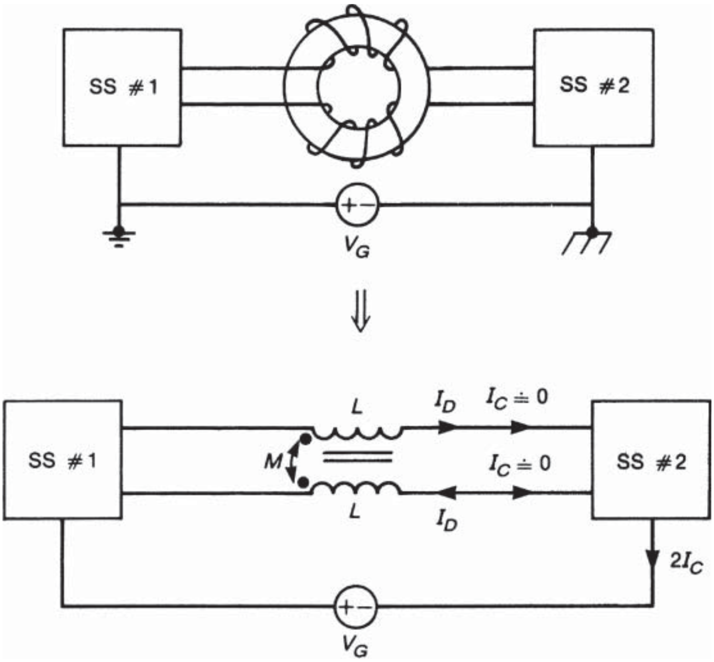

FIGURE 11.32 Use of a common-mode choke to block common mode currents on interconnect cables.

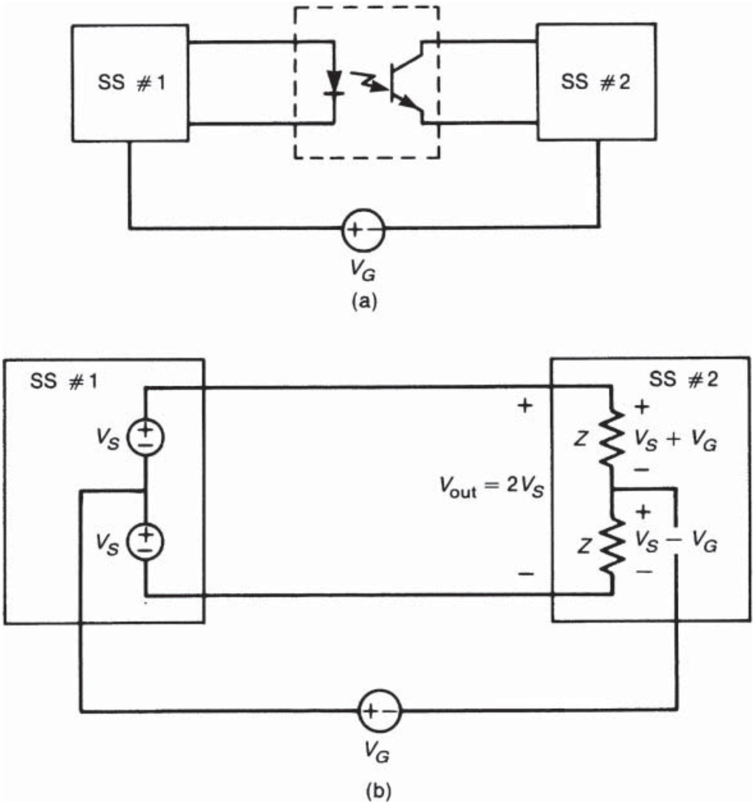

FIGURE 11.33 Methods for decoupling subsystems: (a) the optical isolator; (b) use of balanced terminations (and twisted pairs).

with respect to the common, is $V_{\text{out}} = (V_S + V_G + (V_S - V_G) = 2V_S$. Thus, the ground noise is subtracted out. This is commonly implemented either with center-tapped transformers (often called *baluns*) or with *differential line drivers and line receivers*. These line drivers and receivers utilize operational amplifiers and rely on their *common-mode rejection ratio* when operated in a balanced mode. This is a common method of long distance communication of digital data over wire lines. Balancing also aids elimination of capacitive crosstalk coupling, as discussed in Chapter 9. Twisting the two wires together eliminates the pickup of magnetic fields by the signal wire return wire loop.

The techniques of using common-mode chokes, optical couplers, or balanced transmission are examples of methods of *decoupling subsystems*. We will find numerous other instances where it is important to prevent fluctuations in one sub system from affecting other subsystems. A common example is the use of *decoupling capacitors* to prevent inductive voltage drops along the power and return conductors supplying subsystems from contaminating those subsystems. This important technique will be considered in Section 11.3.5.

11.3 PRINTED CIRCUIT BOARD (PCB) DESIGN

It is this author's opinion that proper PCB layout and design is the most important factor in the ability of an electronic product to comply with the regulations on radiated and conducted emissions, as well as the system's immunity to external sources.

11.3.1 Component Selection

Electronic components on a PCB should be categorized according to their "speed" and "drive." A convenient and meaningful way to categorize components into their potential for creating EMC problems is to rate them by signal speed according to

$$\text{Signal speed} \approx \frac{f_0 I_0}{\tau_r} \tag{11.24}$$

where f_0 is the fundamental frequency (inverse of repetition rate) of its signal, I_0 is the magnitude of its drive current, and τ_r is its rise/falltime. This signal speed is essentially a gauge of the high-frequency spectral content of the component's signals. For example, microprocessors being operated at a clock frequency f_0, generally will have the highest spectral content in the system. ASICs have off chip drivers that, unless they are carefully selected, have unnecessarily large drive current capability that also increase the spectral content of the signals they place on the PCB. In a digital system, we showed in Chapter 3 that the key component of a signal that dictates its high-frequency spectral content is its rise/falltime. In fact, we generated a rule that a digital signal has a "bandwidth" that is essentially the reciprocal of its risetime, $\text{BW} = 1/\tau_r$. Hence, a clock having a 500 ps rise/falltime has significant spectral content up to 2 GHz.

In the initial layout of the PCB, a spreadsheet should be compiled of every part to be placed on the PCB according to its "speed" given by (11.24). This priority list should be given to the layout personnel with instructions to apply the greatest care to placement of the highest speed components at the top of the list and to place the components first according to the highest speed and next to the next lowest speed, and so on. This causes the PCB layout personnel to focus on the proper things during the layout. Numerous automated layout software packages provide for "autorouting" so that the schematic is laid out and parts connected in a rather automatic manner. This can and usually does create severe EMC problems unless it is used judiciously. It is best to place the highest speed components manually and to manually route their connection lands with the previous concepts kept in mind. For example, it is imperative that a clock serving a microprocessor be placed very close to that processor. Furthermore, space and pads might be provided for a plan B to insert a resistor and a capacitor to slow the rise/falltimes if a problem is uncovered during EMC testing. Finally, recognizing that the clock signals will have the highest spectral content in the system, we should manually place "ground" lands on both sides of the clock lands to ensure that the clock signals will not inadvertently return along any unintended and lengthy return paths, thereby creating large loops and radiated emission problems. As the placement continues, the risk of creating EMC problems tends to be reduced. Hence, we should pay attention to the most serious possibilities first.

11.3.2 Component Speed and Placement

As indicated in the previous section the highest speed components should be placed and their connection leads routed with the highest care. As a general principle, recall that the higher the spectral content of a signal, the greater the ability of that signal to couple inadvertently to other conductors and parts. Hence, the highest speed components and the lands they connect should be positioned on the PCB well away from offboard connectors and lands as shown in Fig. 11.34. The author is familiar with a case where the system clock module was placed adjacent to the offboard edge connector of a PCB. When the PCB was plugged into the backplane, it was found that the clock signal inadvertently coupled, via parasitic capacitance, perhaps, to the connector conductors leading to the backplane. Because of the large expanse of the backplane, the signal radiated very well, causing the product to fail the radiated emission requirements. Once the board has been laid out, it is too late to move

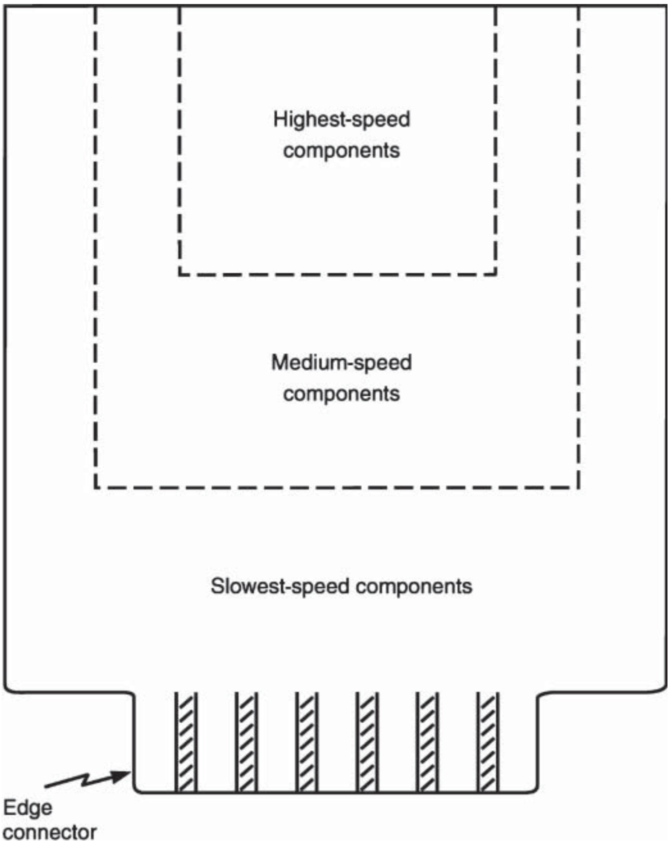

FIGURE 11.34 Keeping the highest-speed components away from offboard connectors.

components; a lengthy re-layout of the board will cause a serious schedule delay of the product. Hence, the initial layout of the PCB is a serious event. It can make or break a product's schedule.

Once again, it is a good practice to place all the components, or at least the higher-speed ones, by hand and not allow automatic software to do this. Perhaps in the future EMC layout rules will be incorporated into these layout tools, but today it seems better to place these components by hand.

It is important to realize that parts "downstream" can increase the speed of a signal that was thought to be "slow speed." Figure 11.35 illustrates this important point.

Finally, when routing the lands, it is important to keep in mind that pins of modules that are thought to be "quiet" can have high-speed signals inadvertently placed on them. Figure 11.36 illustrates a case where the RESET pin of a microprocessor was thought to be quiet and hence the land

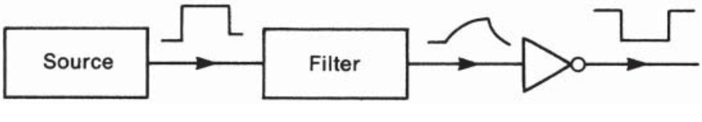

FIGURE 11.35 Illustration of the effect of negating the filtering of a signal with "downstream" components that restore the fast rise/falltimes and radiated emission potential of the signal.

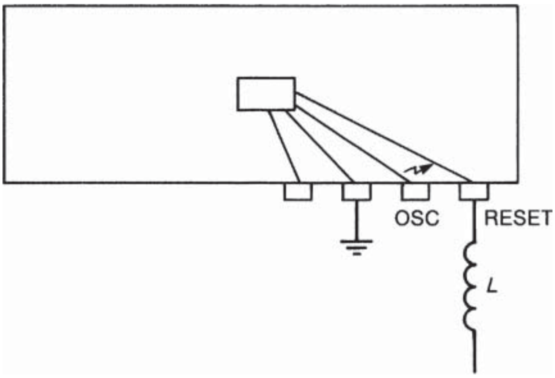

FIGURE 11.36 Illustration of the unintentional coupling of signals between chip bonding wires, causing supposedly quiet module pins to have high-frequency spectral content. A processor pin, the reset pin, was thought to be "quiet" and hence was connected to a long PCB land. Unsuspected coupling caused it to carry the clock signal, thereby creating large radiated emissions. A series inductor was added to prevent this from occurring.

connecting to that pin was routed long distances around the PCB because it was thought to be low priority. It was found that the clock signal inadvertently coupled to the RESET pin bonding wire, causing the long reset land to carry the system clock signal. It goes without saying that this caused the product to fail the radiated emission requirement.

11.3.3 Cable I/O Placement and Filtering

The reader should now be aware of the potential for long offboard cables to create severe radiated emission problems. Quite often common-mode currents on these cables are the main reason for the failure of a product's radiated emissions to comply with the regulations. These common-mode currents tend to be driven by voltage differences on the PCB such as ground bounce. Hence, the cables act like monopole or dipole antennas and the common-mode currents return to their source (on the PCB) via antenna mode or displacement currents. In order to reduce these potentially devastating currents from getting on the offboard cables, we have a number of remedies. Quite often, the cable shields of these cables are "grounded" to a point on the board. As was pointed out before, unless this ground is "quiet" we may have inadvertently created an antenna. Hence, it is important to maintain a quiet ground point. Figure 11.37 shows such an arrangement where a quiet ground is created [16]. The key to creating this quiet ground is to prevent noisy signals from being returned through it creating ground bounce. Physically separating this metal portion from the noisy signal ground of the remainder by connecting the two with a narrow segment of conductor will tend to prevent noisy signal currents from flowing through it. This quiet ground should be connected to "chassis ground" to provide a diversion for ESD-generated signals on the cables. In addition, space and pads should be provided for dual-inline package (DIP) toroids to route all wires of the cable through in order to block common-mode currents. *RC* filter packs can also be provided to block high-frequency differential-mode noise signals. Recall that these *RC* low-pass filters affect only differential-mode currents. So, if common-mode currents on the cables are the problem, these *RC* packs will have little effect on the cable radiation.

In addition, it is a good practice to place I/O cable connectors on only one edge of the PCB. This has the effect of the noise voltages between two points on the PCB not driving cables on opposite edges as a dipole antenna. Figure 11.38 illustrates an adequate design.

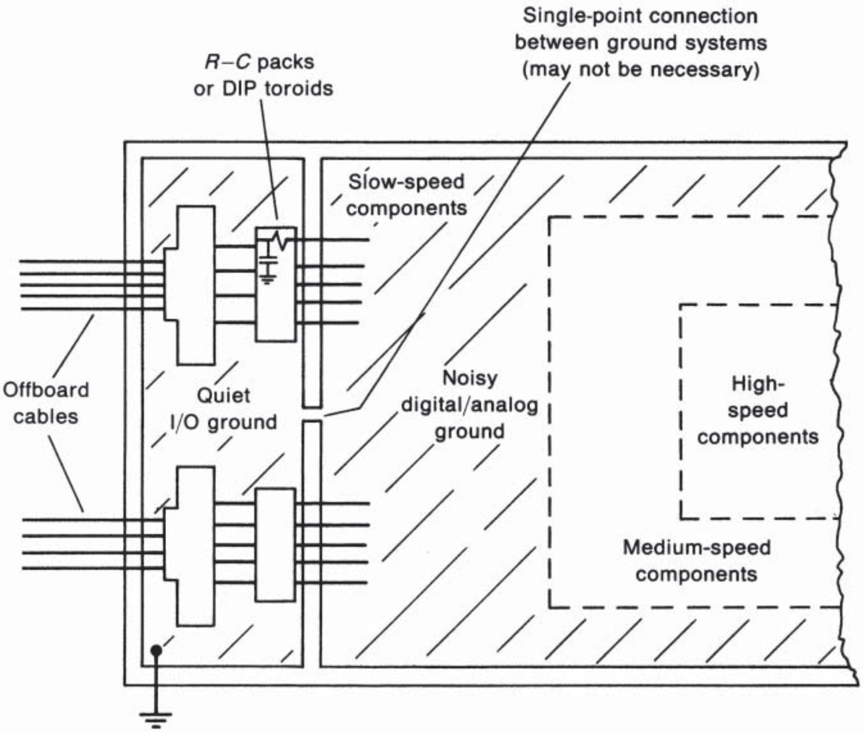
Single-point connection
between ground systems
(may not be necessary)
R–C packs
or DIP toroids
Slow-speed
components
Offboard
cables
Quiet
I/O ground
Noisy
digital/analog
ground
High-
speed
components
Medium-speed
components

FIGURE 11.37 Creation of a quiet ground where connectors enter a PCB. This allows effective termination of shields and filtering of offboard cables [16]. Source: Ott [16]/John Wiley & Sons.

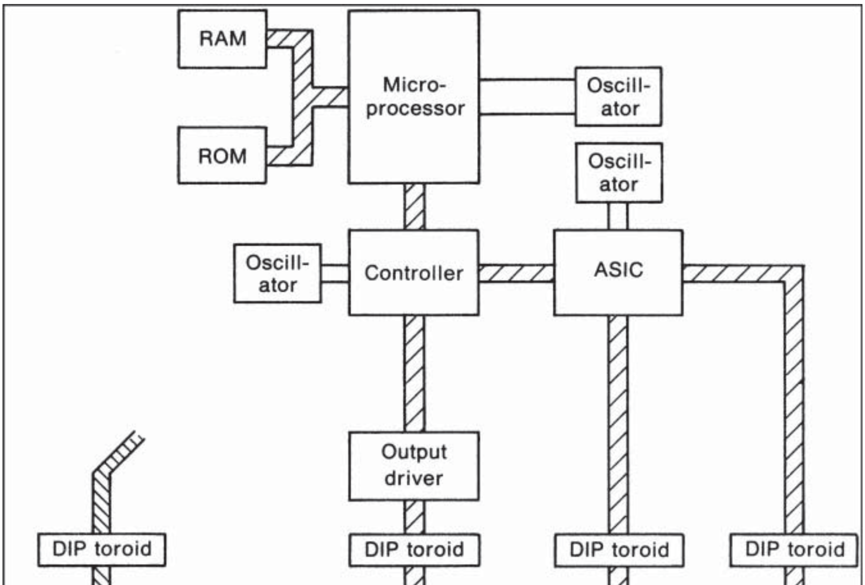
RAM
ROM
Micro-
processor
Oscill-
ator
Oscill-
ator
Oscill-
ator
Controller
ASIC
Output
driver
DIP toroid
DIP toroid
DIP toroid
DIP toroid
Power connector
Disk connector
Keyboard
connector
CRT
connector

FIGURE 11.38 A good PCB layout for a typical digital system.

11.3.4 The Important Ground Grid

On many low-cos products, innerplane boards cannot be afforded. Hence, the important effects of having a ground plane (and a power plane that can act like a ground plane in returning currents) are not present. Having a buried ground plane has the significant advantage of dynamically providing an almost infinite number of potential return paths that each current can select from to enable that current to return close to the going-down current, i.e., directly beneath it. This is why a buried ground plane has such a significant effect; no currents are forced to return along long and circuitous paths having large loop areas with the going-down current such as when the designer neglects to provide a direct return path for the current. On low-cost products where this cannot be afforded, a simple way of achieving this effect is with a *gridded ground system*.

A gridded ground system is similar to a screen door. The ground lands are stitched together as shown in Fig. 11.39a. With all these connected at every possible point, a going-down current I can dynamically select a path through the grid that brings the return current closest to the going-down current. The finer the mesh, the closer this approximates a ground plane. Its effectiveness is dramatic [17]. The effect of the grid spacing was investigated in [18].

On a typical PCB, the lands on the two sides are orthogonal to each other. This is done in order to increase the wiring channels. A gridded ground system would seem to block these wiring channels. However, with the use of vias (connections between the two sides and to any innerplane lands), blockage of wiring channels by the ground grid can be avoided as shown in Fig. 11.39b. A signal land that is blocked by a land of the grid can via down to the other side, proceed on, and via back up to the first side once past the blockage. Of course, this requires more work on the part of the layout personnel, but it is a simple price to pay for passing the regulatory EMC radiated emission requirements. On more complex PCBs this would create considerable layout effort. But in those more complex boards, innerplanes can be afforded, and hence the requirement for a ground grid is replaced by the availability of innerplane ground planes.

11.3.5 Power Distribution and Decoupling Capacitors

Engineers concerned with power distribution concentrate on the power distribution conductors that carry the +5 V to the power pins of the modules so that the IR drop along these distribution conductors will not cause the voltage to drop to unacceptable levels. Hence, they are tending to concentrate on dc performance. In addition, as we now know, the power distribution conductor as well as the power return or “ground” conductors possess an inductance (see Fig. 11.10). Hence, as the modules change state, the current changes at a rate of the rise/falltimes of the digital signal. The $L\,(di/dt)$ voltage drops across these power distribution conductors will therefore cause the voltages at the +5 V pins to be reduced during the time of the signal transition by this inductive voltage drop. Hence, the +5 V at the module power pins can be reduced substantially by this inductive voltage drop, which is often referred to as “power rail collapse.” In addition, the inductance of the ground or return conductors produces ground bounce that causes the voltages of the ground pins of the modules to differ from each other. Both of these effects create the potential for logic errors. It goes without saying that as the rise/falltimes of the digital signals decrease, these problems will tend to increase.

It is helpful to think of the +5 V and ground lands as constituting a transmission line as illustrated in Fig. 11.40a. In Chapter 4, we found that an important parameter of a transmission line is its characteristic impedance, Z_C. The characteristic impedance involves the ratio of the line per-unit-length inductance and capacitance:

$$Z_C = \sqrt{\frac{l}{c}}\ \Omega \tag{11.25}$$

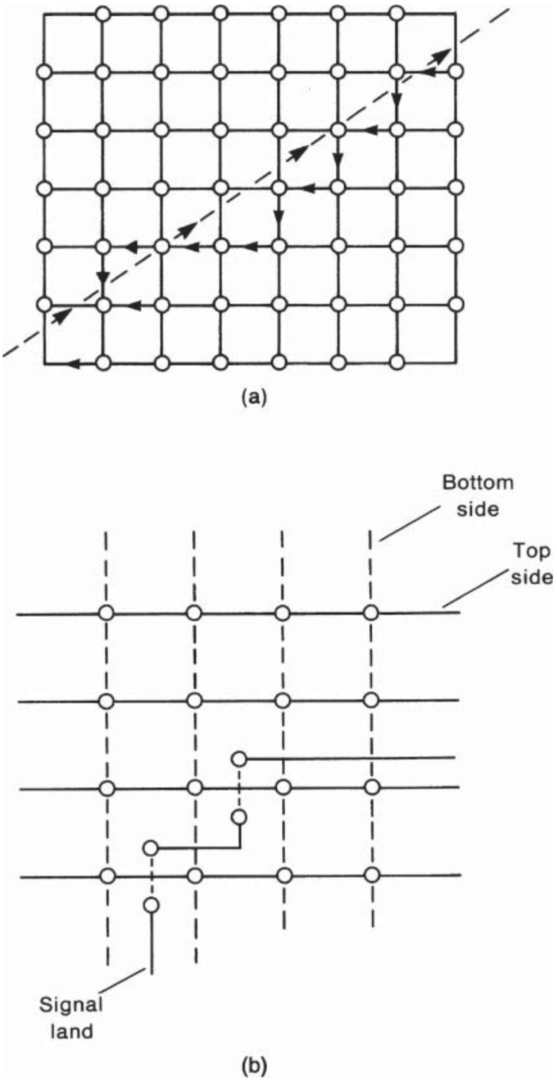

FIGURE 11.39 The important ground grid: (a) providing many alternate paths allows the return currents to select a return path close to the "going-down" path, thereby reducing loop area; (b) vias can be used to interconnect the ground grid without blocking wiring channels.

The inductance here is the "loop" inductance, but we showed that it is related to the partial inductances of each conductor forming the loop. We wish to lower the inductance and raise the capacitance; a larger capacitance between the lands will tend to "hold up" the power voltage during transitions. Lowering the inductance and raising the capacitance has the effect of lowering the characteristic impedance of the transmission line. Hence, a desirable goal in a power distribution design is to *use a transmission line having as low a characteristic impedance as possible*. We now investigate two possibilities shown in Figs. 11.40b, c. We can use the formulas from Chapter 4 to compute the characteristic impedances of these two configurations. For example, consider the case of the two lands being placed on opposite sides of the PCB as shown in Fig. 11.40b. Suppose that the lands have widths $w = 200$ mils and board thickness is $h = 62$ mils. For this we compute Z_C from Eq. (4.43) of

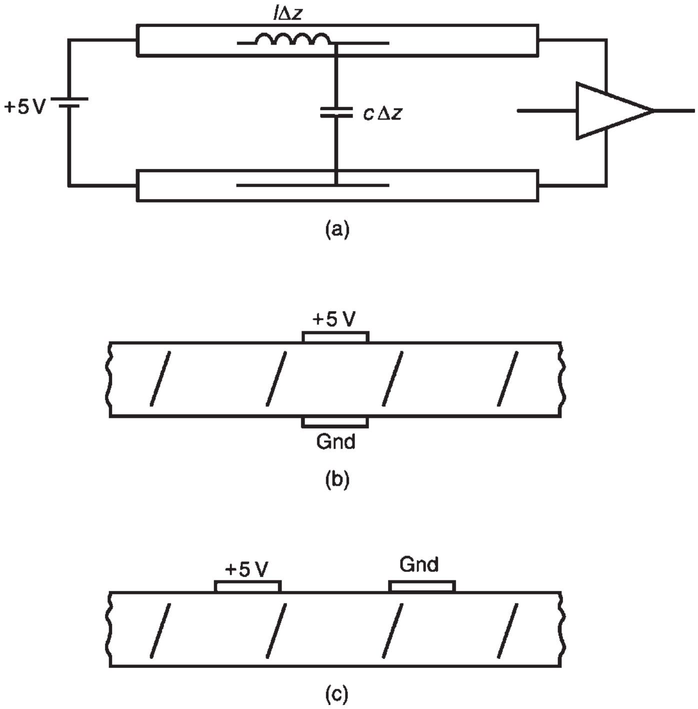

FIGURE 11.40 (a) Power distribution circuits require low-inductance and high-capacitance, specifically, transmission lines having low characteristic impedances; (b) lands on opposite sides of a board can provide lower characteristic impedances than can (c) lands on the same side.

Chapter 4 to be $Z_C = 41.05\ \Omega$. On the other hand, for the case of two lands placed on the same side of the board shown in Fig. 11.40c having widths of $w = 200$ mils and separated by $s = 62$ mils on a board of thickness $h = 62$ mils, Eq. (4.42) of Chapter 4 gives $Z_C = 155.7\ \Omega$. Hence, *pairs of wide lands placed on opposite sides of the board will give characteristic impedances lower than those obtained by placing the lands on the same side of the board*. This intuitively makes sense because there is more capacitance when the land sides face each other than when the edges face each other. So, intelligent design of the power distribution system can contribute to *minimizing the effects of the land inductance*.

2S2P boards will take advantage of the large capacitance between these parallel and extensive conducting planes. An inherent capacitance that depends on the separation between the layers can be utilized advantageously. For example, considering this to be a parallel-plate capacitance, its capacitance is approximately $C = \varepsilon_r \varepsilon_0 (A/d)$ where $\varepsilon_r = 4.7$ is the relative permittivity of the board separating the layers, A is the plate area, and d is the separation between the planes. For a board whose extent is 100 in.^{2} and separation is 5 mils, this gives a capacitance of approximately 0.02 μF. Not all of this area should be utilized in computing this capacitance since the current flowing between two points on the planes will follow a direct path between the points but will spread out around that path a small distance (see Fig. 11.20). This spreading distance is difficult to compute, but suppose that it is, say, 5 times the separation between the planes. For the dimensions given above, plane separation 5 mils and this current width of 25 mils, Eq. (4.43) gives a characteristic impedance of $Z_C = 28.6\ \Omega$, which supports this idea. The larger the relative permittivity, the larger the capacitance and the lower the characteristic impedance. There are some exotic materials being studied that have relative permittivities much larger than those of glass epoxy.

In spite of these helpful design concepts for the power distribution systems, we will probably still need to augment the design with *decoupling capacitors* attached between each module's power and ground pins. As was discussed previously, when modules switch state, current is drawn through the inductances of the +5 V and ground lands from the power supply as illustrated in Fig. 11.41. This causes power rail sag and ground bounce. A decoupling capacitor placed between the power and ground pins of a module acts as a local reservoir of charge. During the time when the module is changing state, the current is drawn from this local decoupling capacitor and not through the long +5 V and ground lands from the power supply as shown in Fig. 11.42. During the quiescent state when the voltage is not changing level, current is drawn through the long power delivery lands at a much slower rate than during the state transition to replenish the local decoupling capacitor preparing it to serve during the next state change. Hence, the effect of the inductances of these long lands is avoided. Of course, this requires that the capacitor be placed very close to the module pins. The traditional placement of the +5 V and ground pins on many DIP packages has been criticized because they are at diagonally opposite corners of the module and require the longest possible connection lead length for the decoupling capacitor. Clearly, this introduces lead inductance albeit much shorter than those of the long lands connecting to the power supply. However, this lead length should be minimized. Figure 11.43a shows a preferred placement. The capacitor is placed close to the +5-V pin of the module and connected to the ground grid. The inductance of the lead to the +5-V pin is minimized, and the ground grid minimizes the inductance of the connection to the module ground pin. *It is important to remember that the inductance of the capacitor connection lead is that of the total conductor length between the capacitor body and the module pins.* A common misconception is that if the visible wires of the decoupling capacitor are kept short, the design is satisfactory. This fails to take into consideration the potentially long *land lengths* that may be required to connect the

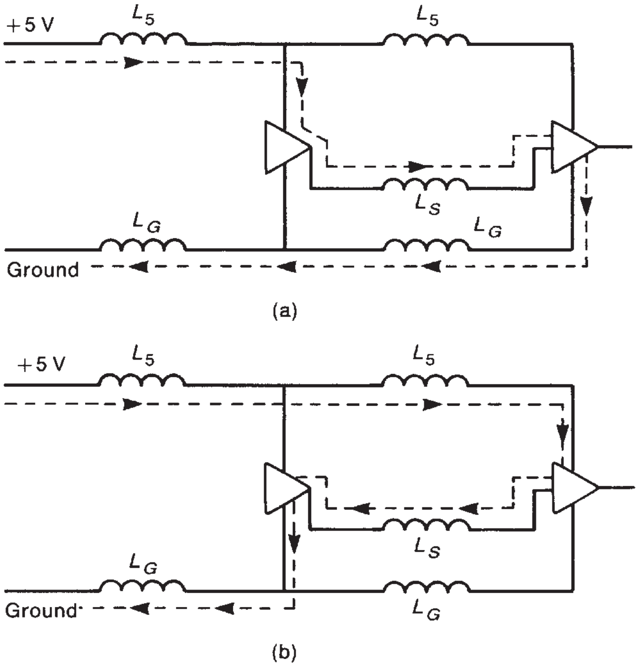

FIGURE 11.41 Loop areas formed when gates switch state: (a) high-to-low; (b) low-to-high.

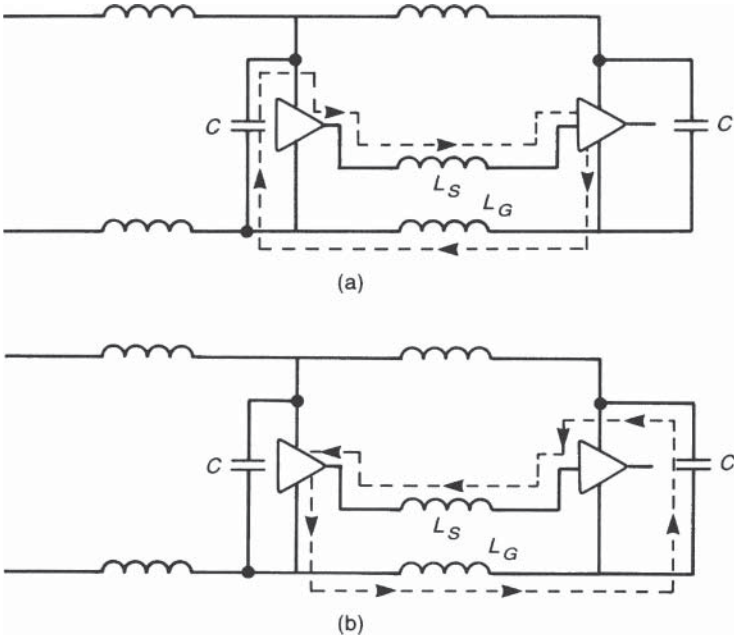

FIGURE 11.42 Use of decoupling capacitors to minimize loop areas when gates switch state: (a) high-to-low; (b) low-to-high.

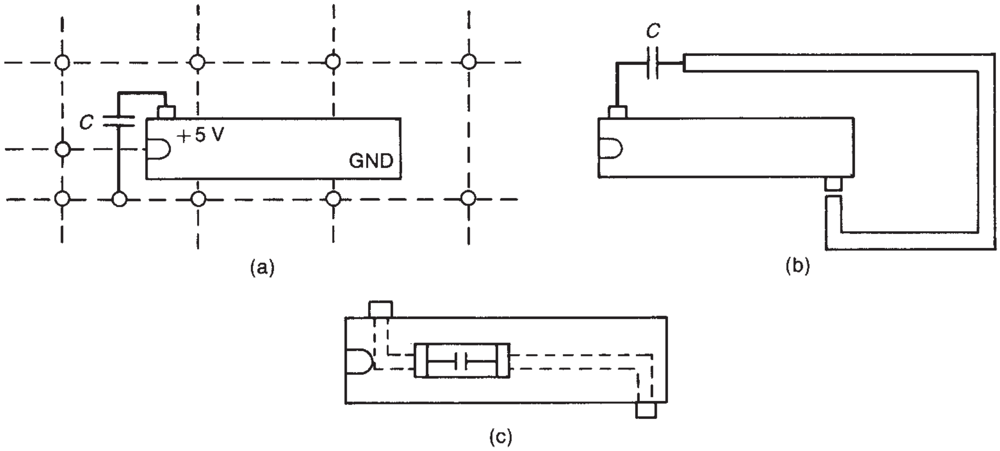

FIGURE 11.43 Decoupling capacitor placement: (a) use of the ground grid to minimize the ground return inductance; (b) the capacitor lead length includes the length of the PCB land required to connect it to the module pin; (c) a surface-mount capacitor on the opposite side of the board minimizes the lead length.

capacitor lead wires to the module pins. An example of this is illustrated in Fig. 11.43b. The fact that the wires of the capacitor are kept short is of little consequence; the long connection land acts like a long lead wire as far as inductance of the total path is concerned. Surface-mount technology (SMT) allows the placement of numerous components such as resistors and capacitors on the opposite side of the PCB. Hence, this can be used to place a SMT capacitor beneath (on the other side of the

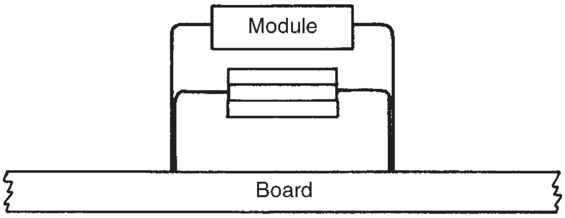

FIGURE 11.44 Distributed (parallel-plate) decoupling capacitors reduce the effect of lead inductance.

board) the module as shown in Fig. 11.43c, thereby minimizing the total connection lead length. In addition, there are "distributed capacitors" that can be inserted beneath the module (plugged into a socket first and the module inserted next) as illustrated in Fig. 11.44. These consist of parallel plates separated by a thin dielectric. Hence, a distributed capacitor (with virtually no "lead length") is inserted between the module pins.

Another way of looking at the effect of this lead length of the decoupling capacitor is in the frequency domain. In Chapter 5, we found that a capacitor C will resonate with the inductance of its leads L_{lead} at a frequency of

$$f_0 = \frac{1}{2\pi\sqrt{L_{\mathrm{lead}}C}} \tag{11.26}$$

The waveform of the switching current contains frequency content up to the reciprocal of the risetime, $f_{\max} = 1/\tau_r$. This spectral content must be retained because the shape of the transition pulse must be preserved. If a significant portion of this spectrum is removed, time-domain parameters such as risetime will be affected. Above the resonant frequency in (11.26), the capacitor will resemble an inductor and its effect will be lost. This is again illustrated in Fig. 11.45. Remember that, for a fixed lead length, *the larger the capacitor value, the lower in frequency the resonant frequency will move*. This emphasizes that one should use as small a value of decoupling capacitor as possible. In some schemes, two capacitors are placed in parallel to overcome this effect. The idea is to use a large value of capacitance to accommodate the lower-frequency part of the spectrum and a small value of capacitance to take over above the resonant frequency of the large capacitor as illustrated in Fig. 11.46a. This, of course, sounds logical until it is examined closely. Figure 11.46b shows the Bode plot of the magnitude of the input impedance to the parallel combination computed by hand assuming the lead inductances are equal, $L = L_1 = L_2$, and $M = 0$, which was published in [19]. The break frequencies are $C_1 \gg C_2$:

$$f_1 = \frac{1}{2\pi\sqrt{LC_1}} \tag{11.27a}$$

$$f_2 = \frac{1}{2\pi\sqrt{2LC_1}} \tag{11.27b}$$

$$\begin{aligned} f_3 &= \frac{1}{2\pi\sqrt{LC_2}} \\ &= \sqrt{2}f_2 \end{aligned} \tag{11.27c}$$

Observe that *the high-frequency asymptote of the parallel combination is reduced by a factor of only 2 or 6 dB from that of the single capacitor* (C_1). What is happening is very clear; at high frequencies above the last break frequency of the smaller capacitor, both capacitors are above their resonant

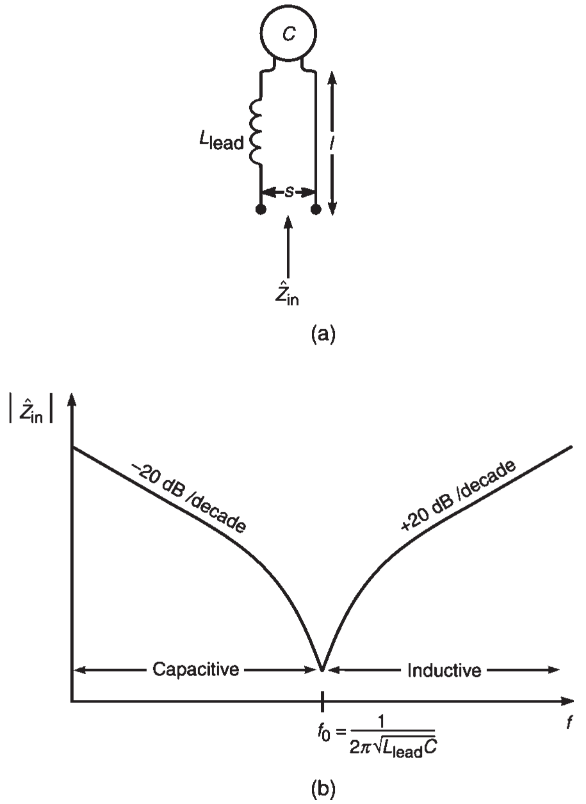

FIGURE 11.45 Effect of component lead inductance: (a) the model; (b) illustration of the fact that above the self-resonant frequency, a capacitor will appear to be an inductor.

frequencies and hence look like inductors of value L. Hence, we essentially have two inductors in parallel, which have a net inductance of $L/2$ that is one-half the inductance of the larger one above its resonant frequency. However, this could have been achieved by using only one capacitor, the larger one (C_1) and *reducing its lead lengths by one-half*! There are, however, cases where this would be more beneficial. If the larger capacitor were of a tantalum or electrolytic type as is common for large capacitors, these would have, in addition to the lead inductance, a substantial internal inductance that is usually much larger than the lead inductance. In this case, the lead inductance of the smaller, high-frequency capacitance in parallel with the large inductance of the larger capacitance would yield a much smaller net inductance than that of the large capacitor alone, thereby achieving a high-frequency reduction of more than 6 dB.

Figure 11.47 shows the computed and experimental results that were published in [19]. The SPICE simulation of two parallel capacitors, $C_1 = 0.01\ \mu\text{F}$ and $C_2 = 100$ pF are shown in Fig. 11.47a. The lead wires are 22-gauge solid wires and the lengths are 0.25 in. (6.35 mm) and are separated by 0.25 in. The loops are placed parallel and separated by 1/8 in. (3.18 mm). The lead self-inductances are $L_{lead} = 11.48$ nH, and the mutual inductance between the two loops formed by the lead wires is $M = 2.046$ nH, giving a coupling coefficient between the loops of $k = 0.178$. Figure 11.47a shows the SPICE simulation of the total impedance (magnitude) of the two in parallel from 10 to 500 MHz. Also shown are their individual impedances. The combination shows a strong resonance around 100 MHz. But away from this resonance, the total curve follows the asymptotic

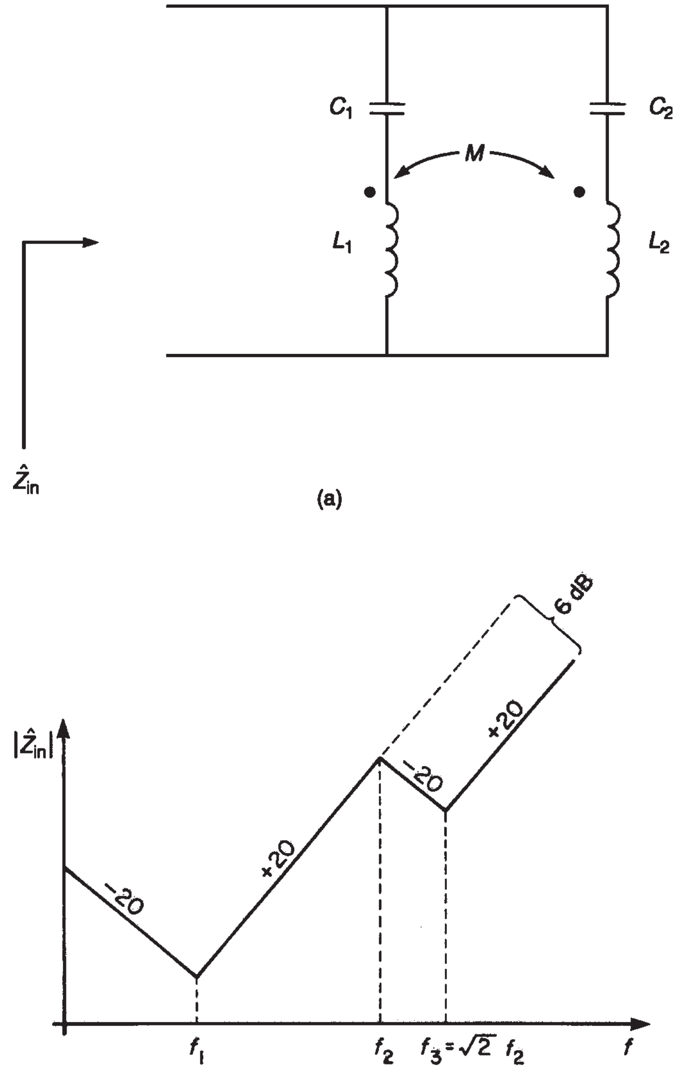

FIGURE 11.46 Use of two parallel capacitors in an attempt to eliminate the effect of lead inductance: (a) the equivalent circuit showing lead inductance and mutual inductance; (b) the Bode plot of the impedance of two parallel decoupling capacitors, including the effect of lead inductance.

plot in Fig. 11.46b. Figure 11.47b shows the experimentally measured impedance of the parallel combination. Comparing Fig. 11.47a,b, we observe excellent predictions. The SPICE predictions are used to plot Fig. 11.47c, which shows the ratio (in decibels) of the impedances of the isolated 0.01 μF capacitor and the parallel combination with a 100 pF capacitor. This illustrates the improvement of the parallel case over the single large capacitor. This clearly shows that the only widespread improvement is above approximately 150 MHz and that is only 6 dB, the rationale for which was discussed previously. This is yet another example of things that “sound right” not turning out to be correct.

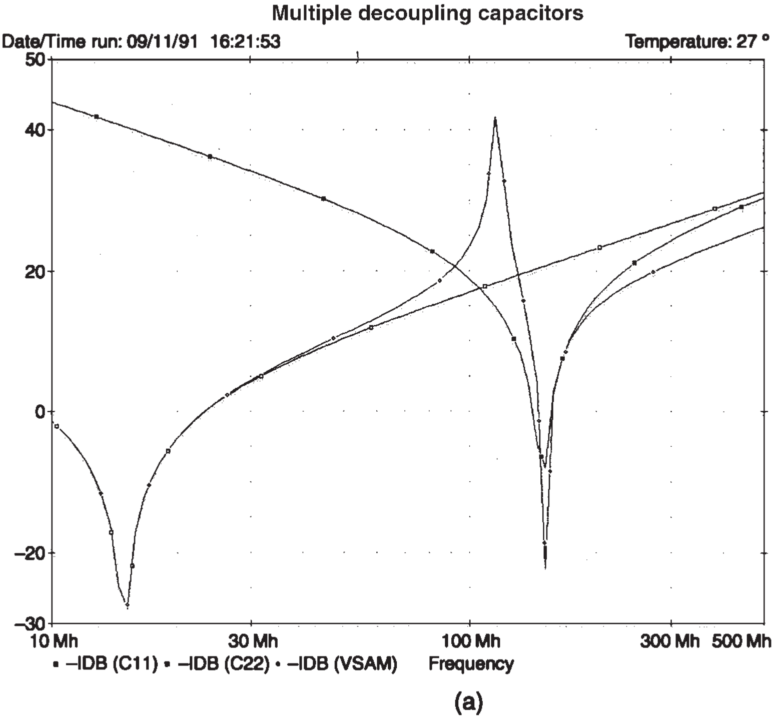

FIGURE 11.47 Frequency response of the impedance of two decoupling capacitors in parallel showing little high-frequency improvement over one: (a) SPICE simulation of the impedance of a 0.01 μF capacitor and a 100 pF capacitor individually and in parallel from 10 to 500 MHz; (b) measured impedances of a 0.01 μF capacitor and a 100 pF capacitor individually and in parallel from 10 to 500 MHz; (c) the ratio (in decibels) of the impedances of the isolated 0.01 μF capacitor and the parallel combination with a 100 pF capacitor. This illustrates the reduction in radiated emissions afforded by the parallel combination (on the order of 6 dB). Source: Paul [19]/IEEE.

We now turn to the computation of the proper value of the decoupling capacitor. This has been the subject of much controversy and research [20]. The reason for this is that the situation is very complicated and relies on knowledge of certain parameters that are unknown to any great degree of accuracy. One thought process is to write the terminal relation of the capacitor as [16]

$$C = \frac{Idt}{dV} \tag{11.28}$$

Next we suppose that during the state change, a current I is required from the capacitor and the voltage across the capacitor (and across the module power and ground pins to which it is attached) are not to be allowed to change by more than dV during the time the state is changing, $dt = \tau_r$. For example, if the supply voltage is not to be allowed to decrease from its value of 5 V by more than 0.1 V in 1 ns and the drive current required is 50 mA, this gives a required value of the decoupling capacitor of 500 pF. Another way of looking at this is shown in Fig. 11.48. The capacitor is to discharge through the +5 V and ground pins of the module, and R is the net resistance seen in this discharge path. The capacitor is initially charged to +5 V and to discharge by only 0.1–4.9 V during the risetime of 1 ns. The value of R is difficult to determine but probably is on the order of 100 Ω

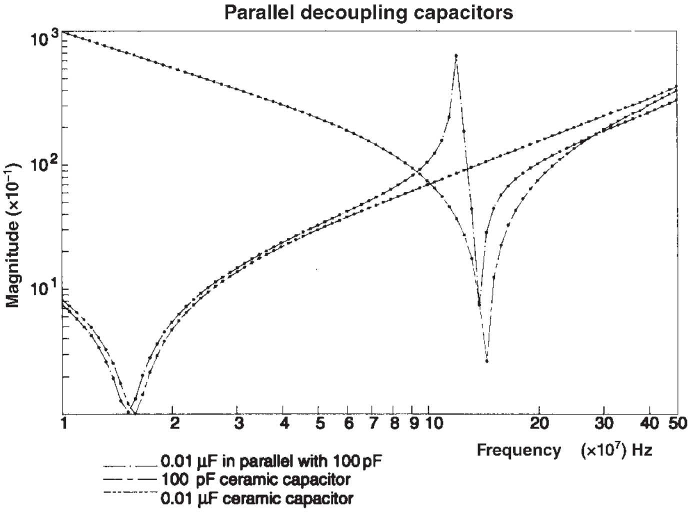

(b)

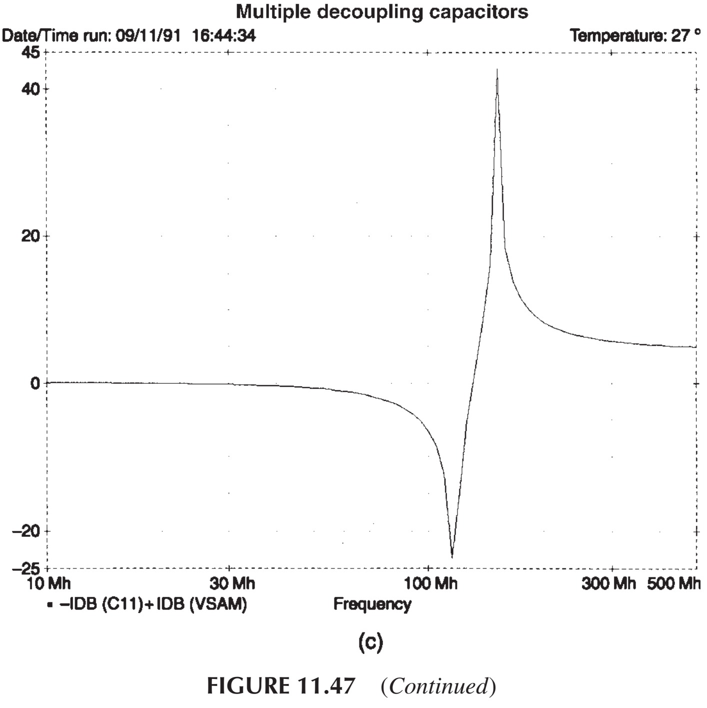

(c)

FIGURE 11.47 (*Continued*)

(see Fig. 11.10, where R is the resistance in the collector of the totem-pole driver). The result for the discharge voltage in Fig. 11.48 is [13]

$$V_0 - \Delta V = V_0 e^{-(\tau_r / RC)} \tag{11.29}$$

Solving this gives the value of C as

$$C = \frac{\tau_r}{R \ln \left[V_0 / \left(V_0 - \Delta V \right) \right]} \tag{11.30}$$

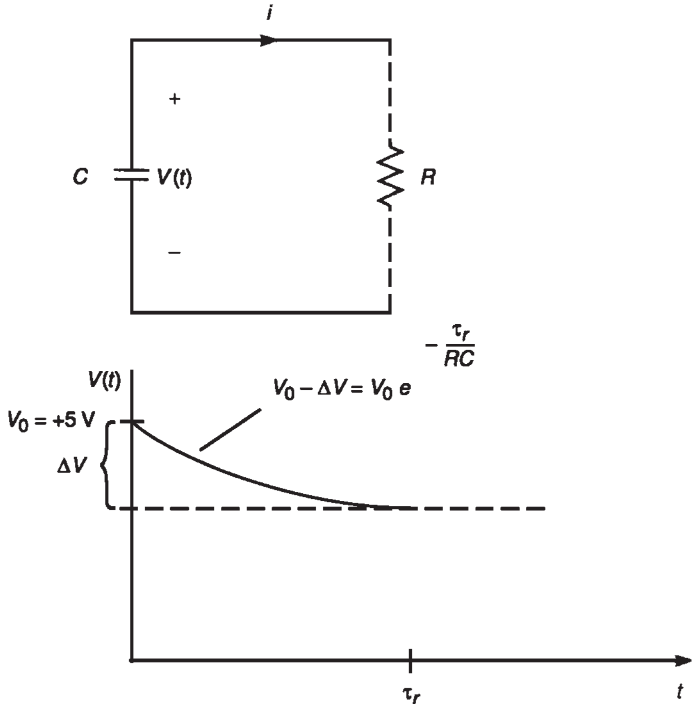

FIGURE 11.48 Transient discharge response of a decoupling capacitor. Source: Paul [13]/John Wiley & Sons.

This gives a value of $C = 495$ pF, which is very close to the value computed with (11.28). Using the approximation of the natural logarithm

$$\ln(1 - x) = -x - \frac{x^2}{2} - \frac{x^3}{3} - \cdots \quad x^2 < 1 \tag{11.31}$$

Equation (11.30) can be approximated by retaining only the first term of (11.31) as

$$C \cong \frac{V_0 \tau_r}{R \Delta V} \tag{11.32}$$

which is identical to (11.28), giving an approximate value of $C \cong 500$ pF. SPICE (PSPICE, LTSPICE, etc.) is a powerful simulation tool. We can simulate actual modules, all known parasitic components, and so on to see how well the rough prediction of the capacitance performs.

11.3.6 Reduction of Loop Areas

We are now sensitized to the effect of large loop areas in the production of radiated emissions; these must be avoided. Figure 11.49 shows some simple examples where a little thought will achieve a reduction of these loop areas in the power distribution circuit with little or no added cost to the product. Figure 11.50 shows a similar loop area reduction for the signal–return path. Of course, not all return paths can be easily seen, as we discussed at the beginning of this chapter. But we should

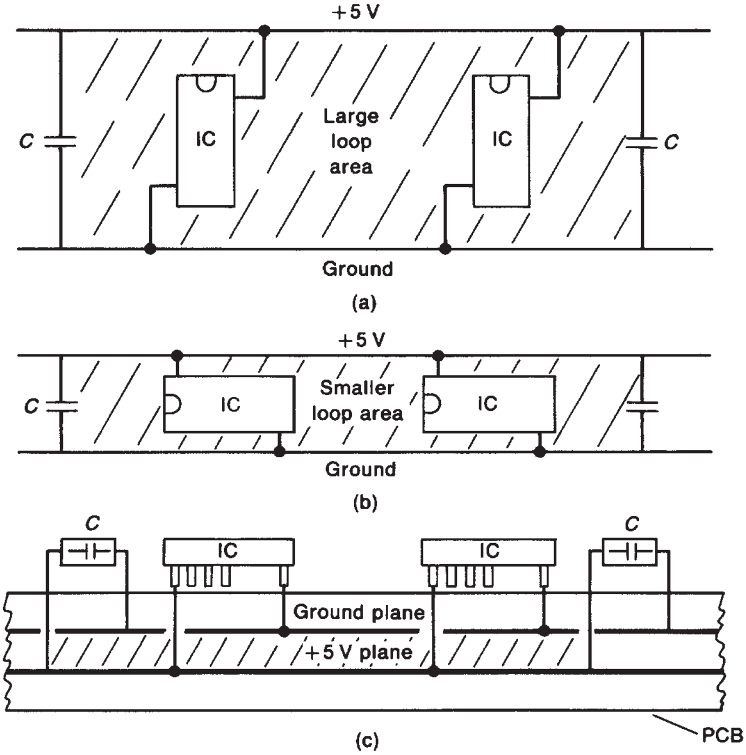

FIGURE 11.49 The important consideration of loop area in minimizing radiated emissions of the power distribution circuits: (a) large loop areas; (b) smaller loop areas; (c) use of an innerplane (multilayer) PCB to reduce the loop area and the characteristic impedance of the power distribution circuit.

nevertheless attempt to identify these on the basis of sound principles and try to observe whether there will be any large loop areas and correct them before production of the prototypes. PCB layout software can generate routing sketches for individual "nets." For example, the lands and their routing for only the +5 V and ground net can be printed. This removes a lot of clutter caused by the presence of the other net lands that can obscure the observation of loops in the power-ground system.

11.3.7 Mixed-Signal PCB Partitioning

As stated earlier, it is preferable to use as few PCBs in the system as possible in order to avoid common-mode currents that would be generated on the cables that would be required to interconnect the boards. Most low-cost electronic systems can be placed on one PCB even though that PCB might be quite large. Most PCBs will have three distinct types of electronic circuitry on them: a *digital section* containing the digital electronics, a *low-level analog section* containing linear ICs such as opamps, and a *high-level noisy section* containing very noisy signals such as motor driver circuits. In order to keep each signal class in its own section so as to not contaminate other sections, we would naturally *partition* the PCB into three *geographically distinct* sections containing these three circuits as illustrated in Fig. 11.30. The intent here is to prevent common impedance coupling when currents of one section flow through another section (in order to return to their source), causing that section to malfunction. Generally, we do not worry about the low-level analog signals corrupting the digital section or the high-level noisy section (motor driver circuitry). However, it is a legitimate

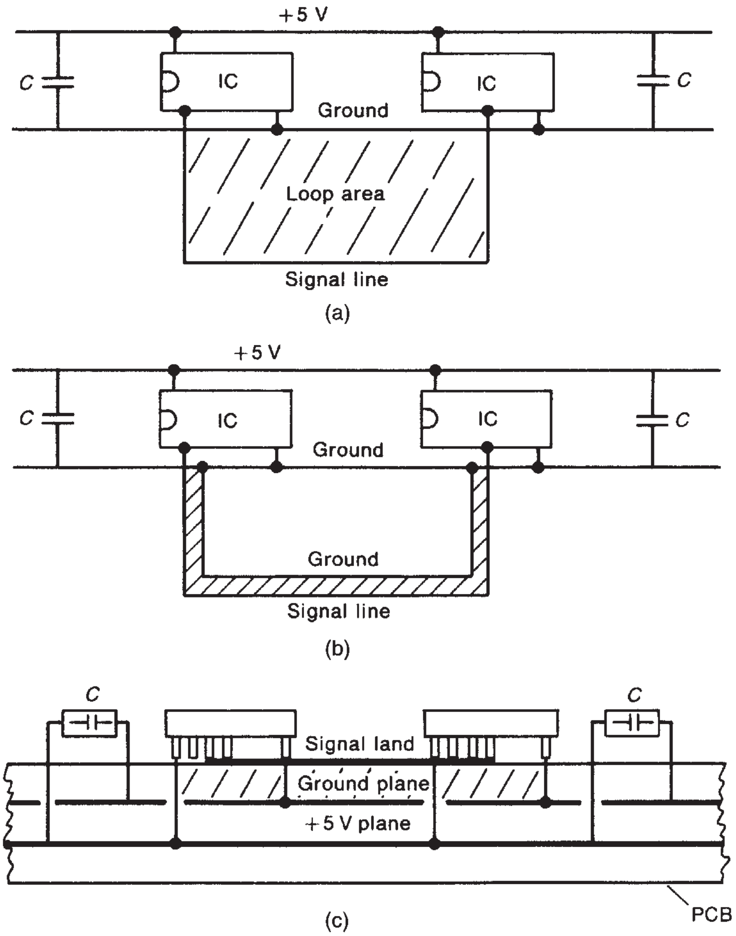

FIGURE 11.50 Large loop areas of the signal–return path should be minimized to reduce radiated emissions: (a) large loop areas; (b) smaller loop areas; (c) use of an innerplane (multilayer) PCB to reduce the loop area and the characteristic impedance of the signal–return circuit.

concern that the digital signals or the high-level noisy signals may (and generally would) contaminate the low-level analog section and cause the electronics in it to malfunction. It is also a legitimate concern that the high-level, noisy motor driver currents may, if permitted to pass through the digital section, cause that section to malfunction. This causes designers to *split ground planes* to try to prevent this as shown in Fig. 11.51a. Passing a trace across the split in the ground plane may cause a large loop area for the return current (back through the power supply common connection or the connection between the two grounds where they enter the board at the power connector). Splitting ground planes or placing a slot in a ground plane and passing a trace over the slot as in Fig. 11.22 has been shown to produce increased radiated emissions [15]. One reason for this is that large loop areas are produced by the return current. In addition, the two planes, which are not connected, are at different high-frequency potentials, thereby producing a dipole antenna; this is an equally bad situation from a radiated emissions standpoint.

We clearly must *physically separate* the voltage distribution planes. In other words, we would need to partition the power plane into three separate, and obviously unconnected, sections: one for

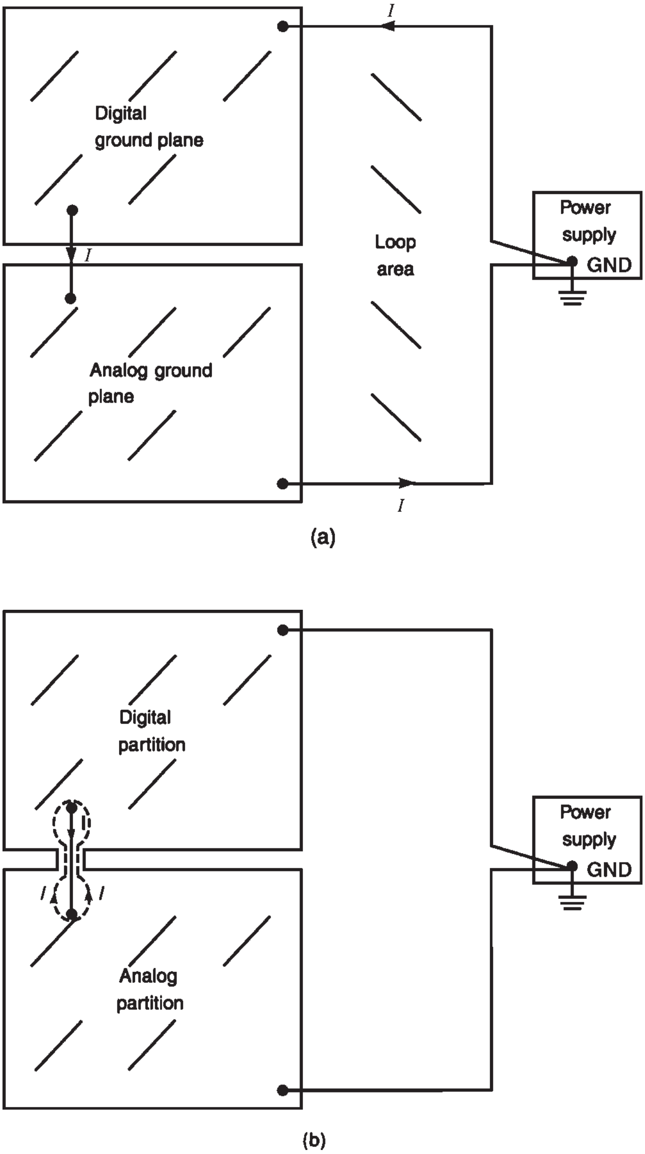
I
Digital
ground plane
I
Loop
area
Power
supply
GND
Analog ground
plane
I
(a)
Digital
partition
Power
supply
GND
I
I
Analog
partition
(b)

FIGURE 11.51 Partitioning analog and digital ground planes, (a) which can create long return paths and large loop areas; (b) providing a connection between partitions beneath the "going-down" land; can reduce the loop area, (c) but are unnecessary since the current will tend to return beneath the "going-down" path if given the opportunity [21]. Source: Based on Ott [21].

the +5 V digital voltages, one for the ±12 V low-level opamp voltages, and one for the +38 V motor driver voltages. But physically splitting the ground plane is a bad idea, as shown by Ott [21].

We showed in Section 11.2.4 that currents on a trace above and close to a conducting plane will return along a path directly below that trace (see Fig. 11.21b). Hence, if we provide a connection between the two ground planes directly beneath any trace that carries a current between them, that current will return directly beneath the trace, thereby minimizing the loop area and hence the radiated emissions as shown in Fig. 11.51b. Ott points out that this suggests that it is better not to split the

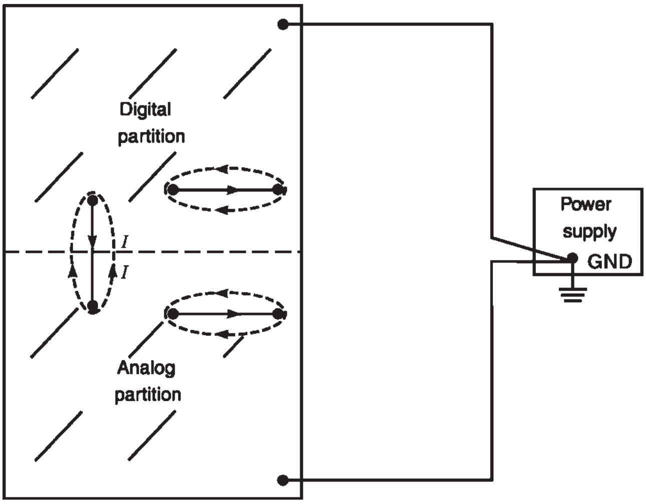

(c)

FIGURE 11.51 (*Continued*)

ground planes as shown in Fig. 11.51c because the currents will then have a path to return that is directly beneath the trace. This again minimizes the loop area and eliminates the dipole antenna formed between the two ground planes if they are unconnected [21]. He also points out that even if the ground plane is contiguous and not split, return currents of other signals in each section will also flow beneath the going-down trace in that section as shown in Fig. 11.51c and will thereby not inadvertently flow in and contaminate the other section.

In low-cost products where only double-sided boards without innerplanes can be afforded, a gridded ground can be used to approximate a ground plane. Hence, these principles can be adhered to in low-cost systems. This use of "image planes" has been shown to significantly reduce radiated emissions presumably by reducing loop areas and/or common-mode currents along otherwise long conductors of a return [14].

11.4 SYSTEM CONFIGURATION AND DESIGN

Perhaps one of the more important aspects of the EMC design of a system is the configuration of the system and its subsystems (location and orientation of the PCBs, cable connectors, power supply and filter, etc.). Quite frequently, improper configuration is the major cause of functional performance problems or failure to comply with regulatory limits. The purpose of this section is to bring attention to this important aspect of EMC design.

11.4.1 System Enclosures

One of the decisions made in the first stage of product development is the external "packaging." The shape and external appearance are typically driven by customer preferences and ergonomic considerations, such as location and shape of a keyboard, and location of the on/off switch. This severely constrains the EMC engineer's options with regard to subsystem placement, internal cable routing, etc. It is therefore important that the EMC engineer be actively involved in the design process from the beginning.

One of the first decisions that must be made has to do with the type of system enclosure: metal or plastic. EMC designers prefer metal enclosures, since shielding of the interior electronics can be more easily achieved. However, metal enclosures are difficult to form into smooth shapes, which gives them a “boxy” appearance that has less appeal to the consumer. Enclosures for large computers and Class A devices such as point-of-sale terminals are usually metallic, since consumer preferences are not as significant for these devices. Seams can be closed quite effectively, reducing radiation from these “slot antennas.” Metallic fingers along the edges of doors reduce the leakage (and points of entry for external signals such as ESD). Knitted-wire gaskets can also be placed along the edges of the seam to close this aperture. It is very important to remember that *any cable that penetrates this shielded enclosure will drastically reduce the shielding effectiveness of the enclosure to internal as well as external signals unless these are treated properly*. For example, peripheral cables that exit the product may require filtering in the form of *RC* packs on each wire or a common-mode choke through which all of the cable wires, including the shield pigtail wire, must pass. Prior to construction of a prototype, it is difficult to determine whether this treatment of all peripheral cables will be necessary. It is therefore wise to allow for the later addition of these components if they are required. For example, pin-through holes that allow insertion of an *RC* pack or a DIP toroid can be provided on a PCB where a peripheral cable exits the board. These connections can be “wired across” with 0 Ω SMT resistors in the initial design. If EMC testing determines that an *RC* pack or a DIP toroid is needed to reduce the signals that exit the board via this cable, the resistors can be removed and the components mounted without a repeated layout of the board. It is quite important to allow space for these components in the initial layout, since board space is often unavailable once the design is completed.

Plastic enclosures are easily molded into any desired shape and present an aesthetically pleasing system enclosure. Such enclosures are cheaper to produce than metal ones (at least before any interior conductive sprays or metal impregnation required for EMC is applied). However, a plastic enclosure provides no shielding, so careful attention to EMC design of the interior electronics is more critical. It is possible to provide some degree of shielding by either coating the interior with a conductive material or by impregnating conductive fibers in the plastic during molding. Conductive paints can be applied, and nickel is a common spray material. There are many other ways of applying this conductive coating, such as flame/arc spraying, vacuum metallization, electroless plating, and metal foil linings. These techniques vary in cost and effectiveness. Conductive fillers can be impregnated in the plastic during molding. A comparison of the shielding effectiveness of these various types of treatment of plastic enclosures is given in [11]. *Even with conductive plastic enclosures, it is important to realize that any penetration of the enclosure such as a peripheral cable or an aperture must be properly treated, or else the ideal shielding effectiveness of the enclosure may be essentially nullified*!

Apertures such as fan vents or other vents must be closed electromagnetically. Screens with many small holes have much better shielding effectiveness than do a few large holes or several long slots, as discussed in Chapter 10. Cathode ray tube (CRT) faces also provide apertures for the internal fields to exist the enclosure. Wire-mesh screens consisting of many small holes can be laminated between two glass sheets to shield the CRT face while only marginally restricting the view.

11.4.2 Power Line Filter Placement

An example of good EMC design is the placement of the power supply filter. The point at which the commercial ac power enters the product is usually chosen for aesthetics, namely, at the rear of the product. The on/off switch is placed at the front of the product with the consumer in mind. Routing the phase and neutral power wires from the rear entrance of the power cord to the front of the product where the switch is located and then back to the rear of the product to pass through the power supply

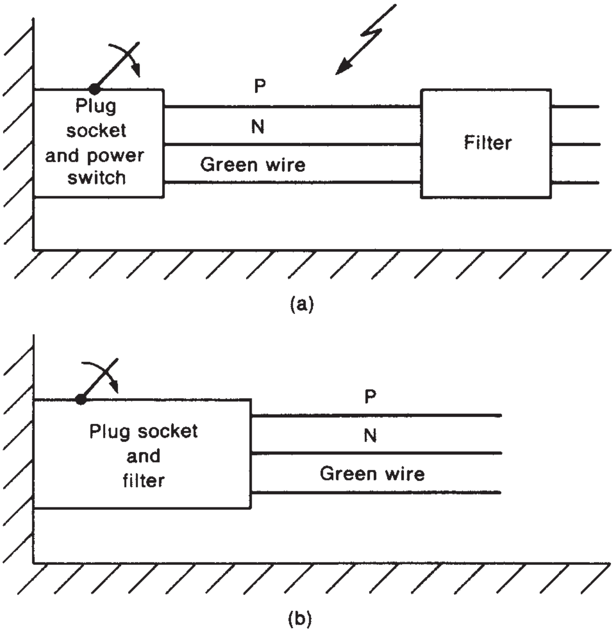

FIGURE 11.52 Effect of power supply filter placement on product emissions: (a) poor placement, allowing coupling to the power cord and bypassing of the filter; (b) proper filter placement.

filter and the power supply creates obvious problems. The exposed section of the wires from the rear entrance to the front switch will pick up signals internal to the product. These signals will then pass *unimpeded* out through the ac power cord, where they are efficiently radiated from the cord or conducted into the LISN in a con ducted emissions test. Either of these situations will likely cause serious problems in complying with the regulatory limits. The actual switch may be placed at the rear of the product where the power cord enters, and a mechanical linkage can be connected between the switch and the on/off switch lever at the front of the product.

In some designs, the power supply filter circuitry may be mounted on the same PCB as the power supply. This also has the possible disadvantage of placing the filter at some distance from the point of entrance of the power cord, as shown in Fig. 11.52a, so that internal noise bypasses the filter. A more desirable placement of the filter is directly at the point where the ac power enters the product, as illustrated in Fig. 11.52b. There exist predesigned, prepackaged integral power sockets and power supply filters. These configurations are the most effective in preventing this bypassing of the filter.

11.4.3 Interconnection and Number of Printed Circuit Boards

The next important decision concerns *the number and interconnection of the PCBs in the product.* As a general rule, *it is preferable to have only one system PCB rather than several smaller PCBs* interconnected by cables. The reason for this is that it is easier to limit the voltage drops developed between the grounds of the parts of the system when they are placed on the same board than when they are placed on separate boards and interconnected by cables. Cables introduce impedance that affects the voltage drop between the two ends of the cable. The impedance between the two subsystems can also be reduced with a *ground grid* if all subsystems are placed on the same board. Trying to achieve the same result in an interconnection cable between PCBs is difficult, since many interspersed ground wires will be required in a ground–signal–ground–signal– … configuration in that

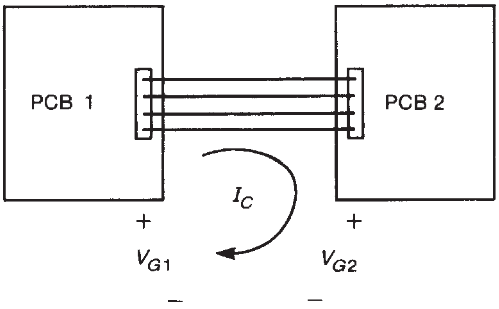

FIGURE 11.53 Illustration that multiple PCBs tend to promote common-mode currents in interconnect cables.

cable, and these ground wires cannot be as closely spaced to their adjacent signal wires as can lands on a PCB. *High-frequency voltages developed between PCBs create common-mode currents flowing between the boards that accentuate radiated and conducted emissions*, as illustrated in Fig. 11.53. Placing all electronics on one board tends to reduce this voltage difference between subsystems on the board.

High-speed signals that pass between PCBs should be buffered where they *enter* the PCB to reduce fan-out problems. For example, suppose that a signal passing from one PCB to another fans out to four other devices. Placing a buffer at the input to the board reduces the current in the interconnect line by a factor of 4 over placing the buffer at the output of the other board, and hence reduces its radiated emission potential, as well as its common-mode current generation potential.

PCBs that must be separated should be connected with low-impedance (*high-frequency-impedance*) connections such as short lands on a motherboard or backplane. The PCBs are interconnected by plugging their edge connectors into this motherboard. Figure 11.24 illustrates some important considerations in the design of these motherboards. Although it is not always strictly necessary, one clock signal may be passed between PCBs along this motherboard. Where possible, this should be avoided, as in asynchronous communication channels. Also various lower-frequency signals are passed between the PCBs on the conductors of this motherboard. Ground conductors should be placed adjacent to these conductors in order to *reduce the radiated emission loop area as well as the inductance and corresponding voltage drop (high frequency) along these conductors*. Figure 11.24a shows a *poor placement* of these ground lands. The return path for the clock signal is at the opposite end of the board, resulting in a large loop area and inductance. Figure 11.24b depicts a *better placement* of these ground lands. Ground or return lands are placed on both sides of and in proximity to the clock signal. Thus, the clock signal should return on these lands, reducing the radiated emission potential as well as the inductance of the path of this important signal. Also, ground or return lands are placed around the signal lands for similar purposes. Since these signals (data, etc.) are usually at a much lower repetition rate than the clock, several signal lands can be contained between ground lands. It is equally important to pay attention to where these return lands are connected on the individual PCBs.

11.4.4 Internal Cable Routing and Connector Placement

The location of cable connectors on PCBs is another critical design consideration. An important aspect of PCB layout is to *place the highest-frequency electronics toward the center of the PCB*. The intent is to take advantage of the natural filtering of the signals by the board as the signals inadvertently pass to the cable connectors. Suppose that the system clock oscillator is placed at the center of the board along with the processor it serves. This high-frequency signal will inadvertently couple to other lands, allowing the possibility of passing out through the cables that are attached to the board, where the signal would contaminate other parts of the system and radiate more efficiently. Maintaining the largest distance between the high-frequency signals and points of exit of the board will place filtering (unintentional but useful filtering) such as parasitic capacitance and inductance in their path. Even though this filtering is not intentionally designed and therefore not as efficient as it can be, it nevertheless should be used to advantage. Placing the connectors at the outer edge of the board and placing the high-frequency electronics at the center will maximize this filtering.

In addition, all connectors should be placed on the same edge of the board. The reason for doing this is to prevent the development of voltage drops between the wires in one cable and another cable that will drive common-mode currents out those cables. The voltage drop across two diagonally opposite corners of a PCB will generally be significant no matter how well laid out the board. Also, if the connectors are all placed on one edge of the PCB, it is easier to provide a "quiet ground" along this local area of the board to which cable shields can be connected. If the point of attachment of the shields is noisy, the shields are then driven as effective antennas and so do not achieve their objective.

Probably one of the simplest yet potentially serious problems to correct is the internal routing of cables within the product. Figure 11.1 illustrates that the potential for indirect but highly efficient coupling to cables can be considerable if those cables are allowed to pass near noisy components of the system. Such inadvertent coupling can virtually invalidate any of the conscientious thought given to PCB layout. This again points out that overall system EMC cannot be accomplished unless all participants in the design discuss the potential for EMC problems in every phase of development.

11.4.5 PCB and Subsystem Placement

Attention should be paid to the *placement and orientation of the PCB* (*s*) *in the system*. For example, placing two PCBs vertically and near each other as shown in Fig. 11.2 allows coupling of signals from one board to another. Not only may this present functional problems, it may also allow for a more efficient exiting of these high-frequency signals onto cables or other parts of the system where the signal may radiate more efficiently. It is a waste of time to take care in the placement of the high-frequency electronics at the center of the board and the connectors at the edge in order to impede the exiting of a high-frequency signal and yet have it couple to another board that is placed nearby. The careful attention to layout in the first board is severely compromised or possibly negated by this board placement. Also, the routing of cables that exit this board should be given consideration to avoid problems of coupling to the cable illustrated in Fig. 11.1. Thus, it is essential that the board designers and the packaging personnel confer in the early stages of the design before the system configuration is "frozen."

11.4.6 PCB and Subsystem Decoupling

Once again, it is important to remember that *noise signals should be confined to their known and desired location and not be allowed to propagate to other parts of the system where they may radiate more efficiently and/or cause functional problems*. These noise signals can couple either by radiation from PCB to PCB or via conducting paths such as interconnect cables or backplanes. Eliminating this coupling is referred to as *decoupling the subsystems*. Common-mode currents flowing between subsystems (PCBs, etc.) can be effectively blocked with ferrite, common-mode chokes, as illustrated in Fig. 11.32. These are available in DIP packages suitable for automatic insertion as with other components of the PCB.

Another method of decoupling subsystems is to insert a filter in the connection wires or lands between the subsystems. This filter can be in the form of *R*–*C* packs, ferrite beads, or a combination.

The significant difference between this method of decoupling and the use of a common-mode choke is that a filter will affect differential-mode (functional) signals and thereby may affect the functional performance of the product. Filtering must be used with care.

High-frequency signals on the power distribution system between subsystems can be reduced by the use of decoupling capacitors. In essence, these serve as local reservoirs of charge for the switching signals.

11.4.7 Motor Noise Suppression

An oft-overlooked component of today's digital systems is the electromechanical motor. Small ac motors are used for cooling fans, whereas small dc motors are used to draw in paper and/or move a print head in printers and electronic typewriters. Stepper motors provide precise positioning such as the rotation of a printer platen. These motors, because of their physical construction, provide very-high-frequency noise sources as well as very pronounced parasitic paths for inadvertently placing high-frequency noise on other parts of the product where they may radiate more efficiently or be conducted out the power cord. The ac motors and the dc motors both share an important physical construction parameter: coils of wire around ferromagnetic cores. These coils are placed in proximity to reduce the reluctance of the airgaps between them, thereby introducing significant parasitic capacitance between them. In the dc motors, the power is provided to the coils on the rotating member, the rotor, producing fields that repel or attract the fields on the stationary member, the stator. Very often the stator is directly connected to the frame of the motor to provide thermal heat sinking. This frame of the motor is then connected to the overall metallic members of the product. High-frequency noise signals on the rotor are thereby coupled to and placed on the large metallic frame of the product by these parasitic capacitances, where they radiate very efficiently and/or introduce noise inadvertently into other portions of the system electronics. The author has measured the impedance between the input leads (tied together) of a small dc motor and the frame of the motor. It was found that the impedance had a minimum of around 1 Ω at around 100 MHz! Hence, noise currents at around 100 MHz were virtually "hard-wired" to the frame. Stepper motors tend to be constructed similarly, except that the power is applied to the stator, and the rotor consists of either rare-earth permanent magnets (PMs) or are formed by induction through the variable reluctance of the path as it rotates (VR).

The motors themselves have *driver* electronics that control the movement and position of the rotor. The small de motors are usually driven by a H-drive electronic circuitry shown in Fig. 5.39a of Chapter 5. The driver transistors turn on and off to change direction. Hence, currents that have very fast changes in polarity and consequently high-frequency content are sent from the driver to the motor. Often, they produce common-mode currents on the attachment wires that radiate very efficiently. A common-mode choke is frequently needed in the drive wires to suppress these as shown in Fig. 5.39b. A stepper motor has a similar problem. Its drive circuitry, shown in Fig. 5.40 of Chapter 5, produces digital signals applied to the phases of the stepper motor that cause it to rotate in precise, discrete increments. These signals also have very-high-frequency spectral content.

Finally, the dc motors have commutators that act to change the magnetic flux in the windings. The brushes across the commutators alternately make and break the connections to the coils on the rotor thereby creating large $L\,(di/dt)$ voltages that appear between the commutator segments. These voltages are quite large and break down the air, resulting in arcing at the commutator. This arcing has an obvious high-frequency spectral content. In order to suppress this arcing, resistive disks can be inserted on the end of the commutator that place resistances between the commutator segments, thereby damping the effect as shown in Fig. 5.38 of Chapter 5. Alternatively, *RC* disks can be similarly attached to the commutator, giving more effective suppression of the arcing.

11.4.8 Electrostatic Discharge (ESD)

An electrostatic discharge begins with the separation of charge between two insulators. If two initially neutral insulators are placed in contact and rubbed together, charge will be transferred from one insulator to the other. When the materials are separated, they become charged: one negatively and the other positively. The degree to which charge is transferred depends on numerous factors. A general idea of the degree of charge transfer is determined by the *triboelectric series* given in Table 11.2. The triboelectric series shows which materials tend to give up electrons and become positively charged (those at the top or positive end of the chart) and which tend to accept electrons and become negatively charged (those at the bottom or negative end of the chart). For example, rubbing nylon against Teflon can cause electrons to be transferred from the nylon to the Teflon. The degree to which this charge transfer takes place depends on a number of factors, and the triboelectric

TABLE 11.2 The Triboelectric Series

	Positive
1	Air
2	Human skin
3	Asbestos
4	Glass
5	Mica
6	Human hair
7	Nylon
8	Wool
9	Fur
10	Lead
11	Silk
12	Aluminum
13	Paper
14	Cotton
15	Wood
16	Steel
17	Sealing wax
18	Hard rubber
19	Mylar
20	Epoxy–glass
21	Nickel, copper
22	Brass, silver
23	Gold, platinum
24	Polystyrene foam
25	Acrylic
26	Polyester
27	Celluloid
28	Orlon
29	Polyurethane foam
30	Polyethylene
31	Polypropylene
32	Polyvinyl chloride (PVC)
33	Silicon
34	Teflon
	Negative

series is only a rough indicator of this. The order of the two materials in the series is an important factor in most such charge separations, but it does not completely determine the degree or type of charge separation. Other factors such as smoothness of the surface, surface cleanliness, contact surface area, contact pressure, degree of rubbing, and speed of separation are more important. In most cases, the charge transfer is probably due more to contact than to the triboelectric series. Charge can also be separated when two like materials come in contact as with the opening of a plastic bag used to carry produce in a grocery store.

Touching an insulator to a conductor can also create charge separation. However, a charged insulator is not the problem since the surface resistivity of insulators is so large that when charge is placed in a region of an insulator, it cannot readily move about on the surface of the insulator to redistribute itself and neutralize. Hence, an electric discharge cannot take place from an insulator. The problem is when the statically charged insulator approaches a conductor. The conductor is electrically neutral (with equal amounts of positive and negative charge). When the insulator approaches the conductor, it causes the charge to separate on the conductor surface with the charge opposite that of the insulator moving to the surface of the conductor closest to the insulator as shown in Fig. 11.54. This process is known as *induction*. If this conductor touches another grounded conductor, the charge on the opposite side of the conductor will be transferred to the other conductor in the form of a current. As the conductors approach each other, the charge separation will also produce an intense voltage and electric field between the two that can cause the air between them to break down, resulting in an intense spark like a miniature lightning bolt. The breakdown electric field of air is around 3 million volts per meter (3×10^6 V/m = 3000 V/mm). Hence, only a small voltage difference between two conductors, such as a human finger and a grounded computer keyboard, can cause an arc if the two conductors are separated by a small distance, on the order of 1 mm.

The ESD event is generally a result of the following sequence [16, 22]. First, charge is placed on an insulator by contact. The charged insulator induces a charge separation on a conductor by induction. This charged conductor is moved near another conductor (grounded or not), and a discharge or arc occurs from one conductor to the other. This is illustrated by walking across a carpet and then touching a computer keyboard. Electrons are transferred from the carpet to the shoes, leaving a positively charged footprint on the carpet and a negative charge on the soles of the shoes. This induces a charge separation (by induction) on the body (a conductor). Positive charge is induced on the soles of the feet in response to the nearby negative charge on the soles of the shoes, and negative charge moves to the upper parts of the body such as the hand. When the negatively charged finger approaches the keyboard, electrons will be drawn through the ground of the keyboard cable and the green wire of the power cord, leaving a net positive charge on the keyboard. As the finger approaches the keyboard, the charge separation between the finger and the keyboard will produce an intense electrostatic field. An arc may be initiated from the finger to the product similar to a miniature lightning stroke as the intense electric field causes the air to break down. This discharge current may pass through the computer and its internal circuitry, resulting in possible

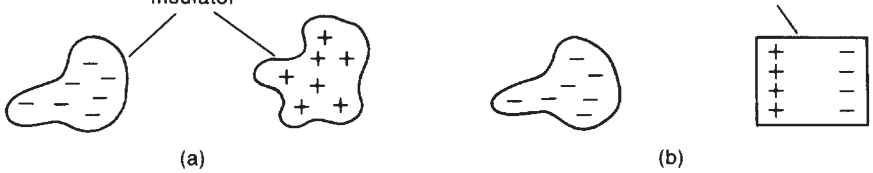

FIGURE 11.54 Illustration of the charging of a conductor by induction: (a) charge separation by contact between two insulators; (b) charge separation on a conductor by induction.

damage to its components or degradation of its function. The speed of approach is an important factor in determining the intensity of the discharge. Formation of the arc requires more time than the discharge. During the formation of the arc, a fast approach will give a narrower arc gap length, resulting in a more intense discharge with faster risetimes and peak currents. It is important to note that ESD voltage discharges of less than 3500 V cannot be felt or seen by humans yet are capable of creating functional problems or even component destruction in electronic circuits.

Figure 11.55 shows typical waveforms of the discharge current in an ESD event. The discharge circuit is represented by a charged capacitance C with an initial voltage V_0 and resistance R of the discharging body. Inductances of the charged body, as well as the green wire of the product, are represented by inductor L. These inductances as well as the resistance cause the arc current waveform to be either overdamped or underdamped. The circuit shown in Fig. 11.55a is a somewhat simplistic model but is sufficient for illustrating the basic phenomenon. More elaborate models are given in the literature [22]. We have been discussing "personnel discharge," i.e., from the human hand to the product. Other types of discharge occur when a metallic chair is moved across a carpet, creating a separation of charge on the chair. When the chair approaches either the product or a metallic table on which the product is placed, a "furniture discharge" may occur. Typical immunity tests try to create personnel, as well as furniture discharges [23]. A furniture discharge typically has smaller resistance in Fig. 11.55a, resulting in underdamped waveforms, whereas personnel discharge typically results in overdamped waveforms because of the higher resistance. Typical risetimes are of order 200 ps to 70 ns, with a total duration of around 100 ns to 2 μs [22]. The peak current levels may approach tens of amperes for a voltage difference of 10 kV. This indicates that *the spectral content of the arc may have large amplitudes and can extend well into the GHz frequency range*!

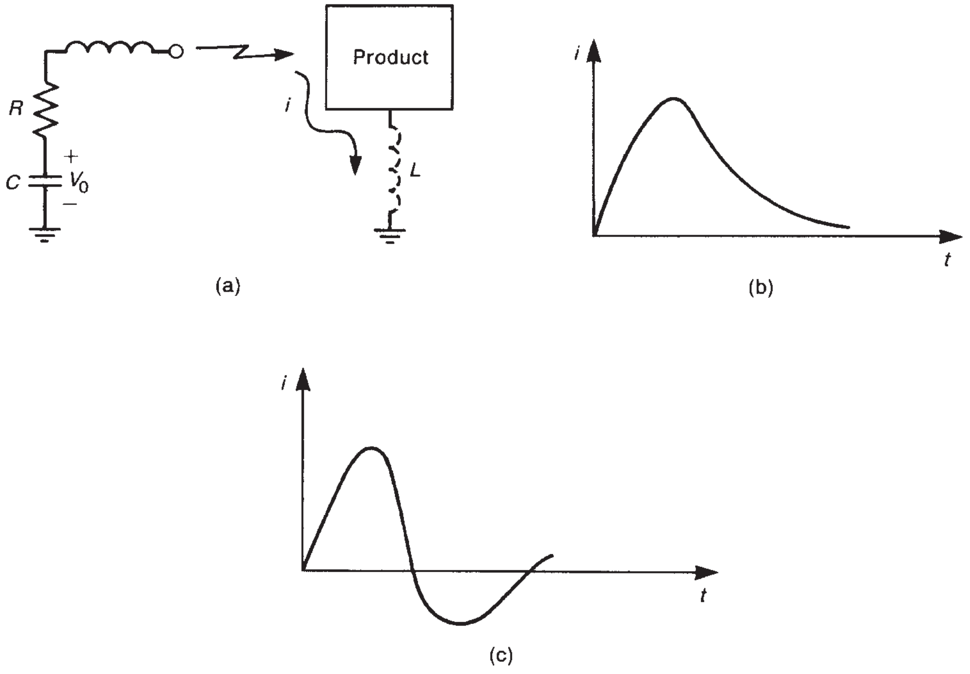

FIGURE 11.55 ESD waveforms: (a) a simple model of human body discharge; (b) the overdamped waveform (typical of human discharges); (c) the underdamped waveform (typical of furniture discharges).

The simple *RLC* circuit of Fig. 11.55a is said to be a single-discharge model. It has been observed that typical ESD discharges can have multiple discharges within a single event. It is interesting to conjecture that this multiple-discharge ESD event is similar to the showering arc discharge associated with the opening or closing of a mechanical switch as discussed in Chapter 5.

This simple scenario represents the typical ESD event. Several mitigating effects will cause the precise discharge generated by one person to differ from that produced by another. For example, as the person walks across the carpet, contact resistance between the soles of the shoes and the carpet will cause a reverse charge flow to occur, which will reduce the charge separated. High humidity will decrease the contact resistance of this path and hence increase the reverse charge flow. Thus, less charge is built up in a humid environment, and hence the ESD event will be of a smaller degree. Antistatic sprays are available that when sprayed on a carpet will tend to increase the conductivity of the shoe–carpet path, facilitating the reduction of stored charge on the body in the same way as high humidity. Nevertheless, the engineer cannot rely on the mitigating effects of such factors as humidity in all potential product installations, so that ESD protection must be included in the product design.

There are basically two primary effects associated with an ESD event:

1. The intense electrostatic field created by the charge separation prior to the ESD arc.
2. The intense arc discharge current.

The extreme differences of potential caused by the intense electrostatic field created by the charge separation prior to the ESD arc can overstress dielectric insulations of electronic components causing their destruction. We will focus on the effects of the arc discharge.

The intense arc discharge current can cause problems ranging from functional upset to component destruction via four secondary processes:

1. Direct conduction through the electronics
2. Secondary arcs or discharges
3. Capacitive coupling to the product's electronic circuits
4. Inductive coupling to the product's electronic circuits

Discharging a large ESD current through the electronics can evidently cause direct damage through thermal heating or can produce large potential differences that can also cause dielectric breakdown, resulting in component destruction. Arc discharges to exposed metallic parts of the product enclosure can result in *secondary discharges* to the interior electronics. The arc current also creates electric and magnetic fields that couple to and induce voltages and currents in the circuits on PCBs and cab ling within the product. These radiated emissions are predominantly a near-field phenomenon due to the proximity of the components to the arc. In high-impedance circuits, the large voltages create capacitive coupling to the electronics. In low-impedance circuits, the large discharge currents create inductive coupling to the electronics. This represents the two mechanisms by which an ESD arc discharge can create functional problems:

1. Conduction
2. Radiation

Conduction tends to produce both malfunction and damage in the electronics. Radiation (near-field radiation here) tends to cause only upset but may also cause damage. The electromagnetic wave created by the arc discharge current may also couple to any peripheral cables and be subsequently conducted into the internal electronics. Thus, there may be a combination of these two mechanisms: radiation followed by conduction. Ordinarily, the term conduction refers to the direct conduction of the arc discharge current through the electronics.

If it were possible to place the electronics in a contiguous metal box having no points of entry such as cables or apertures, the arc discharge would pass along the box exterior through the green-wire connection to ground, thus causing no interference or damage to the components inside the box. In reality, the green wire connection will have a substantial amount of inductance associated with it due to its length. Thus, the potential of the box will rise with respect to ground due to the voltage drop across the green-wire inductance as the discharge current flows through it. If the enclosure is connected to ground via the green wire, the voltage of the enclosure can rise to several thousand volts. If it is not grounded, the voltage of the enclosure can rise to that of the source, which is at most about 25 kV. However, the interior circuitry will also rise to this potential if it is surrounded by a contiguous metallic enclosure having no penetrations. Because there is no difference in potential between different parts of the circuitry, no functional upset would occur. Also, the arc current does not pass through the circuitry, so no damage would occur.

In practice, the enclosure will have numerous penetrations or points of entry such as cables, the power cord, and air vents, as illustrated in Fig. 11.56. All of these points of entry allow the effects of the ESD event to pass into the interior of the enclosure. Intense electric and magnetic fields around these penetrations may result in secondary discharges or field coupling to the internal circuitry. The ESD discharge current may find a lower-impedance path to ground through the electronic circuitry, resulting in damage. Even if the discharge current does not pass directly through the electronic circuitry, the fields may couple to the circuitry via capacitive and/or inductive coupling, causing operational problems.

Arc discharge to keyboards and other exposed parts of the system can conduct the arc current into and through the electronic circuitry, resulting in malfunction or the destruction of components. Even if the discharge does not pass directly through the circuitry, the event essentially bathes it in a traveling wave that couples into that circuitry, possibly causing functional upset.

There are essentially three techniques for preventing problems caused by an ESD event:

1. Prevent occurrence of the ESD event.
2. Prevent or reduce the coupling (conduction or radiation) to the electronic circuitry of the product (hardware immunity).
3. Create an inherent immunity to the ESD event in the electronic circuitry through software (software immunity).

Some or all of these techniques may be appropriate for a system, whereas some may be impractical from the standpoint of cost to implement or the anticipated environment of the installation.

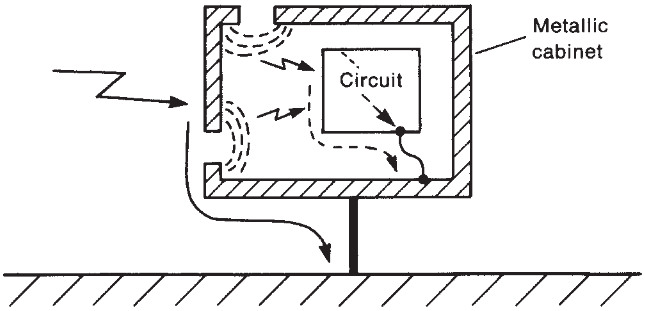

FIGURE 11.56 Illustration of multiple ESD discharge paths.

Electronic components such as ICs are placed in pink polyethylene bags, or their pins are inserted in antistatic foam for transport. The pink polyethylene bags have a lower surface resistivity (of order 10^9 Ω/square) than do ordinary insulating materials, which allows them to redistribute charge fairly rapidly. The static charge distributes itself over the bag surface quickly, preventing concentration of charge. Insulators typically have surface resistivities greater than 10^{14} Ω/square and cannot redistribute the charge rapidly, resulting in charge separation, which may cause an ESD event by, for example, induction.

Some products can utilize charge generation prevention techniques. For example, printers constantly roll paper around a rubber platen. This causes charge to be stripped off the paper, resulting in a buildup of static charge on the rubber platen. Wire brushes contacting the paper or passive ionizers prevent this charge buildup. In many other applications, preventing charge buildup is rarely a practical measure, since the engineer has little control over the installation, and so the design must mitigate the effects of the ESD event.

The various hardware immunity techniques attempt to prevent or reduce the effects of the four basic ESD coupling mechanisms:

1. Secondary arc discharges.
2. Direct conduction.
3. Electric field (capacitive) coupling.
4. Magnetic field (inductive) coupling.

ESD hardware immunity design generally incorporates all of these considerations.

Secondary arc discharges are prevented by (1) grounding exposed metallic parts of the enclosure to chassis ground and/or (2) *insulating* the exposed part from the nearby electronics. *All metallic parts of the enclosure that are exposed should be connected to chassis ground to prevent secondary arc discharges. Interior electronics should be separated from ungrounded parts of the enclosure by 1 cm and from grounded parts by 1 mm to further prevent secondary arc discharges to the electronics.* These recommendations result from the following considerations. Suppose that a metallic item of the enclosure such as a decal or nameplate is isolated. If the operator touches this part, the resulting charge transfer raises its potential, creating a potentially large electric field between the part and nearby electronics. If the electronics is sufficiently close to the part, the intervening air may break down, resulting in a *secondary arc discharge* to the electronics. Secondary discharges of this type can result in more severe arc currents than can arc discharges from the human body, since the resistance of the metallic part is much smaller than that of the human body. The breakdown of electric field strength in air is of order 30 kV/cm, and the human body can be charged to at most around 25 kV. An ungrounded part can rise in potential to the potential of the charged body. Therefore, the maximum voltage between the exposed metal part and nearby electronics is some 25 kV. In order to prevent air breakdown between these parts and adjacent electronics and a secondary discharge, the electronics should be separated by about $d_{\min} = 25\ \text{kV}/(30\ \text{kV/cm}) \cong 1$ cm, as illustrated in Fig. 11.57a. If the metal part is grounded, the voltage across the inductance of the green wire ground due to the passage of the ESD discharge current through it and consequently the voltage of the part may rise to about 1500 V. Therefore, the minimum separation should be of order $d_{\min} = 1500\ \text{V}/(30\ \text{kV/cm}) \cong 1$ mm. These separation distances were predicated on air being the insulation medium. Other insulation media (such as Mylar) have much higher breakdown voltages, and so the minimum separation can be reduced. Another way of preventing this secondary arc discharge is to lengthen the discharge path, as with overlapping joints as illustrated in Fig. 11.57b. Still another technique is to use a secondary shield connected to circuit ground to break up the capacitance between the part and the adjacent electronics, as shown in Figure 11.57c. Plastic parts such as knobs can accumulate charge. The effect

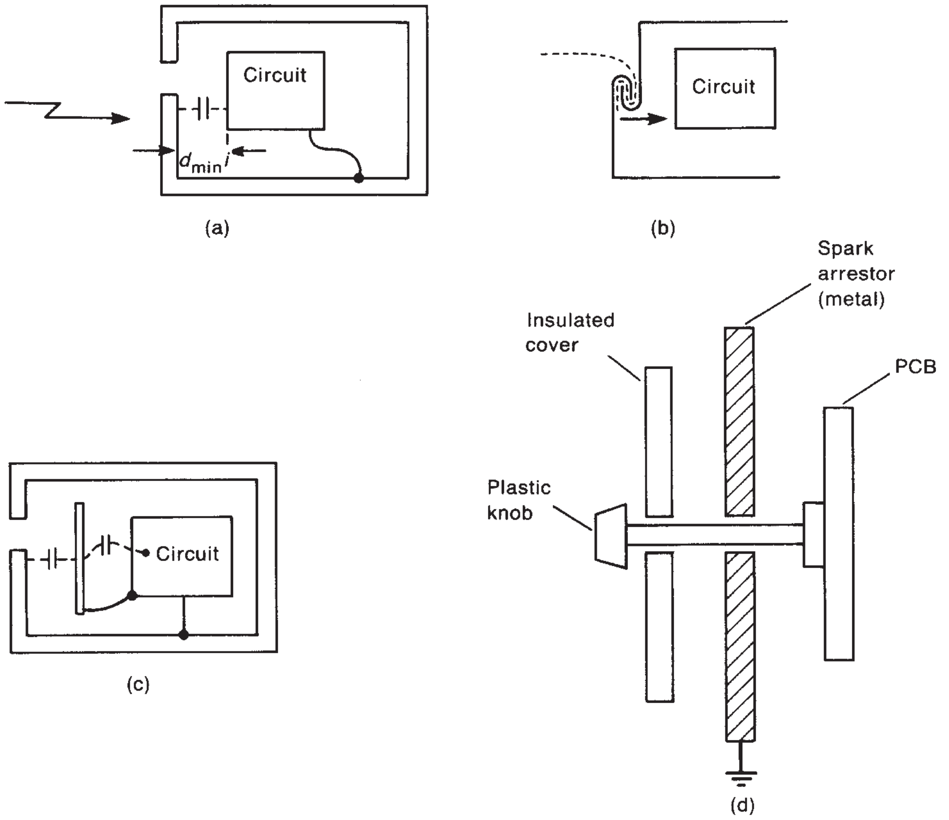

FIGURE 11.57 Methods of reducing secondary arcing: (a) circuit insulation by separation; (b) lengthening the discharge path; (c) use of a secondary shield; (d) a spark arrestor.

of secondary arc discharges from these parts is reduced by placing a grounded metallic shield behind them to safely conduct any discharge away from the sensitive electronics, as Fig. 11.57d illustrates. These are frequently referred to as *spark arrestors* [16].

The first priority in designing for ESD hardware immunity is to *prevent the ESD discharge current from flowing through sensitive circuitry by direct conduction.* There are essentially two ways to accomplish this goal. The first method is to *block the discharge path through the circuitry. Insulating the circuitry* as discussed above is one way of blocking this path. The second method is to *divert the arc discharge current around the electronics to prevent it from flowing through the circuitry.* If the product enclosure is metallic, the enclosure can be used to *divert the discharge current to ground* as depicted in Fig. 11.56. Any penetrations (e.g., apertures and cables) create possible paths through the interior circuitry for the arc current. Properly treating penetrations in metallic enclosures is critical to making the best use of the metallic enclosure. This is virtually no different from preventing electromagnetic fields internal to a shielded region from exiting the shield, as discussed in Chapter 10. Holes in the shield for air vents, etc., should be replaced with many small holes. The degree of coupling through a hole is again more dependent on the maximum dimension than on the hole area. Thus, long, narrow slots such as at panels and doors should be broken into many shorter slots with closely spaced screws or with metallic gaskets. The electromagnetic fields generated by the ESD event as the current flows on the surface of the enclosure tend to be the most intense around apertures. Therefore, sensitive circuitry should not be placed near any aperture regardless of whether the aperture has been properly treated. Virtually all of the techniques that were discussed in Chapter 10 to prevent the degradation of shielding effectiveness should be used and are effective in preventing ESD coupling to the interior of the enclosure. Once these penetrations are properly treated, the only other access points are via the cables.

Once apertures have been properly treated, the cables are the primary mechanisms that allow the effects of the ESD event to penetrate to and affect the internal circuitry. Peripheral cables (including the power cord) are usually quite long, and act as efficient antennas to pick up and couple the fields produced by the ESD event to the interior of the enclosure and thus to the electronic circuitry. Removing all cables (except the power cord) in an ESD test can often determine whether these are the primary points of entry. Shielding all peripheral cables may or may not be an effective prevention measure against coupling the ESD event to the internal electronics. If the cable shield is bonded 360° to the enclosure as illustrated in Fig. 11.58a, it forms an extension of the metallic enclosure and thus is effective. If the shield is terminated in a pigtail as illustrated in Fig. 11.58b, the ESD discharge current flowing through the inductance of the pigtail (approximately 15 nH/in.) can create a large voltage difference between the shield and the other enclosure. This couples to the interior wires and subsequently to the internal circuitry.

Use of shielded cables employing 360° bonding is often impractical from a cost standpoint. This is particularly true for plastic enclosures. There remain two basic methods of preventing these signals from entering the circuitry: (1) *blocking* and (2) *diverting* these signals.

Blocking these signals can be accomplished by placing an impedance in the path. ESD events tend to produce both common-mode and differential-mode currents on the peripheral cables. In order to block the induced common-mode currents, we can use (1) common-mode chokes, (2) optical couplers, or (3) place impedances in series with *every wire of the cable, including the ground wires*. Of these three, the simplest and often most effective is the common-mode choke illustrated in

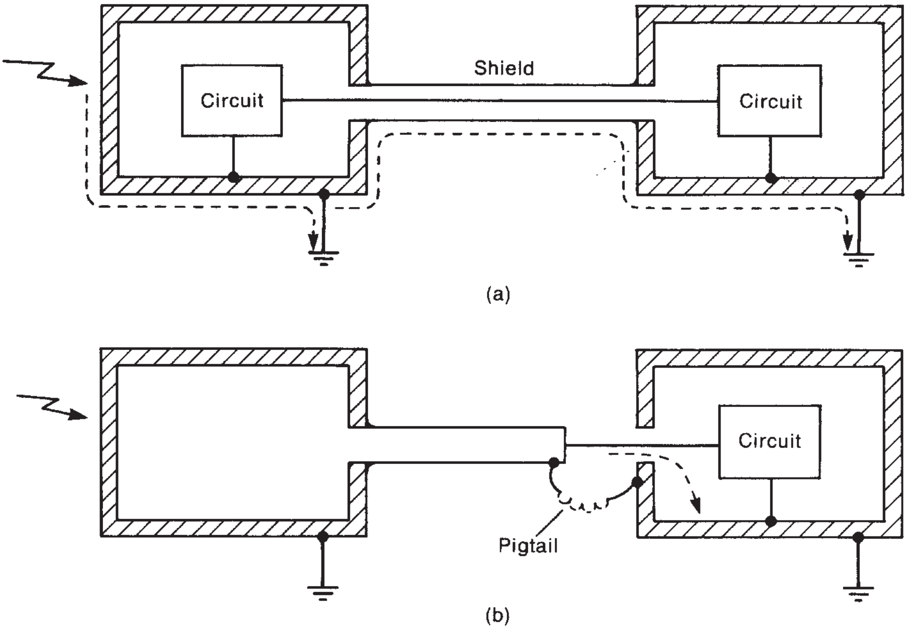

FIGURE 11.58 Use of shielded cables to exclude ESD coupling: (a) circumferentially bonded cables; (b) degradation of shielding due to pigtails.

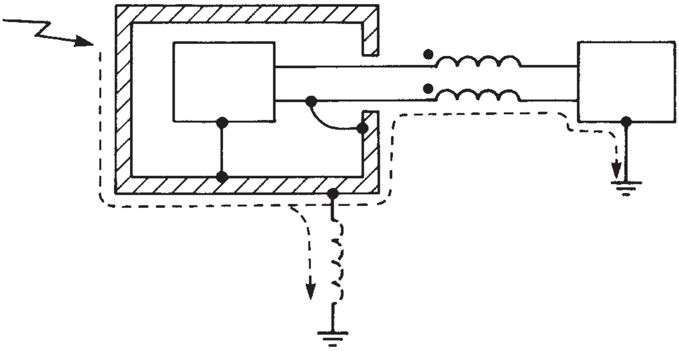

FIGURE 11.59 Use of a common-mode choke to prevent coupling of common-mode ESD signals between subsystems on cables.

Fig. 11.59. A common-mode choke is helpful in preventing common-mode currents from entering a product, as well as from exiting the product on these cables. Consequently, common-mode chokes serve a dual role; they tend to prevent radiated emission problems, as well as ESD problems due to common-mode currents. In this regard, it is important to remember that *all conductors of the cable* (*including the ground wires and the shield pigtail*) *must be routed through the common-mode choke*, as discussed in Chapter 5. Bypassing the common-mode choke with the cable shield connection can effectively defeat the effect of the choke. Common-mode chokes are available in DIP form that allow easy mounting on PCBs where the cables enter.

The other method of preventing ESD-induced currents from penetrating enclosures via peripheral cables is to *divert them*. This method is critically dependent on *geometry*. For example, placing a capacitor between a signal wire and ground tends to divert the induced current to the enclosure, as shown in Fig. 11.60a. The effect of the capacitor on the signal current on the cable must also be considered. The capacitor technique will be effective if the spectral content of the ESD current is higher than that of the signal current. Line-to-line and line-to-ground capacitors may be used to divert differential-mode and common-mode ESD currents, respectively, as in power supply filters. In some cases, multi-element filters such as Tee or Pi configurations may be necessary. Once again, *geometry* is critical. If the enclosure ground connection is at some distance from this entry point, the currents may find another lower-impedance and undesired path. This is another important reason for *placing all cable connectors at one edge of a PCB*. It tends to prevent the formation of lower-impedance paths that are not intended, as illustrated in Fig. 11.60b.

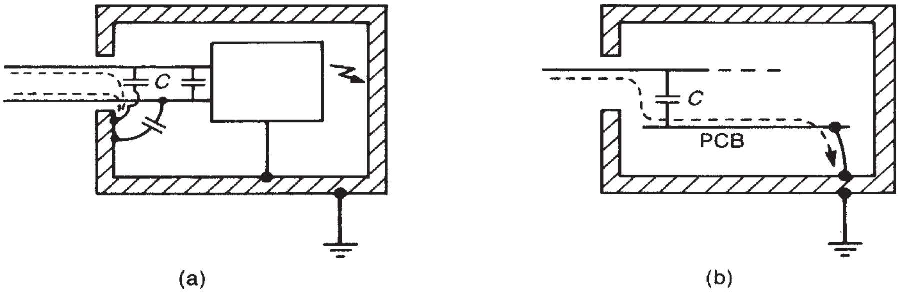

FIGURE 11.60 Use of capacitors to divert ESD discharges: (a) proper capacitor placement; (b) effect of nonlocal grounding of capacitor, forcing discharge through the PCB ground.

As with other uses of diversion elements such as capacitors, the impedance that they are in parallel with determines their effectiveness. Placing capacitors across low-input-impedance devices will probably be ineffective because of current division, as discussed previously. For low-impedance inputs, the technique of *blocking* by placing an impedance in series will be more effective. In this case, a ferrite bead will tend to cause less deterioration of the intended signal, while blocking the higher-frequency components of the ESD signal. On the other hand, a capacitor will serve to effectively divert currents from high-input-impedance devices.

Another method of diversion is the use of *clamping devices* such as zener diodes, often referred to as *transient suppressors*. This is illustrated in Fig. 11.61a. When the input voltage exceeds the threshold of either device, it breaks down. These transient suppressors tend to have activation times inversely proportional to their current-carrying capability: high-current devices have slower response times. Frequently, a parallel combination of a low-current, fast-response device and a high-current, slow-response device is employed. Diodes can be used as shown in Fig. 11.61b to ensure that input voltages to components remain within safe levels. If the signal line voltage exceeds +5 V, the upper diode turns on. Conversely, if the signal voltage attempts to go negative, the lower diode turns on.

The parasitic lead inductance of both the capacitor and the transient absorber are again critical to their success in diverting the ESD signal. It is important to remember that the ESD signal spectral content extends well into the GHz range, so that a small amount of lead inductance can prevent the low-impedance path that these devices are intended to provide.

The previous discussions have concentrated on products that have metallic enclosures where the apertures have been properly treated. Products that are housed in plastic enclosures can utilize these techniques for preventing the penetration of the ESD signal on peripheral cables, but more care is required. In this case, we do not have the advantage of a large metallic path. It is of benefit to have a large metallic plane beneath the product to be used as a diversion for the ESD current and to provide bypass capacitance. It is also important that the plane be connected to all metal parts, including the green-wire ground.

It is also important that (1) the electronic grounds of all peripheral cable connectors be connected to this ground plane where the connector enters the PCB and (2) all PCBs be placed close to and parallel to this ground plane. The first principle is important, because we wish to avoid creating large voltage differences between the cable wires and the ground plane, as illustrated in Fig. 11.62.

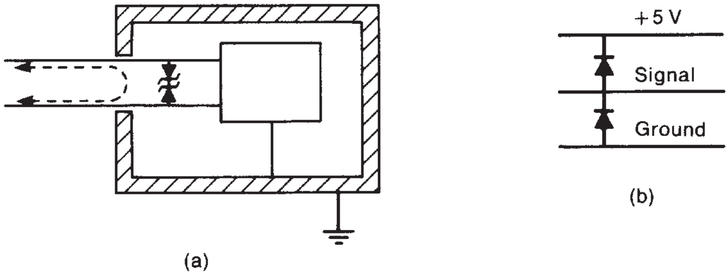

FIGURE 11.61 Use of diodes to clamp ESD-induced voltages to safe levels: (a) zener diodes; (b) back-to-back diodes at circuit inputs to prevent overvoltages.

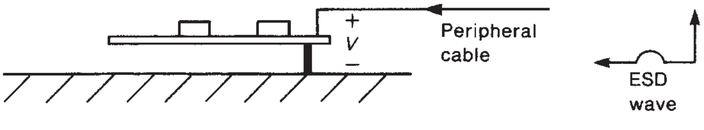

FIGURE 11.62 Illustration of the importance of a local ground where peripheral cables enter the product.

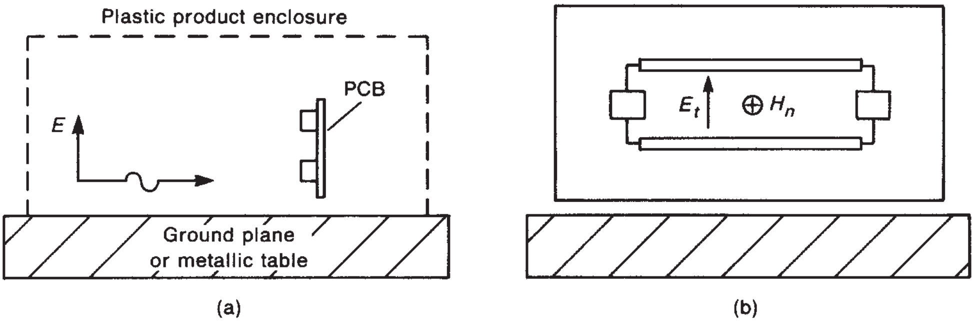

FIGURE 11.63 Illustration of the effect of PCB orientation on its susceptibility to ESD fields: (a) problem dimensions; (b) the ESD fields oriented with respect to the circuit loop for maximum susceptibility.

The reason for the second principle is somewhat subtle but effective. Consider an ESD wave propagating across the table on which a product is placed, as illustrated in Fig. 11.63a. If the table is metallic, the electric field of the wave near the surface of the table must be perpendicular to the table surface in order to satisfy the boundary conditions of zero tangential electric field on the surface of a perfect conductor. Placing the PCB in the product in the vertical direction as illustrated in Fig. 11.63b will mean that the incident electric field will tend to be in the plane of any circuit loops on the PCB (transverse to the transmission-line axis). The magnetic field of the ESD wave will possibly be perpendicular to the plane of the circuit loops on the PCB. In Chapter 8, we showed that transmission lines pick up incident fields most effectively when the electric field is transverse to the line axis, and/or the magnetic field is perpendicular to the plane of the loop. This is precisely the situation when the PCB is oriented vertically to the bottom of the product. A better placement of PCBs is horizontal and near the bottom and ground plane of the product. For this placement, the electric field will be perpendicular to the plane of the circuit loops, and the magnetic field will be parallel to the plane of the circuit loops. Thus, theoretically, the ESD wave will not couple to the circuit loops on the PCB, since the ground plane will force the electric field lines to be perpendicular to the ground plane (at least close to the ground plane). Placing the PCB very close to the ground plane will ensure that any bending of the electric field lines from vertical will be minimized in the vicinity of the circuit loops. This also increases the bypass capacitance to the ground plane. The same holds true for the magnetic field; it will tend to be parallel to the ground plane (near the ground plane).

Proper layout of PCBs in metallic as well as nonmetallic enclosures helps to prevent electric field (capacitive) and magnetic field (inductive) coupling to those circuits from any ESD-induced fields interior to the product. As in the minimization of radiated emissions from a PCB, *loop areas should be kept small to reduce the pickup. Conductor lengths should also be minimized for the same reason.* Ground grids on the PCBs also tend to help. These techniques are very similar to those used to minimize pickup of incident fields, as well as radiated emissions from the currents on the conductors, as discussed in Chapter 8. Providing adjacent returns in proximity to signal lines in a ground–signal–ground– … or ground–signal–signal–ground– … arrangement tends to minimize the loop areas and associated reception of the fields.

Software should be designed to continually verify that faults are detected and recovery action taken. Unlimited wait states should not be used; otherwise, an ESD event can cause the product to “lock up.” Software should include “watchdog” routines that periodically check whether program flow is correct. If an ESD event has interrupted program flow, a recovery routine may be initiated before any damage is done.

The use of parity bits, checksums, and error-correcting codes can prevent the recording of ESD-corrupted data. They cannot restore data, but if correction checks are initiated frequently, much of the stored data will not need to be retransmitted.

Although not properly classified as a software immunity technique, all unused module inputs should be tied to ground or +5 V to prevent false triggering by an ESD event. Also, edge-triggered inputs are very susceptible to “spikes” caused by an ESD event. Thus, all inputs should be latched and strobed. This reduces the likelihood that the occurrence of an ESD event will happen simultaneously with the latching of data and be incorrectly recorded as valid data.

11.5 DIAGNOSTIC TOOLS

As was pointed out many times, *product cost* and *product development schedule* are two of the most important aspects of producing a product that is competitive in the marketplace. Once a prototype of the product is developed, it should receive preliminary EMC testing to determine whether the final product will have significant problems in complying with the government-mandated regulations on radiated and conducted emissions, as well as susceptibility to radiated and conducted emissions and susceptibility to ESD. The key here is *to rapidly and correctly diagnose the source of the problem so that low-cost effective measures can be taken to fix the problem.* This is the point where having effective *diagnostic tools* and a plan of action are critical to keeping the product cost and development schedule within acceptable bounds. For example, suppose that preliminary testing determines that the fifth harmonic of a system clock is causing the product to exceed the radiated emission limits. Determining that the offending signal is the fifth harmonic of one of the clocks is very simple; today’s sophisticated spectrum analyzers can determine the frequency of the emission to within an incredibly large number of digits. The real question to be determined is where this emission is coming from, such as a particular system cable or a particular land on a PCB. The quickest but costliest and probably non-implementable “fix” is to place the product in a contiguous metal shield. Remember that any “fix” added to the product will not increase functionality but will add cost that the customer may be unwilling to bear. Hence, it is preferable to determine which cable the emission is radiating from and its type, i.e., differential-mode current or common-mode current. Using bypass capacitors to keep the offending differential-mode current off the cable or using a ferrite toroid around the cable to block the offending common-mode current is a simple and low-cost “fix.” But the precise source of the emission must be determined first.

It is at this point that we must have effective diagnostic tools. Endlessly testing and hoping that the problem will “go away” severely impacts the development schedule. The typical diagnostic tools that are available to the EMC engineer are:

1. Small E-field probes
2. Small H-field probes
3. High-impedance, high-frequency FET probes attached to a spectrum analyzer
4. Near-field PCB scanners
5. High-frequency current probes
6. “Detective work”

The first five devices are “near-field” measurers. In the near field of the emission, the electric and magnetic fields are not coupled. Hence, a field might be predominantly electric or predominantly magnetic. There are also devices on the market where one places a PCB on its surface and a large number of miniature dipole antennas beneath the surface measure the fields and display them on a computer screen. The different levels of measured field intensity are shown on the screen with different colors denoting the different levels. It is important to point out that *the fields that determine whether the product passes the regulatory test are not near fields but are measured some distance away by the test antenna*. Hence, these near-field levels are difficult to correlate with the regulatory fields. Our intent here is to determine *relative levels* of the near fields to determine where the offending far field is originating from. Figure 11.64a shows how to construct an *E*-field probe. Remove about an inch of the overall shield from a coaxial cable (RG58) exposing the inner wire that is surrounded by its insulation. Leave the insulation around the inner wire intact to prevent inadvertently shorting out (short-circuiting) some component on the board. The *E*-field probe is a simple electric dipole antenna and is not sensitive to magnetic fields. The *H*-field probe shown in Fig. 11.64b is formed by making a loop with a subminiature coaxial cable. Connecting the inner wire to the shield forms a magnetic dipole loop antenna. Retaining the overall shield tends to prevent electric fields

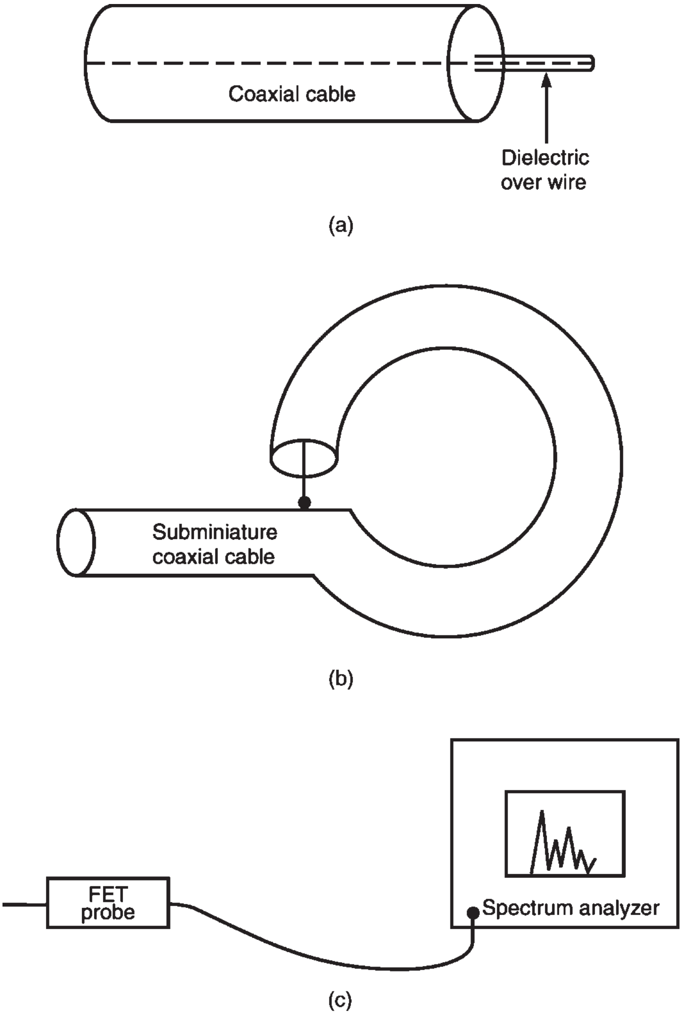

FIGURE 11.64 Diagnostic tools: (a) an electric field probe; (b) a magnetic field probe; (c) a FET (field-effect transistor) probe attached to a spectrum analyzer to determine signals present on the pins of modules.

from being picked up. A high-impedance, high-frequency FET probe connected to a spectrum analyzer as shown in Fig. 11.64c is a very effective tool for determining whether certain pins of ASICs or microprocessors are carrying signals that they are "not supposed to carry." An example of this was cited earlier where the RESET pin of a processor was very close to the CLOCK pin, thereby allowing the clock signal to be inadvertently coupled to the reset line (that was unsuspectingly routed a long distance on the PCB because it was thought to be a low-priority signal). Again the intent is not to measure "accurate voltage levels" but to simply try to determine whether the offending signals are on the pin.

Finally, successful EMC diagnostic work becomes a matter of intelligent "detective work." We may try disconnecting cables individually to see if the offending emission goes away. Once this narrows down a suspect cable, a high-frequency current probe can be clamped around the cable to confirm that common-mode currents on the cable are the culprit. Remember that it was shown that a common-mode current of around 5 μA on a 1-m cable can cause the emissions to fail the FCC Class B (and CISPR 22 Class B) limits. Hence, a great deal of expensive and time-critical testing time in the semi-anechoic chamber can be conserved by giving the product group engineers a current probe and a spectrum analyzer and telling them to work on reducing the common-mode currents on all their product's cables below 5 μA *in their development laboratory*. Once this is done, they can schedule the semi-anechoic chamber to continue testing. Otherwise, the group is likely to tie up the chamber for many hours endlessly trying something, and retesting: a very time-consuming task, particularly with no idea of the source clearly in mind.

From the standpoint of conducted emission testing, it is well advised to construct a common-mode, differential-mode device described in Section 6.2.4 of Chapter 6 to separate the conducted emissions into common-mode or differential-mode components in order to efficiently determine which component of the power supply filter to change to effect a reduction in the *dominant component* of the conducted emission.

The diagnosis of the real problem can be a confusing task. It is important to devise a plan for attacking the diagnosis of the problem and to keep a log of the fixes tried and their outcome. In the course of this work, it is very easy to become frustrated and forget what was done earlier. This log will serve as a snapshot of what was done and provide clues about the problem.

11.5.1 The Concept of Dominant Effect in the Diagnosis of EMC Problems

The discipline of EMC is often accused of being "black magic" where measures taken to reduce the effect of a potential interference source are ineffectual. Quite often, this stems from not understanding the concept of *dominant effect* and not from the ineffectiveness of the measures tried. Suppose that at some frequency f, the radiated or conducted emission being measured is the *sum* of two contributions:

$$E = E_1 + E_2 \tag{11.33}$$

Suppose that $E_1 \gg E_2$. Hence, the total effect is due to E_1, $E \cong E_1$. If we try a suppression measure that *only reduces* E_2*, then the total effect will not be reduced.* Here is where we get into "word games." We say to ourselves that "we tried something and would expect the total to get better or worse; but at least it should change." When we try the suppression measure and observe no change in the total, our mind tells us that "this doesn't make sense." However, if we understood the underlying process, it would make perfect sense; we did not change the dominant effect and hence should not have expected to see a change in the total. Once we understand the underlying process as being contributed by two effects, we clearly understand why reducing one effect might not reduce the total; we did not reduce the dominant effect. Hence, we should focus on determining which effect is the dominant one and concentrate our efforts toward reducing it. There are abundant examples of this throughout this textbook. Here, we will concentrate on three such situations: (1) conducted emissions, (2) radiated emissions, and (3) crosstalk.

In testing a product for compliance with the conducted emissions passing out through the product's power cord, we plug the product into a LISN that is plugged into the commercial power system as shown in Fig. 11.65a. The LISN presents 50 Ω loads (the input impedance to a spectrum analyzer or a dummy load) between phase and green wire and between neutral and green wire. The noise currents passing out the power cord have two components. The differential-mode noise current

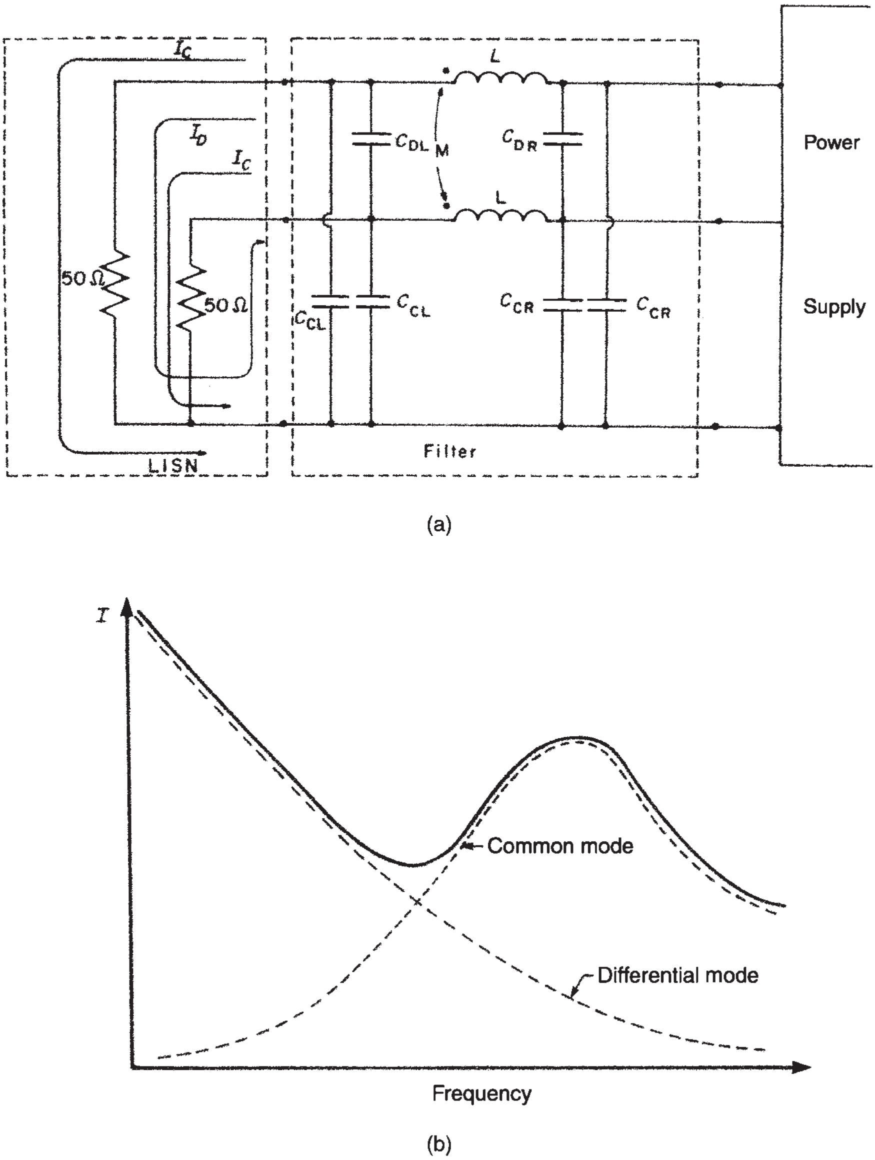
I_C
L
I_D
I_C
C_{DL}
M
C_{DR}
L
Power
50 Ω
50 Ω
C_{CL}
C_{CL}
C_{CR}
C_{CR}
Supply
LISN
Filter
(a)
I
Common mode
Differential mode
Frequency
(b)

FIGURE 11.65 Illustration of the concept of dominant effect in conducted emissions: (a) the power supply filter; (b) determining which element of the filter to change in order to effect a reduction in the total conducted emission.

passes out the phase wire and returns to the product along the neutral wire. The common-mode noise currents pass out the phase and neutral wires, and both return to the product through the green wire. A power supply filter is the key to preventing these noise currents from getting to the LISN and being measured. The filter has components that affect either differential-mode currents or common-mode currents. The line-to-line capacitors between phase and neutral divert the differential-mode noise currents. The line-to-ground capacitors between phase and green wire and between neutral and green wire divert common-mode noise currents. The common-mode choke blocks the common-mode currents but passes the differential-mode currents. In Chapter 6, it was also pointed out that the leakage flux of a common-mode choke that is poorly or not ideally constructed can inadvertently place inductances in both phase and neutral that also tend to block the differential-mode currents. Figure 11.65b shows a typical decomposition of these currents into their differential-mode and common-mode components. Over the lower frequency range, differential-mode currents dominate and therefore determine the total emission. Over this frequency range, we would adjust the line-to-line capacitor values to reduce the total. If we had adjusted only the line-to-ground capacitor values, we would see no net reduction; only the common-mode component would be reduced. So, if we only adjusted the line-to-ground capacitors or the common-mode choke, we would see no effect and suspect “black magic” to be at work. Similarly, at the higher frequencies, the common-mode current emissions dominate. So, over this frequency range, we would have no choice

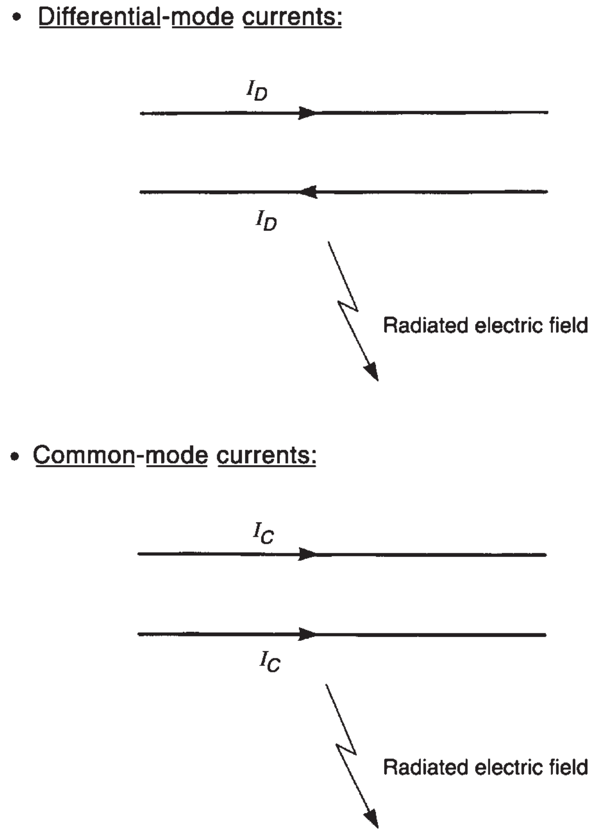

FIGURE 11.66 Illustration that the radiated emissions are due to a combination of differential-mode currents and common-mode currents.

but to adjust the line-to-ground capacitor values and/or the common-mode choke in order to effect a reduction of the total. We also have another very effective option of placing an inductor in the green wire to block the return paths of the common-mode current. Once we understand this situation from the standpoint of the dominant effect, the solution is clear; no random adjustments need to be made.

Figure 11.66 shows how the concept of dominant effect is used to diagnose radiated emission problems. The total currents on cables are composed of differential-mode noise currents that flow out one wire and return on another, and common-mode currents that flow out both wires and return through displacement current. In a radiated emission problem, the total radiated electric field will be dominated by one of these. If the dominant radiated emission is due to differential-mode currents as illustrated in Fig. 11.67a, we have no choice but to try to *divert* them with a capacitor placed between the two wires as shown in Fig. 11.68b. If the dominant radiated emission is due to common-mode currents as illustrated in Fig. 11.67b, we have no choice but to try to *block* them with a common-mode choke inserted into the two wires as shown in Fig. 11.68b. If common-mode current emissions were dominant as in Fig. 11.67b, placing a bypass capacitor between the two wires would show no reduction in the total emission; we would have reduced the component of the emission that was not dominant.

(a) Diiferential-mode current emissions are dominant

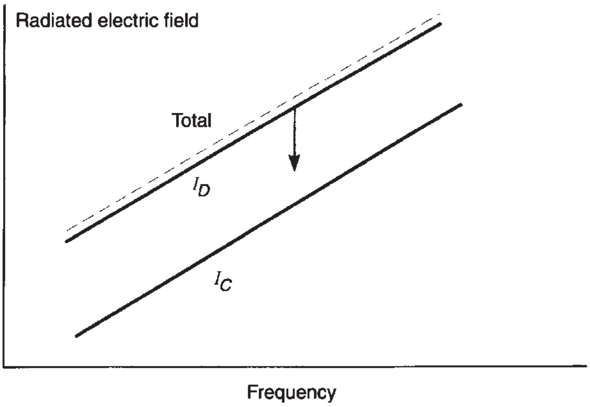

(b) Common-mode current emissions are dominant

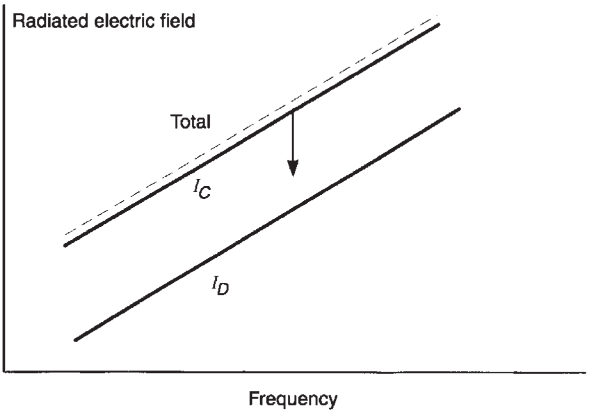

FIGURE 11.67 In order to reduce the total radiated emission, the dominant component must be reduced.

- **Differential-mode current emission dominant:**

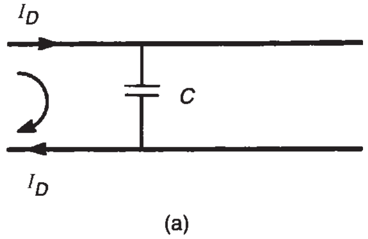

- **Common-mode current emission dominant:**

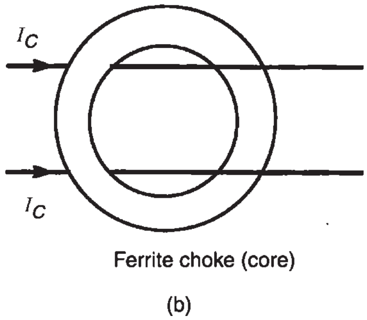

FIGURE 11.68 Different methods affect different components: (a) shunt capacitors can keep differential-mode currents off cables; (b) common-mode chokes can keep common-mode currents off cables.

Finally, we discuss the reduction of crosstalk. In Chapter 9, we learned that at frequencies where a transmission line is *electrically short*, the crosstalk between two transmission lines is composed of the sum of a contribution due to the mutual inductance between the two lines, which we called *inductive coupling*, and a contribution due to the mutual capacitance, which we called *capacitive coupling*. This is illustrated in Fig. 11.69. If the load impedances of the lines are less than their characteristic impedance (low impedance), the inductive coupling component dominates the capacitive coupling component. If the load impedances of the lines are greater than their characteristic impedance (high impedance), the capacitive coupling component dominates the inductive coupling component. This is illustrated in Fig. 11.70. In order to reduce the total crosstalk in wire-type cables, we have two options: replace the generator and/or the receptor wires with either (1) shielded wires or (2) twisted pairs of wires as shown in Fig. 11.71. Placing a shield around a wire inherently eliminates capacitive coupling if it is “grounded” at least one end, but this does not eliminate inductive coupling. In order for a shield to eliminate inductive coupling, it must be grounded at both ends. Similarly, twisting a pair of wires together inherently eliminates inductive coupling but does not affect capacitive coupling. In order for a twisted pair to eliminate capacitive coupling, it must have balanced loads. So, this is an example of another “mysterious” effect. A power supply engineer attempts to reduce crosstalk by shielding a wire and “grounding” the shield at only one end to eliminate ground loops but observes no reduction in the

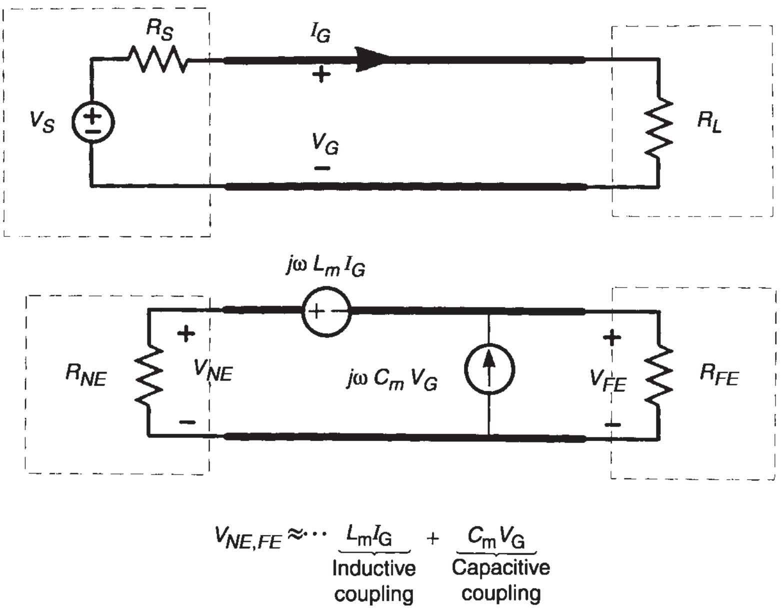
R_S
I_G
+
V_S
V_G
−
R_L
$j\omega L_m I_G$
+
R_{NE}
V_{NE}
−
$j\omega C_m V_G$
+
V_{FE}
−
R_{FE}
$V_{NE,FE} \approx \cdots \underbrace{L_m I_G}_{\text{Inductive coupling}} + \underbrace{C_m V_G}_{\text{Capacitive coupling}}$

FIGURE 11.69 In crosstalk problems, there are two contributions: inductive coupling due to magnetic fields and capacitive coupling due to electric fields.

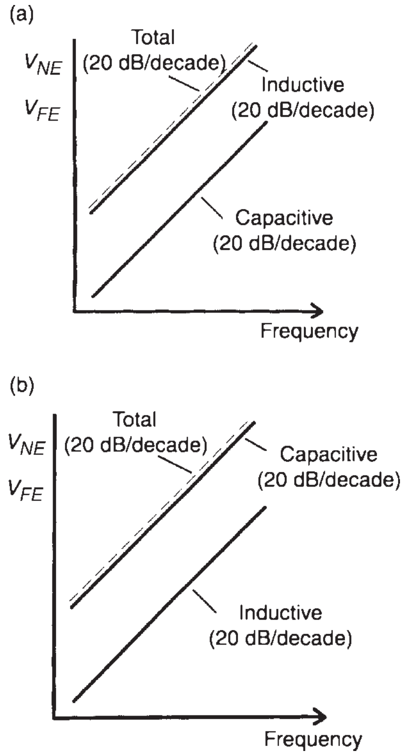

FIGURE 11.70 The dominant crosstalk contribution depends on the circuit termination impedance: (a) in low-impedance circuits, inductive coupling dominates capacitive coupling; (b) in high-impedance circuits, capacitive coupling dominates inductive coupling.

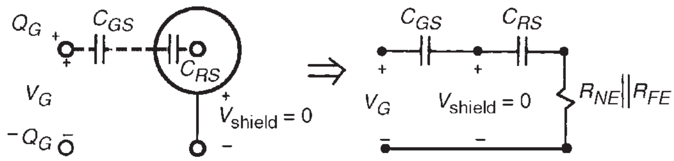

Shielded wires eliminate capacitive coupling !

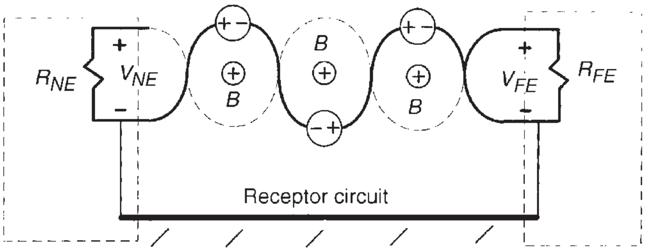

Twisted pairs eliminate inductive coupling !

FIGURE 11.71 Shields "grounded" at only one end eliminate capacitive crosstalk, whereas twisted pairs eliminate inductive crosstalk.

total crosstalk. The reason is now clear; the engineer's circuits and loads were very low impedance and hence the inductive coupling was dominant. The addition of a shield with one end grounded did in fact affect something; it eliminated the capacitive coupling. But since inductive coupling was dominant, the total was not reduced. This is why twisted pairs are typically used in power supply circuits.

It is important to keep this concept of dominant effect in mind while carrying out EMC diagnostics so that frustration will not prevent one from effectively solving the problem. EMC may at times seem to be "mysterious" when in fact there is a logical and scientific principle underlying it.

PROBLEM

This chapter brings together all the ideas and skills of the previous chapters in order to design electronic products that are electromagnetically compatible. Rather than proposing several individual problems at the end of this chapter in order to assess how well the material has been learned, an alternative is proposed. This author is of the opinion that one will gain a more thorough comprehension of new material when we teach the new material to someone else. Hence, the problem for this chapter is as follows. You are employed by a company that designs and manufactures relatively low-cost digital devices and are a member of that company's EMC department. The company has had numerous situations where inattention to EMC design principles has caused disastrous schedule delays and cost overruns. The company management has decreed that this must be stopped. Your manager has tasked you to organize and develop a seminar on EMC design that is to be presented to the product design engineers in the company.

Develop a seminar that will show them how to think about their designs from an EMC perspective. In order to limit the development of this seminar to a reasonable timeframe, design the seminar to last no longer than one hour.

1. You will first need to develop a list of learning objectives that set out what you want to accomplish with the seminar. These should be couched in the form of "At the end of this seminar, the participant will be able to . . . ."
2. Next you will need to develop a detailed outline for the seminar. Do not copy the outline of this book or the outline of this chapter; develop your own, on the basis of what you now view are the important priorities in EMC design.
3. Create slides or "power point" charts for each of the important subareas in your outline. The slides must not be too "busy" with details so that the observer can listen to your discussion. Concentrate on major concepts that you consider to be crucial to EMC design.

REFERENCES

1. C. R. Paul and S. A. Nasar, *Introduction to Electromagnetic Fields*, 2nd ed., McGraw-Hill, New York, 1987.
2. F. W. Grover, *Inductance Calculations*, Dover, New York, 1946.
3. A. E. Ruehli, Inductance calculations in a complex integrated circuit environment, *IBM J. Research Devel.* 16, 470–481 (1972).
4. C. Hoer and C. Love, Exact inductance equations for rectangular conductors with applications to more complicated geometries, *J. Research Natl. Bur. Stand.—C. Eng. Instrum.* 69C, 127–137 (1965).
5. C. R. Paul, Modeling electromagnetic interference properties of printed circuit boards, *IBM J. Research Devel.* 33, 33–50 (1989).
6. D. D. Ling and A. E. Ruehli, Inductance, Section 11.1.4 in *Circuit Analysis, Simulation and Design*, A. E. Ruehli, ed., Elsevier-North Holland, New York, 1987.
7. P. K. Wolff and A. E. Ruehli, Inductance computations for complex three dimensional geometries, *Int. Conf. Circuits and Systems*, Chicago, IL, 1981, pp. 16–19.
8. A. E. Ruehli, Recent progress in circuit oriented techniques for EMC, *Proc. Int. Symp. Technical Exhibition on Electromagnetic Compatibility*, 1995.
9. G. Antonini, A. Orlandi, and C. R. Paul, Internal impedance of conductors of rectangular cross section, *IEEE Trans. Microwave Theory Tech.* MTT-47 (7), 979–985 (1999).
10. H. W. Ott, Ground—a path for current to flow, *Proc. 1979 IEEE Int. Symp. Electro magnetic Compatibility*, San Diego, CA, Oct. 1979.
11. D. R. Bush, A simple way of evaluating the shielding effectiveness of small enclosures, *8th Int. Symp. and Technical Exhibition on Electromagnetic Compatibility*, Zurich, Switzerland, Mar. 1989.
12. C. R. Paul, *Electromagnetics for Engineers: With Applications to Digital Systems and Electromagnetic Compatibility*, Wiley, Hoboken, NJ, 2004.
13. C. R. Paul, *Fundamentals of Electric Circuit Analysis*, Wiley, New York, 2001.
14. R. F. German, H. W. Ott, and C. R. Paul, Effect of an image plane on printed circuit board radiation, *Proc. 1990 IEEE Int. Symp. Electromagnetic Compatibility*, Washington, DC, Aug. 1990.
15. D. C. Smith and E. Nakauchi, ESD immunity in system designs, system field experiences and effects of PWB layout, *Proc. 2000 EOS/ESD Symp*, Anaheim, CA, Sept. 2000.
16. H. W. Ott, *Noise Reduction Techniques in Electronic Systems*, 2nd ed., Wiley-Interscience, New York, 1988.
17. R. F. German, Use of a ground grid to reduce printed circuit board radiation, *Proc. 1985 Int. Symp. Technical Exhibition on Electromagnetic Compatibility*, Zurich, Switzerland, Mar. 1985.

18. T. S. Smith and C. R. Paul, Effect of grid spacing on the inductance of ground grids, *Proc. 1991 IEEE Int. Symp. Electromagnetic Compatibility*, Cherry Hill, NJ, Aug. 1991.
19. C. R Paul, Effectiveness of multiple decoupling capacitors, *IEEE Trans. Electromagn. Compat.* EMC-34 (2), 130–133 (1992).
20. J. C. Englebrecht and K. Hermes, *A Study of Decoupling Capacitors for EMI Reduction*, Technical Report, International Business Machines, TR-51.0152, May 1984.
21. H. W. Ott, Partitioning and layout of a mixed-signal PCB, *Printed Circuit Board Design* 18, 8–11 (2001).
22. W. Boxleitner, *Electrostatic Discharge and Electronic Equipment*, IEEE Press, New York, 1989.
23. R. J. Calcavecchio and D. J. Pratt, A standard test to determine the susceptibility of a machine to electrostatic discharge, *IEEE Int. Symp. Electromagnetic Compatibility*, San Diego, CA, Sept. 1986.
24. R. Morrison, *Grounding and Shielding Techniques in Instrumentation*, Wiley, New York, 1967.
25. C. R. Paul, The concept of dominant effect in EMC, *IEEE Trans. Electromagn. Compat.* 34 (3), 363–367 (1992).

APPENDIX A

The Phasor Solution Method

This appendix is intended as a review of the important phasor methods of solving electric circuits and other linear systems in which the excitation is a single-frequency sinusoidal waveform and the system is in steady state. This method of solution will be used extensively throughout this text. See [1] or any other standard electric circuit analysis text for a more thorough review of this method.

A.1 SOLVING DIFFERENTIAL EQUATIONS FOR THEIR SINUSOIDAL, STEADY-STATE SOLUTION

This important general problem is depicted in Fig. A.1a as a single-input, single-output linear system. It is important to note that this important method applies to a large class of physical systems (electrical, mechanical, chemical, etc.). The input $x(t)$ is a sinusoid, arbitrarily shown as being a cosine, which is described as $A\cos(\omega t + \theta)$. The output or response to this input excitation $y(t)$ is also a sinusoid of the same frequency as the input: $B\cos(\omega t + \phi)$, but having a different amplitude B and phase angle ϕ. The radian frequency of the waveform ω (radians per second) and the cyclic frequency f (Hertz or cycles per second) are related by $\omega = 2\pi f$. The input $x(t)$ and the output $y(t)$ are related by a differential equation. For a lumped system such as an electric circuit, the differential equation is an ordinary differential equation, whereas for a distributed-parameter system such as an electromagnetic field problem, heat flow, or fluid flow, the differential equation is a partial differential equation. In order to illustrate the method, we will use the following example:

$$\begin{aligned}\frac{d^2y(t)}{dt^2} + a\frac{dy(t)}{dt} + by\,(t) &= x(t)\\ &= A\ \cos\,(\omega t + \theta)\end{aligned} \tag{A.1}$$

The general solution to this differential equation is the sum of a homogeneous or transient solution with $x(t) = 0$, and a particular or steady-state solution with $x(t) \neq 0$. We are interested only in the steady-state solution. Hence, the task is to determine a solution $y(t)$ that satisfies (A.1).

The key to this phasor solution is Euler's identity

$$e^{j\theta} = \cos(\theta) + j\sin(\theta) \tag{A.2}$$

Introduction to Electromagnetic Compatibility, Third Edition. Clayton R. Paul, Robert C. Scully, and Mark A. Steffka.

© 2023 John Wiley & Sons, Inc. Published 2023 by John Wiley & Sons, Inc.

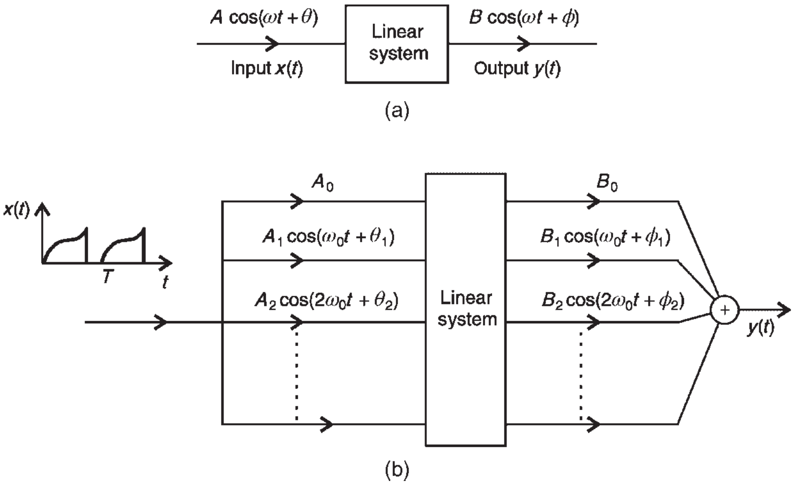

FIGURE A.1 (a) The phasor analysis of linear circuits involves determination of the response to a single-frequency sinusoidal input (source); (b) any other input waveform can be decomposed with the Fourier series into the sum of single-frequency components, and superposition can be used, along with phasor analysis, to indirectly determine the output as the sum of the responses to the individual sinusoidal frequency components.

where $j = \sqrt{-1}$. In order to obtain the solution to (A.1), we solve a different but much easier problem

$$\begin{aligned}\frac{d^2\hat{Y}(t)}{dt^2} + a\frac{d\hat{Y}(t)}{dt} + b\hat{Y}(t) &= \underbrace{A\angle\theta}_{\hat{A}}\, e^{j\omega t} \\ &= A\cos(\omega t + \theta) + jA\sin(\omega t + \theta) \qquad \text{(A.3)}\end{aligned}$$

and we denote a complex-valued phasor quantity having magnitude and phase with a caret over the quantity ($\hat{A} = A\angle\theta$). We have used the important complex algebra equivalence of

$$e^{j\theta} \equiv 1\angle\theta \tag{A.4}$$

to write the right-hand side in an equivalent form. The reason we solve this different problem is that (1) the solution of (A.3) is considerably simpler than the solution of (A.1) and (2) the solution of (A.1) can be easily determined from the solution of (A.3). To show this, we assume a form of the solution to (A.3) of the same form as the right-hand side:

$$\hat{Y}(t) = B\angle\phi\, e^{j\omega t} \tag{A.5}$$

Substituting (A.5) into (A.3) gives

$$[(j\omega)^2 + a(j\omega) + b]B\angle\phi\, e^{j\omega t} = A\angle\theta\, e^{j\omega t} \tag{A.6}$$

Canceling $e^{j\omega t}$ on both sides and noting that $j^2 = -1, j^3 = -j$, etc. gives

$$B\angle\phi = \frac{A\angle\theta}{-\omega^2 + ja\,\omega + b} \tag{A.7}$$

Since we presumably know the frequency of the input ω, as well as its magnitude A and phase θ, we can determine the magnitude B and phase ϕ of the solution to (A.3) using complex algebra.

But how does the solution to (A.3) relate to the solution of the original problem in (A.1)? The answer is simple. The original input $x(t) = A\cos(\omega t + \theta)$ is the real part of the new input:

$$\begin{aligned} x(t) &= \mathscr{Re}\{\hat{X}(t) = \underbrace{A\underline{/\theta}}_{\hat{A}}\, e^{j\omega t}\} \\ &= \mathscr{Re}\{A\ \cos(\omega t + \theta) + jA\ \sin(\omega t + \theta)\} \\ &= A\cos(\omega t + \theta) \end{aligned} \tag{A.8}$$

Hence, the solution to the original problem is

$$\begin{aligned} y(t) &= \mathscr{Re}[\hat{Y}(t)] \\ &= \mathscr{Re}[B\underline{/\phi}\, e^{j\omega t}] \\ &= \mathscr{Re}[B\ \cos(\omega t + \varphi) + jB\ \sin(\omega t + \varphi)] \\ &= B\ \cos(\omega t + \varphi) \end{aligned} \tag{A.9}$$

Hence, if the original input was a cosine, then the output will be a cosine, and if the original input had been a sine, then the output would be a sine, both having the same magnitude and phase:

$$\begin{aligned} x(t) = A\cos(\omega t + \theta) &\Rightarrow y(t) = B\cos(\omega t + \varphi) \\ x(t) = A\sin(\omega t + \theta) &\Rightarrow y(t) = B\sin(\omega t + \varphi) \end{aligned} \tag{A.10}$$

But solving (A.3) using complex algebra is considerably simpler than solving (A.1).

This is referred to as the *phasor method* and is the heart of the solution of electric circuits, as well as all other linear systems. The method was originally developed in the 1930s by a pioneer in electrical engineering, Charles Proteus Steinmetz, while working at General Electric. Note that this solution method applies only to inputs that are sinusoidal and for solutions that are in the steady state, i.e., after all transients have died out. The next and final question is “Why do we invest so much interest and time in analyzing systems whose inputs are single-frequency sinusoids?” A sinusoidal waveform is only one type of possible waveform that could excite this linear system in the real world, so why devote so much interest to determining the response to it? The answer is very simple: *superposition and the Fourier series*. Any periodic waveform can be alternatively represented as an infinite sum of sinusoidal components with the Fourier series (see Chapter 3) as

$$x(t) = A_0 + \sum_{n=1}^{\infty} A_n \cos(n\omega_0 + \theta_n) \tag{A.11}$$

where the $x(t)$ is periodic (but not sinusoidal) with period T and fundamental frequency $\omega_0 = 2\pi f_0$ where $f_0 = 1/T$. A function $x(t)$ is periodic with period T if $x(t \pm mT) = x(t)$ for $m = 1, 2, 3, \cdots$. Hence, *because the system is stipulated to be linear* (the phasor method does not work for nonlinear systems), we can use the important principle of superposition to pass each single-frequency sinusoidal component in (A.11) through the system to determine the response to this general periodic input waveform as the sum of the responses to those sinusoidal components

$$y(t) = B_0 + \sum_{n=1}^{\infty} B_n \cos(n\omega_0 + \phi_n) \tag{A.12}$$

as illustrated in Fig. A.1b. But each of these individual responses can be easily determined using the phasor method. Even if the input waveform is not periodic, a similar process can be used because any nonperiodic waveform can be represented as a smooth continuum of sinusoidal components with the Fourier transform. *This is the essential reason why we invest so much time and effort in learning to analyze the response of a linear system to a single-frequency sinusoidal input.* In addition, as we saw in Chapter 3, by breaking a general, periodic time-domain waveform into its sinusoidal components via the Fourier series, we can more readily understand how these individual sinusoidal components go together to shape the output waveform. This is the essence of the design of electric circuit filters.

Example A.1 Determine the solution to the following differential equation:

$$\frac{d^3y(t)}{dt^3} + \frac{d^2y(t)}{dt^2} + 3\frac{dy(t)}{dt} + 2y(t) = 10\sin(2t + 30^\circ)$$

Solution: Replacing the right-hand side with $10\underline{/30^\circ}\, e^{j2t}$ where $\omega = 2$ and assuming a solution of $\hat{Y}(t) = B\underline{/\phi}\, e^{j2t}$ gives, after canceling the e^{j2t} that is common to both sides, the following equation:

$$\begin{aligned} B\underline{/\phi} &= \frac{10\underline{/30^\circ}}{(j2)^3 + (j2)^2 + 3(j2) + 2} \\ &= \frac{10\underline{/30^\circ}}{-j8 - 4 + j6 + 2} \\ &= \frac{10\underline{/30^\circ}}{-2 - j2} \\ &= \frac{10\underline{/30^\circ}}{2\sqrt{2}\underline{/(-135^\circ)}} \\ &= 3.54\underline{/165^\circ} \end{aligned}$$

Hence, we identify the solution as

$$y(t) = 3.54\sin(2t + 165^\circ)$$

Review Exercise A.1 Determine the sinusoidal steady-state solution for the following differential equation:

$$\frac{d^2y(t)}{dt^2} + 2\frac{dy(t)}{dt} + 4y(t) = 10\sin(4t - 45^\circ)$$

***Answer*:** $y(t) = 0.69\sin(4t - 191.31^\circ) = 0.69\sin(4t + 168.69^\circ)$.

A.2 SOLVING ELECTRIC CIRCUITS FOR THEIR SINUSOIDAL, STEADY-STATE RESPONSE

This phasor method can be used to directly solve for the response of an electric circuit to a sinusoidal source. The reason we investigate the solution for the response to a single-frequency sinusoidal source is, again, because the response to any other source waveform that is periodic can be found using the Fourier series and super position. If the source waveform is not periodic, we use the Fourier transform to decompose the waveform into a continuum of sinusoids in a similar manner. We will acquire great deal of our understanding of EMC through analysis of the sinusoidal response of circuits, and the analysis method will be the phasor method. Hence, the reader should become thoroughly familiar with this technique as applied to linear electric circuits.

Although we may use this method for the analysis of electric circuits, so far it requires that we first derive the differential equation that relates the output (a circuit current or voltage) to the input source. We need not derive that differential equation and can apply the phasor method directly to the circuit in the following manner.

Figure A.2 shows how to transform the circuit elements from the time domain to the frequency (phasor) domain. First consider transforming the independent voltage and current sources. These become complex-valued quantities as

$$V_S \cos(\omega t + \theta_V) \leftrightarrow \hat{V}_S = V_S \underline{/\theta_V} \tag{A.13a}$$

$$I_S \cos(\omega t + \theta_I) \leftrightarrow \hat{I}_S = I_S \underline{/\theta_I} \tag{A.13b}$$

Next consider transforming the circuit elements of the resistor, the inductor, and the capacitor. The time-domain terminal relation for the resistor is Ohm's law: $v(t) = Ri(t)$. Substituting the phasor representation of the voltage and current as $\hat{V}(t) = V\underline{/\phi_V}\, e^{j\omega t}$ and $\hat{I}(t) = I\underline{/\phi_I}\, e^{j\omega t}$ and canceling the common $e^{j\omega t}$ factor yields the phasor relation:

$$\hat{V} = R\hat{I} \tag{A.14}$$

and the resistor remains unchanged in the phasor circuit. Next consider the inductor whose terminal relation is $v(t) = L[di(t)/dt]$. Substituting the phasor representation of the voltage and current as $\hat{V}(t) = V\underline{/\phi_V}\, e^{j\omega t}$ and $\hat{I}(t) = I\underline{/\phi_I}\, e^{j\omega t}$ and canceling the common $e^{j\omega t}$ factor yields the phasor relation:

$$\hat{V} = j\omega L\hat{I} \tag{A.15}$$

Hence, we may replace the inductor with a complex-valued "resistor" having an impedance of

$$\hat{Z}_L = j\omega L \tag{A.16}$$

Next consider the capacitor whose terminal relation is $i(t) = C[dv(t)/dt]$. Substituting the phasor representation of the voltage and current as $\hat{V}(t) = V\underline{/\phi_V}\, e^{j\omega t}$ and $\hat{I}(t) = I\underline{/\phi_I}\, e^{j\omega t}$ and canceling the common $e^{j\omega t}$ factor yields the phasor relation

$$\hat{I} = j\omega C\hat{V} \tag{A.17}$$

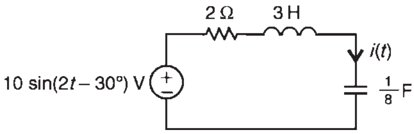

FIGURE A.2 The transformation between the time-domain circuit and the frequency-domain (phasor) circuit.

or

$$\begin{aligned}\hat{V} &= \frac{1}{j\omega C}\hat{I} \\ &= -j\frac{1}{\omega C}\hat{I}\end{aligned} \tag{A.18}$$

and we have used the complex algebra result of $(1/j) = (1/j)(j/j) = -j$. Hence, we may replace the capacitor with a complex-valued "resistor" having an impedance of

$$\hat{Z}_C = -j\frac{1}{\omega C} \tag{A.19}$$

Hence the phasor circuit is essentially a "resistive circuit" having complex-valued "resistors" of impedance $\hat{Z}_R = R, \hat{Z}_L = j\omega L$, and $\hat{Z}_C = -j(1/\omega C)$. Thus, we only need to use resistive circuit solution techniques and complex algebra to solve this phasor circuit, which is much easier than solving the differential equation directly.

Example A.2 Determine the solution for the current $i(t)$ in the circuit of Fig. A.3a.

Solution: The transformed phasor circuit is shown in Fig. A.3b, where the source has radian frequency $\omega = 3$. The inductor transforms as

$$\begin{aligned}\hat{Z}_L &= j\omega L \\ &= j(3)(3) \\ &= j9\ \Omega\end{aligned}$$

The capacitor transforms as

$$\begin{aligned}\hat{Z}_C &= -j\frac{1}{\omega C} \\ &= -j\frac{1}{(3)\left(\frac{1}{21}\right)} \\ &= -j7\ \Omega\end{aligned}$$

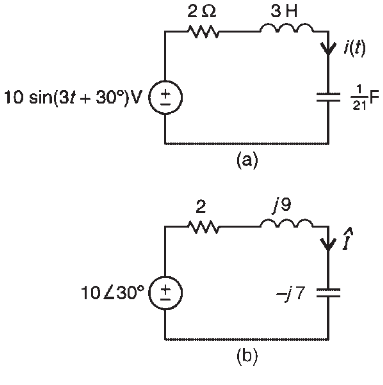

FIGURE A.3 Example A.2; (a) non-transformed circuit; (b) transformed circuit.

Treating this as a “resistive circuit,” the phasor current $\hat{I}$ is the source phasor voltage divided by the sum of the impedances in the loop:

$$\begin{aligned}\hat{I} &= \frac{10\underline{/30^\circ}}{2+j9-j7} \\ &= \frac{10\underline{/30^\circ}}{2+j2} \\ &= \frac{10\underline{/30^\circ}}{2+\sqrt{2}\underline{/45^\circ}} \\ &= 3.54\underline{/(-15^\circ)}\ \text{A}\end{aligned}$$

Therefore, since the source was a sine, the solution is

$$i(t) = 3.54\sin(3t - 15^\circ)\ \text{A}$$

Review Exercise A.2 Determine the sinusoidal steady-state solution for the voltage, $v(t)$, in the circuit of Fig. EA.2.

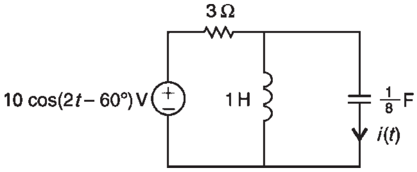

FIGURE EA.2 Review Exercise A.2.

Answer: $v(t) = 17.89\cos(2t - 71.57^\circ)$ V.

PROBLEMS

Solve the following problems by hand and confirm your result using PSPICE (See Appendix D).

A.1 Determine the current $i(t)$ in the circuit of Fig. PA.1. [$3.54\sin(2t - 75^\circ)$ A]

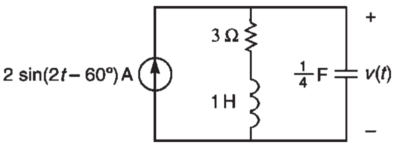

FIGURE PA.1

A.2 Determine the voltage $v(t)$ in the circuit of Fig. PA.2. [$20\cos(t + 45^\circ)$ V]

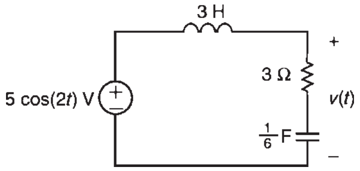
3 H
3 Ω
5 cos(2t) V
+
v(t)
$\frac{1}{6}$ F
−

FIGURE PA.2

A.3 Determine the current $i(t)$ in the circuit of Fig. PA.3. [$2\cos(2t + 66.87°)$ A]

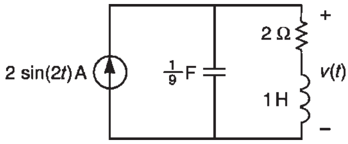
+
2 Ω
2 sin(2t) A
$\frac{1}{9}$ F
v(t)
1 H
−

FIGURE PA.3

A.4 Determine the voltage $v(t)$ in the circuit of Fig. PA.4. [$4.81\sin(2t - 116.31°)$ V]

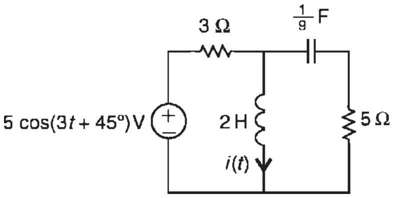
3 Ω
$\frac{1}{9}$ F
5 cos(3t + 45°) V
2 H
5 Ω
i(t)

FIGURE PA.4

A.5 Determine the voltage $v(t)$ in the circuit of Fig. PA.5. [$5\cos(2t - 90°)$ V]

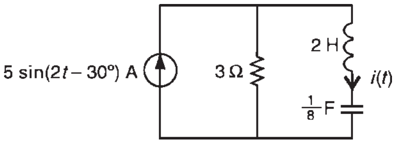
2 H
5 sin(2t − 30°) A
3 Ω
i(t)
$\frac{1}{8}$ F

FIGURE PA.5

A.6 Determine the voltage $v(t)$ in the circuit of Fig. PA.6. [$7.95\sin(2t + 6.34°)$ V]

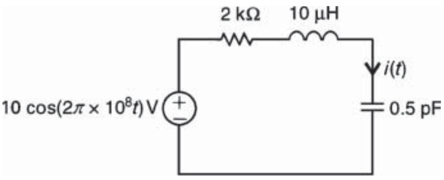
2 kΩ
10 μH
i(t)
10 cos(2π × 10⁸t) V
0.5 pF

FIGURE PA.6

A.7 Determine the current $I(t)$ in the circuit of Fig. PA.7. [$0.57\cos(3t - 35.73°)$ A]

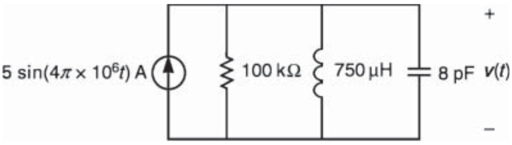
5 sin(4π × 10⁶t) A
100 kΩ
750 μH
8 pF
+
v(t)
–

FIGURE PA.7

A.8 Determine the current $I(t)$ in the circuit of Fig. PA.8. [$5\sin(2t - 30°)$ A]

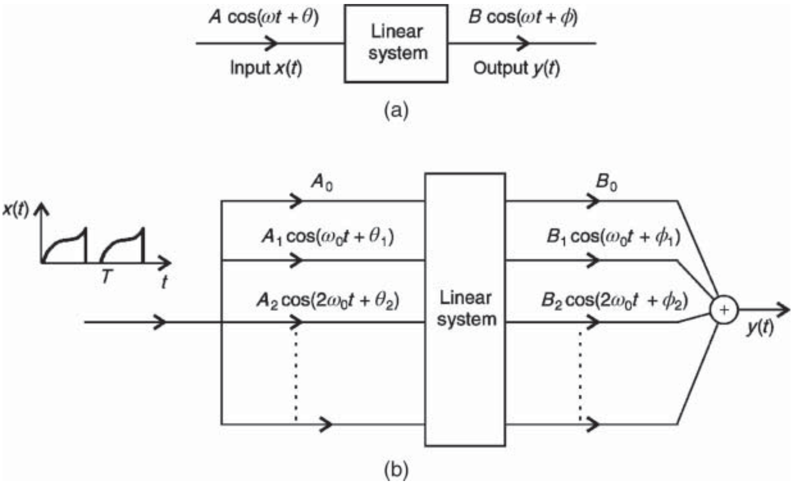
A cos(ωt + θ)
Input x(t)
Linear system
B cos(ωt + ϕ)
Output y(t)
(a)
x(t)
T
t
A₀
A₁ cos(ω₀t + θ₁)
A₂ cos(2ω₀t + θ₂)
Linear system
B₀
B₁ cos(ω₀t + ϕ₁)
B₂ cos(2ω₀t + ϕ₂)
+
y(t)
(b)

FIGURE PA.8

A.9 Determine the voltage $I(t)$ in the circuit of Fig. PA.9. [$2.71\sin(2\pi \times 10^8 t - 57.17°)$ mA]

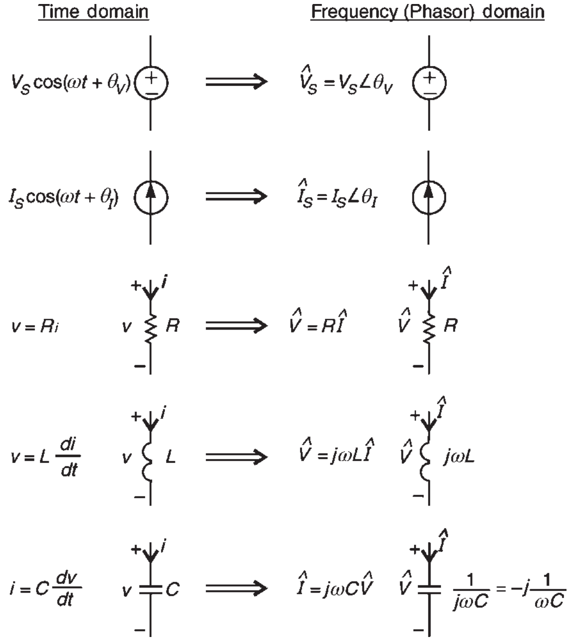
Time domain
Frequency (Phasor) domain
V_S cos(ωt + θ_V)
V̂_S = V_S∠θ_V
I_S cos(ωt + θ_I)
Î_S = I_S∠θ_I
v = Ri
V̂ = RÎ
R
v = L di/dt
V̂ = jωLÎ
L
jωL
i = C dv/dt
Î = jωCV̂
C
1/(jωC) = −j 1/(ωC)

FIGURE PA.9

A.10 Determine the voltage $v(t)$ in the circuit of Fig. PA.10.
$[4.368 \times 10^5 \sin(4\pi \times 10^6 t + 29.13°)$ V]

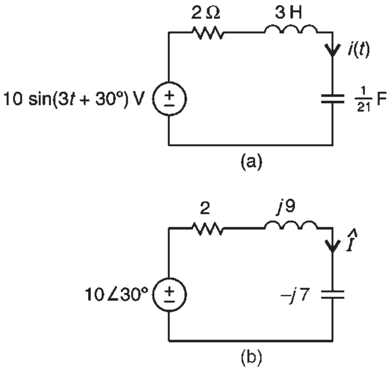
2 Ω
3 H
$i(t)$
10 sin(3t + 30°) V
+
−
$\frac{1}{21}$ F
(a)
2
j9
$\hat{I}$
10∠30°
+
−
−j7
(b)

FIGURE PA.10

REFERENCE

1. C. R. Paul, *Fundamentals of Electric Circuit Analysis*, Wiley, New York, 2001.

APPENDIX B

The Electromagnetic Field Equations and Waves

Electromagnetic field theory and Maxwell's equations underlie all electrical phenomena. This appendix summarizes the essential electromagnetic field concepts necessary for understanding and solving EMC problems, as well as designing modern electronic systems that are electromagnetically compatible with their environment. Standard electrical engineering curricula require at least one semester covering this material. Hence, this appendix will serve as a brief review of that important topic. The reader is referred to [1, 2] or other standard undergraduate electromagnetics texts for a more thorough discussion.

Recall that the frequency range of the regulations is rather large: from 150 kHz to 30 MHz for conducted emissions and from 30 MHz to above 1 GHz for radiated emissions. Thus, the electrical dimensions of an electronic product and its associated connection cables (as well as the ac power cord) may not be electrically small (much less than a wavelength), in which case the usual lumped-circuit notions and analysis principles such as Kirchhoff's laws do not apply. Attempting to analyze electrically large structures using these lumped-circuit analysis principles will lead to erroneous conclusions and faulty designs. The laws governing the behavior of electrically large structures (Maxwell's equations) are not as simple to use as are the lumped-circuit analysis principles. However, for electrically large structures, we have no other recourse. Some problems are sufficiently small, electrically, so that the simpler lumped-circuit analysis techniques will be applicable (in a reasonably approximate sense). An example is the modeling of small, electronic components. Where it is possible, we will utilize the simpler analysis method.

All macroscopic electromagnetic phenomena are governed by *Maxwell's equations*. Maxwell's equations are complex from a mathematical standpoint but are quite easy to describe in conceptual terms. These equations describe the *distributed-parameter* nature of electromagnetic fields; that is, the electromagnetic field quantities are distributed throughout space. Thus, the differential equations that are referred to as Maxwell's equations are a set of *partial differential equations* since the field quantities are functions of spatial parameters x, y, z in three-dimensional space, as well as time t. Where appropriate (electrically small structures), we will use lumped-circuit approximations, and the governing equations become *ordinary differential equations* where the variables are functions of only one parameter, time t.

Introduction to Electromagnetic Compatibility, Third Edition. Clayton R. Paul, Robert C. Scully, and Mark A. Steffka.
© 2023 John Wiley & Sons, Inc. Published 2023 by John Wiley & Sons, Inc.

The material in this appendix constitutes a brief review of basic electromagnetic theory. The reader is referred to [1, 2] or similar texts for additional results and details.

B.1 VECTOR ANALYSIS

Maxwell's equations are described concisely in terms of certain mathematical operations on vector quantities in three-dimensional space. The field quantities are described as *vector* quantities, which will be denoted by bold letters, e.g., $\boldsymbol{A}$, and a vector is represented as a directed line segment. Vector quantities convey two pieces of information: a magnitude and a direction of effect. The magnitude or length of a vector will be denoted as $|\boldsymbol{A}| = A$. To quantitatively describe a vector and perform mathematical operations on it as required by Maxwell's equations, we must describe the vector in a coordinate system. A *rectangular* or *Cartesian* coordinate system consists of three orthogonal planes, $x = x_1 =$ constant, $y = y_1 =$ constant, $z = z_1 =$ constant as illustrated in Fig. B.1. The location of a point is described by the intersection of these three planes as $P = [x_1, y_1, z_1]$. This results in the coordinate system being represented as three orthogonal axes: x, y, z. The vector $\boldsymbol{A}$ has *projections* on each axis: A_x, A_y, A_z. A vector represented in the rectangular coordinate system is written in terms of *unit vectors* $\boldsymbol{a}_x$, $\boldsymbol{a}_y$, $\boldsymbol{a}_z$ in terms of its components as

$$\boldsymbol{A} = A_x \boldsymbol{a}_x + A_y \boldsymbol{a}_y + A_z \boldsymbol{a}_z \tag{B.1}$$

There are other coordinate systems that will be convenient to use. These are the *cylindrical* and *spherical* coordinate systems and will be discussed as needed in the text. Vectors may be added by adding corresponding components as

$$\boldsymbol{A} + \boldsymbol{B} = (A_x + B_x)\boldsymbol{a}_x + (A_y + B_y)\boldsymbol{a}_y + (A_z + B_z)\boldsymbol{a}_z \tag{B.2}$$

Vectors may also have their lengths changed by a factor k by multiplying by that constant that multiplies each component by that factor. If the factor k is a negative number, this has the effect of reversing the direction of the vector. This shows how we may subtract two vectors; simply add

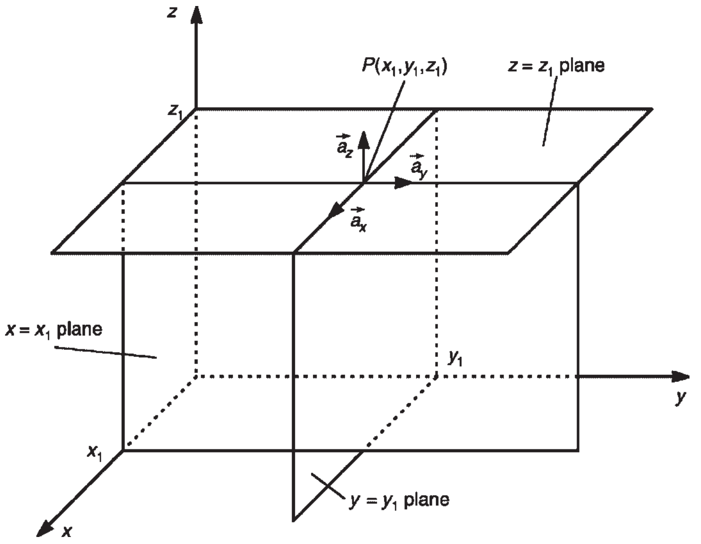

FIGURE B.1 The rectangular coordinate system: locating a point as the intersection of two orthogonal planes.

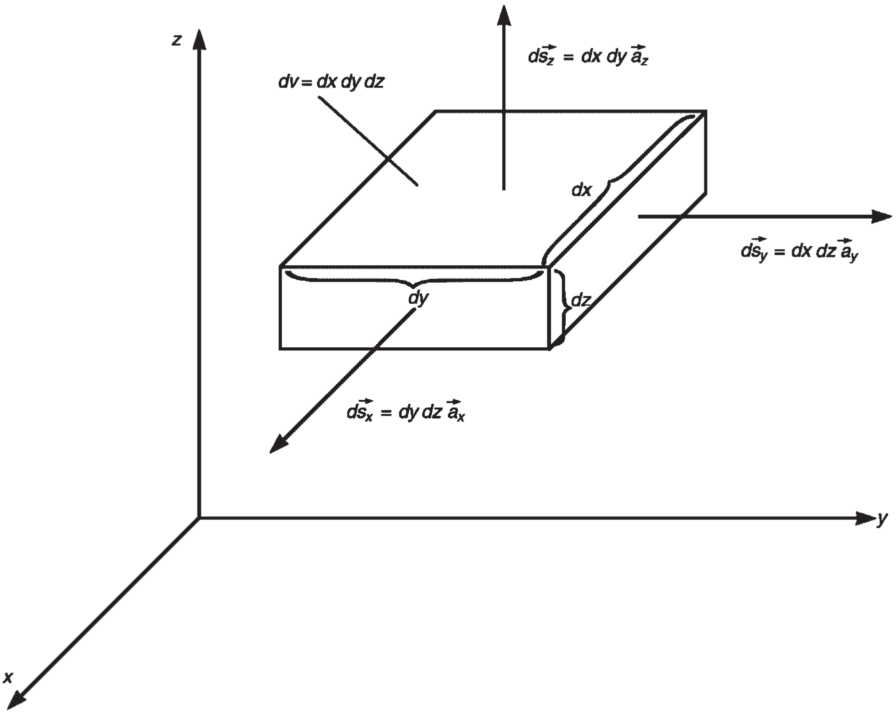
z
dv = dx dy dz
$\vec{ds_z} = dx\, dy\, \vec{a_z}$
dx
$\vec{ds_y} = dx\, dz\, \vec{a_y}$
dy
dz
$\vec{ds_x} = dy\, dz\, \vec{a_x}$
y
x

FIGURE B.2 Differential surfaces and volumes.

$\boldsymbol{A} + k\boldsymbol{B}$ and choose $k = -1$. We will often need differential path lengths $d\boldsymbol{l}$, differential surface areas $d\boldsymbol{s}$, and differential volumes dv as illustrated in Fig. B.2. These become [1, 2]

$$d\boldsymbol{l} = dx\boldsymbol{a}_x + dy\boldsymbol{a}_y + dz\boldsymbol{a}_z \tag{B.3a}$$

$$d\boldsymbol{s} = dydz\boldsymbol{a}_x + dxdz\boldsymbol{a}_y + dxdy\boldsymbol{a}_z \tag{B.3b}$$

$$dv = dxdydz \tag{B.3c}$$

There are two definitions for the product of two vectors: the *dot product* and the *cross product*. The *dot product* of two vectors is defined as [1, 2]

$$\begin{aligned} \boldsymbol{A} \cdot \boldsymbol{B} &= |\boldsymbol{A}||\boldsymbol{B}| \cos\, \theta_{AB} \\ &= A_xB_x + A_yB_y + A_zB_z \end{aligned} \tag{B.4}$$

This represents the product of the length of one vector and the *projection* of the other vector on that vector, as illustrated in Fig. B.3a. The *cross product* of two vectors is defined as [1, 2]

$$\begin{aligned} \boldsymbol{A} \times \boldsymbol{B} &= |\boldsymbol{A}||\boldsymbol{B}| \sin\theta_{AB}\boldsymbol{a}_n \\ &= (A_yB_z - A_zB_y)\boldsymbol{a}_x + (A_zB_x - A_xB_z)\boldsymbol{a}_y + (A_xB_y - A_zB_x)\boldsymbol{a}_z \\ &= -\boldsymbol{B} \times \boldsymbol{A} \end{aligned} \tag{B.5a}$$

where $\boldsymbol{a}_n$ is a unit vector perpendicular to the plane formed by the two vectors, as shown in Fig. B.3b. The direction of this unit vector is determined by the *right-hand rule*; that is, if the fingers of the right

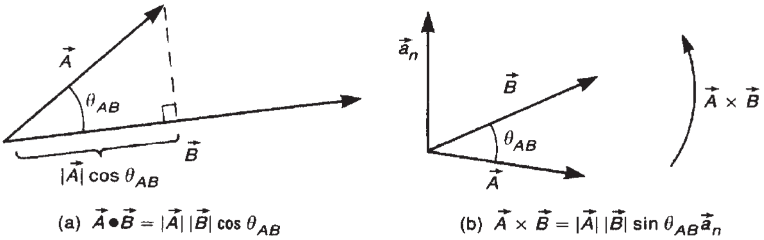
$\vec{A}$
θ_{AB}
$\vec{B}$
$|\vec{A}|\cos\theta_{AB}$
(a) $\vec{A}\bullet\vec{B} = |\vec{A}|\,|\vec{B}|\cos\theta_{AB}$
$\vec{a}_n$
$\vec{B}$
θ_{AB}
$\vec{A}$
$\vec{A}\times\vec{B}$
(b) $\vec{A}\times\vec{B} = |\vec{A}|\,|\vec{B}|\sin\theta_{AB}\vec{a}_n$

FIGURE B.3 Illustration of (a) the dot product and (b) the cross product.

hand are curled from $\boldsymbol{A}$ to $\boldsymbol{B}$, the thumb will point in the direction of $\boldsymbol{a}_n$. Note that the dot product $\boldsymbol{A}\cdot\boldsymbol{B}$ yields a *scalar* and not a vector as the result. The cross product yields a *vector* as the result. Observe that the order of $\boldsymbol{A}$ and $\boldsymbol{B}$ in the cross-product matters, i.e., $\boldsymbol{A}\times\boldsymbol{B} = -\boldsymbol{B}\times\boldsymbol{A}$. An alternative way of computing the cross-product is by evaluating the following determinant:

$$\begin{aligned}\boldsymbol{A}\times\boldsymbol{B} &= \begin{vmatrix}\boldsymbol{a}_x & \boldsymbol{a}_y & \boldsymbol{a}_z\\ A_x & A_y & A_z\\ B_x & B_y & B_z\end{vmatrix}\\ &= (A_yB_z - A_zB_y)\boldsymbol{a}_x + (A_zB_x - A_xB_z)\boldsymbol{a}_y + (A_xB_y - A_zB_x)\boldsymbol{a}_z \qquad \text{(B.5b)}\end{aligned}$$

Example B.1 Determine the dot product and cross product of the following vectors:

$$\boldsymbol{A} = 2\boldsymbol{a}_x + 3\boldsymbol{a}_y - 4\boldsymbol{a}_z$$

$$\boldsymbol{B} = -1\boldsymbol{a}_x - 5\boldsymbol{a}_y + 6\boldsymbol{a}_z$$

Solution: The dot product $\boldsymbol{A}\cdot\boldsymbol{B}$ is

$$\begin{aligned}\boldsymbol{A}\cdot\boldsymbol{B} &= (2)(-1) + (3)(-5) + (-4)(6)\\ &= -41\end{aligned}$$

The cross product $\boldsymbol{A}\times\boldsymbol{B}$ is

$$\begin{aligned}\boldsymbol{A}\times\boldsymbol{B} &= [(3)(6) - (-4)(-5)]\boldsymbol{a}_x + [(-4)(-1) - (2)(6)]\boldsymbol{a}_y\\ &\quad + [(2)(-5) - (3)(-1)]\boldsymbol{a}_z\\ &= -2\boldsymbol{a}_x - 8\boldsymbol{a}_y - 7\boldsymbol{a}_z\end{aligned}$$

or, alternatively

$$\begin{aligned}\boldsymbol{A}\times\boldsymbol{B} &= \begin{vmatrix}\boldsymbol{a}_x & \boldsymbol{a}_y & \boldsymbol{a}_z\\ 2 & 3 & -4\\ -1 & -5 & 6\end{vmatrix}\\ &= [(3)(6) - (-4)(-5)]\boldsymbol{a}_x + [(2)(6) - (-4)(-1)]\boldsymbol{a}_y\\ &\quad + [(2)(-5) - (3)(-1)]\boldsymbol{a}_z\\ &= -2\boldsymbol{a}_x - 8\boldsymbol{a}_y - 7\boldsymbol{a}_z\end{aligned}$$

The cross product $\vec{B} \times \vec{A}$ is

$$\begin{aligned}\boldsymbol{B} \times \boldsymbol{A} &= [(-5)(-4) - (6)(3)]\boldsymbol{a}_x + [(6)(2) - (-4)(-1)]\boldsymbol{a}_y \\ &\quad + [(-1)(3) - (-5)(2)]\boldsymbol{a}_z \\ &= 2\boldsymbol{a}_x + 8\boldsymbol{a}_y + 7\boldsymbol{a}_z \\ &= -\boldsymbol{A} \times \boldsymbol{B}\end{aligned}$$

or, alternatively

$$\begin{aligned}\boldsymbol{B} \times \boldsymbol{A} &= \begin{vmatrix} \boldsymbol{a}_x & \boldsymbol{a}_y & \boldsymbol{a}_z \\ -1 & -5 & 6 \\ 2 & 3 & -4 \end{vmatrix} \\ &= [(-5)(-4) - (6)(3)]\boldsymbol{a}_x + [(6)(2) - (-4)(-1)]\boldsymbol{a}_y \\ &\quad +[(-1)(3) - (-5)(2)]\boldsymbol{a}_z \\ &= 2\boldsymbol{a}_x + 8\boldsymbol{a}_y + 7\boldsymbol{a}_z \\ &= -\boldsymbol{A} \times \boldsymbol{B}\end{aligned}$$

Review Exercise B.1 Determine the dot product and cross product of the following vectors.

$$\boldsymbol{A} = -2\boldsymbol{a}_x + 5\boldsymbol{a}_y + 4\boldsymbol{a}_z$$

$$\boldsymbol{B} = 6\boldsymbol{a}_x - 3\boldsymbol{a}_y + \boldsymbol{a}_z$$

***Answers*:** $\boldsymbol{A} \cdot \boldsymbol{B} = -23,\ \ \boldsymbol{A} \times \boldsymbol{B} = 17\vec{a}_x + 26\vec{a}_y - 24\vec{a}_z$

A number of *vector calculus* operations are important to understand because Maxwell's equations are described mathematically in terms of them. The first is the concept of *line integral* of a vector field $\boldsymbol{F}$ along a contour C [1, 2]

$$\begin{aligned}\int_C \boldsymbol{F} \cdot d\boldsymbol{l} &= \int_C |\,\boldsymbol{F}\,| \cos\theta \, dl \\ &= \int_{C_x} F_x dx + \int_{C_y} F_y dy + \int_{C_z} F_z dz\end{aligned} \tag{B.6}$$

as illustrated in Fig. B.4. The integral in (B.6) symbolizes that we add (integrate) the product of the components of $\boldsymbol{F}$ that are *tangent to the path*, $|\boldsymbol{F}\,| \cos\theta$, and the differential path length dl along the contour C. Perhaps the more obvious use of this result is in the computation of the work required to move an object against a force field from point a to point b.

Example B.2 A force field is given by

$$\boldsymbol{F} = (2y\boldsymbol{a}_x + xy\boldsymbol{a}_y + z\boldsymbol{a}_z)\ \text{N}$$

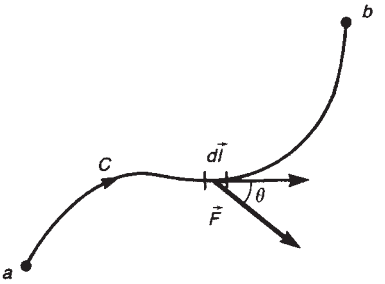

FIGURE B.4 Illustration of the line integral.

Determine the work required to move an object against this field from [x = 1 m, y = 1 m, z = 0 m] to [x = 0 m, y = 2 m, z = 3 m] along a straight-line path between the two points.

Solution: The work required by us is

$$\begin{aligned} W &= -\int_a^b \boldsymbol{F}\cdot d\boldsymbol{l} \\ &= -\left(\int_{x=1}^{0} 2y dx + \int_{y=1}^{2} xy dy + \int_{z=0}^{3} z dz\right) \\ &= -\left[\int_{x=1}^{0} 2(-x+2)dx + \int_{y=1}^{2} (-y+2)y dy + \int_{z=0}^{3} z dz\right] \\ &= \frac{13}{6}\ \text{J} \end{aligned}$$

and we have substituted the equation of the path, $y = -x + 2$, into the appropriate integrand variables to reduce the integrand to a function of only that variable.

Review Exercise B.2 Evaluate the line integral of $\boldsymbol{F} = 2y\boldsymbol{a}_x + 3x\boldsymbol{a}_y + \boldsymbol{a}_z$ along a straight-line path from point a at $x = 0$, $y = 0$, $z = 0$ to point b at $x = 1$, $y = 2$, $z = 3$.

***Answer*:** 8.

The next integral we will find useful is the *surface integral* of a vector field over a surface S, defined by [1, 2]

$$\begin{aligned} \int_S \boldsymbol{F}\cdot d\boldsymbol{s} &= \int_S |\,\boldsymbol{F}\,| \cos\theta\, ds \\ &= \iint F_x dydz + \iint F_y dxdz + \iint F_z dxdy \end{aligned} \tag{B.7}$$

where θ is the angle between $\boldsymbol{F}$ and a normal to the surface. The surface integral in (B.7) symbolizes that we are to add (integrate) the product of the components of $\boldsymbol{F}$ that are *perpendicular to the differential surface* and the differential surface elements as illustrated in Fig. B.5. This gives the *flux*

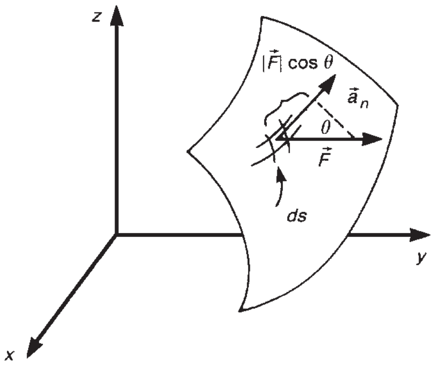

FIGURE B.5 Illustration of the surface integral in the determination of flux through a surface.

of the vector ***F*** *through the surface S*. The surface integral with a circle, $\oint_S$, denotes the surface integral over the *closed surface S*.

Example B.3 A vector field $\boldsymbol{F} = 2x\boldsymbol{a}_x + \boldsymbol{a}_y - \boldsymbol{a}_z$ is to be integrated over the planar surface S defined by the three corners $[x = 2, y = 1, z = 0]$, $[x = 2, y = 3, z = 0]$, and $[x = 2, y = 3, z = 4]$. The surface integral is

$$\begin{aligned}\int_S \boldsymbol{F}\cdot d\boldsymbol{s} &= \int_{y=1}^{3}\int_{z=0}^{z=2y-2} 2x\,dy\,dz + \underbrace{\iint dx\,dz}_{0} - \underbrace{\iint dx\,dy}_{0}\\ &= 16\end{aligned}$$

Since $dx = 0$ over the surface ($x = 2$ at all points on that surface), the second and third integrals are zero. Another way of looking at this is that, because of the orientation of the surface, in the yz plane for $x = 2$, the required flux is that in the positive x direction. The y and z components of the vector are not orthogonal to the surface and therefore contribute nothing to the integral. Observations such as these are important in simplifying the result.

Review Exercise B.3 Determine the net flux of $\boldsymbol{F} = -2x\boldsymbol{a}_x + y\boldsymbol{a}_y - \boldsymbol{a}_z$ out of the closed surface bounded by $-1 \le x \le 1, -2 \le y \le 2$, and $0 \le z \le 3$.

***Answer*:** 24.

There are two additional vector calculus operations that will be useful: the *divergence* and the *curl* of a vector field, The *divergence of a vector field* is defined as [1, 2]

$$\begin{aligned}\operatorname{div}\boldsymbol{F} &= \nabla\cdot\boldsymbol{F}\\ &= \lim_{\Delta v\to 0}\frac{\oint_S \boldsymbol{F}\cdot d\boldsymbol{s}}{\Delta v}\\ &= \frac{\partial F_x}{\partial x} + \frac{\partial F_y}{\partial y} + \frac{\partial F_x}{\partial z}\end{aligned}\tag{B.8}$$

where surface S encloses volume Δv. Therefore, the *divergence of a vector field is the net outward flux of the vector field per unit volume as the volume shrinks to zero*. Essentially, the divergence of a vector field represents the flux of the field from a point that gives an indication of the *net source* of the field at that point and is a *scalar quantity*. An important identity that will prove to be useful is the *divergence theorem* [1]:

$$\int_S \boldsymbol{F} \cdot -d\boldsymbol{s} = \int_v \nabla \cdot \boldsymbol{F} dv \tag{B.9}$$

The divergence theorem shows that the *net flux of a vector field out of a closed surface can be obtained as the integral of the divergence of the vector field throughout the volume bounded by the surface*. This result allows us to interchange surface and volume integrals. The next vector calculus operation that will be required is the *curl of a vector field*, defined as [1, 2]

$$\begin{aligned} curl\, \boldsymbol{F} &= \nabla \times \boldsymbol{F} \\ &= \lim_{\Delta S \to 0} \frac{\oint_C \boldsymbol{F} \cdot d\boldsymbol{l}}{\Delta S} \cdot \boldsymbol{a}_n \\ &= \left(\frac{\partial F_z}{\partial y} - \frac{\partial F_y}{\partial z} \right) \boldsymbol{a}_x + \left(\frac{\partial F_x}{\partial z} - \frac{\partial F_z}{\partial x} \right) \boldsymbol{a}_y + \left(\frac{\partial F_y}{\partial x} - \frac{\partial F_x}{\partial y} \right) \boldsymbol{a}_z \end{aligned} \tag{B.10}$$

where $\boldsymbol{a}_n$ is a unit vector normal to the differential surface.

Equation (B.10) symbolizes that *the curl of a vector field is the line integral of a vector field around a contour C that bounds an open surface S as that surface area shrinks to zero*. Essentially, the curl is the net *circulation of a vector field about a point*. The curl is a *vector quantity* symbolizing the circulation of the vector in three orthogonal planes. A related result is *Stokes' theorem*, which is given by [1]

$$\int_s (\nabla \times \boldsymbol{F}) \cdot d\boldsymbol{s} = \int_C \boldsymbol{F} \cdot d\boldsymbol{l} \tag{B.11}$$

Stokes' theorem symbolizes that *the net flux of the curl of a vector field through an open surface S can be computed by obtaining the line integral of the vector field around the contour C bounding the open surface*. This result allows us to interchange surface and contour integrals.

Example B.4 Determine the divergence and the curl of the vector field $\boldsymbol{F} = F_m \sin x \sin t\, \boldsymbol{a}_y$.

Solution: Writing out the divergence gives

$$\begin{aligned} \nabla \cdot \boldsymbol{F} &= \frac{\partial F_x}{\partial x} + \frac{\partial F_y}{\partial y} + \frac{\partial F_x}{\partial z} \\ &= \frac{\partial}{\partial y}(F_m \sin x \sin t) \\ &= 0 \end{aligned}$$

since F_y is independent of y.

Writing out the curl gives

$$\begin{aligned}\nabla \times \boldsymbol{F} &= \left(\frac{\partial F_z}{\partial y} - \frac{\partial F_y}{\partial z}\right)\boldsymbol{a}_x + \left(\frac{\partial F_x}{\partial z} - \frac{\partial F_z}{\partial x}\right)\boldsymbol{a}_y + \left(\frac{\partial F_y}{\partial x} - \frac{\partial F_x}{\partial y}\right)\boldsymbol{a}_z \\ &= -\frac{\partial F_y}{\partial z}\boldsymbol{a}_x + \frac{\partial F_y}{\partial x}\boldsymbol{a}_z \\ &= -\frac{\partial}{\partial z}[F_m \sin x \sin t]\boldsymbol{a}_x + \frac{\partial}{\partial x}[F_m \sin x \sin t]\boldsymbol{a}_z \\ &= F_m \cos x \sin t\, \boldsymbol{a}_z\end{aligned}$$

Review Exercise B.4 Determine the divergence and curl of the vector field $\boldsymbol{F} = F_m \cos x \cos t\, \boldsymbol{a}_z$.

***Answers*:** $\nabla \cdot \boldsymbol{F} = 0$, $\nabla \times \boldsymbol{F} = F_m \sin x \cos t\, \boldsymbol{a}_y$.

B.2 MAXWELL'S EQUATIONS

Maxwell's equations are stated concisely in terms of the vector calculus operations of the previous section. Maxwell's equations form the cornerstones of electromagnetic phenomena and are therefore essential to our understanding of how to design electronic systems such that they will comply with regulatory requirements and will also not cause interference or be interfered with. Solution of Maxwell's equations is not a simple process, yet this practicality does not diminish their fundamental importance. Quite often we will utilize certain approximations of them, such as lumped-circuit models, in order to simplify the solution of a specific problem. This is permissible so long as the dimensions of the problem are *electrically small*. Nevertheless, we should always be cognizant of the fact that Maxwell's equations govern all electromagnetic phenomena, and their complexity does not change this fact.

B.2.1 Faraday's Law

Faraday's law can be stated concisely in *integral form* as

$$\oint_C \boldsymbol{E} \cdot d\boldsymbol{l} = -\frac{d}{dt}\int_S \boldsymbol{B} \cdot d\boldsymbol{s} \tag{B.12}$$

The parameter $\boldsymbol{E}$ is the *electric field intensity vector*, with units of volts per meter (V/m). The parameter $\boldsymbol{B}$ is the *magnetic flux density vector*, with units of Weber per square meter (Wb/m^2). Faraday's law provides that *the electromotive force (emf) generated around a closed contour C is related to the time rate of change of the total magnetic flux through the open surface S bounded by that contour.* The emf is given by

$$\text{emf} = \oint_C \boldsymbol{E} \cdot d\boldsymbol{l} \tag{B.13}$$

whose units are volts (V). The total magnetic flux through the open surface S that is bounded by the contour C is

$$\psi_m = \int_S \boldsymbol{B} \cdot d\boldsymbol{s} \tag{B.14}$$

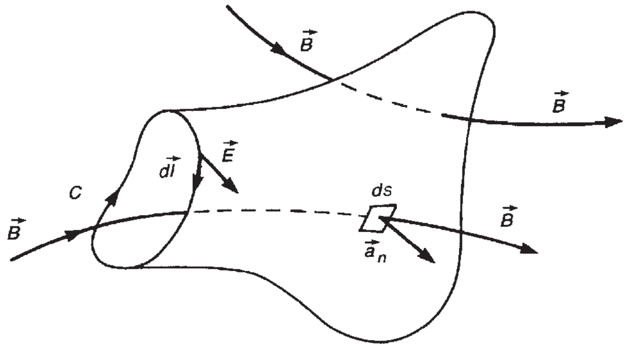

FIGURE B.6 Illustration of Faraday's law.

whose units are Weber (Wb). Therefore, Faraday's law can be written as

$$\text{emf} = -\frac{d\psi_m}{dt} \tag{B.15}$$

The contour C and surface S are intimately related by the right-hand rule, as shown in Fig. B.6. If the fingers of the right hand are directed in the direction of the contour C, the thumb will give the direction of the unit normal to the enclosed surface, $\boldsymbol{a}_n$, and the differential surface is $\boldsymbol{ds} = ds\,\boldsymbol{a}_n$.

The emf in (B.13) can be thought of as a voltage source that is inserted in the loop whose value is the time rate of change of the magnetic flux passing through the loop:

$$V_F = \frac{d\psi_m}{dt} \tag{B.16}$$

This emf is a *distributed-parameter* quantity and cannot be localized (lumped). However, if the dimensions of the loop are electrically small, then we can, as a reasonable approximation, think of this emf as a lumped voltage source. It is vitally important that we get the *polarity* of the inserted Faraday source correct. The negative sign in Faraday's law is referred to as *Lenz's law*. It symbolizes that the emf (and equivalent voltage source) has a polarity so as to generate an induced current in the loop, i_{induced}, which generates an induced magnetic field, $\boldsymbol{B}_{\text{induced}}$, that tends to oppose any *change* in the original magnetic field, $\boldsymbol{B}$. Getting the polarity of the induced source correct is often a confusing issue. A simple yet foolproof way of getting the polarity of the induced source correct is to insert the source so that it will drive an induced current around the loop which will, by the right-hand rule, produce an induced magnetic field, $\boldsymbol{B}_{\text{induced}}$, that is directed *in opposition to* the original magnetic field, $\boldsymbol{B}$. In reality, we want this induced magnetic field to oppose any *change* in the original magnetic field and not just be simply opposite in direction. However, this will be taken care of in the value of the inserted Faraday's law source, V_F. For example, consider Fig. B.7a, where the original magnetic field is directed up. The Faraday source is inserted as shown, which will produce an induced current circulating clockwise around the loop, giving, by the right-hand rule, an induced $\boldsymbol{B}$ field that acts in opposition to the original $\boldsymbol{B}$ field. If the original B field is *increasing* in magnitude, then the Faraday's law source value, $V_F = d\psi_m/dt$, will be *positive* and will oppose further increases in the original magnetic field. Conversely, suppose that the original magnetic field is directed up but is *decreasing* in magnitude. In this case, the Faraday's law source value will be *negative* and will therefore cause the induced current to actually flow in the counterclockwise direction so as to oppose any further

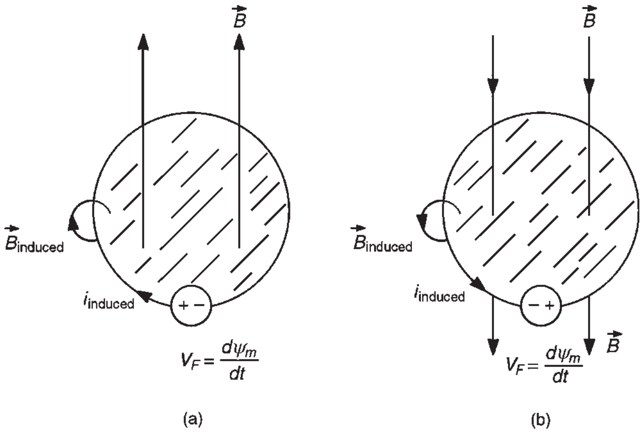
$\vec{B}$
$\vec{B}_{\text{induced}}$
i_{induced}
+ −
$V_F = \frac{d\psi_m}{dt}$
(a)
$\vec{B}$
$\vec{B}_{\text{induced}}$
i_{induced}
− +
$V_F = \frac{d\psi_m}{dt}$
$\vec{B}$
(b)

FIGURE B.7 Illustration of Faraday's law giving the relation between the induced emf and the time rate of change of the magnetic flux through the surface.

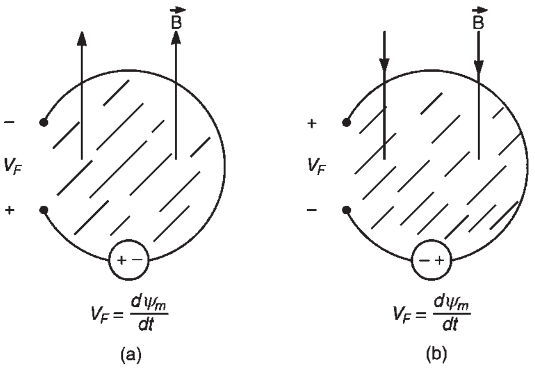

FIGURE B.8 Illustration for the open-circuit voltage induced at the terminals of an open-circuited loop.

decreases in the original magnetic field. So, if we orient the polarity of the source so that it would produce a current, i_{induced}, circulating around the loop, which, by the right-hand rule will produce an induced magnetic field, $\boldsymbol{B}_{\text{induced}}$, which will have a direction *opposite* to the original magnetic field, it will have been inserted properly. The case of the original magnetic field being directed downward is shown in Fig. B.7b.

It is not necessary to have a closed loop in order that a time-changing magnetic field will generate (induce) a voltage in that loop. For example, suppose that the loop of Fig. B.7 is opened at some point as shown in Fig. B.8. A voltage in the form of an induced voltage source is nevertheless induced in the perimeter of the loop and the source is inserted with polarity determined as before as though the loop were closed, allowing a current to flow. That voltage will be present at the terminals of the loop. Although no current will flow because the loop is broken, this voltage will nevertheless appear at the terminals. The polarity of the voltage at the terminals is essentially the *open-circuit voltage* of the loop, which is the induced Faraday source.

Faraday's law essentially shows that a *time-changing magnetic field will generate* (*induce*) *an electric field* in the same fashion as a static charge distribution. However, the induced electric field lines due to a time-changing magnetic field must close on themselves, whereas the electric field lines due to charges originate on positive charge and terminate on negative charge.

Example B.5 Figure B.9a shows an electric circuit that has a magnetic field of $\boldsymbol{B} = 10t\ \ \text{Wb/m}^2$ directed into the page that penetrates the circuit loop. Determine the voltages V_1 and V_2.

Solution: The magnetic flux that penetrates the circuit loop is

$$\begin{aligned}\psi_m &= \int_S \boldsymbol{B}\cdot d\boldsymbol{s}\\ &= 10t\ \ \text{Wb/m}^2 \times 2\ \ \text{m}^2\\ &= 20t\ \ \text{Wb}\end{aligned}$$

This is simply the product of $\boldsymbol{B}$ and the area of the loop, since the $\boldsymbol{B}$ field is assumed to be independent of position across the loop. If the value of the $\boldsymbol{B}$ field had depended on position at various points over the loop, we would have had to perform the integral to determine the flux. The value of the induced source in the circuit loop is

$$\begin{aligned}V_F &= \frac{d\psi_m}{dt}\\ &= 20\ \ \text{V}\end{aligned}$$

This source is inserted with a polarity such that it will produce a current counterclockwise around the circuit so as to produce a magnetic field that opposes the original magnetic field. This enforces Lenz's law. Now the problem becomes an ordinary circuit as shown in Fig. B.9b, where we can readily determine

$$\begin{aligned}I &= \frac{20\ \ \text{V}}{100\ \ \Omega + 50\ \ \Omega}\\ &= \frac{2}{15}\ \ \text{A}\end{aligned}$$

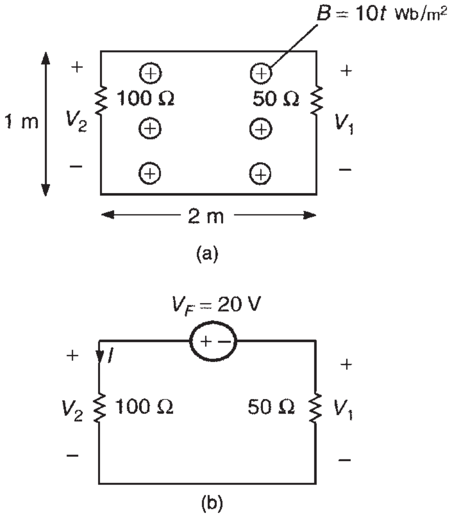

FIGURE B.9 Example B.5: (a) physical dimensions of the circuit; (b) replacing the magnetic field with the induced Faraday voltage source.

Hence, the voltages are

$$\begin{aligned} V_2 &= 100\ \Omega \times I \\ &= 13.33\ \text{V} \end{aligned}$$

and

$$\begin{aligned} V_1 &= -50\ \Omega \times I \\ &= -6.67\ \text{V} \end{aligned}$$

Observe that $V_1 \neq V_2$. In lumped-circuit analysis, we handle this situation by saying that the ***B*** field is due to some adjacent circuit and its flux linking this circuit is represented by a mutual inductance between the two circuits. So the concept of mutual inductance is inherently rooted in Faraday's law.

Example B.6 Figure B.10a shows a circuit wherein a high-impedance voltmeter that draws negligible current is attached across a resistor. In Fig. B.10b, the voltmeter is attached to the same two points, but the voltmeter leads are routed differently. Determine the voltage measured by the voltmeter for these two cases. The magnetic field is directed out of the page.

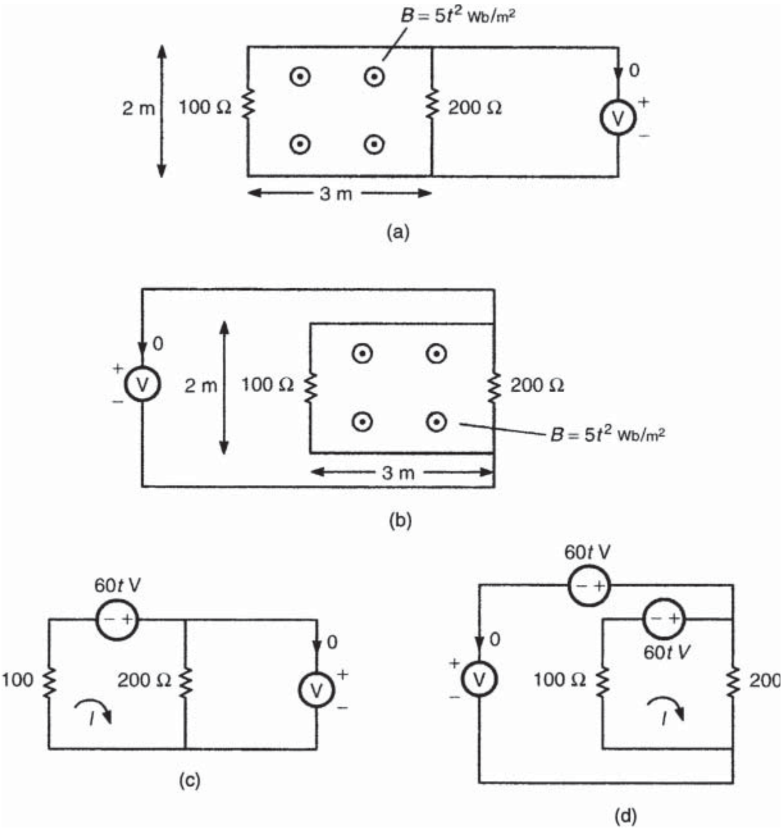

FIGURE B.10 Example B.6: (a) first position of the voltmeter leads; (b) second position of the voltmeter leads; (c) replacement of the magnetic field for the first position of the voltmeter leads with the induced Faraday voltage source; (d) replacement of the magnetic field for the second position of the voltmeter leads with the Faraday voltage sources.

Solution: For the case of Fig. B.10a, the 2 × 3 m circuit loop encloses a total magnetic flux of

$$\begin{aligned}\psi_m &= \int_S \boldsymbol{B}\cdot d\boldsymbol{s}\\ &= 5t^2 \ \ \mathrm{Wb/m^2} \times 6 \ \ \mathrm{m^2}\\ &= 30t^2 \ \ \mathrm{Wb}\end{aligned}$$

Hence, the source induced in that loop is

$$\begin{aligned}V_F &= \frac{d\psi_m}{dt}\\ &= 60t \ \ \mathrm{V}\end{aligned}$$

This source is inserted with polarity shown in Fig. B.10c to enforce Lenz's law (the ***B*** field is out of the page). From that circuit, we obtain

$$\begin{aligned}I &= \frac{60t \ \ \mathrm{V}}{100 \ \ \Omega + 200 \ \ \Omega}\\ &= 0.2t \ \ \mathrm{A}\end{aligned}$$

Hence, the voltage measured is

$$\begin{aligned}V &= 200I\\ &= 40t \ \ \mathrm{V}\end{aligned}$$

The equivalent circuit for Fig. B.10b is shown in Fig. B.10d. Observe that now the voltmeter leads also enclose the flux and another voltage source must be inserted in the loop formed by those leads. Hence, we obtain

$$\begin{aligned}I &= \frac{60t \ \ \mathrm{V}}{100 \ \ \Omega + 200 \ \ \Omega}\\ &= 0.2t \ \ \mathrm{A}\end{aligned}$$

but

$$\begin{aligned}V &= 200I - 60t\\ &= -20t \ \ \mathrm{V}\end{aligned}$$

This can also be obtained by summing KVL around the inner loop of that circuit:

$$\begin{aligned}V &= -60t + 60t - 100 \ \ \Omega \times I\\ &= -100 \ \ \Omega \times I\\ &= -20t \ \ \mathrm{V}\end{aligned}$$

This has shown that for time-varying fields, the position of the voltmeter leads can affect the measured voltage, unlike the case for static fields, where the induced sources are zero because the magnetic fields do not change with time.

Faraday's law was introduced in its *integral form* in (B.12). The integral form is useful from the standpoint of visualization of the meaning of the result. From a computational standpoint, the *point* or *differential form* is more useful. Applying Stokes' theorem to the left-hand side of (B.12) gives the *point form* of Faraday's law as

$$\nabla \times \boldsymbol{E} = -\frac{\partial \boldsymbol{B}}{\partial t} \tag{B.17a}$$

Substituting the result for the curl gives

$$\begin{aligned}&\left(\frac{\partial E_z}{\partial y} - \frac{\partial E_y}{\partial z}\right)\boldsymbol{a}_x + \left(\frac{\partial E_x}{\partial z} - \frac{\partial E_z}{\partial x}\right)\boldsymbol{a}_y + \left(\frac{\partial E_y}{\partial x} - \frac{\partial E_x}{\partial y}\right)\boldsymbol{a}_z\\ &\quad = -\frac{\partial B_x}{\partial t}\boldsymbol{a}_x - \frac{\partial B_y}{\partial t}\boldsymbol{a}_y - \frac{\partial B_z}{\partial t}\boldsymbol{a}_z\end{aligned} \tag{B.17b}$$

Matching components gives three equations:

$$\begin{aligned}\frac{\partial E_z}{\partial y} - \frac{\partial E_y}{\partial z} &= -\frac{\partial B_x}{\partial t}\\ \frac{\partial E_x}{\partial z} - \frac{\partial E_z}{\partial x} &= -\frac{\partial B_y}{\partial t}\\ \frac{\partial E_y}{\partial x} - \frac{\partial E_x}{\partial y} &= -\frac{\partial B_z}{\partial t}\end{aligned} \tag{B.17c}$$

This point form symbolizes that a time-changing magnetic field results in a *circulation* (curl) of the electric field.

Example B.7 As indicated previously, the point form of Faraday's law is most useful in computations. To illustrate this, determine the magnetic field if the electric field is given by

$$\boldsymbol{E} = E_m \cos(\omega t - \beta z)\boldsymbol{a}_x$$

Solution: The electric field has only an x component. Hence, the left side of Faraday's law in (B.17b) becomes

$$\begin{aligned}\nabla \times \boldsymbol{E} &= \left(\frac{\partial E_z}{\partial y} - \frac{\partial E_y}{\partial z}\right)\boldsymbol{a}_x + \left(\frac{\partial E_x}{\partial z} - \frac{\partial E_z}{\partial x}\right)\boldsymbol{a}_y + \left(\frac{\partial E_y}{\partial x} - \frac{\partial E_x}{\partial y}\right)\boldsymbol{a}_z\\ &= \frac{\partial E_x}{\partial z}\boldsymbol{a}_y - \underbrace{\frac{\partial E_x}{\partial y}}_{0}\boldsymbol{a}_z\\ &= \frac{\partial E_x}{\partial z}\boldsymbol{a}_y\end{aligned}$$

Observe that this x component of $\boldsymbol{E}$ depends only on z, so that the z component, $\partial E_x/\partial y$, is zero.

Hence,

$$\begin{aligned}\nabla \times \boldsymbol{E} &= \frac{\partial E_x}{\partial z}\boldsymbol{a}_y\\ &= \beta E_m \sin(\omega t - \beta z)\boldsymbol{a}_y\end{aligned}$$

Since the left-hand side of Faraday's law has only a y component, the right-hand side, $-\partial \boldsymbol{B}/\partial t$, can have only a y component. Therefore, we obtain

$$\beta E_m \sin(\omega t - \beta z) = -\frac{\partial B_y}{\partial t}$$

Integrating this gives

$$B_y = \frac{\beta E_m}{\omega} \cos(\omega t - \beta z)$$

Therefore, the magnetic flux density vector that satisfies Faraday's law is

$$\boldsymbol{B} = \frac{\beta E_m}{\omega} \cos(\omega t - \beta z)\boldsymbol{a}_y$$

Review Exercise B.5 In a laboratory experiment, a high-impedance voltmeter is attached across the parallel combination of two resistors as shown in Fig. EB.5. Nearby, a 60 Hz power transformer causes a magnetic flux to penetrate the circuit as shown. Determine the voltage read by the voltmeter.

Answer: $0.88 \sin(120\pi t)$ mV.

Review Exercise B.6 A square loop is moving to the right as shown in Fig. EB.6. A magnetic field, directed into the page, covers the region 2 m in width. Determine the current in the loop versus time, assuming the right side of the loop enters the magnetic field region at $t = 0$.

Answer: 0.1 A for $0 < t < 1$ s, 0 A for $1 \text{ s} < t < 2$ s, −0.1 A for $2 \text{ s} < t < 3$ s, 0 A for $3 \text{ s} < t$.

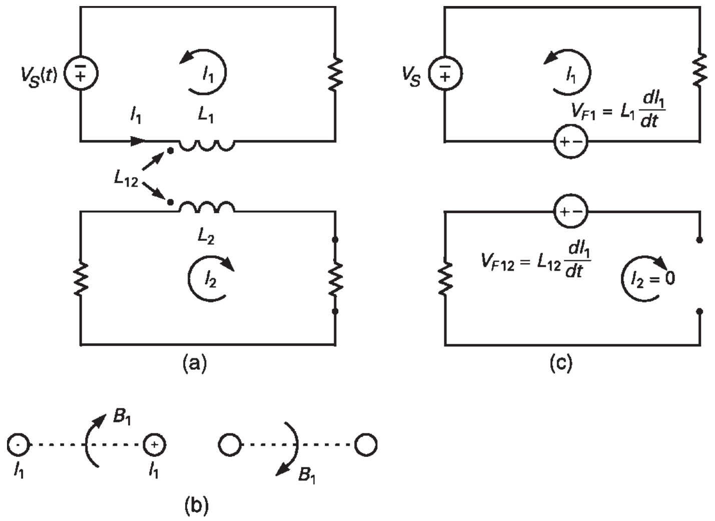

FIGURE EB.5 Review Exercise B.5.

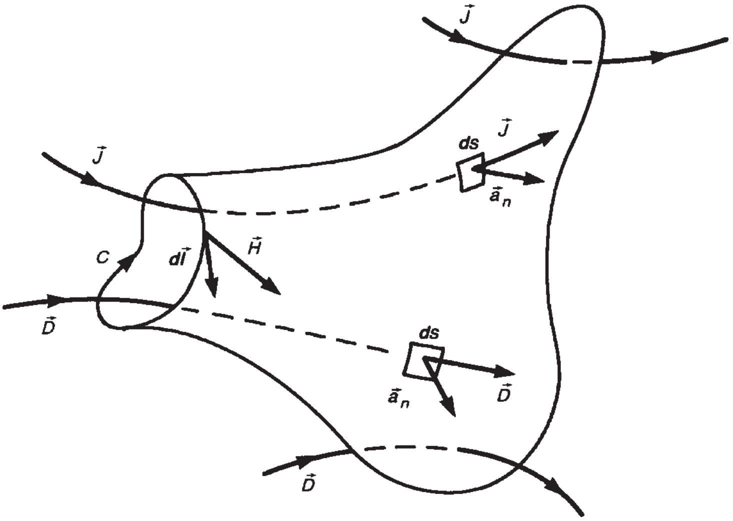

FIGURE EB.6 Review Exercise B.6.

Review Exercise B.7 Determine whether the following fields satisfy Faraday's law:

$$\boldsymbol{E} = E_m \sin x \sin t\, \boldsymbol{a}_y$$

$$\boldsymbol{B} = E_m \cos x \cos t\, \boldsymbol{a}_z$$

Answer: Yes.

Finally, the relation between Faraday's law and inductance (self and mutual) should be emphasized. Consider the two adjacent circuit loops shown in Fig. B.11a. The first loop is driven by a time-varying voltage source, $V_S(t)$, which produces a time-varying current in that loop, $I_1(t)$. The current in the first loop produces a magnetic field, $B_1(t)$, that passes through both loops as illustrated in Fig. B.11b. Similarly, any current in the second loop, $I_2(t)$, will produce a magnetic field, $B_2(t)$, that also passes through each loop. The total magnetic flux passing through each loop is the surface integral over that loop:

$$\psi_{m1} = \int_{S_1} \boldsymbol{B}_1 \cdot d\boldsymbol{s} + \int_{S_1} \boldsymbol{B}_2 \cdot d\boldsymbol{s}$$

and

$$\psi_{m2} = \int_{S_2} \boldsymbol{B}_1 \cdot d\boldsymbol{s} + \int_{S_2} \boldsymbol{B}_2 \cdot d\boldsymbol{s}$$

These total fluxes and the currents producing them are related by

$$\psi_{m1} = L_1 I_1 + L_{12} I_2 \tag{B.18a}$$

$$\psi_{m2} = L_{12} I_1 + L_2 I_2 \tag{B.18b}$$

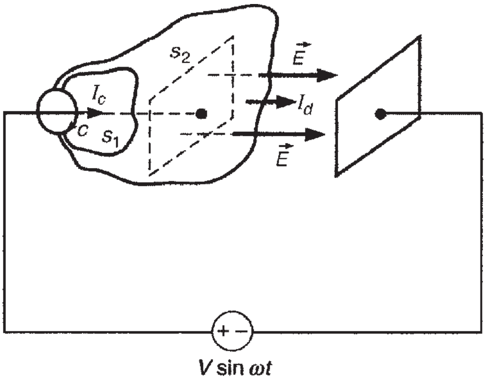

FIGURE B.11 Illustration of inductance (self and mutual); (a) two adjacent circuit loops; (b) magnetic field B1 appears in both loops; (c) induced voltages in each loop as a result of mutual inductance.

where L_1 and L_2 are the self-inductances of the loops and L_{12} is the mutual inductance between the two loops:

$$L_1 = \left.\frac{\psi_{m1}}{I_1}\right|_{I_2=0} \tag{B.19a}$$

$$L_2 = \left.\frac{\psi_{m2}}{I_2}\right|_{I_1=0} \tag{B.19b}$$

$$L_{12} = \left.\frac{\psi_{m2}}{I_1}\right|_{I_2=0} = \left.\frac{\psi_{m1}}{I_2}\right|_{I_1=0} \tag{B.19c}$$

Voltages will be induced in each loop, which are, according to Faraday's law, the time rate of change of the magnetic flux passing through the loop:

$$V_{F1} = \frac{d\psi_{m1}}{dt} = L_1\frac{dI_1}{dt} + L_{12}\frac{dI_2}{dt} \tag{B.20a}$$

$$V_{F2} = \frac{d\psi_{m2}}{dt} = L_{12}\frac{dI_1}{dt} + L_2\frac{dI_2}{dt} \tag{B.20b}$$

If we open-circuit the second loop so that $I_2 = 0$, then

$$\begin{aligned} V_{F1} &= \frac{d\psi_{m1}}{dt} \\ &= L_1\left.\frac{dI_1}{dt}\right|_{I_2=0} \end{aligned} \tag{B.21a}$$

is induced in the first loop and another Faraday voltage source

$$\begin{aligned} V_{F2} &= \frac{d\psi_{m2}}{dt} \\ &= L_{12}\left.\frac{dI_1}{dt}\right|_{I_2=0} \end{aligned} \tag{B.21b}$$

is induced in the second loop as illustrated in Fig. B.11c. Therefore, inductance, either self or mutual, is a consequence of Faraday's law. This is an example of where in circuit analysis we attempt to get away from electromagnetic field principles and laws by defining quantities such as inductance, but we can never completely sever the tie.

B.2.2 Ampere's Law

Faraday's law showed that a time-changing magnetic field can produce (induce) an electric field. Ampere's law shows that the converse is true; that is, *a time-changing electric field can produce* (*induce*) *a magnetic field*. Ampere's law is given in integral form as

$$\oint_C \boldsymbol{H} \cdot d\boldsymbol{l} = \int_S \boldsymbol{J} \cdot d\boldsymbol{s} + \frac{d}{dt}\int_S \boldsymbol{D} \cdot d\boldsymbol{s} \tag{B.22}$$

The quantity $\boldsymbol{H}$ is the *magnetic field intensity vector*, having units of amperes per meter (A/m). The quantity $\boldsymbol{J}$ is the *current density vector*, with units of A/m^2. The quantity $\boldsymbol{D}$ is the *electric flux density vector*, with units of coulombs per square meter (C/m^2). Note that the units of the result in (B.22) after integration are amperes (A). The contour C bounds the open surface S, as illustrated in Fig. B.12. Their directions are related by the right-hand rule. As was the case with Faraday's law, any surface shape is suitable so long as contour C bounds it. Only the $\boldsymbol{J}$ and $\boldsymbol{D}$ that pass through the opening contribute. The line integral of $\boldsymbol{H}$ around the closed contour C is referred to as the *magnetomotive force* or *mmf* around that contour:

$$\text{mmf} = \oint_C \boldsymbol{H} \cdot d\boldsymbol{l} \quad (\text{in A}) \tag{B.23}$$

This is essentially the dual of the emf of Faraday's law. The first term on the right-hand side of Ampere's law is the *total conduction current that penetrates the surface S bounded by the contour C:*

$$I_c = \int_S \boldsymbol{J} \cdot d\boldsymbol{s} \quad (\text{in A}) \tag{B.24}$$

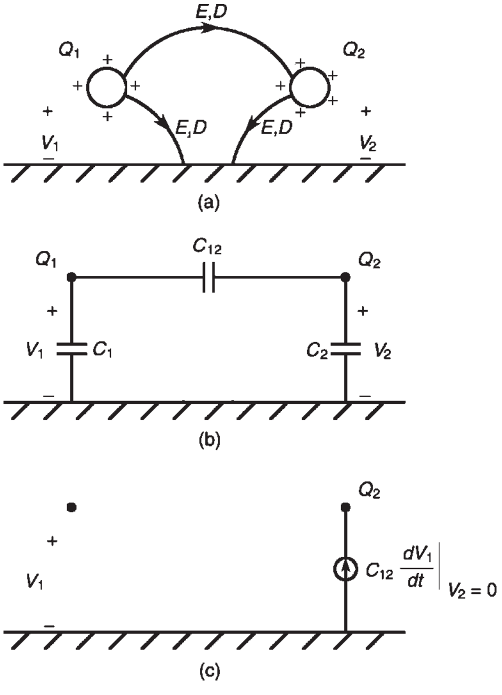

FIGURE B.12 Illustration of Ampere's law.

This is the total current bounded by the contour that is due to free charges. The second term on the right-hand side of Ampere's law is the *total displacement current that penetrates the surface S bounded by the contour C:*

$$I_d = \frac{d}{dt}\int_S \boldsymbol{D} \cdot d\boldsymbol{s} \ \text{(in A)} \tag{B.25}$$

Therefore, Ampere's law can be written as

$$\text{mmf} = I_c + I_d \ \text{(in A)} \tag{B.26}$$

Ampere's law essentially shows that a *time-changing electric flux **D** has the same effect as free current **J*** in producing a magnetic field ***H***. We already know that a static (dc) current will produce a magnetic field. Ampere's law shows that a time-changing electric field will give the same result.

One of James Clerk Maxwell's primary contributions to electromagnetism was the addition of the displacement current term to the existing Ampere's law of that time, which contained only conduction current. Observe that for static (dc) conditions, the displacement current term is zero and hence the revised Ampere's law reduces to the static version.

As a simple example of application of this result, consider a capacitor having a sinusoidal voltage source attached to its terminals as shown in Fig. B.13. The wires attached to the capacitor carry the charges, resulting in a conduction current, I_c. Between the plates of the capacitor, a time-varying electric field (varying at the rate of the source, ω) is directed between the plates. Let us apply Ampere's law given in (B.22) to this situation. Placing the contour about the wire, we obtain several surfaces bounded by that contour. Again, it is helpful to visualize this as a balloon. If we blow up the balloon so that only the wire penetrates the surface, we obtain

$$\begin{aligned}\oint_C \boldsymbol{H} \cdot d\boldsymbol{l} &= \int_S \boldsymbol{J} \cdot d\boldsymbol{s} \\ &= I_c\end{aligned}$$

If we keep the same contour but blow the balloon up so that its surface passes between the capacitor plates, we obtain

$$\oint_C \boldsymbol{H} \cdot d\boldsymbol{l} = \frac{d}{dt}\int_S \boldsymbol{D} \cdot d\boldsymbol{s}$$

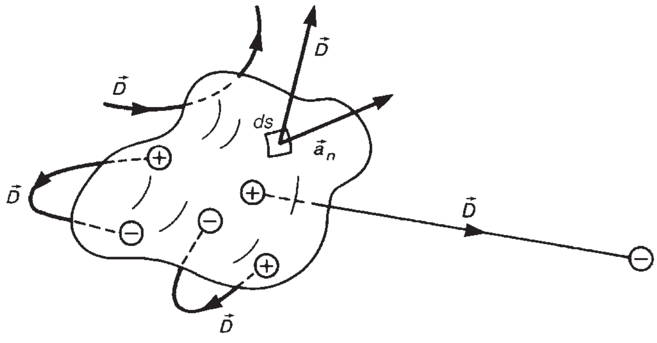

FIGURE B.13 Illustration of Ampere's law and conduction current and displacement current for a capacitor.

If it were not for the addition of the displacement current term to Ampere's law, we would have an obvious problem here. For the same contour C, two different surfaces would yield different results.

Example B.8 In the capacitor situation of Fig. B.13, a 1 μF capacitor has a sinusoidal voltage source $10\sin(\omega t)$ V applied across its terminals, where the frequency of the source is 1 kHz. Verify that the conduction and displacement currents are equal.

Solution: From our electric circuits course, the conduction current in the attachment wires is

$$\begin{aligned} I_c &= \frac{10\ \text{V}}{1/\omega C} \\ &= 62.8\ \text{mA} \end{aligned}$$

The capacitance of a parallel-plate capacitor is approximately $C = \varepsilon A/d$, where A is the plate area, d is the plate separation distance, and ε is the permittivity of the material between the plates. The electric field between the plates is approximately the applied voltage divided by the plate separation distance:

$$E = \frac{10\ \text{V}}{d}$$

Hence,

$$\begin{aligned} D &= \varepsilon E \\ &= \varepsilon \frac{10\ \text{V}}{d} \\ &= \frac{C}{A} 10\ \text{V} \\ &= \frac{10^{-5}}{A} \end{aligned}$$

Hence, the displacement current is

$$\begin{aligned} I_d &= \frac{d}{dt}\int_S \boldsymbol{D} \cdot d\boldsymbol{s} \\ &= \omega \left(\frac{10^{-5}}{A} A \right) \\ &= 62.8\,\text{mA} \end{aligned}$$

Therefore, the displacement current through a capacitor may be symbolized as a current source between the two plates whose value is the displacement current: $I_d = C(dV/dt)$. This is quite similar to the inductor, wherein the terminal relation $V = L(dI/dt)$ amounts to the Faraday's law voltage source, which may be inserted in the inductor loop.

Example B.9 Compare the conduction and displacement currents in a copper conductor at a frequency of 1 GHz. The conductivity of copper is 5.8×107 S/m. The permittivity of copper, like most metals, is that of free space: $\varepsilon = \varepsilon_0 \cong 1/36\pi \times 10^{-9}$.

Solution: The conduction current density is related to the electric field by Ohm's law:

$$J = \sigma E$$

The displacement current density is

$$\varepsilon_0 \frac{\partial E}{\partial t} = \omega \varepsilon_0 E$$

Hence, the ratio of conduction current to displacement current is

$$\begin{aligned} \frac{I_c}{I_d} &= \frac{\sigma}{\omega \varepsilon_0} \\ &= 1.04 \times 10^9 \end{aligned}$$

Therefore, in copper and most other metals the conduction current is many orders of magnitude larger than the displacement current. This is why displacement current can be neglected in conductors.

Review Exercise B.8 Determine the ratio of conduction current to displacement current in seawater at 1 kHz. Seawater has $\varepsilon_r \cong 80$ and $\sigma \cong 4$ S/m at this low frequency.

Answer: 9×10^5.

There is an enormous amount of *duality* throughout electromagnetics and electrical engineering. For example, we determine a law governing voltage (Kirchhoff's voltage law) and a dual law governing current (Kirchhoff's current law). Similarly, Faraday's law and Ampere's law may also be considered duals in a similar fashion. Faraday's law relates the emf (the line integral of the electric field around a closed path) to a time rate of change of magnetic flux penetrating the surface bounded by the closed path. Similarly, Ampere's law relates the mmf (the line integral of the magnetic field around a closed path) to a time rate of change of electric flux (displacement current) penetrating the surface bounded by the closed path. We pointed out that Faraday's law is the basis for induced voltage sources due to self and mutual inductance. Hence, Ampere's law could, by duality, be the basis for induced current sources due to self and mutual capacitance. Observe in Ampere's law in (B.22) if the conduction current is zero, Ampere's law reduces to

$$\oint_C \boldsymbol{H} \cdot d\boldsymbol{l} = \frac{d}{dt} \int_S \boldsymbol{D} \cdot d\boldsymbol{s} \quad (\boldsymbol{J} = 0) \tag{B.27}$$

Hence, the time rate of change of the electric flux passing through the surface

$$\psi_e = \int_S \boldsymbol{D} \cdot d\boldsymbol{s} \tag{B.28}$$

seems to produce a current source, the mmf, through the surface bounded by the contour.

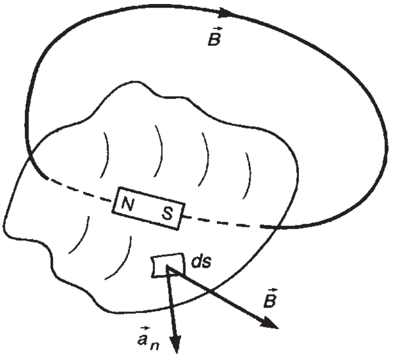

FIGURE B.14 Illustration of capacitance (self and mutual); (a) two objects above an infinite ground plane; (b) equivalent circuit of the capacitances of each of the two objects and the mutual capacitance between them; (c) current injected into the second object.

Capacitance is the dual of inductance. Consider two conducting objects (shown as spheres) above an infinite ground plane to which the voltages are referenced as shown in Fig. B.14a. Charges, Q_1 and Q_2, reside on the spheres. These produce electric fields, $\boldsymbol{E}$ and $\boldsymbol{D}$, some of which terminate on the ground plane and the remainder terminate on the other sphere. We may draw an equivalent circuit in terms of self-capacitances, C_1 and C_2, and a mutual capacitance, C_{12}, as shown in Fig. B.14b. In a fashion similar to that for inductance, we may relate the charges on the two objects to the self- and mutual-capacitances between them and voltages, V_1 and V_2, as

$$Q_1 = C_1 V_1 + C_{12} V_2 \tag{B.29a}$$

$$Q_2 = C_{12} V_1 + C_2 V_2 \tag{B.29b}$$

The current *injected onto each object* is the time derivative of the charge:

$$I_1 = \frac{dQ_1}{dt} = C_1 \frac{dV_1}{dt} + C_{12} \frac{dV_2}{dt} \tag{B.30a}$$

$$I_2 = \frac{dQ_2}{dt} = C_{12} \frac{dV_1}{dt} + C_2 \frac{dV_2}{dt} \tag{B.30b}$$

If we make $V_2 = 0$, then from (B.30b), the current injected onto the second object is due to the time rate of change of the voltage on the first object

$$I_2 = C_{12} \left. \frac{dV_1}{dt} \right|_{V_2=0} \tag{B.31}$$

which we represent as a current source injecting current onto the second object due to the time rate of change of the voltage on the first object as shown in Fig. B.14c. This is the dual to the voltage induced into the second loop due to current in the first loop via mutual inductance as shown in Fig. B.11c. We will frequently use this notion to construct equivalent circuits between two coupled circuits. By duality, if we have an induced voltage due to mutual inductance, we must consider an induced current due to mutual capacitance or else the picture is not complete.

The *point* or *differential form* of Ampere's law can be obtained by applying Stokes' theorem to (B.22) to give

$$\nabla \times \boldsymbol{H} = \boldsymbol{J} + \frac{\partial \boldsymbol{D}}{\partial t} \tag{B.32a}$$

Substituting the result for the curl and matching components gives three equations:

$$\begin{aligned}\frac{\partial H_z}{\partial y} - \frac{\partial H_y}{\partial z} &= J_x + \frac{\partial D_x}{\partial t}\\ \frac{\partial H_x}{\partial z} - \frac{\partial H_z}{\partial x} &= J_y + \frac{\partial D_y}{\partial t}\\ \frac{\partial H_y}{\partial x} - \frac{\partial H_x}{\partial y} &= J_z + \frac{\partial D_z}{\partial t}\end{aligned} \tag{B.32b}$$

Review Exercise B.9 Determine whether the following fields satisfy Ampere's law in free space ($\boldsymbol{J}_c = 0$):

$$\boldsymbol{D} = D_m \sin x \sin t\, \boldsymbol{a}_y, \quad \boldsymbol{H} = D_m \cos x \cos t\, \boldsymbol{a}_z$$

Answer: Yes.

B.2.3 Gauss' Laws

Gauss' law for the electric field is stated in integral form as

$$\oint_S \boldsymbol{D} \cdot d\boldsymbol{s} = \int_v \rho_v dv \tag{B.33}$$

The quantity ρ_v is the *volume free charge density*, whose units are coulombs per cubic meter (C/m^3). Gauss' law for the electric field provides that the *net flux of the electric flux density vector out of the closed surface S is equivalent to the net positive charge enclosed by the surface.* Figure B.15 illustrates this point. Electric field lines that begin on positive charge must terminate on an equal amount of negative charge. Integrating $\boldsymbol{D}$ over a closed surface will only reveal the *net positive charge* enclosed by the surface. Also note that electric field lines can be generated by a time-changing magnetic field, as Faraday's law shows. These lines form closed paths, and as such enter and leave the closed surface and contribute nothing to Gauss' law.

Equation (B.33) is the integral form of Gauss' law. To obtain the point form, we apply the divergence theorem to (B.33) to yield

$$\nabla \cdot \boldsymbol{D} = \rho_v \tag{B.34a}$$

Substituting the result for the divergence gives

$$\frac{\partial D_x}{\partial x} + \frac{\partial D_y}{\partial y} + \frac{\partial D_z}{\partial z} = \rho_v \tag{B.34b}$$

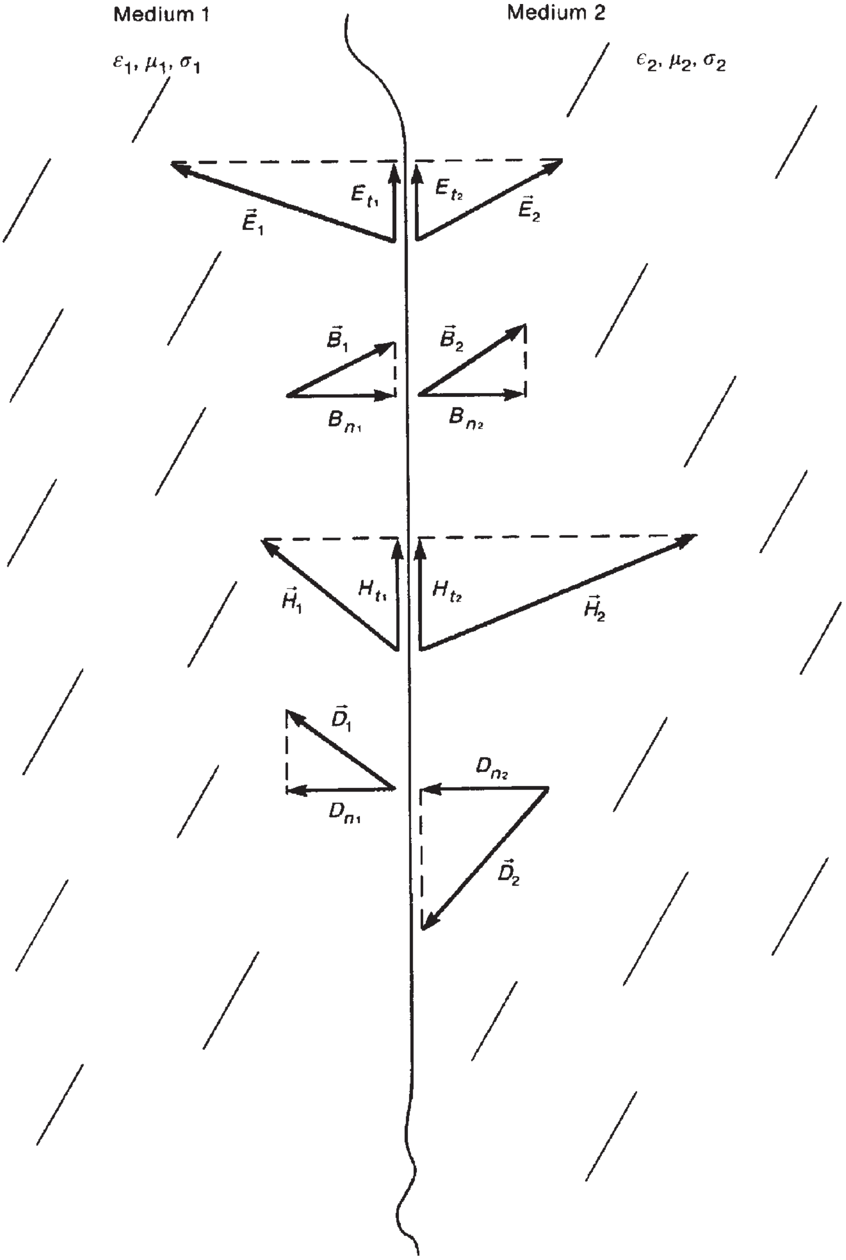
Medium 1
$\varepsilon_1, \mu_1, \sigma_1$
Medium 2
$\epsilon_2, \mu_2, \sigma_2$
E_{t_1}
E_{t_2}
$\vec{E}_1$
$\vec{E}_2$
$\vec{B}_1$
$\vec{B}_2$
B_{n_1}
B_{n_2}
$\vec{H}_1$
H_{t_1}
H_{t_2}
$\vec{H}_2$
$\vec{D}_1$
D_{n_2}
D_{n_1}
$\vec{D}_2$

FIGURE B.15 Illustration of Gauss' law for the electric field. The net flux of $\overrightarrow{D}$ through the closed surface is equal to the net positive charge enclosed by the surface. Electric field lines that begin on positive charge must terminate on negative charge.

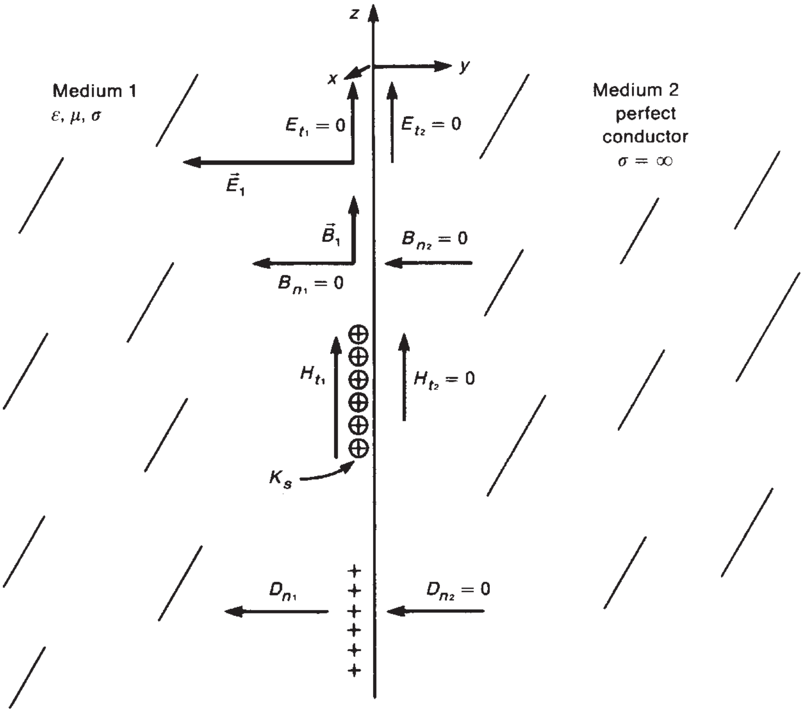

FIGURE B.16 Illustration of Gauss' law for the magnetic field. The net flux of $\vec{B}$ through the closed surface is zero. There are no isolated sources or sinks for the magnetic field; all magnetic field lines must form closed loops.

A related result is Gauss' law for the magnetic field, stated in integral form as

$$\oint_s \boldsymbol{B} \cdot d\boldsymbol{s} = 0 \tag{B.35}$$

This result implies that *all magnetic field lines form closed paths; that is, there are no (known) isolated sources of the magnetic field.* This is illustrated in Fig. B.16. If we try to divide a permanent magnet, we find that new N–S poles are formed at the opposite ends of these pieces. The *point form of Gauss' law for the magnetic field* is obtained by applying the divergence theorem to (B.35) to give

$$\nabla \cdot \boldsymbol{B} = 0 \tag{B.36a}$$

Substituting the result for the divergence gives

$$\frac{\partial B_x}{\partial x} + \frac{\partial B_y}{\partial y} + \frac{\partial B_z}{\partial z} = 0 \tag{B.36b}$$

Review Exercise B.10 Determine whether the following fields in free space ($\rho_v = 0$) satisfy Gauss' laws:

$$\boldsymbol{D} = D_m \sin x \, \sin \, t \boldsymbol{a}_y, \quad \boldsymbol{B} = B_m \cos x \cos t \boldsymbol{a}_z$$

Answer: Yes.

B.2.4 Conservation of Charge

Charge can be neither created nor destroyed. The mathematical statement of this important result is given by

$$\oint_s \boldsymbol{J} \cdot d\boldsymbol{s} = -\frac{d}{dt}\int_v \rho_v dv \tag{B.37}$$

This result is a rather commonsense statement of the fact that *any current leaving a closed surface S implies a decrease of charge within that closed surface in volume v*. The point form of this is obtained by applying the divergence theorem to (B.37) to give

$$\nabla \cdot \boldsymbol{J} = -\frac{\partial \rho_v}{\partial t} \tag{B.38a}$$

Expanding this gives

$$\frac{\partial J_x}{\partial x} + \frac{\partial J_y}{\partial y} + \frac{\partial J_z}{\partial z} = -\frac{\partial \rho_v}{\partial t} \tag{B.38b}$$

It should be pointed out that Faraday's, Ampere's, and Gauss' laws, along with conservation of charge, are collectively referred to as *Maxwell's equations*. These five equations are not all independent. It can be shown that Faraday's law, Ampere's law, and conservation of charge, are all that are required to completely characterize the electromagnetic field [1]. Conservation of charge can be derived from Ampere's and Gauss' laws [1].

B.2.5 Constitutive Parameters of the Medium

Maxwell's equations involve five unknown vector field quantities: $\boldsymbol{E}, \boldsymbol{B}, \boldsymbol{D}, \boldsymbol{H}$, and $\boldsymbol{J}$. The *constitutive relations* relate these quantities. The electromagnetic fields exist in material media and there are various characterizations of those media. The simplest and most common type of medium is the *simple medium*, in which the field vectors are simply related as

$$\boldsymbol{D} = \varepsilon \boldsymbol{E} \tag{B.39a}$$

$$\boldsymbol{B} = \mu \boldsymbol{H} \tag{B.39b}$$

$$\boldsymbol{J}_c = \sigma \boldsymbol{E} \tag{B.39c}$$

The current density $\boldsymbol{J}$ will also consist of impressed currents $\boldsymbol{J}_s$, which can be viewed as the source of the fields. Thus, $\boldsymbol{J} = \boldsymbol{J}_c + \boldsymbol{J}_s$ in Ampere's law. The parameters ε, μ, and σ in these relations are the *permittivity, permeability*, and *conductivity*, respectively, of the medium. The units of ε are farads per meter (F/m) or a capacitance per unit length. The units of μ are henrys per meter (H/m) or an inductance per unit length. The units of σ are siemens per meter (S/m) or a conductance per unit length. Substituting (B.39) into Faraday's and Ampere's laws gives Maxwell's equations for simple media:

$$\nabla \times \boldsymbol{E} = -\mu \frac{\partial \boldsymbol{H}}{\partial t} \tag{B.40a}$$

$$\nabla \times \boldsymbol{H} = \sigma \boldsymbol{E} + \varepsilon \frac{\partial \boldsymbol{E}}{\partial t} + \boldsymbol{J}_s \tag{B.40b}$$

Thus, (B.40) give six equations in the six components of $\boldsymbol{E}$ and $\boldsymbol{H}$. Once these are found, we can obtain $\boldsymbol{D}$, $\boldsymbol{B}$, and $\boldsymbol{J}_c$ from (B.39). Our emphasis in this text will be on electromagnetic fields in simple media, and so the equations in (B.40) will be of paramount importance.

Simple media for which the field vectors are related simply by (B.39) are said to be *linear, homogeneous*, and *isotropic*. A *nonlinear medium* is one in which $\boldsymbol{D}$ is a function of the *magnitude* of $\boldsymbol{E}$, $\boldsymbol{B}$ is a function of the *magnitude* of $\boldsymbol{H}$, and/or $\boldsymbol{J}_c$ is a function of the *magnitude* of $\boldsymbol{E}$. An example of a nonlinear medium is a ferromagnetic one, in which $|\boldsymbol{B}|$ is related to $|\boldsymbol{H}|$ by the familiar nonlinear hysteresis curve. In other words, we may write the parameters as $\varepsilon(E)$, $\mu(H)$, and/or $\sigma(E)$. An *inhomogeneous medium* is one in which the medium parameters are functions of position, e.g., $\varepsilon(x, y, z)$, $\mu(x, y, z)$, and/or $\sigma(x, y, z)$. Examples of inhomogeneous media are dielectric-insulated wires or printed circuit boards where the electric field exists partly in air ($\varepsilon_r = 1$) and partly in the insulating material for which $\varepsilon_r \neq 1$. Finally, an *anisotropic medium* is one in which $\boldsymbol{E}$ is not parallel to $\boldsymbol{D}$, or $\boldsymbol{B}$ is not parallel to $\boldsymbol{H}$, or $\boldsymbol{J}_c$ is not parallel to $\boldsymbol{E}$. Ferrites are examples of anisotropic media. These types of materials are used to construct microwave devices such as circulators. Because of the difficulty in solving Maxwell's equations for media that are not *linear, homogeneous*, and *isotropic*, we will try where possible to approximate media as being simple media.

The permittivity and permeability are related to those of free space:

$$\varepsilon_0 \cong \frac{1}{36\pi} \times 10^{-9} \ \text{F/m} \tag{B.41a}$$

$$\mu_0 = 4\pi \times 10^{-7} \ \text{H/m} \tag{B.41b}$$

as

$$\varepsilon = \varepsilon_r \varepsilon_0 \tag{B.42a}$$

$$\mu = \mu_r \mu_0 \tag{B.42b}$$

where ε_r is the relative permittivity (often called the *dielectric constant*) and μ_r is the relative permeability.

B.3 BOUNDARY CONDITIONS

Maxwell's equations are differential equations, and as such are no different from other differential equations in that they have an infinite number of solutions. Ordinary differential equations such as occur in lumped circuits have an infinite number of solutions and require that certain initial conditions be specified in order to pin down the specific solution. Partial differential equations such as those of Maxwell require the specification of *boundary conditions* in order to pin down which of the infinite number of possible solutions in the particular medium apply. The boundary conditions will be stated, and the reader is referred to [1, 2] for a derivation.

First, we consider the boundary between two physical media shown in Fig. B.17. Medium 1 is characterized by ε_1, μ_1, and σ_1, while medium 2 is characterized by ε_2, μ_2, and σ_2. It is not necessary that the two media be simple media for the following boundary conditions to hold. The *boundary conditions* provide constraints on the components of the field vectors as they transition across the boundary between the two media. The *tangential components of the electric field intensity vector*

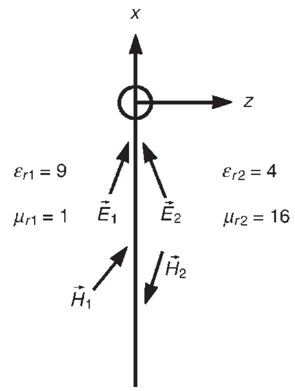

FIGURE B.17 Illustration of the boundary conditions at an interface between two media.

***E** and the magnetic field intensity vector **H** must be continuous across the boundary between two physical media*:

$$E_{t_1} = E_{t_2} \tag{B.43a}$$

$$H_{t_1} = H_{t_2} \tag{B.43b}$$

Also, *the normal components of the electric flux density vector **D** and the magnetic flux density vector **B** must be continuous across the boundary between two physical media*:

$$D_{n_1} = D_{n_2} \tag{B.44a}$$

$$B_{n_1} = B_{n_2} \tag{B.44b}$$

These boundary conditions are illustrated in Fig. B.17. The continuity of the normal components of the electric flux density vector $\boldsymbol{D}$ given in (B.44a) *assumes that no charge has been intentionally placed and resides on the boundary surface*. This may occur, for example, by rubbing cat's fur against nylon, in which case charges are separated, leaving net charge on the two boundaries. This will be important in the examination of electrostatic discharge (ESD) problems.

So far we have been discussing *real, physical media*; that is, media that can exist physically. We will have occasion to utilize the concept of certain idealized mathematical media that, although they do not exist physically, serve to simplify the mathematical calculations and, moreover, are reasonable approximations to certain physical media. The primary such idealized medium is the *perfect conductor*, which may be characterized by an infinite conductivity, $\sigma = \infty$. The impact of an infinite conductivity is to render all the fields in that perfect conductor to be *zero:* $\boldsymbol{E}_2 = 0$, $\boldsymbol{D}_2 = 0$, $\boldsymbol{H}_2 = 0$, and $\boldsymbol{B}_2 = 0$ [1, 2]. Since all the fields in medium 2 (the perfect conductor) are zero, so are the normal and tangential components at the boundary, as illustrated in Fig. B.18. This requires that the tangential component of $\boldsymbol{E}_1$ must be zero at the boundary:

$$E_{t_1} = 0, \quad \sigma_2 = \infty \tag{B.45a}$$

Also the normal component of $\boldsymbol{B}_1$ must be zero at the boundary:

$$B_{n_1} = 0, \quad \sigma_2 = \infty \tag{B.45b}$$

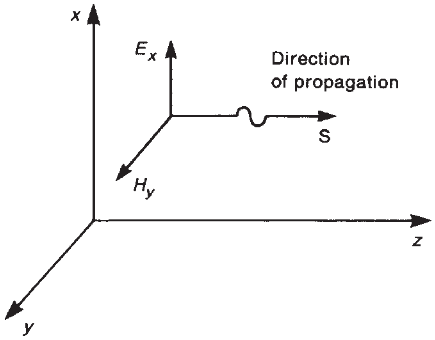

FIGURE B.18 Illustration of the boundary conditions where one medium is a perfect conductor.

It turns out that we cannot similarly require that H_{t_1} and D_{n_1} be zero, or else the resulting fields in medium 1 would be overspecified [1]. The resulting requirements are

$$H_{t_1} = K_s \text{ (in A/m)}, \quad \sigma_2 = \infty \tag{B.45c}$$

and

$$D_{n_1} = \rho_s \text{ (in C/m}^2\text{)}, \quad \sigma_2 = \infty \tag{B.45d}$$

The quantity K_s is the *surface current density existing on the interface*. The units of K_s are amperes per meter (A/m), and this represents a distribution of current along the boundary surface per unit length along the surface [1]. The surface current density K_s is orthogonal to the tangential component of $\boldsymbol{H}$, H_{t_1}. Similarly, the quantity ρ_s given in (B.45d) is the *surface charge density existing on the interface*. The units of ρ_s are coulombs per square meter of the interface (C/m²), and this represents a distribution of charge (free charge) over the boundary surface [1].

Example B.10 Figure B.19 shows the boundary between two media. The boundary lies in the *xy* plane. The electric field intensity vector in medium 1 at the boundary is

$$\boldsymbol{E}_1 = 2\boldsymbol{a}_x + 3\boldsymbol{a}_y + 4\boldsymbol{a}_z \text{ V/m}$$

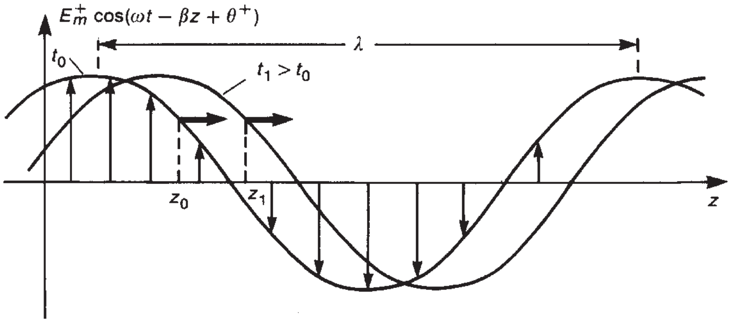

FIGURE B.19 Example B.10.

Determine the electric field intensity vector and electric flux density vector in medium 2 at the boundary.

Solution: Recall that we can convert $\boldsymbol{E}$ to $\boldsymbol{D}$ with $\boldsymbol{D} = \varepsilon_r\varepsilon_0\boldsymbol{E}$. The components of $\boldsymbol{E}$ that are tangent to the boundary are

$$\boldsymbol{E}_{t1} = 2\boldsymbol{a}_x + 3\boldsymbol{a}_y$$

Hence, these are continuous across the boundary, so that

$$\boldsymbol{E}_{t2} = 2\boldsymbol{a}_x + 3\boldsymbol{a}_y$$

The components of $\vec{D}$ that are normal to the boundary are

$$\begin{aligned}\boldsymbol{D}_{n1} &= \varepsilon_{r1}\varepsilon_0\boldsymbol{E}_{n1}\\ &= 9\varepsilon_0(4\boldsymbol{a}_z)\\ &= 36\varepsilon_0\boldsymbol{a}_z\end{aligned}$$

Hence, these are continuous across the boundary, so that

$$\boldsymbol{D}_{n2} = 36\,\varepsilon_0\boldsymbol{a}_z$$

We have the tangential component of $\boldsymbol{E}$ and the normal component of $\boldsymbol{D}$ on the other side of the boundary, so we simply use the relation $\boldsymbol{E}\times\boldsymbol{H}$ in that medium to convert from one to the other. For example, the normal component of $\boldsymbol{E}$ is found from the normal component of $\boldsymbol{D}$ as

$$\begin{aligned}\boldsymbol{E}_{n2} &= \frac{\boldsymbol{D}_{n2}}{\varepsilon_{r2}\varepsilon_0}\\ &= \frac{36\varepsilon_0}{4\varepsilon_0}\boldsymbol{a}_z\\ &= 9\boldsymbol{a}_z\end{aligned}$$

Similarly, we find the tangential component of $\boldsymbol{D}$ from the tangential component of $\boldsymbol{E}$ as

$$\begin{aligned}\boldsymbol{D}_{t2} &= \varepsilon_{r2}\varepsilon_0\,\boldsymbol{E}_{t2}\\ &= 4\varepsilon_0(2\boldsymbol{a}_x + 3\boldsymbol{a}_y)\\ &= 8\varepsilon_0\boldsymbol{a}_x + 12\varepsilon_0\boldsymbol{a}_y\end{aligned}$$

Now, we can form the vectors on the other side of the boundary:

$$\begin{aligned}\boldsymbol{E}_2 &= \boldsymbol{E}_{t2} + \boldsymbol{E}_{n2}\\ &= 2\boldsymbol{a}_x + 3\boldsymbol{a}_y + 9\boldsymbol{a}_z\end{aligned}$$

and

$$\begin{aligned} \boldsymbol{D}_2 &= \boldsymbol{D}_{t2} + \boldsymbol{D}_{n2} \\ &= 8\varepsilon_0 \boldsymbol{a}_x + 12\varepsilon_0 \boldsymbol{a}_y + 36\varepsilon_0 \boldsymbol{a}_z \end{aligned}$$

Observe that $\boldsymbol{D}_2 = \varepsilon_{r2}\varepsilon_0 \boldsymbol{E}_2$ where $\varepsilon_{r2} = 4$.

Review Exercise B.11 In Example B.10, the magnetic flux density vector in medium 1 at the boundary is

$$\boldsymbol{B}_1 = 5\boldsymbol{a}_x + 6\boldsymbol{a}_y + 7\boldsymbol{a}_z \;\; \text{Wb/m}^2$$

Determine the magnetic field intensity vector in medium 2 at the boundary.

Answer: $\boldsymbol{H}_2 = (5/\mu_0)\boldsymbol{a}_x + (6/\mu_0)\boldsymbol{a}_y + (7/16\mu_0)\boldsymbol{a}_z$.

B.4 SINUSOIDAL STEADY STATE

The time variation of the field vectors is not restricted to any particular functional form. However, a major interest in this text will be in the *sinusoidal time variation* of these field vectors. We assume that the fields have been in existence for a sufficient length of time that all transients have decayed to zero, leaving the *sinusoidal steady state*. This has the effect of simplifying the mathematics, and the techniques are virtually no different for sinusoidal steady-state, lumped-circuit analysis as discussed in Appendix A. For example, the phasor form of the x component of the electric field intensity vector is

$$\begin{aligned} \hat{E}_x(x,y,z) &= E_{xm}(x,y,z)e^{j\theta_x(x,y,z)} \\ &= E_{xm}\underline{/\theta_x} \end{aligned} \tag{B.46}$$

Phasor quantities are complex-valued quantities and will be denoted by a caret over the symbol. *The time-domain form of phasor quantities may be obtained by multiplying the phasor form by* $e^{j\omega t}$ *and taking the real part of the result*. This is an important technique and will be used on numerous occasions. For example

$$\begin{aligned} E_x(x,y,z,t) &= \mathcal{R}e\{\hat{E}_x(x,y,z)e^{j\omega t}\} \\ &= \mathcal{R}e\{E_{xm}\underline{/\theta_x}e^{j\omega t}\} \\ &= \mathcal{R}e\{E_{xm}e^{j(\omega t+\theta_x)}\} \\ &= \mathcal{R}e\{E_{xm}\cos(\omega t+\theta_x) + jE_{xm}\sin(\omega t+\theta_x)\} \\ &= E_{xm}\cos(\omega t+\theta_x) \end{aligned} \tag{B.47}$$

where $\mathcal{R}e\{\,\}$ denotes the *real part* of the enclosed complex quantity.

In order to solve Maxwell's equations for sinusoidal excitation, we replace the field vectors with their phasor forms multiplied by $e^{j\omega t}$. Differentiation of these forms of the field vectors with respect to time t gives

$$\frac{\partial}{\partial t}\hat{\boldsymbol{E}}(x, y, z)e^{j\omega t} = j\omega\hat{\boldsymbol{E}}(x, y, z)e^{j\omega t} \tag{B.48}$$

Hence, to convert to phasor form, we replace all time derivatives with $j\omega : \partial/\partial t \Longleftrightarrow j\omega$. This very important property allows a considerable simplification in the solution of Maxwell's equations. Substituting the forms of the field vectors and canceling the $e^{j\omega t}$ that is common to both sides gives the *phasor forms of Maxwell's equations*. If the medium is linear, homogeneous, and isotropic (a simple medium), the phasor Maxwell's equations become

$$\oint_C \hat{\boldsymbol{E}} \cdot d\boldsymbol{l} = -j\omega\mu\int_s \hat{\boldsymbol{H}} \cdot d\boldsymbol{s}, \qquad \nabla \times \hat{\boldsymbol{E}} = -j\omega\mu\hat{\boldsymbol{H}} \tag{B.49a}$$

$$\oint_C \hat{\boldsymbol{H}} \cdot d\boldsymbol{l} = (\sigma + j\omega\varepsilon)\int_s \hat{\boldsymbol{E}} \cdot d\boldsymbol{s} + \int_s \hat{\boldsymbol{J}}_s \cdot d\boldsymbol{s}$$

$$\nabla \times \hat{\boldsymbol{H}} = (\sigma + j\omega\varepsilon)\hat{\boldsymbol{E}} + \hat{\boldsymbol{J}}_s \tag{B.49b}$$

$$\oint_S \hat{\boldsymbol{H}} \cdot d\boldsymbol{s} = 0, \quad \nabla \cdot \hat{\boldsymbol{H}} = 0 \tag{B.49c}$$

$$\oint_S \hat{\boldsymbol{E}} \cdot d\boldsymbol{s} = \frac{1}{\varepsilon}\int_v \hat{\rho}_v dv, \quad \nabla \cdot \hat{\boldsymbol{E}} = \frac{\hat{\rho}_v}{\varepsilon} \tag{B.49d}$$

$$\oint_S \hat{\boldsymbol{J}} \cdot d\boldsymbol{s} = -j\omega\int_v \hat{\rho}_v dv, \qquad \nabla \cdot \hat{\boldsymbol{J}} = -j\omega\hat{\rho}_v \tag{B.49e}$$

Here the permittivity, permeability, and conductivity may be functions of frequency, i.e., $\varepsilon(f)$, $\mu(f)$, and $\sigma(f)$, as they usually are for material media.

B.5 POWER FLOW

The units of the electric field intensity vector $\boldsymbol{E}$ are V/m, while those of the magnetic field intensity vector $\boldsymbol{H}$ are A/m. Thus, the product of these two vectors has the units of power density or watts per square meter (W/m^2). But there are two possibilities for the product of two vectors: dot product and cross product. It turns out that the cross product is more meaningful in that the *power density vector* or *Poynting vector* $\boldsymbol{S}$ relates to power flow and hence must have a direction [1, 2]. The Poynting vector is defined as

$$\boldsymbol{S} = \boldsymbol{E} \times \boldsymbol{H} \quad (\text{in W/m}^2) \tag{B.50}$$

Using certain vector identities, it is possible to show that [1]

$$-\oint_S \boldsymbol{S} \cdot d\boldsymbol{s} = \int_v \boldsymbol{E} \cdot \boldsymbol{J} dv + \int_v \left(\boldsymbol{E} \cdot \frac{\partial \boldsymbol{D}}{\partial t} + \boldsymbol{H} \cdot \frac{\partial \boldsymbol{B}}{\partial t}\right) dv \quad (\text{in W}) \tag{B.51}$$

The term on the left-hand side of (B.51) represents the net inward flux of $\boldsymbol{S}$ into the volume. The first term on the right-hand side represents *power dissipation* within the volume, while the second represents *the time rate of change of the energy stored within the volume* [1]. The Poynting vector

S defined above represents *instantaneous power*. For sinusoidal steady-state excitation, we are interested in *average power*. To determine this average power flow, we define the *phasor Poynting vector* as

$$\hat{\boldsymbol{S}} = \hat{\boldsymbol{E}} \times \hat{\boldsymbol{H}}^{*} \tag{B.52}$$

where the *complex conjugate* of a phasor $\hat{\boldsymbol{A}}$ is denoted by $\hat{\boldsymbol{A}}^{*}$. The *density of average power* is obtained as the *average power density Poynting vector*:

$$\begin{aligned} \boldsymbol{S}_{av} &= \frac{1}{2}\mathcal{R}e\{\hat{\boldsymbol{S}}\} \text{ (in W/m}^2\text{)} \\ &= \frac{1}{2}\mathcal{R}e\{\hat{\boldsymbol{E}} \times \hat{\boldsymbol{H}}^{*}\} \end{aligned} \tag{B.53}$$

The electric and magnetic fields in (B.53) are given in terms of peak values. If they are given in RMS values, the 1/2 factor is removed. This is the only impact of expressing quantities in RMS: the 1/2 does not appear in power expressions.

B.6 UNIFORM PLANE WAVES

We now embark on a discussion of the simplest type of wave propagation: *uniform plane waves*. We initially consider these not only because they are simple but also because wave propagation on transmission lines and waveguides and waves propagated by antennas bears a striking similarity to uniform plane waves. Therefore, the structure and properties of many other forms of wave propagation will be more easily understood.

There are two important terms in the name: *uniform* and *plane*. The term “plane” means that at any point in space the electric and magnetic field intensity vectors lie in a plane and the planes at any two different points are parallel. The term “uniform” means that **E** and **H** are independent of position in each plane. Without any loss of generality, we may assume the electric and magnetic field intensity vectors to lie in the *xy* plane and may choose the electric field intensity vector to be directed in the *x* direction, as shown in Fig. B.20:

$$\boldsymbol{E} = E_x(z,t)\boldsymbol{a}_x \tag{B.54}$$

The criterion that the field vectors be uniform over the *x*, *y* plane means that they must be independent of *x* and *y*.

$$\frac{\partial E_x}{\partial x} = \frac{\partial E_x}{\partial y} = 0 \tag{B.55}$$

and thus, the vectors can be a function of only *z* and, of course time *t*, as indicated in (B.54). Substituting (B.54) into Faraday’s law and using (B.55) show that the magnetic field has only a *y* component:

$$\boldsymbol{H} = H_y(z,t)\boldsymbol{a}_y \tag{B.56}$$

Thus **E** and **H** are orthogonal and lie in the *xy* plane. Similarly, because the wave is uniform over the *xy* plane, we obtain

$$\frac{\partial H_y}{\partial x} = \frac{\partial H_y}{\partial y} = 0 \tag{B.57}$$

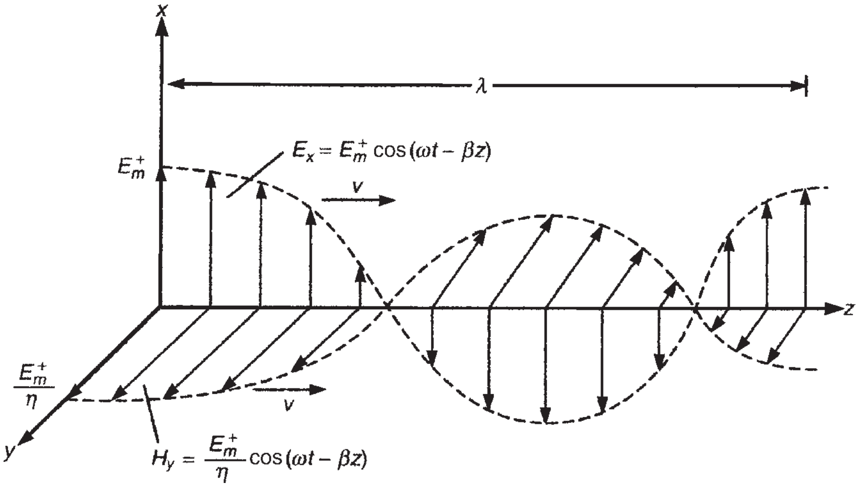
x
λ
E_m^+
$E_x = E_m^+ \cos(\omega t - \beta z)$
v
z
$\frac{E_m^+}{\eta}$
v
y
$H_y = \frac{E_m^+}{\eta} \cos(\omega t - \beta z)$

FIGURE B.20 Illustration of a uniform plane wave.

Substituting these results into Faraday's and Ampere's laws gives the differential equations governing the field vectors for simple media having no impressed sources [1, 2]:

$$\frac{\partial E_x(z,t)}{\partial z} = -\mu \frac{\partial H_y(z,t)}{\partial t} \tag{B.58a}$$

$$\frac{\partial H_y(z,t)}{\partial z} = -\sigma E_x(z,t) - \varepsilon \frac{\partial E_x(z,t)}{\partial t} \tag{B.58b}$$

For sinusoidal, steady-state variation of the field vectors, the results in (B.58) simplify to

$$\frac{d\hat{E}_x(z)}{dz} = -j\omega\mu \hat{H}_y(z) \tag{B.59a}$$

$$\frac{d\hat{H}_y(z)}{dz} = -(\sigma + j\omega\varepsilon)\hat{E}_x(z) \tag{B.59b}$$

Note that we have replaced partial derivatives with ordinary derivatives since the phasor field vectors are functions of only one variable, z. These are a set of coupled first-order ordinary differential equations. They may be reduced to sets of uncoupled second-order ordinary differential equations by differentiating one with respect to z and substituting the other, and vice versa, resulting in

$$\frac{d^2\hat{E}_x(z)}{dz^2} = \hat{\gamma}^2 \hat{E}_x(z) \tag{B.60a}$$

$$\frac{d^2\hat{H}_y(z)}{dz^2} = \hat{\gamma}^2 \hat{H}_y(z) \tag{B.60b}$$

The solutions to these equations are of a simple form [1, 2]:

$$\hat{E}_x = \hat{E}_m^+ e^{-\hat{\gamma} z} + \hat{E}_m^- e^{\hat{\gamma} z} \tag{B.61a}$$

$$\hat{H}_y = \frac{\hat{E}_m^+}{\hat{\eta}} e^{-\hat{\gamma} z} - \frac{\hat{E}_m^-}{\hat{\eta}} e^{\hat{\gamma} z} \tag{B.61b}$$

where the *propagation constant* is

$$\begin{aligned}\hat{\gamma} &= \sqrt{j\omega\mu(\sigma + j\omega\varepsilon)} \\ &= \alpha + j\beta \end{aligned} \tag{B.62}$$

and the *intrinsic impedance* is

$$\begin{aligned}\hat{\eta} &= \sqrt{\frac{j\omega\mu}{\sigma + j\omega\varepsilon}} \\ &= \frac{j\omega\mu}{\hat{\gamma}} \\ &= \eta\underline{/\theta_\eta} \end{aligned} \tag{B.63}$$

The quantity α in (B.62) is referred to as the *attenuation constant*, with units of nepers per meter (Np/m), and the quantity β is referred to as the *phase constant*, with units of radians per meter (rad/m). The quantity $\hat{\eta}$ in (B.63) is referred to as the *intrinsic impedance of the medium*, with units of ohms (Ω). In terms of these quantities, the solutions in (B.61) can be written as

$$\hat{E}_x = \hat{E}_m^+ e^{-\alpha z} e^{-j\beta z} + \hat{E}_m^- e^{\alpha z} e^{j\beta z} \tag{B.64a}$$

$$\hat{H}_y = \frac{\hat{E}_m^+}{\eta} e^{-\alpha z} e^{-j\beta z} e^{-j\theta_\eta} - \frac{\hat{E}_m^-}{\eta} e^{\alpha z} e^{j\beta z} e^{-j\theta_\eta} \tag{B.64b}$$

Writing the complex undetermined constants $\hat{E}_m^+$ and $\hat{E}_m^-$ as a magnitude and angle as $\hat{E}_m^+ = E_m^+ e^{j\theta^+} = E_m^+\underline{/\theta^+}$ and $\hat{E}_m^- = E_m^- e^{j\theta^-} = E_m^-\underline{/\theta^-}$ gives

$$\hat{E}_x = E_m^+ e^{-\alpha z} e^{-j\beta z} e^{j\theta^+} + E_m^- e^{\alpha z} e^{j\beta z} e^{j\theta^-} \tag{B.65a}$$

$$\hat{H}_y = \frac{E_m^+}{\eta} e^{-\alpha z} e^{-j\beta z} e^{-j\theta_\eta} e^{j\theta^+} - \frac{E_m^-}{\eta} e^{\alpha z} e^{j\beta z} e^{-j\theta_\eta} e^{j\theta^-} \tag{B.65b}$$

where we use the identity $1\underline{/\theta} = e^{j\theta}$.

The *time-domain forms* are

$$\begin{aligned} E_x &= \mathcal{R}e\{\hat{E}_x e^{j\omega t}\} \\ &= E_m^+ e^{-\alpha z}\cos(\omega t - \beta z + \theta^+) + E_m^- e^{\alpha z}\cos(\omega t + \beta z + \theta^-) \end{aligned} \tag{B.66a}$$

$$\begin{aligned} H_y &= \mathcal{R}e\{\hat{H}_y\, e^{j\omega t}\} \\ &= \frac{E_m^+}{\eta} e^{-\alpha z}\cos(\omega t - \beta z + \theta^+ - \theta_\eta) \\ &\quad + \frac{E_m^-}{\eta} e^{\alpha z}\cos(\omega t + \beta z + \theta^- - \theta_\eta) \end{aligned} \tag{B.66b}$$

B.6.1 Lossless Media

It is important that we investigate the implications and properties of these equations. To simplify our analysis, we will first consider uniform plane waves in *lossless media*, $\sigma = 0$. For this case, the propagation constant becomes

$$\alpha = 0 \quad (\sigma = 0) \tag{B.67a}$$

$$\beta = \omega\sqrt{\mu\varepsilon} \quad (\sigma = 0) \tag{B.67b}$$

Since $\alpha = 0$, the wave suffers no *attenuation* as it propagates through the (lossless) medium. The intrinsic impedance becomes

$$\eta = \sqrt{\frac{\mu}{\varepsilon}} \quad (\sigma = 0) \tag{B.68a}$$

$$\theta_\eta = 0 \quad (\sigma = 0) \tag{B.68b}$$

Thus, the field vectors become for lossless media

$$E_x = E_m^+ e^{-\alpha z}\cos(\omega t - \beta z + \theta^+) + E_m^- e^{\alpha z}\cos(\omega t + \beta z + \theta^-) \tag{B.69a}$$

$$H_y = \frac{E_m^+}{\eta} e^{-\alpha z}\cos(\omega t - \beta z + \theta^+) - \frac{E_m^-}{\eta} e^{\alpha z}\cos(\omega t + \beta z + \theta^-) \tag{B.69b}$$

Consider the first term of (B.69a), $E_m^+ \cos(\omega t - \beta z + \theta^+)$. This portion of E_x represents a wave traveling in the positive z direction. This can be seen from Fig. B.21, in which $E_m^+ \cos(\omega t - \beta z + \theta^+)$ has been plotted as a function of z for two different instants of time, t_0 and $t_1 > t_0$. Note that *corresponding points on the waveforms occur at positions and times such that the argument of the cosine has the same value*:

$$\omega t_0 - \beta z_0 + \theta^+ = \omega t_1 - \beta z_1 + \theta^+$$

Thus, we observe that *a point on the waveform must move in the positive z direction for increasing time, so that*

$$\omega t - \beta z + \theta^+ = \text{constant}$$

Taking the derivative of this expression with respect to time and position yields the velocity at which the points of constant phase travel and is referred to as the *phase velocity* of the wave:

$$\begin{aligned} v &= \frac{dz}{dt} \quad (\text{in m/s}) \\ &= \frac{\omega}{\beta} = \frac{1}{\sqrt{\mu\varepsilon}} \end{aligned} \tag{B.70}$$

Similarly, we observe that the term $E_m^- \cos(\omega t + \beta z + \theta^-)$ represents a wave traveling in the negative z direction, a *backward-traveling wave*, since, in order to track the movement of a point on the waveform, the argument of the cosine must remain constant. Similar observations hold for the magnetic field intensity vector. However, observe that the magnetic field intensity vector of the backward-traveling wave is in the negative y direction. This is important and sensible because the direction of power flow in the individual waves must be in the same direction as the direction of wave propagation. Figure B.22 shows a plot of the forward-traveling electric and magnetic field traveling waves.

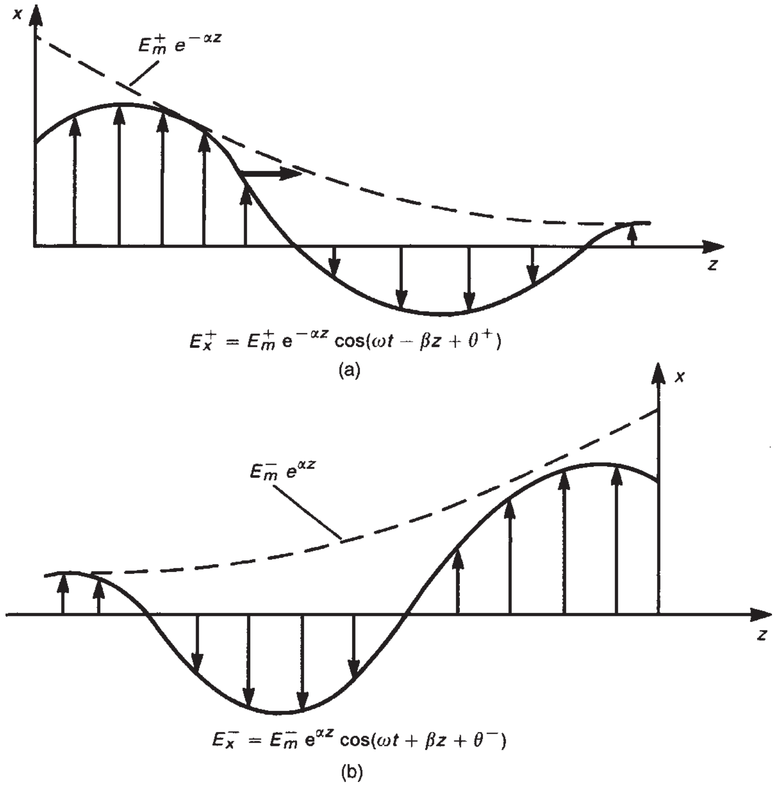
x
$E_m^+ e^{-\alpha z}$
z
$E_x^+ = E_m^+ e^{-\alpha z} \cos(\omega t - \beta z + \theta^+)$
(a)
x
$E_m^- e^{\alpha z}$
z
$E_x^- = E_m^- e^{\alpha z} \cos(\omega t + \beta z + \theta^-)$
(b)

FIGURE B.21 Illustration of a wave distributed in space for a fixed time.

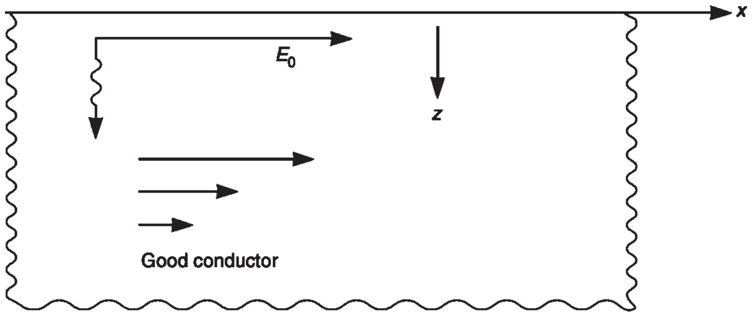
x
E_0
z
Good conductor

FIGURE B.22 Illustration of the electric and magnetic field vectors in a uniform plane wave distributed in space for a fixed time.

The quantity $\beta = \omega\sqrt{\mu\varepsilon}$ is referred to as the *phase constant*. The units are radians per meter, so that β is a change in phase of the wave with distance of propagation. The distance between corresponding adjacent points on the wave is known as the *wavelength* and is denoted as λ. From Fig. B.21, we observe that $\beta\lambda = 2\pi$. Since $\beta = \omega\sqrt{\mu\varepsilon}$ and $v = 1/\sqrt{\mu\varepsilon}$ for this lossless medium, the wavelength becomes

$$\lambda = \frac{2\pi}{\beta} = \frac{v}{f} \tag{B.71}$$

Increased frequencies result in shorter wavelengths. Note that the wavelength is also a function of the properties of the medium since $v = 1/\sqrt{\mu\varepsilon}$. For typical materials, $\mu \geq \mu_0$ and $\varepsilon \geq \varepsilon_0$. Thus, *the phase velocity of propagation is slower than in free space and the wavelength is shorter.*

In free space, $\mu_0 = 4\pi \times 10^{-7}$ H/m and $\varepsilon_0 \cong 1/36\pi \times 10^{-9}$ F/m, so that

$$v_0 \cong 3 \times 10^8 \ \text{m/s}$$

At a frequency of 300 MHz

$$\begin{aligned}\lambda_0 &= \frac{v_0}{f} \\ &= 1 \ \text{m} \quad (f = 300 \ \text{MHz})\end{aligned}$$

Similarly,

$$\lambda_0 = 1 \ \text{cm} \quad (f = 30 \ \text{GHz})$$

$$\lambda_0 = 3107 \ \text{mi} \quad (f = 60 \ \text{Hz})$$

The intrinsic impedance becomes

$$\begin{aligned}\eta_0 &= \sqrt{\frac{\mu_0}{\varepsilon_0}} \\ &= 120\pi \\ &\cong 377 \ \Omega\end{aligned}$$

For any other lossless material medium with $\varepsilon = \varepsilon_r\varepsilon_0$ and $\mu = \mu_r\mu_0$

$$v = \frac{v_0}{\sqrt{\varepsilon_r\mu_r}} \quad (\text{in m/s}) \tag{B.72a}$$

$$\eta = \eta_0\sqrt{\frac{\mu_r}{\varepsilon_r}} \quad (\text{in } \Omega) \tag{B.72b}$$

$$\beta = \beta_0\sqrt{\mu_r\varepsilon_r} \quad (\text{in rad/m}) \tag{B.72c}$$

$$\lambda = \frac{\lambda_0}{\sqrt{\mu_r\varepsilon_r}} \quad (\text{in m}) \tag{B.72d}$$

where we denote the quantities in free space with a subscript zero.

In calculating these quantities in *lossless* material media, one should translate the corresponding results in free space to those in the medium by using these relationships. *One should never again calculate* v_0 and η_0! For example, in order to calculate the wavelength of a 750-MHz signal, we would scale the result of $\lambda = 1$ m at 300 MHz and realize that the wavelength at 750 MHz will be shorter than at 300 MHz:

$$\begin{aligned}\lambda_{750\ \text{MHz}} &= \frac{300}{750} \times \lambda_{300\ \text{MHz}} \\ &= 0.4\ \text{m} \\ &= 40\ \text{cm}\end{aligned}$$

Example B.11 Determine the intrinsic impedance, phase constant, velocity of propagation, and wavelength of a uniform plane wave at 1 GHz in (a) glass-epoxy used to construct printed circuit boards and in (b) silicon used to construct integrated circuits.

Solution:For glass epoxy, $\varepsilon_r = 4.7$, $\mu_r = 1$ so that

$$\begin{aligned}
\eta &= \eta_0 \sqrt{\frac{\mu_r}{\varepsilon_r}} \\
&= 120\pi \sqrt{\frac{1}{4.7}} \\
&\cong 173.9 \ \ \Omega \\
\beta &= \omega\sqrt{\mu\varepsilon} \\
&= 2\pi f \frac{\sqrt{\mu_r \varepsilon_r}}{v_0} \\
&= 2\pi \times 1 \times 10^9 \frac{\sqrt{1 \times 4.7}}{3 \times 10^8} \\
&= 45.41 \ \ \text{rad/m} \\
&= 2601.5 \ \ \text{deg/m} \\
v &= \frac{1}{\sqrt{\mu\varepsilon}} \\
&= \frac{v_0}{\sqrt{\mu_r \varepsilon_r}} \\
&= \frac{3 \times 10^8}{\sqrt{1 \times 4.7}} \\
&= 1.38 \times 10^8 \ \ \text{m/s} \\
\lambda &= \frac{2\pi}{\beta} \\
&= \frac{v}{f} \\
&= 0.138 \ \ \text{m} \\
&= 13.8 \ \ \text{cm}
\end{aligned}$$

For silicon, $\varepsilon_r = 12$, $\mu_r = 1$ so that

$$\begin{aligned}
\eta &= \eta_0 \sqrt{\frac{\mu_r}{\varepsilon_r}} \\
&= 120\pi \sqrt{\frac{1}{12}} \\
&\cong 109 \ \ \Omega
\end{aligned}$$

$$\begin{aligned}\beta &= \omega\sqrt{\mu\varepsilon}\\ &= 2\pi f\frac{\sqrt{\mu_r\varepsilon_r}}{v_0}\\ &= 2\pi\times 1\times 10^9\frac{\sqrt{1\times 12}}{3\times 10^8}\\ &= 72.55 \text{ rad/m}\\ &= 4157 \text{ deg/m}\end{aligned}$$

$$\begin{aligned}v &= \frac{1}{\sqrt{\mu\varepsilon}}\\ &= \frac{v_0}{\sqrt{\mu_r\varepsilon_r}}\\ &= \frac{3\times 10^8}{\sqrt{1\times 12}}\\ &= 8.66\times 10^7 \text{ m/s}\end{aligned}$$

$$\begin{aligned}\lambda &= \frac{2\pi}{\beta}\\ &= \frac{v}{f}\\ &= 8.66 \text{ cm}\end{aligned}$$

Example B.12 Write the phasor and time-domain forms of a uniform plane wave having a frequency of 1 GHz that is traveling in the $+z$ direction in a large block of silicon.

Solution: Using the results of the previous example, the phasor forms are

$$\hat{E}_x = E_m^+ e^{-j72.55z} \text{ V/m}$$

$$\hat{H}_y = \frac{E_m^+}{109}e^{-j72.55z} \text{ A/m}$$

and the time-domain forms are

$$\hat{E}_x = E_m^+ \cos(6.28\times 10^9 t - 72.55z) \text{ V/m}$$

$$\hat{H}_y = \frac{E_m^+}{109}\cos(6.28\times 10^9 t - 72.55z) \text{ A/m}$$

Review Exercise B.12 Determine the intrinsic impedance, phase constant, velocity of propagation, and wavelength of a uniform plane wave at 500 kHz in Teflon ($\varepsilon_r = 2.1$, $\mu_r = 1$). Write the time-domain expressions for the electric and magnetic field intensity vectors. The electric field vector is in the x direction but the wave is propagating in the $-z$ direction.

***Answers*:** $260\Omega, 1.52\times 10^{-2}$ rad/m, 2.07×10^8 m/s, 414 m, $E_x = E_m^- \cos(3.14\times 10^6 t + 1.52\times 10^{-2}z)$ V/m, $H_y = E_m^- \cos(3.14\times 10^6 t + 1.52\times 10^{-2}z)$ A/m.

B.6.2 Lossy Media

There are two important differences between uniform plane waves in lossless media and in *lossy media*. The first difference is that the propagation constant $\hat{\gamma}$ has a nonzero real part, α, in a lossy medium. This results in the waves for the lossy case being multiplied by the exponentials $e^{-\alpha z}$ and $e^{\alpha z}$, as shown in (B.64). These are obviously still forward- and backward-traveling waves, but the *amplitudes* of the forward-traveling waves are $E_m^+ e^{-\alpha z}$ and $(E_m^+/\eta)e^{-\alpha z}$, which are reduced for increasing z (in the direction of propagation). This is shown for a fixed time as a function of z in Fig. B.23. Similarly, the amplitudes of the backward-traveling waves, $E_m^- e^{\alpha z}$ and $(E_m^-/\eta)e^{\alpha z}$, are also reduced, since they are propagating in the $-z$ direction (decreasing z). The real part of $\hat{\gamma}, \alpha$, is referred to as the *attenuation constant* for these reasons.

The second difference between lossless and lossy media is that the intrinsic impedance of a lossy medium has a nonzero phase angle, $\theta_\eta \neq 0$. For the lossless case, $\theta_\eta = 0$, and we observe that the electric and magnetic fields of the forward-traveling wave are in time phase, as are those of the backward-traveling wave as illustrated in Fig. B.22. However, for the lossy case the phase angle of the intrinsic impedance, θ_η, results in the electric and magnetic fields of each traveling wave being out of time phase by the phase angle θ_η. Note from (B.63) that $0 \leq \theta_\eta \leq 45°$. Also, the defining relationships for the phase velocity and wavelength are

$$v = \frac{\omega}{\beta} \tag{B.73}$$

$$\lambda = \frac{2\pi}{\beta} = \frac{v}{f} \tag{B.74}$$

However, *β is the imaginary part of the propagation $\hat{\gamma}$ and is no longer equal to $\omega\sqrt{\mu\varepsilon}$ for the case of a lossy medium.*

Example B.13 Determine the attenuation constant and phase constant in copper ($\sigma = 5.8 \times 10^7$ S/m, $\varepsilon_r = 1$, $\mu_r = 1$) at 1 MHz.

Solution: Form the propagation constant:

$$\begin{aligned}
\hat{\gamma} &= \sqrt{\left(j\underbrace{2\pi \times 10^6}_{\omega} \times \underbrace{1 \times 4\pi \times 10^{-7}}_{\mu}\right)\left(\underbrace{5.8 \times 10^7}_{\sigma} + j\underbrace{2\pi \times 10^6}_{\omega} \times \underbrace{1 \times \frac{1}{36\pi} \times 10^{-9}}_{\varepsilon}\right)} \\
&= \sqrt{-4.39 \times 10^{-4} + j4.58 \times 10^8} \\
&= \sqrt{4.58 \times 10^8 \angle 90°} \\
&= 2.14 \times 10^4 \angle 45° \\
&= \underbrace{1.51 \times 10^4}_{\alpha} + j\underbrace{1.51 \times 10^4}_{\beta}
\end{aligned}$$

Review Exercise B.13 Determine the attenuation constant and phase constant in seawater having $\sigma = 4$ S/m, $\varepsilon_r = 81$, $\mu_r = 1$ at 1 MHz.

Answer: $\alpha = 3.97$, $\beta = 3.98$ rad/m $= 228$ deg/m.

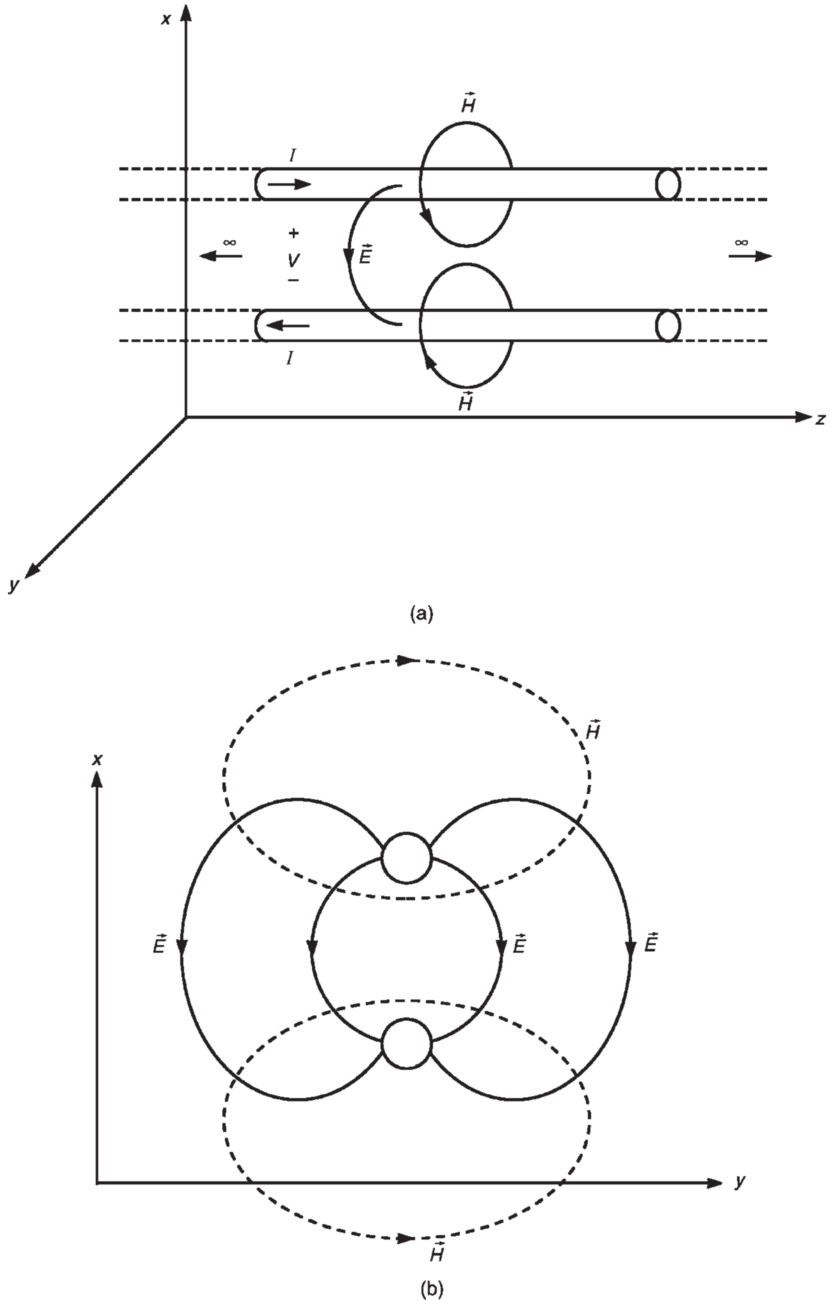
x
$\vec{H}$
I
+
V
−
$\vec{E}$
∞
∞
I
$\vec{H}$
z
y
(a)
$\vec{H}$
x
$\vec{E}$
$\vec{E}$
$\vec{E}$
y
$\vec{H}$
(b)

FIGURE B.23 Spatial properties of a uniform plane wave in a lossy medium: (a) forward traveling wave; (b) backward-traveling wave.

Example B.14 Determine the intrinsic impedance of copper at 1 MHz.

Solution: The conductivity of copper is 5.8×10^7 S/m and the relative permittivity and permeability are unity. Hence, the intrinsic impedance is

$$\begin{aligned}\hat{\eta} &= \sqrt{\frac{j\omega\mu}{\sigma + j\omega\varepsilon}} \\ &= \sqrt{\frac{\left(j\underbrace{2\pi \times 10^0}_{\omega} \times \underbrace{1 \times 4\pi \times 10^{-7}}_{\mu}\right)}{\left(\underbrace{5.8 \times 10^7}_{\sigma} + j\underbrace{2\pi \times 10^6}_{\omega} \times \underbrace{1 \times \frac{1}{36\pi} \times 10^{-9}}_{\varepsilon}\right)}} \\ &= \sqrt{1.36 \times 10^{-7}\angle 90^\circ} \\ &= 3.69 \times 10^{-4}\angle 45^\circ\end{aligned}$$

Hence, $\eta = 3.69 \times 10^{-4}$ and $\theta_\eta = 45^\circ$.

Review Exercise B.14 Determine the intrinsic impedance of seawater ($\sigma = 4$ S/m, $\varepsilon_r = 81$, $\mu_r = 1$) at 1 MHz.

Answer: $\hat{\eta} = 1.4\angle 45^\circ$.

Example B.15 Determine the velocity of propagation and wavelength in copper at 1 MHz.

Solution: Since $\sigma = 5.8 \times 10^7$ S/m, $\varepsilon_r = 1$, $\mu_r = 1$ in copper, we obtain from Example B.13, $\beta = 1.51 \times 10^4$ rad/m so that

$$v = \frac{2\pi \times 10^6}{1.51 \times 10^4} = 416 \text{ m/s}$$

The wavelength is

$$\begin{aligned}\lambda &= \frac{2\pi}{1.51 \times 10^4} \\ &= 4.16 \times 10^{-4} \text{ m} \\ &= \frac{v}{f}\end{aligned}$$

Review Exercise B.15 Determine the velocity of propagation and wavelength in seawater at 1 MHz.

***Answers*:** 1.58×10^6 m/s, 1.58 m

Example B.16 Write the time-domain expressions for the electric and magnetic field vectors for a wave traveling in the $-z$ direction in copper and having a frequency of 1 MHz.

Solution: From (B.66) and the results of the previous example problems, we obtain

$$E_x = E_m^- e^{1.51\times 10^4 z}\cos(6.28\times 10^6 t + 1.51\times 10^4 z)$$

$$H_y = -\frac{E_m^-}{3.69\times 10^{-4}} e^{1.51\times 10^4 z}\cos(6.28\times 10^6 t + 1.51\times 10^4 z - 45°)$$

Observe that since the fields are stipulated to be traveling in the negative z direction ($-z$), the exponent of the attenuation as well as the sign in front of the phase shift term are positive. Also observe that the sign of the angle of the intrinsic impedance is always negative since the intrinsic impedance is in the denominator of the phasor expression for $\hat{H}_y$. Also, the sign of H_y is negative since for this wave traveling in the negative z direction, $\boldsymbol{E}\times\boldsymbol{H}$ must be in the negative z direction.

Review Exercise B.16 Write the time-domain expressions for the electric and magnetic field vectors for a wave traveling in the $-z$ direction in seawater and having a frequency of 1 MHz.

***Answers*:** $E_x = E_m^- e^{3.97x}\cos(6.28\times 10^6 t + 3.98z)$, and $H_y = (-E_m^-/1.4)e^{3.97z}\cos(6.28\times 10^6 t + 3.98z - 45°)$.

B.6.3 Power Flow

The average power density Poynting vector for the uniform plane wave is

$$\begin{aligned}\boldsymbol{S}_{\text{av}} &= \frac{1}{2}\mathcal{R}e\{\hat{\boldsymbol{E}}\times\hat{\boldsymbol{H}}^*\}\\ &= \frac{1}{2}\mathcal{R}e\{\hat{E}_x\boldsymbol{a}_x\times\hat{H}_y^*\boldsymbol{a}_y\}\\ &= \frac{1}{2}\mathcal{R}e\{\hat{E}_x\hat{H}_y^*\}\boldsymbol{a}_z\end{aligned} \tag{B.75}$$

Consider a forward-traveling wave in a lossy medium. The phasor fields are

$$\hat{E}_x = E_m^+ e^{-\alpha z}e^{-j\beta z}e^{j\theta^+} \tag{B.76a}$$

$$\hat{H}_y = \frac{E_m^+}{\eta}e^{-\alpha z}e^{-j\beta z}e^{-j\theta_\eta}e^{j\theta^+} \tag{B.76b}$$

Hence, the Poynting vector becomes

$$\begin{aligned}\boldsymbol{S}_{\text{av}} &= \frac{1}{2}\mathcal{R}e\left\{\frac{E_m^{+2}}{\eta}e^{-2\alpha z}e^{j\theta\eta}\right\}\boldsymbol{a}_z\\ &= \frac{E_m^{+2}}{\eta}e^{-2\alpha z}\cos(\theta_\eta)\boldsymbol{a}_z\end{aligned} \tag{B.77}$$

Example B.17 A 1 MHz, 1 V/m uniform plane wave is traveling through a block of copper. Determine the power dissipated in the copper over a distance of 1 μm with surface area of 2 m^2.

Solution: The attenuation constant and intrinsic impedance were determined in Examples B.13 and B.14 as $\alpha = 1.51 \times 10^4$ and $\hat{\eta} = 3.69 \times 10^{-4} \underline{/45^\circ}$. Hence, the power dissipated in the block is the difference between the power entering the block and the power leaving it using (B.77).

$$\begin{aligned} P_{\text{dissipated}} &= P_{\text{av}}|_{z=0} - P_{\text{av}}|_{z=1\,\mu\text{m}} \\ &= \frac{|\hat{E}_m|^2}{2\eta} \cos(\theta_\eta) A - \frac{|\hat{E}_m|^2}{2\eta} e^{-2\alpha 1\,\mu\text{m}} \cos(\theta_\eta) A \\ &= \frac{|\hat{E}_m|^2}{2_\eta} \cos(\theta_\eta) A (1 - e^{-2\alpha 1\,\mu\text{m}}) \\ &= \frac{1}{2 \times 3.69 \times 10^{-4}} \cos(45^\circ)(2\ \text{m}^2)(1 - e^{-2 \times 1.51 \times 10^4 \times 10^{-6}}) \\ &= 57\ \text{W} \end{aligned}$$

Review Exercise B.17 A 1 MHz, 10 V/m uniform plane wave is traveling through seawater. Determine the power dissipated over a distance of 1 mm with surface area of 2 m^2.

Answer: 0.4 W.

B.6.4 Conductors versus Dielectrics

Note that the only change in Maxwell's equations introduced by losses in the medium occurs in Ampere's law. For ($\sigma \neq 0$), Ampere's law may be written as

$$\nabla \times \hat{\boldsymbol{H}} = (\sigma + j\omega\varepsilon)\hat{\boldsymbol{E}} \tag{B.78}$$

On comparing this expression with the lossless case ($\sigma = 0$):

$$\nabla \times \hat{\boldsymbol{H}} = j\omega\varepsilon\hat{\boldsymbol{E}} \tag{B.79}$$

we see that we could derive the results for the lossless case and "fix up" those results to include losses by replacing ε in the lossless results with a *complex permittivity*:

$$\hat{\varepsilon} = \varepsilon \left(1 - j\frac{\sigma}{\omega\varepsilon}\right) \tag{B.80}$$

The term $\sigma/\omega\varepsilon$ is referred to as the *loss tangent* of the material and is a function of frequency. Values of the loss tangent are experimentally measured for various materials and are tabulated at several frequencies in handbooks. Note that there are two components of current involved in Ampere's law: a conduction current density $\hat{\boldsymbol{J}}_c = \sigma\hat{\boldsymbol{E}}$ and a displacement current density $\hat{\boldsymbol{J}}_d = j\omega\varepsilon\hat{\boldsymbol{E}}$. The conduction current represents an energy loss mechanism, while the displacement current represents energy storage, as we have observed previously. The ratio of these two currents is a measure of the lossy nature of the material. The conduction and displacement current phasors are 90° out of time phase.

The notion of the loss tangent as the ratio of conduction current to displacement current provides a meaningful way of distinguishing between *conductors* and *dielectrics*. Materials are classified as conductors or dielectrics according to whether the conduction current is larger or smaller than the displacement current:

$$\frac{\sigma}{\omega\varepsilon} \ll 1 \quad \text{good dielectric}$$

$$\frac{\sigma}{\omega\varepsilon} \gg 1 \quad \text{good conductor}$$

Calculations of the propagation constant $\hat{\gamma}$ and the intrinsic impedance $\hat{\eta}$ can be simplified, depending on whether the medium can be classified as a good conductor or a good dielectric according to the above criterion.

First, we consider *good dielectrics* where $\sigma/\omega\varepsilon \ll 1$. The propagation constant can be written as

$$\begin{aligned}\hat{\gamma} &= \alpha + j\beta \\ &= \sqrt{j\omega\mu(\sigma + j\omega\varepsilon)} \\ &= j\omega\sqrt{\mu\varepsilon}\sqrt{1 - j\frac{\sigma}{\omega\varepsilon}}\end{aligned} \tag{B.81}$$

For $\sigma/\omega\varepsilon \ll 1$, this essentially simplifies to that of free space: $\hat{\gamma} = j\beta = j\omega\sqrt{\mu\varepsilon}$. The velocity of propagation is also essentially unchanged from that of a lossless medium. The intrinsic impedance can be similarly simplified

$$\begin{aligned}\hat{\eta} &= \sqrt{\frac{j\omega\mu}{\sigma + j\omega\varepsilon}} \\ &= \sqrt{\frac{\mu}{\varepsilon}\frac{1}{1 - j\sigma/\omega\varepsilon}} \\ &\cong \sqrt{\frac{\mu}{\varepsilon}}\end{aligned} \tag{B.82}$$

and the intrinsic impedance is virtually unchanged from the lossless medium case.

Next, we consider the case of *good conductors*, where $\sigma/\omega\varepsilon \gg 1$. The propagation constant can be written as

$$\begin{aligned}\hat{\gamma} &= \sqrt{j\omega\mu(\sigma + j\omega\varepsilon)} \\ &= \sqrt{j\omega\mu\sigma\left(1 + j\frac{\omega\varepsilon}{\sigma}\right)} \\ &\cong \sqrt{j\omega\mu\sigma} \\ &= \sqrt{\omega\mu\sigma}\underline{/45^\circ}\end{aligned} \tag{B.83}$$

so that

$$\alpha = \beta \cong \sqrt{\frac{1}{2}\omega\mu\sigma} \tag{B.84}$$

The velocity of propagation becomes

$$\begin{aligned} v &= \frac{\omega}{\beta} \\ &\cong \sqrt{\frac{2\omega}{\mu\sigma}} \end{aligned} \tag{B.85}$$

The intrinsic impedance becomes

$$\begin{aligned} \hat{\eta} &= \sqrt{\frac{j\omega\mu}{\sigma + j\omega\varepsilon}} \\ &= \sqrt{\frac{j\omega\mu/\sigma}{1 + j\omega\varepsilon/\sigma}} \\ &\cong \sqrt{\frac{j\omega\mu}{\sigma}} \\ &= \sqrt{\frac{\omega\mu}{\sigma}}\underline{/45^\circ} \\ &= \sqrt{\frac{\omega\mu}{2\sigma}}(1 + j1) \end{aligned} \tag{B.86}$$

In addition to conductive loss mechanisms inherent in σ, dielectrics also exhibit another loss mechanism. They are characterized by microscopic dipoles of *bound charge* [1, 2]. As the frequency of the fields is increased, the dipoles of bound charge cannot completely align with the field and tend to lag behind the changes in field direction. This loss phenomenon is also accounted for by ascribing a complex permittivity to the material, $\hat{\varepsilon} = \varepsilon' - j\varepsilon''$.

B.6.5 Skin Depth

The notion of *skin depth* occurs throughout the analysis of electromagnetic field propagation in conductive material media. Consider a wave traveling in a lossy material as illustrated in Fig. B.24. The surface is in the xy plane and the wave is traveling downward in the z direction. The electric field is given by

$$E_x = E_0 e^{-\alpha z} \cos(\omega t - \beta z) \quad z \geq 0 \tag{B.87}$$

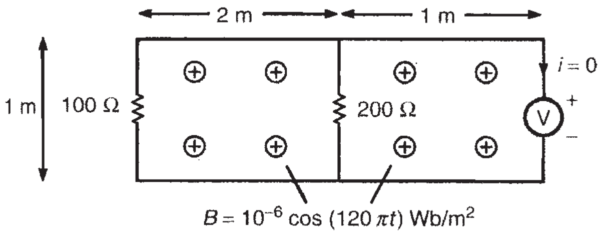

FIGURE B.24 Illustration of skin depth in a conductor.

TABLE B.1 Skin Depth of Copper

f	δ
60 Hz	8.5 mm
1 kHz	2.09 mm
10 kHz	0.66 mm
100 kHz	0.21 mm
1 MHz	2.6 mils
10 MHz	0.82 mils
100 MHz	0.26 mils
1 GHz	0.0823 mils

The current density is

$$\begin{aligned} J_x &= \sigma E_x \\ &= \sigma E_0 e^{-\alpha z}\cos(\omega t - \beta z) \qquad z \geq 0 \end{aligned} \tag{B.88}$$

As the wave travels downward into this conductive material, the amplitude, $\sigma E_0 e^{-\alpha z}$, decreases exponentially. Over a distance of one skin depth, $z = \delta = 1/\alpha$, the amplitude has decreased by $1/e$ or 37%. This distance is called the *skin depth* and is denoted as δ. If the lossy medium qualifies as a good conductor, we may use the relation for the attenuation constant given in (B.84):

$$\begin{aligned} \delta &= \frac{1}{\alpha} \\ &= \sqrt{\frac{2}{\omega\mu\sigma}} \quad \text{(good conductor)} \\ &= \frac{1}{\sqrt{\pi f \mu\sigma}} \end{aligned} \tag{B.89}$$

Values of the skin depth for copper are given in Table B.1, where 1 mil = 0.001 in. = 2.54×10^{-5} m. For increasing frequencies, the skin depth decreases and becomes extremely small for frequencies in the radiated emission limit range. For example, the skin depth for copper at 100 MHz is 0.0066 mm = 6.6 μm = 0.26 mils. For current-carrying conductors, we may consider the current to be essentially concentrated in a depth of a few skin depths on the surface of the conductor that is adjacent to the field that caused the current. The remainder of the conductor has essentially no effect.

B.7 STATIC (DC) ELECTROMAGNETIC FIELD RELATIONS—A SPECIAL CASE

If the fields are not varying with time, then Maxwell's equations and their solution simplify considerably. The reader should be cautioned that a great many mistakes in electromagnetics and EMC in particular are caused by using these static (dc) relations in time-varying situations where they do not apply. However, there are a very large number of cases where the fields vary "slowly" enough that these static results apply to a reasonable approximation. It is important to be able to identify where this can or cannot be done.

B.7.1 Maxwell's Equations for Static (DC) Fields

If the electromagnetic fields do not vary with time, then all time derivatives are zero and Maxwell's equations simplify to the following:

TABLE B.2 Maxwell's Equations for Static (dc) Fields

Law	Integral Form (DC)	Differential Form (DC)
Faraday's law	$\oint_C \boldsymbol{E} \cdot d\boldsymbol{l} = 0$	$\nabla \times \boldsymbol{E} = 0$
Ampere's law	$\oint_C \boldsymbol{H} \cdot d\boldsymbol{s} = \int_S \boldsymbol{J} \cdot d\boldsymbol{s}$	$\nabla \times \boldsymbol{H} = \boldsymbol{J}$
Gauss' law, electric field	$\oint_S \boldsymbol{D} \cdot d\boldsymbol{s} = \int_V \rho_v dv$	$\nabla \cdot \boldsymbol{D} = \rho_v$
Gauss' law, magnetic field	$\oint_S \boldsymbol{B} \cdot d\boldsymbol{s} = 0$	$\nabla \cdot \boldsymbol{B} = 0$
Conservation of charge	$\oint_S \boldsymbol{J} \cdot d\boldsymbol{s} = 0$	$\nabla \cdot \boldsymbol{J} = 0$

Gauss' laws do not involve any time derivatives and are the same for dc or time-varying fields. The right-hand side of Faraday's law involved a time derivative of the magnetic flux through contour C. This is zero for static fields. Hence, the static electric field is conservative; specifically, the line integral of any static electric field around a closed path always yields a result of zero. This allows the unique definition of voltage between two points no matter the path taken between them as [1, 2]

$$V_{ba} = -\int_a^b \boldsymbol{E} \cdot d\boldsymbol{l} \tag{B.90}$$

Note that for dc conditions, Faraday's law states that the line integral of the electric field around a closed loop, i.e., the sum of the voltages around that closed loop, is zero. But this is Kirchhoff's voltage law. As we saw earlier, a time-varying magnetic field that penetrates this loop will induce additional voltages in the loop. But we "fix up" Kirchhoff's voltage law to include these by defining self and mutual inductance.

Ampere's law also contains a time derivative on its right-hand side as the displacement current term. For static conditions, only a flow of free charges, conduction current density, can produce a magnetic field.

Finally, conservation of charge involves the time rate of decrease of free charge on the right-hand side. For static conditions, this is zero, and the result reduces to saying that "no charge can be stored at a point"; whatever current enters a closed surface, it must immediately exit that closed surface. But this is equivalent to Kirchhoff's current law. We "fix up" Kirchhoff's current law by defining capacitance.

B.7.1.1 Range of Applicability for Low-Frequency Fields We can successfully use Kirchhoff's laws and lumped-circuit models to compute currents and voltages in circuits that are excited at the common power frequency of 60 Hz, as well as up to the low megahertz frequency range. But since these frequencies are not strictly dc, how can we apply the static field laws? The answer is the electrical size of the circuit. If the maximum dimension of an electric circuit is electrically small, say, less than $\lambda/10$, then phase shift across the circuit is not significant, and we may get away with the static field relations and lumped circuit modeling and analysis. For example, the phase shift suffered by a wave that propagates a distance d is

$$\begin{aligned}\phi &= \beta d \\ &= 2\pi \frac{d}{\lambda}\end{aligned}$$

If the distance is $\lambda/10$, this amounts to a phase shift of 36°. If the distance is $\lambda/100$, this amounts to a phase shift of 3.6°. Lumped-circuit analysis ignores this phase-shift such as occurs by propagation along the component connection leads. Hence, *if the maximum dimension of a circuit is electrically small, we may ignore this phase shift and use lumped-circuit analysis methods as a valid approximation*. For example, the 60 Hz power frequency has a wavelength of some 3100 mi or 5000 km! Even long power transmission lines are electrically short and may be modeled with only a resistor, a capacitor, and an inductor. Even a simple electronic circuit we construct in laboratories and excited with, say, a 1 MHz source, is electrically small since a wavelength at 1 MHz is 300 m!

Although this discussion is admittedly somewhat course, as engineers we are used to making reasonable assumptions to simplify calculations. This provides some rationale when making such simplifications.

B.7.2 Two-Dimensional Fields and Laplace's Equation

Two-dimensional (2D) electromagnetic field problems occur frequently. For example, transmission-line problems consist of two parallel conductors that are considered to be infinite in length. The electric and magnetic fields lie in the transverse or *xy* plane perpendicular to the line axis, the *z* axis, as demonstrated in Chapter 4. This is said to be the *transverse electromagnetic* (TEM) mode of propagation. For example, the electric and magnetic fields of a two-wire transmission line in the transverse, *xy*, plane are shown in Fig. B.25. For the TEM mode of propagation, these fields are time-varying yet they have the same structure and solution as if they were static (dc). Hence, voltage and current can be uniquely defined [1].

Since the fields in the 2D transverse plane have the same solution as though they were dc, the distribution of voltage in the 2D space surrounding the wires can be determined by solving Laplace's equation in the two-dimensional transverse plane [1]:

$$\nabla^2 V(x,y) = \frac{\partial^2 V(x,y)}{\partial x^2} + \frac{\partial^2 V(x,y)}{\partial y^2} = 0 \tag{B.91}$$

This solution can be used to determine the per-unit-length capacitance and inductance of the transmission-line: the two most important ingredients of the transmission-line equations. Generally,

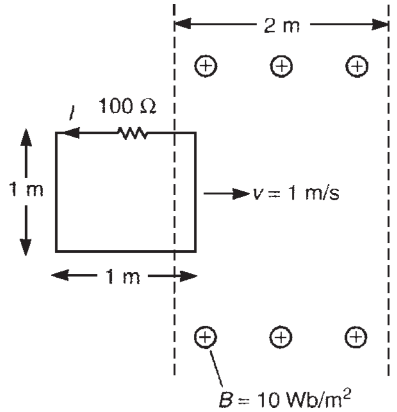

FIGURE B.25 The electric and magnetic fields for the TEM mode of propagation on a transmission line; (a) side view of two wire transmission line illustrating electric and magnetic field lines; (b) end view of two wire transmission line illustrating electric and magnetic field lines.

this solution is a complicated problem. Quite often certain simplifications can be used, but the underlying problem is the solution of Laplace's equation. There are several numerical techniques for solving Laplace's equation [1]. There are also a number of commercially available 2D solvers that make the (numerical) solution of Laplace's equation very straightforward. Some of the more popular numerical methods that are used to essentially solve for the 2D static fields are (1) the method of moments (MoM), (2) the finite-difference method, and (3) the finite-element method (FEM) [1].

PROBLEMS

Section B.1 Vector Analysis

B.1.1 A vector $\boldsymbol{A}(x, y, x)$ is defined in a rectangular coordinate system as being directed from (0, 2, − 4) to (3, − 4, 5) where the units are in meters. Determine (a) an expression for $\boldsymbol{A}$, (b) the distance between the two points, and (c) a unit vector pointing in the direction of $\boldsymbol{A}$. [(a) $3\boldsymbol{a}_x - 6\boldsymbol{a}_y + 9\boldsymbol{a}_z$, (b) 11.22 m, (c) $0.27\boldsymbol{a}_x - 0.53\boldsymbol{a}_y + 0.8\boldsymbol{a}_z$]

B.1.2 Three vectors are given in a rectangular coordinate system as $\boldsymbol{A} = 2\boldsymbol{a}_x + 3\boldsymbol{a}_y - \boldsymbol{a}_3$, $\boldsymbol{B} = \boldsymbol{a}_x + \boldsymbol{a}_y - 2\boldsymbol{a}_z$, and $\boldsymbol{C} = 3\boldsymbol{a}_x - \boldsymbol{a}_y + \boldsymbol{a}_z$. Determine (a) $\boldsymbol{A} + \boldsymbol{B}$, (b) $\boldsymbol{B} - \boldsymbol{C}$, (c) $\boldsymbol{A} + 3\boldsymbol{B} - 2\boldsymbol{C}$, (d) $|\boldsymbol{A}|$, (e) $\boldsymbol{a}_B$, (f) $\boldsymbol{A} \cdot \boldsymbol{B}$, (g) $\boldsymbol{B} \cdot \boldsymbol{A}$, (h) $\boldsymbol{B} \times \boldsymbol{C}$, (i) $\boldsymbol{C} \times \boldsymbol{B}$, (j) $\boldsymbol{A} \cdot \boldsymbol{B} \times \boldsymbol{C}$ [(a) $3\boldsymbol{a}_x + 4\boldsymbol{a}_y - 3\boldsymbol{a}_z$, (b) $-2\boldsymbol{a}_x + 2\boldsymbol{a}_y - 3\boldsymbol{a}_z$, (c) $-\boldsymbol{a}_x + 8\boldsymbol{a}_y - 9\boldsymbol{a}_z$, (d) 3.74, (e) $0.41\boldsymbol{a}_x + 0.41\boldsymbol{a}_y - 0.82\boldsymbol{a}_z$, (f) 7, (g) 7, (h) $-\boldsymbol{a}_x - 7\boldsymbol{a}_y - 4\boldsymbol{a}_z$, (i) $\boldsymbol{a}_x + 7\boldsymbol{a}_y + 4\boldsymbol{a}_z$, (j) −19]

B.1.3 If $\boldsymbol{A} = \boldsymbol{a}_x + 2\boldsymbol{a}_y - 3\boldsymbol{a}_z$ and $\boldsymbol{B} = 2\boldsymbol{a}_x - \boldsymbol{a}_y + \boldsymbol{a}_z$ determine (a) the magnitude of the projection of $\boldsymbol{B}$ onto $\boldsymbol{A}$, (b) the angle (smallest) between $\boldsymbol{A}$ and $\boldsymbol{B}$, (c) a unit vector perpendicular to the plane containing $\boldsymbol{A}$ and $\boldsymbol{B}$. [(a) 0.8, (b) 109.1°, (c) $-0.115\boldsymbol{a}_x - 0.808\boldsymbol{a}_y - 0.577\boldsymbol{a}_z$].

B.1.4 Two vectors are given by $\boldsymbol{A} = \boldsymbol{a}_x + 2\boldsymbol{a}_y - \boldsymbol{a}_z$ and $\boldsymbol{B} = \alpha\boldsymbol{a}_x + \boldsymbol{a}_y + 3\boldsymbol{a}_z$. Determine α such that the two vectors are perpendicular. [$\alpha = 1$]

B.1.5 Two vectors are given by $\boldsymbol{A} = 2\boldsymbol{a}_x + 2\boldsymbol{a}_y + 3\boldsymbol{a}_z$ and $\boldsymbol{B} = \alpha\boldsymbol{a}_x + \beta\boldsymbol{a}_y - 9\boldsymbol{a}_z$. Determine α and β such that the two vectors are parallel. [$\alpha = -3$, $\beta = -6$]

B.1.6 Two vectors are given by $\boldsymbol{A} = 2\boldsymbol{a}_x - 3\boldsymbol{a}_y + \boldsymbol{a}_z$ and $\boldsymbol{B} = -\boldsymbol{a}_x + 2\boldsymbol{a}_y + 4\boldsymbol{a}_z$. Determine a vector $\boldsymbol{C}$ which is perpendicular to both $\boldsymbol{A}$ and $\boldsymbol{B}$ and has a length of 10. [$\boldsymbol{C} = -8.4\boldsymbol{a}_x - 5.4\boldsymbol{a}_y + 0.6\boldsymbol{a}_z$]

B.1.7 Determine the line integral of $\boldsymbol{F} = 2x\boldsymbol{a}_x + 4\boldsymbol{a}_y - y\boldsymbol{a}_z$ from $P_1(-1, 3, -2)$ to $P_2(2, 4, 1)$ where the points are specified in a rectangular coordinate system. [−7/2]

B.1.8 If the force exerted on an object is given by $\boldsymbol{F} = 2x\boldsymbol{a}_x + 3z\boldsymbol{a}_y + 4\boldsymbol{a}_z$ N, determine the work required to move the object in a straight line from $P_1(0, 0, 0)$ to $P_2(1, 1, 2)$ where the points are specified in a rectangular coordinate system in meters. [12 J]

B.1.9 Determine the line integral of $\boldsymbol{F} = x\boldsymbol{a}_x + 2xy\boldsymbol{a}_y - y\boldsymbol{a}_z$ from $P_1(0, 0, 2)$ to $P_2(3, 2, 0)$ along paths consisting of (a) a straight-line path between the two points, and (b) a two segment path consisting of a straight-line path from $P_1(0, 0, 2)$ to the origin and a straight-line path from the origin to $P_2(3, 2, 0)$. The points are specified in a rectangular coordinate system. [(a) 29/2, (b) 25/2]

B.1.10 Determine the flux of the vector field $\boldsymbol{F} = x\boldsymbol{a}_x + y\boldsymbol{a}_y + z\boldsymbol{a}_z$ out of the closed surface consisting of a square volume whose sides are of length 2 and is centered on the origin of a rectangular coordinate system. [24]

B.1.11 Determine the flux of the vector field $\boldsymbol{F} = xy\boldsymbol{a}_x + yz\boldsymbol{a}_y - xz\boldsymbol{a}_z$ out of a closed rectangular surface. The surface has corners at (1, 0, 0), (0, 2, 0), (0, 0, 3), (1, 0, 3), (0, 0, 0), (0, 2, 3), (1, 2, 3), and (1, 2, 0), which are given in rectangular coordinate system variables. [12]

B.1.12 Compute the divergence of the vector field $\boldsymbol{F} = yz\boldsymbol{a}_x + zy\boldsymbol{a}_y + xz\boldsymbol{a}_z$. [$\nabla \cdot \boldsymbol{F} = z + x$]

B.1.13 Compute the curl of the vector field $\boldsymbol{F} = xy\boldsymbol{a}_x + 2\,yz\boldsymbol{a}_y - \boldsymbol{a}_z$. [$\nabla \times \boldsymbol{F} = -2y\boldsymbol{a}_x - x\boldsymbol{a}_z$]

Section B.2 Maxwell's Equations

B.2.1 Determine the voltage V in the circuit of Fig. PB.2.1. [–0.233 mV]

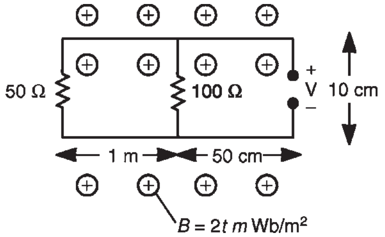
50 Ω
100 Ω
+
V
−
10 cm
1 m
50 cm
B = 2t m Wb/m²

FIGURE PB.2.1

B.2.2 Determine the voltage V in the circuit of Fig. PB.2.2. [0.533 mV]

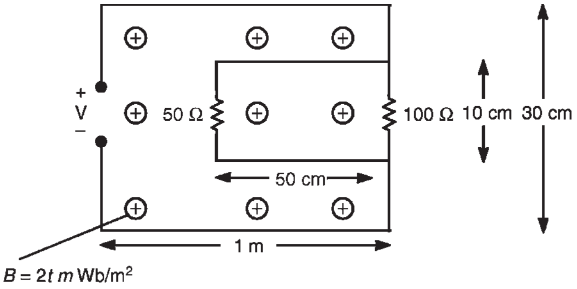
+
V
−
50 Ω
100 Ω
10 cm
30 cm
50 cm
1 m
B = 2t m Wb/m²

FIGURE PB.2.2

B.2.3 Determine the voltage V in the circuit of Fig. PB.2.3. [$301.6\cos(2\pi \times 60t)$ mV]

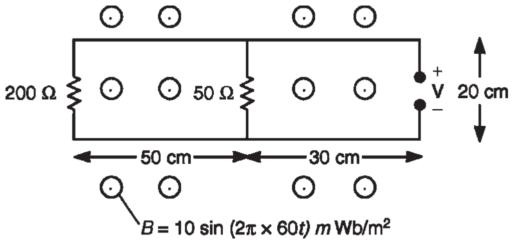
200 Ω
50 Ω
+
V
−
20 cm
50 cm
30 cm
B = 10 sin (2π x 60t) m Wb/m²

FIGURE PB.2.3

B.2.4 Assuming that current I is positive-valued, which of the situations in Fig. PB.2.4 are *not* correct. [b, d]

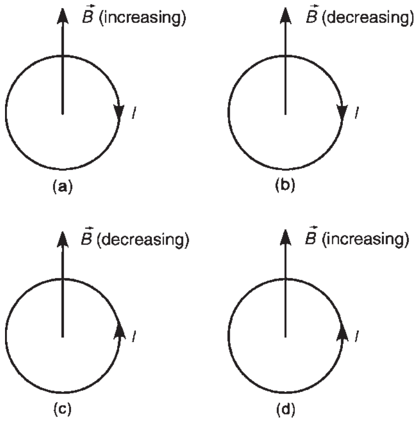
$\vec{B}$ (increasing)
I
(a)
$\vec{B}$ (decreasing)
I
(b)
$\vec{B}$ (decreasing)
I
(c)
$\vec{B}$ (increasing)
I
(d)

FIGURE PB.2.4

B.2.5 Determine the current I in Fig. PB.2.5 if the magnetic field varies as $B = 2\cos(2\pi \times 60t)$ mWb/m^2 and the velocity of the bar is 10 m/s. [$0.1\cos(2\pi \times 60t) - 37.7t\sin(2\pi \times 60t)$ mA]

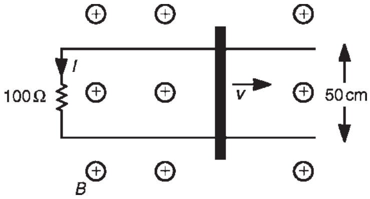
I
100Ω
v
50 cm
B

FIGURE PB.2.5

B.2.6 Determine the current I in Fig. PB.2.5 if the magnetic field is constant at B = 10 mWb/m^2 and the velocity $v = 100\cos(10t)$ m/s. [5 cos (10t) mA]

B.2.7 A rectangular loop rotates about the z axis at an angular speed of $\omega = 5$ rad/s in a constant magnetic field directed in the y direction of $\boldsymbol{B} = 10\,\boldsymbol{a}_y$ mWb/m^2 as shown in Fig. PB.2.7. Determine the current induced to flow around the loop with direction shown, assuming that the loop is in the x direction at $t = 0$. [−2.5 cos(5t) mA]

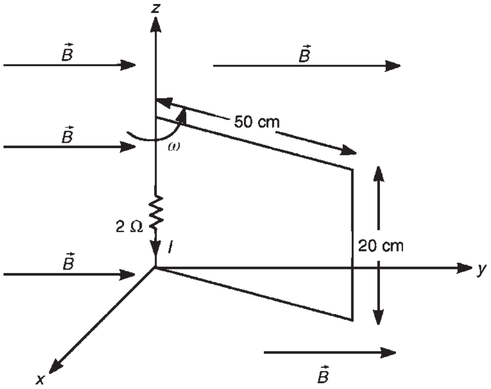
z
$\vec{B}$
$\vec{B}$
50 cm
$\vec{B}$
ω
2 Ω
I
20 cm
$\vec{B}$
y
x
$\vec{B}$

FIGURE PB.2.7

B.2.8 Lightning is particularly detrimental to electronic devices even if those devices do not receive a direct hit. For example, a lightning bolt can be considered as a channel of current, as shown in Fig. PB.2.8, that is very long. Consider modeling the effect of a typical lightning bolt on household wiring. Assume that the lightning channel rises linearly to a peak level of 50 kA in 1 μs and then decays linearly to zero at 10 μs as shown in Fig. PB.2.8. Also assume that the house power wiring has the two wires routed around the floor and the ceiling. Determine the induced voltage at the power input to a digital computer that is connected to the power net for a lightning channel 1 km away. [$V = 2585$ V for $0 < t < 1$ μs and $V = -287$ V for 1 μs $< t < 10$ μs]

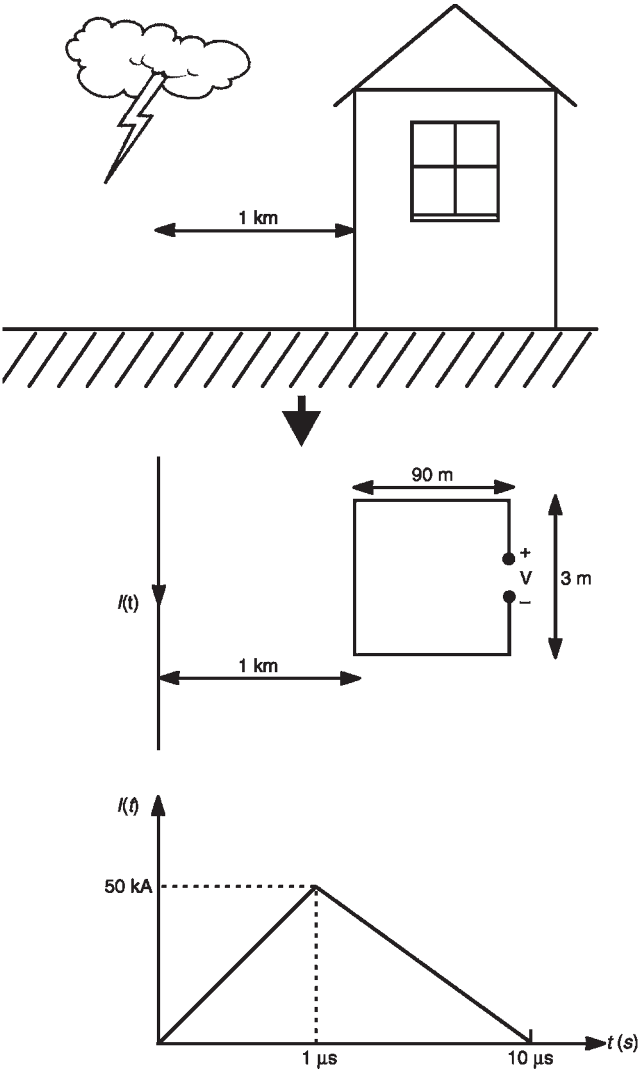

FIGURE PB.2.8

B.2.9 A rectangular loop is moving with velocity v radially away from a wire that carries a dc current I as shown in Fig. PB.2.9. Determine an expression for the current induced in the loop as a function of time.

$$\left[\frac{\mu_0 I l w}{2\pi R(vt+w)t}\right]$$

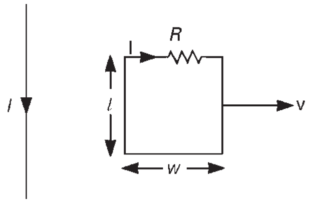

FIGURE PB.2.9

B.2.10 An electric field intensity vector in free space is given in a rectangular coordinate system by $\boldsymbol{E} = E_m \sin\alpha x \sin(\omega t - \beta z)\boldsymbol{a}_y$. Determine the magnetic field intensity vector that satisfies Faraday's law.

$$\left[\boldsymbol{H} = -\frac{E_m\beta}{\omega\mu_0}\sin\alpha x\ \sin(\omega t - \beta z)\boldsymbol{a}_x + \frac{E_m\alpha}{\omega\mu_0}\cos\alpha x\ \cos(\omega t - \beta z)\boldsymbol{a}_z\right]$$

B.2.11 An electric field intensity vector in free space is given in a rectangular coordinate system by $\boldsymbol{E} = E_m \sin\beta z \cos(\omega t)\boldsymbol{a}_x$. Determine the magnetic field intensity vector that satisfies Faraday's law. $[\boldsymbol{H} = -E_m\beta/\omega\mu_0 \cos\beta z \sin(\omega t)\boldsymbol{a}_y]$

B.2.12 Dry soil has $\varepsilon_r \cong 4$ and a conductivity of $\sigma \cong 10^{-5}$ S/m. Determine the frequency above which the displacement current dominates the conduction current. [45 kHz]

B.2.13 A magnetic field intensity vector in free space is given in a rectangular coordinate system as $\boldsymbol{H} = H_x \sin\alpha x \sin(\omega t - \beta z)\boldsymbol{a}_x + H_z \cos\alpha x \cos(\omega t - \beta z)\boldsymbol{a}_z$. Determine the electric field intensity vector that satisfies Ampere's law.

$$\left[\boldsymbol{E} = \frac{(-\beta H_x + \alpha H_z)}{\omega\varepsilon_0}\sin\alpha x\ \sin(\omega t - \beta z)\boldsymbol{a}_y\right]$$

B.2.14 A magnetic field intensity vector in free space is given in a rectangular coordinate system as $\boldsymbol{H} = H_m \cos\beta z \sin(\omega t)\boldsymbol{a}_y$. Determine the electric field intensity vector that satisfies Ampere's law

$$[\boldsymbol{E} = -\beta H_m/\omega\varepsilon_0\ \sin\beta z\ \cos(\omega t)\boldsymbol{a}_x]$$

B.2.15 Show that the $\boldsymbol{E}$ field of Problem B.2.10 satisfies Gauss' law in free space where, unless some is intentionally introduced, there is no free charge density ($\rho_v = 0$).

B.2.16 Show that the $\boldsymbol{E}$ field of Problem B.2.11 satisfies Gauss' law in free space where, unless some is intentionally introduced, there is no free charge density ($\rho_v = 0$).

B.2.17 Show that the $\boldsymbol{H}$ field of Problem B.2.13 satisfies Gauss' law in free space. [Only if $\alpha H_x + \beta H_z = 0$]

B.2.18 Show that the $\boldsymbol{H}$ field of Problem B.2.14 satisfies Gauss' law in free space.

Section B.3 Boundary Conditions

B.3.1 An interface between two media lies in the yz plane at $x = 0$ as shown in Fig. PB.3.1. If the electric field intensity vector in medium 1 at the interface ($x = 0$) is given by $\boldsymbol{E}_1|_{x=0} = \alpha\boldsymbol{a}_x + \beta\boldsymbol{a}_y + \gamma\boldsymbol{a}_z$, determine $\boldsymbol{E}_2|_{x=0}$, that is, the electric field intensity vector in the second medium just across the boundary.

$$\left[\boldsymbol{E}_2|_{x=0} = \alpha\frac{\varepsilon_1}{\varepsilon_2}\boldsymbol{a}_x + \beta\boldsymbol{a}_y + \gamma\boldsymbol{a}_z\right]$$

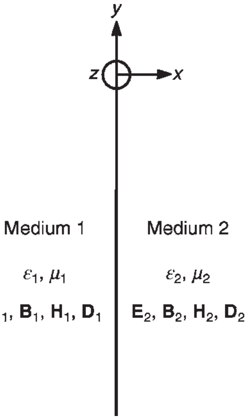

FIGURE PB.3.1

B.3.2 An interface between two media lies in the yz plane at $x = 0$ as shown in Fig. PB.3.1. If the magnetic flux density vector in medium 1 at the interface ($x = 0$) is given by $\boldsymbol{B}_1|_{x=0} = \alpha\boldsymbol{a}_x + \beta\boldsymbol{a}_y + \gamma\boldsymbol{a}_z$, determine $\boldsymbol{B}_2|_{x=0}$, that is, the magnetic flux density vector in the second medium just across the boundary. [$\boldsymbol{B}_2|_{x=0} = \alpha\boldsymbol{a}_x + \beta\mu_2/\mu_1\boldsymbol{a}_y + \gamma\mu_2/\mu_1\boldsymbol{a}_z$]

B.3.3 An interface between two media lies in the yz plane at $x = 0$ as shown in Fig. PB.3.1. If the electric flux density vector in medium 1 at the interface ($x = 0$) is given by $\boldsymbol{D}_1|_{x=0} = \alpha\boldsymbol{a}_x + \beta\boldsymbol{a}_y + \gamma\boldsymbol{a}_z$, determine $\boldsymbol{D}_2|_{x=0}$, that is, the electric flux density vector in the second medium just across the boundary. [$\boldsymbol{D}_2|_{x=0} = \alpha\boldsymbol{a}_x + \beta\varepsilon_2/\varepsilon_1\boldsymbol{a}_y + \gamma\varepsilon_2/\varepsilon_1\boldsymbol{a}_z$]

B.3.4 An interface between two media lies in the yz plane at $x = 0$ as shown in Fig. PB.3.1. If the magnetic field density vector in medium 1 at the interface ($x = 0$) is given by $\boldsymbol{H}_1|_{x=0} = \alpha\boldsymbol{a}_x + \beta\boldsymbol{a}_y + \gamma\boldsymbol{a}_z$, determine $\boldsymbol{H}_2|_{x=0}$, that is, the magnetic field density vector in the second medium just across the boundary.

$$\left[\boldsymbol{H}_2|_{x=0} = \frac{\mu_1}{\mu_2}\alpha\boldsymbol{a}_x + \beta\boldsymbol{a}_y + \gamma\boldsymbol{a}_z\right]$$

Section B.5 Power Flow

B.5.1 A wave traveling in seawater (which is lossy) has its electric and magnetic fields given in a rectangular coordinate system as $\boldsymbol{E} = 10e^{-4z}\cos(\omega t - 4z)\boldsymbol{a}_x$ V/m and $\boldsymbol{H} = 7.15e^{-4z}\cos(\omega t - 4z - \pi/4)\boldsymbol{a}_y$ A/m. Determine the total power exiting a cube surface having sides of length 1 m and corners at (0, 0, 0), (1 m, 0, 0), (0, 0, 1 m), (1 m, 0, 1 m), (0, 1 m, 1 m), (1 m, 1 m, 1 m), (0, 1 m, 0), and (1 m, 1 m, 0). [−25.27 W]

Section B.6 Uniform Plane Waves

B.6.1 A 10 MHz uniform plane wave is traveling in the following lossless dielectric ($\mu_r = 1$) media (a) polyvinyl chloride ($\varepsilon_r = 3.5$), (b) Teflon ($\varepsilon_r = 2.1$), (c) Mylar ($\varepsilon_r = 5$), and (d) polyurethane ($\varepsilon_r = 7$). Determine the phase constant β, the intrinsic impedance η, the phase velocity of propagation v, and the wavelength λ. [(a) $\beta = 0.392$ rad/m, $\eta = 202\ \Omega$, $v = 1.6\times 10^8$ m/s, $\lambda = 16$ m, (b) $\beta = 0.304$ rad/m, $\eta = 260\ \Omega$, $v = 2.07\times 10^8$ m/s, $\lambda = 20.7$ m, (c) $\beta = 0.468$ rad/m, $\eta = 169\ \Omega$, $v = 1.34\times 10^8$ m/s, $\lambda = 13.4$ m, (d) $\beta = 0.554$ rad/m, $\eta = 142\ \Omega$, $v = 1.13\times 10^8$ m/s, $\lambda = 11.3$ m.]

B.6.2 Write the time-domain expressions for a 5 MHz uniform plane wave traveling in free space. The 10 V/m electric field intensity vector is directed in the $+z$ direction and the wave is propagating in the $-y$ direction. [$\boldsymbol{E} = 10\cos(10\pi\times 10^6 t + 0.105y)\ \boldsymbol{a}_z$, $\boldsymbol{H} = -0.0265\cos(10\pi\times 10^6 t + 0.105y)\ \boldsymbol{a}_x$] Hint: Draw a sketch and get the direction of $\boldsymbol{H}$ such that $\boldsymbol{E}\times\boldsymbol{H}$ is in the direction of propagation.

B.6.3 Suppose that a uniform plane wave is traveling in the x direction in a lossless dielectric ($\mu_r = 1$) with a 100 V/m electric field in the z direction. If the wavelength is 25 cm and the velocity of propagation is 2×10^8 m/s, determine the frequency of the wave and the relative permittivity of the medium. Write complete time-domain expressions for the electric and magnetic field vectors. (*Hint*: Draw a sketch and get the direction of $\boldsymbol{H}$ such that $\boldsymbol{E}\times\boldsymbol{H}$ is in the direction of propagation.)

$$\Big[800\ \text{MHz},\ \ \varepsilon_r = 2.25, \boldsymbol{E} = 100\cos(16\pi\times 10^8 t - 25.1x)\boldsymbol{a}_z,$$
$$\boldsymbol{H} = -0.398\ \cos(16\pi\times 10^8 t - 25.1x)\ \boldsymbol{a}_y\Big]$$

B.6.4 Write the time-domain expression for the electric field of a uniform plane wave traveling in silicon ($\varepsilon_r = 12$) if the magnetic field is given by [$\boldsymbol{H} = 0.1\cos(8\pi\times 10^7 t - 2.9y)\boldsymbol{a}_x$]. (*Hint*: Draw a sketch and get the direction of $\boldsymbol{H}$ such that $\boldsymbol{E}\times\boldsymbol{H}$ is in the direction of propagation.) [$\boldsymbol{E} = 10.9\cos(8\pi\times 10^7 t - 2.9y)\ \boldsymbol{a}_z$]

B.6.5 A 2 GHz uniform plane wave is traveling in a medium that is characterized by $\varepsilon_r = 4$ and $\mu = 9$ in the $-z$ direction. The magnetic field intensity vector is directed in the y direction and the magnitude is 0.02 A/m. Write time-domain expressions for the electric and magnetic field vectors. (*Hint*: Draw a sketch and get the direction of $\boldsymbol{H}$ such that $\boldsymbol{E}\times\boldsymbol{H}$ is in the direction of propagation.) [$\boldsymbol{E} = -11.3\cos(4\pi\times 10^9 t + 251z)\ \boldsymbol{a}_x$, $\boldsymbol{H} = 0.02\cos(4\pi\times 10^9 t + 251z)\boldsymbol{a}_y$]

B.6.6 A uniform plane wave has a wavelength of 2 cm in free space and 1 cm in a dielectric ($\mu_r = 1$). Determine the relative permittivity of the dielectric. [$\varepsilon_r = 4$]

B.6.7 A uniform plane wave is propagating in a lossy medium having $\varepsilon_r = 36$, $\mu_r = 4$, and $\sigma = 1$ S/m. The electric field is given by $\boldsymbol{E} = 100e^{-\alpha x}\cos(10\pi\times 10^8 t - \beta x)\boldsymbol{a}_z$. Determine α, β, and $\hat{\eta}$, and write a time-domain expression for the associated magnetic field vector.

$$\Big[\alpha = 57.2,\ \ \beta = 138\ \ \text{rad/m},\ \ \hat{\eta} = 106\underline{/225^\circ},$$
$$\boldsymbol{H} = -0.946e^{-57.2x}\ \cos(10\pi \times 10^8 t - 138x - 22.5^\circ)\,\boldsymbol{a}_y\Big]$$

B.6.8 Determine the phase velocity of propagation, attenuation constant, phase constant, and intrinsic impedance of a uniform plane wave traveling in wet, marshy soil ($\sigma \cong 10^{-2}$ S/m, $\varepsilon_r \cong 15$, $\mu_r = 1$) at 60 Hz (power frequency), 1 MHz (AM radio broadcast frequency), 100 MHz (FM radio broadcast frequency), and 10 GHz (microwave radio relay frequency).

$$[\text{(a)}\ \alpha = 1.54 \times 10^{-3}, \beta = 1.54 \times 10^{-3}\ \ \text{rad/m}, v = \omega/\beta$$
$$= 2.45 \times 10^5\ \ \text{m/s}, \hat{\eta} = 0.22\underline{/45^\circ},\ \ \text{(b)}\ \alpha = 0.19, \beta$$
$$= 0.21\ \ \text{rad/m}, v = \omega/\beta = 3.03 \times 10^7\ \ \text{m/s}, \hat{\eta}$$
$$= 28.05\underline{/42.62^\circ}, \text{(c)}\ \alpha = 0.49, \beta = 8.13\ \ \text{rad/m}, v = \omega/\beta$$
$$= 7.73 \times 10^7\ \ \text{m/s}, \hat{\eta} = 96.99\underline{/3.42^\circ}, \text{(d)}\ \alpha = 0.49, \beta$$
$$= 811.2\ \ \text{rad/m}, v = \omega/\beta = 7.75 \times 10^7\ \ \text{m/s}, \hat{\eta} = 97.34\underline{/0.03^\circ}]$$

B.6.9 If a material has $\sigma = 2$ S/m, $\varepsilon_r = 9$, $\mu_r = 16$, and at a frequency of 1 GHz, calculate the attenuation constant, phase constant, velocity of propagation, and intrinsic impedance.
$[\alpha = 314.06, \beta = 402.25\ \ \text{rad/m}, \sigma$
$= 1.56 \times 10^7\ \ \text{m/s}, \hat{\eta} = 247.55\underline{/37.98^\circ}]$

B.6.10 Write a time-domain expression for the electric field of a uniform plane wave in a lossy dielectric ($\mu_r = 1$) if the magnetic field is given by $\boldsymbol{H} = 0.1e^{-200y}\cos(2\pi \times 10^{10}t - 300y)\,\boldsymbol{a}_x$.

$$[\boldsymbol{E} = 21.9e^{-200y}\ \cos(2\pi \times 10^{10}t - 300y + 33.69^\circ)\ \boldsymbol{a}_z]$$

B.6.11 A 10 MHz uniform plane wave is traveling in the $+z$ direction in a lossless dielectric having $\varepsilon_r = 5$. A 10 V/m electric field is directed in the $+y$ direction. Determine the average power crossing a surface in the xy plane bounded by (3, 2, 2), (3, −1, 2), (−1, 2, 2), (−1, −1, 2), where the coordinates are in meters. [3.56 W]

B.6.12 A 200-MHz uniform plane wave is traveling in the $+z$ direction in a lossless dielectric having $\varepsilon_r = 9$. The 0.2-A/m magnetic field is directed in the $+y$ direction. Determine the average power crossing a surface in the xy plane bounded by (0, 0, 0), (0, 5, 0), (3, 5, 0), (3, 0, 0), where the coordinates are in meters. [37.7 W]

B.6.13 A uniform plane wave is propagating in a lossy medium having $\varepsilon_r = 36$, $\mu_r = 4$, $\sigma = 1$ S/m. The electric field is given by $\boldsymbol{E} = 100e^{-\alpha x}\cos(10\pi \times 10^8 t - \beta x)\,\boldsymbol{a}_z$. Determine the average power lost in propagating through a rectangular volume bounded by (0, 0, 0), (0, 2 m, 0), (20 mm, 2 m, 0), (20 mm, 0, 0), (20 mm, 0, 3 m), (20 mm, 2 m, 3 m), (0, 2 m, 3 m), (0, 0, 3 m). [235 W]

B.6.14 A 1 GHz, 1 V/m uniform plane wave is propagating in a lossy material having parameters of $\sigma = 2$ S/m, $\varepsilon_r = 9$, and $\mu_r = 16$ at a frequency of 1 GHz. Determine the average power lost in propagating across a 100 cm^2 surface perpendicular to it and along a depth in the material of 5 mm. [15.2 μW]

B.6.15 Compare the distances required for a uniform plane wave to travel in seawater ($\sigma = 4$ S/m, $\mu_r = 1$, $\varepsilon_r = 81$) in order that the amplitude of the wave is reduced by 80 dB (a factor of 10,000) at the following frequencies: (a) 1 kHz, (b) 10 kHz, (c) 100 kHz, (d) 1 MHz, (e) 10 MHz, (f) 100 MHz. Show that the attenuation of the amplitude in dB is ($-8.69\ \alpha d$). State whether seawater is a good conductor or a good dielectric at each frequency. This illustrates why communication with submarines uses very low frequencies in the kHz range. [Good conductor for all frequencies, (a) 73.3 m, (b) 23.2 m, (c) 7.33 m, (d) 2.32 m, (e) 0.733 m, (f) 23.2 cm]

REFERENCES

1. C. R. Paul and S. A. Nasar, *Introduction to Electromagnetic Fields*, 2nd ed., McGraw-Hill, New York, 1987.
2. C. R. Paul, *Electromagnetics for Engineers: With Applications to Digital Systems and Electromagnetic Interference*, Wiley, Hoboken, NJ, 2004.

APPENDIX C

Computer Codes for Calculating the Per-Unit-Length (PUL) Parameters and Crosstalk of Multiconductor Transmission Lines

This appendix describes several FORTRAN computer programs for computing the per-unit-length parameters of a multiconductor transmission line using the numerical methods described in Section 9.3. These programs are WIDESEP.FOR (which implements the wide separation approximations for wire-type lines given in Section 9.3.2), RIBBON.FOR (which implements the numerical method for ribbon cables described in Section 9.3.3.1), PCB.FOR (which implements the numerical method for printed circuit boards described in Section 9.3.3.2), MSTRP.FOR (which implements the numerical method for coupled microstrip lines described in Section 9.3.3.2), and STRPLINE.FOR (which implements the numerical method for coupled striplines described in Section 9.3.3.2). The upper diagonal of the per-unit-length inductance matrix, $\boldsymbol{L}$, and the upper diagonal of the per-unit-length capacitance matrix, $\boldsymbol{C}$, are printed to a file PUL.DAT. The upper diagonal of the per-unit-length capacitance matrix *with the dielectric removed*, $\boldsymbol{C}_0$, is printed at the end of PUL.DAT but is not used by subsequent programs.

The program SPICEMTL.FOR reads the per-unit-length parameter matrices $\boldsymbol{L}$ and $\boldsymbol{C}$ from PUL.DAT and computes and prints the SPICE (PSPICE) subcircuit model of the transmission line. This subcircuit model is then imbedded into a SPICE (PSPICE) program written by the user to calculate the exact crosstalk for a lossless multiconductor transmission line as described in Appendix D.

All of these programs are included on the CD supplied with this textbook. These programs along with others are described in more detail in C. R. Paul, *Analysis of Multiconductor Transmission Lines*, Wiley-Interscience, New York, 1994 (ISBN 0-471-02080-X).

This CD also contains the compiled codes designated as XXXXX.EXE, which were compiled with the Lahey FORTRAN compiler. These compiled codes are dimensioned to handle

---

Introduction to Electromagnetic Compatibility, Third Edition. Clayton R. Paul, Robert C. Scully, and Mark A. Steffka.

© 2023 John Wiley & Sons, Inc. Published 2023 by John Wiley & Sons, Inc.

three-conductor lines consisting of a total of three conductors, the generator and receptor line conductors, plus the reference conductor. The array dimensions are determined primarily by the number of conductors in the line and are stored in parameters at the beginning of the code (the uncompiled codes XXXX.FOR can be viewed with an ASCII editor). An example is the parameter MSIZE:

```
PARAMETER (MSIZE=99)
```

The user needs to change these parameters in order to handle larger numbers of conductors in the line. Each uncompiled code, XXXX.FOR, contains at its beginning a brief description of the code, the array dimensions, and the names and contents of the required input files and the name of the output file.

C.1 WIDESEP.FOR FOR COMPUTING THE PUL PARAMETER MATRICES OF WIDELY SPACED WIRES

Required Input Files: WIDESEP.IN

Output File: PUL.DAT. The code computes the entries in the per-unit-length inductance matrix, $\boldsymbol{L}$, for three configurations of widely spaced wires in a homogeneous medium described in Section 9.3.2: (a) $(n+1)$ wires (9.18)–(9.20); (b) n wires above an infinite, perfectly conducting ground plane (9.31), (9.32), (9.35); and (c) n wires within an overall circular cylindrical shield (9.36)–(9.38). The per-unit-length capacitance matrix is obtained from $\boldsymbol{C} = \mu_0\mu_r\varepsilon_0\varepsilon_r\boldsymbol{L}^{-1}$ where μ_r and ε_r are the relative permeability and permittivity, respectively, of the homogeneous medium surrounding the wires. These structures are depicted in Fig. C.1. The first data parameter in WIDESEP.IN is the number of wires, n (exclusive of the reference conductor). The type of reference conductor: wire, ground plane, or overall shield is the next input parameter. The type of structure is input to WIDESEP.IN by the reference conductor parameter: 1 = wire, 2 = ground plane, and 3 = overall shield. The relative permittivity and relative permeability of the surrounding homogeneous medium are the next input parameters. The remaining parameters describe the wire radii and their cross-sectional positions.

The first case, n wires with another wire as the reference wire, is depicted in Fig. C.1a. The reference wire is located at the origin of a rectangular coordinate system. There are five pieces of input data in WIDESEP.IN:

1. The number of wires n (exclusive of the reference wire).
2. The reference conductor type (type = 1).
3. The relative permittivity and permeability of the surrounding homogeneous medium.
4. The radius of the reference wire (in mils).
5. The radii of the other wires (in mils) along with their x coordinates (in meters) and y coordinates (in meters).

The last group are input sequentially for each wire: $r_{w1}, x_1, y_1, r_{w2}, x_2\ y_2, \ldots, r_{wn}, x_n, y_n$. The following input file is for three bare 28-gauge stranded (7×36) wires of radius 7.5 mils in a line, separated

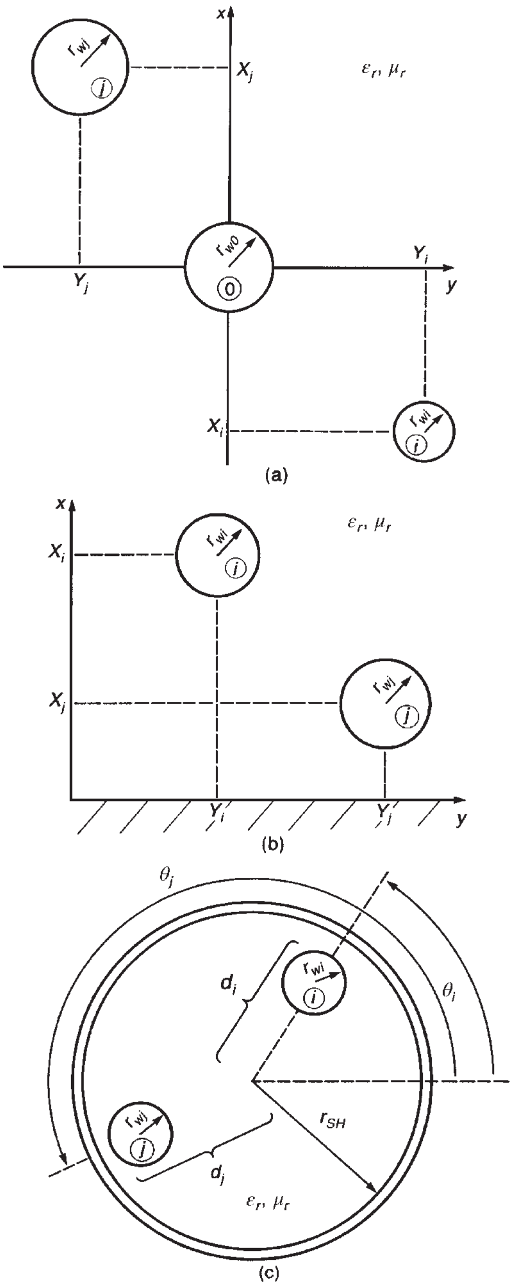
x
r_{wj}
ⓙ
X_j
ε_r, μ_r
r_{w0}
⓪
Y_j
Y_i
y
X_i
r_{wi}
ⓘ
(a)
x
X_i
r_{wi}
ⓘ
ε_r, μ_r
X_j
r_{wj}
ⓙ
Y_i
Y_j
y
(b)
θ_j
d_i
r_{wi}
ⓘ
θ_i
r_{wj}
ⓙ
r_{SH}
d_j
ε_r, μ_r
(c)

FIGURE C.1 Cross-sectional configurations of wire lines for the WIDESEP.FOR FORTRAN program input data: (a) $(n+1)$ wires; (b) n wires above a ground plane; (c) n wires within a cylindrical shield.

by 50 mils (1.27 mm) with the center wire chosen as the reference wire. These were computed by hand in Example 9.1:

```
2        =NUMBER OF WIRES (EXCLUDING REFERENCE
          CONDUCTOR)
1        =REF CONDUCTOR (1=WIRE, 2=GND PLANE, 3=OVERALL
          SHIELD)
1.0      =RELATIVE PERMITTIVITY ER OF HOMOGENEOUS
          MEDIUM
1.0      =RELATIVE PERMEABILITY MUR OF HOMOGENEOUS
          MEDIUM
7.5      =REF WIRE RADIUS OR SHIELD INTERIOR RADIUS
          (mils)
1        =WIRE #1
7.5       =RADIUS OF WIRE #1 (mils)
-1.27E-3 =    1=X1(meters), 2=H1(meters), 3=D1(mils)
0.       =    1=Y1(meters), 2=Y1(meters), 3=THETA1
               (degrees)
2         =WIRE #2
7.5       =RADIUS OF WIRE #2 (mils)
1.27E-3  =    1=X2(meters), 2=H2(meters), 3=D2(mils)
0.       =    1=Y2(meters), 2=Y2(meters), 3=THETA2
               (degrees)
```

The output file is PUL.DAT:

```
1    1     7.58848E-07       =L(  1,   1)
1    2     2.40795E-07       =L(  1,   2)
2    2     7.58848E-07       =L(  2,   2)
1    1     1.63040E-11       =C(  1,   1)
1    2    -5.17352E-12       =C(  1,   2)
2    2     1.63040E-11       =C(  2,   2)


NUMBER OF WIRES= 2
RELATIVE PERMITTIVITY OF HOMOGENEOUS MEDIUM= 1.0
RELATIVE PERMEABILITY OF HOMOGENEOUS MEDIUM= 1.0
REFERENCE CONDUCTOR IS A WIRE WITH RADIUS (mils)= 7.500E+00

WIRE #    WIRE RADIUS     X COORDINATE        Y COORDINATE
            (mils)          (meters)            (meters)
1             7.500E+00      -1.270E-03           0.000E+00
2             7.500E+00       1.270E-03           0.000E+00
```

The second case, *n* wires above an infinite ground plane as the reference conductor, is depicted in Fig. C.1b. The ground plane forms the *y* coordinate axis ($x = 0$) of a rectangular coordinate system. There are four pieces of input data in WIDESEP.IN:

1. The number of wires *n*.
2. The reference conductor type (type = 2).
3. The relative permittivity and permeability of the surrounding homogeneous medium.

4. The radii of the other wires (in mils) along with their x coordinates (height above ground) (in meters) and y coordinates (in meters).

The last group are again input sequentially for each wire: r_{w1}, h_1, y_1, r_{w2}, h_2, y_2, …, r_{wn}, h_n, y_n. (The radius of a reference wire is again input but not read by the code.) The following input file is for Example 9.2, as well as Section 9.6.1, Fig. 9.48. The wires are 20-gauge solid wires with radii of 7.5 mils and are separated by 2 cm and are positioned 2 cm above the ground plane:

```
2        =NUMBER OF WIRES (EXCLUDING REFERENCE CONDUCTOR)
2        =REF CONDUCTOR (1=WIRE, 2=GND PLANE, 3=OVERALL
          SHIELD)
1.0      =RELATIVE PERMITTIVITY ER OF HOMOGENEOUS MEDIUM
1.0      =RELATIVE PERMEABILITY MUR OF HOMOGENEOUS MEDIUM
16.      =REF WIRE RADIUS OR SHIELD INTERIOR RADIUS (mils)
1        =WIRE #1
16.      =RADIUS OF WIRE #1 (mils)
2.E-2    =  1=X1(meters), 2=H1(meters), 3=D1(mils)
0.       =  1=Y1(meters), 2=Y1(meters), 3=THETA1(degrees)
2.       =WIRE #2
16.      =RADIUS OF WIRE #2 (mils)
2.E-2    =  1=X2(meters), 2=H2(meters), 3=D2(mils)
2.E-2    =  1=Y2(meters), 2=Y2(meters), 3=THETA2(degrees)
```

The output file is again PUL.DAT:

```
1     1      9.17859E-07      =L(  1,   1)
1     2      1.60944E-07      =L(  1,   2)
2     2      9.17859E-07      =L(  2,   2)
1     1      1.25068E-11      =C(  1,   1)
1     2     -2.19302E-12      =C(  1,   2)
2     2      1.25068E-11      =C(  2,   2)

NUMBER OF WIRES= 2
RELATIVE PERMITTIVITY OF HOMOGENEOUS MEDIUM= 1.0
RELATIVE PERMEABILITY OF HOMOGENEOUS MEDIUM= 1.0
REFERENCE CONDUCTOR IS A GROUND PLANE
WIRE #        WIRE RADIUS    Y COORDINATE     HEIGHT ABOVE GND
               (mils)          (meters)         (meters)
 1              1.600E+01        0.000E+00         2.000E-02
 2              1.600E+01        2.000E-02         2.000E-02
```

The last case, n wires within an overall shield of radius r_{SH} as the reference conductor, is depicted in Fig. C.1c. There are five pieces of input data in WIDESEP.IN:

1. The number of wires n.
2. The reference conductor type (type = 3).
3. The relative permittivity and permeability of the surrounding homogeneous medium.
4. The (interior) radius of the shield (in mils).
5. The radii of the other wires (in mils) along with their distances from the shield center d_i (in mils) and their angular locations θ_i (in degrees).

The last group are again input sequentially for each wire: r_{w1}, d_1, θ_1, r_{w2}, d_2, $\theta_2 \ldots r_{wn}$, d_n, θ_n. The following input file is for Example 9.3 and consists of two 28-gauge stranded wires (7×36) of radii 7.5 mils at a radius of 15 mils from the center of a shield that has an interior radius of 30 mils. The wires are opposite each other $\theta = 0^\circ$, 180°:

```
2      =NUMBER OF WIRES (EXCLUDING REFERENCE CONDUCTOR)
3      =REF CONDUCTOR (1=WIRE, 2=GND PLANE, 3=OVERALL
        SHIELD)
1.0    =RELATIVE PERMITTIVITY ER OF HOMOGENEOUS MEDIUM
1.0    =RELATIVE PERMEABILITY MUR OF HOMOGENEOUS MEDIUM
30.    =REF WIRE RADIUS OR SHIELD INTERIOR RADIUS (mils)
1      =WIRE #1
7.5    =RADIUS OF WIRE #1 (mils)
15.    =   1=X1(meters), 2=H1(meters), 3=D1(mils)
0.     =   1=Y1(meters), 2=Y1(meters), 3=THETA1(degrees)
2      =WIRE #2
7.5    =RADIUS OF WIRE #2 (mils)
15.    =  1=X2(meters), 2=H2(meters), 3=D2(mils)
180.   =  1=Y2(meters), 2=Y2(meters), 3=THETA2(degrees)
```

The output file is again PUL.DAT:

```
1      1       2.19722E-07         =L(  1,   1)
1      2       4.46287E-08         =L(  1,   2)
2      2       2.19722E-07         =L(  2,   2)
1      1       5.28179E-11         =C(  1,   1)
1      2      -1.07281E-11         =C(  1,   2)
2      2       .28179E-11          =C(  2,   2)

NUMBER OF WIRES= 2
RELATIVE PERMITTIVITY OF HOMOGENEOUS MEDIUM= 1.0
RELATIVE PERMEABILITY OF HOMOGENEOUS MEDIUM= 1.0
REFERENCE CONDUCTOR IS A SHIELD WITH RADIUS (mils)=
3.000E+01
WIRE #     WIRE RADIUS     POSITION          POSITION ANGLE
             (mils)          RADIUS (mils)     (degrees)
1             7.500E+00       1.500E+01         0.000E+00
2             7.500E+00       1.500E+01         1.800E+02
```

The per-unit-length parameter matrices are stored in the output file PUL.DAT. The last items in the PUL.DAT files simply restate the input parameters and are not read by the subsequent application program.

C.2 RIBBON.FOR FOR COMPUTING THE PUL PARAMETER MATRICES OF RIBBON CABLES

Required Input File: RIBBON.IN

Output File: PUL.DAT. Consider the general *N*-wire ribbon cable shown in Fig. C.2. The line consists of *N* identical, dielectric-insulated wires. The wire radii are denoted in the code as RW,

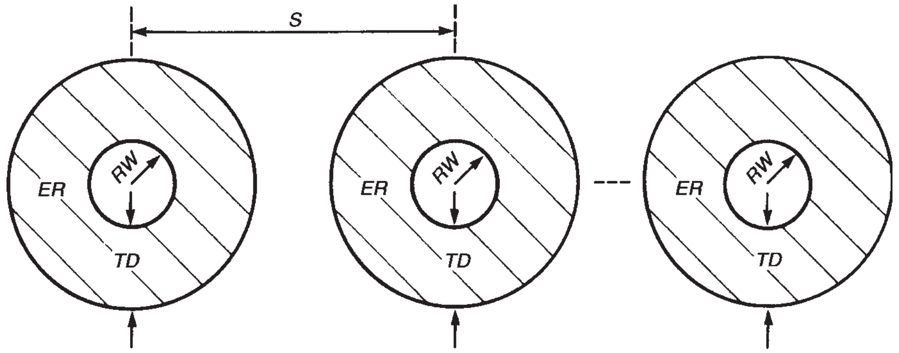

FIGURE C.2 Cross-sectional definition of the ribbon cable parameters for the RIBBON.FOR FORTRAN program input data.

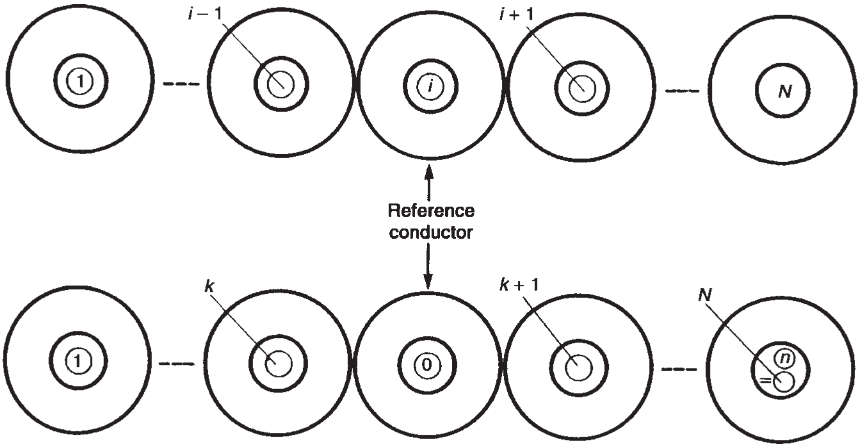

FIGURE C.3 Illustration of the numbering scheme for determining the transmission-line capacitance matrix from the generalized capacitance matrix for a ribbon cable.

the insulation thicknesses are denoted by TD, and the identical adjacent wire spacings are denoted as S. The relative permittivity of the wire insulations is denoted by ER in the code. These data are contained in the input file RIBBON.IN. The per-unit-length parameter matrices are stored in the output file PUL.DAT. The last items in the PUL.DAT files simply restate the input parameters and are not read by the subsequent application program. The scheme for designating the reference wire is illustrated in Fig. C.3. The wires are numbered left to right from 1 to N. With this numbering the reference wire is chosen and then the wires are renumbered left to right from 1 to $N-1=n$.

The following input file, RIBBON.IN, is for the problem of Section 9.4.1.2 and Fig. 9.29, where three identical 28-gauge stranded (7 × 36) wires having radii of 7.5 mils and insulation thicknesses of 10 mils and whose relative permittivity is 4.7, are spaced by 50 mils. The center wire is chosen as the reference wire.

```
3     =TOTAL NUMBER OF WIRES
20    =NUMBER OF FOURIER COEFFICIENTS
2     =NUMBER OF REFERENCE WIRE
7.5   =WIRE RADIUS (mils)
```

```
10.    =INSULATION THICKNESS (mils)
3.5    =RELATIVE DIELECTRIC CONSTANT OF INSULATION
50.    =ADJACENT WIRE SEPARATION (mils)
```

Twenty Fourier expansion coefficients are used to represent the charge distributions around each conductor-dielectric boundary, and 20 coefficients are used to represent the bound-charge distributions around the dielectric-free space boundary.

The output is in PUL.DAT:

```
1     1       7.48501E-07        =L(  1,   1)
1     2       2.40801E-07        =L(  1,   2)
2     2       7.48501E-07        =L(  2,   2)
1     1       2.49819E-11        =C(  1,   1)
1     2      -6.26613E-12        =C(  1,   2)
2     2       2.49819E-11        =C(  2,   2)
1     1       1.65812E-11        =C0(  1,   1)
1     2      -5.33434E-12        =C0(  1,   2)
2     2       1.65812E-11        =C0(  2,   2)
NUMBER OF WIRES= 3
NUMBER OF FOURIER COEFFICIENTS= 20
REFERENCE WIRE= 2
WIRE RADIUS (mils)= 7.500E+00
DIELECTRIC INSULATION THICKNESS (mils)= 1.00E+01
DIELECTRIC CONSTANT OF INSULATION= 3.500E+00
CENTER-TO-CENTER SEPARATION (mils)= 5.000E+01
```

C.3 PCB.FOR FOR COMPUTING THE PUL PARAMETER MATRICES OF PRINTED CIRCUIT BOARDS

Required Input File: PCB.IN

Output File: PUL.DAT. This code computes the per-unit-length parameter matrices for a printed circuit board consisting of N lands on one side of a dielectric substrate as shown in Fig. C.4. The lands have identical width W and are assumed of zero thickness. The edge-to-edge spacings are denoted as S. The board thickness is designated as T and the substrate has relative permittivity of ε_r. The scheme for designating the reference land is illustrated in Fig. C.5. The lands are numbered left to right from 1 to N. With this numbering the reference land is chosen and then the lands are renumbered left to right from 1 to $N-1 = n$.

The following input file, PCB.IN, is used in the problem in Appendix D, section D.7.2. The outer land, land 1, is chosen as the reference land and the land widths are 15 mils and assumed zero

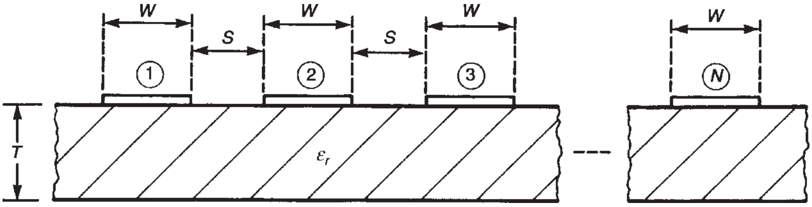

FIGURE C.4 Cross-sectional definition of the printed circuit board parameters for the PCB.FOR FORTRAN program input data.

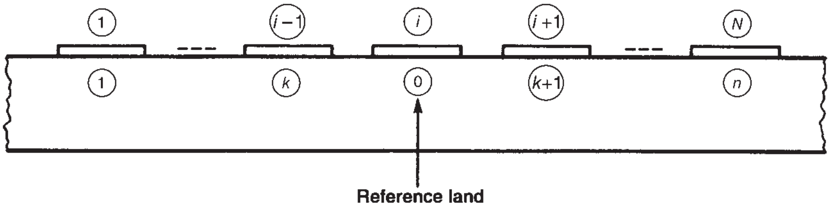

FIGURE C.5 Illustration of the numbering scheme for determining the transmission-line capacitance matrix from the generalized capacitance matrix for a printed circuit board.

thickness. The edge-to-edge separations are 45 mils. The board thickness is 47 mils, and the substrate has a relative permittivity of 4.7. Each land was divided into 30 subsections for the analysis:

```
3      =TOTAL NUMBER OF LANDS
30     =NUMBER OF CONDUCTOR SUBSECTIONS
3      =NUMBER OF REFERENCE LAND
15.0   =LAND WIDTH (mils)
45.0   =EDGE-TO-EDGE LAND SEPARATION (mils)
47.    =BOARD THICKNESS (mils)
4.7    =BOARD RELATIVE DIELECTRIC CONSTANT
```

The output is in PUL.DAT:

```
1     1      1.38315E-06        =L(  1,    1)
1     2      6.91573E-07        =L(  1,    2)
2     2      1.10707E-06        =L(  2,    2)
1     1      2.96949E-11        =C(  1,    1)
1     2     -2.02619E-11        =C(  1,    2)
2     2      4.05238E-11        =C(  2,    2)
1     1      1.16982E-11        =C0(  1,    1)
1     2     -7.30774E-12        =C0(  1,    2)
2     2      1.46155E-11        =C0(  2,    2)


NUMBER OF LANDS=  3
NUMBER OF DIVISIONS PER LAND= 30
REFERENCE LAND=  3
LAND WIDTH (mils)= 1.500E+01
EDGE-TO-EDGE SEPARATION (mils)= 4.500E+01
BOARD THICKNESS (mils)= 4.700E+01
RELATIVE DIELECTRIC CONSTANT= 4.700E+00
```

C.4 MSTRP.FOR FOR COMPUTING THE PUL PARAMETER MATRICES OF COUPLED MICROSTRIP LINES

Required Input File: MSTRP.IN

Output File: PUL.DAT. This code computes the per-unit-length parameter matrices for a coupled microstrip consisting of n lands on one side of a dielectric substrate as shown in Fig. C.6. The reference conductor is a ground plane on the other side of the substrate. The lands have identical width W and are assumed to be of zero thickness. The edge-to-edge spacings are denoted as S. The

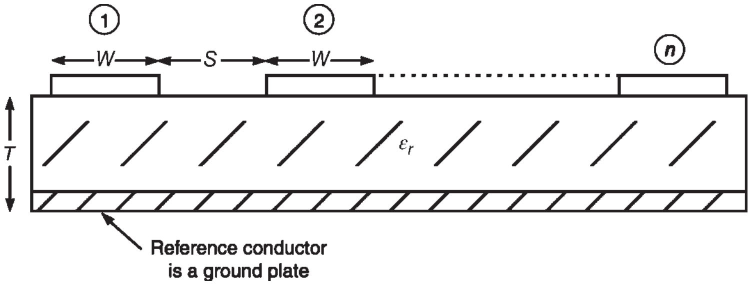

FIGURE C.6 Cross-sectional definition of the coupled microstrip line parameters for the MSTRP.FOR FORTRAN program input data.

board thickness is designated as T, and the substrate has a relative permittivity of ε_r. The following input file, MSTRP.IN, is for the problem in Section 9.4.1.2 and shown in Fig. 9.31. The land widths are 100 mils and assumed to be of zero thickness. The edge-to-edge separations are 100 mils. The board thickness is 62 mils, and the substrate has a relative permittivity of 4.7. Each land was divided into 30 subsections for the analysis:

```
2      =TOTAL NUMBER OF LANDS (EXCLUSIVE OF GND PLANE)
30     =NUMBER OF CONDUCTOR SUBSECTIONS
100.   =LAND WIDTH (mils)
100.   =EDGE-TO-EDGE LAND SEPARATION (mils)
62.    =BOARD THICKNESS (mils)
4.7    =BOARD RELATIVE DIELECTRIC CONSTANT
```

The output file is PUL.DAT:

```
1     1       4.63055E-07        =L(  1,   1)
1     2       9.21843E-08        =L(  1,   2)
2     2       4.63054E-07        =L(  2,   2)
1     1       1.17594E-10        =C(  1,   1)
1     2      -2.34105E-11        =C(  1,   2)
2     2       1.17594E-10        =C(  2,   2)
1     1       2.50201E-11        =C0(  1,   1)
1     2      -4.98097E-12        =C0(  1,   2)
2     2        .50201E-11        =C0(  2,   2)

NUMBER OF LANDS =  2
NUMBER OF DIVISIONS PER LAND = 30
LAND  WIDTH  (mils)=  5.000E+00
EDGE-TO-EDGE SEPARATION (mils)=  5.000E+02
BOARD THICKNESS (mils)= 6.200E+01
RELATIVE DIELECTRIC CONSTANT= 4.700E+00
```

C.5 STRPLINE.FOR FOR COMPUTING THE PUL PARAMETER MATRICES OF COUPLED STRIPLINES

Required Input File: STRPLINE.IN

Output File: PUL.DAT. This code computes the per-unit-length parameter matrices for a coupled stripline consisting of n lands in a dielectric substrate equidistant between two ground planes

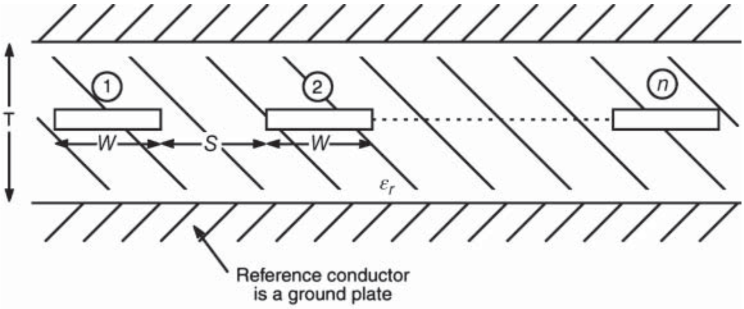

FIGURE C.7 Cross-sectional definition of the coupled stripline parameters for the STRPLINE.FOR FORTRAN program input data.

as shown in Fig. C.7. The lands have identical width *W* and are assumed to be of zero thickness. The edge-to-edge spacings are denoted as *S*. The separation between the ground planes is designated as *T*, and the substrate has a relative permittivity of ε_r. The lands are assumed to be placed equidistant from the ground planes. The following input file, STRPLINE.IN, is for land widths of 5 mils and assumed zero thickness. The edge-to-edge separations are 5 mils. The separation between the two ground planes is 20 mils, and the substrate has a relative permittivity of 4.7. Each land was divided into 30 subsections for the analysis:

```
2      =TOTAL NUMBER OF LANDS (EXCLUSIVE OF GND PLANE)
30.    =NUMBER OF CONDUCTOR SUBSECTIONS
5.     =LAND WIDTH (mils)
5.     =EDGE-TO-EDGE LAND SEPARATION (mils)
20.    =SEPARATION BETWEEN GROUND PLANES (mils)
4.7    =BOARD RELATIVE DIELECTRIC CONSTANT
```

The output file is PUL.DAT

```
1     1     4.63055E-07       =L( 1,  1)
1     2     9.21843E-08       =L( 1,  2)
2     2     4.63054E-07       =L( 2,  2)
1     1     1.17594E-10       =C( 1,  1)
1     2    -2.34105E-11       =C( 1,  2)
2     2     1.17594E-10       =C( 2,  2)
1     1     2.50201E-11       =C0( 1,  1)
1     2    -4.98097E-12       =C0( 1,  2)
2     2     2.50201E-11       =C0( 2,  2)


NUMBER OF LANDS=  2
NUMBER OF DIVISIONS PER LAND= 30
LAND WIDTH (mils)= 5.000E+00
EDGE-TO-EDGE SEPARATION (mils)= 5.000E+00
SEPARATION BETWEEN GROUND PLANES (mils)=  2.000E+01
RELATIVE DIELECTRIC CONSTANT=  4.700E+00
```

APPENDIX D

A SPICE (PSPICE, LTSPICE, etc.) Tutorial and Applications Guide

This Appendix contains brief summaries of the electric circuit analysis program known as SPICE, in particular the older personal computer version PSPICE, and the more recent personal computer version LTSPICE. SPICE is an acronym for *Simulation Program with Integrated-Circuit Emphasis*. The SPICE circuit analysis program or its personal computer version, PSPICE, is a very useful tool for making computations, and for analyzing electric circuit models, plotting their frequency response (Bode plots), analyzing their time-domain behavior, and analyzing the time-domain and frequency-domain responses of transmission lines. We have seen in previous chapters the hand analysis of all these situations in order to gain insight. SPICE can make these sorts of calculations go much faster and provide more immediately available information in comparison. The author highly recommends that the reader become proficient with and use SPICE to analyze circuits.

The original SPICE computer program was developed to analyze complex electric circuits, particularly integrated circuits. It was developed at the University of California at Berkeley in the early 1970s. Note the original SPICE program was developed under US government funding, and it is therefore not proprietary and may be freely copied, used, and distributed. In the first section of this appendix, we will discuss the most common and widely available SPICE2, version G6 code, which was written in FORTRAN. In the second section, we will discuss a recent free version called LTSPICE, from Analog Devices, which uses a graphical user interface to make designs more intuitive. 32-bit and 64-bit versions are available free from www.analog.com for both Windows and MAC OS. The most recent release is version XVII, which contains many predefined electronic components from Analog Devices as well as virtualized components to allow for schematic capture and waveform visualization. Each section provides guidance in entering and executing a SPICE simulation, and several examples are repeated so as to show the comparison between the two approaches. In the third section, we will discuss the application of SPICE to the solution of lumped circuit approximate models. Examples of the original SPICE modeling are provided, and conversion to the more recent LTSPICE version is left as an exercise for the reader.

SPICE was written for use on large mainframe computers of the time. In the 1980s, the MicroSim Corporation developed a personal computer version of SPICE called PSPICE. A number of important modifications were made particularly in the plotting of data via the .PROBE function. Since that time a number of commercial firms have modified and developed their own PC versions. Examples include

---

Introduction to Electromagnetic Compatibility, Third Edition. Clayton R. Paul, Robert C. Scully, and Mark A. Steffka.
© 2023 John Wiley & Sons, Inc. Published 2023 by John Wiley & Sons, Inc.

Micro-CaP, previously offered by Spectrum Software. Micro-Cap is no longer supported, but the last three versions (10, 11, and 12) are still available for download. LTSPICE, discussed in section 2, is now at version 17 and is presently supported and available from Analog Devices, as mentioned previously. Regardless, all of these simulation packages rely on the same core engine as that of the original SPICE code. The MicroSim version of PSPICE was acquired by the OrCAD Corporation, now Cadence Design Systems. A windows-based version known as OrCAD Trial is available free from www.orcad.com. OrCAD Trial provides for free for a limited time a full version of the latest release of OrCAD electronic design software solutions with no functionality limitations, including OrCAD Capture CIS, OrCAD PSpice Designer, OrCAD PCB Designer Professional, OrCAD Sigrity ERC, and more. A number of books [1–6] detail the use of SPICE and PSPICE.

There are generally two methods of entering and executing a SPICE or PSPICE program. The first method is the Direct Method, described here, where one enters the program code using an ASCII text editor (typically supplied with PSPICE). The second method is the Schematic Method (now called Capture) where the user "draws" the circuit diagram directly on the screen and then executes that program. The Direct Method is generally the most rapid method of solving a problem. The Schematic (Capture) Method has the advantage of visually seeing whether the circuit components are connected as intended.

D.1 CREATING A SPICE OR PSPICE SIMULATION

SPICE and PSPICE write the node voltage equations of an electric circuit. One node, the reference node for the node voltages, is designated the zero (0) node. All circuits must contain a zero node. The other nodes in the circuit are labeled with numbers or letters. For example, a node may be labeled 23, or it may be labeled FRED. The voltages with respect to the reference (zero) node are positive at the node and denoted as V(N1), V(N2), etc. as shown in Fig. D.1. The general structure of any SPICE or PSPICE program is as follows:

1. Title
2. Circuit Description
3. Execution Statements
4. Output Statements
5. END Statement

The first line of the SPICE program is the Title and is not processed by SPICE. It is simply written on the output and any plots. A comment line is started with an asterisk (*) and is also not processed by the program. A line may be continued with a plus sign (+) at the beginning of the following line. The next set of lines, Circuit Description, describes the circuit elements and their values and tells

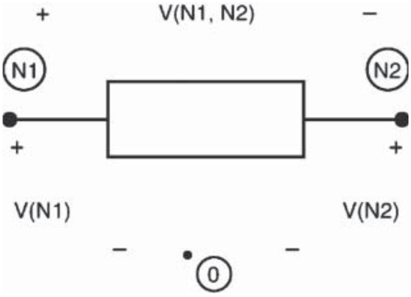

FIGURE D.1 Node voltage and element voltage notation in the SPICE (PSPICE) circuit analysis program.

SPICE how they are connected together to form the circuit. The next set of lines are the Execution Statements that tell SPICE what type of analysis is to be run: dc sources (.DC), sinusoidal steady-state or phasor analysis (.AC), or the full time-domain analysis consisting of the transient and steady-state solution (.TRAN). The next set of statements, Output Statements, tell SPICE what output is desired. The results can be printed to a file with the .PRINT statement or can be plotted with the .PROBE feature. Finally, all programs must end with the .END statement. Actually, the above items 2–4 can appear in any order in the program, but the program must begin with a Title statement and end with the .END statement.

D.1.1 Circuit Description

The basic elements and their SPICE descriptions are shown in Fig. D.2. Figure D.2a shows the independent voltage source. It is named starting with the letter V and then any other letters. For example,

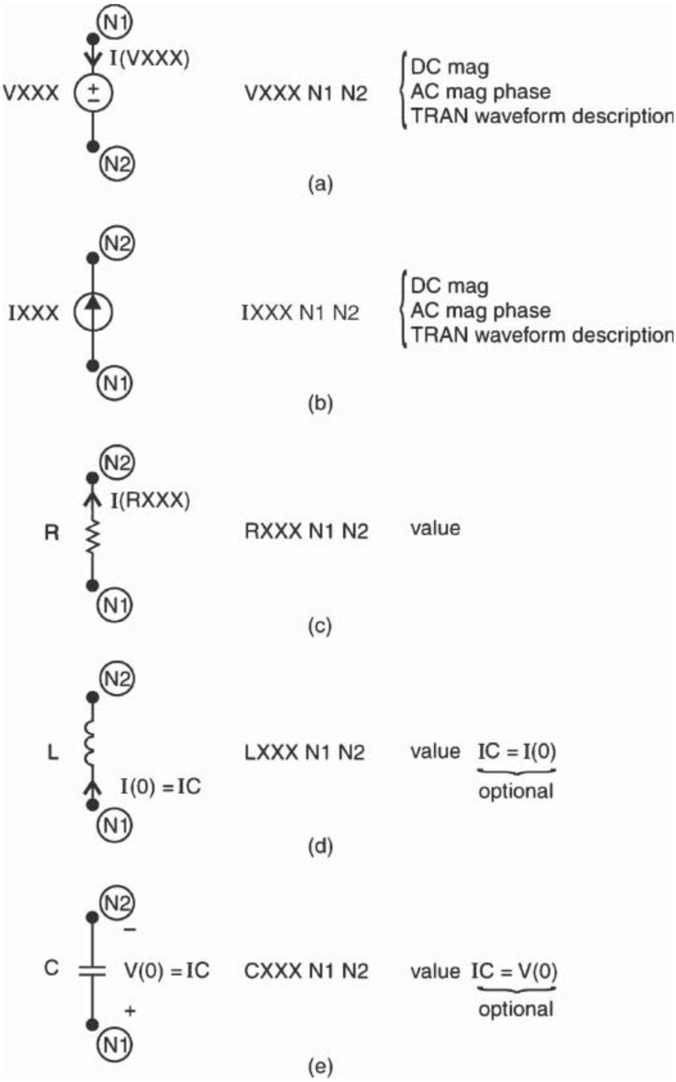
N1
I(VXXX)
VXXX
N2
VXXX N1 N2
DC mag
AC mag phase
TRAN waveform description
(a)
N2
IXXX
N1
IXXX N1 N2
DC mag
AC mag phase
TRAN waveform description
(b)
N2
I(RXXX)
R
N1
RXXX N1 N2
value
(c)
N2
L
I(0) = IC
N1
LXXX N1 N2
value IC = I(0)
optional
(d)
N2
−
C
V(0) = IC
+
N1
CXXX N1 N2
value IC = V(0)
optional
(e)

FIGURE D.2 Coding convention for (a) the independent voltage source, (b) the independent current source, (c) the resistor, (d) the inductor, and (e) the capacitor.

TABLE D.1 Multipliers and the Corresponding SPICE Symbols

Multiplier	SPICE Symbol
10^9	G
10^6 (mega)	MEG
10^3 (kilo)	K
10^{-3} (milli)	M
10^{-6} (micro)	U
10^{-9} (nano)	N
10^{-12} (pico)	P

a voltage source might be called VFRED. It is connected between nodes N1 and N2. It is very important to note that the source is assumed positive at the first-named node. The current through the voltage source is designated as I (VXXX) and is assumed to flow from the first-named node to the last-named node. The source type can be either dc for which we append the terms DC *magnitude*, or a sinusoid, to which we append the terms AC *magnitude phase* (*degrees*). A time-domain waveform is described by several functions that we will describe later, and these descriptions are appended (without the word TRAN). The independent current source is shown in Fig. D.2b. Its name starts with the letter I followed by any other letters. For example, a current source might be designated as ISAD. The current of the source is assumed to flow from the first-named node to the last-named mode. The types of sources are the same as for the voltage source.

The resistor is shown in Fig. D.2c, and its name starts with the letter R, e.g., RHAPPY. The current through the resistor is designated as I(RXXX) and is assumed to flow from the first-named node to the last-named node. SPICE does not allow elements with zero values. Hence, a resistor whose value is 0 Ω (a short circuit) may be represented as having a value of 1E-8 (1×10^{-8}) or any other suitably small value. Similarly, an open circuit may be designated as a resistor having a value of 1E8 or any other suitably large value. SPICE does not allow “floating nodes,” i.e., nodes with no connection. Also, SPICE requires that every source have a dc path to ground.

The inductor is shown in Fig. D.2d and is designated with the letter L, e.g., LTOM. The current through the inductor as well as the initial inductor current at $t = 0^+$, I(0), is assumed to flow from the first-named node to the last-named node. The initial condition can be specified at the end of the statement with IC = I(0). The capacitor is shown in Fig. D.2e and is designated by the letter C, e.g., CME. The initial voltage across the capacitor at $t = 0^+$, V(0), can be specified at the end of the statement with IC = V(0), and this voltage is assumed to be positive at the first-named node.

As shown in Table D.1, all numerical values can be specified in powers of 10 and written in exponential format, e.g., $2 \times 10^{-5} = 2\text{E} - 5$, or by using standard multipliers using standard engineering notation:

For example, 1 mega Ω is written as 1MEG, 1 kΩ is written as 1K, 3 mH is written as 3M, 5 μF is written as 5U, 2 nH is written as 2N, and 7 pF is written as 7P. A 3 Farad capacitor should not be written as 3F since F stands for femto = 10^{-15}. SPICE makes no distinction between uppercase and lowercase letters. Hence, we could write 1 meg, 1k, 3m, 5n, 2n, and 7p.

The four types of controlled sources, G, E, F, and H, are shown in Fig. D.3 along with their descriptions. The polarities of voltage and the currents through the elements conform to the previous rules governing these in terms of the first- and last-named nodes on their description statements. For a current-controlled source, F or H, the controlling current must be through an independent voltage source. Often, we insert a 0 V source to sample the current. Some more recent versions of PSPICE allow the specification of the current through any element as a controlling current. But it is always a simple matter to insert a 0 V voltage source.

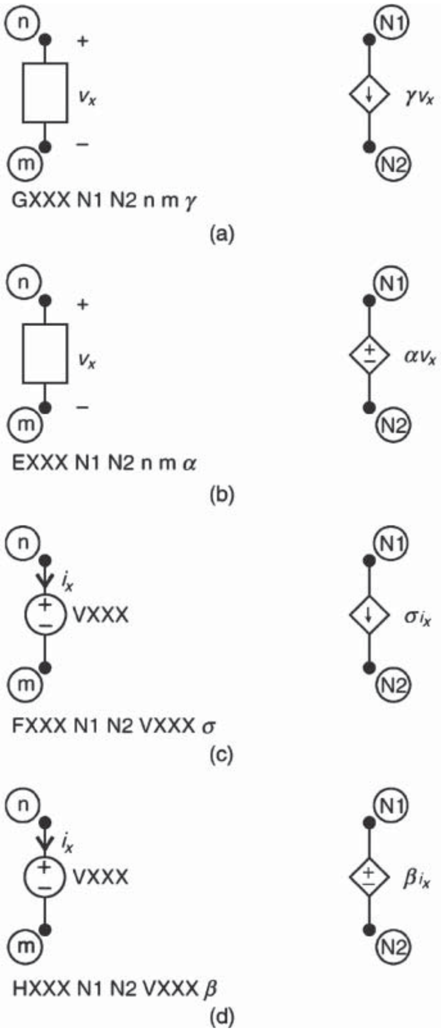
n
+
v_x
–
m
N1
γv_x
N2
GXXX N1 N2 n m γ
(a)
n
+
v_x
–
m
N1
αv_x
N2
EXXX N1 N2 n m α
(b)
n
i_x
VXXX
m
N1
σi_x
N2
FXXX N1 N2 VXXX σ
(c)
n
i_x
VXXX
m
N1
βi_x
N2
HXXX N1 N2 VXXX β
(d)

FIGURE D.3 Coding convention for (a) the voltage-controlled, current source; (b) voltage-controlled, voltage source; (c) the current-controlled, current source; and (d) the current-controlled, voltage source.

Figure D.4 shows how to specify mutual inductance. First the self-inductances that are coupled are specified as before. The mutual inductance is specified in terms of its coupling coefficient:

$$k = \frac{M}{\sqrt{L_1 L_2}}$$

In order to keep the polarities correct, define the self-inductances so that the dots are on the first-named nodes; otherwise a negative coupling coefficient may need to be specified.

Figure D.5 shows the last important element, the transmission line (lossless). There are many ways to specify the important parameters for the line, but the one shown in the figure is the most widely used; specify the characteristic impedance of the line and the line's one-way time delay.

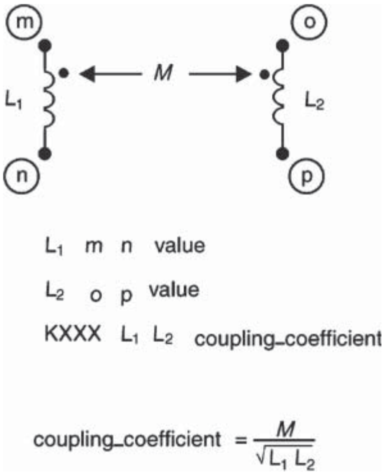
m
o
n
p
M
L1
L2
L1 m n value
L2 o p value
KXXX L1 L2 coupling_coefficient
coupling_coefficient = M / √L1 L2

FIGURE D.4 Coding convention for mutual inductance between two coupled inductors.

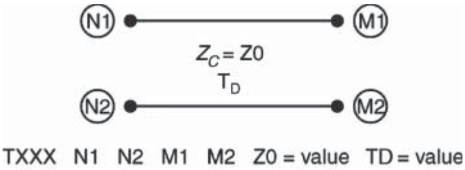
N1
M1
N2
M2
Zc = Z0
TD
TXXX N1 N2 M1 M2 Z0 = value TD = value

FIGURE D.5 Coding convention for the two-conductor, lossless transmission line.

Figure D.6 shows how to specify the important time-domain waveforms. Figure D.6a shows the PWL (piecewise-linear) waveform where straight lines are drawn between pairs of points that are specified by their time location and their value. Observe that the function holds the last specified value, V4 in the figure. Figure D.6b shows the periodic pulse waveform. The function specifies a trapezoidal waveform that repeats periodically with period PER (the reciprocal is the fundamental frequency of the waveform). Note that the pulse width, P_W, is not specified between the 50% points of the pulse as convention. The sinusoidal function is specified by

```
SIN(V0 Va [[Freq [[Td [[Df [[Phase]]]]]]]])
```

which gives the waveform

$$x(t) = v0 + Va\ \sin\left(2\pi\left(\text{Freq}(\text{time} - Td) + \frac{\text{Phase}}{360}\right)\right)e^{-(\text{time}-Td)\ Df}$$

Hence, to specify the general sinusoidal waveform

$$x(t) = A\sin(n\omega_0 t + \theta)$$

we would write

```
SIN(0 A nf 0 0 θ)
```

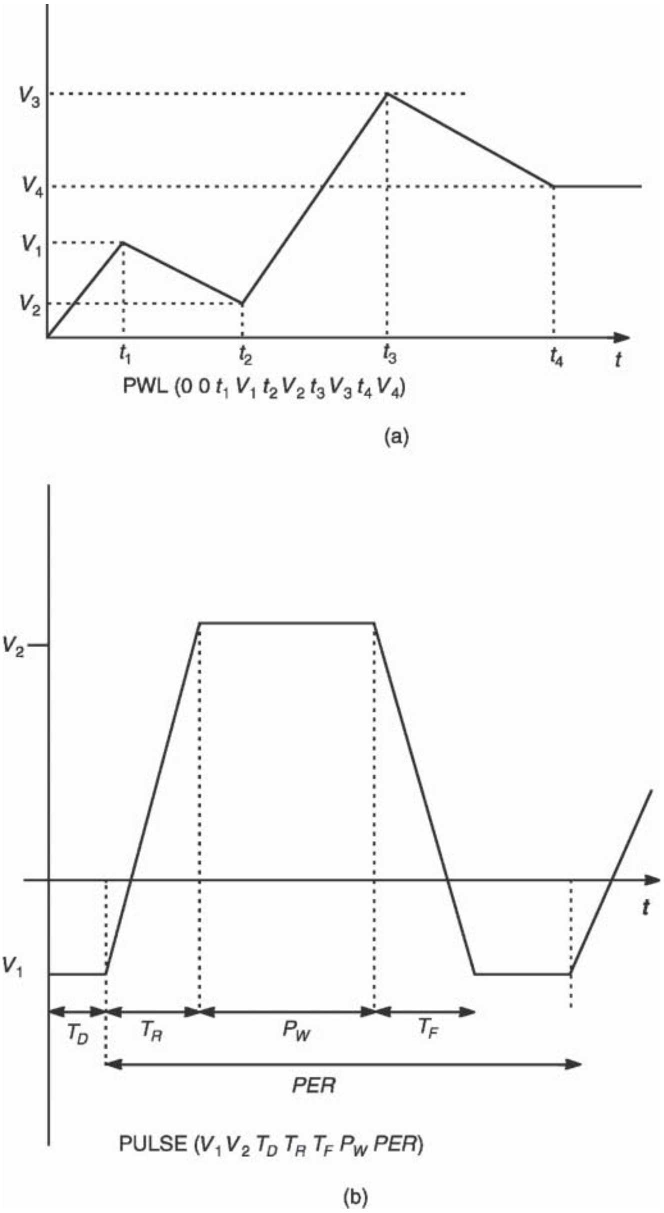
V_3
V_4
V_1
V_2
t_1
t_2
t_3
t_4
t
PWL (0 0 t_1 V_1 t_2 V_2 t_3 V_3 t_4 V_4)
(a)
V_2
t
V_1
T_D
T_R
P_W
T_F
PER
PULSE (V_1 V_2 T_D T_R T_F P_W PER)
(b)

FIGURE D.6 Coding convention for the important source waveforms: (a) the piecewise-linear waveform; (b) the pulse source waveform (periodic).

D.1.2 Execution Statements

There are three types of solutions: dc, sinusoidal steady state, or phasor, and the full time-domain solution (so-called transient, although it contains both the transient and the steady-state parts of the solution).

The dc solution is specified by

```
.DC V, IXXX start_value end_value increment
```

where V,IXXX is the name of a dc voltage or current source in the circuit whose value is to be swept. For example, to sweep the value of a dc voltage source VFRED from 1 to 10 V in increments of 2 V and solve the circuit for each of these source values, we would write

```
.DC VFRED 1 10 2
```

If no sweeping of any source is desired, then we simply choose one dc source in the circuit and iterate its value from the actual value (5 V) to the actual value and use any nonzero increment.

For example

```
.DC VFRED 5 5 1
```

The sinusoidal steady-state or phasor solution is specified by

```
.AC {LIN,DEC,OCT} points start_frequency end_frequency
```

where LIN denotes a linear frequency sweep from *start_frequency* to *end_frequency* and *points* is the total number of frequency points. DEC denotes a log sweep of the frequency where the frequency is swept logarithmically from the *start_frequency* to the *end_frequency* and *points* is the number of frequency points per decade. OCT is a log sweep by octaves where *points* is the number of frequency points per octave.

The time-domain solution is obtained by specifying

```
.TRAN print_step end_time [no_print_time
[step_ceiling]] [UIC]
```

SPICE solves the time-domain differential equations of the circuit by discretizing the time variable and solving the equations in a bootstrapping manner. The first item, *print_step*, governs when an output is requested. Suppose that the discretization used in the solution is every 2 ms. We might not want to see (in the output generated by the .PRINT statement) an output at every 2 ms but only every 5 ms. Hence, we might set the *print_step* time as 5M. The *end_time* is the final time that the solution is obtained for. The remaining parameters are optional. The analysis always starts at $t = 0$. But we may not wish to see a printout of the solution (in the output generated by the .PRINT statement) until after some time has elapsed. If so we would set the *no_print_time* to that starting time. SPICE and PSPICE have a very sophisticated algorithm for determining the minimum step size for discretization of the differential equations in order to get a valid solution. The default maximum step size is *end_time/*50. However, there are some cases where we want the step size to be smaller than what SPICE would allow in order to increase the accuracy of the solution. This is frequently the case when we use SPICE in the analysis of transmission lines (see Chapters 4 and 9). The *step_ceiling* is the maximum time step size that will be used. Although this gives longer run times, there are cases where we need to do this to generate the required accuracy. The last item UIC means that SPICE is to use the initial capacitor voltage or inductor current specified on these element lines with the IC=command. In a transient analysis, SPICE will compute the initial conditions. If some other initial conditions are required, then we should set these and specify UIC on the .TRAN statement. For example

```
.TRAN 0.1N 20N 0 0.01N
```

would command SPICE to do a time-domain (transient analysis) for times from 0 to 20 ns, print out a solution at every 0.1 ns, start printing to the output file at $t = 0$, and use a time discretization time step no larger than 0.01 ns.

D.1.3 Output Statements

The output statements are either for printing to a file with the .PRINT statement or producing a plotted graph of any waveform with the .PROBE statement. The .PRINT statement has three forms depending on the type of analysis being run. For a DC analysis

```
.PRINT DC V(X) I(R)
```

prints the dc solution for the voltage of node X with respect to the reference node and I(R) prints the dc solution for current through resistor R (defined from the first-named node to the last-named node on the specification statement for resistor R). For a sinusoidal steady-state analysis (phasor solution):

```
.PRINT AC VM(NI) VP(NI) IM(RFRED) IP(RFRED)
```

prints the magnitude and phase of node voltages and currents where the magnitude and phase of the node voltage at node NI are VM(NI) and VP(NI), respectively. For the currents through a resistor RFRED, the magnitude is IM(RFRED) and the phase is IP(RFRED). For the time-domain or so-called transient analysis, the print statement is

```
.PRINT TRAN V(NI) I(RFRED)
```

and prints the solutions at all print solution timepoints for the voltage at node NI with respect to the reference node, and the current through resistor RFRED (defined from the first-named node to the last-named node on the specification statement for resistor RFRED).

In addition, the .FOUR statement computes the expansion coefficients for the (one sided) complex exponential form of the Fourier series (magnitude and phase):

```
.FOUR f0 [output_variable(s)]
```

The .FOUR command can be used only in a.TRAN analysis. The fundamental frequency of the *periodic* waveform to be analyzed is denoted as $f_0 = 1/T$, where T is the period of the waveform. The *output_variable(s)* are the desired voltage or current waveforms to be analyzed, e.g., V(2), I(R1). The phase results are with reference to a sine form of the series:

$$x(t) = c_0 + \sum_{n=1}^{\infty} 2|c_n| \sin(n\omega_0 t + \angle c_n + 90^\circ)$$

Hence when one compares the coefficients $c_n = |c_n| \angle c_n$ computed by hand to those computed with .FOUR, one must add 90° to the hand-calculated phases. There is an important consideration in using the .FOUR command. The portion of the waveform that is analyzed to give the Fourier expansion coefficients is the last portion of the solution time of length one period $1/f_0 = T$. In other words, SPICE determines the coefficients from the waveform between *end_time*–$(1/f_0)$ and *end_time*. Hence, *end_time* on the .TRAN command should be at least one period long. In situations where the solution has a transient portion at the beginning of the solution interval and we want to determine the Fourier coefficients for the steady-state solution, we would run the analysis for several periods to ensure that the solution has gotten into steady state. For example, consider an input signal that is periodic with a period of 2 ns or a fundamental frequency of 500 MHz. An output voltage at, for example, node 4, would also have this periodicity but would have a transient period of some five time constants, say, 5 ns. The following commands would be used to obtain the Fourier coefficients of the steady-state response of the node voltage at node 4:

```
.TRAN 0.1N 20N
.FOUR 500MEG V(4)
```

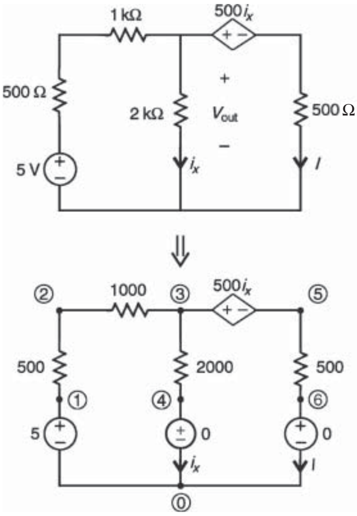

FIGURE D.7 Example D.1.

This would compute the solution for the voltage waveform at node 4 from $t = 0$ to $t = 20$ ns. Since the period (the inverse of 500 MHz) is specified as 2 ns, the portion of the waveform from 18 to 20 ns would be used to compute the Fourier coefficients for the waveform. If we wanted to compute the Fourier coefficients for the initial part of the waveform including the transient, we would specify

```
.TRAN 0.1N 2N
```

which would run for only one period.

All printed output statements are directed to a file named XXXX.OUT if the input file is named XXXX.IN or XXXX.CIR. Plotting waveforms is the greatest enhancement of PSPICE over the original SPICE. This is invoked by simply placing the .PROBE statement in the list. No additional parameters are required. PSPICE stores all variables at all solution timepoints and waits for the user to specify which to plot.

D.1.4 Examples

In this brief tutorial, we have shown the basic commands that one can use to solve the vast majority of electric circuit analysis problems. We have conscientiously tried to minimize the detail and purposely not shown all the possible options in order to simplify the learning. However, there are a myriad of options that can simplify many computations and the reader should consult the references.

Example D.1 Use PSPICE to compute the voltage V_{out} and the current I in the circuit of Fig. D.7.

***Solution*:** The PSPICE coding diagram with nodes numbered is shown in Fig. D.7. Zero-volt voltage sources are inserted to sample the current i_x and I. The PSPICE program is

```
EXAMPLE D.1
VS 1 0 DC 5
R1 1 2 500
R2 2 3 1K
R3 3 4 2K
VTEST1 4 0 DC 0
HSOURCE 3 5 VTEST1 500
```

```
R4 5 6 500
VTEST2 6 0 DC 0
.DC VS 5 5 1
*THE CURRENT I IS I(VTEST2) AND THE VOLTAGE VOUT IS
+V(3) OR V(3,4)
.PRINT DC V(3) I(VTEST2)
.END
```

The result is I=I (VTEST2)=1.875E-3 and the voltage v_{out}=V(3)=2.858E0.

Example D.2 Use PSPICE to plot the frequency response of the band-pass filter shown in Fig. D.8a.

***Solution*:** The nodes are numbered on the circuit diagram, and the PSPICE program is

```
EXAMPLE D.2
VS 1 0 AC 1 0
RES 3 0 100
LIND 1 2 159U
CAP 2 3 1.6P
.AC DEC 50 1MEG 100MEG
.PROBE
*THE MAGNITUDE OF THE OUTPUT IS VM(3) AND THE PHASE
+IS VP(3) .END
```

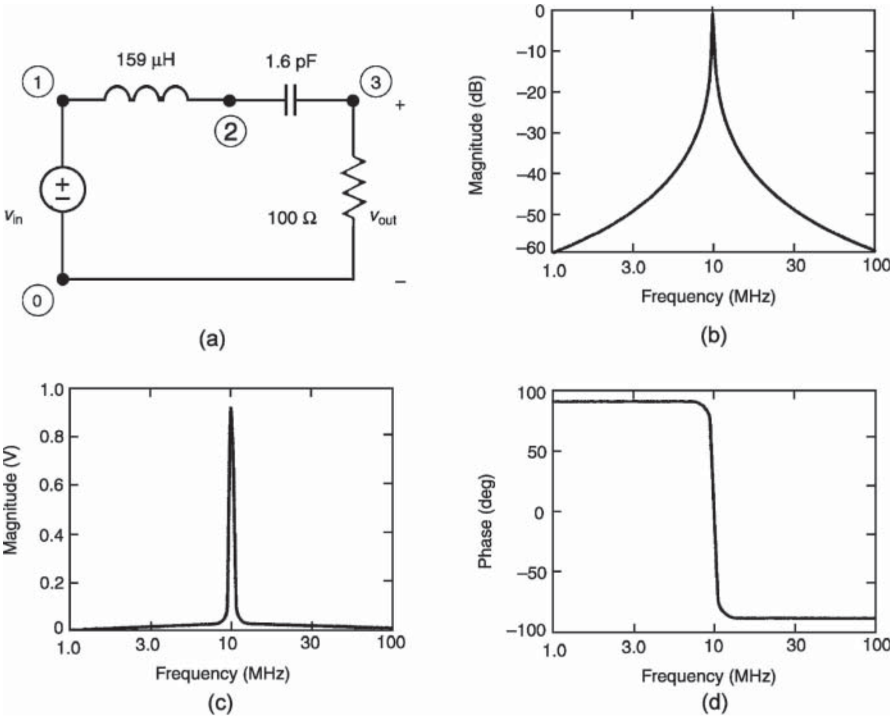

FIGURE D.8 Example D.2: (a) the circuit to be modeled with nodes identified; (b) the magnitude of the output voltage in decibels as a function of frequency; (c) the magnitude of the output voltage in volts as a function of frequency; (d) the phase of the output voltage.

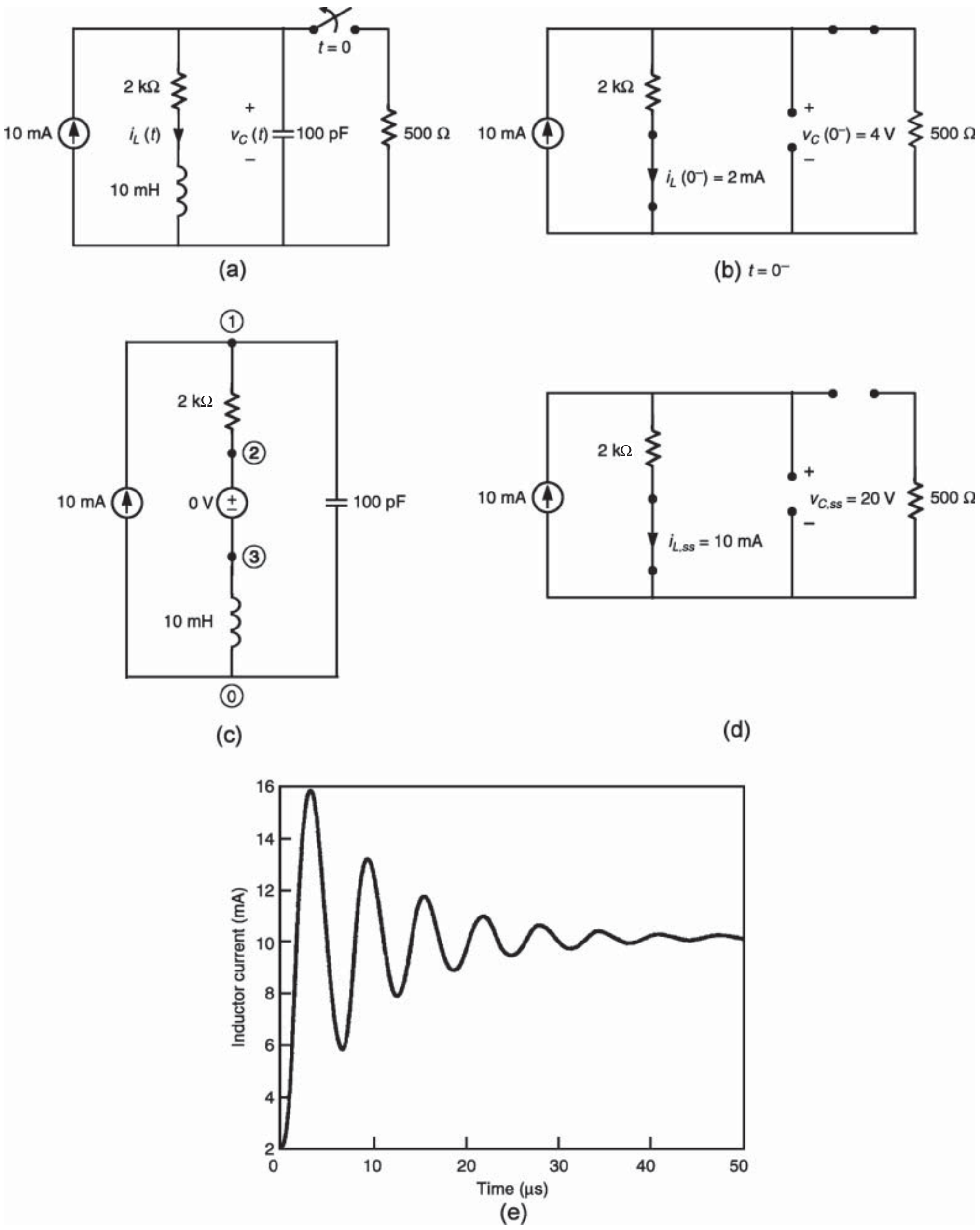
t = 0
2 kΩ
10 mA
$i_L(t)$
+
$v_C(t)$
−
100 pF
500 Ω
10 mH
(a)
2 kΩ
10 mA
+
$v_C(0^-) = 4$ V
−
500 Ω
$i_L(0^-) = 2$ mA
(b) $t = 0^-$
①
2 kΩ
②
10 mA
0 V
③
100 pF
10 mH
⓪
(c)
2 kΩ
10 mA
+
$v_{C,ss} = 20$ V
−
500 Ω
$i_{L,ss} = 10$ mA
(d)
16
14
12
10
8
6
4
2
Inductor current (mA)
0
10
20
30
40
50
Time (μs)
(e)

FIGURE D.9 Example D.3: (a) the circuit to be modeled; (b) the circuit immediately before the switch opens; (c) the PSPICE diagram with the nodes identified immediately before the switch opens; (d) the circuit with the inductor shorted and capacitor open; (e) the inductor current in mA.

The magnitude of the voltage is plotted in Fig. D.8b in decibels using VDB(3), which means

`VDB(3)=20log`$_{10}$`VM(3)`

Figure D.8c shows what we get if we request VM(3): the data are highly compressed outside the band-pass region. The phase is plotted in Fig. D.8d. The resonant frequency is 10 MHz. The phase is +90° below the resonant frequency because of the dominance of the capacitor in this range and is −90° above the resonant frequency, due to the dominance of the inductor in this range. This bears out the important behavior of a series resonant circuit discussed in Chapter 5.

Example D.3 Use PSPICE to plot the inductor current for $t > 0$ in the circuit of Fig. D.9a.

Solution**:** The circuit immediately before the switch opens, i.e., at $t = 0–$, is shown in Fig. D.9b, from which we compute the initial voltage of the capacitor as 4 V and the initial current of the inductor as 2 mA. The PSPICE diagram with nodes numbered is shown in Fig. D.9c, and the PSPICE program is

```
EXAMPLE D.3
IS 0 1 DC 10M
R 1 2 2K
VTEST 2 3
L 3 0 10M IC=2M
C 1 0 100P IC=4
.TRAN .05U 50U 0 .05U UIC
*THE INDUCTOR CURRENT IS I(VTEST) OR I(L)
.PROBE .END
```

We have chosen to solve the circuit out to 50 μs and have directed PSPICE to use a solution time step no larger than 0.05 μs as well as to use the initial conditions given for the inductor and capacitor. The result is plotted using PROBE in Fig. D.9e. The result starts at 2 mA, the initial inductor current, and eventually converges to the steady-state value of 10 mA, which can be confirmed by replacing the inductor with a short circuit and the capacitor with an open circuit in the $t > 0$ circuit as shown in Fig. D.9d.

D.2 CREATING AN LTSPICE SIMULATION

The primary method of entering and executing a SPICE program in LTSPICE is through a graphical user interface, also called Schematic Capture, where a user "draws" the circuit diagram directly on the screen and then executes that program. Other SPICE simulation programs also use a Direct Method, which involves defining a circuit node-by-node through scripting. This Direct Method, while faster, is less intuitive and was discussed in the previous section of this appendix.

At its most fundamental level, LTSPICE Schematic Capture is a lot like drawing a schematic on a piece of paper. Similar schematic symbols are used, and parameters are defined for each component. Common components include resistors, inductors, capacitors, voltage and current sources, and nets, which define points where we can probe our system to view waveforms. For this tutorial, we will focus on an example-based approach and introduce concepts and functions of the program as they are needed.

Example D.4 Use LTSPICE to compute the voltage V_{out} and the current I in the circuit shown in Figure D.7. This should be compared to example D.1 in the previous section.

Solution**:** (Ref. Fig. D.10) The first time you launch LTSPICE you will have an empty workspace. Start a new schematic by selecting *File* menu and then selecting *New Schematic* from the dropdown menu. A blank canvas will appear, and we can start to add our components. We can begin by placing the four resistors above on the schematic. First, click on the resistor icon on the top menu bar and

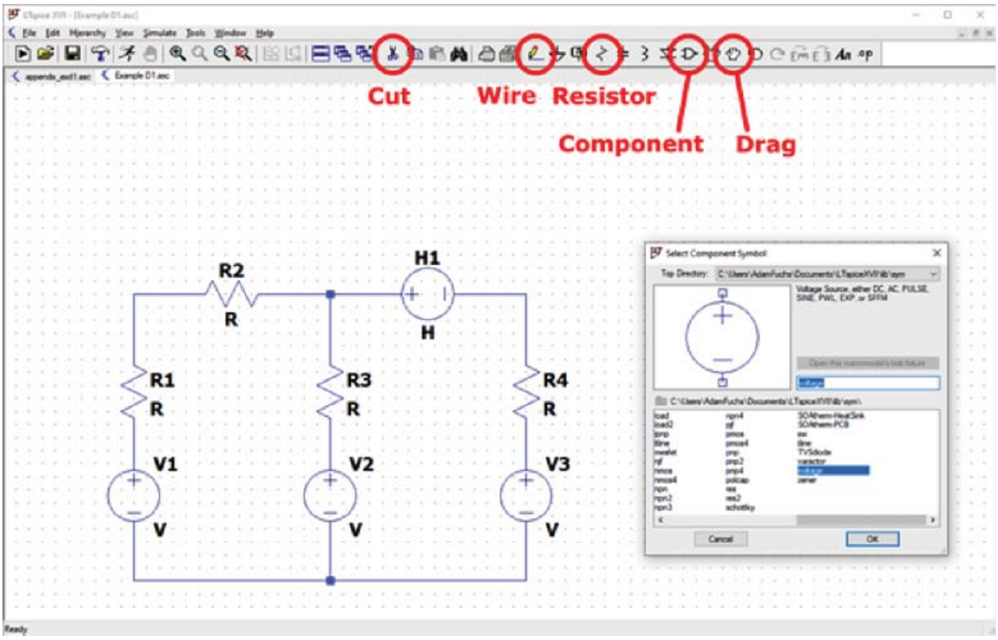

FIGURE D.10 Starting to lay out the schematic.

left click on the schematic to place it. While hovering and deciding where to place a resistor, you can rotate it by pressing *Ctrl* + *R* on the keyboard. As you place the resistors on the schematic LTSPICE will automatically increment the reference designator, in this case R. Next, the 5 V voltage source can be added by pressing the component shortcut. (*Note: most shortcuts we will use for creating the schematic can also be accessed through the Edit menu at the top of the window*). When you select Component, a dialog will appear to *Select Component Symbol*. Scroll all the way to the right and select the "voltage" component, which can act as a source of either AC or DC voltage and other waveforms. Place the voltage source below R1 seen in *Figure 1,* and it will automatically be numbered as V1. Continue to place the rest of the components as shown and note that H1 is labeled as *h* in the Component dialog (it is a *linear current dependent voltage source*). If at some point you make a mistake, you can either remove pieces of your schematic with the *Cut* tool, or you can move them by selecting the *Drag* tool and moving them around.

Next, begin to connect some of the resistors and voltage source together by using the *Wire* tool. When selected, your cursor will turn into a screen-wide cross, signifying that wire mode is enabled. Select and connect all resistors and sources as in the problem statement figure. Notice that as you being to connect components, the blue boxes will disappear. This signifies that the two nodes are successfully connected. Once you have finished making the connections as in the figure above, we can continue to characterize the circuit by assigning values to each component.

Currently, none of the components have any values assigned to them. Right click anywhere on the canvas to turn off any tool you are currently using. Next, right-click on R1 to assign a value to it. We need to assign a value of 500 Ω to this resistor. This can be accomplished by entering "500" in the "Resistance[Ω]:" text box. In this case, we will not need to worry about the tolerance or power rating of the components (Fig. D.11).

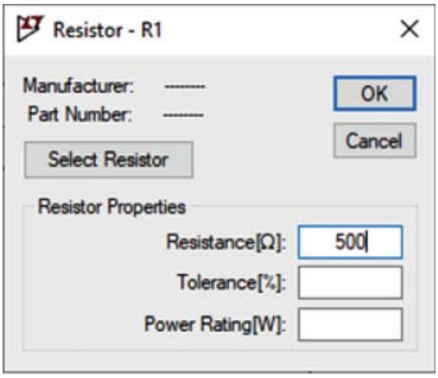

Manufacturer: --------
Part Number: --------
Resistance[Ω]: 500
Tolerance[%]:
Power Rating[W]:

FIGURE D.11 Resistor definition screen.

Note: You can change the magnitude of any value by using the appropriate exponent unit. For example, to enter a 220kΩ resistor, type 220K.

- *K – Kilo* ($\times 10^{3}$)
- *MEG – Mega* ($\times 10^{6}$)
- *G – Giga* ($\times 10^{9}$)
- *T – Tera* ($\times 10^{12}$)
- *M – Milli* ($\times 10^{-3}$)
- *U – Micro* ($\times 10^{-6}$)
- *N – Nano* ($\times 10^{-9}$)
- *P – Pico* ($\times 10^{-12}$)
- *F – Femto* ($\times 10^{-15}$)

When assigning values to the DC power sources, simply input the DC voltage as seen in the problem statement. For V2 input, a DC voltage of 0, as we don't want it to have any impact on the circuit. This voltage source is necessary to include because of LTSPICE's particular use of current-dependent sources.

Important: When assigning the value of H1 (Fig. D.12), be sure to use V2 for Value (or the reference designator of the voltage source attached in series with our 2kΩ resistor). For Value2 input 500, or our scalar. The Linear current dependent voltage source is quite particular in what it can read current from, that is why we had to define the seemingly useless voltage source. The resultant values define the voltage H1 as 500 times the current through R3 and V2. You can then right click on the right side of the table of Value2 under the Vis. column to make it visible in our schematic.

To complete our circuit, we need to define a 0 V reference point. LTSPICE calls this symbol "ground," and although it goes against everything taught in this book, we will continue to call it "ground" in this appendix for the sake of clarity. You can find the "ground" symbol either on the top toolbar, or under Edit -> Place GND. Once the "ground" is placed as in Figure 3, we can begin to define our simulation parameters. To do so, select SPICE Analysis from the Edit menu. This will bring up a list of different types of analysis that can be run on a circuit. For this problem, we will focus on the DC op pnt (DC Operating Point) analysis. Select the DC op pnt tab and press OK to

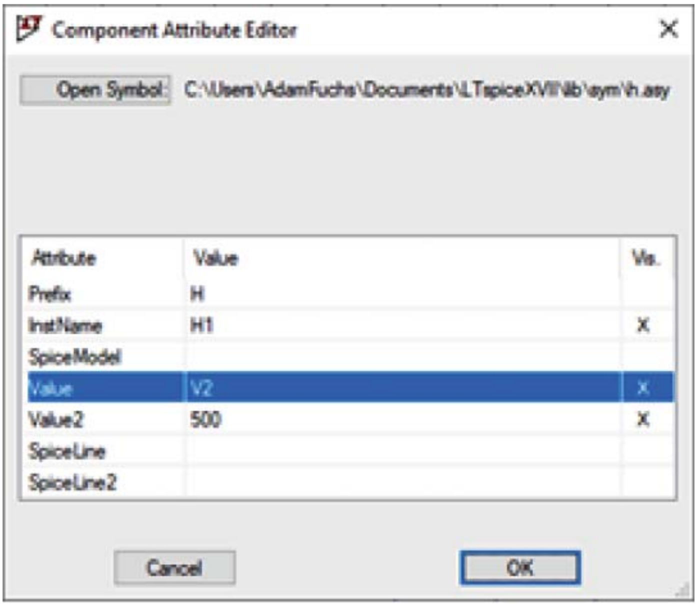

Component Attribute Editor

Open Symbol: C:\Users\AdamFuchs\Documents\LTspiceXVII\lib\sym\h.asy

Attribute	Value	Vis.
Prefix	H	
InstName	H1	X
SpiceModel		
Value	V2	X
Value2	500	X
SpiceLine		
SpiceLine2		

FIGURE D.12 Screen for assigning the value of H1.

place the directive on the circuit. The location does not matter as it is just a directive for our program to run the DC op pnt simulation.

For clarity, it is also a good idea to label each of the important nets in the circuit. We can do so by using the “Label Net” button on the top toolbar and naming a net something descriptive. In this case, we can assign the names 1 through 6 for our important nodes in the circuit. When you enter the name in the form, press OK and you can place the net on a wire where you wish to apply the net name (Fig. D.13). Fig. D.14 illustrates the fully annotated circuit. Fig. D.15 illustrates the “.op” command screen previously discussed.

We are now ready to run the simulation. You can do so by “poking the running man” (pressing the Run button on the left side of the toolbar). What shows up is the results of the DC operating point simulation. Here, we can see the steady-state voltage of each critical node and the current through each component. Each voltage shown is with respect to the “ground” node we defined earlier, so to find the solution to our problem, we need the voltage of Node 3 and the current through R4, which are 1.25V and 1.875mA, respectively (shown as V(3) and I(R4) in Fig. D.16).

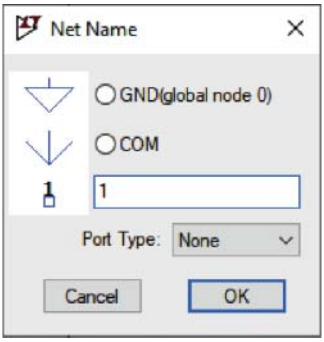

Net Name

○ GND(global node 0)

○ COM

1

Port Type: None

FIGURE D.13 Net name screen.

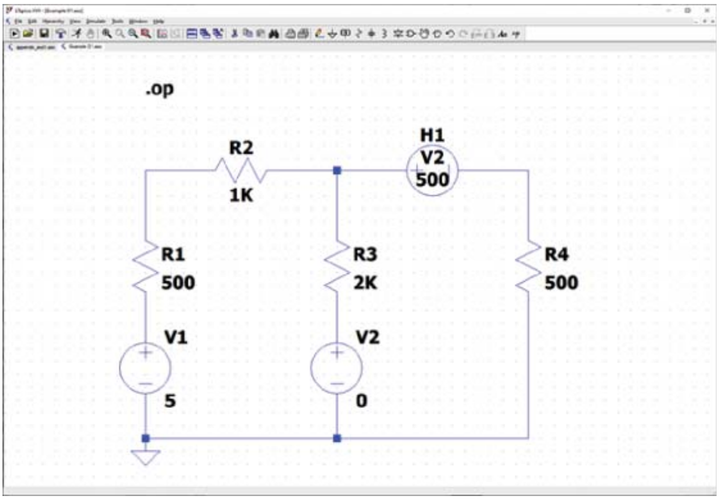
.op
R2
1K
H1
V2
500
R1
500
R3
2K
R4
500
V1
5
V2
0

FIGURE D.14 Fully annotated circuit.

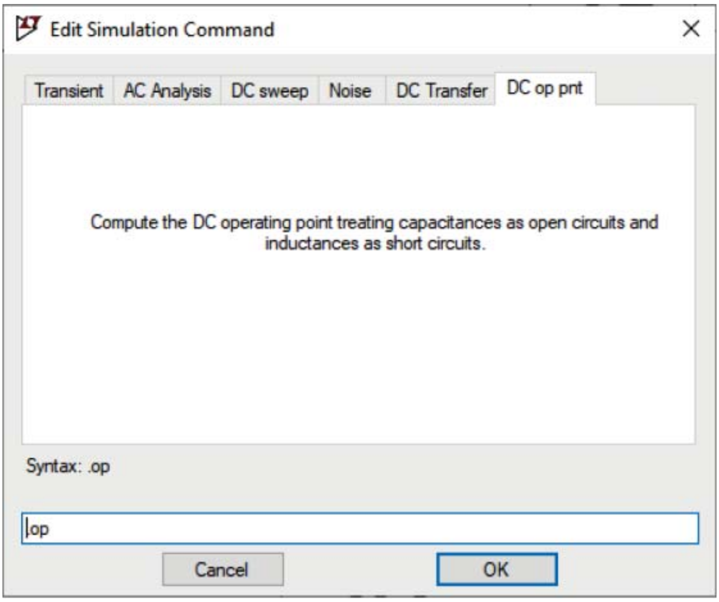
Edit Simulation Command
Transient
AC Analysis
DC sweep
Noise
DC Transfer
DC op pnt
Cancel
OK

Compute the DC operating point treating capacitances as open circuits and inductances as short circuits.

Syntax: .op

.op

FIGURE D.15 Edit simulation command screen.

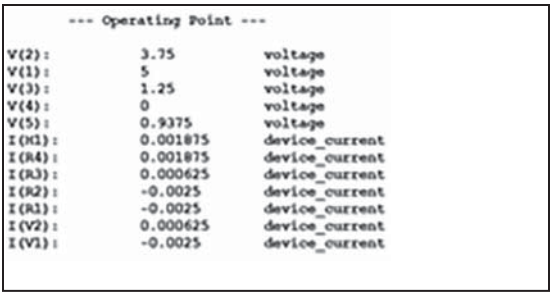

```
       --- Operating Point ---

V(2):          3.75          voltage
V(1):          5             voltage
V(3):          1.25          voltage
V(4):          0             voltage
V(5):          0.9375        voltage
I(H1):         0.001875      device_current
I(R4):         0.001875      device_current
I(R3):         0.000625      device_current
I(R2):         -0.0025       device_current
I(R1):         -0.0025       device_current
I(V2):         0.000625      device_current
I(V1):         -0.0025       device_current
```

FIGURE D.16 Results of DC operating point simulation.

Example D.5 Use LTSPICE to plot the frequency response of the band-pass filter shown in Fig. D.8a.

***Solution*:** When constructing the circuit, we can, for the most part, use the same methodology as in the previous example. L1, C1, V1, and R1 are all basic components found either in the Component or on the top toolbar. When assigning the value of V1 we need to pay special attention due to it being an AC voltage source. In this case, press the "Advanced" button to bring up the full Independent Voltage Source screen. The only field that needs to be entered in this case is the "AC Amplitude." Notice another net is defined in this circuit called VOUT. This net is just an easy way to visualize that the VOUT node is where we want to see the response of our band-pass filter. In this case, select the Port Type to Output to match the example.

Finally, we need to set the simulation settings. Enter the SPICE Analysis options from the Edit menu. To characterize a band-pass filter, we need to find the magnitude of the output voltage at our VOUT node at different frequencies. Fig. D.17 illustrates the configured schematic. Fig. D.18 illustrates the parameter selection screens. This is done in SPICE with an AC Analysis. In this case, the frequency region we are interested in is between 1MHz and 100MHz. We can enter the simulation parameters like so:

By setting the number of points per decade to 50, we ensure that our simulation will not overload the computer with too many calculations. For more precise characterization of a system, it might

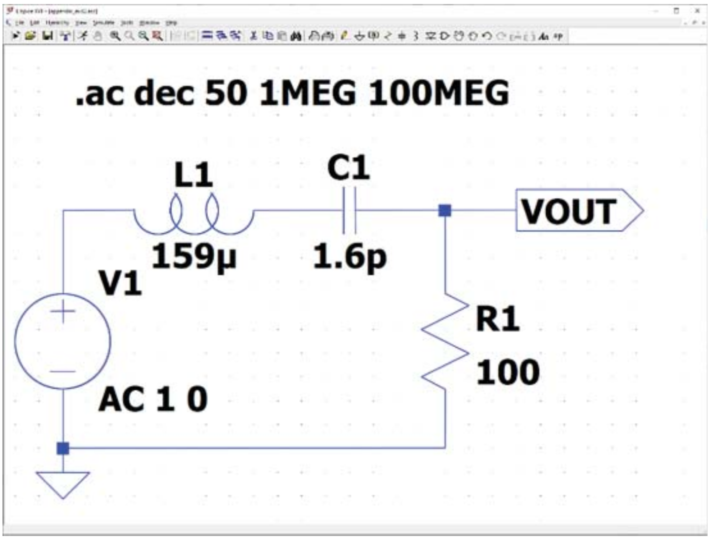

```
.ac dec 50 1MEG 100MEG
```

FIGURE D.17 Circuit from Figure D.8a configured in LTSPICE.

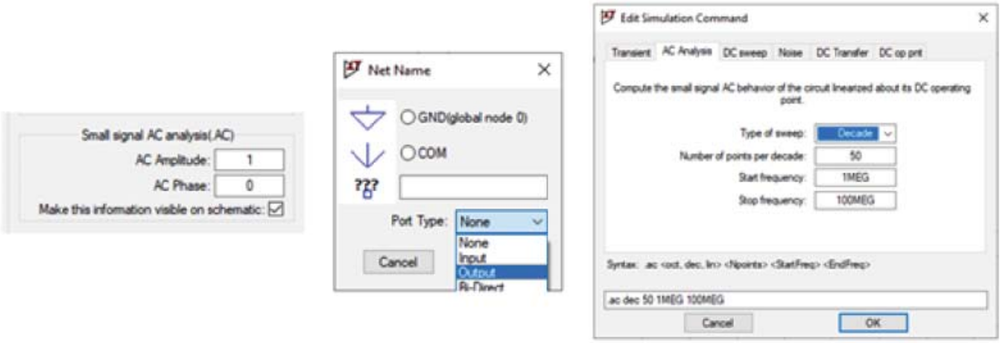

Small signal AC analysis(.AC)
AC Amplitude: 1
AC Phase: 0
Make this information visible on schematic: ☑

Net Name
○ GND(global node 0)
○ COM
Port Type: None
None
Input
Output
Bi-Direct

Edit Simulation Command
Compute the small signal AC behavior of the circuit linearized about its DC operating point.
Type of sweep: Decade
Number of points per decade: 50
Start frequency: 1MEG
Stop frequency: 100MEG
Syntax: .ac <oct, dec, lin> <Npoints> <StartFreq> <EndFreq>

```
.ac dec 50 1MEG 100MEG
```

FIGURE D.18 Simulation parameters for the

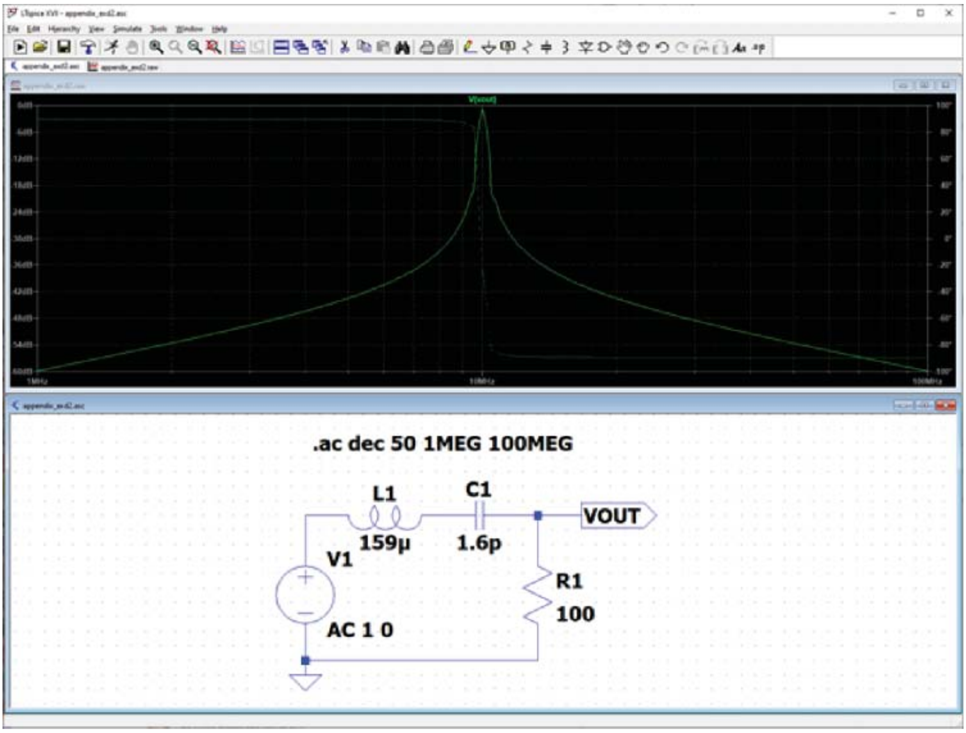

```
.ac dec 50 1MEG 100MEG
```

FIGURE D.19 Plot of VOUT for circuit D.8a.

be beneficial to increase the number of points. Verify that values are entered correctly by making sure that the directive is ".ac dec 50 1MG 100MEG." Place it anywhere on the circuit and "poke the running man" to start the simulation. What you should see is a new blank window. We can populate the graph with data by Left Clicking on the VOUT node. This will graph the magnitude of VOUT across the frequencies we defined in our simulation (Fig. D.19).

In this case, we can see that our system has a cutoff frequency right around 10MHz. You can change the scale of the Y-axis to linear to match your results with Figure D.8c by right clicking on the Y-axis and selecting "Linear" from the available radio switches. Compare the rest of your results to Figure D.8.

Example D.6 Use LTSPICE to plot the inductor current for $t > 0$ in the circuit of Fig. D.9a. The circuit immediately before the switch opens, i.e., at $t = 0^-$, is shown in Fig. D.9b, from which we compute the initial voltage of the capacitor as 4 V and the initial current of the inductor as 2 mA. The LTSPICE diagram with nodes numbered is shown in Fig. D.9c.

Solution**:** To characterize this circuit, it is important to remember that LTSPICE does not magically know the initial conditions of the circuit. This is something that must be explicitly defined through a SPICE Directive. Start by constructing the following circuit (Fig. D.20).

Once defined, select SPICE Directive under the Edit menu and enter the following in the text box provided: ".ic V(C1)=4 I(L1)=2M," ignoring the quotation marks. Press OK and place the directive anywhere on the schematic to apply the initial conditions. This sets the initial conditions (.ic) as 4 V for the voltage across V1 and 2 mA as the current across L1. Next, to see the current through L1 we need to include V1, since LTSPICE does not allow us to plot the current through L1 directly. Since they are in series, it will yield the same result.

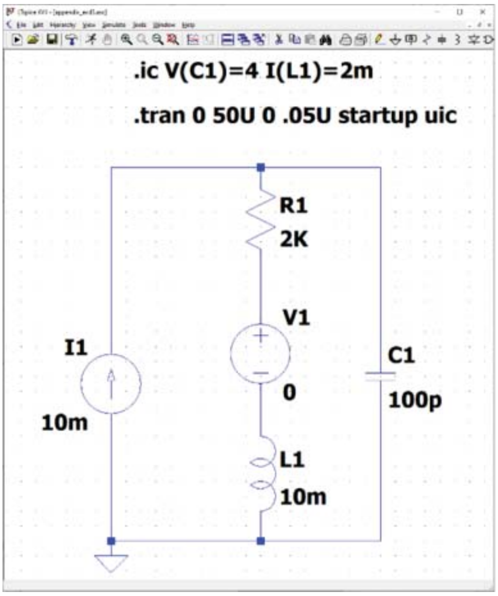

```
.ic V(C1)=4 I(L1)=2m
.tran 0 50U 0 .05U startup uic
```

FIGURE D.20 LTSPICE configured circuit from Figure D.9c.

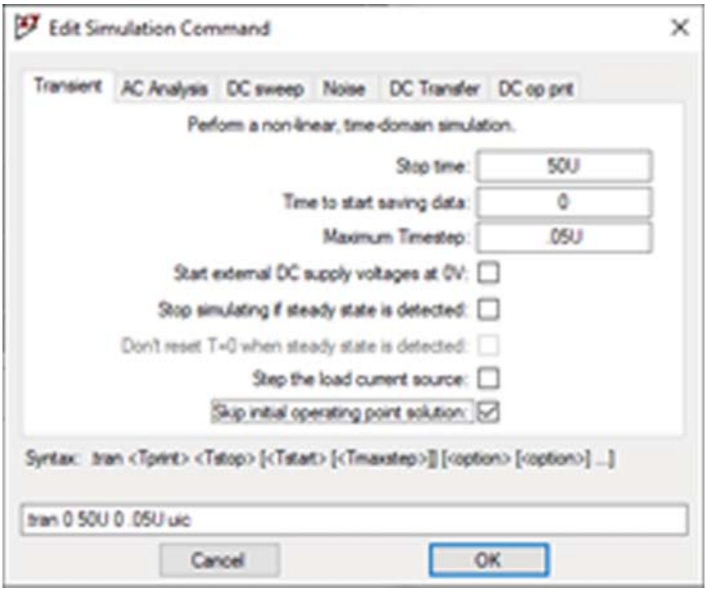

Edit Simulation Command

Perform a non-linear, time-domain simulation.

Stop time: 50U

Time to start saving data: 0

Maximum Timestep: .05U

Start external DC supply voltages at 0V: ☐

Stop simulating if steady state is detected: ☐

Don't reset T=0 when steady state is detected: ☐

Step the load current source: ☐

Skip initial operating point solution: ☑

Syntax: .tran <Tprint> <Tstop> [<Tstart> [<Tmaxstep>]] [<option> [<option>] ...]

```
.tran 0 50U 0 .05U uic
```

FIGURE D.21 Transient simulation screen implementing initial conditions.

To define a time dependent simulation, we will use the transient analysis from the SPICE Analysis menu. A transient analysis is a nonlinear time-domain simulation, which allows us to plot a given signal versus time. Since this circuit will settle rather quickly, we will define our simulation settings to stop the analysis after 50 µs. Fill in the rest of the simulation as shown below and notice that with a maximum timestep of 0.5U, the simulation will record 2500 points and display them. This offers quite a good resolution for such a quick signal. Also, be sure to select the "Skip initial operation point solution" checkbox since we are setting our own initial conditions (Fig. D.21).

When you are ready, “poke the running man” and view the simulation results. You should be able to see that the current settles to 10 mA, which can be analytically confirmed by replacing the capacitor with an open circuit and the inductor with a short circuit, as shown in Figure D9.d.

D.3 LUMPED-CIRCUIT APPROXIMATE MODELS

The SPICE equivalent circuit described in this appendix is an *exact* implementation of the solution of the transmission-line equations for a *lossless* line. A frequently used alternative is the lumped-circuit approximate model. These are similar to those developed for two-conductor lines in Chapter 4, and the lumped-Pi and lumped-T models for three-conductor lines are shown in Fig. D.22. These can be used in lumped-circuit programs such as SPICE for either time-domain or frequency-domain analyses. In these models, we have included the dc resistances of the conductors.

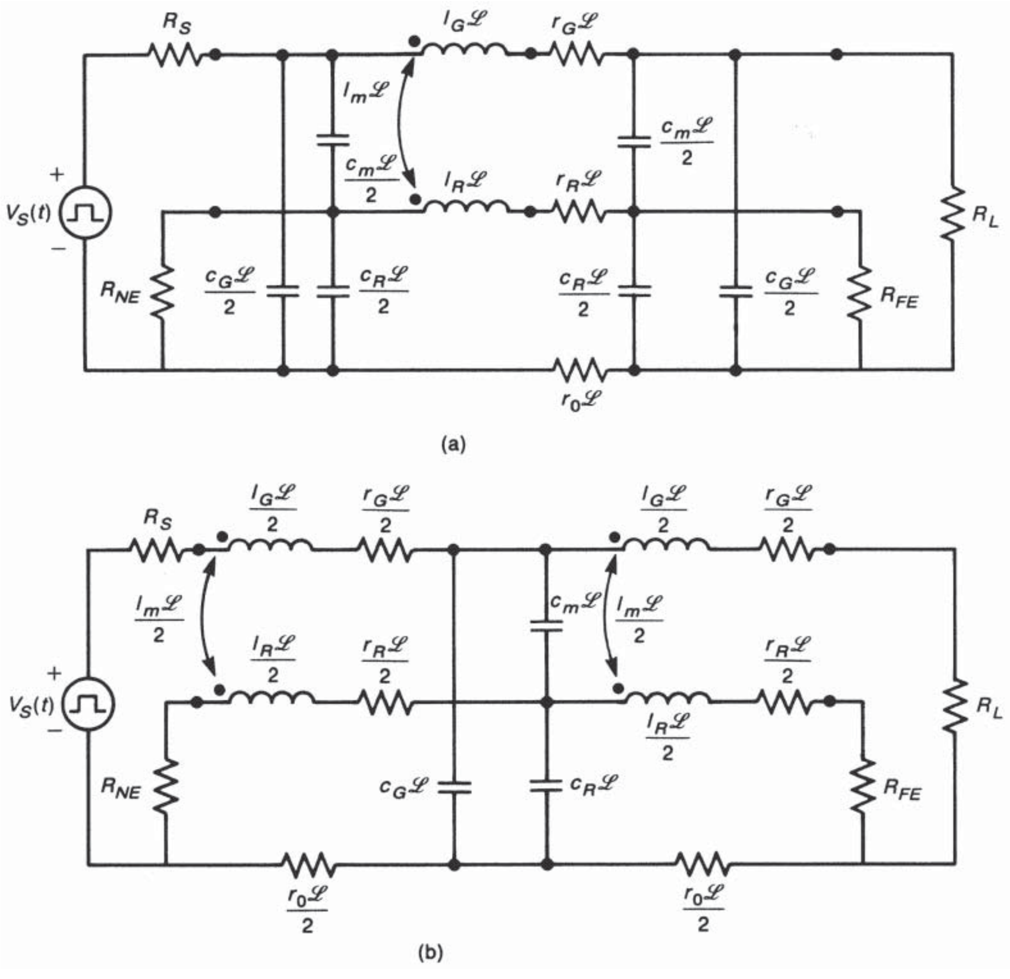
R_S
$l_G\mathcal{L}$
$r_G\mathcal{L}$
$l_m\mathcal{L}$
$\frac{c_m\mathcal{L}}{2}$
$l_R\mathcal{L}$
$r_R\mathcal{L}$
$\frac{c_m\mathcal{L}}{2}$
+
$V_S(t)$
−
R_L
R_{NE}
$\frac{c_G\mathcal{L}}{2}$
$\frac{c_R\mathcal{L}}{2}$
$\frac{c_R\mathcal{L}}{2}$
$\frac{c_G\mathcal{L}}{2}$
R_{FE}
$r_0\mathcal{L}$
(a)
R_S
$\frac{l_G\mathcal{L}}{2}$
$\frac{r_G\mathcal{L}}{2}$
$\frac{l_G\mathcal{L}}{2}$
$\frac{r_G\mathcal{L}}{2}$
$\frac{l_m\mathcal{L}}{2}$
$c_m\mathcal{L}$
$\frac{l_m\mathcal{L}}{2}$
$\frac{l_R\mathcal{L}}{2}$
$\frac{r_R\mathcal{L}}{2}$
$\frac{r_R\mathcal{L}}{2}$
$\frac{l_R\mathcal{L}}{2}$
+
$V_S(t)$
−
R_L
R_{NE}
$c_G\mathcal{L}$
$c_R\mathcal{L}$
R_{FE}
$\frac{r_0\mathcal{L}}{2}$
$\frac{r_0\mathcal{L}}{2}$
(b)

FIGURE D.22 Lumped equivalent circuits for computing crosstalk in a three-conductor line: (a) lumped pi; (b) lumped T.

As an example, consider the ribbon cable shown in Fig. 9.29 that was considered earlier. The frequency-domain predictions of the exact transmission-line model including losses are compared with the predictions of the lumped-Pi model using one and five Pi sections to model the entire line in Fig. D.23. Similar predictions for the coupled microstrip line of Fig. 9.31 are shown in Fig. D.24.

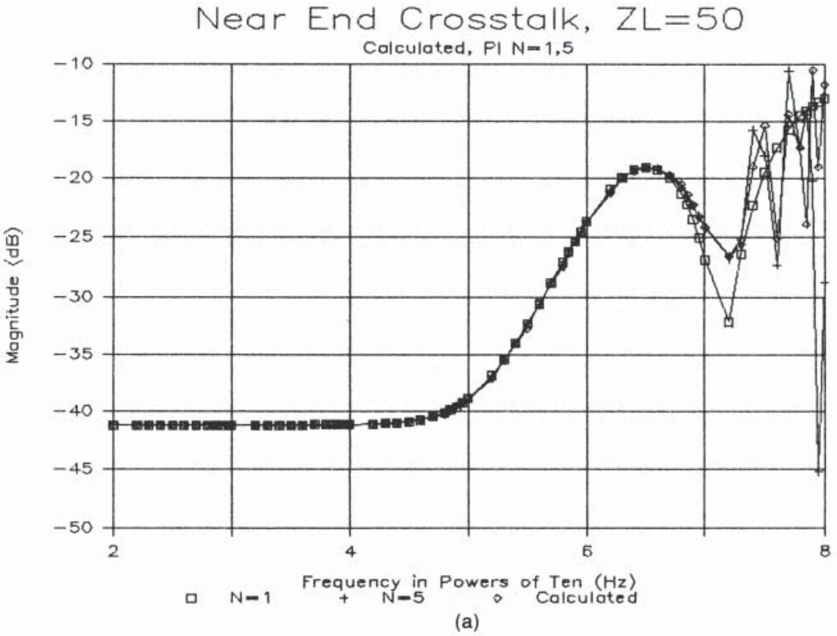

(a)

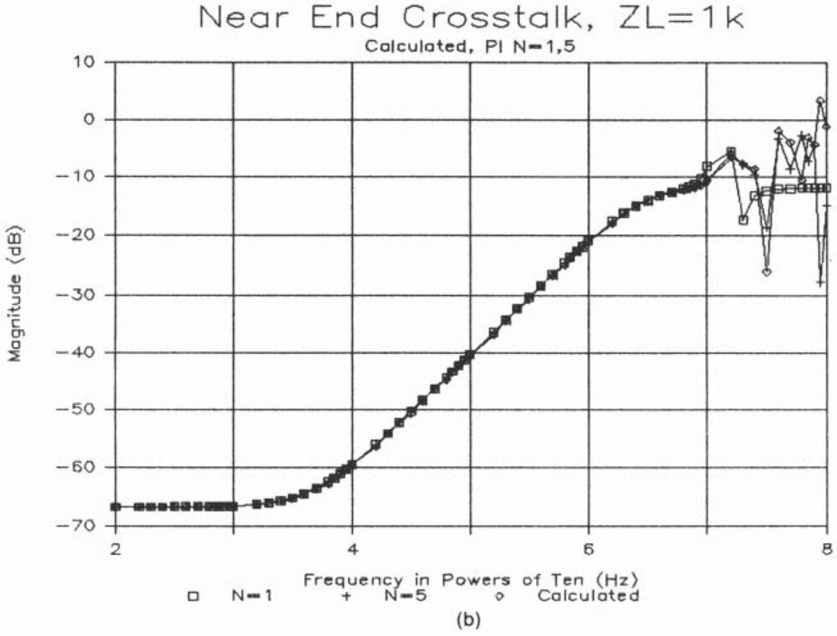

(b)

FIGURE D.23 Predicted crosstalk for the ribbon cable of Fig. 9.29 using the transmission-line model and using the lumped-Pi model with one and five Pi sections for (a) $R = 50\ \Omega$ and (b) $R = 1\ \text{k}\Omega$.

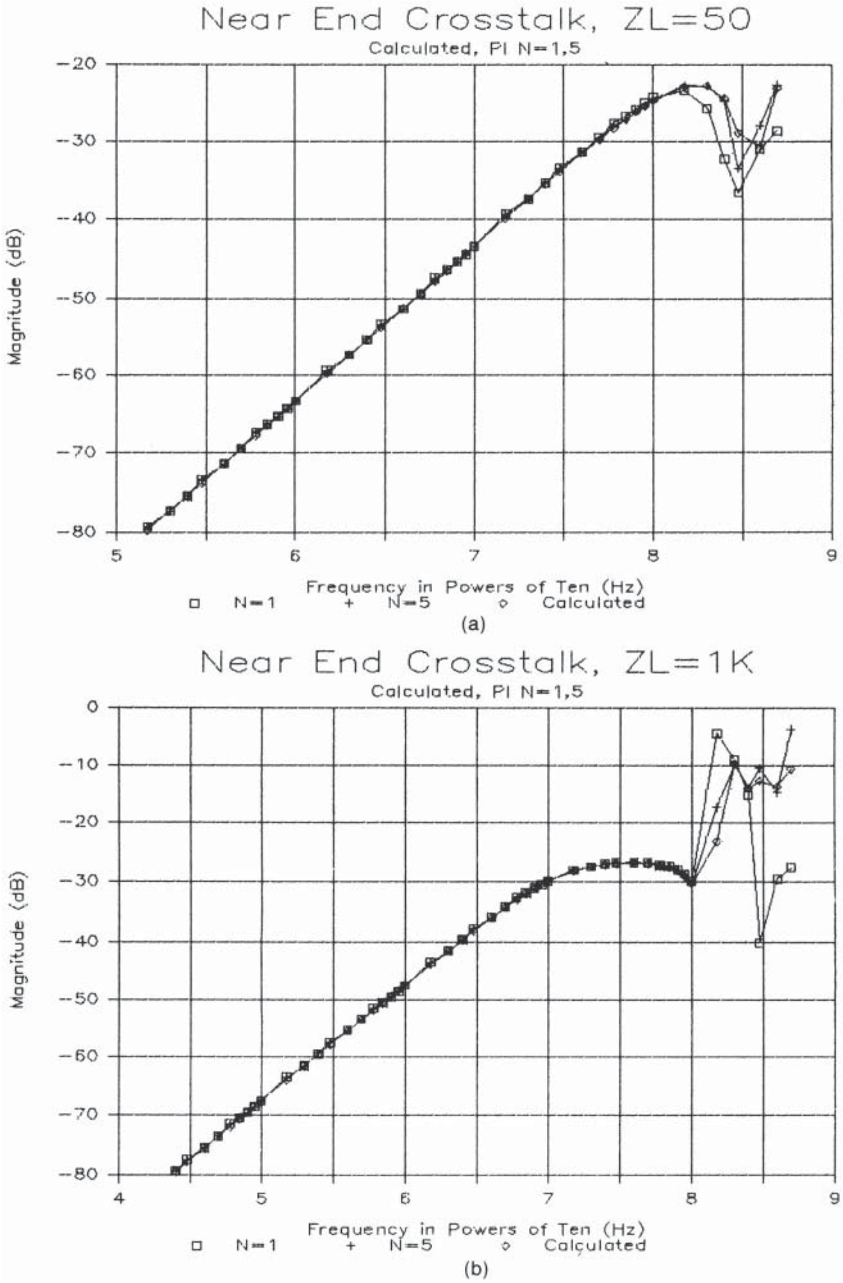

FIGURE D.24 Predicted crosstalk for the printed circuit board of Fig. 9.31 using the transmission-line model and using the lumped-Pi model with one and five Pi sections for (a) $R = 50\ \Omega$ and (b) $R = 1\ \text{k}\Omega$.

A FORTRAN computer program SPICELPI.FOR for producing a SPICE (PSPICE) subcircuit for a lumped-Pi equivalent circuit model of a lossless, multiconductor transmission line is described in this appendix.

D.4 AN EXACT SPICE (PSPICE) MODEL FOR LOSSLESS, COUPLED LINES

In this section, we will give a simple but *exact* solution of the transmission-line equations for *lossless, coupled lines* that is implementable in the SPICE circuit analysis program. This model is implemented in the FORTRAN code SPICEMTL.FOR, described in this appendix. The method will handle lines in homogeneous or inhomogeneous surrounding media. The multiconductor transmission-line equations derived previously can again be written, for *lossless lines*, in matrix form as (variables in bold and not italicized represent matrices)

$$\frac{\partial}{\partial z}\mathbf{V}(z,t) = -\mathbf{L}\frac{\partial}{\partial t}\mathbf{I}(z,t) \tag{D.1a}$$

$$\frac{\partial}{\partial z}\mathbf{I}(z,t) = -\mathbf{C}\frac{\partial}{\partial t}\mathbf{V}(z,t) \tag{D.1b}$$

where the entries in the voltage and current vectors $\mathbf{V}(z, t)$ and $\mathbf{I}(z, t)$ are again given as

$$\mathbf{V}(z,t) = \begin{bmatrix} V_G(z,t) \\ V_R(z,t) \end{bmatrix} \tag{D.2a}$$

and

$$\mathbf{I}(z,t) = \begin{bmatrix} I_G(z,t) \\ I_R(z,t) \end{bmatrix} \tag{D.2b}$$

and

$$\mathbf{L} = \begin{bmatrix} l_G & l_m \\ l_m & l_R \end{bmatrix} \tag{D.3a}$$

and

$$\mathbf{C} = \begin{bmatrix} c_G + c_m & -c_m \\ -c_m & c_R + c_m \end{bmatrix} \tag{D.3b}$$

The key to solving these equations is to decouple them; that is, reduce the coupled pairs of lines to a set of two-conductor lines that do not interact. In order to do this, we define *transformations* that convert these desired line voltages and currents to *mode voltages and currents* $\mathbf{V}_m(z, t)$ and $\mathbf{I}_m(z, t)$ by determining the 2 × 2 transformation matrices $\mathbf{T}_V$ and $\mathbf{T}_I$ as

$$\mathbf{V}(z,t) = \mathbf{T}_V\mathbf{V}_m(z,t) \tag{D.4a}$$

$$\mathbf{I}(z,t) = \mathbf{T}_I\mathbf{I}_m(z,t) \tag{D.4b}$$

where $\mathbf{V}_m$ and $\mathbf{I}_m$ are vectors of *mode voltages and currents*, respectively,

$$\mathbf{V}_m(z,t) = \begin{bmatrix} V_{mG}(z,t) \\ V_{mR}(z,t) \end{bmatrix} \tag{D.5a}$$

$$\mathbf{I}_m(z,t) = \begin{bmatrix} \mathrm{I}_{mG}(z,t) \\ \mathrm{I}_{mR}(z,t) \end{bmatrix} \tag{D.5b}$$

and

$$\mathbf{T}_V = \begin{bmatrix} T_{VGG} & T_{VGR} \\ T_{VRG} & T_{VRR} \end{bmatrix} \tag{D.6a}$$

$$\mathbf{T}_I = \begin{bmatrix} T_{IGG} & T_{IGR} \\ T_{IRG} & T_{IRR} \end{bmatrix} \tag{D.6b}$$

These transformations matrices may not be symmetric. Substituting (D.4) into (D.1) gives the transmission-line equations for these mode quantities as

$$\frac{\partial}{\partial z}\mathbf{V}_m(z,t) = -\mathbf{T}_V^{-1}\mathbf{L}\mathbf{T}_I\frac{\partial}{\partial t}\mathbf{I}_m(z,t) \tag{D.7a}$$

$$\frac{\partial}{\partial z}\mathbf{I}_m(z,t) = -\mathbf{T}_I^{-1}\mathbf{C}\mathbf{T}_V\frac{\partial}{\partial t}\mathbf{V}_m(z,t) \tag{D.7b}$$

Suppose that we can find these transformation matrices such that they *simultaneously diagonalize the per-unit-length inductance and capacitance matrices* as

$$\mathbf{T}_V^{-1}\mathbf{L}\mathbf{T}_I = \mathbf{l}_m = \begin{bmatrix} l_{mG} & 0 \\ 0 & l_{mR} \end{bmatrix} \tag{D.8a}$$

$$\mathbf{T}_I^{-1}\mathbf{C}\mathbf{T}_V = \mathbf{c}_m = \begin{bmatrix} c_{mG} & 0 \\ 0 & c_{mR} \end{bmatrix} \tag{D.8b}$$

If this can be done, the transmission-line equations for the mode voltages and currents are *uncoupled* as

$$\begin{aligned} \frac{\partial}{\partial z}V_{mG}(z,t) &= -l_{mG}\frac{\partial}{\partial t}I_{mG}(z,t) \\ \frac{\partial}{\partial z}I_{mG}(z,t) &= -c_{mG}\frac{\partial}{\partial t}V_{mG}(z,t) \end{aligned} \tag{D.9a}$$

and

$$\begin{aligned} \frac{\partial}{\partial z}V_{mR}(z,t) &= -l_{mR}\frac{\partial}{\partial t}I_{mR}(z,t) \\ \frac{\partial}{\partial z}I_{mR}(z,t) &= -c_{mR}\frac{\partial}{\partial t}V_{mR}(z,t) \end{aligned} \tag{D.9b}$$

These transmission-line equations for the mode quantities represent *two uncoupled two-conductor transmission lines* that have characteristic impedances

$$Z_{CmG} = \sqrt{l_{mG}/c_{mG}} \tag{D.10a}$$

$$Z_{\mathrm{CmR}} = \sqrt{l_{\mathrm{mR}}/c_{\mathrm{mR}}} \tag{D.10b}$$

and velocities of propagation

$$v_{mG} = \frac{1}{\sqrt{l_{mG}c_{mG}}} \tag{D.11a}$$

$$v_{\mathrm{mR}} = \frac{1}{\sqrt{l_{\mathrm{mR}}c_{\mathrm{mR}}}} \tag{D.11b}$$

These uncoupled *mode lines* can be modeled in the SPICE (PSPICE) program using the exact, two-conductor line model that was discussed in Chapter 4. The SPICE model for the mode voltages and currents along the line is solved, and the mode currents and voltages at the endpoints of the line, $z = 0$ and $z = L$, can be converted to the actual line currents and voltages by implementing the transformations given in (D.4) using controlled source models. For example, writing out (D.4a) gives

$$V_G = T_{VGG}V_{mG} + T_{VGR}V_{mR} \tag{D.12a}$$

$$V_R = T_{VRG}V_{mG} + T_{VRR}V_{mR} \tag{D.12b}$$

This can be implemented with voltage-controlled voltage sources as shown in Fig. D.25. Equation (D.4b) can be implemented by inverting this relationship to yield

$$\mathbf{I}_m(z,t) = \mathbf{T}_I^{-1}\mathbf{I}(z,t) \tag{D.13}$$

Writing this out gives

$$I_{mG} = T_{IGG}^{-1}I_G + T_{IGR}^{-1}I_R \tag{D.14a}$$

$$I_{mR} = T_{IRG}^{-1}I_G + T_{IRR}^{-1}I_R \tag{D.14b}$$

where we denote

$$\mathbf{T}_I^{-1} = \begin{bmatrix} T_{IGG}^{-1} & T_{IGR}^{-1} \\ T_{IRG}^{-1} & T_{IRR}^{-1} \end{bmatrix} \tag{D.15}$$

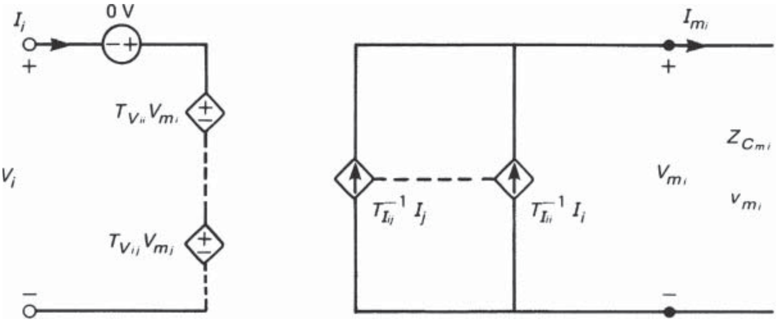

FIGURE D.25 An equivalent circuit for coupled, lossless transmission lines suitable for SPICE implementation.

> *Note:* This symbology for the elements in the inverse, $T^{-1}_{IGG}, T^{-1}_{IGR}, T^{-1}_{IRG}, T^{-1}_{IRR}$, *does not mean that we simply invert the entries in (D.6b) to obtain the inverse of the matrix* $\boldsymbol{T}_I$. *It simply gives a shorthand notation for the entries in* $\boldsymbol{T}_I^{-1}$.

This can be implemented using current-controlled current sources as shown in Fig. D.25. Zero-volt voltage sources are necessary in SPICE to sample the controlling current for current-controlled sources. The complete model of the coupled lines is shown in Fig. D.26. In this model

$$V_{C1} = T_{VGG}V_{mG}(0,t) + T_{VGR}V_{mR}(0,t) \tag{D.16a}$$

$$V_{C2} = T_{VRG}V_{mG}(0,t) + T_{VRR}V_{mR}(0,t) \tag{D.16b}$$

$$V_{C3} = T_{VGG}V_{mG}(L,t) + T_{VGR}V_{mR}(L,t) \tag{D.16c}$$

$$V_{C4} = T_{VRG}V_{mG}(L,t) + T_{VRR}V_{mR}(L,t) \tag{D.16d}$$

according to (D.12) and, according to (D.14),

$$I_{C1} = T^{-1}_{IGG}I_G(0,t) + T^{-1}_{IGR}I_R(0,t) \tag{D.17a}$$

$$I_{C2} = T^{-1}_{IRG}I_G(0,t) + T^{-1}_{IRR}I_R(0,t) \tag{D.17b}$$

$$I_{C3} = T^{-1}_{IGG}I_G(L,t) + T^{-1}_{IGR}I_R(L,t) \tag{D.17c}$$

$$I_{C4} = T^{-1}_{IRG}I_G(L,t) + T^{-1}_{IRR}I_R(L,t) \tag{D.17d}$$

A FORTRAN computer program, SPICEMTL.FOR, is described in this appendix that implements this decoupling and generates a SPICE (PSPICE) subcircuit model representing the line as illustrated in Fig. D.26. The executable file is SPICEMTL.EXE. Once this is run, its output is in the

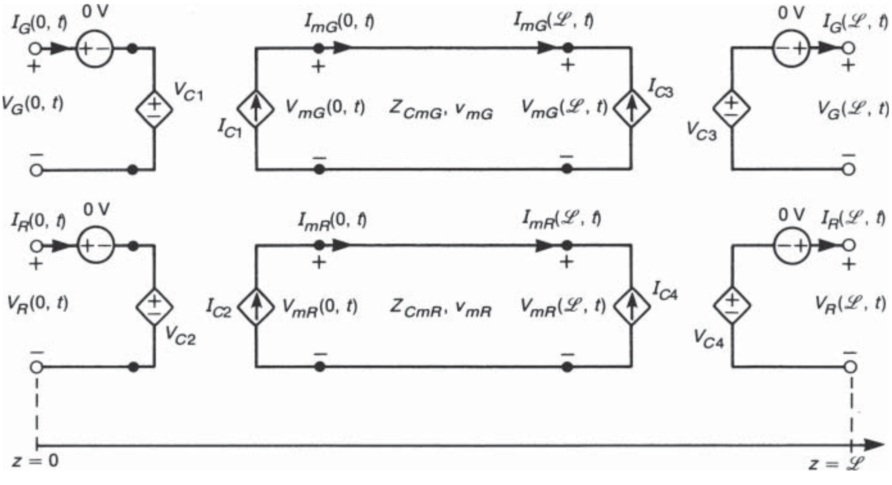
$I_G(0, t)$
0 V
+
$V_G(0, t)$
−
V_{C1}
$I_{mG}(0, t)$
$I_{mG}(\mathcal{L}, t)$
I_{C1}
$V_{mG}(0, t)$
Z_{CmG}, v_{mG}
$V_{mG}(\mathcal{L}, t)$
I_{C3}
V_{C3}
0 V
$I_G(\mathcal{L}, t)$
$V_G(\mathcal{L}, t)$
$I_R(0, t)$
0 V
$V_R(0, t)$
V_{C2}
$I_{mR}(0, t)$
$I_{mR}(\mathcal{L}, t)$
I_{C2}
$V_{mR}(0, t)$
Z_{CmR}, v_{mR}
$V_{mR}(\mathcal{L}, t)$
I_{C4}
V_{C4}
0 V
$I_R(\mathcal{L}, t)$
$V_R(\mathcal{L}, t)$
$z = 0$
$z = \mathcal{L}$

FIGURE D.26 The complete SPICE model for a three-conductor line.

file SPICEMTL.OUT as a SPICE (PSPICE) subcircuit model that acts much like a subroutine. The format of the file begins with

```
.SUBCKT MTL 101 102 201 202
```

and ends with

```
.ENDS MTL
```

This subcircuit holds the model of the line shown in Fig. D.26. The access nodes of this model are denoted as 101, 102, 201, and 202. The nodes beginning with 1 are the near-end nodes (i.e., 101=source end, and 102=near end), whereas the nodes beginning with 2 are the far end nodes (i.e., 201=load end, and 202=far end). The actual line terminations are attached to this subcircuit model through the statement

```
XMTL S NE L FE MTL
```

The correspondence is S=101, NE=102, L=201, and FE=202. This attachment is illustrated in Fig. D.27, where the zero node (0) is the SPICE universal "ground" node. The SPICEMTL.FOR program generates the diagonalization matrices, T_V and T_I, and then generates the SPICE code for the subcircuit. The following experimental results illustrate this application.

D.4.1 Computed Versus Experimental Results for Wires

As an example of a wire-type line, consider the case of two bare 20-gauge solid wires separated by 2 cm and suspended 2 cm above a ground plane that is the reference conductor as shown in Fig. D.28. The line length is 4.674 m. The dielectric insulations of the wires are absent, so this becomes a problem of a homogeneous medium. The per-unit-length inductances and capacitances are computed using the FORTRAN code WIDESEP.FOR in Appendix C, which implements the wide-separation approximations of Section 9.3.2 giving the per-unit-length parameter matrices of

$$\mathbf{L} = \begin{bmatrix} 9.17859 \times 10^{-7} & 1.60944 \times 10^{-7} \\ 1.60944 \times 10^{-7} & 9.17859 \times 10^{-7} \end{bmatrix} \text{H/m}$$

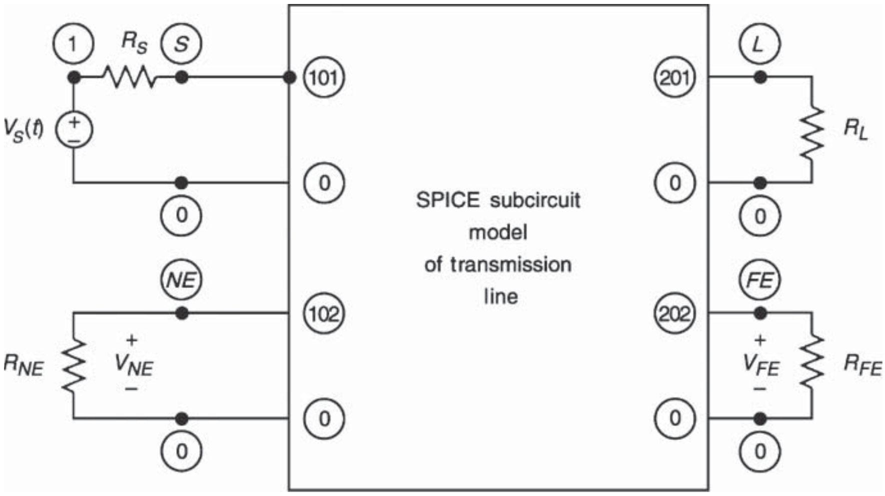

FIGURE D.27 Node numbering for the SPICE subcircuit model for connection of the terminations.

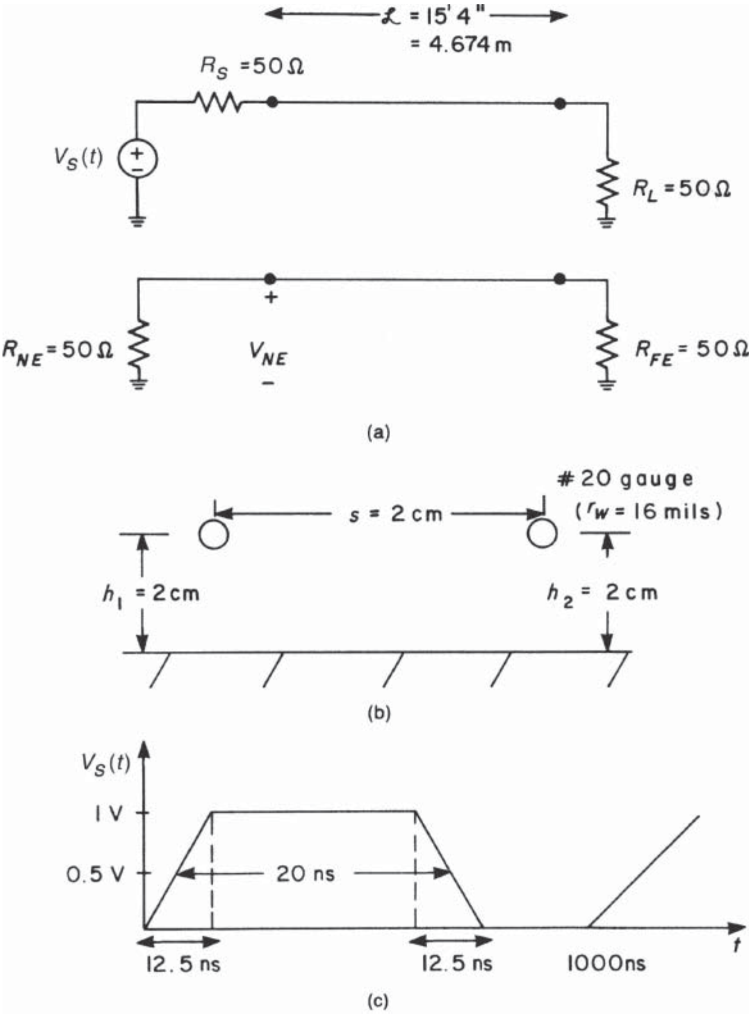
$\mathcal{L}$ = 15' 4"
= 4.674 m
R_S = 50 Ω
$V_S(t)$
R_L = 50 Ω
R_{NE} = 50 Ω
+
V_{NE}
−
R_{FE} = 50 Ω
(a)
# 20 gauge
(r_w = 16 mils)
s = 2 cm
h_1 = 2cm
h_2 = 2cm
(b)
$V_S(t)$
1 V
0.5 V
20 ns
12.5 ns
12.5 ns
1000ns
t
(c)

FIGURE D.28 An experiment consisting of two wires above a ground plane to illustrate the prediction accuracy of the SPICE model of Fig. D.26 for a homogeneous medium: (a) physical configuration; (b) cross-sectional configuration; (c) input voltage specification.

and

$$\mathbf{C} = \begin{bmatrix} 1.25068 \times 10^{-11} & -2.19302 \times 10^{-12} \\ -2.19302 \times 10^{-12} & 1.25068 \times 10^{-11} \end{bmatrix} \text{F/m}$$

(These were computed by hand in Example 9.2.) The output file of WIDESEP.FOR is contained in PUL.DAT (see Appendix C for details). The program SPICEMTL.FOR reads this PUL.DAT file and generates the PSPICE subcircuit model in the output file SPICEMTL.OUT. This file then has the external (to the subcircuit model) line terminations added along with the other SPICE lines required to execute the program. Hence the complete SPICE code is

```
SPICE MTL MODEL; HOMOGENEOUS MEDIUM; FIGURE 9.48
VS 1 0 PULSE (0 1 0 12.5N 12.5N 7.5N 1000N)
RS 1 S 50
```

```
RL L 0 50
RNE NE 0 50
RFE FE 0 50
XMTL S NE L FE MTL
.TRAN .2N 200N 0 .2N
.PROBE
*SUBCIRCUIT MODEL OF A MULTICONDUCTOR TRANSMISSION LINE*
*     NUMBER OF CONDUCTORS= 3
*     TOTAL LINE LENGTH (METERS)= 4.67400E+00
*     L(1, 1)= 9.17859E-07
*     L(1, 2)= 1.60944E-07
*     L(2, 2)= 9.17859E-07
*     C(1, 1)= 1.25068E-11
*     C(1, 2)= -2.19302E-12
*     C(2, 2)= 1.25068E-11
.SUBCKT MTL
+ 101
+ 102
+ 201
+ 202
V101 101 301
EC101 301 0 POLY(2)
+ (501,0)
+ (502,0)
+0
+ 7.084033E-01
+ -7.052552E-01
FC101 0 501 POLY(2)
+ V101
+ V102
+0
+ 7.084033E-01
+ 7.058083E-01
V201 201 401
EC201 401 0 POLY(2)
+ (601,0)
+ (602,0)
+0
+ 7.084033E-01
+ -7.052552E-01
FC201 0 601 POLY(2)
+ V201
+ V202
+0
+ 7.084033E-01
+ 7.058083E-01
V102 102 302
EC102 302 0 POLY(2)
+ (501,0)
+ (502,0)
+0
+ 7.058083E-01
+ 7.089539E-01
FC102 0 502 POLY(2)
+ V101
+ V102
+0
+ -7.052552E-01
+ 7.089539E-01
V202 202 402
EC202 402 0 POLY(2)
+ (601,0)
+ (602,0)
+0
+ 7.058083E-01
+ 7.089539E-01
FC202 0 602 POLY(2)
+ V201
+ V202
+0
+ -7.052552E-01
+ 7.089539E-01
T101 501 0 601 0 Z0= 3.234158E+02 TD= 1.559081E-08
T102 502 0 602 0 Z0= 2.269176E+02 TD= 1.559079E-08
.ENDS MTL
.END
```

Note that both modes have the same one-way time delay and that is $T_D = L/v_0 = 15.59078$ ns. (The program SPICEMTL.FOR uses the value of $v_0 = 2.997925 \times 10^8$ m/s.) The characteristic impedance of one wire above the ground plane is computed using (4.26) and (4.28) as $Z_C = 275.3516\ \Omega$. Hence, the crosstalk has caused the characteristic impedances of the two modes to be different from that of an isolated wire above ground. Hence, *crosstalk effects the propagation properties of each individual line*.

The * is a comment card, and the + represents a continuation card. The source voltage waveform is a 1 V, 1 MHz trapezoidal waveform having a pulsewidth of 20 ns and 12.5 ns rise/falltimes as shown in Fig. D.28. Fig. D.29 shows the predicted near-end crosstalk waveform along with the experimentally obtained waveform. The waveform prediction is quite good.

Review Exercise D.1 Can the time-domain inductive-capacitive coupling model be used in this example to predict the time-domain crosstalk? If not, why not?

***Answer*:** No. The pulse rise/falltimes are 12.5 ns, whereas the line one-way delay is $T_D = L/v_0 =$ 15.6 ns. Hence, the rise/falltimes are not much longer than the line one-way delay.

The SPICE subcircuit model can also be used to predict the frequency-domain response of the coupled line. To do this, we make three changes in the overall SPICE code. First, we replace the time-domain specification of the source voltage waveform with

```
VS 1 0 AC 1 0
```

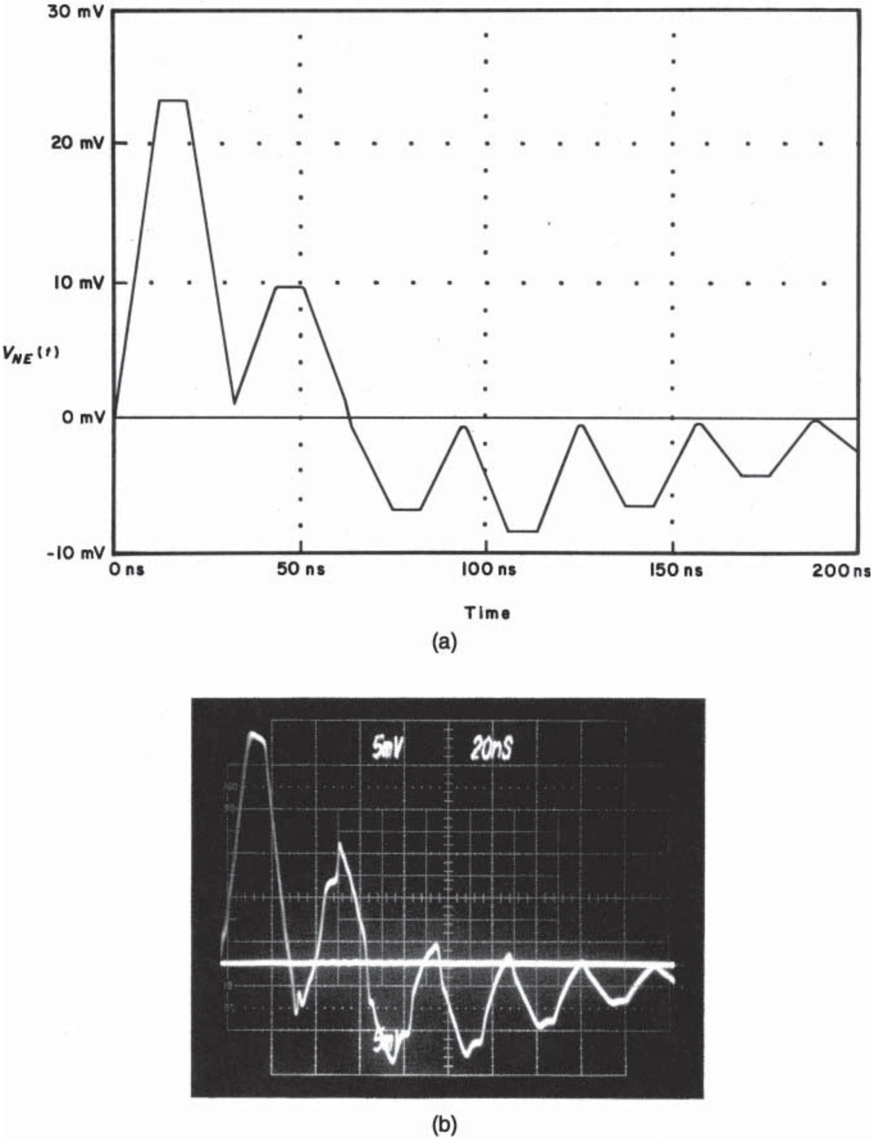

(a)

(b)

FIGURE D.29 Time-domain near-end crosstalk for the configuration of Fig. D.28: (a) prediction of the SPICE subcircuit model; (b) measured.

This replaces the pulse waveform with a sinusoidal waveform of amplitude 1 and phase angle of 0. Next, we replace the execution line .TRAN with

```
.AC DEC 50 1K 100MEG
```

This directs the SPICE program to solve this for the phasor response when the frequency of the sinusoidal source is varied between 1 kHz and 100 MHz in steps of 50 points per decade. And finally, the frequency response is obtained and plotted with .PROBE by plotting

```
VDB (NE) -VDB(S)
```

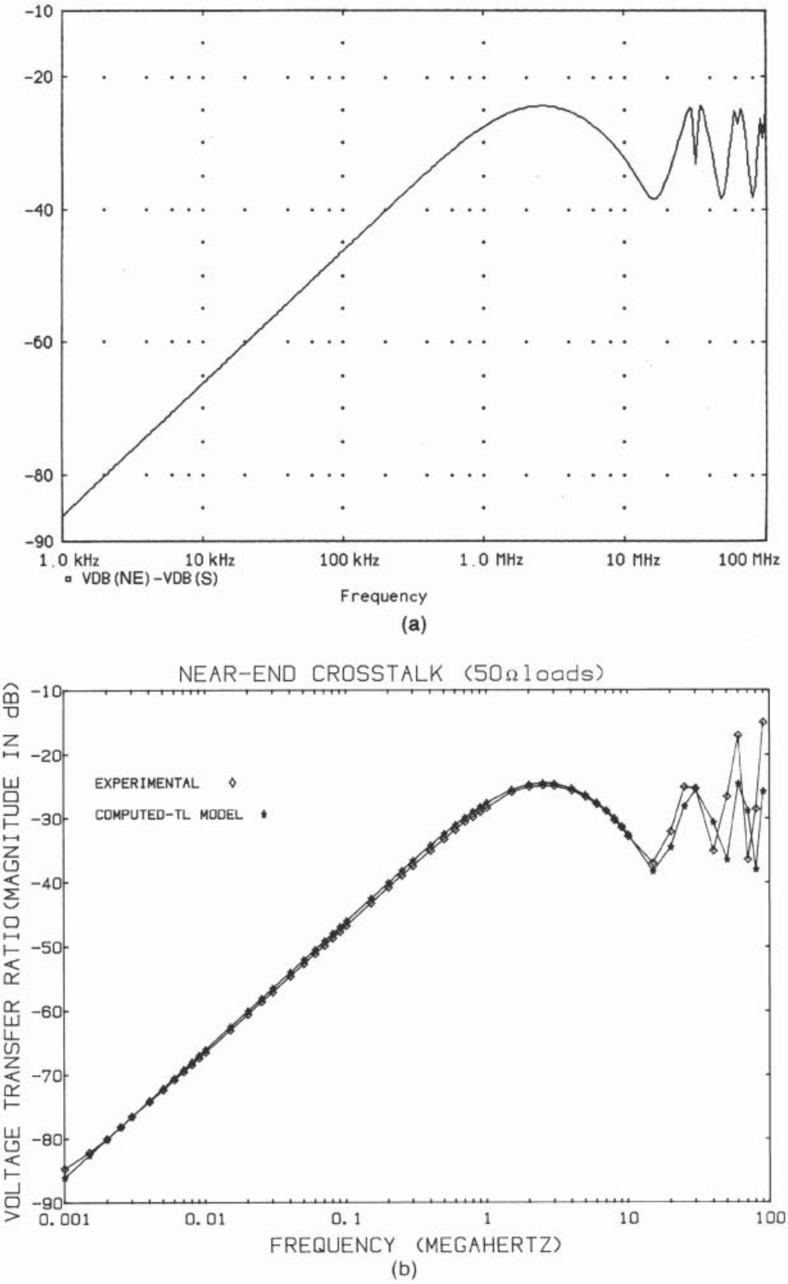

FIGURE D.30 Frequency-domain predictions of the near-end crosstalk transfer function for the configuration of Fig. D.28 using (a) the SPICE subcircuit model and (b) predictions of the transmission-line model versus measured results.

This plots, in dB, the ratio of the node voltage at node NE to the node voltage at node S (the input to the line) as $20\log_{10}(|\hat{V}(NE)/\hat{V}(S)|)$. Fig. D.30a shows this plot. We can verify this frequency response plot using the approximate inductive–capacitive coupling model for frequencies up to around 1 MHz, where the response begins to deviate from a 20 dB/decade behavior. Since the wires are widely separated, the weak coupling assumption in this model is valid. Similarly, it is electrically short for frequencies below approximately 1 MHz. The inductive-capacitive coupling model in Eqs. (9.67) through (9.69) become

$$\frac{\hat{V}(NE)}{\hat{V}(S)} = j2\pi f\ (M_{NE}^{\mathrm{IND}} + M_{NE}^{\mathrm{CAP}})$$

where

$$\begin{aligned} M_{NE}^{\mathrm{IND}} &= \frac{R_{NE}}{R_{NE}+R_{FE}}\frac{L_m = l_m \times 4.674}{R_S = 0 + R_L} \\ &= \frac{50}{50+50}\frac{7.52\times10^{-7}}{50} \\ &= 7.52\times10^{-9} \end{aligned}$$

and

$$\begin{aligned} M_{NE}^{\mathrm{CAP}} &= \frac{R_{NE}R_{FE}}{R_{NE}+R_{FE}}\frac{R_L C_m = c_m \times 4.674}{R_S = 0 + R_L} \\ &= \frac{50\times50}{50+50}\frac{50\times1.03\times10^{-11}}{50} \\ &= 2.56\times10^{-10} \end{aligned}$$

Thus,

$$\begin{aligned} \frac{\hat{V}(NE)}{\hat{V}(S)} &= j2\pi f(7.52\times10^{-9} + 2.56\times10^{-10}) \\ &= j4.89\times10^{-8} f \end{aligned}$$

Evaluating this at 1 kHz gives −86.22 dB, which compares favorably to the SPICE computed value of −86 dB. Similarly at 1 MHz, the inductive–capacitive coupling model gives −26.22 dB, which compares favorably with the SPICE computed value of around −27 dB. Figure D.30b compares the experimentally obtained result to the transmission-line model predictions at the measured frequencies.

D.4.2 Computed Versus Experimental Results for PCBs

As an example of the use of this model for an inhomogeneous medium, consider the PCB shown in Fig. D.31. The board is glass epoxy, and the thickness is 47 mils. The 1 oz copper land widths are 15 mils and are separated edge-to-edge by 45 mils with a length of 10 in. or 25.4 cm. The source voltage waveform is a 10 MHz, 1 V trapezoidal pulse train with a 50% duty cycle and rise/falltimes of 6.25 ns (5 ns 10–90%). The per-unit-length inductance and capacitance matrices

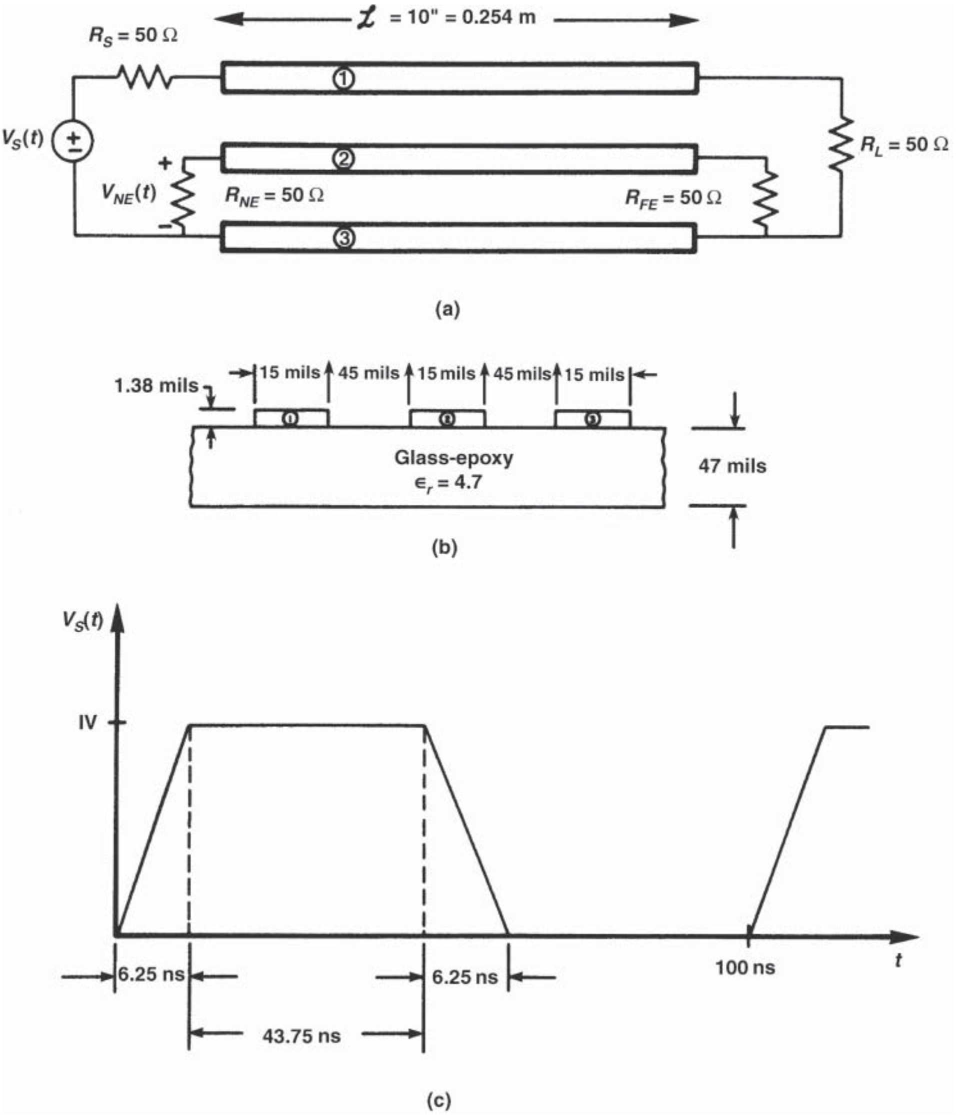
$\mathcal{L}$ = 10" = 0.254 m
R_S = 50 Ω
①
$V_S(t)$
+
$V_{NE}(t)$
−
②
R_{NE} = 50 Ω
R_{FE} = 50 Ω
③
R_L = 50 Ω
(a)
1.38 mils
15 mils
45 mils
15 mils
45 mils
15 mils
Glass-epoxy
ϵ_r = 4.7
47 mils
(b)
$V_S(t)$
IV
6.25 ns
43.75 ns
6.25 ns
100 ns
t
(c)

FIGURE D.31 An experiment consisting of three lands on a PCB to illustrate the prediction accuracy of the SPICE model of Fig. D.26 for an inhomogeneous medium: (a) physical configuration; (b) cross-sectional configuration; (c) input voltage specification.

are computed using the code PCB.FOR in Appendix C, which places them in the output file PUL.DAT as

$$\mathbf{L} = \begin{bmatrix} 1.38315 \times 10^{-6} & 6.91573 \times 10^{-7} \\ 6.91573 \times 10^{-7} & 1.10707 \times 10^{-6} \end{bmatrix} \text{ H/m}$$

and

$$\mathbf{C} = \begin{bmatrix} 2.96949 \times 10^{-11} & -2.02619 \times 10^{-11} \\ -2.02619 \times 10^{-11} & 4.05238 \times 10^{-11} \end{bmatrix} \text{ F/m}$$

The code SPICEMTL.FOR is run, which reads the PUL.DAT file and generates the subcircuit model in the output file SPICEMTL.OUT. This file is then modified by adding the external circuitry and the execution statements to give the SPICE file:

```
SPICE MTL MODEL; INHOMOGENEOUS MEDIUM; FIGURE 9.51
VS 1 0 PULSE (0 1 0 6.25N 6.25N 43.75N 100N)
RS 1 S 50
RL L 0 50
RNE NE 0 50
RFE FE 0 50
XMTL S NE L FE MTL
.TRAN .1N 20N 0 .1N
.PROBE
*SUBCIRCUIT MODEL OF A MULTICONDUCTOR TRANSMISSION LINE*
*     NUMBER OF CONDUCTORS= 3
*     TOTAL LINE LENGTH (METERS)= 2.54000E-01
*     L(1, 1)= 1.38315E-06
*     L(1, 2)= 6.91573E-07
*     L(2, 2)= 1.10707E-06
*     C(1, 1)= 2.96949E-11
*     C(1, 2)=-2.02619E-11
*     C(2, 2)= 4.05238E-11
.SUBCKT MTL
+ 101
+ 102
+ 201
+ 202
V101 101 301
EC101 301 0 POLY(2)
+ (501,0)
+ (502,0)
+0
+ 9.999894E-01
+ -2.372106E-05
FC101 0 501 POLY(2)
+ V101
+ V102
+0
+ 9.999894E-01
+ 5.000049E-01
V201 201 401
EC201 401 0 POLY(2)
+ (601,0)
+ (602,0)
+0
+ 9.999894E-01
+ -2.372106E-05
FC201 0 601 POLY(2)
+ V201
+ V202
+0
+ 9.999894E-01
+ 5.000049E-01
V102 102 302
EC102 302 0 POLY(2)
+ (501,0)
+ (502,0)
+0
+ 5.000049E-01
+ 1.118027E+00
FC102 0 502 POLY(2)
+ V101
+ V102
+0
+ -2.372106E-05
+ 1.118027E+00
V202 202 402
EC202 402 0 POLY(2)
+ (601,0)
+ (602,0)
+0
+ 5.000049E-01
+ 1.118027E+00
FC202 0 602 POLY(2)
+ V201
+ V202
+0
+ -2.372106E-05
+ 1.118027E+00
T101 501 0 601 0 Z0= 2.658983E+02 TD= 1.321285E-09
T102 502 0 602 0 Z0= 1.096490E+02 TD= 1.410790E-09
.ENDS MTL
.END
```

If we compute the characteristic impedance of the board with only two lands, we obtain, using (4.42), $Z_C = 204.525\,\Omega$ and $\varepsilon_r' = 2.6159$ with a time delay of $T_D = L\sqrt{\varepsilon_r'}/v_0 = 1.369$ ns. Hence, again we see that the adjacent land effects the propagation properties of the other land.

The predictions of this SPICE model and the experimentally obtained results are shown in Fig. D.32. The correlation is excellent; the SPICE model predicts a peak voltage of 95 mV occurring slightly past 6 ns, and the experimental peak is 94 mV, occurring at the same time.

Review Exercise D.2 Can the time-domain, inductive–capacitive coupling model be used in this example to predict the time-domain crosstalk? If not, why not?

***Answer*:** No. The pulse rise/falltimes are 6.25 ns. There are two line one-way delays because for this inhomogeneous medium case there are two velocities of propagation of the two modes. From the SPICE subcircuit model these are 1.41 and 1.32 ns. The rise/falltimes are on the order of 4 times the line one-way delays, which is marginally sufficient for the inductive–capacitive coupling model to give valid results.

The SPICE subcircuit model can again be used to predict the frequency-domain response of the coupled line. To do this, we again make three changes in the overall SPICE code. First, we replace the time-domain specification of the source voltage waveform with

```
VS 1 0 AC 1 0
```

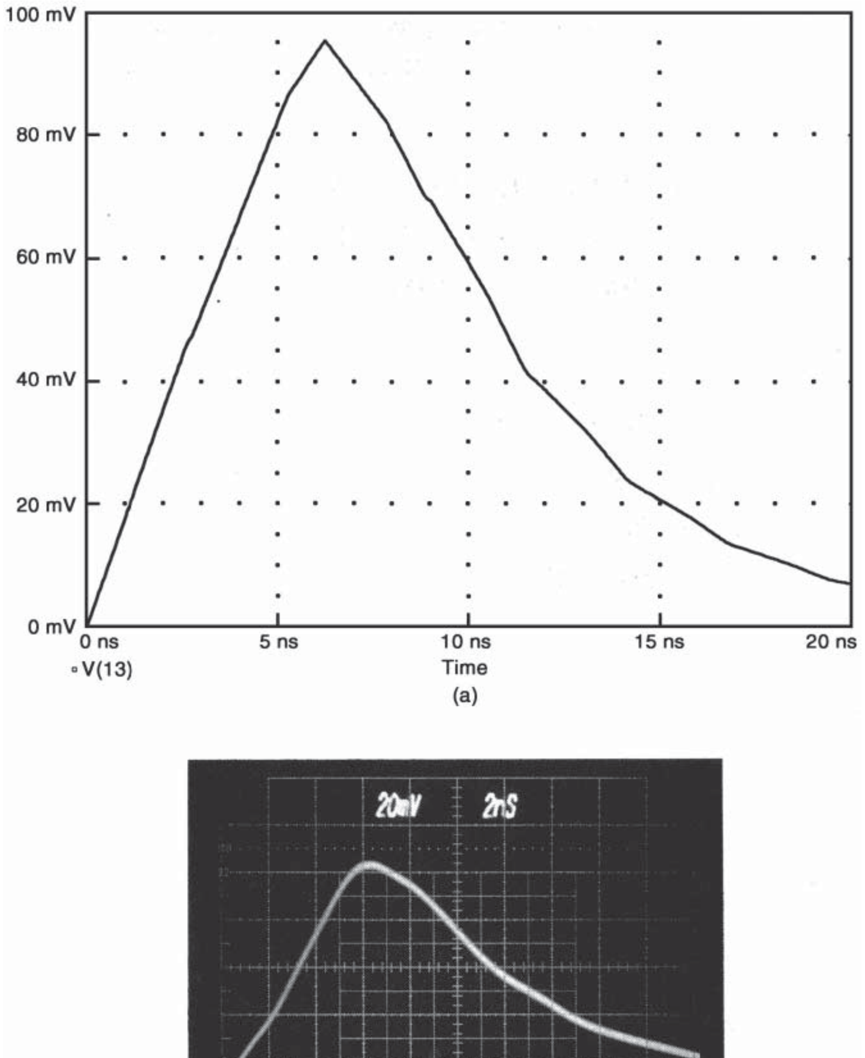

FIGURE D.32 Time-domain near-end crosstalk for the configuration of Fig. D.31: (a) prediction of the SPICE subcircuit model; (b) measured.

This replaces the pulse waveform with a sinusoidal waveform of amplitude 1 and phase angle of 0. Next, we replace the execution line (.TRAN) with

```
.AC DEC 50 10K 1000 MEG
```

This directs the SPICE program to solve this for the phasor response when the frequency of the sinusoidal source is varied between 10 kHz and 1 GHz in steps of 50 points per decade. And finally, the frequency response is obtained and plotted with .PROBE by plotting

```
VDB (NE) −VDB(S)
```

This plots, in dB, the ratio of the node voltage at node NE to the node voltage at node S (the input to the line) as $20\log_{10}(|\hat{V}(NE)/\hat{V}(S)|)$. Fig. D.33a shows this plot. We can verify this frequency response plot using the approximate inductive–capacitive coupling model for frequencies up to around 10 MHz, where the response begins to deviate from a 20 dB/decade behavior. Since the PCB lands are widely separated, the weak coupling assumption in this model is valid. Similarly, it is electrically short for frequencies below approximately 10 MHz. The inductive–capacitive coupling model in Eqs. (9.67) through (9.69) become

$$\frac{\hat{V}(NE)}{\hat{V}(S)} = j2\pi f(M_{NE}^{\text{IND}} + M_{NE}^{\text{CAP}})$$

where

$$\begin{aligned} M_{NE}^{\text{IND}} &= \frac{R_{NE}}{R_{NE}+R_{FE}}\frac{L_m = l_m \times 0.254}{R_S = 0 + R_L} \\ &= \frac{50}{50+50}\frac{1.76\times 10^{-7}}{50} \\ &= 1.76\times 10^{-9} \end{aligned}$$

and

$$\begin{aligned} M_{NE}^{\text{CAP}} &= \frac{R_{NE}R_{FE}}{R_{NE}+R_{FE}}\frac{R_L C_m = c_m \times 0.254}{R_S = 0 + R_L} \\ &= \frac{50\times 50}{50+50}\frac{50\times 5.15\times 10^{-12}}{50} \\ &= 1.29\times 10^{-10} \end{aligned}$$

Thus,

$$\begin{aligned} \frac{\hat{V}(NE)}{\hat{V}(S)} &= j2\pi f(1.76\times 10^{-9} + 1.29\times 10^{-10}) \\ &= j1.18\times 10^{-8} f \end{aligned}$$

Evaluating this at 10 kHz gives −78.5 dB, which compares favorably with the SPICE computed value of −79 dB. Similarly at 10 MHz, the inductive–capacitive coupling model gives −18.53−dB, which compares favorably with the SPICE computed value of around −20 dB. Fig. D.33b compares the experimentally obtained result to the transmission-line model (including losses) predictions at the measured frequencies. Observe that the experimental results show a low-frequency region below approximately 100 kHz, where the resistance of the reference land becomes important and common-impedance coupling becomes dominant. The SPICE model above cannot be readily modified to accommodate losses so that it cannot predict this important aspect of the crosstalk. However, the transmission-line model solution for the frequency domain can be modified to include losses. The predictions of this transmission-line model are plotted against the experimental data in Fig. D.33b and show reasonable correlation. Also shown in Fig. D.33b are the predictions of the lumped-circuit approximate model. The predictions using one and two Pi sections to represent the entire line show the same prediction accuracy as the transmission line model for frequencies where the line is electrically short (below 100 MHz).

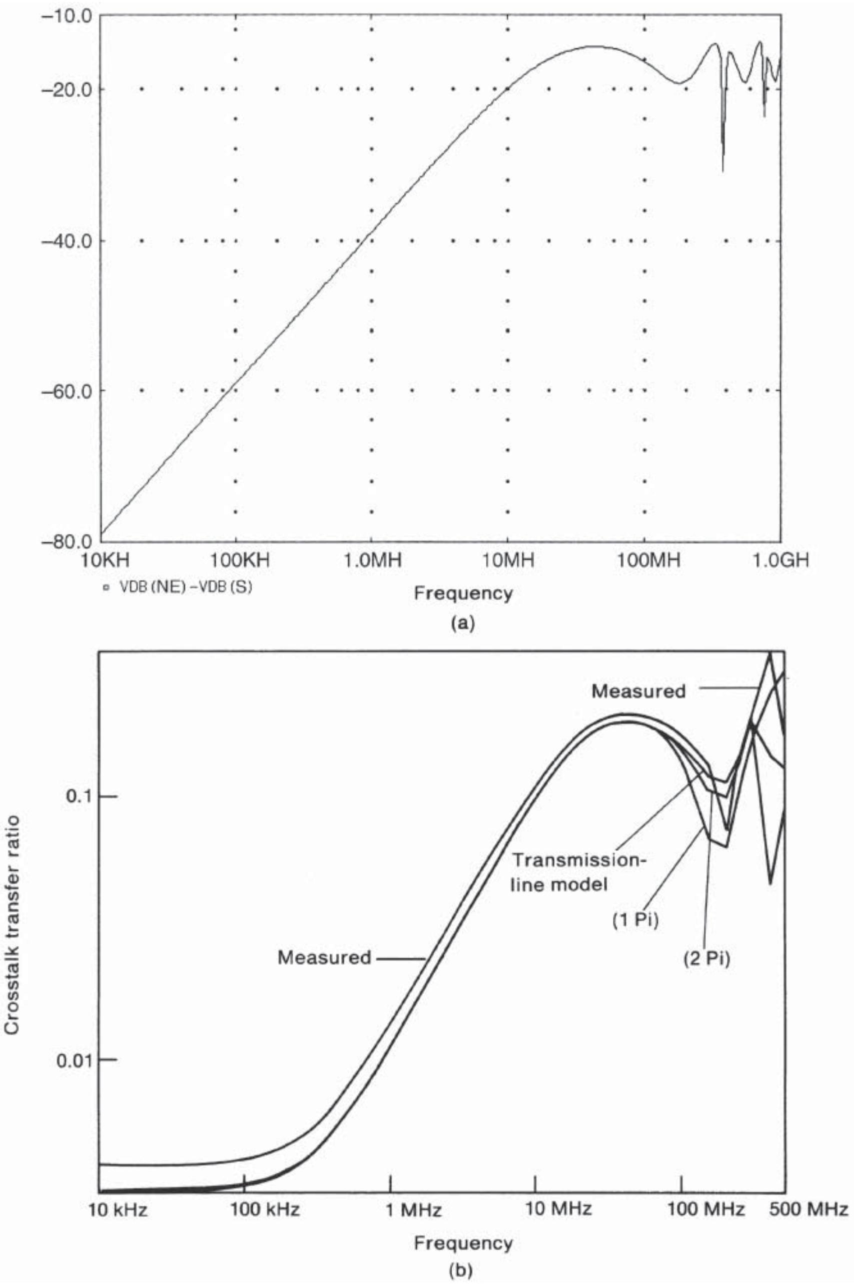

FIGURE D.33 Frequency-domain predictions of the near-end crosstalk transfer function for the configuration of Fig. D.31 using (a) the SPICE subcircuit model and (b) predictions of the transmission-line model and the lumped-Pi model using one and two sections versus measured results.

D.5 USE OF SPICE (PSPICE) IN FOURIER ANALYSIS

One of the more useful features available in SPICE is the Fourier analysis capability. SPICE can calculate the Fourier coefficients (magnitude and phase) and can also plot (with the .PROBE feature) the frequency spectrum. A Fourier analysis is accomplished by adding the .FOUR command to the input list. The .FOUR command can be used only with a .TRAN analysis; that is, it cannot be used when doing a .DC or .AC analysis. The format is

```
.FOUR  f0  [output_variable(s)]
```

The fundamental frequency of the *periodic* waveform to be analyzed is denoted as $f_0 = 1/T$, where T is the period of the waveform. The *output_variable(s)* are the desired voltage or current waveforms to be analyzed, e.g., V(2), I(R1).

In performing the transient (time-domain) analysis, the .TRAN command is used:

```
.TRAN print_step end_time [no_print_time [step_ceiling]] [UIC]
```

SPICE solves the time-domain differential equations of the circuit by discretizing the time variable and solving the equations in a bootstrapping manner. The first item, *print_step*, governs when an output is requested. Suppose the discretization used in the solution is every 2 ms. We might not want to see (in the output generated by the .PRINT statement) an output at every 2 ms but only every 5 ms. Hence, we might set the *print_step* time as 5M. The *end_time* is the final time that the solution is obtained for. The remaining parameters are optional. The analysis always starts at $t = 0$. But we may not wish to see a printout of the solution (in the output generated by the .PRINT statement) until after some time has elapsed. If so we would set the *no_print_time* to that starting time. SPICE and PSPICE have a very sophisticated algorithm for determining the minimum step size for discretization of the differential equations in order to get a valid solution. The default maximum step size is *end_time*/50. However, there are some cases where we want the step size to be smaller than what SPICE would choose in order to increase the accuracy of the solution. This is frequently the case when we use SPICE in the analysis of transmission lines. The *step_ceiling* is the maximum time step size that will be used. Although this gives longer run times, there are cases where we need to do this to generate the required accuracy. The last item *UIC* means that SPICE is to use the initial capacitor voltage or inductor current specified on these element lines with the *IC* = command. In a transient analysis, SPICE will compute the initial conditions. If some other initial conditions are required, then we should set these and specify *UIC* on the .TRAN statement. For example,

```
.TRAN  0.1N  20N  0  0.01N
```

would command SPICE to do a time-domain (transient analysis) for times from 0 to 20 ns, print out a solution at every 0.1 ns, start printing to the output file at $t = 0$, and use a time discretization time step no larger than 0.01 ns. If a printed output is requested via either .PRINT or .FOUR, then the output file containing this is XXXX.OUT if the input file was XXXX.IN or XXXX.CIR.

There is an important consideration in using the .FOUR command. The portion of the waveform that is analyzed to give the Fourier expansion coefficients is the last portion of the solution time of length one period $1/f_0 = T$. In other words, SPICE determines the coefficients from the waveform between *end_time*–[$1/f_0$] and *end_time*. Hence, *end_time* on the .TRAN command should be at least one period long. In situations where the solution has a transient portion at the beginning of the solution interval and we want to determine the Fourier coefficients for the steady-state solution, we would run the analysis for several periods to ensure that the solution has entered into steady state. For example, consider an input signal that is periodic with a period of 2 ns or a fundamental frequency of 500 MHz. An output voltage at node 4 would also have this periodicity but would have a transient period of some five time constants, say, 5 ns. The following commands would be used to obtain the Fourier coefficients of the steady-state response of the node voltage at node 4:

```
.TRAN  0.1N  20N
.FOUR  500MEG  V(4)
```

This would compute the solution for the voltage waveform at node 4 from $t = 0$ to $t = 20$ ns. Since the period (the inverse of 500 MHz) is specified as 2 ns, the portion of the waveform from 18 to 20 ns would be used to compute the Fourier coefficients for the waveform. If we wanted to compute the Fourier coefficients for the initial part of the waveform including the transient, we would specify

```
.TRAN  0.1N  2N
```

which would run for only one period.

Finally, the .FOUR statement generates the dc component of the waveform, as well as the first nine harmonics. Some later versions allow the user to specify any number of harmonics to be calculated. Usually, the first nine harmonics are sufficient to give the major spectral content of the waveform. The phase angles of these Fourier expansion coefficients generated by .FOUR are based on the sine form of the expansion given in (3.19b; repeated here for convenience):

$$x(t) = c_0 + \sum_{n=1}^{\infty} 2|c_n| \sin(n\omega_0 t + \underline{/(c_n + 90^\circ)})$$

Hence, when one compares the coefficients $c_n = |c_n|\underline{/c_n}$ computed by hand to those computed with .FOUR, one must add 90° to the hand-calculated phases.

Example D.7 Determine the Fourier expansion coefficients for the waveform of Example 3.1 shown in Fig. 3.7.

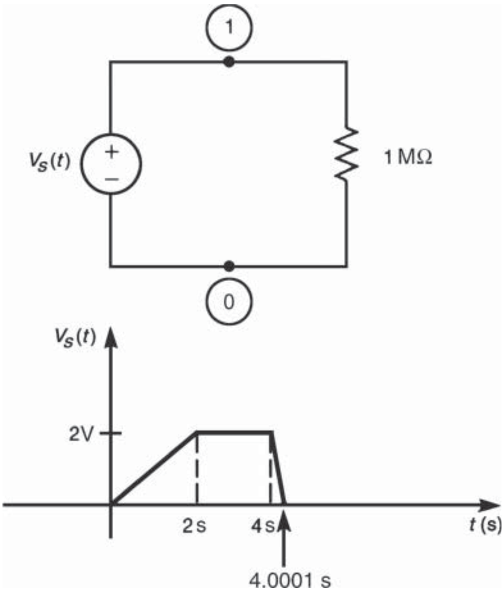

FIGURE D.34 Example D.7 PSPICE coding.

***Solution*:** The coding diagram is shown in Fig. D.34. The PSPICE program is

```
EXAMPLE D.7
VS  1  0  PWL(0  0  2  2  4  2  4.0001  0)
R  1  0  1E6
.TRAN  0.0001  4
.FOUR  0.25  V(1)
.PROBE
.END
```

If we name this file as FOUR.IN, then the printed output is contained in the file FOUR.OUT. We have specified the source voltage waveform with the piecewise-linear (PWL) form, which gives consecutive pairs of time and value points. Note that we needed to specify the end of the waveform that actually drops abruptly from 4 to 0 V at $t = 4$ s with a small but finite slope since the PWL function draws straight lines between these points and hence does not allow specification of an abrupt discontinuity. The Fourier coefficients are contained in the output file FOUR.OUT, shown in Table D.2. The phase angle is based on a sine form of the expansion as shown in (3.19b). The output is

TABLE D.2 Fourier Components of Transient Response V(1)

DC Component = 1.499969E+00

Harmonic No	Frequency (HZ)	Fourier Component	Normalized Component	Phase (DEG)	Normalized Phase (DEG)
1	2.500E−01	7.547E−01	1.000E+00	−1.475E+02	0.000E+00
2	5.000E−01	3.183E−01	4.218E−01	−1.800E+02	−3.247E+01
3	7.500E−01	2.169E−01	2.875E−01	−1.680E+02	−2.049E+01
4	1.000E+00	1.592E−01	2.109E−01	−1.800E+02	−3.246E+01
5	1.250E+00	1.284E−01	1.701E−01	−1.727E+02	−2.520E+01
6	1.500E+00	1.061E−01	1.406E−01	−1.800E+02	−3.245E+01
7	1.750E+00	9.133E−02	1.210E−01	−1.748E+02	−2.725E+01
8	2.000E+00	7.958E−02	1.054E−01	−1.800E+02	−3.244E+01
9	2.250E+00	7.092E−02	9.397E−02	−1.759E+02	−2.839E+01

These data are virtually identical with the hand computations in Example 3.1 for the first seven harmonics.

Example D.8 Determine the Fourier expansion coefficients for the waveform of Example 3.2 shown in Fig. 3.9.

***Solution*:** The coding diagram is shown in Fig. D.35. The PSPICE program is

```
EXAMPLE D.8
VS  1  0  PULSE(0  1  0  0.001  0.001  0.999  2)
R  1  2  1
C  2  0  1
.TRAN  0.001  10
.FOUR  0.5  V(1)  V(2)
.PROBE
.END
```

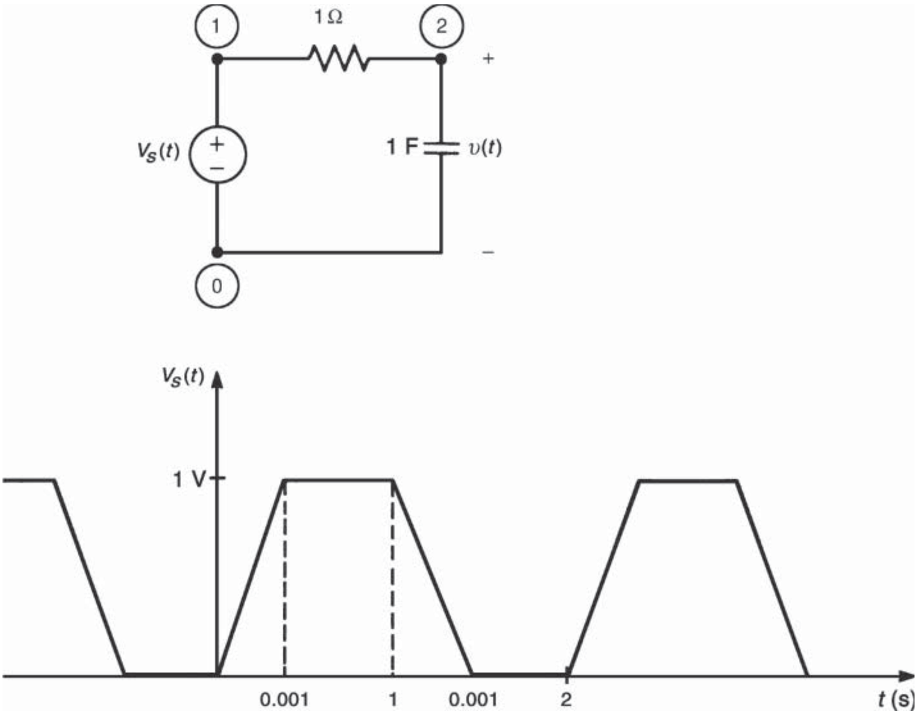

FIGURE D.35 Example D.8 PSPICE coding.

We have specified the source voltage waveform with the PULSE function in order to give a repetitive waveform. The form of the PULSE function is

```
PULSE (initial_level peak_level delay risetime fall-
time pulse_width period)
```

Again, although the ideal square wave has zero rise- and falltimes, we have to specify these with very small (compared to the pulse period) rise- and falltimes of 0.001 s.

If this input file is named FOUR.IN, then the Fourier coefficients are contained in the output file FOUR.OUT, shown in Table D.3. The phase angle is again based on a sine form of the expansion as shown in (3.19b). The expansion coefficients for the source voltage, V(1), are

TABLE D.3 Fourier Components of Transient Response V(1)

DC Component = 5.000000E-01

Harmonic No	Frequency (HZ)	Fourier Component	Normalized Component	Phase (DEG)	Normalized Phase (DEG)
1	5.000E−01	6.366E01	1.000E+00	−9.007E−02	0.000E+00
2	1.000E+00	7.203E−10	1.131E−09	9.843E+01	9.852E+01
3	1.500E+00	2.122E−01	3.333E−01	−2.702E−01	−1.801E−01
4	2.000E+00	7.081E−10	1.100E−09	1.068E+02	1.069E+02
5	2.500E+00	1.273E−01	2.000E−01	−4.504E−01	−3.603E−01
6	3.000E+00	6.882E−10	1.081E−09	1.151E+02	1.152E+02
7	3.500E+00	9.095E−02	1.429E−01	−6.305E−01	−5.404E−01
8	4.000E+00	6.611E−10	1.038E−09	1.233E+02	1.234E+02
9	4.500E+00	7.074E−02	1.990E−01	−8.107E−01	−7.206E−01

and the coefficients for the output voltage, V(2), are shown in Table D.4

TABLE D.4 Fourier Components of Transient Response V(2)

DC Component = 4.999618-01

Harmonic No	Frequency (HZ)	Fourier Component	Normalized Component	Phase (DEG)	Normalized Phase (DEG)
1	5.000E−01	1.930E−01	1.000E+00	−7.290E+01	0.000E+00
2	1.000E+00	1.201E−05	6.224E−05	−1.710E+02	−9.811E+01
3	1.500E+00	2.224E−02	1.152E−01	−8.454E+01	−1.164E+01
4	2.000E+00	6.047E−06	3.133E−05	−1.753E+02	−1.024E+02
5	2.500E+00	8.175E−03	4.235E−02	−8.693E+01	−1.403E+01
6	3.000E+00	4.043E−06	2.095E−05	−1.766E+02	−1.037E+02
7	3.500E+00	4.190E−03	2.171E−02	−8.752E+01	−1.462E+01
8	4.000E+00	3.025E−06	1.567E−05	−1.773E+02	−1.044E+02
9	4.500E+00	2.940E−03	1.523E−02	−8.268E+01	−9.781E+00

These are virtually identical with the hand computations in Example 3.1 for the first seven harmonics. The analysis was run for $t = 0$ to $t = 10$ s in order to allow the output voltage to achieve steady state since the Fourier analysis is valid only for steady state.

Example D.9 Determine the Fourier expansion coefficients for the trapezoidal waveform of Review Exercise 3.1, which has a frequency of 100 MHz, an amplitude of 5 V, a 50% duty cycle, and rise/falltimes of 1 ns.

***Solution*:** The coding diagram is shown in Fig. D.36. The PSPICE program is

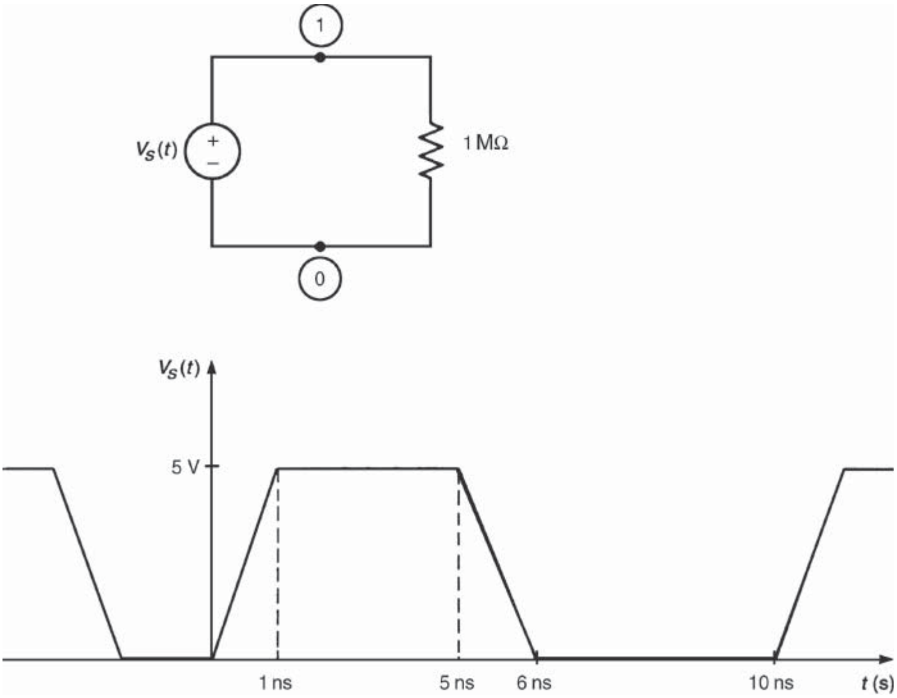

FIGURE D.36 Example D.9 PSPICE coding.

```
EXAMPLE D.9
VS  1  0  PULSE(0  5  0  1N  1N  4N  10N)
R  1  0  1E6
.TRAN  0.0001N  10N
.FOUR  100MEG  V(1)
.PROBE
.END
```

The output in FOUR.OUT is shown in Table D.5

TABLE D.5 Fourier Components of Transient Response V(1)

DC Component = 2.500006E+00

Harmonic No	Frequency (HZ)	Fourier Component	Normalized Component	Phase (DEG)	Normalized Phase (DEG)
1	1.000E+08	3.131E+00	1.000E+00	−1.800E+01	0.000E+00
2	2.000E+08	1.149E−05	3.669E−06	5.321E+01	7.104E+01
3	3.000E+08	9.108E−01	2.909E−01	−5.400E+01	−3.600E+01
4	4.000E+08	9.224E−06	2.946E−06	1.624E+01	3.424E+01
5	5.000E+08	4.053E−01	1.294E−01	−9.000E+01	−7.200E+01
6	6.000E+08	6.035E−06	1.928E−06	−2.129E+01	−3.293E+00
7	7.000E+08	1.673E−01	5.343E−02	−1.260E+02	−1.080E+02
8	8.000E+08	2.633E−06	8.409E−07	−6.143E+01	−4.343E+01
9	9.000E+08	3.865E−02	1.235E−02	−1.620E+02	−1.440E+02

These are virtually identical with the hand computations in Review Exercise 3.1 for the first seven harmonics.

Example D.10 Use PSPICE to recombine the dc and first nine harmonics for the trapezoidal waveform of the previous example to give the time-domain waveform with a truncated spectrum.

***Solution*:** The idea is to use PSPICE to add sinusoidal voltages corresponding to the harmonics as illustrated in Fig. D.37a. The sinusoidal function is specified by

```
SIN (V0  Va  [[Freq  [[Td  [[Df  [[Phase]]]]]]]])
```

which gives the waveform

$$x(t) = v0 + Va\ \sin\left(2\pi\left(\mathrm{Freq}(\mathrm{time} - Td) + \frac{\mathrm{Phase}}{360}\right)\right) e^{-(\mathrm{time}-Td)\ Df}$$

we would write

```
SIN (0  A  nf  0  0  θ)
```

The PSPICE program is

```
EXAMPLE D.10
VS0  1  2  DC  2.5
VS1  2  3  SIN(0  3.131  100MEG  0  0  -180)
VS2  3  4  SIN(0  1.149E-5  200MEG  0  0  53.21)
```

```
VS3  4  5  SIN(0  0.9108  300MEG  0  0  -54)
VS4  5  6  SIN(0  9.224E-6  400MEG  0  0  16.24)
VS5  6  7  SIN(0  0.4053  500MEG  0  0  -90)
VS6  7  8  SIN(0  6.035E-6  600MEG  0  0  -21.29)
VS7  8  9  SIN(0  0.1673  700MEG  0  0  -126)
VS8  9  10  SIN(0  2.633E-6  800MEG  0  0  -61.43)
VS9  10  0  SIN(0  0.03865  900MEG  0  0  -162)
VS  11  0  PULSE(0  5  0  1N  1N  4N  10N)
R1  1  0  1MEG
RS  11  0  1MEG
.TRAN  0.01N  10N
.PROBE
.END
```

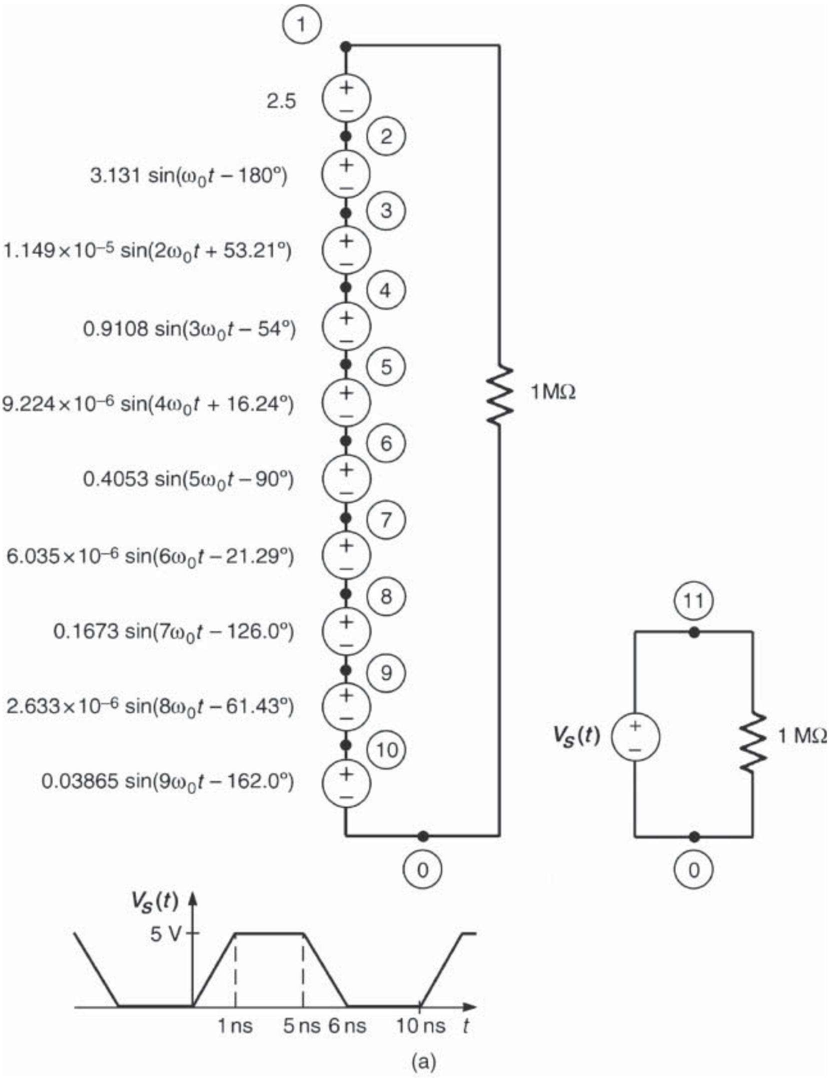
1
2.5
2
3.131 sin(ω0t − 180°)
3
1.149×10−5 sin(2ω0t + 53.21°)
4
0.9108 sin(3ω0t − 54°)
5
9.224×10−6 sin(4ω0t + 16.24°)
6
0.4053 sin(5ω0t − 90°)
7
6.035×10−6 sin(6ω0t − 21.29°)
8
0.1673 sin(7ω0t − 126.0°)
9
2.633×10−6 sin(8ω0t − 61.43°)
10
0.03865 sin(9ω0t − 162.0°)
1MΩ
0
11
Vs(t)
1 MΩ
0
Vs(t)
5 V
1 ns
5 ns 6 ns
10 ns
t
(a)

FIGURE D.37 Example D.10: (a) the PSPICE coding; (b) the PSPICE simulation results showing the components; (c) the PSPICE simulation showing the total summation of the components.

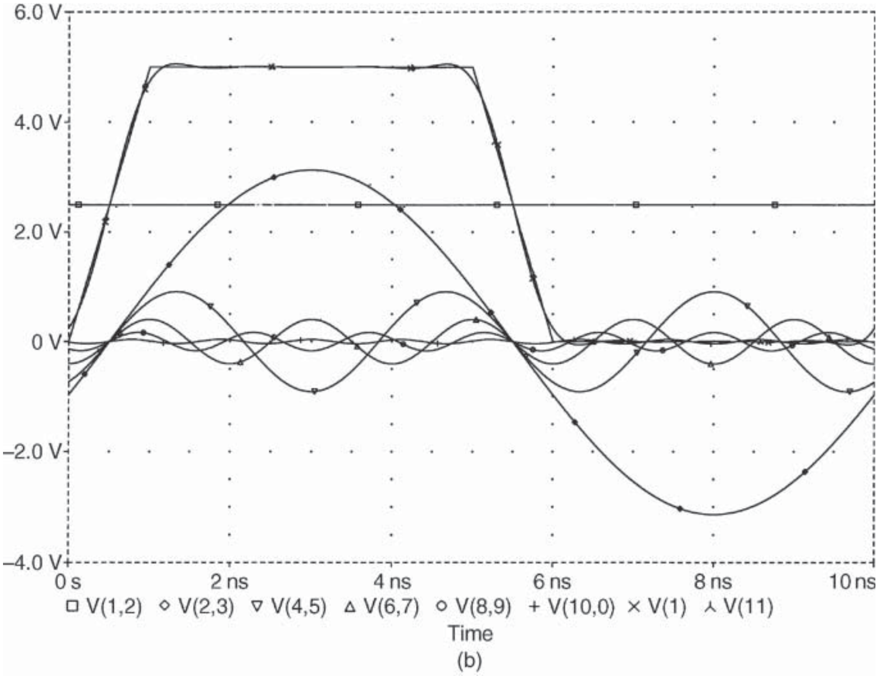

(b)

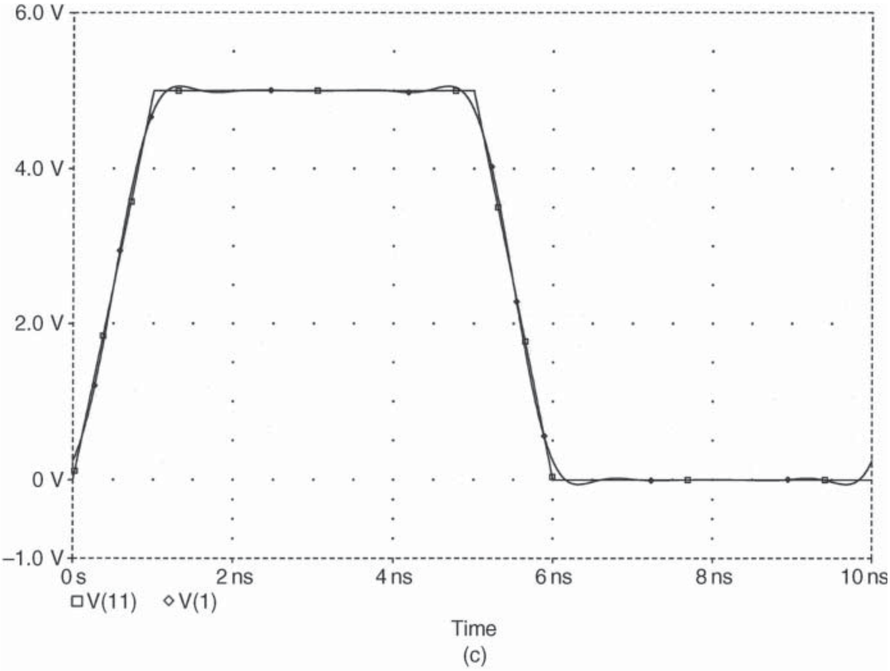

(c)

FIGURE D.37 (*Continued*)

Figure D.37b shows the individual harmonics and how they combine in time to give the composite time-domain waveform. Figure D.37c compares the exact waveform to that obtained by combining the dc term and the first nine harmonics. The reconstruction is quite good. But this is to be expected since the bandwidth for this waveform is $\mathrm{BW} = \frac{1}{\tau_r} = 1$ GHz. Figure D.37c should be compared to Fig. 3.24a, which was constructed using MATLAB and the hand-calculated values of the harmonics.

Hence, to specify the general sinusoidal waveform

$$x(t) = A \ \sin(n\omega_0 t + \theta)$$

Example D.11 In order to simplify our results for the trapezoidal (clock) waveform to aid in the interpretation of the spectrum, we assumed in the exact results in (3.46) that the rise- and falltimes of the pulse were equal, leading to the result in (3.48). In order to assess this assumption, compare the first nine harmonics of a 5 V, 50 MHz trapezoidal waveform having a 50% duty cycle for equal and unequal rise/falltimes: (1) $\tau_r = \tau_f = 5$ ns, (2) $\tau_r = 6$ ns and $\tau_f = 5$ ns, and (3) $\tau_r = 7$ ns and $\tau_f = 5$ ns.

***Solution*:** For the first case, where $\tau_r = \tau_f = 5$ ns, the PSPICE program is

```
EXAMPLE D.11(1)
VS  1  0  PWL(0  0  5N  5  10N  5  15N  0  20N  0)
R  1  0  1MEG
.TRAN  0.01N  20N  0  0.01N
.FOUR  50MEG  V(1)
.PROBE
.END
```

The results for the first nine expansion coefficients are shown Table D.6

TABLE D.6 Fourier Components of Transient Response V(1)

DC Component = 2.500000E+00

Harmonic No	Frequency (HZ)	Fourier Component	Normalized Component	Phase (DEG)	Normalized Phase (DEG)
1	5.000E + 07	2.866E + 00	1.000E + 00	−4.500E + 01	0.000E + 00
2	1.000E + 08	5.594E − 10	1.952E − 10	2.334E + 01	6.834E + 01
3	1.500E + 08	3.184E − 01	1.990E − 01	−1.350E + 02	−9.000E + 01
4	2.000E + 08	5.550E − 10	1.937E − 10	−1.662E + 02	−1.212E + 02
5	2.500E + 08	1.146E − 01	4.000E − 02	−4.500E + 01	8.185E − 08
6	3.000E + 08	1.191E − 09	4.154E − 10	9.100E + 01	1.360E + 02
7	3.500E + 08	5.849E − 02	2.041E − 02	−1.350E + 02	−9.000E + 01
8	4.000E + 08	8.294E − 10	2.894E− 10	2.413E + 01	6.913E + 01
9	4.500E + 08	3.538E − 02	1.235E − 02	−4.500E + 01	1.004E − 07

These are identical to the hand-calculated results using (3.48).

For the second case, where $\tau_r = 7$ ns and $\tau_f = 5$ ns (and still retaining the pulse transition starting halfway in the period at 10 ns), the PSPICE program is

```
EXAMPLE D.11(2)
VS  1  0  PWL(0  0  6N  5  10N  5  15N  0  20N  0)
R  1  0  1MEG
.TRAN  0.01N  20N  0  0.01N
.FOUR  50MEG  V(1)
.PROBE
.END
```

The results for the first nine expansion coefficients are shown Table D.7

TABLE D.7 Fourier Components of Transient Response V(1)

DC Component = 2.375000E + 00

Harmonic No	Frequency (HZ)	Fourier Component	Normalized Component	Phase (DEG)	Normalized Phase (DEG)
1	5.000E+07	2.790E+00	1.000E+00	−4.939E+01	0.000E+00
2	1.000E+08	1.759E−01	6.305E−02	1.348E+02	1.842E+02
3	1.500E+08	2.107E−01	7.616E−02	−1.421E+02	−9.272E+01
4	2.000E+08	6.204E−02	2.223E−02	−3.600E+01	1.339E+01
5	2.500E+08	1.154E−01	4.137E−02	−6.944E+01	−2.005E+01
6	3.000E+08	4.587E−02	1.644E−02	1.191E+02	1.685E+02
7	3.500E+08	2.619E−02	9.385E−03	−1.138E+02	−6.436E+01
8	4.000E+08	2.510E−02	8.993E−03	−7.200E+01	−2.261E+01
9	4.500E+08	2.628E−02	9.419E−03	−8.433E+01	−3.494E+01

These are identical to those computed by hand from (3.46) [where we must double those of (3.46) to get the magnitudes of the one-sided expansion].

For the third case, where $\tau_r = 7$ ns and $\tau_f = 5$ ns (and still retaining the pulse transition starting halfway in the period at 10 ns), the PSPICE program is

```
EXAMPLE D.11(3)
VS  1  0  PWL(0  0  7N  5  10N  5  15N  0  20N  0)
R  1  0  1MEG
.TRAN  0.01N  20N  0  0.01N
.FOUR  50MEG  V(1)
.PROBE
.END
```

The results for the first nine expansion coefficients are shown Table D.8

TABLE D.8 Fourier Components of Transient Response V(1)

DC Component = 2.250000E + 00

Harmonic No	Frequency (HZ)	Fourier Component	Normalized Component	Phase (DEG)	Normalized Phase (DEG)
1	5.000E+07	2.689E+00	1.000E+00	−5.352E+01	0.000E+00
2	1.000E+08	3.200E−01	1.190E−01	1.225E+02	1.761E+02
3	1.500E+08	1.459E−01	5.424E−02	−1.270E+02	−7.346E+01
4	2.000E+08	8.604E−02	3.199E−02	−7.200E+01	−1.848E+01
5	2.500E+08	7.044E−02	2.619E−02	−8.054E+01	−2.702E+01
6	3.000E+08	5.377E−02	1.999E−02	7.730E+01	1.308E+02
7	3.500E+08	5.205E−02	1.936E−02	−1.080E+02	−5.451E+01
8	4.000E+08	1.329E−02	4.944E−03	−1.440E+02	−9.048E+01
9	4.500E+08	2.553E−02	9.494E−03	−3.936E+01	1.416E+01

These are also identical to those computed by hand from (3.46) [where we must double those of (3.46) to get the magnitudes of the one-sided expansion].

Observe that the even harmonics are zero only for a 50% duty cycle *and* equal rise- and falltimes. The ratios of the odd harmonic magnitudes between case (1) and case (2) are $n = 1$, 1.027, $n = 3$, 1.498, $n = 5$, 0.993, $n = 7$, 2.233, and $n = 9$, 1.346. The ratios for $n = 1, 3, 5, 9$ are minor, yet the ratio for $n = 7$ is significant. The ratios of the odd-harmonic magnitudes between cases 1 and 3 are $n = 1$, 1.066, $n = 3$, 2.182, $n = 5$, 1.627, $n = 7$, 1.106, and $n = 9$, 1.386. The ratios for $n = 1, 5, 7, 9$ are minor, yet the ratio for $n = 3$ is significant.

D.6 SPICEMTL.FOR FOR COMPUTING A SPICE (PSPICE) SUBCIRCUIT MODEL OF A LOSSLESS, MULTICONDUCTOR TRANSMISSION LINE

Required Input Files: SPICEMTL.IN, PUL.DAT

Output File: SPICEMTL.OUT. This code implements the exact solution of the multiconductor transmission-line equations for a multiconductor, lossless transmission line by generating a SPICE (PSPICE) subcircuit model of the line. The program reads (1) the total number of conductors and (2) the total line length from the input file SPICEMTL.IN. It also reads the per-unit-length inductance and capacitance matrices, **L** and **C**, from PUL.DAT computed for the specific-line cross-sectional configuration by one of the preceding programs in appendix C. It then diagonalizes these matrices and generates a SPICE subcircuit coding to represent the transmission line as illustrated in Fig. D.26. The user then embeds this subcircuit model in a SPICE (PSPICE) program by attaching the line terminations and providing the computational and output coding as described in Section D.7 and illustrated in Fig. D.27. The subcircuit model has attachment nodes as shown in Fig. D.38. The nodes at $z = 0$ are numbered 101, 102, …, 10n for the nodes of conductors 1, 2, …, n and 201, 202, …, 20n for the nodes of conductors 1, 2, …, n at $z =$ L as illustrated in Fig. D.38.

The following is the input file SPICEMTL.IN for the problem in Section D.7.2 and shown in Fig. D.31:

```
3    =Total Number of Conductors (N+1)
0.254=Total Line Length (m)
```

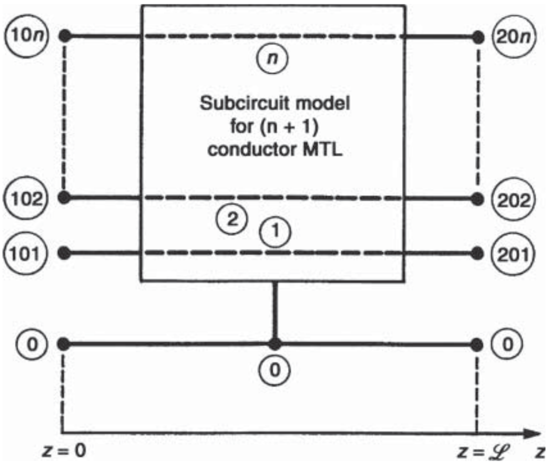

FIGURE D.38 Terminal node numbering scheme for the SPICE subcircuit model generated by the FORTRAN program SPICEMTL.FOR.

The per-unit-length parameter matrices were generated previously by the code PCB.FOR and stored in PUL.DAT. The output file in SPICEMTL.OUT is the SPICE subcircuit model:

```
* SUBCIRCUIT MODEL OF A MULTICONDUCTOR TRANSMISSION LINE*
*  NUMBER OF CONDUCTORS= 3
*  TOTAL LINE LENGTH (METERS)= 2.54000E-01
*  L( 1, 1)= 1.38315E-06
*  L( 1, 2)= 6.91573E-07
*  L( 2, 2)= 1.10707E-06
*  C( 1, 1)= 2.96949E-11
*  C( 1, 2)=-2.02619E-11
*  C( 2, 2)= 4.05238E-11
.SUBCKT MTL
+ 101
+ 102
+ 201
+ 202
V101 101 301
EC101 301 0 POLY( 2)
+     (501,0)
+     (502,0)
+0
+     9.999894E-01
+     -2.372106E-05
FC101 0 501 POLY( 2)
+ V101
+ V102
+0
+     9.999894E-01
+     5.000049E-01
V201 201 401
EC201 401 0 POLY( 2)
+     (601,0)
+     (602,0)
+0
+     9.999894E-01
+     -2.372106E-05
FC201 0 601 POLY   ( 2)
+ V201
+ V202
+0
+     9.999894E-01
+     5.000049E-01
V102 102 302
EC102 302 0 POLY( 2)
+     (501,0)
+     502,0)
+0
+     5.000049E-01
+     1.118027E+00
FC102 0 502 POLY( 2)
+     V101
+     V102
+0
+     -2.372106E-05
+     1.118027E+00
EC    202 402 0 POLY( 2)
+     (601,0)
+     (602,0)
+0
+     5.000049E-01
+     1.118027E+00
FC202 0 602 POLY( 2)
+ V201
+ V202
+0
+     -2.372106E-05
+     1.118027E+00
T101 501 0 601 0 Z0= 2.658983E+02 TD= 1.321285E-09
T102 502 0 602 0 Z0= 1.096490E+02 TD= 1.410790E-09
.ENDS MTL
```

D.7 SPICELPI.FOR FOR COMPUTING A SPICE (PSPICE) SUBCIRCUIT OF A LUMPED-PI MODEL OF A LOSSLESS, MULTICONDUCTOR TRANSMISSION LINE

Required Input Files: SPICELPI.IN, PUL.DAT

Output File: SPICELPI.OUT. This code implements a SPICE (PSPICE) subcircuit for the lumped-Pi model of a lossless, multiconductor transmission line described in Section D.6. The program reads (1) the total number of conductors, and (2) the total line length from the input file SPICELPI.IN. It also reads the per-unit-length inductance and capacitance matrices, **L** and **C**, from PUL.DAT that was computed for the specific line cross-sectional configuration by one of the preceding programs. It then constructs a lumped-Pi approximate model for the line as described in Section D.6. The user then imbeds this subcircuit model in a SPICE (PSPICE) program by attaching the line terminations and providing the computational and output coding as illustrated in Fig. D.27. The subcircuit model has attachment nodes as shown in Fig. D.38. The nodes at $z = 0$ are numbered 101, 102, …, 10n for the nodes of conductors 1, 2, … ,n and 201, 202, …, 20n for the nodes of conductors 1, 2, …, n at $z = \mathrm{L}$ as is illustrated in Figure D.38.

The following is the input file SPICELPI.IN for the problem in Section D.7.2 and shown in Fig. D.31.

```
3 =Total Number of Conductors (N+1)
0.254 =Total Line Length (m)
```

The per-unit-length parameter matrices are generated by the code PCB.FOR in appendix C and stored in PUL.DAT. The output file in SPICELPI.OUT is the SPICE subcircuit model:

```
*SUBCIRCUIT MODEL OF A MULTICONDUCTOR TRANSMISSION LINE*
*LUMPED-PI APPROXIMATE STRUCTURE*
*  TOTAL NUMBER OF CONDUCTORS= 3
*  TOTAL LINE LENGTH (METERS)=2.54000E-01
*  L(1, 1)= 1.38315E-06
*  L(1, 2)= 6.91573E-07
*  L(2, 2)= 1.10707E-06
*  C(1, 1)= 2.96949E-11
*  C(1, 2)=-2.02619E-11
*  C(2, 2)= 4.05238E-11
.SUBCKT LPI
+ 101
+ 102
+ 201
+ 202
L101       101     201     3.51320E-07
C101       101     0       1.19799E-12
C201       201     0       1.19799E-12
L102       102     202     2.81196E-07
C102       102     0       2.57326E-12
C202       202     0       2.57326E-12
K101       L101    L102    5.58877E-01
CM101      101     102     2.57326E-12
CM201      201     202     2.57326E-12
.ENDS LPI
```

PROBLEMS

Section D.5 Use of SPICE (PSPICE) in Fourier Analysis

D.5.1 Use the .FOUR function in PSPICE to verify the expansion coefficients obtained for Problem 3.1.3.

D.5.2 Use the .FOUR function in PSPICE to verify the expansion coefficients obtained for Problem 3.1.4.

D.5.3 Use the .FOUR function in PSPICE to verify the expansion coefficients obtained for Problem 3.1.5.

D.5.4 Use the .FOUR function in PSPICE to verify the expansion coefficients obtained for Problem 3.1.6.

D.5.5 Use the .FOUR function in PSPICE to verify the expansion coefficients obtained for Problem 3.1.7.

Section D.6 Lumped-Circuit Approximate Models

D.6.1 Consider the case of three identical wires having radii of 10 mils and arranged on the vertices of an equilateral triangle with 100 mil sides as shown in Fig. PD.6.1a. The wires are immersed in a homogeneous medium having $\varepsilon_r = 2.1$. It is desired to model a 2 m length of this line using a lumped-Pi circuit as shown in Fig. PD.6.1b. Determine element values in this equivalent circuit. [$L_G = 1.84$ μH, $L_R = 1.84$ μH, $L_m = 0.921$ μH, $C_G = 16.9$ pF, $C_R = 16.9$ pF, $C_m = 16.9$ pF] Above what frequency would you expect this model to be invalid for sinusoidal inputs to the line? [10.35 MHz] For trapezoidal pulse train inputs what would be the rise/falltime of the fastest allowable pulse train for which this model would be expected to yield reasonable predictions. [96.6 ns] Prepare a lumped Pi approximate model by obtaining an LTSPICE subcircuit model using the FORTRAN code SPICELPI.FOR, contained in this appendix. Compute the per-unit-length parameters using the FORTRAN code WIDESEP.FOR in Appendix C.

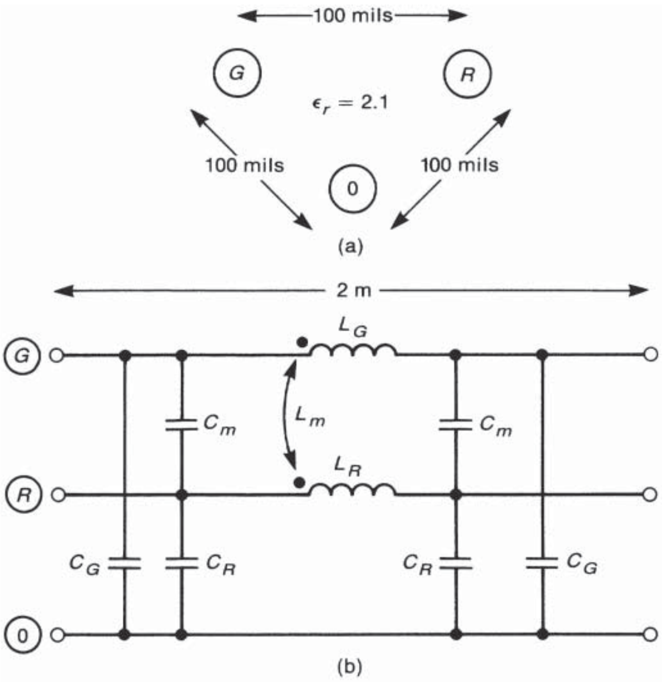

FIGURE PD.6.1

Section D.7 An Exact SPICE (PSPICE) Model for Lossless, Coupled Lines

D.7.1 For the coupled microstrip in Fig. 9.31, generate (1) a PSPICE subcircuit model and (2) a lumped-Pi approximate subcircuit model to represent this structure. Combine these into one PSPICE program and use it to predict the magnitudes of the frequency-domain near-end and far-end cross talk transfer functions, $|\hat{V}_{NE}|/|\hat{V}_S|$ and $|\hat{V}_{FE}|/|\hat{V}_S|$ for $R_S = 0$, $R_L = R_{NE} = R_{FE} = 50\ \Omega$. Plot these in order to compare them from 100 kHz to 1 GHz. Also use this program to predict the time-domain waveshape of the near-end and far-end crosstalk for a source voltage that is a 1 V, 10 MHz trapezoidal waveform having a 50% duty cycle and rise/falltimes of 10 and 1 ns. Compare the levels of the crosstalk pulses predicted to those predicted by the approximate inductive–capacitive coupling model of Section 9.4.2.

D.7.2 For the ribbon cable in Fig. 9.29, generate (1) a PSPICE subcircuit model and (2) a lumped-Pi approximate subcircuit model to represent this structure. Combine these into one PSPICE program and use it to predict the magnitudes of the frequency-domain near-end and far-end crosstalk transfer functions, $|\hat{V}_{NE}|/|\hat{V}_S|$ and $|\hat{V}_{FE}|/|\hat{V}_S|$ for $R_S = 0$, $R_L = R_{NE} = R_{FE} = 50\ \Omega$. Plot these in order to compare them from 100 Hz to 100 MHz. Also use this program to predict the time-domain waveshape of the near-end and far-end crosstalk for a source voltage that is a 1 V, 100 kHz trapezoidal waveform having a 50% duty cycle and rise/falltimes of 200 and 20 ns. Compare the levels of the crosstalk pulses predicted to those predicted by the approximate inductive–capacitive coupling model of Section 9.4.2.

D.7.3 An innerplane PCB has two lands of width 5 mils separated edge-to-edge by 5 mils on a glass epoxy board of thickness 10 mils. Model this as a coupled microstrip. Each land with the group plane connects two CMOS inverters as shown in Fig. PD.7.1. The CMOS inverters are modeled as shown in Fig. P9.6.3c. Assume that one inverter has an open-circuit voltage of 5 V, 10 MHz pulse train, 50% duty cycle, and 10 ns rise/falltimes. Compute the near-end and far-end crosstalk waveforms in the other circuit using the exact transmission-line subcircuit model generated by SPICEMTL.FOR if the total line length is 5 in.

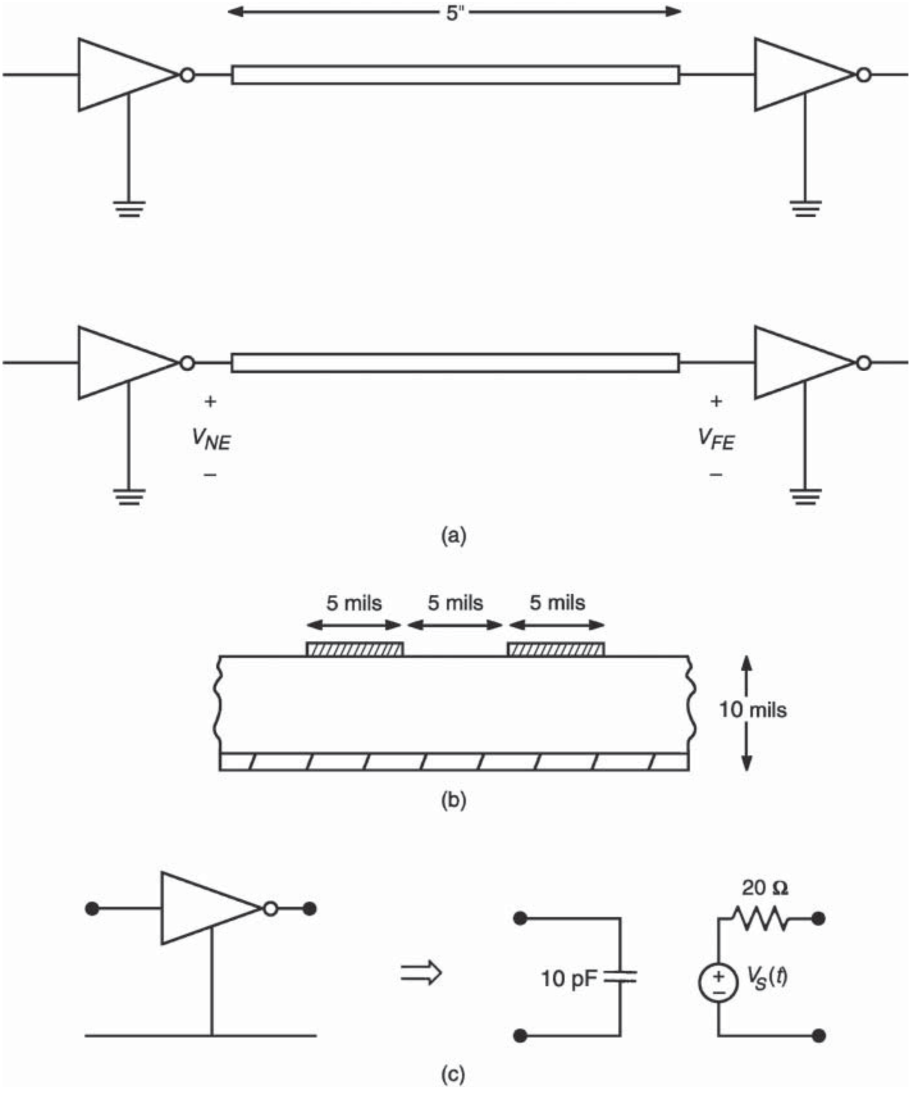

FIGURE PD.7.1

REFERENCES

1. C. R. Paul, *Fundamentals of Electric Circuit Analysis*, Wiley, New York, 2001.
2. P. W. Tuinenga, *SPICE: A Guide to Simulation and Analysis Using PSPICE*, 3rd ed., Prentice-Hall, Englewood Cliffs, NJ, 1995.

3. A. Vladimirescu, *The SPICE Book*, Wiley, New York, 1994.
4. R. Conant, *Engineering Circuit Analysis with PSpice and Probe*, McGraw-Hill, 1993.
5. J. W. Nilsson and S. A. Riedel, *Introduction to PSpice Manual for Electric Circuits Using OrCad Release 9.1*, 4th ed., Prentice-Hall, Englewood Cliffs, NJ, 2000.
6. G. Brocard, *The LTSPICE XVII Simulator Commands and Applications Manual, Methods and Applications*, 1st ed., Wurth Elektronik eiSos GmbH & Co. KG, Waldenburg, Germany, March 2021.

APPENDIX E

A Brief History of Electromagnetic Compatibility

This appendix is intended to provide an overview of electromagnetic compatibility and its origins, complete with some examples of system failures attributed to the lack of electromagnetic compatibility.

E.1 HISTORY OF EMC

It may be said that radio interference and its correction arose with the first spark-gap communications systems of De Forest, Marconi, Popov, and others in the late 1800s and early 1900s. In December 1901, Marconi accomplished the first transatlantic transmission using an array of copper wires. The only receptors of significance at that time were radio receivers. These were few and widely separated, so that the correction of an interference problem was relatively simple. However, technical papers on radio interference began to appear in various technical journals around 1920. The radio receivers and antennas were rather crude and were prone to interference either from external sources or from within as with self-induced oscillations. Improvements in design technology cured many of these problems. Radio interference from electrical apparatus such as electric motors, electric railroads, and electric signs soon began to appear as a major problem around 1930.

During World War II, the use of electronic devices, primarily radios, navigation devices, and radar, accelerated. Instances of interference between radios and navigational devices on aircraft began to increase. These were usually easily corrected by reassignment of transmitting frequencies in an uncrowded spectrum or physically moving cables away from noise emission sources to prevent the cables from picking up those emissions. Because the density of the electronics (primarily vacuum tube electronics) was considerably less than it is today, these interference remedies could be easily implemented on a case-by-case basis to correct any electromagnetic interference (EMI) problem. However, the most significant increases in the interference problem occurred with the inventions of high-density electronic components such as the bipolar transistor in the 1950s, the integrated circuit (IC) in the 1960s, and the microprocessor chip in the 1970s. The frequency spectrum also became more crowded with the increased demand for voice and data transmission. This required considerable planning with regard to *spectrum utilization* and continues today.

Introduction to Electromagnetic Compatibility, Third Edition. Clayton R. Paul, Robert C. Scully, and Mark A. Steffka.

© 2023 John Wiley & Sons, Inc. Published 2023 by John Wiley & Sons, Inc.

Perhaps the primary event that brought the present emphasis on EMC to the forefront was the introduction of digital signal processing and computation. In the early 1960s, digital computers used vacuum tubes as switching elements. These were rather slow (by today's standards) and required large power consumption and considerable "real estate." In the 1970s, the integrated circuit allowed the construction of computers that consumed far less power and required much less physical space. Toward the end of the 1970s, the trend toward replacing *analog signal processing* with *digital signal processing* began to accelerate. Almost all electronic functions were being implemented digitally because of the increased switching speed and miniaturization of the ICs. The implementation of various tasks ranging from computation to word processing to digital control became widespread, and continues today. This meant that the density of noise sources rich in spectral content (switching waveforms) was becoming quite large. Consequently, the occurrence of EMI problems began to rise.

Because of the increasing occurrence of digital system interference with wire and radio communication, the Federal Communications Commission (FCC) in the United States published a regulation in 1979 that required the electromagnetic emissions of all "digital devices" to be below certain limits. The intent of this rule was to try to limit the "electromagnetic pollution" of the environment in order to prevent, or at least reduce, the number of instances of EMI. Because no "digital device" could be sold in the United States unless its electromagnetic emissions met these limits imposed by the FCC, the subject of EMC generated intense interest among the manufacturers of commercial electronics ranging from digital computers to electronic typewriters.

This is not intended to imply that the United States was at the forefront of "cleaning up the electromagnetic environment" in mandating limits on electromagnetic emissions. Countries in Europe imposed similar requirements on digital devices well before the FCC issued its rule. In 1933, a meeting of the International Electrotechnical Commission (IEC) in Paris recommended the formation of the International Special Committee on Radio Interference (CISPR) to deal with the emerging problem of EMI. The committee produced a document detailing measurement equipment for determining potential EMI emissions. The CISPR reconvened after World War II in London in 1946. Subsequent meetings yielded various technical publications, which dealt with measurement techniques, as well as recommended emission limits. Some European countries adopted versions of CISPR's recommended limits. The FCC rule was the first regulation for digital systems in the United States, and the limits follow the CISPR recommendations with variations peculiar to the US environment. Most manufacturers of electronic products within the United States already had internal limits and standards imposed on their products in order to prevent "field problems" associated with EMI. However, the FCC rule made what had been voluntary a matter of legal compliance.

The military community in the United States also imposed limits on the electromagnetic emissions of electronic systems to prevent EMI through MIL-STD-461 prior to the FCC issuing its rule. These had been in effect from the early 1960s and were imposed to insure "mission success." All electronic and electrical equipment ranging from hand drills to sophisticated computers were required to meet the emission limits of these standards. Another aspect of the military's regulations is the imposition of a *susceptibility requirement*. Interfering signals are purposely injected into the equipment, which must then operate properly in the presence of these signals. Even though an electronic product complies with the emission requirements, it could cause interference with or be susceptible to the emissions of another electronic device in proximity. The emission requirements simply attempt to limit electromagnetic pollution. Susceptibility requirements go one step further in attempting to insure electromagnetically compatible operation of all equipment.

These regulations have made EMC a critical aspect in the marketability of an electronic product. If the product does not comply with these regulations for a particular country, it cannot be sold in that country. The fact that the product performs some very desirable task and customers are willing to purchase it is unimportant if it does not comply with the regulatory requirements. Throughout this text, the reader should keep in mind that the evolution of technology has caused the subject of EMC design to be as critical a part of electronic design as any of the traditional aspects.

E.2 EXAMPLES

There are numerous examples of EMI, ranging from the commonplace to the catastrophic. In this section, we will mention a few of these.

Probably one of the more common examples is the occurrence of “lines” across the face of a television screen when a blender, vacuum cleaner, or other household device containing a universal motor is turned on. This problem results from the arcing at the brushes of the universal motor. As the commutator makes and breaks contact through the brushes, the current in the motor windings (an inductance) is being interrupted, causing a large voltage ($L\,di/dt$) across the contacts. This voltage is similar to the Marconi spark-gap generator and is rich in spectral content. The problem is caused by the radiation of this signal to the TV antenna caused by the passage of this noise signal out through the ac power cord of the device. This places the interference signal on the common power net of the household. As mentioned earlier, this common power distribution system is a large array of wires. Once the signal is present on this efficient “antenna,” it radiates to the TV antenna, creating the interference.

A manufacturer of office equipment placed its first prototype of a new copying machine in its headquarters. An executive noticed that when someone made a copy, the hall clocks would sometimes reset or do strange things. The problem turned out to be due to the silicon-controlled rectifiers (SCRs) in the power-conditioning circuitry of the copier. These devices turn on and off to “chop” the ac current to create a regulated dc current. These signals are also rich in spectral content because of the abrupt change in current and were coupled out through the copier’s ac power cord onto the common ac power net in the building. Clocks in hallways are often set and synchronized by use of a modulated signal imposed on the 60 Hz ac power signal. The “glitch” caused by the firing of the SCRs in the copier coupled into the clocks via the common ac power net and caused them to interpret it as a signal to reset.

A new version of an automobile had a microprocessor-controlled emission and fuel monitoring system installed. A dealer received a complaint that when the customer drove down a certain street in the town, the car would stall. Measurement of the ambient fields on the street revealed the presence of an illegal FM radio transmitter. The signals from that transmitter coupled onto the wires leading to the processor and caused it to shut down.

Certain trailer trucks had electronic braking systems installed. Keying a citizen’s band (CB) transmitter in a passing automobile would sometimes cause the brakes on the truck to “lock up.” The problem turned out to be the coupling of the CB signal into the electronic circuitry of the braking system. Shielding the circuitry cured the problem.

A large computer system was installed in an office complex near a commercial airport. At random times, the system would lose or store incorrect data. The problem turned out to be synchronized with the sweep of the airport surveillance radar as it illuminated the office complex. Extensive shielding of the computer room prevented any further interference.

In 1982, the United Kingdom lost a destroyer, the HMS *Sheffield*, to an Exocet missile during an engagement with Argentinian forces in the battle of the Falkland Islands. The destroyer’s radio system for communicating with the United Kingdom would not operate properly while the ship’s antimissile detection system was being operated due to interference between the two systems. To temporarily prevent interference during a period of communication with the United Kingdom, the antimissile system was turned off. Unfortunately, this coincided with the enemy launch of the Exocet missile.

The US Army purchased an attack helicopter designated as the UH-60 Black Hawk. On Sunday, November 8, 1988, various news agencies reported that the helicopter was susceptible to electromagnetic emissions. Evidence revealed in these reports indicated most of the crashes of the Black Hawk since 1982, which killed 22 servicepeople, were caused by flying too close to radar transmitters, radio transmitters, and possibly even a CB transmitter. The susceptibility of the helicopter's electronically controlled flight control system to these electromagnetic emissions was thought to have caused these crashes.

On July 29, 1967, the US aircraft carrier *Forrestal* was deployed off the coast of North Vietnam. The carrier deck contained numerous attack aircraft that were fueled and loaded with 1000-pound bombs, as well as air-to-air and air-to-ground missiles. One of the aircraft missiles was inadvertently deployed, striking another aircraft, and causing an explosion of its fuel tanks and the subsequent death of 134 servicepeople. The problem was thought to be caused by the generation of radio-frequency (RF) voltages across the contacts of a shielded connector by the ship's high-power search radar.

These are a few of the many instances of EMI in our dense electronic world. The life-threatening results clearly demand remedies. The occurrences that merely result in annoyance or loss of data in a computer are not as dramatic, but still create considerable disruption and require resolution.

INDEX

absorption loss, 562, 563, 570, 574, 575, 580, 581
ac motors, 264, 267–268
American National Standards Institute (ANSI), 48
AmericanWire Gauge (AWG), 222
Ampere's law, 711–716
  point form, 719
antenna arrays, 342–349
antenna factor, 356–359
antenna-mode currents, 261
arc discharge, 271, 272, 273, 274, 276, 664–667
arcing at switch contacts, 271–274
arc suppression, 275–278
array factor of antenna array, 376
autocorrelation function, 122, 123, 132
average
  spectrum analyzer detector, 117–118
average detector (AV)
  of measurement receiver, 38

Babinet's principle, 559, 560, 586, 587
balanced systems, 635
balanced vs unbalanced terminations, 549
balancing antennas, 359
baluns, 305, 359–363, 433, 434, 636
bandpass filter, 113–115
bandreject filter, 322
bands on transformers, 584
bandwidth
  of digital waveforms, 105–108
basis functions, 72, 73, 74, 105
bazooka balun, 360, 361
B-H curve, 584
biconical antenna, 51, 381–385, 387
  input impedance to, 381, 383
  for measurement of radiated emissions, 50, 381, 385
Bode plot
  interpolation on, 103
bounce or lattice diagram
  of transmission line, 167
boundary conditions, 368, 371, 372, 378, 388, 431, 432, 473, 586, 671, 720–724
  perfect conductors, 371
  realistic media, 124, 415
bound charge, 204, 468, 469, 470, 475, 740
bowtie antenna, 384
braided shields, 436, 438, 604, 612
bridge rectifier, 314, 315
buck regulator, 313

capacitance of a coaxial cable, 134
capacitance of a two-wire line, 146
capacitance of one wire above a ground plane, 140, 148
capacitance of parallel wires, 229–230
capacitances for a three-wire line, 456, 458
capacitor
  equivalent circuit of, 245
characteristic impedance of a microstrip line, 279
characteristic impedance of a PCB, 151
characteristic impedance of a stripline, 206
characteristic impedance of transmission line, 156
CISPR 12, 63
CISPR 25, 63

Introduction to Electromagnetic Compatibility, Third Edition. Clayton R. Paul, Robert C. Scully, and Mark A. Steffka.
© 2023 John Wiley & Sons, Inc. Published 2023 by John Wiley & Sons, Inc.

CISPR 32, 38–45, 48–51, 54, 55
clock skew, 170, 171
CMOS inverter, 820
coaxial cable
  matched load, 26
coaxial cable transmission line
  capacitance of, 423
  inductance of, 423
common-impedance coupling, 481–484
common-mode choke, 261–264
  in power supply filter, 298–303
common-mode current
  emission model, 405–410
  equivalent circuit in power supply filter, 405–410
conductance of transmission lines, 201
conducted emission limits, FCC and CISPR 32
  graph of, 40–42
  table of for Class A devices, 42
  table of for Class B devices, 42
conducted susceptibility (immunity), 62
conductivities and permeabilities of conductors
  table of, 15
conductivities of metals relative to Copper
  table of, 15
conversion from dBmV to dBμA
  formula for, 19
conversion of mils to meters, 223
conversion to decibels, table of, 22
correction factor for horizontal polarization
  table of, 380
correction factor for vertical polarization
  table of, 380
coupled microstrip line, 449, 549, 761–762
coupled stripline, 447, 449, 475, 549, 762–763
crossover current, 606
crosstalk, 445–549
current gain in decibels, 18
current probes
  transfer impedance of, 410
currents in ground planes, 133

data signals spectra of, 72
dB above a microamp (dBuA), 19
dB above a microvolt (dBuV), 19
dB above a microvolt per meter (dBuV/m), 19
dB above a microwatt (dBuW), (AU:Not Found)
dB above a milliamp (dBmA), 19
dB above a milliwatt (dBmW), 19, 20
dc motors, 265–267
decibels
  power ratios, 29
  voltage and current ratios, 29
decoupling capacitors, 641–651
  in parallel, 648
decoupling the transmission-line equations, 671
diagnostic tools, 672–680
differential-mode current emission model, 402–405
differential-mode current equivalent circuit
  in power supply filter, 293–303
differential-mode currents, 291–294
differentiation of waveforms
  use of in computing Fourier coefficients, 92
digital device
  Class A and Class B, 37, 38, 41
  definition of, 37
diodes
  fast recovery, 315
  snubber circuits, 315, 316
dipole antenna
  current distribution on, 333
  far fields of, 333
directivity of an antenna, 349, 350
discone antenna, 384, 385
dispersion, 206
dominant effect, the concept of, 304, 674–680
duty cycle
  effect on spectrum, 108

E-cores, in transformers, 317
effective aperture of antennas, 354
effective relative permittivity, 135, 140, 153, 154, 180
  microstrip line, 133, 152, 154
effective relative permittivity of a PCB, 135, 140, 153, 154, 180, 234
electrical dimensions, 9–16
electric source, 577, 580, 581
electromagnetic compatibility (EMC)
  definition of, 2
electromagnetic pulse (EMP), 6, 7
electromagnetic wave, 1, 5, 7, 9, 388, 430, 561, 664
electrostatic discharge (ESD), 6, 7, 35, 44, 45, 62–63, 397, 423, 431, 432, 593, 608, 661–672, 721
EMC subproblems, 5
equivalent circuit
  of an inductor, 252
  of a capacitor, 245
  of component attachment leads, 235, 237
  of parallel conductors, 230–232
  of a resistor, 241

equivalent series resistance (ESR), 244
Euler's identity, 74–76, 683

Faraday shield, 318, 319, 596
Faraday's law, 139, 278, 313, 316, 410, 424, 450, 477, 506, 533, 701–711
far-end crosstalk, 481, 492, 498, 499, 500, 535
far field, 38, 39, 326, 327–329, 331, 334, 342, 366, 397, 400, 401
Federal Communications Commission (FCC), 36–38, 40–42, 44, 45, 48, 50, 54, 55, 60, 62, 221
ferrite beads, 258–260
ferromagnetic materials
  saturation and frequency response, 255–258
Fourier series
  expansion coefficients of, 74
  harmonics of, 74
  integral squared error, 105
  one-sided spectrum, 76, 79, 81, 86, 96, 108, 113
Fourier series of derivative of function
  coefficient relations, 74–82
Fourier transform, 119–121
Friis transmission equation, 365–368

gain
  of amplifier, 18, 23
  of an antenna, 351, 353
  of antenna in dB, 357
Gauss' law
  for the electric field, 143, 716
  for the magnetic field, 570, 575, 582
generator conductor, 446, 450, 490
gw discharge, 271, 273, 274, 276
green-wire inductor, 293, 301, 302, 308, 309
ground, 605–636
ground bounce, 607, 612–620
ground grid, 788, 810–811
ground loops, 534, 631, 632, 634–636, 678

half-wave dipole antenna, 335, 367, 586
Hertzian dipole antenna, 355
highpass filter, 322
homogeneous medium
  relation between l and c, 140
  velocity of propagation, 140
homogeneous vs inhomogeneous media, 452–454

impulse function, 82, 89, 90, 121
inductance
  of a coaxial cable, 423
  of one wire above a ground plane, 140, 148
  of parallel wires, 235
  for a three-wire line, 456
  of toroid, 255
  of a two-wire line, 146
induction in ESD, 660
inductive-capacitive coupling model
  frequency-domain model, 479–490
  model for shielded wires, 503–509
  model for twisted pairs, 533–538
  time-domain model, 479
inductors, parasitic elements of, 251
input impedance
  of dipoles and monopoles, 332
  phasor transmission line, 193, 205
input impedance to dipole antenna
  graph of, 194
insertion loss
  of filters, 294
  of pad, 362
  for shields, 364
interference
  definition of, 1, 2
internal inductance
  vs external inductance of wires, 229–230
  of wires, 223–229
International Electrotechnical Committee (IEC), 40
International Special Committee on Radio Interference (CISPR), 40–45, 48, 50, 51, 54
isotropic point source antenna, 353

Laplace's equation
  for static 2D fields, 744
lightning, 1, 6, 7, 62, 63, 287, 321, 423, 662
linearity and superposition, 121
linearity property of, 86
line impedance stabilization network (LISN), 37, 52, 53, 288
  equivalent circuit of, 37, 288
  FCC, impedance of, 36
  for measurement of conducted emissions, 288–291
  purposes of, 50
  simulation of input impedance, 338
  topology and element values, 297, 298
line-to-ground capacitors, 298, 299, 300–304, 307, 669
line-to-line capacitors, 298, 301, 303, 304, 307, 308

LISN for FCC and CISPR 22 tests
  diagram, 42
LISN for MIL-STD-461E tests
  diagram, 68, 824
loading coils, 338
logarithms, properties of, 21
log periodic antenna, 385–387
  for measurement of radiated emissions, 385
long arc, 273, 274
loop antenna, 584, 673
loop areas
  in radiated emissions of differential-mode currents, 651
loss tangent, 205, 206, 738
lossy transmission line equations of, 200–202
low-loss line, approximations for, 210
lowpass filter, 83, 106, 113, 118, 250, 259, 269

magnetic dipole moment, 330
magnetic source, 579–581
matched line, 196
Maxwell's equations, 701–720
  phasor form, 724
mechanical switches, 270–278
method of images, 148, 368
method of moments (MoM), 389, 464, 465, 467, 469, 472
microstrip line, 133, 152, 154, 205, 212, 449
microstrip transmission line
  sketch of, 219
MIL-STD-461, 44–51, 54, 62, 63
MIL-STD-461E
  CE102, RE102, CS101, CS114, RS103, 46
  emission and susceptibility requirements of, 45
  table of requirements, 45, 46
mode voltages and currents, 788–790
MSTRP.FOR, 475, 490, 753, 761–762
multipath effects, 376–381
multiple reflection factor, 563, 567, 570
  approximate solution, 570–572
multipoint ground, 629–634

near-end crosstalk, 481, 485–487
near field vs far field, 576–579
neutral voltage, 290, 292, 305
nonperiodic signal, energy of, 72

one-wire above a ground plane transmission line
  sketch of, 213
open-area test site (OATS)
  for measurement of radiated emissions, 50, 362, 376, 381, 385
open-circuit voltage, of a source, 17, 24, 25, 27, 180, 358
orthogonal functions, 105

pads, 65, 362–364, 596
parallel match, 178, 179, 188, 190
parallel-plate capacitor, 464–467, 469, 713
  graph of approximate vs exact capacitance, 148
parallel-ray approximation
  in antennas, 333
parallel wires
  lumped equivalent circuits of, 230–232
  per-unit-length capacitance of, 137, 139, 148, 151, 153, 232, 447
partial element equivalent circuit (PEEC), 599
partial inductance
  of PCB lands, 620
  of wires, 615–620
path of lowest impedance, 621, 626
pattern factor, of dipole antenna, 335, 337
pattern of antenna, 351
PCB.FOR, 475, 476, 490, 753, 760–761, 799
peak detector, of measurement receiver, 38
peak spectrum analyzer detector, 117–118
perfect conductor, 371, 372, 378, 432, 435, 598, 622
periodic signal
  average power in, 72, 726
  fundamental frequency of, 72
  response of a linear system to, 73, 121, 686
periodic train of impulse functions
  Fourier series of, 90
permeability of free space, 30, 599
permittivity of free space, 30
phase constant
  in lossless media, 729–733
  of wave, 10, 206
phase shift of wave, 12
phase velocity of propagation
  in lossless media, 731
phase voltage, 54
phasor circuit elements, 479, 687, 688
phasor method, 451, 683, 685–687
phasor transfer function, computation of, 83
piecewise-linear functions, 90
piecewise-linear waveforms, 86, 770, 771
pigtail, 435, 518–519, 521, 524
plane waves
  incident on perfect conductor, 372
power gain
  in decibels, 18

power spectral density
  of PCM-NRZ (data) waveform, 121, 124
  of random signal, 123
printed circuit board (PCB lands)
  configurations, three-conductor lines, 446, 447, 454, 785
  impedance of, 232
  per-unit-length resistance of, 234
  transmission line, sketch of, 261
power supply
  linear, 316
  primary-side switcher, 314, 315
  switched mode (SMPS), 312–315
power supply filter
  generic, 297–298
Poynting vector, 199, 329, 337, 370, 725, 726, 737
prevention of interference
  three primary methods, 4
printed circuit board lands,resistance of, 231
proximity effect
  on capacitance, 229
  for parallel wires, 229
PUL.DAT, 753, 756, 758, 759, 761–763, 793, 799
pulsewidth
  effect on spectrum, 96

quarter-wave monopole antenna, 332–342
quasi-peak detector (QP)
  of measurement receiver, 54
  spectrum analyzer detector, 117–118

radiated electric field
  of common-mode currents, 398–401
radiated emission limits
  CISPR 22
    graph of, 54
    table of for Class A devices, 39
    table of for Class B devices, 38, 39
  FCC
    graph of, 41
    table of for Class A devices, 39
    table of for Class B devices, 38, 39
    table of the upper limit for measurement, 40
  graphical comparison of Class A and Class B limits, 37, 38, 41
radiated emissions
  typical for digital product, 37
radiated susceptibility (immunity), 62
radiation intensity,of an antenna, 349
radiation resistance
  of half-wave dipole, 332–342
  of quarter-wave monopole, 332–342
radio frequency device
  FCC definition of, 36
Radio Technical Commission for Aeronautics (RTCA), 63
RC packs, 250, 639, 656
receptor conductor, 446, 447, 450, 457, 490
reciprocity for antennas, 354
reference conductor, 446–450, 459, 471, 472, 483, 487, 500, 518, 519, 529, 530
reflection coefficients
  of plane waves, 157
  of a transmission line, 159
reflection loss
  electric sources, 580
  magnetic sources, 580–581
regulation in power supplies, 313
relative permeabilities of metals, table of, 15
relative permittivities of dielectrics, table of, 15
relative permittivity, table of, 15
reluctance, of ferromagnetic materials, 316
resistance of PCB lands, 222
resistance of wires, 203, 612
resistors
  equivalent circuit of, 222
ribbon cable, 205, 232, 399, 405, 406, 407, 415, 445, 459, 463, 472, 486, 487
  experimental results, 415, 416
  match points in the numerical solution, 467, 744
RIBBON.FOR, 471, 484, 753, 758–760
right-hand rule, 141, 142, 263, 622, 628, 702
ringing (undershoot/overshoot)
  of digital signals, 109–111
RMS vs peak, 17
RTCA DO-160G, 63

SAE J551, 63
SAE J1113, 63
safety ground, 608–610
saturation, 255–258, 260, 264, 317, 583, 584, 606
saturation of ferromagnetic materials, 583, 584
self resonant frequency
  of capacitor, 221, 245
  of inductor, 253
semianechoic chamber (SAC)
  for measurement of radiated emissions, 50, 362, 376, 381, 385
series matching, 188, 217
shielded cables
  break frequency, 508
  surface transfer impedance, 435–438

shielded wires
  capacitive coupling, 533–538
  parameters of, 553
shielding effectiveness
  approximate solution, 567–576
  far field sources, 563–576
  near-field sources, 576–579
shielding factor, 508, 509, 514, 516, 517, 520
shield, in terms of insertion loss, 294, 296
short arc, 273, 274
shorted-turn method, 582
showering arc, 274–275
signal ground, 610–612
signal integrity, 133–211
signal measurers
  equivalent circuit of input, 25
signal source output in dBm, 26
signal source specification
  Thevenin equivalent circuit, 133
single-point ground, 629–634
sinx/x function, 95
skin depth
  of Copper, table of, 226
  effect of adding two signals in the bandwidth, 203
Society of Automotive Engineers (SAE), 63
solenoids, 268
spectral bounds
  use in computing output spectra, 111–113
spectra of digital waveforms, 129–131
spectrum analyzer
  average detector, 38, 51, 118
speed of components, 637, 638
speed of light, 10
SPICE (PSPICE)
  .AC, 767, 775
  coding of circuit elements, 274, 687, 766
  controlled sources, 768, 790, 791
  .DC, 264, 767
  exact model for lossless coupled lines, 788–804
  .FOUR, 806, 807, 810, 813, 814
  in Fourier analysis, 818
  LTSPICE, 765–820
  model of a transmission line, 170
  mutual inductance, 452
  node voltages, 766
  .PRINT, 767, 805
  .PROBE, 765, 767
  PUL.DAT, 762–763, 793, 799, 800, 815–817
  PULSE (pulse waveform), 807, 808, 810, 811
  PULSE function, 808
  PWL (piecewise linear waveform), 86
  PWL function, 807
  SIN function, 810
  sinusoidal waveform, 813
  solution of phasor transmission lines, 193, 205
  SPICELPI.FOR, 193, 205
  SPICEMTL.FOR, 753, 788, 792, 795, 800
  subcircuit model, SUBCKT, 800, 816, 818
  T model of a transmission line, 785
  .TRAN, 767, 772, 773, 794, 796, 800, 805, 806, 813
  transmission line, 815–817
  tutorial, 765–818
  unit multipliers, 768
SPICELPI.FOR, 788, 817–820
SPICEMTL.FOR, 820
square wave
  coefficients of, 76
  Fourier coefficients of, 90
  spectrum of, 96
stepper motors, 267
stranded wires, 222, 463, 553
stripline transmission line
  sketch of, 762–763
STRPLINE.FOR, 762–763
surface mount technology (SMT), 235, 645
surface transfer impedance
  of shielded cables, 435–438
susceptibility model for wires and PCB lands, 442–443

TEM mode of propagation, 199, 449, 743
TEMPEST, 6, 7
time constant, 85, 113, 117, 174, 176, 296, 606, 806
time delay, of a transmission line, 10
time shift
  in Fourier series coefficients, 85, 124
  principle of, 87, 314, 685
Townsend discharge, 271, 272
transfer function, of linear system, 24
transformers
  E-core, 317
  in power supplies, 310–319
transmission coefficients, of plane waves, 183, 185, 192, 375, 568
transmission line discontinuities, 180–192
transmission-line equations
  phasor reflection coefficient, 192
  phasor solution for lossy lines, 202
  for predicting crosstalk, 446
  sinusoidal steady state, 683–686
  time domain, 71–124
  time-domain solution, 155–170
transmission-line parameters

  for a homogeneous medium, 140, 141, 153, 154, 156, 194, 204, 205, 232, 447, 476, 754, 756, 758
transmission lines
  average power flow, 199, 726
  low loss, 206, 207, 210
  lumped-circuit approximate models of, 210–211, 219, 785–788
trapezoidal (clock) waveforms
  Bode plot, 96, 100, 103, 112, 239, 240, 244, 245, 252
  pulse width of, 770, 808
  risetime of, 93, 95
  spectral bounds, 96–111
  spectrum of, 111–113
trapezoidal (digital) waveforms, 119
  spectral bounds, 96–111
  spectrum of, 111–113
triboelectric series, 661, 662
TTL totem-pole outputs, 606
twisted wire pairs, 534, 539
  inductive coupling, 678
two wires above a ground plane
  per-unit-length inductances of, 461
two wires within a shield
  per-unit-length inductances of, 462
two-wire transmission line
two-wire transmission line, capacitance of, 261

Underwriters Laboratory (UL), 298
uniform plane waves, 726–741
units
  conversion of, 22, 266, 388
  English system of, 8, 17
  metric (SI), 8

vector analysis, 694–701
vectors
  cross product, 695–697
  curl, 699, 700
  divergence, 699, 700
  divergence theorem, 700, 716, 718
  dot product, 695
  line integral, 697, 700
  Stokes' theorem, 613, 615, 700, 707
velocity of propagation
  on a transmission line, 9, 10, 14, 135, 140, 156, 159, 166, 205, 206
  of a wave, 9, 10, 14, 134, 135, 140, 151, 156, 193, 199, 205, 206, 207, 212, 213, 733

WILEY END USER LICENSE AGREEMENT

Go to www.wiley.com/go/eula to access Wiley’s ebook EULA.